COMMISSIONS 27 AND 42 OF THE I. A. U.

INFORMATION BULLETIN ON VARIABLE STARS

Nos. 6101 – 6200

2014 March – 2017 February

H–1121 BUDAPEST XII, KONKOLY THEGE ÚT

URL http://www.konkoly.hu/IBVS/IBVS.html

HU ISSN 0374–0676

COPYRIGHT NOTICE

CONTENTS

2014

2015

2016

2017

AUTHOR INDEX

INDEX OF VARIABLES

Star	IBVS No.
BD+09 3111	6124
central star of NGC 6853	6194
central star of NGC 7008	6194
central star of NGC 7076	6194
central star of NGC 7354	6194
GSC 00476-01362	6163
GSC 0191-1282	6150
GSC 03122-02426	6199 6200
GSC 05581-00047	6199 6200
GSC 1489-0914	6122
GSC 1566-2802	6122
GSC 2610-0035	6150
GSC 3851-0240	6150
GSC 4145-0919	6122
GSC 4464-0924	6150
GSC2.3 N1Y0039176	6199 6200
HD 14082	6145
HD 106426	6110
HD 177765	6185
in IC4651	6107
in King 12	6144
IRAS 07001-0230	6188
JCMTSE J053540.0-060838	6187
KIC 2835289	6138
Kronberger PN J1944.9+2245	6194
MASTER OT J132104.04+560957.8	6129
Nova LMC 1968	6162
PSN J07285387+3349106	6140
StH*a* 169	6176
TYC 2505-672-1	6197
TYC 3551-1535-1	6135
TYC 3556-130-1	6105
TYC 3556-299-1	6105
TYC 6083-192-1	6116
TYC 8638-2548-1	6116
USNO-A2.0 1200-08721202	6136
WASP-39b	6177
WISE J194643.44+472029.4	6147

COMMISSIONS 27 AND 42 OF THE IAU
INFORMATION BULLETIN ON VARIABLE STARS

Number 6101

Konkoly Observatory
Budapest
29 March 2014

HU ISSN 0374 – 0676

APASS COLORS FOR 112 SHORT-PERIOD W UMa BINARY CANDIDATES

TERRELL, DIRK

Department of Space Studies, Southwest Research Institute, 1050 Walnut St., Suite 300, Boulder, CO, USA, 80302

e-mail: terrell@boulder.swri.edu

The period distribution of the overcontact binary star systems with convective envelopes, the W UMa binaries, shows a peak at about 0.27 days and a short-period limit at about 0.2 days (Rucinski, 2007). No satisfactory explanation for the short-period limit is yet known, and there is great interest in the discovery and characterization of systems near the limit. Recently, Lohr et al. (2013) published a list of 143 candidate W UMa systems with periods less than 0.23 days discovered in a search of data gathered by the SuperWASP project (Pollacco et al., 2006).

The AAVSO Photometric All-Sky Survey (Henden et al., 2012; hereafter, APASS) is an all-sky survey in five passbands (Johnson B,V and Sloan g',r',i') that covers the 10th-17th magnitude range, making it a complementary source of information for extrasolar planet surveys like SuperWASP and the Kepler mission (Borucki et al., 2010). APASS provides magnitudes and colors with a precision of 0.02 mag to about V=14 for well-sampled observations at a single epoch, with the usual exponential scatter at fainter magnitudes and a precision of about 0.1 mag at V=16.5.

Synoptic surveys like SuperWASP are effective at discovering variable stars, but unfiltered or single-filter observations are ineffective at distinguishing different types of variable stars whose light curve shapes are very similar. For example, in the period range where W UMa systems are found, the light curves of pulsating variables such as δ Scuti stars can be indistiguishable from low-inclination W UMa system light curves. Color information, however, can resolve the identification problem because pulsating stars are of earlier spectral types than the W UMa systems.

With this capability in mind, the APASS database was searched for the 143 sytems in Lohr et al. (2013), and 112 of them were found to have at least two nights of observations. For those systems, the $B-V$ color was measured at each epoch of APASS observation, and then means were formed for all observations of a given star. The larger of the standard deviation of the mean of the $B-V$ values or 0.02 mag (usually for objects with only two APASS observations) was taken as the error in $B-V$.

W UMa systems are known to follow a period-color relation (Terrell, Gross & Cooney, 2012; hereafter, TGC) and this relation can be used to distinguish W UMa systems from pulsating stars. Figure 1 shows the period-color relation for systems from TGC with periods less than 0.3 days (black circles) and the systems from Lohr et al. (2013) that have APASS data (red squares). The short-period blue envelope (SPBE) from Rucinski

(1998) is shown as a solid curve. The dashed curve is a modified SPBE computed as the Rucinski SPBE minus 0.18 mag in $B-V$ to match the bluest systems from TGC that are known to be W UMa systems. Systems significantly below this curve can be ruled out as W UMa systems.

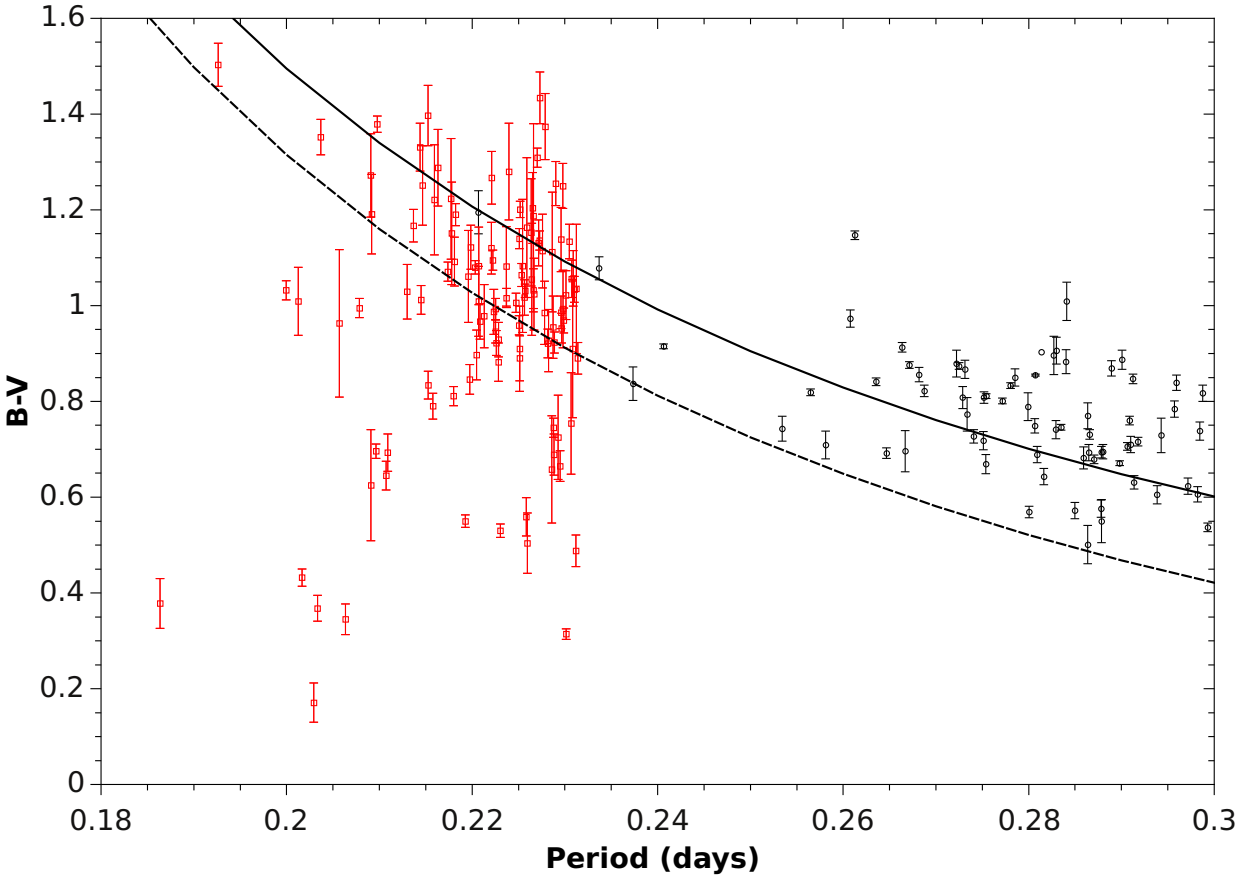

Figure 1. The period-color diagram for W UMa systems (black circles) from Terrell, Gross, and Cooney (2012) and the candidate W UMa systems (red squares) with APASS observations. The upper curve (solid) is the short-period blue envelope (SPBE) from Rucinski (1998) and the lower curve (dashed) is the Rucinski SPBE lowered by 0.18 mag in $B-V$ to include the bluest W UMa systems from Terrell, Gross, & Cooney (2102).

Interstellar reddening can, of course, affect the location of a given object in the period-color diagram. An estimate of the maximum reddening can be determined with the NASA/IPAC Infrared Science Archive's Galactic Dust Redddening and Extinction tool at `http://irsa.ipac.caltech.edu/applications/DUST/` which uses the Schlafly and Finkbeiner (2011) reddening measurements.

Based on the location of an object in the period-color diagram and the error in the $B-V$ color, we can classify the object as unlikely, possibly, or likely to be a W UMa system. For the systems defined as unlikely to be W UMa systems, the APASS $B-V$ is the reddest intrinsic color that the object can have, since dereddening will only make the derived intrinsic color bluer. If the object is lower than the modified SPBE by three times its standard deviation in $B-V$, it is placed in the group of objects unlikely to be W UMa systems. Table 1 gives the APASS $B-V$, the color excess $E(B-V)$, and the

unreddened $B-V$ for these systems.

Table 1. APASS Observations of Objects Unlikely to be W UMa Systems.

SuperWASP ID	Period (d)	Obs.	$B-V$	E($B-V$)	Unreddened $B-V$
J115605.88-091300.5	0.21091	5	0.693±0.039	0.030±0.003	0.663±0.039
J201208.72+083509.8	0.21577	5	0.790±0.027	0.156±0.004	0.634±0.027
J204843.90-350912.7	0.22883	4	0.689±0.043	0.054±0.001	0.634±0.043
J111931.48-395048.2	0.22949	2	0.665±0.032	0.106±0.001	0.559±0.032
J084925.17-151516.5	0.19996	2	1.032±0.020	0.065±0.004	0.968±0.020
J151652.90+004835.8	0.21073	4	0.645±0.030	0.043±0.001	0.603±0.030
J144331.57-421626.8	0.21526	3	0.834±0.029	0.102±0.005	0.731±0.029
J060334.52-283427.1	0.20635	5	0.345±0.032	0.029±0.001	0.315±0.032
J161858.05+261303.5	0.22878	2	0.745±0.020	0.047±0.001	0.698±0.020
J231839.72+352848.2	0.20126	4	1.009±0.071	0.077±0.002	0.932±0.071
J201816.85+112452.8	0.18636	5	0.378±0.052	0.174±0.006	0.204±0.052
J092339.29-412648.9	0.20293	3	0.171±0.041	0.287±0.004	−0.116±0.041
J194726.58-243941.0	0.20334	2	0.368±0.027	0.086±0.002	0.282±0.027
J133105.91+121538.0	0.21801	2	0.811±0.020	0.022±0.000	0.789±0.020
J061011.73-345809.0	0.23014	2	0.314±0.020	0.040±0.000	0.274±0.020
J142312.63-222425.1	0.20964	3	0.696±0.020	0.098±0.002	0.598±0.020
J121359.79-414742.7	0.21927	3	0.550±0.020	0.137±0.007	0.413±0.021
J075149.14+362250.9	0.23119	7	0.488±0.033	0.043±0.001	0.445±0.033
J024148.62+372848.3	0.21975	2	0.846±0.031	0.050±0.001	0.796±0.031
J214046.44+130716.6	0.22596	4	0.504±0.063	0.144±0.005	0.359±0.063
J235935.22+362001.5	0.20167	6	0.432±0.020	0.116±0.002	0.316±0.020
J050128.17-041206.9	0.22584	5	0.559±0.040	0.042±0.001	0.517±0.040
J210423.94+073104.8	0.20909	2	0.625±0.116	0.061±0.002	0.564±0.116
J162117.36+441254.2	0.20785	2	0.995±0.020	0.009±0.001	0.986±0.020
J070953.45+364417.3	0.22305	2	0.530±0.020	0.050±0.000	0.480±0.020

On the other end of the color range, there are objects redder than the SPBE and these are the systems likely to be W UMa systems. Since these objects might be intrinsically bluer because of reddening, we compare their de-reddened $B-V$ with the modified SPBE. If the object is higher than the SPBE in the period-color diagram by more than three times its standard deviation in de-reddened $B-V$, it is placed in the group of objects likely to be W UMa systems, because even with the maximum amount of reddening, they cannot fall below the modified SPBE. Table 2 gives the color data on these systems.

For the remaining systems, the errors in their $B-V$ values are too large to firmly place them in the likely or unlikely W UMa groups. These systems are grouped together as possible W UMa systems, and future observations will have to be made to determine their character. Table 3 lists the color data on these systems. Figure 2 shows the unlikely (black circles), likely (red squares) and possible (green triangles) W UMa systems in the period-color diagram. Note that the upper-leftmost object is BX Trianguli, the W UMa system with the shortest known period (Dimitrov & Kjurkchieva, 2010).

Table 2. APASS Observations of Objects Likely to be W UMa Systems.

SuperWASP ID	Period (d)	Obs.	$B-V$	E($B-V$)	Unreddened $B-V$
J212813.35-520029.1	0.23048	2	1.134±0.036	0.017±0.001	1.117±0.036
J041655.13-492709.8	0.23102	3	1.034±0.027	0.013±0.001	1.021±0.027
J222302.02+195031.8	0.22518	2	1.201±0.020	0.037±0.001	1.164±0.020
J211359.46+122712.4	0.22211	6	1.267±0.055	0.061±0.002	1.206±0.055
J055215.51-551950.8	0.22728	2	1.136±0.020	0.097±0.004	1.039±0.020
J115557.62+072009.1	0.22702	2	1.309±0.020	0.013±0.000	1.295±0.020
J093443.60+420831.9	0.22224	6	1.095±0.021	0.012±0.001	1.083±0.021
J120110.98-220210.8	0.22717	3	1.131±0.048	0.043±0.003	1.088±0.048
J114929.22-423049.0	0.22731	4	1.434±0.054	0.152±0.003	1.282±0.054
J161335.80-284722.2	0.22978	8	1.250±0.047	0.186±0.007	1.064±0.048
J180947.64+490255.0	0.22788	4	1.374±0.069	0.048±0.002	1.326±0.069
J164349.61+325637.8	0.22509	2	1.140±0.021	0.029±0.001	1.110±0.021
J221117.26-150216.6	0.21525	9	1.397±0.063	0.026±0.001	1.372±0.063
J102328.57-153951.7	0.20978	3	1.379±0.020	0.069±0.002	1.310±0.020
J224747.20-351849.3	0.21822	2	1.190±0.023	0.012±0.001	1.177±0.023
J150957.56-115308.4	0.22902	7	1.255±0.046	0.087±0.001	1.168±0.046

Table 3. APASS Observations of Possible W UMa Systems.

SuperWASP ID	Period (d)	Obs.	$B-V$	E($B-V$)	Unreddened $B-V$
J215826.52+253437.4	0.22261	13	0.922±0.026	0.054±0.001	0.867±0.026
J162841.41-334419.8	0.20369	3	1.352±0.037	0.509±0.013	0.843±0.039
J210318.76+021002.2	0.22859	4	0.658±0.112	0.077±0.003	0.581±0.112
J151144.56+165426.4	0.21986	2	1.122±0.046	0.027±0.001	1.095±0.046
J015100.23-100524.2	0.21450	3	1.012±0.030	0.028±0.001	0.984±0.030
J101618.12-085531.0	0.21466	3	1.251±0.083	0.040±0.000	1.211±0.083
J092754.99-391053.4	0.22534	3	1.064±0.024	0.273±0.006	0.792±0.025
J041120.40-230232.3	0.21632	4	1.288±0.080	0.038±0.001	1.250±0.080
J095706.80-201408.7	0.22759	3	1.114±0.077	0.035±0.000	1.079±0.077
J153951.12+105420.7	0.22072	2	1.083±0.081	0.041±0.001	1.042±0.081
J062634.80-385650.1	0.22369	2	1.082±0.083	0.098±0.001	0.984±0.083
J201808.68-231443.0	0.22781	3	0.985±0.066	0.067±0.001	0.918±0.066
J051459.80-021923.6	0.23090	6	1.057±0.058	0.164±0.028	0.893±0.064
J160156.04+202821.6	0.22653	2	1.204±0.074	0.048±0.003	1.156±0.074
J235333.60+455245.8	0.23074	3	1.056±0.039	0.111±0.004	0.945±0.039
J011732.10+525204.9	0.22397	2	1.280±0.101	0.411±0.010	0.869±0.101
J232610.13-294146.6	0.23012	9	1.022±0.051	0.020±0.000	1.002±0.051
J034439.97+030425.5	0.22988	5	0.969±0.026	0.188±0.009	0.780±0.028
J044132.96+440613.7	0.22815	2	1.785±0.101	0.937±0.008	0.848±0.101
J031700.67+190839.6	0.22565	3	1.017±0.037	0.129±0.002	0.888±0.037
J030749.87-365201.7	0.22667	2	1.024±0.075	0.018±0.001	1.005±0.075
J211625.31+251755.4	0.21739	2	1.071±0.020	0.102±0.004	0.969±0.020
J042200.64-450312.5	0.21810	4	1.092±0.051	0.017±0.001	1.076±0.051
J022050.85+332047.6	0.19263	6	1.503±0.045	0.067±0.001	1.437±0.045

SuperWASP ID	Period (d)	Obs.	$B-V$	E$(B-V)$	Unreddened $B-V$
J212009.70-185220.8	0.21780	3	1.151±0.107	0.037±0.001	1.114±0.107
J004050.63+071613.9	0.22927	5	0.725±0.088	0.034±0.002	0.691±0.088
J084408.68-040640.1	0.21773	2	1.223±0.126	0.014±0.000	1.209±0.126
J004545.23-244516.2	0.22034	2	1.080±0.020	0.017±0.001	1.063±0.020
J061850.43+220511.9	0.21439	5	1.331±0.050	0.746±0.031	0.585±0.059
J231943.31+134121.4	0.23084	2	0.910±0.144	0.049±0.002	0.862±0.144
J010642.20-330857.9	0.22208	9	1.120±0.054	0.022±0.002	1.098±0.054
J000205.32+381321.5	0.20908	4	1.272±0.087	0.088±0.002	1.183±0.087
J050904.45-074144.4	0.22958	4	0.986±0.034	0.077±0.002	0.909±0.034
J104942.44+141021.5	0.22980	3	0.993±0.081	0.028±0.002	0.964±0.081
J123148.12-020602.3	0.22661	2	1.032±0.045	0.020±0.001	1.012±0.045
J010340.37-172138.8	0.22824	3	0.927±0.065	0.015±0.000	0.912±0.065
J233120.96-145814.2	0.21594	3	1.221±0.115	0.025±0.000	1.197±0.115
J200756.54-163408.0	0.22253	2	0.946±0.024	0.124±0.002	0.822±0.024
J173003.21+344509.4	0.22371	2	1.016±0.020	0.026±0.001	0.990±0.020
J040615.79-425002.3	0.22234	4	0.987±0.047	0.009±0.000	0.978±0.047
J172717.97+431624.0	0.22507	2	0.959±0.020	0.014±0.001	0.946±0.020
J195730.89+000705.1	0.22643	3	1.055±0.117	0.171±0.002	0.884±0.117
J025054.80+012357.5	0.23067	6	0.754±0.106	0.046±0.002	0.708±0.106
J221058.82+251123.4	0.21300	8	1.029±0.057	0.067±0.003	0.961±0.057
J134430.51-270302.8	0.22965	3	0.953±0.031	0.051±0.000	0.902±0.031
J200059.78+054408.9	0.20569	4	0.963±0.154	0.103±0.006	0.860±0.154
J130920.49-340919.9	0.22284	5	0.882±0.040	0.058±0.001	0.825±0.040
J135403.76-462948.7	0.22873	3	0.955±0.065	0.094±0.003	0.861±0.065
J140533.33+114639.1	0.22512	3	0.910±0.089	0.020±0.000	0.890±0.089
J183738.17+402427.2	0.22131	2	0.978±0.066	0.062±0.002	0.916±0.066
J052036.84+030402.1	0.23140	4	0.890±0.033	0.103±0.006	0.787±0.034
J121906.35-240056.9	0.22637	3	1.153±0.112	0.083±0.002	1.070±0.112
J115326.51+060756.0	0.22864	3	1.112±0.125	0.010±0.001	1.103±0.125
J234401.81-212229.1	0.21368	5	1.167±0.034	0.019±0.000	1.148±0.034
J231505.30-010617.0	0.22959	6	1.138±0.067	0.035±0.001	1.103±0.067
J074658.62+224448.5	0.22085	2	0.967±0.037	0.039±0.001	0.927±0.037
J003033.05+574347.6	0.22662	6	1.187±0.193	0.412±0.009	0.775±0.193
J214510.25-494401.1	0.22816	2	0.921±0.030	0.019±0.001	0.902±0.030
J104125.56-145842.3	0.22572	2	1.031±0.020	0.041±0.002	0.990±0.020
J075102.16+342405.3	0.20917	3	1.191±0.083	0.040±0.001	1.151±0.083
J052825.85+093943.7	0.22070	2	1.009±0.073	0.276±0.013	0.733±0.074
J193537.06-401409.1	0.22590	3	1.163±0.146	0.105±0.002	1.058±0.146
J220734.47+265528.6	0.23124	10	1.035±0.135	0.064±0.001	0.971±0.135
J090758.16-153811.8	0.22888	4	0.923±0.022	0.064±0.001	0.858±0.022
J151146.20-354721.9	0.22254	3	0.993±0.022	0.130±0.007	0.863±0.023
J130111.22+420214.0	0.22544	2	1.083±0.139	0.015±0.000	1.068±0.139
J220235.74+311909.7	0.22048	14	0.897±0.052	0.085±0.002	0.812±0.052
J025959.18-395812.3	0.22285	4	0.929±0.036	0.015±0.001	0.914±0.036
J222514.69+361643.0	0.22473	2	1.006±0.020	0.089±0.001	0.917±0.020
J132308.74+424613.3	0.22513	2	0.890±0.047	0.014±0.001	0.876±0.047
J160202.07+121213.5	0.21960	3	1.061±0.096	0.044±0.001	1.017±0.096

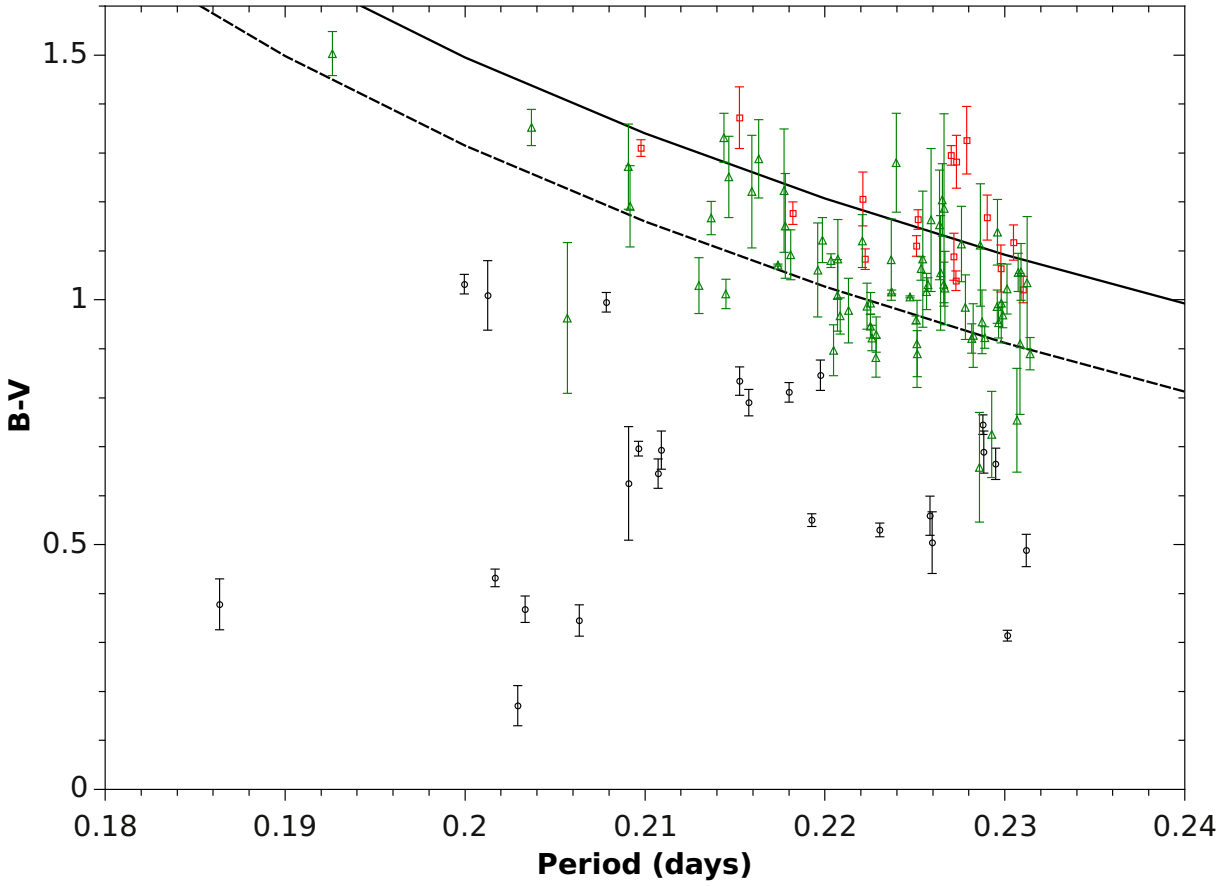

Figure 2. The period-color diagram for objects unlikely to be W UMa systems (black circles) , likely W UMa systems (red squares), and possible W UMa systems (green triangles). The curves are the same as in Figure 1.

In all, 25 objects listed by Lohr et al. (2013) can be ruled out as W UMa systems, while 16 are almost certainly W UMa systems. The remaining 71 could possibly be W UMa systems, and further observations will be needed to characterize them. The 16 likely W UMa systems are good candidates for radial velocity studies to better characterize the properties of overcontact systems near the short-period limit.

Acknowledgement: This research has made use of the APASS database, located at the AAVSO web site. Funding for APASS has been provided by the Robert Martin Ayers Sciences Fund.

References:

Borucki, W. J., et al., 2010, *Science*, **327**, 977
Dimitrov, D. P. & Kjurkchieva, D. P., 2010, *MNRAS*, **406**, 2559
Henden, A. A., Levine, S. E., Terrell, D., Smith, T. C. & Welch, D., 2012, *J. AAVSO*, **40**, 430
Lohr, M. E., Norton, A. J., Kolb, U. C., Maxted, P. F. L., Todd, I., & West, R. G., 2013, *A&A*, **549**, A86
Pollacco, D. L., Skillen, I., Cameron, A. C., et al. 2006, *PASP*, **118**, 1407
Rucinski, S., 1998, *AJ*, **116**, 2998
Rucinski, S., 2007, *MNRAS*, **382**, 393
Schlafly, E. F. & Finkbeiner, D. P., 2011, *ApJ*, **737**, 103
Terrell, D., Gross, J., & Cooney, W. R., 2012, *AJ*, **143**, 99

*This version of the paper contains corrections, and differs from the one appeared on-line originally. Date of last modification: Sun Nov 23 06:57:35 CET 2014

COMMISSIONS 27 AND 42 OF THE IAU
INFORMATION BULLETIN ON VARIABLE STARS

Number 6102

Konkoly Observatory
Budapest
11 April 2014

HU ISSN 0374 – 0676

TIMES OF MINIMA OF ECLIPSING CATACLYSMIC VARIABLES

ATALI, H.B.; ALIS, S.; YELKENCI, K.; SAYGAC, A.T.; AKSOYU NURANOGLU, Y.; FISEK, S.; ULGEN, E.K.

Department of Astronomy and Space Sciences, Faculty of Science, Istanbul University, 34119, Istanbul, Turkey; e-mail: salis@istanbul.edu.tr

Observatory and telescope:
0.6m Ritchey-Chrétien (f/8) telescope (IST60) at Ulupinar Astrophysical Observatory, Canakkale.

Detector:	Apogee Alta U42 CCD camera, 2048 × 2048 pixels with a read-out noise of 10e$^-$ RMS; SBIG STL-1001E CCD camera, 1024 × 1024 pixels with a read-out noise of 14.8e$^-$ RMS.

Method of data reduction:
Reduction of the CCD frames was made in the usual way using IRAF[1] package.

Method of minimum determination:
The minima times were computed with Kwee & Van Woerden (1956) method.

Times of minima:

Star name	Time of min. HJD 2400000+	Error	Type	Filter	Rem.
BH Lyn	56195.5590	0.001	I	White-light	C2
TT Tri	56195.2590	0.002	I	White-light	C2
	56195.3990	0.003	I	White-light	C2
	56570.3250	0.002	I	White-light	C1
HS0455+8315	56193.3580	0.001	I	White-light	C2
	56193.5070	0.001	I	White-light	C2
	56571.2650	0.005	I	White-light	C1
	56571.4140	0.005	I	White-light	C1
PX And	56158.3920	0.002	I	White-light	C1
	56194.5390	0.003	I	White-light	C2
	56570.5200	0.001	I	White-light	C1
V1315 Aql	56159.2930	0.001	I	White-light	C1
	56159.4330	0.001	I	White-light	C1

[1]IRAF is distributed by the National Optical Astronomical Observatories, operated by the Association of the Universities for Research in Astronomy, inc., under cooperative agreement with the National Science Foundation

Explanation of the remarks in the table:
C1 and C2 refer to the CCD cameras Apogee Alta U42 and SBIG STL-1001E, respectively.

Remarks:
These objects were observed in the framework of a project which is carried out at Istanbul University to follow period changes in cataclysmic variables. HS0455+8315 is a SW Sex-type cataclysmic variable which was identified by the Hamburg Quasar Survey (Hagen et al. 1995).

Acknowledgements:
IST60 is a joint project between Canakkale Onsekiz Mart University Astrophysics Research Center and Istanbul University Observatory Research and Application Center and supported by the Research Fund of Istanbul University through the project BAP-3685. Authors would like to thank Ulupinar Astrophysical Observatory for their hospitality.

References:

Hagen, H. J. et al., 1995, *A&AS*, **111**, 195

Kwee, K., van Woerden, H., 1956, *Bulletin of the Astronomical Institutes of the Netherlands*, **12**, 327

COMMISSIONS 27 AND 42 OF THE IAU
INFORMATION BULLETIN ON VARIABLE STARS

Number 6103

Konkoly Observatory
Budapest
12 April 2014

HU ISSN 0374 – 0676

PERIODIC BEHAVIOUR OF THE HeI 6678 Å EMISSION LINE IN γ Cas

POLLMANN, ERNST[1]; GUARRO FLÓ, JOAN[2]

[1] Emil-Nolde-Str. 12, 51375 Leverkusen, Germany

[2] Balmes 2, 08784 Piera (Barcelona), Spain

e-mail: ernst-pollmann@t-online.de; jguarro@telepolis.com

Introduction

The Be star γ Cas (27 Cas, HD 5394, HR 264) is a primary component of a spectroscopic binary and is the very first Be star known, discovered by Secchi (1866). Spectroscopically γ Cas has been investigated mostly in the Balmer lines, mainly in Hα. Recent studies considered He and Fe II lines as well as the kinematics of the circumstellar shell (Hanuschik 1994, Smith 1995). It is believed that a local density enhancement – a one-armed density spiral – is embedded in the disk of γ Cas. Precession of this density enhancement has been observed interferometrically by Berio et al. (1999). They found that this enhanced equatorial density pattern may be located at 1.5 stellar radii from the stellar surface. Stee et al. (1998) proposed that He excitation and ionization region, responsible for the emission in the HeI 6678 Å line, extend to 2.3 stellar radii. Thus, the HeI 6678 Å line has an important diagnostic value of activity close to the stellar surface. The time-dependent mass loss from the primary component of the γ Cas binary system assumes that both photospheric and disk density variations lead to the double peak profile variations of HeI 6678 Å. Recent investigations of Smith (1995), Harmanec et al. (2000), Harmanec (2002), Pollmann & Stober (2005) and Pollmann (2009) give detailed information about the long-term monitoring of the phase and time dependent radial velocities and equivalent widths of the HeI 6678 Å emission line. Further detailed and useful information of the known variations and their time scales, e.g. in context with the orbital period of 203.52 d reported by Harmanec et al. (2000), have been compiled by Miroshnichenko et al. (2002).

Many Be stars often show various periodic phenomena, which can be sometimes strictly periodic, however they can change that behaviour. The periodic V/R variations were explained by one-armed pulsations (Okazaki 1991, 1997), although this is not the only explanation. This V/R ratio is the ratio of the violet-to-red emission peaks that is used as one of the main characteristics describing the double-peak emission lines of Be stars as stated by Stefl et al. (2007).

A cooperative project of amateurs and professionals on π Aqr (Zharikov et al. 2013) shows that the V/R observed in the Hα line can be explained by a local density enhancement that revolves around the primary component of this binary system with the orbital period. Apart from the orbital period, which has been determined on the basis

of radial velocity measurements of the Hα and HeI 6678 Å lines (Harmanec et al. 2000, Miroshnichenko et al. 2002, Nemravová et al. 2012), there is no information about the V/R periodicity of the HeI 6678 Å line in the spectrum of γ Cas. Since spectral lines may form in different places of a circumstellar disk, different V/R periods may be observed. Therefore we cannot a priori expect that these periods coincide with the orbital periods in binary systems. The observations of the V/R variability of the HeI 6678 Å line in the spectrum of γ Cas are presented here for the first time. We found that this variability has a period, which is not equal to the orbital one.

Results

The spectra with a resolution of $R \sim 17000$ were obtained with the Littrow grating spectrograph LHIRES III and the C14 Schmidt-Cassegrain telescope of the Vereinigung der Sternfreunde Köln (Pollmann, 41 spectra) and the Piera-Barcelona observatory Spain (Guarro, 4 spectra). The signal-to-noise (S/N) in the continuum near the HeI 6678 Å line was always higher than 1000 ($>$ 1500 in most spectra). Fig. 1 shows an example spectrum of the HeI 6678 Å double peak emission in γ Cas. To achieve such a high S/N level, 5-10 single spectra with approx. 300 sec exposure time were summed.

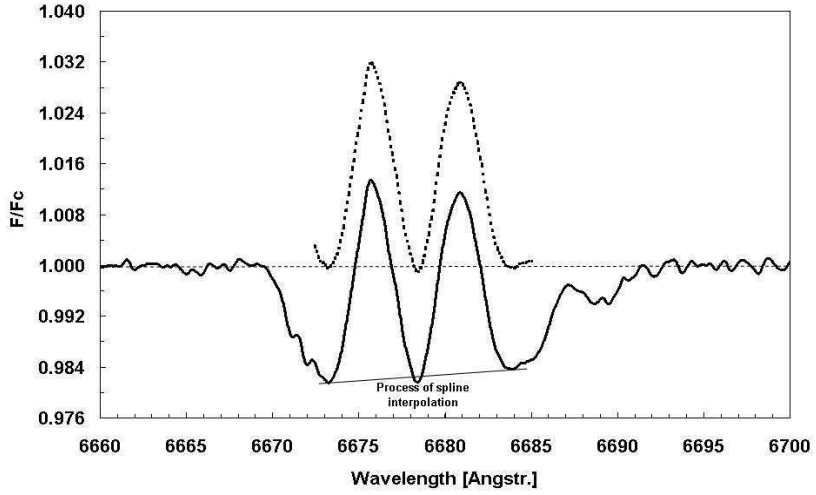

Figure 1. HeI 6678 Å spectrum of γ Cas (2014/02/04), S/N $\approx$ 2200, R = 17000. Solid line: sum spectrum; thin line: spline interpolation between the violet and red absorption minima; dashed line: the double peak emission after spline interpolation.

The accuracy of the V/R evaluation is determined by the S/N ratio and the accuracy of drawing the local continuum. It depends further on the definition of the line wing profiles and on the underlying photospheric absorption line profile. Therefore, as preparation for determining the V/R ratio, the division by a spline interpolation between the violet and red absorption minima serves as a normalizing basis with $F/F_c = 1$. The V and R intensities, separated in this way from the photospheric absorption profile, are then the values of the line maxima related to this basis (Fig. 1). The use of the data reduction program VSpec (`http://www.astrosurf.com/vdesnoux`) for that process and its tool for

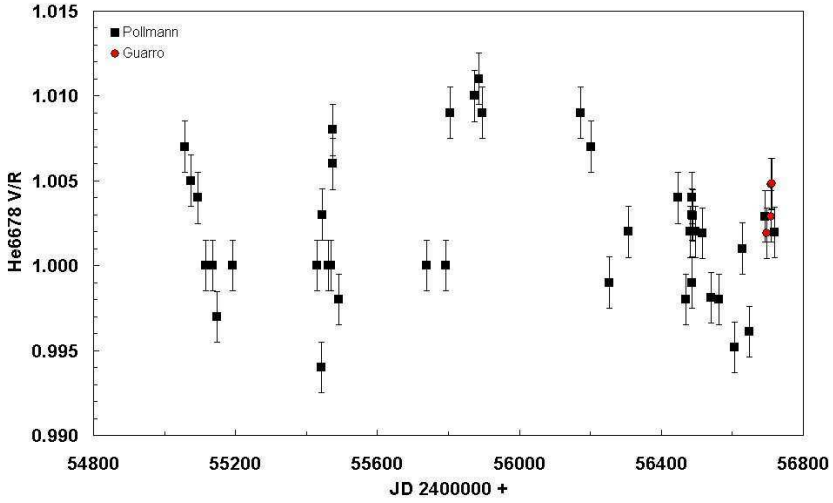

Figure 2. Time series plot of the HeI 6678Å V/R data from 2455058 to 2456719 (08/2009-03/2014).

spline filtering lead to a very precise spectrum normalization and a high level of accuracy of the V/R measurement of the order of approximately 0.2%.

Another way to separate the emission lines from the photospheric absorption profile, is the subtraction of a fitted theoretical absorption line profile. Comparisons of both methods with a same spectrum did lead to deviations to the spline interpolation process of approx. 0.01% in V/R.

As can be seen in Fig. 2, the variation in the V/R ratio of the HeI 6678 Å line is obvious. However the period of the observations (August 2009 through March 2014) covers only eight orbital periods of the binary. This result may motivate observers from different amateur groups (ARAS group for example; `http://www.astrosurf.com/aras`) to take part in this long-term study.

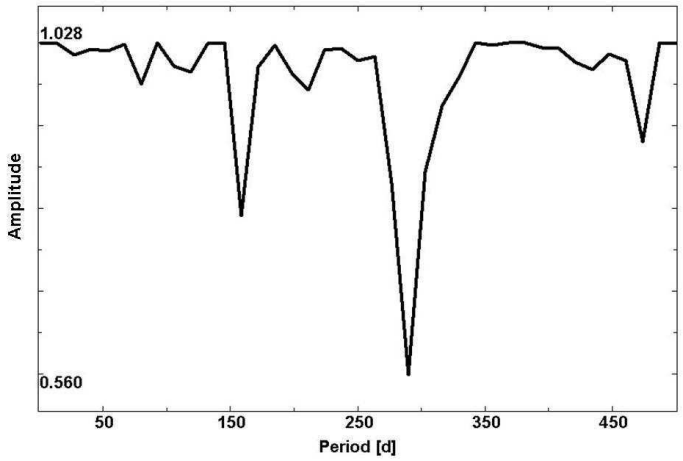

Figure 3. PDM (Phase Dispersion Minimization) periodogram (program AVE) of the data set shown in Fig. 2 points towards a period of 280 days.

The main peak in the PDM power spectrum (that corresponds to a period of 280 d) shown in Fig. 3 is very broad which makes the period evaluation uncertain. Definitely, more data are needed to constrain the period better.

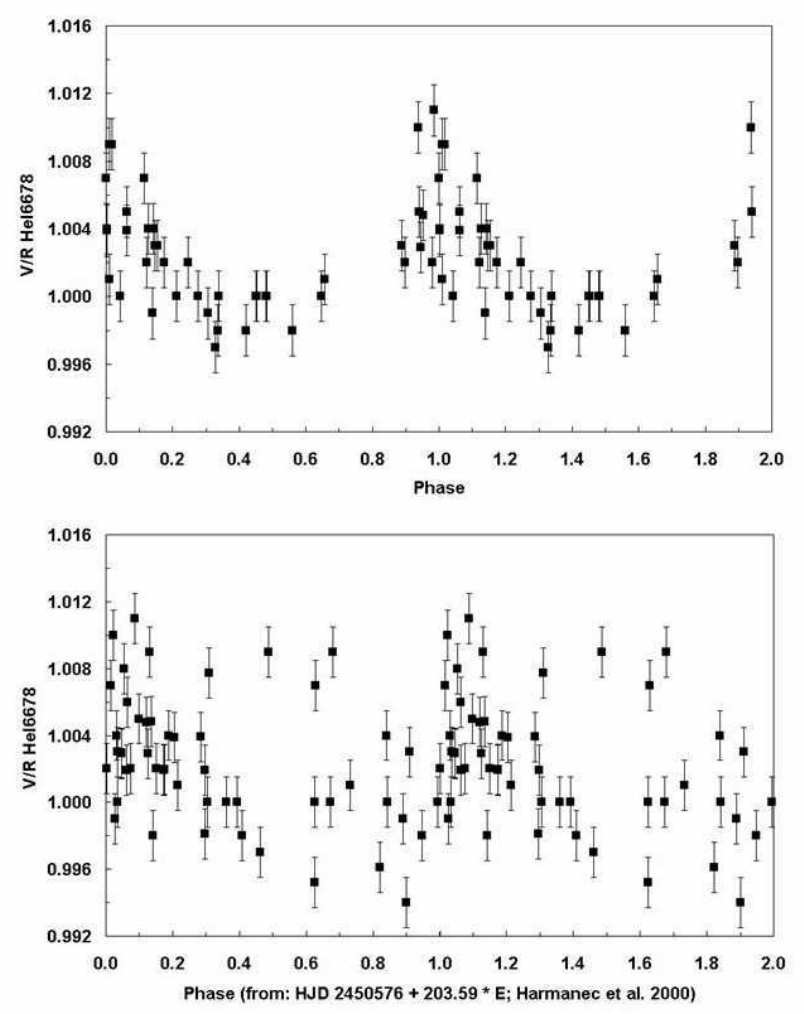

Figure 4. Top panel: phase plot of the V/R data from Figs. 2 & 3; Period: 280 ± 2.98 d; Amplitude: $0.00403 \pm 5.1 \cdot 10^{-4}$; T_0 [JD]: 24554969 ± 14.4; RMS: 0.00235. Bottom panel: phase diagram for the orbital period (203.53 d) by using the same data as in the top panel.

The top panel of Fig. 4 shows the V/R data given in Fig. 2 folded with a period of 280 days. The folding was performed with the program SpecTSA 2.0 by R. Buecke (Hamburg, Germany). In the bottom panel, these data are phased with the orbital period. There is a certain similarity of the V/R variability in the top and bottom panels due to the small difference between the periods of 280 and 203 d, respectively. However, it is clear that the observed variations in the V/R data are independent of the orbital period.

Searching for periodic phenomena (such as those found in π Aqr (Pollmann 2012, Zharikov et al. 2013) & ζ Tau (Pollmann & Rivinius 2008)) in the temporal behaviour of various lines in the spectra of many Be stars would allow us to better understand the structure of their circumstellar disks. Further long-term spectroscopic observations along with the data already stored in the BeSS database (Neiner et al. 2011; `http://basebe.obspm.fr`)

will help to achieve this goal and can also result in finding new binary systems.

Acknowledgements: We are grateful to Prof. Dr. Anatoly Miroshnichenko (Department of Physics and Astronomy, University of North Carolina at Greensboro), whose detailed and critical comments lead to major extensions and improvement of this work.

References:

Berio, P. et al., 1999, *A&A*, **345**, 203
Harmanec, P. et al., 2000, *A&A*, **364**, L85
Harmanec, P., 2002, *ASPC*, **279**, 221
Hanuschik, R. W., 1994, *IAU Symp.*, **162**, 265
Miroshnichenko, A. S., Bjorkman, K. S., Krugov, V. D., 2002, *PASP*, **114**, 1226
Neiner, C., De Batz, B., Cochard, F., Floquet, M., Mekkas, A., Desnoux, V., 2011, *AJ*, **142**, 149
Nemravová, J. et al., 2012, *A&A*, **537**, A59
Okazaki, A. T., 1991, *PASJ*, **43**, 75
Okazaki, A. T., 1997, *A&A*, **318**, 548
Pollmann, E., Stober, B., 2005, *The Be Star Newsletter*, No. 38
Pollmann, E., Rivinius, Th., 2008, *IBVS*, No. 5813
Pollmann, E., 2009, *The Be Star Newsletter*, No. 39
Pollmann, E., 2012, *IBVS*, No. 6023
Secchi, A., 1866, *AN*, **68**, 63
Smith, M. A., 1995, *ApJ*, **442**, 812
Stee, Ph., Vakili, F., Bonneau, D., Mourard, D., 1998, *A&A*, **332**, 268
Stefl, St., Okasaki, A. T., Rivinius, Th., Baade, D., 2007, *ASPC*, **361**, 274
Zharikov, S. V. et al., 2013, *A&A*, **560**, A30

COMMISSIONS 27 AND 42 OF THE IAU
INFORMATION BULLETIN ON VARIABLE STARS

Number 6104

Konkoly Observatory
Budapest
17 April 2014

HU ISSN 0374 – 0676

PHOTOMETRY OF GSC 3408-0735: A W UMa SYSTEM NEAR THE SHORT-PERIOD LIMIT

TERRELL, DIRK[1,2]; GROSS, JOHN[2]

[1] Department of Space Studies, Southwest Research Institute, 1050 Walnut St., Suite 300, Boulder, CO, USA, 80302

[2] Sonoita Research Observatory, 705 W. Millbrook Lane, Tucson, USA, 85704

e-mail: terrell@boulder.swri.edu; johngross3@msn.com

The W UMa stars are short-period overcontact binary systems of main sequence F, G, and K stars. The peak in their period distribution is at about 0.27 days (Rucinski, 2007), with a rapid dropoff in number at shorter periods. Given the small number of known systems with periods less than 0.22 days, any such system that can be well characterized will play an important role in understanding the nature of the short-period limit. In a recent analysis of 143 W UMa candidates with periods less than 0.22 days identified by Lohr et al. (2013) in SuperWASP data (Pollacco et al., 2006), Terrell (2014) found that 25 objects could be ruled out as W UMa systems and 16 were very likely to be W UMa systems, based on their colors from the AAVSO Photometric All-Sky Survey (hereafter, APASS; Henden et al., 2012). Of the remaining systems, the APASS observations are not yet sufficient in number or quality to classify them. In that group, the system GSC 3408-0735 (SuperWASP J080150.03+471433.8) has been observed once by APASS, with a $B-V$ value of 1.06 ± 0.02. Terrell (2014) required at least two observations of a system for inclusion in his analysis, but inspection of the SuperWASP light curve showed deep, potentially complete (total/annular), eclipses (see Figure 1), so it was selected for further photometric observation with the 0.5m telescope of the Sonoita Research Observatory (SRO).

The SRO 0.5m telescope is equipped with a Santa Barbara Instrument Group STL-6303E CCD camera with Johnson-Cousins filters. GSC 3408-0735 was observed on eight nights in February and March of 2014 in the B, V, and I_C passbands. Reduction of the images was performed in the usual manner by subtracting bias and dark frames and flatfielding. GSC 3408-1475 and GSC 3408-1827 were chosen as the comparison and check stars for differential photometry, and no variability greater than 0.01 magnitudes was detected in either star.

The instrumental differential magnitudes were analysed with the 2013 version of the Wilson-Devinney program (hereafter, WD; Wilson & Devinney, 1971; Wilson, 1979). The mean surface temperature of star 1 (T_1) was fixed at 4500 K based on the APASS $B-V$ value and the relatively low interstellar reddening in the field (maximum $E(B-V) = 0.06 \pm 0.01$) as estimated with the NASA/IPAC Infrared Science Archive's Galactic Dust

Reddening and Extinction tool at http://irsa.ipac.caltech.edu/applications/DUST/ which uses the Schlafly and Finkbeiner (2011) reddening measurements.

Initial fits to the light curves resulted in an overcontact configuration for the system, and subsequent iterations were done in WD mode 1 which enforces various constraints appropriate for overcontact binaries (Wilson & Van Hamme, 2013), such as equal surface potentials for the stars, and a smooth variation of surface brightness over the common envelope (hence T_2 is computed from other parameters rather than being adjusted). The adjusted parameters were orbital inclination (i), surface potential of the common envelope (Ω_1), mass ratio ($q = M_2/M_1$), orbital period zero point (HJD_0), orbital period (P), primary star bandpass luminosities (L_1) and third light (l_3). The third light values were always very small compared to their errors, consistent with there being no third light in the system, and in the final solution, third light values were fixed at zero. Local surface computation of limb darkening coefficients (as functions of $T_{\rm eff}$ and log g) was performed as described in Wilson & Van Hamme (2013).

The solution confirms that the eclipses are indeed complete, with a total secondary eclipse, making this an A-type system. While the SuperWASP light curve shows a mild asymmetry between the two maxima, our light curves do not, indicating that spot phenomena may be variable in size and/or location. Table 1 lists the parameters from the solution and Figure 2 shows the fits to the light curves. Figure 3 shows the system at the center of the primary eclipse. The instrumental differential magnitudes are available from the IBVS web site as file 6104-t1.txt.

GSC 3408-0735 is an important system because the eclipses are complete, thus resulting in a more accurate determination of the parameters of the system. The mass ratio, for example, is accurately recovered from the analysis of the photometry, as demonstrated by Terrell & Wilson (2005). With a period of 0.2175 days, it is the shortest-period overcontact binary known to show complete eclipses. The system is faint, V=13.48±0.01 at phase 0.67 for the APASS observation, so measuring accurate radial velocities will be challenging on all but the largest telescopes. But given the small number of systems near the short-period cutoff, and the ability to measure its absolute dimensions very accurately, GSC 3408-0735 is certainly worthy of study on larger instruments.

Acknowledgement: This research was made possible through the use of the AAVSO Photometric All-Sky Survey (APASS), funded by the Robert Martin Ayers Sciences Fund.

References:

Henden, A. A., Levine, S. E., Terrell, D., Smith, T. C. & Welch, D., 2012, *J. AAVSO*, **40**, 430

Lohr, M. E., Norton, A. J., Kolb, U. C., Maxted, P. F. L., Todd, I., and West, R. G., 2013, *A&A*, **549**, A86

Pollacco, D. L., Skillen, I., Cameron, A. C., et al. 2006, *PASP*, **118**, 1407

Rucinski, S., 2007, *MNRAS*, **382**, 393

Schlafly, E. F. & Finkbeiner, D. P., 2011, *ApJ*, **737**, 103

Terrell, D., 2014, *IBVS*, 6101

Terrell, D. & Wilson, R. E., 2005, *ApSpSc*, **296**, 221

Wilson, R. E., 1979, *ApJ*, **234**, 1054

Wilson, R. E. & Devinney, E. J., 1971, *ApJ*, **166**, 605

Wilson, R. E. & Van Hamme, W., 2013, ftp://ftp.astro.ufl.edu/pub/wilson/lcdc2013/ebdoc2013.3apr2013.ps

Table 1. Parameters for GSC 3408-0735.

Parameter	Value
$T_1(K)$	4500 (assumed)
$T_2(K)$	4477 (computed)
i (°)	85.2±0.3
Ω_1	2.715±0.006
q	0.440±0.003
HJD_0	2453383.949±0.006
P (days)	0.2175137±0.0000004
$L_1/(L_1+L_2)_B$	0.686±0.002
$L_1/(L_1+L_2)_V$	0.684±0.002
$L_1/(L_1+L_2)_{I_C}$	0.682±0.001

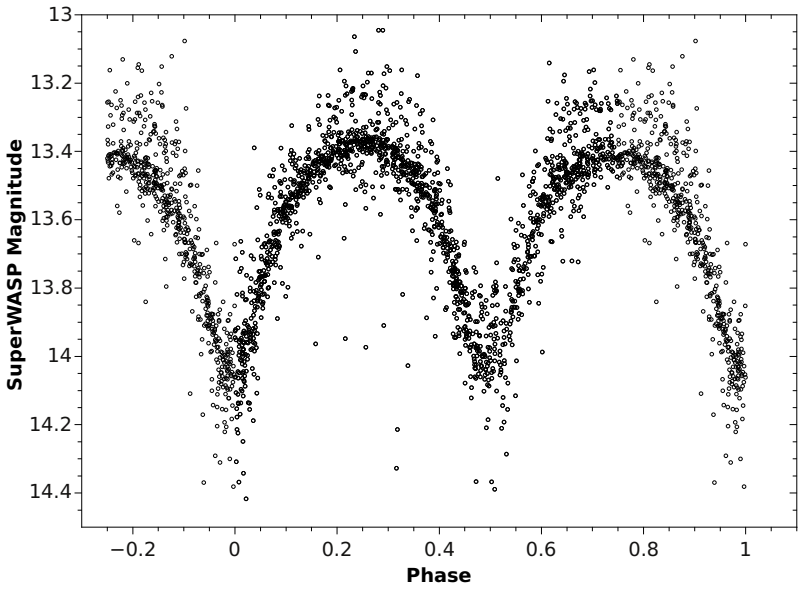

Figure 1. The SuperWASP (data release 1) light curve of GSC 3408-0735.

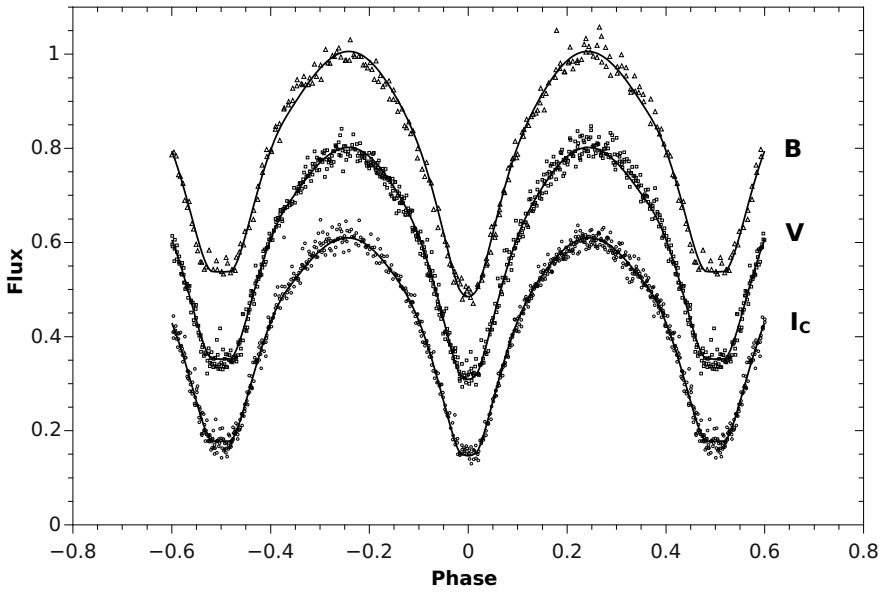

Figure 2. The SRO B, V and I_C light curves of GSC 3408-0735 and the photometric solution using the Wilson-Devinney program.

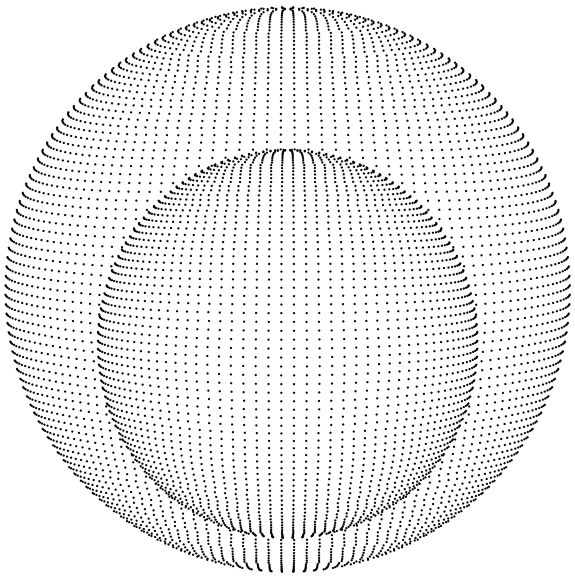

Figure 3. The GSC 3408-0735 system at primary eclipse.

COMMISSIONS 27 AND 42 OF THE IAU
INFORMATION BULLETIN ON VARIABLE STARS

Number 6105

Konkoly Observatory
Budapest
16 May 2014

HU ISSN 0374 – 0676

TYC3556-299-1 AND TYC3556-130-1: A BINARY MEMBER AND A SINGLE δ Sct STAR

SEREBRYANSKIY, A.V. ; GAYNULLINA, E.R.; KHALIKOVA, A.V.

Ulugh Beg Astronomical Institute, Astronomicheskaya str., 33, 100072 Tashkent, Uzbekistan
email: alex@astrin.uz, evelina@astrin.uz

TYC3556-299-1 ($RA_{2000}=19^h35^m36\overset{s}{.}798$; $DEC_{2000}=+46°05'56\overset{''}{.}34$) is a star with V$\approx$ 12 mags and TYC3556-130-1 ($RA_{2000}=19^h38^m08\overset{s}{.}115$; $DEC_{2000}=+46°34'55\overset{''}{.}64$) is a relatively bright star with V$\approx$ 10.7 mags. TYC3556-299-1 is also designated by Kepler ID 9470054 and classified as eclipsing binary system. The premise for designating the star as binary is its light curve variability with period of $1\overset{d}{.}473227$[1].

We observed the field of the open cluster NGC 6811 on Maidanak observatory (Uzbekistan) during several nights in 2010 with Taiwan Automated Telescope (TAT, Chou et al., 2010). The TAT uses a 9-cm Maksutov-type telescope with f=25, manufactured by "Questar". The CCD camera is Apogee Alta U6 16-bit 1024×1024, the CCD chip is a Kodak KAF-1101E, scale is $2\overset{''}{.}18$ per pixel which gives field of view of $0\overset{°}{.}62 \times 0\overset{°}{.}62$. Because the telescope was not originally equipped with standard color filters, observations were made in integrated light, exposure times were either 280 or 320 sec. The main goal of the observations was a search for new variables as well as asteroseismic analysis of known δ Sct stars. Among all nights of observations we had four nights (Aug 26 and Sep 7, 9, 10) when the star TYC3556-299-1 was found in the field of view and two nights (Sep 9, 10) when the star TYC3556-130-1 was found in the field of view. Basic reduction of the frames was done using standard IRAF[2] software.

To obtain light curve of TYC3556-299-1 and TYC3556-130-1 we used method of differential photometry. For this goal we extract photometry of a set of stars across the field of NGC 6811. During the photometric analyses we encountered two main problems: (i) strong coma distortions of the stellar profiles due to a quite wide field of view of the telescope, and (ii) moderate star crowding on the field. To avoid these problems we performed only aperture photometry with aperture radius is being approximately equal to FWHM. Having had the instrumental magnitudes we used method of ensemble photometry (Honeycutt, 1992) realized in "Ensemble-0.7" software by Michael Richmond (`http://spiff.rit.edu/ensemble`). Then we subtracted low-frequency trends (due to possible effects of differential absorption) from all light curves by fitting low-order polynomial. This effectively removes any periodic signal with period longer than several hours. The final light curves contain 119 data points for TYC3556-130-1 and 226 data points for TYC3556-299-1 and are shown in Figure 1.

[1] `http://archive.stsci.edu/kepler`
[2] IRAF is distributed by the NOAO, which are operated by the AURA, Inc., under cooperative agreement with the NSF

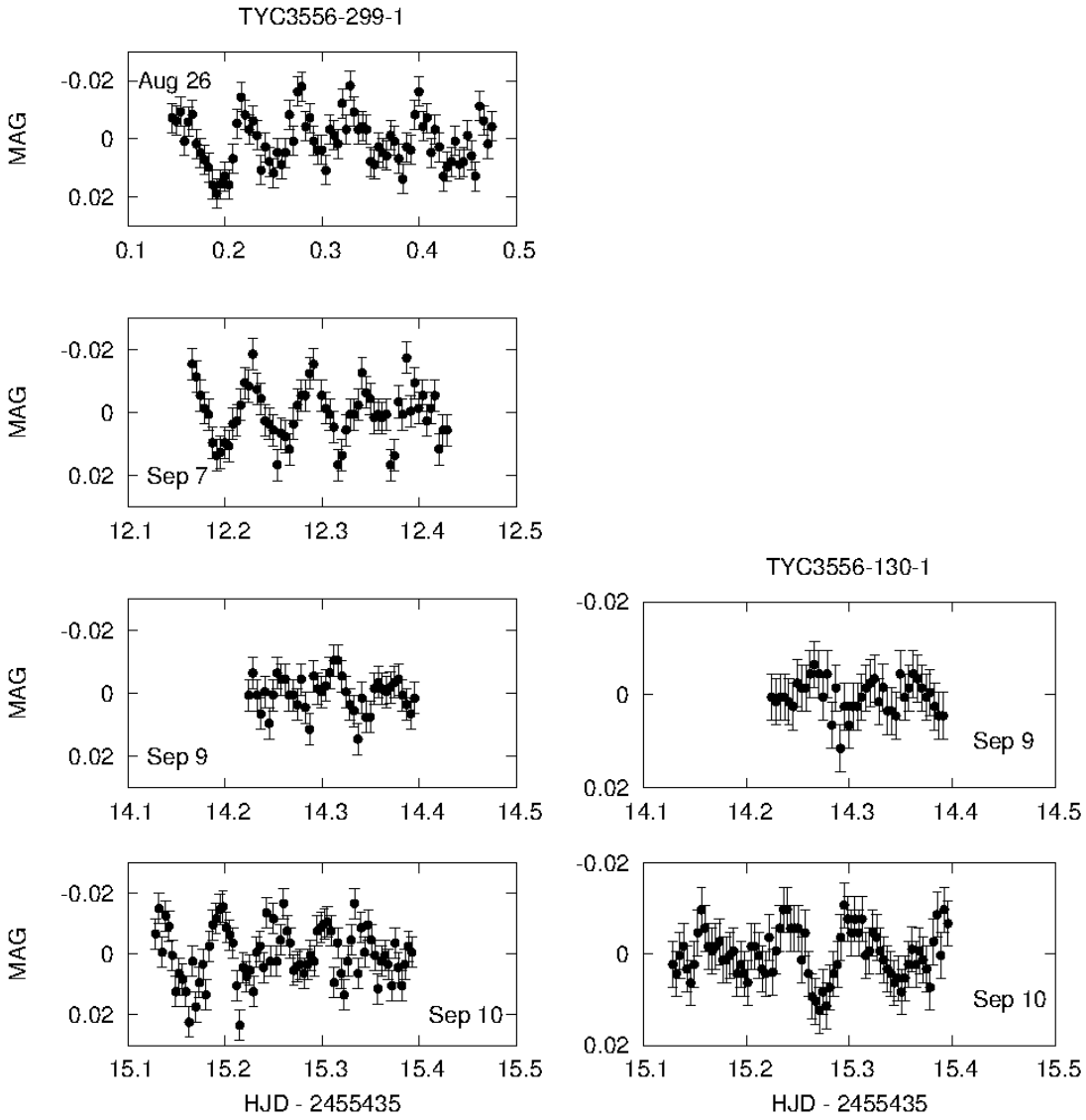

Figure 1. Light curves of the stars TYC3556-299-1 (left column) and TYC3556-130-1 (right column) observed in Maidanak observatory in 2010.

Table 1: Mode parameters for TYC3556-299-1 and TYC3556-130-1

Star	Frequency (c/d))	Amplitude (mmag)	Phase	SNR
TYC3556-299-1	17.233 ± 0.002	6.00 ± 0.53	0.03 ± 0.02	8.60
	15.489 ± 0.003	4.68 ± 0.54	0.35 ± 0.03	7.91
	21.371 ± 0.004	3.07 ± 0.49	0.90 ± 0.05	5.70
	12.432 ± 0.005	2.50 ± 0.51	0.77 ± 0.06	4.57
TYC3556-130-1	13.364	3.75 ± 0.41	0.11 ± 0.017	9.53
	20.409	2.78 ± 0.41	0.50 ± 0.023	9.07
	14.943	2.13 ± 0.42	0.95 ± 0.030	9.79

For the power spectra analysis of the light curves the FAMIAS software package (Zima, 2008) was used. The parameters of the FAMIAS are identical to those used in (Serebryanskiy et al., 2013). The parameters of the modes are listed in Table 1. The errors of the frequency estimation for TYC3556-130-1 are not presented due to low resolution of power spectra used in our analyses. This causes instability of frequencies during pre-whitening in FAMIAS. We fixed the frequency value determined in the previous run to estimate frequency and other parameters of the mode in the subsequent run.

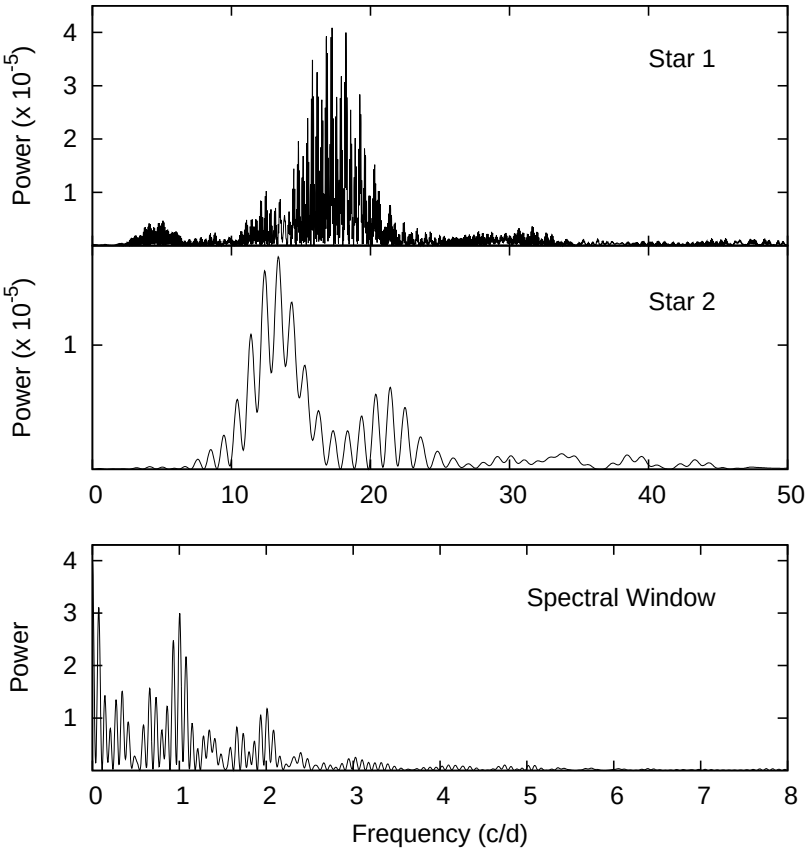

Figure 2. Upper panel (Star 1): power spectrum of TYC3556-299-1. Middle panel (Star 2): power spectrum of TYC3556-130-1. Lower panel: window function of TYC3556-299-1 power spectrum.

Using the available information for these stars, i.e. their magnitudes in different wavelengths from SIMBAD astronomical database and CSOCA catalog (Kharchenko et al., 2004) we found that $(B-V)$ color index for TYC3556-299-1 is in the range of 0.02-0.04 and $(B-V)$ color index for TYC3556-130-1 is in the range of 0.4-0.43. According to Dias et al. (2002) the star TYC3556-299-1 has a high probability due to its proper motion to be a member of NGC 6811 open cluster. From Janes et al. (2013) the color excess E_{B-V} for this cluster is 0.074 ± 0.024. Hence the true $(B-V)_0$ color index for TYC3556-299-1 is ~ -0.04 which make this star to be closer to spectral class A0. Janes et al. (2013) also provide us with color index $(B-V)$ and $(U-B)$ for TYC3556-299-1, which are, respectively, equal to $0.271 \pm 0,002$ and 0.109 ± 0.002. This gives us the possibility to estimate its spectral class using standard color index diagram. We found that this star belongs to spectral class in the range of A8-F0. Considering kinematics the probability that the star

TYC3556-130-1 belongs to the NGC6811 is smaller, but it is high considering photometry and position criteria (Kharchenko et al., 2004). If we assume that this star belongs to the open cluster then the true $(B-V)_0$ color index will be ~ 0.35 which make this star closer to spectral class F0. We assumed that both stars belong to the main sequence.

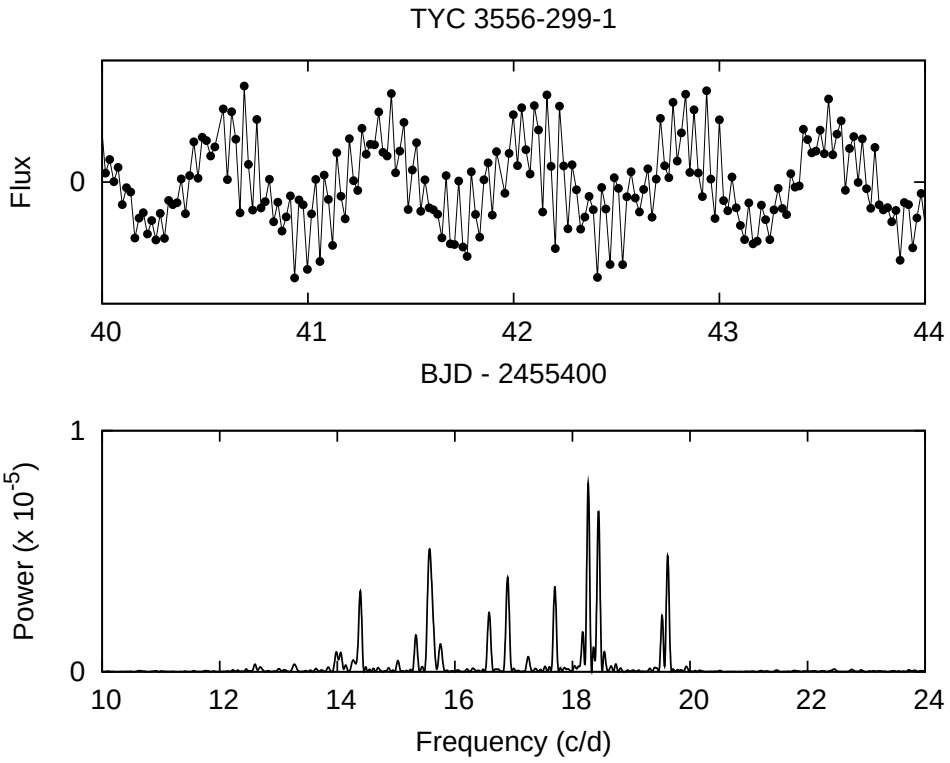

Figure 3. Upper panel: an example of a segment of Kepler light curve. Lower panel: power spectrum for TYC3556-299-1 computed using "Kepler" light curve of the same period of observation (see the text).

We tried to compare our results with results obtained by analyzing part of the Kepler light curve for TYC3556-299-1[3] for the observing period similar to our observations. It should be noted that sampling rate of the Kepler light curve for this star did not allow us to make precise frequency determination. Median value of sampling rate for Kepler observations is ~ 1765 sec, comparing to the sampling rate of the TAT of ~ 300 sec. As a result the possible aliasing did not allow us to select unique modes from power spectrum of Kepler light curve. But we were able to confirm the presence of modes in the range from 12 to 22 c/d with amplitudes higher than 4σ above the noise level; see Fig. 3. On the top panel of Fig. 3 we show only part of Kepler light curve to see clearly oscillation with period of $1\overset{\mathrm{d}}{.}473227$ and superimposed on it the oscillations with shorter periods. The lower panel shows the power spectrum computed using Kepler light curve for the same observing period to our observations.

Considering the amplitudes and periods of oscillations, as well as the spectral type of the stars (A-F) we conclude that TYC3556-299-1 and TYC3556-130-1 could be variables of δ Sct type although the classification of TYC3556-299-1 might be biased by the fact that this system is a binary star.

[3] http://keplerebs.villanova.edu/overview/?k=9470054

Taking into account their brightness and that one of the stars is in a close binary system they will be convenient and interesting targets for a future asteroseismic campaign using small-aperture telescopes.

Acknowledgements: The authors are supported by Fundamental Research Grant FA-F02-F028 of the Uzbek Academy of Sciences. We thanks the anonymous referee for important suggestions and comments.

References:

Chou, D.-Y., Sun, M.-T., Fernandez, F.J. et al., 2010, *Advances in Astronomy*, **2010**, 125340

Dias, W. S., Alessi, B. S., Moitinho, A., Lépine, J. R. D., 2002, *A&A*, **389**, 871

Honeycutt, R.K., 1992, *PASP*, **104**, 435

Janes, K., Barnes, S.A., Meibom, S., Hoq, S., 2013, *Astronomical Journal*, **145**, 7

Kharchenko, N.V., Piskunov, A.E., Röser, S., Schilbach, E., Scholz, R.-D., 2004, *Astr. Nachr.*, **325**, 740

Serebryanskiy, A. V., Gaynullina, E. R., Strel'nikov, D. V., Khalikova, A. V., 2013, *IBVS*, **6047**

Zima, W., 2008, *Communications in Asteroseismology*, **155**, 17

COMMISSIONS 27 AND 42 OF THE IAU
INFORMATION BULLETIN ON VARIABLE STARS
Number 6106

Konkoly Observatory
Budapest
16 May 2014
HU ISSN 0374 – 0676

RR LYRAE STARS IN THE GCVS OBSERVED BY THE QATAR EXOPLANET SURVEY

BRAMICH, D.M.[1]; ALSUBAI, K.A.[1]; ARELLANO FERRO, A.[2]; PARLEY, N.R.[1,3]; COLLIER CAMERON, A.[3]; HORNE, K.[3]; POLLACCO, D.[4]; WEST, R.G.[4]

[1] Qatar Environment and Energy Research Institute, Qatar Foundation, Tornado Tower, Floor 19, P.O. Box 5825, Doha, Qatar

[2] Instituto de Astronomía, Universidad Nacional Autónoma de México, Ciudad Universitaria CP 04510, México

[3] SUPA, School of Physics and Astronomy, University of St Andrews, North Haugh, St Andrews, Fife, KY16 9SS, UK

[4] Department of Physics, University of Warwick, Coventry, CV4 7AL, UK

1 Introduction

The Qatar Exoplanet Survey (QES; Alsubai et al. 2013) is discovering hot Jupiters (Qatar-1b, Alsubai et al. 2011; Qatar-2b, Bryan et al. 2012) and aims to discover hot Saturns and Neptunes that transit in front of relatively bright host stars (8-15 mag). The survey operates a robotic wide-angle multiple-camera system installed at the "New Mexico Skies" observing station in southern New Mexico, USA, and it has been in operation since mid-November 2009. The cameras, which operate without filters for maximum signal-to-noise (S/N), photometrically survey a target field of ∼400 square degrees repeatedly with a cadence of ∼10 minutes. Each target field is followed for ∼3-4 months continuously while it is visible at more than 30° above the horizon. Each year a new set of target fields is designated.

The time-series images of each field are processed by a customised data pipeline (Sec. 4 of Alsubai et al. 2013) to calibrate the images, detect objects, perform astrometry, and extract photometry. Only objects successfully matched with stars in the US Naval Observatory CCD Astrograph Catalog (UCAC3; Zacharias et al. 2010) are considered further in order to avoid faint stars with very low S/N. A reference image, chosen as a best-seeing high-S/N image from the time series, is subtracted from each image in the time series using the image subtraction technique to create difference images (Alard & Lupton 1998; Bramich 2008; Bramich et al. 2013). Photometry is performed on the difference images using point spread function (PSF) fitting at the object positions with a spatially-variable PSF model. The output of this difference image analysis (DIA) is a set of object light curves in differential flux units (ADU/s). These light curves are converted to instrumental magnitudes using reference fluxes for each object as measured on the reference image. The photometric zero point for the reference image is determined using the UCAC3 magnitudes and this is used to calibrate the light curve magnitudes on an absolute scale with

a scatter of ∼0.1 mag. The QES light curves are then stored in a data archive system and trend filtering algorithms are applied to them. However, since the application of trend filtering algorithms to variable star light curves risks distorting their shape, we opted to use the raw QES light curves from the archive (i.e. before detrending is applied) for the study of the variable stars in this paper.

With a typical photometric precision of ∼1-2% over the magnitude range 8-14, a high temporal cadence (∼10 min) sustained over ∼2-7 hours in each 24-hour period, and a time baseline of ∼3-4 months, the QES light-curve archive is a potential gold mine for variability studies. As part of realising the full scientific potential of QES, we have started investigating the variable star content of the archive. This short paper is the first in a series reporting our results. Here we investigate known RR Lyrae variables.

2 Sample selection

We cross-matched UCAC3 with the 47969 variable stars in the General Catalogue of Variable Stars (GCVS4 - version 30/04/2013; Samus et al. 2009) using the CDS X-Match service[1]. The cross-match algorithm simply selects any GCVS star entries within a 5″ radius of any UCAC3 star. This resulted in 43009 matched entries, of which 42973 are unique. Retaining only the unique matches and filtering for variable star type, we obtained 6921 UCAC3 stars classified as RR Lyrae variables.

We then searched in the QES light-curve archive for these UCAC3 RR Lyrae stars and found that we had observed 752 objects in this list. We note that any object observed across multiple target fields and/or cameras will have multiple light curves in the QES archive. Since our analysis requires a reasonable number of data points in each light curve, we rejected light curves with fewer than 100 data points. Furthermore, due to the faint limit of the QES lying at ∼17 mag, we rejected any objects with UCAC3 aperture magnitudes fainter than 16.5. We were left with 724 objects with 2220 light curves.

We inspected plots of the phased (using the GCVS periods where available) and unphased light curves of our object sample. Since RR Lyrae variations have typical amplitudes of 0.1-1.3 mag, we could immediately identify 65 objects with multiple light curves where a subset of the light curves were not showing any variability. This occurs when the QES pipeline misidentifies an object and measures the wrong star, which tends to happen for relatively crowded objects towards the edge of a detector where camera distortions are not sufficiently well-modelled in the astrometric solution. For these cases we simply rejected the 143 light curves that failed to show the variations clearly visible in the remaining light curves for the same object. We also identified 136 objects for which none of their light curves showed variations above the noise level. We found that this was due either to the objects being very faint and therefore exhibiting a large scatter in their light curves, or to the object misidentification problem mentioned already. We rejected these objects from our sample, which left us with 588 photometrically variable objects with 1783 light curves.

3 Analysis and results

Some variables in our data sample do not have GCVS period estimates and/or their GCVS classification as RR Lyrae variables is uncertain or does not distinguish between fundamental mode and first overtone pulsators. Hence our first step was to estimate the

[1] http://cdsxmatch.u-strasbg.fr/xmatch#tab=xmatch&

variable star periods using our light curve data. We applied the string-length method (Burke, Rolland & Boy 1970; Dworetsky 1983) to each of the 1783 light curves in our sample to search for periods in the range 0.1-500 d. For variables with multiple light curves, we adopted the period derived from the light curve with the best combination of the longest time span, the smallest noise, and the most data points (all light curve plots in this paper display this "best" light curve for clarity). We then phase-folded the light curves with our derived periods, and we checked the RR Lyrae classification of our variables.

Apart from being able to improve the GCVS periods and classifications for a large number of variable stars, we also found that some variables in our data sample are not RR Lyrae stars. Consequently we have reclassified these stars using the GCVS classification system described in Samus et al. (2009)[2]. To aid in our reclassification efforts, we searched the literature for previous studies of some of these variables. However, a full literature search for all of the variables in our data sample is beyond the scope of this paper, the purpose of which is to provide a set of concrete updates to the latest version of the GCVS. Therefore we cannot claim that all of our results are guaranteed to be new although we are sure that the majority of the information presented in this paper has not previously been reported in the literature.

Before reporting our results, we mention that due to the coarse pixel scale of the QES camera system (9.26 and 4.64 arcsec/pixel for the 200 and 400 mm lenses, respectively), a relatively high proportion of the variable stars in our sample are likely to be blended with another star. Hence the reference flux for such blended variables as measured on the reference image is systematically overestimated which leads to artificially small amplitudes of variation in the corresponding light curves. Therefore, the amplitudes of our variable star light curves may be systematically too small in a number of cases when compared to light curves derived from higher resolution imaging data.

3.1 Stars that are not RR Lyrae variables

In Table 1, we report the reclassification of 21 variable stars. Our period estimates improve on the GCVS periods in all cases. We reclassify 14 of these variables as eclipsing binaries, where 13 of these are of the W Ursae Majoris type. We plot the phased light curves of the eclipsing binaries in Figure 1 using the best light curve for each variable. Four eclipsing binaries (3UC191-025421, 3UC192-006598, 3UC247-041882 and 3UC308-105518) clearly show the O'Connell effect in our data, which is characterised by two maxima of different brightnesses (O'Connell 1951).

We find that the variable star 3UC205-101683, which is listed in the GCVS as an RR Lyrae star of unknown sub-type, is a known double-lined spectroscopic binary (Mathieu et al. 2003) showing X-ray emission (Belloni, Verbunt & Mathieu 1998) and classed as an RS Canum Venaticorum-type variable (van den Berg et al. 2002). We have updated the record for this star in Table 1, quoting the period derived from our best light curve spanning ∼154 days, which is more precise than the photometric periods quoted in the literature. The phased light curve for this star is shown in Figure 2. We note that the slight variations in the light curve shape and amplitude reported by van den Berg et al. (2002) are also detected in our light curve.

The variable star 3UC171-023140 is a Herbig Ae/Be star of spectral type B9e (Vieira et al. 2003) that exhibits irregular light variations (see Figure 3; Bernhard 2010). We

[2]See also http://www.sai.msu.su/gcvs/gcvs/iii/vartype.txt

were unable to find periodicity in our light curves for this object. Hence we reclassify this star as an irregular variable of early spectral type in Table 1.

We found that four of the variable stars in our sample are most likely classical Cepheids as opposed to RR Lyrae stars. Our new classifications for two of these stars (3UC208-318430 and 3UC225-131002) are based only on the period and the shape of the phased light curve (see Figure 4), which does not definitively distinguish them from other variable types in their period range. Hence our classifications for these two stars are tentative and marked with a colon ":" in Table 1. The variable star 3UC237-053427 was originally classified as a classical Cepheid by Schmidt & Gross (1990) and we confirm that it is most likely pulsating in the first overtone mode as indicated by its smaller pulsation amplitude and relatively symmetric phased light curve. The variable star 3UC268-064903 has also already been classified as a classical Cepheid by Wils, Lloyd & Bernhard (2006).

We also noticed that the variable star 3UC237-121450 has an unusually long period for an RR Lyrae. A literature search revealed that Wallerstein, Kovtyukh & Andrievsky (2009) found this star to be carbon-rich and of relatively high metallicity. These facts lead Andrievsky et al. (2010) to suggest that 3UC237-121450 is more likely to be a short-period type II Cepheid (or BL Her type variable). We adopt this tentative classification for this star in Table 1 and display the phased light curve in Figure 5.

Table 1. Variable stars reclassified as eclipsing binaries, RS Canum Venaticorum-type variables (or RS CVn), irregular variables of early spectral type, classical Cepheids (or type I Cepheids), and type II Cepheids. All of our period estimates improve on the GCVS periods and they are precise to the last decimal place quoted.

UCAC3 ID	GCVS ID	RA	Dec.	Variable Type		UCAC3	Period (d)	
		(J2000.0)	(J2000.0)	GCVS	This Work	Aperture Mag	GCVS	This Work
169-146805	V1018 Oph	16 17 59.22	−05 56 55.3	RRC:	EW	15.244	0.3696396	0.350
171-023140	UY Ori	05 32 00.31	−04 55 53.9	RR:	IA	12.456	-	-
176-102611	V0482 Hya	08 27 38.98	−02 00 34.3	RRC:	EW	15.591	0.190393	0.3808
178-131091	V0593 Vir	14 44 30.11	−01 28 26.2	RRC:	EW	15.473	0.228947	0.3726
179-127893	V0533 Vir	14 12 38.56	−00 53 50.7	RRC:	EW	15.484	0.229537	0.3732
180-101956	V0491 Hya	08 39 55.42	−00 03 50.4	RRC:	EW	14.055	0.263482	0.4170
191-025421	V0651 Ori	05 32 46.49	+05 24 57.8	RR:	EW[a]	14.335	-	0.37827
192-006598	HM Cet	02 07 31.42	+05 41 05.7	RRC	EW[a]	13.017	0.22232	0.44462
192-026024	V1015 Ori	05 28 54.22	+05 39 27.7	RR:	EA	14.627	-	1.8512
205-101683	AG Cnc	08 51 25.30	+12 02 56.5	RR:	RS[b]	13.684	0.313335	2.827[c]
208-318430	HU Peg	23 59 22.17	+13 47 11.5	RR	DCEP:	11.107	-	78[d]
225-131002	V0368 Her	17 10 31.13	+22 23 08.8	RRAB	DCEP:	15.627	0.543689	1.1915
237-053427	CN Tau	05 58 09.42	+28 02 33.5	RRAB	DCEPS[e]	12.645	0.642062	1.794
237-121450	UY CrB	16 06 21.77	+28 07 03.8	RR:	CWB:[f]	13.190	-	0.92916
247-041882	DN Aur	05 07 59.86	+33 23 50.7	RRC	EW[a]	13.535	0.30846	0.61692
263-033768	KN Per	03 22 35.64	+41 19 55.2	RRC	EW	11.615	0.433224	0.8665
268-064903	V0421 Per	04 45 34.83	+43 34 22.2	RR	DCEP[g]	13.643	-	4.3735
270-278831	V0660 And	23 27 52.08	+44 54 14.9	RRC	EW	12.147	0.38542	0.7708
286-145835	V0997 Cyg	19 48 05.07	+52 51 16.3	RRC	EW	13.358	0.22892	0.45823
287-146031	V1017 Cyg	19 56 15.81	+53 19 12.0	RR	EW	15.197	0.96	0.33041
308-105518	V0414 Dra	18 53 30.15	+63 55 03.6	RRC:	EW[a]	11.306	0.348087	0.69619

[a] Clear detection of the O'Connell effect (i.e. unequal brightness of the two maxima).
[b] Classification taken from van den Berg et al. (2002).
[c] Orbital period is 2.823094 d (Mathieu et al. 2003).
[d] This star has a single light curve in our data that spans ∼195 days (or ∼2.5 cycles).
[e] Originally classified as a classical Cepheid by Schmidt & Gross (1990).
[f] Classification taken from Andrievsky et al. (2010).
[g] Also classified as a classical Cepheid by Wils, Lloyd & Bernhard (2006).

3.2 RR Lyrae stars with new sub-type classifications

In Table 2, we report the new sub-type classifications for 61 RR Lyrae stars which have an unspecified or erroneous RR Lyrae sub-type classification in the GCVS. We list our period estimates in the table whenever they improve on the GCVS periods (52 cases). The new sub-type classifications are based on having considered the variable star periods and the

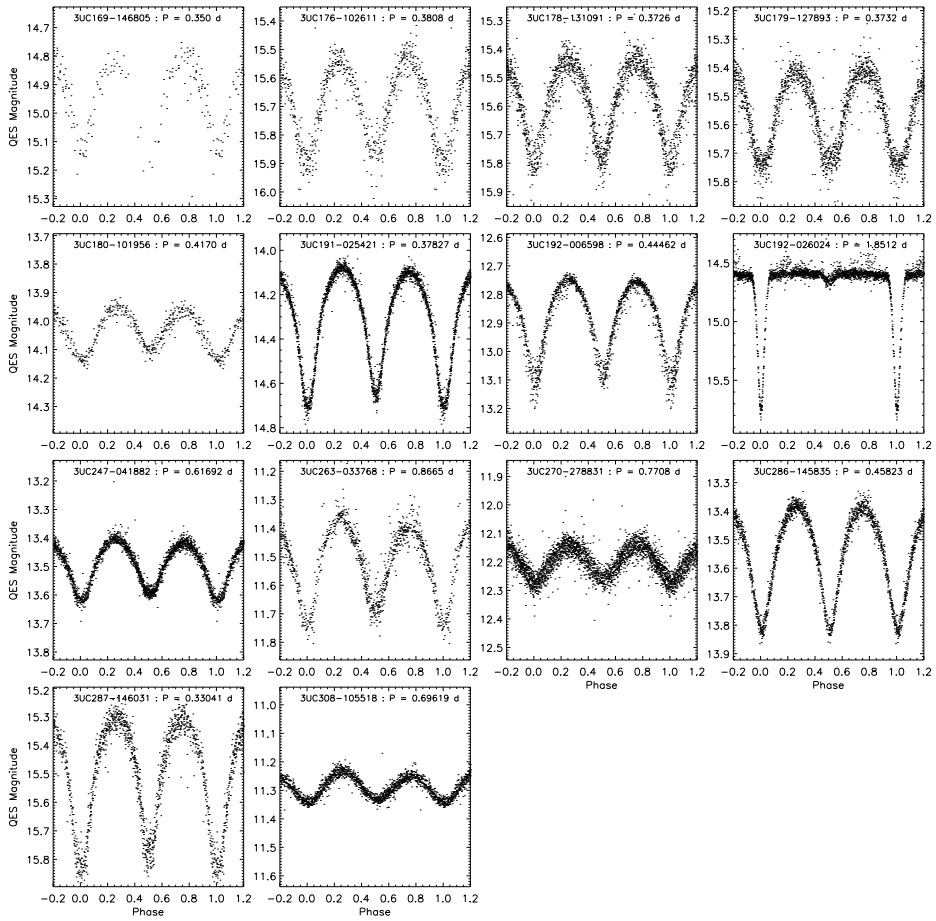

Figure 1. Phased light curves of the variable stars reclassified as eclipsing binaries. The magnitude range in each plot is 0.7 mag except for the stars 3UC191-025421 and 3UC192-026024 which have plots with magnitude ranges of 0.9 and 1.8 mag, respectively.

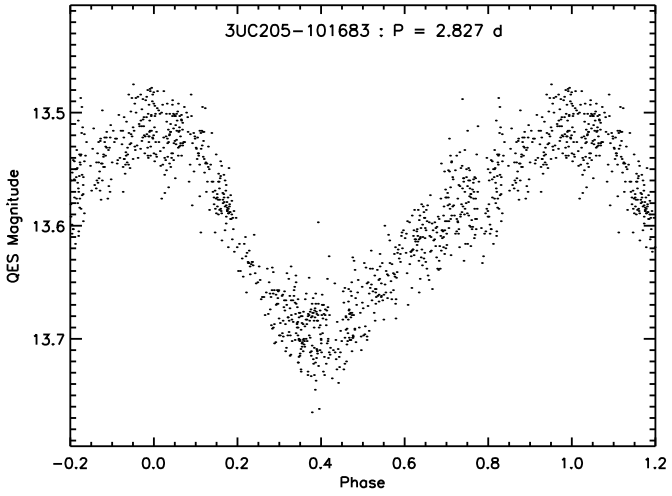

Figure 2. Phased light curve of the variable star 3UC205-101683 reclassified as an RS Canum Venaticorum type variable.

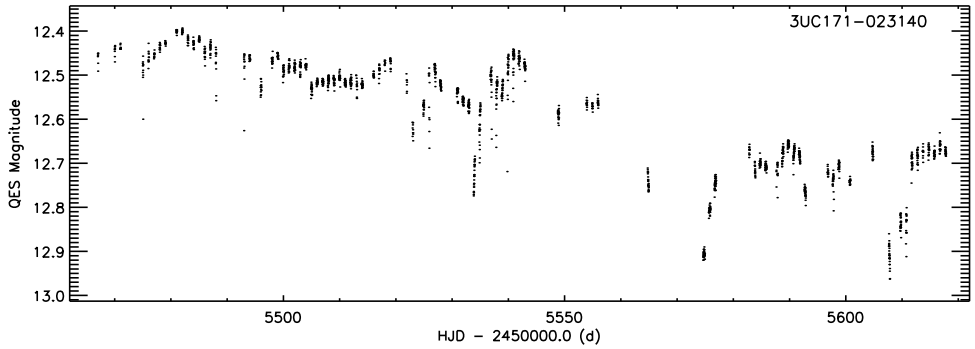

Figure 3. Light curve of the variable star 3UC171-023140 reclassified as an irregular variable of early spectral type.

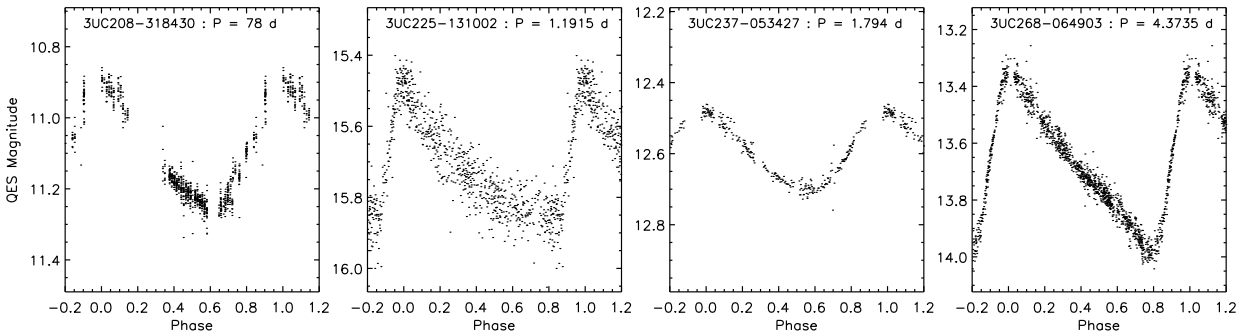

Figure 4. Phased light curves of the variable stars reclassified as classical Cepheids (or type I Cepheids). The magnitude range in each plot is 0.8 mag except for the star 3UC268-064903 which has a plot with a magnitude range of 1.0 mag.

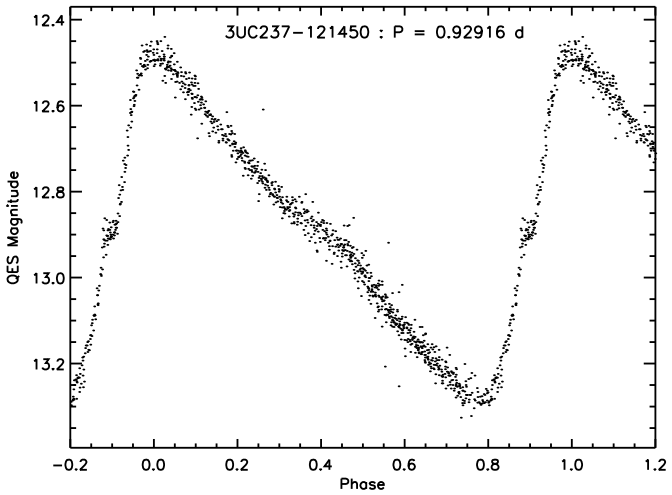

Figure 5. Phased light curve of the variable star 3UC237-121450 reclassified as a type II Cepheid.

phased light curve shapes and amplitudes. We note that some of the GCVS periods fail to properly phase our light curves, which may indicate period changes in these cases (e.g. 3UC167-134566). We clearly detect the Blazhko effect (amplitude and/or phase modulations; Blazhko 1907) in five of these RR Lyrae variables and this is the first detection of the effect in four of them (see the catalogue of known Galactic field Blazhko RR Lyrae stars in Skarka 2013). For 3UC191-097728, 3UC202-143008 and 3UC227-103944, we measure Blazhko periods of 36.2±0.2, 40.0±0.6 and 65.6±1.2 d, respectively, using the power spectrum analysis described in Section 3.5. For 3UC175-133697 we place a lower limit of 80 d on the Blazhko period. Finally we note that the light curve for 3UC236-044458 has a strange shape for an RR Lyrae star, although its period and amplitude are consistent with that of an RRC variable. The phase-folded light curves of all 61 variables are displayed in Figure 6.

3.3 Double-mode RR Lyrae stars

Seven of the variable stars in our sample are double-mode RR Lyrae stars pulsating simultaneously in the fundamental and first overtone modes. The GCVS classification for these stars is wrong in four cases. We checked the literature and all of these stars are known double-mode RR Lyrae stars. We used the program `period04` (Lenz & Breger 2005) to perform a frequency analysis on the best light curve for each star. Our results are reported in Table 3 where we list the correct classification for each star alongside the fundamental and first overtone periods that we measured. For all stars the period ratios between the two modes fall inside the expected range of 0.742-0.748 for this type of variable star (Cox, Hodson & Clancy 1983; Moskalik 2014). The corresponding light curves phased using the first overtone period are plotted in Figure 7.

3.4 RR Lyrae stars with improved periods

For the remaining 499 variables in our sample, the RR Lyrae classifications in the GCVS are correct. However, we have been able to improve on the GCVS period estimates for 83 variables. These stars along with their improved periods are listed in Table 4. Again, period changes in some of these variables may explain the differences between the GCVS and our period estimates (e.g. 3UC204-103494). Note that the GCVS period estimates are the best periods available for the other 416 RR Lyrae variables in our sample. We clearly detect the Blazhko effect in ten of the variables listed in Table 4 and this is the first detection of the effect in seven of them (see Skarka 2013). For 3UC188-089887, 3UC192-101314, 3UC209-135992 and 3UC234-000057, we measure Blazhko periods of 69.7±0.5, 56.6±0.7, 38.8±0.2 and 80±4 d, respectively, using the power spectrum analysis described in Section 3.5. For 3UC232-112040 and 3UC282-145093 we place lower limits of 100 and 80 d, respectively, on the Blazhko periods.

3.5 New detections of the Blazhko effect in RR Lyrae stars

Finally, while inspecting the light curves of the remaining 499 RR Lyrae stars in our sample, we looked for clear indications of amplitude and phase modulations that characterise the Blazhko effect. We then checked our suspected Blazhko RR Lyrae stars against the catalogue of known Galactic field Blazhko stars in Skarka (2013). We found 27 RR Lyrae stars which clearly exhibit the Blazhko effect and which are not in the Skarka (2013) catalogue. This brings the total number of RR Lyrae stars where we have detected the Blazhko effect for the first time to 38 when taking into account the 4 and 7 such stars

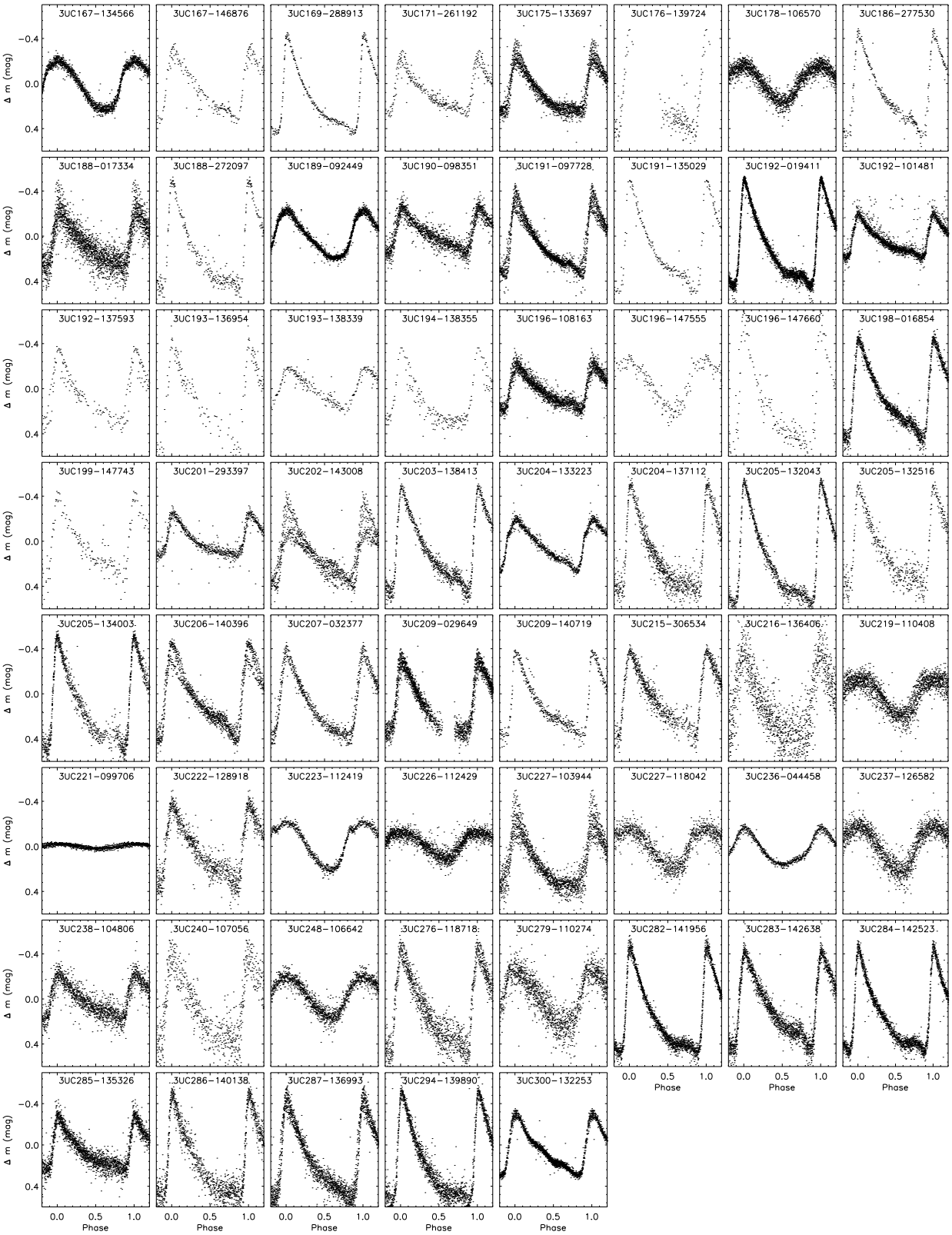

Figure 6. Phased light curves of the RR Lyrae stars with new sub-type classifications. The light curve magnitudes are plotted relative to the mean magnitudes and the same magnitude range of 1.3 mag is used in each plot. See Table 2 for the star brightnesses.

Table 2. RR Lyrae stars with new sub-type classifications. Where listed, our period estimates improve on the GCVS periods and they are precise to the last decimal place quoted.

UCAC3 ID	GCVS ID	RA	Dec.	Variable Type		UCAC3	Period (d)	
		(J2000.0)	(J2000.0)	GCVS	This Work	Aperture Mag	GCVS	This Work
167-134566	KW Lib	14 47 51.53	−06 34 45.9	RRAB	RRC	14.146	0.3143	0.31269
167-146876	V0713 Oph	16 30 10.73	−06 48 02.1	RR	RRAB	14.384	-	0.6858
169-288913	CH Aql	20 33 42.18	−05 38 49.3	RR	RRAB	13.894	0.38918702	-
171-261192	V0909 Aql	20 21 59.39	−04 41 48.7	RR:	RRAB	14.758	0.5756	0.5766
175-133697	FV Lib	14 48 50.96	−02 33 46.4	RR:	RRAB[a,b]	15.028	-	0.5404
176-139724	CI Ser	16 13 41.43	−02 20 23.0	RR	RRAB	15.009	0.5383	0.5385
178-106570	V0494 Hya	08 43 42.26	−01 20 17.0	RRC:	RRC	15.722	0.429765	-
186-277530	EL Del	20 55 23.08	+02 57 35.3	RR	RRAB	14.285	0.595432	-
188-017334	FV Ori	04 50 43.55	+03 47 35.1	RR	RRAB	16.486	0.55218	-
188-272097	V0911 Aql	20 23 47.28	+03 36 49.2	RR	RRAB	15.897	-	0.46156
189-092449	V0516 Hya	09 11 37.56	+04 02 30.4	RRAB:	RRC	13.150	0.346612	0.34666
190-098351	UV Hya	09 38 15.28	+04 45 36.5	RR:	RRAB	14.153	-	0.7072
191-097728	CY Hya	09 10 20.88	+05 20 51.1	RR	RRAB[a,b]	14.615	0.57693446	-
191-135029	V1429 Oph	17 07 15.15	+05 15 08.2	RR	RRAB	14.187	-	0.3651
192-019411	GO Ori	04 56 31.49	+05 35 33.7	RR	RRAB	15.092	-	0.53496
192-101481	IU Hya	09 06 17.78	+05 45 45.3	RR:	RRAB	15.022	-	0.58033
192-137593	V1053 Oph	16 54 46.95	+05 42 16.5	RR:	RRAB	14.921	4.03	0.578
193-136954	V1056 Oph	16 59 23.92	+06 20 15.5	RR:	RRAB	16.249	-	0.593
193-138339	V2598 Oph	17 05 43.58	+06 25 41.5	RRC	RRAB	14.428	0.38749054	0.634
194-138355	V2620 Oph	16 51 05.97	+06 57 47.9	RRAB:	RRAB	15.329	0.456	-
196-108163	BF Cnc	08 42 12.75	+07 48 38.0	RR	RRAB	15.928	-	0.58706
196-147555	V1600 Oph	17 11 41.45	+07 32 11.1	RR	RRC	15.308	-	0.3080
196-147660	V1060 Oph	17 12 16.20	+07 41 25.4	RR:	RRAB	15.475	-	0.4404
198-016854	CK Tau	04 36 44.96	+08 54 24.4	RR	RRAB	14.808	-	0.6009
199-147743	V0612 Her	16 45 06.95	+09 02 33.6	RR	RRAB	15.233	-	0.5807
201-293397	KL Del	20 38 55.50	+10 29 03.2	RR:	RRAB	14.821	-	0.44110
202-143008	V1061 Oph	17 14 29.98	+10 43 07.5	RR	RRAB[a,b]	14.966	-	0.58940
203-138413	V1057 Oph	17 01 06.77	+11 03 17.6	RR	RRAB	15.398	-	0.61805
204-133223	V0605 Her	16 40 41.80	+11 51 58.1	RR	RRAB	13.699	-	0.61129
204-137112	V1322 Oph	17 03 43.25	+11 51 55.5	RR	RRAB	16.071	-	0.46955
205-132043	V0546 Her	16 41 22.37	+12 25 10.8	RR	RRAB	14.706	-	0.467245
205-132516	V0549 Her	16 44 03.55	+12 11 37.9	RR	RRAB	16.112	-	0.58518
205-134003	V1122 Oph	16 53 44.99	+12 24 46.6	RR:	RRAB	16.128	-	0.50378
206-140396	V0461 Her	17 10 49.32	+12 52 50.9	RR	RRAB[a,b]	13.264	0.51301	-
207-032377	EX Tau	05 44 19.60	+13 27 54.3	RR	RRAB	15.159	-	0.5556
209-029649	V0743 Ori	05 34 58.37	+14 25 26.9	RR	RRAB	15.722	-	0.5001
209-140719	V0552 Her	17 30 11.83	+14 22 34.5	RR	RRAB	13.339	-	0.37846
215-306534	HT Del	20 54 39.59	+17 12 02.2	RR	RRAB	16.117	0.362494	0.5699
216-136406	BH Her	17 12 45.04	+17 42 31.0	RR:	RRAB	15.793	-	0.54514
219-110408	MU Boo	14 48 14.73	+19 20 19.1	RRC:	RRC	14.205	0.320375	-
221-099706	GN Cnc	09 16 04.44	+20 04 23.4	RR:	RRC	8.689	-	0.3624
222-128918	V0383 Her	17 16 28.23	+20 58 44.0	RRC	RRAB	15.960	0.39722	0.56801
223-112419	CM Leo	11 56 14.22	+21 15 30.2	RRAB	RRC	13.934	0.361732	-
226-112429	BU Boo	14 01 42.58	+22 30 15.6	RRAB	RRC	14.853	0.445	0.4451
227-103944	AH Leo	11 05 05.30	+23 21 09.0	RR	RRAB[a]	14.717	-	0.4663
227-118042	V0682 Her	16 12 19.89	+23 19 34.7	RR	RRC	15.783	-	0.3102
236-044458	IY Tau	05 42 23.13	+27 56 47.6	RRAB	RRC[c]	12.650	0.3764897	0.37651
237-126582	V0864 Her	16 59 00.56	+28 04 54.7	RRC:	RRC	15.109	-	0.37537
238-104806	NW UMa	11 16 55.26	+28 33 34.3	RRAB:	RRAB	15.650	0.5896	0.5895
240-107056	VZ UMa	11 17 28.28	+29 40 30.1	RR	RRAB	14.452	-	0.5154
248-106642	AT CVn	12 18 17.05	+33 39 56.0	RRAB:	RRC	15.060	-	0.3585
276-118718	BN CVn	12 29 36.75	+47 49 17.3	RR:	RRAB	12.609	-	0.56365
279-110274	DT UMa	08 53 44.85	+49 18 40.1	RR	RRC	15.787	-	0.32114
282-141956	V1104 Cyg	19 18 00.49	+50 45 17.8	RR	RRAB	14.797	0.43626	0.43639
283-142638	V1127 Cyg	19 32 05.81	+51 17 48.8	RR	RRAB	15.536	-	0.64727
284-142523	V1116 Cyg	19 24 03.28	+51 39 52.6	RR	RRAB	15.493	-	0.53853
285-135326	CD Dra	18 54 51.52	+52 28 45.1	RR	RRAB	16.147	-	0.5699
286-140138	V1118 Cyg	19 24 42.97	+52 32 50.8	RR	RRAB	15.860	-	0.50654
287-136993	V1106 Cyg	19 19 01.50	+53 25 15.8	RR	RRAB	15.160	2.04	0.40764
294-139890	CI Dra	19 25 32.47	+56 43 32.4	RR	RRAB	16.243	-	0.47089
300-132253	CY Dra	19 46 05.23	+59 34 26.3	RR:	RRAB	12.775	-	0.53494

[a]Clearly exhibits the Blazhko effect in our data.
[b]Not listed in the set of known Galactic field Blazhko RR Lyrae stars from Skarka (2013).
[c]The light curve has a strange shape for an RR Lyrae star. However, the period and amplitude are consistent with an RRC classification.

listed in Tables 2 and 4, respectively. We confirmed the presence of the Blazhko effect in 19 of these 27 variables by analysing the power spectra of the light curves using `period04`. We did this by prewhitening the power spectrum for the primary frequency f_0 (and the harmonics where necessary) and considered the Blazhko effect to have been detected in the power spectrum if the next highest peak $f_{\rm peak}$ has a significant amplitude (>0.02-0.05

Table 3. Double-mode RR Lyrae stars in our sample that are pulsating simultaneously in the fundamental and first overtone modes. In column 9, we list the fundamental and first overtone periods P_0 and P_1, respectively, along with the period ratio P_1/P_0 that we measure from our data. These periods are precise to the last decimal place quoted.

UCAC3 ID	GCVS ID	RA (J2000.0)	Dec. (J2000.0)	Variable Type GCVS	Variable Type This Work	UCAC3 Ap. Mag	Period (d) GCVS	Period (d) This Work : P_0, P_1, P_1/P_0
173-108416	V0500 Hya	08 47 46.93	−03 39 00.3	RR(B)	RR(B)	10.661	0.42079	0.5639, 0.4208, 0.7462
183-255136	QW Aqr	21 07 26.08	+01 10 17.6	RR(B)	RR(B)	13.794	0.35498	0.4772, 0.3551, 0.7441
201-119785	AQ Leo	11 23 55.28	+10 18 59.1	RR(B)	RR(B)	12.679	0.5497508	0.5498, 0.4102, 0.7461
206-276118	CF Del	20 23 31.36	+12 59 30.5	RR	RR(B)	14.307	0.49923	0.47843, 0.35604, 0.74418
218-133356	V0458 Her	17 08 30.92	+18 31 14.3	RRC	RR(B)	13.305	0.3599801	0.48352, 0.35998, 0.74450
248-100379	WY LMi	09 30 23.25	+33 53 10.6	RRAB	RR(B)	15.391	0.420003	0.4923, 0.3662, 0.7439
263-117859	BN UMa	11 16 22.91	+41 14 01.4	RRC	RR(B)	13.787	0.399901	0.53594, 0.39965, 0.74571

mag depending on light curve quality) and a ratio to the primary frequency in the range ∼0.95-1.05 (Benkő, Szabó & Paparó 2011). The Blazhko period is then estimated via $P_{\rm bl} = 1/\left|f_{\rm peak} - f_0\right|$. We present the details of these Blazhko variables in Table 5 and we plot the phased light curves in Figure 8. In four cases where we could not estimate the Blazhko period from the power spectrum, we were still able to place lower limits on the Blazhko period by inspecting the unphased light curve.

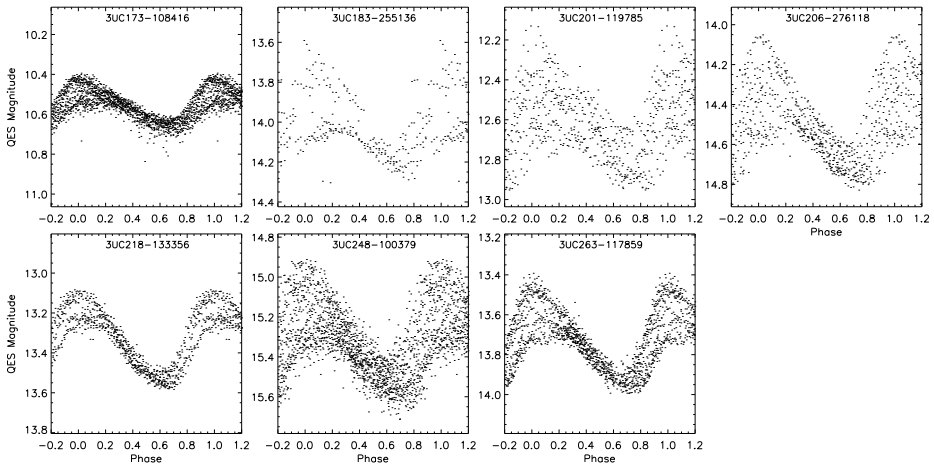

Figure 7. Phased light curves of the double-mode RR Lyrae stars. The light curves are phased with the first overtone period. The magnitude range in each plot is 1.0 mag.

3.6 Electronic light curve data

We provide the 1783 light curves for the sample of 588 photometrically variable objects described in this paper in 6106-d1.txt. The 588 variables breakdown by type as follows: 482 RRAB, 78 RRC, 7 RR(B), 13 EW, 1 EA, 1 RS, 1 IA, 3 DCEP, 1 DCEPS and 1 CWB. An excerpt from the 6106-d1.txt is presented in Table 6. The light curves will also be made available via CDS (Strasbourg) where we hope that the data will be of further use to the astronomical community.

Table 4. RR Lyrae stars with improved periods. Our periods are precise to the last decimal place quoted.

UCAC3 ID	GCVS ID	RA (J2000.0)	Dec. (J2000.0)	Variable Type	UCAC3 Aperture Mag	Period (d) GCVS	Period (d) This Work
170-106909	DG Hya	08 58 06.36	−05 26 25.2	RRAB	12.569	0.429973	0.75425
173-130413	HR Vir	13 42 28.63	−03 37 32.7	RRAB	14.414	-	0.7394
176-019652	V0964 Ori	05 07 54.52	−02 08 48.7	RRAB	13.267	0.5046561	0.50464
177-017006	V1830 Ori	04 49 34.97	−01 42 19.5	RRC	15.955	0.276438	0.2734
177-261611	V0910 Aql	20 23 11.69	−01 33 57.5	RRAB	14.725	1.0	0.50019
179-018625	V1844 Ori	05 03 36.84	−00 59 57.1	RRAB	15.057	0.778216	0.58908
179-140408	V0694 Oph	16 22 47.53	−00 49 37.5	RRAB	14.845	0.62	0.6207
179-141655	V0714 Oph	16 30 03.08	−00 59 56.5	RRAB	14.543	0.556	0.5557
182-001386	BF Cet	00 27 03.97	+00 40 30.3	RRC	13.856	-	0.38034
188-089887	CW Hya	08 55 07.81	+03 39 24.7	RRAB[a,b]	15.904	0.4820734	0.48050
192-101314	V0430 Hya	09 04 48.58	+05 30 08.3	RRAB[a,b]	12.803	0.49691	0.496830
193-135481	V2509 Oph	16 51 29.85	+06 22 26.2	RRAB	13.352	-	0.7786
194-125256	GT Vir	14 56 48.38	+06 48 27.7	RRAB	15.089	0.4080564	0.68931
195-285152	LX Del	20 52 18.98	+07 08 46.8	RRAB	13.876	-	0.5669
197-007736	BP Cet	02 24 52.15	+08 24 05.0	RRAB	14.897	-	0.6924
197-143679	V1013 Her	16 24 49.66	+08 04 14.1	RRAB	13.258	-	0.6448
199-293401	LW Del	20 38 27.40	+09 12 05.4	RRAB	12.890	-	0.5811
200-000971	FF Psc	00 17 48.58	+09 53 22.1	RRAB	12.441	0.70119	0.70110
201-029115	V0944 Ori	05 36 11.40	+10 29 23.0	RRAB	15.456	-	0.5873
201-114082	DL Leo	09 43 03.58	+10 19 01.3	RRAB	13.551	-	0.67378
203-295430	DG Del	20 35 44.20	+11 28 09.0	RRAB	15.797	0.326961	0.4905
203-295942	DI Del	20 36 49.52	+11 20 21.9	RRAB	15.487	0.367221	0.5803
204-103494	AM Cnc	08 56 14.84	+11 37 20.6	RRAB	14.815	0.557615	0.55803
204-113713	GP Leo	11 45 45.53	+11 52 08.5	RRAB	13.952	-	0.6793
204-293402	HV Del	20 33 19.53	+11 32 01.7	RRAB	15.636	0.721265	0.5649
207-115598	LL Leo	11 30 53.62	+13 19 28.4	RRAB	13.144	0.3324	0.33239
209-135992	V1124 Her	17 04 32.86	+14 26 32.7	RRAB[a]	12.426	0.551	0.55103
211-103053	KW Cnc	08 40 47.96	+15 24 52.4	RRAB	14.591	0.60102	0.60044
211-128841	AW Ser	16 06 28.79	+15 22 05.8	RRAB	12.983	0.597097	0.597114
211-291434	CS Del	20 28 54.87	+15 13 14.0	RRC	12.912	0.365737	0.37088
212-310112	V0398 Peg	21 08 57.95	+15 56 55.3	RRAB	13.893	0.55259	0.55136
213-110778	HY Com	12 18 16.02	+16 09 15.9	RRC	10.281	-	0.4488
214-112667	BX Leo	11 38 02.06	+16 32 36.2	RRC	11.771	0.36286	0.36277
215-288176	CH Del	20 23 18.39	+17 06 13.5	RRC	13.176	0.4596	0.31499
216-128398	V0686 Her	16 14 23.25	+17 56 35.2	RRAB	14.800	0.510987	0.511004
216-129723	V0695 Her	16 25 58.65	+17 42 52.0	RRAB[a,b]	14.574	0.678788	0.67884
216-339177	V0611 Peg	23 46 41.17	+17 38 02.6	RRAB	13.794	0.58868	0.588665
216-339421	V0419 Peg	23 50 05.03	+17 53 44.0	RRAB	14.674	0.60373	0.60370
218-287254	EO Del	20 37 47.72	+18 55 30.6	RRAB	14.378	0.580861	0.57990
219-270870	II Del	20 50 01.18	+19 11 43.5	RRC	14.558	0.408021	0.4078
224-130750	SW Her	16 58 27.56	+21 32 51.5	RRAB	14.956	0.49287277	0.492861
225-123239	V0504 Ser	16 01 52.29	+22 22 47.9	RRAB	14.169	0.56396	0.563833
225-131962	V0382 Her	17 16 17.21	+22 01 04.5	RRAB	15.934	0.4556118	0.45554
225-265413	FH Vul	20 40 19.89	+22 13 24.3	RRAB	13.267	0.4054185	0.405412
227-031814	HX Tau	05 10 48.79	+23 12 22.7	RRAB	15.298	0.53875	0.53826
227-119598	V0362 Her	16 30 39.55	+23 26 41.7	RRAB	14.791	0.718297	0.7185
228-098638	EZ Cnc	08 52 57.67	+23 47 54.2	RRAB	12.404	-	0.54578
228-261882	BL Peg	21 22 59.51	+23 53 32.1	RRAB[a,b]	14.433	0.55543	0.55555
229-254073	V0507 Vul	20 49 45.85	+24 12 44.9	RRC	11.848	0.336126	0.33607
230-118556	V0677 Her	16 08 04.15	+24 59 20.2	RRAB	14.387	0.475716	0.475728
230-120541	V1186 Her	16 29 14.78	+24 59 38.7	RRAB	13.894	0.44032	0.44025
231-126743	V0467 Her	17 12 50.79	+25 01 48.6	RRAB	14.850	0.6835066	0.65352
232-094191	AS Cnc	08 25 42.16	+25 43 08.5	RRAB	12.998	0.61752	0.61754
232-096427	SX Cnc	08 51 19.58	+25 33 24.3	RRAB	14.026	0.5101754	0.51016
232-111124	IY Boo	14 19 39.22	+25 47 24.1	RRAB	14.462	0.59165	0.59171
232-112040	LN Boo	14 37 09.05	+25 44 46.6	RRAB[a,b]	13.997	0.46675	0.46667
234-000057	GV Peg	00 00 35.59	+26 39 49.5	RRAB[a,b]	13.600	0.5669237	0.56607
235-118691	CT CrB	16 18 34.34	+27 28 13.2	RRAB[a]	14.271	0.508646	0.50858
236-097672	KV Cnc	08 40 02.43	+27 43 31.5	RRAB[a]	12.916	0.502	0.5020
236-123949	V0860 Her	16 50 38.71	+27 58 40.3	RRAB	16.051	-	0.57083
237-108110	EF Leo	11 49 10.95	+28 00 25.6	RRAB	15.891	-	0.5979
237-274829	V0466 Vul	21 05 22.87	+28 17 49.4	RRAB	14.752	0.4759	0.47592
239-000617	IQ Peg	00 06 05.70	+29 19 12.6	RRAB	16.319	-	0.47993
240-120704	RV CrB	16 19 25.85	+29 42 47.6	RRC	11.387	0.331565	0.33172
245-013999	VX Tri	02 10 00.87	+32 24 08.9	RRAB	14.576	-	0.6331
247-105751	CK Com	12 14 50.60	+33 06 05.9	RRAB	14.727	0.6939962	0.6938
248-104694	V0345 UMa	11 17 49.43	+33 40 14.8	RRAB	14.434	0.57667	0.57662
248-106344	DN CVn	12 09 17.00	+33 39 35.5	RRC	15.083	0.3266873	0.32625
251-289738	DM And	23 32 00.72	+35 11 48.9	RRAB	11.978	0.630387	0.6305
254-099280	VY LMi	09 27 41.32	+36 58 22.4	RRAB	13.838	-	0.52614
255-095249	DQ Lyn	08 23 40.99	+37 28 10.8	RRC	11.670	-	0.4949
257-098638	EN Lyn	08 46 07.04	+38 02 52.7	RRAB	13.554	0.6249	0.6251
262-118704	AO UMa	11 07 39.83	+40 33 57.2	RRAB	15.749	0.561614	0.56265
263-257028	DY And	23 58 42.21	+41 29 19.4	RRAB	13.674	0.603087	0.60323
266-126680	AQ UMa	11 12 59.53	+42 48 41.7	RRAB	16.369	0.644029	0.6433
266-127186	AV UMa	11 29 40.53	+42 44 24.7	RRAB	15.935	0.479483	0.47911
272-115635	AX UMa	11 38 26.84	+45 56 05.9	RRAB	13.591	0.53491	0.53468
278-047793	AN Per	03 08 31.34	+48 32 40.4	RRAB	14.367	0.602818	0.6021
282-136249	DT Dra	18 49 57.25	+50 35 12.8	RRAB	13.625	-	0.52664
282-145093	V1949 Cyg	19 30 12.47	+50 48 21.2	RRAB[a,b]	13.714	-	0.4994
293-139097	XZ Cyg	19 32 29.31	+56 23 17.5	RRAB	9.500	0.4667	0.4666
297-143410	V1035 Cyg	20 05 41.44	+58 02 48.9	RRAB	15.798	0.5321	0.5318
312-073056	V0420 Dra	19 18 09.26	+65 35 17.7	RRC	12.780	0.32963	0.32951

[a] Clearly exhibits the Blazhko effect in our data.
[b] Not listed in the set of known Galactic field Blazhko RR Lyrae stars from Skarka (2013).

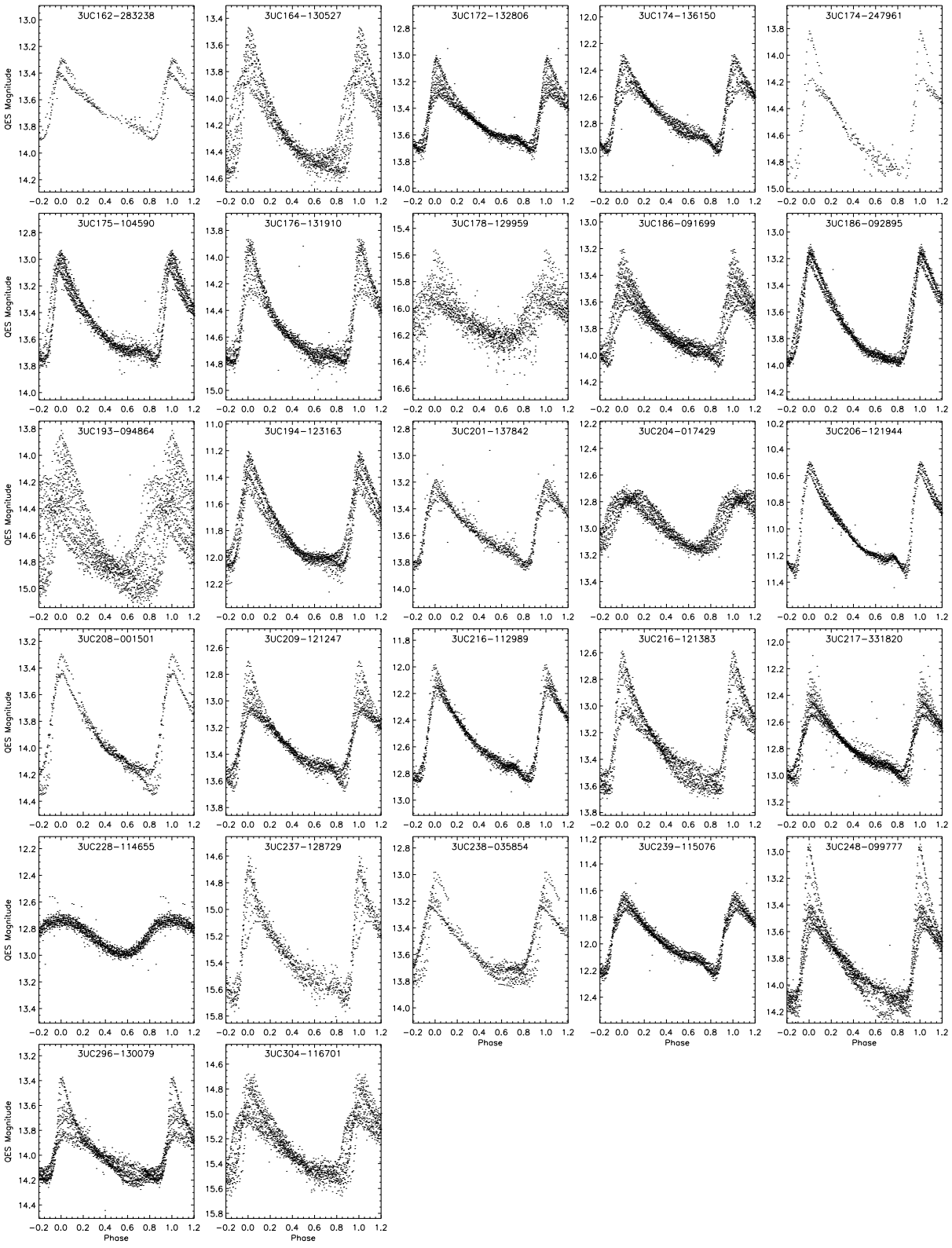

Figure 8. Phased light curves of the RR Lyrae stars exhibiting the Blazhko effect and that are not in the catalogue of Skarka (2013). The magnitude range in each plot is 1.4 mag.

Table 5. New detections of the Blazhko effect in Galactic RR Lyrae stars. These stars are not listed in the catalogue of Skarka (2013).

UCAC3 ID	GCVS ID	RA (J2000.0)	Dec. (J2000.0)	Variable Type	UCAC3 Aperture Mag	Period (d) GCVS	Blazhko Period (d)
162-283238	PQ Aqr	20 43 15.75	−09 09 28.7	RRAB	13.713	0.512286	-
164-130527	V0574 Vir	14 34 30.48	−08 18 32.7	RRAB	14.529	0.47439	26.3±0.3
172-132806	V0586 Vir	14 39 47.52	−04 08 05.3	RRAB	13.376	0.682772	132±3
174-136150	V0585 Vir	14 39 27.36	−03 27 36.6	RRAB	12.872	0.601615	93.8±0.4
174-247961	PS Aqr	20 44 03.69	−03 23 12.3	RRAB	14.411	0.59102	-
175-104590	V0486 Hya	08 30 29.83	−02 42 36.8	RRAB	13.107	0.508655	18.5±1.0
176-131910	MS Lib	14 53 32.99	−02 06 51.5	RRAB	14.445	0.441448	105±10
178-129959	V0561 Vir	14 28 40.65	−01 27 59.4	RRAB	15.893	0.550276	42.0±0.6
186-091699	V0487 Hya	08 32 57.03	+02 59 02.9	RRAB	13.447	0.561485	64.4±0.3
186-092895	GL Hya	08 40 59.22	+02 37 22.2	RRAB	13.409	0.50593	157±10
193-094864	V0425 Hya	08 20 51.78	+06 28 24.2	RRAB	14.829	0.5508	61.1±0.2
194-123163	AF Vir	14 28 09.82	+06 32 43.9	RRAB	11.507	0.48376	35±5
201-137842	V1162 Her	16 17 00.49	+10 17 27.9	RRAB	13.429	0.547925	-
204-017429	V1327 Tau	04 40 09.89	+11 43 17.0	RRC	13.169	0.3312	23.7±0.3
206-121944	UY Boo	13 58 46.34	+12 57 06.5	RRAB	11.001	0.6508964	-
208-001501	FI Psc	00 23 22.80	+13 45 40.8	RRAB	13.590	0.53129	>120
209-121247	LS Boo	14 38 21.77	+14 24 55.1	RRAB	13.624	0.5527108	42.9±1.9
216-112989	AE Leo	11 26 12.19	+17 39 39.7	RRAB	12.508	0.626723	62±4
216-121383	LW Boo	14 40 32.61	+17 35 57.3	RRAB	13.434	0.56342	63.9±0.6
217-331820	V0606 Peg	23 41 58.75	+18 13 01.4	RRAB	12.564	0.52966	26.7±0.3
228-114655	DD Boo	14 51 20.08	+23 32 30.0	RRC[a]	12.889	0.3393397	9.64±0.02
237-128729	V0385 Her	17 16 26.66	+28 05 56.4	RRAB	15.499	0.5281428	>100
238-035854	NU Aur	05 09 02.37	+28 40 52.7	RRAB	13.436	0.53941672	>60
239-115076	XX Boo	14 51 37.56	+29 21 26.7	RRAB	12.061	0.581402	148±7
248-099777	FW Lyn	09 19 51.49	+33 52 23.9	RRAB	13.650	0.52174	>110
296-130079	NQ Dra	18 44 13.17	+57 40 59.4	RRAB	13.752	0.52919	34.5±0.4
304-116701	V0429 Dra	19 59 32.15	+61 31 21.0	RRAB	14.994	0.5862	87.0±2.2

[a] Although the amplitude modulations are small, they are clear to the eye in the unphased light curve and they are strongly detected in the power spectrum. To help confirm our conclusions for this star, we checked the literature and found that Gomez-Forrellad & Garcia-Melendo (1995) also suspected this star of exhibiting the Blazhko effect.

Table 6. Time-series photometry for the 588 variable stars described in this paper. The epoch of mid-exposure (heliocentric Julian date) is listed in column 4. The magnitudes in column 5 are calibrated QES magnitudes. Column 6 contains the uncertainties on the magnitudes. The light curve identifier string is listed in column 7 and consists of a concatenation of the target field name, a camera identifier and an observing campaign identifier.

UCAC3 ID	GCVS ID	Variable Type	HJD (d)	m (mag)	σ_m (mag)	Light Curve Identifier
3UC161-102683	DH Hya	RRAB	2455639.60565	12.265	0.256	084014−044854_416_C5
3UC161-102683	DH Hya	RRAB	2455639.61285	12.347	0.262	084014−044854_416_C5
⋮	⋮	⋮	⋮	⋮	⋮	⋮
3UC161-102683	DH Hya	RRAB	2455639.61110	12.268	0.377	092014−044854_416_C5
3UC161-102683	DH Hya	RRAB	2455639.61810	12.296	0.380	092014−044854_416_C5
⋮	⋮	⋮	⋮	⋮	⋮	⋮
3UC162-107613	SZ Hya	RRAB	2455229.77350	11.529	0.076	091000−071400_403_C2
3UC162-107613	SZ Hya	RRAB	2455229.78082	11.427	0.045	091000−071400_403_C2
⋮	⋮	⋮	⋮	⋮	⋮	⋮

ACKNOWLEDGMENTS: This research made use of the SIMBAD database, the VizieR catalogue access tool, and the cross-match service provided by CDS, Strasbourg, France. This publication was made possible by NPRP grant # X-019-1-006 from the Qatar National Research Fund (a member of Qatar Foundation). The statements made herein are solely the responsibility of the authors. AAF is grateful to DGAPA-UNAM for grant number IN104612. Thanks goes to Noe Kains at STScI in Baltimore for hosting the first author during part of this work and for the many useful discussions.

References:

Alard, C. & Lupton, R.H. 1998, *ApJ*, **503**, 325
Alsubai, K.A., Parley, N.R., Bramich, D.M., Horne, K., Collier Cameron, A., West, R.G., Sorensen, P.M., Pollacco, D., Smith, J.C. & Fors, O., 2013, *Acta Astronomica*, **63**, 465
Alsubai, K.A. et al., 2011, *MNRAS*, **417**, 709
Andrievsky, S.M., Kovtyukh, V.V., Wallerstein, G., Korotin, S.A. & Huang, W., 2010, *PASP*, **122**, 877
Belloni, T., Verbunt, F. & Mathieu, R.D., 1998, *A&A*, **339**, 431
Benkő, J.M., Szabó, R. & Paparó, M., 2011, *MNRAS*, **417**, 974
Bernhard, K., 2010, *BAV Rundbrief*, **59**, 78
Blazhko, S., 1907, *Astronomische Nachrichten*, **175**, 325
Bramich, D.M., 2008, *MNRAS*, **386**, L77
Bramich, D.M., Horne, K., Albrow, M.D., Tsapras, Y., Snodgrass, C., Street, R.A., Hundertmark, M., Kains, N., Arellano Ferro, A., Figuera Jaimes, R. & Giridhar, S., 2013, *MNRAS*, **428**, 2275
Bryan, M.L. et al., 2012, *ApJ*, **750**, 84
Burke, E.W., Rolland, W.W. & Boy, W.R., 1970, *Journal of the Royal Astronomical Society of Canada*, **64**, 353
Cox, A.N., Hodson, S.W. & Clancy, S.P., 1983, *ApJ*, **266**, 94
Dworetsky, M.M., 1983, *MNRAS*, **203**, 917
Gomez-Forrellad, J.M. & Garcia-Melendo, E., 1995, *IBVS*, No. 4247
Lenz, P. & Breger, M., 2005, *Communications in Asteroseismology*, **146**, 53
Mathieu, R.D., van den Berg, M., Torres, G., Latham, D., Verbunt, F. & Stassun, K., 2003, *AJ*, **125**, 246
Moskalik, P., 2014, *IAU Symp.*, **301**, 249
O'Connell, D.J.K., 1951, *Riverview College Observatory Publications*, **2**, 85
Samus, N.N. et al., 2009, *General Catalogue of Variables Stars (Vol. I-III, version 30/04/2013)*,
Schmidt, E.G. & Gross, B.A., 1990, *PASP*, **102**, 978
Skarka, M., 2013, *A&A*, **549**, A101
van den Berg, M., Stassun, K.G., Verbunt, F. & Mathieu, R.D., 2002, *A&A*, **382**, 888
Vieira, S.L.A. et al., 2003, *AJ*, **126**, 2971
Wallerstein, G., Kovtyukh, V.V. & Andrievsky, S.M., 2009, *ApJ*, **692**, L127
Wils, P., Lloyd, C., & Bernhard, K., 2006, *MNRAS*, **368**, 1757
Zacharias, N. et al., 2010, *AJ*, **139**, 2184

*This version of the paper contains corrections, and differs from the one appeared on-line originally. Date of last modification: Tue May 27 11:18:08 CEST 2014

COMMISSIONS 27 AND 42 OF THE IAU
INFORMATION BULLETIN ON VARIABLE STARS
Number 6107

Konkoly Observatory
Budapest
19 May 2014
HU ISSN 0374 – 0676

LONG PERIOD VARIABLES IN STELLAR CLUSTERS: IC4651

SAHAY, ANAND[1]; LEBZELTER, THOMAS[2]; WOOD, PETER[3]

[1] Indian School of Mines, Dhanbad; e-mail: anandsahay@ismu.ac.in

[2] University of Vienna, Department of Astropysics, Türkenschanzstrasse 17, A1180 Vienna, Austria

[3] Australian National University, Research School of Astronomy and Astrophysics

Introduction

The research on long period variables (LPVs) experienced a significant upturn in the past two decades when large photometric surveys led to a huge number of high quality LPV light curves. Major steps forward in our understanding were possible by the observation of stellar samples with known distance, in particular those from the Magellanic Clouds (e.g. Wood 2000, Lebzelter et al. 2002, Fraser et al. 2005, Soszyński et al. 2007). It was found that the pulsation of any LPV follows one of several parallel period-luminosity (PL) relations. To better understand this variability behavior, two of us (TL, PW) initiated a monitoring program to detect and characterize LPVs in stellar clusters. For a detailed description of this program we refer to Lebzelter & Wood (2011) and references therein. Observations and data reduction are briefly summarized below.

Within this program we monitored the open cluster IC4651. Several photometric and spectroscopic studies exist for this cluster in the literature, among the most recent ones being Anthony-Twarog et al. (2000), Meibom et al. (2002), Pasquini et al. (2004), and Mikolaitis et al. (2011). IC4651 is an intermediate age open cluster (1.7 Gyr) at a distance of about 1.01±0.05 kpc and a reddening value of E($B-V$)=0.1 mag (Meibom et al. 2002; Pasquini et al. 2004). Various spectroscopic studies on cluster dwarfs suggest a slightly super-solar metallicity (e.g. Carretta et al. 2004, Pace et al. 2008). A depletion of carbon and an overabundance of nitrogen relative to the sun have been reported by Mikolaitis et al. (2011).

Observation and data reduction

Monitoring of IC4651 started in May 2002 at the 50 inch telescope at Mount Stromlo. The telescope was equipped with a two channel camera used earlier for the MACHO experiment (Alcock et al. 1992) and it obtained red and blue images simultaneously. The wavelength centre of the blue channel was similar to that of Johnson V, while the centre of the red channel was close to that of Johnson R. Observations were obtained once to twice a week. Our monitoring came to an abrupt stop after a few months when Mount Stromlo observatory was destroyed by a bush fire. Altogether we collected 23 frames over 130 days, but only 17 frames were usable for our analysis. All observations were done in queue observing mode.

Since in the blue band the light amplitude of long period variables is typically larger than in the red (e.g. Fox & Wood 1982), the blue range received a higher weight for detecting and characterizing variables. The presence of bad pixels did not allow to search for variability in all the stars in our field of view.

The image subtraction code ISIS 2.1 (Alard 2000) was used for the detection of variable stars and extraction of light curve data. Stellar fluxes of the candidate stars on the reference frame were measured using standard IRAF routines. To determine the photometric zero point, the known V mag of several standard stars from the Guide Star Catalogue (Lasker et al. 2008) were compared with our calculated values. No correction has been made for the difference between Johnson V and MACHO Blue.

Among the 150 variable star candidates detected in the observed field, the long period variables were selected based on the brightness (on the upper giant branch), timescale of the variation (more than 30 days), and a total light amplitude in V of at least 0.05 mag. The period search was done using Period98 (Sperl 1998), a code which computes a discrete Fourier transformation in combination with a least-squares fitting of multiple frequencies on the data. We considered a maximum of two periods for each star. We note that for the typical periods of tens of days found for the variables, the light curves are well sampled so that aliasing should not be a significant problem. Due to the semi-regular nature of LPVs, any periodicity found represents only a snapshot of a possibly more complex light curve, and some non-detected variability of much longer time scales (more than 250 days) may exist as well.

Results

One likely LPV had been detected in IC4651 in the course of the ASAS survey (Pojmanski & Maciejewski 2004). We could confirm that detection and found three new long period variables in the cluster. All four stars are listed in Table 1 with their coordinates, V and DENIS I magnitudes, periods, amplitudes, and 2MASS magnitudes. We used V1 as identifier for the known variable while other variables were named using the prefix 'SLW'.

In Figure 1, the light variations of the four LPVs are plotted against time starting with the first date of our time series. Also shown are synthetic light curves using the periods given in Table 1. From previous work on similar data sets we estimate a typical photometric error around 0.02 mag. The weakest point in the light curve of SLW3 may have a higher photometric uncertainty. As one can see, all the variables have a period exceeding 60-70 days. At least one complete variability cycle has been covered for each star. We cannot say anything about possible long secondary periods in these stars since they are expected to exceed the time span of our monitoring by a factor of about six. The period we find for V1 is in good agreement with the literature value of 93.8 d.

Along with the variable stars for which we can estimate a period, we have listed 3 stars in Table 2 that showed variability but without a clear periodicity. This may be due to a truly irregular nature of their light change, but the length of our time series is not sufficient to clearly classify them as long period variables.

Concerning the membership in IC4651 of the stars in Tables 1 and 2, we can rely on a few studies found in the literature and the stars' locations in the cluster's colour-magnitude diagram (CMD, Fig. 2). Unfortunately, there is very little information available for V1. Based on the CMD, its membership is rather unlikely, since the star is clearly offset to the red from the cluster's giant branch. Much better data exist for the newly discovered variables. SLW1, SLW2, SLW3, SLW5, and SLW6 all show radial velocities very close to the mean cluster velocity (Meibom et al. 2002, Kordopatis et al. 2013). Including also

Table 1: Long period variables in the field of IC4651

Name	RA(2000)	Dec(2000)	$V_{\rm mean}$ [mag]	I^a [mag]	J [mag]	H [mag]	K [mag]	Period [d]	ΔV [mag]
V1	17 25 09.35	−49 52 03.6	12.89	9.413	7.007	6.051	5.646	97	0.75
SLW1	17 25 08.95	−49 53 57.1	9.28	8.641	5.747	4.948	4.660	114	0.06
SLW2	17 24 49.48	−49 57 26.7	11.01	9.809	8.901	8.350	8.209	73	0.4
SLW3	17 24 33.40	−49 54 56.0	10.54	9.109	8.137	7.528	7.341	85	0.27

[a] I-band data taken from DENIS database.

Table 2: Long period variable candidates of IC4651 with unknown periods

Name	RA(2000)	Dec(2000)	$V_{\rm mean}$ [mag]	I^a [mag]	J [mag]	H [mag]	K [mag]
SLW4	17 25 14.50	−50 02 49.2	11.51	10.203	9.408	8.881	8.740
SLW5	17 24 54.16	−49 53 07.5	10.53	9.182	8.081	7.469	7.264
SLW6	17 24 46.71	−49 54 07	11.04	9.728	8.912	8.391	8.247

[a] I-band data taken from DENIS database.

proper motion information, Kharchenko et al. (2004) give a high membership probability to these five stars. However, membership probabilities from proper motion data do not give a homogeneous result (e.g. Dias et al. 2006). SLW4 is probably a field star according to its radial velocity.

While the radial velocity data suggest a membership of most of the newly detected variables, the situation is not as clear when combining variability information and location in the cluster's CMD. Using an age of 1.7 Gyr, a star on the upper giant branch would have had a main sequence mass of about 1.7 $M_\odot$ (Bertelli et al. 2008). The tip of the RGB of IC4651 would then be near K=4.0. SLW1 is therefore located about half a magnitude below the RGB tip, SLW2-6 are 3-4 magnitudes below the RGB tip. Thus these variables could be either RGB or early-AGB stars of the cluster. Two stars, SLW2 and 3, have photometric amplitudes of a few tenths of a magnitude and periods of ≈80 days. However, such an amplitude and period, while typical of an AGB star, is not expected for an object that far below the RGB tip according to results from the Magellanic Clouds (cf. Kiss & Bedding 2003). Their variability behaviour suggests that these stars are more likely background objects. However, considering the cluster's location this would place them ≈700 pc above the Galactic plane, which would be quite unlikely. Further studies of these two stars are needed to clarify their nature. SLW1 has a photometric amplitude of less than 0.1 mag, so we think it is an RGB or AGB star belonging to the cluster.

The number of known long period variables with independently defined masses is still very small, in particular for masses above 1 $M_\odot$. A systematic search of LPVs in open clusters is an important source for increasing this number. In this paper we presented several candidates that are possibly members of the intermediate-age cluster IC4651. Further studies are needed to confirm and characterize their nature.

Acknowledgements: The work of TL has been supported by the FWF under project number P23737-N16. This research has made use of the VizieR catalogue access tool, CDS, Strasbourg, France.

References:

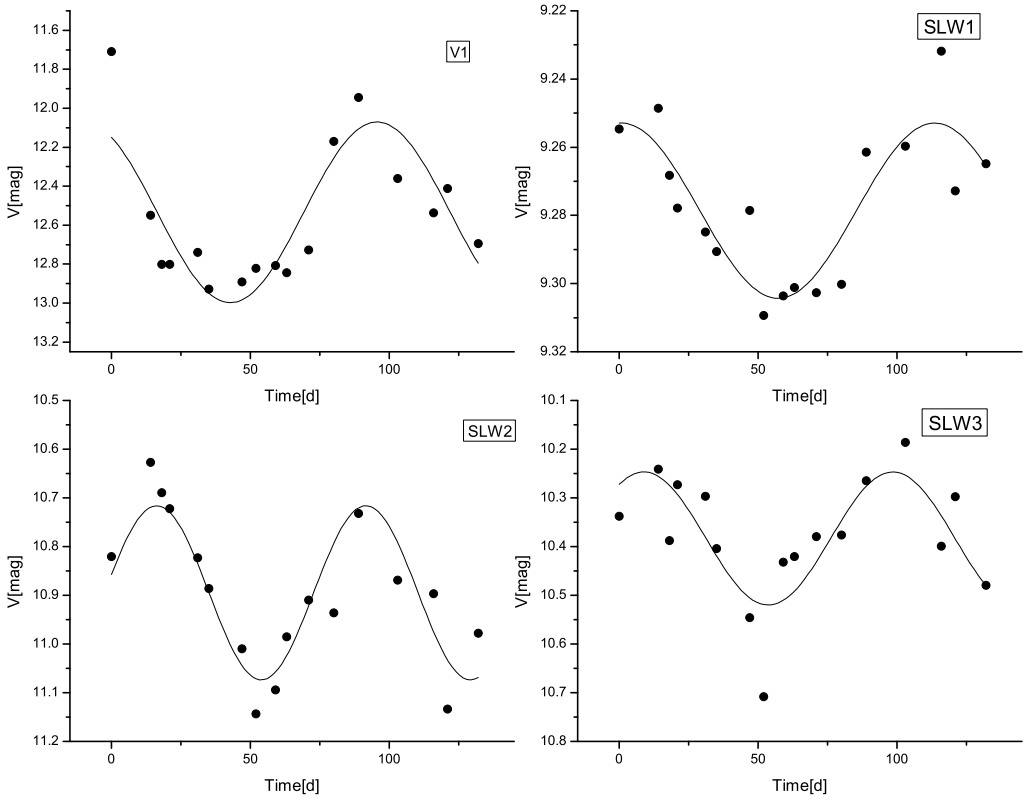

Figure 1. Light curves of the four variables detected in IC4651. Fits to the brightness change are based on the periods given in Table 1. The time axis starts at JD 2452410, the start of our monitoring.

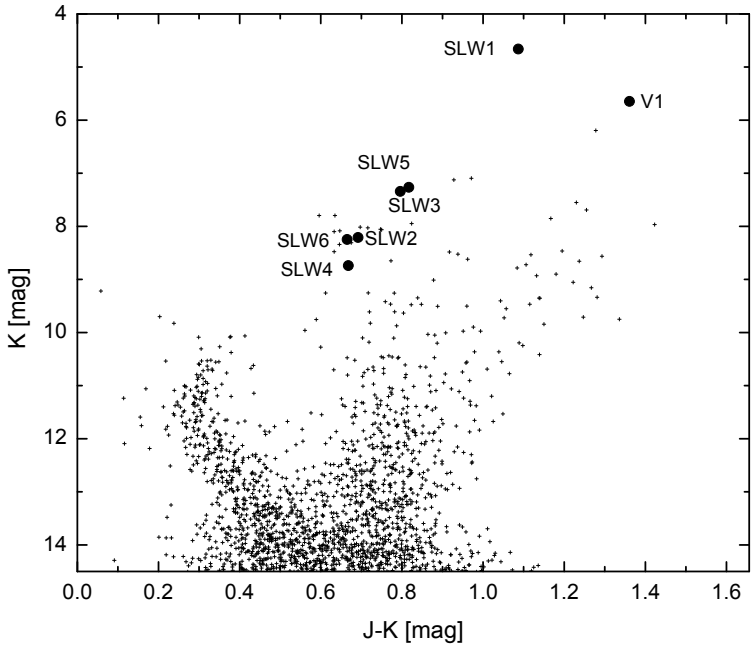

Figure 2. 2MASS colour-magnitude diagram for sources 10 arcminutes around the centre of IC4651. The LPVs from Tables 1 and 2 are marked. The position of the giant branch in this intermediate age cluster is consistent with the positions of variables SLW 1-6 (see the collection of intermediate age giants in Fig. 2 of Bessel et al. (1983), adjusted for a distance modulus of 10.0).

Alard, C. 2000, *A&AS*, **144**, 363.
Alcock, C., Axelrod, T.S., Bennet, D.P., et al. 1992, *ASPC*, **34**, 193.
Anthony-Twarog B. J., Twarog B. A., 2000, *AJ*, **119**, 2282.
Bertelli, G., Girardi, L., Marigo, P., Nasi, E., 2008, *A&A*, **484**, 815.
Bessell, M.S., Wood, P.R., Lloyd Evans, T., 1983, *MNRAS*, **202**, 59.
Carretta E., Bragaglia A., Gratton R., Tosi M., 2004, *A&A*, **422**, 951.
Dias, W.S., Assafin, M., Florio, V., Alessi, B.S., Libero, V., 2006, *A&A*, **446**, 949.
Fox, M.W., Wood, P.R. 1982, *ApJ*, **259**, 198.
Fraser, O.J., Hawley, S.L., Cook, K.H., Keller, S.C., 2005, *AJ*, **129**, 768.
Kharchenko, N.V., Piskunov, A.E., Röser, S., Schilbach, E., Scholz, R.D., 2004, *AN*, **325**, 740.
Kiss, L.L., Bedding, T.R., 2003, *MNRAS*, **343**, L79.
Kordopatis, G., Gilmore, G., Steinmetz, M., et al., 2013, *AJ*, **146**, 134.
Lasker, B.M., Lattanzi, M.G., McLean, B.J., et al., 2008, *AJ*, **136**, 735.
Lebzelter, T., Schultheis, M., Melchior, A.L., 2002, *A&A*, **393**, 573.
Lebzelter, T., Wood, P.R. 2011, *A&A*, **529**, A137.
Meibom S., Andersen J., Nordström B., 2002, *A&A*, **386**, 187.
Mikolaitis, S., Tautvaisiene, G., Gratton, R., Bragaglia, A., Carretta, E., 2011, *MNRAS*, **413**, 2199.
Pace G., Pasquini L., Francois P., 2008, *A&A*, **489**, 403.
Pasquini L., Randich S., Zoccali M., Hill V., Charbonnel C., Nordström B., 2004, *A&A*, **424**, 951.
Pojmanski G., Maciejewski, G., 2004, *AcA*, **54**, 153.
Soszyński I., et al., 2007, *AcA*, **57**, 201.
Sperl, M., 1998, *Comm. in Asteroseismology*, **111**, 1.
Wood, P.R., 2000, *PASA*, **17**, 18.

COMMISSIONS 27 AND 42 OF THE IAU
INFORMATION BULLETIN ON VARIABLE STARS
Number 6108

Konkoly Observatory
Budapest
28 May 2014
HU ISSN 0374 – 0676

CEPHEIDS AND RR LYRAE STARS IN THE K2 FIELDS

MOLNÁR, L.[1,2]; PLACHY, E.[1,2]; SZABÓ, R.[1]

[1] Konkoly Observatory, Research Centre for Astronomy and Earth Sciences, Konkoly Thege Miklós út 15-17, H-1121 Budapest, Hungary

[2] Institute of Mathematics, Physics, and Engineering, Savaria Campus, University of West Hungary, Károlyi Gáspár tér 4, H-9700 Szombathely, Hungary

e-mail: molnar.laszlo@csfk.mta.hu

1 Introduction

The *Kepler* space telescope was launched into orbit in early 2009 with a task to observe about 170 000 stars with unprecedented photometric precision and temporal coverage (Borucki et al. 2010). The original field-of-view was located in the Lyra-Cygnus region at high ecliptic latitudes. *Kepler* observed this field for almost exactly 4 years, providing revolutionary data for several areas, but the failure of its second reaction wheel in May 2013 effectively ended its original mission.

The amount of classical pulsators, Cepheids and RR Lyrae stars, was somewhat limited in the Lyra-Cygnus field. Before the start of the mission, 57 stars were proposed as RR Lyrae targets but 23 of them soon turned out to be other types of stars (Kolenberg et al. 2010). A few targets were discovered later either by the ASAS survey or as contaminants in the pixel apertures of other stars, bringing back the sample size close to 50.

About half of the fundamental-mode RR Lyrae stars turned out to be modulated. The analysis of the 4-year-long rectified data sets revealed that a very high fraction, about 80% shows multiple modulation periods (Benkő et al. 2014). Several of the Blazhko stars show various additional modes and/or period doubling. The sample size, however, is low: Benkő et al. (2014) created rectified data sets for only 15 stars after excluding the blended targets and the bright and heavily saturated RR Lyr, the eponym of the class. A larger population of modulated stars is needed to determine the occurrence rates and especially the various interrelations of the dynamical effects.

Other space photometric missions observed only a handful of RR Lyrae stars. MOST measured AQ Leo, the archetype of the double-mode subclass but most RR Lyraes are too faint for the small telescope (Gruberbauer et al. 2007). Thirteen stars (10 RRab, 2 RRc 1 RRd stars) were identified in the first CoRoT fields (from IR1 to LRC04) and others are expected in the later fields but a thorough search has not been carried out yet (Szabó et al. 2014).

Before the mission, only a single classical Cepheid, V1154 Cyg was known in the *Kepler* field. Despite a thorough search, no other stars were discovered (Szabó et al. 2011). V1154

Cyg itself turned out to be a rewarding target, revealing significant fluctuations in its light curve (Derekas et al. 2012). Similar effects were discovered in two other classical Cepheids with MOST (Evans et al. 2014). A handful of stars have been classified as Cepheids in the early CoRoT data, but those have not been investigated in detail, therefore it is unclear which subtypes are present in the sample (Debosscher et al. 2009).

2 The K2 mission

After the failure of the second reaction wheel, the operators of *Kepler* invited the scientific community to submit white papers detailing the possible uses and techniques for the space telescope. With the help of this feedback, a new mission scenario was devised. Named K2, after both the two-wheel operation mode and the enigmatic and challenging peak in the Karakoram Range, the new mission will carry out shorter-duration campaigns along the ecliptic and will cover several fields in the sky. This setting will allow the telescope to balance against the radiation pressure of the Sun while maintaining attitude in the other two directions with the remaining reaction wheels.

Although the 75-day duration of the campaigns will be much shorter than the time base of the prime mission, the availability of very diverse fields will obviously provide adequate justification for it. Moreover, the 75-day-long campaigns are still longer than most space-based observations. They were only exceeded by the CoRoT long runs that lasted for about 150 days. In the foreseeable future, the regions around the ecliptic poles will be covered by TESS for about one year and after that only PLATO, to be launched in 2024, will carry out multi-year observations (Rauer et al. 2014).

2.1 Target selection

Target selection for the first few fields, including the two-wheel engineering test run, had to be carried out on short time scales, usually within a few weeks. Surveying the fields with new observations was unfeasible, hence we only proposed stars that were already marked as (potential) Cepheid or RR Lyrae stars in various databases.

As a start we queried the stars designated as either RR Lyrae or some subclass of Cepheids from SIMBAD. The main drawback of SIMBAD is that in most cases we cannot verify the classification with actual light curves. Therefore we searched the time-domain photometric databases thoroughly. The All Sky Automated Survey[1] (ASAS; Pojmanski 1997) provides classifications but the photometric accuracy of the data drops considerably below 10-11th magnitudes. We also used the databases of the Northern Sky Variability Survey[2] (NSVS; Woźniak et al. 2004), SuperWASP[3] (Paunzen et al. 2014) and the INTEGRAL Optical Monitoring Camera[4] (IOMC; Mas-Hesse et al. 2003).

The two most valuable sources for RR Lyrae targets were the asteroid-searching surveys that scanned large portions of the sky repeatedly with moderate-sized telescopes to detect faint objects. Most of these data was already mined for RR Lyrae stars to conduct statistical studies and search for stellar streams and other structures in the galactic halo. The LINEAR database[5] contains all types of RR Lyrae stars (Sesar et al. 2013) but covers right ascensions between 8 an 18 hours only and mostly above the celestial equator. The

[1] http://www.astrouw.edu.pl/asas/
[2] http://skydot.lanl.gov/
[3] http://wasp.cerit-sc.cz
[4] http://sdc.cab.inta-csic.es/omc
[5] http://www.astro.washington.edu/users/ivezic/linear/PaperIII/PLV.html

Catalina Survey data[6] covers a larger area, most of the sky above $\delta \sim -20°$, except for a wide band along the Milky Way. A second, deeper survey (Mt. Lemmon Survey, MLS) was carried out along the ecliptic plane as well, but in both cases only the RRab stars were identified (Drake et al. 2013a,b). The LONEOS Phase I data that mostly covered the ecliptic was also mined for RRab stars (Miceli et al. 2008). The distribution of RR Lyrae stars from the various databases are shown in Figure 1. The complete classification of the Catalina data was released only very recently and will be used for target selection from Field 4 onwards (Drake et al. 2014).

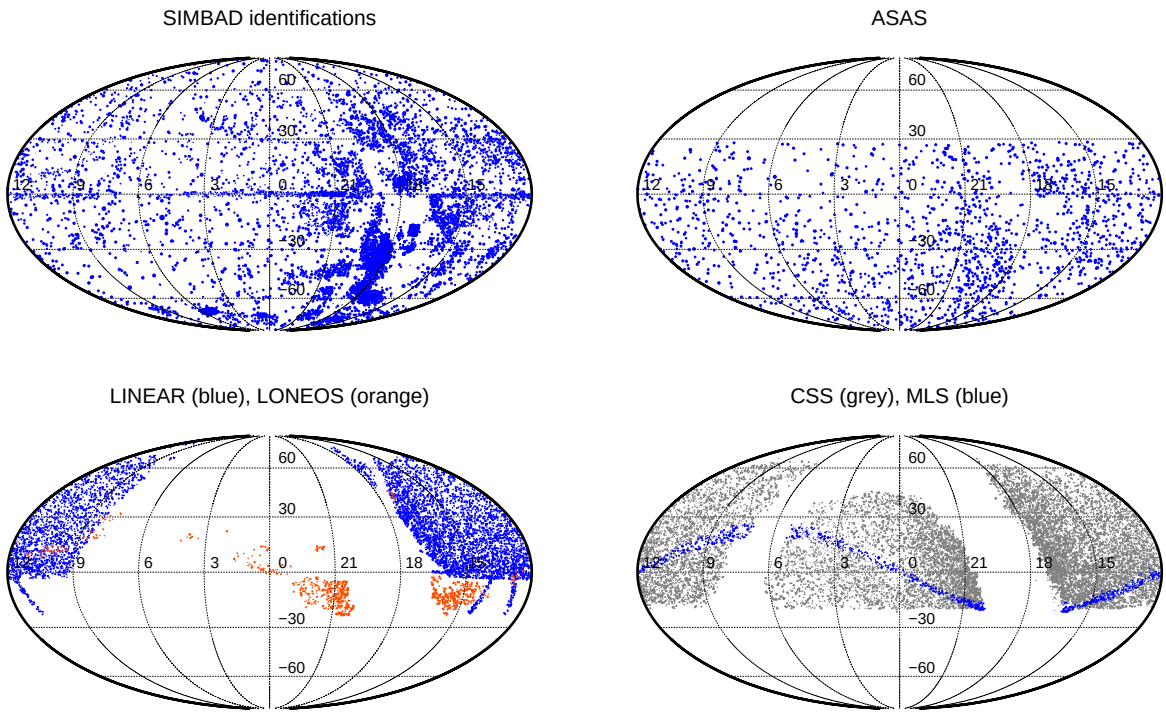

Figure 1. Distribution of RR Lyrae stars in the five major data sets we used for target selection.

Cepheids have been classified only in SIMBAD and the ASAS and NSVS databases (Hoffmann, Harrison & McNamara 2009; Schmidt et al. 2013) so we relied upon those and tried to confirm as many of them as possible with published observations. The distribution is shown in Figure 2.

2.2 Two-wheel engineering test and Field 0

A 9-day engineering test run was carried out in February 2014 to verify the operations with two reaction wheels. *Kepler* observed some 2000 stars in the direction of Pisces. The data suffers from various pointing adjustments and drifts that make the extraction of light curves a complicated task. We found 27 RRab, 3 RRc and a possible Cepheid star among the observations, although the period of the latter star is about 53 days, much longer than the data set itself.

[6] http://catalinadata.org

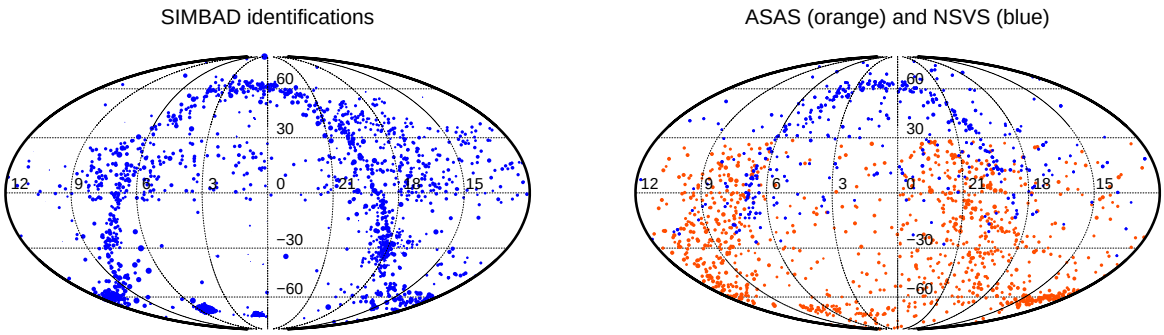

Figure 2. Distribution of various Cepheid and Cepheid-like stars in SIMBAD and the ASAS and NSVS surveys. Most stars are close the plane of the Miky Way.

The brightest RRab star in the sample was ASAS J233637-0212.7 (EPIC 60018644 - EPIC is the *Kepler* Ecliptic Plane Input Catalog). We extracted the light curve of the star with the PyKE toolset to test the stability and quality of the *K2* data. The telescope was repositioned after BJD = 56695.359, shifting the stars by a couple of pixels on the CCDs, therefore we used two pixel masks at different positions to extract the photometric data. The resulting background-corrected light curve can be seen in Figure 3. A detailed summary of the RR Lyrae stars in the engineering-test data will be published in a future paper.

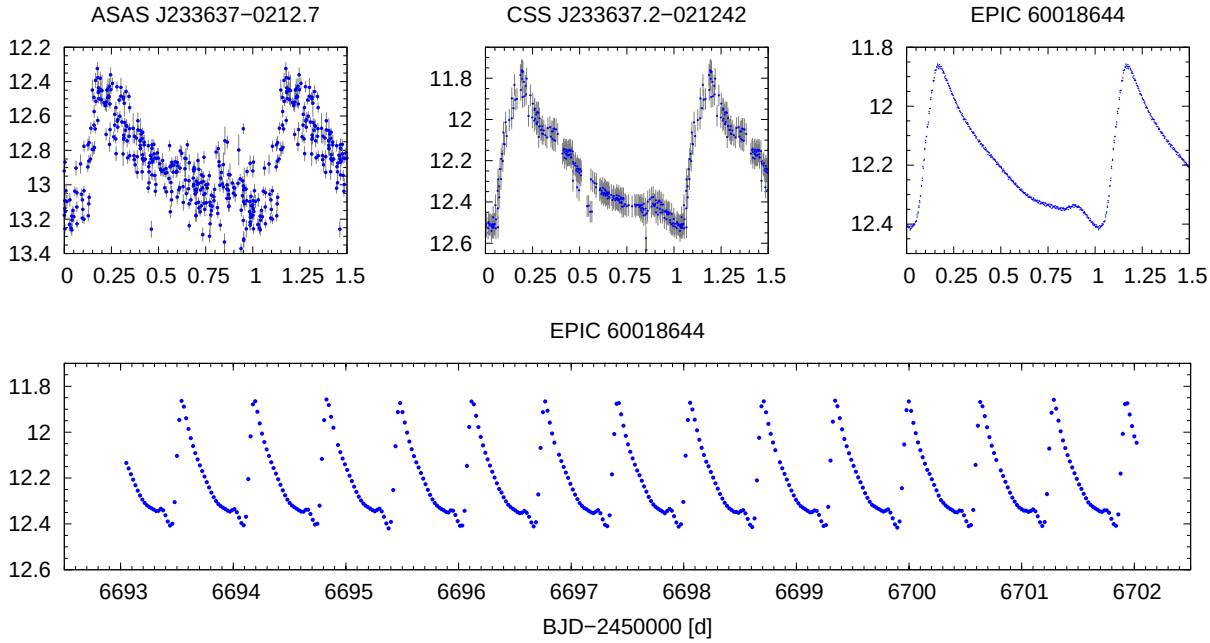

Figure 3. Comparison of the ASAS, Catalina and *K2* long cadence data of the RR Lyrae star ASAS J233637-0212.7. The upper panels show the light curves folded with a pulsation period of $P = 0.6450427$ days. The lower panel contains the extracted *K2* light curve itself.

After the engineering tests, a full-scale performance test was carried out. Campaign 0 was a shakedown that closely resembled the proposed operations of the *K2* mission. Field 0 was set towards the galactic anticenter in Gemini, including the bright open cluster Messier 35. Since the asteroid searching surveys avoided this area we ended up with only 10 RR Lyrae stars that fell on silicon. However, Field 0 was ideally positioned to observe Cepheids: 14 stars were accepted to the long-cadence target list, including fundamental-mode and overtone stars, likely from both Type I and Type II Cepheids. Field 0 in itself will double the number of Cepheids observed with space-based photometry. One RR Lyrae (EW Gem; Schmidt & Reiswig 1993) and one first-overtone Cepheid (NSVS 9770315) were selected for short cadence observations.

2.3 Fields 1 and 3 - galore of RR Lyrae stars

The first science field of the *K2* mission was set towards the Leo-Virgo region and far from the plane of the Galaxy. With the help of the LINEAR and Catalina catalogs, we identified and proposed no less than 133 field RR Lyrae stars. This number far exceeds the approximately 50 stars that were observed in the original *Kepler* field and offered the possibility for an unprecedented opportunity for statistical studies. Moreover, apart from the 118 RRab and 14 RRc stars, we found a single double-mode (RRd) star, LINEAR 2122319, in the field as well (Poleski 2013). Unfortunately, very few stars made it to the final target list, but later fields hopefully will accumulate an expected few hundred stars to carry out the statistical studies. On the other hand, six targets were selected for short cadence observations, including all three types RR Lyrae stars.

In addition, we found three intriguing extragalactic stars. The dwarf spheroidal galaxy Leo IV falls into Field 1 and three RR Lyraes were identified in it by Moretti et al. (2009). These stars, along with the brightest giants and supergiants in the galaxy were included in the target list. The brightness of the three RR Lyraes is below $Kp = 21$ magnitudes so they represent a considerable observational challenge. During the primary mission the estimated precision for a 21st magnitude star was about 0.15 ($P = 148700$ ppm) in a single long-cadence observation. The precision of the *K2* measurements is expected to be within a factor of 2 in fine pointing mode (Howell et al. 2014), therefore the precision of individual points will be around 0.2-0.3 magnitudes. Based on that, the entire data set is expected to provide an accuracy of 5 millimagnitudes for a coherent signal. Most additional-mode peaks fall below this limit, but the strongest ones can be recovered (Benkő et al. 2014; Molnár et al. 2012).

2.4 Field 2 - globular clusters

The speciality of Field 2 is the inclusion of two globular clusters, Messier 4 and 80. *Kepler*, with its 4″/px resolution was not designed to observe dense stellar fields and that leads to various consequences. M4 is fairly spread-out, with a half-light radius (R_h) of 65 pixels, but its bright core would saturate the CCD. Possibly for that reason, only the northern edge falls on silicon. M80 is fainter but also more compact with a half-light radius of only 4 pixels. Still, we identified many pulsating variables in the outskirts of the clusters out to about $7\,R_h$ where we expect the crowding to be acceptable. Several RR Lyrae stars, a few semiregular and SX Phe stars and a single type II Cepheid were proposed for the two clusters.

Apart from the globular clusters, we proposed about 50 field RR Lyrae stars and a few Cepheid/W Vir candidates, as well.

2.5 Future fields

The approximate positions of most of the future fields contain a large number of RR Lyrae stars, including the RRc and RRd classes. Field 7 will be positioned close to the galactic plane and therefore lack asteroid survey data. Nevertheless, the GCVS contains a large amount of otherwise unobserved RR Lyrae stars in that region (Samus et al. 2004).

A comparison of the distribution of various Cepheid stars with the preliminary positions of the *K2* fields suggests that every field will contain a handful of Cepheids (barring misidentifications in the various survey data), including all subtypes: classical Cepheids, BL Her, and W Vir stars.

We identified two galaxies where it is possible to observe extragalactic Cepheids. Fields 7 and 8 may include NGC 6822 and IC 1613, respectively. IC 1613 is closer and contains several Cepheids that are brighter than 21 magnitudes in V band (Bernard et al. 2010). NGC 6822 is somewhat farther away, but about a dozen variables are brighter than 22 magnitudes and therefore we may expect reasonable photometry from those as well (Pietrzyński et al. 2004; Mennickent et al. 2006).

The initial data products of the *K2* campaigns will be the target pixel files: a times series of small CCD subframes containing the image of the star. We already gained experiences with target pixel files to create the rectified RR Lyrae data sets (Benkő et al. 2014), therefore the reduction of the *K2* photometric data will be a relatively straightforward task. An example (EPIC 60018657) from the 9-day engineering run is displayed in Fig. 4.

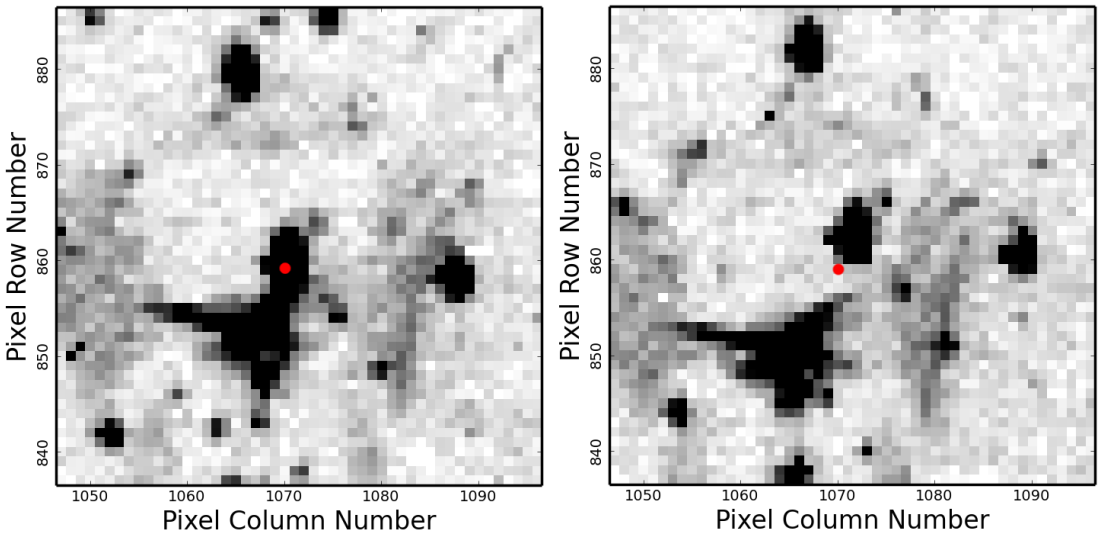

Figure 4. *K2* target pixel files from the 9-day engineering test run. Red dot marks the approximate photocenter of the star during the first 2 days. Left panel: 1st cadence, right panel: the 150th, i.e. after the repositioning of the telescope. There are also four patches of reflected light in the mask, and the brightest one contaminates the star slightly during the first part of the observations. The patches then move to the opposite direction compared to the stars, separating the bright blob from the target.

3 Scientific goals and possibilities in the *K2* mission

The step-and-stare approach of the *K2* mission differs significantly from the original mission scenario. The length of the campaigns seriously limits some applications, e.g. the detection of long Blazhko periods and/or the variations in the modulation cycles. However, the availability of multiple fields opens up several new possibilities compared to the prime mission.

3.1 Cepheids - pulsation and atmospheric dynamics

Continuous observations of space photometric data revealed that classical Cepheids exhibit light curve fluctuations (Derekas et al. 2012). These could possibly be connected to large convective hot spots on the surface of the star (Neilson & Ignace 2014). There are some indications that this effect is stronger in overtone stars than in fundamental-mode pulsators. If this relation exists, it may aid the determination of pulsation modes. Confirmation, however, requires several stars with different periods to be observed.

First-overtone Cepheids may turn out to be double-mode pulsators or can exhibit non-radial modes, according to the OGLE observations (Moskalik & Kołaczkowski 2009). Some of them show strong O–C variations too, but it is not clear if that manifests in the pulsation amplitudes as well or not.

Due to their lower metallicity, light variations of type II Cepheids (W Virginis and BL Herculis stars) exhibit noticeable variations. Period doubling was already detected in one BL Her star, but hydrodynamic models predict other effects such as chaotic pulsation or low-amplitude modulation, too (Smolec et al. 2012; Smolec & Moskalik 2014). Continuous, high-precision data is the best way to detect such irregularities in the pulsation of these stars.

A few anomalous Cepheids were also identified in the fields. These stars lie between the classical and type II Cepheids and follow a separate P-L relation in the period-luminosity diagram (Nemec, Nemec & Lutz, 1994). They have low metallicities and their origin is somewhat uncertain but may involve mass transfer in a binary system with a possible link to blue stragglers (Szabados, Kiss & Derekas 2007). *K2* could be the first space telescope to observe anomalous Cepheids.

3.2 RRab Lyrae stars – mode interactions and the cause of the Blazkho effect

One of the great surprises of the *Kepler* mission was the detection of millimagnitude-level additional modes in almost all modulated RR Lyrae stars (Benkő et al. 2010, 2014). The occurrence of these modes raise serious questions about the mode selection mechanisms in RR Lyrae stars.

Although hydrodynamic models can explain the occurrence of some of the additional modes, there is still discrepancy between the observations and the theoretical results. Based on the sample of the *Kepler* field, most of the stars exhibit period doubling, related to the 9th overtone (Kolláth, Molnár & Szabó 2011), and a frequency peak that may correspond to the second overtone ($P_2/P_0 \approx 0.6$; Benkő et al. 2014). However, in the models, period doubling leads to the destabilization of the first overtone which was detected in very few stars. Finding more stars where the first overtone is excited can lead to accurate comparisons with the models, including the mode amplitudes and the signs of mode interactions, possibly even chaos (Plachy, Kolláth & Molnár 2013). Such nonlinear asteroseismic analysis was attempted only for RR Lyr itself to date (Molnár et al. 2012).

Mode interactions and resonances are the best candidates so far to finally explain the mysterious Blazhko effect (Buchler & Kolláth 2011). Considering that only half of the RRab stars are modulated, a large survey is necessary to understand the relation between these modes. 75 days is long enough to cover at least one modulation cycle for the majority of the Blazhko stars.

Another interesting aspect of the Blazhko effect is the apparent decline of its frequency above $P \sim 0.66 - 0.7$ days (Smolec 2005). It is yet unclear if the typical modulation amplitudes decrease and therefore simply become less detectable by ground-based surveys, or the mechanism of the Blazhko effect itself depends on the pulsation period, e.g. mode resonances may be less likely to occur. All stars in the *Kepler* field have periods below 0.69 days, therefore it could not address this issue (Nemec et al. 2013). If the *K2* campaigns can build up a suitably large sample of modulated stars including long-period ones, the observations may shed light on the origins of this effect and the inner workings of the Blazhko effect.

3.3 RRc and RRd stars

Modulation is present but much less common among the first-overtone (RRc) stars. Only a few RRc stars has been observed from space so far, and none of them turned out to be modulated yet: *Kepler* could be the first space telescope to detect one.

A great surprise of the original *Kepler* field was that all four RRc stars turned out to be multiperiodic. Moreover, they all shared the same properties: the additional mode was detected at $P_X/P_1 = 0.60-0.64$, and showed period doubling in all cases (Moskalik 2014). We note that similar, mysterious modes were detected not only in RRc, but in RRab and LMC Cepheid stars as well, always at the same period ratio (Moskalik 2014). A closer look at the frequency tables of the two RRd stars where additional modes were reported also reveals this mode, although the authors classified them differently. Interestingly, it is connected to the first overtone in both cases (Gruberbauer et al. 2007; Chadid 2012).

The origin of the P_X (or $P_{0.6}$) modes is not yet understood. A thorough survey is required to find out whether all RRc and RRd stars exhibit it, or there is some connection between the mode selection mechanism and the physical properties of the stars. The same is true for the apparent period doubling of this mode. Luckily, the Catalina and LINEAR surveys will provide several RRc and RRd targets, especially from Field 4 onwards.

Double-mode stars are also important on their own right. The two main modes can be modeled accurately with the existing hydrodynamic codes, providing strong constraints on the physical parameters such as the metallicity and the mass of the star.

3.4 Population studies

Field RR Lyrae stars have very different metallities, between [Fe/H]$= -0.05$ and -2.13, with one outlier at -2.54 (Nemec et al. 2013). A change in the metal content can shift the mode resonance regions to different stellar parameters, as in the case of period doubling (Kolláth et al. 2011). If mode resonances are behind the Blazhko effect, this may lead to differences in the modulation properties as well. To detect such metallicity-dependent effects, we need to observe a large number of stars in the Galaxy.

These investigations can be expanded further with the inclusion of stellar populations that share very similar metal content. The globular clusters M4 and M80 have distinctly different metallicities: their [Fe/H] index is –1.16 and –1.75, respectively. The dwarf galaxy Leo IV is very metal poor with [Fe/H] $= -2.4 \pm 0.2$, so it can trace the low end of the metallicity sequence.

4 Conclusions

Although the *K2* mission was born out of the unfortunate failures of the reaction wheels on board the *Kepler* space telescope, the scientific potential of the new campaigns can exceed that of the original field in several areas.

All types of Cepheid variables are rather rare in the Milky Way: only a handful is expected in every *K2* field. Therefore they do not require a large pixel budget per campaign, but the step-and-stare approach can accumulate a good sample of both classical and type II stars. Cepheids also represent a great opportunity for extragalactic *K2* observations in the nearby dwarf galaxies. Light-curve fluctuations and detection of additional modes can provide important insights into these stars.

RR Lyrae stars, like Cepheids, are an important step in the cosmic distance ladder, but they are good tracers of the halo structures and dwarf galaxies around the Milky Way. Therefore the understanding of their pulsations is important for the galactic structure and evolution studies. Yet several open questions still remain: the Blazhko effect, the mysterious $P_{0.6}$ mode, the role of mode interactions and the level of agreement between the observations and the 1D pulsation models. Most of the RR Lyrae stars are faint, below 14th magnitude, therefore the pixel usage would be moderate even for a high number of targets. The capabilities of *Kepler* and the campaign mode of the *K2* mission represent an ideal opportunity to solve these questions, provided that sufficient number of stars (preferably a few hundred in total) will be observed during the mission.

Acknowledgements: The work of L. Molnár leading to this research was supported by the European Union and the State of Hungary, co-financed by the European Social Fund in the framework of TÁMOP 4.2.4. A/2-11-1-2012-0001 'National Excellence Program'. R.Sz. was supported by the János Bolyai Research Scholarship of the Hungarian Academy of Sciences. This work has been supported by the Hungarian OTKA grant K83790, and the 'Lendület-2009' Young Researchers' Programme of the Hungarian Academy of Sciences. The research leading to these results has received funding from the European Community's Seventh Framework Programme (FP7/2007-2013) under grant agreements no. 269194 (IRSES/ASK) and no. 312844 (SPACEINN). This research has made use of the SIMBAD database, operated at CDS, Strasbourg (France), NASA's Astrophysics Data System Bibliographic Services, and PyKE (Still & Barclay 2012), an open source software package developed and distributed by the NASA Kepler Guest Observer Office.

References:

Benkő, J. M., et al., 2010, *MNRAS*, **409**, 1585
Benkő, J. M., Plachy, E., Szabó, R., Molnár, L., Kolláth, Z., 2014, *ApJS*, submitted
Bernard, E. J., et al., 2010, *ApJ*, **712**, 1259
Borucki, W. J., et al., 2010, *Science*, **327**, 977
Buchler J. R., Kolláth Z. 2011, *ApJ*, **731**, 24
Chadid, M., 2012, *A&A*, **540**, A68
Debosscher, J., et al., 2009, *A&A*, **506**, 519
Derekas, A., et al., 2012, *MNRAS*, **425**, 1312
Drake, A. J., et al. 2013a, *ApJ*, **763**, 32
Drake, A. J., et al. 2013b, *ApJ*, **765**, 154
Drake, A. J., et al. 2014, *ApJS*, accepted, arXiv:1405.4290

Evans, N. R., Szabó, R., Szabados, L., Derekas, A., Kiss, L., Matthews, J., Cameron, C., 2014, *IAUS*, **301**, 55
Gruberbauer, M., et al., 2007, *MNRAS*, **379**, 1498
Hoffmann, D. I., Harrison, T. E., McNamara B. J., 2009, *AJ*, **138**, 466
Howell, S. B., et al., 2014, *PASP*, accepted, arXiv:1402.5163
Kolláth, Z., Molnár, L., Szabó, R., 2011, *MNRAS*, 414, 1111
Kolenberg, K., et al., 2010, *ApJ*, **713**, L198
Mas-Hesse, J. M., et al., 2003, *A&A*, **411,** L261
Mennickent, R. E., Gieren, W., Soszyński, I., Pietrzyński, G., 2006, *A&A*, **450**, 873
Miceli, A., et al., 2008, *ApJ*, **678**, 865
Molnár, L., Kolláth, Z., Szabó, R., Bryson, S., Kolenberg, K., Mullally, F., Thompson, S. E., 2012, *ApJ*, **757**, L13
Moretti M. I., et al., 2009, *ApJ*, **699**, L125
Moskalik, P. A., 2014, *IAUS*, **301**, 249
Moskalik, P. A., Kołaczkowski, Z., 2009, *MNRAS*, **394**, 1649
Neilson, H., Ignace, R., 2014, *A&A*, **563**, L4
Nemec, J. M., Nemec, A. F. L., Lutz, T. E., 1994, *AJ*, **108**, 222
Nemec, J. M., Cohen, J. G., Ripepi, V., Derekas, A., Moskalik, P. A., Sesar, B., Chadid, M., Bruntt, H., 2013, *ApJ*, **773**, 181
Paunzen, E., Kuba, M., West, R. G., Zejda, M., 2014, *IBVS*, No. 6090
Pietrzyński, G., Gieren, W., Udalski, A., Bresolin, F., Kudritzki, R-P., Soszyński, I., Szymański, M., Kubiak, M., 2004, *AJ*, **128**, 2815
Plachy, E., Kolláth, Z., Molnár, L., 2013, *MNRAS*, **433**, 3590
Pojmanski, G., 1997, *AcA*, **47**, 467
Poleski, R., 2013, arXiv:1309.1168
Rauer, H., et al., 2014, *Exp. Astr.*, accepted, arXiv:1310.0696
Samus, N. N., et al., 2004, Combined General Catalogue of Variable Stars
Schmidt, E. G., Reiswig, D. E., 1993, *AJ*, **106**, 2429
Schmidt, E. G., et al., 2013, *AJ*, **146**, 61
Sesar, B., et al., 2013, *AJ*, **146**, 21
Smolec, R., 2005, *AcA*, **55**, 59
Smolec, R., Moskalik, P. A., 2014, *MNRAS*, **441**, 101
Smolec, R., et al., 2012, *MNRAS*, **419**, 2407
Still, M., Barclay, T., 2012, Astrophysics Source Code Library, ascl:1208.004
Szabados, L., Kiss, L. L., Derekas, A., 2007, *A&A*, **461**, 613
Szabó, R., et al., 2011, *MNRAS*, **413**, 2709
Szabó, R., et al., 2014, *A&A*, to be submitted
Woźniak, P. R., et al., 2004, *AJ*, **127**, 2436

COMMISSIONS 27 AND 42 OF THE IAU
INFORMATION BULLETIN ON VARIABLE STARS

Number 6109

Konkoly Observatory
Budapest
5 June 2014

HU ISSN 0374 – 0676

LONG-TERM MONITORING OF Hα EMISSION STRENGTH AND PHOTOMETRIC V MAGNITUDE OF γ Cas

POLLMANN, E.[1]; VOLLMANN, W.[2]; HENRY, G. W.[3]

[1] Emil-Nolde-Strasse 12, 51375 Leverkusen, Germany

[2] Dammäckergasse 28/D1/20, A-1210 Wien, Austria

[3] Center of Excellence in Information Systems, Tennessee State University, Nashville, USA

After the discovery of Be stars (Secchi 1867) these stars were systematically monitored in long-term observing programs. Today we know that their spectra vary on time scales of a few days up to several decades. The Hα and Hβ emission lines in particular can sometimes vary unpredictably and dramatically in strength and appearance. An international group consisting mainly of members of the ARAS spectroscopy group (`http://www.astrosurf.com/aras/`) has been observing the Hα emission line strength of the disk of the Be star γ Cas from the year 1994 up to now (2014) (Smith et al. 2012). They continue the professional observations carried out from August 1971 to October 1989 (Horaguchi et al. 1994 and Miroshnichenko et al. 2002) and together cover more than 40 years of data (Fig. 1).

The idea to investigate a possible correlation between the visual magnitude and the spectroscopic Hα equivalent width (EW) emerged from the study of the relationship between γ Cassiopeia's X-ray emission and its circumstellar environment (Smith et al. 2012). The results of the investigation of the X-ray production of the star and its relationship to the intensity of the Hα emission of the disk (Smith et al. 1998) were an additional incentive for our study. Essential to our study was the availability of high precision V magnitudes for a comparable time frame with the spectroscopic Hα EW measures. Fortunately we were able to use the photometric V measures of G. Henry for the time period JD 2451085 to JD 2456702. They are complemented by the 263 DSLR measures by W. Vollmann for the time period JD 2455154 to JD 2456671. The V magnitude measures by G. Henry were already used in the study Rotational and cyclical variability in γ Cas (Smith, Henry, Vishniac 2006; Henry & Smith 2012). The observations were carried out for 15 years with the Automated Photometric Telescope (APT) in Arizona. The accuracy of the DSLR magnitude measures is $\pm$ 0.02 mag while the photoelectric APT measures are accurate to $\pm$ 0.005 mag.

The spectroscopic observations are done by members of the international amateur spectroscopic community. They have been carried out since 1994 with CCDs and telescopes of 20 to 40 cm aperture, first with prism spectrographs then with slit spectrographs with a resolution R between 5000 and 17000. The measurement of the Hα EW was done generally in the wavelength range 6530 to 6610 Å with an accuracy of $\pm$ 3% for the measures of a night (reproducibility of evaluation of two to three sum spectra per night). Today it

is well known that most Be stars are photometric long-term variables, and that at least two characteristic behaviours can be recognized when simultaneous photometry and optical spectroscopy are available: positive and inverse (negative) correlation between the Balmer emission strengths and the stellar brightness (Harmanec, 1983). Indeed, a positive correlation has been observed in several Be stars (e.g. 28 Tau: Pollmann et al. 2012; κ Dra: Juza et al. 1994; 4 Her: Koubsky et al. 1997) as their Hα emission gets stronger when their photometric V magnitude increases.

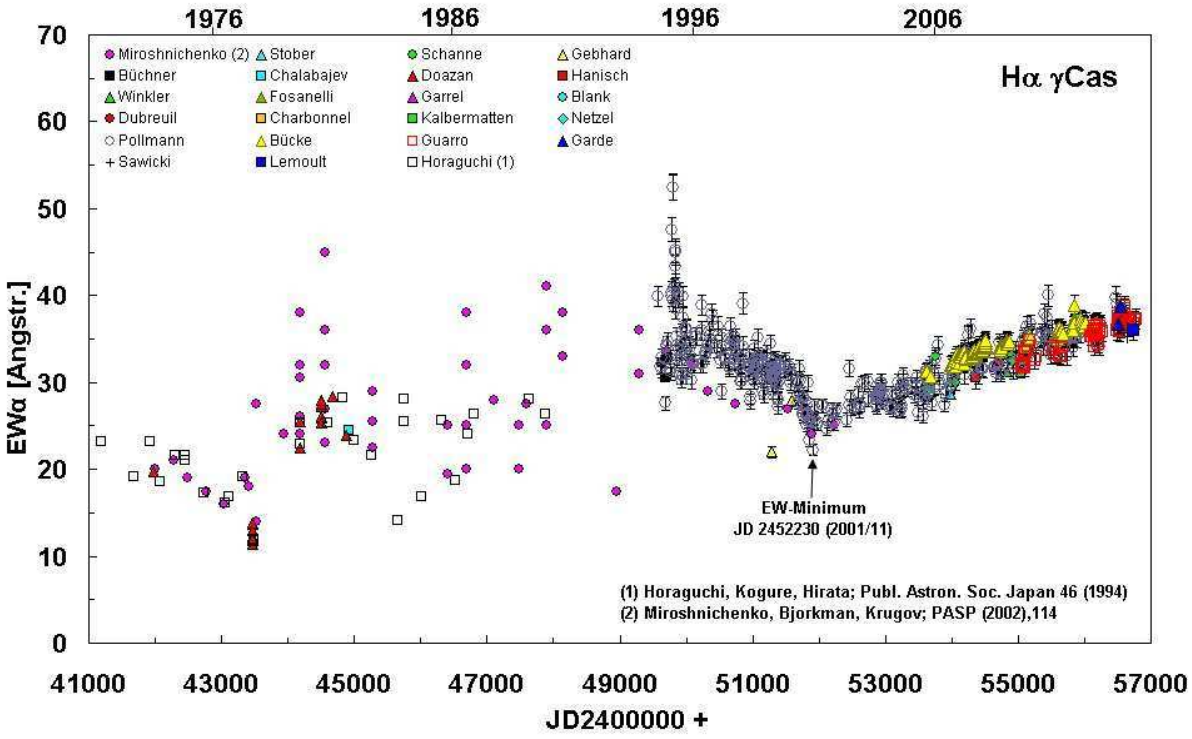

Figure 1. Hα EW long-term monitoring by professional and amateur observers from August 1971 up to now. EWα is the Hα equivalent width – for its definition refer to Pollmann & Rivinius (2010).

These stars are not only seen pole-on but also from different viewing angles. Our study builds on the work by Pollmann et al. (2012) which used visual magnitude estimates superseded now by the significantly more accurate photoelectric measures with the APT. Fig. 2 shows the light curve of γ Cas based on the APT measures by G. Henry, complemented by the DSLR measures by W. Vollmann in 14 observing seasons.

Fig. 3 shows the variable intensity of the Hα EW for the same time span as Fig. 2. To make the visual hints for a correlation between the spectroscopic and photometric time series in these figures and already noted in the studies by Pollmann et al. (2012), Juza et al. (1994) and Koubsky et al. (1997) more concrete, we averaged the data for every observing season (see table in Fig. 4) and plotted them in a correlation diagram (Fig. 4). Hence, a correlation coefficient of 0.86 could be derived for the correlation between the Hα EW and V magnitude.

The diagram in Fig. 4 shows conspicuously that the high correlation coefficient of 0.86 is based primarily on the precision photometric APT measures. The physical cause for

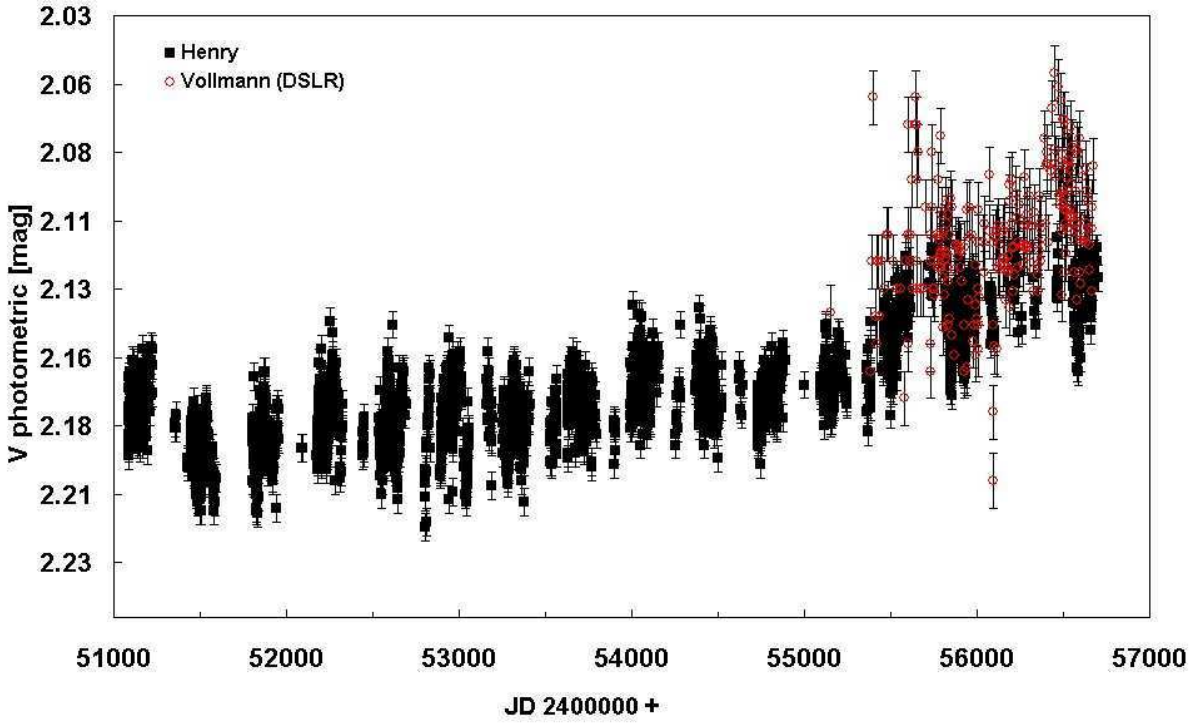

Figure 2. Johnson V magnitude of γ Cas, measured with the T3 40 cm APT at the Fairborn Observatory, Arizona (USA).

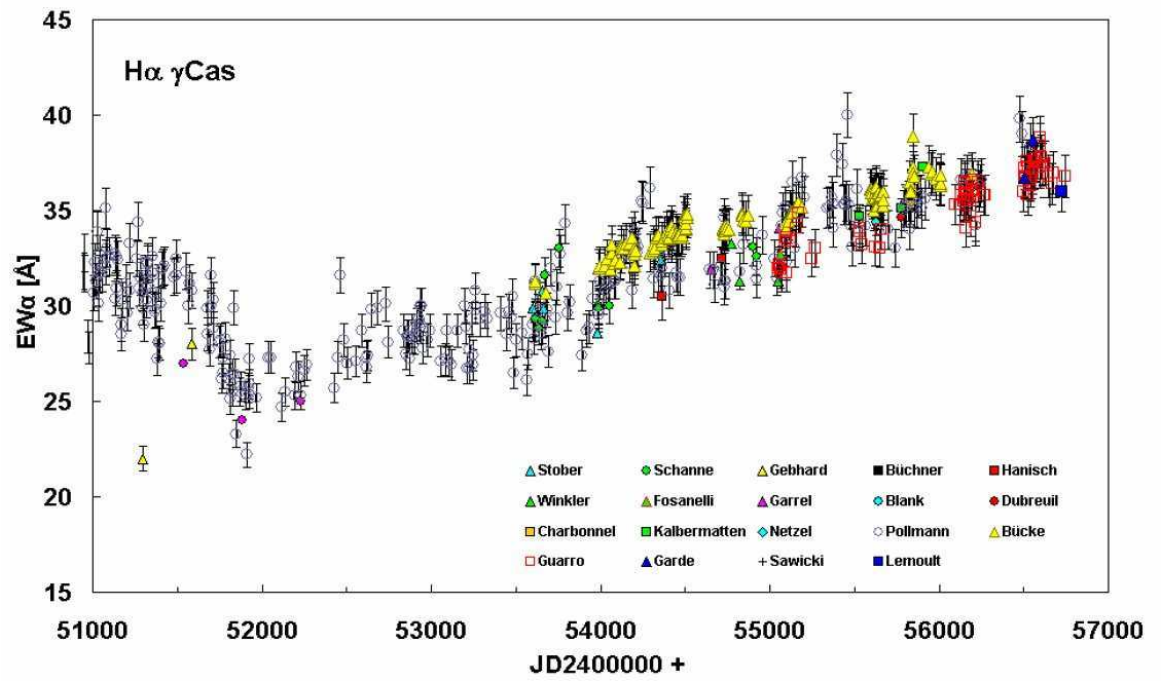

Figure 3. Hα EW measures for the same time period as the photometric measures in Fig. 2 (section of Fig. 1).

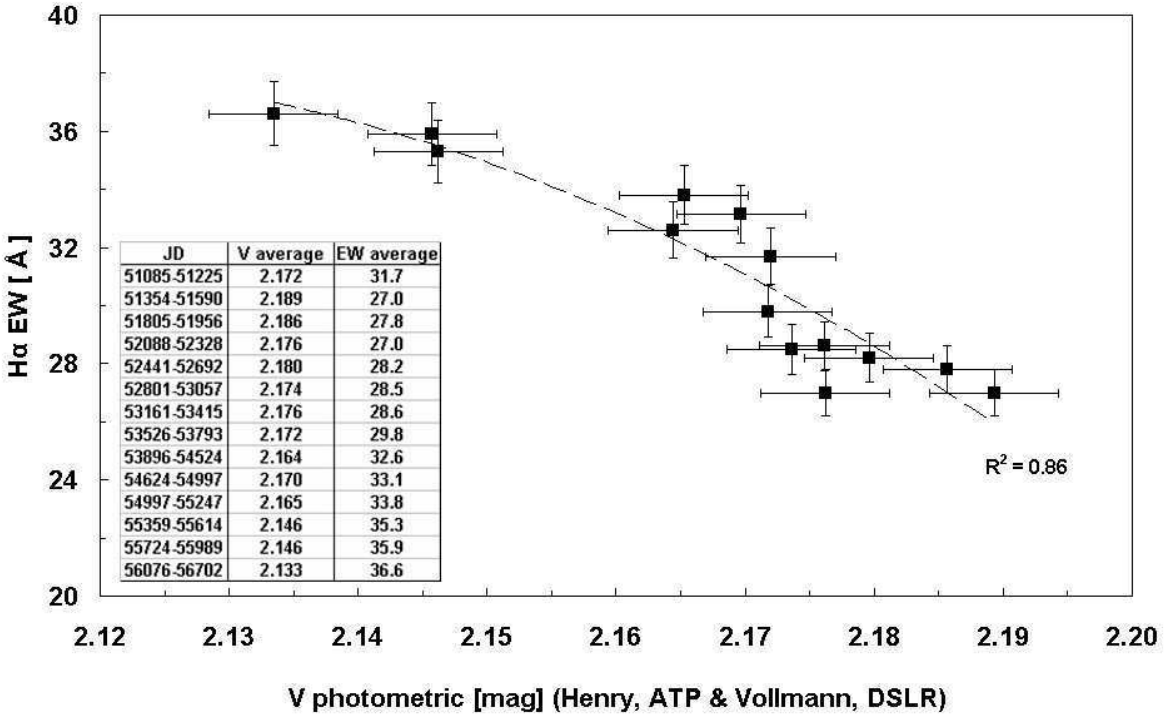

Figure 4. Correlation diagram of Hα equivalent width versus V magnitude (explanation in the text).

the correlation results from the fact that Hα EW is an indicator for the variability of the size, volume and density of the disk around the star, which also gives rise to brightness variations (cf. Pollmann et al. 2012, Juza et al. 1994, Koubsky et al. 1997).

Before our study, it was questionable if magnitude variations of γ Cas would be detectable since we see its disk from a viewing angle of about 45 degrees. However, our data show that the increase of the Hα EW by ca. 10 Å observed during the last 15 years was accompanied by a slight magnitude increase of 0.06 mag. Our observations give evidence for a non-linear relationship between the Hα EW and the V magnitude but it is unknown how long their increase will continue in the future.

The very first investigation of this kind was conducted by Doazan et al. (1983). Their investigations shows, that during and after the spectacular episode of the Be phase from 1932 to 1942, the Balmer lines and the brightness followed the same trend of variations (see Hα in Fig. 5). New correlation model calculations of Hα EW and UBV photometry for Be stars with increasing disk sizes and/or an increasing disk density of Sigut & Patel (2013) are able to explain the positive and negative correlations between long-term variations in Hα EW and V brightness as observed for well known Be stars (Harmanec 1983). However, the need for real observations to examine and refine the model calculations was expressed explicitly. We provide it here.

Acknowledgements: We are grateful to Dr. Dietrich Baade (ESO, Munich) whose critical comments did lead to a clear improvement of this work and to Dr. Myron Smith for the fruitful discussions.

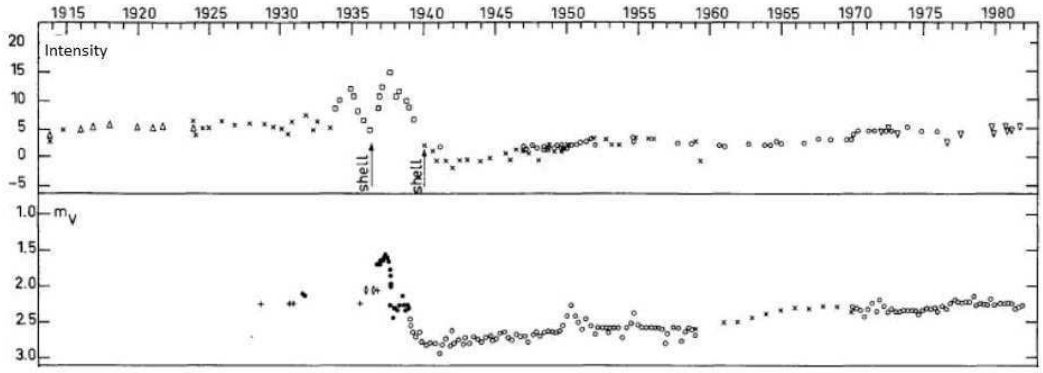

Figure 5. Long-term variations of γ Cas in the visual region: (top panel) intensity variations of the Balmer emission lines (squares: Hα); (bottom panel) long term variations of the visual brightness (Doazan et al. 1980).

References:

Doazan, V., *et al.*, 1980, *ESASP*, **157**, 145
Doazan, V., Franco, M., Rusconi, L., Sedmark, G., Stalio, R., 1983, *A&A*, **128**, 171
Harmanec, P., 1983, *Hvar Observatory Bulletin*, **7**, 55
Henry, G. W., Smith, M. A., 2012, *ApJ*, **760**, 10
Horaguchi, T., Kogure, T., Hirata, R., 1994, *PASJ*, **46**, 9
Juza, K., *et al.*, 1994, *Astron. Astrophys. Suppl. Ser.*, **107**, 403
Koubsky, P., *et al.*, 1997, *A&A*, **328**, 551
Miroshnichenko, A. S., Bjorkman, K. S., Krugov, V. D., 2002, *PASP*, **114**, 1226
Pollmann, E., Rivinus, Th., 2010, *BAV-Rundbrief*, 1/2010
Pollmann, E., Vollmann, W., Puskas, F., 2012, *BAV-Rundbrief*, 1/2012
Secchi, A., 1867, *Astron. Nachrichten*, **68**, 63
Sigut, T., A., A., Patel, P., 2013, *ApJ*, **765**, 41
Smith, M. A., Robinson, R. D., Corbet, R. H. D., 1998, *ApJ*, **503**, 877
Smith, M. A., Lopes de Oliveira, R., Motch, C., Henry, G. W., Richardson, N. D., Bjorkman, K. S., Stee, Ph., Mourard, D., Monnier, J. D., Che, X., Buecke, R., Pollmann, E., Gies, D. R., Schaefer, G. H., ten Brummelaar, T., McAlister, H. A., Turner, N. H., Sturmann, J., Sturmann, L., Ridgway, S. T., 2012, *A&A*, **540**, A53
Smith, M. A., Henry, G. W., Vishniac, E., 2006, *ApJ*, **647**, 1375

COMMISSIONS 27 AND 42 OF THE IAU
INFORMATION BULLETIN ON VARIABLE STARS
Number 6110

Konkoly Observatory
Budapest
26 June 2014
HU ISSN 0374 – 0676

HD 106426, A NEW MULTIPERIODIC δ SCUTI VARIABLE

HOŇKOVÁ, K.[1]; JURYŠEK, J.[1]; MAŠEK, M.[2]; PAUNZEN, E.[3]; ZEJDA, M.[3]

[1] Variable Star and Exoplanet Section of Czech Astronomical Society

[2] Institute of Physics, Czech Academy of Sciences, 182 21 Praha, Czech Republic

[3] Department of Theoretical Physics and Astrophysics, Masaryk University, Kotlářská 2, 611 37 Brno, Czech Republic

The class of δ Scuti stars comprise of pulsating variables of spectral types A to early F with luminosity classes V to III. They pulsate in radial and nonradial p (and also g) modes with periods between about thirty minutes to eight hours and photometric amplitudes less than one magnitude (Breger et al. 2009). Most δ Scuti stars do, however, show very small amplitudes; the smaller the amplitudes become, the more variables are found, for example in space mission data of the Kepler and CoRoT missions (Balona 2014).

During a survey to detect new rapidly rotating Ap stars (Paunzen et al. 2012), we discovered the variability of HD 106426 (CP−62 2642, V = 9.31 mag). Although this star is rather bright, it was hardly investigated in the past. It is also not included in the *Hipparcos* catalogue. Houk & Cowley (1975) list a spectral type of A9 V for this object.

We observed this star in two consecutive nights 18/19 March and 19/20 March 2014 with the F(/Ph)otometric Robotic Atmospheric Monitor (FRAM) telescope of the Pierre Auger Observatory which is located in the Mendoza province in Argentina, in the vicinity of the town Malargüe. The telescope is a Meade 0.3m Schmidt-Cassegrain, with a CCD camera G4-16000 of Moravian Instruments which is also on the wide-field camera (300mm objective Nikkor). The telescope works in fully automated mode. We employed integration times of 40 seconds and a Johnson-Bessell B filter. In addition we analysed the data of the All Sky Automated Survey (ASAS) which are in the V band (Pojmanski 1997).

The basic image reduction (bias and flat correction) as well as the aperture photometry was done within the Windows version of CMunipack[1]. The final light curves of FRAM were generated using different comparison and check stars in order to guarantee the statistical significance of the intrinsic variability of HD 106426.

All light curves were examined in more detail using the Phase-Dispersion-Method within the software Peranso[2]. An analysis with a discrete Fourier algorithm gave the same frequencies and amplitudes. The observation log and the results are listed in Table 1.

[1] http://c-munipack.sourceforge.net/
[2] http://www.peranso.com/

Table 1: Observation log and results.

Source	HJD(start) 2450000+	HJD(end) 2450000+	N	Freq. [c/d]	Ampl. [mmag]
ASAS	1899.84343	5048.51607	521	11.54	11
FRAM	6735.76575	6735.88587	125	10.87	33
	6736.53343	6736.66705	112	6.48	29

The three data sets are of different time base and quality. However, we conclude from the analysis that HD 106426 is multiperiodic. Figure 1 shows the phase folded light curve of the first observing night from FRAM.

Perry (1991) published the following Strömgren $uvby\beta$ photometry for our target: $(b-y) = 0.307$, $m_1 = 0.137$, $c_1 = 0.883$, and $\beta = 2.766$, respectively. Using the photometric calibration by Napiwotzki et al. (1993) gives $E(b-y) = 0.144$ mag, $T_{\rm eff} = 7250 \pm 250$ K, $\log g = 3.65 \pm 0.15$ dex, $M_{\rm V} = 1.50 \pm 0.2$ mag, and solar metallicity. The bolometric correction and magnitude of the Sun taken from Flower (1996) yields $\log L/L_{\odot} = 1.30$ dex. Interpolating in the evolutionary grids for solar metallicity by Schaller et al. (1992), we derive a mass of about $1.9\,{\rm M}_{\odot}$ for HD 106426. It spent about 80% of its main-sequence life-time. These values are typical of an A5 V star.

Because δ Scuti stars obey a period-luminosity-color relationship, we are able to compare our results with the "heuristic" one published by Breger (1979):

$$M_{\rm V} = -3.05 \log P + 8.46\,(b-y)_0 - 3.12.$$

We used a mean logarithmic period of -1 resulting in $M_{\rm V} = 1.3$ mag. Within the errors, this value excellently agrees with that from the photometric calibration. Finally, we calculated the pulsation constant as given by Stellingwerf (1979):

$$\log Q = -6.456 + 0.5 \log g + 0.1 M_{\rm Bol} + \log T_{\rm eff} + \log P.$$

The resulting Q-value of 0.024 for our target would suggest a pulsation in the second or third overtone (Stellingwerf 1979). Further photometric and spectroscopic observations are needed to shed more light on the nature of HD 106426.

Acknowledgements: This project is financed by the SoMoPro II programme (3SGA5916). The research leading to these results has acquired a financial grant from the People Programme (Marie Curie action) of the Seventh Framework Programme of EU according to the REA Grant Agreement No. 291782. The research is further co-financed by the South-Moravian Region. It was also supported by the grants GA ČR P209/12/0217, 14-26115P, 7AMB12AT003, 7AMB14AT015, and the financial contributions of the Austrian Agency for International Cooperation in Education and Research (BG-03/2013, CZ-10/2012, and CZ-09/2014). The operation of the robotic telescope FRAM is supported by the EU grant GLORIA (No. 283783 in FP7-Capacities program) and by the grant of the Ministry of Education of the Czech Republic (MSMT-CR LG13007).

References:

Balona, L. A. 2014, *MNRAS*, **437**, 1476

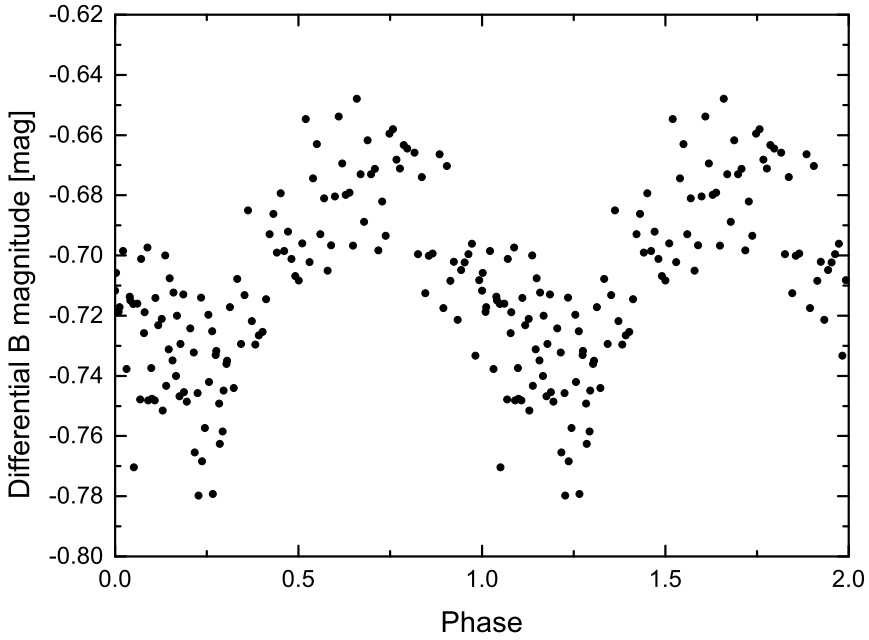

Figure 1. Folded phased light curve of the first observing night from FRAM.

Breger, M. 1979, *PASP*, **91**, 5
Breger, M., Lenz, P., Pamyatnykh, A. A. 2009, *MNRAS*, **396**, 291
Flower, P. J. 1996, *ApJ*, **469**, 355
Houk, N., Cowley, A. P. 1975, University of Michigan Catalogue of two-dimensional spectral types for the HD stars. Volume I
Lenz, P., Breger, M. 2005, *CoAst*, **146**, 53
Napiwotzki, R., Schoenberner, D., Wenske, V. 1993, *A&A*, **268**, 653
Paunzen, E., Netopil, M., Rode-Paunzen, M., et al. 2012, *A&A*, **542**, A89
Perry, C. L. 1991, *PASP*, **103**, 494
Pojmanski, G. 1997, *Acta Astronomica*, **47**, 467
Schaller, G., Schaerer, D., Meynet, G., Maeder, A. 1992, *A&AS*, **96**, 269
Stellingwerf, R. F. 1979, *ApJ*, **227**, 935

COMMISSIONS 27 AND 42 OF THE IAU
INFORMATION BULLETIN ON VARIABLE STARS

Number 6111

Konkoly Observatory
Budapest
28 June 2014

HU ISSN 0374 – 0676

THE 2014 ECLIPSE OF EE Cep: ANNOUNCEMENT FOR A THIRD INTERNATIONAL OBSERVATIONAL CAMPAIGN

GAŁAN, C.[1]; WYCHUDZKI, P.[2]; MIKOŁAJEWSKI, M.[2]; TOMOV, T.[2]; DIMITROV, D.[3]

[1] Nicolaus Copernicus Astronomical Center, Bartycka 18, PL-00-716 Warsaw, Poland;
e-mail: cgalan@astri.uni.torun.pl (CG)

[2] Nicolaus Copernicus University, Centre for Astronomy, Gagarina 11, PL-87-100 Toruń, Poland;
e-mail: adyrbyh@gmail.com (PW); mamiko@astri.uni.torun.pl (MM); tomtom@astri.uni.torun.pl (TT)

[3] Institute of Astronomy and NAO, Bulg. Acad. Sc., 72 Tsarigradsko Chaussee Blvd., 1784 Sofia, Bulgaria
e-mail: dinko@astro.bas.bg (DD)

1 Introduction

The variability of the 11th magnitude star EE Cep was discovered in 1952 (E = 0) by Romano (1956) and soon confirmed by Weber (1956), who reported observations obtained during a previous eclipse in 1947 (E = −1). Thereafter all consecutive eclipses were observed with an orbital period of 5.6 yr. The eclipses vary in an unusual way changing their shape, duration and depth across a wide range of about 0.5 to 2.0 magnitudes (Fig. 1) and simultaneously with very small color variations.

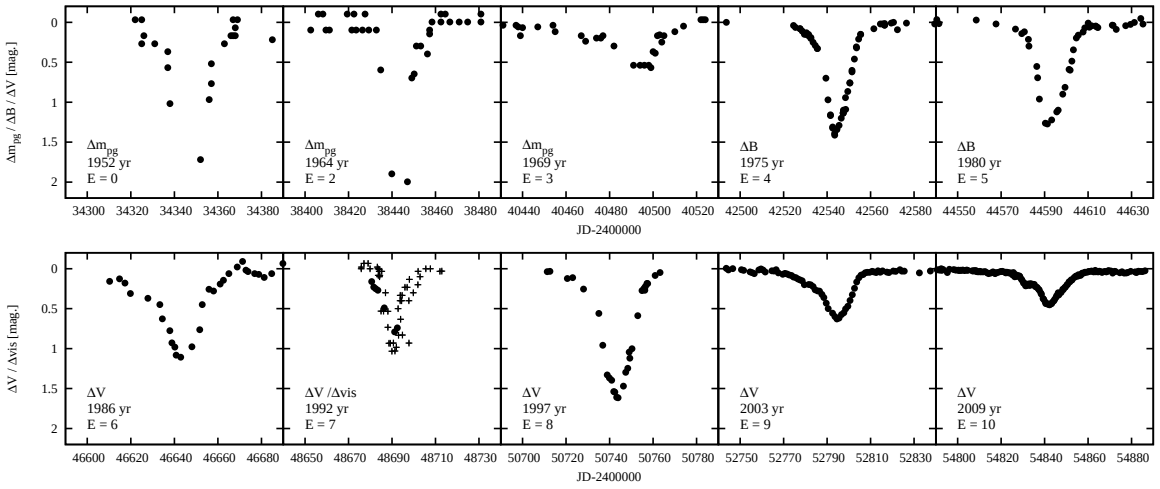

Figure 1. The light curves of ten among the eleven eclipses of EE Cep observed since 1952 are shown. The mean values of Halbach's (1992) visual observations of the 1992 eclipse are marked with crosses.

To explain this unusual behavior Mikolajewski & Graczyk (1999) suggested that the eclipses of the B5 III primary are caused by an invisible secondary component that consists of a dark, opaque, relatively thick disk around a low luminosity central object: a low-mass single star or a close binary. In such a model, the differences between the particular eclipses could be explained by precession, which changes the inclination of the disk to the line of sight and the tilt of its cross-section to the direction of motion. Most of the eclipses have a similar, asymmetrical shape, in which it is possible to distinguish repeatable phases of atmospheric ingress followed by a real ingress, sloped-bottom transit during the central part of the eclipse, and real egress followed by atmospheric eclipse (see for details Fig. 2 in Gałan et al. 2012). The unique flat bottom eclipse, observed in 1969 (E = 3), can be explained by a nearly edge-on and non-tilted projection of the disk.

The last two eclipses, in 2003 (E = 9) and 2008/9 (E = 10) were studied in the framework of wide international campaigns (Mikołajewski et al. 2005ab; Gałan et al. 2010). The results of these campaigns complemented by the historical light curves (Graczyk et al. 2003), enabled us to create a model of the eclipses. According to this model, the eclipses are caused by a dark, geometrically thin disk precessing with period $P_{\rm prec} \approx 11 - 12 P_{\rm orb}$ (Gałan et al. 2012). The model is based on the observations, obtained in an interval of time, almost exactly equal to the predicted precession period. Additional photometric and spectroscopic observations are needed for the model verification.

2 EE Cep – still a unique system

EE Cep is a member of the very rare class of binary systems in which the eclipses are caused by a dark, dusty disk surrounding the orbiting companion. The precursor of this group is the extremely long-period (∼27 yr) ε Aur (see Guinan & Dewarf 2002), extensively studied during its last 2009–2011 eclipse, by the use of photometric, spectroscopic, interferometric, astrometric, and polarimetric observations (Stencel 2013 and references therein). Our photometric and spectroscopic observations are published in Tomov et al. (2012) and Iłkiewiecz et al. (2013). During the last eclipse, the disk in ε Aurigae, was revealed directly by infrared interferometric imaging (Kloppenborg et al. 2010) for the first time. The mechanisms of disk formation in EE Cep and ε Aur seems to be radically different. Containing a B5-type star EE Cep has to be a very young system while ε Aur with an F-type supergiant is significantly evolutionarily advanced. The observations of the eclipses provided indications for a complex structure formed in the ε Aur (Ferluga 1990) and EE Cep (Gałan et al. 2008) disks. The true nature of these structures is not known. In the case of ε Aur a multi-ring structure (Ferluga 1990, Leadbeater & Stencel 2010) was suggested but other corotating inhomogeneities cannot be excluded (Harmanec et al. 2013). The light curve and color variations observed during the last two EE Cep eclipses we interpreted in terms of a multi-ring structure too and speculated that possible planets could be responsible for their formation (Gałan et al. 2010).

For a long time ε Aur and EE Cep remained the only two known systems with dark, dusty disks as obscuring objects. Recently however, new cases of similar systems, with circumstellar or circumbinary disks responsible for obscurations, emerged:
1SWASP J140747.93394542.6 (Mamajek et al. 2012), OGLE-LMC-ECL-11893 (Dong et al. 2014), OGLE-LMC-ECL-17782 (Graczyk et al. 2011), M2-29 (Hajduk et al. 2008), KH 15D (Winn et al. 2006, Herbst et al. 2008). This opens perspectives for studying the dusty disk phenomenon in binary and/or multiple systems and can be helpful to understand the origin of such disks, how they form and evolve in various environments

and on various time scales. EE Cep still remains a unique case of great importance among this small sample, because of its well-documented disk precession history during one, approximately full, precession period (see for details Gałan et al. 2012).

3 Call for observations

The next eclipse (E = 11) approaches and we announce a third observational campaign. According to the ephemeris by Mikolajewski & Graczyk (1999) the minimum should take place on Aug 23, 2014 ($JD_{\rm mid-ecl}$ = 2456893.44). Based on our model of the disk precession (Gałan et al. 2012) we can predict that it should belong to the deepest ones reaching about 2 mag (from 10.8 mag outside of eclipse to ∼13 mag during the minimum in V photometric band). The longest duration eclipses observed so far occurred in 1969 (∼60 days), and 2003 and 2008/9 (∼90 days). So, we propose to conduct systematic photometric monitoring in at least three months time interval (July, August, September) centred on the mid-eclipse moment. During the previous two eclipses the blue maxima in the colors were observed about nine days before and after the mid-eclipse. Therefore, special attention should be paid on precise measurements, covering about one week time intervals around ∼JD 2456884 (Aug 14) and ∼JD 2456902 (Sep 1). However, these moments are subject to change slightly due to changes in the orientation of the disk.

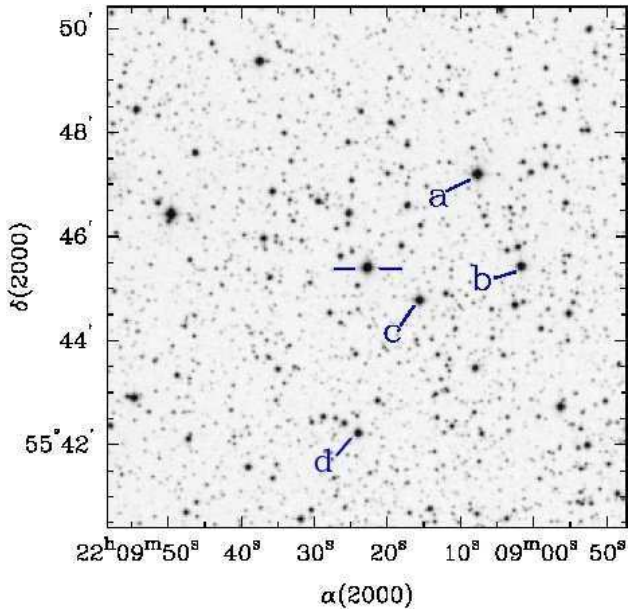

Figure 2. The sky area ($10' \times 10'$) around EE Cep (reprinted from Mikolajewski et al. 2003). The blue color marks the comparison and the check stars recommended for the CCD photometry.

We recommend photometric observations in the standard Johnson-Cousins $UBV(RI)_{\rm C}$ system. At least one measurement per night with an accuracy possibly close to $\sim 0\overset{\rm m}{.}01$ or better is needed. Some multicolour observations, far from the eclipse, should be obtained in order to calibrate systematic differences between the observatories. We propose to use the four brightest objects from the Meinunger's (1975) sequence as comparison stars. This sequence recommended by Mikolajewski et al. (2003) has been used in the observational campaigns during the recent eclipses. These stars are very close in the sky, within $\sim 3'$,

around EE Cep. In the finding chart shown in Figure 2 the sequence stars are marked with Meinunger's designations: "*a*", "*b*", "*c*", and "*d*" for BD+55°2690, GSC-3973 2150, BD+55°2691, and GSC-3973 1261, respectively. Stars "*b*" and "*c*" are designated as New Suspected Variables in the General Catalog of Variable Stars (Samus et al. 2009) – NSV 25842, and NSV 25843, respectively. Baldinelli & Ghedini (1976) were the first who noted $\sim 0\overset{\mathrm{m}}{.}5$ amplitude variations of star "*c*" based on photographic photometry. But they stressed the absolute necessity to confirm this result by photoelectric method. Mikołajewski et al. (2003) used an one channel diaphragm photometer with a cooled photomultiplier to observe the stars "*a*", "*b*", and "*c*" during the EE Cep eclipse in 2003 and found no significant light variations in these stars. Star "*b*" was suggested to be variable on the basis of photographic photometry by Baldinelli & Ghedini (1977), Baldinelli et al. (1981). However, these variations were not discussed and there was no light curve presented.

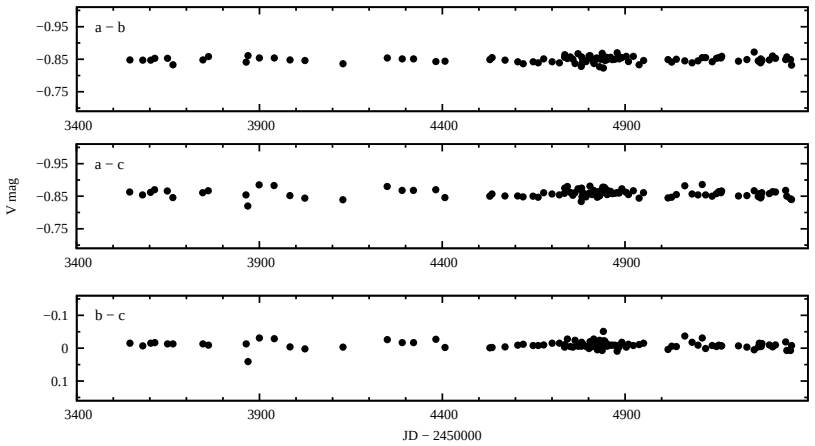

Figure 3. Differential V magnitudes ($a-b$, $a-c$, and $b-c$) of the stars BD+55°2690 (a), GSC-3973 2150 (b), and BD+55°2691 (c) obtained in ∼5 years time interval during and around the 2008/9 eclipse.

We performed $UBV(RI)_{\mathrm{C}}$ CCD photometry of these stars during the last eclipse in 2008/9. The CCD photometry is less weather dependent than the one channel diaphragm photometry and thus offers better accuracy for the $BV(RI)_{\mathrm{C}}$ bands. The differential V magnitudes for stars "*a*", "*b*" and "*c*" obtained during and around the last eclipse are shown in Figure 3. The observed light variations in $a-b$ differential magnitudes are insignificant and the brightness of the stars "*a*" and "*b*" can be recognized as a constant within the accuracy of our photometry, which in the photometric bands $BV(RI)_{\mathrm{C}}$ is typically $\sim 0\overset{\mathrm{m}}{.}01 - 0\overset{\mathrm{m}}{.}02$ (depending on weather conditions during the observations). The differential magnitudes with respect of star c ($a-c$ and $b-c$) demonstrate somewhat larger scatter, in which small changes with a similar pattern can be seen. Small variations of star "*c*" with an amplitude of a few hundredths of a magnitude cannot be excluded. Therefore, we recommend to use "*a*" and "*b*" as comparison stars and "*c*" and "*d*" as check stars.

Any optical and infrared photometric as well as spectroscopic observations obtained before, during and after the EE Cep eclipse could turn out to be very important. They could make it possible to detect the mysterious companion (disk and/or its central star/stars) in the EE Cep system. During the last three orbital epochs we observed about $0\overset{\mathrm{m}}{.}2$ vari-

ations in the I passband, before and after the eclipses, which may prove a significant contribution of a dark body in this band. In the JHK passbands, the cool component can dominate the observed fluxes. Moreover, these variations can reflect in some way the changes in the spatial orientation of the disk.

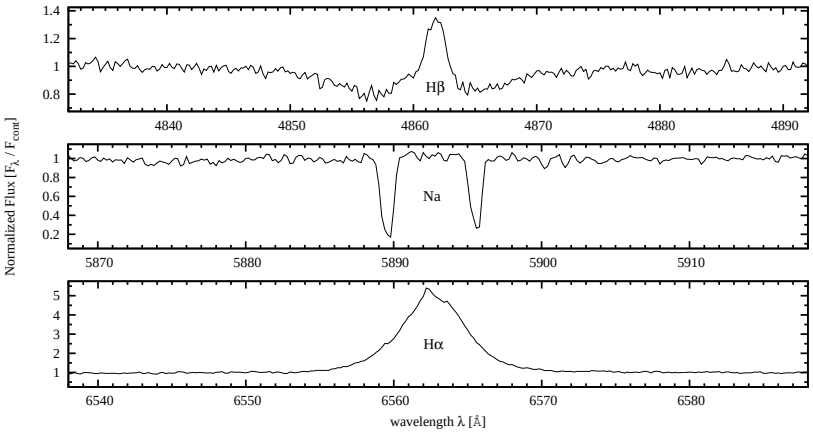

Figure 4. Spectra of EE Cep obtained on April 8, 2014 in the Hα, Hβ and Na I regions (R $\sim$ 16000) using the Coudé spectrograph on the 2m Ritchey–Chrétien telescope at Rozhen Observatory.

The deep EE Cep eclipses have never been well covered with spectroscopic observations. Thus, it will be important to carry out systematic, high and low resolution spectroscopic monitoring of the star during the forthcoming eclipse. Our spectra obtained on April 8, 2014 in the regions of Hα, Hβ, and Na I doublet lines (Fig. 4) do not show changes caused by eclipse in the profiles of these lines (compare with the profiles in Mikołajewski et al. 2005b). Spectroscopic observations obtained during the two previous eclipses in 2003 and 2008/9 show, that the absorption lines, caused by the circumstellar matter were visible up to about 2.5 – 3 months before and after the mid-eclipse. Thus, it is advisable to cover with spectroscopic observations the period from May to November 2014, with increased frequency of observations during the photometric eclipse (July – September), when we can expect significant night to night changes in the profiles of the absorption and the emission lines. At least $S/N \sim 30$ is recommended. In the case of low (R$\sim$1000) resolution observations, it would be advisable to focus mainly on the Balmer lines evolution. Observations of spectrophotometric standard stars are encouraged, because they will permit us to reduce the spectra in fluxes and to study the spectral energy distribution changes during the eclipse.

The observers can use a special web page, prepared to support the campaign coordination `https://sites.google.com/site/eecep2014campaign/`. All interested to participate in collecting of photometric, spectroscopic or any other observations of the forthcoming event are encouraged to contact Piotr Wychudzki at `adyrbyh@gmail.com`.

Acknowledgements: This study is partly supported by the Polish National Science Centre grant No DEC-2013/08/S/ST9/00581. This paper is partly a result of the exchange and joint research project Spectral and photometric studies of variable stars between Polish and Bulgarian Academies of Sciences. We gratefully acknowledge A. Smith for careful reading of the manuscript.

References:

Baldinelli, L., & Ghedini, S., 1976, *IBVS*, No. 1225
Baldinelli, L., & Ghedini, S., 1977, *MmSAI*, **48**, 91
Baldinelli, L., Ferri, A., Ghedini, S., 1981, *IBVS*, No. 1939
Dong, S., Katz, B., Prieto, J. L., et al. 2014, *arXiv:1401.1195v1*
Ferluga, S., 1990, *A&A*, **238**, 278
Gałan, C., Mikołajewski, M., Tomov, T., Cikała, M., 2008, *IBVS*, No. 5866
Gałan, C., Mikołajewski, M., Tomov, T., et al. 2010, *ASPC*, **435**, 423
Gałan, C., Mikołajewski, M., Tomov, T., et al. 2012, *A&A*, **544**, A53
Graczyk, D., Mikolajewski, M., Tomov, T., et al. 2003, *A&A*, **403**, 1089
Graczyk, D., Soszyński, I, Poleski, R., et al. 2011, *Acta Astronomica*, **61**, 103
Guinan, E. F. & Dewarf, L. E., 2002, *ASP Conf. Ser.*, **279**, 121
Hajduk, M., Zijlstra, A. A., Gęsicki, K., 2008, *A&A*, **490**, 7
Halbach, E. A., 1992, *JAAVSO*, **21**, 129
Harmanec, P., Božić, H., Korčáková, D., et al. 2013, *CEAB*, **37**, 99
Herbst, W., Hamilton, C. M., LeDuc, K., et al. 2008, *Nature*, **452**, 194
Iłkiewicz, K., Wychudzki, P., Gałan, C., et al. 2013, *AASP*, **3**, 23
Kloppenborg, B., Stencel, R., Monnier, J. D., et al. 2010, *Nature*, **464**, 870
Leadbeater, R., & Stencel, R., 2010, *arXiv:1003.3617*
Mamajek, E. E., Quillen, A. C., Pecaut, M. J., et al. 2012, *AJ*, **143**, 72
Meinunger, L., 1975, *IBVS*, No. 965
Mikolajewski, M. & Graczyk, D., 1999, *MNRAS*, **303**, 521
Mikolajewski, M., Tomov, T., Graczyk, D., et al. 2003, *IBVS*, No. 5412
Mikołajewski, M., Gałan, C., Gazeas, K., et al. 2005a, *Ap&SS*, **296**, 445 (`http://www.springerlink.com/content/v6t4630310j26300/fulltext.pdf`)
Mikołajewski, M., Tomov, T., Hajduk, M., et al. 2005b, *Ap&SS*, **296**, 451 (`http://www.springerlink.com/content/w28t429p3446p615/fulltext.pdf`)
Romano, G. 1956, *Coelum*, **24**, 135
Samus, N.N., Durlevich O.V., Goranskij V.P., et al. 2009, *General Catalogue of Variable Stars (Samus+ 2007-2013)*
Stencel, R. E., 2013, *CEAB*, **37**, 85
Tomov, T., Wychudzki, P., Mikołajewski, M., et al. 2012, *BlgAJ*, **18**, a3
Weber, R. 1956, *Doc. des Obs. Circ.*, **No. 9**
Winn, J. N., Hamilton, C. M., Herbst, W. J., et al. 2006, *ApJ*, **644**, 510

COMMISSIONS 27 AND 42 OF THE IAU
INFORMATION BULLETIN ON VARIABLE STARS
Number 6112

Konkoly Observatory
Budapest
22 July 2014
HU ISSN 0374 – 0676

SEVEN NEW PERIOD-CHANGE ECLIPSING BINARY STARS

NELSON, ROBERT H.[1,2]

[1] 1393 Garvin Street, Prince George, BC, Canada, V2M 3Z1

[2] Guest User, Canadian Astronomy Data Centre, which is operated by the Dominion Astrophysical Observatory for the National Research Council of Canada's Herzberg Institute of Astrophysics

email: bob.nelson@shaw.ca

In the course of surveying eclipse timing difference (or O−C) plots for a series of papers on period change (Nelson et al. 2014a,b,c), several overcontact systems came to light—not previously noted in the literature—which showed strong evidence of period change. The eclipse timing (ET) data were well modelled by quadratic functions. However, the time interval over which the quadratic relation was evident was short, typically around a decade. Because subsequent data can often prove a relationship wrong, these systems were not included in the main group of 60 to be discussed in detail. Rather, they were simply added as notes at the end of Paper 3. Therefore it was deemed useful to describe the relationships more fully here.

EG CVn

The variability of EG CVn (GSC 3026-1046, ROTSE1 J133726.05+373458.4) was discovered as part of the Robotic Optical Transient Search Experiment I (ROTSE-1, Akerlof et al. 2000). It was identified as EW-type with a period of 0.34927(2) days. Blättler & Diethelm (2002) presented new eclipse timings and an unfiltered CCD light curve. Since then, there have been a number of eclipse timings reported, but no period analysis. As far as is known, there has been no light curve analysis for this system.

In Figure 1, the ET differences from the 32 eclipse timings from 1999 to 2012 are plotted. (The abscissa is the cycle number; the ordinate is the eclipse timing difference (O−C value) in days. Legend: squares—photographic; triangles—visual; open (red) circles—photoelectric; solid circles—CCD timings). The least squares best-fit quadratic curve is shown; its parameters yield the rate of period change as $\mathrm{d}P/\mathrm{d}t = 5.9(4) \cdot 10^{-7}$ days/year. The coefficient of correlation (cc) is 0.992; thus the rate of period change is fairly constant. The first set of timings near cycle 0—showing a large scatter—were given a weight 0.1; the others, 1.

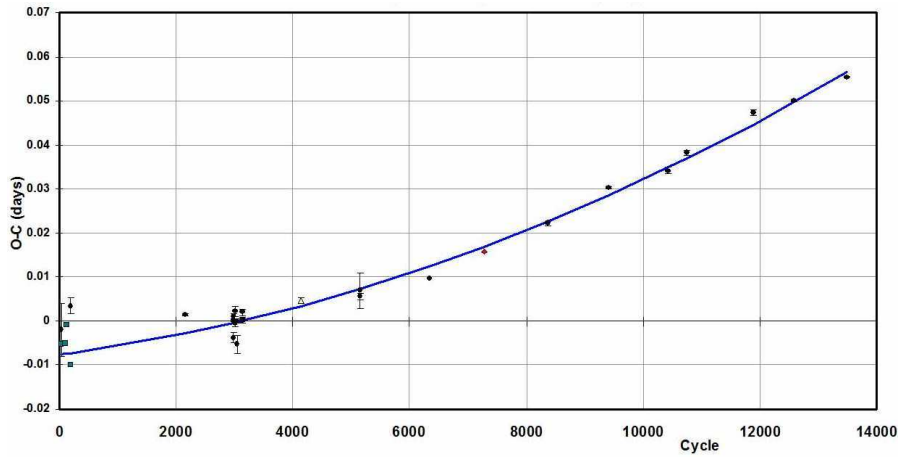

Figure 1. EG CVn: Eclipse timing differences (O−C) using Min I (hel) = 2451246.7820 + 0.349271 E.

V2240 Cyg

The variability of V2240 Cyg (GSC 2684-1255) was discovered by Safár (1999) who presented elements (epoch, period of 0.404194(68) days), six CCD eclipse timings, and an unfiltered light curve. From the shape of the light curve, he identified it as a W UMa variable. Since then, there have been numerous eclipse timings reported in the literature, but no period analysis. As far as is known, there has been no light curve analysis for this system.

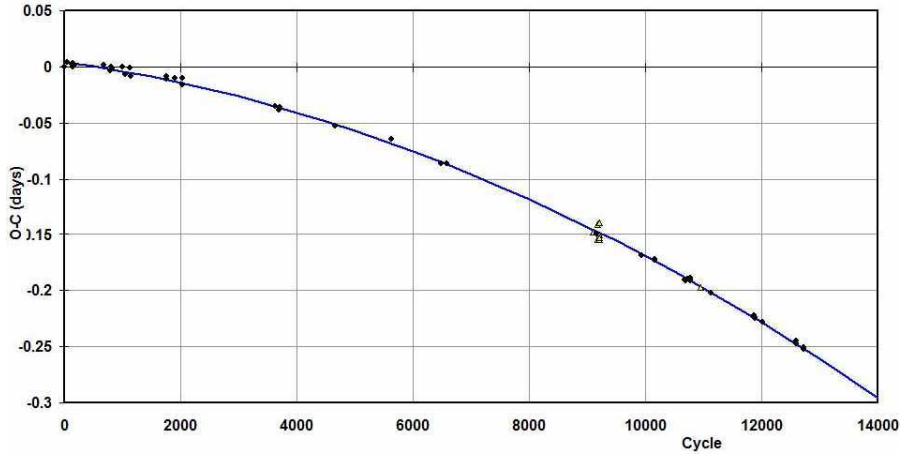

Figure 2. V2240 Cyg: Eclipse timing differences (O−C) using Min I (hel) = 2451375.4523 + 0.404194 E.

In Figure 2, the ET differences from the 63 eclipse timings from 1999 to 2013 are plotted (for the legend, see Section 1). The least squares best-fit quadratic curve is shown; its parameters yield the rate of period change as $\mathrm{d}P/\mathrm{d}t = -1.84(4) \cdot 10^{-6}$ days/year. This is one of the higher rates of period change amongst overcontact binaries. The coefficient of correlation (cc) is 0.999; thus the quadratic equation is a very good fit and the rate of period change very constant in the range.

MS Her

The variability of MS Her (GSC 2101-0313, ROTSE1 J181653.46+273945.4) was discovered by Hoffmeister (1949). The reference is from the CGVS4, but the work is not available. The next reference is the ROTSE-I paper, Akerlof et al. (2000) which lists coordinates and a period of 0.86793(28) days. Since then, there have been numerous eclipse timings reported, but no period analysis. Strangely, the GCVS4 lists the period of this system incorrectly as 0.6052626 days. As far as is known, there has been no light curve analysis for this system.

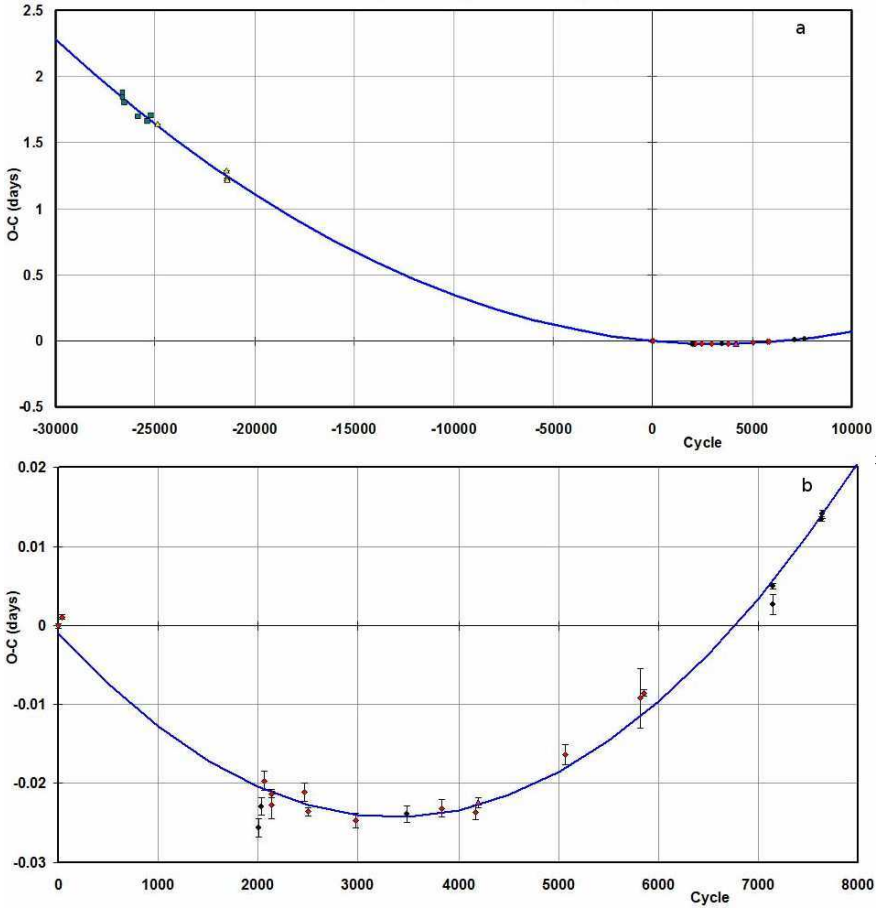

Figure 3. Top: MS Her: eclipse timing differences (O−C) using Min I (hel) = 2449534.4903 + 0.8680423 E. Bottom: eclipse timing differences (O−C) using Min I (hel) = 49534.4903 + 0.8680423 E.

In Figure 3a, the ET differences from the 33 photographic, visual, photoelectric and CCD timings from 1931 to 2012 are plotted. In Figure 3b, the same data and fit are plotted, but for the restricted range cycle 0 (1994) to cycle 7463 (2012). The fact that the quadratic fit—which uses parameters optimized for all the data—fits the restricted range well gives one confidence that the cycle reassignments necessary for Figure 3a are correct.

Weighted least squares fitting for all the data yields a value of $\mathrm{d}P/\mathrm{d}t = 1.74(2) \cdot 10^{-6}$ days/year with a cc of 0.999. Using only the data from cycle 0 or later yields a value of $\mathrm{d}P/\mathrm{d}t = 1.77(7) \cdot 10^{-6}$ days/year with a cc of 0.989. It seems clear that the rate of period change has been constant for the 80 years that timings have been made.

V400 Lyr

This variability of V400 Lyr (GSC 3121-1799, VV 223) was discovered by Miller (1969) who classified it as RRab and supplied a period of 0.3201645 days. Blättler & Diethelm (2000b) presented unfiltered CCD light curves showing the system to be of type EW. They also supplied an updated pair of elements (epoch, period); the latter being 0.2534306(8) days. Marino (2011) obtained CCD light curves and—using PHOEBE software (Prsa & Zwitter 2005)—obtained a Wilson-Devinney fit for BVRI pass bands (Wilson & Devinney 1971). Marino (2011) also displayed an ET difference plot which showed a secular period decrease but did not determine a quadratic fit.

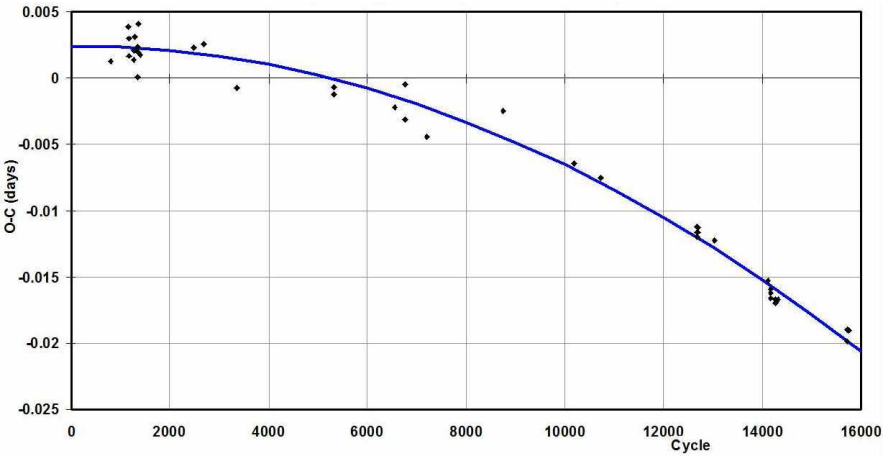

Figure 4. V400 Lyr: Eclipse timing differences (O−C) using Min I (hel) = 2451801.3651 + 0.2534274 E.

In Figure 4, the (all CCD) ET differences from the 43 eclipse timings from 2001 to 2011 are plotted, yielding a value $\mathrm{d}P/\mathrm{d}t = -2.61(23) \cdot 10^{-7}$ days/year with a coefficient of correlation (cc) of 0.992.

V406 Lyr

The variability of V406 Lyr was discovered by Parenago (1946). Meinunger (1970) obtained the first period, 1.51130 days and published a photographic light curve. Agerer et al. (1994) presented new photographic and CCD eclipse timings, and determined that the above period was an alias of the true one, $P = 0.86078384(9)$ days. They also obtained a new light curve with two distinctly unequal minima. Since then, there have been many eclipse timings published but no period analysis.

In Figure 5, the (all CCD) ET differences are plotted for the time interval 1993-2013; the earlier photographic and visual timings are not plotted because the gaps impose an uncertainty as to the correct cycle count. Plotted are 29 points yielding a value $\mathrm{d}P/\mathrm{d}t = 8.35(29) \cdot 10^{-7}$ days/year with a coefficient of correlation (cc) of 0.989. As far as is known, there has been no light curve analysis for this system.

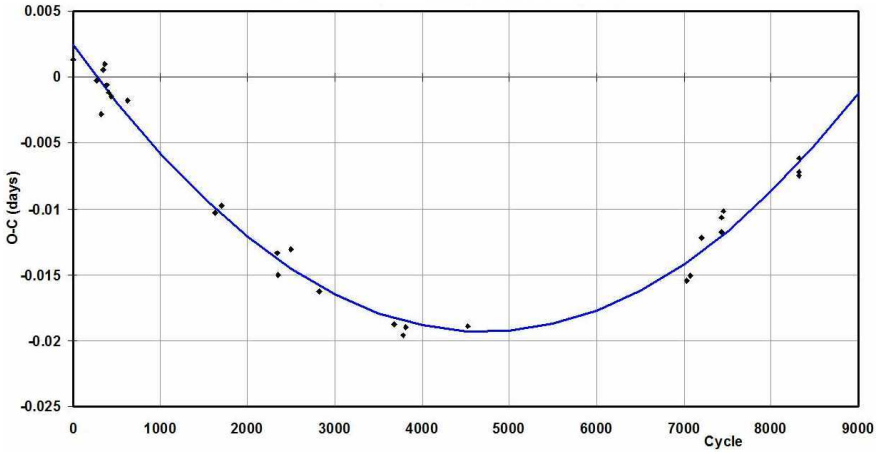

Figure 5. V406 Lyr: Eclipse timing differences (O−C) using Min I (hel) = 2449250.4582 + 0.8607838 E.

V579 Lyr

The variability of V579 Lyr (GSC 3131-0476) was discovered by Akerlof et al. (2000) in the ROTSE-1 all-sky survey for variable stars. Blättler & Diethelm (2000a) presented unfiltered CCD light curves showing the system to be of type EW. They also supplied an updated pair of elements (epoch, period); the latter being 0.2429100(25) days. Since then, there have been many eclipse timings published but no period analysis.

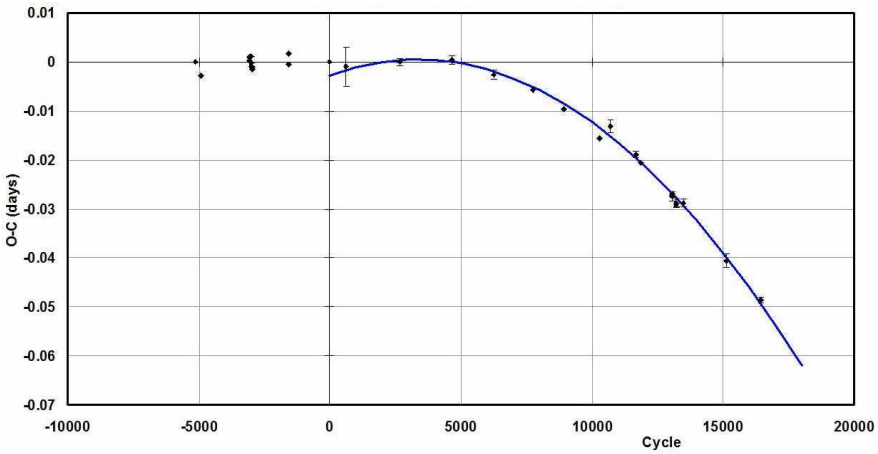

Figure 6. V579 Lyr: Eclipse timing differences (O−C) using Min I (hel) = 2452500.0623 + 0.2429093 E.

In Figure 6, the (all photometric-CCD) ET differences are plotted for the time interval 1999-2013, but only the eclipse timings since cycle 0 (2002) were used to compute the period change, $\mathrm{d}P/\mathrm{d}t = -8.78(48) \cdot 10^{-7}$ days/year with a cc = 0.998. The timings before cycle 0 represent a discrepancy to the quadratic fit. It is possible that the period change is caused by the light time effect from the orbit of a companion (rather than—say—mass interchange), in which case the relationship would be a good deal more complex. In

any case, future eclipse timings over several decades are required to establish the true relationship. As far as is known, there has been no light curve analysis for this system.

KN Vul

The variability of KN Vul (GSC 2148-3403) was discovered by Wachmann (1966) in a survey of the southern stars in Cygnus. Kreiner (2004) provided a set of elements (epoch, period). Since then, there have been a number of eclipse timings published, but no period analysis.

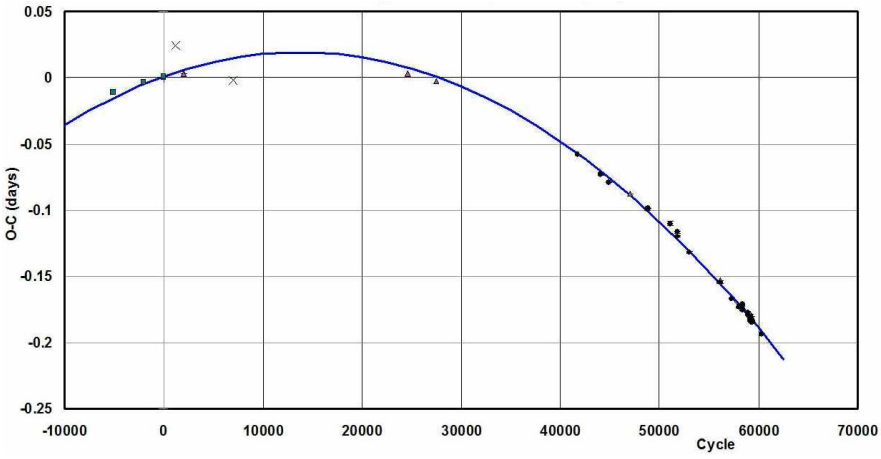

Figure 7. KN Vul: Eclipse timing differences (O−C) using Min I (hel) = 2434634.2821 + 0.3573325 E.

In Figure 7, the ET differences from the 85 eclipse timings from 1948 to 2012 are plotted. The rate of period change is $\mathrm{d}P/\mathrm{d}t = 2.00(2) \cdot 10^{-7}$ days/year with a cc of 0.999. As far as is known, there has been no light curve analysis for this system.

Acknowledgements: This research has made use of the SIMBAD database, operated at CDS, Strasbourg, France. Also useful were the Lichtenknecker—Database of the BAV (http://www.bav-astro.de/LkDB/index.php?lang=en) and the O−C Gateway (http://var.astro.cz/ocgate/).

References:

Agerer, F., Kleikamp, W. & Moschner, W., 1994, *IBVS* No. 4132
Akerlof, C., et al., 2000, *AJ*, **119**, 1901
Blättler, E. & Diethelm, R., 2000a, *IBVS*, No. 4982
Blättler, E. & Diethelm, R., 2000b, *IBVS*, No. 4995
Blättler, E. & Diethelm, R., 2002, *IBVS*, No. 5269
GCVS4, General Catalogue of Variable Stars, http://www.sai.msu.su/gcvs/
Hoffmeister, C., 1949, *Veröff. Sternw. Sonneberg*, **1**, N3
Kreiner, J. M., 2004, *AcA*, **54**, 207
Marino, G., 2011, *IBVS*, No. 6002
Meinunger, L., 1970, *Mitt. Ver. Sterne*, **5**, 128

Miller, W. J., 1969, *Ricerche Astronomiche*, **7**, 459
Nelson, R. H., Terrell, D. & Milone, E.F., 2014a, *New Astr. Rev.*, **59**, 1 (Paper 1)
Nelson, R. H., Terrell, D. & Milone, E.F., 2014b, *New Astr. Rev.*, (Paper 2), submitted
Nelson, R. H., Terrell, D. & Milone, E.F., 2014c, *New Astr. Rev.*, (Paper 3), in preparation
Parenago, P., 1946, *Perem. Zvezdy*, **6**, 25
Prsa, A. & Zwitter, T., 2005, *ApJ*, **628**, 426
Safár, J., 1999, *IBVS*, No. 4818
Wachmann, A. A., 1966, *Astron. Abh. Hamburg. Sternw.*, **6**, 281
Wilson, R. E. & Devinney, E.J., 1971, *ApJ*, **166**, 605

COMMISSIONS 27 AND 42 OF THE IAU
INFORMATION BULLETIN ON VARIABLE STARS

Number 6113

Konkoly Observatory
Budapest
10 August 2014

HU ISSN 0374 – 0676

ASAS 000709+2621.5 IS AN OVERCONTACT ECLIPSING BINARY, NOT A δ Sct VARIABLE

KJURKCHIEVA, D. P.[1]; DIMITROV, D. P.[2]; IBRYAMOV, S. I.[2]

[1] Department of Physics, Faculty of Natural Sciences, Shumen University, 9700 Shumen, Bulgaria, e-mail: d.kyurkchieva@shu-bg.net

[2] Institute of Astronomy and NAO, Bulgarian Academy of Sciences, 72 Tsarigradsko Shose Blvd., 1784 Sofia, Bulgaria, e-mail: dinko@astro.bas.bg; sibryamov@astro.bas.bg

Recently the discovery of new variable stars has been accelerating due to large observing programs such as ROTSE, MACHO, ASAS, OGLE, etc. However the low precision of these data as well as their automatic reduction and fitting led to the wrong classification of many targets. This refers especially to the cases of almost sinusoidal light curves which are appropriate both for δ Sct variables and for W UMa systems. Their right classification often requires follow-up observations and analysis.

The star ASAS 000709+2621.5 (further shortly ASAS 0007) is such a case. It was classified as a δ Sct variable with a pulsation period of P=0.2017 d and amplitude of 0.49 mag on the base of the ASAS data (Pojmanski 2000). We built folded curves of these data with periods $1P$ and $2P$ (Fig. 1) but they did not allow us to conclude if the target is a δ Sct variable or a W UMa binary.

To answer this question we carried out follow-up photometric observations of ASAS 0007 with the 60-cm Cassegrain telescope using the FLI PL09000 CCD camera (3056×3056 pixels, 12 μm/pixel, field of view 27.0×27.0 arcmin with focal reducer) of the Rozhen National Astronomical Observatory (Table 1). The average photometric precision per data point was below 0.01 mag.

Table 1. Journal of the Rozhen observations

Date	exposures (s)	filters	number
Aug 20 2010	60, 60	V, I	120, 120
Aug 22 2010	60, 60	V, I	176, 177
Aug 23 2010	60, 60	V, I	16, 16
Sept 17 2010	70	I	420

Table 2. Coordinates, magnitudes and colors of the target and standard stars

Star	GSC1ID	RA (2000)	DEC (2000)	V	$V-I$
ASAS 0007	0173200262	00 07 09.00	+26 21 30.0	11.55	0.86
C1	0173200564	00 07 24.71	+26 16 38.1	12.87	1.20
C2	0173201665	00 07 15.61	+26 23 33.1	11.10	1.25
C3	0173200140	00 07 10.20	+26 15 49.9	14.14	1.25

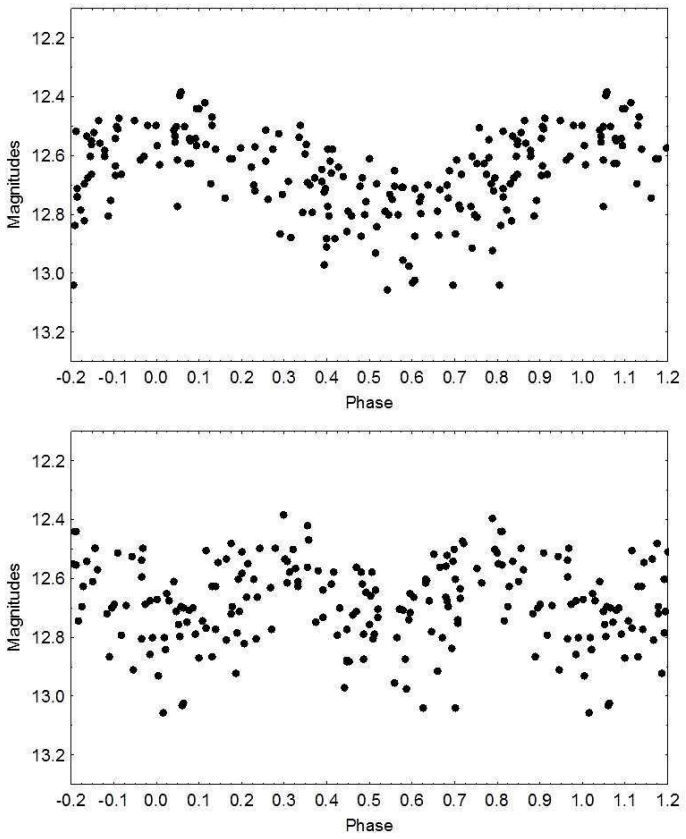

Figure 1. Folded light curves of the ASAS data with periods $1P$ (top) and $2P$ (down)

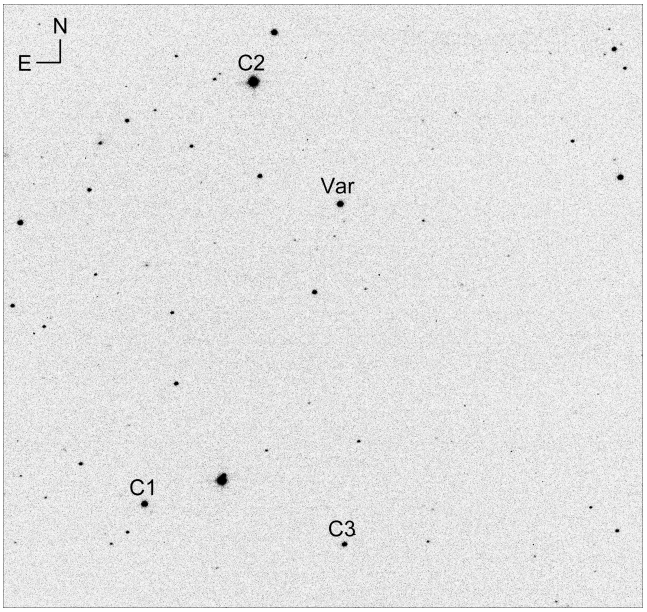

Figure 2. The field 10×10 arcmin around ASAS 0007

The standard procedures were used for reduction of the photometric data. The standard stars in the observed field (Fig. 2) were chosen by the criterion to be constant within 0.01 mag during the observations in all filters and all nights. Table 2 presents their V magnitudes and $V-I$ colors from USNO-B1 catalog.

The periodogram analysis of our I data (which are considerably more numerous than the V data, see Table 1) with a software PERSEA led to the ephemeris

$$\mathrm{HJD(MinI)} = 2455429.744 + 0.4034 \times E \quad (1)$$

and Figure 3 presents the corresponding folded light curves of ASAS 0007.

The amplitudes of the light variability in V and I filters are correspondingly 0.32 mag and 0.30 mag. The previous bigger V amplitude of 0.49 mag (Pojmanski 2000) probably due to the rough automate reduction of the ASAS data.

The qualitative analysis of the Rozhen data revealed binary nature of ASAS 0007 rather than δ Sct variability due to the following reasons:

(a) There are two light minima with different depths (visible in I filter);

(b) The brightness minima seem slightly sharper than the maxima;

(c) We calculated the de-reddened color index $(V-I)_0$=0.86 of the target by the Galactic Reddening and Extinction Calculator (Schlafly & Finkbeiner 2011). It corresponds to temperature T_m=5870 K according to the tables of VandenBerg & Clem (2003). This value is quite low for a δ Sct star (see Table 2 and Figure 2 of McNamara 2000) but appropriate for a W UMa star.

Another important criterion for the binary nature of ASAS 0007 could be the successful reproducing of its light curve by eclipses. That is why we tried to model the Rozhen data of ASAS 0007 using the code PHOEBE (Prša & Zwitter 2005) by the following procedure.

Initially the primary temperature was fixed as T_1=T_m. We adopted coefficients of gravity brightening 0.32 and reflection 0.5 appropriate for late stars while the limb-darkening coefficients for each component were taken from the tables of VanHamme (1993) according to its temperature. The fitted parameters were: secondary temperature T_2, mass ratio q, orbital inclination i and potentials $\Omega_{1,2}$ (and correspondingly relative radii $r_{1,2}$ and fillout factors $f_{1,2}$). Finally we varied the temperatures of the two components around T_m to reach a best fit of the observations.

The parameter values corresponding to our light curve solution are: orbital inclination $i = 61\overset{\circ}{.}30 \pm 0\overset{\circ}{.}06$; mass ratio $q = 0.953 \pm 0.003$; temperatures $T_1 = 5940 \pm 113$ K and $T_2 = 5673 \pm 105$ K; relative radii $r_1^{\mathrm{mean}} = 0.395 \pm 0.005$ and $r_2^{\mathrm{mean}} = 0.386 \pm 0.005$ (potentials $\Omega_1 = \Omega_2 = 3.595 \pm 0.007$); relative luminosities $l_1 = 0.55$ and $l_2 = 0.45$. The cited values of the parameter errors are the formal ones obtained by PHOEBE.

The synthetic curves corresponding to these parameters (Fig. 3) revealed that the Rozhen data can be well-reproduced by partial eclipses of an overcontact binary (with fillout factor $f_{1,2}$=0.147) whose components are not in thermal contact. Hence, the analysis of our observations of ASAS 0007 allowed us confidently to conclude that it is an eclipsing star but not a δ Sct variable, as it was previously classified.

This investigation is a new emphatic illustration of the proposition that the morphological classifications given in large data sets, especially for variable stars with almost sinusoidal light variability, might be wrong. Hence, the results of the statistical investigations on the base of such classifications should be assumed rather as approximate estimations.

Acknowledgement: This research was supported partly by funds of the project RD-08-244 of Shumen University. It used the SIMBAD database, operated at CDS, Stras-

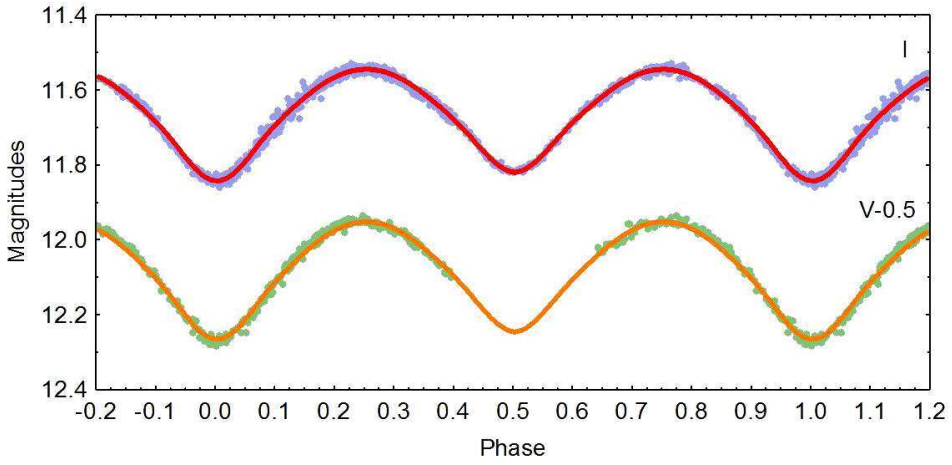

Figure 3. Rozhen VI folded light curves of ASAS 0007

bourg, France, USNO-B1.0 catalogue (`http://www.nofs.navy.mil/data/fchpix/`), and NASA's Astrophysics Data System Abstract Service.

References:

McNamara D., 2000, *ASPC*, **210**, 373
Pojmanski G., 2000, *AcA*, **50**, 177
Prśa A., Zwitter T., 2005, *ApJ*, **628**, 426
Schlafly E., Finkbeiner D., 2011, *ApJ*, **737**, 103
VandenBerg D., Clem J., 2003, *AJ*, **126**, 778
Van Hamme W., 1993, *AJ*, **106**, 2096

COMMISSIONS 27 AND 42 OF THE IAU
INFORMATION BULLETIN ON VARIABLE STARS

Number 6114

Konkoly Observatory
Budapest
11 September 2014

HU ISSN 0374 – 0676

COLLECTION OF MINIMA OF ECLIPSING BINARIES

ZASCHE, P.[1]; UHLAŘ, R.[2]; KUČÁKOVÁ, H.[1]; SVOBODA, P.[3]; MAŠEK, M.[4]

[1] Institute of Astronomy, Charles University, Prague, V Holešovičkách 2, Prague 8, CZ-18000 Czech Republic; e-mail: zasche@sirrah.troja.mff.cuni.cz

[2] Private Observatory, Pohoří 71, Jílové u Prahy, CZ-25401 Czech Republic

[3] Private observatory, Výpustky 5, Brno, CZ-614 00 Czech Republic

[4] Variable Star and Exoplanet Section of Czech Astronomical Society, Czech Republic

Observatory and telescope:

CCD photometry with various ground-based and automatic survey telescopes were used for the times of minima determination.

Method of data reduction:

The C-Munipack and IRAF routines were used for the reduction of the CCD frames.

Method of minimum determination:

The minima times were computed with the Kwee–van Woerden method (Kwee & van Woerden, 1956).

Explanation of the remarks in the table:

$BVRI$ filters by the specification by Bessell (1990), C: unfiltered. Observers: PZ: Petr Zasche, RU: Robert Uhlař, HK: Hana Kučáková, PS: Petr Svoboda, MM: Martin Mašek. Instruments: OND: 65 cm telescope in Ondřejov observatory, RF34/135: 34 mm refractor, RF75/300: 75 mm refractor, N150/750: 150 mm Newton reflector, N200/1000: 200 mm Newton reflector, Carona: 120 mm telescope located in Carona, Switzerland. For the double eclipsing systems their A/B pairs were designated according to the published ephemerides of both pairs. For the newly discovered systems their ephemerides (hence also primary/secondary distinction) are mostly not known yet. In Figure 1 we show evident pulsations of the star GQ Dra.

Acknowledgements:

Based on data from the OMC Archive at LAEFF, pre-processed by ISDC. We are also grateful to the ESO team at the La Silla Observatory for their help in maintaining and operating the 1.54 m Danish telescope. We thank the ASAS, CRTS, NSVS, SWASP, PI of the sky, and Integral OMC teams for making all of the observations available and easily accessible. This work was supported by the Czech Science Foundation grant no. P209/10/0715 and also by the grant LG12001 of the Ministry of Education of the Czech Republic. The use of "O-C gateway" (Paschke & Brát 2006) is also acknowledged.

Table 1: Times of minima of eclipsing binaries

Star Name	HJD 24.....	Error	Type	Filter	Instrument/Source	Observer
AD And	54303.72574	0.00099	Prim	W	SWASP	–
AD And	54304.71515	0.00022	Prim	W	SWASP	–
AD And	54305.70116	0.00024	Prim	W	SWASP	–
AD And	54306.68668	0.00031	Prim	W	SWASP	–
AD And	54307.67336	0.00036	Prim	W	SWASP	–
AD And	54308.66188	0.00069	Prim	W	SWASP	–
AD And	54312.59903	0.00163	Prim	W	SWASP	–
AD And	54316.54573	0.00091	Prim	W	SWASP	–
AD And	54318.51642	0.00033	Prim	W	SWASP	–
AD And	54320.49302	0.00117	Prim	W	SWASP	–
AD And	54322.46972	0.00073	Prim	W	SWASP	–
AD And	54334.79197	0.00039	Sec	W	SWASP	–
AD And	54335.77729	0.00011	Sec	W	SWASP	–
AD And	54337.74962	0.00120	Sec	W	SWASP	–
AD And	54338.73485	0.00079	Sec	W	SWASP	–
AD And	54339.72202	0.00024	Sec	W	SWASP	–
AD And	54340.70936	0.00025	Sec	W	SWASP	–
AD And	54344.65274	0.00043	Sec	W	SWASP	–
AD And	54345.63896	0.00029	Sec	W	SWASP	–
AD And	54346.62759	0.00046	Sec	W	SWASP	–
AD And	54347.61315	0.00043	Sec	W	SWASP	–
AD And	54348.60256	0.00175	Sec	W	SWASP	–
AD And	54349.58698	0.00023	Sec	W	SWASP	–
AD And	54350.57138	0.00027	Sec	W	SWASP	–
AD And	54351.55816	0.00027	Sec	W	SWASP	–
AD And	54352.54419	0.00019	Sec	W	SWASP	–
AD And	54353.53023	0.00027	Sec	W	SWASP	–
AD And	54354.51572	0.00031	Sec	W	SWASP	–
AD And	54355.50221	0.00028	Sec	W	SWASP	–
AD And	54356.48869	0.00019	Sec	W	SWASP	–
AD And	54357.47372	0.00021	Sec	W	SWASP	–
AD And	54358.45966	0.00052	Sec	W	SWASP	–
AD And	54359.44527	0.00017	Sec	W	SWASP	–
AD And	54360.43254	0.00055	Sec	W	SWASP	–
AD And	54361.41967	0.00036	Sec	W	SWASP	–
AD And	54362.40450	0.00071	Sec	W	SWASP	–
AD And	54363.39052	0.00129	Sec	W	SWASP	–
AD And	54364.37835	0.00042	Sec	W	SWASP	–
AD And	54381.63425	0.00076	Prim	W	SWASP	–
AD And	54382.62115	0.00043	Prim	W	SWASP	–
AD And	54383.60836	0.00026	Prim	W	SWASP	–
AD And	54384.59394	0.00047	Prim	W	SWASP	–
AD And	54387.55242	0.00025	Prim	W	SWASP	–
AD And	54388.53840	0.00029	Prim	W	SWASP	–
AD And	54389.52477	0.00017	Prim	W	SWASP	–
AD And	54392.48402	0.00023	Prim	W	SWASP	–
AD And	54393.47126	0.00045	Prim	W	SWASP	–
AD And	54394.45812	0.00023	Prim	W	SWASP	–
AD And	54395.44424	0.00070	Prim	W	SWASP	–
AD And	54396.42879	0.00006	Prim	W	SWASP	–
AD And	54397.41436	0.00044	Prim	W	SWASP	–
AD And	54398.40127	0.00016	Prim	W	SWASP	–
AD And	54399.38725	0.00055	Prim	W	SWASP	–
AD And	54402.34385	0.00074	Prim	W	SWASP	–

Table 1: cont...

Star Name	HJD 24.....	Error	Type	Filter	Instrument/Source	Observer
AD And	54405.30235	0.00184	Prim	W	SWASP	–
AD And	54406.28939	0.00098	Prim	W	SWASP	–
AD And	54407.27384	0.00130	Prim	W	SWASP	–
AD And	54408.26358	0.00170	Prim	W	SWASP	–
AD And	54420.59152	0.00115	Sec	W	SWASP	–
AD And	54421.57523	0.00211	Sec	W	SWASP	–
AD And	54427.49021	0.00031	Sec	W	SWASP	–
AD And	54437.35397	0.00011	Sec	W	SWASP	–
AD And	54438.34028	0.00018	Sec	W	SWASP	–
AD And	54439.32658	0.00015	Sec	W	SWASP	–
AD And	54441.29665	0.00065	Sec	W	SWASP	–
AD And	54444.25582	0.00044	Sec	W	SWASP	–
BX And	56155.51490	0.00025	Prim	C	RF34/135	RU
BX And	56291.26506	0.00034	Sec	R	N200/1000	RU
BX And	56584.42061	0.00030	Prim	C	N150/750	RU
BX And	56585.33607	0.00043	Sec	C	N150/750	RU
GZ And	56179.53745	0.00027	Prim	R	N200/1000	RU
V389 And	56203.58618	0.00125	Prim	C	RF34/135	RU
V389 And	56564.47946	0.00032	Prim	C	N150/750	RU
V392 And	56190.37142	0.00080	Sec	C	RF34/135	RU
V392 And	56540.37470	0.00215	Prim	C	RF34/135	RU
RY Aqr	56179.46711	0.00015	Prim	C	RF34/135	RU
RY Aqr	56533.44918	0.00029	Prim	C	RF34/135	RU
RY Aqr	56538.35712	0.00163	Sec	C	RF34/135	RU
RY Aqr	56540.34402	0.00189	Sec	R	N200/1000	RU
RY Aqr	56884.46938	0.00254	Sec	C	RF34/135	RU
RY Aqr	56889.39632	0.00071	Prim	C	RF34/135	RU
SU Aqr	56163.42425	0.00082	Prim	C	RF34/135	RU
SU Aqr	56209.39248	0.00066	Prim	R	N200/1000	RU
SU Aqr	56889.48945	0.00019	Prim	R	N200/1000	RU
DX Aqr	56491.47481	0.00072	Prim	C	RF34/135	RU
DX Aqr	56499.50366	0.00178	Sec	C	RF34/135	RU
V342 Aql	56486.43700	0.00216	Prim	R	RF34/135	RU
V342 Aql	56494.94264	0.00191	Sec	C	RF34/135	RU
V346 Aql	56076.50136	0.00009	Prim	R	N200/1000	RU
V346 Aql	56486.40148	0.00029	Sec	C	RF34/135	RU
V346 Aql	56835.46479	0.00009	Prim	C	N150/750	RU
V346 Aql	56892.44137	0.00119	Sec	R	RF34/135	RU
V822 Aql	56863.44725	0.00079	Prim	R	RF34/135	RU
V1461 Aql	56492.39943	0.00290	Prim	R	N200/1000	RU
V1461 Aql	56856.47416	0.00039	Sec	C	RF34/135	RU
V1461 Aql	56864.39947	0.00156	Prim	C	RF34/135	RU
V1470 Aql	56108.51261	0.00086	Prim	R	RF34/135	RU
V1470 Aql	56457.53690	0.00073	Prim	R	N200/1000	RU
V1470 Aql	56460.46962	0.00108	Sec	R	N200/1000	RU
V1470 Aql	56824.50902	0.00127	Sec	C	N150/750	RU
V1470 Aql	56827.41037	0.00432	Prim	C	RF34/135	RU
Sigma Aql	56148.46751	0.00028	Prim	C	RF34/135	RU
Sigma Aql	56460.51061	0.00049	Prim	I	RF34/135	RU
Sigma Aql	56461.48516	0.00029	Sec	I	RF34/135	RU
Sigma Aql	56853.49992	0.00037	Sec	I	RF34/135	RU
Sigma Aql	56856.41853	0.00119	Prim	I	RF34/135	RU
AL Ari	56670.28377	0.00009	Prim	R	N200/1000	RU
BQ Ari	56573.48279	0.00046	Sec	R	N200/1000	RU

Table 1: cont...

Star Name	HJD 24.....	Error	Type	Filter	Instrument/Source	Observer
BQ Ari	56573.62509	0.00023	Prim	R	N200/1000	RU
IU Aur	56666.40412	0.00078	Prim	R	RF34/135	RU
LY Aur	56624.40894	0.00062	Prim	C	RF34/135	RU
LY Aur	56630.41758	0.00123	Sec	C	RF34/135	RU
V424 Aur	54066.64236	0.00142	Sec	W	SWASP	–
V424 Aur	54067.56285	0.00054	Prim	W	SWASP	–
V424 Aur	54114.40006	0.00125	Sec	W	SWASP	–
V424 Aur	52682.58752	0.00064	Prim	V	OMC	–
V424 Aur	54056.53865	0.00119	Prim	W	SWASP	–
V424 Aur	56230.44289	0.00331	Prim	R	N200/1000	RU
V424 Aur	56566.59114	0.00081	Prim	R	RF34/135	RU
V424 Aur	56670.36163	0.00135	Sec	C	N150/750	RU
V462 Aur	56245.68524	0.00149	Sec	R	RF34/135	RU
V462 Aur	56246.56003	0.00063	Prim	R	RF34/135	RU
V462 Aur	56673.47149	0.00087	Prim	C	N150/750	RU
V462 Aur	56709.48583	0.00119	Sec	R	N200/1000	RU
V560 Aur	56565.46324	0.00389	Sec	R	RF34/135	RU
V560 Aur	56584.58070	0.00113	Prim	R	N200/1000	RU
V560 Aur	56597.55781	0.00059	Sec	R	N200/1000	RU
V560 Aur	56624.31504	0.00053	Prim	R	N200/1000	RU
V560 Aur	56692.31118	0.00039	Sec	C	N150/750	RU
AC Boo	56354.50618	0.00048	Prim	C	RF34/135	RU
EM Boo	56073.43912	0.00083	Sec	C	RF34/135	RU
EM Boo	56035.51007	0.00237	Prim	R	N200/1000	RU
EM Boo	56726.57129	0.00045	Sec	C	N150/750	RU
EM Boo	56737.58714	0.00102	Prim	R	N150/750	RU
EM Boo	56835.43792	0.00025	Prim	C	RF34/135	RU
ET Boo	55969.68608	0.00038	Sec	R	N200/1000	RU
ET Boo	56052.57374	0.00031	Prim	R	N200/1000	RU
ET Boo	56354.44953	0.00043	Prim	C	RF34/135	RU
ET Boo	56451.53023	0.00028	Sec	R	N200/1000	RU
ET Boo	56783.40212	0.00017	Prim	R	N200/1000	RU
ET Boo	56842.42313	0.00021	Sec	C	N150/750	RU
ET Boo	48462.70103	0.00109	Sec	Hp	Hipparcos	–
ET Boo	48463.02693	0.00102	Prim	Hp	Hipparcos	–
GK Boo	55963.56529	0.00016	Sec	R	N200/1000	RU
GK Boo	56019.46442	0.00028	Sec	R	N200/1000	RU
GK Boo	56026.39127	0.00011	Prim	R	N200/1000	RU
GK Boo	56094.47494	0.00010	Sec	R	N200/1000	RU
GK Boo	56354.62239	0.00084	Prim	R	RF34/135	RU
GK Boo	56366.56507	0.00039	Prim	R	N200/1000	RU
GK Boo	56421.50960	0.00029	Prim	C	RF34/135	RU
GK Boo	56461.40374	0.00036	Sec	C	RF34/135	RU
GK Boo	56483.38116	0.00017	Sec	R	N200/1000	RU
GK Boo	56709.60623	0.00027	Prim	C	N150/750	RU
GK Boo	56750.45464	0.00012	Sec	R	N200/1000	RU
GK Boo	56781.51017	0.00024	Sec	C	N150/750	RU
i Boo	56035.38947	0.00043	Prim	C	RF34/135	RU
i Boo	56035.52326	0.00039	Sec	C	RF34/135	RU
i Boo	56471.39774	0.00038	Prim	C	RF34/135	RU
i Boo	56714.44248	0.00027	Sec	I	RF34/135	RU
i Boo	56714.57675	0.00025	Prim	I	RF34/135	RU
SZ Cam	56204.61063	0.00069	Prim	C	RF34/135	RU
SZ Cam	56536.51531	0.00149	Prim	C	RF34/135	RU

Table 1: cont...

Star Name	HJD 24.....	Error	Type	Filter	Instrument/Source	Observer
SZ Cam	56563.46902	0.00162	Prim	I	RF34/135	RU
SZ Cam	56590.47196	0.00109	Prim	I	N200/1000	RU
SZ Cam	56602.61669	0.00428	Sec	C	RF34/135	RU
SZ Cam	56625.55333	0.00124	Prim	C	RF34/135	RU
CV Cam	56356.34765	0.00039	Prim	C	RF34/135	RU
CV Cam	56587.49120	0.00297	Sec	C	RF34/135	RU
DT Cam	55977.46852	0.00011	Prim	C	RF34/135	RU
DT Cam	56203.58753	0.00016	Prim	C	RF34/135	RU
S Cnc	56717.48067	0.00790	Sec	R	RF34/135	RU
TX Cnc	56650.49065	0.00032	Prim	R	RF34/135	RU
TX Cnc	56650.68542	0.00036	Sec	R	RF34/135	RU
GU CMa	56269.59472	0.00430	Prim	R	RF34/135	RU
KL CMa	56283.64326	0.00073	Prim	C	RF34/135	RU
KL CMa	56638.50902	0.00025	Sec	C	RF34/135	RU
LT CMa	55992.28577	0.00035	Sec	C	RF34/135	RU
LT CMa	56007.29484	0.00138	Prim	R	RF34/135	RU
RW CMi	55966.28398	0.00015	Prim	R	OND	PZ
CX CVn	56367.56827	0.00018	Prim	R	N200/1000	RU
CX CVn	56395.47355	0.00411	Sec	C	RF34/135	RU
CX CVn	56700.64099	0.00257	Sec	C	N150/750	RU
CX CVn	56728.54328	0.00030	Prim	C	N150/750	RU
YZ Cas	56184.50555	0.00060	Prim	C	RF34/135	RU
AR Cas	56515.50590	0.00172	Prim	I	RF34/135	RU
CC Cas	56199.52561	0.00092	Prim	R	RF34/135	RU
CC Cas	56241.57926	0.00520	Sec	R	RF34/135	RU
CC Cas	56534.46070	0.00133	Sec	C	RF34/135	RU
DN Cas	54750.48812	0.00267	Prim	BVRI	RF34/135	RU
DN Cas	54758.57793	0.00218	Sec	BVRI	RF34/135	RU
DO Cas	56190.42806	0.00056	Prim	R	RF34/135	RU
DO Cas	56203.43703	0.00037	Prim	R	RF34/135	RU
DO Cas	56252.39251	0.00085	Sec	C	RF34/135	RU
DO Cas	56558.43863	0.00148	Sec	C	RF34/135	RU
V368 Cas	56199.39101	0.00162	Prim	R	RF34/135	RU
V649 Cas	56206.35452	0.00027	Sec	C	RF34/135	RU
V649 Cas	56291.25352	0.00239	Prim	C	RF34/135	RU
V649 Cas	56451.46692	0.00226	Prim	R	RF34/135	RU
V649 Cas	56500.47558	0.00077	Sec	C	RF34/135	RU
V649 Cas	56543.53379	0.00206	Sec	V	RF34/135	RU
V649 Cas	56555.48536	0.00258	Sec	C	RF34/135	RU
V649 Cas	56561.46503	0.00290	Prim	C	RF34/135	RU
V649 Cas	56891.45712	0.00095	Prim	C	RF34/135	RU
V745 Cas	56152.41060	0.00318	Sec	R	N200/1000	RU
V745 Cas	56154.52673	0.00049	Prim	R	N200/1000	RU
V745 Cas	56501.56986	0.00519	Prim	C	RF34/135	RU
V745 Cas	56602.39233	0.00317	Sec	R	N200/1000	RU
V776 Cas	56155.40894	0.00033	Prim	R	N200/1000	RU
V776 Cas	56500.48298	0.00035	Sec	C	RF34/135	RU
V776 Cas	56542.53555	0.00030	Prim	R	RF34/135	RU
V779 Cas	56159.45785	0.00033	Prim	C	RF34/135	RU
V779 Cas	56572.43769	0.00172	Prim	C	RF34/135	RU
V791 Cas	56190.43766	0.00583	Prim	R	RF34/135	RU
V791 Cas	56545.50681	0.00205	Prim	R	RF34/135	RU
V791 Cas	56558.49919	0.00053	Sec	C	RF34/135	RU
U Cep	56245.41607	0.00073	Sec	C	RF34/135	RU

Table 1: cont...

Star Name	HJD 24.....	Error	Type	Filter	Instrument/Source	Observer
U Cep	56478.50130	0.00073	Prim	C	RF34/135	RU
U Cep	56564.51645	0.00256	Sec	C	RF34/135	RU
VW Cep	56201.26896	0.00058	Prim	R	RF34/135	RU
VW Cep	56201.41269	0.00149	Sec	R	RF34/135	RU
VW Cep	56201.54908	0.00021	Prim	R	RF34/135	RU
VW Cep	56541.36200	0.00014	Prim	C	RF34/135	RU
VW Cep	56541.50175	0.00014	Sec	C	RF34/135	RU
VW Cep	56851.39648	0.00047	Prim	C	RF34/135	RU
VW Cep	56851.53729	0.00026	Sec	C	RF34/135	RU
ZZ Cep	56187.34548	0.00017	Prim	C	RF34/135	RU
ZZ Cep	56461.49619	0.00023	Prim	C	RF34/135	RU
CW Cep	56038.50913	0.00037	Prim	C	RF34/135	RU
DP Cep	56495.57778	0.00019	Prim	R	OND	HK
LP Cep	55945.22399	0.00012	Prim	R	OND	PZ
LP Cep	56166.30797	0.00017	Prim	R	OND	PZ
NN Cep	56692.57443	0.00248	Prim	BVR	RF34/135	PS
V357 Cep	55957.52344	0.00005	Prim	R	OND	PZ
V383 Cep	56190.47788	0.00051	Prim	C	RF34/135	RU
V442 Cep	56486.49893	0.00046	Prim	I	N200/1000	RU
V442 Cep	56568.46910	0.00049	Sec	V	RF34/135	RU
V453 Cep	56158.51632	0.00150	Prim	C	RF34/135	RU
V453 Cep	56237.30337	0.00261	Sec	C	RF34/135	RU
V453 Cep	56510.38193	0.00069	Prim	R	RF34/135	RU
V453 Cep	56527.55888	0.00062	Sec	R	RF34/135	RU
KK Com	55993.49319	0.00024	Sec	R	N200/1000	RU
KK Com	56747.42602	0.00229	Sec	C	N150/750	RU
KK Com	56755.42920	0.00022	Prim	C	N200/1000	RU
KR Com	55923.64835	0.00145	Prim	C	RF34/135	RU
KR Com	56030.32507	0.00079	Sec	R	RF34/135	RU
KR Com	56048.47990	0.00052	Prim	I	N200/1000	RU
KR Com	56105.39669	0.00207	Sec	I	N200/1000	RU
KR Com	56273.68164	0.00057	Prim	C	RF34/135	RU
KR Com	56340.58372	0.00049	Prim	C	RF34/135	RU
KR Com	56433.39291	0.00526	Sec	C	RF34/135	RU
KR Com	56692.65630	0.00096	Prim	V	RF75/300	RU
RV Crt	56729.45004	0.00050	Sec	C	N150/750	RU
CG Cyg	56101.51576	0.00024	Sec	R	N200/1000	RU
V749 Cyg	55945.27742	0.00024	Prim	R	OND	PZ
V796 Cyg	51275.34192	0.00220	Sec	V	NSVS	–
V796 Cyg	51276.03205	0.00205	Prim	V	NSVS	–
V796 Cyg	53128.59346	0.00037	Prim	W	SWASP	–
V796 Cyg	54232.63881	0.00426	Sec	W	SWASP	–
V796 Cyg	54249.62796	0.00077	Prim	W	SWASP	–
V796 Cyg	54252.58835	0.00056	Prim	W	SWASP	–
V796 Cyg	54260.77600	0.00102	Sec	W	SWASP	–
V796 Cyg	54261.47377	0.00056	Prim	W	SWASP	–
V796 Cyg	54269.65701	0.00123	Sec	W	SWASP	–
V796 Cyg	54272.61719	0.00056	Sec	W	SWASP	–
V796 Cyg	54275.57953	0.00099	Sec	W	SWASP	–
V796 Cyg	54278.54265	0.00093	Sec	W	SWASP	–
V796 Cyg	54280.72737	0.00106	Prim	W	SWASP	–
V796 Cyg	54281.50339	0.00101	Sec	W	SWASP	–
V796 Cyg	54283.68759	0.00082	Prim	W	SWASP	–
V796 Cyg	54284.46353	0.00070	Sec	W	SWASP	–

Table 1: cont...

Star Name	HJD 24.....	Error	Type	Filter	Instrument/Source	Observer
V796 Cyg	54286.64854	0.00022	Prim	W	SWASP	–
V796 Cyg	54287.42867	0.00044	Sec	W	SWASP	–
V796 Cyg	54289.60962	0.00037	Prim	W	SWASP	–
V796 Cyg	54290.38939	0.00038	Sec	W	SWASP	–
V796 Cyg	54292.57242	0.00092	Prim	W	SWASP	–
V796 Cyg	54606.52007	0.00130	Prim	W	SWASP	–
V796 Cyg	54608.76715	0.00215	Sec	W	SWASP	–
V796 Cyg	54629.50120	0.00278	Sec	W	SWASP	–
V796 Cyg	54631.69083	0.00056	Prim	W	SWASP	–
V796 Cyg	54632.46578	0.00060	Sec	W	SWASP	–
V796 Cyg	54635.42420	0.00074	Sec	W	SWASP	–
V796 Cyg	54637.62028	0.00086	Prim	W	SWASP	–
V796 Cyg	54640.58241	0.00109	Prim	W	SWASP	–
V796 Cyg	54643.54231	0.00073	Prim	W	SWASP	–
V796 Cyg	54645.78778	0.00037	Sec	W	SWASP	–
V796 Cyg	54646.50625	0.00037	Prim	W	SWASP	–
V796 Cyg	54657.63733	0.00023	Sec	W	SWASP	–
V796 Cyg	54660.59886	0.00074	Sec	W	SWASP	–
V796 Cyg	54663.56280	0.00056	Sec	W	SWASP	–
V796 Cyg	54666.52437	0.00117	Sec	W	SWASP	–
V796 Cyg	54669.48535	0.00087	Sec	W	SWASP	–
V796 Cyg	54671.68293	0.00112	Prim	W	SWASP	–
V796 Cyg	54672.44591	0.00056	Sec	W	SWASP	–
V796 Cyg	54674.64323	0.00056	Prim	W	SWASP	–
V796 Cyg	54683.52700	0.00093	Prim	W	SWASP	–
V796 Cyg	54686.48992	0.00148	Prim	W	SWASP	–
V1187 Cyg	56563.32657	0.00027	Prim	C	N150/750	RU
V1191 Cyg	56500.50883	0.00017	Sec	R	N200/1000	RU
V1191 Cyg	56563.34304	0.00016	Prim	C	N150/750	RU
V2083 Cyg	56134.50378	0.00030	Sec	C	RF34/135	RU
V2083 Cyg	56458.51203	0.00115	Prim	R	RF34/135	RU
V2083 Cyg	56768.51290	0.00121	Prim	R	RF34/135	RU
V2154 Cyg	56070.50625	0.00022	Prim	I	N200/1000	RU
V2154 Cyg	56199.40535	0.00039	Prim	C	RF34/135	RU
V2154 Cyg	56433.53282	0.00147	Prim	C	RF34/135	RU
V2154 Cyg	56800.50207	0.00105	Sec	R	RF34/135	RU
V2165 Cyg	56101.51766	0.00041	Prim	C	RF34/135	RU
V2169 Cyg	56108.42379	0.00037	Prim	C	RF34/135	RU
V2169 Cyg	56496.43491	0.00129	Sec	I	N200/1000	RU
V2169 Cyg	56562.44527	0.00043	Prim	C	RF34/135	RU
V2486 Cyg	56495.56871	0.00167	Sec	R	N200/1000	RU
V2486 Cyg	56497.47701	0.00015	Prim	R	N200/1000	RU
MR Del	56094.49253	0.00048	Sec	R	RF34/135	RU
MR Del	56100.49176	0.00010	Prim	R	N200/1000	RU
MR Del	56148.48803	0.00050	Prim	R	N200/1000	RU
MR Del	56205.35315	0.00028	Prim	R	RF34/135	RU
MR Del	56210.30800	0.00048	Sec	R	RF34/135	RU
MR Del	56232.21862	0.00035	Sec	R	RF34/135	RU
MR Del	56239.26196	0.00017	Prim	C	RF34/135	RU
MR Del	56256.21676	0.00018	Sec	R	N200/1000	RU
MR Del	56449.50223	0.00038	Prim	C	RF34/135	RU
MR Del	56454.45779	0.00046	Sec	C	RF34/135	RU
MR Del	56510.53952	0.00017	Prim	R	N200/1000	RU
MR Del	56542.36330	0.00064	Prim	C	RF34/135	RU

Table 1: cont...

Star Name	HJD 24.....	Error	Type	Filter	Instrument/Source	Observer
MR Del	56572.35832	0.00082	Sec	R	N200/1000	RU
MR Del	56827.46691	0.00109	Sec	C	N150/750	RU
MR Del	56863.46028	0.00016	Sec	C	RF34/135	RU
RR Dra	56349.47808	0.00185	Prim	R	OND	PZ
WW Dra	56076.46598	0.00054	Prim	C	RF34/135	RU
WW Dra	56495.45204	0.00210	Sec	R	RF34/135	RU
WW Dra	56826.50036	0.00119	Prim	C	RF34/135	RU
BH Dra	56040.56931	0.00016	Prim	R	RF34/135	RU
BH Dra	56041.47096	0.00053	Sec	C	RF34/135	RU
BH Dra	56539.40253	0.00059	Sec	C	RF34/135	RU
BV Dra	55992.58077	0.00107	Prim	R	N200/1000	RU
BV Dra	56390.43932	0.00031	Sec	R	N200/1000	RU
BV Dra	56390.61095	0.00072	Prim	R	N200/1000	RU
BV Dra	56650.71207	0.00026	Prim	R	N200/1000	RU
BV Dra	56656.65299	0.00035	Prim	R	RF34/135	RU
BV Dra	56754.33927	0.00019	Prim	R	RF34/135	RU
BV Dra	56754.50548	0.00018	Sec	R	RF34/135	RU
BW Dra	55992.54855	0.00039	Prim	R	N200/1000	RU
BW Dra	55992.69390	0.00030	Sec	R	N200/1000	RU
BW Dra	56390.46449	0.00101	Prim	R	N200/1000	RU
BW Dra	56390.61451	0.00048	Sec	R	N200/1000	RU
BW Dra	56650.64198	0.00031	Sec	R	N200/1000	RU
CM Dra	56729.53018	0.00006	Prim	R	N200/1000	RU
CM Dra	56731.43152	0.00021	Sec	R	N200/1000	RU
GQ Dra	56043.55365	0.00064	Sec	R	N200/1000	RU
GQ Dra	56052.36294	0.00018	Prim	R	N200/1000	RU
GQ Dra	56357.57243	0.00053	Sec	C	RF34/135	RU
GQ Dra	56755.46212	0.00029	Prim	C	N150/750	RU
GQ Dra	56783.41372	0.00052	Sec	C	N150/750	RU
GZ Dra	56035.45695	0.00056	Prim	R	RF34/135	RU
GZ Dra	56462.46881	0.00034	Sec	R	RF34/135	RU
GZ Dra	56747.51675	0.00043	Prim	C	RF34/135	RU
GZ Dra	56782.43185	0.00138	Sec	C	RF34/135	RU
HI Dra	56096.51142	0.00190	Prim	C	RF34/135	RU
HI Dra	56499.46535	0.00039	Sec	R	N200/1000	RU
HI Dra	56755.46633	0.00076	Prim	R	RF34/135	RU
HI Dra	56766.51588	0.00040	Sec	C	N150/750	RU
CI Eri	51918.23600	0.00077	Prim	V	ASAS	–
CI Eri	51918.84956	0.01238	Sec	V	ASAS	–
CI Eri	52158.44555	0.00076	Prim	V	ASAS	–
CI Eri	52159.06045	0.00507	Sec	V	ASAS	–
CI Eri	52589.33945	0.00028	Prim	V	ASAS	–
CI Eri	52589.95478	0.00331	Sec	V	ASAS	–
CI Eri	52986.80061	0.00209	Prim	V	ASAS	–
CI Eri	52987.41039	0.00822	Sec	V	ASAS	–
CI Eri	53598.46692	0.00061	Prim	V	ASAS	–
CI Eri	53599.07916	0.00179	Sec	V	ASAS	–
CI Eri	54322.80851	0.00078	Prim	V	ASAS	–
CI Eri	54323.43271	0.00156	Sec	V	ASAS	–
CI Eri	54762.36627	0.00161	Prim	V	ASAS	–
CI Eri	54762.98463	0.00282	Sec	V	ASAS	–
CI Eri	55068.20169	0.00308	Prim	V	ASAS	–
CI Eri	55068.81999	0.00950	Sec	V	ASAS	–
CI Eri	54077.64545	0.00043	Prim	C	PI of the sky	–

Table 1: cont...

Star Name	HJD 24.....	Error	Type	Filter	Instrument/Source	Observer
CI Eri	54098.69548	0.00139	Prim	C	PI of the sky	–
CI Eri	54113.55527	0.00800	Prim	C	PI of the sky	–
CI Eri	54768.55785	0.00600	Prim	C	PI of the sky	–
CI Eri	54823.65100	0.00175	Sec	C	PI of the sky	–
CI Eri	54824.27425	0.00127	Prim	C	PI of the sky	–
KP Eri	56290.44934	0.00114	Sec	C	RF34/135	RU
YY Gem	56630.50029	0.00012	Prim	R	N200/1000	RU
V337 Gem	55970.33537	0.00032	Prim	C	RF34/135	RU
AK Her	56835.42140	0.00021	Sec	R	RF34/135	RU
V819 Her	56778.40769	0.00034	Prim	I	RF34/135	RU
V819 Her	56798.47402	0.00035	Prim	I	RF34/135	RU
V819 Her	56818.53929	0.00113	Prim	I	RF34/135	RU
V819 Her	56827.45966	0.00036	Prim	I	RF34/135	RU
V822 Her	56100.45416	0.00158	Prim	R	RF34/135	RU
V822 Her	56415.53648	0.00153	Sec	C	RF34/135	RU
V822 Her	56783.49759	0.00027	Prim	R	RF34/135	RU
V822 Her	56792.54156	0.00177	Sec	R	RF34/135	RU
V994 Her^{A}	56368.61655	0.00029	Sec	I	N200/1000	RU
V994 Her^{A}	56463.37125	0.00081	Prim	C	RF34/135	RU
V994 Her^{A}	56465.45059	0.00259	Prim	C	RF34/135	RU
V994 Her^{B}	56450.37231	0.00204	Prim	C	RF34/135	RU
V994 Her^{B}	56457.46946	0.00054	Prim	C	RF34/135	RU
V994 Her^{B}	56455.43271	0.00040	Sec	C	RF34/135	RU
V994 Her^{B}	56354.60974	0.00207	Sec	C	RF34/135	RU
V994 Her^{A}	56441.53093	0.00020	Sec	R	RF34/135	RU
V994 Her^{B}	56736.59690	0.00049	Sec	R	RF34/135	RU
V994 Her^{B}	56758.50910	0.00259	Prim	R	RF34/135	RU
V994 Her^{A}	56766.52219	0.00090	Sec	R	RF34/135	RU
V994 Her^{A}	56767.53147	0.00027	Prim	R	RF34/135	RU
V994 Her^{B}	56827.48758	0.00078	Sec	I	N200/1000	RU
V994 Her^{A}	56839.44646	0.00247	Sec	C	N150/750	RU
V994 Her^{A}	56842.53174	0.00132	Prim	C	N150/750	RU
HS Hya	56356.45155	0.00144	Sec	C	RF34/135	RU
HS Hya	56730.4260	0.00439	Prim	R	N200/1000	RU
CY Lac	56673.39907	0.00450	Sec	R	OND	HK
CY Lac	56645.29574	0.00320	Prim	R	OND	HK
V394 Lac	56490.48697	0.00151	Prim	C	RF34/135	RU
V394 Lac	56188.52829	0.00159	Prim	C	RF34/135	RU
V394 Lac	56853.49534	0.00144	Prim	C	N150/750	RU
V401 Lac	56097.50644	0.00021	Prim	C	RF34/135	RU
V401 Lac	56180.34094	0.00060	Sec	R	N200/1000	RU
V401 Lac	56486.49818	0.00040	Sec	C	RF34/135	RU
V401 Lac	56489.48043	0.00015	Prim	C	RF34/135	RU
V401 Lac	56878.45447	0.00048	Sec	I	N200/1000	RU
V402 Lac	56163.43315	0.00016	Prim	I	N200/1000	RU
V402 Lac	56511.38248	0.00097	Prim	C	RF34/135	RU
V402 Lac	56821.51566	0.00046	Prim	R	RF34/135	RU
TX Leo	55920.62784	0.00115	Prim	C	RF34/135	RU
TX Leo	56397.42535	0.00245	Prim	C	RF34/135	RU
TX Leo	56634.58728	0.00296	Prim	C	RF34/135	RU
AM Leo	56724.38495	0.00052	Prim	C	N150/750	RU
BV Leo	55957.39709	0.00042	Sec	R	OND	PZ
T LMi	56368.50591	0.00011	Prim	R	OND	HK
GV Lib	52556.85068	0.00201	Prim	V	ASAS	–

Table 1: cont...

Star Name	HJD 24.....	Error	Type	Filter	Instrument/Source	Observer
GV Lib	52557.30163	0.00078	Sec	V	ASAS	–
GV Lib	53651.54359	0.00086	Prim	V	ASAS	–
GV Lib	53651.94942	0.02982	Sec	V	ASAS	–
GV Lib	54617.30562	0.00175	Prim	V	ASAS	–
GV Lib	54617.74349	0.00030	Sec	V	ASAS	–
GV Lib	51446.84206	0.00143	Prim	V	NSVS	–
GV Lib	51447.31431	0.00172	Sec	V	NSVS	–
GV Lib	53782.41226	0.00248	Prim	V	CRTS	–
GV Lib	53782.90780	0.00544	Sec	V	CRTS	–
GV Lib	54596.27621	0.00262	Prim	V	CRTS	–
GV Lib	54596.75552	0.00676	Sec	V	CRTS	–
GV Lib	55857.19271	0.00286	Prim	V	CRTS	–
GV Lib	55857.67318	0.00845	Sec	V	CRTS	–
IV Lib	56482.35429	0.00345	Prim	R	N200/1000	RU
Delta Lib	56026.42928	0.00036	Prim	C	RF34/135	RU
Delta Lib	56062.50697	0.00342	Sec	C	RF34/135	RU
Delta Lib	56368.55095	0.00040	Prim	I	RF34/135	RU
DI Lyn	55930.62256	0.00031	Sec	C	RF34/135	RU
DI Lyn	55963.41722	0.00076	Prim	R	N200/1000	RU
DI Lyn	56006.29657	0.00081	Sec	R	RF34/135	PS
DI Lyn	56006.29662	0.00121	Sec	V	RF34/135	RU
DI Lyn	56037.40065	0.00055	Prim	R	RF34/135	RU
DI Lyn	56337.57130	0.00249	Sec	C	RF34/135	RU
DI Lyn	56354.37518	0.00049	Sec	V	RF34/135	RU
DI Lyn	56590.64339	0.00039	Prim	I	N200/1000	RU
DI Lyn	56703.30766	0.00048	Prim	V	RF34/135	RU
DI Lyn	56713.39681	0.00039	Prim	I	N200/1000	RU
DI Lyn	56750.39042	0.00051	Prim	V	RF34/135	RU
TZ Lyr	56076.45591	0.00011	Prim	R	N200/1000	RU
TZ Lyr	56108.45047	0.00033	Sec	R	N200/1000	RU
TZ Lyr	56510.35925	0.00021	Sec	R	N200/1000	RU
TZ Lyr	56765.51808	0.00013	Prim	C	N150/750	RU
TZ Lyr	56778.47445	0.00028	Sec	R	N200/1000	RU
UZ Lyr	56864.51503	0.00070	Prim	R	RF34/135	RU
V380 Mon	52739.87642	0.00217	Sec	V	ASAS	PZ
V380 Mon	52740.36440	0.00559	Prim	V	ASAS	PZ
V380 Mon	54335.77963	0.00478	Prim	V	ASAS	PZ
V380 Mon	54336.27605	0.00558	Sec	V	ASAS	PZ
V380 Mon	51545.82077	0.00559	Sec	V	NSVS	PZ
V498 Mon	55894.60455	0.00007	Prim	B	OND	PZ
V684 Mon	56270.62494	0.00047	Sec	C	RF34/135	RU
V684 Mon	56273.42636	0.00104	Prim	C	RF34/135	RU
V684 Mon	56633.50668	0.00057	Sec	C	RF34/135	RU
V684 Mon	56634.46013	0.00117	Prim	C	RF34/135	RU
V684 Mon	56709.41608	0.00052	Sec	C	N150/750	RU
V727 Mon	55996.33538	0.00188	Prim	C	RF34/135	RU
V727 Mon	56643.47558	0.00291	Sec	R	N200/1000	RU
V727 Mon	56701.37002	0.00048	Prim	C	N150/750	RU
V730 Mon	56624.60168	0.00187	Sec	C	RF34/135	RU
V730 Mon	56654.47885	0.00123	Sec	C	RF34/135	RU
V730 Mon	56713.35270	0.00046	Prim	C	RF34/135	RU
V879 Mon	56648.47861	0.00083	Sec	C	RF34/135	RU
V879 Mon	56717.36788	0.00022	Prim	C	N150/750	RU
U Oph	56060.50860	0.00025	Prim	C	RF34/135	RU

Table 1: cont...

Star Name	HJD 24.....	Error	Type	Filter	Instrument/Source	Observer
U Oph	56455.52815	0.00048	Sec	I	RF34/135	RU
U Oph	56461.39534	0.00035	Prim	C	RF34/135	RU
V456 Oph	56471.55608	0.00022	Sec	B	OND	HK
V456 Oph	56497.46596	0.00005	Prim	B	OND	HK
V456 Oph	56582.29963	0.00040	Sec	B	OND	HK
V456 Oph	56728.60346	0.00010	Sec	R	OND	PZ
V456 Oph	56814.45986	0.00088	Prim	R	OND	PZ
V456 Oph	56842.39531	0.00004	Sec	R	OND	PZ
V456 Oph	56876.43658	0.00022	Prim	C	Sonnar 180	MM
V456 Oph	56878.46847	0.00014	Prim	R	OND	HK
V2388 Oph	56797.48623	0.00056	Prim	I	RF34/135	RU
V2388 Oph	56856.46397	0.00052	Sec	I	N200/1000	RU
V2388 Oph	56891.35642	0.00059	Prim	I	RF34/135	RU
V2610 Oph	56451.45721	0.00099	Sec	C	RF34/135	RU
V2610 Oph	56455.50853	0.00041	Prim	C	RF34/135	RU
V2610 Oph	56802.47289	0.00042	Sec	C	N150/750	MM
V2610 Oph	56818.46715	0.00029	Prim	C	N150/750	MM
V2610 Oph	56888.41359	0.00038	Prim	C	RF34/135	RU
V645 Ori	55957.32312	0.00003	Prim	R	OND	PZ
V1804 Ori	56270.46918	0.00063	Prim	C	RF34/135	RU
V1804 Ori	56573.59898	0.00285	Prim	C	RF34/135	RU
V1804 Ori	56621.51598	0.00119	Sec	C	RF34/135	RU
V1834 Ori	55901.46847	0.00170	Sec	C	RF34/135	RU
V1834 Ori	56318.38089	0.00250	Sec	R	RF34/135	RU
V1834 Ori	56629.55264	0.00089	Sec	I	N200/1000	RU
V1834 Ori	56639.37757	0.00032	Prim	C	RF34/135	RU
Delta Ori	55787.36327	0.00527	Sec	I	RF34/135	RU
Eta Ori	56291.34125	0.00108	Sec	I	RF34/135	RU
Eta Ori	56311.24483	0.00500	Prim	C	RF34/135	RU
AW Peg	56148.59965	0.00218	Prim	R	RF34/135	RU
KP Peg	56499.45219	0.00230	Prim	C	RF34/135	RU
PU Peg	56181.50092	0.00065	Prim	C	RF34/135	RU
PU Peg	56525.45138	0.00180	Prim	I	N200/1000	RU
PU Peg	56541.38508	0.00159	Sec	R	N200/1000	RU
PU Peg	56588.35958	0.00127	Prim	R	N200/1000	RU
PU Peg	56884.47120	0.00113	Sec	C	N150/750	RU
V415 Peg	56515.51081	0.00415	Sec	I	N200/1000	RU
V416 Peg	56105.55212	0.00234	Sec	C	Carona	RU
V416 Peg	56147.58159	0.00044	Prim	C	RF34/135	RU
V416 Peg	56541.52876	0.00126	Sec	R	N200/1000	RU
V416 Peg	56566.46445	0.00029	Prim	R	N200/1000	RU
ST Per	56205.40262	0.00079	Prim	R	N200/1000	RU
ST Per	56565.57532	0.00065	Prim	C	RF34/135	RU
AG Per	55930.27950	0.00048	Sec	C	RF34/135	RU
AG Per	55937.39904	0.00033	Prim	C	RF34/135	RU
AG Per	56288.37119	0.00055	Prim	C	RF34/135	RU
AG Per	56291.39123	0.00046	Sec	C	RF34/135	RU
AG Per	56578.48239	0.00032	Prim	C	RF34/135	RU
AG Per	56583.52706	0.00057	Sec	C	RF34/135	RU
IQ Per	56180.55097	0.00039	Sec	R	RF34/135	RU
IQ Per	56181.49456	0.00065	Prim	R	RF34/135	RU
LX Per	55906.31001	0.00119	Prim	C	RF34/135	RU
V366 Per	55901.37281	0.00011	Prim	R	OND	PZ
V436 Per	55908.37358	0.00013	Prim	C	RF34/135	RU

Table 1: cont...

Star Name	HJD 24.....	Error	Type	Filter	Instrument/Source	Observer
V590 Per	56588.60338	0.00175	Sec	I	N200/1000	RU
V593 Per	56279.60463	0.00439	Prim	C	RF34/135	RU
V593 Per	56563.43930	0.00243	Sec	R	N200/1000	RU
V593 Per	56584.53011	0.00218	Prim	R	RF34/135	RU
V736 Per	56585.34636	0.00049	Prim	R	N200/1000	RU
V871 Per	56276.22899	0.00060	Sec	R	OND	PZ
V871 Per	56323.48420	0.00007	Prim	R	OND	HK
V871 Per	56584.67553	0.00030	Sec	B	OND	HK
V871 Per	56586.55520	0.00096	Prim	R	OND	HK
Beta Per	56266.43745	0.00305	Sec	C	RF34/135	RU
Zeta Phe	52819.48535	0.00648	Prim	V	ASAS	–
Zeta Phe	53733.67671	0.01494	Sec	V	ASAS	–
Zeta Phe	53734.51918	0.00394	Prim	V	ASAS	–
Zeta Phe	54248.80812	0.00287	Prim	C	PI of the sky	–
Zeta Phe	54563.55669	0.00344	Sec	V	ASAS	–
Zeta Phe	54564.39547	0.00815	Prim	V	ASAS	–
Zeta Phe	54709.66918	0.01578	Prim	C	PI of the sky	–
Zeta Phe	54784.79817	0.00800	Prim	C	PI of the sky	–
Zeta Phe	54820.69055	0.00079	Sec	C	PI of the sky	–
Zeta Phe	56210.79039	0.00105	Prim	C	La Silla all-sky cam	PZ
Zeta Phe	56215.79640	0.01109	Prim	C	La Silla all-sky cam	PZ
Zeta Phe	56559.76998	0.00977	Prim	C	La Silla all-sky cam	PZ
Zeta Phe	56560.59702	0.00599	Sec	C	La Silla all-sky cam	PZ
UV Psc	56152.60033	0.00036	Prim	C	RF34/135	RU
SZ Psc	56541.56062	0.00124	Prim	C	RF34/135	RU
SZ Psc	56559.44636	0.00205	Sec	C	RF34/135	RU
SZ Psc	56892.51119	0.00509	Sec	I	N200/1000	RU
SZ Psc	56894.51652	0.00269	Prim	V	N200/1000	RU
ET Psc	56159.55935	0.00028	Prim	R	N200/1000	RU
ET Psc	56293.32668	0.00042	Sec	C	RF34/135	RU
ET Psc	56545.48485	0.00022	Sec	R	N200/1000	RU
ET Psc	56545.48540	0.00037	Sec	R	N200/1000	RU
ET Psc	56573.37683	0.00045	Prim	C	RF34/135	RU
EU Psc	56187.55283	0.00106	Prim	I	RF34/135	RU
EU Psc	56288.25303	0.00248	Sec	C	RF34/135	RU
EU Psc	56545.55796	0.00315	Sec	C	RF34/135	RU
EU Psc	56573.46934	0.00048	Prim	R	RF34/135	RU
PV Pup	56342.44639	0.00025	Prim	C	RF34/135	RU
DM Sge	51449.99623	0.00155	Sec	V	NSVS	PZ
DM Sge	51451.38814	0.00608	Prim	V	NSVS	PZ
DM Sge	56495.53238	0.00080	Sec	R	OND	HK
DM Sge	56728.66084	0.00010	Sec	R	OND	PZ
V505 Sgr	56136.45681	0.00021	Prim	I	N200/1000	RU
V505 Sgr	56152.42663	0.00076	Sec	R	RF34/135	RU
V505 Sgr	56155.38240	0.00040	Prim	C	RF34/135	RU
V505 Sgr	56450.50214	0.00114	Sec	C	RF34/135	RU
V505 Sgr	56460.55882	0.00022	Prim	C	RF34/135	RU
V505 Sgr	56466.47343	0.00019	Prim	C	RF34/135	RU
V505 Sgr	56479.48444	0.00018	Prim	C	RF34/135	RU
V505 Sgr	56489.53481	0.00057	Sec	I	N200/1000	RU
V505 Sgr	56835.52293	0.00009	Prim	R	RF34/135	RU
V1301 Sco	56347.85040	0.00038	Sec	R	DK154	PZ
V1301 Sco	56383.89541	0.00077	Prim	R	DK154	PZ
PS Ser	56396.41343	0.00072	Prim	R	RF34/135	RU

Table 1: cont...

Star Name	HJD 24.....	Error	Type	Filter	Instrument/Source	Observer
V413 Ser	56065.51298	0.00045	Sec	R	N200/1000	RU
V413 Ser	56159.37241	0.00120	Prim	I	N200/1000	RU
V413 Ser	56421.50170	0.00086	Prim	R	RF34/135	RU
V413 Ser	56456.45424	0.00046	Sec	R	RF34/135	RU
V413 Ser	56856.42651	0.00049	Sec	C	N150/750	RU
V413 Ser	56864.41296	0.00175	Prim	C	N150/750	RU
CD Tau	56201.56843	0.00226	Prim	C	RF34/135	RU
CD Tau	56225.61730	0.00019	Prim	C	RF34/135	RU
CD Tau	56639.55152	0.00012	Sec	C	RF34/135	RU
V1128 Tau	56292.25090	0.00018	Prim	C	RF34/135	RU
V1128 Tau	56292.40413	0.00032	Sec	C	RF34/135	RU
V1128 Tau	56566.47276	0.00028	Prim	C	RF34/135	RU
V1128 Tau	56566.62711	0.00023	Sec	C	RF34/135	RU
V1154 Tau	56292.31253	0.00087	Prim	C	RF34/135	RU
V1154 Tau	56556.62256	0.00249	Sec	C	RF34/135	RU
V1154 Tau	56656.50366	0.00057	Prim	C	RF34/135	RU
Ksi Tau	56278.29207	0.00759	Prim	C	RF34/135	RU
Ksi Tau	55917.41664	0.00097	Sec	C	RF34/135	RU
Ksi Tau	56210.43013	0.00085	Sec	I	RF34/135	RU
Ksi Tau	56285.44436	0.00145	Prim	C	RF34/135	RU
Ksi Tau	56535.58620	0.00089	Prim	C	RF34/135	RU
Ksi Tau	56560.59679	0.00195	Sec	C	RF34/135	RU
VV UMa	56006.38137	0.00041	Prim	C	RF34/135	RU
W UMa	56006.33529	0.00011	Prim	C	RF34/135	RU
W UMa	56006.50233	0.00014	Sec	C	RF34/135	RU
W UMa	56643.40780	0.00015	Sec	C	RF34/135	RU
W UMa	56643.57335	0.00015	Prim	C	RF34/135	RU
AC UMa	56416.43087	0.00233	Prim	R	OND	HK
AC UMa	56039.41622	0.00023	Prim	R	N200/1000	RU
AW UMa	56008.51449	0.00014	Prim	C	RF34/135	RU
AW UMa	56292.58695	0.00029	Sec	C	RF34/135	RU
AW UMa	56293.68393	0.00021	Prim	C	RF34/135	RU
AW UMa	56728.45986	0.00022	Prim	V	RF34/135	RU
AW UMa	56730.43381	0.00029	Sec	V	RF34/135	RU
DN UMa	56023.49296	0.00021	Prim	C	RF34/135	RU
DN UMa	56043.39102	0.00008	Sec	I	N200/1000	RU
DN UMa	56272.67141	0.00077	Prim	C	RF34/135	RU
DN UMa	56285.64928	0.00078	Sec	C	RF34/135	RU
DN UMa	56357.46389	0.00049	Prim	R	RF34/135	RU
DN UMa	56390.33259	0.00035	Prim	C	RF34/135	RU
DN UMa	56460.43606	0.00143	Sec	C	RF34/135	RU
DN UMa	56638.65705	0.00052	Sec	C	RF34/135	RU
DN UMa	56709.60384	0.00224	Sec	V	RF34/135	RU
DN UMa	56729.51191	0.00078	Prim	V	RF34/135	RU
GT UMa	56026.56655	0.00043	Prim	R	RF34/135	RU
GT UMa	56290.37226	0.00042	Sec	C	RF34/135	RU
GT UMa	56644.44444	0.00072	Sec	C	RF34/135	RU
GT UMa	56725.39150	0.00020	Prim	R	N200/1000	RU
HR UMa	55969.45907	0.00017	Sec	C	RF34/135	RU
HR UMa	55991.56678	0.00056	Sec	R	RF34/135	RU
HR UMa	55992.30224	0.00053	Prim	R	N200/1000	RU
HR UMa	56291.55036	0.00053	Prim	C	RF34/135	RU
HR UMa	56367.46972	0.00027	Sec	C	RF34/135	RU
HR UMa	56644.60348	0.00050	Sec	C	RF34/135	RU

Table 1: cont...

Star Name	HJD 24.....	Error	Type	Filter	Instrument/Source	Observer
HR UMa	56726.41880	0.00026	Prim	R	N200/1000	RU
HR UMa	56771.38002	0.00021	Sec	C	RF34/135	RU
HV UMa	56272.65753	0.00022	Sec	C	RF34/135	RU
HV UMa	56638.70040	0.00026	Sec	C	RF34/135	RU
II UMa	56057.47533	0.00040	Prim	C	RF34/135	RU
II UMa	56319.48641	0.00059	Sec	C	RF34/135	RU
II UMa	56713.53442	0.00069	Prim	R	N200/1000	RU
II UMa	56725.49983	0.00025	Sec	R	N200/1000	RU
NU UMa	56713.54861	0.00027	Sec	C	RF34/135	RU
NU UMa	56727.30304	0.00020	Prim	R	N200/1000	RU
AH Vir	56319.71358	0.00021	Prim	C	RF34/135	RU
AH Vir	56367.60030	0.00027	Sec	R	RF34/135	RU
AH Vir	56701.57173	0.00025	Prim	C	N150/750	RU
AH Vir	56727.44880	0.00018	Sec	R	RF34/135	RU
AZ Vir	56367.42446	0.00055	Sec	R	RF34/135	RU
DL Vir	55992.60284	0.00079	Prim	C	RF34/135	RU
DL Vir	56367.51750	0.00037	Prim	C	RF34/135	RU
DL Vir	56421.45190	0.00188	Prim	I	N200/1000	RU
DL Vir	56425.39663	0.00146	Prim	C	RF34/135	RU
HT Vir	56367.43401	0.00022	Prim	R	RF34/135	RU
HT Vir	56449.37603	0.00019	Prim	C	RF34/135	RU
HT Vir	56713.54838	0.00014	Prim	R	RF34/135	RU
HT Vir	56727.61304	0.00041	Sec	R	RF34/135	RU
HT Vir	56790.39604	0.00080	Sec	R	RF34/135	RU
HY Vir	56712.61157	0.00029	Sec	C	N150/750	RU
HY Vir	56771.35769	0.00046	Prim	C	N150/750	RU
LV Vir	56727.54318	0.00038	Prim	C	N150/750	RU
LV Vir	56758.45504	0.00032	Sec	C	N150/750	RU
Z Vul	56060.49958	0.00068	Sec	C	RF34/135	RU
Z Vul	56470.47174	0.00045	Sec	C	RF34/135	RU
Z Vul	56481.51879	0.00027	Prim	I	N200/1000	RU
Z Vul	56783.47369	0.00014	Prim	C	RF34/135	RU
Z Vul	56799.43381	0.00035	Sec	C	RF34/135	RU
BU Vul	56206.36421	0.00013	Prim	R	RF34/135	RU
V402 Vul	56487.52707	0.00019	Prim	R	N200/1000	RU
BD+58 2217	56131.42852	0.00021	Prim	R	N200/1000	RU
CSS_J172513.9+512625	56783.36740	0.00118	Prim	C	N150/750	RU
CSS_J172513.9+512625	56783.53025	0.00159	Sec	C	N150/750	RU
GSC 01742-01524	56564.37886	0.00048	Sec	R	N200/1000	RU
GSC 01742-01524	56564.54856	0.00047	Prim	R	N200/1000	RU
GSC 02405-01886^{B}	56728.40728	0.00038	Prim	R	OND	PZ
HD 6421	56569.51686	0.00047	Prim	R	N200/1000	RU
HD 24105	56569.45179	0.00046	Sec	C	RF34/135	RU
HD 24105	56596.60432	0.00019	Prim	R	N200/1000	RU
HD 24105	53174.07695	0.00253	Sec	V	ASAS	PZ
HD 24105	53174.70913	0.00081	Prim	V	ASAS	PZ
HD 24105	54630.22723	0.00293	Sec	V	ASAS	PZ
HD 24105	54630.85921	0.00260	Prim	V	ASAS	PZ
HD 24105	51520.28839	0.00136	Prim	V	NSVS	PZ
HD 24105	53322.46318	0.00450	Prim	C	PI of the sky	PZ
HD 24105	53323.08292	0.00375	Sec	C	PI of the sky	PZ
HD 24105	53347.72078	0.00351	Prim	C	PI of the sky	PZ
HD 24105	54451.51948	0.00378	Prim	C	PI of the sky	PZ
HD 24105	54452.15660	0.00125	Sec	C	PI of the sky	PZ

Table 1: cont...

Star Name	HJD 24.....	Error	Type	Filter	Instrument/Source	Observer
HD 24105	54005.71085	0.00055	Prim	W	SWASP	PZ
HD 24105	54007.60357	0.00142	Sec	W	SWASP	PZ
HD 24105	54031.60261	0.00077	Sec	W	SWASP	PZ
HD 24105	54050.54545	0.00098	Sec	W	SWASP	PZ
HD 24105	54057.49242	0.00037	Prim	W	SWASP	PZ
HD 24105	54067.59252	0.00053	Prim	W	SWASP	PZ
HD 24105	54069.49010	0.00059	Sec	W	SWASP	PZ
HD 24105	54076.43438	0.00116	Prim	W	SWASP	PZ
HD 24105	54083.37959	0.00087	Sec	W	SWASP	PZ
HD 24105	54093.48330	0.00052	Sec	W	SWASP	PZ
HD 24105	54095.38069	0.00259	Prim	W	SWASP	PZ
HD 24105	54124.42511	0.00165	Prim	W	SWASP	PZ
HD 55338	56631.48423	0.00088	Prim	C	RF34/135	RU
HD 55338	56293.49066	0.00078	Prim	C	RF34/135	RU
HD 55338	56318.33284	0.00039	Sec	R	N200/1000	RU
HD 55338	56623.62199	0.00171	Sec	C	RF34/135	RU
HD 55338	52411.37498	0.00286	Sec	V	ASAS	–
HD 55338	52411.97647	0.00199	Prim	V	ASAS	–
HD 55338	53023.15906	0.00144	Sec	V	ASAS	–
HD 55338	53023.76225	0.00108	Prim	V	ASAS	–
HD 55338	53402.94869	0.00172	Prim	V	ASAS	–
HD 55338	53403.56107	0.00235	Sec	V	ASAS	–
HD 55338	53765.78686	0.00409	Sec	V	ASAS	–
HD 55338	53766.38500	0.00137	Prim	V	ASAS	–
HD 55338	54358.78660	0.00130	Prim	V	ASAS	–
HD 55338	54359.40109	0.00235	Sec	V	ASAS	–
HD 55338	54951.80879	0.00413	Prim	V	ASAS	–
HD 55338	54952.40097	0.00240	Sec	V	ASAS	–
HD 63238	56718.52476	0.00270		C	RF34/135	RU
HD 63238	56758.41959	0.00035		C	Carona	RU
HD 63238	56272.50469	0.00148		C	RF34/135	RU
HD 63238	56292.45844	0.00130		C	RF34/135	RU
HD 99666	56356.43455	0.00026	Prim	R	RF34/135	RU
HD 99666	56712.47870	0.00033	Prim	R	N200/1000	RU
HD 174343	56504.37794	0.00145	Prim	C	RF34/135	RU
HD 174343	56523.45644	0.00098	Sec	C	RF34/135	RU
HD 174343	56750.49370	0.00572	Prim	C	N150/750	RU
HD 178661	56501.53501	0.00159	Sec	R	RF34/135	RU
HD 178661	56525.41503	0.00041	Prim	C	RF34/135	RU
HD 179923	56490.53827	0.00066	Prim	R	N200/1000	RU
HD 179923	56491.41459	0.00037	Prim	R	N200/1000	RU
HD 179923	56501.51355	0.00265	Sec	R	N200/1000	RU
HD 180848	56462.55338	0.00026	Prim	C	RF34/135	RU
HD 180848	56472.44618	0.00078	Prim	C	RF34/135	RU
HD 180848	56474.52932	0.00026	Prim	C	RF34/135	RU
HD 180848	56486.50586	0.00045	Prim	R	RF34/135	RU
HD 180848	56497.43930	0.00028	Prim	R	RF34/135	RU
HD 180848	56510.45725	0.00033	Prim	C	RF34/135	RU
HD 180848	56514.36159	0.00083	Sec	C	RF34/135	RU
HD 180848	56515.40269	0.00038	Sec	C	RF34/135	RU
HD 180848	56516.44247	0.00075	Sec	V	N200/1000	RU
HD 180848	56516.44255	0.00100	Sec	I	N200/1000	RU
HD 180848	56516.44274	0.00079	Sec	R	N200/1000	RU
HD 180848	56516.44285	0.00104	Sec	B	N200/1000	RU

Table 1: cont...

Star Name	HJD 24.....	Error	Type	Filter	Instrument/Source	Observer
HD 180848	56517.48441	0.00143	Sec	C	RF34/135	RU
HD 180848	56526.33798	0.00186	Sec	R	N200/1000	RU
HD 180848	56527.37837	0.00030	Sec	R	N200/1000	RU
HD 180848	56528.41989	0.00032	Sec	C	RF34/135	RU
HD 180848	56831.45467	0.00112	Sec	C	N150/750	RU
HD 180848	56851.50195	0.00025	Prim	C	N150/750	RU
HD 180848	56892.37354	0.00069	Sec	C	RF34/135	RU
HIP 57810	56272.61369	0.00170	Prim	C	RF34/135	RU
HIP 57810	56272.71907	0.00259	Sec	C	RF34/135	RU
HIP 57810	56285.61265	0.00179	Prim	C	RF34/135	RU
HIP 57810	56285.72596	0.00199	Sec	C	RF34/135	RU
HIP 57810	56638.59355	0.00257	Prim	C	RF34/135	RU
HIP 57810	56638.71449	0.00306	Sec	C	RF34/135	RU
HIP 57810	54573.42500	0.00521	Sec	W	SWASP	–
HIP 57810	54574.40155	0.00279	Prim	W	SWASP	–
HIP 57810	54575.44622	0.00252	Prim	W	SWASP	–
NSV 2698	56658.48132	0.00039	Prim	C	RF34/135	RU
NSV 2698	52067.65294	0.00184	Prim	V	ASAS	–
NSV 2698	52068.05427	0.00212	Sec	V	ASAS	–
NSV 2698	52810.21560	0.00113	Prim	V	ASAS	–
NSV 2698	52810.61692	0.00157	Sec	V	ASAS	–
NSV 2698	53624.53899	0.00178	Prim	V	ASAS	–
NSV 2698	53624.92717	0.00514	Sec	V	ASAS	–
NSV 2698	54343.71701	0.00138	Prim	V	ASAS	–
NSV 2698	54344.11337	0.01711	Sec	V	ASAS	–
NSV 2698	54884.71611	0.00059	Prim	V	ASAS	–
NSV 2698	54885.10116	0.01676	Sec	V	ASAS	–
NSV 2698	51534.71384	0.00083	Prim	V	NSVS	–
NSV 2698	51535.11375	0.00318	Sec	V	NSVS	–
NSVS 16400408	55707.57552	0.00018	Prim	R	OND	PZ
NSVS 16400408	56046.51711	0.00010	Sec	R	OND	PZ
NSVS 16400408	56400.55763	0.00010	Prim	R	OND	PZ
NSVS 16400408	56778.50287	0.00012	Prim	R	OND	HK
NSVS 7826147	55966.52660	0.00009	Prim	R	OND	PZ
SAO 34132	56568.51433	0.00080		V	RF34/135	RU
SAO 90888	56105.54807	0.00122		C	Carona	RU
TYC 2696-2866-1	56101.54752	0.00161	Sec	R	N200/1000	RU
TYC 2696-2866-1	54280.59938	0.00741	Sec	W	SWASP	PZ
TYC 2696-2866-1	54337.51365	0.00074	Prim	W	SWASP	PZ
TYC 2696-2866-1	54344.49644	0.00117	Prim	W	SWASP	PZ
TYC 3807-759-1^A	54439.61055	0.00087	Prim	W	SWASP	–
TYC 3807-759-1^A	54501.54810	0.00056	Prim	W	SWASP	–
TYC 3807-759-1^A	54501.66102	0.00055	Sec	W	SWASP	–
TYC 3807-759-1^A	54502.45885	0.00015	Prim	W	SWASP	–
TYC 3807-759-1^A	54503.48248	0.00172	Sec	W	SWASP	–
TYC 3807-759-1^A	54504.50841	0.00042	Prim	W	SWASP	–
TYC 3807-759-1^A	54524.43242	0.00142	Sec	W	SWASP	–
TYC 3807-759-1^A	54525.45700	0.00017	Prim	W	SWASP	–
TYC 3807-759-1^A	54530.46776	0.00001	Prim	W	SWASP	–
TYC 3807-759-1^A	54530.57760	0.00009	Sec	W	SWASP	–
TYC 3807-759-1^A	54534.45291	0.00087	Sec	W	SWASP	–
TYC 3807-759-1^A	54536.50225	0.00044	Sec	W	SWASP	–
TYC 3807-759-1^A	54539.46229	0.00064	Sec	W	SWASP	–
TYC 3807-759-1^A	54539.57600	0.00018	Prim	W	SWASP	–

Table 1: cont...

Star Name	HJD 24.....	Error	Type	Filter	Instrument/Source	Observer
TYC 3807-759-1^{A}	54540.37297	0.00057	Sec	W	SWASP	–
TYC 3807-759-1^{A}	54544.58336	0.00030	Prim	W	SWASP	–
TYC 3807-759-1^{A}	54545.49594	0.00011	Prim	W	SWASP	–
TYC 3807-759-1^{A}	54547.43181	0.00155	Sec	W	SWASP	–
TYC 3807-759-1^{A}	54553.35032	0.00034	Sec	W	SWASP	–
TYC 3807-759-1^{A}	54553.46761	0.00015	Prim	W	SWASP	–
TYC 3807-759-1^{A}	54555.40135	0.00026	Sec	W	SWASP	–
TYC 3807-759-1^{A}	54555.51810	0.00051	Prim	W	SWASP	–
TYC 3807-759-1^{A}	54556.42758	0.00010	Prim	W	SWASP	–
TYC 3807-759-1^{A}	54558.47720	0.00007	Prim	W	SWASP	–
TYC 3807-759-1^{A}	56241.51283	0.00088	Prim	R	N200/1000	RU
TYC 3807-759-1^{A}	56241.62948	0.00104	Sec	R	N200/1000	RU
TYC 3807-759-1^{A}	56282.50216	0.00027	Prim	R	N200/1000	RU
TYC 3807-759-1^{A}	56292.52156	0.00019	Prim	R	N200/1000	RU
TYC 3807-759-1^{A}	56354.46021	0.00014	Prim	R	N200/1000	RU
TYC 3807-759-1^{A}	56355.37105	0.00019	Prim	R	N200/1000	RU
TYC 3807-759-1^{A}	56357.30799	0.00012	Sec	R	N200/1000	RU
TYC 3807-759-1^{A}	56357.42041	0.00018	Prim	R	N200/1000	RU
TYC 3807-759-1^{A}	56367.32729	0.00011	Sec	R	N200/1000	RU
TYC 3807-759-1^{A}	56367.43950	0.00016	Prim	R	N200/1000	RU
TYC 3807-759-1^{A}	56395.33610	0.00026	Sec	R	N200/1000	RU
TYC 3807-759-1^{A}	56395.44887	0.00057	Prim	R	N200/1000	RU
TYC 3807-759-1^{A}	56397.38565	0.00015	Sec	R	N200/1000	RU
TYC 3807-759-1^{A}	56397.49805	0.00015	Sec	R	N200/1000	RU
TYC 3807-759-1^{A}	56666.31538	0.00021	Sec	R	N200/1000	RU
TYC 3807-759-1^{A}	56666.42946	0.00018	Prim	R	N200/1000	RU
TYC 3807-759-1^{A}	56666.54276	0.00017	Sec	R	N200/1000	RU
TYC 3807-759-1^{A}	56673.37364	0.00017	Sec	R	N200/1000	RU
TYC 3807-759-1^{A}	56673.48843	0.00017	Prim	R	N200/1000	RU
TYC 3807-759-1^{A}	56683.28042	0.00027	Sec	R	N200/1000	RU
TYC 3807-759-1^{A}	56683.39486	0.00035	Prim	R	N200/1000	RU
TYC 3807-759-1^{A}	56692.27457	0.00017	Prim	R	N200/1000	RU
TYC 3807-759-1^{A}	56692.38881	0.00014	Sec	R	N200/1000	RU
TYC 3807-759-1^{A}	56692.50293	0.00023	Prim	R	N200/1000	RU
TYC 3807-759-1^{A}	56701.49740	0.00012	Sec	R	N200/1000	RU
TYC 3807-759-1^{A}	56701.61116	0.00036	Prim	R	N200/1000	RU
TYC 3807-759-1^{A}	56706.62052	0.00021	Sec	R	N200/1000	RU
TYC 3807-759-1^{B}	54427.63955	0.02002	Prim	W	SWASP	PZ
TYC 3807-759-1^{B}	54436.77003	0.02749	Prim	W	SWASP	PZ
TYC 3807-759-1^{B}	54438.73127	0.01582	Sec	W	SWASP	PZ
TYC 3807-759-1^{B}	54527.51440	0.00171	Sec	W	SWASP	PZ
TYC 3807-759-1^{B}	54533.38838	0.00087	Prim	W	SWASP	PZ
TYC 3807-759-1^{B}	54535.35024	0.00034	Sec	W	SWASP	PZ
TYC 3807-759-1^{B}	54544.48276	0.00066	Sec	W	SWASP	PZ
TYC 3807-759-1^{B}	56245.60618	0.00063	Sec	R	N200/1000	RU
TYC 3807-759-1^{B}	56292.60644	0.00102	Sec	R	N200/1000	RU
TYC 3807-759-1^{B}	56354.61749	0.00019	Prim	R	N200/1000	RU
TYC 3807-759-1^{B}	56356.57558	0.00060	Sec	R	N200/1000	RU
TYC 3807-759-1^{B}	56366.36772	0.00015	Prim	R	N200/1000	RU
TYC 3807-759-1^{B}	56368.32861	0.00133	Sec	R	N200/1000	RU
TYC 3807-759-1^{B}	56396.39603	0.00027	Prim	R	N200/1000	RU
TYC 3807-759-1^{B}	56396.47477	0.00021	Sec	R	N200/1000	RU
TYC 3807-759-1^{B}	56398.35323	0.00069	Sec	R	N200/1000	RU
TYC 3807-759-1^{B}	56428.37839	0.00183	Sec	R	N200/1000	RU

Table 1: cont...

Star Name	HJD 24.....	Error	Type	Filter	Instrument/Source	Observer
TYC 3807-759-1^B	56647.70805	0.00151	Sec	R	N200/1000	RU
TYC 3807-759-1^B	56657.50441	0.00010	Prim	R	N200/1000	RU
TYC 3807-759-1^B	56695.36398	0.00140	Prim	R	N200/1000	RU
TYC 3807-759-1^B	56700.58736	0.00011	Prim	R	N200/1000	RU
TYC 3807-759-1^B	56706.46126	0.00014	Sec	R	N200/1000	RU
TYC 4046-00154-1	55096.41329	0.00169		V	RF34/135	RU
TYC 4046-00154-1	56211.51118	0.00040		C	RF34/135	RU
TYC 4046-00154-1	56272.41334	0.00034		C	RF34/135	RU
TYC 4046-00154-1	56554.56461	0.00124		C	RF34/135	RU
TYC 4046-00154-1	56622.44040	0.00023		C	RF34/135	RU
TYC 4046-00154-1	56622.64379	0.00035		C	RF34/135	RU
TYC 4048-01455-1	56181.50509	0.00069	Sec	R	N200/1000	RU
TYC 4048-01455-1	56201.58395	0.00070	Prim	R	N200/1000	RU
TYC 4048-01455-1	56203.48295	0.00042	Sec	R	N200/1000	RU
TYC 4315-01566-1	56542.51481	0.00082		R	RF34/135	RU
TYC 5112-00252-1	56456.43123	0.00039		R	RF34/135	RU
TYC 5423-01246-1	56342.42845	0.00095		C	RF34/135	RU

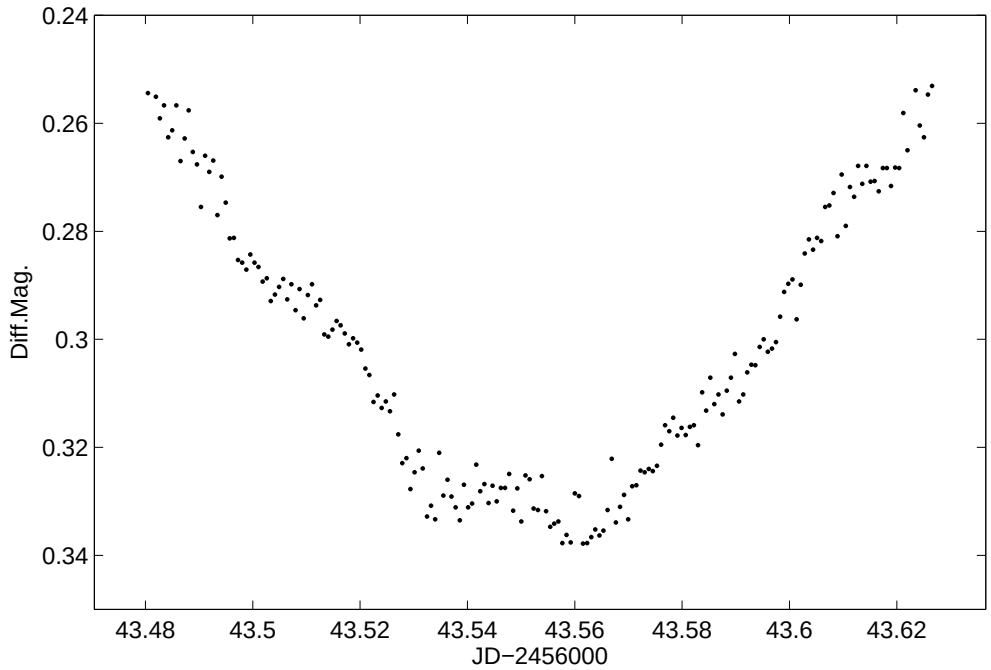

Figure 1. Primary minimum of GQ Dra, the periodic pulsations are clearly visible.

References:

Bessell, M. S. 1990, PASP, **102**, 1181
Kwee, K. K., van Woerden, H., 1956, *Bull. Astron. Inst. Neth.*, **12**, 327.
Paschke, A., Brát, L., 2006, *OEJV*, **23**, 13

COMMISSIONS 27 AND 42 OF THE IAU
INFORMATION BULLETIN ON VARIABLE STARS

Number 6115

Konkoly Observatory
Budapest
30 September 2014

HU ISSN 0374 – 0676

V363 And – A DETACHED ECLIPSING BINARY

NELSON, ROBERT H.[1,2]

[1] 1393 Garvin Street, Prince George, BC, Canada, V2M 3Z1 email: bob.nelson@shaw.ca

[2] Guest investigator, Dominion Astrophysical Observatory, Herzberg Institute of Astrophysics, National Research Council of Canada

V363 And (= TYC 2305-272-1 = HIP 7122 = SAO 54757) is listed in the General Catalogue of Variable Stars (Samus et al., 2007-2012) as a β Lyrae (EB) type with an epoch of 2448500.3980, a period of 1.27799 days and a spectral type of A2. Its photometric variability was discovered from the data of the Hipparcos mission. Accordingly, it was added to the author's observing programme.

The first task was to establish the proper elements (epoch, period) for phasing. All available eclipse timings—together with two new timings—are listed in Table 1.

Table 1. All available eclipse timings for V363 And.

Source	Type	HJD−2400000	Error (d)	Detector	Filters
Selam et al. (2003)	II	52855.2955	0.0002	Photomultiplier	B, V
Aksu et al. (2005)	II	52925.3790	0.0007	Photomultiplier	B, V
Senavci et al. (2007)	I	53640.3931	0.0005	Photomultiplier	B, V
Senavci et al. (2007)	I	53649.3501	0.0006	Photomultiplier	B, V
Paschke (2011)	I	55856.413	0.01	CCD	??
This work	II	56545.8793	0.0003	CCD	V, R, I
This work	I	56547.7958	0.0005	CCD	V, R, I

These yielded the eclipse timing (ET) diagram (a.k.a. O–C diagram) of Fig. 1. (The value labelled 'BAD?' is the third timing in Table 1 and was not included in the least-square fit.)

The least-squares best fit relation to fit the curve was found to be:

$$\mathrm{HJD\,(min\,I)} = 2456547.7963(6) + 1.2779742(3)\,\mathrm{E} \qquad (1)$$

Accordingly, these elements were used for all phasing.

In September of 2011, the author took 10 medium resolution spectra at the DAO. The grating (#21181) was 1800 lines/mm, blazed at 5000 Å and used in first order, reciprocal linear dispersion = 10 Å/mm, resolving power = 10000. The camera used was the SITe-2. The spectral range covered was from 4995 to 5256 Å, approximately.

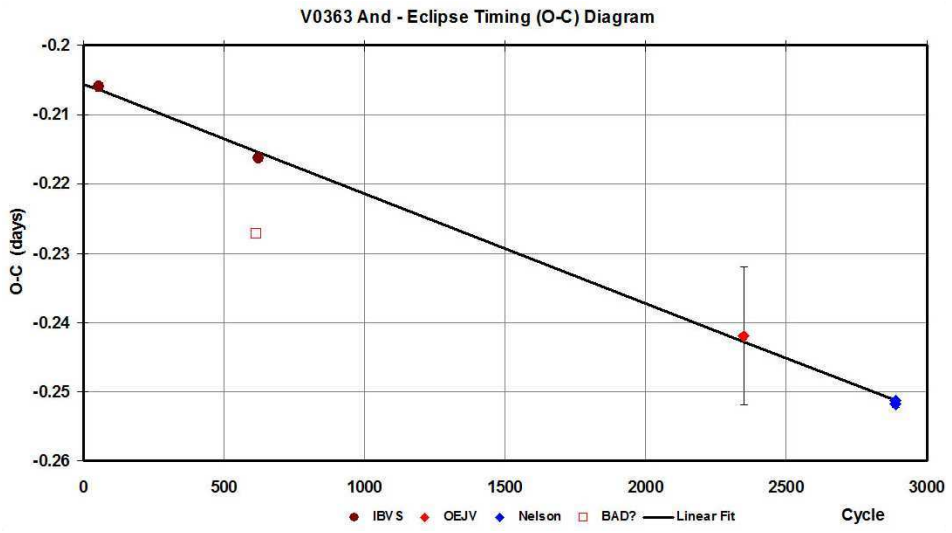

Figure 1. Eclipse timing diagram for V363 And.

The author then used the Rucinski broadening functions (Rucinski, 2004) to obtain radial velocity (RV) curves (see Nelson, et al. (2006) and Nelson (2010) for details). A log of DAO observations and RV results is presented in Table 2. In order to correct for the small phase smearing, the RVs were increased by 1% (in this case) in the following way: the RVs were divided by the factor $f = (\sin X)/X$ (where $X = 2\pi\, t/P$ and t = exposure time, P = period). For spherical stars, the correction is exact; in other cases, it can be shown to be close enough for any deviations to fall below observational errors.

Table 2. Log of DAO observations.

DAO Image #	Mid Time (HJD−2400000)	Exposure (sec)	Phase at mid-exp	V1 (km/s)	V2 (km/s)
7833	55808.7963	3600	0.741	151.3	−127.3
7895	55810.8335	3600	0.335	−114.7	131.5
7945	55811.9451	1800	0.205	−124.5	147.5
7995	55813.8675	1800	0.709	131.5	−138.4
8063	55815.8617	1800	0.270	−136.9	141.2
8065	55815.8840	1800	0.287	−129.7	141.8
8102	55816.9864	1200	0.150	−106.7	123.8
8116	55817.7711	1800	0.764	146.6	−131.5
8121	55817.7932	1800	0.781	142.7	−128.9
8127	55817.8497	1800	0.825	131.6	−119.2

In fitting two simple sine functions to the data, an overall rms deviation of 3.4 km/s was noted. These two best-fit functions yielded the following parameters:

$$K_1 = 141.0 \pm 1.0\,\text{km/s},\ \text{K}_2 = 139.6 \pm 0.9\,\text{km/s},\ \text{and}\ \text{V}_\gamma = 6.6 \pm 4.3\,\text{km/s}.$$

In September-October of 2013, the author took a total of 775 frames in V, 737 in R_C (Cousins) and 771 in the I_C (Cousins) band at his private observatory in Prince

George, BC, Canada. (The telescope was a 33 cm f/4.5 Newtonian on a Paramount ME mount; the camera was an SBIG ST-10XME. Standard reductions were then applied. The comparison and check stars are listed in Table 3. The coordinates and magnitudes are from the Tycho Catalogue, Hog, et al., 2000.)

Table 3. Details of variable, comparison and check stars.

Type of target	GSC 2305-	R.A. J2000	Dec. J2000	V (Tycho) mag	$B-V$ mag
Variable	0272	$01^h31^m46^s.573$	$+36°05'37''.99$	9.06	0.25
Comparison	0270	$01^h31^m50^s.457$	$+36°03'40''.07$	9.90	1.02
Check	1196	$01^h31^m09^s.6886$	$+36°04'56''.961$	11.12	0.98

In view of the number of data points, the author binned the data into phase bins of width 0.01. He then used the 2004 version of the Wilson-Devinney (WD) light curve and radial velocity analysis program with Kurucz atmospheres (Wilson and Devinney, 1971, Wilson, 1990, Kallrath et al., 1998) as implemented in the Windows front-end software WDwint (Nelson, 2009) to analyze the data. To get started, a spectral type A2 (SIMBAD; no reference given) was used. If the system were main sequence, this would correspond to a temperature $T_1 = 9000$ K (Cox, 2000). However, best-fit models using this temperature yielded masses of 1.70 $M_\odot$, too low for the interpolated standard value of 2.50 $M_\odot$ given in Cox (2000). From an inspection of the interpolated table, a spectral type of A8-9 was found to yield masses of 1.75 and 1.67 solar masses, respectively more in keeping with the computed values. Therefore a temperature of $T_1 = 7554 \pm 255K$ (the mean of 7640 and 7468) and $\log g = 4.285 \pm 0.003$ [cgs] (the mean of 4.284 and 4.286) were adopted. (The errors correspond to an error of one spectral sub-class.) An interpolation program by Terrell (1994, available from Nelson 2009) gave the Van Hamme (1993) limb darkening values; and finally, a square root (LD = 3) law for the limb-darkening coefficients was selected, appropriate for hotter temperatures (ibid).

From the GCVS 4 designation and from the shape of the light curve mode 2 (detached binary) was used. Convergence by the method of multiple subsets was reached in a small number of iterations. Radiative envelopes for both stars were used, appropriate for hotter stars (hence the values of gravity exponent, g = 1.00 and albedo, A = 1.00 were used for each). The limb darkening coefficients are listed in Table 4.

Table 4. Limb darkening values from Van Hamme (1993).

Band	x1	x2	Y1	y2
Bol	0.210	0.224	0.525	0.512
V	0.120	0.132	0.684	0.675
R_C	0.070	0.084	0.634	0.625
I_C	0.026	0.040	0.563	0.548

During the initial stages of modelling, it was discovered that no solution was possible without third light (see below). It was tempting to add a spot to improve the fit of the computed solution at the shoulders of the secondary minimum; however, the fit improved

only very slightly at the expense of adding four new parameters. Therefore, the spot was abandoned.

The model is presented in Table 5. Note again that the quoted error in T_2 listed above, output by the WD program, refers to the error relative to T_1. This error, when added statistically to the error in T_1 quoted below, yields an absolute error of 85 K for T_2 (see Table 6). If the error in classification is a full spectral sub-class, the estimated errors in T_1 and T_2 would rise to 255 K.

Detailed reflections were eventually used, with nref = 3, but little or no change in parameters ensued. The binned and unbinned light curve data and the their fits are displayed in Figures 2 and 3, respectively.

Table 5. Wilson-Devinney parameters.

WD Quantity	Binned Value	Binned error	Unbinned Value	Unbinned error	Unit
$q = M_2/M_1$	0.9896	0.0038	0.9896	0.0036	—
Temperature T_1	7554	[fixed]	7554	[fixed]	K
Temperature T_2	7534	7	7529	4	K
Potential Ω_1	4.722	0.013	4.725	0.007	—
Potential Ω_2	4.939	0.017	4.938	0.011	—
Inclination, i	72.83	0.13	72.83	0.08	deg
Semi-maj. axis a	7.463	0.017	7.463	0.024	s.u.
V_γ	6.60	0.28	6.60	0.43	km/s
Phase shift	-0.0002	0.0003	-0.0002	0.0002	—
3rd light EL3 (V)	0.019	0.008	0.019	0.005	—
3rd light EL3 (R)	0.029	0.008	0.029	0.005	—
3rd light EL3 (I)	0.036	0.009	0.036	0.004	—
$L_1/(L_1+L_2)$ (V)	0.5366	0.0022	0.5367	0.0012	—
$L_1/(L_1+L_2)$ (R_C)	0.5354	0.0022	0.5354	0.0013	—
$L_1/(L_1+L_2)$ (I_C)	0.5495	0.0022	0.5341	0.0012	—
r_1 (pole)	0.2656	0.0010	0.2654	0.0006	s.u.
r_1 (point)	0.2822	0.0013	0.2819	0.0008	s.u.
r_1 (side)	0.2707	0.0011	0.2705	0.0006	s.u.
r_1 (back)	0.2781	0.0012	0.2779	0.0007	s.u.
r_2 (pole)	0.2497	0.0012	0.2498	0.0009	s.u.
r_2 (point)	0.2623	0.0015	0.2625	0.0011	s.u.
r_2 (side)	0.2537	0.0013	0.2538	0.0009	s.u.
r_2 (back)	0.2595	0.0014	0.2596	0.0010	s.u.
$\Sigma\omega\,\mathrm{res}^2$	0.00300	—	0.0538	—	—

The radial velocities are shown in Fig. 4. A three dimensional representation from Binary Maker 3 (Bradstreet, 1993) is shown in Fig. 5.

The WD output fundamental parameters and errors are listed in Table 6. Most of the errors are output or derived estimates from the WD routines. The fill factor $f = (\Omega^I - \Omega)/(\Omega^I - \Omega^O)$, where Ω is the modified Kopal potential of the system, Ω^I is that

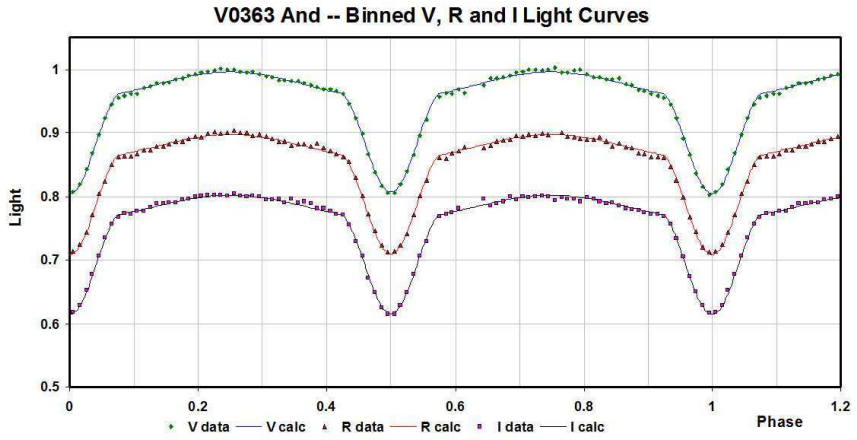

Figure 2. V363 And: V, R_C, and I_C light curves – binned data and WD fit.

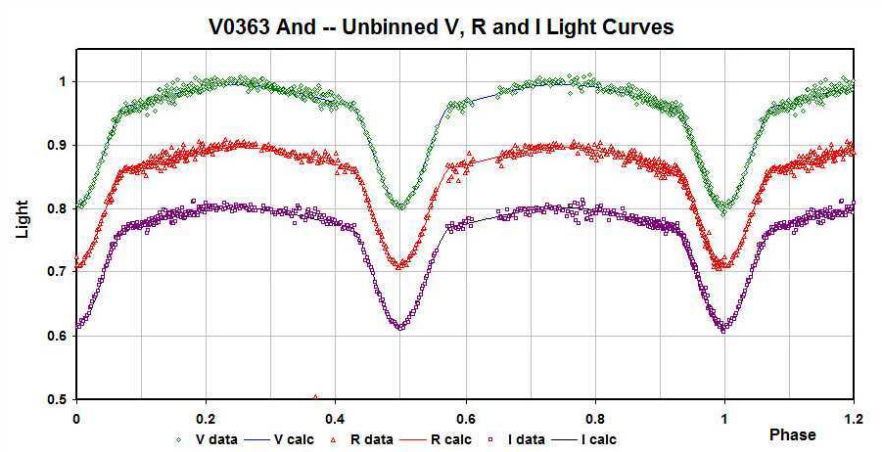

Figure 3. V363 And: V, R_C, and I_C light curves – unbinned data and WD fit.

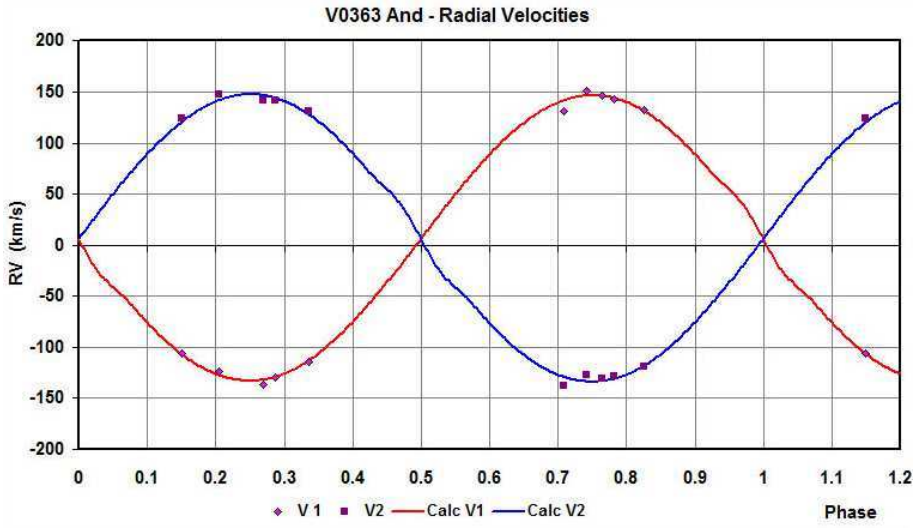

Figure 4. V363 And: radial velocity curves – data and WD fit.

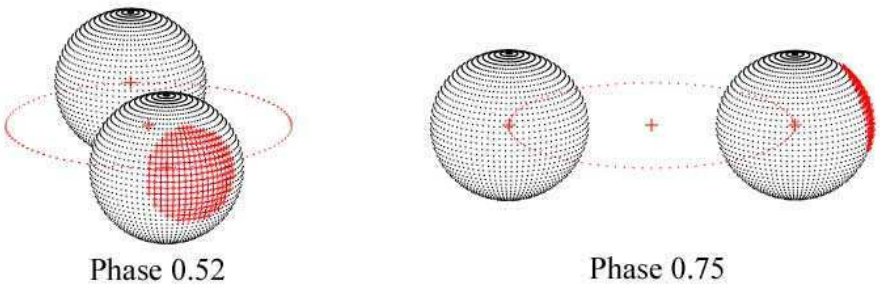

Figure 5. Binary Maker 3 representation of the system – at phases 0.52 and 0.75.

of the inner Lagrangian surface, and Ω^O, that of the outer Lagrangian surface, was also calculated.

Table 6. Fundamental parameters.

Quantity	Value	Error	unit
Temperature, T_1	7554	255	K
Temperature, T_2	7534	255	K
Mass, M_1	1.722	0.026	$M_\odot$
Mass, M_2	1.704	0.025	$M_\odot$
Radius, R_1	2.03	0.01	$R_\odot$
Radius, R_2	1.90	0.01	$R_\odot$
M_{bol}, 1	2.09	0.02	mag
M_{bol}, 2	2.24	0.02	mag
Log g_1	4.06	0.01	cgs
Log g_2	4.11	0.01	cgs
Luminosity, L_1	12.0	0.2	$L_\odot$
Luminosity, L_2	10.5	0.2	$L_\odot$
Distance, r	280	12	pc

To determine the distance r, the following procedure was followed: first the WD routine gave the absolute bolometric magnitudes of each component; these were then converted to the absolute visual magnitudes of both, $M_{V,1}$ and $M_{V,2}$, using the bolometric correction BC $= -0.108$. The latter datum was taken from interpolated tables in Cox (2000). The absolute V magnitudes of the total system were then determined by the usual rules for addition, getting $M_V = 1.518 \pm 0.037$ magnitude. The apparent magnitude in the V passband was 9.06 ± 0.02 magnitudes taken from the Tycho catalogue (Hog et al., 2000) and converted to the Johnson system (Kidger, no date) yielding $V = 9.01 \pm 0.02$ magnitude. However, the author's ensemble magnitude (taken using all the Tycho stars as standards and at phases 0.25 and 0.75) yielded $V = 8.91 \pm 0.02$ magnitudes. This was considered more reliable because it was not known at what phase the Tycho value was determined.

It was then necessary to estimate the galactic extinction $A_V = R \cdot E[B-V]$ where $E[B-V] = (B-V)_{\rm obs} - (B-V)_{\rm tables}$ is the colour excess, and $R =$ the reddening coefficient. (The value 3.1 was adopted.) Unfortunately, the Tycho B and V values

lacked the precision to give meaningful results (unreasonable values near $A_V = 0.2$ were obtained). Fortunately, the dust maps of Schlegel et al (1998) (images available at Schlegel et al., (2013)) provided a maximum value of $E[B-V] = 0.051$ magnitudes[1] for the galactic coordinates of V363 And. Adopting that value, distances were obtained from the standard relation:

$$r = 10^{0.2\times(V-M_V-A_V+5)} \text{ parsecs}$$

The errors were assigned as follows: $\delta M_{bol,1} = \delta M_{bol,2} = 0.02$, $\delta BC_1 = \delta BC_2 = 0.017$ (1.5x the variation of a spectral sub-class), $\delta V = 0.02$, $\delta E(B-V) = 0.026$, all in magnitudes, and $\delta R = 0.1$. Combining the errors rigorously yielded estimated errors in r of 17 pc. It was noted that the result was not overly sensitive to the value of $E[B-V]$ that was chosen. Dropping the value of $E[B-V]$ to half the Schlegel et al.'s value raised the distance by only 10 pc.

Van Leeuwen (2007), in a new reduction of Hipparcos data, derived a parallax value of 2.18 ± 1.02 mas, which yields a distance of $r = 459 \pm 214$ pc. The value for the distance presented here certainly lies within this large range. Also (as pointed out by an anonymous referee) it is not clear whether the Hipparcos value is valid for binary systems.

Reference to the evolutionary tracks of Schaller et al. (1992) for metallicity $Z = 0.02$ (approximately solar) and the derived masses revealed a reasonable fit at age $8.7 \cdot 10^8$ years for the luminosities and temperatures (see Table 7).

Table 7. Luminosities and temperatures compared to theoretical evolved values of Schaller et al. (1992).

Star	Mass ($M_\odot$)	Luminosity this paper	Luminosity Schaller	Temperature this paper	Temperature Schaller
1	1.722	12.0	10.80	7554	7544
2	1.704	10.5	10.17	7534	7537

In conclusion, this detached system of two stars, nearly equal in mass, is evolved and has an approximate age of $8.7 \cdot 10^8$ years. The luminosity of each star falls close to the theoretical value; discrepancies may result from differences in the metallicity from the assumed value of $Z = 0.02$.

An anonymous referee has pointed out that the primary is close to the delta Scuti instability strip and hence it is a candidate to δ Scuti stars in eclipsing binaries (Soydugan et al., 2006), and the star was also observed to search forδ Scuti-like pulsations for a short time (Liakos et al., 2012).

Acknowledgements:

It is a pleasure to thank the staff members at the DAO (especially Dmitry Monin and Les Saddlemyer) for their usual splendid help and assistance.

[1]Since the $E[B-V]$ values were derived from the far-infrared all-sky images, this means that the former apply for a light path from the observer all the way through the Galaxy (in the specified direction), and therefore represent an upper limit for the appropriate value for a star lying somewhat closer than the far edge. The error estimate in this quantity has been set to 50% of this value, and is then an appreciable contributor to the overall error in r.

References:

Aksu, O., et al., 2005, *IBVS*, No. 5588

Bradstreet, D.H., 1993, "Binary Maker 2.0 – An Interactive Graphical Tool for Preliminary Light Curve Analysis", in Milone, E.F. (ed.) Light Curve Modelling of Eclipsing Binary Stars, pp 151-166 (Springer, New York)

Cox, A.N., ed., 2000, Allen's Astrophysical Quantities, 4th ed., (Springer-Verlag, New York, NY)

Hog, E. et al., 2000, *A&A*, **355**, L27

Kallrath, J., Milone, E.F., Terrell, D., Young, A.T., 1998, *ApJ*, **508**, 308.

Kidger, M., `http://www.britastro.org/asteroids/Tycho%20Photometry.htm`

Liakos, A., Niarchos, P., Soydugan, E., Zasche, P., 2012, *MNRAS*, **422**, 1250

Nelson, R.H., Terrell, D., and Gross, J., 2006, *IBVS*, No. 5715

Nelson, R.H., 2009, Software, by Bob Nelson, `http://members.shaw.ca/bob.nelson/software1.htm`

Nelson, R.H., 2010, "Spectroscopy for Eclipsing Binary Analysis" in The Alt-Az Initiative, Telescope Mirror & Instrument Developments (Collins Foundation Press, Santa Margarita, CA), R.M. Genet, J.M. Johnson and V. Wallen (eds)

Paschke, A., 2012, *OEJV*, 142

Rucinski, S. M. 2004, *IAU Symp.*, **215**, 17

Samus N.N., et al., 2007-2012, General Catalogue of Variable Stars, `http://www.sai.msu.su/gcvs/cgi-bin/search.htm`

Schaller, G., Schaerer, D., Meynet, G. and Maeder, A., 1992, *A&AS*, **96**, 269

Schlegel, D.J., Finkbeiner, D.P., Davis, M., 1998, *ApJ*, **500**, 525

Schlegel, D.J., Finkbeiner, D.P. & Krigel, A., 2013, `http://www.astro.princeton.edu/~schlegel/dust/data/data.html`

Selam, S. O., et al., 2003, *IBVS*, No. 5471

Senavci, H.V., et al., 2007, *IBVS*, No. 5754

Soydugan, E., Soydugan, F., Demircan, O., Ibanoglu, C., 2006, *MNRAS*, **370**, 2013

Terrell, D., 1994, Van Hamme Limb Darkening Tables, vers. 1.1.

Van Hamme, W., 1993, *AJ*, **106**, 2096

Van Leeuwen, F., 2007, *A&A*, **474**, 653

Wilson, R.E., & Devinney, E.J., 1971, *ApJ*, **166**, 605

Wilson, R.E., 1990, *ApJ*, **356**, 613

COMMISSIONS 27 AND 42 OF THE IAU
INFORMATION BULLETIN ON VARIABLE STARS

Number 6116

Konkoly Observatory
Budapest
10 October 2014

HU ISSN 0374 – 0676

NEW GALACTIC DOUBLE PERIODIC VARIABLES

MENNICKENT, R.E.; ROSALES, J.

Astronomy Department, University of Concepción, Concepción, Chile. e-mail: rmennick@udec.cl

We have searched the ASAS[1] catalogue of semi-detached eclipsing binaries (Pojmański 1997) for interacting binaries of the type Double Periodic Variable (DPV). These are intermediate-mass binaries characterized by a long photometric period lasting about 33 times the orbital period (Mennickent et al. 2003, 2012a, 2013, Poleski et al. 2010). This long periodicity has been interpreted as evidence of mass loss cycles (Mennickent et al. 2008, 2012b). We performed a visual inspection of the light curves provided by ASAS, and selected DPV candidates characterized by long-term tendencies in the upper and lower boundaries of the forest of data points. We determined the orbital and long periods by using the PDM IRAF[2] program (Stellingwerf 1978). Errors for the orbital periods were estimated by visually inspecting the light curves phased with trial periods near the minimum of the periodogram. Then we disentangled the two main photometric frequencies by using a code specially designed for this purpose by Zbigniew Kołaczkowski. The code adjusts the orbital signal with a Fourier series consisting of the fundamental frequency plus their harmonics. Then it removes this signal from the original time series letting the long periodicity present in a residual light curve. The program fits this remaining signal with another Fourier series consisting of a fundamental frequency and harmonics and removes it. As result we obtain the cleaned light curve with no additional frequencies and two light curves for the isolated orbital and long frequencies. Following this procedure we found two new DPVs and 3 DPV candidates. In the second group the long cycle is observed almost once and it is of low amplitude, so the classification is uncertain. The result of this search is summarized in Tables 1 and 2. The disentangled light curves are shown in Figures 1 and 2.

The two confirmed new DPVs are V495 Cen and V4142 Sgr. They show a total primary eclipse and have relatively long orbital periods. They are ideal targets for follow-up spectroscopic studies and light curve modeling. All stars in Table 1 show longer orbital period than those 11 Galactic DPVs reported by Mennickent et al. (2012a). For the suspected DPVs half of the orbital period was also a possible solution; we followed the ASAS choice, giving a period ratio around 33. We checked the WISE image survey[3] (Wright et al. 2010), especially in the band W4, and find that none of these targets show evidence of close nebulosity, which could be relevant when discussing systemic mass loss and evolutionary stage.

[1] http://www.astrouw.edu.pl/asas/

[2] IRAF is distributed by the National Optical Astronomy Observatories, which are operated by the Association of Universities for Research in Astronomy, Inc., under cooperative agreement with the National Science Foundation.

[3] http://irsa.ipac.caltech.edu/applications/wise/

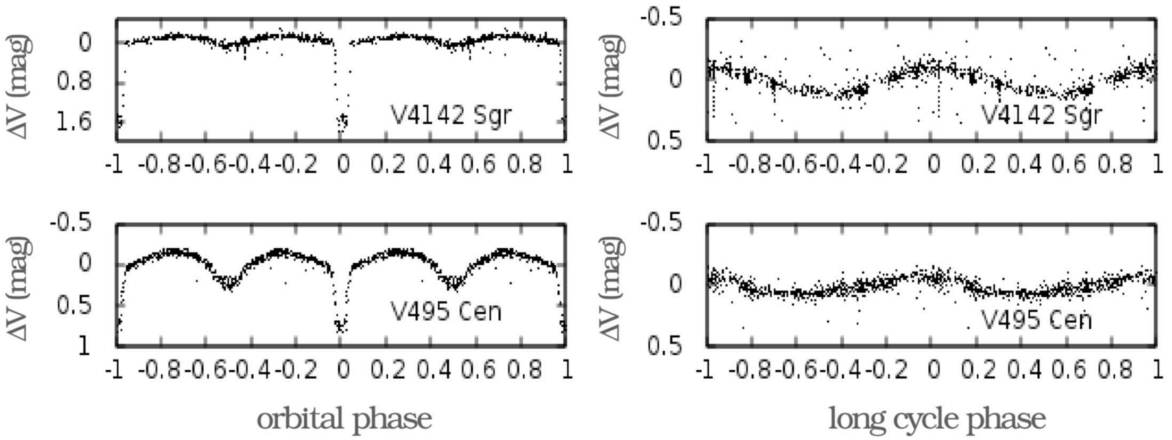

Figure 1. Disentangled ASAS V-band light curves of the new confirmed Double Periodic Variables.

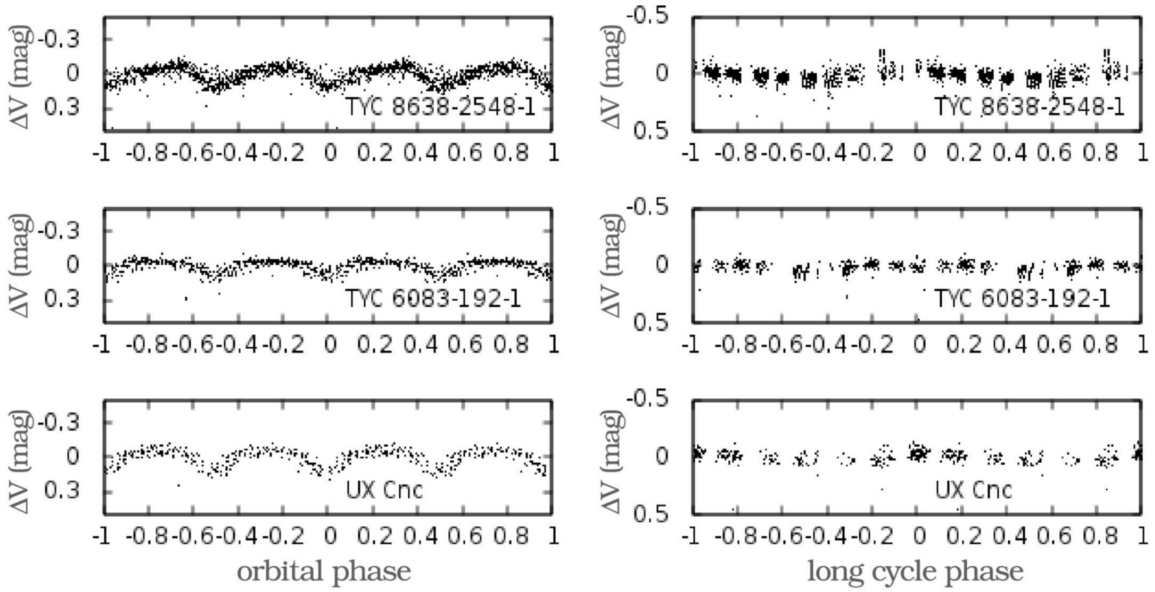

Figure 2. Disentangled ASAS V-band light curves of the new candidate Double Periodic Variables.

Table 1: New confirmed Double Periodic Variables and their orbital (P_o) and long (P_l) periods. Epochs for the minimum brightness of the orbital light curve and the maximum brightness of the long-cycle light curve are also given.

ASAS-ID	Other ID	RA (2000)	DEC (2000)	P_o (days)	P_l (days)	$T_0(min_o)$ −2450000	$T_0(max_l)$ −2450000	V (ASAS) (mag)
130135−5605.5	V0495 Cen	13:01:35	−56:05:30	33.490(18)	1283	4609.8460	4894.6	9.9
180745−2824.1	V4142 Sgr	18:07:45	−28:24:06	30.633(27)	1206	4726.5550	3546.7	10.95

Table 2: New candidates Double Periodic Variables and their orbital (P_o) and long (P_l) periods. Epochs for the minimum brightness of the orbital light curve and the maximum brightness of the long-cycle light curve are also given. Brightness values are from the ASAS database.

ASAS-ID	Other ID	RA (2000)	DEC (2000)	P_o (days)	P_l (days)	$T_0(min_o)$ −2450000	$T_0(max_l)$ −2450000	V (mag)
090329+0735.7	UX Cnc	09:03:29	07:35:42	84.761(10)	2158:	2715.5975	2703.4	11.75
111014−2007.1	TYC 6083-192-1	11:10:14	−20:07:06	90.386(60)	3497:	3125.4230	3799.8	9.37
114033−5641.8	TYC 8638-2548-1	11:40:33	−56:41:48	101.295(22)	3400:	3423.3300	2471.0	10.51

Acknowledgements: We acknowledge support by VRID-Enlace 214.016.001-1.0 and the BASAL Centro de Astrofísica y Tecnologías Afines (CATA) PFB–06/2007.

References:

Mennickent R. E., Pietrzyński G., Diaz M., Gieren W., 2003, *A&A*, **399**, L47

Mennickent R. E., Kołaczkowski Z., Michalska G., Pietrzyński G., Gallardo R., Cidale L., Granada A., Gieren W., 2008, *MNRAS*, **389**, 1605

Mennickent R. E., Djurašević G., Kołaczkowski Z., Michalska G., 2012a, *MNRAS*, **421**, 862

Mennickent R. E., Kołaczkowski Z., Djurašević G., Niemczura E., Diaz M., Curé M., Araya I., Peters G. J., 2012b, *MNRAS*, **427**, 607

Mennickent R. E., 2013, *Central European Astrophysical Bulletin*, **37**, 41

Pojmański G., 1997, *AcA*, **47**, 467

Poleski R., Soszyński I., Udalski A., Szymański M. K., Kubiak M., Pietrzyński G., Wyrzykowski Ł., Ulaczyk K., 2010, *AcA*, **60**, 179

Stellingwerf R. F., 1978, *ApJ*, **224**, 953

Wright E. L., Eisenhardt R. M., Mainzer A. K., et al. 2010, *AJ*, **140**, 1868

*This version of the paper contains corrections, and differs from the one appeared on-line originally. Date of last modification: Wed Oct 29 13:24:24 CET 2014

COMMISSIONS 27 AND 42 OF THE IAU
INFORMATION BULLETIN ON VARIABLE STARS
Number 6117

Konkoly Observatory
Budapest
10 October 2014

HU ISSN 0374 – 0676

CH CYGNI: NEW BRIGHTENING IN 2014

RSPAEV, F.; KONDRATYEVA, L.; AIMURATOV, E.

Fessenkov Astrophysical Institute, Almaty, Kazakhstan. e-mail: kondr.lud@gmail.com; lu_kondr@mail.ru

The brightest symbiotic object CH Cygni has undergone several outbursts. Numerous papers are devoted to the study of this object. A summary of observational history of CH Cyg was presented in the paper of Contini et al. (2009). The last flash took place in 1998-2000 (Skopal et al. 2004) and was followed by a quiescent phase. Then in 2006 a drop to a very low optical state was registered. Later it was interrupted by two short brightenings up to $\sim 8^{\rm m}$ in V filter, observed during 2009 July and from 2009 September to the end of the year (Skopal et al. 2012). Spectral observations are discussed in many papers as well (e.g., Burmeister et al. 2009, and Wallerstein et al. 2010).

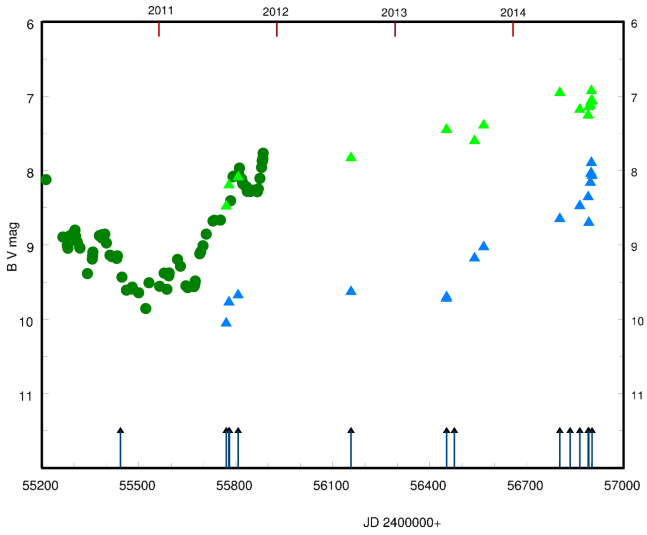

Figure 1. Light curve of CH Cyg from 2010 to 2014. Photoelectric data and results of CCD photometry from Skopal et al. (2012) are signed by circles and our values by triangles, blue color is used for B magnitudes and green for V magnitudes. Dates of our spectroscopic observations are marked by arrows.

Our observations of CH Cyg in Fessenkov Astrophysical Institute were made in 2011-2014. Photometric observations were carried out with two telescopes: 1-meter Carl-Zeiss Jena reflector, equipped with CCD ST-7 (765×510, 9 μm) and 70 cm telescope AZT-8, equipped with CCD ST-8 (1530×1020, 9 μm) and samples of $BVR_{\rm C}$ filters. All

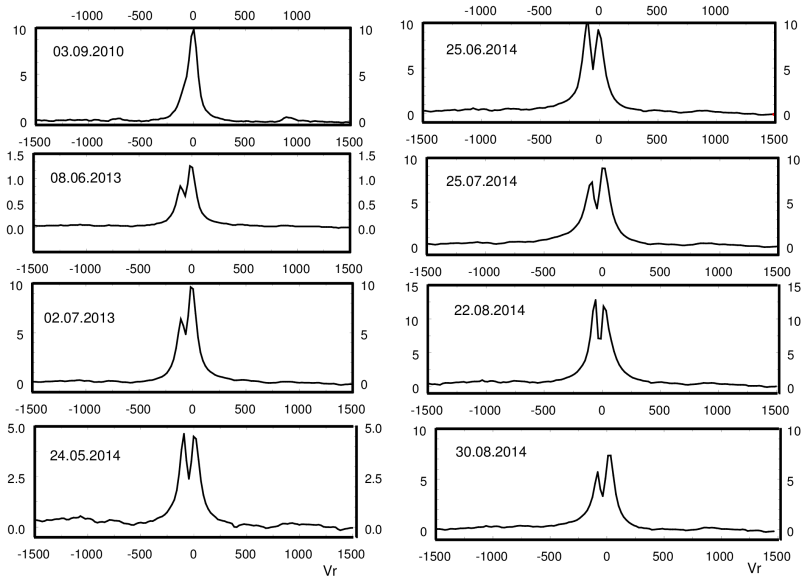

Figure 2. Evolution of the Hα profiles from a quiescent stage in 2010 to the recent active phase. X-axis shows the heliocentric radial velocity in km/s, Y-axis gives a ratio $(I_\lambda - I_{\rm cont})/I_{\rm cont}$.

Table 1: Photometric results

Date	HJD	B	V	R
	2400000+	mag	mag	mag
27.07.2011	55770.479	10.04±0.05	8.47±0.03	5.02±0.01
04.08.2011	55778.521	9.76±0.05	8.19±0.02	4.64±0.01
02.09.2011	55807.125	9.67±0.04	8.08±0.03	4.71±0.01
16.08.2012	56156.190	9.62±0.04	7.82±0.01	4.52±0.01
07.06.2013	56451.400	9.72±0.04	7.44±0.02	4.51±0.01
08.06.2013	56452.260	9.69±0.04	7.43±0.01	4.51±0.01
02.09.2013	56538.370	9.17±0.03	7.59±0.02	5.00±0.02
01.10.2013	56567.085	9.02±0.02	7.38±0.02	4.21±0.01
24.05.2014	56802.383	8.64±0.02	6.94±0.02	4.41±0.01
25.07.2014	56864.250	8.46±0.01	7.17±0.01	4.47±0.01
20.08.2014	56890.208	8.35±0.01	7.25±0.02	4.27±0.01
22.08.2014	56892.153	8.69±0.02	7.14±0.02	4.22±0.01
27.08.2014	56897.149	8.15±0.03	7.11±0.02	4.82±0.01
28.08.2014	56898.177	8.03±0.01	7.06±0.02	4.86±0.01
29.08.2014	56899.142	8.02±0.01	7.06±0.01	4.84±0.01
30.08.2014	56900.148	7.88±0.02	6.92±0.01	4.86±0.01
01.09.2014	56902.129	8.06±0.03	7.05±0.02	4.22±0.01

Table 2: Log of spectral observations

Date	HJD 2400000+	$\Delta\lambda$ Å	Telescope	$R = \lambda/\Delta\lambda$ Å
03.09.2010	55443.140	4400-5200	1-meter	10000
		6100-6900	1-meter	13000
27.07.2011	55770.208	6100-7100	AZT-8	9000
04.08.2011	55778.267	6100-7100	AZT-8	9000
06.08.2011	55780.275	4300-5300	AZT-8	7000
02.09.2011	55807.108	4300-5300	AZT-8	7000
16.08.2012	56156.240	6100-7100	AZT-8	9000
08.06.2013	56452.210	4400-5200	1-meter	10000
		6100-6900	1-meter	13000
02.07.2013	56476.317	6100-6900	1-meter	13000
24.05.2014	56802.346	6100-6900	1-meter	13000
25.06.2014	56834.288	4400-5200	1-meter	10000
		6100-6900	1-meter	13000
25.07.2014	56864.229	4400-5200	1-meter	10000
		6100-6900	1-meter	13000
20.08.2014	56890.200	4300-5300	AZT-8	7000
		6100-7100	AZT-8	9000
22.08.2014	56892.217	4400-5200	1-meter	10000
		6100-6900	1-meter	13000
30.08.2014	56900.150	4400-5200	1-meter	10000
		6100-6900	1-meter	13000

obtained images were dark subtracted and flat fielded. The stars HD195307, HD196330 and HD191418 were adopted as standards. Our observations of CH Cyg were infrequent because the object was in stable stage. The $BVR_{\rm C}$ magnitudes are compiled in Table 1. The light curve of CH Cyg for 2010-2014 is presented in Fig. 1. It can be seen that our earlier data, obtained in 2010-2012, agree with values of Skopal et al. (2012) very well.

In the end of May, 2014 the brightening of CH Cyg has started. The maximal values of B and V magnitudes ($B = 7\overset{\rm m}{.}88 \pm 0\overset{\rm m}{.}02$, $V = 6\overset{\rm m}{.}92 \pm 0\overset{\rm m}{.}02$) are similar to those observed during previous active phases, 1992-1995 and 1998-2000 (Skopal et al. 1997; Skopal 2004). High level of brightness with some fluctuations has been detected to the present.

Spectral observations have been carried out with two spectrographs, attached to the mentioned telescopes and equipped with the CCD cameras ST-8. The slit width equals to 3–4″. Wavelength calibration was done using a laboratory source of HeI, NeI and ArI emission lines. Spectra of standard stars obtained just before or after the target were used for the flux calibration. All spectrograms were corrected for atmospheric extinction. The list of observations is presented in Table 2. Spectrograms with a dispersion of 0.5 Å/pixel (1-meter telescope) and 0.75 Å/pixel (AZT-8) were obtained in the "blue" and "red" spectral ranges (Table 2). Emission lines of HI, HeI, [OIII], [NII], FeII, [FeII] were observed in the spectra of CH Cyg. The results of spectral observations are presented in Table 3. Absolute fluxes $F_{\rm abs}$ are expressed in 10^{-10} erg cm^{-2}sec^{-1} for Hα and 10^{-11} erg cm^{-2}sec^{-1} for other lines. Errors are $\leq$10% for EWs and about 25% for $F_{\rm abs}$ because of non-uniform late-type continuum.

Significant strengthening of all emissions began in 2012. The maximal flux of Hα was

Table 3: Spectral results

HJD	Hβ		HeI, 4921		[OIII], 5007		Hα		[NII], 6583		[OI], 6300	
2400000+	$F_{\rm abs}$	EW	$F_{\rm abs}$	EW	$F_{\rm abs}$	EW	$F_{\rm abs}$	EW	$F_{\rm abs}$	EW	$F_{\rm abs}$	EW
	10^{-11}	Å	10^{-11}	Å	10^{-11}	Å	10^{-10}	Å	10^{-11}	Å	10^{-11}	Å
55443.140	1.06	40			0.34	15	0.84	35	0.60	2.8	0.91	7.6
55770.208							0.43	7.5	0.69	1.7		
55778.267							0.41	7.9	0.64	1.3	0.91	4.3
55780.275	0.45	12.3			0.19	7.1						
55807.108	0.39	9.3			0.16	4.1						
56156.240							2.36	47	1.64	3.3	1.30	3.2
56452.210	2.81	16	0.74	2.0	2.00	9.3	3.03	22	0.41	0.3	2.83	6.3
56476.317							3.78	43	0.59	0.7	2.23	8.7
56802.346							17.6	17	1.82	2.4	2.19	4.3
56834.288	5.00	26	1.08	2.4	0.75	4.4	5.34	36	2.70	2.7	2.77	6.8
56864.229	7.30	29	2.28	1.4	2.94	3.5	6.15	49	3.85	3.7	2.09	4.3
56890.200	7.96	18	4.70	4.1	1.26	2.7	6.27	64	5.00	5.1	2.15	4.2
56892.217	9.1	26	3.75	2.9	1.52	2.9	7.19	78	4.35	4.8	2.50	5.8
56900.150	5.08	11	1.73	3.5	0.90	2.8	6.80	63	7.30	7.7	4.94	5.2

Table 4: Radial velocities of the absorption component in the Hα profiles

Date	08.06.2013	02.07.2013	24.05.2014	25.06.2014	25.07.2014	22.08.2014	30.08.2014
$V_{\rm r}$	−63	−63	−46	−53	−49	−34	−36

registered on 24 May 2014. New increase in the emission fluxes of HI, [NII], HeI and [OI] was observed in the end of August. The emission line [OIII], at 5007 Å was the strongest earlier – on July, 25, and then its flux decreased (Table 3).

The type of Hα profile can be recognized only on spectrograms obtained on the 1-meter telescope with a dispersion of 0.5 Å/pixel. Thus, we know that in 2010, Hα had a single-peaked profile. Beginning from June, 2013, double-peaked profiles have been observed with variable ratio of "blue" to "red" intensities (Fig. 2). Three possible types of profile are presented in Fig. 2: $V < R$, $V = R$ and $V > R$. Heliocentric radial velocities of absorption lines were measured with an uncertainty of about 0.5 Å or ± 20 km/sec. The obtained values are presented in Table 4.

All observable characteristics of CH Cyg: increasing brightness, strengthening of the emission lines, and double-peaked profiles of Balmer lines testify a new active phase of the object.

References:

Burmeister, M., Leedjarv, L., 2009, *A&A*, **504**, 171
Contini, M., Angeloni, R., and Rafanelli, P., 2009, *AN*, **330**, 816
Skopal, A., 1997, *IBVS*, **4495**
Skopal, A., Pribulla, T., Vanko, M. et al., 2004, *CoSka*, **34**, 45
Skopal, A., Shugarov, S. et al. 2012, *AN*, **333**, 242
Wallerstein, G., Munari, U., Siviero, A. et al., 2010, *PASP*, **122**, 12

COMMISSIONS 27 AND 42 OF THE IAU
INFORMATION BULLETIN ON VARIABLE STARS

Number 6118

Konkoly Observatory
Budapest
30 October 2014

HU ISSN 0374 – 0676

BAV RESULTS OF OBSERVATIONS – PHOTOELECTRIC MINIMA OF SELECTED ECLIPSING BINARIES AND MAXIMA OF PULSATING STARS

(BAV MITTEILUNGEN NO. 234)

HÜBSCHER, JOACHIM

Bundesdeutsche Arbeitsgemeinschaft für Veränderliche Sterne e.V. (BAV), Munsterdamm 90, 12169 Berlin, Germany, www.bav-astro.de, publikat@bav-astro.de

In this 77th compilation of BAV results, photoelectric observations obtained mostly in the years 2013 and 2014 are presented on 591 variable stars giving 962 minima on eclipsing binaries and maxima on pulsating stars. All moments of minima and maxima are heliocentric UTC. The errors are tabulated in column "±". The values in column "$O-C$" are determined without incorporating nonlinear terms. The references are given in the section "Remarks". All information about photometers and filters are specified in the columns "Fil" and "Rem". The observations were made at private observatories. The photoelectric measurements and all the light curves with evaluations can be obtained from the office of the BAV for inspection.

Please use the following link for an easy access to all the publications of the BAV including the "Lichtenknecker Database of the BAV": `http://www.bav-astro.de/sfs`.

Table 1: Times of minima of eclipsing binaries

Variable	HJD 24.....	±	Obs	$O-C$		Ref	Fil	n	Rem
RT And	56584.2995	0.0020	AG	+0.0595	s	⟨7⟩	-I	44	10)
UU And	53252.4169	0.0001	MS FR	+0.0064		⟨7⟩	o	220	4)
	55850.4871	0.0001	RAT RCR	+0.0365		⟨7⟩	-U-I	283	12)
	56568.3616	0.0001	MS FR	+0.0315		⟨7⟩	o	366	18)
	56596.6008	0.0016	AG	+0.0311		⟨7⟩	-I	47	10)
AA And	56494.5286	0.0021	AG	−0.0003		⟨7⟩	-I	22	10)
AB And	56539.3341	0.0008	AG	−0.0076	s	⟨7⟩	-I	44	10)
	56539.4988	0.0006	AG	−0.0089		⟨7⟩	-I	44	10)
AD And	56615.3749	0.0022	JU	−0.0324	s	⟨7⟩	o	51	2)
BD And	54360.3373	0.0001	MS FR	−0.0051		⟨7⟩	o	254	4)
	56569.3061	0.0002	MS FR	−0.0223		⟨7⟩	o	224	18)
	56637.3528	0.0009	JU	−0.0227		⟨7⟩	o	90	2)
BL And	56541.3489	0.0012	AG	−0.0031		⟨7⟩	-I	36	10)
BX And	56643.2945	0.0090	AG	−0.0158	s	⟨7⟩	-I	54	10)
CN And	56588.4081	0.0014	AG	−0.0138		⟨7⟩	-I	29	10)
	56592.3428	0.0025	AG	−0.0129	s	⟨7⟩	-I	44	10)
	56592.5749	0.0027	AG	−0.0122		⟨7⟩	-I	44	10)
CO And	56650.3332	0.0081	AG	+0.0026		⟨7⟩	-I	39	10)
DO And	55430.4495	0.0003	MS FR	+0.0219		⟨7⟩	o	611	4)
DS And	56592.2715	0.0034	AG	−0.0025		⟨7⟩	-I	45	10)
	56596.3190	0.0022	AG	+0.0029		⟨7⟩	-I	36	10)
	56643.3080	0.0056	AG	+0.0028	s	⟨7⟩	-I	54	10)
EP And	56650.4151	0.0009	AG	+0.0700	s	⟨7⟩	-I	44	10)
	56650.6140	0.0027	AG	+0.0668		⟨7⟩	-I	44	10)
GK And	56520.4508	0.0091	AG	+0.0738		⟨7⟩	-I	31	10)
GZ And	56630.3521	0.0035	AG	−0.0028		⟨7⟩	-I	67	10)

Table 1: cont.

Variable	HJD 24.....	±	Obs	$O-C$		Ref	Fil	n	Rem
	56630.5014	0.0016	AG	−0.0061	s	⟨7⟩	-I	67	10)
HS And	56612.3159	0.0002	MS FR	−0.0037		⟨7⟩	o	300	11)
LM And	54365.3219	0.0006	MS FR	−0.0087		⟨7⟩	o	294	4)
LO And	56629.3713	0.0005	RAT RCR	−0.0140	s	⟨7⟩	V	70	12)
QW And	56650.3778	0.0013	AG	+0.0050		⟨7⟩	-I	40	10)
QX And	56592.4803	0.0022	AG	+0.1056		⟨7⟩	-I	44	10)
	56596.3968	0.0098	AG	−0.0961		⟨7⟩	-I	36	10)
	56643.3779	0.0144	AG	−0.0620		⟨7⟩	-I	54	10)
V372 And	56630.3832	0.0152	AG				-I	68	10)
V404 And	56642.3772	0.0009	JU	+0.0077		⟨7⟩	o	71	2)
	56644.4054	0.0018	AG	+0.0078		⟨7⟩	-I	29	10)
V444 And	56650.4616	0.0013	AG				-I	38	10)
V473 And	56520.4017	0.0021	AG				-I	32	10)
	56520.6031	0.0005	AG				-I	32	10)
V487 And	56596.4001	0.0171	AG				-I	45	10)
V502 And	56596.2782	0.0025	AG				-I	46	10)
	56596.4386	0.0010	AG				-I	46	10)
V506 And	56596.4361	0.0013	AG				-I	41	10)
V509 And	56596.3721	0.0045	AG				-I	46	10)
V510 And	56596.3409	0.0011	AG				-I	46	10)
V512 And	56596.4657	0.0008	AG	+0.0745		⟨7⟩	-I	46	10)
V514 And	56596.4047	0.0036	AG	−0.0041		⟨7⟩	-I	46	10)
	56596.5801	0.0046	AG	−0.0122	s	⟨7⟩	-I	46	10)
V546 And	56650.4264	0.0019	AG				-I	39	10)
V547 And	56643.3267	0.0003	AG				-I	54	10)
V560 And	56650.4386	0.0029	AG				-I	42	10)
V565 And	56650.2879	0.0045	AG				-I	42	10)
	56650.4397	0.0028	AG				-I	42	10)
HS Aqr	56495.4975	0.0009	AG	−0.0020		⟨7⟩	-I	25	10)
IO Aqr	56506.5508	0.0008	AG				-I	21	10)
LL Aqr	56174.4120	0.0035	PGL	−3.7020	s	⟨7⟩	V	562	9)
MU Aqr	56501.4104	0.0003	RAT RCR	+0.0012		⟨7⟩	V	68	12)
FK Aql	56461.4743	0.0005	RAT RCR	−0.0261		⟨7⟩	V	126	12)
KP Aql	56496.3884	0.0017	AG	−0.0227		⟨7⟩	-I	29	10)
	56506.4908	0.0010	AG	−0.0228		⟨7⟩	-I	23	10)
V417 Aql	56560.4176	0.0006	QU	+0.0755	s	⟨7⟩	V	61	3)
V640 Aql	55352.4944	0.0001	MS FR	+0.0511	s	⟨7⟩	o	700	4)
V688 Aql	56500.4170	0.0008	AG	+0.0113		⟨7⟩	-I	22	10)
V1045 Aql	56542.4616	0.0023	AG	−0.0110	s	⟨7⟩	-I	31	10)
V1075 Aql	56133.3892	0.0001	MS FR	−0.0412		⟨7⟩	o	450	4)
V1798 Aql	56462.4864	0.0004	RAT RCR				V	154	12)
V1799 Aql	56458.5026	0.0002	RAT RCR				V	147	12)
RX Ari	56630.2269	0.0021	AG	+0.0696		⟨7⟩	-I	70	10)
BN Ari	56630.2929	0.0012	AG	−0.0383		⟨7⟩	-I	68	10)
	56630.4432	0.0010	AG	−0.0377	s	⟨7⟩	-I	68	10)
	56630.5905	0.0013	AG	−0.0401		⟨7⟩	-I	68	10)
BO Ari	56630.2810	0.0025	AG				-I	68	10)
	56630.4406	0.0018	AG				-I	68	10)
BQ Ari	56563.4596	0.0009	RAT RCR	−0.0257		⟨7⟩	V	150	12)
	56563.6016	0.0010	RAT RCR	−0.0248	s	⟨7⟩	V	150	12)
CL Ari	56656.3386	0.0015	AG	−0.0557		⟨7⟩	-I	31	10)
RZ Aur	56630.4233	0.0026	AG	−0.0397		⟨7⟩	-I	47	10)
SX Aur	56654.5375	0.0031	AG	−0.0039		⟨7⟩	-I	52	10)
	56656.3492	0.0051	AG	−0.0073	s	⟨7⟩	-I	32	10)
TT Aur	56650.3543	0.0020	AG	+0.0058		⟨7⟩	-I	62	10)
	56656.3495	0.0027	AG	+0.0037	s	⟨7⟩	-I	32	10)
	56666.3486	0.0019	AG	+0.0072		⟨7⟩	-I	18	10)
WW Aur	56670.6210	0.0029	AG	+0.0001		⟨7⟩	-I	47	10)
	56698.3970	0.0022	AG	+0.0009		⟨7⟩	-I	46	10)
AP Aur	56384.3711	0.0003	RAT RCR	+0.0976		⟨7⟩	V	95	12)
AR Aur	56650.5351	0.0017	AG	+0.0207	s	⟨7⟩	-I	61	10)
BF Aur	56654.5441	0.0023	AG	+0.0080		⟨7⟩	-I	52	10)
	56670.3694	0.0003	AG	+0.0011	s	⟨7⟩	-I	37	10)
FO Aur	56630.5479	0.0031	AG	−0.0051		⟨7⟩	-I	48	10)
FR Aur	56630.4009	0.0361	AG	+0.0154	s	⟨7⟩	-I	47	10)
GX Aur	54830.330 :	0.000	MS FR	−0.004	s	⟨7⟩	o	484	4)
HL Aur	56356.3898	0.0001	RAT RCR	+0.0046		⟨7⟩	V	98	12)
IM Aur	56650.4521	0.0008	AG	+0.0006		⟨7⟩	-I	61	10)
IU Aur	56657.3486	0.0164	AG	+0.0016		⟨7⟩	-I	51	10)
IY Aur	56668.3970	0.0263	AG	−0.0263	s	⟨7⟩	-I	64	10)
	56675.3967	0.0030	QU	−0.0100		⟨7⟩	V	76	3)

Table 1: cont.

Variable	HJD 24.....	±	Obs	$O-C$		Ref	Fil	n	Rem
	56689.3691	0.0007	QU	−0.0045		⟨7⟩	I_C	86	3)
LY Aur	56654.4195	0.0270	AG	−0.0040	s	⟨7⟩	-I	52	10)
	56668.4220	0.0011	AG	−0.0103		⟨7⟩	-I	64	10)
	56670.4305	0.0337	AG	−0.0030	s	⟨7⟩	-I	45	10)
MU Aur	56630.5423	0.0037	AG	+0.0054		⟨7⟩	-I	47	10)
V364 Aur	56567.5316	0.0001	MS FR	−0.0004		⟨7⟩	o	432	18)
V410 Aur	56670.4770	0.0025	AG	+0.0160	s	⟨7⟩	-I	36	10)
	56700.3351	0.0033	AG	+0.0157		⟨7⟩	-I	24	10)
V425 Aur	56654.3309	0.0126	AG	+0.0075		⟨7⟩	-I	52	10)
V455 Aur	56670.6190	0.0029	AG	−0.0578		⟨7⟩	-I	40	10)
V459 Aur	56670.3799	0.0074	AG				-I	47	10)
V567 Aur	56630.3643	0.0032	AG				-I	48	10)
V618 Aur	53765.5555	0.0010	FR				-I	39	8)
	56630.3798	0.0146	AG				-I	47	10)
V620 Aur	55851.3872	0.0009	MS FR				o	570	4)
V636 Aur	56630.3237	0.0063	AG				-I	47	10)
	56630.4936	0.0014	AG				-I	47	10)
V641 Aur	56365.3762	0.0004	JU				o	80	2)
TU Boo	54199.4045	0.0003	MS FR	−0.0001		⟨7⟩	o	285	4)
TY Boo	54224.3811	0.0002	MS FR	+0.0023	s	⟨7⟩	o	259	4)
VW Boo	54222.3662	0.0002	MS FR	−0.0001	s	⟨7⟩	o	342	4)
BG Boo	55682.377	0.001	MS FR	−0.028		⟨7⟩	o	396	4)
GN Boo	54220.4309	0.0001	MS FR	+0.0020		⟨7⟩	o	364	4)
	55310.4132	0.0001	MS FR	+0.0034		⟨7⟩	o	581	4)
GQ Boo	55273.5139	0.0010	MS FR	+0.0061		⟨7⟩	o	380	4)
GR Boo	55266.4557	0.0004	MS FR	−0.0042		⟨7⟩	o	434	4)
	55309.3962	0.0002	MS FR	−0.0041		⟨7⟩	o	456	4)
GS Boo	56015.3421	0.0001	MS FR	−0.0173		⟨7⟩	o	610	4)
GT Boo	55943.6359	0.0003	MS FR	−0.0025		⟨7⟩	o	720	4)
XZ Cam	56535.5116	0.0083	AG	+0.1076		⟨7⟩	-I	26	10)
AK Cam	56281.3185	0.0015	JU	−0.2144		⟨7⟩	o	90	2)
AO Cam	56354.3317	0.0004	JU	+0.0035	s	⟨7⟩	o	90	2)
	56650.2728	0.0011	AG	+0.0091	s	⟨7⟩	-I	57	10)
	56650.4381	0.0019	AG	+0.0094		⟨7⟩	-I	57	10)
	56650.6024	0.0015	AG	+0.0087	s	⟨7⟩	-I	57	10)
AT Cam	56623.3774	0.0016	JU	−0.1199		⟨7⟩	o	115	2)
AV Cam	56535.3614	0.0013	AG	−0.0640		⟨7⟩	-I	26	10)
AW Cam	56698.4825	0.0024	AG	−0.0084		⟨7⟩	-I	43	10)
CD Cam	56654.3046	0.0089	AG	+0.0071	s	⟨6⟩	-I	57	10)
	56654.6885	0.0046	AG	+0.0089		⟨6⟩	-I	57	10)
NQ Cam	56654.3880	0.0027	AG	−0.0488		⟨7⟩	-I	56	10)
	56654.5665	0.0007	AG	−0.0514	s	⟨7⟩	-I	56	10)
NS Cam	56654.2722	0.0101	AG	−0.0721		⟨7⟩	-I	57	10)
PP Cam	56541.4474	0.0002	RAT RCR	−0.0514		⟨7⟩	V	210	12)
V366 Cam	56565.5891	0.0003	RAT RCR	+0.1101	s	⟨7⟩	V	223	12)
V369 Cam	56334.4456	0.0003	RAT RCR				V	107	12)
V378 Cam	56535.5870	0.0004	AG				-I	25	10)
V381 Cam	56562.4701	0.0002	RAT RCR	−0.0149		⟨7⟩	V	209	12)
V394 Cam	56535.4417	0.0015	AG				-I	26	10)
V396 Cam	56535.4935	0.0027	AG				-I	26	10)
V418 Cam	56535.3464	0.0006	AG				-I	24	10)
	56535.5015	0.0001	AG				-I	24	10)
V420 Cam	56535.3773	0.0031	AG				-I	25	10)
V428 Cam	56535.4602	0.0008	AG	−0.0659	s	⟨7⟩	-I	26	10)
V429 Cam	56535.3851	0.0013	AG	+0.0671	s	⟨7⟩	-I	26	10)
V438 Cam	56535.3850	0.0033	AG	+0.0038	s	⟨7⟩	-I	25	10)
V447 Cam	56354.3958	0.0003	RAT RCR				V	113	12)
V452 Cam	56654.3870	0.0034	AG				-I	56	10)
	56654.5854	0.0014	AG				-I	56	10)
V454 Cam	56654.5039	0.0015	AG				-I	58	10)
V466 Cam	56654.3400	0.0007	AG				-I	58	10)
	56654.5392	0.0016	AG				-I	58	10)
V473 Cam	56357.4061	0.0002	RAT RCR	+0.0137		⟨7⟩	V	314	12)
	56357.5544	0.0002	RAT RCR	+0.0128	s	⟨7⟩	V	314	12)
	56654.3525	0.0005	AG	+0.0143		⟨7⟩	-I	56	10)
	56654.5009	0.0009	AG	+0.0135	s	⟨7⟩	-I	56	10)
	56654.6506	0.0004	AG	+0.0139		⟨7⟩	-I	56	10)
V474 Cam	56367.4380	0.0002	RAT RCR				V	77	12)
V479 Cam	56654.3453	0.0007	AG	+0.0285	s	⟨7⟩	-I	57	10)
	56654.5071	0.0007	AG	+0.0276		⟨7⟩	-I	57	10)
	56654.6715	0.0017	AG	+0.0293	s	⟨7⟩	-I	57	10)

Table 1: cont.

Variable	HJD 24.....	±	Obs	$O-C$		Ref	Fil	n	Rem
V489 Cam	56365.4679	0.0002	RAT RCR	+0.0237		⟨7⟩	V	295	12)
	56654.2774	0.0009	AG	+0.0283		⟨7⟩	-I	57	10)
	56654.5852	0.0010	AG	+0.0262	s	⟨7⟩	-I	57	10)
HN Cnc	56596.6169	0.0010	MS FR	−0.0346		⟨7⟩	o	141	11)
IL Cnc	56643.5313	0.0001	MS FR	−0.0485	s	⟨7⟩	o	200	11)
KY Cnc	56690.4841	0.0040	AG				-I	26	10)
BI CVn	56407.4871	0.0071	AG	−0.0261		⟨7⟩	-I	36	10)
DF CVn	56305.6018	0.0002	RAT RCR	−0.0021		⟨6⟩	V	154	12)
EX CVn	56305.6018	0.0002	RAT RCR	+0.0577		⟨7⟩	V	142	12)
FI CVn	56427.5203	0.0020	RAT RCR				V	116	12)
RW CMi	56713.3366	0.0037	AG	−1.2505		⟨6⟩	-I	32	10)
AK CMi	56712.3335	0.0010	WTR	−0.0505	s	⟨7⟩	o	106	1)
TV Cas	56596.3709	0.0019	AG	−0.0276		⟨7⟩	-I	36	10)
TW Cas	56644.4226	0.0022	AG	−0.0007		⟨7⟩	-I	45	10)
AB Cas	56596.5543	0.0020	AG	+0.1213		⟨7⟩	-I	36	10)
	56644.3958	0.0020	AG	+0.1222		⟨7⟩	-I	45	10)
AE Cas	56274.3137	0.0005	JU	+0.0716		⟨7⟩	o	49	2)
	56567.3344	0.0008	JU	+0.0724		⟨7⟩	o	57	2)
AH Cas	56596.4093	0.0008	JU	−0.2181		⟨7⟩	o	58	2)
	56629.3704	0.0019	SCI	−0.2102	s	⟨7⟩	o	38	2)
AX Cas	56342.4027	0.0016	JU	−0.0972	s	⟨7⟩	o	103	2)
	56507.5037	0.0035	AG	−0.0996	s	⟨7⟩	-I	24	10)
	56526.4198	0.0015	AG	−0.0953		⟨7⟩	-I	30	10)
	56538.4273	0.0009	JU	−0.0953		⟨7⟩	o	72	2)
	56540.5295	0.0027	AG	−0.0944	s	⟨7⟩	-I	36	10)
BS Cas	56507.4354	0.0016	AG	−0.1027		⟨7⟩	-I	24	10)
	56526.5948	0.0011	AG	−0.1044	s	⟨7⟩	-I	30	10)
	56540.4693	0.0009	AG	−0.1051		⟨7⟩	-I	37	10)
BU Cas	56507.5338	0.0004	AG	−0.0244		⟨7⟩	-I	24	10)
	56568.4244	0.0003	RAT RCR	−0.0241		⟨7⟩	V	75	12)
BZ Cas	56540.5134	0.0089	AG	+0.3023	s	⟨7⟩	-I	31	10)
DN Cas	56585.3814	0.0140	AG	−0.0297		⟨7⟩	-I	26	10)
	56592.3166	0.0021	AG	−0.0273		⟨7⟩	-I	57	10)
	56644.3099	0.0089	AG	−0.0305	s	⟨7⟩	-I	39	10)
DO Cas	56644.3618	0.0019	AG	−0.0014		⟨7⟩	-I	45	10)
DZ Cas	56640.2247	0.0011	MS FR	−0.1958		⟨7⟩	o	176	11)
EG Cas	56585.4120	0.0012	AG	+0.0765	s	⟨7⟩	-I	26	10)
EP Cas	56567.3653	0.0001	MS FR	−0.0383		⟨7⟩	o	280	18)
EY Cas	56585.4303	0.0022	AG	+0.0478	s	⟨7⟩	-I	27	10)
GK Cas	56540.5509	0.0004	AG	−0.3445		⟨7⟩	-I	37	10)
GT Cas	54381.3884	0.0003	MS FR	+0.1760		⟨7⟩	o	930	4)
IL Cas	56526.4532	0.0028	AG	−0.0881		⟨7⟩	-I	30	10)
IQ Cas	56610.2679:	0.0022	MS FR	−0.2763		⟨7⟩	o	130	18)
IR Cas	56541.3786	0.0008	AG	+0.0091		⟨7⟩	-I	36	10)
LR Cas	56596.4931	0.0099	AG	−0.0025		⟨7⟩	-I	35	10)
MM Cas	55087.4583	0.0010	MS FR	+0.0946		⟨7⟩	o	190	4)
MN Cas	56584.5837	0.0007	AG	+0.0104		⟨7⟩	-I	46	10)
NU Cas	56613.3203	0.0006	MS FR	−0.1336	s	⟨7⟩	o	200	11)
OX Cas	56295.3449	0.0014	JU	+0.0369		⟨7⟩	o	58	2)
	56585.3453	0.0073	AG	−0.0010	s	⟨7⟩	-I	24	10)
	56590.3245	0.0066	AG	−0.0005	s	⟨7⟩	-I	35	10)
	56590.3265	0.0018	JU	−0.0015	s	⟨7⟩	o	62	2)
	56596.5642	0.0012	AG	+0.0457		⟨7⟩	-I	40	10)
PV Cas	56494.4902	0.0003	AG	−0.0306		⟨7⟩	-I	21	10)
	56579.4192	0.0020	JU	−0.0356	s	⟨7⟩	o	51	2)
	56592.5120	0.0017	AG	−0.0351		⟨7⟩	-I	37	10)
	56650.2773	0.0006	JU	−0.0353		⟨7⟩	o	47	2)
V336 Cas	56713.3732	0.0013	SCI	−0.0185	s	⟨7⟩	o	39	2)
	56713.6745	0.0013	SCI	−0.0158		⟨7⟩	o	49	2)
V337 Cas	55063.4150	0.0004	MS FR	−0.0670		⟨7⟩	o	310	4)
V344 Cas	56675.5250	0.0018	SCI	−0.1080		⟨7⟩	o	27	2)
V359 Cas	56132.512 :	0.000	MS FR	+0.150		⟨7⟩	o	310	4)
V361 Cas	56640.2982	0.0002	MS FR	−0.2175		⟨7⟩	o	220	11)
V366 Cas	56507.4015	0.0015	AG	+0.0288		⟨7⟩	-I	24	10)
V375 Cas	54316.4782	0.0001	MS FR	+0.1225		⟨7⟩	o	577	4)
	55097.3956	0.0005	MS FR	+0.1462		⟨7⟩	o	517	4)
V380 Cas	56584.4698	0.0071	AG	−0.0732		⟨7⟩	-I	45	10)
	56592.6182	0.0013	AG	−0.0685		⟨7⟩	-I	54	10)
V381 Cas	56584.5804	0.0026	AG	−0.0108		⟨7⟩	-I	49	10)
	56647.4284	0.0015	JU	−0.0169		⟨7⟩	o	112	2)
V448 Cas	56722.3573	0.0024	SCI				o	26	2)

Table 1: cont.

Variable	HJD 24.....	±	Obs	$O-C$		Ref	Fil	n	Rem
V471 Cas	56540.4575	0.0008	AG	−0.0465	s	⟨7⟩	-I	37	10)
V473 Cas	56526.4411	0.0005	AG	−0.0024		⟨6⟩	-I	30	10)
	56630.3051	0.0001	MS FR	−0.0032		⟨6⟩	o	228	11)
V520 Cas	56585.4646	0.0012	AG	+0.0213		⟨7⟩	-I	29	10)
V523 Cas	56520.3645	0.0019	AG	−0.0185	s	⟨7⟩	-I	32	10)
	56520.4814	0.0016	AG	−0.0184		⟨7⟩	-I	32	10)
	56520.5984	0.0008	AG	−0.0182	s	⟨7⟩	-I	32	10)
V541 Cas	56644.3881	0.0025	AG	+0.0132		⟨7⟩	-I	42	10)
V559 Cas	56592.4832	0.0021	AG				-I	57	10)
V821 Cas	56585.3804	0.0038	AG				-I	27	10)
V969 Cas	56526.4669	0.0242	AG	−0.6098		⟨7⟩	-I	30	10)
V1030 Cas	56520.4170	0.0014	AG	−0.0402		⟨7⟩	-I	31	10)
	56520.5689	0.0015	AG	−0.0404	s	⟨7⟩	-I	31	10)
V1044 Cas	56590.4230	0.0139	AG				-I	35	10)
V1046 Cas	56644.3755	0.0007	QU	−0.0100		⟨7⟩	V	70	3) 24)
V1060 Cas	56526.4307	0.0066	AG	−0.0210		⟨7⟩	-I	30	10)
	56584.5390	0.0082	AG	−0.0256		⟨7⟩	-I	50	10)
V1094 Cas	56540.5256	0.0017	AG	+0.0881	s	⟨7⟩	-I	37	10)
V1107 Cas	56342.3157	0.0015	JU	−0.0697		⟨7⟩	o	103	2)
	56342.4528	0.0015	JU	+0.0674		⟨7⟩	o	103	2)
	56507.4582	0.0024	AG	−0.0644		⟨7⟩	-I	24	10)
	56526.4595	0.0014	AG	−0.0649	s	⟨7⟩	-I	30	10)
	56526.5967	0.0015	AG	−0.0644		⟨7⟩	-I	30	10)
	56540.4040	0.0010	AG	−0.0641	s	⟨7⟩	-I	36	10)
	56540.5404	0.0028	AG	−0.0644		⟨7⟩	-I	36	10)
V1115 Cas	56540.3706	0.0030	AG	−0.0759		⟨7⟩	-I	37	10)
	56540.5345	0.0021	AG	−0.0736	s	⟨7⟩	-I	37	10)
V1138 Cas	56507.5104	0.0025	AG	+0.0046		⟨7⟩	-I	24	10)
V1139 Cas	56526.4745	0.0010	AG	+0.0043		⟨7⟩	-I	30	10)
V1160 Cas	56610.5274	0.0004	RAT RCR				V	256	12)
SU Cep	56494.4643	0.0329	AG	+0.0059		⟨7⟩	-I	22	10)
	56521.5095	0.0138	AG	+0.0091		⟨7⟩	-I	44	10)
	56596.3229	0.0036	AG	+0.0062		⟨7⟩	-I	26	10)
VW Cep	56539.4138	0.0029	AG	+0.0625		⟨7⟩	-I	44	10)
	56539.5520	0.0018	AG	+0.0615	s	⟨7⟩	-I	44	10)
VZ Cep	56540.3931	0.0033	AG	−0.0095	s	⟨7⟩	-I	42	10)
WX Cep	56506.4736	0.0020	AG	+0.0083	s	⟨7⟩	-I	20	10)
XX Cep	56540.4607	0.0017	AG	+0.0015		⟨7⟩	-I	42	10)
XZ Cep	56596.5405	0.0010	AG	+0.0650		⟨7⟩	-I	68	10)
AI Cep	56539.5157	0.0010	ALH	+0.1931	s	⟨7⟩	V	511	5)
BE Cep	54318.5237	0.0001	MS FR	−0.0949		⟨7⟩	o	686	4)
CW Cep	56584.3425	0.0069	AG	+0.0168		⟨7⟩	-I	43	10)
	56629.3261	0.0019	JU	+0.0297	s	⟨7⟩	o	80	2)
	56644.3857	0.0049	JU	+0.0189		⟨7⟩	o	92	2)
DN Cep	56590.3139	0.0046	AG	−0.0389		⟨7⟩	-I	42	10)
EY Cep	56596.3800	0.0036	AG	+0.6217	s	⟨7⟩	-I	35	10)
IW Cep	56568.4466	0.0012	AG	+0.0592		⟨7⟩	-I	37	10)
V397 Cep	56534.5499	0.0072	AG				-I	41	10)
	56535.4942	0.0034	AG				-I	38	10)
V736 Cep	56535.4212	0.0059	AG	−0.0164		⟨7⟩	-I	38	10)
	56568.4477	0.0032	AG	−0.0171	s	⟨7⟩	-I	34	10)
V808 Cep	56564.5738	0.0003	RAT RCR				V	173	12)
AQ Com	55279.3836	0.0002	MS FR	−0.0025		⟨7⟩	o	195	4)
CN Com	56013.3969	0.0002	MS FR	+0.0615		⟨7⟩	o	343	4)
DD Com	54828.5778	0.0003	MS FR	−0.0583	s	⟨7⟩	o	516	4)
	54828.7126	0.0004	MS FR	−0.0581		⟨7⟩	o	516	4)
LL Com	54909.4648	0.0001	MS FR	−0.0006		⟨6⟩	o	357	4)
LO Com	56390.3289	0.0020	RAT RCR	−0.0027	s	⟨6⟩	V	52	12)
LT Com	56642.6864	0.0002	MS FR	−0.0022		⟨6⟩	o	230	11)
MM Com	55944.4795	0.0002	MS FR	−0.0207		⟨7⟩	o	464	4)
MR Com	55942.6757	0.0001	MS FR	−0.0480		⟨7⟩	o	640	4)
TU CrB	54861.5823	0.0002	MS FR	+0.1214	s	⟨7⟩	o	626	4)
Y Cyg	56560.3897	0.0035	JU	+0.1244	s	⟨7⟩	o	77	2)
	56584.3581	0.0030	AG	+0.1221	s	⟨7⟩	-I	35	10)
	56590.3538	0.0062	AG	+0.1252	s	⟨7⟩	-I	33	10)
VV Cyg	56533.4470	0.0019	SCI	+0.0166		⟨7⟩	o	46	2)
BR Cyg	56499.5065	0.0004	AG	+0.0097	s	⟨7⟩	-I	30	10)
CG Cyg	56590.3351	0.0011	AG	+0.0712		⟨7⟩	-I	33	10)
DK Cyg	56506.5299	0.0014	AG	+0.0997	s	⟨7⟩	-I	20	10)
DL Cyg	56540.3677	0.0020	AG	+0.1261		⟨7⟩	-I	41	10)
DO Cyg	56568.5647	0.0005	AG	−0.0266		⟨7⟩	-I	37	10)

Table 1: cont.

Variable	HJD 24.....	±	Obs	$O-C$		Ref	Fil	n	Rem
DP Cyg	56600.3730	0.0008	AG	+0.1780	s	⟨7⟩	-I	46	10)
GO Cyg	56494.4538	0.0054	AG	+0.0659	s	⟨7⟩	-I	22	10)
GV Cyg	56588.5421	0.0061	AG	+0.1460		⟨7⟩	-I	28	10)
	56666.3061	0.0017	AG	+0.1419	s	⟨7⟩	-I	27	10)
KR Cyg	56494.4181	0.0022	AG	+0.0191		⟨7⟩	-I	22	10)
	56496.5367	0.0062	AG	+0.0248	s	⟨7⟩	-I	29	10)
	56535.4043	0.0115	AG	+0.0155	s	⟨7⟩	-I	31	10)
MR Cyg	56534.4390	0.0015	AG	−0.0008		⟨7⟩	-I	40	10)
	56539.4707	0.0037	AG	−0.0002		⟨7⟩	-I	44	10)
QU Cyg	56012.6075	0.0001	MS FR	−0.0719		⟨7⟩	o	456	4)
QX Cyg	54922.644 :	0.006	MS FR	−0.155	s	⟨7⟩	o	550	4)
V346 Cyg	55309.5931	0.0004	MS FR	+0.1470		⟨7⟩	o	594	4)
V366 Cyg	56158.434	0.011	AG	+0.011	s	⟨7⟩	-I	29	10)
	56495.4383	0.0030	AG	−0.0101		⟨7⟩	-I	23	10)
V379 Cyg	56528.6012	0.0042	SCI				o	33	2)
V382 Cyg	56534.5372	0.0018	SCI	+0.1122	s	⟨7⟩	o	180	2)
V385 Cyg	56487.5290	0.0004	RAT RCR	−0.1394		⟨7⟩	V	134	12)
V388 Cyg	56535.3935	0.0020	AG	−0.1003		⟨7⟩	-I	30	10)
	56584.3553	0.0050	AG	−0.1036		⟨7⟩	-I	33	10)
V398 Cyg	54684.4569	0.0002	FR	+2.0859		⟨7⟩	-I	89	10)
	55050.4590	0.0079	FR	+4.2061	s	⟨7⟩	-I	31	10)
	56650.2652	0.0002	FR	+1.0895	s	⟨7⟩	-I	50	10)
V401 Cyg	54199.6094	0.0002	MS FR	+0.0569		⟨7⟩	o	448	4)
V442 Cyg	56535.5314	0.0022	AG	−0.0423	s	⟨7⟩	-I	30	10)
	56584.4401	0.0030	AG	−0.0455		⟨7⟩	-I	33	10)
V477 Cyg	56494.5048	0.0026	AG	−0.0308		⟨7⟩	-I	24	10)
	56534.4037	0.0013	AG	−0.0308		⟨7⟩	-I	40	10)
V478 Cyg	56534.4471	0.0174	AG	+0.0215		⟨7⟩	-I	40	10)
V483 Cyg	56534.4857	0.0378	AG	−0.0067		⟨7⟩	-I	39	10)
V488 Cyg	55339.4779	0.0008	MS FR	+0.0590		⟨7⟩	o	710	4)
V490 Cyg	56559.3730	0.0003	FR	+0.1618		⟨7⟩	-I	33	10)
V498 Cyg	56534.5665	0.0007	AG	+0.1517		⟨7⟩	-I	40	10)
V548 Cyg	56534.4427	0.0180	AG	−0.8671		⟨7⟩	-I	35	10)
V687 Cyg	56534.3907	0.0007	AG	−0.0080		⟨7⟩	-I	38	10)
V693 Cyg	55311.4960	0.0005	MS FR	+0.0072		⟨7⟩	o	102	4)
V700 Cyg	56540.3518	0.0002	WTR	−0.0667		⟨7⟩	o	101	1)
	56541.3682	0.0010	WTR	−0.0705		⟨7⟩	o	121	1)
V703 Cyg	56666.2800	0.0036	AG				-I	23	10)
V726 Cyg	56061.4361	0.0001	MS FR	+0.0361		⟨7⟩	o	770	4)
V749 Cyg	55341.4125	0.0003	MS FR	−0.0456		⟨7⟩	o	352	4)
V789 Cyg	56494.4519	0.0018	AG	−0.0713		⟨7⟩	-I	30	10)
V828 Cyg	56495.5087	0.0049	AG	−0.1445		⟨7⟩	-I	19	10)
V836 Cyg	56506.4633	0.0011	AG	+0.0198		⟨7⟩	-I	22	10)
V850 Cyg	55340.3854	0.0012	MS FR	+0.6592		⟨7⟩	o	784	4)
V859 Cyg	56463.4698	0.0002	RAT RCR	+0.0295		⟨7⟩	V	133	12)
	56494.4519	0.0004	AG	+0.0290	s	⟨7⟩	-I	29	10)
V877 Cyg	56507.4363	0.0004	FR	+0.0257		⟨7⟩	-I	40	10)
V884 Cyg	56494.5205	0.0036	AG	+0.0205		⟨7⟩	-I	30	10)
V909 Cyg	56495.4267	0.0010	AG	−0.1767	s	⟨7⟩	-I	25	10)
V912 Cyg	56014.5355	0.0001	MS FR	−0.1251		⟨7⟩	o	612	4)
V1034 Cyg	56535.3907	0.0043	AG	+0.0060		⟨7⟩	-I	31	10)
	56559.3280	0.0009	FR	+0.0085	s	⟨7⟩	-I	49	10)
V1047 Cyg	55333.4775	0.0004	MS FR				o	384	4)
V1061 Cyg	56521.4831	0.0006	AG	−0.0128		⟨7⟩	-I	44	10)
	56534.3906	0.0063	AG	+1.1614		⟨7⟩	-I	39	10)
V1141 Cyg	56465.4681	0.0002	RAT RCR	+0.0292	s	⟨7⟩	V	133	12)
V1171 Cyg	56535.4967	0.0050	AG	−0.0595		⟨7⟩	-I	31	10)
V1401 Cyg	56588.4756	0.0067	AG	+0.2974		⟨7⟩	-I	28	10)
V1411 Cyg	56592.2741	0.0009	AG	−0.1464	s	⟨7⟩	-I	45	10)
V1414 Cyg	56505.5148	0.0022	AG	+0.0490		⟨7⟩	-I	26	10)
	56588.4827	0.0047	AG	+0.0480		⟨7⟩	-I	28	10)
V1417 Cyg	56495.4014	0.0016	AG	+0.1429	s	⟨7⟩	-I	24	10)
	56521.5640	0.0024	AG	+0.1416	s	⟨7⟩	-I	44	10)
V1425 Cyg	56535.4581	0.0065	AG	+0.0124		⟨7⟩	-I	38	10)
V1437 Cyg	55826.4652	0.0014	FR	−0.0721		⟨7⟩	-I	30	10)
	56474.3937	0.0012	FR	−0.0620	s	⟨7⟩	-I	31	10)
	56507.5746	0.0020	FR	−0.0611	s	⟨7⟩	-I	66	10)
V1815 Cyg	56534.3700	0.0110	AG	+0.0026	s	⟨6⟩	-I	40	10)
V1877 Cyg	55050.3641	0.0005	FR	−0.1868	s	⟨6⟩	-I	63	10)
	56650.3159	0.0006	FR	+0.0417	s	⟨6⟩	-I	41	10)
	56654.3360	0.0006	FR	+0.0262	s	⟨6⟩	-I	41	10)

Table 1: cont.

Variable	HJD 24.....	±	Obs	$O-C$		Ref	Fil	n	Rem
	56657.2140	0.0009	FR	+0.0792		⟨6⟩	-I	87	10)
V1918 Cyg	54299.4459	0.0001	MS FR	+0.0027	s	⟨6⟩	o	674	4)
	54300.4787	0.0001	MS FR	+0.0025		⟨6⟩	o	732	4)
	54316.387	0.002	MS FR	+0.004	s	⟨6⟩	o	209	4)
V2021 Cyg	56588.3875	0.0035	AG	+0.0024		⟨6⟩	-I	28	10)
	56590.2881	0.0012	AG	+0.0009		⟨6⟩	-I	33	10)
V2181 Cyg	56559.4253	0.0005	FR	+0.0011		⟨6⟩	-I	61	10)
V2247 Cyg	56650.3272	0.0006	FR				-I	35	10)
	56657.2290	0.0014	FR				-I	36	10)
V2263 Cyg	56495.5007	0.0029	AG				-I	23	10)
V2278 Cyg	56515.4075	0.0035	SCI				o	62	2)
	56540.4233	0.0035	SCI				o	73	2)
	56560.3378	0.0017	SCI				o	50	2)
	56560.5472	0.0030	SCI				o	43	2)
	56568.5083	0.0017	SCI				o	79	2)
	56579.3358	0.0024	SCI				o	48	2)
	56596.3739	0.0018	SCI				o	61	2)
	56608.2982	0.0013	SCI				o	58	2)
	56623.3262	0.0010	SCI				o	50	2)
	56647.2140	0.0019	SCI				o	25	2)
	56675.2948	0.0017	SCI				o	53	2)
V2282 Cyg	56563.4685	0.0020	JU	+0.0071	s	⟨6⟩	o	90	2)
V2477 Cyg	56568.3896	0.0013	AG	+0.0009		⟨7⟩	-I	30	10)
V2545 Cyg	56535.3560	0.0028	AG				-I	30	10)
V2546 Cyg	56535.3723	0.0035	AG	−0.0062		⟨7⟩	-I	30	10)
V2619 Cyg	56491.5399	0.0020	RAT RCR				V	142	12)
TY Del	56489.5147	0.0001	RAT RCR	+0.0594		⟨7⟩	V	154	12)
	56495.4706	0.0015	AG	+0.0596		⟨7⟩	-I	21	10)
	56539.5424	0.0010	AG	+0.0597		⟨7⟩	-I	42	10)
BG Del	56539.4603	0.0013	AG	+0.0807		⟨7⟩	-I	45	10)
DM Del	56496.5335	0.0010	AG	−0.0988		⟨7⟩	-I	29	10)
EX Del	56500.3795	0.0004	AG	−0.0775		⟨7⟩	-I	24	10)
	56500.5468	0.0022	AG	+0.0898		⟨7⟩	-I	24	10)
FZ Del	56490.4815	0.0001	RAT RCR	−0.0348		⟨7⟩	V	120	12)
	56506.5349	0.0018	AG	−0.0372	s	⟨7⟩	-I	20	10)
Z Dra	56418.4498	0.0001	RAT RCR	−0.1950		⟨7⟩	V	223	12)
RZ Dra	56496.5283	0.0028	AG	+0.0574	s	⟨7⟩	-I	28	10)
TZ Dra	56496.5066	0.0019	AG	−0.0355		⟨7⟩	-I	29	10)
BH Dra	56499.4174	0.0063	AG	+0.8998		⟨7⟩	-I	23	10)
EX Dra	56541.5030	0.0035	PGL	+0.0015		⟨6⟩	V	177	9)
LN Dra	56516.4919	0.0003	RAT RCR	−0.0033	s	⟨6⟩	V	206	12)
LZ Dra	56397.4922	0.0002	RAT RCR	−0.0077		⟨6⟩	V	192	12)
MY Dra	56431.5167	0.0004	RAT RCR	+0.0351		⟨7⟩	V	200	12)
V381 Dra	56509.4910	0.0004	RAT RCR				V	197	12)
V738 Dra	56539.3828	0.0072	AG				-I	22	10)
S Equ	56540.4879	0.0016	AG	+0.0632		⟨7⟩	-I	37	10)
U Gem	56639.4369	0.0035	PGL	−0.0030		⟨6⟩	V	44	17)
RW Gem	56700.3172	0.0038	AG	−0.0003		⟨7⟩	-I	24	10)
AL Gem	56690.4907	0.0012	AG	+0.0812		⟨7⟩	-I	31	10)
AZ Gem	56643.4555	0.0018	AG	+0.0913	s	⟨7⟩	-I	50	10)
CW Gem	56643.5046	0.0019	AG	+0.2856		⟨7⟩	-I	49	10)
CX Gem	56643.6041	0.0278	AG	−0.0241	s	⟨7⟩	-I	49	10)
DG Gem	56643.4242	0.0072	AG	+0.7288	s	⟨7⟩	-I	50	10)
EY Gem	56643.5101	0.0016	AG	−0.2319		⟨7⟩	-I	50	10)
FG Gem	56643.4494	0.0023	AG	−0.0189		⟨7⟩	-I	48	10)
GP Gem	56642.5314	0.0006	MS FR	+0.0977		⟨7⟩	o	152	11)
GW Gem	56698.4993	0.0069	AG	+0.0306	s	⟨7⟩	-I	44	10)
GX Gem	56568.5228	0.0004	MS FR	−0.0628		⟨7⟩	o	450	18)
KV Gem	56643.4323	0.0024	AG	+0.0473		⟨7⟩	-I	50	10)
	56643.6126	0.0018	AG	+0.0091		⟨7⟩	-I	50	10)
V372 Gem	56643.5387	0.0032	AG				-I	49	10)
V404 Gem	56643.4419	0.0027	AG	+0.0082		⟨7⟩	-I	50	10)
	56643.6172	0.0027	AG	+0.0091	s	⟨7⟩	-I	50	10)
V414 Gem	56643.5566	0.0070	AG				-I	50	10)
V416 Gem	56643.4143	0.0011	AG				-I	49	10)
	56643.5415	0.0022	AG				-I	49	10)
	56643.6695	0.0021	AG				-I	49	10)
RX Her	56495.4888	0.0035	AG	+0.0031	s	⟨7⟩	-I	20	10)
TX Her	56540.3915	0.0016	AG	−0.0034		⟨7⟩	-I	22	10)
UX Her	56494.5165	0.0016	AG	+0.1009		⟨7⟩	-I	24	10)
DI Her	56539.3746	0.0033	AG	−0.0008		⟨7⟩	-I	35	10)

Table 1: cont.

Variable	HJD 24.....	±	Obs	$O-C$		Ref	Fil	n	Rem
DK Her	56494.4442	0.0012	SCI	−0.1548		⟨7⟩	o	136	2)
HS Her	56527.4830	0.0006	AG	−0.0248		⟨7⟩	-I	29	10)
MX Her	56518.4324	0.0003	RAT RCR	+0.5436	s	⟨7⟩	V	176	12)
V338 Her	56540.3605	0.0164	AG	−0.5430		⟨7⟩	-I	24	10)
V342 Her	56540.4044	0.0059	AG	+0.0209		⟨7⟩	-I	31	10)
V450 Her	56495.4530	0.0024	AG	+0.0897	s	⟨7⟩	-I	25	10)
V728 Her	56540.3792	0.0073	AG	+0.0275	s	⟨7⟩	-I	22	10)
V732 Her	56390.4668	0.0028	SCI	−0.0060	s	⟨7⟩	o	36	2)
	56492.5187	0.0022	SCI	+0.0967	s	⟨7⟩	o	55	2)
	56496.4227	0.0027	SCI	+0.0594		⟨7⟩	o	53	2)
	56506.4385	0.0025	SCI	+0.0905		⟨7⟩	o	54	2)
V994 Her	56539.4483	0.0089	AG				-I	33	10)
	56540.4583	0.0068	AG				-I	31	10)
V1055 Her	56494.4920	0.0002	RAT RCR	+0.0070		⟨6⟩	V	172	12)
	56540.3854	0.0025	AG	+0.0087	s	⟨6⟩	-I	22	10)
V1073 Her	56527.4102	0.0003	AG	−0.0037		⟨6⟩	-I	24	10)
V1103 Her	56506.3850	0.0003	RAT RCR	−0.0131	s	⟨7⟩	V	209	12)
	56506.5286	0.0002	RAT RCR	−0.0151		⟨7⟩	V	209	12)
V1302 Her	56507.4476	0.0002	RAT RCR				V	156	12)
	56540.3425	0.0041	AG				-I	24	10)
V1309 Her	56540.3713	0.0050	AG				-I	24	10)
V1355 Her	56450.4576	0.0003	RAT RCR				V	140	12)
DF Hya	54515.3224	0.0001	MS FR	+0.0251	s	⟨7⟩	o	420	4)
	54829.3985	0.0004	MS FR	+0.0333	s	⟨7⟩	o	675	4)
	54829.5627	0.0001	MS FR	+0.0322		⟨7⟩	o	675	4)
	54831.5463	0.0001	MS FR	+0.0322		⟨7⟩	o	410	4)
RT Lac	56596.4248	0.0089	AG	−0.3006	s	⟨7⟩	-I	28	10)
SW Lac	56539.4525	0.0019	AG	+0.0661		⟨7⟩	-I	44	10)
	56539.6108	0.0007	AG	+0.0640	s	⟨7⟩	-I	44	10)
	56597.3423	0.0008	DIE	+0.0657	s	⟨7⟩	o	24	14)
UY Lac	56505.4921	0.0010	AG	+0.5431		⟨7⟩	-I	27	10)
VV Lac	56568.3309	0.0031	AG	+0.7987	s	⟨7⟩	-I	47	10)
	56592.5069	0.0041	AG	+0.7918	s	⟨7⟩	-I	44	10)
VY Lac	56505.5307	0.0037	AG	−0.1738		⟨7⟩	-I	27	10)
AG Lac	56600.5127	0.0031	AG	−0.0326		⟨7⟩	-I	44	10)
BS Lac	56505.4302	0.0021	AG	−0.1576		⟨7⟩	-I	27	10)
CG Lac	56588.4301	0.0001	AG	−0.1585		⟨7⟩	-I	28	10)
	56592.5271	0.0020	AG	−0.1585		⟨7⟩	-I	47	10)
CM Lac	56496.4733	0.0015	AG	−0.0039		⟨7⟩	-I	29	10)
	56590.3504	0.0039	AG	−0.0013	s	⟨7⟩	-I	35	10)
CN Lac	56588.4470	0.0012	AG	−0.1010		⟨7⟩	-I	28	10)
CO Lac	56568.4360	0.0025	AG	−0.0063	s	⟨7⟩	-I	37	10)
DG Lac	55345.4546	0.0003	MS FR	−0.2209		⟨7⟩	o	660	4)
EO Lac	56541.4766	0.0305	AG	+0.2931	s	⟨7⟩	-I	36	10)
EP Lac	56541.3952	0.0009	AG	−0.3688		⟨7⟩	-I	36	10)
EQ Lac	56134.4269	0.0004	MS FR	+0.0205		⟨7⟩	o	620	4)
ER Lac	56541.4940	0.0041	AG	−0.5839		⟨7⟩	-I	37	10)
	56600.3995	0.0054	AG	−0.5874		⟨7⟩	-I	48	10)
EU Lac	56541.4503	0.0010	AG	+0.2118		⟨7⟩	-I	37	10)
	56590.4314	0.0026	AG	+0.2107		⟨7⟩	-I	41	10)
EX Lac	56541.3429	0.0007	AG	+0.2371		⟨7⟩	-I	36	10)
	56600.4782	0.0046	AG	+0.2364		⟨7⟩	-I	44	10)
FL Lac	56535.4735	0.0018	AG	+0.2160		⟨7⟩	-I	29	10)
	56568.4339	0.0027	AG	−0.0433		⟨7⟩	-I	37	10)
	56600.5454	0.0044	AG	−0.0442		⟨7⟩	-I	44	10)
GX Lac	56568.5297	0.0083	AG	−0.0534	s	⟨7⟩	-I	37	10)
HR Lac	56505.4483	0.0022	AG	−0.1026	s	⟨7⟩	-I	27	10)
HX Lac	56135.5087	0.0005	MS FR	+0.0346	s	⟨7⟩	o	576	4)
IL Lac	56495.5091	0.0039	AG	+0.0034		⟨6⟩	-I	24	10)
IP Lac	56505.4937	0.0010	AG	+0.0856		⟨7⟩	-I	27	10)
	56568.5430	0.0013	AG	+0.0862		⟨7⟩	-I	46	10)
IU Lac	56590.5623	0.0024	AG	+0.0125		⟨7⟩	-I	42	10)
	56592.5013	0.0012	AG	+0.0134		⟨7⟩	-I	43	10)
	56600.2539	0.0027	AG	+0.0135		⟨7⟩	-I	46	10)
IZ Lac	56568.3878	0.0056	AG	+0.0989	s	⟨7⟩	-I	47	10)
	56600.3425	0.0047	AG	+0.0984	s	⟨7⟩	-I	46	10)
MZ Lac	56590.3277	0.0091	AG	−0.4134	s	⟨7⟩	-I	42	10)
NR Lac	56505.4657	0.0029	AG	+0.0695		⟨7⟩	-I	27	10)
NW Lac	56590.5594	0.0029	AG	−0.1563		⟨7⟩	-I	41	10)
OO Lac	56600.2764	0.0015	AG	+0.1611		⟨7⟩	-I	46	10)
OS Lac	56541.3984	0.0026	AG	+0.3031	s	⟨7⟩	-I	36	10)

Table 1: cont.

Variable	HJD 24.....	±	Obs	$O-C$		Ref	Fil	n	Rem
PP Lac	56588.4503	0.0005	AG	−0.0574		⟨7⟩	-I	27	10)
	56588.6510	0.0017	AG	−0.0573	s	⟨7⟩	-I	27	10)
V339 Lac	56495.5007	0.0016	AG	+0.1812		⟨7⟩	-I	23	10)
	56541.4892	0.0008	AG	+0.1550		⟨7⟩	-I	37	10)
V342 Lac	56568.5624	0.0030	AG	−0.0639		⟨7⟩	-I	47	10)
	56600.4390	0.0045	AG	−0.0636	s	⟨7⟩	-I	46	10)
V343 Lac	56592.2558	0.0014	AG				-I	70	10)
V441 Lac	56590.2932	0.0017	AG	+0.0074		⟨6⟩	-I	42	10)
	56590.4460	0.0017	AG	+0.0058	s	⟨6⟩	-I	42	10)
	56592.3027	0.0025	AG	+0.0090	s	⟨6⟩	-I	43	10)
	56592.4559	0.0015	AG	+0.0077		⟨6⟩	-I	43	10)
	56600.3327	0.0013	AG	+0.0071	s	⟨6⟩	-I	46	10)
	56600.4870	0.0017	AG	+0.0070		⟨6⟩	-I	46	10)
V455 Lac	56590.2927	0.0029	AG				-I	42	10)
	56592.2782	0.0028	AG				-I	48	10)
WY Leo	56408.4011	0.0027	SCI	+0.3894		⟨7⟩	o	56	2)
BW Leo	55260.3530	0.0002	MS FR	+0.0559	s	⟨7⟩	o	504	4)
	56712.4064	0.0022	SCI	+0.0357	s	⟨7⟩	o	26	2)
	56712.5784	0.0017	SCI	+0.0390		⟨7⟩	o	16	2)
CE Leo	55877.7115	0.0001	MS FR	−0.0123		⟨7⟩	o	306	4) 22)
	56006.3687	0.0003	MS FR	−0.0090		⟨7⟩	o	368	4)
FM Leo	54911.3841	0.0006	MS FR	−0.0071		⟨6⟩	o	372	4)
XX LMi	56356.5880	0.0008	RAT RCR	+0.0085		⟨7⟩	V	186	12)
XY LMi	56356.5373	0.0002	RAT RCR	−0.0234		⟨7⟩	V	188	12)
SW Lyn	56698.2843	0.0015	AG	+0.0659		⟨7⟩	-I	46	10)
SX Lyn	56690.4535	0.0042	AG	+0.0205		⟨7⟩	-I	26	10)
CN Lyn	56670.3685	0.0028	AG				-I	41	10)
	56713.3879	0.0031	AG				-I	53	10)
DE Lyn	56384.3876	0.0008	JU	−0.0050		⟨6⟩	o	78	2)
DY Lyn	56698.5009	0.0021	AG	−0.2070	s	⟨7⟩	-I	45	10)
DZ Lyn	56670.4792	0.0034	AG	−0.0142		⟨7⟩	-I	51	10)
	56690.5176	0.0054	AG	−0.0107		⟨7⟩	-I	28	10)
	56698.4488	0.0011	AG	−0.0179		⟨7⟩	-I	41	10)
	56700.3458	0.0048	AG	−0.0110		⟨7⟩	-I	23	10)
EK Lyn	56713.3406	0.0041	AG				-I	53	10)
FI Lyn	56670.2799	0.0026	AG	+0.0149	s	⟨7⟩	-I	47	10)
	56670.4697	0.0005	AG	+0.0180		⟨7⟩	-I	47	10)
	56690.4363	0.0012	AG	+0.0152	s	⟨7⟩	-I	27	10)
FN Lyn	56698.3840	0.0005	AG	+0.0634		⟨7⟩	-I	44	10)
UZ Lyr	56499.4981	0.0010	AG	−0.0334		⟨7⟩	-I	25	10)
	56535.4341	0.0033	AG	−0.0316		⟨7⟩	-I	31	10)
AA Lyr	56577.2958	0.0015	FR	+0.2912	s	⟨7⟩	-I	36	10)
	56579.3658	0.0009	FR	+0.2145	s	⟨7⟩	-I	37	10)
BN Lyr	55380.4792	0.0006	FR				-I	30	10)
BV Lyr	56454.4438	0.0004	RAT RCR	+0.0278		⟨7⟩	V	150	12)
DT Lyr	55418.4735	0.0037	FR	+0.1306	s	⟨7⟩	-I	48	10)
	56568.4232	0.0003	FR	+0.1344		⟨7⟩	-I	50	10)
PV Lyr	56015.5961	0.0003	MS FR	+0.0075		⟨7⟩	o	660	4)
V401 Lyr	54258.4670	0.0003	MS FR	−0.0462	s	⟨7⟩	o	480	4)
V412 Lyr	55380.5306	0.0024	FR	+0.2031	s	⟨7⟩	-I	40	10)
	55387.5200	0.0009	FR	+0.2065		⟨7⟩	-I	29	10)
V412 Lyr	55409.4121	0.0012	FR	+0.2091	s	⟨7⟩	-I	42	10)
	56136.4353	0.0018	FR	+0.2207		⟨7⟩	-I	33	10)
	56579.3557	0.0018	FR	+0.2276	s	⟨7⟩	-I	37	10)
V417 Lyr	55338.4244	0.0002	MS FR	+0.0550		⟨7⟩	o	325	4)
RW Mon	56656.4276	0.0040	AG	−0.0790		⟨7⟩	-I	25	10)
V453 Mon	56612.4847	0.0020	MS FR	+0.1433		⟨7⟩	o	99	11)
V454 Mon	54508.3479	0.0006	MS FR	+0.0835		⟨7⟩	o	510	4)
V527 Mon	55874.5804	0.0003	MS FR	−0.0273		⟨7⟩	o	468	4)
V714 Mon	56596.5219	0.0002	RAT RCR	−0.0038	s	⟨6⟩	V	134	12)
V456 Oph	56495.4332	0.0068	AG	+0.0189		⟨7⟩	-I	25	10)
	56527.4356	0.0015	AG	+0.0174	s	⟨7⟩	-I	20	10)
V839 Oph	56480.4889	0.0002	RAT RCR	+0.0729	s	⟨7⟩	o	293	19)
ES Ori	56640.3886	0.0005	MS FR	−0.0084	s	⟨7⟩	o	93	11)
EW Ori	56650.3498	0.0050	SIR	−0.0291		⟨7⟩	o	143	7)
V668 Ori	56706.3366	0.0001	SCI				o	37	2)
V2735 Ori	56668.3480	0.0042	AG	−0.0173		⟨7⟩	-I	59	10)
V2759 Ori	56668.2602	0.0050	AG				-I	59	10)
V2762 Ori	56666.2517	0.0027	AG				-I	22	10)
AT Peg	56592.3834	0.0007	AG	+0.0111		⟨7⟩	-I	33	10)
BB Peg	56542.3388	0.0016	DIE	−0.0094		⟨7⟩	o	25	14)

Table 1: cont.

Variable	HJD 24.....	±	Obs	$O-C$		Ref	Fil	n	Rem
	56563.3053	0.0001	DIE	−0.0100		⟨7⟩	o	25	14)
BN Peg	56506.4868	0.0010	AG	+0.0008		⟨7⟩	-I	21	10)
	56540.3740	0.0105	AG	+0.0063	s	⟨7⟩	-I	40	10)
DI Peg	56501.5600	0.0001	RAT RCR	−0.0024		⟨7⟩	V	100	12)
	56588.4035	0.0009	AG	−0.0006		⟨7⟩	-I	28	10)
EH Peg	56597.3583	0.0003	SCI	−0.3405		⟨7⟩	o	137	2)
EU Peg	56132.4214	0.0002	MS FR	+0.0377		⟨7⟩	o	459	4)
GP Peg	56539.3807	0.0102	AG	−0.0506	s	⟨7⟩	-I	42	10)
IP Peg	56539.3867	0.0006	SCI	−0.0010		⟨6⟩	o	23	2)
	56539.4757	0.0021	SCI	+0.0089	s	⟨6⟩	o	23	2)
	56539.5437	0.0008	SCI	−0.0022		⟨6⟩	o	22	2)
	56539.6283	0.0021	SCI	+0.0033	s	⟨6⟩	o	15	2)
	56541.4438	0.0006	SCI	−0.0006		⟨6⟩	o	25	2)
	56541.5984	0.0018	SCI	−0.0042		⟨6⟩	o	50	2)
	56559.3222	0.0006	SCI	+0.0006		⟨6⟩	o	16	2)
	56559.4121	0.0018	SCI	+0.0114	s	⟨6⟩	o	25	2)
	56559.4792	0.0006	SCI	−0.0006		⟨6⟩	o	33	2)
	56567.4751	0.0013	SCI	+0.0059	s	⟨6⟩	o	23	2)
	56567.5477	0.0007	SCI	−0.0006		⟨6⟩	o	17	2)
	56588.2705	0.0004	SCI	−0.0028		⟨6⟩	o	13	2)
	56629.2473	0.0003	SCI	−0.0014		⟨6⟩	o	17	2)
	56644.2775	0.0015	SCI	−0.0007		⟨6⟩	o	33	2)
LX Peg	56212.2836	0.0009	BHE				-I	181	15)
V396 Peg	56133.5284	0.0010	MS FR	−0.0029		⟨6⟩	o	321	4)
V407 Peg	56588.3723	0.0038	AG				-I	26	10)
V523 Peg	56493.4808	0.0003	RAT RCR				V	161	12)
V560 Peg	56539.3836	0.0270	AG				-I	42	10)
	56539.6130	0.0023	AG				-I	42	10)
V573 Peg	56539.4090	0.0047	AG				-I	42	10)
	56539.6127	0.0003	AG				-I	42	10)
Z Per	56643.3452	0.0045	AG	−0.2657		⟨7⟩	-I	56	10)
RT Per	56592.3751	0.0020	AG	−0.3421		⟨7⟩	-I	53	10)
	56630.6026	0.0020	AG	−0.3377		⟨7⟩	-I	72	10)
	56650.5630	0.0013	AG	+0.0865		⟨7⟩	-I	51	10)
ST Per	56650.3219	0.0008	AG	+0.2273		⟨7⟩	-I	50	10)
AG Per	56643.4047	0.0049	AG	+0.1752		⟨7⟩	-I	56	10)
	56650.4742	0.0083	AG	−0.8702		⟨7⟩	-I	52	10)
	56654.5347	0.0122	AG	−0.8671		⟨7⟩	-I	52	10)
BR Per	54396.5869	0.0001	MS FR	−0.0029		⟨6⟩	o	682	4)
	56629.4432	0.0002	MS FR	+0.0013		⟨6⟩	o	189	11)
	56642.3437	0.0004	MS FR	+0.0014		⟨6⟩	o	184	11)
DK Per	56540.4771	0.0140	AG	+0.0205	s	⟨7⟩	-I	33	10)
DM Per	56643.4412	0.0191	AG	−0.0043	s	⟨7⟩	-I	50	10)
	56650.2535	0.0010	SCI	−0.0114		⟨7⟩	o	90	2)
IQ Per	56643.5406	0.0034	AG	+0.0003		⟨7⟩	-I	59	10)
	56645.2823	0.0035	PGL	−0.0015		⟨7⟩	V	218	17)
	56650.5147	0.0037	AG	+0.0002		⟨7⟩	-I	53	10)
IT Per	56597.3480	0.0020	JU	−0.0281		⟨7⟩	o	50	2)
	56643.3590	0.0033	AG	−0.0289		⟨7⟩	-I	59	10)
KN Per	56567.4723	0.0010	QU	+0.0657		⟨7⟩	V	70	3)
KR Per	56692.4015	0.0029	AG	−0.0206	s	⟨7⟩	-I	23	10)
	56698.3770	0.0047	AG	−0.0216	s	⟨7⟩	-I	36	10)
V427 Per	56650.4303	0.0074	AG	+0.0094		⟨7⟩	-I	50	10)
V462 Per	56629.2870	0.0005	MS FR	+0.2510		⟨7⟩	o	204	11)
V505 Per	56592.5084	0.0008	AG	+0.0029	s	⟨6⟩	-I	56	10)
	56630.5098	0.0034	AG	+0.0062	s	⟨6⟩	-I	69	10)
V736 Per	56630.5497	0.0065	AG				-I	70	10)
V740 Per	56643.3444	0.0047	AG	+0.0058		⟨7⟩	-I	56	10)
	56643.5292	0.0048	AG	+0.0041	s	⟨7⟩	-I	56	10)
	56650.2447	0.0008	AG	+0.0049	s	⟨7⟩	-I	52	10)
	56650.4301	0.0016	AG	+0.0037		⟨7⟩	-I	52	10)
	56654.3473	0.0029	AG	+0.0040	s	⟨7⟩	-I	52	10)
	56654.5338	0.0029	AG	+0.0040		⟨7⟩	-I	52	10)
V753 Per	56540.3101	0.0011	AG				-I	37	10)
V873 Per	56643.2961	0.0005	AG	−0.0183	s	⟨7⟩	-I	56	10)
	56643.4445	0.0013	AG	−0.0173		⟨7⟩	-I	56	10)
V887 Per	56630.3512	0.0053	AG	−0.0163		⟨7⟩	-I	72	10)
	56650.2980	0.0018	AG	−0.0172		⟨7⟩	-I	50	10)
V959 Per	56338.4140	0.0003	RAT RCR	+0.0210		⟨7⟩	V	120	12)
	56642.5647	0.0001	RAT RCR	+0.0222		⟨7⟩	V	203	12)
	56654.4534	0.0026	AG	+0.0223		⟨7⟩	-I	51	10)

Table 1: cont.

Variable	HJD 24.....	±	Obs	$O-C$		Ref	Fil	n	Rem
	56656.4345	0.0007	AG	+0.0220		⟨7⟩	-I	31	10)
	56670.3041	0.0006	AG	+0.0216		⟨7⟩	-I	39	10)
FY Psc	56596.3630	0.0009	AG				-I	46	10)
	56596.5417	0.0010	AG				-I	46	10)
GK Psc	56596.3714	0.0011	AG				-I	45	10)
	56596.5565	0.0022	AG				-I	45	10)
HO Psc	56521.5418	0.0001	RAT RCR				V	140	12)
U Sge	56526.4380	0.0029	FR	−0.0208	s	⟨7⟩	-I	38	10)
V Sge	56534.5458	0.0048	AG	−0.0803		⟨7⟩	-I	41	10)
	56542.5130	0.0046	AG	−0.0831	s	⟨7⟩	-I	35	10)
CP Sge	56500.4341	0.0167	AG	+0.0702	s	⟨7⟩	-I	23	10)
CW Sge	56539.3539	0.0025	AG	+0.0650		⟨7⟩	-I	43	10)
DK Sge	56539.5385	0.0019	AG	−0.1405		⟨7⟩	-I	45	10)
	56542.3325	0.0027	AG	−0.1447	s	⟨7⟩	-I	35	10)
V365 Sge	56539.4421	0.0016	AG	−0.0658	s	⟨7⟩	-I	43	10)
V368 Sge	56500.4032	0.0035	AG				-I	23	10)
	56539.4952	0.0032	AG				-I	42	10)
	56542.4069	0.0026	AG				-I	32	10)
V369 Sge	56500.4629	0.0069	AG				-I	22	10)
	56542.4203	0.0025	AG				-I	32	10)
V374 Sge	56500.4618	0.0042	AG				-I	23	10)
	56539.5237	0.0021	AG				-I	44	10)
U Sct	56481.4185	0.0002	RAT RCR	−0.0130		⟨7⟩	o	136	19)
V384 Ser	56505.3579	0.0015	FR	−0.0042	s	⟨7⟩	-I	56	10)
	56505.4949	0.0005	FR	−0.0016		⟨7⟩	-I	56	10)
V505 Ser	56505.4843	0.0024	FR	+0.0286	s	⟨3⟩	-I	35	10)
V554 Ser	56449.4419	0.0004	RAT RCR				V	127	12)
RW Tau	56723.2914	0.0007	SCI	−0.2601		⟨7⟩	o	62	2)
RZ Tau	56657.3860	0.0014	AG	+0.0730	s	⟨7⟩	-I	54	10)
	56668.3981	0.0018	AG	+0.0697		⟨7⟩	-I	64	10)
TY Tau	54380.5777	0.0001	MS FR	+0.2465		⟨7⟩	o	870	4)
AH Tau	56643.2775	0.0003	MS FR	+0.0272		⟨7⟩	o	156	11)
AM Tau	56656.4160	0.0014	AG	−0.0642		⟨7⟩	-I	31	10)
AN Tau	56654.2669	0.0026	AG	+0.3171		⟨7⟩	-I	52	10)
CF Tau	56654.3145	0.0184	AG	−0.1156	s	⟨7⟩	-I	52	10)
CT Tau	56657.3931	0.0035	AG	−0.0606	s	⟨7⟩	-I	50	10)
	56692.4016	0.0034	AG	−0.0607		⟨7⟩	-I	29	10)
	56700.4033	0.0009	AG	−0.0610		⟨7⟩	-I	31	10)
CU Tau	56643.2246	0.0004	MS FR	−0.0554	s	⟨7⟩	o	159	11)
EQ Tau	56654.3451	0.0010	WTR	−0.0294		⟨7⟩	o	83	1)
GR Tau	56654.2908	0.0069	AG	−0.0426	s	⟨7⟩	-I	52	10)
	56654.4968	0.0019	AG	−0.0447		⟨7⟩	-I	52	10)
	56657.2988	0.0130	AG	−0.0436	s	⟨7⟩	-I	53	10)
	56713.3875	0.0007	QU	−0.0438		⟨7⟩	V	127	3)
HU Tau	56654.4159	0.0052	AG	+0.0285		⟨7⟩	-I	52	10)
V781 Tau	56657.2701	0.0033	AG	−0.0485		⟨7⟩	-I	50	10)
	56657.4458	0.0040	AG	−0.0453	s	⟨7⟩	-I	50	10)
	56668.3084	0.0019	AG	−0.0473		⟨7⟩	-I	64	10)
	56668.4810	0.0029	AG	−0.0472	s	⟨7⟩	-I	64	10)
V1123 Tau	56643.3277	0.0033	AG	+0.0042	s	⟨6⟩	-I	58	10)
	56643.5258	0.0027	AG	+0.0024		⟨6⟩	-I	58	10)
V Tri	56592.4372	0.0025	AG	−0.0048	s	⟨7⟩	-I	44	10)
	56596.5329	0.0048	AG	−0.0056	s	⟨7⟩	-I	37	10)
RS Tri	56592.5321	0.0004	AG	−0.0484		⟨7⟩	-I	54	10)
	56596.3496	0.0026	AG	−0.0488		⟨7⟩	-I	37	10)
AW Tri	56596.4456	0.0030	AG				-I	38	10)
BC Tri	56596.4786	0.0531	AG	+0.1071	s	⟨7⟩	-I	37	10)
CU Tri	56698.3492	0.0008	MZ				-I	167	3)
W UMa	56698.2904	0.0015	AG	−0.0814		⟨7⟩	-I	41	10)
	56698.4561	0.0007	AG	−0.0825	s	⟨7⟩	-I	41	10)
TY UMa	56354.4398	0.0004	JU	−0.0274	s	⟨7⟩	o	103	2)
UY UMa	56355.3936	0.0023	JU	−0.0566		⟨7⟩	o	100	2)
AA UMa	56397.4657	0.0015	JU	+0.0443	s	⟨7⟩	o	84	2)
ES UMa	56384.5276	0.0002	RAT RCR	+0.0030	s	⟨6⟩	V	223	12)
MS UMa	56408.3750	0.0005	RAT RCR	+0.0469	s	⟨7⟩	V	220	12)
	56408.5763	0.0002	RAT RCR	+0.0430		⟨7⟩	V	220	12)
PZ UMa	56698.3779	0.0013	AG				-I	32	10)
QT UMa	56698.5269	0.0003	AG	−0.0569	s	⟨7⟩	-I	32	10)
V342 UMa	56387.4512	0.0045	JU	−0.0189		⟨7⟩	o	69	2)
	56390.3725	0.0016	JU	−0.0203	s	⟨7⟩	o	61	2)
VY UMi	56390.5549	0.0001	RAT RCR	+0.0285		⟨7⟩	V	224	12)

Table 1: cont.

Variable	HJD 24.....	±	Obs	$O-C$		Ref	Fil	n	Rem
CG Vir	56427.4308	0.0005	QU	+0.1268	s	⟨7⟩	V	58	3) 23) 24)
RS Vul	56535.4116	0.0083	AG	+0.0157		⟨7⟩	-I	30	10)
AX Vul	56521.4882	0.0009	FR	−0.0342	s	⟨7⟩	-I	37	10)
BE Vul	56534.4293	0.0241	AG	+0.0947	s	⟨7⟩	-I	40	10)
BP Vul	56534.4385	0.0028	AG	−0.0542	s	⟨7⟩	-I	41	10)
	56535.4479	0.0012	AG	−0.0150		⟨7⟩	-I	27	10)
CS Vul	56542.4893	0.0018	AG				-I	33	10)
FF Vul	55338.5130	0.0001	MS FR	−0.0762	s	⟨7⟩	o	469	4)
FM Vul	56494.4732	0.0096	AG	+0.0301	s	⟨7⟩	-I	28	10)
FO Vul	56542.3362	0.0004	FR	−0.1541		⟨7⟩	-I	56	10)
FR Vul	56494.3825	0.0002	AG	−0.0092		⟨7⟩	-I	24	10)
	56527.3487	0.0009	AG	−0.0080		⟨7⟩	-I	24	10)
	56542.4206	0.0002	FR	−0.0058		⟨7⟩	-I	70	10)
V511 Vul	56492.5082	0.0003	RAT RCR				V	136	12)
ASAS J055920+2801.7	56657.3575	0.0110	AG				-I	50	10)
ASAS J164358+2617.7	56540.3359	0.0003	FR				-I	40	10)
	56541.3850	0.0002	FR				-I	38	10)
ASAS J191610+1918.3	56526.4015	0.0008	FR				-I	74	10)
ASAS J214320+2215.2	56592.4078	0.0019	AG				-I	30	10)
ASAS J202741+2145.0	56534.4206	0.0083	AG				-I	41	10)
	56535.4352	0.0108	AG				-I	26	10)
GSC 01643-01880	56542.5097	0.0050	AG				-I	35	10)
GSC 01721-01591	55415.4770	0.0003	MS FR	−0.0530	s	⟨5⟩	o	900	4)
	55428.5519	0.0001	MS FR	+0.0162	s	⟨5⟩	o	650	4)
	55429.5086	0.0001	MS FR	−0.2094	s	⟨5⟩	o	754	4)
GSC 02134-00028	55385.4709	0.0009	FR				-I	32	10)
	55387.3804	0.0008	FR				-I	123	10)
	55409.4080	0.0017	FR				-I	41	10)
	55418.3806	0.0026	FR				-I	99	10)
	55429.5313	0.0011	FR				-I	52	10)
	56568.4223	0.0005	FR				-I	53	10)
	56577.3955	0.0018	FR				-I	38	10)
	56579.3030	0.0002	FR				-I	42	10)
GSC 02135-02603	56500.4950	0.0009	FR				-I	94	10)
	56568.3645	0.0004	FR				-I	57	10)
	56579.4060	0.0015	FR				-I	52	10)
	56590.2639	0.0005	FR				-I	25	10)
	56596.2371	0.0015	FR				-I	68	10)
	56624.2891	0.0007	FR				-I	51	10)
	56630.2613	0.0034	FR				-I	21	10)
GSC 02161-01310	56521.6045	0.0008	FR	−0.0042		⟨4⟩	-I	56	10) 21)
GSC 02361-02410	56629.3604	0.0002	MS FR				o	189	11)
	56642.4086	0.0001	MS FR				o	177	11)
GSC 02409-00305	53765.3856	0.0006	FR				-I	42	8)
	53765.5555	0.0011	FR				-I	42	8)
GSC 02695-03163	54682.5165	0.0007	FR				-I	50	10)
	54684.4721	0.0005	FR				-I	39	10)
	54719.3582	0.0009	FR				-I	46	10)
	56159.4049	0.0004	FR				-I	80	10)
GSC 02696-02034	54719.3454	0.0004	FR				-I	88	10)
	56159.5389	0.0008	FR				-I	78	10)
	56650.3203	0.0008	FR				-I	70	10)
GSC 03619-00047	56521.4244	0.0022	AG	+0.0145		⟨2⟩	-I	44	10)
	56541.5554	0.0033	AG	+0.0222	s	⟨2⟩	-I	37	10)
	56600.4641	0.0050	AG	+0.0158		⟨2⟩	-I	47	10)
GSC 03628-00260	56592.3888	0.0040	AG				-I	42	10)
GSC 03674-01587	56540.3579	0.0038	AG				-I	37	10)
	56540.4808	0.0073	AG				-I	37	10)
	56540.5962	0.0020	AG				-I	37	10)
GSC 03944-01954	56568.3506	0.0071	AG				-I	29	10)
GSC 04009-00670	56567.3965	0.0006	MS FR	−0.0097		⟨2⟩	o	295	18)
	56585.3212	0.0136	AG	−0.0022		⟨2⟩	-I	27	10)
GSC 04190-01948	54136.6045	0.0024	SCI				o	147	2)
	54210.3485	0.0021	SCI				o	113	2)
	54210.5966	0.0029	SCI				o	69	2)
	55643.5744	0.0031	SCI				o	120	2)
	55650.4075	0.0022	SCI				o	114	2)
GSC 04339-01166	56540.4624	0.0020	RAT RCR	+0.0233	s	⟨1⟩	V	163	12)
	56541.6163	0.0020	RAT RCR	+0.0460	s	⟨1⟩	V	204	12)
GSC 04500-00730	56167.4211	0.0013	AG				-I	27	10)
	56167.5791	0.0009	AG				-I	27	10)

Table 1: cont.

Variable	HJD 24.....	±	Obs	$O-C$		Ref	Fil	n	Rem
NSVS 1272103	56539.4036	0.0093	AG				-I	44	10)
NSVS 1824689	56644.3133	0.0042	AG				-I	45	10)
	56644.4707	0.0007	AG				-I	45	10)
NSVS 1841163	56585.3294	0.0023	AG				-I	26	10)
NSVS 1916718	56643.4058	0.0065	AG				-I	50	10)
NSVS 2432473	56692.4364	0.0040	AG				-I	28	10)
NSVS 296349	56592.5729	0.0009	AG				-I	49	10)
NSVS 3971593	56643.4363	0.0424	AG				-I	54	10)
NSVS 4116978	56630.3623	0.0043	AG				-I	71	10)
	56630.5157	0.0031	AG				-I	71	10)
	56650.3650	0.0013	AG				-I	51	10)
NSVS 4116978	56650.5159	0.0044	AG				-I	51	10)
NSVS 4732433	56700.3221	0.0086	AG				-I	23	10)
NSVS 6386566	56596.3564	0.0080	AG				-I	46	10)
NSVS 6867860	56657.3200	0.0115	AG				-I	45	10)
NSVS 755884	56354.5031	0.0007	RAT RCR				V	36	12)
NSVS 8209613	56568.3109	0.0003	FR				-I	50	10)
	56579.2664	0.0021	FR				-I	53	10)
NSVS 8299112	56535.4190	0.0025	AG				-I	31	10)
ROTSE1_J175527.44+440654.3	56540.4014	0.0065	AG				-I	24	10)
TYC 4038-0836	56596.4312	0.0151	AG				-I	36	10)
UCAC3 323-013086	56629.3591	0.0028	SCI				o	29	2)
	56629.5933	0.0028	SCI				o	27	2)
U-B1 1113-0498137	56539.3990	0.0068	AG				-I	45	10)
	56542.3629	0.0038	AG				-I	34	10)
	56542.5718	0.0058	AG				-I	34	10)
U-B1 1398-0469064	56588.5786	0.0031	AG	−0.0076	s	⟨2⟩	-I	28	10)
U-B1 1400-0455467	56495.4100	0.0163	AG	−0.0748	s	⟨1⟩	-I	23	10)
	56541.5377	0.0101	AG	−0.0106	s	⟨1⟩	-I	36	10)
U-B1 1416-0454010	56495.5252	0.0020	AG				-I	24	10)
	56521.3779	0.0014	AG				-I	44	10)
	56521.5383	0.0036	AG				-I	44	10)
	56541.4388	0.0034	AG				-I	37	10)
	56541.5954	0.0013	AG				-I	37	10)
	56600.3587	0.0019	AG				-I	48	10)
	56600.5153	0.0023	AG				-I	47	10)
U-B1 1440-0411990	56495.4244	0.0018	AG				-I	24	10)
U-B1 1441-0441871	56541.3633	0.0026	AG	+0.0172		⟨1⟩	-I	36	10)
	56541.5358	0.0028	AG	+0.0212	s	⟨1⟩	-I	36	10)
VSX J190933.7+290329	55074.3950	0.0007	FR				-I	47	10)
	55387.3833	0.0018	FR				-I	59	10)
	55418.4367	0.0007	FR				-I	38	10)
	55429.5780	0.0005	FR				-I	205	10)
	56568.4338	0.0007	FR				-I	37	10)
	56590.3428	0.0015	FR				-I	36	10)
	56596.3031	0.0012	FR				-I	38	10)

Table 2: Times of maxima of pulsating stars

Variable	HJD 24.....	±	Obs	$O-C$	Ref	Fil	n	Rem
XX And	56608.5358	0.0020	ALH	+0.0033	⟨7⟩	V	504	5)
CC And	56541.4273	0.0035	PGL	+0.0366	⟨7⟩	V	75	17)
GP And	56541.4207	0.0035	PGL	+0.0061	⟨7⟩	V	73	17)
	56564.4745	0.0005	WLH	+0.0060	⟨7⟩	-U-I	61	6)
HK And	56520.429	0.001	AG			-I	31	10)
OV And	56592.299	0.001	AG	−0.003	⟨7⟩	-I	43	10)
V460 And	56635.3161	0.0021	PGL	+0.0036	⟨7⟩	V	50	17)
V550 And	56650.358	0.001	AG			-I	40	10)
V341 Aql	56584.3566	0.0035	PGL	+0.0427	⟨7⟩	V	324	17)
RV Ari	56569.4399	0.0008	WLH	−0.0016	⟨7⟩	-U-I	75	6)
	56631.3651	0.0035	PGL	−0.0067	⟨7⟩	V	47	17)
TZ Aur	56638.3918	0.0007	QU	+0.0012	⟨7⟩	V	70	3) 24)
UY Cam	56654.284	0.001	AG	−0.090	⟨7⟩	-I	57	10)
	56654.546	0.001	AG	−0.095	⟨7⟩	-I	57	10)
	56710.3619	0.0012	MZ	−0.0907	⟨7⟩	-I	111	3)
X CMi	56713.350	0.001	AG	−0.089	⟨7⟩	-I	32	10)

Table 2: cont.

Variable	HJD 24.....	±	Obs	$O-C$	Ref	Fil	n	Rem
PS Cas	56526.494	0.001	AG	−0.160	⟨7⟩	-I	30	10)
RZ Cep	56541.5316	0.0015	ALH	−0.1152	⟨7⟩	o	703	5) 25)
NS Cyg	56534.3887	0.0015	MZ	+0.2522	⟨7⟩	-I	107	3)
	56535.4855:	0.0100	MZ	+0.2484	⟨7⟩	-I	79	3)
	56539.3356	0.0013	MZ	+0.2464	⟨7⟩	-I	120	3)
NS Cyg	56540.4349	0.0012	MZ	+0.2451	⟨7⟩	-I	174	3)
	56562.4641	0.0012	MZ	+0.2623	⟨7⟩	-I	148	3)
	56567.4154	0.0013	MZ	+0.2609	⟨7⟩	-I	131	3)
V833 Cyg	56639.2785	0.0009	MZ	−0.1734	⟨7⟩	-I	117	3)
V2455 Cyg	56496.410	0.001	AG	+0.037	⟨7⟩	-I	28	10)
	56496.506	0.001	AG	+0.039	⟨7⟩	-I	28	10)
	56530.4188	0.0014	PGL	+0.0372	⟨7⟩	V	226	17)
LW Del	56565.3368	0.0014	MZ			-I	102	3)
RW Dra	56640.3242	0.0035	PGL	−0.1998	⟨7⟩	V	73	17)
SX For	56155.6140	0.0002	WLH HUN	+0.0496	⟨7⟩	-U-I	283	3)
RR Gem	56640.4371	0.0035	PGL	−0.1148	⟨7⟩	V	45	17)
SZ Gem	56712.3968	0.0010	QU	−0.0735	⟨7⟩	V	71	3) 24)
EW Gem	55622.3566	0.0090	MZ	+0.1435	⟨7⟩	-I	62	3)
	55944.4650	0.0016	MZ	+0.1868	⟨7⟩	-I	133	3)
V403 Gem	56643.322	0.001	AG			-I	50	10)
	56643.665	0.001	AG			-I	50	10)
AR Her	56154.5261	0.0035	PGL	+0.0534	⟨7⟩	V	260	13)
V497 Her	56490.473	0.003	FR			-I	44	10)
V862 Her	56506.3935	0.0020	MZ			-I	102	3)
CH Lac	56588.576	0.002	AG	+0.019	⟨7⟩	-I	28	10)
KZ Lac	56592.318	0.001	AG			-I	43	10)
CM Leo	56710.4965	0.0019	MZ	−0.1435	⟨7⟩	-I	78	3)
AN Lyn	56006.3445	0.0035	PGL			V	137	9)
	56046.4424	0.0014	PGL			V	290	9)
	56243.4862	0.0035	PGL			V	90	9)
BE Lyn	56371.3649	0.0028	PGL			V	229	16)
ZZ Lyr	56568.3210	0.0014	MZ	+0.0072	⟨7⟩	-I	84	3)
	56589.3230	0.0016	MZ	+0.0080	⟨7⟩	-I	70	3)
CN Lyr	56532.4473	0.0056	PGL	+0.0164	⟨7⟩	V	30	13)
V1162 Ori	56343.3898	0.0035	HPF			V	116	16)
VV Peg	56211.4523	0.0035	PGL	−0.0270	⟨7⟩	V	60	17)
VZ Peg	56568.4606	0.0055	MZ	−0.0916	⟨7⟩	-I	119	3)
BH Peg	56219.4298	0.0035	PGL	−0.1202	⟨7⟩	V	290	17)
	56220.3058	0.0035	PGL	+0.1148	⟨7⟩	V	324	17)
	56540.5551	0.0015	ALH	−0.1323	⟨7⟩	V	510	5)
	56549.5346	0.0035	PGL	−0.1267	⟨7⟩	V	137	9)
BP Peg	56569.3034	0.0008	WLH	+0.0467	⟨7⟩	-U-I	59	6)
DY Peg	56190.3965	0.0035	PGL	−0.0092	⟨7⟩	V	119	16)
	56495.4445	0.0069	PGL	−0.0119	⟨7⟩	V	279	13)
	56514.4034	0.0035	PGL	−0.0138	⟨7⟩	V	52	17) 20)
	56622.3342	0.0035	PGL	−0.0139	⟨7⟩	V	99	17)
KV Per	56596.4499	0.0020	MZ	−0.0060	⟨7⟩	-I	86	3)
BO Tau	56639.4390	0.0015	MZ	+0.1907	⟨7⟩	-I	162	3)
SX Tri	55944.2932	0.0013	MZ	+0.1317	⟨7⟩	-I	83	3)
UU Tri	56217.3985	0.0017	MZ	+0.0383	⟨7⟩	-I	109	3)
	56222.4154	0.0017	MZ	+0.0775	⟨7⟩	-I	178	3)
	56229.3002	0.0030	MZ	+0.0489	⟨7⟩	-I	103	3)
	56248.4080	0.0015	MZ	+0.0757	⟨7⟩	-I	205	3)
	56305.3240	0.0018	MZ	+0.0253	⟨7⟩	-I	162	3)
	56656.2962	0.0013	MZ	+0.0733	⟨7⟩	-I	86	3)
	56661.5169	0.0013	MZ	+0.0398	⟨7⟩	-I	128	3)
	56693.3246	0.0020	MZ	+0.0459	⟨7⟩	-I	128	3)
	56698.3259	0.0020	MZ	+0.0696	⟨7⟩	-I	165	3)
RV UMa	56639.5309	0.0035	PGL	+0.1296	⟨7⟩	V	55	17)
TU UMa	56367.4872	0.0005	QU	−0.0571	⟨7⟩	V	224	3) 23) 24)
	56706.5441	0.0031	SCI	−0.0567	⟨7⟩	o	97	2)
AE UMa	56623.4625	0.0035	PGL	−0.0031	⟨7⟩	V	47	17)
	56642.4776	0.0009	SCI	+0.0023	⟨7⟩	o	33	2)
	56642.5585	0.0006	SCI	−0.0028	⟨7⟩	o	33	2)
	56642.6487	0.0011	SCI	+0.0013	⟨7⟩	o	41	2)
	56643.5061	0.0035	PGL	−0.0014	⟨7⟩	V	170	17)
BN Vul	56538.5028	0.0010	ALH	+0.0764	⟨7⟩	V	363	5)
GSC 00144-03031	56333.4301	0.0021	PGL			V	66	16)
	56625.4602	0.0035	PGL			V	72	17)
	56641.4286	0.0035	PGL			V	71	17)
GSC 02671-02149	56559.416	0.003	FR	−0.003	⟨1⟩	-I	39	10)

Table 2: cont.

Variable	HJD 24.....	±	Obs	$O-C$	Ref	Fil	n	Rem
GSC 02847-00586	56629.3903	0.0010	ALH			V	159	5)
	56629.5327	0.0013	ALH			V	159	5)
GSC 02861-00970	56634.2991	0.0008	ALH			V	604	5)
	56634.4086	0.0006	ALH			V	604	5)
	56634.5189	0.0006	ALH			V	604	5)
	56634.6281	0.0006	ALH			V	604	5)
GSC 03428-01497	56331.4160	0.0035	PGL			V	83	16)
GSC 03682-00018	56540.340	0.001	AG			-I	37	10)
GSC 03755-00845	56629.3363	0.0004	ALH			V	69	5)
	56629.4117	0.0004	ALH			V	69	5)
	56629.4879	0.0004	ALH			V	69	5)
ROTSE1 J164316.86+264815.8	56540.350	0.003	FR			-I	40	10)
ROTSE1 J172802.42+231648.3	56490.433	0.003	FR			-I	47	10)
TYC 1698-01052-1	56178.4491	0.0021	PGL			V	112	9)
	56179.4497	0.0035	PGL			V	112	9)
	56179.4722	0.0035	PGL			V	112	9)
	56211.3568	0.0035	PGL			V	152	9)
	56549.4557	0.0035	PGL			V	117	9)
	56638.2976	0.0035	PGL			V	47	17)
U-B1 1424-0504416	56600.241	0.001	AG	−0.017	⟨1⟩	-I	44	10)
	56600.389	0.001	AG	−0.021	⟨1⟩	-I	44	10)
	56600.537	0.001	AG	−0.025	⟨1⟩	-I	44	10)

Observers:

AG:	Agerer, F., Tiefenbach	MZ:	Maintz, Dr. G., Bonn
ALH:	Alich, K., Schaffhausen	PGL:	Pagel, L., Klockenhagen
BHE:	Böhme, D., Nessa	QU:	Quester, W., Esslingen
DIE:	Dietrich, M., Radebeul	RAT:	Rätz, M., Herges-Hallenberg
FR:	Frank, P., Velden	RCR:	Rätz, K., Herges-Hallenberg
HPF:	Hopfer, R., Dresden	SCI:	Schmidt, U., Karlsruhe
HUN:	Hunger, T., Warstein	SIR:	Schirmer, J., Harsefeld
JU:	Jungbluth, H., Karlsruhe	WLH:	Wollenhaupt, G., Oberwiesenthal
MS:	Moschner, W., Lennestadt	WTR:	Walter, F., München

Remarks:

n	number of measurements
:	uncertain
s	secondary minimum
(21)	normal minimum
(22)	assembled from the observations of two nights
(23)	maximum determination as described by Wade et al. (1999)
(24)	mean error in this case: standard deviation
(25)	double maximum: time of the second maximum

Photometers:

(1)	CCD camera ST-6: chip 375×242 uncoated	(11)	CCD camera STL-6303E
(2)	CCD camera ST-7	(12)	CCD camera Moravian G2-1600
(3)	CCD camera ST-7E	(13)	CCD camera QHY8
(4)	CCD camera ST-9E	(14)	CCD camera ATIK 314 L+
(5)	CCD camera ST-8 XMEI	(15)	CCD camera Mead DSI Pro 3
(6)	CCD camera ST-9XE: chip 512×512	(16)	camera Canon EOS 1100D
(7)	CCD camera ST-8 XME	(17)	CCD camera QHY8L
(8)	CCD camera OES-LcCCD12	(18)	CCD camera STXL-6303E
(9)	CCD camera Artemis 4021	(19)	CCD camera ST-8
(10)	CCD camera Sigma 1603		

Filters:

o	without filter
V	V-filter
I_C	I-filter Cousins
-I	IR cut-off filter
-U-I	U and IR cut-off filter

References:

Agerer, F., 2010, *PZP*, **10**, 13 ⟨1⟩
Agerer, F., 2010, *PZP*, **10**, 4 ⟨2⟩
BAV Services for Scientists, 2013, `http://www.bav-astro.de/sfs/index.php/`
Bernhard, K., Frank, P., 2006, *IBVS*, No. 5719 *BAV Mitt.*, **177** ⟨3⟩
Bernhard, K., Frank, P., 2010, *BAV Rb.*, **59**, 2 ⟨4⟩
Bernhard, K., Frank, P., Moschner, W., 2011, *BAV Rb.*, **60**, 2 ⟨5⟩
Kreiner, J. M., 2004, *Acta Astr.*, **54**, 207 ⟨6⟩
Lichtenknecker Database of the BAV, `http://www.bav-astro.de/LkDB/index.php/`
Samus, N. N., et al., 2011, `http://www.sai.msu.su/gcvs/gcvs/index.htm` ⟨7⟩
Wade, R. A., Donley, J., Fried, R., White, R. E., Saha, A., et al., 1999, *AJ*, **118**, 2442

ERRATUM FOR IBVS 5643 (BAVM 172)

VV UMa 53106.4463 PC has to be deleted

ERRATUM FOR IBVS 6026 (BAVM 225)

UU And 55850.4181 RAT RCR has to be deleted
KW Per 55879.2817 BHE has to be deleted

ERRATUM FOR IBVS 6070 (BAVM 231)

SX For 56155.5723 WLH HUN has to be deleted

ERRATUM FOR IBVS 6084 (BAVM 232)

BI CVn 56407.4389 AG has to be deleted

ERRATUM FOR IBVS 6118 (BAVM 234)

FL Lac 56535.4735 AG has to be deleted

COMMISSIONS 27 AND 42 OF THE IAU
INFORMATION BULLETIN ON VARIABLE STARS

Number 6119

Konkoly Observatory
Budapest
8 November 2014

HU ISSN 0374 – 0676

LIGHT TIME EFFECT IN THE SYSTEM V2294 Cyg

LIŠKA, J.

Department of Theoretical Physics and Astrophysics, Masaryk University, Kotlářská 2, 611 37 Brno, Czech Republic, e-mail: jiriliska@post.cz

The eclipsing binary star V2294 Cyg (GSC 03564-03059, 2MASS J19402932+5025522, KIC 12019674, ROTSE1 J194028.86+502554.7, ASAS J194029+5026.0) was discovered as a variable object by Akerlof et al. (2000) in data from the ROTSE all-sky survey. They found a preliminary, but incorrect period of variability of 0.26168(4) d. Follow-up observations were performed by Blättler & Diethelm (2000). They detected brightness changes in the range of 13.25–13.58 mag (unfiltered). Subsequently, they determined a better period of 0.35436(4) d, and found the star to be a W UMa type eclipsing binary. The binary star was included in a catalogue of contact binary stars (Pribulla, Kreiner & Tremko 2003) and in the same year it obtained the name V2294 Cyg in the GCVS (Kazarovets et al. 2003). Several different periods have been published up to now, e.g. 0.354317(3) d (Kreiner 2004) or 0.3544890 d (Pigulski et al. 2009). The latter value is taken from a catalogue of variable stars in the Kepler field of view, which is based on ASAS measurements. This catalogue contains information about average brightness in the V-band of 13.158 mag (amplitude 0.37 mag) and in the I-band of 12.210 mag (amplitude 0.31 mag), respectively.

The system V2294 Cyg was measured by the Kepler Space Telescope and the most information about the eclipsing binary come from this great project. Preliminary parameters from the first 44 days of Kepler operations, e.g. period 0.35450 d, effective temperature 5841 K, ratio of temperatures $T_2/T_1 = 0.91126$ and mass ratio 1.06290, were published by Prša et al. (2011). Updated values from a larger dataset (125 days) include the period 0.354492 d, ratio of temperatures $T_2/T_1 = 1.047$ and mass ratio $M_2/M_1 = 0.760$ (Slawson et al. 2011).

The eclipsing binary V2294 Cyg shows fast and irregular changes with an amplitude of about 2.5 hours in its O–C diagram (Fig. 1). This variability is supported by different published periods. Better orbital elements provided information about cyclic changes in the O–C diagram, which can be explained by the Light Time Effect (LiTE) with an ~ 8 yr period (see below).

The latest results from the Kepler project (Conroy et al. 2014) also describe the variability of the period of the V2294 Cyg in terms of LiTE. Unfortunately their results from LiTE modelling are based on measurements obtained over only a short time interval (4 years), therefore the parameters that they found (period of LiTE $P_3 = 1088.4(34.7)$ d $= 2.980(95)$ yr, eccentricity $e_3 = 0.346(1)$ and semi-amplitude of LiTE $A = 198(4)$ s $= 0.00229(5)$ d) are less reliable.

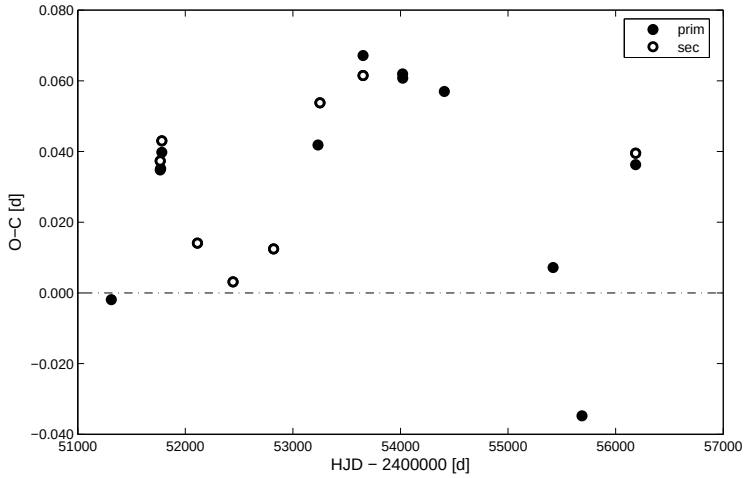

Figure 1. O–C diagram of V2294 Cyg constructed with elements $E_0 = 2451781.365$ and $P = 0.354328\,\mathrm{d}$ adopted from O–C Gateway (Paschke & Brát 2006).

For our study of LiTE in the system, the non-linear least squares method described in Liška et al. (2014) was used. All the mid-eclipse timings were used from the O–C Gateway (Paschke & Brát 2006) and are listed in Table 2 with the corrected types of minima according to our model and original source. All the minima were obtained from CCD light curves and the same value of weights were used for this reason. The best found solution, with the lowest sum of squares of residuals $R = 0.000122$ and corresponding average uncertainty of individual measurement ($0.0024\,\mathrm{d}$), is shown in Fig. 2. Individual parameters together with their uncertainties, determined by the bootstrap method, are summarized in Table 1.

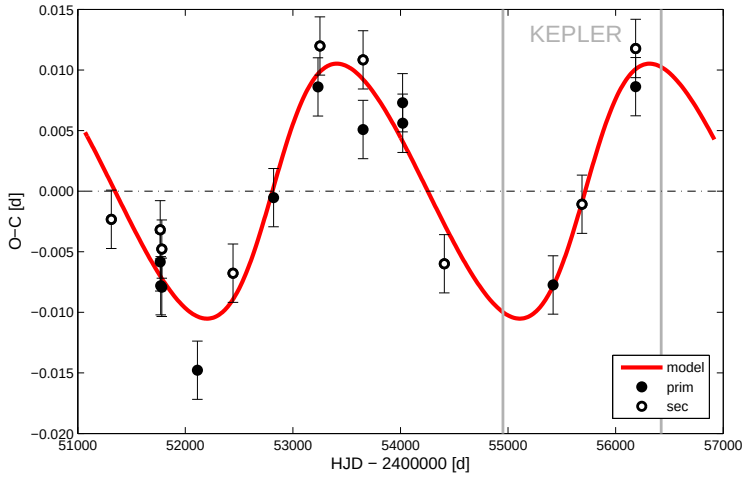

Figure 2. O–C diagram of V2294 Cyg with model of 8 years long LiTE according to parameters from Table 1. Baseline of Kepler observations from JD 2454953 to 2456424 is displayed (area between gray lines).

Despite the fact that our preliminary solution is based on only 20 times of minima from ground-based observations, it seems that our solution for the three-body system is more convincing than the solution based on the parameters from Conroy et al. (2014). The middle ephemeris for eclipses of the binary system in Heliocentric Julian Date (HJD) can be expressed in the form

$$T_{\min} = 2453363.5350^{+17}_{-20} + 0.35449748^{+21}_{-24}\,\mathrm{d} \cdot E. \quad (1)$$

The orbit of the third body with a period of $P_3 \sim 8$ years can be described by parameters from Table 1; time of periastron passage T_0, eccentricity e_3, argument of periastron ω_3 and semi-amplitude of LiTE A. The estimation of the lowest limit of a third body mass from the mass function $f(M_3)$ was performed for an assumed total mass of the eclipsing system of $M_{1+2} = 0.982^{0.173}_{0.111}\,\mathrm{M}_\odot$ (Huber et al. 2014). Unfortunately, the total mass of the star V2294 Cyg was determined only from its total brightness in different bands without taking into account that this is a multiple star system. Therefore, the value of $M_{3\,\min}$ of about $0.66\,\mathrm{M}_\odot$ is only a rough estimate. All three stars could have similar masses and contributions to the total flux.

LiTE allows us to estimate the shape of variations in γ-velocity of an eclipsing binary system caused by the orbit of a third body. Based on our model, the semi-amplitude of these changes is about $8\,\mathrm{km\,s^{-1}}$. Unfortunately no value for radial velocity for V2294 Cyg has been published yet. High-resolution spectroscopic measurements are necessary for a correct analysis of this system.

Table 1: Determined parameters from LiTE model for the three-body system V2294 Cyg. Mass limit of the third body was estimated from mass function $f(M_3)$, inclination of orbit ($i_3 = 90°$) and mass of eclipsing binary $M_{1+2} = 0.982^{0.173}_{0.111}\,\mathrm{M}_\odot$ adopted from Huber et al. (2014).

Parameter	Value
P_{ecl} [d]	0.35449748^{+21}_{-24}
E_0 [HJD]	2453363.5350^{+17}_{-20}
P_3 [y]	7.96^{+30}_{-28}
T_0 [d]	2452820^{+320}_{-390}
e_3	0.27^{+26}_{-5}
ω_3 [°]	2^{+42}_{-52}
A [light day]	0.0109^{+20}_{-8}
R	0.000122
$a_{12}\,\sin i$ [AU]	1.89^{+34}_{-14}
$f(M_3)$ [$\mathrm{M}_\odot$]	0.107^{+63}_{-27}
$M_{3\,\min}$ [$\mathrm{M}_\odot$]	0.66^{+16}_{-10}
K_{12} [$\mathrm{km\,s^{-1}}$]	$7.6^{+2.2}_{-0.5}$

Our results suggest that the use of the short-time interval data from Kepler could lead to misinterpretations as in Conroy et al. (2014). As in the case of similar projects, this high-accuracy photometric project is limited by the length of its time baseline. The approximately 4-year-long interval was insufficient to cover the whole LiTE cycle (see Fig. 2). In addition, the part of the cycle (from minimal value O–C to maximal) covered by the available Kepler data caused confusion in the determination of the length of the orbital period of the third body. We propose that other systems from the publication (Conroy et al. 2014) be investigated as well. Suspect systems occur in the second or third

part of their Table 4 which therefore have LiTE periods longer than half of the baseline of Kepler observations (more than 2 years). Based on our multi-colour photometry of V2294 Cyg (initiated in 2010) together with high-accuracy Kepler measurements, a more comprehensive study on V2294 Cyg is being prepared.

Table 2: Minima used from the O–C Gateway together with information about corrected minimum-type and used publication.

HJD	Type	Source
2451311.8785	sec	Blättler & Diethelm (2000)
2451766.3434	sec	BBSAG 123[a]
2451766.5180	prim	BBSAG 123[a]
2451771.4790	prim	BBSAG 123[a]
2451781.4048	prim	BBSAG 123[a]
2451781.5852	sec	BBSAG 123[a]
2452112.4986	prim	BBSAG 126[a]
2452443.4300	sec	BBSAG 128[a]
2452820.4443	prim	Diethelm (2004)
2453233.4430	prim	Diethelm (2005)
2453251.3485	sec	Diethelm (2005)
2453652.2840	sec	Diethelm (2006)
2453652.4555	prim	Diethelm (2006)
2454019.3626	prim	Diethelm (2007)
2454020.4244	prim	Hübscher & Walter (2007)
2454407.3468	sec	Diethelm (2008)
2455418.5491	prim	Hübscher (2011)
2455687.4421	sec	BAVM 220[b]
2456186.4070	prim	BAVM 231[b]
2456186.5874	sec	BAVM 231[b]

Notes: [a]BBSAG Bulletins from http://www.astroinfo.ch/bbsag/bbsag_e.html,
[b]BAV Mitteilungen from http://www.bav-astro.de/rb/mitteilungen.php

Acknowledgements: This work was supported by the grant MUNI/A/0773/2013. The author thanks Miloslav Zejda for useful comments and Stephan N. de Villiers for carefully reading and language corrections.

References:

Akerlof, C., Amrose, S., Balsano, R., et al., 2000, *AJ*, **119**, 1901
Blättler, E. & Diethelm, R., 2000, *IBVS*, **4995**, 1
Conroy, K. E., Prša, A., Stassun, K. G., et al., 2014, *AJ*, **147**, 45
Diethelm, R., 2004, *IBVS*, **5543**, 1
Diethelm, R., 2005, *IBVS*, **5653**, 1
Diethelm, R., 2006, *IBVS*, **5713**, 1
Diethelm, R., 2007, *IBVS*, **5781**, 1
Diethelm, R., 2008, *IBVS*, **5837**, 1
Huber, D., Silva Aguirre, V., Matthews, J. M., et al., 2014, *ApJS*, **211**, 2

Hübscher, J. & Walter, F., 2007, *IBVS*, **5761**, 1
Hübscher, J., 2011, *BAVSM*, **215**, 1
Kazarovets, E. V., Kireeva, N. N., Samus, N. N., Durlevich, O. V., 2003, *IBVS*, **5422**, 1
Kreiner, J. M., 2004, *AcA*, **54**, 207
Liška, J., Skarka, M., Mikulášek, Z., Zejda, M., 2014, in prep.
Paschke, A. & Brát, L., 2006, *OEJV*, **23**, 13
Pigulski, A., Pojmanski, G., Pilecki, B., Szczygiel, D. M., 2009, *AcA*, **59**, 33
Pribulla, T., Kreiner, J. M. & Tremko, J., 2003, *CoSka*, **33**, 38
Prša, A., Batalha, N., Slawson, R. W., et al., 2011, *AJ*, **141**, 83
Slawson, R. W., Prša, A., Welsh, W. F., et al., 2011, *AJ*, **142**, 160

COMMISSIONS 27 AND 42 OF THE IAU
INFORMATION BULLETIN ON VARIABLE STARS

Number 6120

Konkoly Observatory
Budapest
10 November 2014

HU ISSN 0374 – 0676

ANOTHER COMPONENT IN THE V523 CASSIOPEIAE ECLIPSING BINARY SYSTEM

CASTELAZ, M. W.[1,2]

[1] Brevard College, One Brevard College Drive, Brevard, NC USA 28712, e-mail: michael.castelaz@brevard.edu

[2] Pisgah Astronomical Research Institute, One PARI Drive, Rosman, NC 28772

V523 Cassiopeiae is a W UMa type eclipsing binary. Samec et al. (2004) used 160,000 orbits measured over a period of 102 years for a comprehensive period study. Their O–C diagram strongly suggests a sinusoidal term which is indicative of a third star in the binary system. According to Samec et al. (2004), if a third star were present, it would be about 0.41 solar masses with a period of 101 ± 5 years. However, the difference in the O–C curve calculated from linear light elements and from light elements that include the sinusoidal term could not be clearly distinguished in their O–C diagram. Extrapolating the Samec et al. (2004) linear and sinusoidal ephemerides from 2004 to 2013 shows that a departure from their O–C curves will begin in 2013, after 40,000 orbits since 2004, if a third component exists. We set out to observe the V523 Cas light curve through many orbits in 2012 and 2013 and calculated the O–C diagram through 2013. If a third component is present, it should be clear from the new O–C diagram.

V523 Cas is located at $\alpha_{2000} = 0^{\rm h}40^{\rm m}06\overset{\rm s}{.}2$, $\delta_{2000} = +50°14'16\overset{''}{.}0$ and is fairly bright with $V \sim 10.9$ magnitudes and about 1.0 magnitude difference between minimum and maximum. The system was observed using the Pisgah Astronomical Research Institute 0.4-m telescope equipped with an Apogee E42 2048×2048 CCD camera and VRI filters. Exposure times were 40 seconds in each filter. The number of images per filter per night varied from 80 to 120. Observations were made on UT 2012 October 22, 23, 24, 25, November 2, 9, 11, 14, 16, 18, 19, 21, 22, 25, 26, 29, and UT 2013 October 10, 11, 12, 24, November 4, 8, 11, 14, 15. A total of 1,833 images were made in each filter over the two year period.

The telescope and camera have a 30 arcminute field of view. Three stars in this field of view were selected as the comparison and check stars. Table 1 lists the coordinates and magnitudes of these stars and Figure 1 is the finding chart. The V magnitudes are from the Tycho-2 Catalog (Hog et al. 2000) and the R and I magnitudes are from the USNO B1.0 Catalog (Monet et al. 2003).

Table 1. Comparison and check stars.

Star	RA (J2000)	Dec (J2000)	V	R	I
BD+49 151 (Comparison)	00 40 15.01	+50 07 14.6	9.75	9.63	9.53
BD+49 154 (Check 1)	00 40 26.17	+50 06 16.0	9.84	9.69	9.56
TYC 3257-747-1 (Check 2)	00 40 49.02	+50 22 49.13	10.27	9.93	9.67

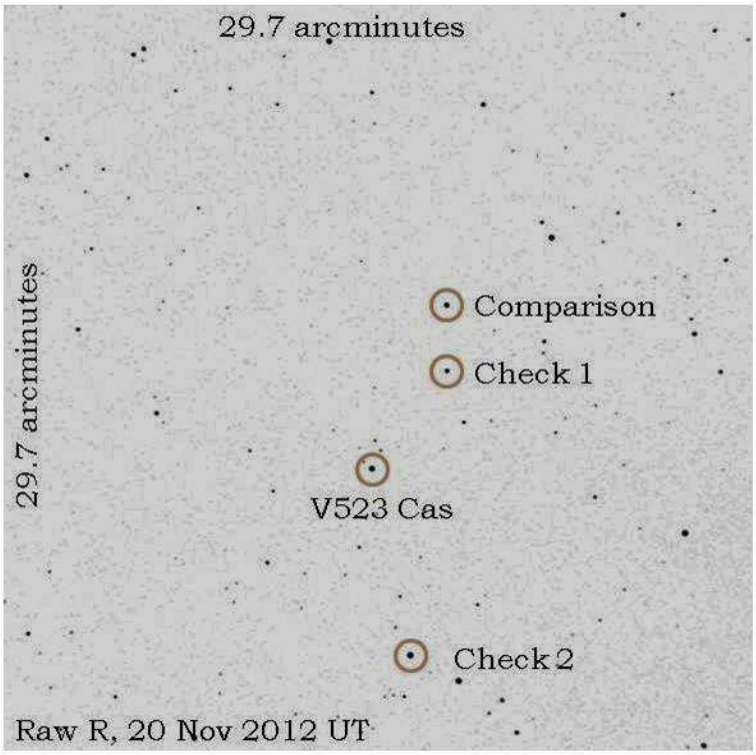

Figure 1. Finding chart for V523 Cas.

The images were bias, dark, and flat field corrected. Photometry of V523 Cas and comparison and check stars was done with an aperture radius of 12 arcseconds for star brightness measurement, and a concentric outer annulus from 14 arcseconds to 17 arcseconds for sky measurements. The magnitude measurement error was 0.010, 0.008, and 0.006 in V, R, and I, respectively. The time of measurement was converted to heliocentric Julian date. Phase was calculated from the ephemeris $2446708.786 + 0.^{\rm d}233691049E$ (Samec et al. 2004). Figure 2 shows the light curve of V523 Cas from all observations made in 2012 and 2013. The V, R, and I observations are given in Tables 2, 3 and 4 as HJD, orbital phase (based on the ephemeris) and magnitude. (The tables are available through the IBVS website as `6120-t1.txt`, `6120-t2.txt`, and `6120-t3.txt`.)

Over the total of 25 days of observations in two years, 30 primary minima were measured. Two primary minima were observed in one night on 2012 October 23, November 11, 14, 18 and 2013 October 12, 24, and November 14. On all other days, only one primary minimum was observed. The opportunity exists to precisely measure the period of the V523 Cas directly on 7 separate occasions. In order to measure the period and calculate the O–C curve, the time of minimum must be determined. Table 5 lists the dates of observations, times of minima measured with bisector of chords method of Kwee and van Woerden (1956) and the error in determining the primary minima. Also included in Table 5 are all (48) published primary minima measured between 2004 and the observations presented here. Note that the bisector of chords method was used by Samec et al. (2004) in their period analysis that led to the suggestion of a third component in the system.

The linear light ephemeris used to calculate times of minima without a third component was determined from Samec et al. (2004) and is

HJD min. I $= 2446708.7773 + 0.^{\rm d}233689935E$

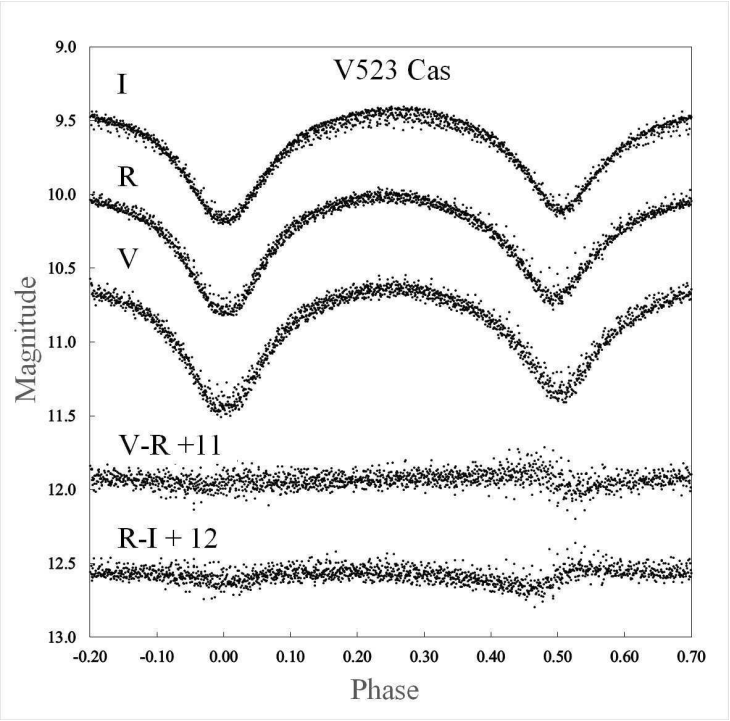

Figure 2. V523 Cas VRI light curves.

The linear light ephemeris was applied to all recorded times of primary minima given in the Brno Regional Network of Observers O–C Gateway database (Paschke & Brat 2006), plus the current set of observed primary minima. Figure 3 shows the O–C values. The best fit which includes the effect of a third component to the O–C values is given by the ephemeris with a sinusoidal term (Samec et al. 2004):

HJD min. I = $2446708.8030+0^{\rm d}.233691049E+1.1\cdot10^{-11}E^2+(0^{\rm d}.041)[\sin(3.90\cdot10^{-5}E-1.04]$

The sinusoidal fit, as well as a parabolic fit, are shown in Figure 3. Figure 4 is the same O–C diagram, but showing the data only from 2004 through 2013. Figure 4 clearly shows the deviation between the parabolic and sinusoidal models of the O–C diagram. Table 5 lists the current O–C residuals and those measured since 2004 for both the parabolic and sinusoidal models. (Table 5 is available through the IBVS website as `6120-t4.txt`.)

The sinusoidal fit of the O–C residuals does not deviate and represents a better model than a parabolic fit, strongly suggesting the presence of a third component. We adopt the sinusoidal ephemeris as best predicting the times of minima of V523 Cas.

Kepler's third law and using the sinusoidal component with an amplitude of 0.041 days implies the mass of the third component according to this ephemeris is 0.6 solar masses and the orbital period of the larger system is 70 years, assuming all three stars are in the same orbital plane.

An orbital period of 70 years implies a semimajor axis of 17 AU or a maximum angular separation of 0.25 arcseconds at the distance of V523 Cas of 69 pc (Samec et al. 2004). Rucinski et al. (2007) searched eclipsing binaries for companions using an adaptive optics method. Their resolution was 0.07–0.08 arcseconds in separation and magnitude difference in the K filter up to 6 magnitudes. V523 Cas was included in their search. They did not

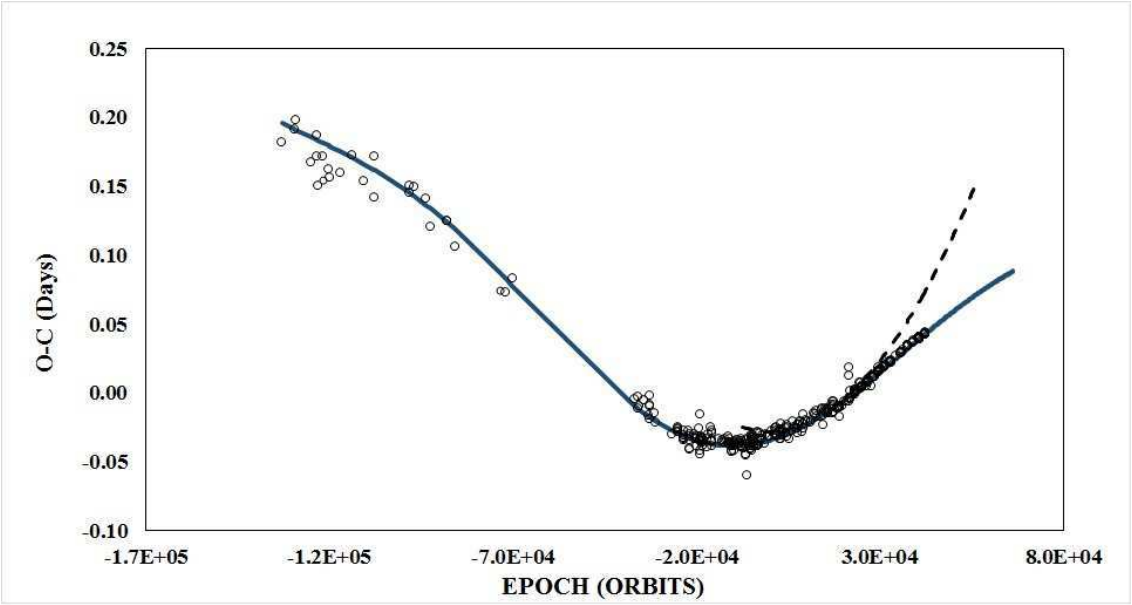

Figure 3. V523 Cas O–C diagram from to 2013. The circles represent the O–C values, the dashed line is the ephemeris without a third component and the solid line is the ephemeris that includes a third component.

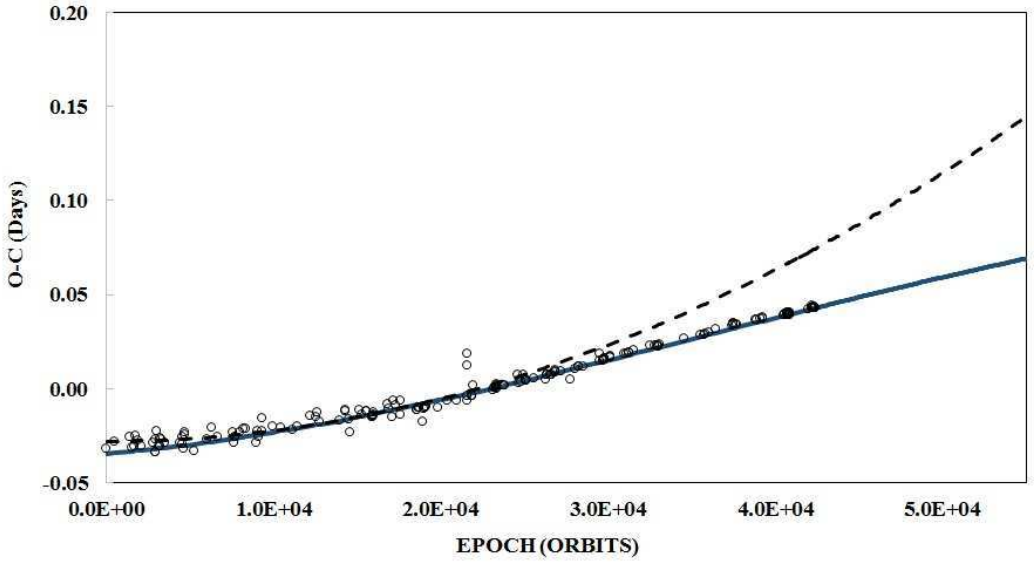

Figure 4. V523 Cas O–C diagram from 2004 to 2013. The circles represent the O–C values, the dashed line is the ephemeris without a third component and the solid line is the ephemeris that includes a third component

detect the third component which implies that the third component must be nearly along the line of sight to the eclipsing binary system of V523 Cas. However, a quarter of a period later, or in about 18 years, the third component should be clearly visible with current spatial resolution imaging capabilities.

Table 5. Times of Minima and O–C residuals.

Date	Primary Minimum (HJD 2450000+)	Error[a] (days)	Parabolic O–C residuals	Sinusoidal O–C residuals	Ref[b]
2004 Feb 20	3056.3286	0.008	−0.00473	0.00042	1
2004 Jul 07	3193.501	—	−0.01081	−0.00512	2
2004 Sep 14	3263.1465	—	−0.00619	−0.00021	3
2004 Nov 06	3316.429	—	−0.00598	0.00023	3
2004 Nov 07	3316.6628	—	−0.00587	0.00033	3
2004 Dec 29	3369.0099	0.0003	−0.00629	0.00014	4
2005 Aug 16	3599.436	—	−0.00283	0.00467	2
2005 Aug 19	3602.2365	—	−0.00666	0.00085	3
2005 Oct 05	3648.508	—	−0.00666	0.00108	3
2005 Oct 06	3650.3771	—	−0.00711	0.00063	3
2005 Oct 07	3651.3117	—	−0.00729	0.00046	1
2005 Oct 07	3661.5948	—	−0.00675	0.00105	3
2005 Oct 08	3662.2965	—	−0.00613	0.00167	3
2005 Oct 08	3662.5295	—	−0.00682	0.00098	3
2005 Oct 25	3669.307	—	−0.00646	0.00137	4
2006 Jan 09	3745.2573	—	−0.00686	0.00135	1
2006 Jan 09	3745.4916	0.0011	−0.00626	0.00196	3
2006 Jul 26	3943.4294	0.0001	−0.00772	0.00153	5
2006 Sep 08	3987.3632	0.0001	−0.00851	0.00099	6
2006 Oct 09	4018.211	0.0001	−0.00839	0.00127	3
2006 Oct 10	4019.3796	—	−0.00827	0.00141	7
2006 Dec 16	4086.4499	0.0004	−0.00833	0.00173	6
2007 Aug 02	4314.5347	—	−0.00956	0.00185	5
2007 Sep 22	4366.4144	—	−0.01010	0.00163	3
2007 Oct 27	4401.2344	—	−0.01062	0.00133	3
2007 Nov 17	4422.0319	—	−0.01196	0.00012	3
2007 Nov 24	4429.0432	—	−0.01150	0.00062	3
2007 Dec 07	4441.6632	0.0001	−0.01102	0.00118	8
2008 Nov 08	4779.3502	0.0001	−0.01316	0.00132	9
2009 Jul 04	5017.4829	0.0001	−0.01571	0.00051	10
2009 Aug 10	5054.4066	0.0001	−0.01584	0.00066	10
2009 Sep 02	5076.6077	—	−0.01577	0.00090	10
2009 Oct 21	5126.3843	0.0001	−0.01624	0.00082	3
2010 Jan 24	5221.2646	—	−0.01618	0.00162	10
2010 Sep 21	5461.0338	—	−0.01832	0.00146	3
2010 Sep 28	5468.2785	—	−0.01817	0.00167	3
2010 Oct 08	5478.3278	—	−0.01777	0.00216	3
2010 Oct 09	5478.5615	0.0001	−0.01777	0.00216	3
2010 Oct 30	5500.2942	0.0003	−0.01873	0.00138	10
2010 Nov 17	5517.5877	0.0002	−0.01869	0.00158	11
2011 Aug 04	5778.3891	—	−0.02137	0.00122	12
2011 Aug 21	5794.514	—	−0.02145	0.00128	3
2011 Oct 15	5850.3669	—	−0.02178	0.00148	3
2011 Nov 17	5883.0837	—	−0.02235	0.00121	3
2011 Nov 17	5883.3178	0.0002	−0.02195	0.00162	3
2012 Sep 12	6183.3786	0.0002	−0.02629	0.00020	12
2012 Sep 18	6189.4547	—	−0.02628	0.00027	12
2012 Sep 19	6219.6015	—	−0.02622	0.00064	3
2012 Oct 22	6222.63863	0.00022	−0.02761	−0.00072	13
2012 Oct 23	6223.57480	0.00175	−0.02587	0.00103	13
2012 Oct 23	6223.80757	0.00014	−0.02697	−0.00006	13
2012 Oct 24	6224.74323	0.00059	−0.02661	0.00030	13

Table 5. Continued Times of Minima and O–C residuals.

Date	Primary Minimum (HJD 2450000+)	Error[a] (days)	Parabolic O–C residuals	Sinusoidal O–C residuals	Ref[b]
2012 Nov 02	6233.62264	0.00022	−0.02747	−0.00047	13
2012 Nov 09	6240.63314	0.00011	−0.02718	−0.00010	13
2012 Nov 11	6242.50281	0.00015	−0.02714	−0.00005	13
2012 Nov 11	6242.73649	0.00014	−0.02703	0.00007	13
2012 Nov 14	6245.54068	0.00053	−0.02750	−0.00038	13
2012 Nov 14	6245.77544	0.00043	−0.02671	0.00041	13
2012 Nov 16	6247.64421	0.00014	−0.02755	−0.00040	13
2012 Nov 18	6249.51396	0.00026	−0.02693	0.00023	13
2012 Nov 18	6249.74730	0.00007	−0.02720	−0.00003	13
2012 Nov 19	6250.68245	0.00025	−0.02707	0.00011	13
2012 Nov 21	6252.55234	0.00012	−0.02671	0.00049	13
2012 Nov 22	6253.48601	0.00048	−0.02767	−0.00046	13
2012 Nov 25	6256.52497	0.00029	−0.02702	0.00021	13
2012 Nov 29	6260.49747	0.00021	−0.02720	0.00008	13
2013 Aug 14	6519.4294	—	−0.02999	0.00002	3
2013 Oct 10	6575.74935	0.00016	−0.03074	−0.00012	13
2013 Oct 11	6576.68531	0.0004	−0.02956	0.00108	13
2013 Oct 12	6577.61881	0.00021	−0.03083	−0.00018	13
2013 Oct 12	6577.85236	0.00008	−0.03096	−0.00031	13
2013 Oct 24	6589.53704	0.00024	−0.03092	−0.00014	13
2013 Oct 24	6589.77115	0.00025	−0.03047	0.00032	13
2013 Nov 04	6600.75474	0.00015	−0.03058	0.00032	13
2013 Nov 08	6604.72680	0.00015	−0.03127	−0.00032	13
2013 Nov 11	6607.76530	0.00001	−0.03103	−0.00005	13
2013 Nov 14	6610.56932	0.00014	−0.03126	−0.00025	13
2013 Nov 14	6610.80309	0.00021	−0.03147	−0.00045	13
2013 Nov 15	6611.50413	0.00055	−0.03120	−0.00018	13

[a] Errors are stated when given in the reference.
[b] 1) Brat et al. 2007, 2) Locher 2005, 3) Paschke & Brat 2006, 4) Kim et al. 2006, 5) Parimucha et al. 2007, 6) Dogru et al. 2007a, 7) Csizmadia 2006, 8) Dogru et al. 2007b, 9) Hübscher et al. 2009, 10) Parimucha et al. 2011, 11) Diethelm 2011, 12) Parimucha et al. 2013, 13) This paper.

References:

Brat, L., Zejda, M., Svoboda, P. 2007, *Open European Journal on Variable Stars*, No. 74, 1

Csizmadia, Sz. et al. 2006, *IBVS*, No. 5736

Diethelm, R. 2011, *IBVS*, No. 5960

Dogru, S.S. et al. 2007a, *IBVS*, No. 5746

Dogru, S. S., Dogru, D., Dönmez, A. 2007b, *IBVS*, No. 5795

Hog, E. et al. 2000, *A&A*, **355**, L27

Hübscher, J., Steinbach, H-M., Walter, F. 2009, *IBVS*, No. 5889

Kim, Chun-Hwey et al. 2006, *IBVS*, No. 5694

Kwee, K. K. & van Woerden, H., 1956, *BAN*, **12**, 327

Locher, K. 2005, *Open European Journal on Variable Stars*, No. 3, 1

Monet, D. et al. 2003, *AJ*, **125**, 984

Paschke, A. & Brat, L. 2006, *Open European Journal on Variable Stars*, No. 23, 13

Parimucha, S. et al. 2007, *IBVS*, No. 5777

Parimucha, S., Dubovsky, P., Vanko, M., Pribulla, T., Kudzej, I., Barsa, R. 2011, *IBVS*, No. 5980

Parimucha, S., Dubovsky, P., Vanko, M. 2013, *IBVS*, No. 6044

Rucinski, S. M., Pribulla, T., & van Kerkwijk, M. H. 2007, *AJ*, **134**, 2353

Samec, R. G., Faulkner, D. R., & Williams, D. B., 2004, *AJ*, **128**, 2997

COMMISSIONS 27 AND 42 OF THE IAU
INFORMATION BULLETIN ON VARIABLE STARS

Number 6121

Konkoly Observatory
Budapest
6 December 2014

HU ISSN 0374 – 0676

NEW SPECTROSCOPY OF MULTIPLE STARS RR LYNCIS AND HT VIRGINIS

BENSCH, KATARZYNA[1,2]; DIMITROV, WOJCIECH[1]; ŻYWUCKA, NATALIA[2]; FAGAS, MONIKA[1]; KAMIŃSKI, KRZYSZTOF[1]; PRZYBYSZEWSKA, ANNA[1]; MALICZAK, MATEUSZ; KURZAWA, KRYSTIAN[1]; KRUSZEWSKI, ADRIAN[1]; KOWALCZYK, TOMASZ; BORCZYK, WOJCIECH[1]; BĄKOWSKA, KAROLINA[1]; BARTCZAK, PRZEMYSŁAW[1]; KWIATKOWSKI, TOMASZ[1]; SCHWARZENBERG-CZERNY, ALEKSANDER[3]

[1] Astronomical Observatory Institute, Faculty of Physics, A. Mickiewicz University, Słoneczna 36, 60-186 Poznań, Poland, email: `katarzyna.bensch@gmail.com`

[2] Astronomical Observatory, Jagiellonian University, Orla 171, 30-244 Kraków, Poland

[3] Nicolaus Copernicus Astronomical Center, Polish Academy of Sciences, Bartycka 18, 00-716 Warsaw, Poland

In this paper we present radial velocity measurements as a result of new spectroscopic observations of RR Lyncis and HT Virginis. Both systems are worth to be the objects of a long-term monitoring. The observations made during a long period of time reveal the apsidal motion and the movements around the center of mass of the systems. Long-term measurements enable us to measure the light-time effect in the eclipsing binaries as well. Data were collected using the Poznań Spectroscopic Telescope (PST1) at Borowiec station (Baranowski et al. 2009) covering a range of wavelength $4280 - 7500$ Å. The telescope is equipped with an echelle spectrograph thermally stabilized to 0.1°C. The data were calibrated with ThAr (Thorium-Argon) lamp. Data reduction was performed with IRAF[1] (Image Reduction and Analysis Facility) `echelle` package based scripts. The one-dimensional cross-correlation technique (Cross Correlation Function) was used to determine radial velocities of components with IRAF FXCOR task.

RR Lyncis

RR Lyn is listed in SIMBAD database as an eclipsing binary of Algol type with V magnitude of $5\overset{\mathrm{m}}{.}54$, color index $(B-V) = 0\overset{\mathrm{m}}{.}22$ and with equatorial coordinates $\mathrm{RA}_{2000} = 06^{\mathrm{h}}26^{\mathrm{m}}26^{\mathrm{s}}$, $\mathrm{Dec}_{2000} = +56°17'06''$. It is one of the the nearest eclipsing binaries in the northern sky at the distance of 73.5 ± 2.8 pc (Khaliullin et al. 2001).

First spectroscopic observations of RR Lyncis were made in 1915 by Harper (1915) while the first light curve was presented by Huffer (1931). Spectroscopic orbits for the object were derived by Popper (1971) and Kondo (1976). In 2001 Khaliullin et al. carried out accurate WBVR photoelectric photometry of RR Lyn and obtained light curves of the eclipsing system (Khaliullin et al. 2001). Khaliullin and Khaliullina (2002) detected quasi-periodic co-phased oscillations of times of the primary and secondary minima of

[1] IRAF is distributed by the National Optical Astronomy Observatory, which is operated by the Association of Universities for Research in Astronomy, Inc., under a cooperative agreement with the National Science Foundation.

RR Lyn, based on photoelectric observations which were published during the previous 70 years. The presence of a third body with an estimated mass of $M < 0.9\ M_{\odot}$ was suggested as an explanation. The latest spectroscopic measurements (Tomkin & Fekel 2006) do not confirm the presence of a third component in the system.

The following ephemeris was derived based on high-precision $WBVR$ photoelectric measurements and other published photoelectric timings of minima of RR Lyn (Khaliullin et al. 2001):

$$\text{Min. I} = \text{HJD}2444988.49594(30) + 9\overset{\text{d}}{.}9450738(7) \times E.$$

The light curve obtained by Khaliullin et al. (2001) was typical of detached binaries of Algol type. The spectral types obtained from $WBVR$ photometry for eclipsing binary components are A6 IV for primary component and F0 V for the second one.

Our spectroscopic data (15 nights) were acquired in April 2010 and during the period between January and June 2011. The exposure times were $600 - 1800$ s. The cross-correlation function for RR Lyn shows the presence of two components (Figure 1). Two narrow peaks are connected with the eclipsing pair. The results of measurements are presented in Table 1. The radial velocities for component 2 measured in certain phases (near 0 and 0.5) were impossible to derive due to the blending of CCF (Cross-Correlation Function) peaks. The results for component 1 in corresponding phases are also affected by blending.

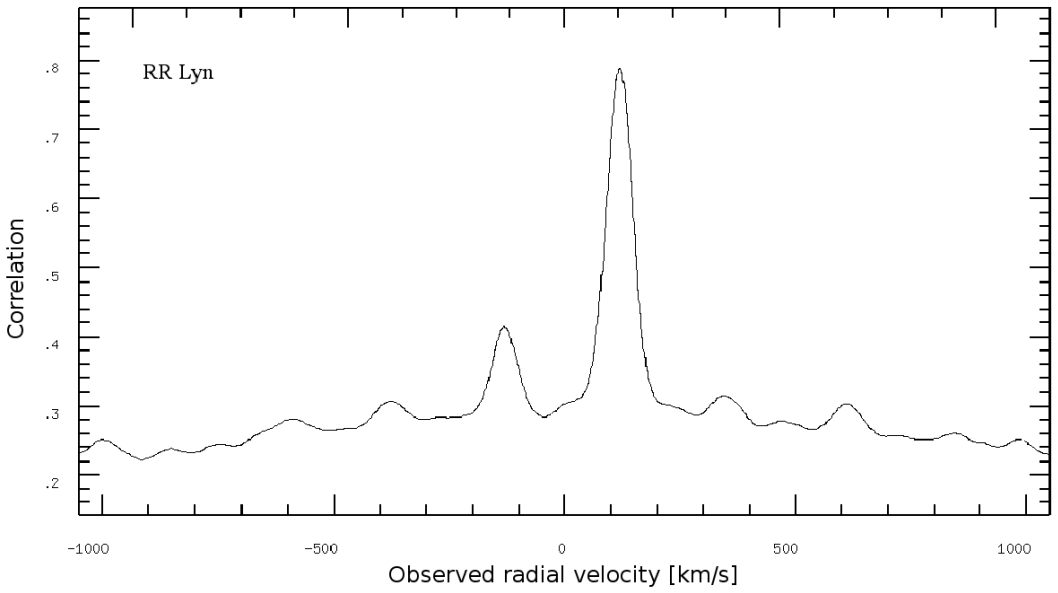

Figure 1. The cross-correlation function for RR Lyn. There are two peaks of the eclipsing pair.

We used the PHOEBE code (Prša & Zwitter 2005) based on the Wilson-Devinney method (Wilson & Devinney 1971) in order to derive preliminary solution for the system parameters from this radial velocities. We used Tomkin & Fekel (2006) values for inclination and surface potential (fixed parameters). The measurements made during phases of the minimal radial velocities were not taken into account during modeling due to the blending effect. The radial velocity solution for RR Lyn is well defined (Figure 2) because of the narrow shape of the peaks which are well separated in CCF. The dispersion of data

is equal to $\sigma = 0.36\,\mathrm{km/s}$. The results from the radial velocity curve modelling (Table 2) are the preliminary solution. We present the preliminary solution in order to provide a reader with the orders of magnitude of the results obtained using our measurements.

The spectroscopic data we obtained is shifted with respect to the ephemeris ($ph_{\mathrm{shift}} = -0.004 \pm 0.003$). The ephemeris might have been affected by the light-time effect.

Table 1. Heliocentric radial velocity measurements for two eclipsing components of RR Lyn - PST1. (The values given in the table are plotted in the chart in Fig. 2.)

HJD	RV_1	RV_2	HJD	RV_1	RV_2
-2455000	[km/s]	[km/s]	-2455000	[km/s]	[km/s]
304.38946	−74.0	73.0	624.41394	−10.7	−*
304.39930	−75.7	−**	624.43784	−10.1	−*
304.42738	−73.0	73.3	629.35782	−3.2	−*
305.35812	−42.2	33.4	629.38278	−4.2	−*
305.38691	−41.0	31.4	629.42699	−5.9	−*
605.35305	21.9	−50.8	629.45110	−6.7	−*
605.37696	22.7	−52.1	629.47628	−7.4	−*
605.40829	23.6	−53.9	629.49952	−8.1	−*
605.43169	24.4	−54.7	650.36610	−45.1	35.4
614.25972	−17.0	−*	650.38209	−45.7	36.5
614.28042	−16.3	−*	705.37704	36.9	−71.1
614.30271	−15.6	−*	705.39313	37.3	−71.9
616.27191	44.2	−80.9	707.34378	43.5	−80.3
616.28857	44.6	−80.9	707.35998	43.6	−80.3
616.30449	44.8	−81.0	707.38418	42.8	−80.3
621.31289	−73.0	70.2	707.40148	42.9	−79.8
621.33188	−73.3	71.1	716.37329	50.1	−87.5
624.36039	−12.2	−*	716.38878	50.1	−87.3
624.38715	−11.3	−*			

* - There is no RV value derived in this phase due to the blending of CCF peaks,
** - no values due to higher dispersion of the measurements.

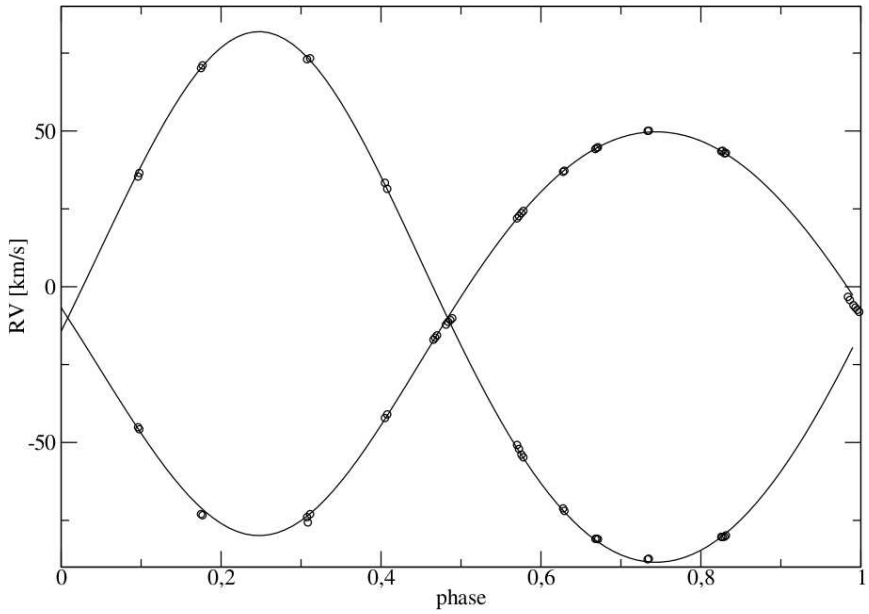

Figure 2. Radial velocity measurements (PST1) for two components of the eclipsing pair RR Lyn. The solid line presents the synthetic curve based on the derived model.

Table 2. Preliminary solution for the eclipsing pair RR Lyn and formal errors outputted by the PHOEBE code.

Parameter	Value
HJD_0	2455629.530±0.004
P (days)	9.9453±0.0002
a ($R_\odot$)	29.55±0.04
e	0.087±0.002
ω (rad)	3.17±0.02
V_γ (km s^{-1})	−10.06±0.08
q	0.769±0.002
i^* (deg)	87.45 (fixed)
$\Omega^*_{R_1}$	12.176 (fixed)
$\Omega^*_{R_2}$	15.570 (fixed)

* - fixed values based on results of Tomkin & Fekel (2006).

HT Virginis

HT Vir is listed in SIMBAD database as an eclipsing binary of W UMa type. The visual magnitude of the object is $7\overset{\mathrm{m}}{.}16$, color index is $(B-V) = 0\overset{\mathrm{m}}{.}54$ and the equatorial coordinates are $\mathrm{RA}_{2000} = 13^{\mathrm{h}}46^{\mathrm{m}}07^{\mathrm{s}}$, $\mathrm{Dec}_{2000} = +05°06'56''$.

The first photometric measurements of this object were made by Walker & Chambliss (1985). The spectroscopic measurements published by Lu et al. (2001) showed that HT Vir is a quadruple system with a contact binary (HT Vir B - eclipsing pair of SB2 type) and a component HT Vir A which is actually also a binary of SBI type. The analysis of the data from the Hipparcos indicated the separation between the component HT Vir B and HT Vir A equal to 0.56 arcsec (Fabricius & Makarov 2000).

The orbital period of the contact binary is 0.407670 d and the period of single-lined binary is 32.45 d (Lu et al. 2001). Zola et al. (2005) obtained BVR photometric measurements of HT Vir B. The light curve is typical of W UMa-type stars. Lu et al. derived F8 V spectral type for HT Vir B.

The spectra used for the measurements presented in this paper were acquired during 5 nights of observations in May 2011. The exposure time of each spectrum was 1800 s. There are three peaks in the CCF of HT Vir (Figur 3). Two peaks which are related to the eclipsing pair are broad because of fast rotation of both components. The narrow peak is connected with the third component. The results of radial velocity measurements are presented in Table 3. The RV measurements for both components of the eclipsing pair close to phases 0 and 0.5 were impossible to derive due to the blending of CCF peaks. The results for third body in these phases are affected by blending as well.

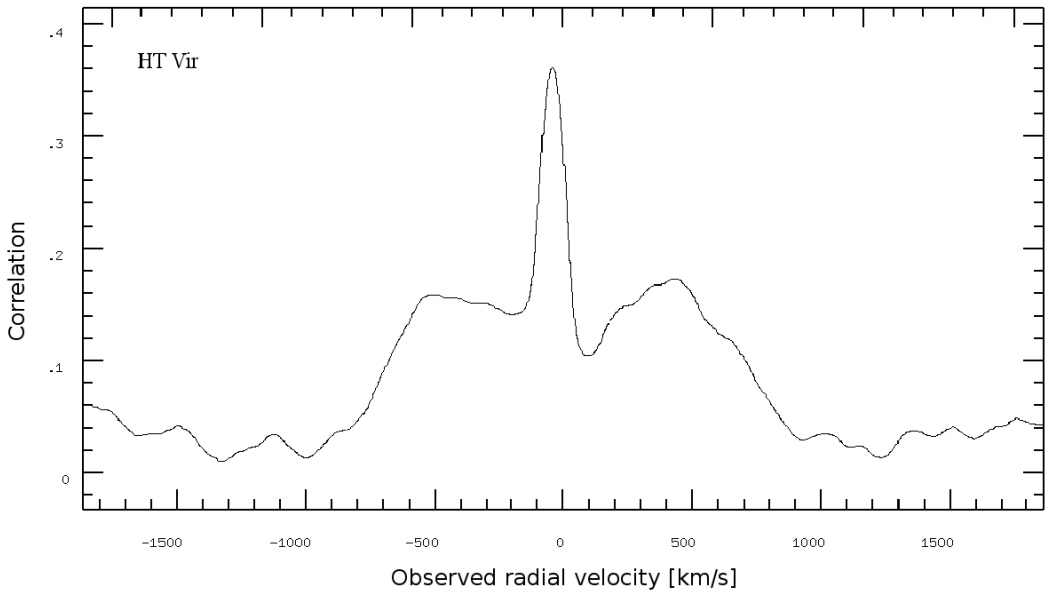

Figure 3. The cross correlation function for HT Vir. The two broad peaks of the eclipsing pair and one narrow are shown (component A).

We derived preliminary parameters of the HT Vir B system from radial velocities using PHOEBE code. As the input fixed values we used parameters of i, Ω_1 and Ω_2 from Zola et al. (2005). As a starting point for adjusting the parameter of HJD_0 we used the value $HJD_0 = 2455691.528$ of one of the measurements close to the phase 0. The adjusted radial velocity curve is shown in Figure 4. We present the parameters of the model adjusted to the radial velocities in Table 4. The large dispersion of data $\sigma = 11.0\,\mathrm{km/s}$ is due to the fast rotation of the components of the eclipsing pair which causes the broad and not well defined shape of the peaks on the CCF.

The broadening function (Rucinski 1992) method or TODCOR (Mazeh & Zucker 1992) could improve the radial velocity measurements for HT Vir. The spectra will be available at CDS for future analysis.

Table 3. Heliocentric radial velocity measurements for three components of HT Vir - PST1. (The values are plotted in the chart in Fig. 4.)

HJD	RV_1	RV_2	RV_3	HJD	RV_1	RV_2	RV_3
−2455000	[km/s]	[km/s]	[km/s]	−2455000	[km/s]	[km/s]	[km/s]
688.37647	−201.8	153.5	−23.6	693.37783	82.1	−128.3	−31.0
688.40044	−167.5	122.4	−23.6	693.40186	137.7	−152.6	−31.2
691.34020	99.9	−96.4	-27.1	693.43032	169.9	−187.9	−31.0
691.36410	131.1	−144.0	−27.5	693.45378	184.6	−210.9	−31.2
691.39680	165.0	−202.1	−28.5	693.47730	158.9	−166.4	−30.5
691.42198	143.2	−191.4	−28.4	703.37042	−152.5	85.9	−28.8
691.44844	142.0	−180.8	−28.5	703.39398	−174.1	99.7	−28.7
691.47214	113.4	−155.4	−28.6	703.41970	−205.7	135.8	−28.5
691.52809	−*	−*	−28.5	703.44765	−178.3	99.8	−28.8
692.34068	−*	−*	−29.5	703.47494	−183.6	143.8	−28.7
692.36357	−139.2	111.1	−29.4	703.49766	−152.4	90.7	−28.8
693.35396	−*	−*	−30.9				

*There is no RV value derived in this phase due to the blending of CCF peaks.

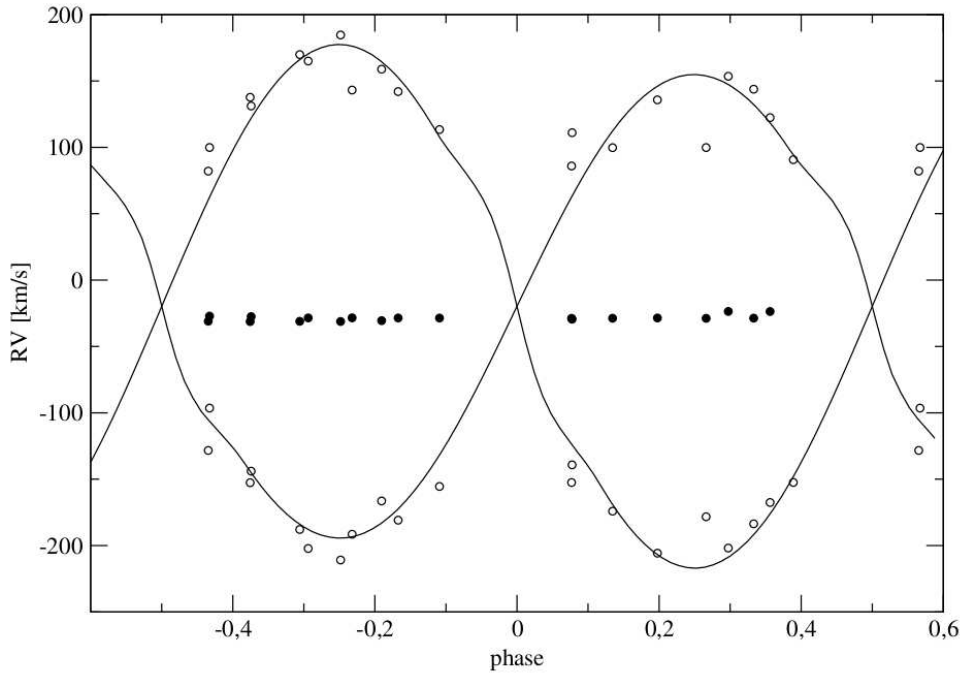

Figure 4. Radial velocity measurements for the three components of HT Vir (the eclipsing pair and third body) made by PST1 are presented in the figure. The empty circles indicate the radial velocity values of the eclipsing pair and the filled circles are connected to the third component. The solid line shows the synthetic curve based on the derived model of eclipsing pair.

Table 4. Preliminary solution for the eclipsing pair HT Vir B and formal errors outputted by the PHOEBE code.

Parameter	Value
HJD_0	2455691.511±0.002
P (days)	0.4077±0.0001
a ($R_\odot$)	3.04±0.06
V_γ (km s^{-1})	−19.6±2.8
q	1.11±0.04
i^* (deg)	84.3 (fixed)
Ω_1^*	4.067 (fixed)
Ω_2^*	4.067 (fixed)

* - PHOEBE program input values not adjust (Zola et al. 2005)

Acknowledgements: This work was supported by the Polish National Science Centre through grant UMO-2011/01/D/ST9/00427.

References:

Baranowski, R. et al., 2009, *MNRAS*, **396**, 2194
Fabricius C. & Makarov V. V., 2000, *A&A*, **356**, 141
Harper, W. E., 1915, *JRASC*, **9**, 168
Huffer, C. M., 1931, *PAAS*, **6**, 25
Khaliullin, Kh. F. et al., 2001, *Astron. Rep.*, **45**, 888
Khaliullin, Kh. F. et al., 2002, *Astron. Rep.*, **46**, 119
Kondo, M., 1976, *Tokyo Ann.*, **16**, 1
Lu, W.A. et al., 2001, *AJ*, **122**, 402
Mazeh, T. & Zucker, S., 1992, *ASPCS*, **32**, 164
Popper, D. M., 1971, *ApJ*, **169**, 549
Prša, A. & Zwitter, T., 2005, *ApJ*, **628**, 426
Rucinski, S. M., 1992, *AJ*, **104**, 1968
Tomkin, J. & Fekel, F., 2006, *AJ*, **131**, 2652
Walker, R. L., Chambis, C., 1985, *AJ*, **90**, 346
Wilson, R. E. & Devinney, E. J., 1971, *ApJ*, **166**, 605
Zola, S. et al., 2005, *AcA*, **55**, 389

COMMISSIONS 27 AND 42 OF THE IAU
INFORMATION BULLETIN ON VARIABLE STARS

Number 6122

Konkoly Observatory
Budapest
10 December 2014

HU ISSN 0374 – 0676

PHOTOMETRY OF HIGH-AMPLITUDE DELTA SCUTI STARS IN 2013

WILS, PATRICK[1]; AYIOMAMITIS, ANTHONY[2,3]; ROBERTSON, C.W.[4]; HAMBSCH, FRANZ-JOSEF[1,5]; VANLEENHOVE, MAARTEN[1]; NIEUWENHOUT, FRANS[6]; VAN DE STADT, INGE[6]; BAILLIEN, ANTOINE[1]; LAMPENS, PATRICIA[7]; VAN CAUTEREN, PAUL[1,7]; VAN WASSENHOVE, JEROEN[1]; PICKARD, ROGER D.[8]; KLEIDIS, STELIOS[2,9]; STAELS, BART[1,10]

[1] Vereniging Voor Sterrenkunde, Belgium; e-mail: patrickwils@yahoo.com

[2] Helliniki Astronomiki Enosi, Greece

[3] Perseus Observatory, Athens, Greece

[4] SETEC Observatory, Goddard, Kansas, USA

[5] Bundesdeutsche Arbeitsgemeinschaft für Veränderliche Sterne e.V. Germany

[6] Werkgroep Veranderlijke Sterren, The Netherlands

[7] Koninklijke Sterrenwacht van België (ROB), Brussel, Belgium

[8] British Astronomical Association, UK

[9] Zagori Observatory, Epirus, Greece

[10] Center for Backyard Astrophysics Flanders

This report is the sixth paper in a series on photometry of High-Amplitude Delta Scuti (HADS) Stars (see Wils et al., 2013 for references to the earlier papers in this series). It presents details on 390 times of maximum for 75 HADS, obtained during 2013. The method used to calculate the times of maximum is described in the first paper of the series (Wils et al., 2009).

Table 1 lists the code used for the observers and their instruments. We list the observed maxima in Table 2 with star name (Col. 1), the epoch of the observed maximum (Col. 2), the uncertainty of the epoch (Col. 3), the observer's code (Col. 4) and the filter used (Col. 5) for the observations. When a maximum was observed in more than one filter by the same observer, the table shows the average value of the times obtained in each filter individually (note that there may be a significant delay between the maximum times when observed in different filters).

We found that the observed times of maximum deviated considerably from their ephemeris for some stars. Insufficient precision in the original determination of the period is often the cause. We give new elements for these stars in Table 3. To obtain the highest possible precision, we used data from the ASAS (Pojmański, 2002), NSVS (Woźniak et al., 2004), CRTS (Drake et al., 2009) and SuperWASP surveys (Butters et al., 2010) in conjunction with our own data.

We detected a sudden change in the period of V376 Cam, likely at the beginning of 2013. A plot of the $O-C$ data calculated from our observations using a linear ephemeris are given in Fig. 1. Assuming a constant period before and after the change, the period shortened by 0.282 ± 0.006 seconds, or $\Delta P/P = 2.3 \times 10^{-5}$. Sweigart and Renzini (1979) proposed small random mixing events in a semiconvective zone and at the edge of the

Table 1: List of instruments used for the observations.

Code	Observer(s)	Telescope	Observatory	CCD
AA	AA	Catadioptric 30 cm	Perseus Observatory	SBIG ST-10XME
AB	AB	Catadioptric 35 cm	Carpe Noctem Observatory	SBIG ST-9E
FN	FN	Catadioptric 40 cm	Alkmaar, Nederland	SBIG ST-7XME
FNA	FN	Catadioptric 25 cm	ABT Metius	SBIG ST402XME
HMBW	FJH	Catadioptric 30 cm	Astrokolkhoz, New Mexico	SBIG ST-9XE
HMBC	FJH	Catadioptric 40 cm	Chile Remote Obs. Atacama Desert	FLI ML16803
HO40	PL+PVC	Newton 40 cm	R.O.B.-Humain	SBIG ST-10XME
IS	IS	Catadioptric 25 cm	ABT Metius	SBIG ST402XME
MAV	MV	Maksutov 26 cm	Leest Observatory	SBIG ST-10XME
MAVN	MV	Newton 35 cm	Leest Observatory	QSI583 WSG
RP	RDP	Catadioptric 36 cm	Shobdon, UK	Starlight XPress SXV-H9
SBL	BS	Cassegrain 28 + 23.5 cm	Alan Guth Observatory	Starlight XPress MX-716
SK	SK	Catadioptric 30 cm	Zagori Observatory	SBIG ST-7XMEI
SO30	CWR	Catadioptric 30 cm	SETEC Observatory	SBIG ST-8iXME
SO40	CWR	Catadioptric 40 cm	SETEC Observatory	SBIG ST-8XME
VWSR	JVW	Refractor 15.2 cm	Hooglede, Belgium	SBIG ST-7XME
VWS	JVW	Catadioptric 23.5 cm	Hooglede, Belgium	SBIG ST-8XME

convective core as the cause of sudden period changes in RR Lyrae stars. A similar mechanism may be at work here. Alternatively the light time effect from the passage through periastron of a companion in a highly elliptic orbit may mimick a sudden change in period. In that case these events should reoccur at regular intervals.

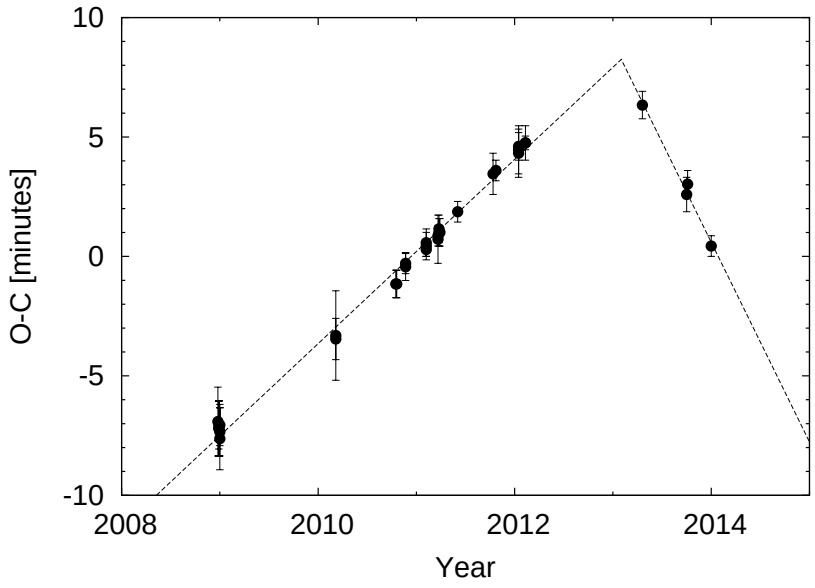

Figure 1. $O-C$ values for the maxima of V376 Cam with respect to the ephemeris Max HJD = $2454823.4194 + 0\overset{\mathrm{d}}{.}14032268 \times E$. The straight lines indicate the instantaneous period before and after the change.

Four of the observed stars observed turned out be multiperiodic variables. We found V879 Her (observed by AA), GSC 1489-0914 (observed by AA) and GSC 4145-0919 (observed by JVW and AA) to be double-mode pulsators while GSC 1566-2802 (observed by AA and MV) showed at least one other pulsation mode, probably a non-radial mode. Table 4 lists details about the independent frequencies f_0, the fundamental radial mode, and f_1, the first overtone mode in the case of the double-mode pulsators and a non-radial

mode for GSC 1566-2802. The frequencies, amplitudes and phases, and their uncertainties were determined using Period04 (Lenz & Breger, 2005). The uncertainties were derived using Monte Carlo simulations. We also detected a number of linear combinations of the independent frequencies in all stars. In 2014 Hümmerich independently discovered the double-mode behaviour of GSC 1489-0914[1]. Data of these four stars are available from the IBVS website: `6122-t1.txt` (V879 Her); `6122-t2.txt` (GSC 1489-0914); `6122-t3.txt`, `6122-t4.txt` (GSC 4145-0919); `6122-t5.txt`, `6122-t6.txt` (GSC 1566-2802).

One of us (JVW) found one of the comparison stars used for LW Dra, GSC 4431-0698, to be a W UMa type variable with a period of 0.36949 days. GSC 4431-0698 is a close pair of two stars (2MASS J19053535+6840195 and 2MASS J19053648+6840169) 6.″7 apart. We could not determine which one of these stars is the variable. The data are available online (`6122-t7.txt`).

Acknowledgements:
This work has made use of the SIMBAD database, operated at CDS, Strasbourg, France. Part of the equipment used at SETEC Observatory was purchased with a grant from the American Astronomical Society. FN is grateful to the University of Amsterdam for providing a CCD camera with filter wheel. IS and FN thank the Prins Bernhard Fonds for helping to fund the ABT Metius system. PL acknowledges support from the Royal Observatory of Belgium (ROB) for operating a small optical telescope at the radio-astronomy station of Humain under the project HOACS (HOACS stands for the Humain Optical Observatory for Astrophysics of Coeval Stars). The HOACS data were also acquired thanks to equipment financed by the Belgian National Lottery (1999). PVC is grateful for support from Baader Planetarium and Astrotechniek.

References:

Butters, O.W. et al., 2010, *A&A*, **520**, L10
Drake, A.J. et al., 2009, *ApJ*, **696**, 870
Lenz, P., Breger, M., 2005, *Comm. in Asteroseismology*, **146**, 53
Pojmański, G., 2002, *Acta Astron.*, **52**, 397
Sweigart, A.V., Renzini, A., 1979, *A&A*, **71**, 66
Wils, P. et al., 2009, *IBVS*, No. 5878
Wils, P. et al., 2013, *IBVS*, No. 6049
Woźniak, P.R. et al., 2004, *AJ*, **127**, 2436

[1]AAVSO VSX: "Fundamental period and epoch are tabulated. First overtone period: 0.0419105 d. Period ratio: 0.7734. J-K=0.15 (2MASS); B-V=0.21 (APASS)" (`http://www.aavso.org/vsx`)

Table 2: Observed times of maximum (Epoch = HJD − 2400000).

Star	Epoch	Unc.	Obs.	Filter	Star	Epoch	Unc.	Obs.	Filter
GP And	56573.6020	0.0005	SO30	V	V792 Cep	56460.5081	0.0012	AA	C
	56573.6808	0.0006	SO30	V		56497.3300	0.0013	AA	C
	56573.7592	0.0005	SO30	V		56497.4624	0.0012	AA	C
	56573.8381	0.0005	SO30	V	XX Cyg	56487.5234	0.0003	MAV	V
	56573.9166	0.0007	SO30	V	V2455 Cyg	56482.4685	0.0004	MAV	V
	56577.6149	0.0007	SO30	V	LW Dra	56403.4120	0.0010	VWSR	V
	56577.6931	0.0005	SO30	V		56410.3829	0.0012	VWSR	V
	56577.7718	0.0005	SO30	V		56423.4980	0.0006	VWSR	V
	56577.8508	0.0008	SO30	V		56451.5004	0.0007	VWSR	V
	56577.9295	0.0004	SO30	V	V1116 Her	56352.9694	0.0017	HMBW	V
	56604.6032	0.0007	SO30	V		56404.3796	0.0018	SBL	V
	56604.6819	0.0006	SO30	V		56404.4768	0.0016	SBL	V
	56604.7606	0.0007	SO30	V		56404.5702	0.0016	SBL	V
	56604.8389	0.0006	SO30	V		56466.3973	0.0010	AA	C
	56615.4615	0.0006	RP	V		56466.4922	0.0010	AA	C
	56641.6626	0.0004	SO30	V	V1209 Her	56351.9971	0.0004	HMBW	V
V460 And	56506.5001	0.0005	MAV	V		56404.3703	0.0004	MAVN	V
	56566.3358	0.0004	MAV	V		56404.4218	0.0004	MAVN	V
	56566.4090	0.0009	MAV	V		56404.4728	0.0003	MAVN	V
V524 And	56573.5811	0.0005	SO40	V		56404.5241	0.0003	MAVN	V
	56573.6753	0.0003	SO40	V	KZ Lac	56483.4106	0.0018	MAV	V
	56573.7698	0.0003	SO40	V		56483.5146	0.0014	MAV	V
	56573.8644	0.0002	SO40	V		56507.4263	0.0010	MAV	V
	56573.9590	0.0003	SO40	V		56508.4705	0.0017	MAV	V
V528 And	56543.5202	0.0012	AA	C		56508.5747	0.0020	MAV	V
	56590.2982	0.0013	AA	C		56541.3611	0.0004	AB	C
	56590.3870	0.0011	AA	C		56577.5934	0.0012	SO40	V
	56590.4761	0.0011	AA	C		56577.6979	0.0012	SO40	V
V544 And	56581.2459	0.0012	AA	C		56577.8026	0.0015	SO40	V
	56581.3541	0.0008	AA	C		56577.9072	0.0013	SO40	V
	56587.2341	0.0005	AA	C	SZ Lyn	56299.6526	0.0005	SO30	V
	56587.3408	0.0005	AA	C		56299.7733	0.0009	SO30	V
	56587.4482	0.0004	AA	C		56299.8940	0.0007	SO30	V
	56587.5549	0.0003	AA	C		56309.6568	0.0009	SO30	BV
CY Aqr	56559.4172	0.0008	AB	C		56309.7770	0.0005	SO30	BV
YZ Boo	56339.8669	0.0006	HMBW	V		56309.8979	0.0010	SO30	BV
	56339.9708	0.0007	HMBW	V		56310.0187	0.0016	SO30	BV
	56385.3547	0.0006	MAVN	V		56310.6211	0.0010	SO30	BV
	56385.4589	0.0005	MAVN	V		56310.7416	0.0008	SO30	BV
V336 Boo	56340.9529	0.0005	HMBW	V		56310.8622	0.0008	SO30	BV
BL Cam	56584.2339	0.0007	AA	C		56310.9827	0.0008	SO30	BV
	56584.2731	0.0005	AA	C	V593 Lyr	56451.4583	0.0017	AB	C
	56584.3120	0.0004	AA	C		56478.4267	0.0007	RP	V
	56584.3509	0.0005	AA	C		56478.5296	0.0005	RP	V
	56584.3900	0.0006	AA	C	V1162 Ori	56355.3484	0.0022	HO40	V
	56584.4289	0.0004	AA	C		56356.2932	0.0025	HO40	V
	56584.4681	0.0003	AA	C		56356.3731	0.0027	HO40	V
	56584.5073	0.0003	AA	C		56636.4933	0.0042	HO40	V
	56584.5466	0.0005	AA	C		56637.5167	0.0027	HO40	V
V367 Cam	56356.4964	0.0011	FN	C		56638.3805	0.0028	HO40	V
V376 Cam	56403.5975	0.0004	IS	V		56638.4612	0.0032	HO40	V
	56568.4741	0.0005	IS	V		56638.5386	0.0035	HO40	V
	56568.6147	0.0004	IS	V		56639.4055	0.0040	HO40	V
	56656.3146	0.0003	MAV	V		56639.4817	0.0042	HO40	V
V435 Cam	56589.4995	0.0010	AA	C		56639.5635	0.0029	HO40	V
AD CMi	56349.6838	0.0009	HMBW	V		56654.6679	0.0022	SO30	V
	56349.8067	0.0011	HMBW	V		56654.7476	0.0032	SO30	V

Table 2: Observed times of maximum (continued).

Star	Epoch	Unc.	Obs.	Filter	Star	Epoch	Unc.	Obs.	Filter
V1162 Ori	56654.8262	0.0022	SO30	V	GSC 0632-0812	55851.7790	0.0007	HMBC	V
	56654.9084	0.0034	SO30	V		55851.8627	0.0008	HMBC	V
V465 Peg	56560.3500	0.0007	AB	C		55852.7904	0.0005	HMBC	V
V536 Peg	56567.4058	0.0003	AB	C		55852.8747	0.0007	HMBC	V
DW Psc	56558.8889	0.0003	HMBC	V		55855.7406	0.0006	HMBC	V
	56560.8568	0.0004	HMBC	V		55855.8254	0.0010	HMBC	V
	56564.8539	0.0002	HMBC	V	GSC 0753-1489	56341.3893	0.0015	AB	C
	56637.2662	0.0004	HO40	C		56637.4594	0.0008	AB	C
AX Tri	56591.2745	0.0004	AA	C		56656.3897	0.0005	AB	C
	56591.3434	0.0005	AA	C	GSC 0914-0684	56414.3073	0.0010	AA	C
	56591.4122	0.0004	AA	C		56414.3847	0.0007	AA	C
	56591.4812	0.0006	AA	C		56414.4623	0.0009	AA	C
	56591.5501	0.0005	AA	C		56414.5399	0.0008	AA	C
	56599.2081	0.0005	AA	C	GSC 0933-0651	56341.9448	0.0006	HMBW	V
	56599.2769	0.0006	AA	C		56460.3215	0.0013	AA	C
	56599.3458	0.0006	AA	C		56460.4259	0.0007	AA	C
	56599.4150	0.0005	AA	C	GSC 1061-1651	56503.3033	0.0008	AA	C
	56599.4838	0.0004	AA	C		56503.4396	0.0004	AA	C
GW UMa	56379.5664	0.0007	IS	V	GSC 1076-0158	56458.4368	0.0006	AB	C
	56386.4748	0.0006	IS	V		56483.4509	0.0010	AB	C
YZ UMi	56389.4098	0.0004	VWSR	V		56528.3585	0.0047	AB	C
	56541.3789	0.0004	VWS	V		56533.3987	0.0008	AB	C
GSC 0191-1282	56309.4144	0.0010	IS	V	GSC 1220-1131	56320.2791	0.0007	FN	V
	56357.3552	0.0006	FN	C		56320.3601	0.0009	FN	V
	56357.4016	0.0006	FN	C		56337.2794	0.0016	FN	C
	56357.4487	0.0005	FN	C		56578.3817	0.0007	AA	C
	56366.3632	0.0003	IS	C		56578.4628	0.0007	AA	C
	56384.3344	0.0007	FN	C		56605.2256	0.0007	AA	C
	56384.3826	0.0006	FN	C		56605.3065	0.0006	AA	C
	56384.4301	0.0006	FN	C		56605.3878	0.0004	AA	C
	56384.4773	0.0006	FN	C		56605.4693	0.0004	AA	C
	56638.4485	0.0005	AB	C		56622.4697	0.0019	RP	V
	56638.4963	0.0003	AB	C		56646.3853	0.0009	FN	C
GSC 0321-0314	56364.8096	0.0008	HMBW	V	GSC 1306-0466	56309.3121	0.0036	FNA	V
GSC 0435-3806	56461.3768	0.0013	AA	C		56366.3820	0.0014	FN	C
	56461.4407	0.0010	AA	C		56639.3443	0.0009	HO40	V
	56461.5063	0.0009	AA	C		56639.4307	0.0010	HO40	V
GSC 0513-0624	56460.8962	0.0007	HMBC	V		56656.3212	0.0019	AB	C
	56461.9095	0.0007	HMBC	V	GSC 1442-1358	56354.8875	0.0004	HMBW	V
	56540.3876	0.0005	AB	C		56358.8290	0.0006	HMBW	V
	56573.3272	0.0007	SO40	C	GSC 1594-2234	56470.4074	0.0012	SK	V
GSC 0632-0812	55829.6929	0.0005	HMBC	V		56470.5470	0.0007	SK	V
	55829.7762	0.0008	HMBC	V		56494.3294	0.0007	AA	C
	55829.8617	0.0008	HMBC	V		56494.4662	0.0006	AA	C
	55830.7895	0.0010	HMBC	V		56541.3488	0.0006	AA	C
	55830.8728	0.0005	HMBC	V		56543.4000	0.0005	AA	C
	55831.8002	0.0007	HMBC	V	GSC 1716-1598	56571.5260	0.0009	RP	V
	55831.8844	0.0006	HMBC	V	GSC 1750-1237	56637.2991	0.0011	AB	C
	55833.8230	0.0008	HMBC	V	GSC 2043-1201	56378.5892	0.0018	IS	V
	55837.7013	0.0006	HMBC	V		56378.6677	0.0013	IS	V
	55837.7850	0.0005	HMBC	V		56402.5160	0.0017	IS	V
	55839.8081	0.0008	HMBC	V		56402.5933	0.0024	IS	V
	55841.8315	0.0007	HMBC	V		56412.5688	0.0010	RP	C
	55843.7707	0.0006	HMBC	V	GSC 2080-0986	56448.4316	0.0004	AB	C
	55843.8551	0.0009	HMBC	V	GSC 2194-2001	56493.3230	0.0007	AA	C
	55850.7670	0.0005	HMBC	V		56493.4375	0.0012	AA	C
	55850.8512	0.0008	HMBC	V		56552.3756	0.0011	AA	C

Table 2: Observed times of maximum (continued).

Star	Epoch	Unc.	Obs.	Filter	Star	Epoch	Unc.	Obs.	Filter
GSC 2194-2001	56552.4907	0.0014	AA	C	GSC 2977-0238	56310.8165	0.0006	SO40	BV
	56554.3287	0.0012	AA	C		56310.8922	0.0006	SO40	BV
	56554.4431	0.0016	AA	C		56310.9682	0.0006	SO40	BV
	56555.3627	0.0013	AA	C		56390.3188	0.0011	FN	C
	56555.4774	0.0013	AA	C		56390.3948	0.0006	FN	C
	56589.2553	0.0008	AA	C		56390.4708	0.0009	FN	C
	56589.3692	0.0012	AA	C	GSC 3004-0870	56337.3446	0.0006	AB	C
GSC 2290-1195	56638.2632	0.0025	MAV	V		56365.8537	0.0008	HMBW	V
	56638.3413	0.0031	MAV	V		56385.4079	0.0007	FN	C
GSC 2496-0118	56305.4470	0.0020	IS	V		56385.4901	0.0007	FN	C
	56337.3564	0.0029	IS	V		56385.5724	0.0007	FN	C
	56337.4255	0.0031	IS	V		56385.6540	0.0008	FN	C
	56379.3635	0.0006	FN	C		56400.2784	0.0005	AA	C
	56379.4309	0.0008	FN	C		56400.3605	0.0005	AA	C
	56379.4990	0.0010	FN	C		56400.4429	0.0005	AA	C
	56379.5664	0.0009	FN	C		56400.5247	0.0009	AA	C
	56379.6333	0.0013	FN	C		56416.3819	0.0007	FN	C
	56395.2830	0.0003	AA	C		56416.4642	0.0009	FN	C
	56395.3504	0.0004	AA	C		56416.5464	0.0011	FN	C
	56395.4177	0.0003	AA	C	GSC 3031-0307	56356.4387	0.0006	AB	C
	56403.4143	0.0007	FN	C		56411.2798	0.0013	AA	C
	56403.4825	0.0009	FN	C		56412.2777	0.0013	AA	C
	56403.5501	0.0014	FN	C		56412.3794	0.0010	AA	C
	56638.4419	0.0009	MAV	V		56412.4785	0.0009	AA	C
	56638.5092	0.0006	MAV	V		56414.4764	0.0012	RP	C
GSC 2566-1398	56384.6074	0.0009	IS	V		56414.5745	0.0016	RP	C
GSC 2696-1396	56481.4575	0.0005	MAV	V		56439.3485	0.0014	AA	C
GSC 2843-1999	56254.2503	0.0007	MAV	V		56439.4491	0.0013	AA	C
	56254.3122	0.0013	MAV	V		56447.3395	0.0011	AA	C
GSC 2861-0970	56307.3960	0.0006	FNA	V		56447.4391	0.0010	AA	C
	56335.3628	0.0007	FN	C		56447.5399	0.0011	AA	C
	56573.3003	0.0013	MAV	V	GSC 3428-1497	56323.3263	0.0009	MAV	V
	56573.4100	0.0008	MAV	V		56323.4025	0.0012	MAV	V
	56577.4843	0.0006	AA	C		56379.3857	0.0018	IS	V
	56579.3563	0.0006	AA	C	GSC 3489-0868	56349.8601	0.0005	HMBW	V
	56579.4663	0.0006	AA	C		56349.9467	0.0004	HMBW	V
	56579.5764	0.0004	AA	C		56385.3868	0.0010	MAV	V
	56592.3488	0.0007	AA	C		56385.4731	0.0005	MAV	V
	56592.4588	0.0006	AA	C	GSC 3755-0845	56309.2795	0.0011	MAV	V
	56592.5689	0.0005	AA	C		56315.2901	0.0016	MAV	V
	56637.2714	0.0006	MAV	V		56315.3665	0.0019	MAV	V
	56637.2725	0.0012	FN	C		56638.3258	0.0006	HO40	V
	56637.3814	0.0014	FN	C		56638.4020	0.0006	HO40	V
	56637.3815	0.0005	MAV	V		56638.4779	0.0005	HO40	V
GSC 2977-0238	56299.6544	0.0004	SO40	V		56638.5541	0.0005	HO40	V
	56299.7306	0.0005	SO40	V		56639.3150	0.0008	MAV	V
	56299.8066	0.0006	SO40	V	GSC 3810-1553	56349.8406	0.0003	HMBW	V
	56299.8817	0.0009	SO40	V		56351.8206	0.0003	HMBW	V
	56299.9584	0.0003	SO40	V		56351.8914	0.0003	HMBW	V
	56305.5773	0.0006	IS	V		56389.3690	0.0006	FN	C
	56309.6776	0.0008	SO40	BV		56389.4394	0.0012	FN	C
	56309.7533	0.0006	SO40	BV	GSC 3832-0152	56308.6560	0.0012	IS	V
	56309.8293	0.0004	SO40	BV		56308.7475	0.0005	IS	V
	56309.9052	0.0006	SO40	BV		56336.6076	0.0011	IS	V
	56309.9810	0.0007	SO40	BV		56336.6984	0.0009	IS	V
	56310.6644	0.0006	SO40	BV		56378.3493	0.0003	MAV	V
	56310.7405	0.0006	SO40	BV	GSC 3850-0137	56413.2733	0.0003	AA	C

Table 2: Observed times of maximum (continued).

Star	Epoch	Unc.	Obs.	Filter	Star	Epoch	Unc.	Obs.	Filter
GSC 3850-0137	56413.3366	0.0004	AA	C	GSC 4552-1498	56356.5917	0.0003	IS	V
	56413.3999	0.0004	AA	C		56356.6476	0.0003	IS	V
	56413.4633	0.0004	AA	C		56385.5020	0.0002	IS	V
	56413.5265	0.0004	AA	C		56385.5576	0.0003	IS	V
GSC 3863-0740	56378.4134	0.0014	MAVN	V		56506.4449	0.0006	MAV	V
GSC 3934-1904	56489.4786	0.0003	MAV	V	GSC 4556-1113	56306.3133	0.0004	VWSR	V
	56496.3620	0.0005	SK	V		56371.3312	0.0007	MAV	V
	56496.4712	0.0006	SK	V		56371.4173	0.0004	MAV	V
	56496.5799	0.0008	SK	V		56384.3690	0.0003	VWSR	V
GSC 4163-0984	56409.2712	0.0003	AA	C		56410.2718	0.0006	AA	C
	56409.3505	0.0005	AA	C		56410.3577	0.0008	AA	C
	56409.4300	0.0003	AA	C		56410.4446	0.0013	AA	C
	56409.5095	0.0003	AA	C		56410.5304	0.0007	AA	C
GSC 4196-1784	56463.3685	0.0012	AA	C		56487.4614	0.0004	VWSR	V
	56463.5395	0.0008	AA	C		56494.4553	0.0005	VWSR	V
GSC 4417-0394	56384.4256	0.0007	AB	C		56538.4052	0.0003	VWS	V
GSC 4464-0924	56398.5990	0.0007	IS	V		56559.2999	0.0005	VWS	V
	56485.4400	0.0009	MAV	V		56559.3861	0.0003	VWS	V
	56485.5182	0.0015	MAV	V		56637.3526	0.0004	VWS	V
	56581.3087	0.0006	IS	V	GSC 4923-0693	56353.8649	0.0004	HMBW	V
	56581.3895	0.0022	IS	V	GSC 5018-1085	56385.6112	0.0014	IS	V
GSC 4500-0083	56496.4233	0.0036	MAV	V		56418.5891	0.0014	IS	V
GSC 4552-1498	56305.6922	0.0004	IS	V	NSVS 14243430	56489.4929	0.0004	AB	C
	56336.4999	0.0004	IS	V		56539.4189	0.0004	AB	C

Table 3: Updated linear elements for some HADS. Uncertainties are given in units of the last decimal.

Star	Max (HJD)	Period (d)
GSC 1061-1651	2452383.172(7)	0.13693601(3)
GSC 1220-1131	2452625.8155(4)	0.081343587(9)
GSC 1442-1358	2452638.0670(10)	0.08211246(3)
NSVS 14243430	2452206.7164(9)	0.08607561(3)

Table 4: Independent frequencies detected in multiperiodic HADS. Uncertainties are given in units of the last decimal. The phase is given with respect to HJD = 2450000. For radial double-mode pulsators the period ratio is also listed.

Star		Frequency c/d	Semi-Amplitude Mag.	Phase	Period ratio
V879 Her	f_0	17.576979(4)	0.197(5)	0.499(4)	
	f_1	22.66134(2)	0.034(5)	0.51(3)	0.77564
GSC 1489-0914	f_0	18.453211(2)	0.120(2)	0.475(2)	
	f_1	23.860353(10)	0.0283(2)	0.175(9)	0.77338
GSC 1566-2802	f_0	16.538388(2)	0.1926(10)	0.5495(10)	
	f_1	21.97807(3)	0.0161(12)	0.2878(10)	0.75250
GSC 4145-0919	f_0	15.614244(5)	0.189(5)	0.276(4)	
	f_1	20.15552(3)	0.033(5)	0.16(3)	0.77469

COMMISSIONS 27 AND 42 OF THE IAU
INFORMATION BULLETIN ON VARIABLE STARS

Number 6123

Konkoly Observatory
Budapest
12 December 2014

HU ISSN 0374 – 0676

INVESTIGATION OF THE ECLIPSING BINARY SYSTEM OT Lyr

BAV MITTEILUNGEN NR. 237

AGERER, F.

Bundesdeutsche Arbeitsgemeinschaft für Veränderliche Sterne e.V. (BAV), Munsterdamm 90, D-12169 Berlin, Germany, email: agerer.zweik@t-online.de

This star (AN 61.1930 = USNO-B1.0 1192-0326799 = 2MASS J19081152+2913576) was discovered to be a variable of Algol type by Hoffmeister (1930). A range from 14 to 15 mag was given. The same author gave this variable the 1855.0 coordinates RA = $19^{\rm h}02^{\rm m}28^{\rm s}$, Dec = $+29°0\farcm1$. Richter (1961) determined the first ephemeris as

$$\text{Min I} = \text{JD } 2425303.646 + 0\fd471095 \times E \tag{1}$$

and a magnitude range between $13\fm9$ and $14\fm9$.

OT Lyr is listed in the GCVS with these information (Samus et al. 2014). OT Lyr has been included in 'A Catalogue of Eclipsing Variables'(Malkov et al. 2006). In 2007 a minimum of OT Lyr was observed by the author (Hübscher 2007). Further observations of this variable showed only small amplitude variation of DSCT-type.

Extensive photoelectric monitoring (C14, -IR and -UV-filter, KAF 1603 CCD) has confirmed the Algol type of variability and revealed a period of approximately 8.3 days (Figure 1). TYC 2135-2336 ($12\fm597$) and GSC 2135-1552 ($12\fm5$) has been used as comparison star and check star, respectively.

Observed minima

Number	HJD hel.	Weight	Epoch	$(O-C)$	Source
1	2425303.646	0	−3692.0	−1.346	[1]
2	2454222.4568	1	−222.0	+0.001	[2]
3	2456072.5023	1	0.0	−0.004	[3]
4	2456897.5191	1	99.0	−0.010	[3]
5	2456918.360	0	101.5	−0.003	[3]
6	2456964.210	1	107.0	+0.012	[3]

Sources: [1] Richter (1961), [2] Hübscher (2007), [3] Agerer (this paper).

Using only CCD-measured primary minimum timings the following first ephemeris could be derived:

$$\begin{array}{l} \text{Min I} = \text{HJD } 2456072.5063 + 8\fd333563 \times E \\ \qquad\qquad\qquad\qquad\quad \pm 13 \qquad\quad \pm 10 \end{array} \tag{2}$$

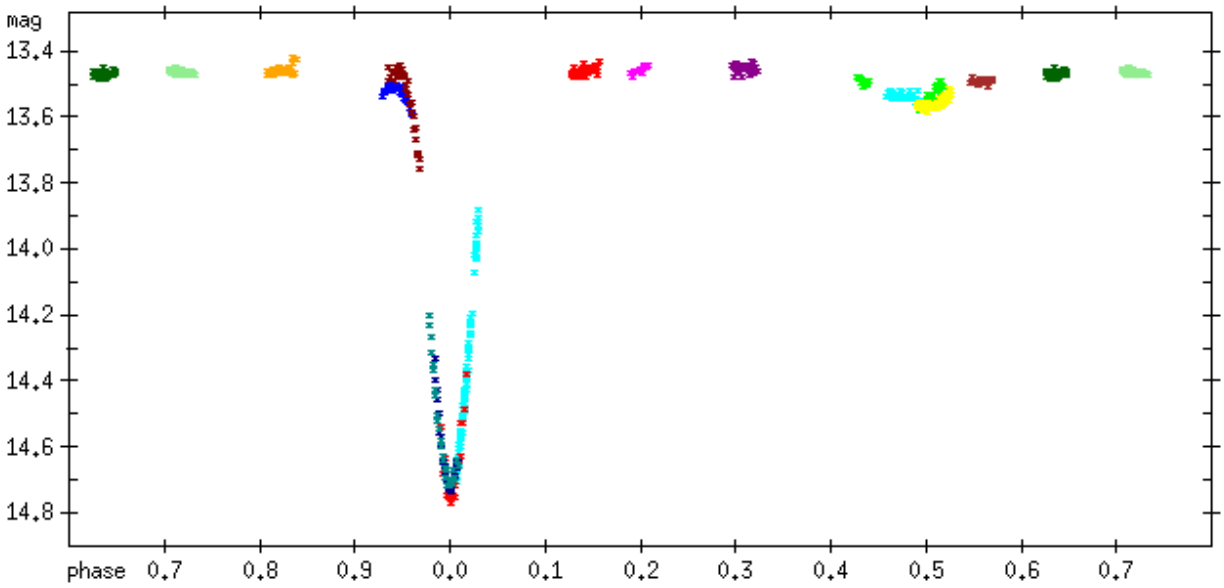

Figure 1. Photoelectric observations folded with the ephemeris (2), after removing the variations caused by the DSCT component.

In the instrumental system, OT Lyr is $13\overset{m}{.}45$ out of eclipse and $14\overset{m}{.}75$ in primary minimum. The secondary minimum seems to be somewhat displaced at a phase about 0.48 and is about $0\overset{m}{.}07$ deep.

A closer view to the data made clear, that the δ Scuti variations can be followed through the whole period of the eclipsing binary. During primary minima the amplitude of the light variation is reduced to about $\pm 0\overset{m}{.}2$ (Figure 2), whereas in normal light and in times of secondary eclipses the amplitude is about $\pm 0\overset{m}{.}4$ (Figure 3).

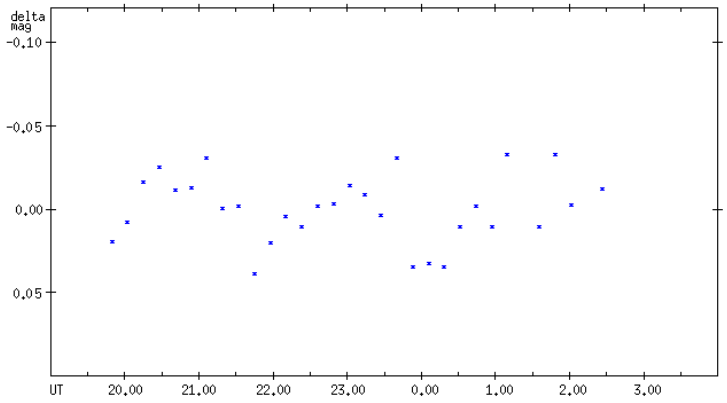

Figure 2. The δ Scuti variations in primary eclipse, after removing the variation caused by the eclipse.

From this it is obvious that the hotter component of the binary is the pulsating one and that the eclipse is not total.

The following first elements for the δ Scuti component could be derived:

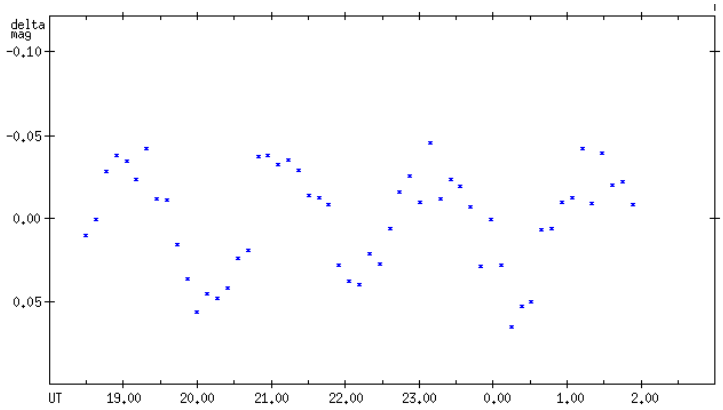

Figure 3. DSCT component in secondary eclipse, after removing the variation caused by the eclipse.

$$\text{Max} = \text{HJD } 2455451.3375 + 0\overset{\text{d}}{.}086495 \times E. \quad (3)$$

Figure 4 shows the corresponding phased light curve.

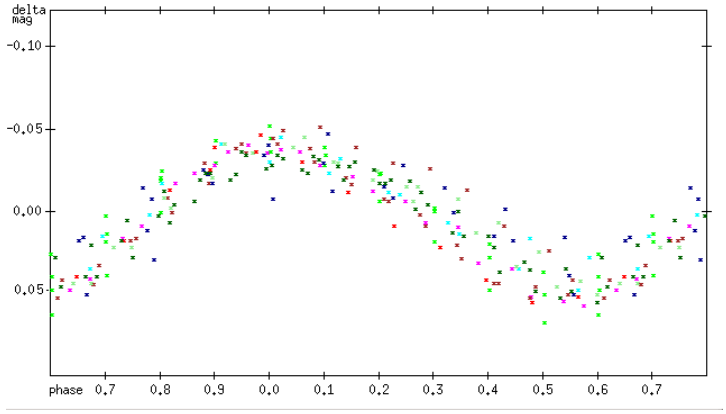

Figure 4. The δ Scuti component out of eclipse, folded with the ephemeris (3), and displayed with respect to the constant brightness level.

Acknowledgements: This research made use of the SIMBAD data base, operated by the CDS at Strasbourg, France.

References:

Hoffmeister, C., 1930, *AN*, **238**, 189
Hoffmeister, C., 1933, *Sonn. Mitt.*, **N22**, 191
Hübscher, J., 2007, *IBVS*, **5802**
Malkov O.Y., et al., 2006, *A&A*, **446**, 785
Richter, G., 1961, *MVS*, **565**
Samus, N. N. et al., 2014, *General Catalogue of Variable Stars*, Moscow

*This version of the paper contains corrections, and differs from the one appeared on-line originally. Date of last modification: Thu Dec 18 13:34:50 CET 2014

COMMISSIONS 27 AND 42 OF THE IAU
INFORMATION BULLETIN ON VARIABLE STARS

Number 6124

Konkoly Observatory
Budapest
20 December 2014

HU ISSN 0374 – 0676

CzeV615 – A NEW ECLIPSING BINARY

LIŠKA, J.[1]; LIŠKOVÁ, Z.[2,3]

[1] Department of Theoretical Physics and Astrophysics, Masaryk University, Kotlářská 2, 611 37 Brno, Czech Republic, e-mail: jiriliska@post.cz

[2] CEITEC – Central European Institute of Technology, Brno University of Technology, Technická 3058/10, 616 00 Brno, Czech Republic, e-mail: zuzana.liskova@ceitec.vutbr.cz

[3] Institute of Physical Engineering, Brno University of Technology, Technická 2896/2, 616 69 Brno, Czech Republic

The field of an RR Lyrae star, AT Serpentis (discovered by Hoffmeister, 1935), was observed at a private observatory in Brno during 7 nights in June and July 2014. The determination of maxima timings of the pulsating star was the main aim of the observations. One of stars in the field, CzeV615[1](Ser) = BD+09 3111 = USNO-A2.0 0975-08030166 (RA=$15^{\rm h}53^{\rm m}23\overset{\rm s}{.}634$, DEC=$+08°47'22\overset{''}{.}32$), was identified as a new variable object from our CCD measurements. Light changes of about 0.1 mag in V-band were detected.

A small Malokuk telescope was used. The telescope comprises an ATIK 16IC CCD camera (659×494 pix, Sony ICX 424AL chip), a Sonnar $f/4$ 135 mm photographic camera lens, and an EQ-1 Table Top mount. The field of view of the telescope is about 2.1°×1.6°, and the angular resolution is 11.3″/pix. The CCD camera is equipped with a *green* filter with a transmission similar to the Johnson V-band (see Fig. 1).

All CCD frames were calibrated in the standard way including dark and flat corrections. Groups of 5 consecutive frames were combined into a single image with a time resolution of about 150 s to achieve a better signal-to-noise ratio. An exposure time of 30 s was used for each frame. These procedures, as well as differential aperture photometry, were performed using C-Munipack[2] (Motl 2009) based on Daophot (Stetson 1987). HD 142799 and BD+08 3106 were used as comparison and check star, respectively. The list of observations is given in Table 1.

Own photometric data[3] are insufficient to determine the type of variability and for period estimation. Nevertheless, an eclipse explanation is proposed based on the detected dip in brightness. Fortunately, data for CzeV615 were found in the archives of the following projects: ASAS-3 (Pojmanski 2002, V band), NSVS (Woźniak et al. 2004, unfiltered measurements) and WISE (Wright et al. 2010, 4 infrared bands).

We verified transmission of our filter to be able to compare our measurements with data from sky-surveys. For this reason, transmission measurements were made with an Avantes AVS-S2000 spectrometer (wavelength range: 190–856 nm, resolution: 0.37–0.27 nm px^{-1}). The sensitivity of our ATIK 16IC CCD camera and the relative transmission function

[1]star included in Czech catalogue of discovered variable stars (Brát 2006), http://var2.astro.cz/czev.php
[2]http://c-munipack.sourceforge.net/
[3]available on-line at the IBVS website (`6124-t1.txt`)

Table 1: List of observations. N is the number of combined images.

Night	Start UTC	Exp. [s]	N
9 June 2014	23:46	30	29
15 June 2014	20:19	30	89
18 June 2014	20:18	30	46
19 June 2014	22:10	30	16
20 June 2014	22:00	30	67
24 June 2014	20:10	30	37
18 July 2014	20:56	30	10

of our filter were compared with that of the V-filters of the Johnson & Morgan (1953) UBV photometric system, the Johnson (1965) $UBVRI$ system and the Bessell (1990) $UBVRI$ system. Data for the individual filters were taken from the ADPS[4] (Moro & Munari 2000). The shape of the transmission function of our filter is evidently different than the transmission functions of the standard V-filters (Fig. 1). We also detected a red leak in wavelengths longer than 750 nm, which contributes about 20 % to the total signal (relative spectral response of our CCD is less than 40 % in this area). Nevertheless, these differences are negligible for our purpose. Our data are comparable with ASAS-3 measurements (similar photometric bands).

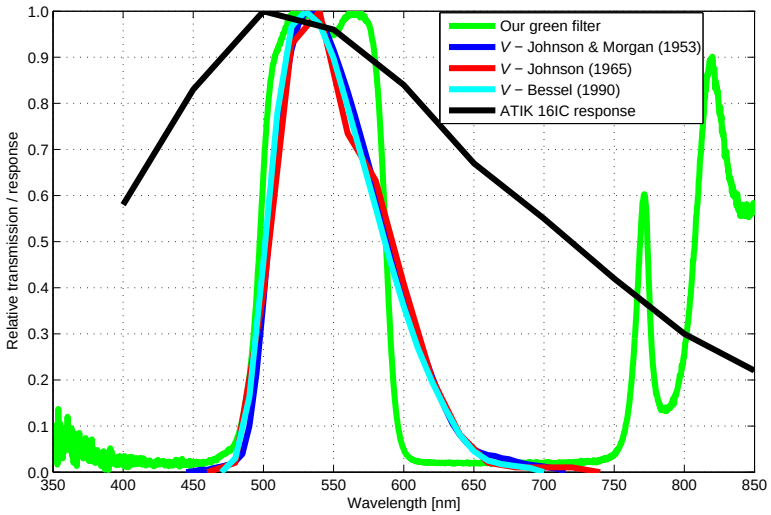

Figure 1. Relative transmission in the range of 350–850 nm for our *green* filter (own measurement) and for the standard photometric filters from the Asiago database together with the relative spectral response of the used ATIK 16IC CCD camera.

Using Period04 (Lenz & Breger 2005), the period was found to be about 0.7435 d based on data from ASAS-3 and NSVS (Fig. 2). The data set from the WISE project was omitted from period analysis and fitting of the light variations, because it contains only a small number of measurements (28 points in $W1$, $W2$ bands, 12 points in $W3$, $W4$). In addition, the shape of the infrared light curve could be very different from that in the optical band.

[4]Asiago Database on Photometric Systems, http://ulisse.pd.astro.it/Astro/ADPS/

The shape of variations with this period evidently corresponds to eclipsing binary behaviour, but no significant depression of a secondary minimum is visible in the phase diagram. We tested two possible scenarios: a semi-detached system with two different components (different radius, surface temperature, brightness) and orbital period close to 0.75 day; a detached binary system with similar components causing similar depths of eclipses and a period of double the value (about 1.5 day). Period analysis could not assist in selecting the correct solution, because the double-period value is not visible in the frequency spectra from PERIOD04 (Fig. 2). This is generally a problem for eclipsing binaries with similar eclipses – only half the value of the period is present in the frequency spectrum from PERIOD04. The other methods, e.g. Renson or a similar method implemented in PERANSO software[5] (Vanmunster 2011), show both values of the period in the spectrum to be of nearly the same strength (Fig. 3).

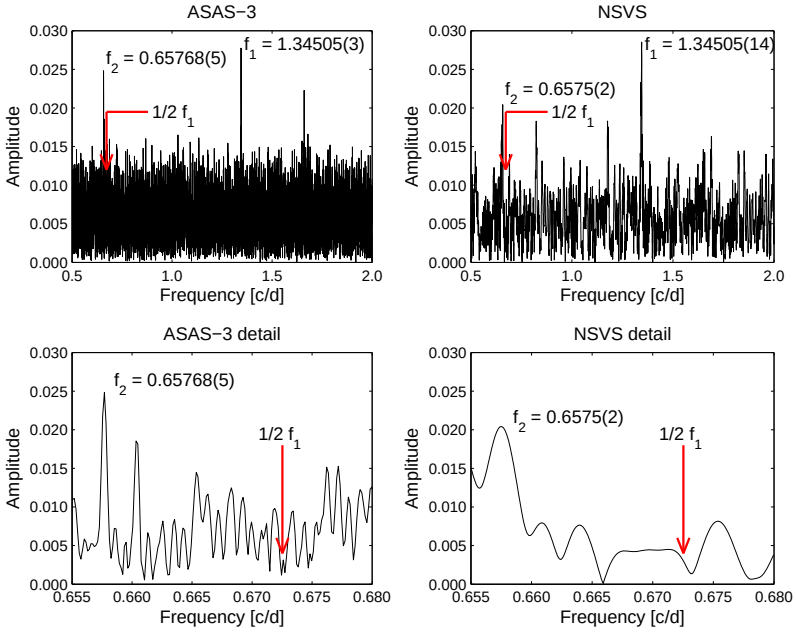

Figure 2. Frequency spectra from ASAS-3 and NSVS data (PERIOD04) contain the strongest frequency $f_1 = 1.34505\,\mathrm{c\,d^{-1}}$ which corresponds to the period 0.7435 d (figures on the top). The half value of the frequency $1/2\,f_1 = 0.67253\,\mathrm{c\,d^{-1}}$(double period 1.487 d) has a very low amplitude and it is at the bottom of the frequency spectra in the noise (clear visible in the detail of the figures at the bottom). The frequency marked as f_2 suggests a very blurred phase light curve.

We decided to give priority to the latter explanation ($P \sim 1.5\,\mathrm{d}$) due to the following reasons. The primary and secondary eclipses have slightly different depths from our model for a 1.5 d period (more below). We did not detect a secondary minimum for the period of 0.75 d. The last indication is given by proximity effects which are visible in the phase light curve. A typical light curve influenced by proximity effects has two maxima close to phases 0.25 and 0.75 and minima close to phases 0.0 and 0.5. The maximum brightness for our 0.75-day period is at phase 0.5, which is contrary to the mentioned statement and

[5] http://www.peranso.com/

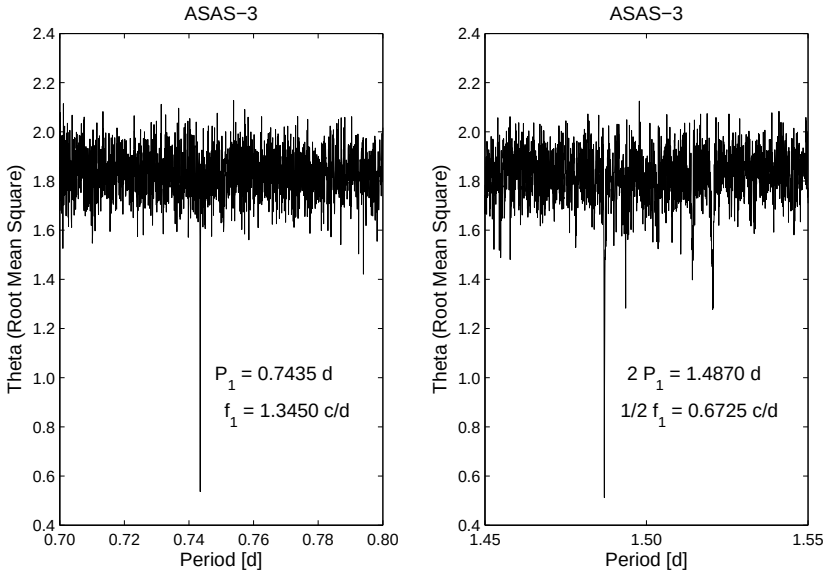

Figure 3. Frequency (period) spectrum for ASAS-3 data obtained from the PERANSO software and the Renson method contains both periods with nearly identical strengths (minimum value of dispersion).

supports the correctness of the double-period preference. Nevertheless, it is necessary to verify our preliminary results using more accurate photometry or spectroscopy.

The observed light variations were fitted using a non-linear least-squares method based on the work of Mikulášek, Zejda & Janík (2012), Mikulášek & Zejda (2013), Chrastina, Mikulášek & Zejda (2014). The function $m(t)$ for describing an eclipsing binary light curve was chosen in the form

$$m(t) = m_{0\,i} + a_1 \, \exp\left[\frac{-\varphi_1^2(t)}{2\,\sigma^2}\right] + a_2 \, \exp\left[\frac{-\varphi_2^2(t)}{2\,\sigma^2}\right] + a_3 \, \cos[4\,\pi\,\vartheta(t)], \qquad (1)$$

where $m_{0\,i}$ is the zero point for the i-th dataset and $a_{1,2}$ are the amplitudes of the primary and secondary eclipses, respectively. Eclipses are represented by a Gaussian function including constant σ to control their widths. Parameter a_3 is the amplitude of correction for small changes in brightness outside of the eclipses (proximity effects). Finally, the phase function $\vartheta(t)$ and the phases of the primary or secondary eclipses $\varphi_{1,2}(t)$ can be written as

$$\vartheta(t) = \frac{t - E_0}{P}, \;\; \varphi_1(t) = \vartheta(t) - \mathrm{round}[\vartheta(t)], \;\; \varphi_2(t) = \left[\vartheta(t) - \frac{1}{2}\right] - \mathrm{round}\left[\vartheta(t) - \frac{1}{2}\right], \quad (2)$$

where the time t is in heliocentric Julian date, E_0 is the zero epoch and P is the period in days. The input parameter σ was quasi-randomly generated. The model with the lowest χ^2 (for the data without evident outliers) was selected as the best solution (Fig. 4). The uncertainties of parameters were subsequently determined using the bootstrap method.

Brightness variation was determined from our model in the range of 10.008(2)–10.121(5) mag in the V-band (ASAS-3) and 10.306(2)–10.419(5) mag (NSVS, close to the R-band). The semi-amplitude a_3 of brightness changes outside of the eclipses was found to be 0.006^{+2}_{-2}. The time of minimum light (mid-eclipse) can be expressed in the form

$$T_{\min} = 2453144.9028^{+11}_{-14} + 1.4869803^{+14}_{-15}\,\mathrm{d} \cdot E. \qquad (3)$$

Nevertheless, primary and secondary minima have similar amplitudes of $a_1 = 0.100^{+6}_{-5}$ mag, $a_2 = 0.091^{+6}_{-5}$ mag. Due to the low accuracy of measurements, it is difficult to differentiate between primary and secondary minima. Similar depths of minima from ASAS-3 and NSVS measurements for the period 1.4869803 d indicate that CzeV615 is a detached binary system with both components of similar surface temperature and spectral type. It could be an advantage for future spectroscopic analysis, because the spectral lines of both components could be easily detected in the spectrum. The duration of both eclipses is about 3.5 h ($\sigma = 0.0211^{+11}_{-11}$). Eclipses are also detectable in the infrared region. Four measured values from WISE ($W1$, $W2$) obtained in phases close to mid-eclipse, are about 0.1 mag fainter than outside the eclipses.

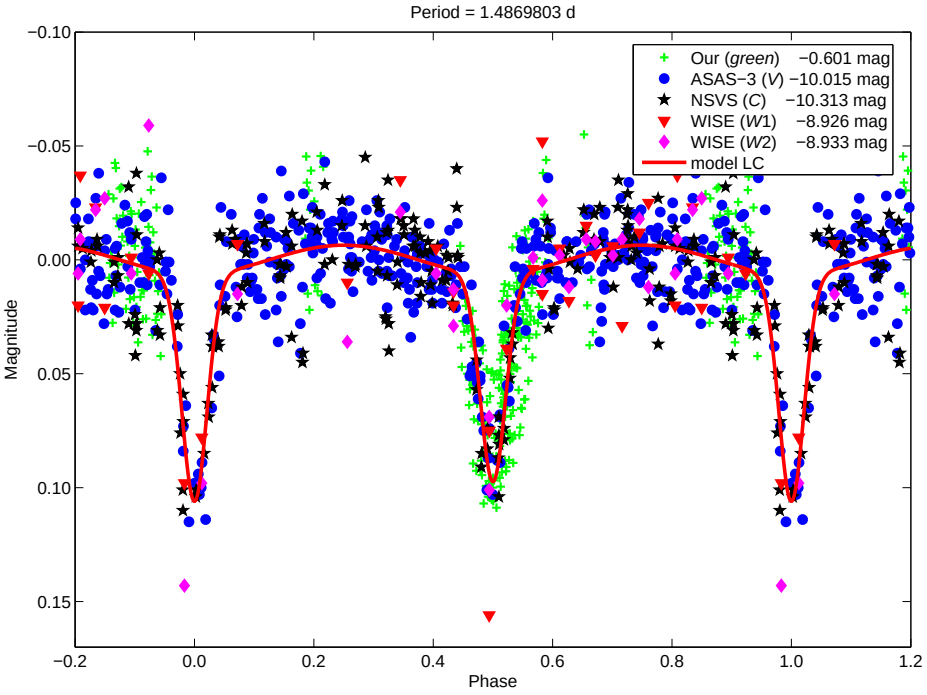

Figure 4. Own measurements together with data from ASAS-3, NSVS and WISE database and our model of the light curve phased according to eq. (3).

Data from WISE can also be useful for possible elimination of the half value for the orbital period (0.7434902 d). The phase curve constructed with this period does not contain a secondary minimum in optical photometry (ASAS-3, NSVS). This can be explained as a semi-detached system where secondary eclipses are not visible in the optical band, but they are detectable in infrared wavelengths (components with very different surface temperatures). WISE photometry also does not show a depression in phases outside of the primary minimum. Unfortunately, the number of WISE measurements is not high and values have low accuracy.

Literature, found in the VizieR database (Ochsenbein, Bauer & Marcout 2000), does not contain much information about the object CzeV615. Its spectral type is probably F0 (Heckmann 1975), colour $B - V = 0.319(83)$ mag (ESA 1997) and effective temperature about 7000 K, e.g. Wright et al. (2003) give 7200 K, Ammons et al. (2006) give 6698 K or 6564 K. The distance of CzeV615 is very uncertain. Measurements from the Hipparcos

satellite have very large uncertainty (parallax 27.00(32.09) mas, ESA 1997) resulting in a distance of 37(44) pc. These values are completely different from the values of Pickles & Depagne (2010), who give the distance as 347 pc and the spectral type as F5IV. Additional photometric and spectroscopic observations are therefore needed.

Acknowledgements: This publication makes use of data products from the Wide-field Infrared Survey Explorer, which is a joint project of the University of California, Los Angeles, and the Jet Propulsion Laboratory/California Institute of Technology, funded by the National Aeronautics and Space Administration. This research made use of the VizieR catalogue access tool, CDS, Strasbourg, France. We acknowledge the financial support of MUNI/A/0773/2013, LH14300 and the project "CEITEC – Central European Institute of Technology" (CZ.1.05/1.1.00/02.0068) from the European Regional Development Fund. ZL was supported by Brno Ph.D. Talent Scholarship Holder - Funded by the Brno City Municipality. We thank Marek Skarka, Zdeněk Mikulášek and Miloslav Zejda for useful comments, Zdeněk Liška and Pavel Wilk for their help with the compilation of the Malokuk telescope and Stephan N. de Villiers for carefully reading and language corrections.

References:

Ammons, S. M., Robinson, S. E., Strader, J., et al., 2006, *ApJ*, **638**, 1004
Bessell, M. S., 1990, *PASP*, **102**, 1181
Brát, L., 2006, *OEJV*, **23**, 55
Chrastina, M., Mikulášek, Z. & Zejda, M., 2014, *CoSka*, **43**, 422
ESA 1997, The Hipparcos and Tycho Catalogs, ESA SP–1200
Heckmann, O., 1975, Hamburg-Bergedorf: Hamburger Sternwarte, edited by Dieckvoss, W.
Hoffmeister, C., 1935, *Astron. Nachr.*, **255**, 401
Johnson, H. L. & Morgan, W. W., 1953, *ApJ*, **117**, 313
Johnson, H. L., 1965, *ApJ*, **141**, 923
Lenz, P. & Breger, M., 2005, *Comm. Asteroseismology*, **146**, 53
Mikulášek, Z., Zejda, M. & Janík, J., 2012, *IAUS*, **282**, 391
Mikulášek, Z. & Zejda, M., 2013, Úvod do studia proměnných hvězd, Masarykova univerzita, muni PRESS, Brno
Moro, D. & Munari, U., 2000, *A&AS*, **147**, 361
Motl, D., 2009, C-Munipack, `http://c-munipack.sourceforge.net/`
Ochsenbein, F., Bauer, P., & Marcout, J. 2000, *A&AS*, **143**, 23
Pickles, A. & Depagne, É., 2010, *PASP*, **122**, 1437
Pojmanski, G., 2002, *Acta Astronomica*, **52**, 397
Stetson, P. B., 1987, *PASP*, **99**, 191
Vanmunster, T., 2011, Peranso, `http://www.peranso.com/`
Woźniak, P. R., Vestrand, W. T., Akerlof, C. W., et al., 2004, *AJ*, **127**, 2436
Wright, C. O., Egan, M. P., Kraemer, K. E. & Price, S. D., 2003, *AJ*, **125**, 359
Wright, E. L., Eisenhardt, P. R. M., Mainzer, A. K., et al., 2010, *AJ*, **140**, 1868

COMMISSIONS 27 AND 42 OF THE IAU
INFORMATION BULLETIN ON VARIABLE STARS

Number 6125

Konkoly Observatory
Budapest
20 December 2014

HU ISSN 0374 – 0676

TIMES OF MINIMA OF ECLIPSING BINARIES AND MID-TRANSIT TIMES OF TRANSITING EXOPLANETS

BAŞTÜRK, Ö.[1,2]; BAHAR, E.[1,2]; ŞENAVCI, H.V.[1,2]; KILIÇOĞLU, T.[1,2]; ÖZAVCI, İ.[1,2]; BURDANOV, A.[3]; YILMAZ, M.[1,2]; ÇALIŞKAN, Ş.[1,2]; TEZCAN, C.T.[1,2]; YÖRÜKOĞLU, O.[1,2]; ÖZKELEŞ, A.[1,2]; İZCİ, D.D.[1,2]; GÜMÜŞ, D.[1,2]; AVCI, Z.[1,2]; ÖZTÜRK, D.[1,2]; SELAM, S.O.[1,2]; EKMEKÇİ, F.[1,2]; ALBAYRAK, B.[1,2]

[1] Ankara University Ankara University, Faculty of Science, Department of Astronomy and Space Sciences, TR-06100, Tandoğan, Ankara, Turkey; e-mail: obasturk@ankara.edu.tr

[2] Ankara University Kreiken Observatory, TR-06873, Ahlatlıbel, Ankara, Turkey

[3] Kourovka Astronomical Observatory of Ural Federal University, Mira Str. 19, 620002 Ekaterinburg, Russia

Observatory and telescope:
16" Schmidt-Cassegrain telescope of the Ankara University Kreiken Observatory

Detector:	Apogee ALTA U47+ CCD camera. 1024 x 1024 pixels.

Method of data reduction:
Reduction of the CCD frames and differential photometry were performed with the standard tasks of IRAF[1] package

Method of minimum determination:
The minima times of eclipsing binaries were calculated using Kwee & van Woerden's (1956) method. Mid-transit times were calculated by making use of a model-fitting algorithm available via the Exoplanet Transit Database (Poddaný et al. 2010)[2].

[†]Based on the observations performed at Ankara University Kreiken Observatory

[1]IRAF is distributed by the National Optical Astronomical Observatories, operated by the Association of the Universities for Research in Astronomy, inc., under cooperative agreement with the National Science Foundation

[2]http://var2.astro.cz/ETD/

Table 1: Minima Times of Eclipsing binaries

Star name	Time of min. HJD 2400000+	Error	Type	Filter	Obs.
RT And	56515.4310	0.0001	I	$BVRI$	IO
	56617.3173	0.0001	I	$BVRI$	KS
AB And	56504.4851	0.0001	II	VRI	AUU
	56257.2270	0.0001	II	BVR	OY
	56645.2063	0.0001	II	VRI	SC
BD And	56847.51139	0.00008	I	$BVRI$	SO
OO Aql	56852.34508	0.00008	II	$BVRI$	OO
V417 Aql	56891.47788	0.00009	II	$BVRI$	AAUU
SS Ari	56885.4908	0.0001	II	$BVRI$	MBD
AR Aur	56336.2991	0.0003	II	$BVRI$	CTT
IU Aur	56264.2627	0.0003	I	BVR	YN
EL Boo	56420.4498	0.0002	I	$BVRI$	DO
	56441.3421	0.0002	II	$BVRI$	ZA
	56444.4470	0.0002	I	$BVRI$	RO
	56477.3406	0.0002	II	$BVRI$	AO
V776 Cas	56638.5450	0.0002	I	$BVRI$	DDI
GW Cep	56737.3880	0.0001	II	$BVRI$	DG
RW Com	56385.5154	0.0001	I	$BVRI$	MBD
CC Com	56690.59636	0.00009	I	VRI	BK
YY CrB	56532.3252	0.0001	I	$BVRI$	BE
WZ Cyg	56826.46413	0.00006	I	$BVRI$	OV
ZZ Cyg	56853.48273	0.00004	I	$BVRI$	OY
MY Cyg	56821.3628	0.0002	I	$BVRI$	KA
V2280 Cyg	56513.4856	0.0001	II	VRI	RO
	56483.4532	0.0002	II	R	MA
V2294 Cyg	56483.2961	0.0002	I	R	OK
	56499.4310	0.0002	II	$BVRI$	RO
YY Del	56835.4604	0.0002	I	$BVRI$	CTT
AK Her	56880.3126	0.0001	I	$BVRI$	ZA
	56840.4806	0.0004	II	$BVRI$	MU
CC Her	56416.4795	0.0002	II	VRI	EB
PP Lac	56866.4549	0.0001	I	$BVRI$	ZA
AP Leo	56687.56866	0.00008	I	$BVRI$	YK
UV Lyn	56653.5820	0.0001	II	$BVRI$	CTT
	56653.5792	0.0001	II	$BVRI$	UD
U Peg	56482.4965	0.0001	I	$BVRI$	OU
	56616.2924	0.0002	I	$BVRI$	UB
KL Per	56228.3409	0.0002	I	$BVRI$	MMK
CU Sge	56804.4717	0.0004	I	$BVRI$	MAK
CW Sge	56839.4860	0.0001	I	$BVRI$	EB
CU Tau	56690.2423	0.0002	I	VRI	DT
V781 Tau	56325.2965	0.0002	II	$BVRI$	CTT
	56638.2995	0.0001	I	$BVRI$	AUU
	56325.2961	0.0002	II	$BVRI$	ND
HH UMa	56357.2530	0.0002	I	$BVRI$	ZA
AX Vir	56408.4600	0.0001	I	$BVRI$	AO
	56409.5153	0.0004	II	$BVRI$	TG
	56413.3764	0.0001	I	$BVRI$	TK
HW Vir	56809.33987	0.00002	I	R	OB

Table 2: Transit Mid-Times of Transiting Exoplanets

Star name	Transit mid-time HJD 2400000+	Error	Filter	Obs.
Qatar-1b	56407.3494	0.0017	*R*	AOE
Qatar-1b	56478.3449	0.0007	*R*	SG
Qatar-1b	56576.3267	0.0007	*R*	HVS
Qatar-1b	56884.4733	0.0006	*R*	HVY
TrES-1b	56562.3023	0.0008	*R*	MY
TrES-1b	56880.4611	0.0010	*R*	BAS
TrES-2b	56497.4296	0.0009	*R*	BC
TrES-2b	56875.4270	0.0011	*R*	BA
TrES-3b	56867.5116	0.0006	*R*	MHT
TrES-3b	56892.3285	0.0005	*R*	OB
WASP-2b	56845.3667	0.0009	*R*	OB
WASP-3b	56476.3998	0.0006	*R*	SOS
WASP-3b	56537.3456	0.0017	*R*	OB
WASP-3b	56838.3867	0.0008	*R*	MHT
WASP-3b	56849.4633	0.0009	*R*	HVS
WASP-33b	56217.4783	0.0012	*I*	MY
WASP-33b	56217.4782	0.0012	*R*	MY
WASP-33b	56217.4709	0.0013	*V*	DGT

Observers:			
AUU:	A. Ulus Uludağ	MMK:	M. Metin Keklik
AOE:	Ali Öğer	MU:	Murat Uzundağ
AO:	Anıl Özkeleş	MY:	Mesut Yılmaz
BA:	Büşra Akerdem	ND:	Nermin Demircioğlu
BAS:	Büşra Aslan	OEA :	Ö. Ezgi Aydoğdu
BC:	Burcu Çelikoğlu	OB:	Özgür Baştürk
BE:	Başak Esmer	OK:	Oğuzhan Karadeniz
BK:	Burak Keten	OO:	Özge Özata
CTT:	C. Tuğrul Tezcan	OU:	Özge Ünal
DDI:	D. Dilan İzci	OV:	Özge Varol
DG:	Damla Gümüş	OY:	Onur Yörükoğlu
DGT:	Dilem Göktaş	RO:	Reyhan Orhan
DO:	Derya Öztürk	SO:	Sercan Öz
DT:	Damla Tire	SOS:	Selim O. Selam
EB:	Engin Bahar	SC:	Şeyma Çalışkan
HKA:	H. Kübra Aygören	SG:	Serdar Gökçeğaçlı
HVS:	H. Volkan Şenavcı	TG:	Tolga Günday
HVY:	H. Volkan Yıldırım	TK:	Tolgahan Kılıçoğlu
IO:	İbrahim Özavcı	UB:	Ufuk Bostancı
KS:	Koray Sevim	UD:	Utku Demirhan
MA:	Mihriban Akı	YN:	Yahya Nasolo
MAK:	Merih Akgünay	YK:	Yasemin Karademirci
MBD:	M. Burak Doğruel	ZA:	Zeynep Avcı
MHT:	M. Hayri Türkyılmaz		

Acknowledgements:

We would like to thank all the observers and the staff at the Ankara University Kreiken Observatory. Authors from Ankara University acknowledge the support by the research fund of Ankara University (BAP) through the project 13B4240006.

References:

Kwee, K.K., van Woerden, H., 1956, BAN, 12, 327
Poddaný S., Brát L., Pejcha O., 2010, NewA, 15, 297

COMMISSIONS 27 AND 42 OF THE IAU
INFORMATION BULLETIN ON VARIABLE STARS

Number 6126

Konkoly Observatory
Budapest
6 January 2015

HU ISSN 0374 – 0676

RESOLVED PHOTOMETRY OF THE BINARY COMPONENTS OF RW Aur

ANTIPIN, S.; BELINSKI, A.; CHEREPASHCHUK, A.; CHERJASOV, D.; DODIN, A.; GORBUNOV, I.; LAMZIN, S.; KORNILOV, M.; KORNILOV, V.; POTANIN, S.; SAFONOV, B.; SENIK, V.; SHATSKY, N.†; VOZIAKOVA, O.

Sternberg Astronomical Institute, Lomonosov Moscow State University, Russia. †kolja@sai.msu.ru

1 Introduction

RW Aur is one of the objects from the initial list of T Tauri type stars composed by Joy (1945). Joy & van Biesbroeck (1944) discovered that the star has a companion, RW Aur B, which was at that moment $1\overset{\mathrm{m}}{.}5$ fainter than the primary star RW Aur A. The current position of the companion RW Aur B is: $\rho \simeq 1.45''$, PA$\simeq 256^\circ$ (Bisikalo et al. 2012). It was found later that both A and B components were classical T Tauri stars (Duchêne et al. 1999), i.e. pre-main sequence low mass stars surrounded by accretion disks. Spectral types of the main component and the companion are K1-K4 (Petrov et al. 2001) and K5 (Duchêne et al. 1999), respectively.

Variability of RW Aur was discovered more than a century ago by L.P. Ceraski (Ceraski 1906). Historical light curve of the star (Beck & Simon 2001; Grankin et al. 2007; Rodriguez et al. 2013) reflects the total brightness of both components due to their proximity. In $UBVRI$ bands the star demonstrates irregular variability, whose amplitude increases from I to U band, that is typical of classical T Tauri stars. In particular, average brightness of RW Aur during 1985-2003 in the V band was near $10\overset{\mathrm{m}}{.}5$ with an average amplitude of seasonal variations $\simeq 1\overset{\mathrm{m}}{.}4$ (Grankin et al. 2007).

It is commonly accepted to interpret the variability of RW Aur as that of the brighter component A. We found the only paper by White & Ghez (2001) where a quantitative information on the brightness of RW Aur B in the $UBVR_{\mathrm{c}}I_{\mathrm{c}}$ bands is presented (from November 9, 1994 HST observations).

Petrov & Kozack (2007) concluded that the brightness and color of RW Aur A are governed by variations of the circumstellar extinction rather than of the accretion. It looks strange because the inclination of RW Aur A disk midplane to the line of sight lies between 30° and 45° (Cabrit et al. 2006). Unexpected confirmation of Petrov & Kozack conclusion appeared in 2010 when a long and deep dimming of RW Aur happened. The dimming had a depth of 2 magnitudes, a duration of 180 days and presumably was due to occultation of RW Aur A by a dust cloud (Rodriguez et al. 2013).

The V magnitude of RW Aur during the dimming event fell down to $\simeq 13^{\mathrm{m}}$, that is close to brightness of RW Aur B, so it is not clear what was the real amplitude of RW

Aur A dimming. It was not possible to answer this question due to the lack of resolved photometry of this double system.

According to the AAVSO database (`http://www.aavso.org`), in a period from April 2011 to the end of April 2014 RW Aur demonstrated its usual (pre-dimming) behavior, e.g. its V magnitude varied in an irregular way around the average value of $10\overset{\mathrm{m}}{.}5$. Then the star was not observed till October, 23 when it appeared that RW Aur dimmed again down to $V \simeq 12.6^{\mathrm{m}}$.

2 Observations and results

Multicolor imaging of RW Aur was performed on November 13/14, 2014 with a newly installed 2.5 meter telescope ($F_{\mathrm{equiv}} = 20$ m) of the Caucasus observatory of Lomonosov Moscow State University at the mount Shatzhatmaz[1] in course of test precommissioning observations aimed at checking the image quality provided by the instrument. The telescope was equipped with a mosaic CCD camera manufactured by Niels Bohr Institute based on two E2V CCD44-82 detectors (pixel size 15 μm) and a set of standard Bessel $UBVR_{\mathrm{c}}I_{\mathrm{c}}$ filters from Asahi Spectra Co.

In course of observations the image quality with FWHM between 0.5 and 0.7 arcsec was routinely obtained confirming the excellent optics quality of the instrument, delivered by the REOSC company of Safran group, France (Poutriquet et al. 2012). The binary was clearly resolved (see Fig. 1): the wings of a brighter component image contribute $< 7\,\%$ to the central intensity of a fainter component in all bands. This time of year at the site is known to be characteristic of exceptionally stable atmospheric turbulence conditions (Kornilov et al. 2014), so this result was not unexpected. The exposure time varied from 5 sec in the I_{c} band to 300 sec in the U band, the middle date of measurements is JD 2456975.56.

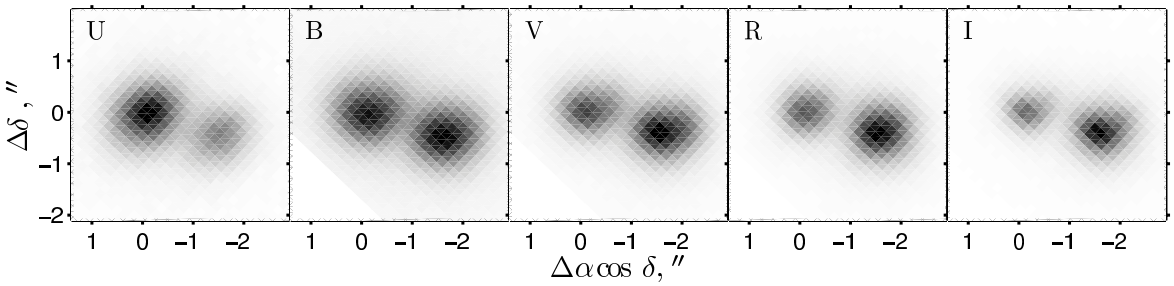

Figure 1. Images of RW Aur binary in the $UBVRI$ photometric bands. The primary component, RW Aur A, is placed in the origin of the coordinate system.

Primary data processing and PSF photometry were performed in a standard way in the ESO-MIDAS environment with the DAOPHOT program package (Stetson 1987). Stars 127 and 129 from the AAVSO chart for RW Aur were used as $BVR_{\mathrm{c}}I_{\mathrm{c}}$ photometric standards. The $U-B$ colors for these standards and transformation of magnitudes and colors from the instrumental to the standard $UBVR_{\mathrm{c}}I_{\mathrm{c}}$ system were made based on quasi-

[1]Webpage of the observatory, in Russian: `http://lnfm1.sai.msu.ru/kgo/`. An English report can be found at the following link:
`http://phys.org/wire-news/180021829/lomonosov-moscow-state-university-opens-new-observatory-in-the-c.html` .

simultaneous observations of Landolt standard fields (Landolt 2009) using formulae from Hardie (1964). The results of our measurements are presented in Table 1.

Table 1: $UBVRI$ photometry of RW Aur

	U	B	V	R_c	I_c
RW Aur A	14.26 ± 0.3	14.50 ± 0.06	13.80 ± 0.05	13.18 ± 0.07	12.46 ± 0.1
RW Aur B	14.97 ± 0.3	14.26 ± 0.05	12.92 ± 0.03	11.97 ± 0.07	11.01 ± 0.1

The results are non-trivial, as follows from the comparison of our data with that of White & Ghez (2001) obtained 20 years ago (see Fig. 2). First of all, during our observations RW Aur A became $\simeq 3^{\rm m}$ fainter in all spectral bands (the dot-dashed curve at the left panel of the figure) which may be interpreted as gray extinction. A better fit can be obtained assuming that the extinction is a sum of two components: a gray extinction with $A_V = 2.87$ and a selective standard one (Savage & Mathis, 1979) with $A_V = 0.44$ – see open circles in the panel. It seems natural to explain current RW Aur A dimming as a result of an eclipse of the star by dust particles, with predominantly large enough size r to produce gray extinctions up to at least 0.7 μm, which means that $r > 1$ μm (Krügel 2003).

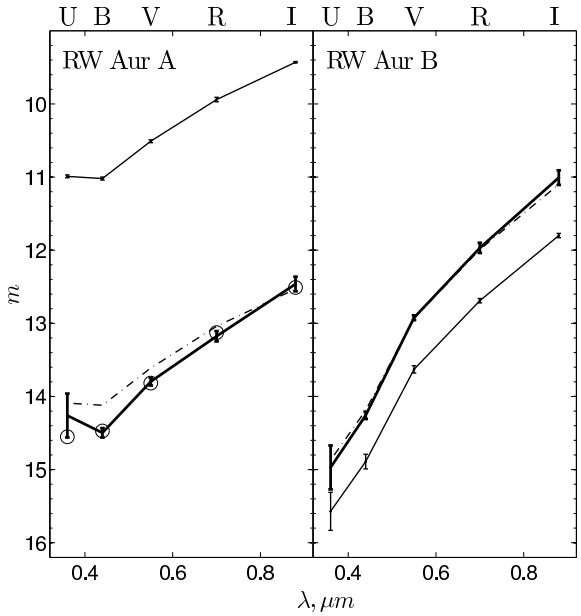

Figure 2. $UBVRI$-photometry for A and B components of RW Aur for two epochs: the thin lines are for HST observation (Nov. 1994), the thick lines are for our observation. The dash-dotted line corresponds to the HST data shifted down by $3\overset{\rm m}{.}1$ and up by $0\overset{\rm m}{.}7$ for A and B components, respectively. The circles are obtained from HST data by applying a sum of gray extinction with $\Delta m = 2.87$ and selective extinction with $A_V = 0.44$ using a standard reddening curve.

Our results indicate that RW Aur B is also a variable star: at the moment of our observations it was brighter than 20 years ago at $\Delta m \simeq 0\overset{\rm m}{.}7$ in each of $UBVRI$ band (gray brightening). Explanation is the same as for RW Aur A, but in the opposite sense: in 1994, RW Aur B was eclipsed by a cloud that consisted of dust particles with size $r > 1$ μm and now the cloud has passed away from the line of sight.

It follows also from our data that at the moment of observations the relative contribution of RW Aur B to the total brightness monotonically decreases from I to U band: it dominates at long wavelengths but becomes fainter than RW Aur A in the ultraviolet (see Fig. 1).

And last but not the least: our test observations indicate that the optics of the new 2.5 m telescope is good as well as the seasonal astroclimate at the site.

Acknowledgements: We thank an anonymous referee for valuable comments. This research was carried out in the frame of Lomonosov Moscow State University Program of Development.

References:

Beck T.L., Simon M., 2001, AJ, **122**, 413
Bisikalo D.V., Dodin A.V., Kaigorodov P.V. et al., 2012, *Astron. Rep.*, **56**, 686
Cabrit S., Pety J., Pesenti N. and C. Dougados C., 2006, *A&A*, **452**, 897
Ceraski W., 1906, *AN*, **170**, 339
Duchêne G., Monin J.-L., Bouvier J. and Ménard F., 1999, *A&A*, **351**, 954
Grankin K., Melnikov S., Bouvier J. et al. 2007, *A&A*, **461**, 183
Hardie R.H., 1964, *Photoelectric Reductions* in *Astronomical Techniques*, ed. W.A. Hiltner, University of Chicago, p. 178
Joy A.H., van Biesbroeck G., 1944, *PASP*, **56**, 123
Joy A.H., 1945, *ApJ*, **102**, 168
Kornilov, V., Safonov, B., Kornilov, M. et al., 2014, *PASP*, **126**, 482
Krügel E., 2003, *The Physics of Interstellar Dust*, IoP Series in Astronomy and Astrophysics, Bristol, UK: The Institute of Physics
Landolt A.U., 2009, *AJ*, **137**, 4186
Petrov P.P., Gahm G.F., Gameiro J.F. et al., 2001, *A&A*, **369**, 993
Petrov P.P., Kozack B.S., 2007, *Astron. Rep.*, **51**, 500
Poutriquet F., Plainchamp P., Billet J. et al., 2012, *Proc. SPIE* **8444**, 84441W
Rodriguez J.E., Pepper J., Stassun K.G. et al., 2013, *AJ*, **146**, 112
Savage B.D., Mathis J.S., 1979, *Ann. Rev. Astr. Ap.*, **17**, 73
Stetson P.B., 1987, *PASP*, **99**, 191
White R.J., Ghez A.M., 2001, *ApJ*, **556**, 265

COMMISSIONS 27 AND 42 OF THE IAU
INFORMATION BULLETIN ON VARIABLE STARS

Number 6127

Konkoly Observatory
Budapest
12 January 2015

HU ISSN 0374 – 0676

NULL CORRELATION BETWEEN THE O'CONNELL EFFECT AND ORBITAL PERIOD CHANGE FOR SW Lac, CN And, AND V502 Oph

KOJU, VIJAY[1]; BEAKY, MATTHEW M.[2]

[1] Computational Science Program, Middle Tennessee State University, 1301 East Main Street, Murfreesboro, TN 37132, USA

[2] Physics and Engineering Physics, Juniata College, 1700 Moore Street, Huntingdon, PA 16652, USA
e-mail: vk2g@mtmail.mtsu.edu

Introduction

One peculiar feature observed in the light curves of some eclipsing binaries is the asymmetry in the heights of the maxima, known as the O'Connell effect. Although it has been called "one of the celebrated difficult problems in the field of close binary systems" (Liu and Yang 2003), the O'Connell effect has still not been conclusively explained for the majority of the systems exhibiting it.

The first careful study of this phenomenon was carried out by Mergentaler (1950), followed by a statistical study of the asymmetry by O'Connell (1951). O'Connell searched for correlations between the size of the asymmetry and other parameters, such as the orbital period and the depths of the eclipses, the relative dimensions of the component stars, and their atmospheric densities. He found that the size of the asymmetry tended to be greater at shorter optical wavelengths. A similar result was found by Davidge and Milone (1984), although the color correlation they determined was opposite in sign.

Eclipsing binary systems such as SX Cassiopeiae, ST Centauri, and RV Ophiuchi have maintained a constant O'Connell effect over many decades (Davidge and Milone 1984). However, in many other systems, e.g. CG Cygni, YY Eridani, RT Lacertae, and XY Ursae Majoris (Milone et al. 1979; Yang and Liu 1999; Cakirli et al. 2003; and Pribulla et al. 2001), this effect is observed to vary significantly over many cycles.

Many theoretical models have been developed for explaining the O'Connell effect, such as the presence of starspots on one or both components in the binary system (see Berdyugina 2005 for an introduction to starspot theory), the impact of a mass-transferring gas stream flowing from one component to the other, circumstellar matter, and asymmetric circumfluence due to Coriolis forces (Liu and Yang 2003).

In this paper, we present the results of our investigations of three eclipsing binary systems that exhibit a variable O'Connell effect: SW Lacertae, CN Andromedae, and V502 Ophiuchi. Each of these systems is known to also have a variable orbital period. In addition to making new photometric observations of these systems, we looked for evidence of correlation between the change in the orbital period of the systems and the size of the asymmetry in the maxima.

Remarks on Individual Systems

SW Lacertae

Photometric variability of SW Lacertae was discovered by Miss Ashall (Leavitt 1918) on plates taken at Harvard Observatory. Since that time, the system has been observed photoelectrically and photometrically by many observers, including Jordan (1929), Schilt (1924), Serkowski (1956), Brownlee (1957), Hinderer (1960), Broglia (1962), Bookmyer (1965), Faulkner and Bookmyer (1980), Essam (1992), Lee et al. (1991), Djuraševic et al. (2005), Gazeas et al. (2005), and Alton & Terrell (2006). The system has been of continuous interest due to its short orbital period of 0.3207209 d, conspicuous changes in the period of the system, and variability in the light of the system at out-of-eclipse phases. Panchatsaram and Abhyankar (1981) and Pribulla et al. (1999) suggest that the variation in the orbital period of the binary system is due to the presence of two additional unseen components, making it a quadruple system. Light curve variations in this system are usually attributed to the presence of starspots in one or both of the components of the system (Stepien 1980, Binnendijk 1984, Leung et al. 1984, Lee et al. 1991, Eaton 1986, Jeong et al. 1994, Djuraševic and Erkapic 1997, Pribulla et al. 1999, Djuraševic et al. 2005). SW Lac belongs to the W-type subclass of W UMa binaries (Binnendijk 1984) with spectral type G5V (Gazeas et al. 2005).

CN Andromedae

Variability of CN Andromedae was discovered by Hoffmeister (1949) and was first classified as an Algol-type binary with an orbital period of 2.599 d (Tsesevich 1956). Löchel (1960) later classified it as a W UMa-type binary with the period of 0.462798 d. Additional photometric observations of the systems have been carried out by Bozkurt et al. (1976), Seeds and Abernethy (1982), Kaluzny (1983), Michaels et al. (1984), Evren et al. (1987), Keskin (1989), Samec et al. (1998), Van Hamme et al. (2001), Zola et al. (2005), Jassur and Khodadadi (2006), and Lee & Lee (2006). Kaluzny (1983) reclassified the system as β Lyrae-type because of the difference in the depths of the minima. The change in the orbital period of the system has been explained by the mass transfer from the primary to the secondary component and/or by magnetic breaking as a result of strong system activity (Samec et al. 1998). CN And is an active solar type binary with components of spectral type in the F5 to G5 range (Zola et al. 2005). Flare events (Yang and Liu 1985) and X-ray emission (Shaw et al. 1996) have also been detected in the system.

V502 Ophiuchi

V502 Ophiuchi was discovered by Hoffmeister (1935) to be an eclipsing binary. Photometric observations of the system have been carried out by Kwee (1968), Wilson (1967), Binnendijk (1969), Vader & van der Wal (1973), Maceroni et al. (1982), Rovithis et al. (1988), Zola and Krzesinski (1988), and recently by Selam et al. (2009). The system has an orbital period of 0.453388 d, but its period variation has not been observed over as long a time as the other systems examined in this paper. This change in the period of the system can be explained in terms of the mass transfer from more massive to less massive component, or angular momentum loss from the system by magnetically driven wind (Vilhu 1982). The asymmetric maxima of the light curves have been attributed to the existence of the cool spot on the secondary component (Rovithis et al. 1988). The

primary and the secondary component have been classified as having the spectral type of G1V and F9V, respectively (Struve and Zebergs 1959).

New Photometric Observations

We observed the three eclipsing binary systems V502 Oph, SW Lac, and CN And, using a 20-cm Meade LX200GPS telescope at the Truman State University Observatory in Kirksville, Missouri. An SBIG ST-9XE CCD camera with Johnson BVRI filters was used for all observations.

V502 Oph was observed for 11 nights between June 29 and July 18, 2010. SW Lac and CN And were observed for 7 nights between July 10 and 19, 2010 and 4 nights between August 7 and 12, 2010, respectively. Astronomers Control Panel (ACP) was used to communicate between the telescope, CCD camera, focuser, and observatory dome. The telescope and CCD camera were controlled by Maxim DL, which was also used to analyze the acquired images and to create the light curves.

The resulting differential light curves for SW Lac, CN And, and V502 Oph in *B, V, R,* and *I* filters are shown in Figures 1, 2, and 3 respectively. Some of the light curves have been adjusted by adding a constant offset in order to improve the legibility of the figures.

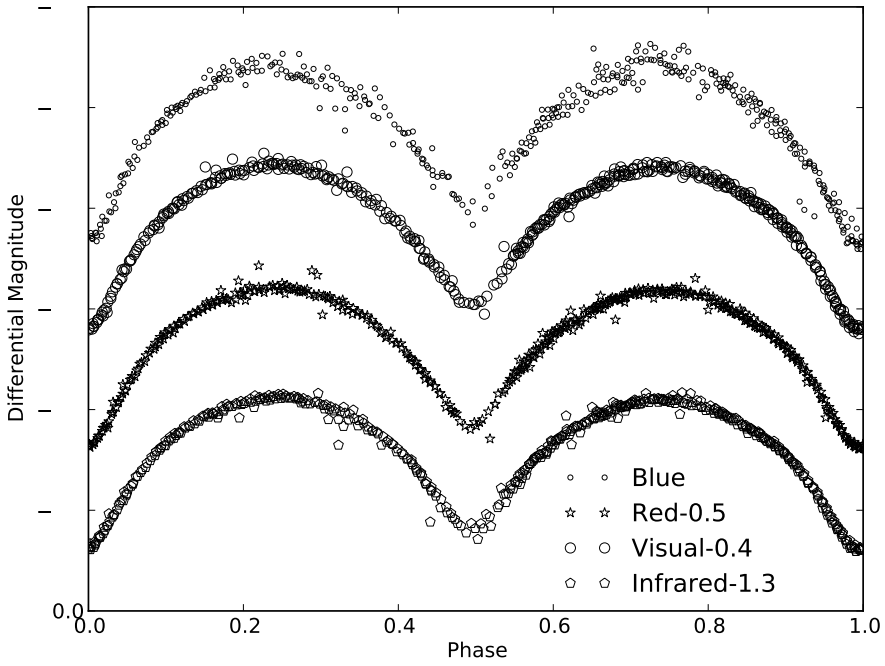

Figure 1. *BVRI* light curves of SW Lac acquired in 2010, August. Data for the *V, R,* and *I* filters are offset for clarity.

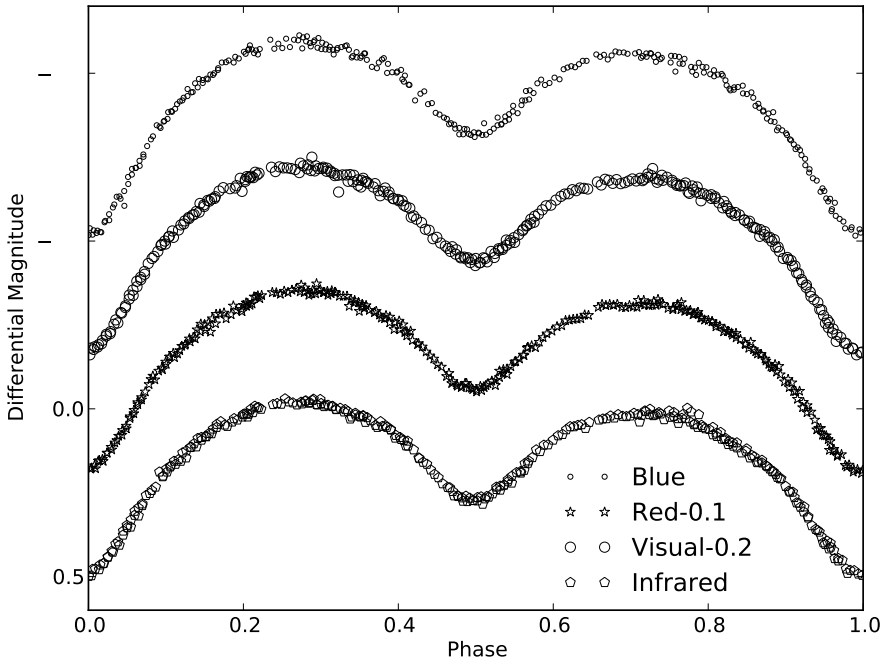

Figure 2. *BVRI* light curves of CN And acquired in 2010, July. Data for the V and R filters are offset for clarity.

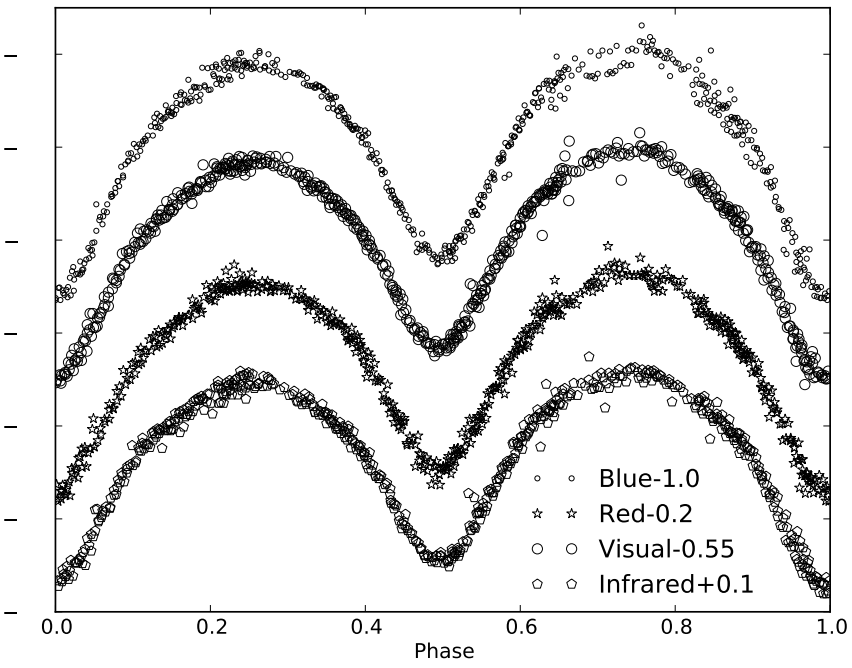

Figure 3. *BVRI* light curves of V502 Oph acquired in 2010, June-July. Data for the V and R filters are offset for clarity.

Analysis of Historical Data

A key element of our study is the investigation of the relationship between the change in the orbital period and the variation in the asymmetry in the maxima in some eclipsing binaries. For this reason, we chose the well-studied O'Connell effect systems SW Lac, CN And, and V502 Oph. We have combined our new photometric data with a reexamination of light curves from the literature in order to explore relationships between the size and sign of the O'Connell effect and variations in the orbital period of the binary systems.

To compute the O'Connell effect (Δm), we fit a 16-term Fourier series to the observational data (Wilsey and Beaky 2009). Using the fitted curve, Δm is calculated as the difference between the two maxima given as

$$\Delta m = (\text{magII} - \text{magI}) \times 1000 \text{ mmag},$$

where magI and magII are the magnitudes of primary and secondary maxima respectively. Thus, the brighter primary maximum corresponds to the positive O'Connell effect, whereas the brighter secondary maximum corresponds to the negative O'Connell effect. Table 1 gives the values of the O'Connell effect of the three systems studied in all filters based on our photometric data from 2010.

Table 1: Δm (millimagnitudes) for the light curves in Figs. 1, 2, and 3.

Star Name	B	V	R	I
SW Lac	-1 ± 10	18 ± 6	18 ± 6	11 ± 7
CN And	32 ± 3	34 ± 3	41 ± 5	38 ± 4
V502 Oph	-27 ± 5	-23 ± 5	-24 ± 4	-15 ± 6

Figures 4, 5, and 6 show the measure of the O'Connell effect in SW Lac, CN And, and V502 Oph, respectively, together with the Eclipse Timing Variations (ETV) data for the systems, plotted against the year of observation. In all cases the size of the O'Connell effect varied only slightly between measurements made with different filters. Figure 4 through 6 contain the data for V filter (left) and B filter (right). ETV data for each of the three systems was acquired from the website (`var.astro.cz/ocgate/`), using the default ephemeris provided. The ETV data for SW Lac represent an average value per year, but those for CN And and V502 Oph are not averaged due to the lack of sufficient data points.

Discussion

Observational Light Curves

The O'Connell effect in SW Lac has switched from positive and negative several times in the past 60 years. During our observation period in the summer of 2010, SW Lac was observed to have a small positive O'Connell effect, which is difficult to detect visually in the light curves shown in Figure 1. The light curve in the B filter is comparatively noisier than those in other filters, especially at the secondary maximum. Its effect can be seen in the value of Δm for the B filter, which has a different sign than the values for VRI filters.

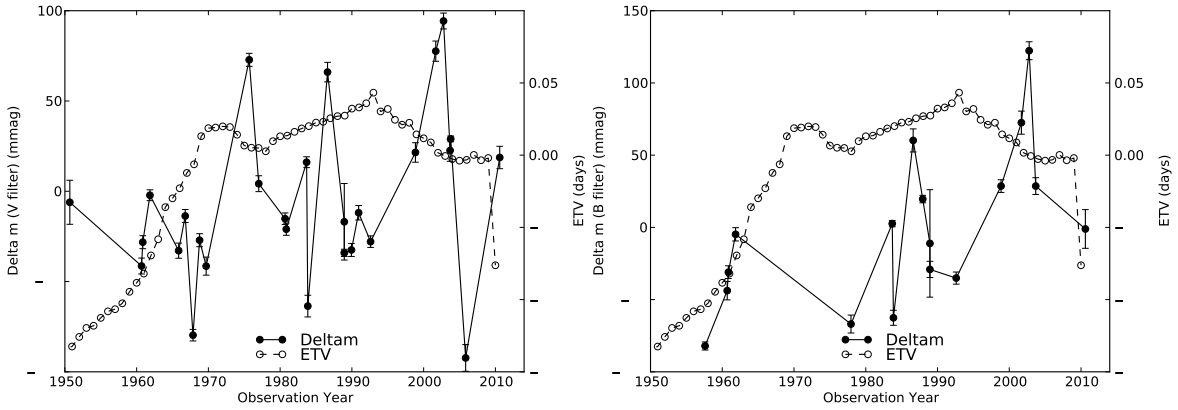

Figure 4. Measurement of the O'Connell effect Δm (left axis) and ETV values (right axis) for SW Lac between 1949 and 2010. The left and right plots represent the data for Visual and Blue filters respectively. The list of references and observation dates for SW Lac is presented in Table 2. Each ETV data point represents an average value per year.

Table 2: Observers and dates of observation for the photometric data on SW Lac in Figure 4.

Reference	Observation Date
Eaton (1986)	Dec., 1976
Eaton (1986)	Oct. and early Nov., 1980
Lafta & Grainger (1985)	Aug. 6 - Sept. 7, 1983
Lee et al. (1991)	Oct. 9 - Nov. 21, 1988
Mikolajewska & Mikolajewski (1981)	Autumn 1975
Mikolajewska & Mikolajewski (1981)	Autumn 1980
Muthsam & Rakos (1974)	Autumn 1960
Gazeas et al. (2005)	Sept. 20 - 21, 2003
Semeniuk (1971)	Aug. 28 - Sept. 26, 1968
Semeniuk (1971)	Aug. 6 - Sept. 8, 1969
Serkowski (1956)	July 10 - Oct. 5, 1950
Bookmyer (1965)	Aug. 29 - Nov. 23, 1960
Bookmyer (1965)	Aug. - Nov., 1961
Essam et al. (1992)	July 1 - 14, 1986
Albayrak et al. (2004)	2001
Albayrak et al. (2004)	2002
Djuraševic et al. (2005)	2003
Hrivnak & Goehring (1991)	Oct. - Nov., 1990
Jeong et al. (1994)	Oct. 9 - Nov. 21, 1988
Alton & Terrell (2006)	Oct. 1, 2005
Zhang et al. (1992)	July 29 - 30, 1992
Niarchos (1987)	Oct. 1 - 4, 1983
Peña et al. (1993)	Nov. 1 - 6, 1989
Pribulla et al. (1999)	Aug. - Dec., 1998
Ruciński (1968)	Oct. 5 - 7, 1965
Ruciński (1968)	Sept. 10 - 25, 1966
Stepien (1980)	Sept. 26 - Oct. 9, 1967

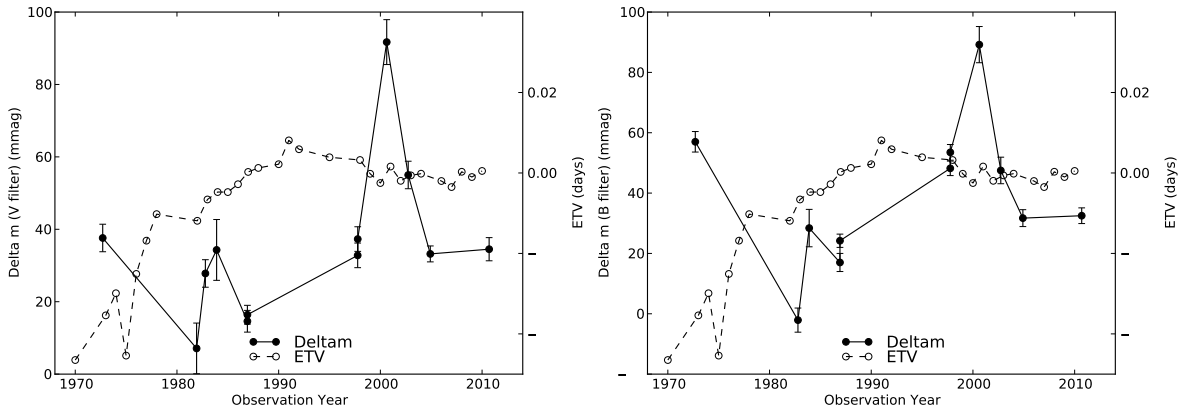

Figure 5. Measurement of the O'Connell effect Δm (left axis) and ETV values (right axis) for CN And between 1970 and 2010. The left and right plots represent the data for Visual and Blue filters respectively. The list of references and observation dates for CN And is presented in Table 3. Each ETV data point represents an average value per year.

Table 3: Observers and dates of observation for the photometric data on CN And in Figure 5.

Reference	Observation Date
Van Hamme et al. (2001)	Sept. 7 - 11, 1997
Jassur & Khodadadi (2006)	Summer 2000
Kaluzny (1983)	Aug. 15 - Oct. 18, 1982
Keskin (1989)	Oct. 8 - Nov. 27, 1986
Bozkurt et al. (1976)	July 13 - Sept. 12, 1972
Michaels et al. (1984)	Sept. 30 - Nov. 15, 1984
Evren et al. (1987)	Oct. 8 - Nov. 28, 1986
Lee & Lee (2006)	Sept. 24 - Dec. 1, 2004
Samec et al. (1998)	Sept. 4 - 10, 1997
Seeds & Abernethy (1982)	Oct. 3 - Dec. 7, 1981
Zola et al. (2005)	Aug. 19 - Sept. 4, 2002

Like SW Lac, the O'Connell effect in both CN And and V502 Oph have varied significantly over the past several decades. In 2010, CN And exhibited a positive O'Connell effect, while V502 Oph had a negative O'Connell effect. For both systems, the sign and magnitude of our new values of Δm is consistent across all filters and with the most recently observed light curves (2004 for CN And, and 2005 for V502 Oph). The O'Connell effect in CN And has always been observed to be positive, but has varied from a few millimagnitudes to almost 100 mmag. Likewise, V502 Oph has also exhibited large swings in the size of the O'Connell effect. At some point between 1987 and 2005, the value of Δm changed from positive to negative, and remained negative in our 2010 measurements.

The variations in the O'Connell effect (Figures 4, 5 and 6) suggest that the cause of the light curve asymmetries in the three systems is highly dynamic. Ideally, a model which accounts for the change in the asymmetry as some function of time (Lanza et al. 1993, 1994) should be adopted, though no such model currently exists. In the case of SW Lac, a recent Doppler imaging study has identified the presence and location of starspots on both components (Şenavcı et al. 2011).

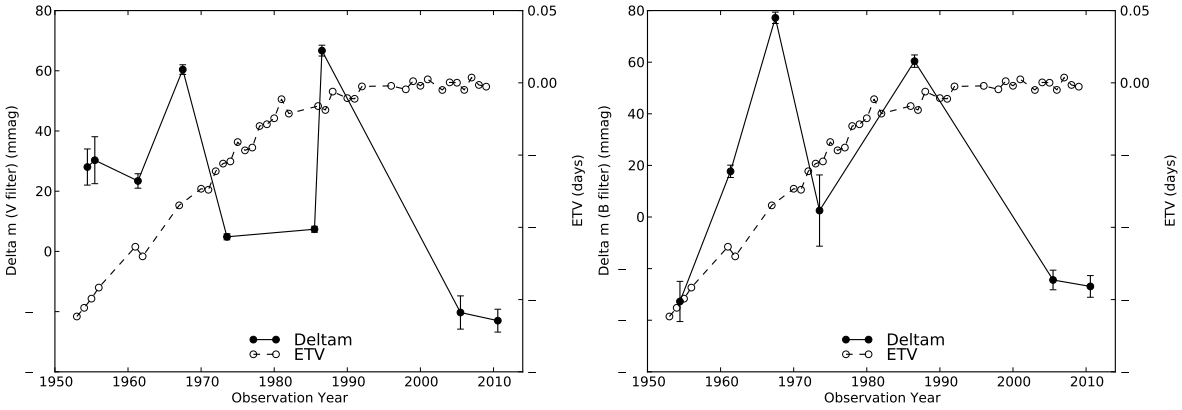

Figure 6. Measurement of the O'Connell effect Δm (left axis) and ETV values (right axis) for V502 Oph between 1953 and 2010. The left and right plots represent the data for Visual and Blue filters respectively. The list of references and observation dates for V502 Oph is presented in Table 4. Each ETV data point represents an average value per year.

Table 4: Observers and dates of observation for the photometric data on V502 Oph in Figure 6.

Reference	Observation Date
Binnendijk (1969)	May 20 - June 3, 1967
Kwee (1968)	April - June, 1955
Rovithis et al. (1988)	May - June, 1986
Selam et al. (2009)	2005
Vader & van der Wal (1973)	May 30 - June 26, 1973
Wilson (1967)	Apr. 4 - 16, 1961
Zola & Krzesinski (1988)	1985

Orbital Period Change and the O'Connell effect

In addition to a varying O'Connell effect, SW Lac, CN And, and V502 Oph have exhibited a continuous change in their orbital period for as long as they have been observations. The ETV diagrams for CN And and V502 Oph are close to parabolic, while that for SW Lac is more irregular.

The variation in the period of SW Lac might be due to the existence of a third component or may be attributed to the intrinsic variability of the system, mainly to mass-loss by one or both components caused by dynamic instability (Kopal 1959). A detailed analysis of the ETV diagram performed by Pribulla et al. (1999) revealed the presence of two possible extraneous bodies, and they suggested a mass transfer rate of $2.32 \times 10^{-7} M_{\odot} y^{-1}$ to explain the period increase observed in SW Lac. The decrease in the orbital period of CN And could be interpreted in terms of mass transfer form the Roche lobe-filling primary to the slightly underfilling secondary component at the rate of $4.82(6) \times 10^{-8} M_{\odot} y^{-1}$. Similarly, the decrease of the period in V502 Oph can be explained in terms of the mass transfer from more massive to less massive component, or angular momentum loss from the system by magnetically driven wind (Vilhu 1981, 1982), or the presence of a third body (Derman et al. 1991).

The magnetically induced structural variations during the magnetic cycle of a convective component of a close binary system, together with tidal spin-orbit coupling, has an effect in the period of such systems (Applegate 1989). Thus, a correlation between variations in orbital period change and other measures of the magnetic activity might be expected. If the asymmetry in the maxima is alleged to be caused by starspot, which is an indicator of magnetic, activity, then there may be a correlation between changes in the orbital period and the light curve asymmetry (Derman et al. 1991; Lanza & Rodonò, 2004).

Figures 4 through 6 do not indicate any strong correlation between the orbital period change and the size of the asymmetry in the maxima of the light curves in any of the three systems over the past 60 years. Variations in Δm appear to be largely random, while the ETV diagrams indicate a generally steady change in orbital period. One could make the claim for periodicity in the Δm values for SW Lac, with a period of about 10 to 15 years. Likewise, the meandering nature of the ETV diagram for SW Lac could arguably arise from a superposition of a parabolic term and an oscillating term with a period of 10 to 20 years.

Future Directions

The greatest impediment to identifying patterns in long-term variations of the O'Connell effect in contact binaries over time is the irregularity with which light curves have been acquired. Both CN And and V502 Oph are interesting and dynamic systems, yet their light curves have been obtained only once or twice per decade, on average. Even SW Lac, one of the best observed contact binaries, has gaps spanning several years between successive photometric observations. As a consequence, it is impossible to extract information about starspot cycles or differential rotation, if indeed such phenomena are present in the binary system.

A superior approach to monitoring the dynamical evolution of starspots on a contact binary system would be through uninterrupted photometric coverage, such as that provided by the NASA Kepler Space Mission. The Prša et al. (2011) catalog contains 1879 unique objects, out of $\sim$ 150,000 stars, identified as eclipsing binaries, and a check of even a few of the observational light curves available through the Kepler Eclipsing Binary

Catalog (`http://keplerebs.villanova.edu`) shows that many of these systems exhibit a variable O'Connell effect. Clearly, this is a unique and invaluable resource for studying the real-time evolution and migration of starspots in contact eclipsing binaries.

The visual inspection of the historical light curves that we conducted in the course of this project revealed clearly that in addition to an asymmetry in the light curve maxima, the classical O'Connell effect, there was also a significant variation in the depth of the minima. Figure 7 shows the variation of the difference between the primary minimum and the secondary minimum, represented by $\Delta m_{\rm min}$, for SW Lac, using the same light curves for which $\Delta m_{\rm max}$ was determined in Figure 4. The degree of variation is dramatic, ranging over 300 millimagnitudes and even becoming negative in 1991, meaning that the secondary minimum was deeper than the primary (Hrivnak & Goehring 1991). While such phenomena have been noted occasionally in the literature (e.g. Ruciński, 1968), it is more often overlooked. The light curve minima of EBs are generally of different depths, however their difference is of constant magnitude which is attributed to the difference in temperatures of the component stars. The large and random variations in the difference between the two minima over time (Figure 7) can potentially be significant in understanding the temporal dynamics of EBs. One possible cause for this random variations can be the presence of different sized starspots on the visible (front) star during the eclipses.

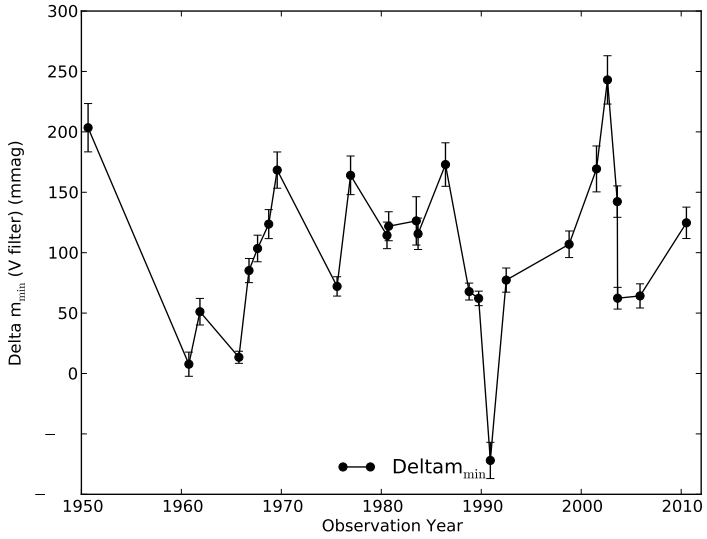

Figure 7. Difference between the primary and secondary minima of SW Lac, denoted $\Delta m_{\rm min}$, between 1949 and 2010.

Acknowledgements: This work was funded Truman State University under the TruScholars Summer Undergraduate Research Program, 2010.

References:

Albayrak, B., et al., 2004, *A&A*, **420**, 1039
Alton, K. B., & Terrell, D., 2006, *JAAVSO*, **34**, 188
Applegate, J. H., 1989, *ApJ*, **337**, 865

Berdyugina, S. V., 2005, *Living Rev. Solar Phys*, **2**, 8
Binnendijk, L., 1969, *AJ*, **74**, 218
Binnendijk, L., 1984, *PASP*, **96**, 646
Bookmyer, B. B., 1965, *AJ*, **70**, 415
Bozkurt, S., et al., 1976, *IBVS*, **1087**, 1
Broglia, P., 1962, *Mem. Soc. Astron. Ital.*, **33**, 43
Brownlee, R. R., 1957, *ApJ*, **125**, 372
Çakirli, Ö., et al., 2003, *A&A*, **405**, 733
Davidge, T. J., & Milone, E. F., 1984, *ApJS*, **55**, 571
Derman, E., et al., 1991, *A&AS*, **90**, 301
Djurašević, G., & Erkapić, S., 1997, *Bull. Astr. de Belgrade*, **155**, 55
Djurašević, G. et al., 2005, *ApSS*, **296**, 261
Eaton, J. A., 1986, *AcA*, **36**, 79
Essam, A., et al., 1992, *Ap&SS*, **188**, 117
Evren, S., et al., 1987, *IBVS*, **3109**, 1
Faulkner, D. R., & Bookmyer, B. B., 1980, *PASP*, **92**, 92
Gazeas, K. D., et al., 2005, *AcA*, **55**, 123
Hinderer, F., 1960, *JO*, **43**, 161
Hoffmeister, C., 1935, *AN*, **255**, 401
Hoffmeister, C., 1949, *AN*, **278**, 24
Hrivnak, B. J., & Goehring, C. A., 1991, *IAPPP Comm.*, **45**, 29
Jassur, D. M. Z., & Khodadadi, A., 2006, *JApA*, **27**, 47
Jeong, J. H., et al., 1994, *ApJ*, **421**, 779
Jordan, F. C., 1929, *PAllO*, **7**, 125
Kaluzny, J., 1983, *AcA*, **33**, 345
Keskin, V., 1989, *Ap&SS*, **153**, 191
Kopal, Z., 1959, Close binary systems, *The international Astrophysics Series*, Chapman & Hall, London
Kwee, K. K., 1968, *BANS*, **2**, 277
Lafta, S. J., & Grainger, J. F., 1985, *Ap&SS*, **114**, 23
Lanza, A. F. et al., 1993, *A&A*, **269**, 351
Lanza, A. F. et al., 1994, *A&A*, **290**, 861
Lanza, A. F. and Rodonò, M., 2004, *AN* **325**, 393
Leavitt, H. S., 1918, *Harvard Circ.*, 207
Lee, W. B., et al., 1991, *Proc. ASA*, **9**, 297
Lee, C.-U., & Lee, J. W., 2006, *JKAS*, **39**, 25
Leung, K.-C., et al., 1984, *PASP*, **96**, 634
Liu, Q.-Y., & Yang, Y.-L., 2003, *ChJAA*, **3**, 142
Löchel, K., 1960, *M.V.S.*, 457
Maceroni, C., et al., 1982, *A&AS*, **49**, 123
Mergentaler, J., 1950, *Contr. Wroclaw Astron. Obs.*, **4**, 1
Michaels, E. J., et al., 1984, *IBVS*, **2474**, 1
Mikolajewska, J., & Mikolajewski, M., 1981, *IBVS*, **1953**, 1
Milone, E. F., et al., 1979, *AJ*, **84**, 417
Muthsam, H., & Rakos, K. D., 1974, *A&AS*, **13**, 127
Niarchos, P. G., 1987, *A&AS*, **67**, 365
O'Connell, D. J. K., 1951, *PRCO*, **2**, 85
Panchatsaram, T., & Abhyankar, K. D., 1981, *Bull. Astron. Soc. India*, **9**, 31
Peña, J. H., et al., 1993, *Rev. Mex. Astron. Astrofis.*, **25**, 63

Pribulla, T., et al., 1999, *Contrib. Astron. Obs. Skalnaté Pleso*, **29**, 111
Pribulla, T., et al., 2001, *A&A*, **371**, 997
Prša, A., et al., 2011, *AJ*, **141**, 83
Rovithis, P., et al., 1988, *A&AS*, **74**, 265
Ruciński, S. M., 1968, *AcA*, **18**, 49
Samec, R. G., et al., 1998, *IBVS*, **4616**, 1
Schilt, J., 1924, *BAN*, **2**, 175
Seeds, M. A., & Abernethy, D. K., 1982, *PASP*, **94**, 1001
Selam, S. O., et al., 2009, *Journal of Arts & Science*, **12**, 151
Semeniuk, I., 1971, *AcA*, **21**, 49
Şenavcı, H. V., et al., 2011, *A&A* **529**, A11
Serkowski, K., 1956, *AcA*, **6**, 95
Shaw, J. S., et al., 1996, *ApJ*, **461**, 951
Stepien, K., 1980, *AcA*, **30**, 315
Struve, O., & Zebergs, V., 1959, *ApJ*, **130**, 789
Tsesevich, W., 1956, *A.C.Kasan*, **170**, 14
Vader, P., & van der Wal, N. A., 1973, *IBVS*, **842**, 1
Van Hamme, W., et al., 2001, *AJ*, **122**, 3436
Vilhu, O., 1981, *Ap&SS*, **78**, 401
Vilhu, O., 1982, *A&A*, **109**, 17
Wilsey, N. J., & Beaky, M. M., 2009, *SASS*, **28**, 107
Wilson, E. R., 1967, *AJ*, **72**, 1028
Yang, Y.-L., & Liu, Q.-Y., 1985, *IBVS*, **2705**, 1
Yang, Y., & Liu, Q., 1999, *A&AS*, **136**, 139
Zhang, R.-X., et al., 1992, *IBVS*, **3772**, 1
Zola, S., & Krzesinski, J., 1988, *IBVS*, **3218**, 1
Zola, S., et al., 2005, *AcA*, **55**, 389

Light curves from the new photometric observations are accessible online at the IBVS website:

Star	Filter	File Name
CN And	B	6127-t5.txt
CN And	I	6127-t6.txt
CN And	R	6127-t7.txt
CN And	V	6127-t8.txt
SW Lac	B	6127-t9.txt
SW Lac	I	6127-t10.txt
SW Lac	R	6127-t11.txt
SW Lac	V	6127-t12.txt
V502 Oph	B	6127-t13.txt
V502 Oph	I	6127-t14.txt
V502 Oph	R	6127-t15.txt
V502 Oph	V	6127-t16.txt

COMMISSIONS 27 AND 42 OF THE IAU
INFORMATION BULLETIN ON VARIABLE STARS

Number 6128

Konkoly Observatory
Budapest
14 January 2015

HU ISSN 0374 – 0676

MINIMA TIMES OF SOME ECLIPSING BINARY STARS

TERZİOĞLU, Z.; GÜRSOYTRAK, H.; SARAL,G.; BAĞIRAN, N.; GÖKAY, G.; KILIÇ, Y.; DEMİRCAN, Y.; OKAN, A.; DOĞRUEL, M.B.; ALPSOY, M.; CERİT, S.; ŞEMUNİ, M.; YILDIRIM, C.; GÜROL, B.

Ankara University Observatory, Faculty of Science, Astronomy and Space Sciences Department 06100, Tandoğan, Ankara, TÜRKİYE; e-mail: zterzioglu@ankara.edu.tr

We present several CCD minima observations of eclipsing binaries. Observations were done with an Apogee ALTA U47+ back illuminated CCD camera attached to an 16″ Schmidt/Cassegrain telescope at Ankara University Observatory. Reduction of the CCD frames was made with the IRAF[1] `ccdred` and `daophot` packages.

The minima times were computed with several methods in Minima25b (Nelson 2006) (parabolic fit, tracing paper, bisectors of chords, Kwee and van Woerden method (Kwee & van Woerden 1956), Fourier fit and sliding integrations technique). Then weighted mean minimum-time values were calculated for all filters used.

Table 1: Times of minima of eclipsing binaries

Variable	HJD 24.....	±	Obs	$O-C$		Ref	Fil
V1713 Aql	56132.5218	0.0002	AO-ŞŞŞ-YŞ	−0.0034	p	⟨12⟩	BVRI
HH Boo	56091.3859	0.0001	ZT	+0.0012	p	⟨2⟩(T_0), ⟨11⟩(P)	BVRI
	56092.3429	0.0006	HG-GG	+0.0022	p		BVRI
	56092.5024	0.0008	HG-GG	+0.0024	s		BVRI
V1046 Cas	56161.4792	0.0020	MA	+0.0115	s	⟨6⟩(T_0), ⟨11⟩(P)	BVRI
	56189.4234	0.0003	MNB	+0.0114	p		BVRI
EF Cep	56156.4346	0.0007	MSH	+0.0010	p	⟨1⟩(T_0), ⟨11(P)⟩	BVRI
	56173.4064	0.0002	MBD	+0.0017	p		BVRI
	56194.3155	0.0003	MBD	+0.0001	s		BVRI
EG Cep	56197.4147	0.0002	GG-Eİ-BE	+0.0116	p	⟨9⟩(T_0), ⟨11⟩(P)	BVRI
ASAS J013630+0150.3	56196.5554	0.0005	HG	+0.0203	s	⟨13⟩	BVRI
TW CrB	56090.4767	0.0002	AO-ŞŞŞ-YŞ	−0.0004	p	⟨2⟩(T_0), ⟨11⟩(P)	BVRI
V859 Cyg	56126.3023	0.0004	CY-MA	+0.0038	p	(a)	BVRI
	56126.5052	0.0002	CY-MA	+0.0042	s		BVRI
TYC 3069-1654-1	56094.4952	0.0004	ŞŞŞ	+0.0719	s	⟨4⟩	BVRI
	56127.4039	0.0005	GG-Eİ-BE	+0.0730	p		BVRI
GSC 2750-0854	56174.5653	0.0004	AO	−0.1119	p	⟨7⟩	BVRI
	56195.5498	0.0077	AO	−0.1160	s		BVRI
TYC 2220-704-1	56169.3903	0.0003	GG	−0.0327	p	⟨13⟩	BVRI
	56169.5509	0.0007	GG	−0.0320	s		BVRI
	56175.3059	0.0006	AY-YD	−0.0322	s		BVRI
	56175.4653	0.0004	AY-YD	−0.0326	p		BVRI
ASAS J212915+1604.9	56134.3443	0.0003	GG-Eİ-BE	+0.0005	s	(b)	BVRI
	56134.4846	0.0003	GG-DDİ-KÖÜ	−0.0007	p		BVRI
	56139.2950	0.0002	AO-YŞ	−0.0007	p		BVRI
	56139.4378	0.0005	AO-YŞ	+0.0006	s		BVRI
	56155.4242	0.0002	MA-BE-Eİ	−0.0002	p		BVRI
	56155.5665	0.0002	MA-BE-Eİ	+0.0006	s		BVRI

[1]IRAF is distributed by the National Optical Astronomical Observatories, operated by the Association of the Universities for Research in Astronomy, inc., under cooperative agreement with the National Science Foundation

Table 1: cont.

Variable	HJD 24.....	±	Obs	$O-C$		Ref	Fil
ASAS J225956+1418.2	56196.4051	0.0005	HG	−0.0599	p	⟨13⟩	BVRI
V882 Per	56162.5056	0.0002	GG	+0.0145	p	⟨8⟩	BVRI
	56171.5003	0.0005	MNB-MBD	+0.0155	p		BVRI
	56198.4814	0.0009	MNB	+0.0153	p		BVRI
V384 Ser	56087.3527	0.0003	YK-SC	−0.0040	p	⟨3⟩(T_0), ⟨11⟩(P)	BVRI
	56087.4848	0.0008	YK-SC	−0.0062	s		BVRI
GSC 2140-1485	56111.3167	0.0006	AO-YŞ	−0.0025	p	(c)	BVRI
ASAS J205847+2731.9	56157.3047	0.0003	YK	+0.0076	s	⟨13⟩	BVRI
	56157.4380	0.0005	YK	+0.0069	p		BVRI
	56157.5728	0.0007	YK	+0.0076	s		BVRI
	56166.4192	0.0003	MMK	+0.0077	s		BVRI
	56166.5521	0.0002	MMK	+0.0066	p		BVRI
	56195.2359	0.0003	AO	+0.0069	p		BVRI
	56195.3702	0.0005	AO	+0.0071	s		BVRI
ASAS J211538+2454.2	56138.3995	0.0003	MA-MBD	−0.0221	p	⟨13⟩	BVRI

(a): New elements: T_0=2451041.4457, P=0.4050062 d.
(b): New elements: T_0=2455407.5576, P=0.28296136 d.
(c): New elements: T_0=2456111.3192, P=0.30120202 d.

Observers:

AO:	Abdullah OKAN	MBD:	Mustafa Burak DOĞRUEL
AY:	Arzu YOLKOLU	MHT:	Mustafa Hayri TÜRKYILMAZ
BE:	Başak ESMER	MMK:	Metehan Metin KEKLİK
CY:	Ceren YILDIRIM	MNB:	Mehmet Naim BAĞIRAN
DDİ:	Didem Dilan İZCİ	MSH:	Muhammed ŞEMUNİ
Eİ:	Elif İMDAT	SC:	Sonay CERİT
GG:	Gökhan GÖKAY	ŞŞŞ:	Şakir Şenol ŞAHİN
GS:	Gözde SARAL	YD:	Yahya DEMİRCAN
HG:	Hande GÜRSOYTRAK	YK:	Yücel KILIÇ
HS:	Hatice SARAÇ	YŞ:	Yunus ŞENDAĞ
KÖÜ:	Kübra Özge ÜNAL	ZT:	Zahide TERZİOĞLU
MA:	Mehmet ALPSOY		

References:

Diethelm, R., 2012a, *IBVS*, No. 6011 ⟨1⟩
Diethelm, R., 2012b, *IBVS*, No. 6029 ⟨2⟩
Hübscher, J. et al., 2012, *IBVS*, No. 6026 ⟨3⟩
Khruslov, A. V., 2007, *Perem. Zvezdy Prilozh.*, **7**, 6 ⟨4⟩
Kwee, K. K., van Woerden, H., 1956, *Bull. Astron. Inst. Neth.*, **12**, 327 ⟨5⟩
Locher, K., 2005, *OEJV*, **3**, 1 ⟨6⟩
Maciejewski, G. et al., 2004, IBVS, No. 5518 ⟨7⟩
Nagai, K., 2009, VSOLJ 48 ⟨8⟩
Nagai, K., 2012, VSOLJ 53 ⟨9⟩
Nelson, B., 2006, `http://www.members.shaw.ca/bob.nelson/software1.htm` ⟨10⟩
Paschke, A., Brat, L., 2006, *OEJV*, **23**, 13, `http://var.astro.cz/ocgate` ⟨11⟩
Paschke, A., 2012, *OEJV*, **142**, 1 ⟨12⟩
Pojmanski, G., 1997, *Acta Astronomica*, **47**, 467 ⟨13⟩

COMMISSIONS 27 AND 42 OF THE IAU
INFORMATION BULLETIN ON VARIABLE STARS

Number 6129

Konkoly Observatory
Budapest
5 February 2015

HU ISSN 0374 – 0676

HIGH-AMPLITUDE, RAPID PHOTOMETRIC VARIATION OF THE NEW POLAR MASTER OT J132104.04+560957.8

LITTLEFIELD, COLIN;[1,2] GARNAVICH, PETER;[1] MAGNO, KATRINA;[1] MURISON, MARC;[3] DEAL, SHANEL;[4] MCCLELLAND, COLIN;[1] ROSE, BENJAMIN[1]

[1] Department of Physics, University of Notre Dame, Notre Dame, IN 46556, USA

[2] Department of Astronomy, Wesleyan University, Middletown, CT 06459, USA

[3] United States Naval Observatory Flagstaff Station, Flagstaff, AZ 86001, USA

[4] North Carolina Agricultural and Technical State University, Greensboro, NC 27411, USA

Polars are cataclysmic variables (CVs) in which the magnetic field of the white dwarf (WD) synchronizes the WD's spin period with the orbital period of the binary (see Cropper (1990) for a thorough review). In contrast to non-magnetic CVs, there is no accretion disk in a polar. Instead, as the accretion stream flows from the L1 point toward the WD, the magnetic pressure from the WD rapidly increases until it matches the stream's ram pressure. The stream then threads onto the WD's magnetic field lines, which channel the captured material onto cyclotron-emitting accretion regions near the WD's magnetic poles. Because cyclotron emission is heavily beamed, it appears brightest when the observer's line of sight is perpendicular to the field lines of the emitting material; thus, changes in the viewing angle of the cyclotron-emitting region can produce dramatic photometric variability modulated at the WD's spin period (*e.g.*, Gänsicke et al. 2001). A polar can undergo a precipitous drop in optical brightness if the accretion region rotates behind the limb of the WD or is eclipsed by the donor star.

The optical transient MASTER OT J132104.04+560957.8 (hereinafter, "J1321") was reported as a possible eclipsing polar by Yecheistov et al. (2012) on the basis of rapid (∼30 min), high-amplitude (∼2 mag) variation. To investigate this classification, we obtained follow-up photometry with a 28-cm Schmidt-Cassegrain telescope on 2012 December 23. We used the APASS survey (Henden et al. 2012) to find the Johnson V magnitudes of our comparison stars so that we could infer V-band magnitudes of J1321 from our unfiltered data. During the 5.7-hour time series, J1321 peaked at V ∼17 and dropped below V ∼18.5 during each photometric cycle, becoming so faint that we could no longer detect it. The data showed a period of roughly 91 minutes with each cycle having two unequal maxima, but the modest signal-to-noise precluded a more rigorous analysis. Based on this time series, the system was reported as a non-eclipsing polar with possible two-pole accretion in vsnet-alert 15204 (Kato 2012).

By itself, the high-amplitude, short-term variation does not establish J1321 as a polar, so we obtained seven spectra of J1321 using the 1.8-m Vatican Advanced Technology Telescope (VATT) and the "VattSpec" spectrometer on 2013 June 28. We used the 300 lines/mm grating and a 1 arcsec slit, and the resulting spectra have a dispersion of

1.5 Å/px with a resolution of 4.8 Å (FWHM). The exposures were 300 seconds long and began at 5:40 UT. Though the spectra were too noisy for meaningful individual analysis, the average spectrum, which is presented in Figure 1, shows a strong continuum which decreases blueward of 500 nm as well as Balmer, He I and He II emission lines. The continuum's shape is not significantly affected by interstellar reddening, estimated to be just $E(B-V) = 0.013$ mag near J1321's position (Schlafly & Finkbeiner 2011). The single-peaked lines and the strong He II λ4686 Å emission are classic characteristics of polars, providing strong evidence that J1321 is indeed a polar. Follow-up polarimetric observations of J1321 could detect the polarized cyclotron emission from the accretion region, conclusively verifying this classification.

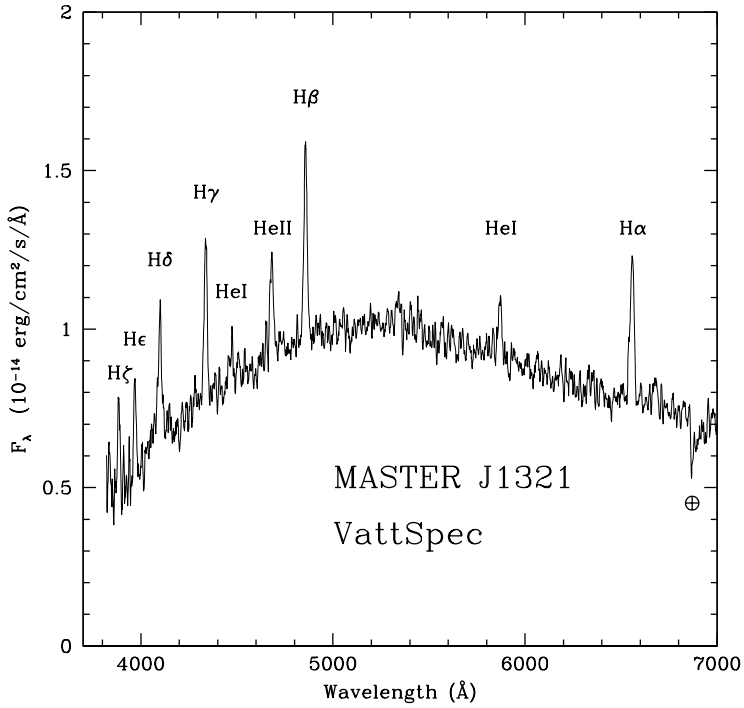

Figure 1. The average spectrum of J1321, obtained with the VATT. The strong He II emission and single-peaked lines are typical of polars.

We also performed time-resolved V-band photometry of J1321 with the VATT on 2013 February 7 and on four consecutive nights in 2014, beginning on June 28 and ending on July 1. Additional photometry was obtained with the United States Naval Observatory Flagstaff Station's 1.3-m telescope on seven nights in 2013 (May 25–28 and June 5–7) and Wesleyan University's 60-cm Perkin Telescope on 2014 November 29. The USNO data used an SDSS r filter, while the Perkin data were unfiltered. In the combined dataset, J1321 did not exhibit any noticeable long-term variation and consistently peaked at $V \sim 16.5$. The light curves themselves display complex variation with an ephemeris of

$$T_{\max}[HJD] = 2456330.9670(13) + 0.06323501(7) \times E, \quad (1)$$

where $\phi = 0.0$ corresponds with the system's peak brightness. In addition, we also downloaded the 61 observations of the system from the Catalina Real-Time Transient Survey (Drake et al. 2009) obtained between 2007 and 2013 to study J1321's long-term

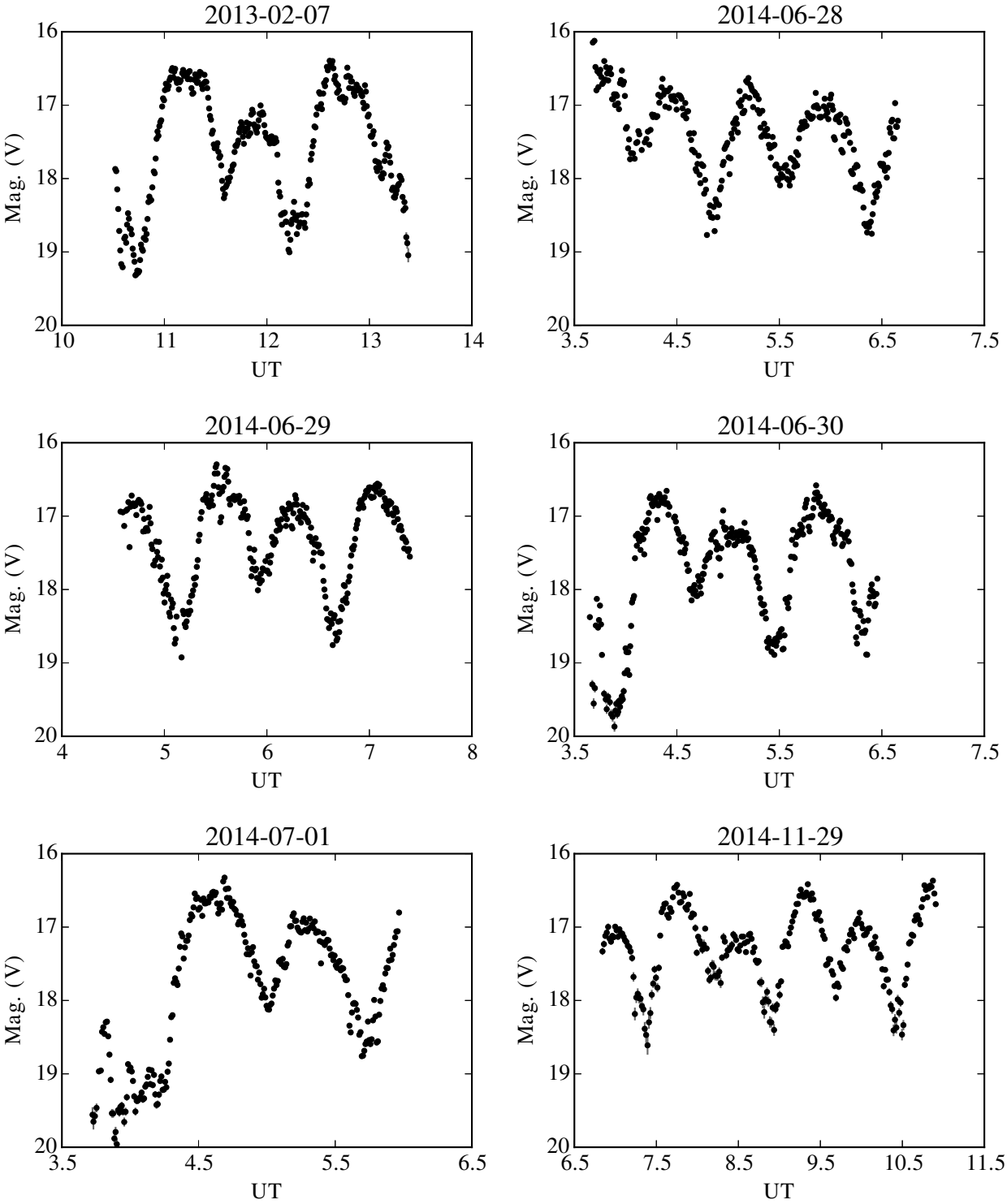

Figure 2. Six light curves of J1321. With the exception of the unfiltered light curve from 2014 November 29, which was obtained with the 60-cm Perkin Telescope at Wesleyan University, all data were in V-band and obtained with the VATT. There are dramatic night-to-night changes in the light curves obtained on consecutive nights between 2014 June 28 and 2014 July 1. In the data from July 1, the secondary maximum is very weak in one orbital cycle and strong in the next.

variation. Although the sparse data coverage precludes us from drawing any sweeping conclusions about J1321's long-term behavior, the phased Catalina data do not show evidence of significant variations in the overall brightness of the system.

Each cycle contains two unequal maxima as well as two unequal minima. To quantify the duration of the maxima, we measured the full width of each maximum one magnitude below its peak brightness and found that the two maxima have comparable widths on average (∼0.35 phase units). The secondary maximum is centered on $\phi \sim 0.45$ and usually peaks near $V \sim 17.0$, making it roughly ∼0.5 mag dimmer on average than the primary maximum. The deepest minimum occurs at $\phi \sim 0.7$, with the other minimum appearing near $\phi \sim 0.25$. The phase of the midpoint of the secondary minimum is highly variable, ranging from $0.15 < \phi < 0.30$. The system's changes in brightness are dramatic; we observed the system to brighten by as much as much as 2.8 magnitudes in just under 14 minutes. Additionally, significant flickering was apparent in almost all light curves, with some strong flares occurring even during deep minima. We also occasionally observed non-periodic dips during the maxima with a depth of up to a half-magnitude and a duration of no more than several minutes. All five VATT light curves, along with the Perkin light curve, are presented in Figure 2 and shown in a phase plot in Figure 3.

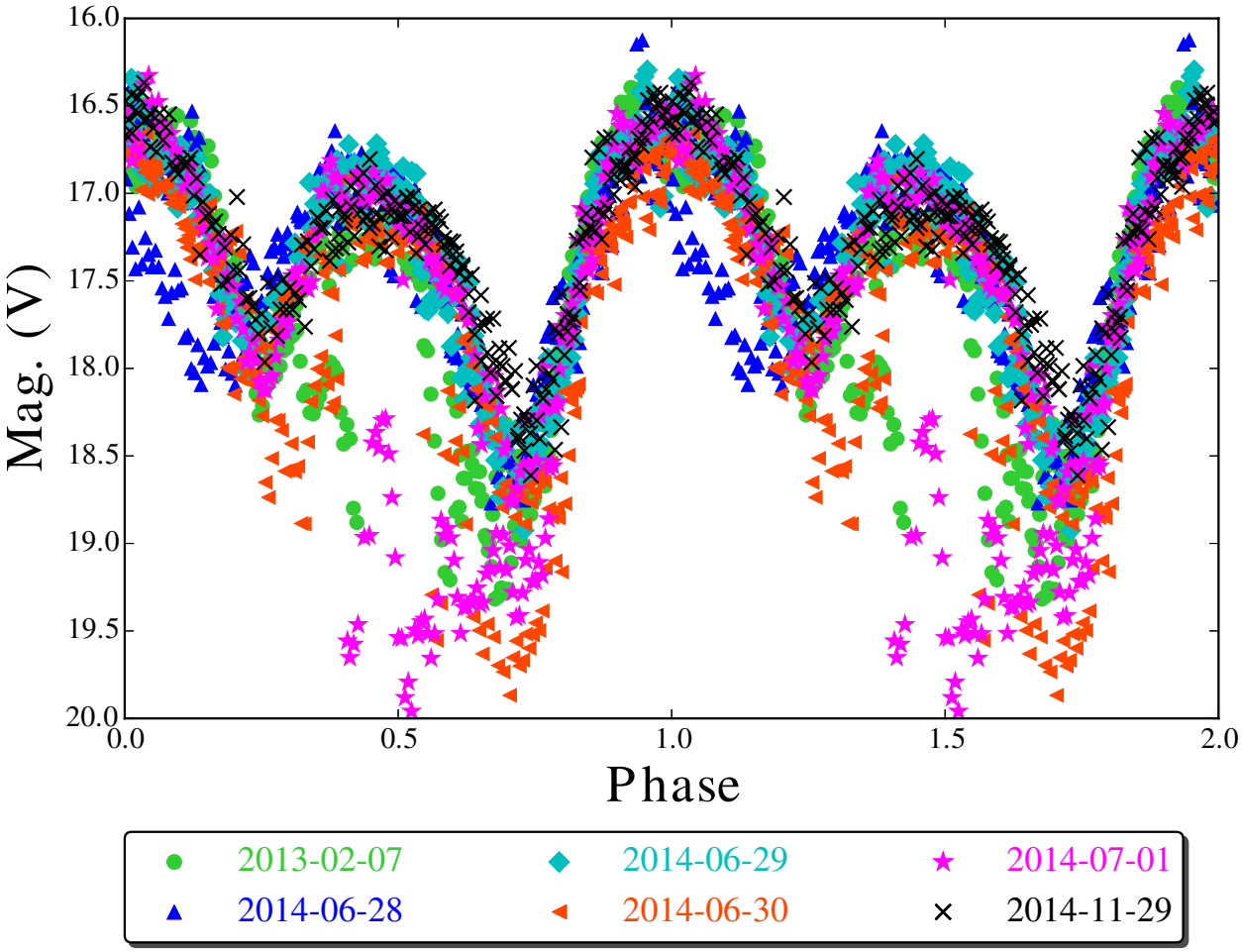

Figure 3. The phase plot of the six light curves from Figure 2. Note the extreme variation near $\phi \sim 0.5$, as well as the phase shifts of the secondary minimum near $\phi \sim 0.2$ and the variable depth of the primary minimum at $\phi \sim 0.7$.

The behavior of the secondary maximum is perhaps the most curious phenomenon in our photometry. For example, in a VATT light curve obtained on July 1, the secondary maximum appeared as a flare-like feature with a width of just 0.06 phase units and a peak brightness of $V \sim 18.3$—fully 1.3 magnitudes fainter than normal. But during the very next photometric cycle, the secondary maximum was again prominent, with its peak magnitude and width both returning to the average values of $V \sim 17.0$ and 0.35 phase units, respectively. The same phenomenon was present in one of the USNO light curves; the secondary maximum was strong in one cycle but was abruptly replaced by a brief flare in the next. Thus, either the accretion geometry or the accretion rate can be highly variable on a timescale of less than 90 minutes.

The morphology of the minima also shows great variation from night-to-night. For instance, as shown in Figure 2, the shape of the secondary minimum changed from flat-bottomed (2014 June 28) to V-shaped (2014 July 1) in a matter of days.

The overall photometric variation resembles that of polars with intense cyclotron beaming. For example, Gänsicke et al. (2001) modeled the cyclotron emission in the polar AM Her, and their synthetic light curves exhibited a double-humped structure with rapid increases and decreases in brightness, in agreement with their observations of the system (see their Figure 5). Considering that our spectra and photometry are consistent with J1321 being a polar, it is likely that a similar mechanism is at least partially responsible for J1321's rapid brightness variations, but our data are not conclusive in this regard.

Although Yecheistov et al. (2012) speculated that J1321 might be an eclipsing polar, our data show that it is very unlikely that J1321's variation is the result of an eclipse of the WD by the donor star. In a typical eclipsing polar such as HU Aqr, the accretion region is so compact that the donor eclipses it in a matter of seconds, causing the system to fade by several magnitudes on that timescale (Harrop-Allin et al. 1999). When compared to the seconds-long ingresses and egresses of eclipsing polars, the dips in J1321 are not sufficiently rapid to be consistent with the eclipse of a small, luminous accretion region by a stellar body.

An unresolved mystery, however, is the immense cycle-to-cycle variation of the secondary maximum. As the phase plot in Figure 3 exemplifies, the secondary maximum is highly variable on a timescale of just one photometric cycle, whereas the primary maximum is not. Additional observations are necessary to determine the cause of these variations. Furthermore, the phase of the secondary minimum and the shape of the primary minimum are quite variable, too. A logical first step would be to obtain intensive time-resolved photometry of J1321 to ascertain whether there is a discernible pattern to these phenomena.

References:

Cropper M. 1990, *SSRv*, **54**, 195
Drake, A. J., Djorgovski, S. G., Mahabal, A., et al. 2009, *ApJ*, **696**, 870
Gänsicke, B. T., Fischer, A., Silvotti, R., & de Martino, D. 2001, *A&A*, **372**, 557
Harrop-Allin, M. K., Cropper, M., Hakala, P. J., Hellier, C., Ramseyer, T. 1999, *MNRAS*, **308**, 807
Henden, A. A., Levine, S. E., Terrell, D., Smith, T. C., Welch, D. 2012, *JAAVSO*, **40**, 430
Kato, T. 2012, vsnet-alert 15204
Schlafly, E. F. & Finkbeiner, D. P. 2011, *ApJ*, **737**, 103
Yecheistov, V. et al. 2012, *ATel*, **4662**, 1

COMMISSIONS 27 AND 42 OF THE IAU
INFORMATION BULLETIN ON VARIABLE STARS

Number 6130

Konkoly Observatory
Budapest
7 February 2015

HU ISSN 0374 – 0676

NEW TIMES OF MINIMA OF SOME ECLIPSING VARIABLES

LACY, C.H.S.

Department of Physics, University of Arkansas, Fayetteville, Arkansas 72701, USA; e-mail: clacy@uark.edu

Observatory and telescope:
NFO WebScope near Silver City, NM, USA (`www.nfo.edu`); 24-inch classical Cassegrain.

Detector:	2102 × 2092 pixels Kodak KAF 4300E CCD cooled to (typ.) −20 C; 0.78 arcsec square pixels; 27' square field of view, used with a Bessell V filter.

Method of data reduction:
Virtual measuring engine (Multi-Measure 2.2) written by C.H.S. Lacy (2013).

Method of minimum determination:
Kwee & van Woerden (1956)

Times of minima:

Star name	Time of min. HJD 2400000+	Error	Type	Filter	Rem.
BX CMi	56715.7056	0.0004	II		
	56738.7331	0.0004	II		
	56748.7117	0.0002	I		
	56978.9737	0.0004	II		
	57018.8873	0.0005	II		
V361 Cas	56942.6282	0.0014	II		
	56953.6917	0.0005	I		
	56980.7270	0.0004	I		

Times of minima:					
Star name	Time of min. HJD 2400000+	Error	Type	Filter	Rem.
LO Gem	56969.7755	0.0005	I		
	56980.9620	0.0006	I		
	56988.7958	0.0003	II		
V501 Her	56731.9059	0.0005	I		
NS Mon	56722.6555	0.0004	I		
	56746.6503	0.0005	II		
V501 Mon	56697.7380	0.0009	II		
NP Per	56955.7795	0.0021	II		
V514 Per	56706.6769	0.0008	II		
AQ Tau	56971.8104	0.0009	II		
	56977.8890	0.0009	I		
TYC 1077-828-1	56915.7467	0.0003	I		
	56956.6792	0.0003	I		
TYC 1323-169-1	56736.6603	0.0003	II		
	56942.9212	0.0005	I		
TYC 279-35-1	56724.8131	0.0003	I		
TYC 4985-74-1	56715.9012	0.0002	II		
TYC 5085-1264-1	56827.6753	0.0007	I		
TYC 54-504-1	56925.8056	0.0005	II		
	56943.8918	0.0005	II		
TYC 687-1139-1	56985.8619	0.0008	I		
TYC 740-8-1	56717.7548	0.0002	II		
	56982.9923	0.0002	I		
TYC 950-560-1	56733.9612	0.0004	I		
	56738.8895	0.0004	I		
	56746.9011	0.0008	II		
	56754.9128	0.0006	I		
	56764.7733	0.0007	I		
	56772.7835	0.0013	II		
	56780.7956	0.0003	I		

Acknowledgements:
Construction and operation of the NFO telescope were partially funded by the National Science Foundation, the Arkansas Center for Space and Planetary Sciences, the NASA Arkansas Space Grant Consortium, the University of Arkansas, Fayetteville, the University of Arkansas at Little Rock, and the Harvard-Smithsonian Center for Astrophysics. We are grateful to Dr. Bill Neely for initial processing of the images and construction, maintenance, and operation of the NFO equipment and software.

Reference:

Kwee, K. K. & van Woerden, H. 1956, *BAN*, **12**, 327

COMMISSIONS 27 AND 42 OF THE IAU
INFORMATION BULLETIN ON VARIABLE STARS

Number 6131

Konkoly Observatory
Budapest
7 February 2015

HU ISSN 0374 – 0676

CCD MINIMA FOR SELECTED ECLIPSING BINARIES IN 2014

NELSON, ROBERT H.

1393 Garvin Street, Prince George, BC, Canada, V2M 3Z1 e-mail: bob.nelson@shaw.ca

Observatory and telescope:
Sylvester Robotic Observatory (SyRO): 33 cm f/4.5 Newtonian on a Paramount ME

Detector:	SyRO: SBIG ST-10XME, 6.8″ pixels, 34.4′ × 23.2′ FOV, $-10 < T < -30$ °C

Method of data reduction:
Bias and dark subtraction, flat-fielding using light-box flats; aperture photometry– all using MIRA, by Mirametrics. Check stars were used throughout.

Method of minimum determination:
Digital tracing paper method, bisection of chords, curve fitting, and (occasionally) Kwee and van Woerden (1956)

Times of minima:

Star name	Time of min. HJD 2400000+	Error	Type	Filter	Rem.
AD And	56955.6161	0.0001	II	c	−0.0016
G2837-1343 And	56921.7652	0.0003	II	c	0.0002
BO Ari	56928.7461	0.0002	II	*R*	0
EP Aur	56955.815	0.002	II	c	-0.0074
V0562 Aur	56661.7792	0.002	I	c	0.0002
V0644 Aur	56661.6217	0.0003	I	c	−0.0007
TY Boo	56692.8944	0.0002	I	c	−0.0018
GN Boo	56697.9477	0.0001	II	c	−0.0005
HH Boo	56690.9585	0.0002	II	c	0.0014
PU Boo	56692.9662	0.0005	II	c	0
V0339 Boo	56691.9254	0.0003	II	c	0

Times of minima:					
Star name	Time of min. HJD 2400000+	Error	Type	Filter	Rem.
LO Com	56696.88	0.0003	I	c	0.001
V0403 Cam	56676.6103	0.0003	II	c	0
V0405 Cam	56964.7495	0.0004	I	c	0
V0473 Cam	56674.6461	0.0004	I	c	0
V0474 Cam	56695.6407	0.0002	II	c	0.0001
V0517 Cam	56688.8892	0.0002	I	c	0.0001
V0608 Cas	57007.6716	0.0002	I	c	0
V1137 Cas	56917.7017	0.0002	I	c	0.0027
UZ CMi	56697.7449	0.0004	I	c	0.0009
EH Cnc	56691.6848	0.0003	II	c	0.0005
HN Cnc	56695.7625	0.0004	II	c	0.0012
IL Cnc	56677.791	0.0002	I	c	0.0009
IT Cnc	56703.7034	0.0008	I	c	−0.001
DX CVn	56693.9601	0.0005	I	c	0.0006
EY CVn	56697.8519	0.0004	I	c	0.0006
GM CVn	57021.002	0.0002	II	R	−0.0003
CV Cyg	56848.807	0.002	II	VRI	−0.0012
V1034 Cyg	56810.8846	0.0005	I	VRI	−0.0016
V1941 Cyg	56929.7176	0.0004	I	c	0
V2545 Cyg	56801.9137	0.0005	I	c	−0.0021
LS Del	56866.819	0.0007	I	VRI	−0.0004
LS Del	56852.8119	0.0007	II	VRI	0.0004
DG Dra	56782.9385	0.0005	I	R	0.0047
FX Dra	56788.794	0.002	II	VRI	0.0026
NV Dra	56693.7686	0.0002	I	c	0.0004
OX Dra	56695.9017	0.0001	I	c	−0.0008
SX Gem	56662.705	0.002	I	c	0.005
V0348 Gem	57021.7189	0.0004	II	R	0
V0404 Gem	56693.6557	0.0003	I	c	0.0002
V0405 Gem	56693.6365	0.0005	I	c	−0.0009
V0435 Gem	56676.7644	0.001	II	c	0.0004
V1023 Her	56687.9718	0.0002	II	c	0
V1094 Her	56801.8301	0.0002	I	c	0.0004
V1302 Her	56794.8016	0.0005	II	c	0.0024
UW Hya	57007.9233	0.0003	I	c	0.001
AV Hya	56687.843	0.001	0	c	0.0022
SW Lac	56794.9078	0.0005	I	VRI	−0.0002
UZ Leo	56689.878	0.0003	I	c	0.0059
AP Leo	56694.8847	0.0002	I	R	0.0005
RT LMi	57022.8386	0.0003	II	R	−0.0009
FI Lyn	56698.6491	0.0003	II	c	−0.0007
V1833 Ori	56925.9474	0.0007	I	R	0
V1847 Ori	57007.7649	0.0002	I	c	−0.0003
V1848 Ori	56696.6346	0.0001	I	c	0.0013
G1721-1141 Peg	56951.6555	0.0002	I	c	0.001

Times of minima:					
Star name	Time of min. HJD 2400000+	Error	Type	Filter	Rem.
IM Per	56927.8424	0.0002	II	R	0.0008
V0432 Per	56675.6133	0.0005	II	VRI	−0.0003
V0873 Per	56658.6316	0.0002	II	R	−0.0009
EQ Tau	56929.8123	0.0003	I	c	−0.0002
V1295 Tau	56935.8288	0.0003	I	c	0
AV Tri	56928.8622	0.0002	I	c	0
HH UMa	57021.8797	0.0002	II	R	0.004
KM UMa	57020.9033	0.0004	I	R	−0.0009
V0354 UMa	57022.9616	0.0005	II	R	−0.001
V0354 UMa	57023.11045	0.001	I	R	0.001
AW Vir	56688.9961	0.0003	I	c	0.0001

Remarks:

To save space, GSC star names have been shortened to a leading "G" only; times of minimum are heliocentric Julian dates with the leading 24 removed.
O-C values were computed using elements computed from the O-C database listed in the references (Nelson, 2014).

Acknowledgements:

Thanks are due to Environment Canada for the website satellite views (see reference below) that were essential in predicting clear times for observing runs in this cloudy locale. Thanks are also due to Attilla Danko for his 'Clear Sky Charts', (see below). This research has made use of the SIMBAD database, operated at CDS, Strasbourg, France

References:

Danko, A., Clear Sky Charts, `http://cleardarksky.com/`
Kwee, K.K., & van Woerden, H., 1956, *BAN*, **12**, (464), 327
Nelson, R.H. 2014, Bob Nelson's O−C Files, `http://www.aavso.org/bob-nelsons-o-c-files`
Satellite Images for North America,`http://weather.gc.ca/satellite/index_e.html`

COMMISSIONS 27 AND 42 OF THE IAU
INFORMATION BULLETIN ON VARIABLE STARS

Number 6132

Konkoly Observatory
Budapest
16 February 2015

HU ISSN 0374 – 0676

AR Ser: PHOTOMETRIC OBSERVATIONS OF A BLAZHKO STAR

BONNARDEAU, MICHEL[1]; HAMBSCH, FRANZ-JOSEF[2]

[1] MBCAA Observatory, Le Pavillon, 38930 Lalley, France, email: arzelier1@free.fr

[2] ROAD Observatory, 12 Oude Bleken, Mol, 2400, Belgium

We observed AR Serpentis (RA=$15^{\rm h}33^{\rm m}30\overset{\rm s}{.}8$ DEC=$+2°46'38''$ (2000.0) average V=$12\overset{\rm m}{.}0$) between 2010 and 2014, with Johnson V filters and CCD cameras. 2195 photometric measurements over 58 nights were gathered in 2010-2014 with a 20 cm telescope located in France (MB), and 4599 measurements over 74 nights in 2014 with a 40 cm telescope in Chile (Hambsch, HMB).

For the differential photometry, the comparison star is UCAC4 464-053185 with a V magnitude of 11.551. Because the instruments are different, there is a magnitude offset between the two observers. Owing to 3 pairs of overlapping times-series with the two setups (as shown in Figure 1), this offset is evaluated to be 20 mmag, that is added to the measurements obtained with the 20 cm telescope.

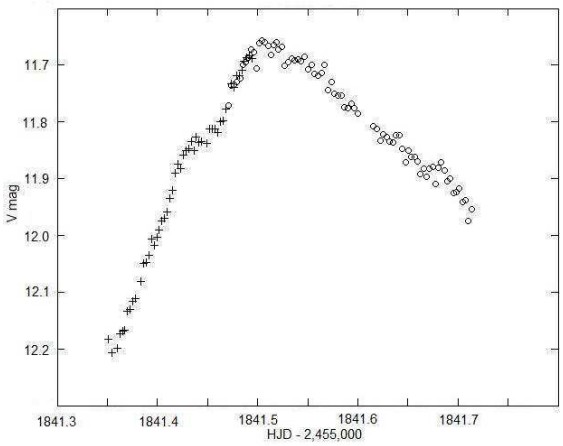

Figure 1. An example of a pair of overlapping times-series. Cross: data with the 20 cm telescope, circle: those with the 40 cm one.

The data are analysed with the PERIOD04 software program (Lenz & Breger, 2005) which provides simultaneously sine-wave fitting and least-squares fitting algorithms. This yields the pulsation frequency:
$F_{\rm p} = 1.7385671 \pm 3.9 \times 10^{-6}$ day^{-1}
(or the pulsation period: $P_{\rm p} = 0.5751863$ day $\pm$ 0.12 s).

There is no evidence for a variation of this period during our observations. The ephemeris for the maxima of the pulsation is then:
$t(n) = 2,456,135.181 + nP_{\rm p}$ HJD

Owing to the PERIOD04 software program, the data are fitted with a sine-wave function of time t, with the number of harmonics of up to the 7th order:
$f(t) = z + \Sigma_{i=1}^{8} A_i \sin[2\pi(F_i t + \Phi_i)]$
with $z = 11.9597 \pm 0.0014$ mag and the other parameters given in Table 1, components F1-F8.

The resulting phase plot is shown in Figure 2 and the residuals of the observations from the $f(t)$ function in Figure 3.

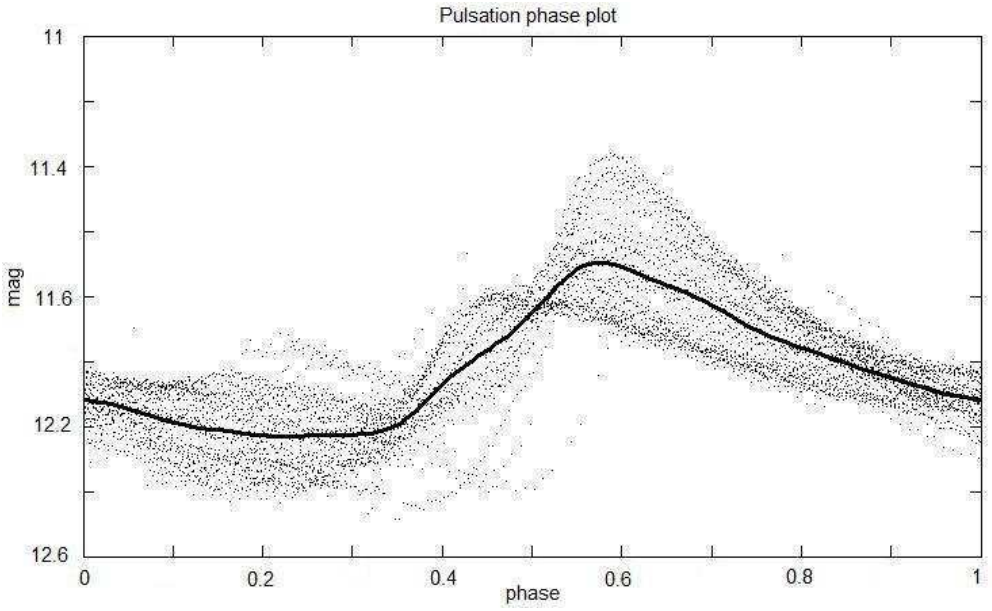

Figure 2. Dots: the observations, Solid line: the $f(t)$ function. The phase origin is arbitrary.

The deviations around the fit $f(t)$ are due to the Blazhko effect.

The Blazhko modulation is expected to show up as side peaks around multiples of the pulsation frequency $F_{\rm p}$ in the Fourier spectrum (Breger & Kolenberg, 2006 and Szeidl & Jurcsik, 2009). The two strongest signals in the residuals of the pulsation (prewhitening) correspond to the frequencies $F_{\rm B1} = 1/89$ day^{-1} and $F_{\rm B2} = 1/109$ day^{-1}. Peaks are clearly seen at $nF_{\rm p} \pm F_{\rm B1}$ and $nF_{\rm p} \pm F_{\rm B2}$ with n=1, 2, 3, as shown in Figures 4, 5, 6. Hence, AR Ser has two Blazhko modulations.

There are many small peaks in the spectra and we refrain from interpreting them. However there is a possibility for signals at $nF_{\rm p} \pm 2F_{\rm B2}$ (see Figures 4, 5, 6), although fitting the data including them does not much improve the residuals. Such quintuplets may imply a magnetic origin for the modulation (Shibahashi, 2000) or may be due to a non-radial pulsation (Dziembowski & Mizerski, 2004). The first star where a Blazhko effect was discovered with quintuplets was RV UMa (Hurta et al., 2008) and a number of them have been found since, especially owing to satellite observations (Chadid et al., 2010).

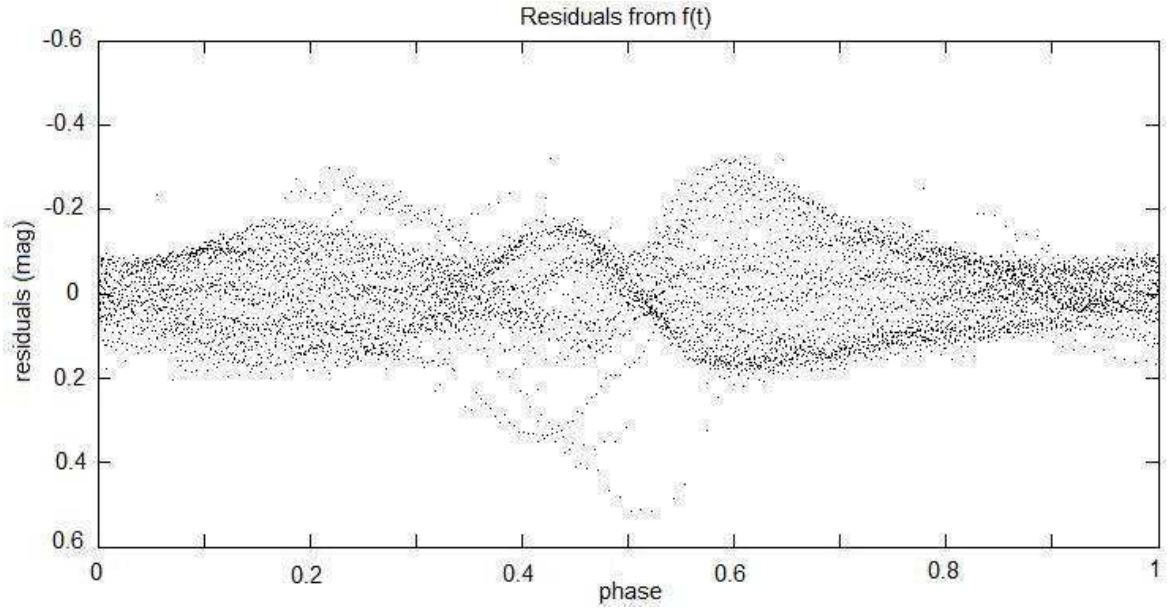

Figure 3. The difference between the observations and the $f(t)$ function.

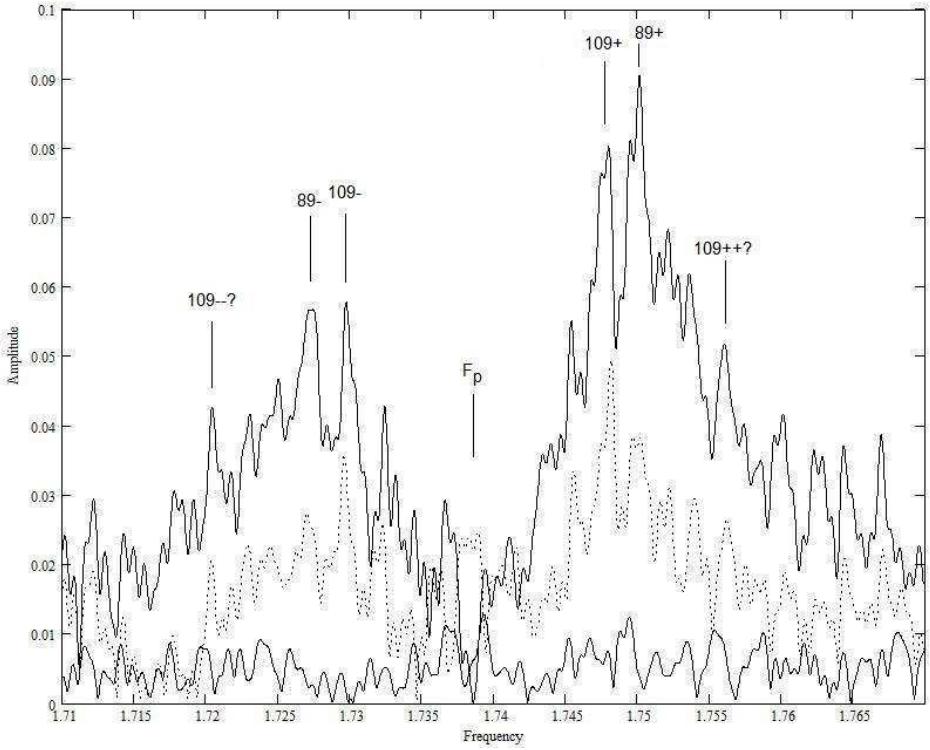

Figure 4. The Fourier spectra of the residuals around $F_{\rm p}$. The upper solid line is after prewhitening with the $F_{\rm p}$ pulsation. The triplet at $F_{\rm B1}$ is noted 89+ and 89-, the one at $F_{\rm B2}$, 109+ and 109- (there is a hint for a quintuplet with $F_{\rm B2}$, hence the 109++ and 109- -). The middle dotted line is after prewhitening with both the $F_{\rm p}$ pulsation and the $F_{\rm B1}$ modulation: the triplets at $F_{\rm B2}$ are clearly visible. The bottom solid line is after prewhitening with the pulsation and the modulations at $F_{\rm B1}$ and $F_{\rm B2}$: only noise is left.

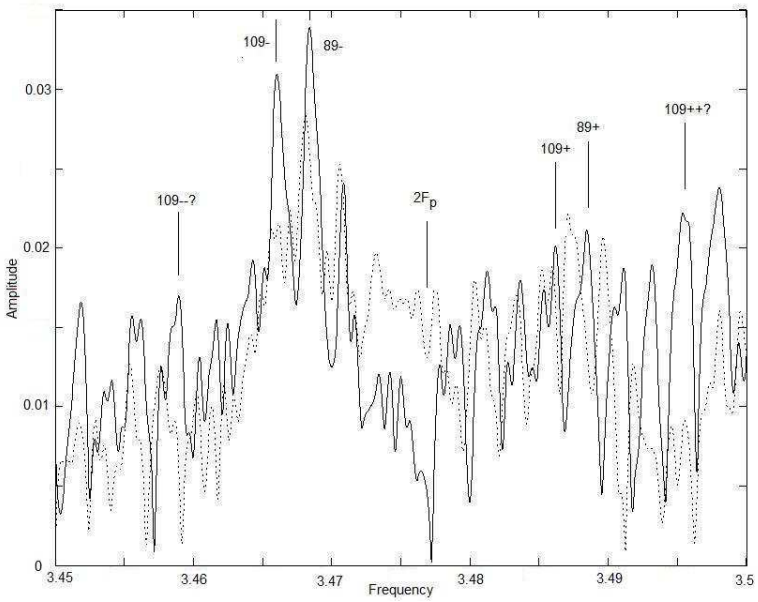

Figure 5. The Fourier spectrum around $2F_{\rm p}$. Solid line: prewhitening with the pulsation only, dotted line: prewhitening with the pulsation and the $F_{\rm B1}$ modulation.

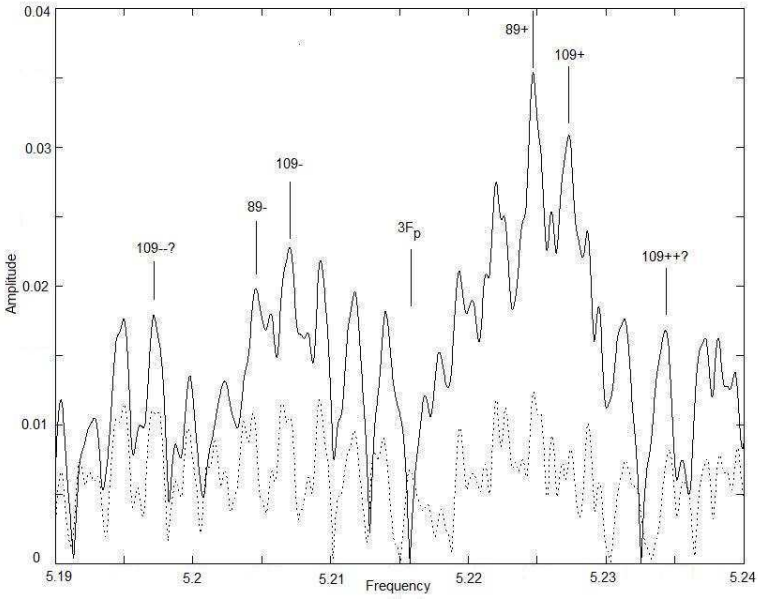

Figure 6. The same as Fig. 5 for $3F_{\rm p}$.

The observations are not evenly distributed, with most of them concentrated over a time interval of about $1/F_{\rm B1}$ (the data obtained from Chile). We checked that the signals at $F_{\rm B1}$ are not spurious by computing the Fourier spectrum of the data obtained from France only, that span 5 years: the strongest signals are still at $F_{\rm B1}$.

Using the PERIOD04 software program, the observations are then fitted with the frequencies $nF_{\rm p} \pm F_{\rm B1}$ and $nF_{\rm p} \pm F_{\rm B2}$. The results are shown in Table 1, components F9 through F20.

Table 1: Sinusoidal decomposition with PERIOD04.

Name	Component	Frequency F	Uncertainty on F	Amplitude A	Uncert. on A	Phase Φ	Uncert. on Φ
F1	$F_{\rm p}$	1.7385671	3.9e-006	0.2155	0.0018	0.1017	0.0013
F2	$2F_{\rm p}$			0.0726	0.0018	0.6056	0.0042
F3	$3F_{\rm p}$			0.0206	0.0019	0.078	0.013
F4	$4F_{\rm p}$			0.0063	0.0019	0.525	0.061
F5	$5F_{\rm p}$			0.0052	0.0018	0.730	0.043
F6	$6F_{\rm p}$			0.0069	0.0016	0.356	0.039
F7	$7F_{\rm p}$			0.0066	0.0021	0.833	0.046
F8	$8F_{\rm p}$			0.0049	0.0020	0.380	0.053
F9	$F_{\rm p} + F_{\rm B1}$	1.7500584	7.8e-006	0.0762	0.0018	0.5796	0.0039
F10	$F_{\rm p} - F_{\rm B1}$	1.727451	1.9e-005	0.0295	0.0017	0.8223	0.0092
F11	$F_{\rm p} + F_{\rm B2}$	1.7481126	9.9e-006	0.0557	0.0019	0.4206	0.0050
F12	$F_{\rm p} - F_{\rm B2}$	1.7296166	9.5e-006	0.0413	0.0018	0.6841	0.0048
F13	$2F_{\rm p} + F_{\rm B1}$	3.488479	1.6e-005	0.0276	0.0013	0.2376	0.0069
F14	$2F_{\rm p} - F_{\rm B1}$	3.466037	1.5e-005	0.0299	0.0014	0.2942	0.0069
F15	$2F_{\rm p} + F_{\rm B2}$	3.485996	3.4e-005	0.0168	0.0013	0.454	0.016
F16	$2F_{\rm p} - F_{\rm B2}$	3.468079	1.6e-005	0.0242	0.0013	0.241	0.047
F17	$3F_{\rm p} + F_{\rm B1}$	5.226968	2.1e-005	0.0240	0.0013	0.787	0.011
F18	$3F_{\rm p} - F_{\rm B1}$	5.204693	2.5e-005	0.0128	0.0013	0.643	0.012
F19	$3F_{\rm p} + F_{\rm B2}$	5.224864	2.5e-005	0.0121	0.0013	0.830	0.013
F20	$3F_{\rm p} - F_{\rm B2}$	5.206496	2.6e-005	0.0143	0.0012	0.077	0.012

The data from Chile have a very dense coverage. Their Fourier spectrum was then searched for a high frequency Blazhko modulation, with a negative result.

The residuals of the observations and of this modelling (the $F(t)$ function, see below) were searched for signals at $F_{\rm B1}$ and $F_{\rm B2}$, in the low frequency end of their Fourier spectrum, with negative results. The spectrum was also searched for half-integer multiples of the pulsation frequency $F_{\rm p}$ (this is connected to the period doubling, see Szabó, 2014), with negative results.

The fit function $F(t)$ is:
$F(t) = Z + \Sigma_{i=1}^{20} A_i \sin[2\pi(F_i t + \Phi_i)]$
with $Z = 11.95590 \pm 0.00057$ mag.

The difference between the $F(t)$ and the $f(t)$ represents the Blazhko modulations. It is shown in Figure 7.

The two Blazhko periods may be computed from the F9, F10, F13, F14, F17 and F18 components of Table 1 for the first period, and from the other components starting from F11 for the second period. The average and standard deviations are:

$1/F_{B1} = 89.1 \pm 1.3$ days
$1/F_{B2} = 109.6 \pm 2.6$ days.

AR Ser was reported in the literature having one Blazhko modulation close to F_{B2} (Firmanyuk, 1977, Kolenberg et al., 2008) and also an uncertainty pulsation of 63 days (Wils et al., 2006), not seen in our data. We observe it with two modulations of comparable amplitude. The first Blazhko star discovered as having two modulations of comparable amplitude is CZ Lac (Sódor et al., 2011). Such stars are not very common in ground-based observations (Skarka, 2014) although they seem to be ubiquitous in satellite observations (Benkő et al., 2014).

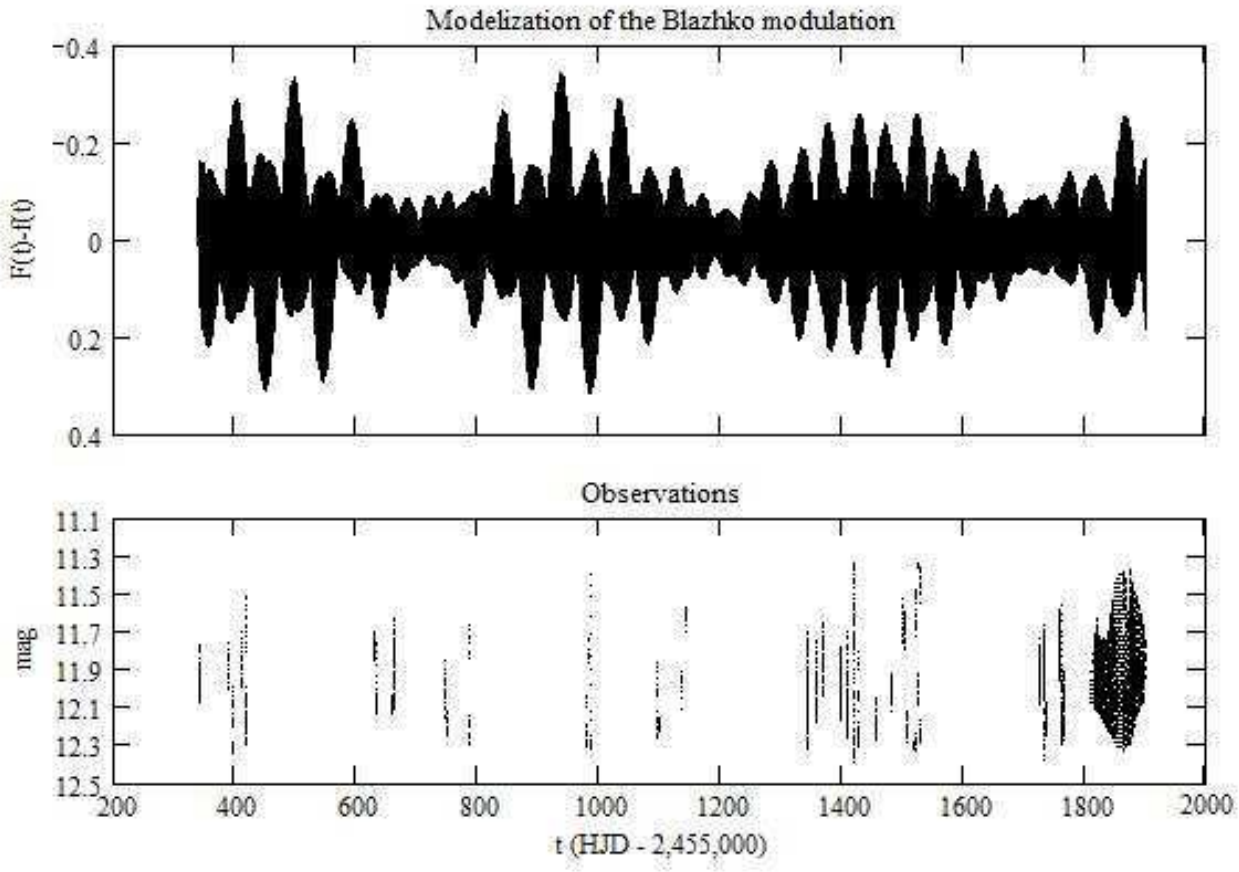

Figure 7. The Blazhko modulations and the observations.

The ratio of the two frequencies may be expressed as the ratio of two small integers, $F_{B1}/F_{B2} = 6/5$, a common occurrence for Blazhko stars with two modulations (Skarka, 2014, Benkő et al., 2014, Sódor et al., 2011).

The residuals of the observations and of the $F(t)$ function are shown in Figure 8. Although they are much improved compared to Figure 3, there are a few time-series that do not fit the model $F(t)$ and are out of phase or with too large amplitudes. Such discrepant observations appear suddenly, that means the time series obtained a few weeks or days before or after fit the model. This suggests irregularities or glitches, which is a behaviour observed in many Blazhko stars (Szabó, 2014).

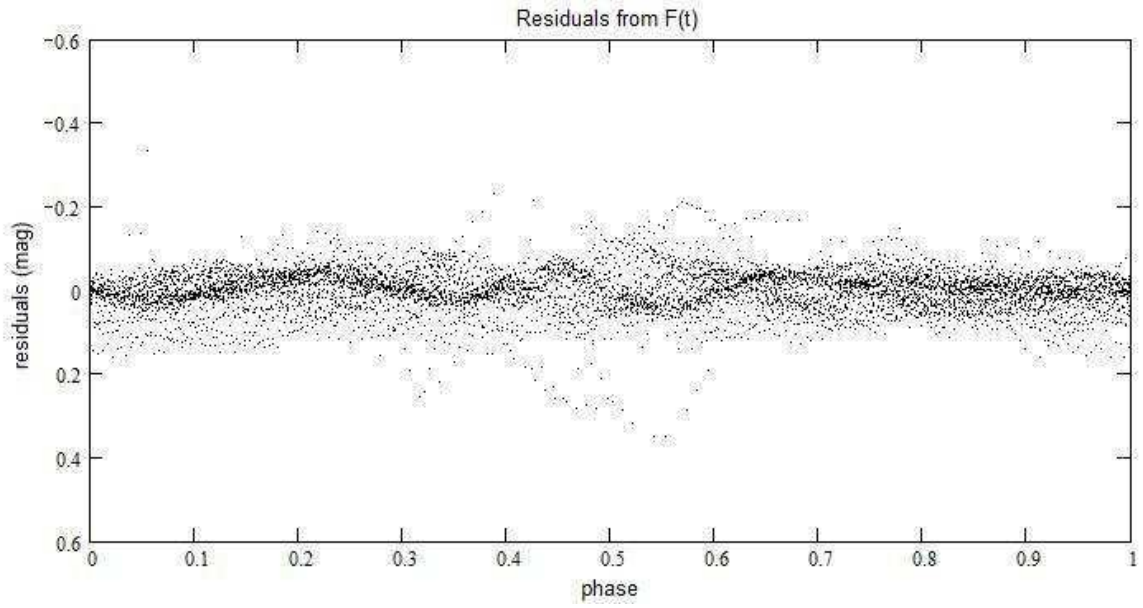

Figure 8. Residuals of the observations and of the F(t) function.

References:

Benkő, J.M., Plachy, E., Szabó, R., Molnár, L., Kolláth, Z., 2014, *ApJS*, **213**, 31
Breger, M., Kolenberg, K., 2006, *A&A*, **460**, 167
Chadid, M., Benkő, J.M., Szabó, R. et al., 2010, *A&A*, **510**, A39
Dziembowski, W.A., Mizerski, T., 2004, *Acta Astronomica*, **54**, 363
Firmanyuk, B.N., 1977, *IBVS*, **1245**
Hurta, Zs., Jurcsik, J., Szeidl, B., Sódor, Á., 2008, *AJ*, **135**, 957
Kolenberg, K., Guggenberger, E., Medupe, T., 2008, *Comm. Asteroseismology*, **153**, 67
Lenz, P., Breger, M., 2005, *Comm. Asteroseismology*, **146**, 53
Shibahashi, H., 2000, *ASP Conf. Series*, **203**, 299
Skarka, M., 2014, *A&A*, **562**, A90
Sódor, Á., Jurcsik, J., Szeidl, B., Váradi, M., Henden, A., Vida, K., Hurta, Zs., Posztobányi, K., Dékány, I., Szing, A., 2011, *MNRAS*, **411**, 1585
Szabó, R., 2014, *IAU Symposium*, **301**, 241
Szeidl, B., Jurcsik, J., 2009, *Comm. Asteroseismology*, **160**, 17
Wils, P., Lloyd, C., Bernhard, K., 2006, *MNRAS*, **368**, 1757

COMMISSIONS 27 AND 42 OF THE IAU
INFORMATION BULLETIN ON VARIABLE STARS

Number 6133

Konkoly Observatory
Budapest
18 February 2015

HU ISSN 0374 – 0676

CCD TIMES OF MINIMA OF ECLIPSING BINARIES

KUBICKI, D.

Torun Centre for Astronomy, Faculty of Physics, Astronomy and Applied Informatics, N. Copernicus University, Grudziadzka 5, 87-100 Torun, Poland; e-mail: kubicki@ca.umk.pl

Observatory and telescope:
T1: 60-cm Cassegrain telescope (f/12.5) at the Nicolaus Copernicus University Observatory (53.0943 °N, 18.5532 °E).

Detector:	STL-1001E CCD camera, Peltier cooling, KAF-1001E chip, $11.4' \times 11.4'$ 1024×1024 pixels.

Method of data reduction:
Differential photometry with the software MUNIWIN v.2.0.14 (David Motl, 2003).

Method of minimum determination:
Kwee & van Woerden (1956).

Times of minima:

Star name	Time of min. HJD 2400000+	Error	Type	Filter	$O-C$ [day]	Rem.
NY Vir	2456398.467422	0.000023	I	Clear	−0.00047	1
	56398.517741	0.000068	II	Clear	−0.00043	1
	56398.568440	0.000021	I	Clear	−0.00047	1
	56404.478110	0.000099	II	Clear	−0.00023	1
	56404.528422	0.000019	I	Clear	−0.00043	1
HW Vir	56418.446210	0.000022	I	Clear	−0.00043	1
	56418.387933	0.000082	II	Clear	0.00001	1
V470 Cam	56417.386458	0.000041	II	Clear	0.00171	1
	56417.434424	0.000029	I	Clear	0.00153	1
	56404.331281	0.000019	I	Clear	0.00197	1
	56398.305544	0.000015	I	Clear	0.00197	1
	56398.353436	0.000064	II	Clear	0.00236	1
	57029.477794	0.000094	I	Clear	0.00218	1
	57029.287029	0.00043	I	R	0.0027	1

Explanation of the remarks in the table:
1. Ephemeris references: O-C gateway, an online database of all known eclipsing binaries (`http://var.astro.cz/ocgate`).

Acknowledgements:
This work made use of Kreiner (2014). Special thanks to Krzysztof Goździewski for his invaluable help.

References:

Kreiner, J.M., 2004, *Acta Astronomica*, **54**, 207
Kwee, K., van Woerden, H., 1956, *BAN*, **12**, 327

COMMISSIONS 27 AND 42 OF THE IAU
INFORMATION BULLETIN ON VARIABLE STARS

Number 6134

Konkoly Observatory
Budapest
30 March 2015

HU ISSN 0374 – 0676

LO ANDROMEDAE – A W-TYPE OVERCONTACT ECLIPSING BINARY

NELSON, ROBERT H.[1,2]; ROBB, RUSSELL M.[2,3]

[1] 1393 Garvin Street, Prince George, BC, Canada, V2M 3Z1, email: bob.nelson@shaw.ca

[2] Guest investigator, Dominion Astrophysical Observatory, Herzberg Institute of Astrophysics, National Research Council of Canada

[3] Department of Physics and Astronomy, University of Victoria, Victoria, B.C., Canada, V8P 2W7

The variability of LO And (= TYC 3637-416-1= NSV 14569 = NSVS 3561083 = CSV 8853 = WR 136) was discovered photographically by Weber (1963), who classified the system as a probable Cepheid variable. Diethelm & Gautschy (1980) determined a period of 0.190429 days (half the modern value) and supplied a full photoelectric light curve displaying only one minimum. The General Catalogue of Variable Stars (Samus et al., 1985-2013) lists the type as EW and a period of 0.3804427 days, with a reference to Kreiner (2004). From 1995 to 2014 there have been numerous eclipse timings. Gürol & Müyesseroğlu (2005) [hereafter G&M (2005)] presented five new times of minima of their own, collected a total of 15 photographic (pg), 164 visual (vis), 17 photoelectric (PE), and 10 charge-coupled device (CCD) eclipse timings from the literature, and performed the first period study of the system. Plotting an eclipse timing (ET) diagram (a.k.a. O−C diagram), they first determined a quadratic fit (which they attributed to mass exchange), noting that it was not sufficient to explain the period variation completely. They then went on to solve for the parameters of the orbit of the putative third star, listed in Table 1. (They considered, then rejected, that an alternate explanation might be magnetic cycles – the Applegate effect (Applegate, 1992)).

Assuming that the residual variation is due to the light time effect (LTE) resulting from a third orbiting body, the new times of minima, T can be predicted by the equation

$$T = \mathrm{HJD}_0 + P_0 E_0 + (c_0 + c_1 E + c_2 E^2) + \Delta T \qquad (1)$$

where HJD_0 (= 24 45071.059) is the starting epoch, P_0 (= 0.38043556 days) is initial period, c_0, c_1 and c_2 are the coefficients for the quadratic fit, and ΔT is the time delay due to orbital motion of the close eclipsing pair about the centre of mass of the triple system. The latter is given by (Irwin, 1952, 1959):

$$\Delta = A \frac{(1 - e^2)\sin(\nu + \omega)}{(1 + e\cos\nu) + e\sin\omega} \qquad (2)$$

where A = semi-amplitude = $\frac{1}{2}[(\mathrm{O-C})_{\max} - (O-C)_{\min}] = (a_{13}\sin i_3)/c$; i_3 = inclination of the 3rd star orbit (90°= edge-on); e = eccentricity; ν = true anomaly; c = speed of light, and ω = argument of periastron.

Quantity	G&M (2004)	This study	unit
Constant, c_0	1.00	4.68	10^{-3} days
Slope, c_1	0	−9.69	10^{-6} days/cycle
Quadratic coeff., c_2	1.281	1.167	10^{-10} days/cycle^2
Amplitude, $A = a_{13} \sin i/c$	0.00829	0.00755	days
$a_{13} \sin i$	1.435	1.31	astron. units
Eccentricity, e	0.275	0.262	—
Period, P_3	37.08	29.6	years
Arg. of periastron, ω	198	80.4	degrees
Periastron time, $T_{\rm p}$	41919.1	46431.0	HJD−2400000
dP/dt	2.46	2.24	10^{-7} days/year
Mass transfer rate, dm_1/dt	+1.686	+1.537	10^{-7} M$_\odot$/year
Mass function, $f(m_3)$	0.002150	0.00256	M$_\odot$
Mass, m_3	0.21	0.22	M$_\odot$

Table 1: Parameters for the quadratic + LTE fit from the analysis of G&M (2005) and the present paper, plus some derived quantities.

With the benefit of 48 new PE and CCD subsequent eclipse timings, we have re-determined a quadratic + LTE fit using the linear elements (HJD$_0$, P_0) given above; both sets of resulting parameters are given in Table 1, column 3. An ET difference plot is displayed in Figure 1. Weights of 0.1 were assigned to the visual estimates, and 1 to the photographic, photoelectric and CCD eclipse timings. The residuals from quadratic fits of both studies are displayed in Figs. 2 and 3. (Note that the latter two cannot be displayed in the same figure because constants c_0, c_1 and c_2 are different in each case.)

It will be seen that, visually, the present solution fits the augmented data set better than that of G&M (2005). As in their work, we have solved for the intrinsic rate of period change, dP/dt by equation 3.

$$\frac{dP}{dt} = 2c_2 \left(\frac{365.24}{P_0} \right) \ . \tag{3}$$

One can show, under the conditions of mass and angular momentum conservation for the system as a whole, for masses m_1, m_2 and period P, that:

$$(m_1 m_2)^3 P = \text{constant} \tag{4}$$

Therefore, differentiating equation 4, one obtains:

$$\frac{dm_1}{dt} = \frac{1}{3P \left(\frac{1}{m_2} - \frac{1}{m_1} \right)} \frac{dP}{dt} \ . \tag{5}$$

Both values of dm_1/dt (from G&M (2005) and from this work) are presented in Table 1.

We have also solved for the mass function defined in Mayer (1990), assuming that the orbital inclination of the third-star orbit, i_3 is the same as the inclination of the binary pair orbit, i given in Table 5.

$$f(m_3) = \frac{(a_{13} \sin i)^3}{P_3^2} = \frac{(m_3 \sin i_3)^3}{(m_1 + m_2 + m_3)^2} \ . \tag{6}$$

From equation (6) one can iterate for m_3:

$$m_3 = \frac{a_{13} \sin i_3}{\sin i_3} \left(\frac{m_1 + m_2 + m_3}{P_3} \right)^{\frac{2}{3}} \quad . \tag{7}$$

The corresponding values for m_3 are also presented in Table 1.

It should be firmly borne in mind, however, that – due to the scatter in the early timings (before cycle 10000) – all the fit parameters and derived quantities are very tentative, and that new data over the next decade or so may very well render their values obsolete. By comparison, a much more robust quadratic + LTE fit, in the case of ER Orionis, may be found in Nelson (2015). The O−C file for LO And may be obtained from the AAVSO website (Nelson, 2013).

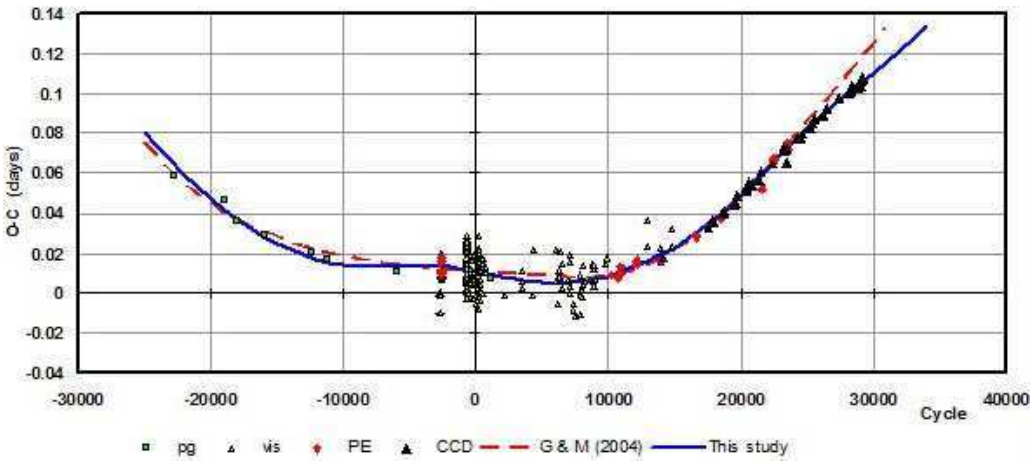

Figure 1. Eclipse timing diagram for LO And showing the fit of G&M (2005) [dashed line] and that of the present study [solid line].

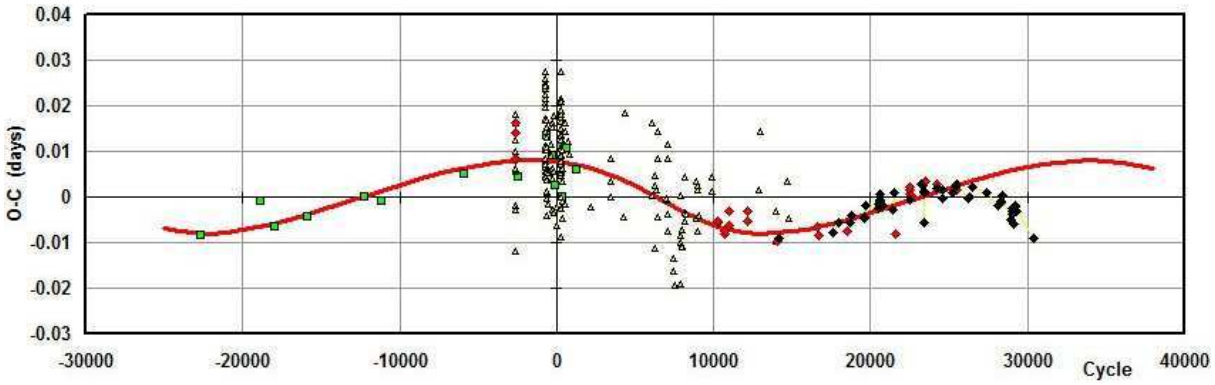

Figure 2. Residuals from the quadratic fit of G&M (2005) plus their LTE fit. See Fig. 1 for the legend.

Using the 2003 Wilson-Devinney code (see references below), G&M (2005) went on to perform a light curve analysis on B & V photometric data that they had obtained at Ankara University Observatory. They determined a value for the important parameter mass ratio ($q = m_2/m_1$) indirectly by the "q-search" method. [The latter entails fixing

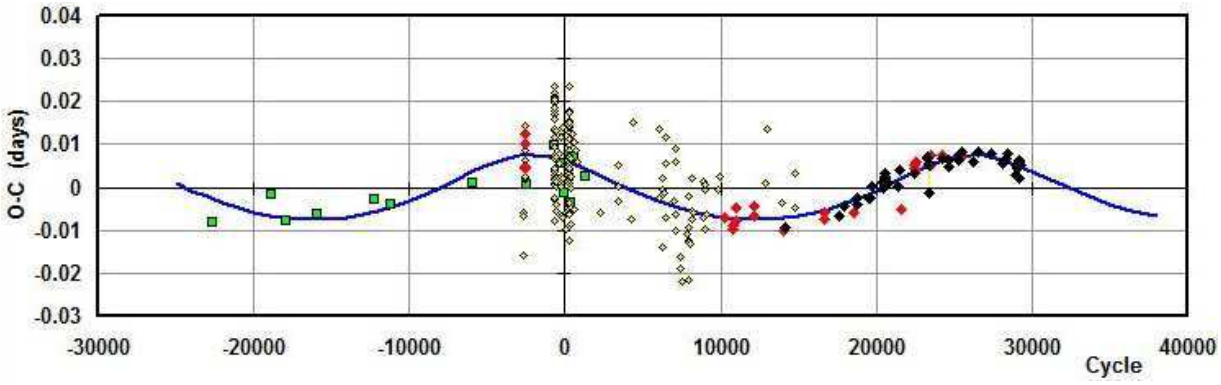

Figure 3. Residuals from the quadratic fit of this study plus our LTE fit. See Fig. 1 for the legend.

the mass ratio for a range of values, varying the remaining parameters (such as orbital inclination i, temperature T_2, system potential Ω, light value L_1, and – if used – spot parameters) to obtain solutions. The residuals from the best fit obtained in each case versus the corresponding value of q are plotted, and the q corresponding to the minimum is adopted.] The problem with the q-search method is that the value of q obtained is not as robust as that obtained spectroscopically, and, in the case of overcontact binaries undergoing partial eclipses, the value of q obtained is only determinable to about $\pm$10%. (Terrell & Wilson, 2005).

In order to improve on this study, one of the authors (R.H.N.) secured, in the months of September in 2007, 2009, 2010, and 2013, a total of 13 medium resolution ($R \sim 10000$ on average) spectra of LO And at the Dominion Astrophysical Observatory (DAO) in Victoria, British Columbia, Canada using the Cassegrain spectrograph attached to the 1.85 m Plaskett Telescope. He used the 21181 grating with 1800 lines/mm, blazed at 5000 Å giving a reciprocal linear dispersion of 10 Å/mm in the first order. The wavelength ranged from 5000 to 5260 Å, approximately. A log of observations is given in Table 2. The following elements were used for both RV and photometric phasing:

$$\text{JD (Hel) Min I} = 24\ 56226.6792 + 0.380441888458\ E \tag{8}$$

Frame reduction was performed by software RaVeRe (Nelson 2009). See Nelson et al. (2014) for further details. Radial velocities were determined using the Rucinski broadening functions (Rucinski, 2004, Nelson, 2010b, Nelson et al., 2014). An Excel worksheet with built-in macros (written by him) was used to do the necessary radial velocity conversions to geocentric and back to heliocentric values (Nelson 2010a). The resulting RV determinations are also presented in Table 2. These results were corrected 7.7% up in this case to allow for the small phase smearing. Correction was achieved by dividing the RVs by the factor $f = (\sin X)/X$; where $X = 2\pi t/P$ and t denotes exposure time, and P denotes the orbital period. For spherical stars, this correction is exact; in other cases, it can be shown to be close enough for any deviation to fall below observational errors. The mean rms error for each RV is 8.3 km/s and the rms deviation from the curves of best fit is 11.4 km/s. The best fit yielded the values $K_1 = 76.4(2.8)$ km/s, $K_2 = 272.4(3.3)$ km/ s and $V_\gamma = 3.7(1.9)$ km/s.

In May-July of 2012, the same author (R.H.N.) took a total of 169 frames in V, 172 in R_c (Cousins) and 169 in the I_c (Cousins) band at his private observatory in Prince George, BC, Canada. The telescope was a 33 cm f/4.5 Newtonian on a Paramount ME

DAO Image #	Mid Time (HJD−2400000)	Exposure (sec)	Phase at Mid-exp	V_1 (km/s)	V_2 (km/s)
11183	54365.9451	3600	0.019	1.7	—
11188	54365.9897	3600	0.136	−58.9	185.1
11203	54366.9663	3600	0.703	62.8	−256.0
11205	54367.0166	3600	0.835	76.2	−248.9
11211	54367.6466	3600	0.491	−2.6	—
11213	54367.6717	617	0.557	19.7	—
11219	54367.7539	3600	0.773	69.5	−259.5
11262	54369.8917	3600	0.393	−45.5	—
19073	55100.8404	3600	0.708	86.7	−277.8
19149	55102.9667	3600	0.297	−68.6	247.2
17272	55469.6910	3600	0.240	−69.8	278.2
9670	56545.9697	3600	0.262	−91.1	258.3
9692	56546.9266	3600	0.778	67.7	−294.9

Table 2: Log of DAO observations

Object	GSC	RA (J2000)	Dec (J2000)	V (mag)	$B-V$ (mag)
Variable	3637-0416	$23^{\rm h}27^{\rm m}06\overset{\rm s}{.}672$	$45°33'22\overset{''}{.}00$	11.25	+0.70
Comparison	3637-0299	$23^{\rm h}26^{\rm m}26\overset{\rm s}{.}518$	$45°30'37\overset{''}{.}77$	10.53	+1.00
Check	3636-0116	$23^{\rm h}25^{\rm m}56\overset{\rm s}{.}429$	$45°32'28\overset{''}{.}82$	10.18	+1.26

Table 3: Details of variable, comparison and check stars.

mount; the camera was an SBIG ST-10XME. Standard reductions were then applied. The comparison star (the same as for G&M, 2005) and check star are listed in Table 3. The coordinates and magnitudes are from the Tycho Catalogue, Hog et al. (2000).

For classification purposes, one of the authors (R.M.R.) took two low resolution spectra, on 2013 March 9 (HJD=24 56360.4608) and 2013 June 22 (HJD=24 56465.3077). He used the 1.85 m Plaskett telescope at the Dominion Astrophysical Observatory (DAO) in Victoria, British Columbia, Canada with the Cassegrain spectrograph in the 2131 configuration, resulting in a reciprocal dispersion of 60 Å/mm. The two spectra were very similar. The strength of the Calcium H&K lines, G-band, Hγ, Fe I 4384, Ca I 4227, and Hδ lines all indicated a F5 ±1 spectral classification for LO And.

R.H.N. used the 2003 version of the Wilson-Devinney (WD) light curve and radial velocity analysis program with Kurucz atmospheres (Wilson and Devinney, 1971, Wilson, 1990, Kallrath, et al., 1998) as implemented in the Windows front-end software WDwint (Nelson, 2009) to analyse the data. To get started, the spectral type F5 V, mentioned above, was adopted. Interpolated tables from Cox (2000) gave a temperature $T1 = 6650 \pm 100$ K and $\log g = 4.355$. An interpolation program by Terrell (1994, available from Nelson 2009) gave the Van Hamme (1993) limb darkening values; and finally, a logarithmic (LD=2) law for the limb darkening coefficients was selected, appropriate for temperatures < 8500 K (ibid.).

From the GCVS 4 designation (EW) and from the shape of the light curve, mode 3 (overcontact binary) mode was used. Early on, it was noted that the maxima between eclipses were unequal. This is the O'Connell effect (Davidge & Milone, 1984, and

Band	x_1	x_2	y_1	y_2
Bol	0.640	0.641	0.243	0.243
V	0.705	0.705	0.280	0.280
R_c	0.632	0.632	0.287	0.287
I_c	0.549	0.548	0.275	0.275

Table 4: Limb darkening values from Van Hamme (1993)

WD Quantity	G & M Value	G & M error	This work Value	This work error	Unit
Temperature, T_1	6500	[fixed]	6650	[fixed]	K
Temperature, T_2	6465	184	6690	24	K
$q = m_2/m_1$	0.371	0.002	0.305	0.004	—
Potential, $\Omega_1 = \Omega_2$	2.548	0.026	2.401	0.009	—
Inclination, i	78.67	0.62	80.1	0.6	deg
Semi-maj. axis, a	—	—	2.74	0.02	sol. rad.
V_γ	—	—	-3.0	0.8	km/s
Spot co-latitude	—	—	97	10	deg
Spot longitude	—	—	45	5	deg
Spot radius	—	—	33	2	deg
Spot temp factor	—	—	0.9765	0.005	—
$L_1/(L_1+L_2)(V)$	0.7061	0.0025	0.7330	0.0010	—
$L_1/(L_1+L_2)(R_c)$	na	na	0.7339	0.0009	—
$L_1/(L_1+L_2)(I_c)$	na	na	0.7348	0.0008	—
r_1 (pole)	0.4524	0.0058	0.4706	0.0003	orb. rad.
r_1 (side)	0.4873	0.0081	0.5103	0.0005	orb. rad.
r_1 (back)	0.5189	0.0115	0.5414	0.0008	orb. rad.
r_2 (pole)	0.2911	0.0099	0.2795	0.0012	orb. rad.
r_2 (side)	0.3055	0.0124	0.2937	0.0015	orb. rad.
r_2 (back)	0.3501	0.0251	0.3427	0.0035	orb. rad.
Phase shift	—	—	-0.0012	0.0004	—
$\Sigma\omega^2_{res}$	0.04039	—	0.02872	—	—

Table 5: Wilson-Devinney parameters

references therein) and is usually explained by the presence of one or more star spots. Accordingly, one was added first to star 1, and this gave good results. (Moving the spot to star 2 gave poorer results and was abandoned.)

Convergence by the method of multiple subsets was reached in a small number of iterations. (The subsets were: (a, L_1), (T_2, q), and (V_γ, i, q). The spots were handled separately.) Convective envelopes for both stars were used, appropriate for cooler stars (hence values gravity exponent $g = 0.32$ and albedo $A = 0.500$ were used for each). Detailed reflections were tried, with $n_{ref} = 3$, but there was little – if any – difference in the fit from the simple treatment. The limb darkening coefficients are listed in Table 4. There are certain uncertainties in the process (see Csizmadia et al., 2013, Kurucz, 2002). On the other hand, the solution is weakly dependent on the exact values used.

The model is presented in Table 5. Note that estimating the uncertainties in temper-

Quantity	G & M Value	G & M Error	This work Value	This work Error	unit
Temperature, T_1	6500	[fixed]	6650	200	K
Temperature, T_2	6465	184	6690	200	K
Mass, m_1	1.31	0.18	1.468	0.048	$M_\odot$
Mass, m_2	0.49	0.07	0.447	0.022	$M_\odot$
Radius, R_1	1.30	0.05	1.40	0.01	$R_\odot$
Radius, R_2	0.85	0.14	0.84	0.01	$R_\odot$
$M_{\rm bol}$, 1	3.67	0.08	3.45	0.02	mag
$M_{\rm bol}$, 2	4.62	0.39	4.53	0.02	mag
$\log g_1$	4.32	0.71	4.32	0.01	cgs
$\log g_2$	4.26	0.75	4.24	0.01	cgs
Luminosity, L_1	2.70	0.08	3.44	0.06	$L_\odot$
Luminosity, L_2	1.13	0.35	1.27	0.02	$L_\odot$
Fill-out factor	0.306	—	0.398	0.062	—
Distance, r	—	—	343	45	pc

Table 6: Fundamental parameters

atures T_1 and T_2 are somewhat problematic. A common practice is to quote the temperature difference over half a spectral sub-class (assuming that the classification is good to one spectral sub-class, which precision might be rare). In addition, various different calibrations have been made (Cox, 2000, page 388-390 and references therein, and Flower, 1996), and the variations between the various calibrations can be significant. In our case the classification is ± one sub-class. Therefore, we propose to assign an uncertainty of ± 200 K to the absolute temperatures of each, which would roughly span this range. The modelling error in temperature T_2, relative to T_1, is indicated by the WD output to be much smaller, around 24 K.)

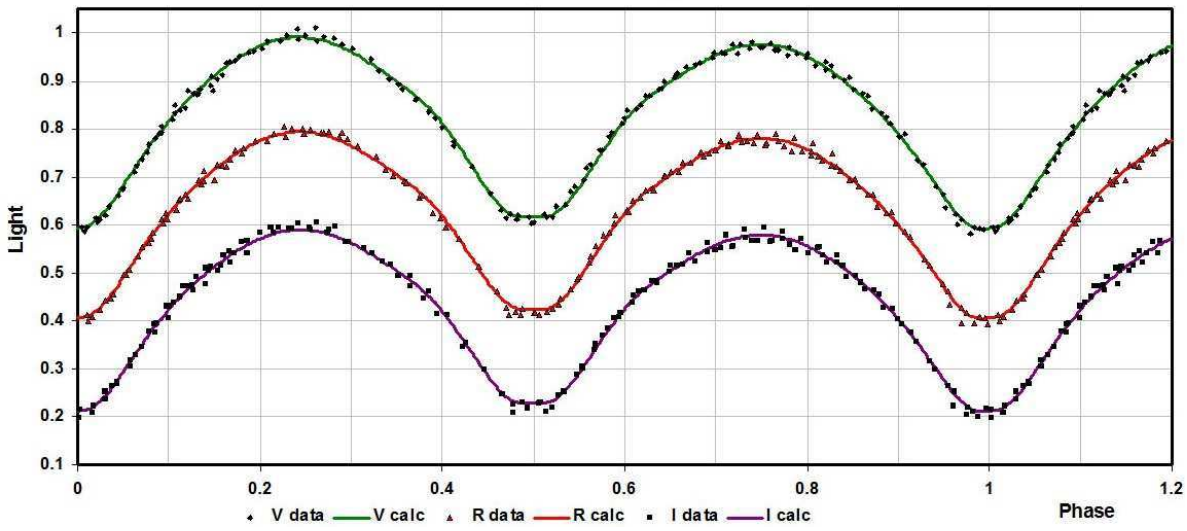

Figure 4. V, $R_{\rm c}$, and $I_{\rm c}$ light curves – data and WD fit

The WD output fundamental parameters and errors are listed in Table 6. Most of the errors are output or derived estimates from the WD routines. The fill-out factor $f = (\Omega^{\rm I} - \Omega)/(\Omega^{\rm I} - \Omega^{\rm O})$, where Ω is the modified Kopal potential of the system, $\Omega^{\rm I}$ is that of the inner Lagrangian surface, and $\Omega^{\rm O}$, that of the outer Lagrangian surface, was also calculated.

The light curve data and the fitted curves are depicted in Figure 4. The presence of third light was tested for, but found not to be significant.

The RVs are shown in Fig. 5. A three-dimensional representation from Binary Maker 3 (Bradstreet, 1993) is shown in Fig. 6.

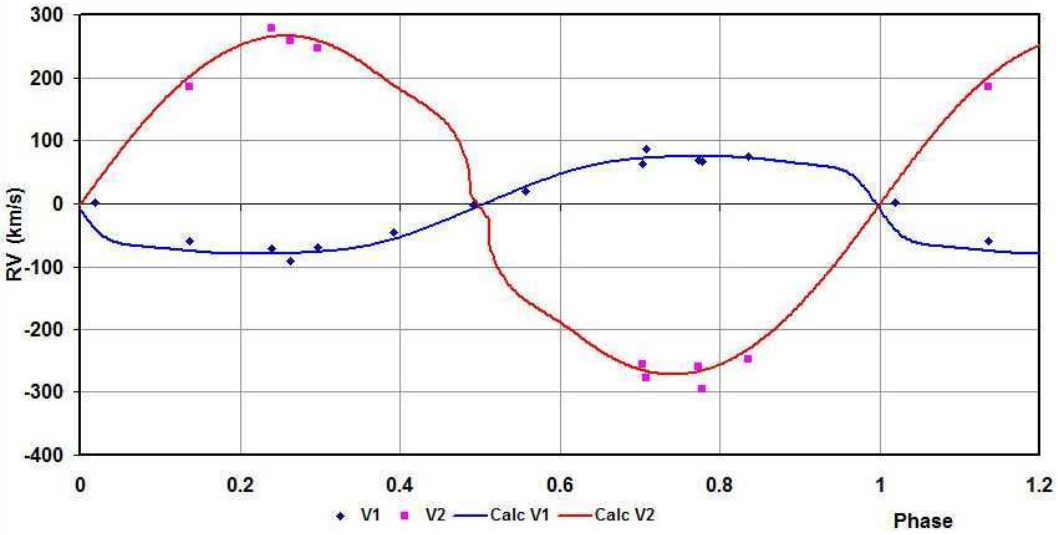

Figure 5. LO And: radial velocity curves – data and WD fit.

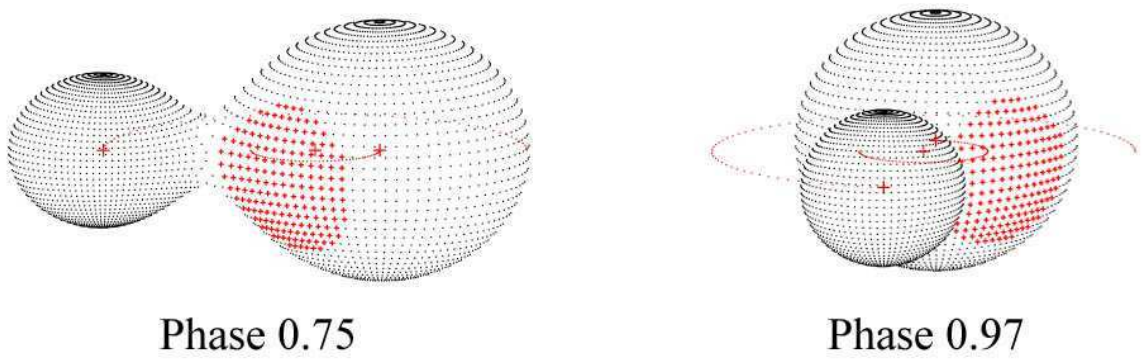

Figure 6. Binary Maker 3 representation of the system – at phases 0.75 and 0.97.

To determine the distance r in column 4, we proceeded as follows: First the WD routine gave the absolute bolometric magnitudes of each component; these were then converted to the absolute visual (V) magnitudes of both, $M_{V,1}$ and $M_{V,2}$, using the bolometric correction BC = −0.140 for each. The latter was taken from interpolated tables in Cox (2000). The absolute V magnitude was then computed in the usual way, getting M_V =

3.25±0.03 magnitudes. The apparent magnitude in the V passband was $V = 11.19 \pm 0.09$, taken from the Tycho values (Hog et al., 2000) and converted to a Johnson magnitude using relations due to Henden (2001). The colour excess (in $B - V$) was obtained in the usual way, by subtracting the tabular value of $B - V$ (for that spectral class) from the observed (converted Tycho) value. This gave $E[B-V] = 0.26$ magnitudes. However, reference to the dust tables of Schlegel et al. (1998) revealed a value of $E[B-V] = 0.1711$ for those galactic coordinates. Since the $E[B-V]$ values have been derived from full-sky far-infrared measurements, they therefore apply to objects outside of the Galaxy; this value of $E[B-V]$ so derived then represents an upper limit for closer objects within the Galaxy. Hence the higher value of 0.26 cannot be regarded as reliable. Again, since the value of $E[B-V] = 0.1711$ represents an upper limit, objects closer than the edge of the galaxy should have a lower value; hence $E[B-V] = 0.086$ (half) was adopted and the error estimate also set to this value. Galactic extinction was obtained from the usual relation $A_V = RE[B-V]$, using $R = 3.1$ for the reddening coefficient. Hence, distance $r = 343$ pc was calculated from the standard relation:

$$r = 10^{0.2(V - M_V - A_V + 5)} \text{ parsecs} . \quad (9)$$

The errors were assigned as follows: $\delta M_{\rm bol,1} = \delta M_{\rm bol,2} = 0.02$, $\delta {\rm BC}_1 = \delta {\rm BC}_2 = 0.01$ (the variation of 1.5 spectral sub-classes), $\delta V = 0.09$, $\delta E(B-V) = 0.086$, all in magnitudes, and $\delta R = 0.1$. Combining the errors rigorously yielded an estimated error in r of 45 pc.

In conclusion, the fundamental parameters of this system have been determined. One of these is the mass ratio, defined by the WD routine as $q = m_2/m_1$. As to eclipse sub-type (A or W), the deeper eclipse, by convention, defines phase 0; therefore the star eclipsed at that phase – the primary – is the hotter one. However, in this case, detailed modelling using a spot results in a slightly higher temperature for the secondary, making the system type-W.

It is interesting to note that Gürol & Müyesseroğlu (2005), although they noted a magnitude difference in maxima (Max II − Max I) of −0.010 in V, made no attempt to include any spots in their WD modelling. They also the classified the system as type-A, which classification might have been different if they had added a spot as we have done. (However, in our case, we noted a magnitude difference (Max II − Max I) ≈ +0.03 in the V band–the opposite. Clearly the spot, if it exists, has migrated in the time interval of nine years.)

Acknowledgements: It is a pleasure to thank the staff members at the DAO (especially Dmitry Monin and Les Saddlemyer) for their usual splendid help and assistance.

References:

Applegate, J.H., 1992, *ApJ*, **385**, 621

Bradstreet, D.H., 1993, "Binary Maker 2.0 - An Interactive Graphical Tool for Preliminary Light Curve Analysis", in Milone, E.F. (ed.) Light Curve Modelling of Eclipsing Binary Stars, pp 151-166 (Springer, New York, N.Y.)

Cox, A.N., ed, 2000, Allen's Astrophysical Quantities, 4th ed., (Springer, New York, NY)

Csizmadia, S., Pasternacki, T., Dreyer, C., Cabrera, A., Erikson, A. & Rauer, H., 2013, *A&A*, **549**, A9

Davidge, T.J., & Milone, E.F., 1984, *ApJS*, **55**, 571

Diethelm, R. & Gautschy, A., 1980, *IBVS*, **1767**

Flower, P.J., 1996, *ApJ*, **469**, 355
Gürol, B. & Müyesseroğlu, Z., 2005, *AN*, **326**, 43
Henden, A., 2001, `http://www.tass-survey.org/tass/catalogs/tycho.old.html`
Hog, E., et al., 2000, *A&A*, **355**, L27
Irwin, J.B., 1952, *ApJ*, **116**, 211
Irwin, J.B., 1959, *AJ*, **64**, 149
Kallrath, J., Milone, E.F., Terrell, D., and Young, A.T., 1998, *ApJ*, **508**, 308
Kreiner, J.M., 2004, *AcA*, **54**, 207
Kurucz, R.L., 2002, *BaltA*, **11**, 101
Mayer, P., 1990, *BAICz*, **41**, 231
Nelson, R.H., 2009, Software, by Bob Nelson,
`http://members.shaw.ca/bob.nelson/software1.htm`
Nelson, R.H., 2010a, Spreadsheets, by Bob Nelson,
`http://members.shaw.ca/bob.nelson/spreadsheets1.htm`
Nelson, R.H., 2010b, "Spectroscopy for Eclipsing Binary Analysis" in The Alt-Az Initiative, Telescope Mirror & Instrument Developments (Collins Foundation Press, Santa Margarita, CA), R.M. Genet, J.M. Johnson and V. Wallen (eds)
Nelson, R.H., 2013, Bob Nelsons O−C Files,
`http://www.aavso.org/bob-nelsons-o-c-files`
Nelson, R. H., Şenavcı, H.V. Baştürk, Ö. & Bahar, E., 2014, *NewA*, **29**, 57
Nelson, R.H., 2015, *NewA*, **34**, 159
Rucinski, S. M. 2004, "Advantages of the Broadening Function (BF) over the Cross-Correlation Function (CCF)", in Stellar Rotation, Proc. IAU Symp. 215., 14
Samus N.N., Durlevich O.V., Goranskij V.P., Kazarovets E. V., Kireeva N.N., Pastukhova E.N., Zharova A.V., 1985-2013, General Catalogue of Variable Stars
Schlegel, D.J., Finkbeiner, D.P. & Davis, M., 1998, *ApJ*, **500**, 525
Terrell, D., 1994, Van Hamme Limb Darkening Tables, vers. 1.1.
Terrell, D. & Wilson, R.E., 2005, *Ap&SS*, **296**, 221
Van Hamme, W., 1993, *AJ*, **106**, 2096
Weber, R., 1963, *IBVS*, **21**
Wilson, R.E., 1990, *ApJ*, **356**, 613
Wilson, R.E., & Devinney, E.J., 1971, *ApJ*, **166**, 605

COMMISSIONS 27 AND 42 OF THE IAU
INFORMATION BULLETIN ON VARIABLE STARS

Number 6135

Konkoly Observatory
Budapest
15 April 2015

HU ISSN 0374 – 0676

TYC3551-1535-1: A NEW VARIABLE STAR OF δ SCT TYPE

GAYNULLINA, E.R.; SEREBRYANSKIY, A.V.; KHALIKOVA, A.V.

Ulugh Beg Astronomical Institute, Astronomicheskaya str., 33, 100072 Tashkent, Uzbekistan
email: alex@astrin.uz, evelina@astrin.uz

In 2013 some close double stars were observed on Maidanak Observatory of Uzbekistan. The star V2364 Cyg (RA_{2000}=$19^h22^m11\overset{s}{.}73$; DEC_{2000}=$+49°28'34\overset{''}{.}43$) was observed in July 2013. The star TYC3551-1535-1 was in the field of view during 12 nights and indicated variability with amplitude about 0.02-0.03 magnitudes.

The observations were done with the 60-cm telescope Zeiss-600 with focal length of 7200 mm. The CCD camera is FLI MicroLine, the chip is a Kodak KAF-1001E, scale is $0\overset{''}{.}687$ per pixel which gives the field of view of $11\overset{'}{.}7 \times 11\overset{'}{.}7$. Observations were carried out in Bessell filter R. We provide some observational information in Table 1: start and end times of observation (at middle time of exposure), the exposure time, air mass for the first and the last frames and average Full Width on Half Maximum (FWHM) of a stellar profile. The air mass initially decreased till its minimal value 1.018 and then increased again.

Basic reduction of the frames was done using standard IRAF† software. We did the aperture photometry for all stars which can be used as the comparison stars. In the end, we decided that the star marked as $C1$ in the Figure 1 is more suitable to be a comparison star. During few days this star was located on bad CCD column and as a result we used $C2$ star as the comparison star. Since we used different comparison stars, nightly average values were subtracted from each light curve. Neither linear nor parabolic trends were removed and no differential extinction corrections were applied.

We plot the light curves of the variable star in Figure 2. The final light curve contains 8067 data points. Both the close binary system V2364 Cyg and TYC3551-1535-1 are located very close but not on the *Kepler*'s field and as a result we were not able to compare our light curve with *Kepler*'s ones. For the power spectral analysis of the light curves the FAMIAS software package (Zima, 2008) was used. Figure 3 presents the spectral window and the power spectra of two modes. The width of the smoothing window for noise level estimation (box size) was set to 8 c/d. Only two modes exceed 4σ criteria. We show the results in Table 2.

In order to classify the type of variability of TYC3551-1535-1 we need to know its spectral type. We estimated it from the $J-H$ color of TYC3551-1535-1 using templates by Stead & Hoare (2011). The resulting value is F2. Considering the amplitude and period of oscillations as well as spectral type we tend to assume that TYC3551-1535-1 could be a variable star of δ Sct type.

Table 1: Observational info

Date	Start time (UTC) hh:mm:ss	End time (UTC) hh:mm:ss	Exp. time sec	Air mass start : end	FWHM arcsec
July 7	18:05:11.0	22:36:45.0	20	1.076 : 1.170	1.8
July 11	17:11:45.5	23:28:21.5	25	1.129 : 1.350	1.7
July 12	17:06:07.5	23:18:58.5	25	1.131 : 1.332	1.7
July 14	17:00:07.5	23:31:29.0	25	1.128 : 1.404	1.7
July 15	16:54:47.5	23:24:02.5	25	1.131 : 1.391	1.8
July 17	16:40:46.5	22:52:09.5	25	1.141 : 1.309	1.8
July 18	16:35:46.0	19:49:39.0	30	1.143 : 1.027	2.5
July 19	16:41:28.0	23:30:05.0	30	1.127 : 1.480	1.9
July 20	17:41:39.5	23:30:47.5	25	1.067 : 1.501	1.6
July 21	16:31:57.0	21:17:19.0	30	1.077 : 1.137	2.0
July 25	16:52:09.5	23:43:06.0	30	1.077 : 1.679	1.9
July 26	16:30:05.0	22:06:46.0	30	1.102 : 1.279	2.0

Table 2: Mode parameters

Mode	P c/d	σ_P c/d	A mmag	σ_A mmag	S/N
f1	8.9039	0.0004	4.77	0.07	13.3
f2	8.9659	0.0013	1.76	0.07	4.9

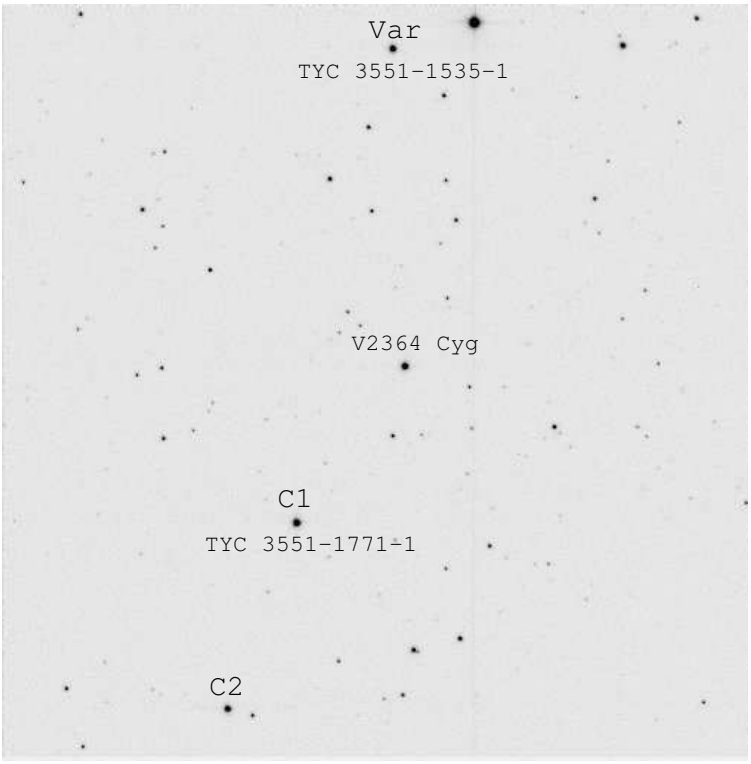

Figure 1. Finding chart for variable and comparison stars. North is up and East is to the left.

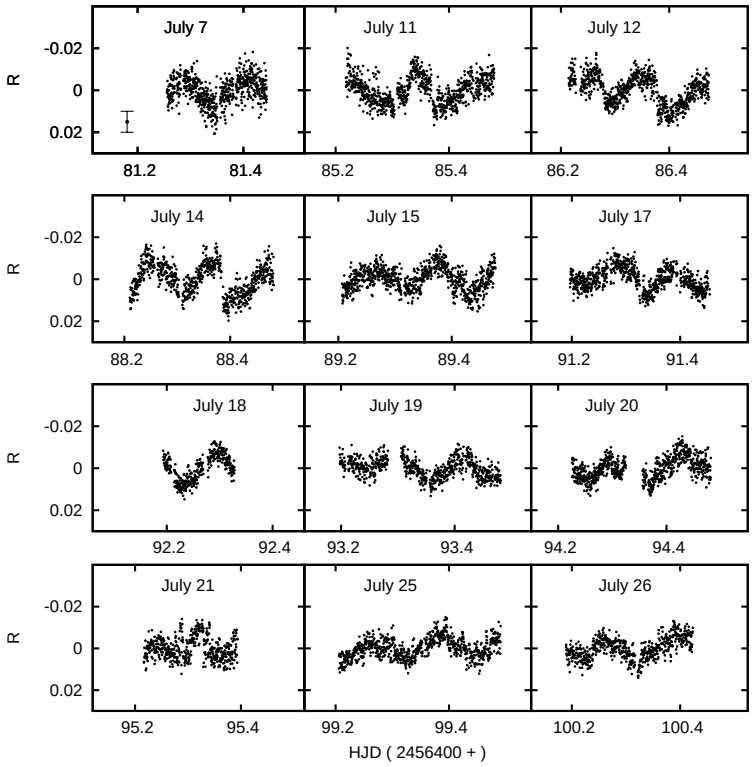

Figure 2. Light curves of TYC3551-1535-1. On the top left panel we show the largest error bar.

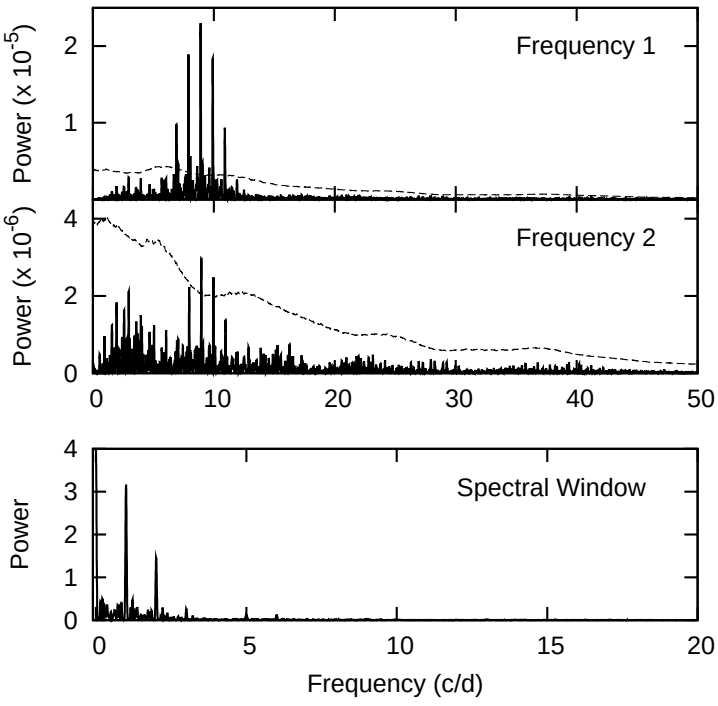

Figure 3. Spectral window and power spectra. The dashed line is 4σ significance level.

Acknowledgements: The authors are supported by Fundamental Research Grants FA-F02-F027 and FA-F02-F028 of the Uzbek Academy of Sciences. We used the Simbad database and the 2MASS All-Sky Survey in our work. We thank the observer Parmonov O. The authors also thank the anonymous referee for important suggestions and comments.

References:

Stead, J. J., Hoare, M. G., 2011, *MNRAS*, **418**, 2219 (VizieR Online Data Catalog: J/MNRAS/418/2219/tablea1)

Zima, W., 2008, *Communications in Asteroseismology*, **155**, 17

[†]IRAF is distributed by the NOAO, which are operated by the AURA, Inc., under cooperative agreement with the NSF

COMMISSIONS 27 AND 42 OF THE IAU
INFORMATION BULLETIN ON VARIABLE STARS

Number 6136

Konkoly Observatory
Budapest
15 April 2015

HU ISSN 0374 – 0676

A VARIABLE STAR IN THE FIELD AROUND TRES-4

GAYNULLINA, E.R.; SEREBRYANSKIY, A.V.; KHALIKOVA, A.V.; KARIMOV, R.G.

Ulugh Beg Astronomical Institute, Astronomicheskaya str., 33, 100072 Tashkent, Uzbekistan
email: alex@astrin.uz, evelina@astrin.uz

Transits of exoplanets were occasionally observed on Maidanak Observatory of Uzbekistan in the period from 2010 to 2013 using Zeiss-600 telescope equipped with FLI IMG1001E (in 2010) and FLI MicroLine (2012-2013) with FoV equal to $11\farcm7 \times 11\farcm7$. Observations of exoplanet host star TrES-4 ($RA_{2000}=17^h53^m13\fs058$; $DEC_{2000}=+37°12'42\farcs36$) was performed in 2010 in filter Cousins R and in 2012 and 2013 using filter Bessell R. We also provide with additional information on observation in Table 1: start and end times of observation (at middle time of exposure), the exposure time, air mass for the first and the last frames for each night and average Full Width on Half Maximum (FWHM) of a star profile. In 2012 the air mass initially decreased down to 1.001 and then increased again.

Table 1: Observational info

Date (UTC)	Start time (UTC)	End time (UTC)	Exp. time	Air mass	FWHM
	hh:mm:ss	hh:mm:ss	sec	start : end	arcsec
Aug 30, 2010	15:11:37	20:41:04	30	1.003 : 2.489	2.02
July 23, 2012	15:58:21	21:10:03	60	1.039 : 1.415	2.00
June 12, 2013	16:32:58	19:15:26	40, 60	1.414 : 1.012	1.73

Table 2: Mode parameters

Date	Frequency c/d	σ_F c/d	Amplitude mmag	σ_A mmag	SNR
2010	11.802	-	19.9	0.4	18.4
2012	11.781	-	19.8	0.3	18.8
2013	11.511	-	19.5	0.5	42.8
All	11.805823	0.000005	19.8	0.2	28.2

Basic reduction of the frames was done using standard IRAF† software. We did the aperture photometry for all stars which can be used as the comparison stars. In the end, we selected 7 stars for further analyses. In Figure 1 we show our field of view in 2012 and mark the comparison stars as Sn, $n = 1, 2....$ In 2010 and 2013 we used $S1$, $S2$ and $S3$

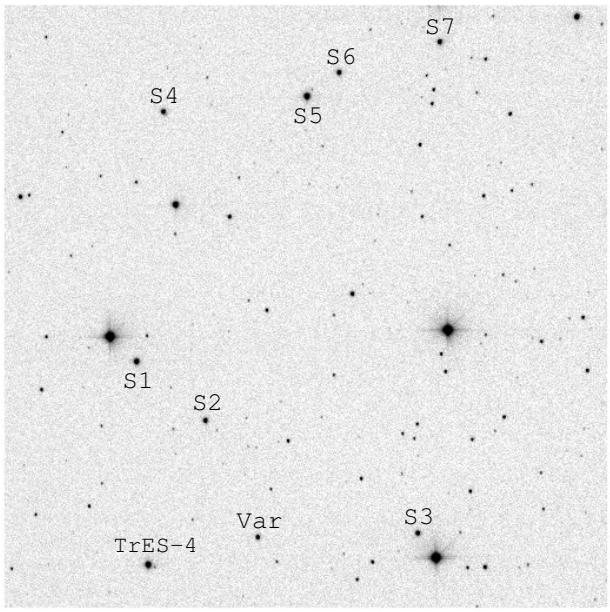

Figure 1. Image taken on July 23, 2012. TrES-4, the new variable star (Var) and comparison stars are marked. North is up and East is to the left.

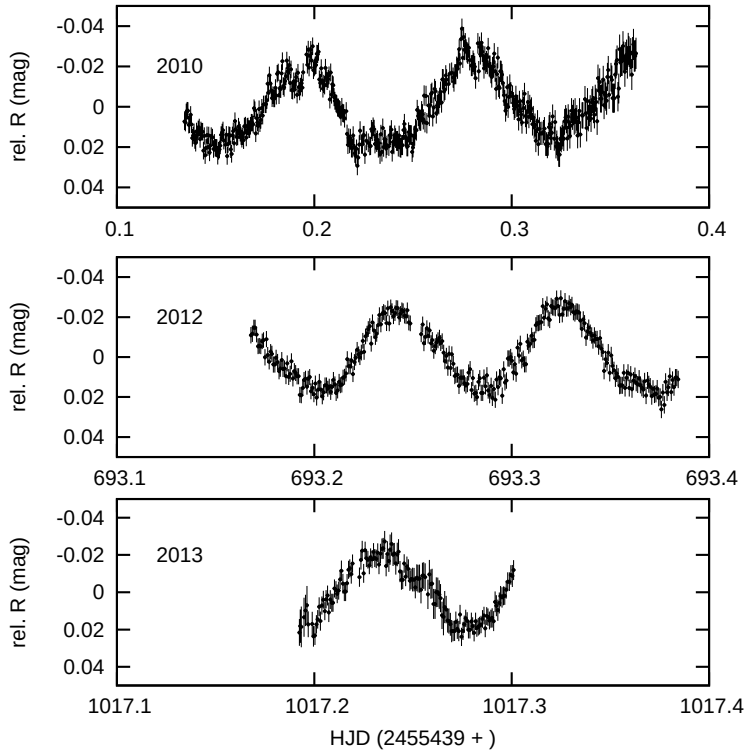

Figure 2. The light curves of the new variable star.

comparison stars and in 2012 we used all seven stars. One star marked as Var has shown variability with an amplitude of ≈ 0.04 mag. Because we used different comparison stars, nightly average values were subtracted from each light curve. Neither linear nor parabolic trends were removed and no differential extinction corrections were applied. We plot the light curves of the variable star in Figure 2. The final light curves contain 509 data points in 2010, 300 data points in 2012 and 147 data points in 2013. The `6136-t3.txt` file containing the photometry is available online.

This Var star is not included in any of catalogues. We did not find any reference on it in the publications devoted to TrES-4. But we have found the short report (DeCoster et al., 2011) where the authors wrote about searching for variable stars in the archival mid-infrared data (4.5-micron) from the Spitzer Space Telescope. They found one star in the TrES-4 field that displayed periodic variability (P = 0.082 days) when phase-folded.

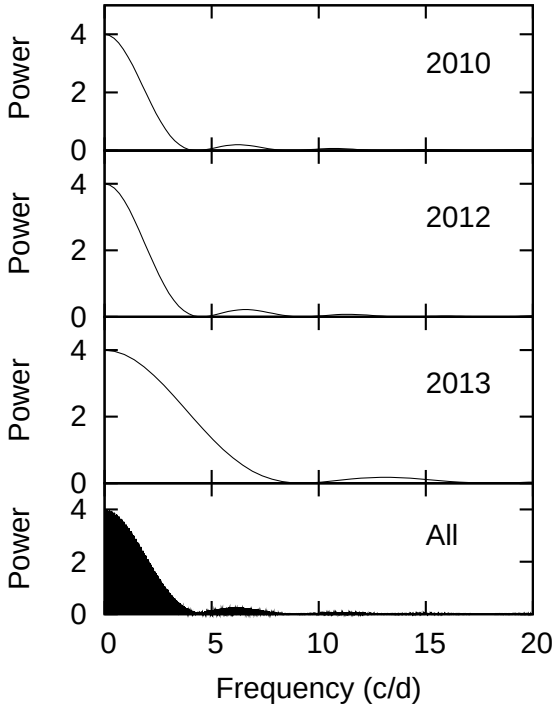

Figure 3. The spectral windows.

For the power spectral analysis of the light curves the FAMIAS software package (Zima, 2008) was used. Figure 3 presents the spectral windows. The width of the smoothing window for noise level estimation (box size) was set to 16 c/d. Amplitudes in power spectra of several modes exceeded 4σ for each light curve. Only one mode was present for all light curves. We show the results in Table 2. The errors of the frequency estimation for individual light curve are not presented due to the low resolution of power spectra which caused instability of frequencies. The spectral analyses of the total light curve (for all 3 years data points) gives the period of P=0.085 days which is very close to that reported in (DeCoster et al., 2011). This suggests that we are probably dealing with the same star.

[†]IRAF is distributed by the NOAO, which are operated by the AURA, Inc., under cooperative agreement with the NSF

Considering the amplitude and period of oscillations we tend to assume that this variable star could belong to δ Sct type.

Acknowledgements: The authors are supported by Fundamental Research Grants FA-F02-F027 and FA-F02-F028 of the Uzbek Academy of Sciences. We thank the observers Khafizov B., Fayziev S. and Parmonov O. We also thank the anonymous referee for important suggestions and comments.

References:

DeCoster, R., Piper, P., Thomas, B. et al., 2011, *Bulletin of the American Astronomical Society*, **43**, 342

Zima, W., 2008, *Communications in Asteroseismology*, **155**, 17

COMMISSIONS 27 AND 42 OF THE IAU
INFORMATION BULLETIN ON VARIABLE STARS

Number 6137

Konkoly Observatory
Budapest
15 April 2015

HU ISSN 0374 – 0676

NEW VARIABLES IN M5 (NGC 5904) AND SOME IDENTIFICATION CORRECTIONS

ARELLANO FERRO, A.[1]; BRAMICH, D.M.[2]; GIRIDHAR, S.[3]; LUNA, A.[1]; MUNEER, S.[3]

[1] Instituto de Astronomía, Universidad Nacional Autónoma de México, Ciudad Universitaria CP 04510, México: armando@astro.unam.mx; aluna@astro.unam.mx

[2] Qatar Environment and Energy Research Institute, Qatar Foundation, P.O. Box 5825, Doha, Qatar: dan.bramich@hotmail.co.uk

[3] Indian Institute of Astrophysics, Koramangala 560034, Bangalore, India: giridhar@iiap.res.in

1 Introduction

The bright globular cluster M5 (NGC 5904) has been the subject of many variable star searches for more than a hundred years. The first variables were discovered by Solon I. Bailey with the 13-inch Boyden Telescope at the Arequipa station in 1896 (see Pickering 1896 and Bailey 1899). The catalogue of variable stars in globular clusters (CVSGC; Clement et al. 2001) lists 169 variables, mostly of the RR Lyrae type, with 5 SX Phe stars, one W Virginis star (CW), one RV Tau, one (possibly two) eclipsing binaries, and one U Gem type star. However, there are also a number of uncertain classifications and some variables have an unknown type, or it is not even clear if they are truly variable. A new study of the variable stars in M5 is therefore pertinent.

As part of our program of CCD time-series observations of variable star populations in globular clusters (GC), we performed CCD V and I photometry of the globular cluster M5. Difference image analysis (DIA) has proven to be very efficient in identifying variable stars even in the crowded central regions of GCs (e.g. Arellano Ferro et al. 2013 and references therein). Exploration of our collection of light curves of all stars in the field of our images down to $V \sim 18.5$ mag allowed us to identify twelve variables not previously detected; one SX Phe and eleven semi-regular variables (SR). In the present note, we report on their identifications, equatorial coordinates, ephemerides, and light curves. We argue that the known variable V155, previously classified as RRc, is in fact a contact eclipsing binary or EW. Furthermore, we have explored the light curves of a group of stars whose variability has not been confirmed and that are marked as probable non-variables in the CVSGC. Finally, we offer detailed identifications for some of the known variables in crowded regions that were misidentified in previous studies. We shall also address the cases of the cataclysmic variable or U Gem type V101 and of the variable blue straggler V159.

2 Observations and reductions

The observations were acquired on 11 nights between 29 February 2012 and 9 April 2014 with the 2.0m telescope of the Hanle Observatory, India. A total of 385 and 384 images in V and I, respectively, were obtained. Image data were calibrated using bias and flat-field correction procedures. We used DIA to extract high-precision time-series photometry employing the `DanDIA` pipeline for the data reduction process (Bramich et al. 2013), which includes an algorithm that models the convolution kernel matching the PSF of a pair of images of the same field as a discrete pixel array (Bramich 2008). We have also applied a post-calibration method developed by Bramich & Freudling (2012) which determines appropriate per-image magnitude offsets to correct for errors in the fitted value of the photometric scale factor p. We derived offsets of the order of ~ 0.02 and ~ 0.03 mag in V and I, respectively. The instrumental magnitudes are calculated via the difference flux, the reference flux and the photometric scale factor by the equation;

$$m_{\rm ins}(t) = 25.0 - 2.5 \log \left[f_{\rm ref} + \frac{f_{\rm diff}(t)}{p(t)} \right]. \quad (1)$$

The difference fluxes $f_{\rm diff}$ are measured by scaling the known PSF to the difference images at the position of each star. Since the constant stars have been fully subtracted in the difference images, the difference fluxes for the variables are very precise. The reference fluxes $f_{\rm ref}$ are, however, measured on the reference image by PSF fitting and they have the potential to suffer from the usual problems caused by blending. For the variables in the most crowded parts of the reference image, where the probability of blending is high, the brightness of a variable star may be overestimated, and its amplitude underestimated (see Section 2.3 of Bramich et al. 2011 for a more in-depth discussion of the caveats of DIA).

The instrumental magnitudes were transformed to the standard Johnson-Kron-Cousins magnitudes using secondary photometric standards in the field of view (FoV) from Stetson (2000) covering the full range of colours.

All of our VI photometry for the stars discussed in this paper is provided in Table 1. Just a small portion of this table is given in the printed version of this paper, while the full table is only available in electronic form.

3 Exploration of suspected non-variables in the CVSGC

In the CVSGC there are 23 stars classified as (probably) non-variables or "constant" (CST, CST? or ?); these are V22, V23, V46, V48, V49, V51, V124, V136, V138, V140, V141, V143-V154. Except for V22 and V141, which are outside of the FoV of our images, we have VI light curves for all of them. We have carried out a quick exploration of the light curves to comment on their possible variability or otherwise.

Firstly we have identified the 21 stars in our FoV on the colour-magnitude diagram (CMD) of Fig. 1 and the RMS diagram of Fig. 2. All of them are marked with red squares. In the RMS diagram we draw an arbitrarily set line above which all variables seem to fall and hence it can serve as a guide of detectability when judging the variability of a given candidate. While true variables are expected to have significantly larger rms values than this upper limit, we note however that non-true variables may lie above that limit if they are near a true variable due to flux contamination (e.g. V140, see below), or that true variables may be found below that limit, particularly those of very small amplitude (e.g. the SX Phe star V164). Thus, individual explorations of the light curves of specific

Table 1: Time-series V and I photometry for all stars discussed in this paper. The standard $M_{\rm std}$ and instrumental $m_{\rm ins}$ magnitudes are listed in columns 4 and 5, respectively, corresponding to the variable star in column 1. Filter and epoch of mid-exposure are listed in columns 2 and 3, respectively. The uncertainty on $m_{\rm ins}$ is listed in column 6, which also corresponds to the uncertainty on $M_{\rm std}$. For completeness, we also list the quantities $f_{\rm ref}$, $f_{\rm diff}$ and p from Eq. 1 in columns 7, 9 and 11, along with the uncertainties $\sigma_{\rm ref}$ and $\sigma_{\rm diff}$ in columns 8 and 10. This is an extract from the full table, which is available with the electronic version of the article (`6137-t1.txt`).

Variable Star ID	Filter	HJD (d)	$M_{\rm std}$ (mag)	$m_{\rm ins}$ (mag)	σ_m (mag)	$f_{\rm ref}$ (ADU s^{-1})	$\sigma_{\rm ref}$ (ADU s^{-1})	$f_{\rm diff}$ (ADU s^{-1})	$\sigma_{\rm diff}$ (ADU s^{-1})	p
V23	V	2455987.37467	14.402	15.567	0.002	5984.932	11.137	−51.549	9.416	1.0195
V23	V	2455987.37903	14.404	15.569	0.002	5984.932	11.137	−59.403	9.521	0.9697
⋮	⋮	⋮	⋮	⋮	⋮	⋮	⋮	⋮	⋮	⋮
V23	I	2455987.37248	13.353	14.622	0.002	14205.530	25.101	−44.978	27.407	1.0588
V23	I	2455987.37686	13.370	14.639	0.002	14205.530	25.101	−278.790	30.268	1.0423
⋮	⋮	⋮	⋮	⋮	⋮	⋮	⋮	⋮	⋮	⋮
V25	V	2455987.37467	14.632	15.826	0.003	2449.232	15.883	+2267.438	12.352	1.0195
V25	V	2455987.37903	14.625	15.819	0.003	2449.232	15.883	+2186.565	11.576	0.9697
⋮	⋮	⋮	⋮	⋮	⋮	⋮	⋮	⋮	⋮	⋮
V25	I	2455987.37248	14.253	15.542	0.004	3901.695	29.242	+2298.204	26.254	1.0588
V25	I	2455987.37686	14.310	15.599	0.005	3901.695	29.242	+1939.003	29.961	1.0423
⋮	⋮	⋮	⋮	⋮	⋮	⋮	⋮	⋮	⋮	⋮

cases are required. In Table 2 we list the mean magnitudes and rms values in the V light curves. In the last column we list the value of the upper limit rms corresponding to the mean magnitude. Except for V140, all the stars listed above fall below the threshold. From the individual explorations we found that V140 does in fact show some variations. However we argue that these are due to flux contamination by a nearby variable (V175) as it will be discussed in § 5. For the rest, we found no signs of variability confirming their classification as non-variables (or CST) in the CVSGC.

4 Comments, identification and classification correction for some previously known variables

During the process of variable star identification we noticed that stars V25, V36, V53, V74, V102 and V108 are all very close to a neighbour of similar brightness or much brighter. While checking the finding charts of the discovery papers, we found that their identifications are dubious or definitely wrong, mainly due to the fact that the stars are not resolved in old plates and/or that they are close to the cluster central regions. Here we offer a precise identification and a few comments on each variable. We have confirmed the variable nature of these stars by phasing the light curves of the two candidates and by blinking the difference images. It was also noted that the equatorial coordinates in the CVSGC of the variable V140 point to a non-variable star. We address the cases of V50 whose variability has not been clearly established and of V155 that needs a reclassification. To avoid confusion in future work we include here in Table 3 the correct equatorial coordinates of all these stars. Below we offer a brief comment on individual stars including the U Gem type star V101, and binary V159.

V25 is a very close pair that in our images is heavily blended. In the finding chart of the discovery paper (Bailey 1902), the star looks like a single one. Careful blinking of the difference images makes it clear that the true variable is the western star of the pair, as

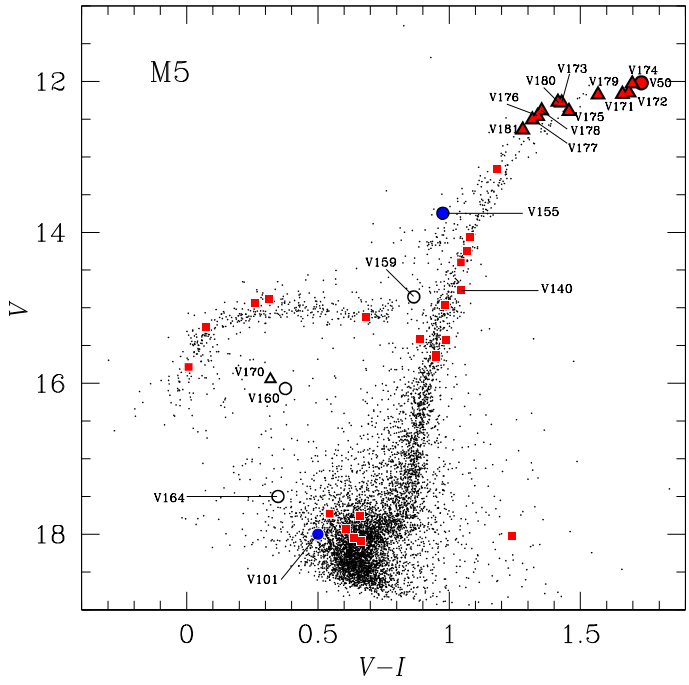

Figure 1. Colour-magnitude diagram of M5 with the new variables marked with triangles. The colour code is: empty symbols for blue straggler variables, the position of binary V159 is biased since it is heavily blended; red triangles for tip of the RGB variables; blue filled circles for two previously known variables V101 and V155. The cataclysmic variable V101 is plotted at its approximate position during outburst. No other known variables are shown. Red squares are stars listed as variables but whose variability has not been confirmed. See the text for a detailed discussion.

Table 2: Mean magnitudes and rms for stars whose variability is not confirmed. Local rms refers to the upper limit of the main rms distribution for a given value of $\langle V \rangle$, represented by the continuous line in Fig. 2.

Var ID	$\langle V \rangle$	rms V	local rms	Var ID	$\langle V \rangle$	rms V	local rms
V23	14.40	0.017	0.023	V145	15.26	0.017	0.033
V46	17.93	0.150	0.184	V146	15.65	0.019	0.040
V48	14.24	0.012	0.022	V147	15.12	0.015	0.031
V49	15.78	0.013	0.043	V148	15.62	0.018	0.040
V51	14.06	0.013	0.020	V149	17.75	0.062	0.160
V124	14.88	0.015	0.028	V150	18.08	0.056	0.208
V136	14.93	0.018	0.028	V151	18.02	0.054	0.198
V138	13.17	0.011	0.016	V152	17.72	0.043	0.160
V140	14.76	0.072	0.028	V153	18.05	0.049	0.203
V143	15.42	0.029	0.036	V154	17.93	0.046	0.184
V144	15.41	0.020	0.036				

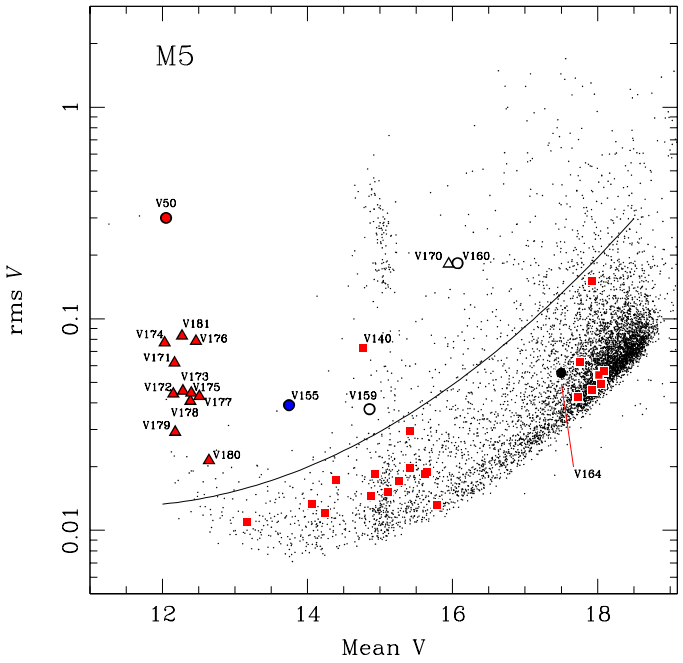

Figure 2. The rms V magnitude deviations calculated for 8431 stars in our FoV of M5 as a function of mean magnitude V. The sybols and colour code are as in Fig 1. The continuous line represents an arbitrary threshold for variability detectability (see text in § 3).

identified in Fig. 4.

V36 is also called V135 (see CVSGC for M5, 2014 update). The star is incorrectly identified in the chart of Caputo et al. (1999), labelled as V135, as the south-western star of the pair. The RRab variable is actually the north-eastern and brighter star of the pair.

V50 sits on the tip of the RGB. Bailey (1917) suggested a period of 106 d that was not confirmed by Oosterhoff (1941) who described the variation as irregular. Our data suggest a period of 107.6 d, in good agreement with Bailey's result. Therefore we classify the star as a semi-regular late-type variable (SRA). Its light curve, phased with the above period, is shown in Fig. 3.

V53 is not resolved in the finding chart of Bailey (1902) and not identified afterwards. The correct variable is the eastern star of the pair.

V74 is not resolved in the finding chart of Bailey (1902) and not identified afterwards. The correct variable is the western star of the pair.

V101 is a cataclysmic variable of the U Gem type. It was discovered by Oosterhoff (1941) who classified it as SS Cyg (or dwarf nova). Two outbursts of amplitude 2.7 mag within 100 days in the V light curve were detected by Kaluzny et al. (1999) who argue in favour of a short duty cycle with a characteristic time of about 3.4 hours. Our VI light curves, displayed in the mosaic of Fig. 3, span 770 days and two outbursts are clearly seen at HJD 2456029.4 and 2456312.5 d reaching 18.5 and 18.0 mag in V, and 18.0 and 17.0 mag in I respectively.

V102 The identification chart in Oosterhoff (1941) shows a strong blend close to the saturated central region that prevents an accurate identification. The authentic variable is the SE star of the pair.

V108 The variability of this star was announced by Kadla et al. (1987) (see also

Gerashchenko 1987). It was identified by Drissen & Shara (1998) in their *Hubble Space Telescope (HST)* image but mistakenly labelled as V22. The identification of the star by Caputo et al. (1999), now labelled as V108, points to the wrong star to the east of the real variable. We confirm that the variable star is the western star of the pair, in agreement with Drissen & Shara's (1998) identification.

Table 3: Known variables with corrected classifications, equatorial coordinates and identifications in Fig. 4.

Var ID	Variable type	RA(J2000.0)	Dec.(J2000.0)
V25	RRab	15 18 30.98	+02 02 42.5
V36	RRab	15 18 32.66	+02 03 58.9
V50	SRA	15 18 36.04	+02 06 37.8
V53	RRc	15 18 37.92	+02 05 06.8
V74	RRab	15 18 47.19	+02 07 25.7
V101	U Gem	15 18 14.51	+02 05 35.7
V102	RRab	15 18 34.37	+02 04 34.4
V108	RRc	15 18 33.79	+02 04 47.0
V140	CST	15 18 36.18	+02 05 13.2
V155	EW	15 18 33.40	+02 05 12.2
V159	E	15 18 32.88	+02 04 36.5

V140 is identified by Caputo et al. (1999) but the equatorial coordinates given in the CVSGC have a typo error producing some confusion in the identification and in the variable nature of the star which is classified as a probable non-variable. The star pointed to by the CVSGC at 15:18:36.18; +02:03:13.1 is not variable. The correct coordinates of the star identified by Caputo et al. (1999) are given in Table 3. However, this V140 is very close to a much brighter star and a careful blinking of the difference images clearly reveals that the authentic variable is the brighter star, which we have identified as the new SRA variable V175 (see §5). Both the light curves for V140 and V175 are shown in the mosaic of Fig. 3. The light curve of V140 has been contaminated by the real variations in the much brighter star V175. We conclude that V140 is not a variable star while V175 is an SRA variable.

V155 was discovered by Drissen & Shara (1998) and they classified it as RRc. However, the star lies near the RGB on the CMD (see Fig. 1) and the light curve in Fig. 3 is similar to that of an eclipsing binary of the EW type, or contact binary, when phased with the ephemerides P= 0.664865 days and the epoch 245 6504.2067 d. Note that two different depths of the minima, particularly visible in the V light curve, are implied.

V159 is classified in the CVSGC as a probable eclipsing binary. The star was identified as variable by Drissen & Shara (1998) on their HST images and labelled as V28. The V159 name was given by Caputo et al. (1999) on their finding chart. We find that this star is highly blended in our images, which affects the star's position on the CMD. We detected two clear eclipses in the V band at JD 2455989.52 and 2456750.44, of about 0.15 mag depth (see Fig. 3). However, we are not able to determine the periodicity although we confirm the star as an eclipsing binary.

5 New variable stars in M5

To search for new variables in the field of M5 we have used several approaches. We isolated all stars in regions of the CMD where most variable stars in a GC tend to be found. This includes the horizontal branch, the blue stragglers region and the RGB. We identified all previously known variables in the field of our images and studied in detail the light curves of the rest of the stars. This procedure allowed us to identify a new large amplitude ($A_V \sim 0.6$ mag) SX Phe star V170, for which we identify only one period. Then we explored the difference images for clear variations; this approach allowed us to discover the variability of six SRA (V171, V172, and V174-V177). A third approach was via the rms diagram of Fig. 2. It can be seen from this diagram that our photometry achieves uncertainties between 7 and 20 mmag at the bright end. High values of rms are generally produced by variable stars. For instance the group of stars with rms above 0.1 mag and with $V \sim 15$ are all RR Lyrae stars which are not discussed in the present paper. Through this procedure we identified five additional SRA stars V173 and V178-V181. For some of these new SRA stars we have been able to estimate a periodicity.

The new variables, their equatorial coordinates, periods and epochs are listed in Table 4 and their position on the CMD and the rms diagram are displayed in Figs. 1 and 2 respectively. Their light curves in the V and I bands, phased whenever possible or as a function of HJD otherwise, are displayed in Fig. 3.

In the identification chart of Fig. 4, we have marked a detailed identification for all variable stars discussed in this paper. No effort has been made to identify the numerous known variables listed in the CVSGC since that will be the subject of a future paper.

Table 4: New variable stars found in M5, V170-V181.

Name	Variable type	RA (J2000.0)	Dec. (J2000.0)	Period days	Epoch (−245 0000.)	$\langle V \rangle$ mag	$\langle I \rangle$ mag	A_V mag	A_I mag
V170	SX Phe	15 18 32.14	+02 04 20.4	0.089467	6063.3361	15.95	15.63	0.57	0.41
V171	SRA	15 18 34.26	+02 04 24.2	28.8	6312.5083	12.17	10.50	0.25	0.14
V172	SRA	15 18 31.59	+02 04 41.4	–	–	12.15	10.47	0.23	0.13
V173	SRA	15 18 28.42	+02 04 29.8	43.1	6504.1686	12.28	10.86	0.13	0.13
V174	SRA	15 18 34.18	+02 06 25.5	80.6	6063.4183	12.03	10.33	0.33	0.15
V175	SRA	15 18 36.22	+02 05 11.3	–	–	12.40	10.94	0.18	0.13
V176	SRA	15 18 37.38	+02 06 08.2	133.3	5989.3064	12.46	11.13	0.22	0.20
V177	SRA	15 18 41.40	+02 06 00.9	–	–	12.51	11.19	0.13	0.10
V178	SRA	15 18 33.10	+02 04 58.0	141.6	5987.4759	12.39	11.03	0.12	0.10
V179	SRA	15 18 33.42	+02 04 59.6	–	–	12.18	10.61	0.12	0.11
V180	SRA	15 18 35.82	+02 03 42.4	–	–	12.27	10.86	0.24	0.24
V181	SRA	15 18 45.40	+02 04 30.9	–	–	12.64	11.36	0.07	0.08

Acknowledgements: We are thankful to the referee, Dr. Ádám Sódor for his valuable comments and suggestions. We acknowledge the support from DGAPA-UNAM, Mexico grant through projects IN104612 and IN106615 and from NPRP grant # X-019-1-006 from the Qatar National Research Fund (a member of Qatar Foundation).

References:

Arellano Ferro, A., Bramich, D.M., Figuera Jaimes, R., et al. 2013, *MNRAS*, **434**, 1220
Bailey, S. I., 1899, *ApJ*, **10**, 255
Bailey, S. I., 1902, *Harv. Ann.*, **38**, 1
Bailey, S. I., 1917, *Harv. Ann.*, **78**, 99
Bramich, D.M., 2008, *MNRAS*, **386**, L77

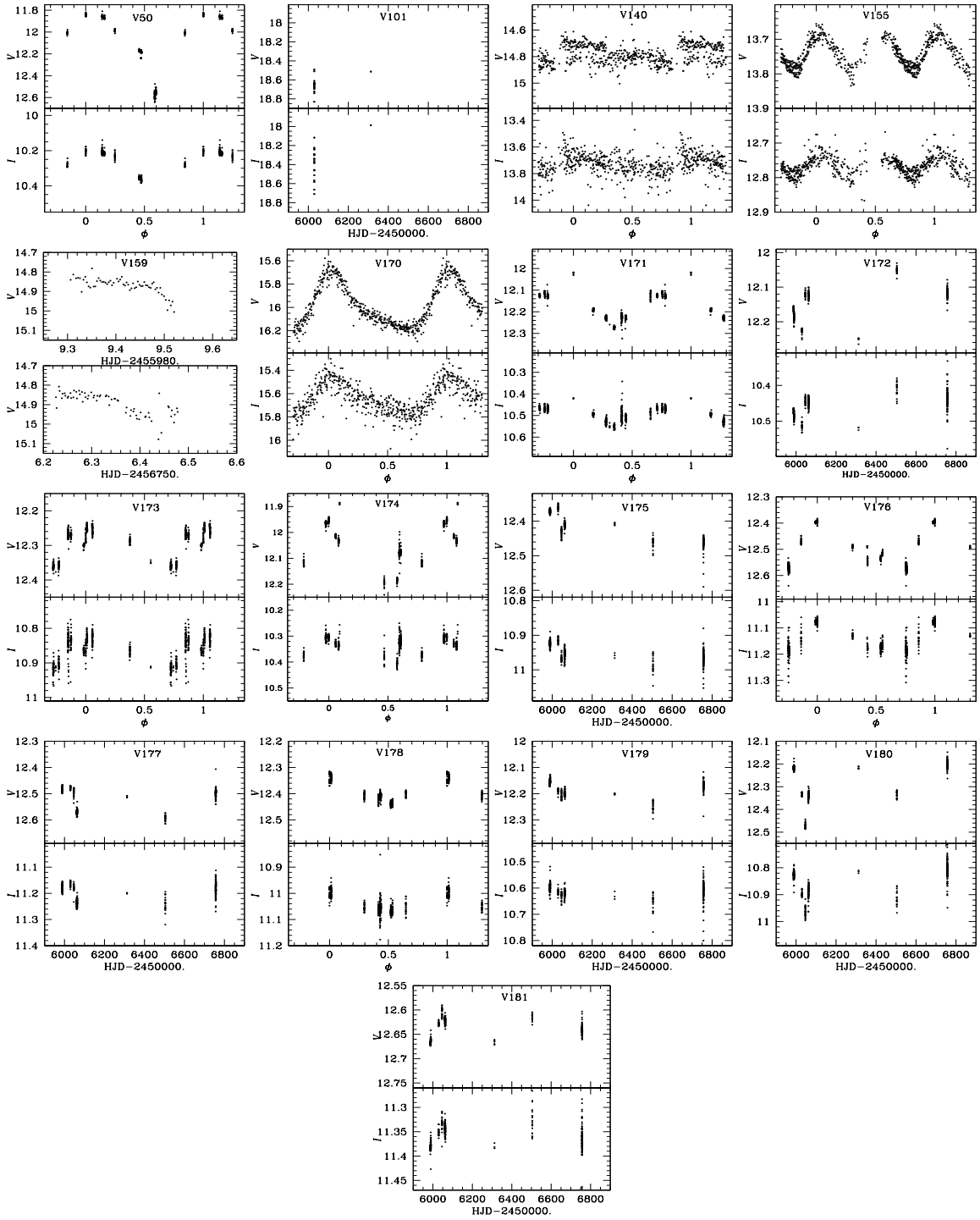

Figure 3. V and I light curves of the variable stars found in this work (V170-V181). V50, V101, V140, V155 and V159 are discussed in the text. For V101 only the data during outburst are displayed. For V159 the two panels are V light curves during eclipses. When the period is known, light curves are phased with the ephemerides in Table 4.

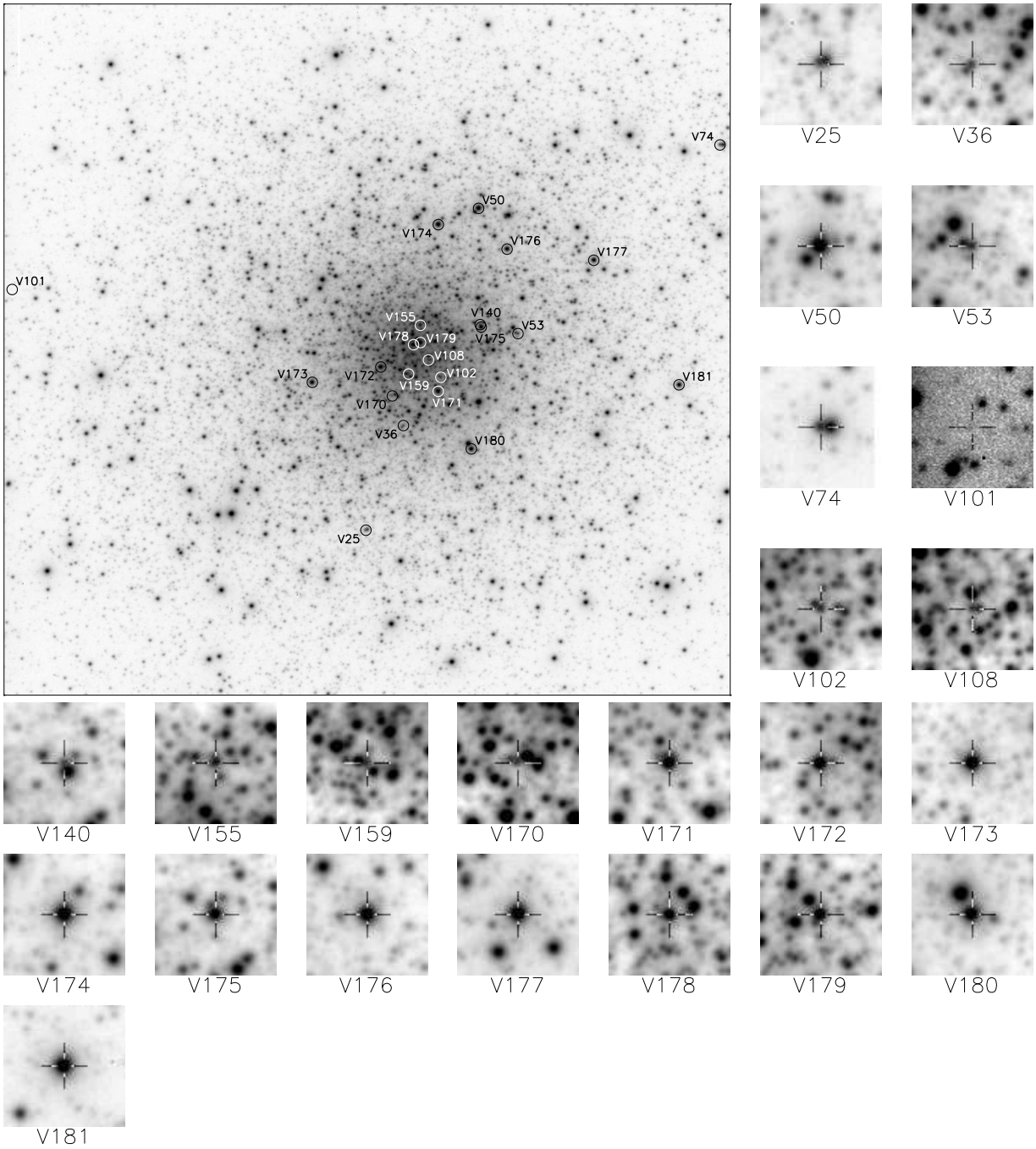

Figure 4. Finding charts from our V reference image; North is up and east is to the right. The cluster image is 8.39 × 8.39 arcmin^2 and the individual stamps are 24.0 × 24.0 arcsec^2.

Bramich, D. M., Figuera Jaimes R., Giridhar S., Arellano Ferro A., 2011, *MNRAS*, **413**, 1275

Bramich D. M., Freudling W., 2012, *MNRAS*, **424**, 1584

Bramich, D.M., Horne, K., Albrow, M.D., Tsapras, Y., Snodgrass, C., Street, R.A., Hundertmark, M., Kains, N., Arellano Ferro, A., Figuera Jaimes, R. & Giridhar, S., 2013, *MNRAS*, **428**, 2275

Caputo, F., Castellani, V., Marconi, M., Ripepi, V. 1999, *MNRAS*, **306**, 815

Clement, C.M., Muzzin, A., Dufton, Q., Ponnampalam, T., Wang, J., Burford, J., Richardson, A., Rosebery, T., Rowe, J., Sawyer-Hogg, H., 2001, *AJ*, **122**, 2587

Drissen, L., Shara, M. M. 1998, *AJ*, **115**, 725

Gerashchenko, A. 1987, *IBVS*, 3044

Kadla, Z. I., Gerashchenko, A. N., Yablokova, N. V., Irkaev, B. N. 1987, *Astr. Tsirk.*, **1502**, 7

Kaluzny, J., Thompson, I., Krzeminski, W., Pych, W. 1999, *A&A*, **350**, 469

Oosterhoff, P. Th. 1941, *Leiden Ann.*, **17**, Part 4

Pickering, E.C., 1896, *AN*, **140**, 285

Stetson, P.B., 2000, *PASP*, **112**, 925

COMMISSIONS 27 AND 42 OF THE IAU
INFORMATION BULLETIN ON VARIABLE STARS

Number 6138

Konkoly Observatory
Budapest
16 April 2015

HU ISSN 0374 – 0676

CALL FOR FOLLOW-UP OBSERVATIONS OF THE DYNAMICALLY CHANGING TRIPLE STAR KIC 2835289

CONROY, K.[1,2]; PRŠA, A.[2]; STASSUN, K.[1]; OROSZ, J.[3]

[1] Vanderbilt University, Department of Physics and Astronomy, Nashville, TN 37235, USA, email: aprsa@villanova.edu

[2] Villanova University, Dept. of Astrophysics and Planetary Science, Villanova PA 19085, USA

[3] San Diego State University, Department of Astronomy, San Diego, CA 92182, USA

KIC 2835289 (2MASS J19072623+3801389; $\alpha_{2000} = 19^{\rm h}07^{\rm m}26\overset{\rm s}{.}231$, $\delta_{2000} = +38°01'38\overset{''}{.}92$) is a V∼13 ellipsoidal variable with an orbital period of ∼0.86 days, observed by the *Kepler* mission (Borucki et al. 2010) and cataloged in the *Kepler* Eclipsing Binary Catalog (Prša et al. 2011, `http://keplerEBs.villanova.edu`). *Kepler* observations are available in long cadence (30-min exposure times) for all 17 quarters spanning 4 years, and in short cadence (1-min exposure times) for Quarter 17. It is incorrectly classified in the *Simbad* database as an overcontact binary of the W UMa type.

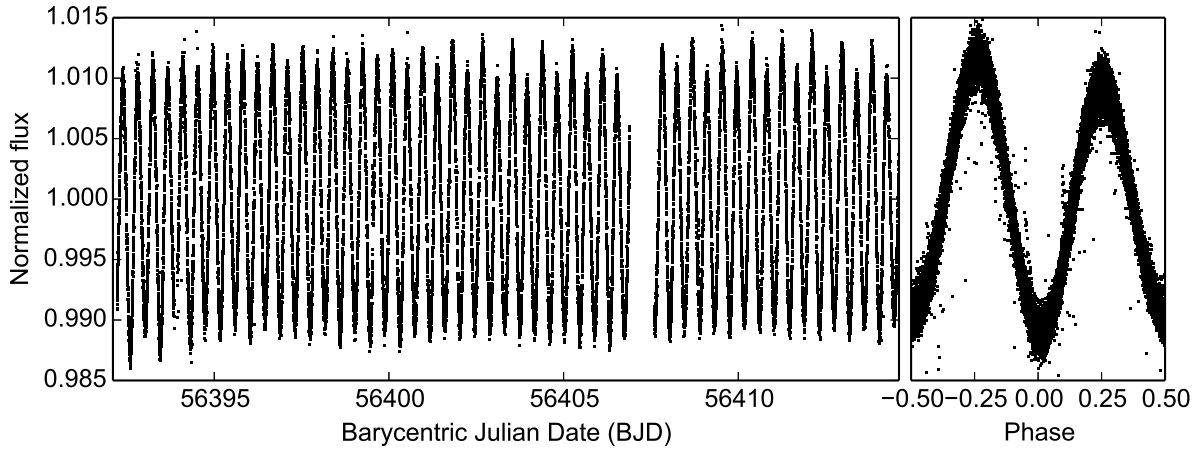

Figure 1. *Kepler* light curve of KIC 2835289 in time (left) and phase (right). Chromospheric activity complicates the modeling of this ellipsoidal variable, but with 4 years of uninterrupted data, the intrinsic ellipsoidal signal can be extracted to a high precision.

Two features make this binary star interesting: strong chromospheric activity and the presence of a third stellar component. Fig. 1 depicts a light curve segment from Quarter 17 in time (left) and phase (right), where the "smear" in the phased light curve is a consequence of chromospheric activity. Spots account for the time-varying O'Connell effect –

asymmetric light curve maxima – that are clearly evident in the data, and interesting in their own right. The remarkable feature of this system, however, is the detection of two eclipse events in quarters Q9 and Q17 (cf. Fig. 2) separated by ∼750 days, attesting to the presence of the third stellar component in this system. We also measured the timings of ellipsoidal minima (akin to eclipse timing variations in eclipsing binary systems; Conroy et al. 2014) and found clear evidence of a moderately eccentric outer orbit (Fig. 3). This circumstance is particularly appealing for further study, since it directly tests the Kozai-Lidov model of close binary evolution. According to the model, three-body systems with eccentric outer orbits undergo oscillations in inner eccentricity and mutual inclination angle (Fabrycky & Tremaine 2007). While in a state of higher inner eccentricity, tidal friction at periastron increases and circularization ensues (Kiseleva et al. 1998). In consequence, the inner binary is tightened while the outer star settles into a wide, eccentric, inclined orbit, much like KIC 2835289.

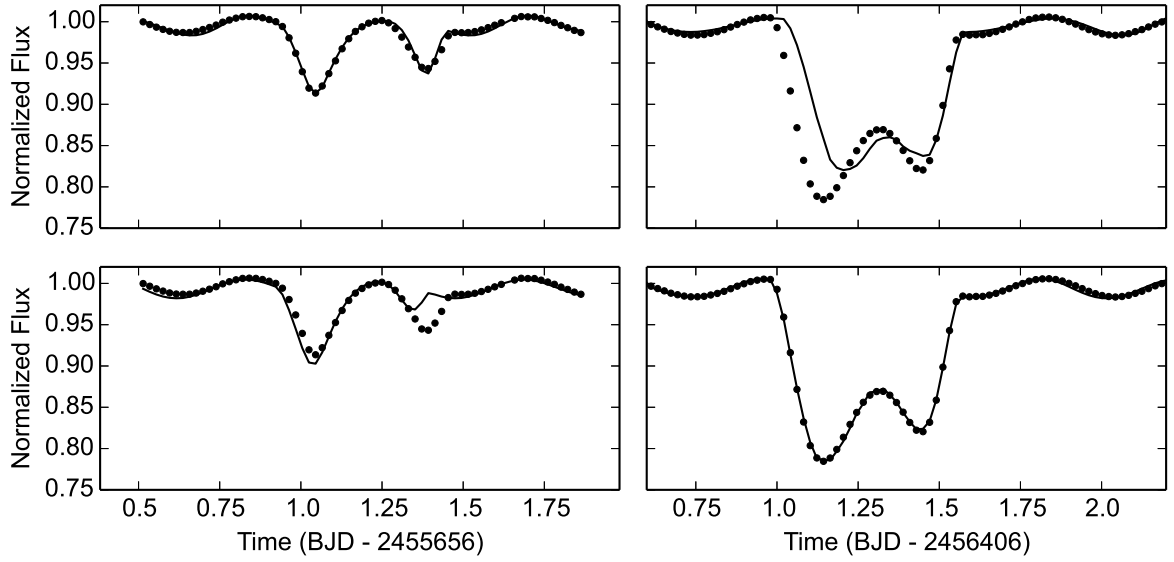

Figure 2. Eclipse events in *Kepler* Quarters 9 (left) and 17 (right). Filled circles are long cadence observations and solid lines are model fits. No single model was found to fit both eclipse events, but allowing the inner eccentricity and mutual inclination to vary, a family of solutions was found that can describe observations. The model fit to Q9 data is plotted in the top panels, and the model fit to Q17 data is plotted in the bottom panels.

An ongoing detailed photodynamical analysis (Conroy et al. 2015, in preparation) using a new version of the PHOEBE code (Prša & Zwitter 2005, Conroy et al. 2013) provided a uniquely interesting first look into the dynamics in this system. While quite a few triple systems have been successfully modeled recently based on the dynamical effects in timing variations (cf. Borkovits et al. 2015, who analyzed mutual inclinations of 26 triple stars in the *Kepler* data-set), the near-circular nature of the tight inner binary in this system excluded it from their analysis. We ran the photodynamical model in PHOEBE and found that there seems to be no consistent set of orbital and physical parameters that would successfully describe *both* eclipse events. However, by allowing the inner eccentricity and mutual inclination to vary slightly, a family of plausible solutions can be obtained. Thus,

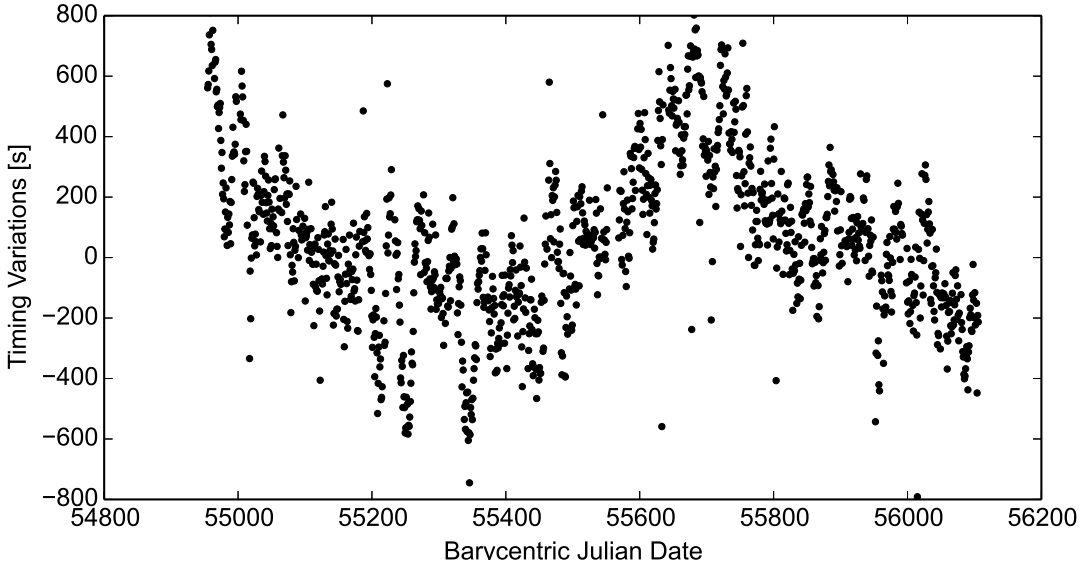

Figure 3. Timings of ellipsoidal minima. The dominant trend is the light time travel effect due to third body interaction. Chromospheric activity causes secular variations.

if these preliminary results are confirmed, we may be seeing a case of Kozai cycles with tidal friction in action. Two eclipse events, unfortunately, are not enough to break the degeneracy between possible solutions and fully determine the extent of dynamics in the system.

From the measured period of the outer orbit, the timings of the two observed tertiary events and the photodynamical model, we can calculate the times of past eclipse events and predict the times of future eclipse events. The eclipse preceding the Q9 event should have occurred shortly before the beginning of the *Kepler* mission (centered around BJD 2454907.25). The next event is expected to occur on May 14, 2015, motivating this brief communication. By observing this and other future events, we will be able to further constrain the model and determine the exact degree and nature of the tentative dynamical effects in the system.

Our preliminary photodynamical models that fit each observed eclipse are depicted by a solid line in Fig. 2. By extrapolating both models to the time of the next eclipse event, we can obtain a reasonable estimate of the duration and shape of the upcoming event (Fig. 4). The exact times of ingress and egress, as well as the shape of the event, depend on the exact nature of these dynamical effects. It is thus important to observe the entire event so that a comprehensive model can be fully constrained.

The next event is expected to occur on May 14, from Barycentric Julian Date 2457157.1 to 2457157.9. The amplitude of ellipsoidal variability is ∼2% while the depth of the triple eclipse event is predicted to ∼5-10%. Photometric follow up effort is being organized; Table 1 lists the time spans of several upcoming events and we solicit help from the community in observing them via this communication. For further coordination of this effort please contact the authors.

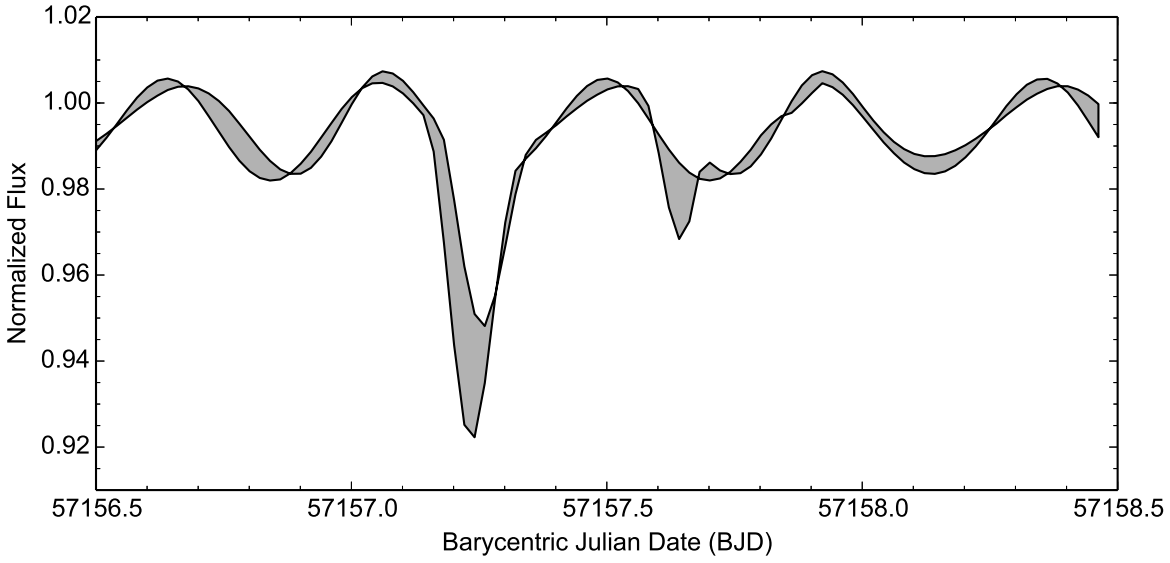

Figure 4. Light curve of the upcoming event. Solid lines depict predictions of the best-fit models to the Q9 eclipse event and the Q17 eclipse event. The shaded region represents the uncertainty of the prediction. This event is expected to occur on May 14: BJD 2457157.1–2457157.9.

Start Date (UTC)	BJD Start	BJD End
May 14, 2015	2457157.1	2457157.9
June 2, 2017	2457907.2	2457908.3
June 23, 2019	2458657.5	2458658.5
July 12, 2021	2459407.5	2459408.5
August 1, 2023	2460157.8	2460158.6

Table 1: Predicted earliest times of ingress and latest times of egress for the next several triple eclipse events by extending both the model to the Kepler Q9 and Q17 events.

References:

Borkovits, T., Rappaport, S., Hajdu, T., & Sztakovics, J., 2015, *MNRAS*, **448**, 946
Borucki, W.J., et al., 2010, *Science*, **327**, 977
Conroy, K., et al., 2013, *EAS*, **64**, 295
Conroy, K., et al., 2014, *AJ*, **147**, 45
Fabrycky, D., & Tremaine, S., 2007, *ApJ*, **669**, 1298
Kiseleva, L., Eggleton, P.P., & Mikkola, S., 1998, *MNRAS*, **300**, 292
Prša, A., & Zwitter, T., 2005, *ApJ*, **628**, 426
Prša, A., et al., 2011, *AJ*, **141**, 83

COMMISSIONS 27 AND 42 OF THE IAU
INFORMATION BULLETIN ON VARIABLE STARS

Number 6139

Konkoly Observatory
Budapest
18 April 2015

HU ISSN 0374 – 0676

PHOTOMETRIC EVOLUTION AND PECULIAR DUST FORMATION IN THE GAMMA-RAY NOVA Sco 2012 (V1324 Sco)

MUNARI, U.[1]; WALTER, F. M.[2]; HENDEN, A.[3]; DALLAPORTA, S.[4]; FINZELL, T.[5]; CHOMIUK, L.[5]

[1] INAF Osservatorio Astronomico di Padova, Sede di Asiago, I-36032 Asiago (VI), Italy

[2] Dept. of Physics and Astronomy, Stony Brook University, Stony Brook, NY 11794-3800, USA

[3] AAVSO, 49 Bay State Rd. Cambridge, MA 02138, USA

[4] ANS Collaboration, c/o Astronomical Observatory, 36012 Asiago (VI), Italy

[5] Dept. of Physics and Astronomy, Michigan State Univ., 567 Wilson Road, East Lansing, MI 48824-2320, USA

Nova Sco 2012 was discovered on 2012 May 22.80 UT by Wagner et al. (2012) as the optical transient MOA 2012 BLG-320 during the Microlensing Observations in Astrophysics (MOA) survey (Abe et al. 1997). It appeared at equatorial coordinates RA = 17:50:53.90 and DEC = −32:37:20.46 (J2000), corresponding to Galactic coordinates l=357.4255 and b=−02.8723 deg, and has no obvious counterpart on DSS plates. Pre-outburst MOA photometry reported by Wagner et al. (2012) shows the progenitor varying around 19.0-19.5 mag in I band. Between May 14 and 16 UT, the source began a slow monotonic increase in brightness, modulated with an amplitude of about 0.1 mag and a period of about 1.6 hr, with the real outburst starting between June 1.77 and 2.55 UT. High-resolution spectroscopy obtained on June 4.08 UT by Wagner et al. (2012) with the ESO-VLT+UVES telescope confirmed the transient to be an FeII-class nova, with a FWHM∼800 km/s for the Hα and Hβ lines.

The Fermi/LAT satellite detected γ-ray emission at >100 MeV from Nova Sco 2012 from June 16 to June 30, with the highest flux during June 18-24 (Cheung et al. 2012, Metzger et al. 2015). Only a very few other novae have been so far detected in γ-rays (Ackermann et al. 2014).

No description of the optical and infrared photometric evolution of Nova Sco 2012 has been provided to date. In this paper we present $BVR_{\rm c}I_{\rm c}JHK$ photometry of Nova Sco 2012 and discuss its light curve covering the evolution from pre-maximum to day +34 past optical maximum, when the nova had declined by more than 5 magnitudes below V maximum, plus some later B, V data. Our photometry is given in Tables 1 and 2. It was collected with ANS Collaboration telescope 036 (Munari et al. 2012), during the APASS all-sky survey (Henden et al. 2012), with AAVSOnet OC61 telescope (Mt. John University Observatory, NZ), and with the CTIO SMARTS 1.3 m telescope (Walter et al. 2012). The light and color-curves of Nova Sco 2012 are presented in Figure 1, with pre-maximum data from Wagner et al. (2012) and observations retrieved from VSNET and AAVSO international databases included. The AAVSO data are presented as the mean nightly value for a single observer when multiple entries are present. AAVSO and VSNET data have had obviously deviating points removed, and offsets have been applied to bring

their zero points to agree with ANS, APASS and SMARTS properly calibrated data (0.15, −0.05 and −0.17 mag have been added to VSNET B, V and R_c data, respectively, and 0.05 mag to AAVSO B data). At 8 arcsec distance from the nova lies a field star, measured by APASS at B=16.23, V=15.32, g'=15.69, r'=14.95, i'=13.05.

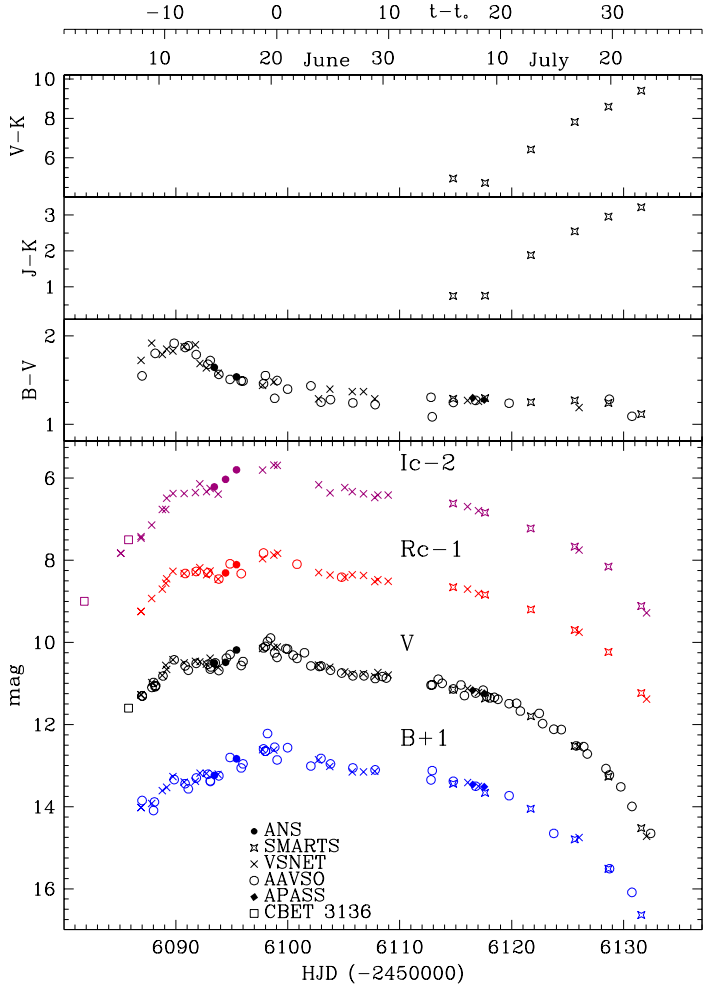

Figure 1. BVR_cI_c light curves and $B-V$, $J-K$ and $V-K$ evolution of Nova Sco 2012.

The rise of Nova Sco 2012 toward maximum in the I_c band covered the last 2.65 mag before the pre-max halt at a constant speed of 0.33 mag/day. The pre-max halt in Figure 1 is obvious in V, R_c and I_c and lasted ∼3 days (from day −9 to −6), after which the final ∼0.5 mag rise to maximum was completed in ∼6 days with superimposed large variability. The presence of the pre-max halt is much less obvious in B band.

The initial decline from maximum of Nova Sco 2012 was smooth and slow, with decline times of t_1^B=19, t_1^V=17 days, and a decline slope suggesting t_2^V ≈40 days (t_n is the time required to decline from maximum by n magnitudes in the given band). Initial JHK photometry (cf Figure 1, data points for days +16 and +19) is consistent with normal photospheric emission under heavy interstellar reddening. Around day +20, dust begun to form in the ejecta, which caused a rapid and large increase in $J-K$ and $V-K$ color indexes and a parallel drop in optical brightness. It is worth noticing that, as observed in many novae (e.g. Nova Aql 1993 by Munari et al. 1994; Nova Sct 2009 by Raj et al. 2012; Nova Cep 2013 by Munari et al. 2014), the dust condensation did not cause a reddening

Table 1: Optical photometry of Nova Sco 2012.

HJD	id	B	±	V	±	R_c	±	I_c	±
6093.438	ANS	12.239	0.013	10.501	0.006	8.213	0.008		
6094.438	ANS	10.483	0.004	9.306	0.008	8.028	0.014		
6095.419	ANS	11.833	0.017	10.184	0.006	9.105	0.008	7.795	0.014
6114.775	SMARTS	12.438	0.002	11.148	0.002	9.656	0.001	8.617	0.001
6116.511	APASS	12.464	0.004	11.164	0.002				
6117.547	APASS	12.515	0.004	11.236	0.002				
6117.628	SMARTS	12.661	0.002	11.365	0.002	9.840	0.001	8.840	0.001
6121.709	SMARTS	13.051	0.003	11.799	0.003	10.199	0.001	9.222	0.001
6125.640	SMARTS	13.794	0.004	12.523	0.004	10.698	0.002	9.665	0.001
6128.646	SMARTS	14.512	0.006	13.270	0.006	11.234	0.002	10.153	0.001
6131.584	SMARTS	15.638	0.012	14.523	0.011	12.231	0.004	11.115	0.002
6384.034	OC61	16.842	0.020						
6389.128	OC61	18.428	0.021	16.829	0.015				
6396.004	OC61	18.424	0.026	16.883	0.020				

of optical colors of Nova Sco 2012 (cf Figure 1). The fact that the wavelength-dependent absorption efficiency of the dust turned from neutral to selective at $\lambda \geq$6000 Å suggests a prevalent carbon composition with a diameter of dust grains of the order of 0.1 μm (Draine and Lee 1984; Kolotilov et al. 1996). In many novae forming dust, the dust condensation starts quite suddenly causing a marked knee in the light curve (cf the recent case of Nova Cep 2013, Munari et al. 2014). Such a knee is absent in the light curve of Nova Sco 2012 and substituted by a gradual *acceleration* of the extinction, suggesting a more gradual condensation of the dust grains. Nova Sco 2012 differs from many other dust condensing novae in two other respects: (1) dust formation usually occurs at the time of the transition from optically thick to optically thin ejecta, about 3-4 mag below maximum brightness, which led Shore and Gehrz (2004) to suggest that it is the photo-ionization from the central star that triggers dust grain condensation in the ejecta. In Nova Sco 2012, dust begun to condense at a much earlier phase, only 1 mag below maximum; (2) the slower a nova, the later dust begins to condense, as illustrated by the compilation of data for M31 and Galactic novae of Shafter et al. (2011). Their relation, applied to the predicted t_2^V ≈40 days for Nova Sco 2012, indicates that dust should have begun to condense ∼60 days past maximum (±10 days given the dispersion of the plotted data) and ∼60 days is also estimated from the theoretical modeling presented by Williams et al. (2013). Such a ∼60 day delay is much longer than the observed 20 days for Nova Sco 2012. The dust extinction caused the V magnitude of Nova Sco 2012 to drop below 19-20 mag (SMARTS and AAVSO data). When we re-observed the nova in April 2013 (day +285, see Table 1) the nova had rebrightened to V=16.8 and recovered the normal brightness decline, meaning the dust extinction had already cleared.

According to van den Bergh and Younger (1987), typical novae display $(B-V)_\circ = +0.23$ at B, V maximum brightness and $(B-V)_\circ = -0.02$ at t_2. The corresponding values for Nova Sco 2012 were $B-V$=+1.44 and $B-V$=+1.23 (from spline interpolation of the data in Figure 1), that provide E_{B-V}=1.21 and 1.25, respectively. The average E_{B-V}=1.23 is in excellent agreement with the E_{B-V}=1.23 derived by Finzell et al. (2015) from the intensity of interstellar NaI and KI in high resolution spectra of Nova Sco 2012. The corresponding extinction is A_V=4.18 mag from Fiorucci and Munari (2003) relations appropriate for the intrinsic colors of the nova and standard R_V=3.1 extinction law.

Table 2: SMARTS infrared photometry of Nova Sco 2012.

HJD	J	$\pm$	H	$\pm$	K	$\pm$
6114.773	6.942	0.006	6.637	0.004	6.193	0.005
6117.626	7.392	0.006	6.837	0.004	6.635	0.004
6121.707	7.252	0.006	6.380	0.003	5.370	0.003
6125.638	7.243	0.006	5.903	0.003	4.700	0.002
6128.644	7.635	0.007	5.960	0.003	4.675	0.002
6131.583	8.326	0.009	6.347	0.003	5.110	0.002

Nova Sco 2012 reached a maximum brightness of B=11.60, V=10.14, $R_{\rm c}$ = 8.85 and $I_{\rm c}$ = 7.68 around JD=2456099.0 ($\pm$0.5), 2012 June 20.5 UT, and the observed decline times were t_2^B=26, t_2^V=25, t_3^B=30.5, t_3^V=29.5, with t_3 times too short with respect to t_2 because of the undergoing extinction by dust condensing in the ejecta. These decline times are a popular means to estimate the distance to a nova. The most recent calibration of the absolute magnitude at maximum versus rate of decline (MMRD) relation has been presented by Downes and Duerbeck (2000). The distance to Nova Sco 2012, with the A_V=4.18 mag extinction, is 5.5 kpc for t_2^V=25 and the linear MMRD and 5.3 kpc for the S-shaped MMRD. For t_3^V=29.5, the linear MMRD yields 6.9 kpc. The large discrepancy of the distances estimated from t_2^V and t_3^V is a sign of the disturbance from the condensing dust. Considering t_2^V $\approx$40 days, estimated above as a feasible value in absence of condensing dust, the corresponding distance to Nova Sco 2012 would be 4.3 kpc from linear MMRD and 3.7 kpc from S-shaped MMRD.

References:

Abe, F., et al. 1997, in *"Variable Stars and the Astrophysical Returns of the Microlensing Surveys"*, R. Ferlet, J.-P. Maillard and B. Raban eds., Editions Frontieres, p.75
Ackermann, M., et al., 2014, *Science*, **345**, 554
Cheung, C. C., et al., 2012, *ATel*, **4310**
Downes, R. A., Duerbeck, H. W., 2000, *AJ*, **120**, 2007
Draine B. T., Lee H. M., 1984, *ApJ*, **285**, 89
Finzell, T., et al., 2015, in preparation
Fiorucci, M., Munari, U., 2003, *A&A*, **401**, 781
Henden, A. A., et al., 2012, *JAAVSO*, **40**, 430
Kolotilov E. A., et al., 1996, *ARep.*, **40**, 81
Metzger, B. D., et al., 2015, *MNRAS*, in press (arXiv 1501.05308)
Munari, U., et al., 1994, *A&A*, **284**, L9
Munari, U., et al., 2012, *BaltA*, **21**, 13
Munari, U., et al., 2014, *MNRAS*, **440**, 3402
Raj, A. et al., 2012, *MNRAS*, **425**, 2576
Shafter, A. W., et al., 2011, *ApJ*, **727**, 50
Shore, S. N., Gehrz, R. D., 2004, *A&A*, **417**, 695
van den Bergh S., Younger P. F., 1987, *A&AS*, **70**, 125
Wagner, R. M., et al., 2012, *CBET*, **3136**
Walter F. M., et al., 2012, *PASP*, **124**, 1057
Williams, S. C., et al., 2013, *ApJL*, **777**, L32

COMMISSIONS 27 AND 42 OF THE IAU
INFORMATION BULLETIN ON VARIABLE STARS

Number 6140

Konkoly Observatory
Budapest
20 April 2015

HU ISSN 0374 – 0676

PSN J07285387+3349106 IN NGC 2388: AN EXTREMELY RAPIDLY DECLINING LUMINOUS SUPERNOVA

TSVETKOV, D. YU.; VOLKOV, I. M.; PAVLYUK, N. N.

Sternberg Astronomical Institute, M.V. Lomonosov Moscow State University, Universitetskij pr.13, 119992 Moscow, Russia, e-mail: tsvetkov@sai.msu.su

Supernova in NGC 2388 was discovered by Lick Observatory Supernova Search (LOSS) on 2015 February 13.338 UT at an unfiltered magnitude of 16.9. The variable was designated PSN J07285387+3349106 when it was posted at the Central Bureau's TOCP webpage. The new object was located at RA=7:28:53.87, DEC=+33:49:10.6 (2000), which is 5″E and 2″N from the center of the host galaxy. Spectroscopic observation on 2015 February 18.79 UT was reported by Ochner et al. (2015). The spectrum was almost featureless, with strong interstellar Na I D absorption, which allowed to estimate a reddening value of $E(B-V) \approx 1$ mag. Unresolved emission lines of He I (587.6 and 706.5 nm) were detected, and a black-body temperature of about 15300 K was inferred for the transient. The characteristics were consistent with those of a very young core-collapse SN, and a tentative classification as Type Ibn SN was suggested for the object.

We performed photometric observations of PSN J07285387+3349106 in the $BVRI$ bands with the 0.7-m reflector in Moscow (M70), equipped with Apogee AP-7p CCD camera, and the 1.0-m reflector of Simeiz Observatory (S100) with FLI PL09000 CCD. First images were obtained on February 17, and the last ones were collected on March 17, 2015. The standard image reductions and photometry were made using IRAF[1]. Photometric measurements of the SNe were made relative to 6 nearby local standard stars using PSF-fitting with IRAF DAOPHOT package. The BV and $g'r'i'$ magnitudes of these stars were taken from the AAVSO Photometric All-Sky Survey (Henden et al., 2012; hereafter, APASS). The RI magnitudes were computed using relations presented by Munari[2]. Besides, on one photometric night we calibrated VR magnitudes of the local standards using data from the M70 telescope. The agreement between the APASS data and our calibration was excellent, confirming the reliability of the calibration. Subtraction of the host galaxy background was necessary for reliable photometry, because the SN occurred in one of the spiral arms of the galaxy and close to the nucleus. As the SN was practically undetectable in the images obtained on March 17, we used these frames to subtract the galaxy background from the images collected in February, when the SN was bright. For the images obtained in March we used the SDSS[3] images for subtraction. We plan to obtain new deep images of the host galaxy with our telescopes and improve the quality

[1]IRAF is distributed by the National Optical Astronomy Observatory, which is operated by AURA under cooperative agreement with the National Science Foundation

[2]https://1337870331699155271 5.googlegroups.com/

[3]http://www.sdss.org

of subtraction. The instrumental magnitudes were transformed to the standard Johnson-Cousins system using linear colour equations. The photometry for the SN is presented in Table 1, the light curves are shown in Fig. 1.

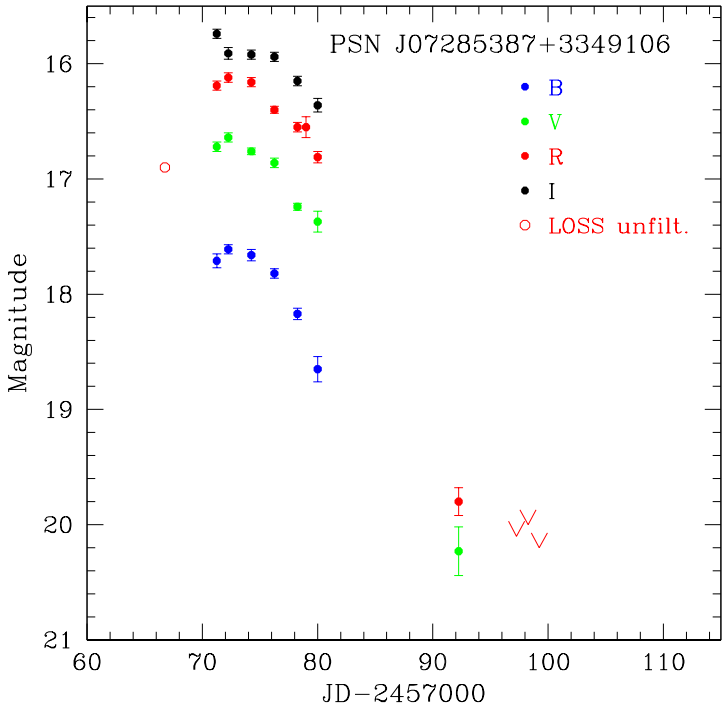

Figure 1. The $BVRI$ light curves for PSN J07285387+3349106.

The maximum light in the BVR bands was reached at about JD 2457072-73 (February 18-19), and perhaps some days earlier in the I band. The magnitudes at maximum are $B_{\max} = 17.6$, $V_{\max} = 16.65$, $R_{\max} = 16.15$, with about ± 0.1 mag uncertainty . The red colour of $(B - V) \approx 1$ mag at maximum confirms the high value of interstellar reddening reported by Ochner et al. (2015). For the first week past maximum the brightness declined quite slowly, but then a very fast decline occurred. We can approximately estimate the values of brightness decline for the first 15 days after peak (Δm_{15}), which are usually used to describe the rate of photometric evolution for SNe Ia and SNe of other types with similar light curve shapes: $\Delta m_{15}(V) \approx 2.6$, $\Delta m_{15}(R) \approx 2.5$. Such high values were observed only for three among all well-studied SNe: SN 2002bj (Type Ib)(Poznanski et al., 2010), 2005ek (Ic)(Drout et al., 2013) and 2010X (Ic-pec)(Kasliwal et al., 2010).

Fig. 2 presents comparison of the R-band light curve of PSN J07285387+3349106 with the light curves for the three fastest declining SNe listed above and also with the type Ibn SN 2010al (Pastorello et al., 2015), and one of the fastest decliners among SNe Ic SN 1994I (Richmond et al., 1996). The left panel compares the shape of the light curves which are normalized to the peak. It is shown that the R-band light curve of PSN J07285387+3349106 near maximum is matched by that for SNe 1994I, 2002bj and 2010X, while SN 2005ek has sharper peak, and for SN 2010al the peak is much broader. The fast decline after the peak is similar for SNe 2002bj, 2005ek, 2010X and PSN J07285387+3349106.

The right panel shows the absolute magnitude light curves. We accepted the following

Table 1: *BVRI* photometry of PSN J07285387+3349106

JD − 2457000	B	σ_B	V	σ_V	R	σ_R	I	σ_I	Telescope
71.22	17.71	0.06	16.72	0.04	16.19	0.04	15.74	0.04	M70
72.31	17.61	0.04	16.64	0.04	16.12	0.04	15.91	0.05	S100
74.31	17.66	0.05	16.76	0.03	16.16	0.04	15.92	0.04	S100
76.39	17.82	0.04	16.86	0.04	16.40	0.03	15.94	0.04	S100
78.28	18.17	0.05	17.24	0.03	16.55	0.04	16.15	0.04	S100
79.15					16.55	0.09			M70
80.16	18.65	0.11	17.37	0.09	16.81	0.05	16.36	0.06	M70
92.22			20.23	0.21	19.80	0.12			M70
97.27					>20.1				M70
98.26					>20.0				M70
99.24					>20.2				M70

values of distance moduli and total extinction A_R for the SNe used for comparison: SN 1994I: 29.62, 1.05; SN 2002bj: 33.48, 0.2; SN 2005ek: 34.12, 0.44; SN 2010X: 34.0, 0.4; SN 2010al: 34.27, 0.15. For PSN J07285387+3349106 we adopted a distance modulus of $\mu = 33.84 \pm 0.15$ from the NED database, which is calculated from the redshift of the galaxy, corrected for Virgo and Great Attractor infall, with $H_0 = 73$ km/sec/Mpc. We adopted Galactic extinction $A_R = 0.13$ (Schlafly & Finkbeiner, 2011) and the host galaxy interstellar reddening $E(B-V) = 1$ mag from Ochner et al. (2015). To calculate absolute magnitudes we need the value of $R_V = A_V/E(B-V)$. It is well known that for SNe R_V may differ from the standard Galactic value of 3.1, and can be as low as ~ 1.5, especially for SNe with high $E(B-V)$ (see e.g. Tsvetkov et al., 2014; Wang et al., 2008). So we calculated absolute magnitudes using two values of R_V: 3.1 and 1.5. It is difficult to estimate uncertainty of the data on the host galaxy extinction, as Ochner et al. (2015) does not provide such information. Assuming this uncertainty to be about 10%, and adding in quadratures the errors of distance modulus (± 0.15) and peak magnitude (± 0.1) we derive uncertainty of absolute magnitude ~ 0.3 mag. The right panel plot demonstrates that with $R_V = 3.1$ PSN J07285387+3349106 reaches peak magnitude of $M_R = -20.15$ mag and is definitely much brighter than all other SNe of our sample. If $R_V = 1.5$, than the maximum luminosity of PSN J07285387+3349106 $M_R = -18.8$ mag is close to that for SNe 2010al and 2002bj, it is higher than for SN 1994I by about 0.8 mag, and exceeds that for SNe 2005ek and 2010X by about 1.8 mag.

We conclude that PSN J07285387+3349106 belongs to a rare class of extremely fast declining SNe and is similar to SNe 2002bj, 2005ek and 2010X regarding the shape of the light curves. The estimate of the peak luminosity for a heavily reddened SN depends strongly on the presently unknown value of R_V. We show that even if R_V is close to the minimal observed value, PSN J07285387+3349106 still belongs to the brightest objects among SNe of similar classes.

PSN J07285387+3349106 may represent an extreme case of fast declining SNe, combining very fast decay and high maximum luminosity. Unfortunately, it is now too faint for our instruments, and we want to attract attention of all interested observers to this object. We should note that for SNe 2002bj, 2005ek and 2010X there are practically no data on the radioactive tail of the light curve. PSN J07285387+3349106 presents the opportunity to obtain such data for the first time for a SN of this class. Observations at largest telescopes are needed to help reveal the nature of this object and for all class of

fast declining SNe.

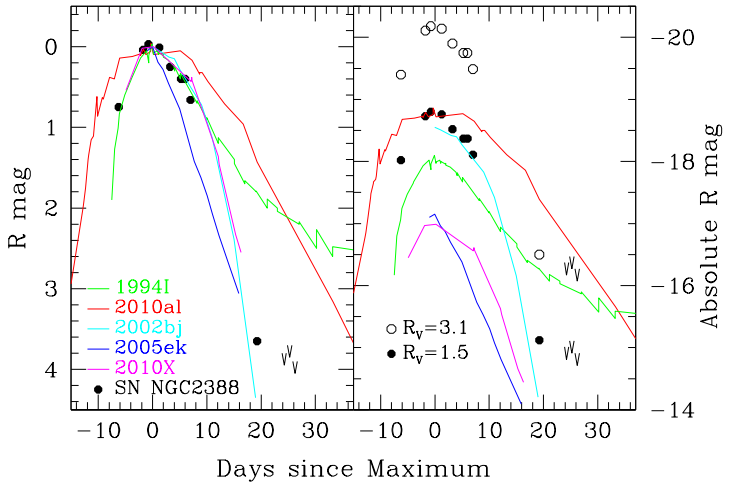

Figure 2. Comparison of the *R*-band light curves for PSN J07285387+3349106 with those for 5 SNe.

Acknowledgements: This research has made use of the APASS database, located at the AAVSO web site. Funding for APASS has been provided by the Robert Martin Ayers Sciences Fund. This research has made use of the NASA/IPAC Extragalactic Database (NED) which is operated by the Jet Propulsion Laboratory, California Institute of Technology, under contract with NASA. We are grateful to the anonymous referee for important suggestions and comments.

References:

Drout, M. R., Soderberg, A. M., Mazzali, P. A., et al., 2013, *ApJ*, **774**, 58
Henden, A. A., Levine, S. E., Terrell, D., Smith, T. C. & Welch, D., 2012, *J. AAVSO*, **40**, 430
Kasliwal, M. M., Kulkarni, S. R., Gal-Yam, A., et al., 2010, *ApJ*, **723**, L98
Ochner, P., Benetti, S., Pastorello, A., et al., 2015, *ATel*, **7105**
Pastorello, A., Benetti, S., Brown, P. J., et al., 2015, *MNRAS*, **449**, 1921
Poznanski, D., Chornock, R., Nugent, P. E., et al., 2010, *Science*, **327**, 58
Richmond, M. W., VanDyk, S. D., Ho, W., et al., 1996, *AJ*, **111**, 327
Schlafly, E. F. & Finkbeiner, D. P., 2011, *ApJ*, **737**, 103
Tsvetkov, D. Yu., Metlov, V. G., Shugarov, S. Yu., Tarasova, T. N., & Pavlyuk, N. N., 2014, *CoSka*, **44**, 67
Wang, X., Li, W., Filippenko, A.V., et al., 2008, *ApJ*, **675**, 626

COMMISSIONS 27 AND 42 OF THE IAU
INFORMATION BULLETIN ON VARIABLE STARS

Number 6141

Konkoly Observatory
Budapest
22 April 2015

HU ISSN 0374 – 0676

NEW RESULTS ON SPECTRAL AND PHOTOMETRIC VARIABILITY OF V806 CASSIOPEIAE

KONDRATYEVA, L.; RSPAEV, F.; AIMURATOV, E.

Fessenkov Astrophysical Institute, Almaty, Kazakhstan. e-mail: kondr.lud@gmail.com; lu_kondr@mail.ru

V806 Cas = HD 236071 = MWC 1076 is a star with emission lines. For the first time its spectrum was described by Merrill et al. (1948) and Burbidge & Burbidge (1954). On the slit spectrograms, obtained in 1948, H I lines were observed in emission, and lines of He I in absorption (Merrill et al., 1948). Later the object has been included in some catalogues of eclipsing variable stars (Kohoutek & Wehmeyer, 1999, Malkov et al., 2006, Avvakumova et al., 2013). The information on its brightness is quite limited: $V = 8\overset{\mathrm{m}}{.}7$ (Merrill et al., 1948), $B = 8\overset{\mathrm{m}}{.}99$; $B - V = +0\overset{\mathrm{m}}{.}25$ (Haupt & Schroll, 1974), $V_{\max} = 9\overset{\mathrm{m}}{.}0$; $V_{\min} = 9\overset{\mathrm{m}}{.}20$ (Malkov et al., 2006). Estimations of the spectral class of the object vary from B3 (Burbidge & Burbidge, 1954) up to A0pe (Malkov et al., 2006, Avvakumova et al., 2013). It was supposed by Avvakumova et al. (2013), that changes of brightness may be connected with periodic eclipses of a hot component by a red giant or a supergiant. The orbital period is unknown.

Our quasi-simultaneous photometric and spectroscopic observations of V806 Cas were carried out in 2008-2014. Photometric observations were made with two telescopes: 1-meter Carl-Zeiss Jena reflector, equipped with CCD ST-7 (765×510, 9 μm) and 70 cm telescope AZT-8, equipped with CCD ST-8 (1530×1020, 9 μm, and samples of BVR_{C} filters). Usually two series of BVR_{C} images of the studied object were obtained successively. All images were dark subtracted and flat fielded. The resulting BVR_{C} magnitudes are compiled in Table 1. Errors of measurements do not exceed $0\overset{\mathrm{m}}{.}01$. Rapid (within 5 minutes) decrease by about 0.15 mag has been registered in V filter on 26.09.2011. We consider this variation to be real, because the brightness of a control star remained constant.

It is important to note, that the brightness of the object in different filters varies practically synchronously. Colour indices change within $0\overset{\mathrm{m}}{.}16 - 0\overset{\mathrm{m}}{.}19$ for $(B - V)$ and $0\overset{\mathrm{m}}{.}27 - 0\overset{\mathrm{m}}{.}31$ for $(V - R_{\mathrm{C}})$, and they do not correlate with the brightness level. Typical light curves of eclipsing variables exhibit deep minima caused by eclipses of the binary components. During our observation similar event was not observed, because our data were probably too scanty. However a periodicity is suggested by the brightness variations. The time intervals between two observed minima and two maxima correspond to 1117 ± 10 days (Figure 1). Such variations can be connected with pulsation of the star or with a non-uniform surface brightness (spots?) on a rotating star. If V806 Cas is a double system, it is possible to expect some changes of absorption on the line of sight for different orbital positions.

Table 1: Photometric B, V, R_C observations of V806 Cas

Date	HJD	B	V	R
	2400000+	mag	mag	mag
31.11.2008	54801.097	9.22	9.05	8.81
14.10.2009	55119.210	9.29	9.08	8.84
16.10.2009	55121.169	9.38	9.17	8.88
11.08.2010	55420.304	9.24	9.06	8.74
02.09.2011	55807.300	9.40	9.11	8.83
26.09.2011	55831.267	9.39	9.23	8.95
26.09.2011	55831.271	9.41	9.38	8.94
10.10.2012	56211.090	9.38	9.20	8.92
17.11.2012	56249.101	9.24	9.08	8.82
02.09.2013	56538.331	9.16	8.98	8.72
03.10.2013	56569.228	9.28	9.09	8.83
04.11.2013	56601.156	9.27	9.06	8.81
27.08.2014	56897.295	9.48	9.21	8.82
20.09.2014	56921.249	9.39	9.14	8.84
17.10.2014	56948.234	9.45	9.18	8.91

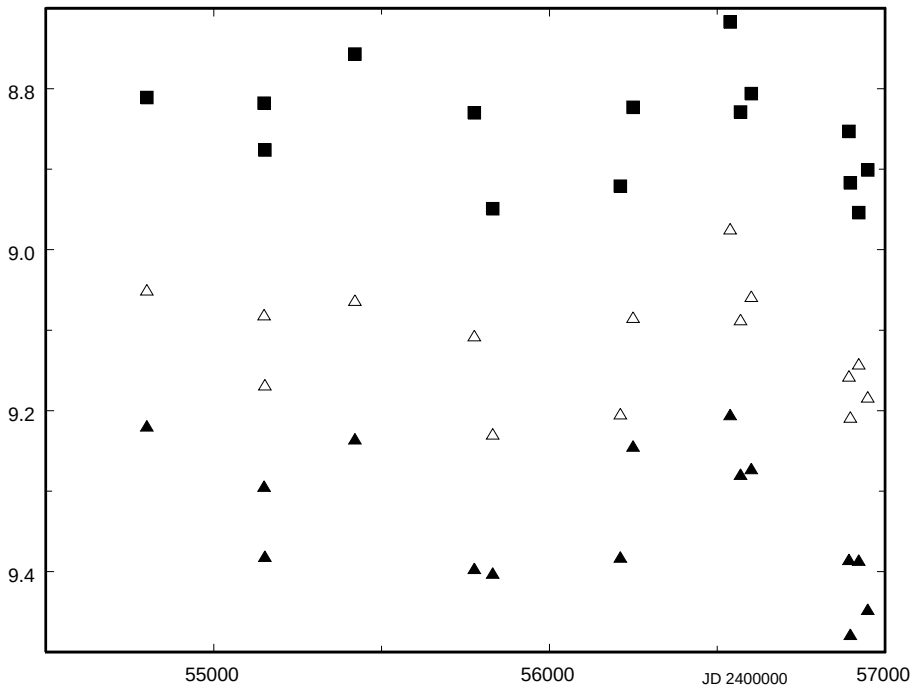

Figure 1. Light curve of V806 Cas from 2008 to 2014. BVR magnitudes are marked by full, empty triangles and squares.

Table 2: List of spectral observations

Date	HJD 2400000+	Range Å	Telescope	$R = \lambda/\Delta\lambda$
28.09.2008	54738.104	4000-4800	1-meter	9000
	54738.125	4400-5200	1-meter	10000
	54738.146	6100-6900	1-meter	13000
27.11.2008	54798.090	4300-5400	AZT-8	7000
	54798.110	6000-7200	AZT-8	9000
30.11.2008	54801.082	4400-5200	1-meter	10000
	54801.103	6100-6900	1-meter	13000
14.10.2009	55119.196	6100-7300	AZT-8	9000
16.10.2009	55121.185	4400-5200	1-meter	10000
	55121.206	6100-7300	1-meter	13000
18.10.2009	55123.202	3950-5200	AZT-8	7000
12.08.2010	55421.308	4400-5200	1-meter	10000
	55421.330	6100-6900	1-meter	13000
26.09.2011	55831.235	4400-5200	1-meter	10000
	55831.256	6100-7300	1-meter	13000
10.10.2012	56211.165	4400-5200	1-meter	10000
	56211.186	6100-7300	1-meter	13000
17.11.2012	56249.077	4400-5200	1-meter	10000
02.09.2013	56538.264	4300-5400	AZT-8	7000
	56538.285	6000-72000	AZT-8	9000
03.10.2013	56569.150	4000-5200	AZT-8	7000
	56569.172	4400-5200	1-meter	10000
	56569.190	6100-6900	1-meter	13000
04.11.2013	56601.094	4400-5200	1-meter	10000
	56601.115	4400-5200	1-meter	10000
	56601.137	6100-6900	1-meter	13000
27.08.2014	56897.327	4400-5200	1-meter	10000
	56897.284	6100-6900	1-meter	13000
20.09.2014	56921.214	4400-5200	1-meter	10000
	56921.235	6100-6900	1-meter	13000
17.10.2014	56948.226	4400-5200	1-meter	10000
	56948.246	6100-6900	1-meter	13000

Spectral observations have been carried out with two spectrographs, attached to the mentioned telescopes and equipped with the CCD cameras ST-8. The slit width equals to 3 - 4″. A standard procedure of dark subtraction, flattening and wavelength calibration with a laboratory source of HeI, NeI and ArI emission lines was applied. Spectra of standard stars HD 218376 and 224572, obtained just before or after the target, were used for the flux calibration. All results were corrected for atmospheric extinction. The list of spectral observations is given in Table 2.

There were only three nights, when the spectral range of observation was extended up to 3950 - 4000 Å. Lines Hϵ, Hδ and Hγ were in absorption. Their radial velocities were measured with an accuracy $\sim$ 50-55 km/sec, which is limited by dispersion of 0.75 Å per pixel. The following heliocentric velocities have been obtained:

28.09.2008 V_r(Hγ)=−10 km/sec
18.10.2009 V_r(Hϵ)=−240 km/sec, V_r(Hδ)=−220 km/sec, V_r(Hγ)=−180 km/sec
03.10.2013 V_r(Hδ)=−180 km/sec, V_r(Hγ)=−140 km/sec.

Table 3: Characteristics of the Hβ line

HJD	Hβ profiles			Radial Velocities of Hβ components		
2400000+	$F_{\rm abs}$	EW	V/R	Emission	Absorption	Emission
	10^{-12}	Å		V		R
54738.125	0.92±0.09	0.9±0.1	0.19	−175	−85	+35
54801.082	2.02±0.15	2.1±0.1	0.26	−165	−75	+20
55152.185	1.00±0.08	0.9±0.1	0.02	−195	−110	+50
55421.308	0.47±0.16	0.4±0.1	0.24	−190	−85	+55
55831.235	0.73±0.03	0.8±0.1	0.31	−210	−120	+35
56211.165	1.10±0.09	1.1±0.1	0.58	−180	−75	+45
56249.077	0.69±0.11	0.6±0.1	0.83	−160	−85	+40
56538.254	0.90±0.11	0.9±0.1	0.36	−155	−65	+75
56569.150	1.28±0.02	1.2±0.1	<0.05	—	−100	+50
56601.094	0.75±0.10	0.9±0.1	<0.05	−155	−90	+45
56896.261	0.80±0.11	0.9±0.1	0.25	−215	−125	+30
56921.214	0.24±0.06	0.3±0.1	0.62	−210	−105	+10
56948.226	1.17±0.07	1.2±0.1	<0.1	−200	−105	+60

Emission profiles of Hβ and Hα displayed double-peaked profiles. Weak line HeI, 6678 Å was observed in absorption on all our spectrograms. The results of spectral observations are presented in Table 3 and Table 4. Absolute emission fluxes $F_{\rm abs}$, equivalent widths in Å and the ratio of fluxes of the blue (V) to the red (R) emission component, V/R are presented in columns 3-5. Fluxes are in erg cm^{-2}sec^{-1} with the multipliers 10^{-11} for Hα and 10^{-12} for Hβ. Heliocentric radial velocities of profile components are given in columns 6-8 with the errors ±30 km/sec for Hβ and ±20 km/sec for Hα.

Observed profiles of the Hβ and FeII, 4924 Å lines are shown in Figure 2. The ratio $V/R < 1$, and sometimes the "blue" component disappeared completely. Broad absorption wings are recognized at the blue or at the red sides of Hβ components. Average positions of emission components correspond to values: V_r(blue) $= -185 \pm 6$ km/sec and V_r(red) $= +55 \pm 4$ km/sec. Profiles of FeII, 4924, 5018 Å are similar to those of Hβ, although sometimes instead of the emission component, an additional absorption in the FeII profile appeared (see for example, 28.09.2008 and 20.09.2014). The following values are obtained for the narrow absorption in Hβ and FeII: V_r(abs) $= -95 \pm 5$ km/sec and -90 ± 5 km/sec.

Profiles of Hα line vary slightly from date to date. Some examples of profiles are given in Figure 3. The ratio V/R is about 0.35. Disappearance of the blue Hβ component on 03.10.2013 and 17.10.2014, was accompanied by only a small decrease of V/R in the Hα profile. Average positions of Hα components correspond to values: V_r(blue) $= -180 \pm 3$ km/sec, V_r(abs) $= -98 \pm 2$ km/sec and V_r(red) $= +15 \pm 2$ km/sec.

The observed Hβ profile consists of three components: a broad absorption, forming in the stellar photosphere, emission from circumstellar envelope and narrow absorption, formed in the external neutral layers.

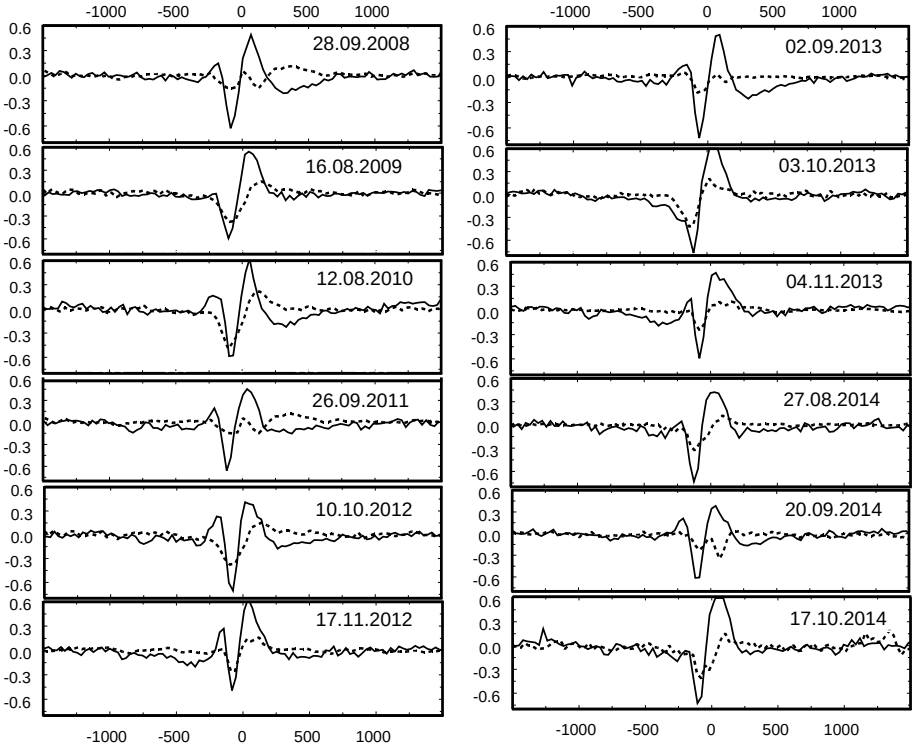

Figure 2. Variation of the Hβ (solid line) and FeII (dashed line) profiles in 2008-2014. X-axis shows heliocentric radial velocity (km/sec), Y-axis gives the ratio $(I_\lambda - I_{\rm cont})/I_{\rm cont}$.

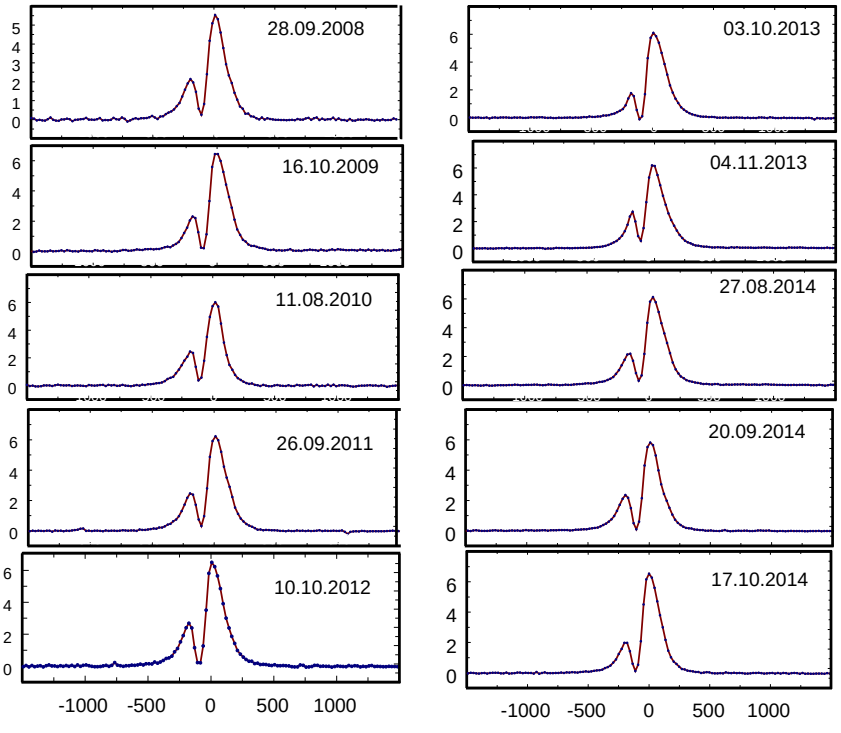

Figure 3. Variation of the Hα profiles in 2008 - 2014. X-axis shows heliocentric radial velocity (km/sec), Y-axis gives the ratio $(I_\lambda - I_{\rm cont})/I_{\rm cont}$.

Table 4: Characteristics of Hα line

HJD	Hα profiles			Radial Velocities of the Hα components		
2400000+	$F_{\rm abs}$	EW	V/R	Emission	Absorption	Emission
	10^{-11}	Å		V		R
54738.146	1.85±0.05	31.2±0.1	0.38	−175	−85	+30
54794.110	1.29±0.20	31.6±0.2	0.40	—	—	—
54801.103	1.07±0.20	33.4±0.1	0.43	−155	−90	+5
55150.196	1.45±0.08	33.1±0.2	0.37	—	—	—
55152.206	1.44±0.08	35.0±0.2	0.36	−185	−110	+5
55421.330	1.22±0.16	31.6±0.2	0.41	−185	−115	+20
55831.256	1.57±0.05	50.8±0.1	0.39	−195	−100	+10
56211.186	1.95±0.02	35.6±0.5	0.41	−175	−95	+6
56538.285	2.04±0.01	31.2±0.2	0.38	−175	−95	+40
56569.190	1.80±0.03	31.5±0.6	0.28	−175	−105	+10
56601.137	1.97±0.03	33.9±0.2	0.44	−160	−90	+10
56896.284	1.25±0.04	32.8±0.1	0.38	−165	−65	+30
56921.235	2.67±0.10	32.8±0.1	0.40	−190	−100	+10
56948.246	1.85±0.02	34.0±0.4	0.30	−195	−110	+5

Radial velocities of the broad Hγ and Hδ absorption lines, in spite of their low accuracy, reflect an orbital motion of the star. However, radial velocities of emission and sharp absorption components of Hβ vary within narrower limits and do not correlate with the variation of the stellar absorption. This suggests that the envelope, which is the source of the emission components and the narrow absorption, does not follow the orbital motion. It is probable that emission lines are formed in the circumstellar environment of the binary.

References:

Avvakumova, E., Malkov, O., Kniazev, A., 2013, *AN*, **334**, 860
Burbidge, M., Burbidge, G., 1954, *ApJ*, **119**, 501
Haupt, H., Schroll, A., 1974, *A&AS*, **15**, 311
Kohoutek, L., Wehmeyer, R., 1999, *A&AS*, **134**, 255
Malkov, O.Yu., Oblak, E., Snegireva, E.A., Torra, J., 2006, *A&A*, **446**, 785
Merrill, P., Burwell, C., Miller, W., 1948, *PASP*, **60**, 68

COMMISSIONS 27 AND 42 OF THE IAU
INFORMATION BULLETIN ON VARIABLE STARS

Number 6142

Konkoly Observatory
Budapest
29 April 2015

HU ISSN 0374 – 0676

AN UPDATED PERIOD ANALYSIS FOR AC BOOTIS

NELSON, ROBERT H.

11393 Garvin Street, Prince George, BC, Canada, V2M 3Z1 e-mail: bob.nelson@shaw.ca

AC Bootis (=BD +46°2004 = TYC 3474-905-1 = HIP 73103, Sp. F8V) was discovered to be variable by Geyer (1955, as reported by Mauder, 1964). The system was identified as a member of the W-UMa class by Zessewitch (1956), and the correct period first determined by Mauder (1964). Since then, numerous photoelectric light curves have been obtained, and variations over time noted. Several light curve analyses have been preformed using various codes, most recently those of Wilson-Devinney (Wilson & Devinney, 1971, Wilson, 1990; hereafter WD). (See Nelson, 2010 for a more complete set of references.) Radial velocity curves were obtained by Hrivnak (1993) using a cross-correlation technique. Nelson (2010) performed a full WD analysis (using radial velocities and multi-filter CCD light curves determined by him), solving for the fundamental parameters. Independently, Alton (2010) presented a photometric WD analysis of his own light curve data and also those from five other authors, arriving at a unified model with closely similar values for the parameters, differing only in those for the spots, which varied over time.

Both authors (Nelson and Alton) also undertook separate period analyses, concluding that the period had changed over the interval from 1929 (cycle −54880) to 2012 (cycle 31000). Based on visual, photoelectric and CCD eclipse timings, Nelson (2010) concluded that the period was constant from 1929 to 1982, after which there was a "sudden rise in the period; after that, the period displayed a slow, steady increase over time". He suggested that the abrupt change in period could be explained by an episodic mass interchange possibly as the two stars established contact. After that, there was a continuous period increase at a constant rate. See Fig. 1.

Alton (2010) also performed a period analysis, noting a "continual increase in orbital period over the last 48 years or longer, thereby suggesting an ongoing exchange of mass. Fourier analysis also revealed possible periodicity in $O-C$ residuals which was "heavily influenced by a putative sinusoidal-like wave most apparent over the past twenty years." He gave the opinion that the variation was not due to an unseen component but rather due to spot formation on either stellar component.

The system was also discussed briefly in the review paper by Nelson et al. (2014).

A new period analysis has now been completed allowing for the light time effect (LTE) due to a possible third star. The full set of equations for period change study were given in Nelson (2015a), but two are reproduced here:

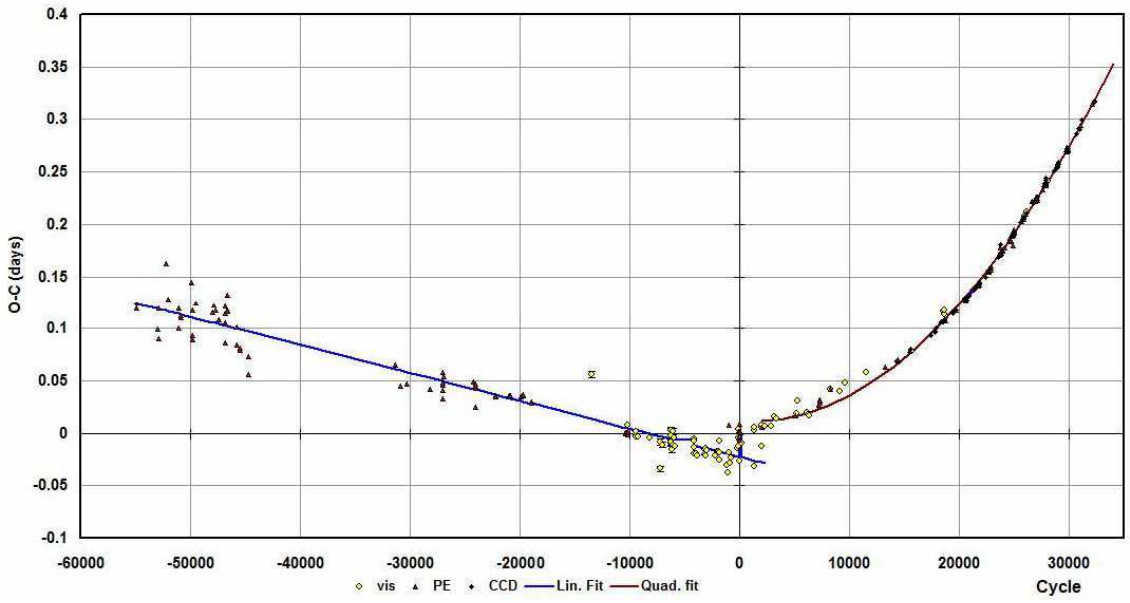

Figure 1. AC Boo – ET diagram (Nelson, 2010)

The equation of a best-fit parabola in the eclipse timing diagram is:

$$Y_1 = c_0 + c_1 n + c_2 n^2 \tag{1}$$

where n is the cycle number. The equation for the difference in time due to the light time effect (Irwin 1952, 1959) is:

$$Y_2 = A \left[\frac{1 - e^2}{1 + e \cos \nu} \sin(\nu + \omega) + e \sin \omega \right] \tag{2}$$

where A = semi-amplitude in days ($= a_{12} \sin i/c$), a_{12} = semi-major axis of the 1-2 pair about the centre of mass of the triple system, c = speed of light = 300 000 km/s, e = eccentricity of the (1,2)-3 orbit, ν = the true anomaly (varies), ω = argument of periastron (constant). Additional parameters are P_3 = period of the (1,2)-3 system and T_0 = time of periastron passage.

As in Nelson (2010), the elements of Schieven et al. (1983) were used:

$$\text{J.D.Hel.minI} = 24\,45117.781(1) + 0.3524321(2)n \tag{3}$$

A note about the method used to obtain a solution may be of use. In the present study, all of the available eclipse timings were entered into an Excel worksheet, each with the standard weighting $w_i \sim 1/e_i^2$. Analysis of deviations from the curve of best fit (see Fig. 3) yielded weights of 0.02 for group 1 (cycle < -40000), 0.1 for group 2 ($-40000 <$ cycle < -10000) and 1 for PE/CCD data for group 3 (cycle > -15000). (The visual data were initially given weights of 0.1 but were eventually excluded from the fit.)

All eight parameters (c_0, c_1, c_2, A, e, ω, P_3, and T_0) were listed in adjacent cells, and additional equations given in Nelson (2015a) were used to compute expected values $C = Y_1 + Y_2$ for each row in the worksheet, which corresponded to one data point. The weighted sum of the differences squared, $\sum w_i (O - C)^2$ was then minimized using the 'Solver' tool.

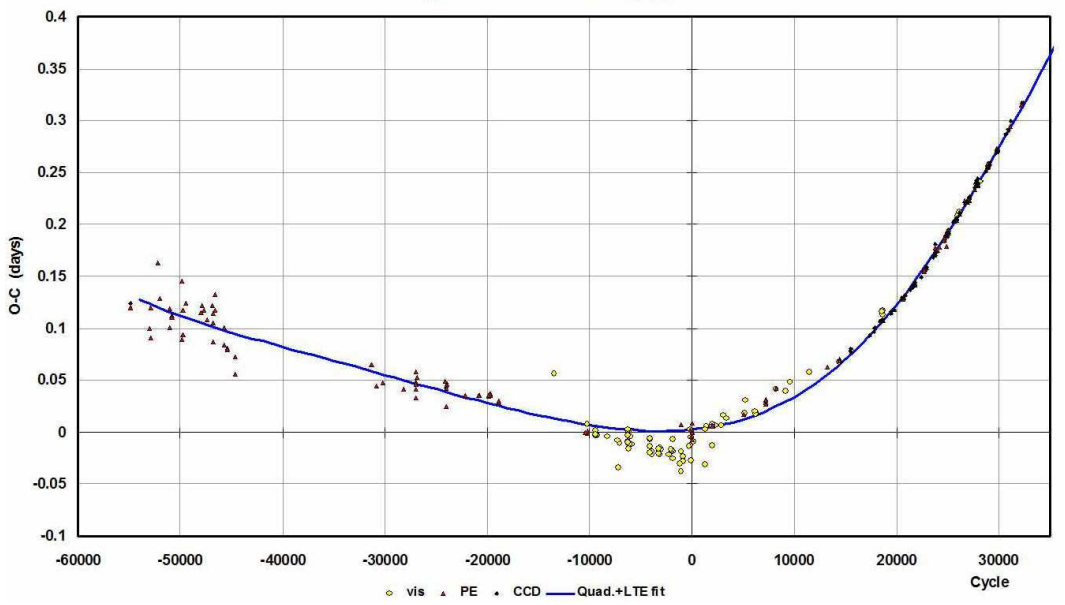

Figure 2. AC Boo – ET diagram

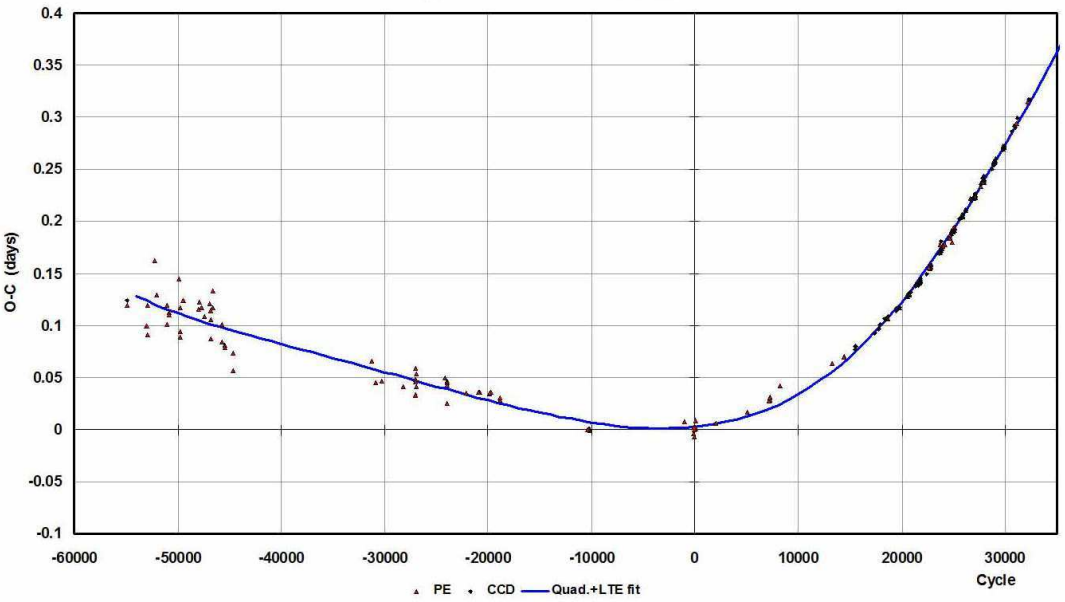

Figure 3. AC Boo – ET diagram

Table 1: Parameters for the quadratic + LTE fit for the eclipse timing differences of AC Bootis

Quantity	Coeff.	error	Unit
Constant, c_0	2.4	0.7	10^{-2} days
Slope, c_1	4.26	0.06	10^{-6} days/cycle
Quadratic coefficient, c_2	1.28	0.11	10^{-10} days^2/cycle
dP/dt	2.67	0.23	10^{-7} days/year
Amplitude, $A = (a_3 \sin i)/c$	0.047	0.004	days
$a_{12} \sin i$	8.11	0.54	AU
Eccentricity, e	0.35	0.05	—
Period, P_3	72.4	2.5	years
Argument of periastron, ω	348	11	degrees
Periastron time, T_p	53710	2154	HJD−2400000
Mass function, $f(m_3)$	0.10	0.02	$M_\odot$

It was noted that, to the eye, the first solution did not match all the data very well (see Fig. 2). The problem seemed to lie with the visual data. Using only photoelectric and CCD data led to a much better fit visually (see Fig. 3).

The residuals from the LTE fit are displayed in Fig. 4 along with the fitted quadratic function. The residuals from the quadratic fit are displayed in Fig. 5 along with the fitted LTE function.

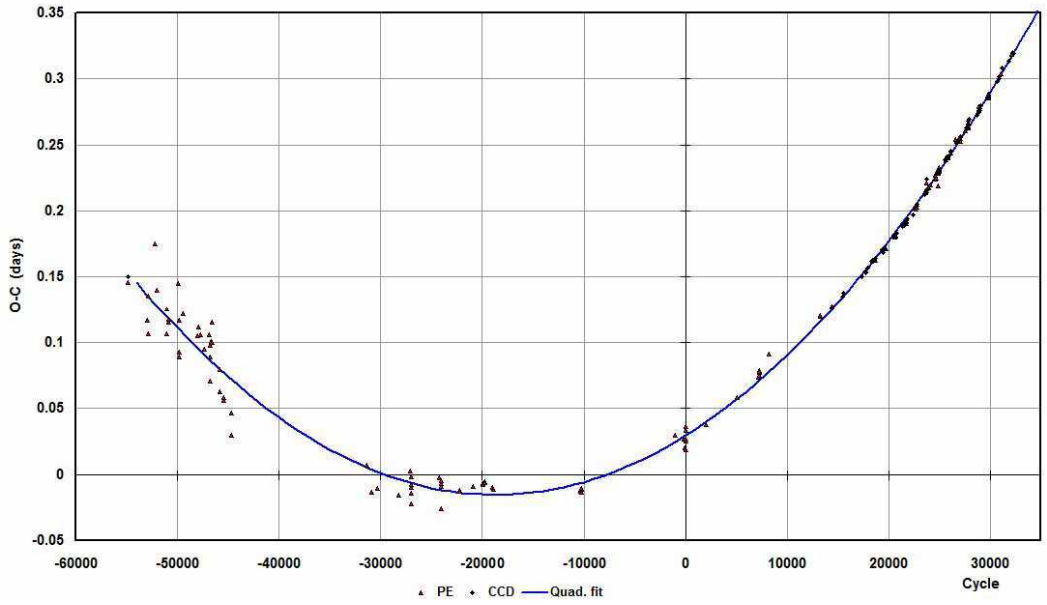

Figure 4. AC Boo – residuals from the LTE fit

The best-fit parameter set is given in Table 1. The procedure used in the error analysis was described in Nelson (2015a).

Nelson (2010) derived masses $m_1 = 0.36(3)\ M_\odot$, $m_2 = 1.20(5)\ M_\odot$ for the system. Using the well-known equation

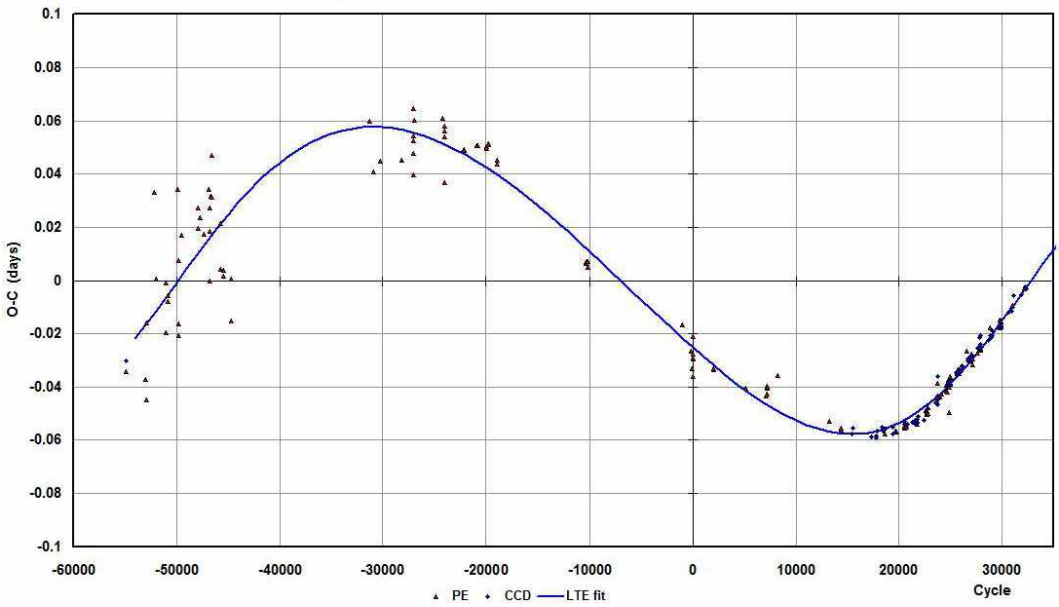

Figure 5. AC Boo – residuals from the quadratic fit

$$\frac{dm_1}{dt} = \frac{1}{3P(\frac{1}{m_2} - \frac{1}{m_1})}\frac{dP}{dt} \tag{4}$$

and the value for dP/dt in Table 1, one obtains the mass transfer rate $dm_1/dt = (-1.3 \pm 0.3) \times 10^{-7}\ M_\odot$/year. Since the system is of the W-type subclass (the star having the lesser mass is the brighter and is therefore eclipsed at the primary eclipse and is designated as star 1), this means that the more massive star is gaining mass at the expense of the less massive one.

Obtaining reliable values for the mass exchange rates in overcontact eclipsing binaries is problematic. This is because both magnetic cycles (Applegate, 1992) and the light time effect can mimic the quadratic function in the eclipse timing difference $(O-C)$ plot occurs when mass is exchanged at a constant rate.

This topic, dealt with in review papers by Nelson et al. (2014, 2015a, 2015b), is all the more important because of the finding by Pribulla & Rucinski (2006) that most contact binary stars exist in multiple systems. Therefore, one might expect the light time effect to be common with such systems.

However, if it is true that the light time effect as modelled above adequately explains the somewhat complex (viz. non-linear or quadratic) features in the ET plots of Figs. 1-3 and that magnetic cycles can be ruled out, then the residuals, as displayed in Fig. 4, are due entirely to mass exchange, and the value $dm_1/dt = (-1.30 \pm 0.27) \times 10^{-7}\ M_\odot$/year is reliable.

It is noted, as stressed in Nelson et al. (2014, 2015a, 2015b), that subsequent eclipse timing data will often demand a new fit. Sometimes the fit is completely wrong. In a sense all fits are tentative, to some level of uncertainty. In any case, the results in Table 1 should be treated with caution, especially since little more than one period of the putative third star has been observed. The error estimates are mathematically sound, but real errors may be larger. On the other hand, repeated tests with existing data have failed to reveal any other plausible values for P_3 (and hence the other parameters).

The $O - C$ file for this system may be obtained at the URL given below in Nelson (2015b).

References:

Alton, K.B., 2010, *JAAVSO*, **38**, 57
Applegate, J.H., 1992, *ApJ*, **385**, 621
Geyer, E., 1955, *Kleine Veröff. Bamberg*, **9**, 4
Hrivnak, B.J., 1993, *ASP Conf. Series*, **38**, 269
Irwin, J.B., 1952, *ApJ*, **116**, 211
Irwin, J.B., 1959, *AJ*, **64**, 149
Mauder, H., 1964, *ZA*, **60**, 222
Mayer, P., 1990, *BAICz*, **41**, 231
Nelson, R.H., 2010, *IBVS*, **5951**
Nelson, R.H., 2015a, *NewA*, **34**, 159
Nelson, R.H., 2015b, `http://www.aavso.org/bob-nelsons-o-c-files` [updated annually]
Nelson, R.H., Terrell, D., Milone, E.F., 2014, *NewAR*, **59**, 1 (paper 1)
Nelson, R.H., Terrell, D., Milone, E.F., 2015a, *NewAR*, (paper 2) submitted
Nelson, R.H., Terrell, D., Milone, E.F., 2015b, *NewAR*, (paper 3) in preparation
Pribulla, T. & Rucinski, S.M., 2006, *AJ*, **131**, 2986
Schieven, G., Morton, J.C., McLean, B.J., Hughes, V.A., 1983, *A&AS*, **52**, 463
Wilson, R.E., 1990, *ApJ*, **356**, 613
Wilson, R.E., and Devinney, E.J., 1971, *ApJ*, **166**, 605
Zessewitsch, W.P., 1956, *AZ Kasan*, **171**

COMMISSIONS 27 AND 42 OF THE IAU
INFORMATION BULLETIN ON VARIABLE STARS

Number 6143

Konkoly Observatory
Budapest
2 June 2015

HU ISSN 0374 – 0676

HOT DUST REVEALED DURING THE DIMMING OF THE T TAURI STAR RW Aur A

SHENAVRIN, V.I.[1]; PETROV, P.P.[2]; GRANKIN, K.N.[2]

[1] Lomonosov Moscow State Univ., Sternberg Astron. Inst., Universitetsky pr. 13, 119234 Moscow, Russia

[2] Crimean Astrophysical Observatory, 298409 Nauchny, Republic of Crimea

email: vshen@msu-crimea.ru, petrogen@rambler.ru, kgrankin@crao.crimea.ua

T Tauri stars (TTS) are young pre-main sequence objects of low mass ($M < 2\ M_\odot$), located in star forming regions. During the first ~ 10 Myr of their evolution TTS are surrounded by circumstellar disks, where processes of planet formation are going on. TTS are distinguished by irregular light variability and the characteristic emission line spectrum of low excitation. The light variability of TTS with accretion discs is caused by three processes: obscuration of stellar light by dust clouds in the circumstellar disc, variable mass accretion – infall of matter from the disc to the stellar surface, and cool magnetic spots which often cause rotational modulation of stellar brightness (Herbst et al. 1994).

RW Aur A is one of the brightest TTS, located in the Taurus-Auriga star forming region at the distance of 140 pc. It is a K1-K3 star of about solar mass ($1.4\ M_\odot$) with strong emission line spectrum and clear signatures of accretion and wind (Petrov et al. 2001, Alencar et al. 2005). RW Aur is a visual binary with a separation of $1\farcs4$ between A and B components. The secondary, RW Aur B, is a TTS of lower mass, $0.8\ M_\odot$, and of later spectral type, K7. It is nearly a weak-line TTS, with Hα equivalent width of ≈ 7 Å, which indicates a low rate of mass accretion. The B component is also a binary with separation of $0\farcs12$ and mass of the secondary below $0.045\ M_\odot$ (Ghez et al. 1997).

RW Aur has been intensively observed photometrically during ~ 50 yr. The range of visual light variability is typically from V=$10\fm0$ to V=$12\fm0$ on a time scale of a few days. The first long-lasting dimming event was recorded in 2010, when the star faded by about 2^m and remained in a low state with some fluctuations during several months. Rodriguez et al. (2013) presented a detailed investigation of this phenomenon and concluded that the star was obscured by a distant cloud, supposedly a remnant of tidally disrupted disc of the star. Recently, Dai et al. (2015) performed MHD simulations which reproduced the morphology of the molecular cloud around RW Aur as a result of tidal encounter with the secondary star.

In 2014 the dimming event repeated: RW Aur A faded by $\approx 3^m$ and has remained in the low state until now (April 2015). Resolved photometry of the two components was made by Antipin et al. (2015) in November 2014. They showed that RW Aur A underwent a grey extinction in $UBVR$ bands. The secondary component was found to be variable within $\approx 1^m$. Resolved spectroscopy of the two components in December 2014

(Petrov et al. 2015) showed that the emission line spectrum of RW Aur A remained as usual, but the wind features in some resonance lines have increased considerably. The spectrum of the secondary remained unchanged. The authors proposed that the dimming might be caused by extinction of light in a dusty wind of the primary component.

In this paper we present results of infrared (IR) photometry of RW Aur in 2010-2015, which provides additional information about the cause of the dimming events. IR-photometry of RW Aur was carried out at the 125-cm telescope at the Crimean observatory of the Moscow University. InSb-photometer with a standard $JHKLM$ system was used. Technical parameters of the photometer, methods of observations and calculations of magnitudes were described in details by Shenavrin et al. (2011). The star BS 1791 was used as a photometrical standard. Its JK magnitudes were taken from the catalogue of Johnson et al. (1966), and HLM magnitudes were calculated from relations given in Koornneef (1983). The standard error of the measured magnitudes of RW Aur is about $0\overset{m}{.}02$ in $JHKL$ bands, and about $0\overset{m}{.}05$ in M band. In our observations, the A and B components of RW Aur were not resolved.

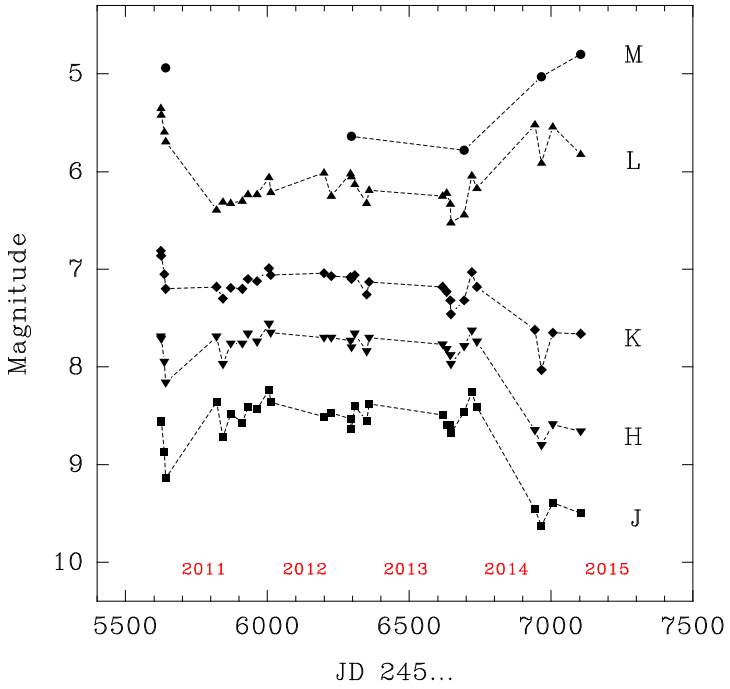

Figure 1. Light curves of RW Aur in $JHKLM$ bands in 2010-2015. Note the brightening of the star in L and M bands, while fading in JHK bands.

Fig. 1 shows the IR light curves of RW Aur in 2010-2015, starting from the very end of the dimming event of 2010 and covering the dimming event of 2014-2015. Comparison of spectral energy distribution in the bright and low states of RW Aur is shown in Fig. 2. The $UBVRI$ data at the bright state are from our Crimean database.

Note the different slopes at 2-5 μm (KLM bands) at low and bright states, indicating appearance of additional source of IR-radiation when the star has faded in visual range. This additional flux can be attributed to radiation of hot dust at the temperature of about 1000 K. The IR source is most probably associated with the primary component

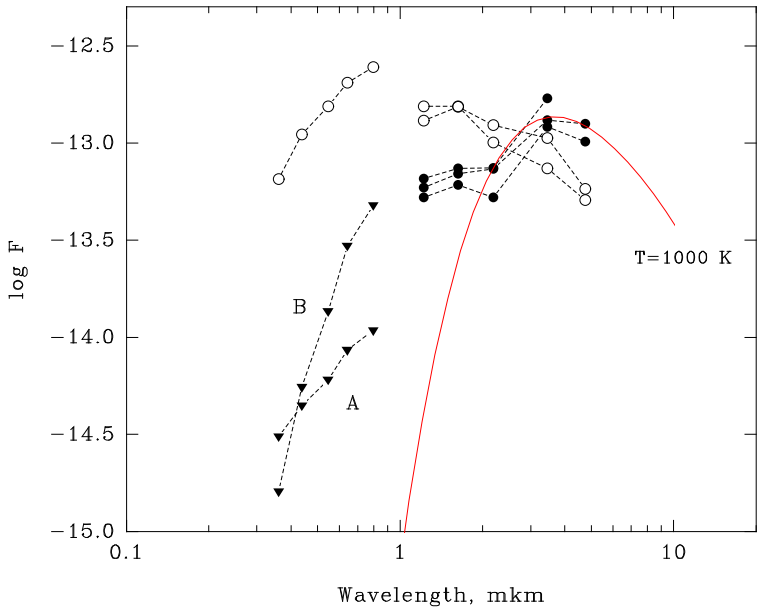

Figure 2. Spectral energy distribution in bright and low states of RW Aur. The flux scale is $\log \lambda F(\lambda)$, in units erg cm^{-2} s^{-1}. Open circles – $UBVRI$ and $JHKLM$ photometry in bright state of 2013, filled circles – $JHKLM$ photometry in the low state of 2014–2015 (JD 2456965 – 2457104), triangles – resolved photometry of A and B components of RW Aur in the low state of 2014 (JD 2456975), from Antipin et al. (2015). The solid curve is the Planck function (T=1000 K) fitting the additional flux in KLM bands during the dimming of 2014-2015.

(RW Aur A), because the secondary is much fainter in K band: at normal brightness of the primary, the K magnitude of the secondary was $\approx 1\overset{\mathrm{m}}{.}6$ fainter (Eisner et al. 2007).

Hot dust is present in the inner regions of accretion discs of TTS, at the distance of about 0.1 AU, where the dust is near the temperature of sublimation, 1500-2000 K (Millan-Gabet et al. 2007). From IR-interferometry of RW Aur the inner radius of the dusty disc was determined as 0.10-0.23 AU (Akeson et al. 2005; Eisner et al. 2007). If dimmings of RW Aur at the optical wavelength were caused by extinction of light in a distant cloud, as was suggested by Rodriguez et al. (2013), one would expect that not only the central star is obscured, but the inner disc is too, at least partly, is screened by the cloud, like, e.g., in V2492 Cyg, where occultation of the central star and the inner disk causes large amplitude variations in optical and IR bands (Hillenbrand et al. 2013). In RW Aur, the observed *increase* of the IR flux during the deep dimming event of 2014 is not compatible with the hypothesis of a distant cloud. Most probably, the extinction of starlight is due to the same dust which radiates at 3-5 μm, not far from the star.

Light variability related to dusty clouds in the circumstellar disks is usually observed in UXors – intermediate mass pre-main sequence stars of earlier spectral types as compared to the low mass TTS. Correlated variations in optical and near-IR bands were observed in some UXors, while others demonstrated anti-correlation (Shenavrin et al. 2012). The variations similar to that shown in Fig. 1 were observed in the UXor type stars UX Ori and AK Sco (Hutchinson et al. 1994). Explanation of this kind of variability was suggested by Grinin et al. (2009) for another UXor, V1184 Tau, in the context of the model of accretion disk with the puffed-up inner rim in the dust sublimation zone. The authors supposed that an enhancement of the accretion results in increase of geometrical thickness of the

rim and the dusty atmosphere of the inner disk, which obscures the starlight. At the same time, the near-IR radiation from the inner rim remains the same or even increases.

Although this model is natural for an UXor, it is questionable whether it can be applied to a later spectral type TTS. Another point is that the disk plane of RW Aur A is inclined by between 30 to 45 degrees to the line of sight (Cabrit et al. 2006). It was shown by Rodriguez et al. (2013) that with such inclination the inner rim can hardly obscure the star. And, finally, the emission line spectrum of RW Aur A has not changed during the dimming event, i.e. the accretion rate remained as usual. Nevertheless, a hot dust in atmosphere of the inner disk is the most probable agent which obscures the star and radiates in near-IR. Petrov et al. (2015) revealed the enhanced wind features during the dimming event of RW Aur A. Note, that inclination of the star is close to the opening angle of a conical wind (Romanova et al. 2009). We suggest that the hot dust, responsible for the dimming event, was carried into the wind of RW Aur A, streaming from the inner disk towards the observer.

References:

Akeson, R. L., Boden, A. F., Monnier, J. D., et al., 2005, *ApJ*, **635**, 1173
Alencar, S. H. P., Basri, G., Hartmann, L., Calvet, N. 2005, *A&A*, **440**, 595
Antipin, S., Belinski, A., Cherepashchuk, A., et al., 2015, *IBVS*, **6126**
Cabrit, S., Pety, J., Pesenti, N., Dougados, C., 2006, *A&A*, **452**, 897
Dai, F., Facchini, S., Clarke, C., et al., 2015, *MNRAS*, **449**, 1996
Eisner, J. A., Hillenbrand, L. A., White, R. J., et al., 2007, *ApJ*, **669**, 1072
Ghez, A. M., White, R. J., and Simon, M., 1997, *ApJ*, **490**, 353
Grinin, V. P., Arkharov, A. A., Barsunova, O. Yu., Sergeev, S. G., Tambovtseva, L. V., 2009, *AstL*, **35**, 114
Herbst, W., Herbst, D. K., Grossman, E. J., Weinstein, D., 1994, *AJ*, **108**, 1906
Hillenbrand, L. A., Miller, A. A., Covey, K. R., et al., 2013, *AJ*, **145**, 59
Hutchinson, M. G., Albinson, J. S., Barrett, P., Davies, J. K., Evans, A., Goldsmith, M. J., Maddison, R. C., 1994, *A&A*, **285**, 883
Johnson, H. L., Mitchell, R. I., Iriarte, B., et al., 1966, *Comm. Lunar Planet. Lab.*, **4**, 99
Koornneef, J., 1983, *A&A*, **128**, 84
Millan-Gabet, R., Malbet, F., Akeson, R., et al., 2007, in "Protostars and Planets V", eds. Reipurth, B., Jewitt, D., and Keil K., University of Arizona Press, Tucson, p. 539
Petrov, P. P., Gahm, G. F., Gameiro, J. F., Duemmler, R., Ilyin, I. V., Laakkonen, T., Lago, M. T. V. T., Tuominen, I., 2001, *A&A*, **369**, 993
Petrov, P. P., Gahm, G. F., Djupvik, A. A., et al., 2015, *A&A*, **577**, A73
Rodriguez, J. E., Pepper, J., Stassun, K. G., et al., 2013, *AJ*, **146**, 112
Romanova, M. M., Ustyugova G. V., Koldoba A. V., Lovelace R. V. E., 2009, *MNRAS*, **399**, 1802
Shenavrin, V. I., Taranova, O. G. and Nadzhip, A. E., 2011, *Astron. Rep.*, **55**, 31
Shenavrin, V. I., Grinin, V. P., Rostopchina-Shakhovskaja, A. N., Demidova, T. V., Shakhovskoi, D. N. 2012, *Astron. Rep.*, **56**, 379

COMMISSIONS 27 AND 42 OF THE IAU
INFORMATION BULLETIN ON VARIABLE STARS

Number 6144

Konkoly Observatory
Budapest
10 June 2015

HU ISSN 0374 – 0676

SEARCH FOR VARIABLES IN THE OPEN CLUSTER KING 12

PAUNZEN, E.[1]; NETOPIL, M.[1]; RODE-PAUNZEN, M.[2]; BOZIC, H.[3]

[1] Department of Theoretical Physics and Astrophysics, Masaryk University, Kotlářská 2, 611 37 Brno, Czech Republic

[2] Institut für Astrophysik der Universität Wien, Türkenschanzstr. 17, A-1180 Wien, Austria

[3] Hvar Observatory, Faculty of Geodesy, University of Zagreb, Kaciceva 26, HR-10000 Zagreb, Croatia

Open clusters are physically related groups of stars held together by mutual gravitational attraction. Therefore, these populate a limited region of space, typically much smaller than their distance from the Sun, so that the members are all approximately at the same distance. They are believed to originate from large cosmic gas and dust clouds, and to continue to orbit the Milky Way through the disk. Also, as all the stars in a cluster are formed from the same diffuse nebula, they are all of similar initial chemical composition. In many clouds visible as bright diffuse nebulae, star formation still takes place, so that we can observe the birth of new young star clusters (Massi et al. 2015).

Variable stars play an important role in stellar astrophysics. They offer, in general, the only possibility to look inside stars (asteroseismology), and they represent an important way to measure distances (Zejda et al. 2012).

We searched for variables in the central region of the young open cluster King 12 (C 2350+616) which, to our knowledge, was never done, up to now. This cluster is located in the Galactic disk ($l = 116\overset{\circ}{.}121$ and $b = -0\overset{\circ}{.}151$) at a distance of about 2.9 kpc from the Sun (Lata et al. 2014). The most interesting fact is that it still contains pre-main sequence stars at an age of approximately 12 Myr (Davidge 2012).

The observations were performed in August and September 2010 at the Hvar Observatory, University of Zagreb, using the 1 m Austrian-Croatian Telescope (ACT). The telescope was equipped with a Apogee Alta U47 CCD camera of 1024×1024 pixels, resulting in a field-of-view of about $3'$ square. The integration times for the observations in the Bessell I filter system were set either to 20 or 45 s, depending on the weather conditions. In total, 674 frames of about 500 minutes of photometry in six nights were secured. After the basic CCD reductions (bias-subtraction and flat fielding), we applied point spread function (PSF) photometry within IRAF. The further reduction steps were performed using the standard technique for time series CCD observations. The complete observation log is listed in Table 1.

All differential light curves were examined in more detail using the Phase Dispersion Minimization method (PDM, Stellingwerf 1978) within the software Peranso[1]. An analysis with a discrete Fourier algorithm gave the same noise level over the searched frequency range as PDM.

[1] http://www.peranso.com/

Table 1: Observation log.

JD(start) 2455400+	JD(end) 2455400+	N	JD(start) 2455400+	JD(end) 2455400+	N
20.464288	20.620203	266	60.381684	60.405388	33
21.554554	21.620735	115	63.424560	63.447975	82
26.545666	26.611418	118	67.348276	67.363623	60

Primarily, we were searching for variations on times scales of a few hours (typical δ Scuti type pulsation) but also for very high amplitude variations on the time scales of weeks and months. For the latter, we would not be able to retrieve the exact periods put to sort out good candidates. In total, we investigated 54 stars in the central part of King 12.

Figure 1 shows the upper limits of non-variability for the investigated stars. The dependency of them on the apparent magnitude is caused by the photon noise. The detection limits is about 8 mmag for the brightest stars and decreases to about 0.04 mag for the faintest ones. We found no star which shows a statistically significant peak in its frequency spectrum in the range from 12 h down to 20 min. Of course, we are not able to exclude variability on other time scales and/or with lower amplitudes than reported here.

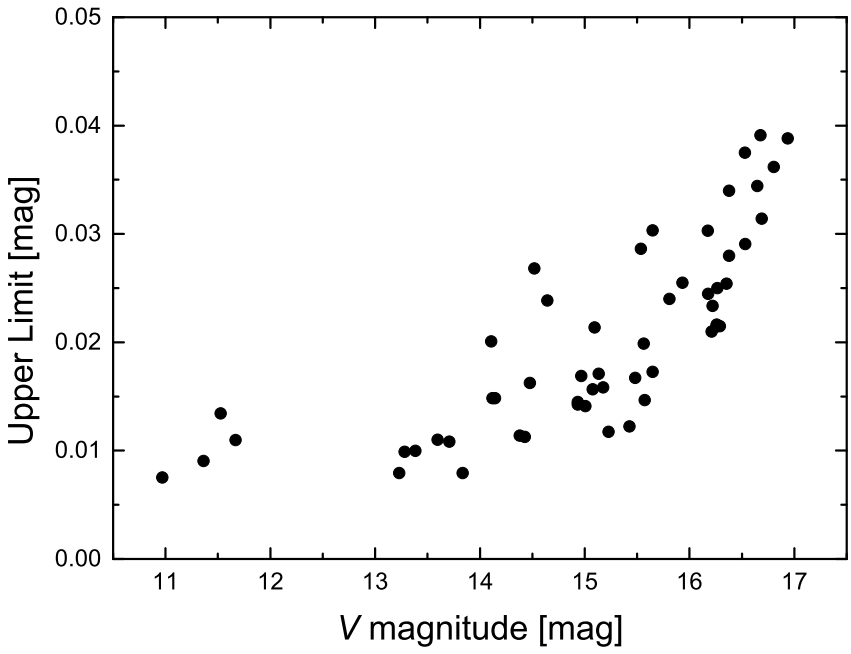

Figure 1. Upper limits of variability of stars in the field of King 12.

Acknowledgements: This project is financed by the SoMoPro II programme (3SGA5916). The research leading to these results has acquired a financial grant from the People Programme (Marie Curie action) of the Seventh Framework Programme of EU according to the REA Grant Agreement No. 291782. The research is further co-financed by the South-Moravian Region. It was also supported by the grants 7AMB14AT015,

14-26115P, and the financial contributions of the Austrian Agency for International Cooperation in Education and Research (BG-03/2013 and CZ-09/2014). HB acknowledges financial support by Croatian Science Foundation under the project 6212 "Solar and Stellar Variability". This research has made use of the WEBDA database, operated at the Department of Theoretical Physics and Astrophysics of the Masaryk University.

References:

Davidge, T. J. 2012, *ApJ*, **761**, 155
Lata, S., Pandey, A. K., Sharma, S., Bonatto, C., Yadav, R. K. 2014, *New Astronomy*, **26**, 77
Massi, F., Giannetti, A., Di Carlo, E., Brand, J., Beltrán, M. T., Marconi, G. 2015, *A&A*, **573**, A95
Stellingwerf, R. F. 1978, *ApJ*, **224**, 953
Zejda, M., Paunzen, E., Baumann, B., Mikulášek, Z., & Liška, J. 2012, *A&A*, **548**, A97

COMMISSIONS 27 AND 42 OF THE IAU
INFORMATION BULLETIN ON VARIABLE STARS
Number 6145

Konkoly Observatory
Budapest
23 June 2015

HU ISSN 0374 – 0676

HIP10680/HIP10679: A VISUAL BINARY IN THE β PICTORIS ASSOCIATION WITH THE FASTEST ROTATING MEMBER

MESSINA, S.[1]; HENTUNEN V.-P.[2]; ZAMBELLI, R.[3]

[1] INAF- Catania Astrophysical Observatory, via S. Sofia, 78 I-95123 Catania, Italy, e-mail: sergio.messina@oact.inaf.it

[2] Taurus Hill Observatory, Varkaus, Finland, e-mail: veli-pekka.hentunen@kassiopeia.net

[3] Canis Mayor Observatory, La Spezia, Italy, e-mail: robertozambelli.rz@libero.it

Introduction

We are carrying out a photometric monitoring of confirmed and candidate members of the young β Pictoris association. Particular emphasis is given to multiple stellar systems to study the distribution of the rotation periods of their components. We want to investigate what causes significant differences among the rotation periods. Causes can be either different initial rotation periods or primordial disc lifetimes. Specifically, we find that components with very close either stellar or sub-stellar mass companions tend to exhibit a rotation period shorter than more distant components (see, e.g. Messina et al. 2014, 2015). In this paper, we present the case of the wide visual binary HIP 10680/HIP 10679 for which we have measured for the first time the rotation periods.

Literature information

HIP 10680 (RA = 02:17:25.3, DEC = +28:44:42.1, J2000, V = 6.95 mag) and HIP 10679 (RA = 02:17:24.73, DEC = +28:44:30.3, J2000, V = 7.75 mag) are components of a common proper motion visual binary (also named HD 14082AB, BD+28 382AB) consisting of F5V + G2V dwarfs. An angular separation $\rho = 13.8''$ between the two components is reported in The Washington Visual Double Star Catalog (Mason et al. 2001). The parallaxes measured by Hipparcos have an uncertainty of the order of 15%, and correspond to distances $d = 34.5$ pc for HIP 10680 and $d = 27.3$ pc for HIP 10679. The most reliable distance determination was recently provided by Pecaut & Mamajek (2013), who report for both components a kinematic distance $d = 37.62 \pm 2.73$ pc. This measurement is based on UCAC4 proper motions (Zacharias et al. 2013), the assumption of membership to the β Pictoris association, and the use the convergent point solution. In fact, this visual binary system is a well known member of β Pictoris association. Its membership was first proposed by Zuckerman & Song (2004), and subsequently confirmed by Torres et al. (2006), Lépine & Simon (2009), Kiss et al. (2011), and more recently by Malo et al. (2014).

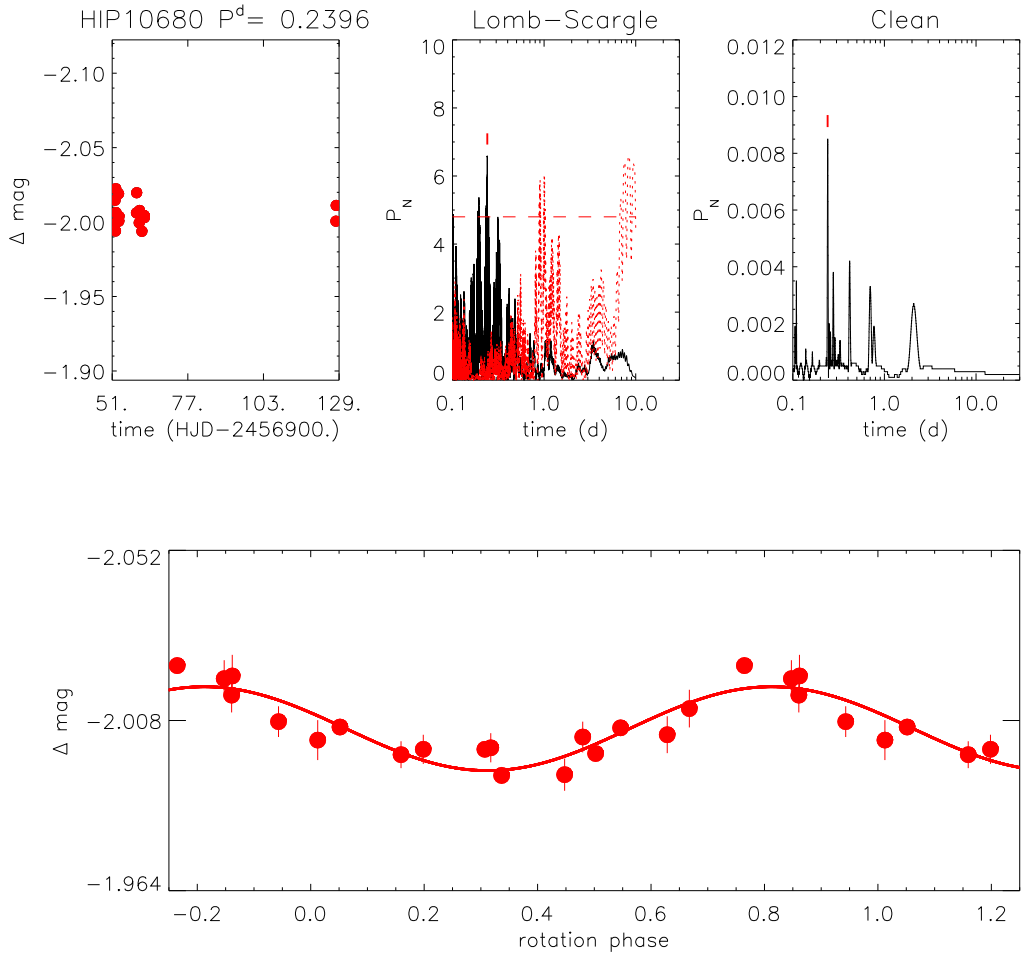

Figure 1. *top panels:* (left) Our new observations (combined B, V, and R magnitudes; see text) of HIP 10680 collected at the Taurus Hill Observatory; (middle) LS periodogram (dotted line is the window function and horizontal dashed line the power corresponding to a 99% confidence level); (right) CLEAN periodogram. *bottom panel:* light curve phased with the $P = 0.2396$ d rotation period and with overplotted (solid line) a sinusoidal fit with an amplitude of Δmag $= 0.026$ mag.

The cooler G2V component HIP 10679 hosts a debris disc first detected based on its infrared excess using the MIPS (Multiband Imaging Photometer for Spitzer) instrument onboard the Spitzer Space Telescope (Rebull et al., 2008). They derived a disc radius of 20 AU and a luminosity ratio $L_{\rm d}/L_\star = 80 \times 10^{-4}$. The disc was subsequently detected by Herschel Space Observatory, whose observations allowed Riviere-Marichalar et al. (2014) to infer an inner radius of 8.5 AU, mass $3.7 \times 10^{-3} M_\oplus$, and $T_{\rm dust} = 97$ K. In contrast, the same observations did not detect any evidence of disc around the hotter F5V component HIP10680. Both components were observed by Brandt et al. (2014) as part of the SEEDS high-contrast imaging survey of exoplanets and disks, but no companion was detected within a projected separation of 7.5″ (∼210 AU).

HIP 10680 and HIP 10679 have projected equatorial velocities $v \sin i = 37.6\,{\rm kms}^{-1}$ and $v \sin i = 7.8\,{\rm kms}^{-1}$, respectively (Valenti & Fischer 2005). Similar values, $v \sin i = 45\,{\rm kms}^{-1}$ and $v \sin i = 8\,{\rm kms}^{-1}$, respectively, are measured by Torres et al. (2006). Both components have well detected Li line. Mentuch et al. (2008) measured EW = 132 mÅ and EW = 172 mÅ for HIP 10680 and HIP 10679, respectively; da Silva et al. (2009) measured EW = 140 mÅ and EW = 160 mÅ for HIP 10680 and HIP 10679, respectively. Fast rotation and high lithium content are indicators of youth and are well consistent with the young age of 23 Myr inferred by Mamajek & Bell (2014) for the β Pictoris association.

HIP 10680 is reported in the Hipparcos catalogue as likely Algol-type eclipsing binary with period $P = 7.06$ d. However, a note to the catalogue reports the possibility that this photometry has been contaminated at some epochs by the presence of the close companion generating a spurious variability.

Consistently with the young age and their low-mass, we expect that both components exhibit photometric variability, possibly periodic, caused by the presence of surface temperature inhomogeneities. The photometric variability can in principle allow us to measure the rotation period. Multi-band photometric observations are suited to infer the rotation period and can add information on the nature of surface inhomogeneities, i.e. on their temperature, and on a lower limit on their covering fraction.

Observations

To measure the photometric rotation periods of both components we carried out a multi-filter photometric monitoring at the Taurus Hill Observatory (62°18′54″N and 28°23′21″E, 160 m a.s.l., Varkaus, Finland). Observations were collected with a 35-cm f/11 Celestron telescope on a Paramount ME German equatorial mount, and equipped with a SBIG ST-8XME CCD camera (1530×1020, 9 μm pixels size), and Johnson-Bessell BVR filters.

The visual binary HIP 10680/HIP 10679 was observed from October 21, 2014 until January 5, 2015 for a total of 7 nights. We observed in the B, V, and R filters and collected a total of 90 frames in each filter. On a few nights, we observed the binary up to four times at distance of about 2 hours from one pointing to the subsequent one. On each pointing, we collected five consecutive frames per filter. Exposure times were set to 15, 6, and 2 sec for the B, V, and R filters, respectively. Bias subtraction and flat fielding of science frames were performed with MaxIm DL 5.0 (Diffraction Limited, Canada) and the magnitude time series of each component and other nearby stars were extracted using aperture photometry. Each series of five consecutive magnitudes was averaged for the subsequent analysis. After averaging, we were left with 17 averaged magnitudes per filter whose photometric precisions turned out to be $\sigma_B = 0.006$, $\sigma_V = 0.006$, and

$\sigma_R = 0.007$ mag. The stars BD+28 381 (RA = 02:17:10.77, DEC = +28:40:55.60, J2000.0, $V = 9.09$, $B - V = 1.06$) and GSC 1777-01383 (RA = 02:17:24, DEC = 28:40:39, J2000, $V = 12.82$) turned out to be well suited to be used as comparison (C) and check (CK) stars to get differential magnitudes of our targets. The standard deviation of the CK−C magnitude time series turned out to be $\sigma_{\mathrm{CK-C}} = 0.009$ mag.

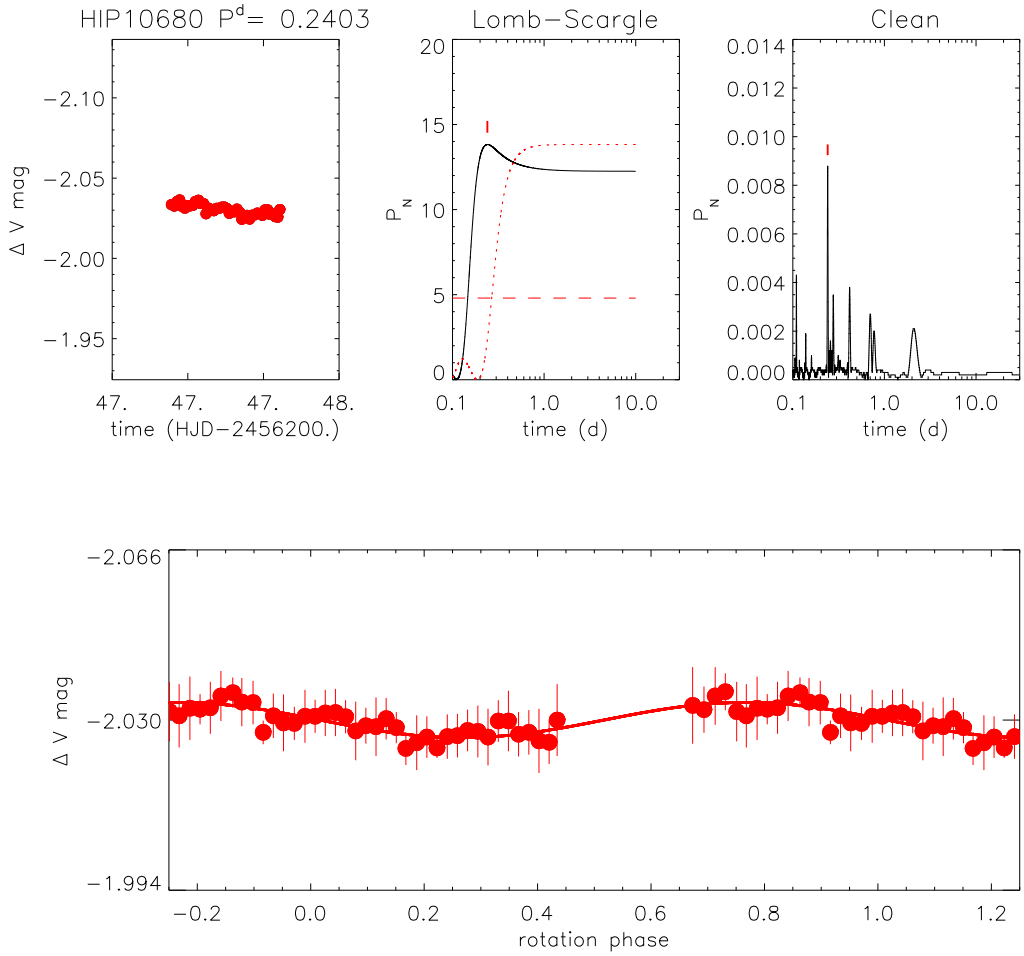

Figure 2. The same as in Fig. 1, but for data collected at Canis Mayor Observatory in the V band and phased with the rotation period $P = 0.2403$ d.

On one night, November 15, 2012, we could get a series of 390 frames in the V filter at the Canis Mayor Observatory (44°06′17″ N and 10°00′29″ E, 190 m a.s.l., La Spezia, Italy). Observations were collected by a 40-cm f/8 telescope equipped with a SBIG STL 6303 CCD camera (0.58″/pixel plate scale and 29.5′ × 19.7′ field of view) using 10-s exposure. Frame reduction was done as already described for the data collected at the Taurus Hill Observatory.

Search for rotation periods

HIP 10680

We carried out a Pearson linear correlation analysis among the magnitude variations in different filters and found that B, V, and R magnitude variations were well correlated (we measured the following linear correlation coefficients: $r_{BV} = 0.61$; $r_{BR} = 0.54$; $r_{VR} = 0.57$ with significance level $> 99.9\%$). To improve the S/N ratio of the magnitude time series for the periodogram analysis, we averaged the B, V, and R band light curves. The Lomb-Scargle (LS; Scargle 1982) and CLEAN (Roberts et al. 1987) periodogram analyses revealed a significant (FAP $< 1\%$) power peak at $P = 0.2396 \pm 0.0005$ d which we consider the stellar rotation period. For instance, this is to date the shortest rotation period ever measured in a member of the β Pictoris association. The light curve amplitudes inferred from the amplitude of the sinusoidal fit are $\Delta B = 0.035$, $\Delta V = 0.026$, $\Delta R = 0.021$ mag. An estimate of the False Alarm Probability (FAP), that is the probability that a peak of given power in the periodogram is caused by statistical variations, i.e., by Gaussian noise, was done using Monte Carlo simulations according to the approach outlined by Herbst et al. (2002). The uncertainty on the rotation period determination was estimated following Lamm et al. (2004; see also Messina et al. 2010). The results are summarized in Fig. 1.

The results of the periodogram analysis of the data collected at the Canis Mayor Observatory are summarized in Fig. 2. In this case, we note that the observations lasted about 0.19 d, and, therefore, were not long enough to measure the rotation period of HIP 10680 (the time span of observations should be at least longer than 1.5 times the searched rotation period). Nonetheless, thanks to the dense sampling we could retrieve the correct rotation period and, consistently with the other datasets, we presented the same analysis. In this case the results can be considered as a confirmation rather than an independent determination of the rotation period of HIP 10680.

We could retrieve observations of this binary system also from the SuperWASP (Butters et al. 2010) and Hipparcos (Turon et al. 1993) public archives. This binary system was observed by SWASP (1SWASP J021725.28 +284442.1) on three nights only, from 19 to 21 July, 2008. A total of 21 V-band frames were collected, where the two components are not spatially resolved. Owing to the stellar brightness, the photometric precision was very high ($\sigma_V = 0.003$ mag). The LS and Clean periodogram analyses revealed the most significant power peak at $P = 0.2405$ d, which is in very good agreement with our independent period determination. Although the components are unresolved in the SuperWASP photometry, the flux variability is likely dominated by the brighter F5V component (HIP 10680). The results are summarized in Fig. 3.

This binary system was also observed by Hipparcos from January 1990 to March 1992. After removing outliers, and averaging consecutive observations collected within 20 min, a total of 33 magnitudes were left for the subsequent analysis. Owing to the stellar brightness, the photometric precision was very high ($\sigma_V = 0.007$ mag). The LS and CLEAN periodogram analyses revealed the most significant power peak at P = 0.2805 d, and P = 0.2005 d. A note to the Hipparcos catalogue reports the possibility that this photometry has been contaminated at some epochs by the presence of the close companion generating a spurious variability. This may explain the about 10% discrepancy with respect to the period derived from our own and the SuperWASP photometry. The results are summarized in Fig. 4.

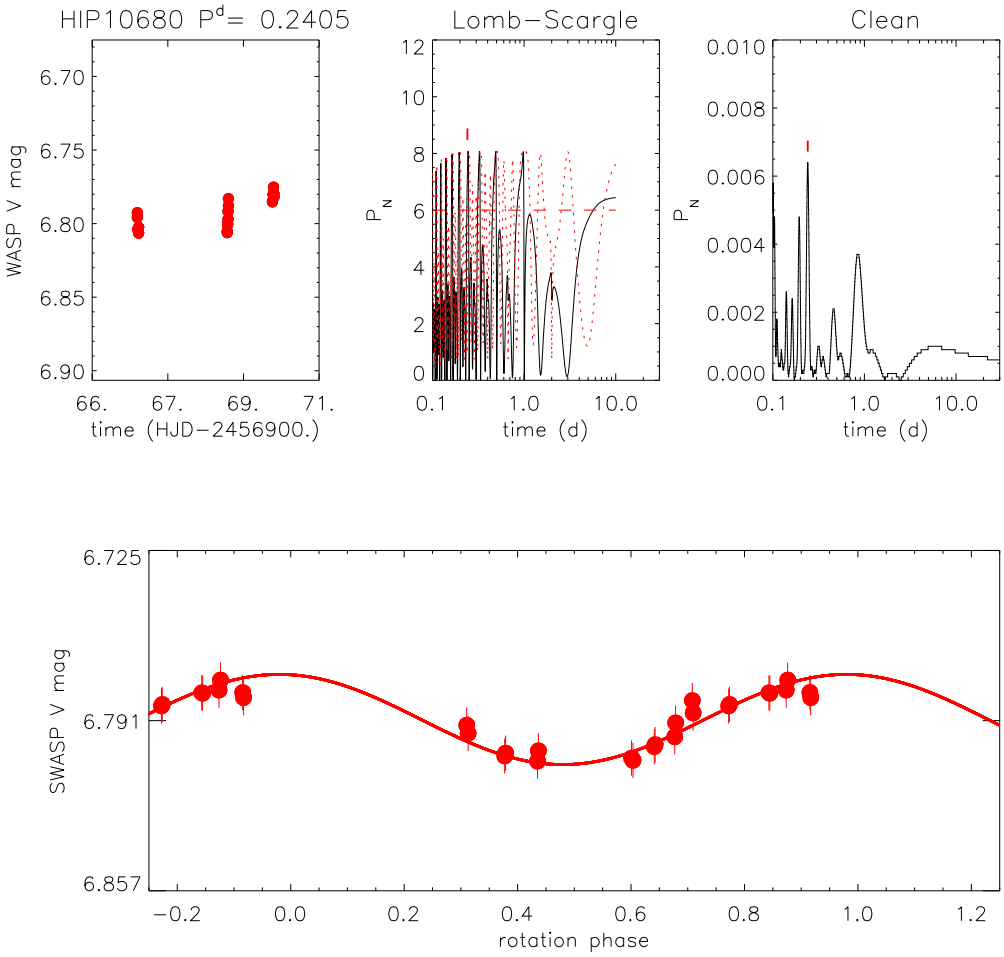

Figure 3. The same as in Fig. 1, but for data collected by SuperWASP for the unresolved system HIP10680+HIP10679. The light curve is phased with the P = 0.240 d rotation period and with overplotted (solid line) a sinusoidal fit with an amplitude of $\Delta V = 0.035$ mag.

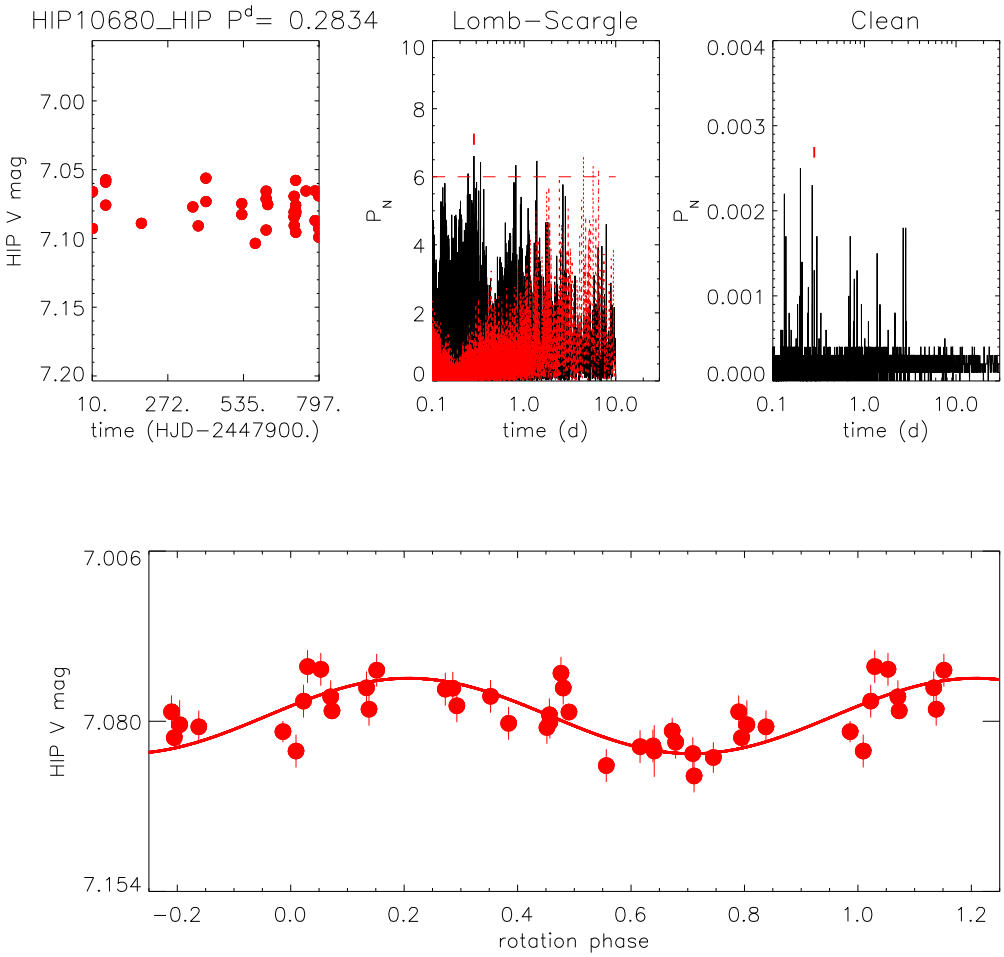

Figure 4. The same as in Fig. 1, but for data collected by Hipparcos. The light curve is phased with the $P = 0.240\,\mathrm{d}$ rotation period and with overplotted (solid line) a sinusoidal fit with an amplitude of $\Delta V = 0.030\,\mathrm{mag}$.

HIP10679

We carried out a Pearson linear correlation analysis among the magnitude variations in different filters and found that the correlation coefficients are $r > 0.70$ with confidence level $> 99.8\%$. As done for HIP 10680, we averaged the multi-band light curves. The LS and CLEAN periodograms revealed the highest power peak to be at $P = 0.777 \pm 0.005$ d with FAP $< 1\%$. This is the stellar rotation period of HIP 10679. The light curves have peak-to-peak amplitudes $\Delta B = 0.06$, $\Delta V = 0.07$, and $\Delta R = 0.07$ mag. The results are summarized in Fig. 5.

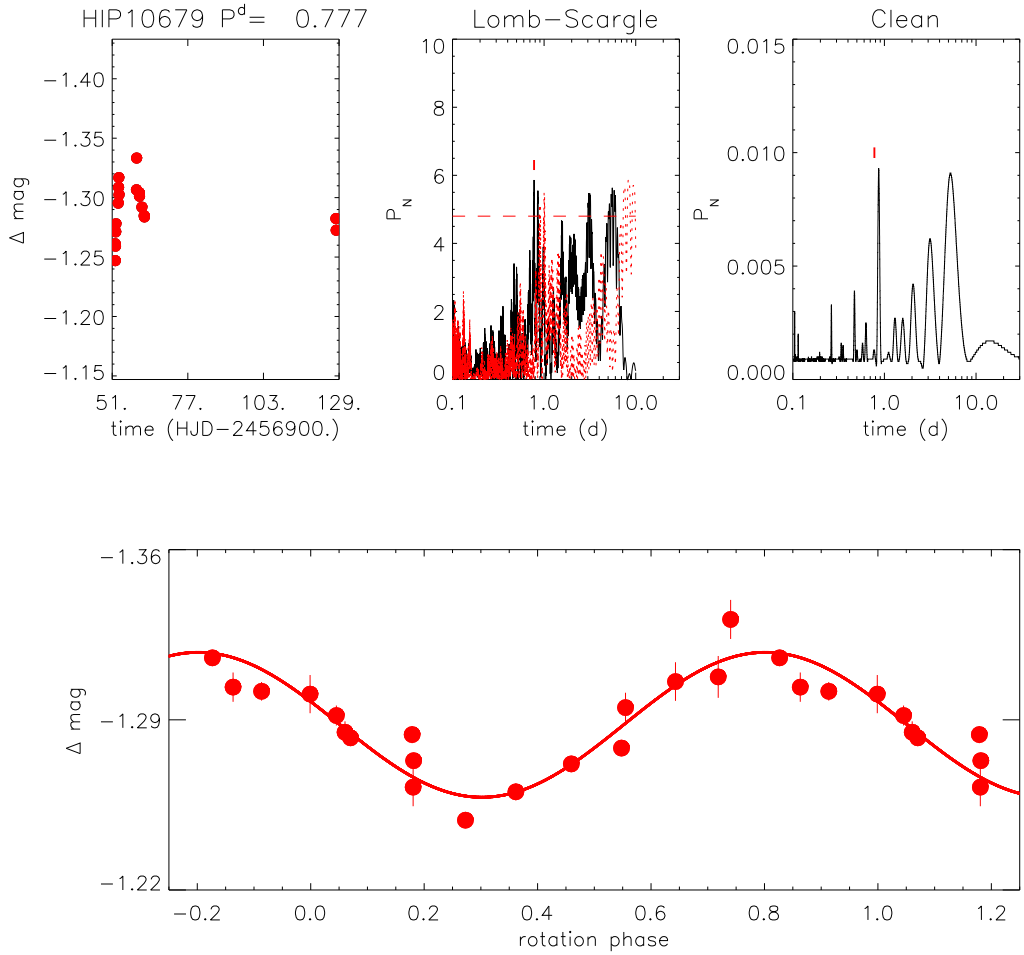

Figure 5. *top panels:* Our new observations (combined B, V, and R magnitudes; see text) of HIP 10679; LS periodogram (dotted line is the window function and horizontal dashed line the power corresponding to a 99% confidence level); and CLEAN periodograms. *bottom panel:* light curve phased with the $P = 0.777\,d$ rotation period and with overplotted (solid line) a sinusoidal fit with an amplitude of Δmag $= 0.07$ mag.

We could retrieve also the magnitude time series of HIP 10679 collected by Hipparcos.

Although the magnitudes are to some level contaminated by the flux from the nearby brighter star, we could retrieve from our periodogram analysis about the same rotation period $P = 0.78 \pm 0.02$ d. The results are summarized in Fig. 6. No similar rotation period was found in the short SuperWASP time series.

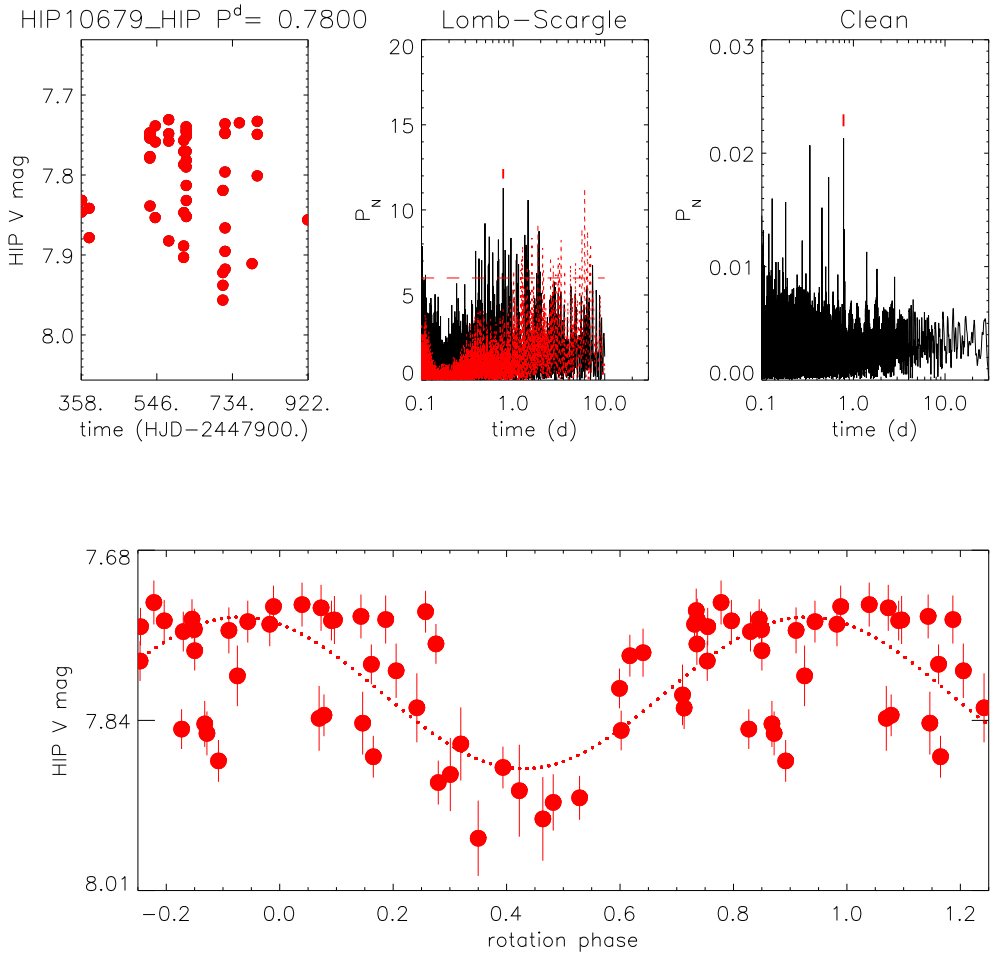

Figure 6. The same as in Fig. 5, but for data collected by Hipparcos. A mentioned in the text, this photometry may be contaminated by the flux from the brighter component.

Discussion

Using the observed V magnitude, the distance from Pecaut & Mamajek (2013), the bolometric correction and effective temperature proper for their spectral types from Pecaut & Mamajek (2013) we could estimate the luminosity and radius of both components. For HIP 10680, we derive a luminosity $L = 1.88 \pm 0.17\, L_{\odot}$, a radius $R = 1.11 \pm 0.10\, R_{\odot}$. Combining radius and average projected stellar velocity, we estimate an inclination of the

stellar rotation axis $i \sim 10°$.

For HIP 10679, we derive a luminosity $L = 0.96 \pm 0.09\, L_{\odot}$, a radius $R = 0.95 \pm 0.09\, R_{\odot}$. Combining radius and average projected stellar velocity we estimate an inclination of the stellar rotation axis $i \sim 10°$. The same inclination likely arises from the common formation and early evolution processes of the two stars in the same binary system. An interesting aspect presented by this system is that the two components have a significant difference in their rotation periods. This difference may be due to the different masses. However, we find from a comparison with the evolutionary models of Siess et al. (2000) that this difference is not larger than about 15%. Different initial rotation periods may also have caused the presently observed difference. However, we note that the slower rotating G2V component hosts a debris disc. There is evidence of an anti-correlation between the presence of IR excess, revealing the presence of primordial discs, and the rotation period in very young stars (see, e.g. Bouvier et al. 1993, Rebull et al. 2004). In fact, the magnetic disc-locking should lock the rotation of the external star's envelope with the disc rotation and prevent the star to spin-up despite the stellar radius contraction. By the age of β Pictoris, such an anti-correlation is not as significant as in younger stars, and it appears as a weak tendency of fast rotators to have smaller IR excess (see Rebull et al. 2008). However, the available sample is not large and $v \sin i$ is used to measure the rotation rate, instead of the more robust rotation period. In our specific case, one possibility to explain the rotation period difference is that the component with IR excess HIP10679 may have had a disc-locking phase longer than the other component, for which no IR excess is detected. The shorter disc-locking phase of HIP10680 may have allowed this star to start the rotation spin-up, owing to radius contraction towards the ZAMS, earlier than HIP10679, and therefore reaching a shorter rotation period at the present age. However, we just propose it as one possibility.

What may have caused different disc-lifetimes for the two components and different rotation periods is currently unknown. In fact, neither binarity nor the presence of sub-stellar companion have been reported for either star, that may have gravitationally perturbed the primordial disc of HIP 10680, enhancing its dispersal.

Conclusions

We have carried out a multi-filter photometric monitoring of the wide visual binary HIP10680/HIP10679. We found that HIP10680 has a rotation period $P = 0.2396 \pm 0.0005$ d, which is the shortest value ever measured in the β Pictoris association, whereas HIP10679 has a rotation period $P = 0.777 \pm 0.005$ d. Combining stellar radii and projected rotational velocities, we found that both components have same inclinations of their rotation axes, $i \sim 10°$ and, therefore, they are seen almost pole-on. Despite the low inclination, both components exhibit a significant photometric variability whose amplitudes in the V band are $\Delta V = 0.03$ mag and $\Delta V = 0.07$ mag, for HIP10680 and HIP10679, respectively. The G2V star, having a deeper convection zone, and consequently, a more efficient dynamo action, shows a larger amplitude variability. Although the two components have a mass difference not larger than 15%, they exhibit a significant difference between their rotation periods. Such difference may arise either from different initial rotation periods or to different disc life times. For instance, the slower component HIP 10679 hosts a well known debris disc.

Acknowledgements: The extensive use of the SIMBAD database operated by the CDS, Strasbourg, France, and the ADS database operated by the Smithsonian Astrophys-

ical Observatory (SAO) under a NASA grant, are gratefully acknowledged. We thank the Super-WASP consortium for the use of their public archive in this research. We also thanks the anonymous Referee for useful comments and suggestions.

References:

Bouvier, J., Cabrit, S., Fernandez, M., Martin, E. L., & Matthews, J. M., 1993, *A&A*, **272**, 176
Brandt, T.D., Kuzuhara, M., McElwain, M.W., et al., 2014, *ApJ*, **786**, 1
Butters, O.W., West, R.G., Anderson, D.R., et al., 2010, *A&A*, **520**, L10
da Silva, L. Torres, C.A.O., de la Rez, R., et al., 2009, *A&A*, **508**, 833
Herbst, W., Bailer-Jones, C. A. L., Mundt, R., Meisenheimer, K., & Wackermann, R., 2002, *A&A*, **396**, 513
Kiss, L. L., Moór, A., Szalai, T., et al., 2011, *MNRAS*, **411**, 878
Lamm, M. H., Bailer-Jones, C. A. L., Mundt, R., Herbst, W., & Scholz, A., 2004, *A&A*, **417**, 557
Lépine, S. & Simon, M., 2009, *AJ*, **137**, 3632
Malo, L., Doyon, R., Lafreniére, D., et al., 2013, *ApJ*, **762**, 88
Mamajek, E.E. & Bell, C. P. M., 2014, *MNRAS*, **445**, 2169
Mason, B.D., Wycoff, G.L., Hartkopf, W.I., et al., 2001, *AJ*, **122**, 3466
Mentuch, E., Brandeker, A., van Kerkwijk, M.H., et al., 2008, *ApJ*, **689**, 1127
Messina, S., Desidera, S., Turatto, M., Lanzafame, A. C., & Guinan, E. F., 2010, *A&A*, **520**, A15
Messina, S., Monard, B., Biazzo, K., Melo, C. H. F., & Frasca, A., 2014, *A&A*, **570**, A19
Messina, S., Monard, B., Worters, H.L., Bromage, G.E., Zanmar, R.S., 2015, submitted to New Astronomy
Pecaut, M. J. & Mamajek, E. E., 2013, *ApJS*, **208**, 9
Rebull, L. M., Wollfs S. C., & Strom, S. E., 2004, *AJ*, **127**, 1029
Rebull, L. M., Stapelfeldt, K. R., Werner, M. W., et al., 2008, *ApJ*, **681**, 1484
Riviere-Marichalar, P., Barrado, D., Montesinos, B., et al., 2014, *A&A*, **565**, A68
Roberts, D. H., Lehar, J., & Dreher, J. W., 1987, *AJ*, **93**, 968
Scargle, J. D., 1982, *ApJ*, **263**, 835
Siess L., Dufour E., Forestini M., 2000, *A&A*, **358**, 593
Torres, C. A. O., Quast, G. R., da Silva, L., et al., 2006, *A&A*, **460**, 695
Turon C., Egret D., Gomez A., et al., 1993, *BICDS*, **43**, 5
Valenti, J.A. & Fischer, D.A., 2005, *ApJS*, **159**, 141
Zacharias N., Finch C.T., Girard T.M., et al., 2013, *Astron. J.*, **145**, 44
Zuckerman, B. & Song, I., 2004, *ARA&A*, **42**, 685

COMMISSIONS 27 AND 42 OF THE IAU
INFORMATION BULLETIN ON VARIABLE STARS

Number 6146

Konkoly Observatory
Budapest
27 July 2015

HU ISSN 0374 – 0676

AO Psc TIME KEEPING

BONNARDEAU, MICHEL

MBCAA Observatory, Le Pavillon, 38930 Lalley, France, email: arzelier1@free.fr

AO Piscium (RA=$22^{\rm h}55^{\rm m}17\overset{\rm s}{.}99$ DEC=$-03°10'40\overset{''}{.}0$ J2000.) is an intermediate polar, that is a subclass of cataclysmic systems in which the white dwarf is magnetized enough to module the accretion. Furthermore, the period of rotation (or spin) of the white dwarf is shorter than the orbital period and there is an accretion disc. AO Psc is one of the brightest cataclysmic, with a V mag as high as 13.2.

The orbital period is $P_{\rm orb} = 3\overset{\rm h}{.}59$, the rotation period of the white dwarf is $P_{\rm rot} = 805\,{\rm s}$ and the accretion X-ray beam is reprocessed on the secondary star atmosphere, giving rise to a synodic modulation with the period $P_{\rm syn}$ such that:
$1/P_{\rm syn} = 1/P_{\rm orb} - 1/P_{\rm rot}$
i.e. $P_{\rm syn} = 859\,{\rm s}$ (Patterson & Price, 1981, Motch & Pakull, 1981, van Amerongen et al., 1985 (hereafter vA85), Taylor et al., 1997).

All these periodicities are visible by photometry as modulations in the light curves, the synodic modulation being usually the strongest one.

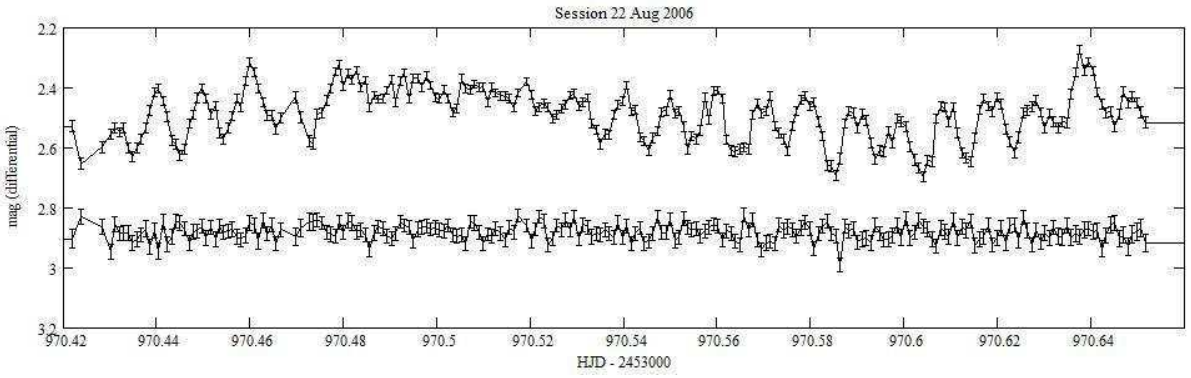

Figure 1. Upper light curve: AO Psc, Lower: the check star shifted by −0.2 mag. The error bars are the quadratic sum of the 1-sigma statistical uncertainties on the variable/check star and on the comparison star.

Photometric observations of AO Psc were carried out over eleven seasons, from 2004 to 2014, with a 203 mm f/6.3 Schmidt-Cassegrain telescope, a Clear filter and an SBIG

ST7E camera (KAF401E CCD). The exposures were 60 s long. The images were dark substracted (using master darks of the same duration than the images and at the same temperatures) and flat corrected (MaximDL software program). For the aperture differential photometry (AstroMB software package), the comparison star is GSC 5238-462. A check star, GSC 5238-347, is used to compare the standard deviations to the statistical uncertainties so as to make sure that the systematic errors are low. An example of a light curve is given Figure 1. A total of 8744 images were obtained over 74 nights.

Table 1: Results of the fits and cycle counts

Season	$t_{\rm syn}$	$N_{\rm syn}$	$t_{\rm rot}$	$N_{\rm rot}$	$t_{\rm orb}$	$N_{\rm orb}$	A_0	$A_{\rm syn}$	$A_{\rm rot}$	$A_{\rm orb}$
2004	322.3748	(a)	323.2710	(b)	346.3534	(c)	2.614	-0.120	-0.054	0.033
	±10		±22		±68		±0.002	±0.001	±0.001	±0.002
2005	612.6533	29,209	612.6264	31,050	701.2596	2,372	2.488	-0.117	-0.051	0.063
	±7		±25		±40		±0.001	±0.001	±0.001	±0.001
2006	970.4400	36,002	970.4118	38,393	970.5857	1,800	2.530	-0.117	-0.063	0.068
	±12		±13		±49		±0.001	±0.001	±0.002	±0.001
2007	1301.5420	33,317	1356.4425	41,424	1296.6073	2,179	2.214	-0.044	-0.016	0.091
	±9		±36		±39		±0.001	±0.001	±0.001	±0.001
2008	1709.5149	41,052	1681.5259	34,884	1681.6001	2,573	2.271	-0.036	-0.038	0.062
	±18		±15		±9		±0.001	±0.001	±0.001	±0.001
2009	2041.5198	33,408	2041.5171	38,630	2041.5900	2,406	2.227	-0.029	-0.028	0.080
	±16		±21		±44		±0.001	±0.001	±0.001	±0.001
2010	2415.5229	37,634	2454.5989	44,327	2415.5044	2,499	2.292	-0.032	-0.040	0.075
	±30		±22		±33		±0.002	±0.002	±0.001	±0.001
2011	2744.5262	33,106	2748.5909	31,548	2744.5315	2,199	2.207	-0.041	-0.024	0.100
	±17		±16		±23		±0.001	±0.001	±0.001	±0.001
2012	3140.4698	39,842	3140.4705	42,052	3126.5269	2,553	2.218	-0.028	-0.020	0.063
	±38		±35		±13		±0.001	±0.001	±0.001	±0.001
2013	3489.5265	35,124	3489.4897	37,453	3559.3922	2,893	2.189	-0.049	-0.017	0.083
	±10		±51		±61		±0.001	±0.001	±0.001	±0.001
2014	3836.4857	34,913	3836.4863	37,236	3865.5218	2,046	2.173	-0.067	-0.007	0.087
	±11		±72		±72		±0.001	±0.001	±0.003	±0.001

the $t_{\rm xxx}$ are in HJD − 2,453,000 with the uncertainties in seconds,
the $N_{\rm xxx}$ for one season is the difference with the previous season,
the $A_{\rm xxx}$ are in mag.
(a) 819,882 cycles from the 0 of vA85, 83,170 cycles from the 2002 measurement of Williams (2003) (hereafter W03).
(b) 905,581 cycles from the 0 of vA85, 711,933 cycles from the 1986 measurement of Kaluzny & Semeniuk (1988) (hereafter KS88).
(c) 56,689 cycles from the 0 of vA85 + $P_{\rm orb}/2$, 44,495 cycles from the 1986 measurement of KS88 + $P_{\rm orb}/2$.

The magnitudes as a function of time t are fitted by the following $H(t)$ function:
$H(t) = A_0 + H_{\rm syn}(t) + H_{\rm rot}(t) + H_{\rm orb}(t)$
where A_0 is a constant, $H_{\rm syn}(t)$ is the synodic modulation:
$H_{\rm syn}(t) = A_{\rm syn}[\cos(\pi(t - t_{\rm syn})/P_{\rm syn}]^2$

$H_{\rm rot}(t)$ is the rotation modulation:
$H_{\rm rot}(t) = A_{\rm rot}[\cos(\pi(t - t_{\rm rot})/P_{\rm rot}]^2$
and $H_{\rm orb}(t)$ is the orbital modulation:
$H_{\rm orb}(t) = A_{\rm orb}[1 + \cos(2\pi(t - t_{\rm orb})/P_{\rm orb})]$

The $H(t)$ function is fitted to the observations owing to a Monte Carlo method to test the parameters relative to the timing and, for each trial, the amplitudes are determined by a least squares method. The magnitudes are weighted with the uncertainties.

Each Monte Carlo run is made of 10 millions trials. The averages and standard deviations for 10 runs are given in Table 1, along with the number of cycles, $N_{\rm xxx}$.

In 2007 the synodic and rotation modulations become fainter, especially the synodic one, and the orbital modulation and the non-modulated part A_0 become brighter, as shown Figures 2-5.

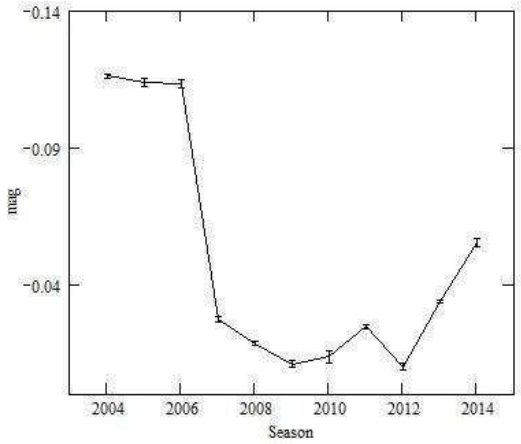

Figure 2. The amplitude $A_{\rm syn}$

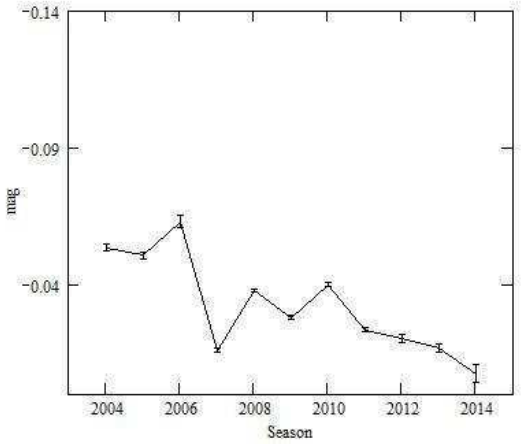

Figure 3. The amplitude $A_{\rm rot}$

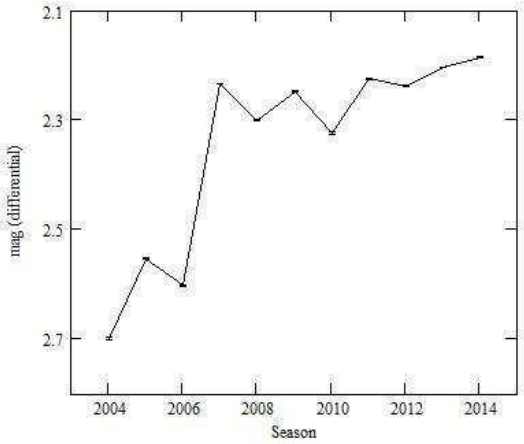

Figure 4. The amplitude A_0

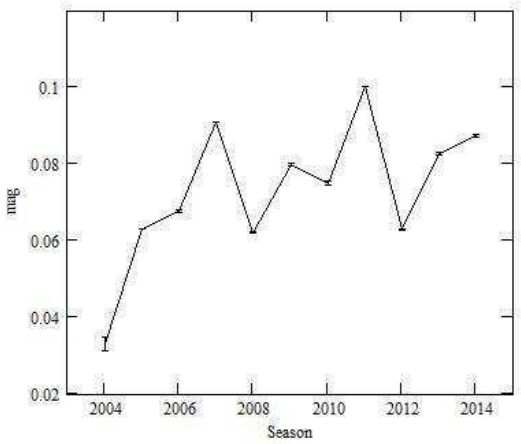

Figure 5. The amplitude $A_{\rm orb}$

The times of maxima of the synodic modulation may be fitted with the function $\mathrm{ToM}(n) = T_{\rm syn} + P_{\rm syn}n + b_{\rm syn}n^2$. There are 26 such maxima (9 from vA85, 1 from KS88, 5 from W03 and 11 from this paper). With only the data from vA85 and of W03, there is an ambiguity in the cycle count and two fits are possible (W03). Indeed, the residuals (weighted with the uncertainties) are then 8.1 s for the Fit 1 of W03 and 10.4 s for the

Fit 2. But adding the data presented here allow lifting the ambiguity: 8.9 s for the Fit 1, 15.6 s for the Fit 2. Adding the measurement of KS88 gives 9.2 s and 15.4 s respectively. Therefore, the cycle count of the Fit 1 of W03 is the right one.

The fit of the 2004-14 synodic maxima gives $b_{\rm syn} = -(2.544 \pm 0.043) \times 10^{-13}$ day. This is larger (smaller in absolute value) that the fits of W03, themselves larger than the ones of KS88 and of vA85. All the 26 maxima are then fitted with a supplementary term, $\gamma_{\rm syn} n^3$. Furthermore, they are corrected for the leap seconds due to the Earth rotation slowing down (Eastman et al., 2010). For $T_{\rm syn}$ in 1982 this correction is 21 s, for the first maximum the correction is 19 s, 35 s for the last one. $T_{\rm syn}$ is to be expressed in HJD, the corrections are then between -2 s and $+14$ s. The barycentric effect of Jupiter and Saturn is neglected as it is only $\pm$ 4 s and cyclic (unlike the leap seconds that keep accumulating), and the other general relativistic corrections are much smaller. The least squares method gives:
$b_{\rm syn} = -3.020 \times 10^{-13}$ day
$\gamma_{\rm syn} = 1.44 \times 10^{-21}$ day.

The fit is also done with a Monte Carlo method, so as to have a result that is independent of the least squares method and to evaluate the uncertainties. For a Monte Carlo run, $T_{\rm syn}$, $P_{\rm syn}$, $b_{\rm syn}$ and $\gamma_{\rm syn}$ are chosen each in its own range; for $\gamma_{\rm syn}$ the range is $[-10, +10] \times 10^{-21}$. 10 millions trials are computed for a run. The averages and standard deviations of 10 runs are:
$T_{\rm syn} = 2,445,174.181,13(2)$ HJD
$P_{\rm syn} = 0.009,938,498,0(4)$ day
$b_{\rm syn} = -3.031(8) \times 10^{-13}$ day
$\gamma_{\rm syn} = 2.13(44) \times 10^{-21}$ day.

Therefore the spinning up is slowing down. The derivative of the period is:
$\dot{P}_{\rm syn} = 2b_{\rm syn}/P_{\rm syn} = -6.10 \times 10^{-11}$
and the secondary derivative of the period is:
$\ddot{P}_{\rm syn} = 6\gamma_{\rm syn}/P_{\rm syn}^2 = 1.30 \times 10^{-16}\,{\rm day}^{-1}$.
This gives the time scale:
$\tau = P_{\rm syn}/(2\dot{P}_{\rm syn}) = -223$ kyr
and the breaking index:
$n = P_{\rm syn}\ddot{P}_{\rm syn}/\dot{P}_{\rm syn}^2 = 346$.
(By comparison, for FO Aqr, one has from W03: $\tau = 194$ kyr, $n = -6431$).

There are 7 orbital maxima from vA85 and one from KS88. In order to fit them with the 11 orbital minima presented here, they are corrected by adding $P_{\rm orb}/2$. A Monte Carlo method (rather than a least squares method, so as to evaluate the uncertainties) gives the ephemeris, for the orbital minima, taking into account the leap seconds:
$t(n) = T_{\rm orb} + P_{\rm orb} n$
with:
$T_{\rm orb} = 2,444,864.21809(1)$ HJD
$P_{\rm orb} = 0.149,625,502,2(1)$ day
This is within the error bars of the ephemeris of KS88, with a better precision. An ephemeris with a quadratic term was also searched for, but with no significant improvement.

As the rotation modulation is related to the synodic modulation and the orbital period, the number of rotations of the white dwarf may be calculated unambiguously. The results are given in Table 1 at (b).

References:

Eastman J., Siverd R. and Gaudi B.S., 2010, *PASP*, **122**, 935
Kaluzny J. and Semeniuk I., 1988, *IBVS*, 3145
Motch C. and Pakull M.W., 1981, *A&A*, **101**, L9
Patterson J. and Price C.M., 1981, *ApJ*, **243**, L83
Taylor P., Beardmore A.P., Norton A.J., Osborne J.P. and Watson M.G., 1997, *MNRAS*, **289**, 349
van Amerongen S., Kraakman H., Damen E., Tjemkes S. and van Paradijs J., 1985, *MNRAS*, **215**, P45
Williams G., 2003, *PASP*, **115**, 618

*This version of the paper contains corrections, and differs from the one appeared on-line originally. Date of last modification: Mar 13 2016

COMMISSIONS 27 AND 42 OF THE IAU
INFORMATION BULLETIN ON VARIABLE STARS

Number 6147

Konkoly Observatory
Budapest
3 August 2015

HU ISSN 0374 – 0676

A NEW CONTACT ECLIPSING BINARY IN THE FIELD OF KOI 1152

SAFSTEN, EMILY D.[1]; LARA, PAMELA[1,2]; JONER, MICHAEL D.[1]; STEPHENS, DENISE C.[1]; RAWLINS, JOSEPH[1]

[1] Department of Physics and Astronomy, Brigham Young University, N283 ESC, Provo, UT, USA, 84602

[2] Department of Physics, Utah Valley University, MS-179, 800 W. University Parkway, Orem, UT, USA, 84058

A new contact eclipsing binary star, designated in the WISE catalog as J194643.44+472029.4, was discovered during research on the transiting planet candidate KOI 1152. A search in the General Catalog of Variable Stars as well as a literature search in the SAO/NASA Astrophysics Data System revealed that this star has not yet been documented as a variable.

This field was observed on multiple nights from 2011-2014 with the 0.9 m optical telescope at Brigham Young University's West Mountain Observatory. Data were taken in the B, V, R, and I filters of the Johnson/Cousins system. The images were reduced using standard procedures in IRAF, and differential aperture photometry was performed using the BRIGHTER program (Ranquist 2013) that was developed at BYU. J194643.44+472029.4 has an apparent V magnitude ranging from about 16.25 to 16.75.

Initially, it was thought that this new variable was of the δ Scuti type. A closer inspection of the light curve, however, revealed characteristics, particularly the brief plateaus of the minima, that suggested the object is instead a contact eclipsing binary. The eclipses have very similar depths, indicating that the components have about the same effective temperature. Figure 1 shows phased light curves for the object in all four filters we used. From our observations and analysis, we estimated a color index of $B - V = 0.51$ mag, corresponding to a temperature of 6240 K according to the table for main sequence stars in Flower (1996). The 2MASS catalog lists J and K magnitudes for this object of 15.314 and 15.035, respectively, giving $J - K = 0.279$ (Skrutskie et al. 2006). According to Bessell & Brett (1988), this corresponds to approximately an F5 spectral type, which has a temperature of 6400 K. This corroborates our estimate of temperature from the $B - V$ color index.

We used the AoV period search algorithm in the VARTOOLS program to determine the period of this system and found it to be $P = 0.346178$ d (Schwarzenberg-Czerny 1989, Devor 2005, Hartman et al. 2008). It was difficult for the algorithm to acknowledge the presence of two different eclipses, due to their very similar depths and the scatter of our data, and the half-period of $P = 0.173089$ d was also a strong result. We thus recognize that J194643.44+472029.4 could indeed be an intrinsically variable star with a period of 0.173089 d, and spectral data may be needed to confirm the binary nature of this object. We also detected a period change in J194643.44+472029.4 towards the end

of our available data. A period decrease of about 10 s occurred sometime between HJD 2456960.779091 and HJD 2456967.609178. The new period is $P \approx 0.346062$ d, or, if it is in fact an intrinsically variable star, $P \approx 0.173031$ d. We have one good observed time of minimum after this change, determined by the Kwee & van Woerden (1956) method to be HJD 2456969.6782, though it is unclear whether this is a primary or secondary minimum. We have not further analyzed the state of the system after this happens, due to our lack of data during this time, and thus leave that to future work.

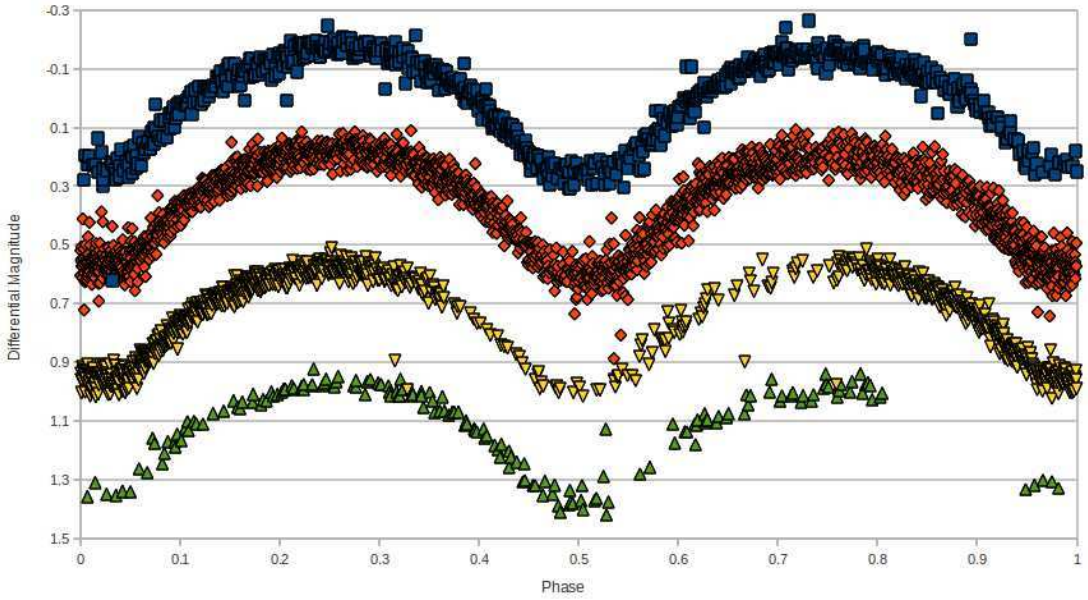

Figure 1. Phased light curves of J194643.44+472029.4 in, from top to bottom, B, V, R, and I filters.

We used the package PHOEBE, which makes use of the Wilson-Devinney code, to find a model for this object (Prša and Zwitter 2005). We worked with several of the different models that the program provides. In accordance with the determined color index, we fixed the temperature of the primary component at 6240 K in each model. The secondary temperature, T_2, was left free to vary except where doing so led to exorbitant parameter values, in which case it also was fixed at 6240 K. Other free parameters included the mass ratio q, the inclination i, the luminosities in each filter of the primary star, and the stars' dimensionless potential. Most of the results from the different models are in good general agreement with each other, giving a mass ratio of about 4-5 and an inclination of 85°-90°. The larger component is about 0-100 K warmer than its companion. The best fit comes from the overcontact binary of the W UMa type model. The results from this fit are a mass ratio of $q = 4.5$, an inclination of $i = 85°$, and a degree of contact $f \approx 34\%$. The secondary temperature T_2 was fixed at 6240 K. The semidetached model with the secondary component filling its lobe converged to a solution with a significant degree of contact and also gives a very good fit to the data. It is in good agreement with the W UMa model, giving $q = 5.2$, $i = 87°$, $T_2 = 6312$ K, and degree of contact of $f \approx 67\%$. Figure 2 shows the best fit solution, from the W UMa model, with our observed light curves in the B, V, R, and I filters, and Figure 3 gives a visual interpretation of the system at phase 0.25, as generated by PHOEBE.

The model described above provides the best fit to our observed curves, most notably in the plateaus of the minima. However, other models were found which, though they do

not give the best fit, perhaps should not be entirely discarded. A system with $q \approx 3.2$, $T_2 \approx 6188$ K, and $i \approx 70°$, or a system with $q \approx 1.3$, $T_2 \approx 4616$ K, and $i \approx 70°$, both provide solutions which do not have flat minima but are within the scatter of our data. Thus, though the first model we described gives the best fit, perhaps other models should not be entirely ruled out, as they may also give valid solutions. We will further work with the models to refine our solution, explore other possible factors such as spots and a third light, and more precisely determine the parameter values.

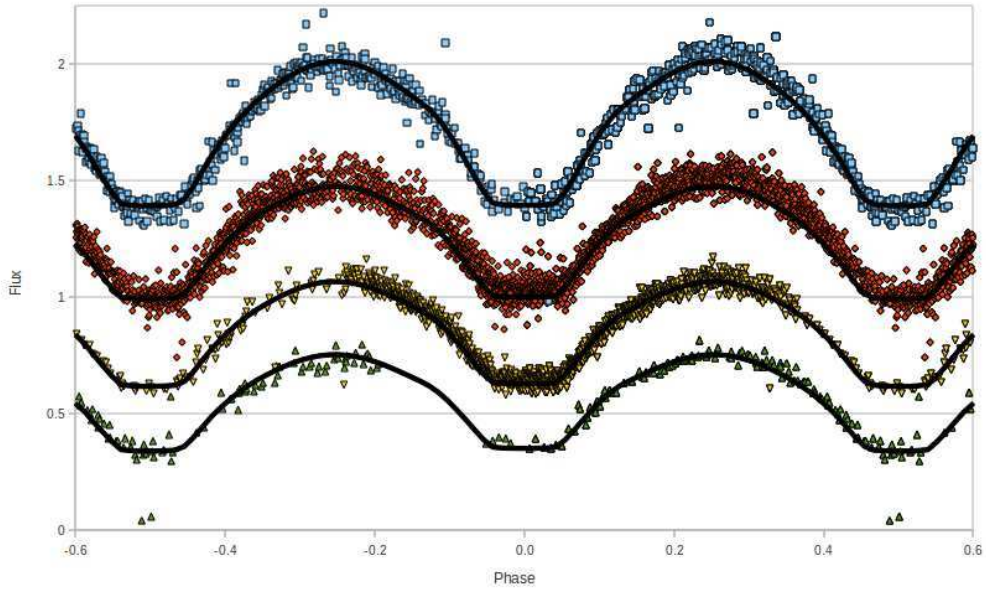

Figure 2. Observed data and solution light curves in, from top to bottom, B, V, R, and I filters. The calculated curves are shown as solid lines.

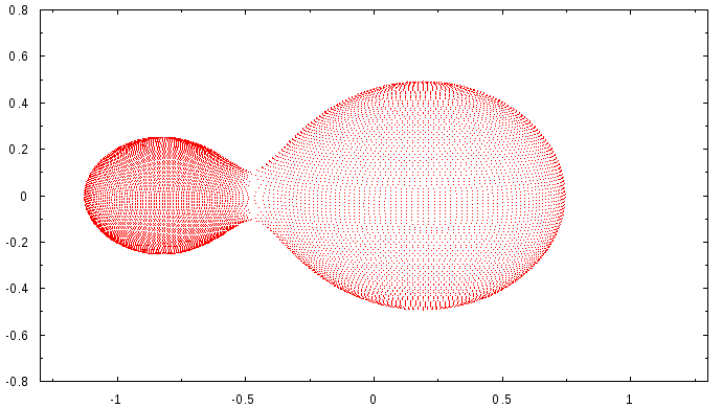

Figure 3. Geometric representation of J194643.44+472029.4.

Acknowledgements: This research has made use of the VizieR catalogue access tool, CDS, Strasbourg, France. The original description of the VizieR service was published in

A&AS 143, 23. This publication makes use of data products from the Two Micron All Sky Survey, which is a joint project of the University of Massachusetts and the Infrared Processing and Analysis Center/California Institute of Technology, funded by the National Aeronautics and Space Administration and the National Science Foundation. The research was also made possible by use of the facilities at Brigham Young University's West Mountain Observatory with NSF grant AST-0618209. It was also funded in part by the Physics and Astronomy REU program at BYU during the summer of 2013 with NSF grant PHY-1157078.

References:

Bessell M. S., Brett J. M., 1988, *PASP*, **100**, 1134
Devor, J., 2005, *ApJ*, **628**, 411
Flower, P. J., 1996, *ApJ*, **469**, 355
Hartman et al., 2008, *ApJ*, **675**, 1254
Kwee K. K., van Woerden H., 1956, *BAN*, **12**, 327
Prša A., Zwitter T., 2005, *ApJ*, **628**, 426
Ranquist, E. A. 2013. A Compilation and Description of Scripts Written for the Optimization of Photometric Procedures. Bachelors Thesis, Brigham Young University, Provo, Utah. 45 p.
Schwarzenberg-Czerny, A., 1989, *MNRAS*, **241**, 153
Skrutskie, M. F. et al., 2006, *AJ*, **131**, 1163

ERRATUM FOR IBVS 6147

We had initially reported a period change in this binary system that occurred toward the end of our available data. Analysis of images obtained later on, however, did not show the new period to persist. Through further investigation, we found that, unbeknownst to us, there had been an error in the time in the telescope computer during the acquisition of the data at the end of our original set. This caused the observation times of these images to be off, which led to our interpretation of a period change. We have since corrected the error, and the binary's period remains consistent with the original value of $P = 0.346178$ d.

The authors

COMMISSIONS 27 AND 42 OF THE IAU
INFORMATION BULLETIN ON VARIABLE STARS

Number 6148

Konkoly Observatory
Budapest
14 September 2015

HU ISSN 0374 – 0676

STUDY OF PULSATION SPECTRUM OF MASS-ACCRETING COMPONENT OF ALGOL-TYPE SYSTEM VV UMa

GUNSRIWIWAT, K.[1]; MKRTICHIAN, D.E.[2]

[1] Department of Physics and Materials Science, Faculty of Science, Chiang Mai University, Muang, 50200 Chiang Mai, Thailand

[2] National Astronomical Research Institute of Thailand, 191 Siriphanich Bldg., Huay Kaew Rd., Suthep, Muang, 50200 Chiang Mai, Thailand

VV UMa is an eclipsing, semi-detached (Algol-type) close binary system with a short period of 0.6873801 day. It was found to be a variable by Gitz (1936) based on the photographic plates taken at the Moscow Observatory. Afterwards, Struve (1950) classified VV UMa as a single-lined spectroscopic binary with spectral type A0V, a mass ratio q$\sim$0.23 and semi-amplitude $K_1 = 59\,\mathrm{km\,s^{-1}}$. Hill et al. (1975) classified the primary component as A2V. The first set of complete uvby light curves of VV UMa was acquired in 2000 January and analyzed by Lázaro et al. (2001). They reported about detection of pulsational light variations with periodicity of about 0.048 days (20.88 c/d) and 0.020 days (50.76 c/d). Later, with new observations, Lázaro et al. (2002) confirmed the periodicity of about 0.0216 days (46.2 c/d) and derived effective temperatures of the primary and the secondary as $T_{\rm eff}$=9250$\pm$150 K and $T_{\rm eff}$=5600$\pm$100 K, respectively. Kim et al. (2005) confirmed the pulsations and assign VV UMa system to so called new class of oEA stars suggested by Mkrtichian et al. (2002, 2004). Kim et al. *B*-filter CCD photometric light curve and period search analysis definitely show of 51.239 c/d (0.0195 day) and 47.46 c/d (0.0211 day) pulsations.

We conducted a new photometric observations of VV UMa within frames of Thai Sky Survey for oEA Stars (THASSOS) in order to get improved information about oscillation spectrum. The photometric observations were acquired from 26 December 2013 to 23 March 2014 at the Thai National Observatory (TNO, 18° 35′ 17″ N, 98° 29′ 11″ E). The 0.5 meter Cassegrain Telescope, the Apogee Alta U9000 3056 × 3056 pixels CCD camera and 10 seconds exposure times though V filter were used. The data were reduced by using Maxim DL5 program. Comparison stars are listed in Table 1. The phased, differential light curve folded with the period of 0.6873801 day is plotted in Figure 1.

Table 1: Data on VV UMa, comparison and check stars.

Star	RA (J2000)	DEC (J2000)	*V*
VV UMa	$09^{\rm h}38^{\rm m}06\overset{\rm s}{.}72$	$+56°01'07\overset{''}{.}25$	10.28
TYC 3810-1503-1 (Comparison Star)	$09^{\rm h}38^{\rm m}32\overset{\rm s}{.}22$	$+55°52'06\overset{''}{.}52$	10.17
TYC 3810-1120-1 (Check Star)	$09^{\rm h}37^{\rm m}43\overset{\rm s}{.}28$	$+55°49'19\overset{''}{.}76$	10.36

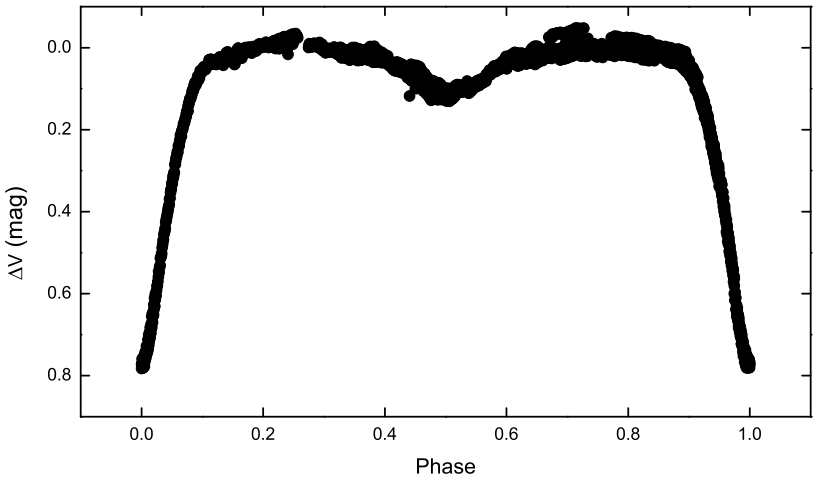

Figure 1. The phased V-filter light curve of VVUMa folded on the period of 0.68738 days.

Times of binary curve minima were measured using quadratic polynomial fitting method and are presented in the Table 2. The residuals from the out-of-eclipse light curves were obtained by removal of low-degree polinomial fits to the light curves of every night and are shown in Figure 2. Residuals exhibit strong amplitude modulation – an indicator of multiperiodiciy of pulsations.

Table 2: Times of light minima of VV UMa.

Date	Minima HJD time	Type of eclipse
3 January 2014	2456661.44963	primary
9 February 2014	2456698.23069	secondary
11 February 2014	2456700.28931	secondary
13 March 2014	2456730.18678	primary

Table 3: Pulsation frequencies and amplitudes found in the primary component.

Frequency (c/d)	Amplitude (mag)
F_1=48.8483±0.0003	0.0028±0.0001
F_2=47.0152±0.0005	0.0018±0.0001
F_3=19.4359±0.0008	0.0018±0.0001

The Discrete Fourier Transform (DFT) analysis was applied to the residual data to find the pulsation frequencies of the primary component. We use a pre-whitening technique for consecutive detections of signals. The periodograms of consecutive steps of the DFT analyses of the primary component of VV UMa are shown in Figure 3 from top to bottom. We detected three oscillation frequencies listed in Table 3.

In summary, during new photometric study of pulsations in a primary, mass-accreting component of Algol-type system VV UMa we found four new times of binary light minima. We confirmed pulsations of the primary component and found three pulsation periods at

frequencies of 48.8483 c/d (0.0205 d), 47.0152 c/d (0.0213) and 19.4359 c/d (0.0515 d). First two frequencies are close to the values reported by Kim et al. (2005), but we believe that our frequencies are more accurate. We are going to combine our photometric results with results of spectroscopic observations of VV UMa obtained by us in 2014-2015 using 2.4 m telescope at TNO in order to get accurate orbital parameters of VV UMa system.

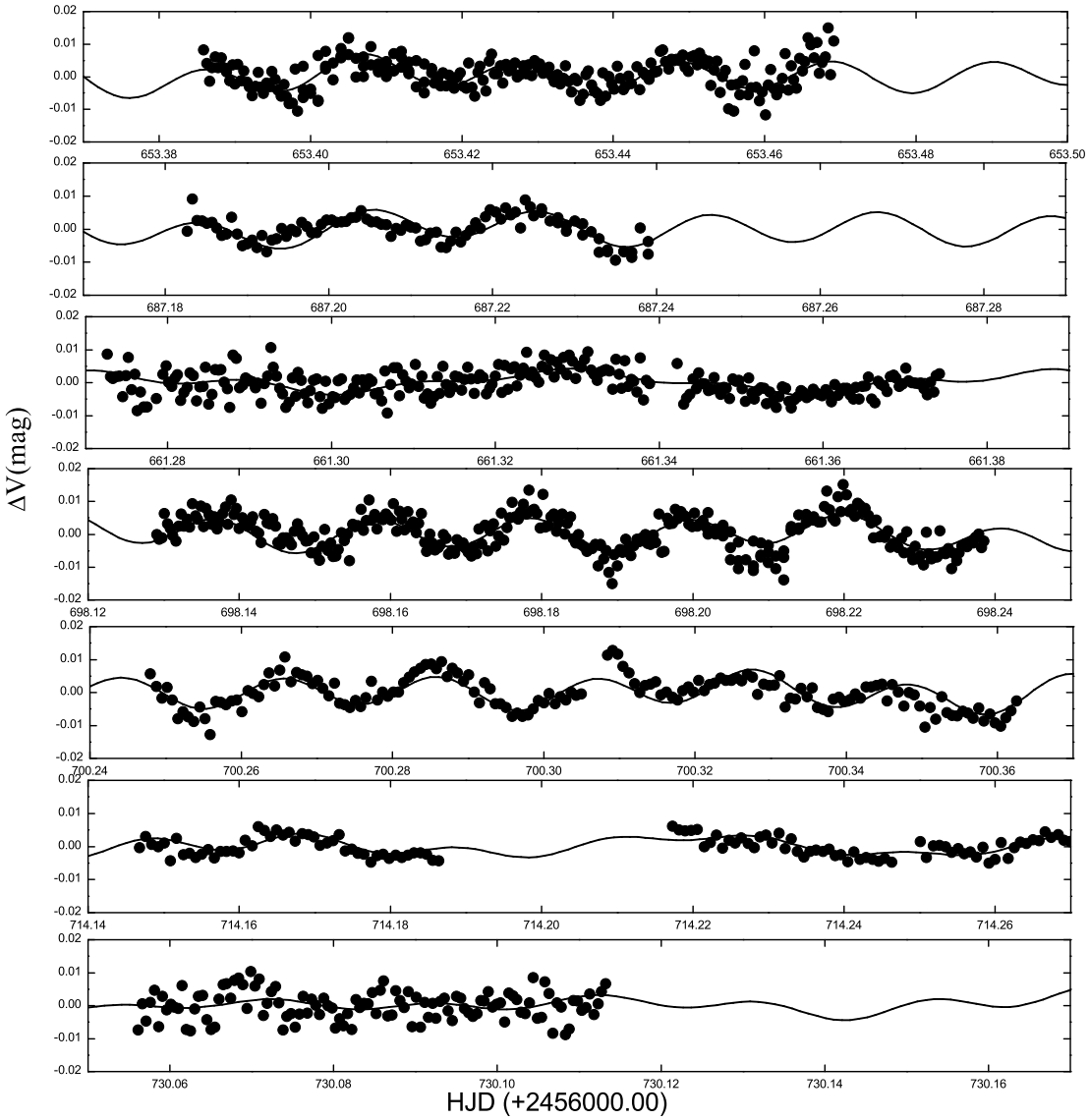

Figure 2. The nightly residual light variations (HJD time zero point is 2456000). Pulsational multiperiodic fits to the light curves are shown by solid line.

Acknowledgements: Department of Physics and Materials Science Chiang Mai University thanked for support, this work is a part of research activity of the National Astronomical Research Institute of Thailand (NARIT).

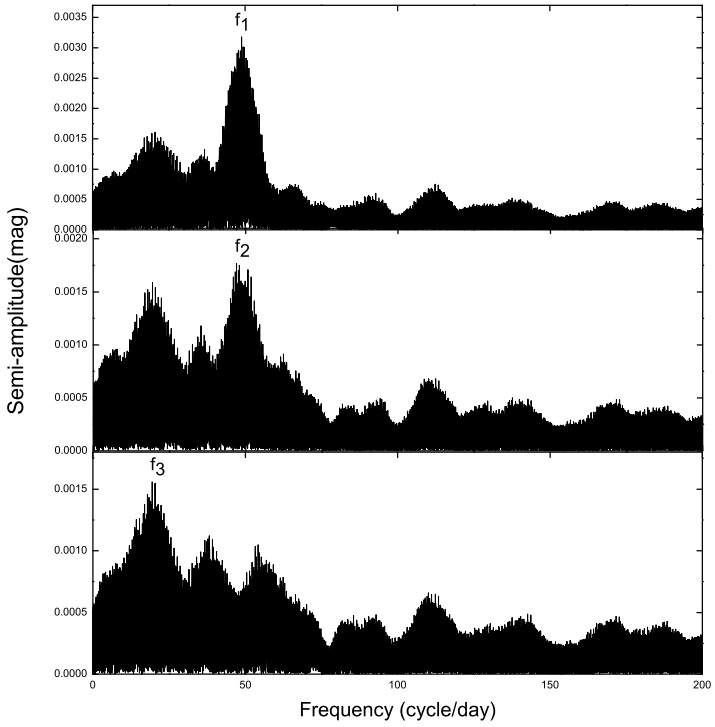

Figure 3. The DFT amplitude spectra of the primary component after consecutive (from top to bottom) pre-whitening procedures.

References:

Gitz, H., 1936, *Perem. Zvezdy*, **5**, 65

Hill, G., Hilditch, R. W., Younger, F., & Fisher, W. A., 1975, *MmRAS*, **79**, 131

Kim, S.-L., Lee, J.W., Lee, C.-U., Kang, Y.B., Koo, J-R., Mkrtichian, D.E., 2005, *IBVS*, **5598**

Lázaro, C., & Arévalo, M. J., Martínez-Pais, I.G., Domínguez, R.M., 2002, *AJ*, **123**, 2733

Lázaro, C., Arévalo, M. J., Claret, A., Rodriguez, E., & Olivares, I., 2001, *MNRAS*, **325**, 617

Mkrtichian, D. E., Kusakin, A. V., Gamarova, A. Yu. & Nazarenko, V., 2002, *ASPC*, **259**, 96

Mkrtichian, D.E., Kusakin, A.V., Rodriguez, E., et al., 2004, *A&A*, **419**, 1015

Struve, O., 1950, *ApJ*, **112**, 184

COMMISSIONS 27 AND 42 OF THE IAU
INFORMATION BULLETIN ON VARIABLE STARS

Number 6149

Konkoly Observatory
Budapest
15 September 2015

HU ISSN 0374 – 0676

BAV-RESULTS OF OBSERVATIONS - PHOTOELECTRIC MINIMA OF SELECTED ECLIPSING BINARIES AND MAXIMA OF PULSATING STARS

(BAV MITTEILUNGEN NO. 238)

HÜBSCHER, JOACHIM; LEHMANN, PETER B.

Bundesdeutsche Arbeitsgemeinschaft für Veränderliche Sterne e.V. (BAV), Munsterdamm 90, 12169 Berlin, Germany, www.bav-astro.de, publikat@bav-astro.de

In this 80th compilation of BAV results, photoelectric observations obtained mostly in the year 2014 are presented on 637 variable stars giving 1,108 minima on eclipsing binaries and maxima on pulsating stars. All moments of minima and maxima are heliocentric UTC. The errors are tabulated in column "±". The values in column "$O-C$" are determined without incorporating nonlinear terms. The references are given in the section "Remarks". All information about photometers and filters are specified in the columns "Fil" and "Rem". The observations were made at private observatories. The photoelectric measurements and all the light curves with evaluations can be obtained from the office of the BAV for inspection.

Please use the following link for an easy access to all the publications of the BAV including the "Lichtenknecker Database of the BAV": `http://www.bav-astro.de/sfs`.

Table 1: Times of minima of eclipsing binaries

Variable	HJD 24.....	±	Obs	$O-C$		Ref	Fil	n	Rem
RT And	56842.4757	0.0005	AG	+0.0634		⟨6⟩	-I	27	33)
	56871.4054	0.0013	AG	+0.0627		⟨6⟩	-I	28	33)
AA And	56876.4974	0.0120	AG	+0.4490		⟨6⟩	-I	23	33)
AB And	56870.3942	0.0024	AG	−0.0090		⟨6⟩	-I	27	33)
	56870.5600	0.0007	AG	−0.0092	s	⟨6⟩	-I	27	33)
	56876.3675	0.0008	AG	−0.0098		⟨6⟩	-I	25	33)
	56876.5330	0.0009	AG	−0.0102	s	⟨6⟩	-I	25	33)
CN And	56876.4991	0.0047	AG	−0.0102	s	⟨6⟩	-I	25	33)
	56877.4227	0.0022	AG	−0.0122	s	⟨6⟩	-I	30	33)
HS Aqr	56877.5753	0.0011	AG	−0.0051		⟨6⟩	-I	29	33)
KP Aql	56831.4523	0.0029	AG	−0.0230	s	⟨6⟩	-I	31	33)
V337 Aql	56870.4121	0.0091	AG	+0.1660	s	⟨6⟩	-I	26	33)
V343 Aql	56871.4718	0.0038	AG	+0.8780		⟨6⟩	-I	28	33)
V346 Aql	56871.4303	0.0042	AG	+0.5504		⟨6⟩	-I	27	33)
	56876.3995	0.0028	AG	−0.0123		⟨6⟩	-I	23	33)
	56877.5071	0.0011	AG	−0.0110		⟨6⟩	-I	30	33)
V415 Aql	56834.4989	0.0004	AG	+0.1752		⟨6⟩	-I	22	33)
V417 Aql	56834.4495	0.0004	QU	+0.0270		⟨6⟩	V	75	30) 2)
V1353 Aql	56822.4748	0.0042	AG	+0.0650		⟨6⟩	-I	21	33)
	56834.5011	0.0015	AG	+0.0655	s	⟨6⟩	-I	22	33)
V1700 Aql	56870.4438	0.0063	AG				-I	27	33)
V1825 Aql	56871.4034	0.0021	AG				-I	27	33)
V1826 Aql	56897.4224	0.0010	AG				-I	31	33)

Table 1: cont.

Variable	HJD 24.....	±	Obs	$O-C$		Ref	Fil	n	Rem
AH Aur	56713.3592	0.0019	JU	−0.0264	s	⟨6⟩	o	72	29)
	56734.3594	0.0020	AG	−0.0257		⟨6⟩	-I	34	33)
AP Aur	56686.4319	0.0014	JU	+0.1063	s	⟨6⟩	o	89	29)
CI Aur	56725.4462	0.0041	AG	+0.0042		⟨6⟩	-I	33	33)
CL Aur	56725.4595	0.0069	AG	+0.0246	s	⟨6⟩	-I	34	33)
DN Aur	56701.4287	0.0024	AG	+0.0009	s	⟨6⟩	-I	30	33)
FN Aur	56709.4899	0.0007	FR	+0.0074		⟨6⟩	-I	47	33)
	56730.3446	0.0041	FR	+0.0043	s	⟨6⟩	-I	26	33)
FO Aur	56709.5137	0.0004	FR	−0.0360	s	⟨6⟩	-I	56	33)
	56725.3683	0.0009	AG	−0.0418	s	⟨6⟩	-I	35	33)
GI Aur	56734.3247	0.0019	AG	+0.0015		⟨6⟩	-I	35	33)
HP Aur	56701.4011	0.0008	AG	+0.0018		⟨6⟩	-I	31	33)
IM Aur	56713.4393	0.0044	AG	−0.0002	s	⟨6⟩	-I	35	33)
KO Aur	56728.3665	0.0006	AG	+0.0000		⟨6⟩	-I	28	33)
KU Aur	56729.3444	0.0014	JU	+0.0244		⟨6⟩	o	29	29)
MO Aur	56725.4328	0.0070	AG	−0.0054		⟨6⟩	-I	40	33)
NN Aur	56729.4596	0.0005	FR	−0.0039		⟨6⟩	-I	50	33)
OZ Aur	56701.3643	0.0188	AG				-I	30	33)
V410 Aur	56701.4348	0.0021	AG	+0.0163		⟨6⟩	V	30	33)
V432 Aur	56713.3069	0.0075	AG	−0.0053	s	⟨6⟩	-I	39	33)
V459 Aur	56698.5448	0.0018	AG				-I	64	33)
V562 Aur	56701.4374	0.0018	AG				-I	30	33)
V599 Aur	56701.2845	0.0016	AG	+0.0055	s	⟨6⟩	-I	29	33)
	56701.4446	0.0003	AG	+0.0073		⟨6⟩	-I	29	33)
V610 Aur	56725.4057	0.0071	AG				-I	40	33)
V618 Aur	56709.3049	0.0008	FR				-I	136	33)
V640 Aur	56747.2862	0.0004	FR	−0.0202		⟨6⟩	-I	113	33)
	56747.4502	0.0020	FR	−0.0202	s	⟨6⟩	-I	113	33)
SU Boo	56747.5087	0.0022	AG	−0.0081		⟨6⟩	-I	43	33)
TY Boo	56817.3745	0.0010	WTR	−0.0105	s	⟨6⟩	o	66	28)
TZ Boo	56736.5085	0.0007	AG	−0.0075	s	⟨6⟩	-I	43	33)
	56736.6558	0.0002	AG	−0.0088		⟨6⟩	-I	43	33)
	56744.3858	0.0021	AG	−0.0050		⟨6⟩	-I	49	33)
	56744.5334	0.0012	AG	−0.0060	s	⟨6⟩	-I	49	33)
	56815.4053	0.0010	WTR	−0.0071		⟨6⟩	o	81	28)
UW Boo	56772.5736	0.0151	AG	+0.0086	s	⟨6⟩	-I	182	33)
VW Boo	56798.4489	0.0001	AG	−0.0067		⟨6⟩	-I	29	33)
YY Boo	56728.4899	0.0021	AG	+0.0161		⟨3⟩	-I	34	33)
AC Boo	56725.6408	0.0014	SCI	+0.0100	s	⟨6⟩	o	78	29)
	56728.4608	0.0003	FR	+0.0103	s	⟨6⟩	-I	100	33)
	56728.6354	0.0002	FR	+0.0087		⟨6⟩	-I	100	33)
	56730.3968	0.0044	AG	+0.0079		⟨6⟩	-I	46	33)
	56730.5760	0.0026	AG	+0.0109	s	⟨6⟩	-I	46	33)
	56734.6256	0.0014	SCI	+0.0073		⟨6⟩	o	138	29)
	56736.3884	0.0025	AG	+0.0079		⟨6⟩	-I	43	33)
	56736.5674	0.0014	AG	+0.0107	s	⟨6⟩	-I	43	33)
	56744.3220	0.0033	AG	+0.0114	s	⟨6⟩	-I	50	33)
	56744.4964	0.0024	AG	+0.0096		⟨6⟩	-I	50	33)
	56747.3157	0.0021	AG	+0.0093		⟨6⟩	-I	41	33)
	56747.4926	0.0008	AG	+0.0100	s	⟨6⟩	-I	41	33)
	56757.3653	0.0028	SCI	+0.0141	s	⟨6⟩	o	79	29)
	56757.5408	0.0031	SCI	+0.0134		⟨6⟩	o	63	29)
	56782.3844	0.0023	SCI	+0.0093	s	⟨6⟩	o	100	29)
	56782.5613	0.0016	SCI	+0.0100		⟨6⟩	o	104	29)
AD Boo	56798.4446	0.0010	AG	+0.0013		⟨6⟩	-I	28	33)
BW Boo	56730.3639	0.0023	AG	−0.0056		⟨6⟩	-I	46	33)
CK Boo	56750.4725	0.0056	AG	−0.0180		⟨6⟩	V	66	33)
CV Boo	56746.5405	0.0004	AG	−0.0002		⟨6⟩	-I	59	33)
	56764.3268	0.0066	AG	−0.0008		⟨6⟩	-I	27	33)
	56783.3850	0.0019	AG	+0.0001	s	⟨6⟩	-I	36	33)
DU Boo	56730.4753	0.0175	AG	+0.0230	s	⟨6⟩	-I	46	33)
	56747.3752	0.0093	AG	+0.0287	s	⟨6⟩	-I	41	33)
EF Boo	56728.5183	0.0014	SCI	+0.0058		⟨6⟩	o	166	29)
	56730.4099	0.0017	AG	+0.0051	s	⟨6⟩	-I	46	33)
	56730.6205	0.0014	AG	+0.0054		⟨6⟩	-I	46	33)
	56736.5072	0.0019	AG	+0.0049		⟨6⟩	-I	43	33)
	56747.4409	0.0030	AG	+0.0052		⟨6⟩	-I	39	33)
EM Boo	56764.4955	0.0023	AG				-I	32	33)
ET Boo	56728.5749	0.0002	FR	−0.0076		⟨6⟩	-I	68	33)
	56730.5103	0.0015	AG	−0.0074		⟨6⟩	-I	46	33)
	56736.6392	0.0010	AG	−0.0063	s	⟨6⟩	-I	43	33)

Table 1: cont.

Variable	HJD 24.....	±	Obs	$O-C$		Ref	Fil	n	Rem
ET Boo	56742.4402	0.0036	AG	−0.0107	s	⟨6⟩	V	28	33)
	56744.3769	0.0035	AG	−0.0091	s	⟨6⟩	-I	51	33)
EW Boo	56730.6219	0.0117	AG	+0.0080	s	⟨6⟩	-I	44	33)
	56736.5134	0.0037	AG	+0.0082		⟨6⟩	-I	43	33)
FI Boo	56729.4897	0.0017	SCI	−0.0181		⟨6⟩	o	166	29)
	56729.6547	0.0017	SCI	−0.0481	s	⟨6⟩	o	79	29)
	56730.4561	0.0013	SCI	−0.0267	s	⟨6⟩	o	133	29)
	56730.6515	0.0017	SCI	−0.0263		⟨6⟩	o	73	29)
FP Boo	56728.5575	0.0061	AG				V	30	33)
	56764.4309	0.0004	MS FR				o	245	39)
	56812.4628	0.0013	AG				-I	21	33)
GK Boo	56730.3885	0.0012	AG	−0.0003	s	⟨6⟩	-I	46	33)
	56730.6270	0.0012	AG	−0.0007		⟨6⟩	-I	46	33)
	56736.5982	0.0013	AG	−0.0016	s	⟨6⟩	-I	43	33)
	56744.4822	0.0016	AG	−0.0009		⟨6⟩	-I	50	33)
	56747.3488	0.0012	AG	−0.0009		⟨6⟩	-I	40	33)
	56747.3499	0.0012	AG	+0.0002		⟨6⟩	-I	47	33)
	56747.5861	0.0007	AG	−0.0025	s	⟨6⟩	-I	47	33)
	56747.5894	0.0011	AG	+0.0008	s	⟨6⟩	-I	40	33)
	56749.4984	0.0388	AG	−0.0013	s	⟨6⟩	-I	48	33)
	56798.4717	0.0014	AG	+0.0003		⟨6⟩	-I	27	33)
GN Boo	56747.4118	0.0007	AG	+0.0307	s	⟨6⟩	-I	47	33)
	56747.5622	0.0018	AG	+0.0303		⟨6⟩	-I	47	33)
GP Boo	56783.5103	0.0153	AG	+0.0035	s	⟨6⟩	-I	36	33)
GT Boo	56746.3877	0.0094	AG	−0.0009		⟨6⟩	-I	61	33)
	56798.4429	0.0041	AG	−0.0021	s	⟨6⟩	-I	28	33)
GV Boo	56770.3473	0.0016	MS FR	−0.0262		⟨6⟩	o	124	39)
GW Boo	56764.3830	0.0015	AG	+0.0067	s	⟨6⟩	-I	31	33)
HH Boo	56764.4127	0.0017	AG	+0.0001		⟨6⟩	-I	32	33)
	56764.5717	0.0004	AG	−0.0002	s	⟨6⟩	-I	32	33)
	56772.3786	0.0017	AG	−0.0006		⟨6⟩	-I	182	33)
	56772.5381	0.0031	AG	−0.0005	s	⟨6⟩	-I	182	33)
IK Boo	56747.3805	0.0006	AG	−0.0184	s	⟨6⟩	-I	46	33)
	56747.5323	0.0023	AG	−0.0181		⟨6⟩	-I	46	33)
IN Boo	56747.4139	0.0015	AG	+0.0008		⟨6⟩	-I	46	33)
	56747.5548	0.0016	AG	−0.0012	s	⟨6⟩	-I	46	33)
NY Boo	56742.5429	0.0025	AG	+0.0808		⟨6⟩	V	28	33)
OS Boo	56742.5070	0.0020	AG				-I	28	33)
	56742.6430	0.0006	AG				-I	28	33)
	56746.3669	0.0031	AG				-I	60	33)
	56746.5046	0.0016	AG				-I	60	33)
	56746.6408	0.0008	AG				-I	60	33)
PR Boo	56728.4941	0.0016	AG				-I	34	33)
	56742.4161	0.0006	AG				-I	28	33)
	56742.6033	0.0011	AG				-I	28	33)
PS Boo	56745.4094	0.0019	AG				-I	35	33)
	56745.5515	0.0008	AG				-I	35	33)
PT Boo	56728.6293	0.0033	AG	−0.0777		⟨6⟩	-I	34	33)
PU Boo	56728.4157	0.0053	AG	−0.0202		⟨6⟩	V	35	33)
PY Boo	56745.4220	0.0008	AG	+0.0410	s	⟨6⟩	-I	36	33)
	56745.5569	0.0014	AG	+0.0368		⟨6⟩	-I	36	33)
PZ Boo	56728.4488	0.0073	AG				-I	34	33)
	56742.4427	0.0024	AG				-I	28	33)
	56745.5542	0.0021	AG				-I	35	33)
	56746.5034	0.0063	AG				-I	61	33)
QQ Boo	56728.4165	0.0016	AG				-I	35	33)
	56728.5538	0.0008	AG				-I	35	33)
	56745.4181	0.0011	AG				-I	35	33)
	56745.5599	0.0014	AG				-I	35	33)
QT Boo	56745.4294	0.0052	AG				-I	36	33)
	56745.5873	0.0027	AG				-I	36	33)
QW Boo	56728.5356	0.0009	AG				-I	35	33)
	56742.4970	0.0013	AG				-I	28	33)
	56742.6442	0.0003	AG				-I	28	33)
QX Boo	56742.4306	0.0010	AG				-I	28	33)
	56742.6110	0.0024	AG				-I	28	33)
	56745.4946	0.0014	AG				-I	35	33)
QY Boo	56728.5695	0.0029	AG				-I	35	33)
	56742.4222	0.0005	AG				-I	28	33)
	56742.5853	0.0025	AG				-I	28	33)
	56812.5067	0.0022	AG				-I	21	33)

Table 1: cont.

Variable	HJD 24.....	±	Obs	$O-C$		Ref	Fil	n	Rem
V339 Boo	56728.5697	0.0029	AG				V	32	33)
	56742.5377	0.0020	AG				V	28	33)
i Boo	56733.3217	0.0021	SCI	−0.0061		⟨6⟩	o	54	29)
	56733.3217	0.0021	SCI	−0.0061		⟨6⟩	o	54	29)
	56733.4548	0.0013	SCI	−0.0069	s	⟨6⟩	o	66	29)
	56733.4548	0.0013	SCI	−0.0069	s	⟨6⟩	o	66	29)
	56733.5996	0.0020	SCI	+0.0040		⟨6⟩	o	99	29)
	56733.5996	0.0020	SCI	+0.0040		⟨6⟩	o	99	29)
	56747.3908	0.0004	SCI	+0.0025	s	⟨6⟩	o	105	29)
	56747.5132	0.0004	SCI	−0.0090		⟨6⟩	o	165	29)
	56758.3747	0.0028	SCI	+0.0058	s	⟨6⟩	o	76	29)
WW Cam	56727.3836	0.0030	AG	−0.0260		⟨6⟩	-I	55	33)
AK Cam	56725.5760	0.0232	AG	−0.2105	s	⟨6⟩	-I	49	33)
	56734.4850	0.0013	AG	−0.2088	s	⟨6⟩	-I	40	33)
AL Cam	56764.5760	0.0027	AG	−0.0282	s	⟨6⟩	-I	32	33)
AN Cam	56887.5481	0.0001	AG	−4.8625		⟨6⟩	-I	25	33)
AS Cam	56712.4190	0.0011	AG	+1.5019		⟨6⟩	-I	49	33)
AT Cam	56713.4138	0.0016	AG	−0.1191	s	⟨6⟩	-I	42	33)
AY Cam	56726.5729	0.0061	AG	+0.0138	s	⟨6⟩	-I	58	33)
	56729.3052	0.0015	AG	+0.0112	s	⟨6⟩	-I	61	33)
	56737.5124	0.0006	AG	+0.0135	s	⟨6⟩	-I	56	33)
AZ Cam	56729.6100	0.0013	AG	+0.0216	s	⟨6⟩	-I	59	33)
	56737.5231	0.0010	AG	+0.0193	s	⟨6⟩	-I	54	33)
DN Cam	56713.3816	0.0008	AG	+0.0012	s	⟨4⟩	-I	62	33)
	56713.6321	0.0011	AG	+0.0026		⟨4⟩	-I	62	33)
FN Cam	56731.3381	0.0006	AG	−0.0011	s	⟨4⟩	-I	39	33)
	56734.3871	0.0007	AG	+0.0008		⟨4⟩	-I	39	33)
	56737.4312	0.0009	AG	−0.0022	s	⟨4⟩	-I	56	33)
	56744.5443	0.0013	AG	+0.0009		⟨4⟩	-I	52	33)
	56745.5578	0.0013	AG	−0.0013	s	⟨4⟩	-I	44	33)
QU Cam	56887.5048	0.0034	AG	−0.0504		⟨6⟩	-I	29	33)
V337 Cam	56713.4312	0.0015	AG				-I	55	33)
	56727.4305	0.0216	AG				V	56	33)
V345 Cam	56727.3457	0.0022	AG				-I	56	33)
	56727.5731	0.0009	AG				-I	56	33)
V352 Cam	56727.3655	0.0026	AG				-I	56	33)
	56727.5543	0.0021	AG				-I	56	33)
V356 Cam	56727.3445	0.0044	AG				-I	56	33)
	56727.5500	0.0071	AG				-I	56	33)
V362 Cam	56727.5509	0.0048	AG				-I	55	33)
V369 Cam	56727.2876	0.0017	AG				-I	55	33)
	56727.4613	0.0009	AG				-I	55	33)
	56727.6330	0.0009	AG				-I	55	33)
V372 Cam	56727.3584	0.0106	AG				-I	55	33)
V374 Cam	56727.3309	0.0006	AG				-I	55	33)
V514 Cam	56764.4389	0.0014	AG	+0.0277		⟨6⟩	-I	32	33)
V517 Cam	56814.4219	0.0012	AG				-I	25	33)
RY Cnc	56743.3902	0.0025	AG	+0.0782		⟨6⟩	-I	32	33)
TU Cnc	56727.3487	0.0106	AG	−0.0549		⟨6⟩	-I	40	33)
TX Cnc	56709.4549	0.0030	AG	+0.0441		⟨6⟩	-I	26	33)
	56743.3407	0.0014	AG	+0.0449	s	⟨6⟩	V	31	33)
	56743.5340	0.0026	AG	+0.0468		⟨6⟩	V	31	33)
WY Cnc	56706.5078	0.0009	AG	−0.0390		⟨6⟩	-I	45	33)
	56712.3120	0.0025	AG	−0.0404		⟨6⟩	-I	94	33)
	56745.4867	0.0029	AG	−0.0405		⟨6⟩	-I	38	33)
	56746.3170	0.0020	AG	−0.0396		⟨6⟩	-I	33	33)
AH Cnc	56736.3440	0.0003	MS FR	+0.0211	s	⟨6⟩	o	93	39)
EH Cnc	56743.5210	0.0013	AG	+0.0012	s	⟨4⟩	-I	32	33)
FF Cnc	56743.4774	0.0020	AG	−0.0003	s	⟨4⟩	V	30	33)
IL Cnc	56743.3679	0.0011	AG	−0.0453	s	⟨6⟩	-I	34	33)
	56743.5003	0.0011	AG	−0.0468		⟨6⟩	-I	34	33)
IM Cnc	56743.3582	0.0020	AG	−0.0422		⟨6⟩	-I	35	33)
IR Cnc	56743.3579	0.0064	AG				-I	31	33)
IT Cnc	56743.3435	0.0075	AG	+0.0789	s	⟨6⟩	-I	32	33)
	56743.5230	0.0035	AG	+0.0766		⟨6⟩	-I	31	33)
KY Cnc	56709.5309	0.0027	AG				-I	25	33)
	56746.4291	0.0045	AG				-I	27	33)
RS CVn	56746.3956	0.0008	AG	−0.7587		⟨6⟩	-I	38	33)
VZ CVn	56736.5527	0.0009	AG	−0.0019		⟨6⟩	-I	42	33)
	56742.4503	0.0003	AG	−0.0016		⟨6⟩	-I	12	33)
	56744.5586	0.0022	AG	+0.0006	s	⟨6⟩	-I	50	33)

Table 1: cont.

Variable	HJD 24.....	±	Obs	$O-C$		Ref	Fil	n	Rem
VZ CVn	56749.6112	0.0022	AG	−0.0016	s	⟨6⟩	-I	52	33)
	56750.4530	0.0008	AG	−0.0023	s	⟨6⟩	-I	46	33)
BI CVn	56729.4634	0.0014	AG	+0.0241		⟨6⟩	-I	57	33)
	56729.6559	0.0007	AG	+0.0245	s	⟨6⟩	-I	57	33)
	56734.4597	0.0010	AG	+0.0263		⟨6⟩	-I	48	33)
BO CVn	56730.5970	0.0035	AG	+0.0008	s	⟨4⟩	-I	46	33)
	56737.3256	0.0015	AG	+0.0024	s	⟨4⟩	-I	56	33)
	56737.5836	0.0033	AG	+0.0016		⟨4⟩	-I	56	33)
DF CVn	56783.3602	0.0014	AG	−0.0015	s	⟨4⟩	-I	35	33)
	56783.5214	0.0007	AG	−0.0037		⟨4⟩	-I	35	33)
FU CVn	56737.5613	0.0012	AG				-I	56	33)
GZ CMa	56726.2917	0.0026	FR				-I	55	33)
SX CMi	56726.3864	0.0062	AG	−0.2992	s	⟨6⟩	-I	28	33)
TT CMi	56713.4472	0.0017	AG	+0.0646	s	⟨6⟩	-I	33	33)
TX CMi	56713.3747	0.0031	AG	−0.0373		⟨6⟩	-I	33	33)
	56726.4123	0.0012	AG	−0.0312	s	⟨6⟩	-I	29	33)
TY CMi	56713.3927	0.0311	AG	+0.1756		⟨6⟩	-I	33	33)
	56726.3915	0.0182	AG	+0.1835		⟨6⟩	-I	29	33)
TZ CMi	56713.3364	0.0011	AG	+2.5754	s	⟨6⟩	-I	33	33)
UZ CMi	56725.3141	0.0018	AG	+0.1359		⟨6⟩	-I	32	33)
XZ CMi	56725.3687	0.0014	AG	+0.0002		⟨6⟩	-I	32	33)
	56727.3874	0.0129	AG	−0.0069	s	⟨6⟩	-I	29	33)
YY CMi	56726.4129	0.0059	AG	+0.0180	s	⟨6⟩	-I	38	33)
AK CMi	56713.4658	0.0074	AG	+0.2612		⟨6⟩	-I	32	33)
BB CMi	56726.3692	0.0061	AG	−0.0509		⟨6⟩	-I	29	33)
BH CMi	56726.3318	0.0023	AG	+0.0056	s	⟨4⟩	V	28	33)
DS CMi	56713.4174	0.0016	AG				-I	30	33)
DW CMi	55621.3567	0.0031	AG	+0.0088		⟨6⟩	-I	49	33)
	55621.5096	0.0006	AG	+0.0079	s	⟨6⟩	-I	49	33)
	55625.3539	0.0014	AG	+0.0078		⟨6⟩	-I	39	33)
	55625.5033	0.0031	AG	+0.0034	s	⟨6⟩	-I	39	33)
	56713.3313	0.0008	AG	+0.0093	s	⟨6⟩	-I	33	33)
	56713.4843	0.0005	AG	+0.0086		⟨6⟩	-I	33	33)
	56726.4008	0.0013	AG	+0.0078		⟨6⟩	-I	29	33)
EI CMi	56726.4342	0.0017	AG				-I	29	33)
EL CMi	56726.3371	0.0026	AG				-I	29	33)
TV Cas	56683.3760	0.0035	PGL	−0.0271		⟨6⟩	V	97	35) 5)
DN Cas	56682.4393	0.0035	PGL	−0.0318		⟨6⟩	V	62	38) 6)
DO Cas	56725.4947	0.0024	SCI	−0.0014	s	⟨6⟩	o	64	29)
NU Cas	56875.5302	0.0002	MS FR	−0.1288	s	⟨6⟩	o	343	39)
OX Cas	56682.4353	0.0104	PGL	+0.0046	s	⟨6⟩	V	78	35)
QQ Cas	56891.4701	0.0053	AG	+0.2194	s	⟨6⟩	-I	30	33)
V445 Cas	56886.3862	0.0027	AG	+0.0671		⟨6⟩	-I	18	33)
V1044 Cas	56887.4823	0.0150	AG				-I	28	33)
SU Cep	56814.4614	0.0003	AG	+0.0056		⟨6⟩	-I	24	33)
	56877.5603	0.0011	AG	+0.0064		⟨6⟩	-I	30	33)
VW Cep	56814.3832	0.0016	AG	+0.0570		⟨6⟩	-I	25	33)
	56814.5220	0.0019	AG	+0.0567	s	⟨6⟩	-I	25	33)
VZ Cep	56834.4569	0.0016	AG	−0.0118		⟨6⟩	-I	22	33)
AI Cep	56877.5281	0.0283	AG	+0.1825	s	⟨6⟩	-I	30	33)
CQ Cep	56877.5477	0.0075	AG	−0.0848	s	⟨6⟩	-I	30	33)
EG Cep	56747.4829	0.0009	AG	+0.0129		⟨6⟩	-I	40	33)
EK Cep	56862.4313	0.0095	AG	−2.0080		⟨6⟩	-I	34	33)
GK Cep	56824.4507	0.0014	AG	+0.1279		⟨6⟩	-I	27	33)
NN Cep	56897.3745	0.0049	AG	+0.0043	s	⟨6⟩	-I	35	33)
	56898.4081	0.0085	AG	+0.0087		⟨6⟩	-I	47	33)
V397 Cep	56870.5284	0.0037	AG				-I	27	33)
RW Com	56746.4010	0.0010	MS FR	−0.0008	s	⟨6⟩	o	132	39)
RZ Com	56730.5146	0.0009	AG	+0.0474	s	⟨6⟩	-I	46	33)
	56736.4388	0.0010	AG	+0.0478		⟨6⟩	-I	43	33)
	56736.6070	0.0012	AG	+0.0467	s	⟨6⟩	-I	43	33)
	56744.3942	0.0017	AG	+0.0483	s	⟨6⟩	-I	51	33)
	56744.5631	0.0036	AG	+0.0479		⟨6⟩	-I	51	33)
	56746.4241	0.0016	AG	+0.0471	s	⟨6⟩	-I	37	33)
	56746.5908	0.0036	AG	+0.0446		⟨6⟩	-I	37	33)
EK Com	56737.3705	0.0001	MS FR	+0.0017		⟨4⟩	o	168	39)
MZ Com	56744.5330	0.0258	AG				-I	51	33)
RT CrB	56783.4682	0.0212	AG	−0.0262	s	⟨6⟩	-I	35	33)
RW CrB	56764.3783	0.0194	AG	−0.0016	s	⟨6⟩	-I	33	33)
	56776.3656	0.0002	AG	−0.0001		⟨6⟩	-I	20	33)
TU CrB	56736.5840	0.0019	SCI	+0.0120	s	⟨6⟩	o	99	29)

Table 1: cont.

Variable	HJD 24.....	±	Obs	$O-C$		Ref	Fil	n	Rem
TU CrB	56737.3878	0.0022	SCI	+0.0089		⟨6⟩	o	78	29)
TW CrB	56782.4056	0.0036	AG	+0.0495		⟨6⟩	-I	30	33)
	56797.4241	0.0012	SCI	+0.0517	s	⟨6⟩	o	163	29)
	56812.4381	0.0012	AG	+0.0494		⟨6⟩	-I	20	33)
	56855.4267	0.0006	JU	+0.0503		⟨6⟩	o	52	29)
YY CrB	56742.4431	0.0014	AG	+0.0051		⟨4⟩	-I	12	33)
	56749.4108	0.0005	AG	+0.0065	s	⟨4⟩	-I	52	33)
	56749.5994	0.0008	AG	+0.0069		⟨4⟩	-I	52	33)
	56754.4963	0.0035	AG	+0.0086		⟨4⟩	-I	24	33)
AR CrB	56782.4637	0.0006	AG	−0.0055		⟨6⟩	-I	30	33)
AS CrB	56764.5789	0.0003	MS FR	+0.0240		⟨6⟩	o	96	39)
WZ Cyg	56814.4821	0.0013	AG	+0.0657	s	⟨6⟩	-I	24	33)
ZZ Cyg	56559.2912	0.0009	FR	−0.0649		⟨6⟩	V	51	37)
	56799.4220	0.0022	AG	−0.0656		⟨6⟩	-I	23	33)
	56810.4190	0.0077	AG	+0.2449		⟨6⟩	-I	24	33)
CG Cyg	56811.5520	0.0007	AG	+0.0732	s	⟨6⟩	-I	19	33)
	56841.5312	0.0013	AG	+0.0732		⟨6⟩	-I	43	33)
CV Cyg	56157.4793	0.0041	FR	+0.2046		⟨6⟩	V	28	37)
	56810.4559	0.0063	AG	+0.1831		⟨6⟩	-I	24	33)
DK Cyg	56817.4254	0.0009	AG	+0.1041		⟨6⟩	-I	21	33)
GO Cyg	56821.3933	0.0011	AG	+0.0640		⟨6⟩	-I	24	33)
	56822.4724	0.0075	AG	+0.0664	s	⟨6⟩	-I	24	33)
KR Cyg	56810.5034	0.0016	AG	+0.0177		⟨6⟩	-I	24	33)
LO Cyg	56891.4480	0.0077	AG	−0.0611		⟨6⟩	-I	28	33)
MR Cyg	56830.4359	0.0078	AG	+0.8382		⟨6⟩	-I	30	33)
MY Cyg	56877.4339	0.0033	AG	−0.0001		⟨6⟩	-I	30	33)
V366 Cyg	56815.4849	0.0018	AG	−0.0009		⟨6⟩	-I	32	33)
V382 Cyg	56815.4761	0.0013	AG	+0.1094	s	⟨6⟩	-I	32	33)
	56864.4974	0.0034	AG	+0.1073	s	⟨6⟩	-I	26	33)
V388 Cyg	56815.4320	0.0013	AG	−0.1079		⟨6⟩	-I	31	33)
V401 Cyg	56799.4517	0.0038	AG	+0.0850	s	⟨6⟩	-I	24	33)
V453 Cyg	56871.5477	0.0019	AG	+0.0626		⟨6⟩	-I	59	33)
V456 Cyg	56799.4598	0.0024	AG	+0.0484	s	⟨6⟩	-I	23	33)
	56811.4922	0.0005	AG	+0.0498		⟨6⟩	-I	18	33)
V463 Cyg	56886.4624	0.0010	AG	+0.0570		⟨6⟩	-I	18	33)
V466 Cyg	56821.4141	0.0011	AG	+0.0065		⟨6⟩	-I	27	33)
	56862.4656	0.0004	AG	+0.0068	s	⟨6⟩	-I	35	33)
V477 Cyg	56886.4501	0.0023	AG	−0.0329		⟨6⟩	-I	26	33)
V478 Cyg	56799.4951	0.0089	AG	+0.0268		⟨6⟩	-I	23	33)
V498 Cyg	56799.4520	0.0118	AG	+0.1897		⟨6⟩	-I	23	33)
V541 Cyg	56876.4377	0.0026	AG	+0.0639		⟨6⟩	-I	24	33)
V548 Cyg	56811.5407	0.0002	AG	+0.0302		⟨6⟩	-I	18	33)
V628 Cyg	56783.5650	0.0013	MS FR	−0.0058		⟨6⟩	o	66	39)
V675 Cyg	56891.4196	0.0052	AG	+0.6454		⟨6⟩	-I	29	33)
V687 Cyg	56831.4518	0.0018	AG	−0.0051		⟨6⟩	-I	33	33)
V700 Cyg	56799.4466	0.0012	AG	−0.0871		⟨6⟩	-I	23	33)
V704 Cyg	56891.3820	0.0031	AG	+0.0346		⟨6⟩	-I	28	33)
V728 Cyg	56862.4389	0.0024	AG	+0.0448		⟨6⟩	-I	35	33)
V787 Cyg	56822.4536	0.0021	AG	+0.0028		⟨6⟩	-I	25	33)
V796 Cyg	56834.4788	0.0018	AG	−0.0360	s	⟨6⟩	-I	22	33)
V828 Cyg	56817.4390	0.0025	AG	−0.2088		⟨6⟩	-I	26	33)
V836 Cyg	56817.4884	0.0004	AG	+0.0207		⟨6⟩	-I	24	33)
	56864.5345	0.0019	AG	+0.0211		⟨6⟩	-I	27	33)
V874 Cyg	56897.4245	0.0016	AG	+0.0019	s	⟨6⟩	-I	34	33)
V889 Cyg	56821.4204	0.0011	AG	−0.1994		⟨6⟩	-I	25	33)
	56862.4953	0.0083	AG	−0.2010	s	⟨6⟩	-I	35	33)
V891 Cyg	56812.5011	0.0010	AG	+0.0479		⟨6⟩	-I	21	33)
V1034 Cyg	56871.4557	0.0057	AG	+0.0068		⟨6⟩	-I	28	33)
V1061 Cyg	56886.3843	0.0052	AG	+1.1567		⟨6⟩	-I	19	33)
V1073 Cyg	56830.5077	0.0039	AG	−0.1481		⟨6⟩	-I	30	33)
V1171 Cyg	56799.4113	0.0036	AG	−0.0582	s	⟨6⟩	-I	24	33)
V1305 Cyg	56157.4916	0.0040	FR	−0.1199	s	⟨6⟩	V	26	37)
V1356 Cyg	56871.4742	0.0096	AG	+0.2592	s	⟨6⟩	-I	28	33)
V1414 Cyg	56891.5307	0.0022	AG	+0.0487		⟨6⟩	-I	27	33)
V1417 Cyg	56891.4862	0.0028	AG	+0.1360	s	⟨6⟩	-I	26	33)
V1508 Cyg	56816.4409	0.0014	SCI	−0.0849	s	⟨6⟩	o	61	29)
	56817.4431	0.0028	SCI	−0.0800		⟨6⟩	o	58	29)
V1723 Cyg	56877.4122	0.0007	JU	+0.0637		⟨6⟩	o	50	29)
V2021 Cyg	56877.5072	0.0027	AG	+0.0005		⟨4⟩	-I	30	33)
V2197 Cyg	56814.4311	0.0006	AG	−0.0017		⟨4⟩	-I	24	33)
V2247 Cyg	56877.4568	0.0073	AG				-I	30	33)

Table 1: cont.

Variable	HJD 24.....	±	Obs	$O-C$		Ref	Fil	n	Rem
V2278 Cyg	56815.4613	0.0023	SCI				o	58	29)
	56821.4305	0.0028	SCI				o	41	29)
V2477 Cyg	56842.4477	0.0007	AG	+0.0033	s	⟨6⟩	-I	24	33)
V2486 Cyg	56898.3880	0.0010	AG				-I	57	33)
V2524 Cyg	55829.5321	0.0004	FR				-I	63	33)
	55831.3352	0.0006	FR				-I	74	33)
	55831.5597	0.0006	FR				-I	74	33)
	55834.4894	0.0004	FR				-I	75	33)
	55851.3906	0.0005	FR				-I	88	33)
	55851.6137	0.0004	FR				-I	88	33)
V2540 Cyg	56559.3789	0.0019	FR				V	31	37)
V2546 Cyg	56864.5149	0.0042	AG	−0.0081	s	⟨6⟩	-I	26	33)
V2643 Cyg	56891.3823	0.0027	AG				-I	32	33)
W Del	56891.3969	0.0005	AG	+0.0332		⟨6⟩	-I	27	33)
TY Del	56841.4913	0.0209	AG	+0.0580	s	⟨6⟩	-I	43	33)
AV Del	56864.4358	0.0010	AG	+0.0436		⟨6⟩	-I	25	33)
CN Del	56841.5470	0.0005	MS FR				o	212	39)
	56842.4317	0.0003	MS FR				o	185	39)
FZ Del	56871.5187	0.0095	AG	−0.0305	s	⟨6⟩	-I	27	33)
Z Dra	56764.6004	0.0005	AG	−0.1956		⟨6⟩	-I	32	33)
RR Dra	56870.4356	0.0010	AG	+0.0130		⟨6⟩	-I	27	33)
RX Dra	56871.4449	0.0042	AG	+0.0584	s	⟨6⟩	-I	28	33)
RZ Dra	56750.4836	0.0018	AG	+0.0599	s	⟨6⟩	-I	46	33)
	56871.4011	0.0013	AG	+0.0606		⟨6⟩	-I	28	33)
SX Dra	56750.5366	0.0011	AG	+0.0960		⟨6⟩	-I	62	33)
TW Dra	56747.4570	0.0005	AG	−0.0016		⟨6⟩	-I	41	33)
TZ Dra	56810.4441	0.0030	AG	−0.0356	s	⟨6⟩	-I	24	33)
	56891.4163	0.0029	JU	−0.0376		⟨6⟩	o	56	29)
AI Dra	56782.5096	0.0089	AG	−0.5769		⟨6⟩	-I	29	33)
	56809.4918	0.0053	AG	+0.0314		⟨6⟩	-I	26	33)
	56812.4917	0.0043	AG	−0.5652		⟨6⟩	-I	22	33)
AR Dra	56729.3499	0.0015	AG	+0.0251	s	⟨6⟩	-I	46	33)
AX Dra	56729.4783	0.0020	AG	−0.0623	s	⟨6⟩	-I	45	33)
	56764.4196	0.0011	AG	−0.0631		⟨6⟩	-I	32	33)
BH Dra	56817.4377	0.0017	AG	+0.9034		⟨6⟩	-I	25	33)
BS Dra	56747.4964	0.0018	AG	+0.0017		⟨6⟩	-I	41	33)
BU Dra	56737.5723	0.0019	AG	+0.1684		⟨6⟩	-I	52	33)
	56783.5132	0.0018	AG	+0.1692		⟨6⟩	-I	35	33)
CK Dra	56771.3347	0.0009	AG				-I	86	33)
CV Dra	56750.3872	0.0026	AG	+0.0045		⟨4⟩	-I	38	33)
FU Dra	56764.4553	0.0005	AG	−0.0072		⟨4⟩	-I	32	33)
	56764.6092	0.0002	AG	−0.0066	s	⟨4⟩	-I	32	33)
	56776.4167	0.0024	AG	−0.0078		⟨4⟩	-I	20	33)
GQ Dra	56750.4832	0.0032	AG	−0.0054	s	⟨4⟩	-I	33	33)
KK Dra	56871.4804	0.0029	AG	−0.0216		⟨4⟩	-I	28	33)
MW Dra	56764.3849	0.0063	AG				-I	33	33)
NW Dra	56729.3057	0.0003	AG				-I	45	33)
OQ Dra	56729.3394	0.0018	AG	+0.0702		⟨6⟩	-I	45	33)
	56729.5099	0.0016	AG	+0.0709	s	⟨6⟩	-I	45	33)
V338 Dra	56771.5005	0.0063	AG	−0.0342		⟨6⟩	-I	25	33)
V339 Dra	56771.5784	0.0021	AG				-I	25	33)
V341 Dra	56731.5197	0.0026	AG	+0.0097	s	⟨6⟩	-I	35	33)
	56736.4640	0.0196	AG	+0.0027	s	⟨6⟩	-I	43	33)
	56745.5452	0.0011	AG	+0.0066		⟨6⟩	-I	41	33)
	56746.3726	0.0070	AG	+0.0088	s	⟨6⟩	-I	39	33)
	56750.4949	0.0009	AG	+0.0050		⟨6⟩	-I	46	33)
V342 Dra	56771.5266	0.0042	AG				-I	26	33)
V344 Dra	56771.4645	0.0032	AG	−0.0452	s	⟨6⟩	-I	25	33)
V422 Dra	56897.3633	0.0053	AG				-I	25	33)
WW Gem	56689.4324	0.0021	JU	+0.0357		⟨6⟩	o	85	29)
	56725.3291	0.0032	MOO	+0.0359		⟨6⟩	V	80	35)
YY Gem	56764.4491	0.0035	PGL	−0.0070	s	⟨6⟩	V	666	38) 7)
BT Gem	56734.3121	0.0080	AG	−0.0096	s	⟨6⟩	-I	35	33)
EY Gem	56734.3411	0.0015	SCI	−0.2212	s	⟨6⟩	o	51	29)
GW Gem	56706.4099	0.0058	AG	+0.0279	s	⟨6⟩	-I	42	33)
	56714.3250	0.0096	AG	+0.0297	s	⟨6⟩	-I	64	33)
HR Gem	56734.3106	0.0025	AG	+0.0124	s	⟨6⟩	-I	35	33)
V396 Gem	56734.3588	0.0129	AG				-I	35	33)
Z Her	56887.4118	0.0025	AG	−0.0232		⟨6⟩	-I	22	33)
RX Her	56808.5151	0.0037	AG	+0.0006	s	⟨6⟩	-I	27	33)
	56809.4021	0.0032	AG	−0.0017		⟨6⟩	-I	25	33)

Table 1: cont.

Variable	HJD 24.....	±	Obs	$O-C$		Ref	Fil	n	Rem
SZ Her	56810.5283	0.0051	AG	+0.3857		⟨6⟩	-I	24	33)
TT Her	56810.5196	0.0036	AG	+0.0445	s	⟨6⟩	-I	24	33)
TU Her	56782.5058	0.0095	AG	−0.2295	s	⟨6⟩	-I	30	33)
	56799.5099	0.0022	AG	−0.2279		⟨6⟩	-I	25	33)
TX Her	56782.4174	0.0065	AG	−0.0051	s	⟨6⟩	-I	29	33)
	56886.4392	0.0153	AG	−0.0037		⟨6⟩	-I	18	33)
UX Her	56810.4887	0.0015	AG	+0.1082		⟨6⟩	-I	23	33)
AK Her	56798.5363	0.0006	AG	+0.0158		⟨6⟩	-I	29	33)
	56808.4427	0.0026	AG	+0.0165	s	⟨6⟩	-I	27	33)
	56809.4958	0.0018	AG	+0.0158		⟨6⟩	-I	27	33)
AW Her	56812.652	0.001	AG	+0.133		⟨6⟩	-I	195	33)
CC Her	56814.4455	0.0004	AG	+0.2541		⟨6⟩	-I	25	33)
DD Her	56737.6024	0.0017	SCI	+0.3682		⟨6⟩	o	78	29)
DH Her	56808.4359	0.0047	AG	+0.0074		⟨6⟩	-I	28	33)
DI Her	56887.5372	0.0021	AG	+0.0062		⟨6⟩	-I	28	33)
DK Her	56796.4742	0.0022	SCI	−0.1531	s	⟨6⟩	o	85	29)
HS Her	56798.4906	0.0035	SCI	+0.8061		⟨6⟩	o	126	29)
	56821.4149	0.0045	AG	+0.8063		⟨6⟩	-I	24	33)
LT Her	56812.5078	0.0017	AG	−0.1380		⟨6⟩	-I	22	33)
MM Her	56783.4206	0.0013	SCI	−0.0151		⟨6⟩	o	113	29)
MT Her	56808.5313	0.0028	AG	+0.0137	s	⟨6⟩	-I	28	33)
V338 Her	56782.5827	0.0002	AG	+0.1175		⟨6⟩	-I	29	33)
	56799.5584	0.0004	AG	+0.1186		⟨6⟩	-I	24	33)
V342 Her	56841.4948	0.0072	AG	+0.0248	s	⟨6⟩	-I	40	33)
V359 Her	56764.4339	0.0039	AG	+0.2417		⟨6⟩	-I	32	33)
	56799.5507	0.0031	AG	+0.2438		⟨6⟩	-I	24	33)
V450 Her	56798.4857	0.0018	AG	+0.0964	s	⟨6⟩	-I	27	33)
V728 Her	56764.4788	0.0022	AG	+0.1052	s	⟨6⟩	-I	32	33)
	56782.3888	0.0034	AG	−0.0582		⟨6⟩	-I	28	33)
V829 Her	56772.5987	0.0010	SCI	+0.0014		⟨4⟩	o	67	29)
V842 Her	56749.4290	0.0008	AG	−0.0003	s	⟨4⟩	-I	50	33)
	56750.4787	0.0008	AG	+0.0019		⟨4⟩	-I	41	33)
V857 Her	56764.4443	0.0040	AG	+0.0030		⟨4⟩	-I	32	33)
V861 Her	56764.4459	0.0027	AG	−0.0113		⟨4⟩	-I	32	33)
V878 Her	56750.5524	0.0026	AG	−0.0014	s	⟨4⟩	-I	36	33)
	56799.5203	0.0024	AG	−0.0099		⟨4⟩	-I	24	33)
	56808.5199	0.0028	AG	−0.0114		⟨4⟩	-I	27	33)
V994 Her	56815.4382	0.0041	AG				-I	32	33)
V1023 Her	56745.4881	0.0022	AG				-I	36	33)
V1038 Her	56764.4655	0.0009	AG	+0.0051	s	⟨4⟩	-I	32	33)
	56764.5999	0.0004	AG	+0.0054		⟨4⟩	-I	32	33)
V1044 Her	56764.3734	0.0008	AG	−0.0010	s	⟨4⟩	-I	32	33)
	56764.4936	0.0033	AG	−0.0011		⟨4⟩	-I	32	33)
	56764.6128	0.0004	AG	−0.0022	s	⟨4⟩	-I	32	33)
V1049 Her	56809.5186	0.0053	AG	−0.0131	s	⟨4⟩	-I	28	33)
V1053 Her	56764.4508	0.0017	AG	−0.0036		⟨4⟩	-I	32	33)
	56764.5952	0.0007	AG	−0.0031	s	⟨4⟩	-I	32	33)
V1055 Her	56764.4836	0.0018	AG	+0.0023		⟨4⟩	-I	32	33)
	56835.4516	0.0017	JU	+0.0034		⟨4⟩	o	60	29)
	56886.3907	0.0016	AG	+0.0040	s	⟨4⟩	-I	17	33)
V1073 Her	56814.4808	0.0015	AG	−0.0054	s	⟨4⟩	-I	25	33)
	56886.4310	0.0002	AG	−0.0072		⟨4⟩	-I	19	33)
V1091 Her	56764.5864	0.0046	AG	−0.0745	s	⟨6⟩	-I	32	33)
V1097 Her	56810.5413	0.0020	AG				-I	24	33)
	56831.4728	0.0040	AG				-I	32	33)
V1119 Her	56808.4815	0.0036	AG				-I	27	33)
V1138 Her	56745.5695	0.0026	AG				-I	35	33)
V1140 Her	56745.4816	0.0015	AG				-I	36	33)
V1302 Her	56799.3916	0.0055	AG				-I	24	33)
	56799.5475	0.0007	AG				-I	24	33)
V1306 Her	56475.4057	0.0028	FR				V	49	37)
V1309 Her	56799.4766	0.0067	AG				-I	24	33)
V1355 Her	56822.4637	0.0103	AG				-I	22	33)
u Her	56814.4457	0.0022	AG	−0.0161		⟨6⟩	-I	25	33)
WY Hya	56743.4461	0.0011	AG	+0.0318		⟨6⟩	-I	20	33)
AV Hya	56725.4273	0.0111	AG	−0.1117	s	⟨6⟩	-I	42	33)
	56726.4562	0.0024	AG	−0.1079		⟨6⟩	-I	64	33)
	56728.5032	0.0044	AG	−0.1111		⟨6⟩	-I	61	33)
EU Hya	56743.3734	0.0046	AG	−0.0352		⟨6⟩	-I	25	33)
FG Hya	56743.4426	0.0016	AG	−0.0675	s	⟨6⟩	-I	24	33)
	56745.4071	0.0022	AG	−0.0700	s	⟨6⟩	-I	27	33)

Table 1: cont.

Variable	HJD 24.....	±	Obs	$O-C$		Ref	Fil	n	Rem
RT Lac	56842.5056	0.0021	AG	−0.3063		⟨6⟩	-I	26	33)
VX Lac	56897.4698	0.0015	AG	+0.0826		⟨6⟩	-I	35	33)
	56898.5442	0.0004	AG	+0.0825		⟨6⟩	-I	54	33)
VY Lac	56876.5052	0.0009	AG	−0.1768		⟨6⟩	-I	24	33)
AW Lac	56830.5039	0.0026	AG	+0.1903	s	⟨6⟩	-I	29	33)
CM Lac	56841.4817	0.0023	AG	−0.0042		⟨6⟩	-I	43	33)
	56886.4136	0.0017	AG	−0.0037		⟨6⟩	-I	21	33)
CO Lac	56683.3397	0.0035	PGL	+0.0029		⟨6⟩	V	72	38) 8)
	56834.4762	0.0010	AG	+0.0031		⟨6⟩	-I	22	33)
DG Lac	56830.4459	0.0008	AG	−0.2270		⟨6⟩	-I	27	33)
HR Lac	56891.3990	0.0016	AG	−0.1022		⟨6⟩	-I	26	33)
IP Lac	56891.4578	0.0020	AG	+0.0890		⟨6⟩	-I	28	33)
NS Lac	56835.4939	0.0002	MS FR	−0.2425		⟨6⟩	o	176	39)
Y Leo	56711.3721	0.0021	AG	−0.0430		⟨6⟩	-I	23	33)
RT Leo	56726.5370	0.0081	AG	−0.0050		⟨6⟩	-I	60	33)
RW Leo	56746.3429	0.0010	WTR	−0.1412		⟨6⟩	o	81	28)
UV Leo	56709.4456	0.0016	AG	+0.0383	s	⟨6⟩	-I	26	33)
	56713.3491	0.0002	DIE	+0.0412		⟨6⟩	o	25	36)
	56723.5492	0.0007	AG	+0.0399		⟨6⟩	-I	95	33)
	56725.3498	0.0023	AG	+0.0402		⟨6⟩	-I	51	33)
	56725.6479	0.0012	AG	+0.0383	s	⟨6⟩	-I	51	33)
	56726.5503	0.0020	AG	+0.0406		⟨6⟩	-I	57	33)
	56728.3499	0.0021	AG	+0.0399		⟨6⟩	-I	74	33)
	56728.6493	0.0017	AG	+0.0393	s	⟨6⟩	-I	74	33)
UZ Leo	56723.5624	0.0066	AG	−0.0585		⟨6⟩	-I	95	33)
	56725.4164	0.0037	AG	−0.0587		⟨6⟩	-I	51	33)
	56726.3446	0.0043	AG	−0.0575	s	⟨6⟩	-I	57	33)
	56726.6523	0.0043	AG	−0.0589		⟨6⟩	-I	57	33)
	56728.5072	0.0049	AG	−0.0581		⟨6⟩	-I	74	33)
VZ Leo	56727.4609	0.0030	FR	−0.0554	s	⟨6⟩	-I	62	33)
WY Leo	56727.5023	0.0015	SCI	+0.4008		⟨6⟩	o	63	29)
	56727.5067	0.0026	FR	+0.4053		⟨6⟩	-I	49	33)
XY Leo	56723.4300	0.0023	AG	−0.0278	s	⟨6⟩	-I	84	33)
	56723.5722	0.0020	AG	−0.0277		⟨6⟩	-I	84	33)
	56725.4193	0.0025	AG	−0.0272	s	⟨6⟩	-I	53	33)
	56725.5612	0.0024	AG	−0.0274		⟨6⟩	-I	53	33)
	56726.4136	0.0022	AG	−0.0273		⟨6⟩	-I	52	33)
	56726.5552	0.0021	AG	−0.0277	s	⟨6⟩	-I	52	33)
XZ Leo	56723.5034	0.0068	AG	+0.0629	s	⟨6⟩	-I	84	33)
	56725.4548	0.0053	AG	+0.0634	s	⟨6⟩	-I	53	33)
	56726.4302	0.0029	AG	+0.0633	s	⟨6⟩	-I	52	33)
AL Leo	56725.6029	0.0053	AG	−0.8355		⟨6⟩	-I	53	33)
	56726.4048	0.0052	AG	−0.0336		⟨6⟩	-I	52	33)
AM Leo	56723.4699	0.0024	AG	+0.0133	s	⟨6⟩	-I	78	33)
	56723.6548	0.0036	AG	+0.0153		⟨6⟩	-I	78	33)
AP Leo	56723.5046	0.0036	AG	−0.0137	s	⟨6⟩	-I	77	33)
	56728.4531	0.0004	QU	−0.0143		⟨6⟩	V	182	30)
	56736.4167	0.0013	SCI	−0.0123	s	⟨6⟩	o	75	29)
VW LMi	56709.5339	0.0018	AG	+0.0011	s	⟨4⟩	-I	26	33)
WZ LMi	56744.4814	0.0069	AG	+0.0920	s	⟨6⟩	V	42	33)
XX LMi	56744.4450	0.0043	AG	+0.0073	s	⟨6⟩	V	42	33)
XY LMi	56744.4928	0.0023	AG	−0.0260		⟨6⟩	V	43	33)
AE LMi	56744.4359	0.0009	AG	+0.0090	s	⟨6⟩	-I	42	33)
	56744.4214	0.0023	AG	−0.0461	s	⟨6⟩	-I	43	33)
AF LMi	56744.6271	0.0025	AG	−0.0437		⟨6⟩	-I	43	33)
SW Lyn	56714.3870	0.0015	AG	+0.0670		⟨6⟩	-I	72	33)
TY Lyn	56731.4834	0.0086	AG	+0.0561		⟨6⟩	-I	36	33)
	56744.4810	0.0017	AG	+0.0587		⟨6⟩	-I	37	33)
UV Lyn	56713.3410	0.0030	AG	+0.0878	s	⟨6⟩	-I	60	33)
	56713.5464	0.0017	AG	+0.0858		⟨6⟩	-I	60	33)
	56714.3765	0.0048	AG	+0.0859		⟨6⟩	-I	84	33)
	56714.5840	0.0043	AG	+0.0859	s	⟨6⟩	-I	84	33)
	56729.3173	0.0016	AG	+0.0874		⟨6⟩	-I	53	33)
	56729.5242	0.0054	AG	+0.0868	s	⟨6⟩	-I	53	33)
CC Lyn	56748.4029	0.0024	SCI	+0.0512	s	⟨4⟩	o	112	29)
CD Lyn	56706.4448	0.0066	AG	−0.0048		⟨4⟩	-I	46	33)
	56706.4472	0.0016	ALH	−0.0024		⟨4⟩	R	961	31)
CN Lyn	56709.4772	0.0032	AG				-I	26	33)
	56711.4310	0.0009	AG				-I	17	33)
	56712.4102	0.0014	AG				-I	54	33)
	56714.3648	0.0071	AG				-I	72	33)

Table 1: cont.

Variable	HJD 24.....	±	Obs	$O-C$		Ref	Fil	n	Rem
DE Lyn	56764.3831	0.0011	JU	−0.0062	s	⟨4⟩	o	60	29)
DY Lyn	56714.2589	0.0004	AG	−0.2078	s	⟨6⟩	-I	72	33)
	56746.4332	0.0018	AG	−0.2079		⟨6⟩	-I	25	33)
DZ Lyn	56714.3322	0.0056	AG	−0.0113		⟨6⟩	-I	72	33)
	56714.5205	0.0096	AG	−0.0120	s	⟨6⟩	-I	72	33)
TT Lyr	56811.4992	0.0002	AG	+0.0147		⟨6⟩	-I	19	33)
TZ Lyr	56475.4586	0.0019	FR	+0.0086	s	⟨6⟩	V	42	37)
	56541.5626	0.0059	FR	+0.0092	s	⟨6⟩	V	38	37)
	56809.4123	0.0025	AG	+0.0081		⟨6⟩	-I	27	33)
	56811.5254	0.0032	AG	+0.0059		⟨6⟩	-I	20	33)
UZ Lyr	56830.4700	0.0027	AG	−0.0342		⟨6⟩	-I	30	33)
	56830.4703	0.0004	QU	−0.0339		⟨6⟩	V	74	30)
AA Lyr	56897.5153	0.0035	AG	+0.1220		⟨6⟩	-I	32	33)
AH Lyr	56897.4031	0.0045	AG	−0.1431	s	⟨6⟩	-I	34	33)
EW Lyr	56541.4647	0.0006	FR	+0.2540		⟨6⟩	V	27	37)
FL Lyr	56841.5041	0.0048	AG	−0.0013	s	⟨6⟩	-I	43	33)
MN Lyr	56745.5418	0.0003	MS FR	+0.0523		⟨6⟩	o	183	39)
PS Lyr	56897.3748	0.0384	AG	+0.0175	s	⟨6⟩	-I	34	33)
PY Lyr	56897.5077	0.0030	AG	−0.0725	s	⟨6⟩	-I	35	33)
V412 Lyr	56897.4653	0.0021	AG	+0.2405		⟨6⟩	-I	34	33)
V507 Lyr	56811.4701	0.0030	MS FR				o	132	39)
V563 Lyr	56541.4603	0.0011	FR	+0.0023		⟨4⟩	V	53	37)
	56811.5078	0.0029	AG	+0.0018	s	⟨4⟩	-I	18	33)
	56842.4109	0.0009	AG	+0.0010		⟨4⟩	-I	27	33)
V572 Lyr	56541.6002	0.0025	FR				V	54	37)
V574 Lyr	56856.4360	0.0017	JU	+0.0033	s	⟨4⟩	o	60	29)
	56871.4577	0.0005	JU	+0.0030	s	⟨4⟩	o	42	29)
V576 Lyr	56541.5443	0.0020	FR	+0.0047	s	⟨4⟩	V	38	37)
V581 Lyr	56490.3950	0.0013	FR				V	54	37)
V664 Lyr	56490.4593	0.0016	FR				V	29	37)
BO Mon	56725.3613	0.0001	WTR	−0.0383		⟨6⟩	o	131	28)
	56725.3626	0.0023	AG	−0.0370		⟨6⟩	-I	20	33)
HM Mon	56713.4343	0.0007	AG	+0.0066		⟨6⟩	-I	30	33)
NN Mon	56713.3791	0.0048	AG	+0.2170		⟨6⟩	-I	31	33)
V532 Mon	56713.3753	0.0034	AG	−0.0494		⟨6⟩	-I	30	33)
V864 Mon	56726.3868	0.0012	AG	−0.0112	s	⟨6⟩	-I	29	33)
	56728.3585	0.0021	AG	−0.0108		⟨6⟩	-I	29	33)
V868 Mon	56713.3257	0.0057	AG				-I	41	33)
	56727.3556	0.0129	AG				-I	29	33)
V936 Mon	56713.2731	0.0003	AG	−0.0362	s	⟨6⟩	-I	31	33)
	56713.4574	0.0006	AG	−0.0364		⟨6⟩	-I	30	33)
V948 Mon	56726.3599	0.0005	AG				-I	28	33)
V953 Mon	56726.4923	0.0034	AG				-I	29	33)
U Oph	56809.4511	0.0056	AG	−0.0075	s	⟨6⟩	-I	26	33)
V456 Oph	56815.4763	0.0005	AG	+0.0222		⟨6⟩	-I	31	33)
V501 Oph	56808.4180	0.0045	AG	−0.0060	s	⟨6⟩	-I	28	33)
V508 Oph	56808.3828	0.0005	AG	−0.0233	s	⟨6⟩	-I	28	33)
	56810.4521	0.0012	AG	−0.0228	s	⟨6⟩	-I	23	33)
V566 Oph	56812.5115	0.0008	AG	+0.0034		⟨6⟩	-I	22	33)
V839 Oph	56814.4416	0.0006	AG	+0.0810		⟨6⟩	-I	25	33)
V2612 Oph	56815.3991	0.0017	AG	−0.0635	s	⟨6⟩	-I	31	33)
V2735 Ori	56701.4672	0.0002	AG	−0.0184		⟨6⟩	-I	39	33)
AT Peg	56887.5063	0.0103	AG	+0.0193	s	⟨6⟩	-I	29	33)
BN Peg	56877.4015	0.0013	AG	+0.0005		⟨6⟩	-I	30	33)
GH Peg	56891.5531	0.0013	AG	+0.0056		⟨6⟩	-I	25	33)
GP Peg	56876.4573	0.0018	AG	−0.0500		⟨6⟩	-I	22	33)
V478 Peg	56897.4111	0.0021	AG				-I	36	33)
V481 Peg	56897.4644	0.0021	AG				-I	36	33)
V535 Peg	56898.4850	0.0021	AG				-I	52	33)
V560 Peg	56887.4433	0.0111	AG				-I	31	33)
V573 Peg	56876.4938	0.0011	AG				-I	22	33)
IQ Per	56706.3079	0.0017	JU	−0.0009		⟨6⟩	o	75	29)
V482 Per	56722.3247	0.0026	JU	−0.0002		⟨4⟩	o	86	29)
MP Pup	56713.4668	0.0017	FR				-I	46	33)
U Sge	56815.5027	0.0008	AG	+0.0010		⟨6⟩	-I	32	33)
V Sge	56891.3994	0.0026	AG	−0.0780		⟨6⟩	-I	24	33)
SY Sge	56891.5099	0.0006	AG	+0.1789		⟨6⟩	-I	22	33)
CU Sge	56871.3748	0.0029	AG	+0.0246	s	⟨6⟩	-I	45	33)
GN Sge	56834.4324	0.0037	AG	+0.0016		⟨6⟩	-I	21	33)
AO Ser	56810.5040	0.0077	AG	−0.0117	s	⟨6⟩	-I	23	33)
AU Ser	56782.5374	0.0009	AG	+0.0766		⟨6⟩	-I	30	33)

Table 1: cont.

Variable	HJD 24.....	±	Obs	$O-C$		Ref	Fil	n	Rem
AU Ser	56783.5018	0.0007	AG	+0.0747	s	⟨6⟩	-I	36	33)
	56812.4894	0.0009	AG	+0.0747	s	⟨6⟩	-I	23	33)
V384 Ser	56834.4254	0.0008	FR	+0.0046		⟨6⟩	-I	43	33)
	56856.4598	0.0004	FR	+0.0032		⟨6⟩	-I	49	33)
V505 Ser	56834.4169	0.0063	FR	+0.0090	s	⟨2⟩	-I	34	33)
	56856.4576	0.0014	FR	+0.0039		⟨2⟩	-I	35	33)
Y Sex	56723.5145	0.0076	AG	−0.0103	s	⟨6⟩	-I	60	33)
	56728.3443	0.0041	AG	−0.0085		⟨6⟩	-I	40	33)
	56728.5535	0.0009	AG	−0.0092	s	⟨6⟩	-I	40	33)
WZ Sex	56743.4050	0.0060	AG				-I	32	33)
WY Tau	56731.3223	0.0007	SCI	+0.0658	s	⟨6⟩	o	60	29)
AL Tau	56727.3077	0.0015	SCI	+0.0564		⟨6⟩	o	61	29)
AM Tau	56701.3811	0.0054	AG	−0.0654		⟨6⟩	-I	38	33)
AN Tau	56729.3315	0.0017	SCI	−0.2525	s	⟨6⟩	o	73	29)
BV Tau	56725.4061	0.0039	SCI	+0.1641	s	⟨6⟩	o	82	29)
CD Tau	56701.3818	0.0081	AG	+0.0053	s	⟨6⟩	-I	44	33)
	56713.4055	0.0044	AG	+0.0060		⟨6⟩	-I	38	33)
V1374 Tau	56725.3883	0.0022	AG	+0.0371		⟨6⟩	-I	33	33)
	56725.5080	0.0013	AG	+0.0314	s	⟨6⟩	-I	33	33)
W UMa	56706.2998	0.0002	DIE	−0.0793		⟨6⟩	o	34	37)
	56706.4640	0.0011	AG	+0.0849		⟨6⟩	-I	45	33)
	56714.3024	0.0036	AG	+0.0828	s	⟨6⟩	-I	83	33)
	56714.4717	0.0011	AG	+0.0853		⟨6⟩	-I	83	33)
	56714.6364	0.0004	AG	+0.0832	s	⟨6⟩	-I	83	33)
TX UMa	56727.4814	0.0033	AG	+0.1948		⟨6⟩	-I	52	33)
TY UMa	56710.4123	0.0008	JU	−0.0116	s	⟨6⟩	o	68	29)
VV UMa	56714.3784	0.0014	AG	−0.0554		⟨6⟩	-I	84	33)
	56759.4031	0.0035	JU	−0.0541	s	⟨6⟩	o	53	29)
XY UMa	56723.3976	0.0019	JU	+0.0395		⟨6⟩	o	80	29)
	56745.4325	0.0008	JU	+0.0407		⟨6⟩	o	36	29)
	56757.4093	0.0016	JU	+0.0426		⟨6⟩	o	56	29)
XZ UMa	56706.5335	0.0087	AG	−0.1244	s	⟨6⟩	-I	45	33)
	56711.4288	0.0018	AG	−0.1184	s	⟨6⟩	-I	18	33)
	56714.4800	0.0021	AG	−0.1230		⟨6⟩	-I	84	33)
ZZ UMa	56725.2961	0.0005	AG	−0.0020		⟨6⟩	-I	50	33)
	56727.5946	0.0005	AG	−0.0028		⟨6⟩	-I	52	33)
AC UMa	56745.4684	0.0178	AG	−0.1376		⟨6⟩	-I	34	33)
AF UMa	56712.4752	0.0014	AG	+0.5872		⟨6⟩	-I	77	33)
AW UMa	56727.5824	0.0051	AG	−0.0955		⟨6⟩	-I	52	33)
	56729.3356	0.0052	AG	−0.0972		⟨6⟩	-I	60	33)
	56729.5567	0.0055	AG	−0.0955	s	⟨6⟩	-I	60	33)
	56731.3166	0.0083	AG	−0.0905	s	⟨6⟩	-I	37	33)
	56731.5290	0.0023	AG	−0.0975		⟨6⟩	-I	37	33)
BM UMa	56730.4095	0.0018	AG	+0.0134	s	⟨6⟩	-I	43	33)
	56730.5433	0.0007	AG	+0.0116		⟨6⟩	-I	43	33)
	56737.3235	0.0005	AG	+0.0113		⟨6⟩	-I	43	33)
	56737.4605	0.0024	AG	+0.0127	s	⟨6⟩	-I	43	33)
	56737.5947	0.0007	AG	+0.0113		⟨6⟩	-I	43	33)
BQ UMa	56730.6064	0.0035	AG	−0.1444		⟨6⟩	-I	44	33)
	56737.5713	0.0040	AG	−0.1441		⟨6⟩	-I	38	33)
BS UMa	56730.4683	0.0014	AG	−0.0263		⟨6⟩	-I	43	33)
	56730.6435	0.0006	AG	−0.0697	s	⟨6⟩	-I	43	33)
	56737.4584	0.0004	AG	−0.0285		⟨6⟩	-I	42	33)
	56737.6354	0.0006	AG	−0.0700	s	⟨6⟩	-I	42	33)
DW UMa	56728.4484	0.0004	JU	−0.0005		⟨4⟩	o	75	29)
GT UMa	56712.5855	0.0009	AG				-I	78	33)
	56725.3892	0.0088	AG				-I	51	33)
	56747.5207	0.0023	AG				-I	35	33)
LO UMa	56744.5178	0.0029	AG	+0.0119		⟨4⟩	-I	43	33)
LP UMa	56728.3748	0.0027	JU	+0.0048	s	⟨4⟩	o	69	29)
MQ UMa	56730.4830	0.0036	AG	+0.0917		⟨6⟩	-I	44	33)
	56737.3880	0.0055	AG	+0.0938	s	⟨6⟩	-I	38	33)
MT UMa	56730.3762	0.0040	AG				-I	43	33)
	56737.5796	0.0026	AG				-I	38	33)
PZ UMa	56706.3902	0.0042	AG				-I	45	33)
	56709.5398	0.0015	AG				-I	25	33)
	56711.3772	0.0167	AG				-I	22	33)
QT UMa	56706.5770	0.0046	AG	−0.0567	s	⟨6⟩	-I	45	33)
	56709.4202	0.0004	AG	−0.0546	s	⟨6⟩	-I	47	33)
	56711.3104	0.0011	AG	−0.0585	s	⟨6⟩	-I	22	33)
V342 UMa	56761.3883	0.0011	JU	−0.0230	s	⟨6⟩	o	77	29)

Table 1: cont.

Variable	HJD 24.....	±	Obs	$O-C$		Ref	Fil	n	Rem
V342 UMa	56783.3940	0.0012	JU	−0.0239	s	⟨6⟩	o	40	29)
V343 UMa	56387.4932	0.0084	JU	−0.0097		⟨6⟩	o	62	29)
	56761.4354	0.0042	JU	−0.0170		⟨6⟩	o	76	29)
W UMi	56734.5302	0.0009	AG	−0.1794		⟨6⟩	-I	43	33)
RU UMi	56725.4827	0.0065	AG	−0.0137	s	⟨6⟩	-I	50	33)
	56729.4199	0.0020	AG	−0.0134		⟨6⟩	-I	61	33)
VW UMi	56734.6014	0.0021	AG	+0.0983	s	⟨6⟩	-I	41	33)
BH Vir	56782.4992	0.0020	AG	−0.0098		⟨6⟩	-I	27	33)
NN Vir	56782.511	0.003	AG				-I	28	33)
V355 Vir	56745.6374	0.0030	FR				-I	201	33)
V589 Vir	56750.4869	0.0020	AG				-I	62	33)
	56750.6169	0.0018	AG				-I	62	33)
V591 Vir	56750.4283	0.0053	AG				-I	63	33)
	56750.6062	0.0031	AG				-I	63	33)
Z Vul	56864.4870	0.0015	AG	−0.0115		⟨6⟩	-I	28	33)
RR Vul	56864.4933	0.0055	AG	−0.0691		⟨6⟩	-I	28	33)
RS Vul	56817.5052	0.0012	AG	+0.0165		⟨6⟩	-I	27	33)
AW Vul	56831.4112	0.0014	AG	−0.0189		⟨6⟩	-I	29	33)
BB Vul	56840.4805	0.0001	MS FR	+0.0001		⟨4⟩	o	248	39)
BE Vul	56842.5071	0.0018	AG	+0.0918		⟨6⟩	-I	20	33)
BO Vul	56870.5202	0.0006	AG	−0.0310		⟨6⟩	-I	26	33)
BP Vul	56891.4621	0.0013	AG	+0.9153		⟨6⟩	-I	23	33)
BQ Vul	56815.4409	0.0006	MS FR	+0.7465		⟨6⟩	o	280	39)
BS Vul	56817.4554	0.0012	AG	−0.0327	s	⟨6⟩	-I	23	33)
	56862.4368	0.0006	AG	−0.0306		⟨6⟩	-I	35	33)
BU Vul	56817.4606	0.0008	AG	+0.0150		⟨6⟩	-I	20	33)
	56862.4119	0.0003	AG	+0.0159		⟨6⟩	-I	35	33)
DR Vul	56886.3658	0.0021	AG	+0.2027	s	⟨6⟩	-I	22	33)
FM Vul	56897.3882	0.0014	AG	+0.0321		⟨6⟩	-I	33	33)
FR Vul	56817.4425	0.0007	AG	−0.0067		⟨6⟩	-I	25	33)
	56864.5338	0.0027	AG	−0.0083		⟨6⟩	-I	28	33)
GO Vul	56795.4455	0.0004	MS FR	−0.0457		⟨6⟩	o	264	39)
GP Vul	56822.4046	0.0048	AG	−0.0769	s	⟨6⟩	-I	24	33)
NO Vul	56834.5079	0.0001	MS FR	+0.0830	s	⟨6⟩	o	200	39)
NP Vul	56834.5407	0.0004	MS FR				o	200	39)
V496 Vul	56870.4975	0.0018	AG				-I	25	33)
2MASS J07254451-0007409	56713.4469	0.0023	AG				-I	30	33)
ASAS J053222+2521.1	56728.3373	0.0014	AG				-I	30	33)
ASAS J093305+0441.8	56725.4733	0.0124	AG				-I	42	33)
ASAS J182856+1141.8	56809.4499	0.0088	AG				-I	24	33)
ASAS J183952+4323.1	56541.3411	0.0051	FR				V	39	37)
	56541.5725	0.0040	FR				V	39	37)
ASAS J185538+4207.9	56490.4497	0.0014	FR				V	31	37)
	56541.4402	0.0022	FR				V	48	37)
ASAS J190139+3902.5	56490.4524	0.0013	FR				V	30	37)
ASAS J190934+4305.9	56490.5443	0.0019	FR				V	30	37)
ASAS J191745+0846.9	56864.5191	0.0009	AG				-I	27	33)
ASAS J191751+1822.7	56834.4628	0.0005	AG				-I	22	33)
ASAS J195605+4713.2	56559.4351	0.0030	FR				V	37	37)
ASAS J201225+0959.4	56871.5397	0.0013	AG				-I	27	33)
ASAS J203921+1746.2	56891.4677	0.0005	AG				-I	27	33)
ASAS J220226+4831.3	56830.4309	0.0047	AG				-I	30	33)
GSC 00279-00695	56745.3999	0.0008	FR				-I	65	33)
	56745.5804	0.0007	FR				-I	65	33)
GSC 00279-00822	55280.4467	0.0002	FR				-I	72	33)
	55627.5730	0.0001	FR				-I	58	33)
	56002.4868	0.0003	FR				-I	49	33)
	56745.4592	0.0003	FR				-I	80	33)
	56745.6428	0.0020	FR				-I	80	33)
GSC 01337-01137	56712.4081	0.0004	FR				-I	80	33)
GSC 01403-01508	56754.4600	0.0024	SCI				o	80	29)
GSC 02695-03163	56877.4742	0.0099	AG				-I	30	33)
GSC 02753-01017	55386.4761	0.0009	FR				-I	46	33)
	55386.5648	0.0025	FR				-I	145	33)
GSC 02757-01475	55386.4579	0.0011	FR				-I	60	33)
GSC 03110-00482	56475.4271	0.0009	FR				V	24	37)
	56541.4275	0.0017	FR				V	57	37)
GSC 03111-00566	56541.3954	0.0038	FR				V	64	37)
	56541.5770	0.0040	FR				V	64	37)
GSC 03619-00047	56891.4089	0.0071	AG	+0.0217		⟨1⟩	-I	28	33)
GSC 03679-02129	56526.5620	0.0048	AG				-I	30	33)

Table 1: cont.

Variable	HJD 24.....	±	Obs	$O-C$	Ref	Fil	n	Rem
GSC 03944-01954	56842.4602	0.0061	AG			-I	24	33)
GSC 03948-02316	55831.4641	0.0014	FR			-I	49	33)
	55834.4403	0.0030	FR			-I	43	33)
	55839.4718	0.0012	FR			-I	66	33)
GSC 03949-00122	55829.4027	0.0010	FR			-I	48	33)
	55835.5560	0.0014	FR			-I	59	33)
	55839.3377	0.0006	FR			-I	53	33)
	55851.6315	0.0027	FR			-I	154	33)
GSC 03949-00631	55831.4861	0.0013	FR			-I	61	33)
	55834.5415	0.0008	FR			-I	44	33)
GSC 03949-01667	55829.3184	0.0011	FR			-I	82	33)
	55831.3048	0.0009	FR			-I	76	33)
	55831.4694	0.0008	FR			-I	76	33)
	55831.6392	0.0030	FR			-I	76	33)
	55832.2993	0.0005	FR			-I	77	33)
	55832.4652	0.0005	FR			-I	77	33)
	55832.6303	0.0030	FR			-I	77	33)
	55834.2904	0.0013	FR			-I	77	33)
	55834.4564	0.0006	FR			-I	77	33)
	55834.6238	0.0025	FR			-I	77	33)
	55839.2658	0.0013	FR			-I	73	33)
	55839.4366	0.0007	FR			-I	73	33)
	55851.3824	0.0010	FR			-I	73	33)
	55851.5504	0.0007	FR			-I	73	33)
HAT 199-12392	55832.3500	0.0025	FR			o	43	37)
HAT 199-36558	56157.4343	0.0076	FR			o	29	33)
HD 55338	56728.4151	0.0144	AG			-I	28	33)
NSV 2146	55887.4108	0.0021	FR			-I	46	33)
NSVS 10123419	56743.5102	0.0015	AG			-I	29	33)
NSVS 2554499	56783.4712	0.0034	AG			-I	24	33)
NSVS 2560518	56711.3639	0.0045	AG			-I	20	33)
	56725.3184	0.0048	AG			-I	50	33)
	56725.4833	0.0117	AG			-I	50	33)
	56725.6468	0.0041	AG			-I	50	33)
	56727.3078	0.0045	AG			-I	51	33)
	56727.4782	0.0081	AG			-I	51	33)
	56727.6388	0.0011	AG			-I	51	33)
NSVS 2745595	56737.4419	0.0033	AG			-I	52	33)
	56737.5797	0.0031	AG			-I	52	33)
	56783.3955	0.0024	AG			-I	35	33)
	56783.5377	0.0023	AG			-I	35	33)
NSVS 3009580	56870.4178	0.0070	AG			-I	27	33)
NSVS 3067305	56897.3669	0.0028	AG			-I	25	33)
NSVS 3068865	56897.3488	0.0022	AG			-I	25	33)
	56897.5161	0.0007	AG			-I	25	33)
NSVS 4863977	56711.3345	0.0020	AG			-I	22	33)
NSVS 4873889	56709.5240	0.0023	AG			-I	25	33)
	56711.4236	0.0033	AG			-I	18	33)
NSVS 4992380	56727.3942	0.0030	AG			-I	52	33)
	56727.5420	0.0012	AG			-I	52	33)
	56749.4329	0.0051	AG			-I	53	33)
	56749.5770	0.0047	AG			-I	53	33)
NSVS 5381032	56541.3759	0.0008	FR			V	50	37)
	56541.5774	0.0019	FR			V	50	37)
NSVS 5475619	56541.4453	0.0017	FR			V	38	33)
NSVS 8097163	56475.4423	0.0011	FR			V	49	37)
NSVS 8229881	56541.4929	0.0081	FR			V	41	37)
NSVS 8744913	56737.4254	0.0023	AG			-I	56	33)
	56737.6172	0.0058	AG			-I	56	33)
ROTSE1 J125947.50+365843.6	56729.4207	0.0110	AG			-I	57	33)
ROTSE1 J143602.90+370529.4	56744.4824	0.0029	AG			-I	50	33)
ROTSE1 J175527.44+440654.3	56782.4841	0.0049	AG			-I	29	33)
	56799.4592	0.0048	AG			-I	24	33)
ROTSE1 J181032.62+403847.4	56541.4427	0.0012	FR			V	46	37)
ROTSE1 J181628.90+375019.3	56541.4451	0.0035	FR			V	32	37)
ROTSE1 J181631.43+371103.0	56475.4806	0.0006	FR			V	24	37)
ROTSE1 J185450.96+401407.7	56490.4400	0.0026	FR			V	43	37)
TYC 3864-0488	56737.3652	0.0002	AG			-I	52	33)
	56737.5222	0.0076	AG			-I	52	33)
TYC 3973-1124	56830.4891	0.0040	AG			-I	29	33)
UCAC3 294-12179	56875.4871	0.0018	MS FR			o	264	39)

Table 1: cont.

Variable	HJD 24.....	±	Obs	$O-C$	Ref	Fil	n	Rem
U-B1 1135-0102876	56734.3220	0.0028	AG			-I	35	33)
U-B1 1416-0453013	56891.5601	0.0026	AG			-I	26	33)
U-B1 1416-0454010	56891.5257	0.0014	AG			-I	28	33)

Table 2: Times of maxima of pulsating stars

Variable	HJD 24.....	±	Obs	$O-C$	Ref	Fil	n	Rem
OV And	56870.4066	0.0035	PGL	−0.0084	⟨6⟩	V	138	32) 9)
SX Aqr	56870.4698	0.0035	PGL	−0.0056	⟨6⟩	V	161	32) 10)
BH Aur	56725.326	0.001	AG	+0.005	⟨6⟩	-I	34	33)
V574 Aur	56747.4431:	0.0030	FR	−0.0727	⟨6⟩	-I	57	33)
RS Boo	56745.5246	0.0035	PGL	−0.0469	⟨6⟩	V	204	38) 11)
	56764.4325	0.0007	QU	−0.0059	⟨6⟩	V	88	30) 2)
	56782.5512	0.0007	ALH	+0.0005	⟨6⟩	o	454	31)
SW Boo	56747.634	0.001	AG	+0.016	⟨6⟩	-I	39	33)
UU Boo	56746.630	0.001	AG	+0.008	⟨6⟩	-I	61	33)
WW Boo	56832.4232	0.0011	MZ	−0.0239	⟨6⟩	-I	115	30)
	56855.4262	0.0009	MZ	−0.0257	⟨6⟩	-I	113	30)
WZ Boo	56764.4661	0.0014	MZ	+0.0409	⟨6⟩	-I	120	30)
	56842.4228	0.0008	MZ	+0.0359	⟨6⟩	-I	148	30)
	56853.3930:	0.0030	MZ	+0.0337	⟨6⟩	-I	110	30)
	56857.4418	0.0015	MZ	+0.0400	⟨6⟩	-I	87	30)
YZ Boo	56746.344	0.001	AG	−0.035	⟨6⟩	V	61	33)
	56746.449	0.001	AG	−0.035	⟨6⟩	V	61	33)
	56746.554	0.001	AG	−0.034	⟨6⟩	V	61	33)
	56754.362	0.001	AG	−0.033	⟨6⟩	-I	24	33)
	56764.248	0.001	AG	−0.035	⟨6⟩	-I	27	33)
	56783.403	0.001	AG	−0.033	⟨6⟩	-I	36	33)
	56783.505	0.001	AG	−0.035	⟨6⟩	-I	36	33)
CQ Boo	56783.4523	0.0015	ALH	−0.0647	⟨6⟩	o	535	31) 3)
	56783.4877	0.0019	ALH	−0.0293	⟨6⟩	o	535	31) 4)
IQ Boo	56811.5107	0.0013	MZ			-I	118	30)
	56840.4042	0.0010	MZ			-I	111	30)
MZ Boo	56747.472	0.007	AG			-I	41	33)
NN Boo	56808.4279	0.0016	MZ	+0.0166	⟨6⟩	-I	133	30)
PQ Boo	56771.449	0.001	AG			-I	25	33)
V336 Boo	56799.4000	0.0007	ALH			o	471	31)
	56799.5133	0.0007	ALH			o	471	31)
CN Cam	56737.526	0.001	AG	+0.000	⟨5⟩	-I	56	33)
EW Cam	56729.539	0.001	AG			-I	52	33)
	56731.418	0.001	AG			-I	37	33)
HU Cam	56601.3880	0.0013	MZ			-I	67	30)
V354 Cam	56727.456	0.001	AG			-I	56	33)
RW Cnc	56725.4465	0.0011	ALH	+0.2167	⟨6⟩	R	410	31)
	56754.4486	0.0035	PGL	+0.2172	⟨6⟩	V	170	38) 12)
AQ Cnc	56726.3647	0.0035	PGL	−0.0852	⟨6⟩	V	273	32) 13)
	56727.4641	0.0015	ALH	−0.0829	⟨6⟩	R	416	31)
EF Cnc	56745.383	0.001	AG			-I	34	33)
LQ Cnc	56722.4302	0.0019	MZ			-I	90	30)
W CVn	56764.5305	0.0010	ALH	−0.1492	⟨6⟩	R	759	31)
Z CVn	56737.5938	0.0018	ALH	+0.1161	⟨6⟩	R	481	31)
RR CVn	56783.3873	0.0015	MZ	+0.0204	⟨6⟩	-I	102	30)
RZ CVn	56746.4353	0.0011	ALH	−0.1329	⟨6⟩	R	487	31)
	56814.5283	0.0035	PGL	−0.1292	⟨6⟩	V	153	38) 14)
AP CVn	56820.423	0.002	MZ	−0.276	⟨6⟩	-I	87	30)
AD CMi	56726.356	0.001	AG	+0.014	⟨6⟩	B	29	33)
	56726.476	0.001	AG	+0.011	⟨6⟩	B	29	33)
V1040 Cas	56875.378	0.002	MS FR	+0.013	⟨6⟩	o	318	39)
	56875.452	0.002	MS FR	+0.014	⟨6⟩	o	318	39)
	56875.525	0.002	MS FR	+0.013	⟨6⟩	o	318	39)
S Com	56736.5053	0.0013	ALH	−0.1063	⟨6⟩	R	489	31)
ST Com	56776.4300	0.0035	PGL	−0.0344	⟨6⟩	V	410	32) 15)
BD Com	56781.5295	0.0009	MZ			-I	164	30)
BT Com	56821.4478	0.0016	MZ	+0.1051	⟨6⟩	-I	91	30)
DL Com	56795.3908	0.0013	MZ	+0.0885	⟨6⟩	-I	86	30)
HY Com	56743.504	0.002	AG			-I	62	33)

Table 2: cont.

Variable	HJD 24.....	±	Obs	$O-C$	Ref	Fil	n	Rem
LY Com	56764.3516	0.0022	MZ			-I	76	30) 4)
	56802.4128	0.0015	MZ			-I	118	30) 3)
	56802.4506	0.0022	MZ			-I	118	30) 4)
	56810.3926	0.0015	MZ			-I	99	30) 3)
	56810.4230	0.0021	MZ			-I	99	30) 4)
	56815.4016	0.0010	MZ			-I	97	30) 3)
	56815.4337	0.0010	MZ			-I	97	30) 4)
RV CrB	56814.5424	0.0009	ALH	−0.0548	⟨6⟩	V	511	31) 3)
	56814.5816	0.0017	ALH	−0.0155	⟨6⟩	V	511	31) 4)
TV CrB	56808.451	0.001	AG	+0.044	⟨6⟩	-I	28	33)
XX Cyg	56870.4033	0.0006	ALH	+0.0008	⟨6⟩	R	388	31)
	56870.5385	0.0040	ALH	+0.0012	⟨6⟩	R	388	31)
XZ Cyg	56855.5176	0.0007	ALH	−0.0317	⟨6⟩	V	615	31)
V2369 Cyg	56157.3939	0.0030	FR			V	48	37)
V2455 Cyg	56862.3963	0.0006	ALH	+0.0275	⟨6⟩	V	708	31)
	56862.4903	0.0005	ALH	+0.0273	⟨6⟩	V	708	31)
	56862.5842	0.0007	ALH	+0.0270	⟨6⟩	V	708	31)
RW Dra	56863.5199	0.0013	ALH	+0.2087	⟨6⟩	o	410	31)
SU Dra	56729.464	0.001	AG	+0.079	⟨6⟩	-I	45	33)
	56737.372	0.001	AG	+0.062	⟨6⟩	-I	56	33)
SW Dra	56754.4005	0.0010	ALH	+0.0620	⟨6⟩	V	396	31)
	56754.403	0.001	AG	+0.065	⟨6⟩	-I	27	33)
VZ Dra	56815.5290	0.0021	ALH	+0.0513	⟨6⟩	V	348	31)
OS Dra	56729.568	0.001	AG			-I	46	33)
OW Dra	56731.376	0.001	AG	+0.017	⟨6⟩	-I	39	33)
PY Dra	56771.530	0.001	AG			-I	25	33)
QS Dra	56771.403	0.001	AG			-I	27	33)
	56771.482	0.001	AG			-I	27	33)
QV Dra	56771.449	0.001	AG			-I	22	33)
RR Gem	56727.4422	0.0016	MOO	−0.1207	⟨6⟩	V	56	35)
V397 Gem	56737.3407	0.0013	MZ	−0.0238	⟨6⟩	-I	118	30)
VX Her	56816.4401	0.0008	ALH	−0.0266	⟨6⟩	V	336	31)
VZ Her	56801.4366	0.0010	ALH	+0.0764	⟨6⟩	o	523	31)
AR Her	56733.5537	0.0035	PGL	+0.0065	⟨6⟩	V	126	35) 16)
	56796.5392	0.0020	ALH	+0.0082	⟨6⟩	V	609	31)
	56819.5722	0.0035	PGL	+0.0099	⟨6⟩	V	136	38) 17)
	56820.5158	0.0035	PGL	+0.0134	⟨6⟩	V	226	38) 18)
	56873.5850	0.0035	PGL	−0.0305	⟨6⟩	V	237	38) 19)
	56875.4930	0.0035	PGL	−0.0027	⟨6⟩	V	190	38) 20)
DY Her	56797.4635	0.0007	ALH			o	383	31)
LS Her	56810.435	0.001	AG	−0.007	⟨6⟩	-I	23	33)
	56812.500	0.001	AG	−0.019	⟨6⟩	-I	22	33)
DE Lac	56877.3637	0.0017	ALH	+0.0592	⟨6⟩	V	621	31)
RR Leo	56723.4750	0.0007	ALH	+0.1351	⟨6⟩	R	580	31)
	56727.547	0.001	AG	+0.136	⟨6⟩	-I	52	33)
SS Leo	56743.427	0.001	AG	−0.090	⟨6⟩	-I	29	33)
WY LMi	56746.4359	0.0013	MZ			-I	85	30)
AB LMi	56744.464	0.001	AG			-I	43	33)
SZ Lyn	56704.284	0.001	AG	+0.031	⟨6⟩	-I	19	33)
	56712.3578	0.0009	ALH	+0.0285	⟨6⟩	R	101	31)
	56712.4792	0.0007	ALH	+0.0294	⟨6⟩	R	101	31)
	56712.5989	0.0007	ALH	+0.0285	⟨6⟩	R	101	31)
TT Lyn	56727.497	0.001	AG	−0.043	⟨6⟩	-I	43	33)
AN Lyn	56713.3420	0.0015	ALH			R	723	31)
	56713.4420	0.0015	ALH			R	723	31)
	56713.5398	0.0013	ALH			R	723	31)
	56713.6402	0.0024	ALH			R	723	31)
	56734.5683	0.0035	PGL			V	128	38) 21)
DQ Lyn	56727.4345	0.0020	MZ			-I	144	30)
	56729.4096	0.0020	MZ			-I	161	30)
RR Lyr	56854.4739	0.0039	ALH	+0.2794	⟨6⟩	V	935	31)
RZ Lyr	56830.4652	0.0016	ALH	−0.0427	⟨6⟩	R	318	31)
ZZ Lyr	56861.4591	0.0008	MZ	+0.0228	⟨6⟩	-I	70	30)
DD Lyr	56870.3888	0.0014	MZ	−0.1353	⟨6⟩	-I	125	30)
	56889.3933	0.0010	MZ	−0.1343	⟨6⟩	-I	125	30)
EZ Lyr	56817.4409	0.0018	ALH	−0.1419	⟨6⟩	V	328	31)
KM Lyr	56541.5573	0.0040	FR	−0.1537	⟨6⟩	V	30	37)
LX Lyr	56490.4216	0.0020	FR	+0.0066	⟨6⟩	V	32	37)
NR Lyr	56490.4359	0.0020	FR	−0.0290	⟨6⟩	V	31	37)
V593 Lyr	56475.4656	0.0020	FR	−0.0036	⟨6⟩	V	43	37)
	56490.3836	0.0020	FR	+0.0018	⟨6⟩	V	50	37)

Table 2: cont.

Variable	HJD 24.....	±	Obs	$O-C$	Ref	Fil	n	Rem
V593 Lyr	56490.4806	0.0020	FR	−0.0033	⟨6⟩	V	50	37)
	56541.5593	0.0020	FR	+0.0049	⟨6⟩	V	29	37)
TU Per	56643.4264	0.0035	PGL			V	567	34) 22)
AR Per	56665.3900	0.0035	PGL	+0.0621	⟨6⟩	V	96	38) 23)
	56722.4188	0.0022	JU	+0.0673	⟨6⟩	o	98	29)
	56870.5055	0.0035	PGL	+0.0630	⟨6⟩	V	156	32) 24)
AN Ser	56812.466	0.001	AG	+0.006	⟨6⟩	-I	23	33)
BH Ser	56814.4413	0.0012	MZ	+0.1259	⟨6⟩	-I	126	30)
T Sex	56728.467	0.001	AG	−0.086	⟨6⟩	-I	47	33)
UX Tri	56682.4634	0.0069	PGL			V	30	38) 25)
RV UMa	56728.4645	0.0010	ALH	+0.1317	⟨6⟩	R	325	31)
	56736.420	0.001	AG	+0.130	⟨6⟩	-I	42	33)
	56750.462	0.001	AG	+0.130	⟨6⟩	-I	44	33)
TU UMa	56725.5019	0.0005	QU	−0.0593	⟨6⟩	V	163	30) 1) 2)
	56729.4048	0.0010	ALH	−0.0600	⟨6⟩	R	718	31)
	56729.4056	0.0007	QU	−0.0592	⟨6⟩	V	187	30) 1) 2)
	56729.407	0.001	AG	−0.058	⟨6⟩	-I	60	33)
	56734.4249	0.0069	PGL	−0.0588	⟨6⟩	V	63	38) 26)
	56744.4621	0.0007	QU	−0.0595	⟨6⟩	V	165	30) 1) 2)
AB UMa	56731.510	0.002	AG	+0.135	⟨6⟩	-I	39	33)
	56737.502	0.002	AG	+0.132	⟨6⟩	-I	53	33)
AE UMa	56683.5091	0.0035	PGL	+0.0037	⟨6⟩	V	110	38) 27)
	56734.3460	0.0010	ALH	+0.0045	⟨6⟩	R	686	31)
	56734.4267	0.0005	ALH	−0.0009	⟨6⟩	R	686	31)
	56734.5116	0.0010	ALH	−0.0020	⟨6⟩	R	686	31)
	56746.3877	0.0007	SCI	+0.0038	⟨6⟩	o	89	29)
	56746.4688	0.0004	SCI	−0.0011	⟨6⟩	o	50	29)
	56746.5532	0.0005	SCI	−0.0028	⟨6⟩	o	50	29)
	56746.6464	0.0005	SCI	+0.0044	⟨6⟩	o	41	29)
AP UMa	56730.620	0.001	AG			-I	43	33)
AU UMa	56730.542	0.002	AG			-I	43	33)
	56737.376	0.001	AG			-I	38	33)
AV UMa	56737.579	0.001	AG	+0.105	⟨6⟩	-I	38	33)
AX UMa	56730.401	0.001	AG	+0.261	⟨6⟩	-I	43	33)
	56737.353	0.001	AG	+0.259	⟨6⟩	-I	38	33)
BN UMa	56737.438	0.001	AG			-I	41	33)
MO UMa	56730.410	0.001	AG	−0.123	⟨6⟩	-I	43	33)
	56737.401	0.001	AG	−0.129	⟨6⟩	-I	39	33)
MU UMa	56737.426	0.001	AG			-I	38	33)
YZ UMi	56734.507	0.001	AG			-I	39	33)
2MASS J18294745+3745005	56541.3804	0.0030	FR			V	34	37)
	56541.4914	0.0030	FR			V	34	37)
ASAS J084144+2530.6	56709.517	0.001	AG			-I	25	33)
CSS J093057.0+155713	55623.4793	0.0030	FR			-I	63	33)
GSC 02696-02177	54682.377	0.000	FR			-I	72	33)
	54682.450	0.001	FR			-I	72	33)
	54682.523	0.000	FR			-I	72	33)
	54684.487	0.001	FR			-I	64	33)
	54684.556	0.001	FR			-I	64	33)
	54719.338	0.000	FR			-I	87	33)
	54719.408	0.000	FR			-I	87	33)
	54719.478	0.001	FR			-I	87	33)
	55050.397	0.001	FR			-I	64	33)
	55050.468	0.001	FR			-I	64	33)
	56159.392	0.002	FR			-I	94	33)
	56159.463	0.002	FR			-I	94	33)
	56159.535	0.001	FR			-I	94	33)
	56650.206	0.001	FR			-I	67	33)
	56650.274	0.002	FR			-I	67	33)
	56650.348	0.001	FR			-I	67	33)
	56654.271	0.001	FR			-I	66	33)
	56654.345	0.001	FR			-I	66	33)
	56657.251	0.002	FR			-I	62	33)
	56657.324	0.001	FR			-I	62	33)
GSC 02977-00238	56724.3502	0.0007	ALH			R	656	31)
	56724.4264	0.0011	ALH			R	656	31)
	56724.5016	0.0007	ALH			R	656	31)
	56724.5773	0.0005	ALH			R	656	31)
GSC 03074-00114	56809.4044	0.0004	ALH			o	301	31)
	56809.4554	0.0004	ALH			o	301	31)
	56809.5065	0.0031	ALH			o	301	31)

Table 2: cont.

Variable	HJD 24.....	±	Obs	$O-C$	Ref	Fil	n	Rem
GSC 03074-00114	56809.5577	0.0005	ALH			o	301	31)
GSC 03428-01497	56726.3619	0.0013	ALH			R	929	31)
	56726.4373	0.0012	ALH			R	929	31)
	56726.5124	0.0012	ALH			R	929	31)
	56726.5882	0.0014	ALH			R	929	31)
GSC 03577-02495	56559.3014	0.0040	FR			V	67	37)
GSC 03755-00845	56629.3363	0.0004	ALH			V	69	31)
	56629.4117	0.0004	ALH			V	69	31)
	56629.4879	0.0004	ALH			V	69	31)
GSC 03832-00152	56758.3343	0.0009	ALH			V	480	31)
	56758.4247	0.0007	ALH			V	480	31)
	56758.5160	0.0004	ALH			V	480	31)
	56758.6073	0.0004	ALH			V	480	31)
GSC 03851-00240	56761.4284	0.0049	ALH			R	416	31)
	56761.4946	0.0010	ALH			R	416	31)
	56761.5629	0.0008	ALH			R	416	31)
	56761.6323	0.0008	ALH			R	416	31)
GSC 03863-00740	56757.4080	0.0017	ALH			V	153	31)
	56757.6073	0.0022	ALH			V	153	31)
GSC 03934-01904	56856.3971	0.0006	ALH			R	521	31)
	56856.5056	0.0006	ALH			R	521	31)
	56856.6154	0.0008	ALH			R	521	31)
GSC 04372-00436	56654.245	0.001	AG			-I	31	33)
	56654.519	0.001	AG			-I	26	33)
GSC 04552-01498	56668.4064	0.0005	JU			o	18	29)
ROTSE1 J181449.65+400948.5	56541.4430	0.0030	FR			V	52	37)
TYC 4556-1113	56764.365	0.001	AG			-I	32	33)
	56764.450	0.001	AG			-I	32	33)
	56764.538	0.001	AG			-I	32	33)

Observers:

AG:	Agerer, F., Tiefenbach
ALH:	Alich, K., Schaffhausen
DIE:	Dietrich, M., Radebeul
FR:	Frank, P., Velden
JU:	Jungbluth, H., Karlsruhe
MOO:	Moos, C., Netphen
MS:	Moschner, W., Lennestadt
MZ:	Maintz, G., Bonn
PGL:	Pagel, L., Klockenhagen
QU:	Quester, W., Esslingen
SCI:	Schmidt, U., Karlsruhe
WTR:	Walter, F., München

Remarks:

n	number of measurements
:	uncertain
s	secondary minimum
(1)	maximum determination as described by Wade et al. (1999)
(2)	mean error in this case: standard deviation
(3)	double maximum: time of the first maximum
(4)	double maximum: time of the second maximum
(5)	8.172 mag
(6)	10.859 mag
(7)	9.228 mag
(8)	10.953 mag
(9)	10.806 mag
(10)	11.707 mag
(11)	9.458 mag
(12)	11.110 mag
(13)	11.518 mag
(14)	10.744 mag
(15)	10.958 mag
(16)	10.329 mag
(17)	10.522 mag
(18)	10.462 mag
(19)	10.734 mag
(20)	10.747 mag
(21)	10.231 mag
(22)	11.854 mag
(23)	10.029 mag
(24)	9.920 mag
(25)	12.925 mag
(26)	9.210 mag
(27)	10.961 mag

Photometers:

(28) CCD camera ST-6: chip 375×242
(29) CCD camera ST-7
(30) CCD camera ST-7E
(31) CCD camera ST-8 XMEI
(32) CCD camera Artemis 4021
(33) CCD camera Sigma 1603
(34) CCD camera Moravian G2-1600
(35) CCD camera QHY8
(36) CCD camera ATIK 314 L+
(37) camera Canon EOS 450D
(38) CCD camera QHY8L
(39) CCD camera STXL-6303E

Filters:

o without filter
V V-filter
B B-filter
R R-filter
-I IR cut-off filter

References:

Agerer, F., 2010, *PZP*, **10**, 4 ⟨1⟩
BAV Services for Scientists, 2013, `http://www.bav-astro.de/sfs/index.php/`
Bernhard, K., Frank, P., 2006, *IBVS*, No. 5719 *BAV Mitt.*, **177** ⟨2⟩
Bernhard, K., Frank, P., 2010, *BAV Rb.*, **59**, 31 ⟨3⟩
Kreiner, J. M., 2004, *Acta Astr.*, **54**, 207 ⟨4⟩
Lichtenknecker Database of the BAV, `http://www.bav-astro.de/LkDB/index.php/`
Maintz, G., 2012, *BAV Rb.*, **61**, 83 ⟨5⟩
Samus, N. N., et al., 2011, `http://www.sai.msu.su/gcvs/gcvs/index.htm` ⟨6⟩
Wade, R. A., Donley, J., Fried, R., White, R. E., Saha, A., et al., 1999, *AJ*, **118**, 2442

ERRATUM FOR IBVS 6118 (BAVM 234)

FL Lac 56535.4735 AG has to be deleted

COMMISSIONS 27 AND 42 OF THE IAU
INFORMATION BULLETIN ON VARIABLE STARS

Number 6150

Konkoly Observatory
Budapest
28 September 2015

HU ISSN 0374 – 0676

PHOTOMETRY OF HIGH-AMPLITUDE DELTA SCUTI STARS IN 2014

WILS, PATRICK[1]; HAMBSCH, FRANZ-JOSEF[1,2]; VANLEENHOVE, MAARTEN[1]; LAMPENS, PATRICIA[3]; VAN CAUTEREN, PAUL[1,3]; VAN DE STADT, INGE[4]; PICKARD, ROGER D.[5]; VAN WASSENHOVE, JEROEN[1]; BAILLIEN, ANTOINE[1]; DUBOIS, FRANKY[1,6]; LOGIE, LUDWIG[1,6]; RAU, STEVE[1,6]; VANAVERBEKE, SIEGFRIED[1,6]; NIEUWENHOUT, FRANS[4]; BENAVIDES PALENCIA, RAFAEL[7]; ROBERTSON, C.W.[8]; AYIOMAMITIS, ANTHONY[9,10]; GONZALEZ CARBALLO, JUAN-LUIS[11]; KANTOLA, TIMO[12]

[1] Vereniging Voor Sterrenkunde, Belgium; e-mail: patrickwils@yahoo.com

[2] Bundesdeutsche Arbeitsgemeinschaft für Veränderliche Sterne e.V. Germany

[3] Koninklijke Sterrenwacht van België (ROB), Brussel, Belgium

[4] Werkgroep Veranderlijke Sterren, The Netherlands

[5] British Astronomical Association, UK

[6] Astrolab IRIS, Ieper, Belgium

[7] Observatorio Posadas, Córdoba, Spain

[8] SETEC Observatory, Goddard, Kansas, USA

[9] Helliniki Astronomiki Enosi, Greece

[10] Perseus Observatory, Athens, Greece

[11] Observatorio Cerro del Viento, Badajoz, Spain

[12] Pieksämäki, Finland

This paper continues the series of reports on photometry of High-Amplitude Delta Scuti (HADS) stars (see Wils et al., 2014 for the previous paper). It presents details on 409 times of maximum for 70 HADS, most of them obtained during 2014. In the first paper of the series (Wils et al., 2009), the method used to calculate the times of maximum is described.

We list the observed maxima in Table 1 with the star name (Col. 1), the epoch of the observed maximum (Col. 2), the uncertainty of the epoch (Col. 3), the observer/instrument code (Col. 4) and the filter used for the observations (Col. 5). The index to the observer/instrument code is given in Table 2. It lists the observer's initials, the location and the instruments used.

The period of KZ Lac has been found to vary rather erratically. An $O-C$ plot with respect to a linear ephemeris based on all our data (from this and previous papers in the series) is given in Fig. 1. The elements themselves are given in Table 3. It is possible that the period of KZ Lac shows cyclical changes on a timescale of about 10 years. However, for the moment the timespan of our observations is too short to confirm this.

Changes in the period of GSC 0191-1282 (= ASAS J073758+0552.3) have been detected as well. In the $O-C$ plot given in Fig. 2 our data are supplemented with maxima calculated from yearly phase plots of ASAS (Pojmański, 2002) and NSVS (Woźniak et al., 2004) data. This shows shorter term period changes in addition to a longer term

Table 1: Observed times of maximum (Epoch = HJD − 2400000).

Star	Epoch	Error	Obs.	Filter	Star	Epoch	Error	Obs.	Filter
GP And	56904.3841	0.0010	HMB	V	LW Dra	56814.4654	0.0020	IS	C
	56949.3125	0.0004	HO40	V		56904.3821	0.0007	VWS	V
	56949.3913	0.0004	HO40	V		56962.3946	0.0009	VWS	V
	56949.4698	0.0005	HO40	V	DY Her	56741.5839	0.0006	HMB	V
	56949.5485	0.0004	HO40	V		56750.5022	0.0023	HMB	V
V460 And	56742.3147	0.0004	HMB	V		56750.6505	0.0007	HMB	V
	56912.4453	0.0004	MAV	V		56796.5782	0.0021	HMB	V
	56912.5204	0.0004	MAV	V	V1086 Her	56745.5587	0.0013	HMB	V
	56962.3075	0.0004	AB	C		56767.6298	0.0016	HMB	V
	56962.3832	0.0008	AB	C		56781.6039	0.0013	HMB	V
	57000.4732	0.0005	RP	V	V1116 Her	56113.4295	0.0012	GCJ	C
	57006.3208	0.0004	AB	C		56113.5235	0.0017	GCJ	C
V524 And	56862.5369	0.0005	MAVR	V		56113.5257	0.0012	PNQ	C
	56908.3657	0.0015	HMB	V		56742.4880	0.0015	HMB	V
	56908.4594	0.0014	HMB	V		56742.5841	0.0018	HMB	V
	56935.4850	0.0006	RP	V		56749.5894	0.0013	HMB	V
	56935.5798	0.0006	RP	V		56791.5334	0.0022	HMB	V
	56935.6742	0.0004	RP	V	V1209 Her	56745.4912	0.0003	HMB	V
V544 And	56928.3646	0.0010	AB	C		56745.5424	0.0003	HMB	V
	56928.4713	0.0005	AB	C		56745.5935	0.0002	HMB	V
	57004.2907	0.0006	RP	V		56745.6450	0.0004	HMB	V
	57004.3983	0.0008	RP	V		56763.5477	0.0003	HMB	V
CY Aqr	56928.3955	0.0003	HO18	V		56763.5989	0.0002	HMB	V
	56928.4565	0.0004	HO18	V		56782.5271	0.0004	HMB	V
YZ Boo	56691.6967	0.0006	IS	C		56782.5783	0.0003	HMB	V
	56722.5072	0.0014	HO18	V	KZ Lac	56165.4640	0.0008	KTU	V
	56726.6710	0.0006	IS	C		56176.5318	0.0007	KTU	V
V336 Boo	56728.5098	0.0018	IS	C		56180.2909	0.0010	KTU	V
	56728.6237	0.0008	IS	C		56794.5734	0.0018	MAVR	V
V367 Cam	56721.4044	0.0041	RP	V		56856.4944	0.0019	MAV	V
	57006.3038	0.0013	MAV	V		56903.3793	0.0022	MAV	V
V376 Cam	56676.3804	0.0005	IS	C		56909.3305	0.0043	MAV	V
	56700.6559	0.0005	IS	C		56909.4330	0.0040	MAV	V
	56724.6506	0.0006	IS	C		56910.4773	0.0025	RP	V
	56743.4534	0.0006	IS	C		56910.5829	0.0026	RP	V
	56764.3602	0.0006	VWS	V		56913.4018	0.0012	HMB	V
	56764.5009	0.0003	VWS	V		56962.3738	0.0011	HMB	V
	56796.4940	0.0008	IS	C	EH Lib	56729.6669	0.0004	IS	C
	56928.3953	0.0005	MAV	V		56796.5080	0.0006	HO18	V
	56928.5357	0.0005	MAV	V	SZ Lyn	56728.3898	0.0009	HMB	V
	56940.3226	0.0006	MAV	V		56728.5104	0.0009	HMB	V
	57005.4316	0.0003	ALI	V		56728.6302	0.0009	HMB	V
	57011.3249	0.0004	ALI	V		56745.3849	0.0011	HMB	V
AD CMi	56699.5445	0.0013	HMBC	V		56757.4377	0.0008	HMB	V
	56699.6682	0.0014	HMBC	V		56763.3443	0.0008	HMB	V
V792 Cep	56869.4133	0.0009	MAVR	V		56763.4651	0.0008	HMB	V
	56869.5469	0.0011	MAVR	V	V593 Lyr	56823.3922	0.0010	MAV	V
	56944.2573	0.0016	MAV	V		56823.4937	0.0008	MAV	V
	56944.3905	0.0007	MAV	V	V1162 Ori	56654.6679	0.0022	SO30	V
XX Cyg	56890.5010	0.0011	RP	V		56654.7476	0.0032	SO30	V
V2455 Cyg	56862.4019	0.0004	MAV	V		56654.8262	0.0022	SO30	V
	56862.4960	0.0003	MAV	V		56654.9084	0.0034	SO30	V
	56862.5901	0.0003	MAV	V		56691.2572	0.0041	HO40	V
	56863.4380	0.0010	MAV	V		56691.3347	0.0027	HO40	V
	56863.5324	0.0005	MAV	V		56691.4166	0.0039	HO40	V
LW Dra	56781.3840	0.0012	VWS	V		56711.3220	0.0026	HO40	V
	56781.5024	0.0007	VWS	V		56711.4027	0.0037	HO40	V

Table 1: Observed times of maximum (continued).

Star	Epoch	Error	Obs.	Filter	Star	Epoch	Error	Obs.	Filter
V1162 Ori	56712.3458	0.0031	HO40	V	GSC 0321-0314	56795.3857	0.0005	HO40	C
	56722.3396	0.0032	HO40	V	GSC 0429-2098	56764.6231	0.0018	HMB	V
	56722.4183	0.0032	HO40	V	GSC 0612-0771	56913.5020	0.0005	HMB	V
	56723.3606	0.0032	HO40	V		56913.5650	0.0005	HMB	V
	56725.3302	0.0035	HO40	V		56952.4911	0.0008	RP	V
	56728.3185	0.0031	HO40	V	GSC 0628-0348	56973.3852	0.0009	LP11	V
	56728.3995	0.0044	HO40	V	GSC 0753-1489	56701.6175	0.0013	HMBC	V
	56729.3422	0.0041	HO40	V		56701.7104	0.0007	HMBC	V
	56729.4187	0.0045	HO40	V		57004.4994	0.0008	RP	V
	56730.2841	0.0042	HO40	V		57004.5923	0.0007	RP	V
	56730.3644	0.0030	HO40	V		57004.6858	0.0007	RP	V
	56949.5817	0.0022	HO40	V	GSC 0933-0651	56733.5775	0.0015	HMB	V
	56973.4976	0.0032	LP11	V		56794.4527	0.0018	HMB	V
	56973.5797	0.0033	LP11	V		56794.5579	0.0013	HMB	V
	56973.6567	0.0028	LP11	V	GSC 1061-1651	56548.4931	0.0020	PNQ	V
	56973.7370	0.0030	LP11	V	GSC 1220-1131	56912.6238	0.0027	HMB	V
DY Peg	56900.4755	0.0011	RP	V		56962.4869	0.0008	HMB	V
	56900.5479	0.0004	RP	V		56962.5678	0.0009	HMB	V
	56900.6210	0.0003	RP	V		56962.6485	0.0011	HMB	V
	57002.3529	0.0004	ALI	V	GSC 1306-0466	56722.3077	0.0006	FN	C
V536 Peg	56875.4535	0.0004	AB	C		56722.3946	0.0006	FN	C
	56912.3949	0.0005	HMB	V		56968.4248	0.0016	MAV	V
	56912.4592	0.0005	HMB	V	GSC 1442-1358	56711.5844	0.0010	FN	C
	56940.2929	0.0005	HMB	V		56721.6023	0.0020	RP	V
	56940.3581	0.0004	HMB	V		56729.3217	0.0013	HMB	V
DW Psc	56913.4989	0.0007	HMB	V		56729.4030	0.0009	HMB	V
	56913.5574	0.0006	HMB	V		56729.4838	0.0015	HMB	V
	56917.4953	0.0005	HO40	C	GSC 1716-1598	56264.3726	0.0014	PNQ	C
	56917.5546	0.0003	HO40	C		56904.4033	0.0014	AB	C
	56928.5296	0.0004	HO40	C	GSC 1750-1237	56917.4539	0.0012	AB	C
GW UMa	56702.4418	0.0009	MAV	V	GSC 2043-1201	56742.5398	0.0016	HMB	V
	56728.4505	0.0009	HMB	V		56742.6174	0.0014	HMB	V
	56767.4635	0.0009	HMB	V		56795.4565	0.0015	HMB	V
	56791.4399	0.0007	HMB	V		56795.5341	0.0021	HMB	V
YZ UMi	56711.5120	0.0011	IS	C	GSC 2080-0986	56746.5173	0.0007	HMB	V
	56711.6087	0.0008	IS	C		56792.5441	0.0006	HMB	V
	56722.3320	0.0005	VWS	V	GSC 2194-2001	56911.5199	0.0018	RP	V
	56722.4285	0.0004	VWS	V		56912.4405	0.0019	HMB	V
	56746.3884	0.0010	VWS	V	GSC 2290-1195	56912.4217	0.0013	AB	C
	56757.4025	0.0005	VWS	V		56958.2891	0.0050	MAV	V
	56797.4956	0.0015	IS	C		56958.3677	0.0031	MAV	V
	56810.4416	0.0011	IS	C		57011.2478	0.0012	ALI	V
	56810.5391	0.0020	IS	C	GSC 2496-0118	56711.3423	0.0006	FN	C
	56958.3536	0.0009	IS	C		56711.4100	0.0004	FN	C
	56958.4501	0.0005	IS	C		56730.3118	0.0014	HMB	V
	56958.5465	0.0005	IS	C		56730.3799	0.0016	HMB	V
	56961.4450	0.0006	VWS	V		56730.4477	0.0017	HMB	V
GSC 0191-1282	56660.4026	0.0004	AB	C		56746.3684	0.0007	HMB	V
	56660.4501	0.0003	AB	C		56746.4362	0.0007	HMB	V
	56660.4976	0.0003	AB	C		56757.3437	0.0023	HMB	V
	56660.5447	0.0006	AB	C		56757.4118	0.0024	HMB	V
	56700.5666	0.0005	HMBC	V		56757.4790	0.0017	HMB	V
	56700.6139	0.0005	HMBC	V		56764.3904	0.0017	HMB	V
	56700.6613	0.0007	HMBC	V		56764.4579	0.0013	HMB	V
	56700.7089	0.0004	HMBC	V	GSC 2566-1398	56690.6609	0.0009	IS	C
GSC 0321-0314	56738.6587	0.0005	IS	C		56690.7511	0.0006	IS	C
	56767.5300	0.0009	IS	C		56726.5812	0.0007	IS	C

Table 1: Observed times of maximum (continued).

Star	Epoch	Error	Obs.	Filter	Star	Epoch	Error	Obs.	Filter
GSC 2696-1396	56912.5217	0.0008	RP	V	GSC 3428-1497	56745.5290	0.0017	HO18	B
GSC 2843-1999	56938.3431	0.0011	MAV	V		56745.6051	0.0008	HO18	B
	56938.4053	0.0013	MAV	V		56746.3520	0.0008	HO18	B
	56940.3297	0.0017	MAVR	V		56746.4266	0.0018	HO18	B
	56940.3920	0.0014	MAVR	V		56746.5008	0.0008	HO18	B
	56942.3788	0.0010	AB	C		56746.5746	0.0030	HO18	B
GSC 2861-0970	56742.3120	0.0007	HMB	V		56750.3916	0.0024	HMB	V
	56949.3102	0.0004	MAV	V		56763.4149	0.0038	HMB	V
	56949.4200	0.0004	MAV	V		56763.4886	0.0022	HMB	V
	56949.5301	0.0004	MAV	V		56792.3841	0.0017	HMB	V
	56962.5226	0.0004	HMB	V		56792.4589	0.0019	HMB	V
	56962.6327	0.0004	HMB	V	GSC 3489-0868	56730.5108	0.0004	HMB	V
	56991.2601	0.0006	MAV	V		56730.5976	0.0006	HMB	V
	56991.3702	0.0006	MAV	V		56730.6841	0.0003	HMB	V
	56999.4081	0.0006	RP	V		56793.5048	0.0006	HMB	V
GSC 2977-0238	56014.3723	0.0008	PNQ	C		56793.5918	0.0005	HMB	V
	56014.4482	0.0004	PNQ	C	GSC 3755-0845	56669.4499	0.0010	RP	V
	56711.2900	0.0003	MAV	V		56669.5258	0.0017	RP	V
	56711.3658	0.0004	MAV	V		56968.3618	0.0008	MAVR	V
	56711.4417	0.0005	MAV	V		56968.4379	0.0011	MAVR	V
	56713.3402	0.0003	MAV	V		56997.4324	0.0015	RP	V
	56713.4160	0.0004	MAV	V		56997.5077	0.0012	RP	V
	56726.3240	0.0006	FN	C		56997.5845	0.0013	RP	V
	56726.3996	0.0003	FN	C		56997.6602	0.0013	RP	V
	56726.4755	0.0002	FN	C		57020.2595	0.0025	MAV	V
	56749.3325	0.0003	HMB	V	GSC 3810-1553	56690.4583	0.0004	MAV	V
	56749.4084	0.0004	HMB	V		56690.5290	0.0003	MAV	V
	56764.4434	0.0004	HMB	V		56696.3276	0.0005	MAV	V
	56972.6527	0.0008	LP11	V		56696.3982	0.0005	MAV	V
GSC 3004-0870	56691.3675	0.0014	MAV	V		56767.3926	0.0004	HMB	V
	56691.4494	0.0012	MAV	V		56767.4631	0.0004	HMB	V
	56691.5316	0.0012	MAV	V		56781.3934	0.0005	HMB	V
	56725.3813	0.0007	FN	C	GSC 3832-0152	56690.5568	0.0008	IS	V
	56725.4634	0.0006	FN	C		56725.4496	0.0004	RP	V
	56725.5455	0.0007	FN	C		56725.5409	0.0010	RP	V
	56725.6273	0.0008	FN	C		56725.6320	0.0004	IS	C
GSC 3031-0307	56709.6583	0.0020	RP	V		56725.6322	0.0006	RP	V
	56722.3449	0.0041	MAV	V		56725.7235	0.0013	RP	V
	56722.4445	0.0033	MAV	V		56764.5438	0.0005	IS	C
	56722.5418	0.0013	HO18	C	GSC 3863-0740	56726.3690	0.0013	MAV	V
GSC 3097-0583	56787.4183	0.0005	MAV	V		56746.3373	0.0019	MAV	V
	56794.4191	0.0008	MAV	V		56746.5352	0.0015	MAV	V
	56794.5032	0.0007	MAV	V		56795.5572	0.0056	RP	V
	56794.5875	0.0006	MAV	V	GSC 3934-1904	56797.3957	0.0008	MAV	V
	56796.5271	0.0004	HO40	C		56797.5052	0.0004	MAV	V
	56824.4448	0.0006	MAV	V	GSC 4163-0984	56693.3806	0.0004	MAV	V
	56824.5289	0.0005	MAV	V		56693.4602	0.0003	MAV	V
GSC 3428-1497	56728.3166	0.0025	HMB	V		56730.3346	0.0011	MAV	V
	56728.3898	0.0020	HMB	V		56747.4214	0.0005	RP	V
	56728.4664	0.0029	HMB	V		56747.5009	0.0003	RP	V
	56728.5417	0.0025	HMB	V		56747.5802	0.0003	RP	V
	56728.6139	0.0028	HMB	V	GSC 4417-0394	56713.5831	0.0007	IS	C
	56730.3350	0.0010	HO18	V		56713.7146	0.0006	IS	C
	56730.4088	0.0008	HO18	V		56727.3372	0.0016	MAV	V
	56730.4842	0.0009	HO18	V		56728.3947	0.0012	MAV	V
	56730.5581	0.0013	HO18	V		56729.3207	0.0010	MAV	V
	56745.4558	0.0012	HO18	V		56729.4527	0.0009	MAV	V

Table 1: Observed times of maximum (continued). The catalogue name USNO-A2.0 is abbreviates as U.

Star	Epoch	Error	Obs.	Filter	Star	Epoch	Error	Obs.	Filter
GSC 4417-0394	56753.3889	0.0012	MAV	V	GSC 4552-1498	56741.4090	0.0005	MAV	V
	56753.5207	0.0009	MAV	V		56741.4652	0.0003	MAV	V
GSC 4464-0924	56782.4017	0.0009	ALI	C		56749.6123	0.0002	IS	C
	56880.4504	0.0013	VWS	V		56749.6684	0.0002	IS	C
	56901.4138	0.0012	ALI	C		56757.4261	0.0002	ALI	C
	56912.3804	0.0007	VWS	V		56903.4282	0.0004	ALI	V
	56912.3807	0.0012	MAV	V		56958.6246	0.0003	IS	C
	56912.4602	0.0024	VWS	V		56958.6810	0.0002	IS	C
	56912.5419	0.0007	VWS	V		56968.2804	0.0005	ALI	V
	56961.3213	0.0019	ALI	C		56968.3362	0.0007	ALI	V
	56972.2888	0.0009	ALI	V	GSC 4556-1113	56669.3004	0.0003	VWS	V
	56972.2888	0.0008	VWS	V		56690.3685	0.0005	VWS	V
	56972.3699	0.0015	VWS	V		56690.4551	0.0003	VWS	V
	56972.4498	0.0009	VWS	V		56711.3497	0.0003	VWS	V
	56991.3166	0.0005	VWS	V		56711.4364	0.0003	VWS	V
	56991.3995	0.0008	VWS	V		56723.3514	0.0005	MAV	V
	56991.4776	0.0005	VWS	V		56723.4378	0.0004	MAV	V
	57011.3961	0.0010	VWS	V		56729.3952	0.0004	VWS	V
GSC 4500-0083	56628.4467	0.0024	PNQ	V		56794.4105	0.0003	VWS	V
	56628.5329	0.0023	PNQ	V		56794.4970	0.0004	VWS	V
	56733.3359	0.0017	VWS	V		56811.5069	0.0015	IS	C
	56853.5373	0.0025	MAV	V		56913.3918	0.0004	VWS	V
	56855.4940	0.0030	MAV	V		56958.2897	0.0004	VWS	V
	56886.3727	0.0019	MAVR	V		56958.3760	0.0004	VWS	V
	56913.3384	0.0018	MAV	V	GSC 4923-0693	56723.4130	0.0009	AB	C
	56913.4239	0.0024	MAV	V		56723.4795	0.0004	AB	C
	56913.5087	0.0022	MAV	V		56741.3804	0.0006	AB	C
GSC 4552-1498	56692.6857	0.0005	IS	V		57007.7773	0.0005	HMBC	V
	56692.7419	0.0007	IS	V	GSC 5018-1085	56736.6365	0.0009	IS	C
	56725.3351	0.0004	MAV	V		56736.7059	0.0006	IS	C
	56725.3909	0.0006	MAV	V	U 1425-04240809	56990.4183	0.0017	AB	C
	56725.4465	0.0005	MAV	V		57023.2611	0.0011	AB	C
	56741.3534	0.0004	MAV	V		57023.3182	0.0010	AB	C

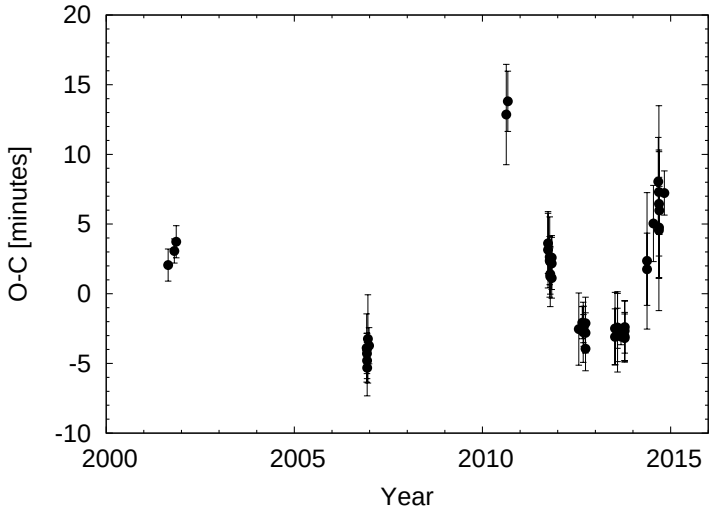

Figure 1. $O - C$ values for the maxima of KZ Lac with respect to the ephemeris of Table 3.

change. Changes in the light curve shape or amplitude have not been detected. The origin of the period changes is unknown at this time.

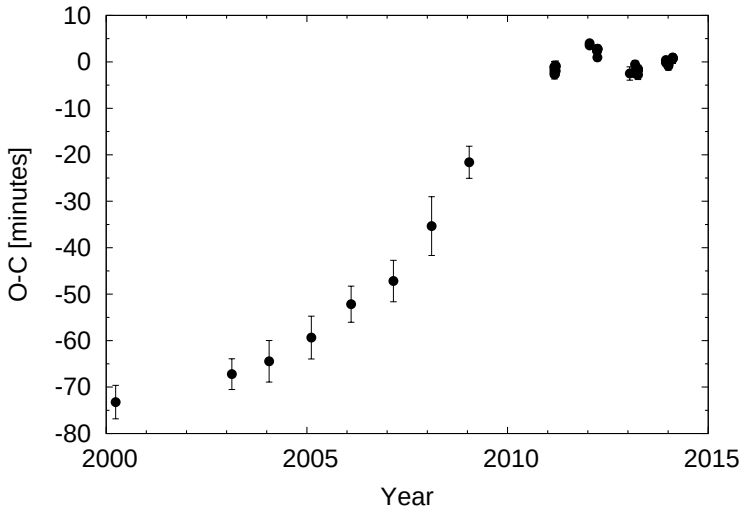

Figure 2. $O-C$ values for the maxima of GSC 0191-1282 with respect to the ephemeris of Table 3.

Of the HADS observed in 2014, two were found to be multiperiodic variables. GSC 3851-0240 was observed by AA, JGC, PL, PVC and RPB and turned out to be a double-mode pulsator with a frequency ratio of 0.774. Such a ratio is indicative of the fundamental to first overtone radial mode pulsation (Stellingwerf, 1979). Modulations in the light curve were already found by Hoffman and Monninger (2011). GSC 2610-0035 (= CSS_J173401.0+320716; discovered by Drake et al., 2014) was observed by JGC and RPB and showed at least one other pulsation frequency, likely a non-radial mode because of the unusual frequency ratio of 0.750. Table 4 lists details about the independent frequencies f_0, the fundamental radial mode, and the secondary frequency f_1 of both stars. The frequencies, amplitudes and phases, and their uncertainties were calculated using Period04 (Lenz & Breger, 2005). The uncertainties were derived using Monte Carlo simulations by Period04. For GSC 2610-0035 data from the Catalina Real-time Transient Survey (Drake et al., 2009) were used. A number of linear combinations of the independent frequencies were also detected in GSC 3851-0240. Our data for these two stars are available as electronic tables from the IBVS website.

The HADS GSC 4464-0924 was previously already found to have an additional non-radial mode (Wils et al., 2012). Updated frequencies for this star, based on all the data available, are given in Table 4. The amplitude of the secondary frequency in this star is relatively small compared to the amplitude of the radial mode. It is therefore still possible to calculate individual times of maxima for GSC 4464-0924 using our standard procedure. We can see the effect of the beat frequency $f_1 - f_0$ of about 6.14 cycles/day and with semi-amplitude of 1.6 ± 0.4 min on the $O-C$ diagram under the form of a larger than usual scatter in Fig. 3. Subtracting this beat signal from the original data shows a less-scattered $O-C$ diagram in which a period change (of the main period f_0) becomes much more evident (cf. Fig. 4). The observations of GSC 4464-0924 obtained by JVW are also available from the IBVS website.

Table 2: List of instruments used for the observations.

Code	Observer(s)	Telescope	Observatory	CCD
AA	AA	Catadioptric 30 cm	Perseus Observatory	SBIG ST-10XME
AB	AB	Catadioptric 35 cm	Carpe Noctem Observatory	SBIG ST-9E
ALI	FD+LL+SR+SV	Newton 68 cm	Astrolab Iris, Belgium	SBIG STL-6303E
FN	FN	Catadioptric 40 cm	Alkmaar, Nederland	SBIG ST-7XME
GCJ	GCJ	Catadioptric 20 cm	Observatorio Cerro del Viento, Badajoz, Spain	Atik 16HR
HMB	FJH	Catadioptric 28 cm	Mol, Belgium	SBIG ST-8XME
HMBC	FJH	Catadioptric 40 cm	Remote Observatory Atacama Desert, Chile	FLI ML16803
HO18	PL+PVC	Refractor 18 cm	ROB-Humain	SBIG ST-10XME, STL6303
HO40	PL+PVC	Newton 40 cm	ROB-Humain	SBIG ST-10XME
IS	IS	Catadioptric 25 cm	ABT Metius	SBIG ST402XME
KTU	TK	Newton 30 cm	Pieksämäki, Finland	Starlight XPress MX716
LP11	PL+PVC	Refractor 11 cm	Roque de los Muchachos Observatory, La Palma	SBIG ST-10XME
MAV	MV	Maksutov 26 cm	Leest Observatory	SBIG ST-10XME
MAVR	MV	Ritchey-Chrétien 40 cm	Leest Observatory	QSI583
PNQ	PNQ	Catadioptric 28 cm	Observatorio Posadas, Córdoba, Spain	Luna-QHY 9
RP	RDP	Catadioptric 36 cm	Shobdon, UK	Starlight XPress SXV-H9
SO30	CWR	Catadioptric 30 cm	SETEC Observatory	SBIG ST-8iXME
VWS	JVW	Catadioptric 23.5 cm	Hooglede, Belgium	SBIG ST-8XME

Table 3: Current linear elements for HADS that have shown period changes. Uncertainties are given in units of the last decimal. These elements are used to plot the $O-C$ diagrams in Figures 1 to 3.

Star	Max (HJD)	Period (d)
KZ Lac	2454075.5781(6)	0.10441606(3)
GSC 0191-1282	2455635.3714(3)	0.04741785(2)
GSC 4464-0924	2451342.8888(11)	0.08063078(2)

Table 4: Independent frequencies detected in multiperiodic HADS. Uncertainties are given in units of the last decimal. The phase is given with respect to HJD = 0. The period ratio f_1/f_0 is listed in the last column.

Star		Frequency c/d	Semi-Amplitude Mag.	Phase	Period ratio
GSC 3851-0240	f_0	14.718110(2)	0.1385(7)	0.2043(8)	
	f_1	19.01133(2)	0.0122(7)	0.413(9)	0.77418
GSC 2610-0035	f_0	12.206842(5)	0.059(2)	0.720(4)	
	f_1	16.25726(2)	0.012(2)	0.81(2)	0.75085
GSC 4464-0924	f_0	12.4022022(7)	0.1812(6)	0.5436(6)	
	f_1	18.54319(8)	0.0160(6)	0.284(6)	0.66883

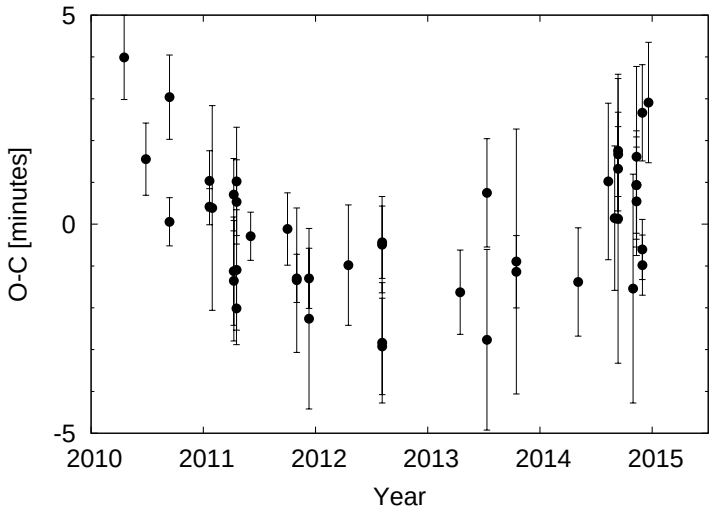

Figure 3. $O - C$ values for the maxima of GSC 4464-0924 with respect to the ephemeris in Table 3.

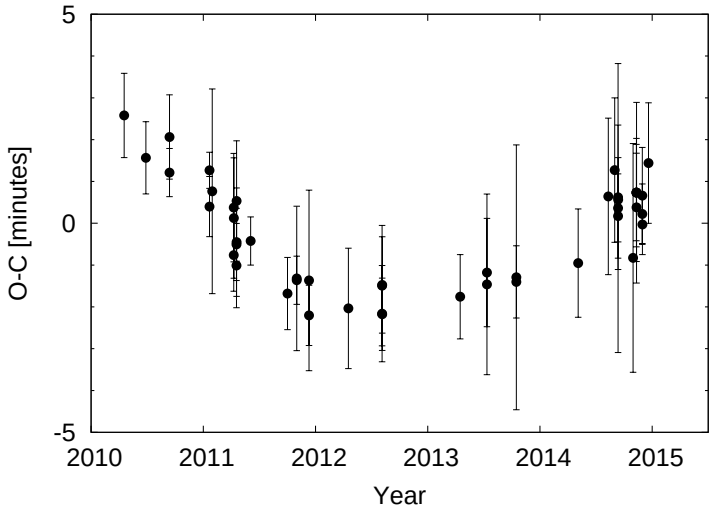

Figure 4. The same data as in Fig. 3, but in this case a sine wave with a frequency equal to the beat frequency and a semi-amplitude of 1.6 minutes has first been subtracted from the data.

Acknowledgements: This work has made use of the SIMBAD database, operated at CDS, Strasbourg, France. PL acknowledges support from the Royal Observatory of Belgium (ROB) for operating a small optical telescope at the radio-astronomy station of Humain under the project HOACS (HOACS stands for the Humain Optical Observatory for Astrophysics of Coeval Stars). The HOACS data were also acquired thanks to equipment financed by the Belgian National Lottery (1999). PVC is grateful for support from Baader Planetarium and Astrotechniek. IS and FN thank the Prins Bernhard Fonds for helping to fund the ABT Metius system. FN is grateful to the University of Amsterdam for providing a CCD camera with filter wheel. Part of the equipment used at SETEC Observatory was purchased with a grant from the American Astronomical Society.

References:

Drake A.J., Djorgovski S.G., Mahabal A., et al., 2009, *ApJ*, **696**, 870

Drake A.J., Graham M.J., Djorgovski S.G., et al., 2014, *ApJS*, **213**, 9

Hoffman D.I., Monninger G., 2011, *IBVS*, **5999**

Lenz P., Breger M., 2005, *CoAst*, **146**, 53

Pojmański G., 2002, *AcA*, **52**, 397

Stellingwerf, R.F., 1979, *ApJ*, **227**, 935

Wils P., Kleidis S., Hambsch F.-J., Vidal-Sáinz J., Vanleenhove M., Lampens P., Van Cauteren P., Robertson C.W., Staels B., Pickard R.D., Rozakis I., Dufoer S., Groenendaels R., Gómez-Forrellad J.M., García-Melendo E., Hautecler H., Van der Looy J., 2009, *IBVS*, **5878**

Wils P., Panagiotopoulos K., Van Wassenhove J., Ayiomamitis A., Nieuwenhout F., Robertson C.W., Vanleenhove M., Hambsch F.-J., Hautecler H., Pickard R.D., Baillien A., Staels B., Kleidis S., Lampens P., Van Cauteren P., 2012, *IBVS*, **6015**

Wils P., Ayiomamitis A., Robertson C.W., Hambsch F.-J., Vanleenhove M., Nieuwenhout F., van de Stadt I., Baillien A., Lampens P., Van Cauteren P., Van Wassenhove J., Pickard R.D., Kleidis S., Staels B., 2014, *IBVS*, **6122**

Woźniak P.R., Vestrand W.T., Akerlof C.W., et al., 2004, *AJ*, **127**, 2436

COMMISSIONS 27 AND 42 OF THE IAU
INFORMATION BULLETIN ON VARIABLE STARS

Number 6151

Konkoly Observatory
Budapest
27 October 2015

HU ISSN 0374 – 0676

THE 81ST NAME-LIST OF VARIABLE STARS. PART I — RA 00^h TO 17^{h}30^m

KAZAROVETS, E.V.[1]; SAMUS, N.N.[1,2]; DURLEVICH, O.V.[2]; KIREEVA, N.N.[1]; PASTUKHOVA, E.N.[1]

[1] Institute of Astronomy, Russian Academy of Sciences, 48, Pyatnitskaya Str., Moscow 119017, Russia
[helene@inasan.ru, samus@sai.msu.ru, kireeva@sai.msu.ru, pastukhova@sai.msu.ru]

[2] Sternberg Astronomical Institute, M.V. Lomonosov University of Moscow, 13, University Ave., Moscow 119992, Russia
[gcvs@sai.msu.ru]

Since 1946, the General Catalogue of Variable Stars (GCVS) has been a project of the International Astronomical Union performed by Moscow astronomers in the USSR Academy of Sciences (now in the Institute of Astronomy, Russian Academy of Sciences) and in M.V. Lomonosov University of Moscow (Sternberg Astronomical Institute). Till 2015, Commissions 27 (Variable Stars) and 42 (Close Binary Stars) were the bodies of the IAU supporting the project.

The recent re-organization of the IAU scientific bodies at the Hawaii IAU General Assembly (2015) created a new situation when there is no IAU body that would cover the whole topic of variable stars. The IBVS was also a bulletin published on behalf of the IAU Commissions 27 and 42 that exist no longer. Nevertheless, we continue our GCVS work: during the recent years, the variable-star community has repeatedly express its interest in official GCVS names for new variable stars. We work in a good contact with the International Register of Variable Stars (VSX) that is being compiled by the American Association of Variable Star Observers; in our opinion, the GCVS and VSX projects supplement each other quite well.

It is still unclear how the IAU will coordinate the variable-star projects in future. The Presidents of the IAU Division G "Stars and Stellar Systems" (C. Charbonnel) and Commission G4 "Pulsating Stars" (S. Jeffery), in their correspondence with the GCVS team, confirmed that their IAU bodies are interested in the GCVS project.

Because of its large volume, the 80th Name-List of Variable Stars (NL 80, Kazarovets et al., 2011ab, 2013) consists of three parts ordered (with the exception of several stars that got their designations quickly) by their right ascension (2000.0). Numerous new discoveries make it necessary for us to split also the present, 81th Name-List, this time in two parts. The division between the two parts was put at the right ascension of 17 hours 30 minutes (2000.0).

This publication, Part I of the 81st Name-List of Variable Stars, contains information on 1952 stars newly named in the system of the General Catalogue of Variable Stars (GCVS; Samus et al., 2015), 14 of them being extraordinary namings for Novae and

other unusual stars. The total number of named variable stars, not counting designated non-existing stars or stars subsequently identified with earlier-named variables, is now 49 763.

Like in the case of NL 80, we separate the catalogue of newly designated variables (to be presented at the GCVS web site) from the Name-List proper. Table 1 of the current Name-List contains the new GCVS name, equatorial coordinates (rounded to an accuracy sufficient for identification), and variability type for each star. The order of stars in Table 1 corresponds to the order of stars in the GCVS. The electronic version of the Name-List at http://www.sai.msu.su/gcvs/gcvs/nl81, to be presented in the nearest future, will additionally contain variability ranges, light elements, spectral types, identifications with astronomical catalogues, detailed remarks, bibliographic references for the newly named variable stars, accurate coordinates and proper motions (with references to corresponding positional catalogs or sources in the literature).

We continued naming Novae and variables of special interest upon requests from the IAU Bureau of Astronomical Telegrams and in other extraordinary cases requiring quick naming. Part I of the 81th Name-List contains fourteen such stars (twelve Novae, an FU Orionis star, and a possible symbiotic star). They are included in Table 1 and, besides, listed in Table 2 that contains, along with GCVS names, preliminary "constellation+year" designations for Novae. (Note that the ZAND: star V1534 Sco also has a preliminary Nova designation, N Sco 2014.) The GCVS names for thirteen of these stars (with the exception of V2944 Oph), with additional information concerning variability types, variation ranges, and references, were announced in Kazarovets and Samus (2015).

Finally, we would like to announce a correction to the NL 80, Part 3 (Kazarovets et al., 2013). In the list of variable stars detected in the WASP0 database, Kane et al. (2005) announced stars No. 18 and No. 36. Kazarovets et al. (2012) studied No. 18 using ROTSE-I/NSVS data and No. 36, using Catalina data. The stars got the GCVS designations V0504 Peg and V0503 Peg, respectively. Otero (2015) informed us that, as noted by Tamas Zalezsak, the two stars had virtually the same period; V0503 Peg is the real variable, and the "variability" of V0504 Peg is due to blending in the WASP0 and ROTSE-I/NSVS data. Thus, the EW type given in NL No. 80, Pt. 3 for V0503 Peg is correct, while the star at the coordinates of V0504 Peg does not vary (type CST).

This study was supported in part by Russian Foundation for Basic Research and by the Programme "Non-stationary Phenomena of Objects in the Universe" of the Presidium of Russian Academy of Sciences.

References:

Kane, S.R., Lister, T.A., Collier Cameron, A., et al. 2005, *MNRAS*, **362**, 117

Kazarovets, E.V., Pastukhova, E.N., Samus, N.N., Bogdanova, E.M. 2012, *Peremennye Zvezdy*, **32**, 4

Kazarovets, E.V. and Samus, N.N. 2015, *Peremennye Zvezdy*, **35**, 3

Kazarovets, E.V., Samus, N.N., Durlevich, O.V., Kireeva, N.N., Pastukhova, E.N. 2011a, *Inform. Bull. Var. Stars*, No. 5969

Kazarovets, E.V., Samus, N.N., Durlevich, O.V., Kireeva, N.N., Pastukhova, E.N. 2011b, *Inform. Bull. Var. Stars*, No. 6008

Kazarovets, E.V., Samus, N.N., Durlevich, O.V., Kireeva, N.N., Pastukhova, E.N. 2013, *Inform. Bull. Var. Stars*, No. 6052

Otero, S. 2015, Private communication

Samus, N.N., Durlevich, O.V., Kazarovets, E.V., Kireeva, N.N., Pastukhova, E.N., et al. 2015, *General Catalogue of Variable Stars* (GCVS database, version September 2015), Strasbourg Center of Astronomical Data: CDS B/gcvs, GCVS site: http://www.sai.msu.su/gcvs/gcvs

Table 1

Name	R.A., Decl., 2000.0	Type	Name	R.A., Decl., 2000.0	Type
	h m s o ' "			h m s o ' "	
V0716 And	00 10 46.2 +28 50 44	EW	V0367 Aps	14 12 48.3 -74 14 23	M
V0717 And	00 12 16.5 +31 22 33	EW	V0368 Aps	14 32 39.2 -73 46 34	EW
V0718 And	00 15 40.1 +23 28 28	SR	V0369 Aps	14 39 36.7 -73 59 43	EB
V0719 And	00 17 01.0 +33 57 23	RS	V0370 Aps	14 50 04.2 -71 11 37	RRC
V0720 And	00 18 50.3 +40 04 04	EB	V0371 Aps	15 19 43.4 -77 38 40	E
V0721 And	00 19 59.0 +40 32 31	EW	V0372 Aps	15 20 30.9 -78 40 15	RRC
V0722 And	00 27 22.8 +25 10 02	EW	V0373 Aps	16 12 57.0 -71 18 23	M
V0723 And	00 27 27.8 +36 50 08	EW	V0374 Aps	16 13 30.2 -70 38 46	M
V0724 And	00 32 43.8 +25 06 42	EW	V0375 Aps	16 14 40.1 -73 48 27	EW
V0725 And	00 36 35.7 +42 18 19	EA/RS	V0376 Aps	16 14 45.1 -70 23 10	EA:
V0726 And	00 36 54.1 +42 20 22	EW	V0377 Aps	16 14 46.0 -76 01 50	RS
V0727 And	00 42 53.7 +36 30 01	LB	V0378 Aps	16 18 20.8 -73 33 16	SRB
V0728 And	00 43 29.8 +42 13 54	EW	V0379 Aps	16 20 43.8 -71 39 38	EW
V0729 And	00 45 05.9 +36 43 35	SR	V0380 Aps	16 31 23.8 -71 34 46	LB
V0730 And	00 46 25.6 +41 07 14	UG:	V0381 Aps	16 45 23.6 -79 31 03	LB
V0731 And	00 48 16.6 +34 39 49	SRB	V0382 Aps	16 47 03.5 -71 59 22	M
V0732 And	00 49 20.2 +23 25 17	EW	V0383 Aps	17 01 43.9 -70 13 52	SR
V0733 And	00 51 23.0 +42 50 34	EW	V0384 Aps	17 18 47.6 -73 25 13	RS
V0734 And	00 54 45.4 +33 57 22	EB	V0385 Aps	17 23 29.6 -75 38 58	BY
V0735 And	00 56 17.2 +38 11 00	EA	V1830 Aql	19 02 33.4 +03 15 19	NA
V0736 And	00 57 30.9 +37 38 19	EW	V0916 Ara	16 35 54.3 -52 57 55	M
V0737 And	00 59 05.6 +34 00 01	LB	V0917 Ara	16 36 12.9 -55 39 40	LB
V0738 And	01 16 51.9 +35 00 40	EW	V0918 Ara	16 38 07.4 -59 44 38	LB
V0739 And	01 17 43.2 +36 48 42	SR	V0919 Ara	16 39 07.8 -58 21 25	RS
V0740 And	01 18 32.7 +44 37 02	LB	V0920 Ara	16 40 15.9 -48 18 28	LB
V0741 And	01 20 53.0 +43 38 57	EW	V0921 Ara	16 41 18.6 -47 40 48	EB
V0742 And	01 25 22.9 +44 48 47	LB	V0922 Ara	16 41 20.0 -47 39 39	DCEP
V0743 And	01 28 19.5 +34 08 29	EW	V0923 Ara	16 41 58.4 -57 43 56	M
V0744 And	01 29 40.1 +38 42 10	AM	V0924 Ara	16 42 14.3 -52 58 18	M
V0745 And	01 32 27.6 +41 36 34	EB	V0925 Ara	16 42 44.7 -54 07 11	M
V0746 And	01 33 21.1 +39 37 23	EA	V0926 Ara	16 44 36.3 -54 12 01	M
V0747 And	01 34 09.6 +42 02 29	EW	V0927 Ara	16 46 49.8 -56 03 38	M
V0748 And	01 37 28.1 +40 08 36	EW	V0928 Ara	16 48 55.1 -58 47 43	LB
V0749 And	01 41 53.8 +37 09 13	BY	V0929 Ara	16 50 56.2 -58 42 27	SRB
V0750 And	01 56 07.3 +44 01 18	EW	V0930 Ara	16 51 05.5 -58 50 44	SRA:
V0751 And	01 56 51.5 +44 05 36	EA	V0931 Ara	16 51 47.6 -54 56 24	SRA:
V0752 And	01 57 17.2 +37 40 52	EA	V0932 Ara	16 52 52.7 -51 23 29	M
V0753 And	01 57 18.9 +44 29 21	EA	V0933 Ara	16 53 35.4 -61 23 58	EB
V0754 And	01 58 26.7 +44 44 53	EW	V0934 Ara	16 54 13.4 -56 40 05	LB
V0755 And	02 05 12.7 +39 10 25	EW	V0935 Ara	16 54 47.5 -59 07 48	LB
V0756 And	02 12 02.2 +47 23 28	EW	V0936 Ara	16 56 09.9 -47 04 19	LB
V0757 And	02 12 13.8 +45 33 15	EW	V0937 Ara	16 57 05.4 -57 09 55	M:
V0758 And	02 22 20.5 +37 59 05	GDOR:	V0938 Ara	16 57 13.5 -58 04 06	LB
V0759 And	02 22 39.4 +50 18 59	LB	V0939 Ara	16 59 12.0 -55 00 16	SRA
V0760 And	02 30 50.1 +49 37 57	EW	V0940 Ara	16 59 18.1 -53 39 57	M
V0761 And	02 31 00.7 +48 49 35	LB	V0941 Ara	17 00 00.7 -56 40 09	EW
V0762 And	02 35 51.5 +49 18 02	LB	V0942 Ara	17 00 20.5 -52 02 45	M
CG Ant	09 31 49.3 -32 26 33	M:	V0943 Ara	17 01 01.4 -50 15 35	RCB:
CH Ant	09 46 23.3 -39 56 57	DSCT	V0944 Ara	17 02 41.2 -48 17 13	M
CI Ant	10 17 39.5 -34 51 53	EW	V0945 Ara	17 03 27.8 -54 52 24	LB
CK Ant	10 20 21.8 -36 12 13	RS	V0946 Ara	17 04 51.7 -60 57 06	M:
CL Ant	10 22 30.4 -39 50 14	RS	V0947 Ara	17 05 40.0 -51 43 19	M
CM Ant	10 32 10.2 -39 05 47	RS:	V0948 Ara	17 06 33.9 -57 42 52	SRD
CN Ant	10 32 45.9 -34 23 08	RRC	V0949 Ara	17 08 38.6 -62 16 38	M

Table 1 (continued)

Name	R.A., Decl., 2000.0 h m s o ' "	Type	Name	R.A., Decl., 2000.0 h m s o ' "	Type
V0950 Ara	17 10 05.2 -53 47 04	M	DI Ari	02 58 38.9 +29 44 04	EW
V0951 Ara	17 10 21.8 -55 53 53	SR	DK Ari	03 02 24.4 +30 04 30	EW
V0952 Ara	17 10 22.0 -54 15 05	DSCT	DL Ari	03 14 57.7 +19 48 49	EW
V0953 Ara	17 11 11.0 -57 49 29	M:	V0655 Aur	04 51 37.7 +44 23 37	LB
V0954 Ara	17 11 32.9 -60 14 37	SR	V0656 Aur	04 59 18.2 +45 13 20	EW
V0955 Ara	17 12 47.6 -47 39 14	M	V0657 Aur	05 00 05.3 +45 27 19	EW
V0956 Ara	17 12 59.3 -50 08 42	SRB	V0658 Aur	05 00 43.6 +45 10 57	EB
V0957 Ara	17 13 13.6 -47 38 29	M	V0659 Aur	05 01 13.3 +44 55 41	EW
V0958 Ara	17 13 55.7 -48 13 31	M	V0660 Aur	05 01 16.4 +45 20 46	EW
V0959 Ara	17 15 32.8 -55 54 23	SRB	V0661 Aur	05 01 17.4 +45 10 58	EB
V0960 Ara	17 17 47.9 -53 23 55	LB:	V0662 Aur	05 02 10.2 +45 14 18	EA
V0961 Ara	17 18 45.8 -57 46 30	EB	V0663 Aur	05 02 13.4 +44 52 47	EW
V0962 Ara	17 18 57.0 -48 09 32	M	V0664 Aur	05 02 15.9 +45 33 39	EA/RS:
V0963 Ara	17 18 59.3 -45 57 56	SR	V0665 Aur	05 02 22.1 +44 52 21	EB
V0964 Ara	17 21 01.0 -51 48 54	M	V0666 Aur	05 02 42.4 +35 57 45	EA
V0965 Ara	17 21 17.2 -63 26 05	M	V0667 Aur	05 02 57.2 +35 33 41	EA
V0966 Ara	17 22 15.4 -57 40 26	SRB	V0668 Aur	05 03 00.1 +35 55 56	EW
V0967 Ara	17 22 27.3 -60 14 55	EW	V0669 Aur	05 03 09.7 +36 19 31	BY
V0968 Ara	17 22 45.3 -61 20 29	LB	V0670 Aur	05 03 15.9 +35 56 27	EA
V0969 Ara	17 23 02.4 -50 10 07	M	V0671 Aur	05 03 16.9 +35 48 13	EW
V0970 Ara	17 23 23.9 -57 22 56	SRB	V0672 Aur	05 03 34.9 +36 17 41	EW
V0971 Ara	17 23 57.5 -49 29 28	SRA:	V0673 Aur	05 03 38.3 +35 34 04	EA
V0972 Ara	17 24 13.3 -64 01 51	M	V0674 Aur	05 03 38.8 +45 19 56	RRC:
V0973 Ara	17 24 19.4 -53 08 59	M	V0675 Aur	05 04 23.8 +35 40 00	EW
V0974 Ara	17 24 21.1 -59 23 43	SR	V0676 Aur	05 04 24.7 +35 54 02	BY:
V0975 Ara	17 24 37.2 -61 11 17	LB	V0677 Aur	05 04 25.4 +36 06 03	EB
V0976 Ara	17 25 49.0 -55 55 48	SRB	V0678 Aur	05 04 29.4 +36 21 37	EA/RS
V0977 Ara	17 25 57.6 -59 50 50	SR	V0679 Aur	05 04 30.9 +36 00 30	EA
V0978 Ara	17 26 07.6 -58 54 31	SRB	V0680 Aur	05 04 35.3 +36 13 15	EW
V0979 Ara	17 26 10.9 -61 43 24	SRB	V0681 Aur	05 04 51.3 +35 51 17	RRAB
V0980 Ara	17 26 35.4 -61 16 45	SR	V0682 Aur	05 05 02.6 +35 41 06	DSCTC
V0981 Ara	17 27 21.1 -53 05 49	RRAB	V0683 Aur	05 05 20.6 +35 36 01	EB
V0982 Ara	17 27 54.6 -58 39 55	SR	V0684 Aur	05 05 30.5 +36 15 56	EW
V0983 Ara	17 28 43.3 -48 54 59	SR	V0685 Aur	05 05 50.6 +36 11 45	EW
V0984 Ara	17 29 51.0 -51 53 45	SRB	V0686 Aur	05 05 51.9 +36 17 54	ELL:
CM Ari	01 49 27.9 +17 50 32	EW	V0687 Aur	05 05 54.9 +35 43 31	EB
CN Ari	01 54 19.7 +21 53 21	SRS:	V0688 Aur	05 06 03.6 +36 20 05	BY:
CO Ari	02 01 45.8 +20 38 44	EW	V0689 Aur	05 06 14.9 +36 10 26	RRC
CP Ari	02 03 52.7 +18 21 12	EW	V0690 Aur	05 06 26.8 +35 31 05	EW
CQ Ari	02 05 34.8 +14 46 30	EW	V0691 Aur	05 06 29.4 +35 51 07	BY
CR Ari	02 06 17.2 +14 52 13	DSCTC:	V0692 Aur	05 06 49.1 +35 42 28	BY
CS Ari	02 06 27.3 +11 12 46	SRB	V0693 Aur	05 06 51.4 +35 46 35	EW
CT Ari	02 07 30.2 +14 56 23	EW	V0694 Aur	05 10 24.2 +35 45 36	EA
CU Ari	02 14 08.7 +26 31 29	RRAB	V0695 Aur	05 12 19.0 +33 25 50	EW
CV Ari	02 14 21.4 +18 52 25	EW	V0696 Aur	05 12 26.7 +33 39 11	EA
CW Ari	02 19 35.2 +18 56 30	EB	V0697 Aur	05 12 46.9 +29 39 00	EB
CX Ari	02 25 50.6 +26 33 14	EB	V0698 Aur	05 12 50.6 +33 36 37	EA
CY Ari	02 26 01.4 +22 26 45	EW	V0699 Aur	05 13 23.9 +33 35 36	EA
CZ Ari	02 34 20.5 +14 55 20	EW	V0700 Aur	05 14 39.0 +39 14 49	EA
DD Ari	02 38 08.8 +16 59 30	EB:	V0701 Aur	05 14 44.2 +39 22 42	EW
DE Ari	02 50 58.2 +29 09 58	EW	V0702 Aur	05 14 51.1 +39 13 09	EW
DF Ari	02 51 39.4 +19 10 54	EW	V0703 Aur	05 15 00.7 +38 58 58	EW
DG Ari	02 55 21.1 +15 39 23	RS	V0704 Aur	05 15 03.9 +39 18 47	EA
DH Ari	02 58 16.2 +29 43 59	EW	V0705 Aur	05 15 20.2 +39 29 44	RS:

Table 1 (continued)

Name	R.A., Decl., 2000.0 h m s o ' "	Type	Name	R.A., Decl., 2000.0 h m s o ' "	Type
V0706 Aur	05 15 22.1 +39 20 32	EW	V0760 Aur	05 59 06.4 +35 20 28	EA
V0707 Aur	05 15 58.5 +39 10 58	EB	V0761 Aur	05 59 16.5 +51 34 45	EW
V0708 Aur	05 16 09.2 +38 40 56	EW	V0762 Aur	05 59 17.7 +34 37 16	EW
V0709 Aur	05 16 11.9 +39 03 52	EA	V0763 Aur	05 59 19.8 +34 48 11	EA
V0710 Aur	05 16 18.7 +38 55 11	DSCTC	V0764 Aur	05 59 28.6 +35 09 45	EA
V0711 Aur	05 16 22.2 +38 50 55	BY:	V0765 Aur	05 59 59.3 +29 26 43	EA
V0712 Aur	05 16 23.6 +39 04 46	BY:	V0766 Aur	06 00 10.2 +29 07 12	EW
V0713 Aur	05 16 29.8 +38 41 25	EW	V0767 Aur	06 00 12.6 +34 37 31	BY:
V0714 Aur	05 16 30.6 +30 13 31	EW	V0768 Aur	06 00 23.5 +42 16 54	RS
V0715 Aur	05 16 45.7 +39 16 25	EW	V0769 Aur	06 00 51.1 +39 43 14	CEP
V0716 Aur	05 17 04.8 +39 04 21	EA	V0770 Aur	06 01 03.7 +34 34 35	EW
V0717 Aur	05 17 16.7 +38 49 05	EW	V0771 Aur	06 01 05.9 +35 20 07	EB
V0718 Aur	05 17 17.2 +39 08 42	EA	V0772 Aur	06 01 06.8 +28 58 21	EW
V0719 Aur	05 17 17.9 +39 14 53	BY:	V0773 Aur	06 01 22.3 +29 33 21	EB
V0720 Aur	05 17 42.0 +39 06 34	EA	V0774 Aur	06 01 24.8 +29 21 21	EB:
V0721 Aur	05 17 51.3 +38 46 29	BY:	V0775 Aur	06 01 26.8 +28 11 36	EW
V0722 Aur	05 17 55.0 +38 44 06	SR:	V0776 Aur	06 01 29.3 +29 27 46	DSCTC
V0723 Aur	05 17 57.9 +39 15 13	EW	V0777 Aur	06 01 34.5 +34 37 39	SR:
V0724 Aur	05 18 38.0 +38 41 51	EA	V0778 Aur	06 01 38.3 +28 14 54	EA
V0725 Aur	05 21 51.4 +28 38 42	EW	V0779 Aur	06 01 54.3 +35 06 52	SR:
V0726 Aur	05 22 45.7 +29 07 05	EW	V0780 Aur	06 02 02.4 +28 14 51	LB
V0727 Aur	05 27 11.4 +35 15 09	EB	V0781 Aur	06 02 19.6 +28 57 48	BY:
V0728 Aur	05 30 54.8 +35 56 32	SR:	V0782 Aur	06 02 29.5 +29 31 34	EA
V0729 Aur	05 30 56.5 +36 52 20	SR	V0783 Aur	06 02 46.3 +30 12 01	EW
V0730 Aur	05 31 17.7 +32 11 03	LB	V0784 Aur	06 02 52.8 +28 25 13	EW
V0731 Aur	05 39 08.5 +39 17 13	EB	V0785 Aur	06 03 03.0 +29 35 28	EA:
V0732 Aur	05 42 35.6 +31 13 15	EA	V0786 Aur	06 03 06.2 +30 01 03	LB
V0733 Aur	05 43 50.6 +38 42 07	SR	V0787 Aur	06 03 16.4 +30 09 17	LB
V0734 Aur	05 44 05.8 +31 06 44	DSCT	V0788 Aur	06 03 19.7 +28 09 24	EW
V0735 Aur	05 45 01.9 +38 39 40	LB	V0789 Aur	06 03 21.2 +30 10 05	EB
V0736 Aur	05 45 10.6 +38 22 23	LB	V0790 Aur	06 03 21.5 +30 18 16	DSCTC:
V0737 Aur	05 47 35.1 +53 21 06	LB	V0791 Aur	06 03 23.5 +28 45 15	BY:
V0738 Aur	05 48 09.5 +38 08 35	SR:	V0792 Aur	06 03 26.0 +29 06 02	DSCT
V0739 Aur	05 54 16.6 +53 37 25	SR	V0793 Aur	06 03 33.4 +39 19 38	EW
V0740 Aur	05 54 38.4 +30 04 24	EB	V0794 Aur	06 03 37.9 +38 14 30	LB
V0741 Aur	05 55 23.2 +30 05 27	DSCTC	V0795 Aur	06 03 38.1 +28 19 59	EW
V0742 Aur	05 55 44.4 +29 12 49	EW:	V0796 Aur	06 03 57.6 +28 49 37	EW
V0743 Aur	05 55 57.9 +28 50 33	DSCT	V0797 Aur	06 04 00.5 +30 07 45	BY:
V0744 Aur	05 56 24.3 +30 03 57	EW	V0798 Aur	06 04 26.3 +28 57 44	EW
V0745 Aur	05 56 46.1 +29 49 25	EB	V0799 Aur	06 05 01.9 +55 09 52	DSCT
V0746 Aur	05 56 57.5 +29 47 07	DSCTC	V0800 Aur	06 09 54.2 +44 36 02	RRC
V0747 Aur	05 56 58.8 +28 41 08	EW	V0801 Aur	06 10 16.3 +40 11 05	EB
V0748 Aur	05 57 13.2 +53 35 50	SRB	V0802 Aur	06 11 32.6 +32 09 21	BY
V0749 Aur	05 57 22.8 +28 44 44	EB	V0803 Aur	06 12 13.9 +31 48 24	DSCT:
V0750 Aur	05 57 35.3 +51 38 17	DSCT	V0804 Aur	06 26 06.6 +27 55 58	EW
V0751 Aur	05 57 40.0 +29 22 50	EW	V0805 Aur	06 27 03.8 +39 52 49	UGSU
V0752 Aur	05 58 10.7 +51 33 36	EW	V0806 Aur	06 31 09.3 +29 45 20	EA
V0753 Aur	05 58 11.9 +34 53 12	EB	V0807 Aur	06 39 48.8 +46 57 15	DSCT
V0754 Aur	05 58 18.5 +34 54 08	EW	V0808 Aur	07 11 26.0 +44 04 05	AM+EA
V0755 Aur	05 58 20.2 +28 56 01	LB	V0809 Aur	07 11 49.5 +42 47 22	EW
V0756 Aur	05 58 21.0 +28 45 50	LB:	V0810 Aur	07 14 56.5 +43 29 04	EA
V0757 Aur	05 58 48.6 +35 07 28	EW	V0811 Aur	07 17 52.0 +40 58 27	ELL
V0758 Aur	05 58 49.5 +28 40 19	DSCTC	V0812 Aur	07 18 11.5 +44 06 48	EB
V0759 Aur	05 59 04.0 +30 09 05	LB	V0813 Aur	07 19 48.9 +40 53 32	UG

Table 1 (continued)

Name	R.A., Decl., 2000.0	Type	Name	R.A., Decl., 2000.0	Type
	h m s o ' "			h m s o ' "	
V0814 Aur	07 22 29.9 +41 03 17	EW	V0430 CMa	06 39 35.6 -15 59 48	EW
V0815 Aur	07 23 12.6 +42 33 37	EB	V0431 CMa	06 48 19.1 -15 06 10	EA
V0816 Aur	07 23 33.6 +40 58 33	EW	V0432 CMa	06 50 10.1 -13 52 45	EA
V0817 Aur	07 26 31.5 +40 24 35	EA	V0433 CMa	06 51 20.2 -11 13 45	EW
V0818 Aur	07 26 32.8 +40 51 33	EW	V0434 CMa	07 13 42.4 -17 37 13	DCEP
V0819 Aur	07 26 33.6 +40 32 23	EA	ES CMi	07 08 39.7 +12 14 43	EW
V0820 Aur	07 28 19.7 +41 13 58	EW	ET CMi	07 09 20.8 +12 12 14	EW
V0821 Aur	07 29 28.5 +40 15 11	BY:	EU CMi	07 12 14.1 +08 40 10	EW
V0822 Aur	07 30 08.3 +42 44 12	EA	EV CMi	07 13 10.9 +02 24 26	EW:
V0823 Aur	07 30 09.3 +40 29 17	EW:	EW CMi	07 17 35.5 +07 04 12	EW
V0824 Aur	07 30 13.5 +41 47 13	EW	EX CMi	07 24 21.5 +11 27 43	EW
V0825 Aur	07 30 16.1 +40 57 30	EA	EY CMi	07 26 03.3 +08 36 47	EW
V0341 Boo	13 52 57.0 +16 51 15	EW	EZ CMi	07 26 18.1 +08 37 59	EW
V0342 Boo	13 59 53.5 +17 53 57	EW	FF CMi	07 26 59.3 +08 38 41	EW
V0343 Boo	14 03 31.4 +08 30 43	RRC	FG CMi	07 27 43.8 +08 18 04	EA
V0344 Boo	14 03 45.0 +28 27 02	RRAB	FH CMi	07 29 02.7 +08 19 40	EW
V0345 Boo	14 04 10.5 +28 19 38	EB	FI CMi	07 36 00.5 +03 16 48	BY
V0346 Boo	14 04 18.0 +28 24 03	EW	FK CMi	07 36 41.9 +03 54 20	RS
V0347 Boo	14 06 02.9 +28 11 41	EA	FL CMi	07 48 55.8 +03 24 10	RS
V0348 Boo	14 06 32.0 +52 36 11	RRC	FM CMi	07 55 30.0 +01 25 02	EB
V0349 Boo	14 06 57.5 +20 56 25	RRAB	GP CVn	12 27 40.7 +51 39 25	UGSU+EA
V0350 Boo	14 08 30.5 +31 17 00	LB	GQ CVn	12 43 12.1 +43 32 00	UGSU
V0351 Boo	14 09 25.5 +51 26 54	BY	GR CVn	12 43 22.8 +34 57 17	RR(B)
V0352 Boo	14 10 22.3 +25 44 33	RRC	GS CVn	13 05 08.4 +39 15 33	RRC
V0353 Boo	14 11 51.6 +45 31 08	ELL	GT CVn	13 30 03.2 +43 30 13	DSCT
V0354 Boo	14 13 40.6 +32 56 48	EW	GU CVn	13 33 21.0 +50 31 04	EA/RS
V0355 Boo	14 15 09.3 +33 52 22	EB	GV CVn	13 48 10.3 +43 15 47	SRD:
V0356 Boo	14 20 44.3 +11 21 07	EW	GW CVn	13 48 17.9 +44 30 17	SR
V0357 Boo	14 24 06.2 +48 51 16	EW	GX CVn	13 49 08.8 +44 16 06	SR
V0358 Boo	14 25 55.9 +14 12 10	BY	GY CVn	13 50 13.0 +47 40 42	SR
V0359 Boo	14 26 09.4 +46 16 07	RS	GZ CVn	13 58 23.9 +46 51 02	E:
V0360 Boo	14 27 17.7 +24 31 56	RRC	HH CVn	13 58 27.0 +43 48 20	SR
V0361 Boo	14 29 10.1 +41 07 04	EW	HI CVn	14 02 27.0 +34 17 45	RRAB
V0362 Boo	14 31 08.0 +24 39 23	SR	SZ Cae	04 29 52.4 -39 20 05	RRC
V0363 Boo	14 32 13.1 +45 36 29	BY	TT Cae	04 42 55.9 -31 31 19	RRAB
V0364 Boo	14 33 03.4 +40 28 46	EW	TU Cae	04 43 14.9 -41 06 19	RS
V0365 Boo	14 36 31.7 +38 43 35	EB	TV Cae	04 43 57.9 -37 56 09	RRC
V0366 Boo	14 36 39.8 +12 10 33	RRAB	TW Cae	04 53 19.3 -31 31 57	RRAB
V0367 Boo	14 39 01.4 +45 48 42	EW	TX Cae	04 53 38.1 -29 06 37	EW
V0368 Boo	14 41 54.9 +53 56 48	RRAB	V0520 Cam	03 15 53.3 +57 34 26	EW
V0369 Boo	14 43 39.1 +53 47 37	EW	V0521 Cam	03 17 05.9 +57 46 57	EW
V0370 Boo	14 47 25.3 +22 50 12	EW	V0522 Cam	03 17 26.6 +57 38 01	EW
V0371 Boo	14 49 22.2 +09 48 40	RRAB	V0523 Cam	03 19 42.4 +57 04 50	EB
V0372 Boo	14 54 04.2 +20 43 06	EW	V0524 Cam	03 19 59.8 +57 19 10	EA/RS
V0373 Boo	14 55 41.5 +15 49 03	EW	V0525 Cam	03 20 05.0 +57 07 32	EA/RS
V0374 Boo	15 00 06.4 +12 48 48	RRAB	V0526 Cam	03 20 23.6 +57 06 45	EA
V0375 Boo	15 08 05.7 +46 10 30	EW	V0527 Cam	03 23 12.1 +60 54 45	LB
V0376 Boo	15 17 24.3 +35 03 56	EW	V0528 Cam	03 44 50.8 +68 37 53	UG:
V0377 Boo	15 22 21.5 +32 58 45	DSCT	V0529 Cam	03 47 35.6 +75 57 29	EW
V0378 Boo	15 30 57.5 +47 03 38	EA	V0530 Cam	03 49 13.0 +74 36 50	EW
V0379 Boo	15 41 49.0 +44 46 41	SR	V0531 Cam	03 49 36.7 +78 06 34	EW
V0380 Boo	15 46 52.0 +51 52 39	EA	V0532 Cam	03 51 21.8 +74 39 23	RRC
V0428 CMa	06 34 36.4 -21 33 05	RS:	V0533 Cam	03 56 32.3 +55 14 53	SR
V0429 CMa	06 38 47.6 -31 07 56	EW	V0534 Cam	03 56 52.8 +53 16 41	EA

Table 1 (continued)

Name	R.A., Decl., 2000.0	Type	Name	R.A., Decl., 2000.0	Type
	h m s o ' "			h m s o ' "	
V0535 Cam	04 02 30.7 +52 51 18	EB	V0851 Car	09 55 15.1 -62 03 32	BY:
V0536 Cam	04 03 43.5 +53 19 12	LB	V0852 Car	10 02 31.2 -62 03 29	RS
V0537 Cam	04 07 54.5 +74 28 19	EW	V0853 Car	10 03 55.8 -70 53 54	RS
V0538 Cam	04 18 59.8 +77 38 49	EW	V0854 Car	10 10 36.8 -58 17 47	DCEP
V0539 Cam	04 34 46.3 +66 59 46	SR	V0855 Car	10 19 53.7 -59 01 06	SR:
V0540 Cam	04 38 31.0 +67 06 42	SR	V0856 Car	10 29 57.3 -69 51 17	M
V0541 Cam	04 49 13.4 +79 00 25	SR	V0857 Car	10 30 44.3 -69 00 33	SR
V0542 Cam	04 53 46.5 +68 28 26	DSCT	V0858 Car	10 32 00.9 -58 16 02	EA
V0543 Cam	05 09 53.2 +72 49 12	LB	V0859 Car	10 48 41.7 -64 09 51	SR:
V0544 Cam	05 13 03.3 +75 46 44	BY	V0860 Car	10 57 17.1 -62 20 32	M
V0545 Cam	05 23 28.8 +69 04 58	BY:	V0861 Car	11 05 11.5 -61 44 57	EA
V0546 Cam	05 24 36.1 +68 44 02	EW	V0862 Car	11 05 23.7 -61 08 22	RS
V0547 Cam	05 25 43.7 +72 28 40	EA	V0863 Car	11 05 24.4 -61 06 03	RS
V0548 Cam	05 27 43.2 +65 59 15	BY	V0864 Car	11 05 26.7 -61 48 37	EW
V0549 Cam	05 28 08.0 +72 56 06	EW	V0865 Car	11 05 50.0 -61 31 52	EA
V0550 Cam	05 28 25.5 +73 21 14	EW	V0866 Car	11 05 53.6 -61 06 06	RS
V0551 Cam	05 30 44.4 +72 51 14	EA	V0867 Car	11 05 55.5 -60 58 47	EB/RS
V0552 Cam	05 33 00.1 +73 27 26	EW	V0868 Car	11 05 59.0 -61 22 54	EW
V0553 Cam	05 34 44.5 +73 40 06	EW	V0869 Car	11 05 59.2 -61 50 59	EA
V0554 Cam	05 34 55.0 +71 01 09	SR	V0870 Car	11 06 27.6 -61 13 44	EB
V0555 Cam	05 35 14.6 +73 31 24	EW	V0871 Car	11 06 29.0 -61 10 39	EA
V0556 Cam	05 49 50.4 +58 42 08	EW	V0872 Car	11 06 35.6 -61 40 12	EA
V0557 Cam	05 51 04.5 +69 18 14	EW	V0873 Car	11 06 44.8 -61 27 25	EA
V0558 Cam	05 53 22.5 +57 17 35	EW	V0874 Car	11 06 51.2 -61 14 07	EA
V0559 Cam	06 07 55.3 +69 56 01	LB	V0875 Car	11 07 04.0 -61 26 45	EA
V0560 Cam	06 10 09.3 +69 59 27	EB	V0876 Car	11 07 11.5 -61 31 23	EA
V0561 Cam	06 10 33.7 +68 56 17	SR	V0877 Car	11 07 16.0 -61 52 00	EW
V0562 Cam	06 11 32.1 +81 52 55	EW	V0878 Car	11 07 31.9 -61 26 38	EW
V0563 Cam	06 28 02.2 +76 55 30	SR	V0879 Car	11 07 46.9 -61 08 15	EA
V0564 Cam	06 28 23.7 +72 57 16	LB	V0880 Car	11 07 57.2 -61 03 52	EW
V0565 Cam	06 34 05.6 +76 31 33	EW	V0881 Car	11 07 59.0 -61 34 03	EA
V0566 Cam	06 53 57.8 +83 16 03	SR	V0882 Car	11 08 03.1 -61 45 59	EA
V0567 Cam	06 57 31.3 +72 49 48	E:	V0883 Car	11 08 04.5 -61 43 29	EA
V0568 Cam	07 09 22.2 +75 47 16	EW:	V0884 Car	11 08 05.6 -61 47 08	EA
V0569 Cam	07 30 27.2 +77 44 36	EW	V0885 Car	11 08 31.2 -61 34 18	EA
V0570 Cam	08 02 57.3 +78 34 48	EB	V0886 Car	11 08 37.8 -61 46 29	EA
V0571 Cam	09 34 22.8 +82 21 39	SRD:	V0887 Car	11 08 41.8 -60 57 30	EA
V0572 Cam	12 03 17.3 +80 33 43	DSCT	V0888 Car	11 08 42.6 -61 28 40	EA
V0835 Car	07 05 12.3 -57 34 14	RS	V0889 Car	11 08 48.4 -61 40 07	EA
V0836 Car	07 08 54.2 -50 57 49	RS	V0890 Car	11 08 50.9 -61 43 35	EA
V0837 Car	07 12 25.0 -53 56 42	RS	V0891 Car	11 08 51.4 -61 31 45	EA
V0838 Car	07 43 42.9 -61 07 17	BY	V0892 Car	11 09 13.3 -61 07 29	EW
V0839 Car	07 58 57.4 -55 06 56	EA	V0893 Car	11 09 26.8 -60 49 29	ELL:
V0840 Car	08 02 48.9 -59 13 28	BY	V0894 Car	11 09 28.1 -60 27 47	EW
V0841 Car	08 39 11.6 -58 34 28	RS	V0895 Car	11 09 30.8 -60 43 02	EA
V0842 Car	08 42 00.5 -62 18 26	RS	V0896 Car	11 09 36.6 -60 51 59	EA
V0843 Car	08 45 08.3 -55 58 04	RS	V0897 Car	11 09 46.3 -60 30 12	EB
V0844 Car	08 49 41.3 -60 15 18	EB	V0898 Car	11 09 47.6 -61 01 17	EA
V0845 Car	09 12 47.3 -58 39 17	RS	V0899 Car	11 09 52.2 -60 57 57	DSCT
V0846 Car	09 14 55.6 -64 01 33	DSCT	V0900 Car	11 10 36.3 -61 19 57	EA
V0847 Car	09 18 14.8 -57 22 17	M	V0901 Car	11 10 41.7 -61 09 00	EA
V0848 Car	09 46 56.7 -70 22 32	M	V0902 Car	11 10 43.3 -60 40 08	EA
V0849 Car	09 47 03.8 -65 35 05	BY	V0903 Car	11 10 51.9 -58 51 46	M
V0850 Car	09 48 19.9 -57 48 38	DCEP	V0904 Car	11 11 28.5 -63 00 24	M

Table 1 (continued)

Name	R.A., Decl., 2000.0 h m s o ' "	Type	Name	R.A., Decl., 2000.0 h m s o ' "	Type
V0905 Car	11 20 26.5 -58 34 02	RS	V1383 Cen	12 47 55.7 -44 57 35	RS
V1245 Cas	00 01 21.5 +51 12 14	M	V1384 Cen	13 14 00.2 -62 29 54	DCEP
V1246 Cas	00 01 29.2 +64 23 17	LB	V1385 Cen	13 14 19.8 -46 38 04	M
V1247 Cas	00 05 07.6 +50 49 05	EA	V1386 Cen	13 15 16.7 -50 58 07	RS
V1248 Cas	00 11 29.0 +60 04 02	EB	V1387 Cen	13 27 50.3 -47 54 23	SRD
V1249 Cas	00 15 10.6 +60 21 21	DSCT:	V1388 Cen	13 29 18.6 -47 22 51	RS
V1250 Cas	00 15 21.0 +53 42 50	EW	V1389 Cen	13 34 31.9 -42 09 31	RS:
V1251 Cas	00 16 02.5 +53 54 20	EA	V1390 Cen	13 43 31.1 -35 20 25	RS
V1252 Cas	00 17 30.2 +55 11 15	EB	V1391 Cen	13 48 09.7 -49 05 57	M
V1253 Cas	00 19 29.8 +53 39 58	EW	V1392 Cen	13 53 14.3 -37 23 14	EB
V1254 Cas	00 21 58.8 +59 13 27	EW	V1369 Cen	13 54 45.4 -59 09 04	NA
V1255 Cas	00 24 30.5 +61 05 15	EW:	V1393 Cen	13 57 15.6 -52 55 23	DSCT
V1256 Cas	00 28 35.0 +68 15 19	LB	V1394 Cen	13 57 22.0 -63 19 06	EA
V1257 Cas	00 30 24.4 +69 47 39	LB	V1395 Cen	13 57 30.5 -35 53 56	M
V1258 Cas	00 38 10.2 +67 32 38	LB	V1396 Cen	13 57 54.9 -63 05 47	EA
V1259 Cas	00 39 21.5 +68 16 26	SR	V1397 Cen	13 58 12.7 -42 15 10	RRAB
V1260 Cas	00 47 52.3 +67 21 10	LB	V1398 Cen	13 59 26.8 -62 50 24	EA
V1261 Cas	00 48 03.7 +60 51 30	EW	V1399 Cen	14 06 13.8 -49 36 32	M
V1262 Cas	00 49 53.9 +71 23 05	SR	V1400 Cen	14 07 47.9 -39 45 43	E:/RS
V1263 Cas	00 50 56.4 +71 39 39	SR:	V1401 Cen	14 12 46.9 -38 31 22	BY
V1264 Cas	00 51 18.5 +50 22 58	EW	V1402 Cen	14 32 08.3 -63 42 15	RS
V1265 Cas	00 52 49.8 +57 24 24	LB	V1403 Cen	14 38 48.3 -36 46 43	RRAB
V1266 Cas	00 55 28.6 +70 00 54	SR	V0963 Cep	00 02 55.6 +70 34 42	LB
V1267 Cas	00 58 26.8 +68 29 06	SR	V0964 Cep	00 06 23.3 +69 48 26	EA/RS
V1268 Cas	00 58 37.6 +66 34 56	EW	V0965 Cep	00 09 49.4 +80 21 41	DSCT
V1269 Cas	01 00 05.5 +67 37 23	LB	V0966 Cep	00 13 46.5 +68 17 30	SR:
V1270 Cas	01 01 05.0 +67 03 20	LB	V0967 Cep	00 49 44.7 +77 53 35	EB
V1271 Cas	01 01 54.3 +67 08 49	EA	V0968 Cep	02 45 36.3 +79 13 35	EW
V1272 Cas	01 01 56.3 +66 19 37	EW	V0969 Cep	04 42 13.1 +82 06 08	RS
V1273 Cas	01 05 53.4 +53 56 06	EA	V0962 Cep	20 54 23.8 +60 17 07	NA
V1274 Cas	01 10 05.2 +61 24 31	EW	HX Cet	00 05 13.8 -07 32 36	EW
V1275 Cas	01 11 08.9 +61 07 45	EW	HY Cet	00 28 21.4 -14 53 17	EW
V1276 Cas	01 22 26.4 +59 12 36	RRC	HZ Cet	00 35 13.5 -04 15 01	RRC
V1277 Cas	01 31 57.9 +59 30 14	DSCTC	II Cet	00 41 45.8 -03 00 28	RRC
V1278 Cas	01 32 01.9 +59 29 13	EA	IK Cet	00 55 29.6 -11 06 35	EW
V1279 Cas	01 32 02.8 +59 27 52	EA	IL Cet	00 57 11.8 -19 35 51	RRAB
V1280 Cas	01 32 09.7 +59 28 01	DSCTC	IM Cet	01 01 45.3 -12 08 03	RS
V1281 Cas	01 48 50.4 +67 57 44	SR:	IN Cet	01 04 25.2 -00 30 41	EW
V1282 Cas	02 35 29.3 +57 44 56	DSCT	IO Cet	01 34 16.3 -07 24 38	EW
V1283 Cas	03 07 55.7 +60 31 25	EW	IP Cet	01 36 29.4 +01 50 20	EW
V1284 Cas	03 15 05.4 +57 47 15	EW	IQ Cet	01 43 05.3 +01 05 49	RR(B)
V1370 Cen	11 13 29.3 -50 19 21	M	IR Cet	01 46 51.8 -05 47 15	RS
V1371 Cen	11 20 26.4 -43 38 47	EW	IS Cet	01 54 37.7 -04 09 08	EW
V1372 Cen	11 20 39.1 -61 49 52	DCEP	IT Cet	01 57 44.4 -20 53 46	RRAB
V1373 Cen	11 40 27.9 -62 01 34	BY	IU Cet	02 03 14.9 +01 12 21	RR(B)
V1374 Cen	11 45 38.8 -36 22 54	EW	IV Cet	02 04 32.6 -01 21 18	EW
V1375 Cen	11 51 13.0 -62 37 29	XND	IW Cet	02 12 35.4 +05 53 24	EW
V1376 Cen	11 58 23.3 -45 57 32	RS	IX Cet	02 12 59.5 +05 41 16	EA
V1377 Cen	12 00 36.3 -39 15 35	EW	IY Cet	02 18 59.6 -23 05 32	EW
V1378 Cen	12 26 02.2 -54 21 16	RS	IZ Cet	02 19 47.4 -10 25 41	RS
V1379 Cen	12 32 20.7 -44 57 41	M	KK Cet	02 28 46.0 -02 29 16	EB
V1380 Cen	12 36 17.7 -50 42 42	BY	KL Cet	02 38 47.8 -05 26 51	SR
V1381 Cen	12 38 11.9 -44 22 32	RRAB	KM Cet	02 42 27.1 +01 13 32	RR(B)
V1382 Cen	12 39 11.0 -54 29 25	RS	KN Cet	02 42 42.9 -11 46 45	UG+EA

Table 1 (continued)

Name		R.A., Decl., 2000.0 h m s o ' "	Type	Name		R.A., Decl., 2000.0 h m s o ' "	Type
KO	Cet	02 57 39.0 +07 10 44	EB	CV	CrB	15 57 33.7 +28 32 25	RRC
KP	Cet	03 08 26.0 +08 05 03	BY	CW	CrB	16 02 08.0 +27 03 32	RRAB
KQ	Cet	03 11 41.2 -00 43 48	EW	CX	CrB	16 16 28.4 +27 52 01	RRAB
KR	Cet	03 13 33.1 +00 42 55	RR(B)	CY	CrB	16 22 12.5 +34 11 47	UG
IU	Cha	11 25 48.0 -76 30 29	RS	CZ	CrB	16 22 58.9 +36 34 24	RRC
IV	Cha	12 30 34.2 -77 03 53	RCB:	AQ	Crt	11 14 51.4 -20 07 04	RRAB
EZ	Cir	14 19 54.1 -64 38 18	RS	AR	Crt	11 27 15.5 -25 10 20	RRAB:
FF	Cir	14 41 09.7 -70 32 07	SR	FM	Cru	11 59 49.9 -61 36 25	BY
FG	Cir	14 48 10.4 -60 00 45	EA	FN	Cru	12 07 42.4 -62 27 28	BY
FH	Cir	15 03 06.7 -60 27 58	DSCT	FO	Cru	12 17 04.7 -57 43 56	RS
FI	Cir	15 16 32.2 -58 55 24	BY	FP	Cru	12 21 30.8 -64 03 53	BY
FK	Cir	15 17 51.6 -59 49 34	EA:	FQ	Cru	12 22 40.2 -62 09 36	DCEP
FL	Cir	15 20 21.3 -58 07 20	DCEP	FR	Cru	12 24 09.8 -60 03 42	BY
LW	Cnc	08 02 10.1 +17 29 15	EB	FS	Cru	12 27 19.9 -58 18 34	BY:
LX	Cnc	08 12 07.6 +13 18 25	UGSU	FT	Cru	12 56 09.4 -61 27 25	INT
LY	Cnc	08 13 31.3 +24 51 53	EW	YZ	Crv	12 30 45.6 -23 58 10	RRC
LZ	Cnc	08 13 37.5 +15 27 15	RS	ZZ	Crv	12 36 36.5 -23 32 39	RRAB
MM	Cnc	08 38 02.2 +16 59 25	EW	AA	Crv	12 42 00.5 -22 08 10	RRAB
MN	Cnc	08 38 47.7 +31 45 22	EW	V2659	Cyg	20 21 42.3 +31 03 30	NB
MO	Cnc	08 40 30.8 +12 36 18	EW	V0339	Del	20 23 30.7 +20 46 04	NA
MP	Cnc	08 41 21.5 +19 00 26	EW	BG	Dor	04 52 12.7 -56 20 47	RRC
MQ	Cnc	08 48 27.0 +07 27 54	EW	BH	Dor	05 05 36.5 -57 55 36	RS
MR	Cnc	08 51 47.2 +07 23 54	RR(B)	BI	Dor	05 26 06.2 -67 10 57	EB
MS	Cnc	08 53 48.9 +11 43 53	EW	BK	Dor	06 23 10.8 -67 25 24	RS
MT	Cnc	08 54 39.0 +11 33 00	EB	V0450	Dra	11 11 28.9 +73 06 55	EW
MU	Cnc	08 57 09.7 +18 56 44	EW	V0451	Dra	11 24 25.4 +77 42 15	DSCT
MV	Cnc	09 00 42.4 +28 17 31	RS	V0452	Dra	11 28 25.3 +68 37 17	EB
MW	Cnc	09 04 52.7 +20 24 54	EA	V0453	Dra	11 37 27.3 +72 24 03	EW
MX	Cnc	09 15 34.9 +08 13 56	UG:	V0454	Dra	11 40 30.0 +71 11 02	EW
MY	Cnc	09 18 17.0 +31 58 49	RRC	V0455	Dra	11 48 36.5 +71 07 51	EW
MZ	Cnc	09 18 31.6 +09 07 43	EA	V0456	Dra	11 55 58.3 +73 00 25	EW
BF	Col	05 06 06.0 -31 09 54	RRAB	V0457	Dra	12 06 41.3 +71 32 46	EW
BG	Col	05 07 12.8 -38 29 56	RRC	V0458	Dra	13 20 53.7 +68 39 51	EW:
BH	Col	05 12 07.8 -40 58 00	RRAB	V0459	Dra	13 22 58.3 +65 24 58	EA/RS
BI	Col	05 30 22.4 -32 34 47	RRC:	V0460	Dra	13 24 55.5 +64 33 16	RRC:
BK	Col	05 36 28.3 -38 36 59	RRC	V0461	Dra	13 41 32.7 +65 43 37	EB
BL	Col	05 38 30.4 -35 54 20	RRAB	V0462	Dra	13 49 56.2 +66 28 28	EW
BM	Col	05 40 49.0 -31 24 07	RS	V0463	Dra	13 54 35.0 +65 12 08	EA
BN	Col	05 51 04.6 -39 26 21	RRAB	V0464	Dra	14 28 55.1 +57 30 24	RRAB
BO	Col	05 56 46.3 -33 10 26	XN	V0465	Dra	14 39 24.7 +64 59 30	EA
BP	Col	06 12 43.6 -36 37 55	RS	V0466	Dra	14 40 33.9 +65 27 24	EW
BQ	Col	06 28 38.0 -38 48 27	RRAB	V0467	Dra	14 41 38.2 +56 26 17	DSCT:
PS	Com	11 59 16.0 +14 14 09	EW	V0468	Dra	14 42 52.6 +63 12 25	RRC
PT	Com	12 13 40.8 +17 14 38	DSCT	V0469	Dra	14 46 21.4 +62 33 14	SRD
PU	Com	12 21 52.1 +18 02 34	EW	V0470	Dra	14 54 53.9 +64 38 44	SRD:
PV	Com	12 32 49.9 +15 17 35	EW	V0471	Dra	15 06 17.4 +56 41 07	EW
PW	Com	12 35 57.4 +13 29 25	RS	V0472	Dra	15 14 00.9 +64 55 34	EA
PX	Com	12 43 05.9 +14 48 32	EW	V0473	Dra	15 21 13.9 +54 23 15	EW
PY	Com	12 43 42.8 +15 31 37	EW	V0474	Dra	15 28 12.7 +62 01 23	EW
PZ	Com	12 46 43.4 +28 28 10	RRC	V0475	Dra	15 45 16.1 +65 49 47	EW
QQ	Com	13 07 53.9 +22 10 07	RRC	V0476	Dra	15 58 53.9 +61 27 33	EW:
QR	Com	13 15 01.2 +21 13 54	EW	V0477	Dra	16 01 59.8 +57 47 45	EW
QS	Com	13 18 20.1 +24 52 20	EW	V0478	Dra	16 03 47.0 +57 41 48	RRAB
QT	Com	13 18 36.8 +15 18 40	SR	V0479	Dra	16 06 14.8 +62 40 15	RRAB

Table 1 (continued)

Name	R.A., Decl., 2000.0	Type	Name	R.A., Decl., 2000.0	Type
	h m s o ' "			h m s o ' "	
V0480 Dra	16 07 37.4 +57 32 09	RRAB	NX Eri	04 16 49.6 -29 51 29	RR(B)
V0481 Dra	16 07 42.5 +62 49 36	EA	NY Eri	04 19 46.3 -05 18 00	EW
V0482 Dra	16 09 27.5 +62 51 09	EW	NZ Eri	04 27 01.2 -09 33 26	EA
V0483 Dra	16 10 44.1 +62 26 10	LB	OO Eri	04 34 33.2 -09 19 15	EW
V0484 Dra	16 10 47.4 +61 12 20	BY	OP Eri	04 36 12.5 -01 50 25	RS
V0485 Dra	16 16 26.9 +66 31 17	EW	OQ Eri	04 36 39.1 -09 23 09	EW
V0486 Dra	16 16 30.8 +54 23 22	RRC	OR Eri	04 39 39.2 -05 01 51	BY
V0487 Dra	16 17 59.5 +67 55 36	BY	OS Eri	04 45 05.9 -25 08 23	RRAB
V0488 Dra	16 21 13.8 +64 09 44	SR	OT Eri	04 48 53.1 -09 11 56	EB
V0489 Dra	16 21 48.3 +65 30 05	EW	OU Eri	04 54 50.1 -11 35 37	EW
V0490 Dra	16 22 21.5 +64 22 52	EW:	OV Eri	05 09 04.5 -07 41 44	EW
V0491 Dra	16 23 42.1 +60 03 23	EA	BB For	01 47 54.6 -29 31 31	RRC
V0492 Dra	16 24 57.2 +63 40 58	EW:	BC For	01 49 26.7 -30 15 59	RRAB
V0493 Dra	16 25 23.4 +52 41 44	SR	BD For	02 12 37.7 -37 21 13	RRAB
V0494 Dra	16 26 58.9 +53 24 35	BY	BE For	02 24 40.3 -24 54 04	RRC
V0495 Dra	16 27 48.0 +60 10 56	SRB	BF For	02 48 07.9 -36 58 54	RS
V0496 Dra	16 28 15.6 +62 43 03	EA	BG For	02 52 12.1 -31 38 28	RRC
V0497 Dra	16 28 48.9 +61 37 23	LB	BH For	03 05 34.6 -31 16 07	RRAB
V0498 Dra	16 34 50.7 +51 17 03	EW	BI For	03 14 08.3 -34 46 22	RRC
V0499 Dra	16 49 38.5 +64 19 12	EW	BK For	03 16 16.4 -28 25 35	RRAB
V0500 Dra	16 50 12.9 +71 46 46	EB:	V0437 Gem	06 01 00.4 +23 56 15	EW
V0501 Dra	17 07 08.1 +64 14 02	RRAB	V0438 Gem	06 28 49.9 +15 22 34	EW
V0502 Dra	17 11 06.0 +72 15 13	RRAB	V0439 Gem	06 33 43.2 +17 52 51	EA
V0503 Dra	17 12 23.5 +54 02 52	EW	V0440 Gem	06 36 40.6 +16 33 13	SRB
V0504 Dra	17 13 00.6 +61 37 21	EW	V0441 Gem	06 39 57.1 +20 00 16	RS
V0505 Dra	17 13 29.2 +70 37 27	EA	V0442 Gem	06 40 33.0 +21 48 57	DSCT
V0506 Dra	17 13 53.7 +56 40 51	RRC	V0443 Gem	06 40 46.9 +28 04 48	EW
V0507 Dra	17 14 53.0 +67 42 10	SR	V0444 Gem	06 40 51.3 +19 24 16	EB
V0508 Dra	17 14 56.8 +58 51 28	EB	V0445 Gem	06 44 02.3 +12 22 34	EW
V0509 Dra	17 15 20.9 +58 28 38	EW	V0446 Gem	06 47 19.1 +33 34 25	UG
V0510 Dra	17 16 26.2 +69 35 04	EW	V0447 Gem	06 49 05.1 +19 59 54	RS
V0511 Dra	17 17 33.3 +64 59 52	EW	V0448 Gem	06 50 01.7 +22 21 28	EW
V0512 Dra	17 19 36.5 +70 53 16	SR	V0449 Gem	06 50 17.4 +22 30 22	EW
V0513 Dra	17 19 41.7 +70 32 09	EB	V0450 Gem	06 58 30.2 +13 11 31	EW
V0514 Dra	17 19 54.8 +69 47 43	EW	V0451 Gem	06 58 50.5 +20 31 33	EA
V0515 Dra	17 28 12.4 +72 39 23	RS	V0452 Gem	06 59 20.3 +14 09 10	EA
V0516 Dra	17 28 48.1 +65 12 35	EW	V0453 Gem	07 00 32.9 +14 07 12	EW
MT Eri	02 26 36.5 -41 19 44	BY	V0454 Gem	07 05 47.6 +15 01 21	RS
MU Eri	02 48 10.6 -15 18 04	EW	V0455 Gem	07 08 53.9 +19 19 38	GDOR
MV Eri	02 51 11.5 -47 53 08	BY	V0456 Gem	07 10 36.7 +13 33 23	EW
MW Eri	02 55 35.2 -02 19 57	EA	V0457 Gem	07 16 12.7 +32 48 02	EW
MX Eri	03 10 00.1 -12 06 19	EA	V0458 Gem	07 17 56.6 +34 12 05	BY
MY Eri	03 12 52.0 -07 44 20	EW	V0459 Gem	07 24 24.0 +33 57 04	RS
MZ Eri	03 13 48.0 -23 22 40	RRC	V0460 Gem	07 30 20.4 +20 21 49	EA
NN Eri	03 24 38.4 -23 34 43	RRAB	V0461 Gem	07 30 29.0 +26 42 55	EW
NO Eri	03 34 09.6 -41 43 50	RS	V0462 Gem	07 31 56.4 +25 54 57	BY:
NP Eri	03 34 19.1 -21 20 00	RRAB	V0463 Gem	07 32 03.6 +26 33 45	EW
NQ Eri	03 36 23.4 -07 55 32	EB	V0464 Gem	07 33 35.5 +26 11 26	EB
NR Eri	03 52 56.9 -35 03 28	RRC	V0465 Gem	07 33 41.6 +25 55 44	EW
NS Eri	03 57 16.1 -08 15 59	EA	V0466 Gem	07 33 57.4 +26 26 51	BCEP:
NT Eri	04 02 48.9 -09 26 01	EA	V0467 Gem	07 34 06.2 +25 55 59	RRAB
NU Eri	04 07 59.4 -00 18 57	EB	V0468 Gem	07 34 13.0 +25 59 00	EB
NV Eri	04 13 59.0 -31 32 40	RS	V0469 Gem	07 34 38.6 +26 11 22	EW
NW Eri	04 14 43.3 -18 52 12	RS:	V0470 Gem	07 35 56.0 +19 14 46	EW

Table 1 (continued)

Name	R.A., Decl., 2000.0	Type	Name	R.A., Decl., 2000.0	Type
	h m s o ' "			h m s o ' "	
V0471 Gem	07 37 38.8 +14 11 45	EB	AM Hor	03 59 36.7 -39 53 15	RS
V0472 Gem	07 40 54.9 +21 09 03	EW	AN Hor	04 04 59.8 -44 57 06	RRAB
V0473 Gem	07 42 54.8 +20 19 58	EW	V0564 Hya	08 11 56.0 +01 07 34	SRB
V0474 Gem	07 45 16.4 +20 23 17	RS	V0565 Hya	08 13 11.2 -05 13 28	EA
V0475 Gem	07 48 49.1 +19 15 27	EB	V0566 Hya	08 28 22.9 +05 36 53	EW
V0476 Gem	07 52 57.3 +21 48 34	EW	V0567 Hya	08 31 25.1 -08 16 38	EA
V1361 Her	15 55 06.1 +42 54 02	EA	V0568 Hya	08 39 47.8 -06 57 20	EA
V1362 Her	15 58 54.2 +46 35 49	EW	V0569 Hya	08 49 54.2 -10 32 14	EB
V1363 Her	16 04 18.0 +47 32 52	EW	V0570 Hya	08 50 59.8 -04 21 07	EA
V1364 Her	16 08 51.3 +46 18 47	EW	V0571 Hya	08 52 54.4 -03 00 17	RRC
V1365 Her	16 11 14.7 +23 05 07	SRB	V0572 Hya	08 56 50.6 +02 30 24	EW
V1366 Her	16 13 24.7 +41 09 48	RRC	V0573 Hya	09 08 32.2 -04 43 15	EW
V1367 Her	16 14 04.2 +10 57 35	EA	V0574 Hya	09 08 38.7 -16 42 44	EA:
V1368 Her	16 20 11.2 +23 20 10	EW	V0575 Hya	09 09 00.1 -04 10 25	RRC
V1369 Her	16 23 44.3 +12 33 01	EW	V0576 Hya	09 09 10.5 -13 13 47	EW
V1370 Her	16 26 15.1 +47 49 34	LB	V0577 Hya	09 12 43.3 -08 08 53	EW
V1371 Her	16 26 28.4 +43 38 09	RRC	V0578 Hya	09 13 52.1 +02 57 35	EB
V1372 Her	16 26 34.2 +42 04 57	RRAB	V0579 Hya	09 19 12.6 -12 16 51	EA
V1373 Her	16 31 22.6 +39 38 11	RRC	V0580 Hya	09 22 36.2 -10 45 31	EB
V1374 Her	16 31 25.3 +32 24 27	LB	V0581 Hya	09 24 34.1 -09 24 22	EW
V1375 Her	16 31 34.2 +36 08 07	RRAB	V0582 Hya	09 25 48.2 -15 35 25	EW
V1376 Her	16 31 37.5 +39 47 35	RRAB	V0583 Hya	09 26 31.4 -01 23 13	EW
V1377 Her	16 31 58.9 +38 45 39	RRC	V0584 Hya	09 28 20.1 -12 50 52	EB
V1378 Her	16 32 50.2 +08 08 01	EW	V0585 Hya	09 28 28.8 -13 26 33	EA
V1379 Her	16 33 14.3 +11 45 21	EW	V0586 Hya	09 28 29.5 -09 22 58	BY
V1380 Her	16 34 55.5 +09 19 11	EW	V0587 Hya	09 32 56.6 +01 56 46	EA
V1381 Her	16 37 13.8 +10 46 15	EW	V0588 Hya	09 37 31.4 -18 16 13	RRAB
V1382 Her	16 38 31.5 +35 35 39	EB	V0589 Hya	09 38 04.9 +04 47 59	EW
V1383 Her	16 38 37.7 +13 28 58	EW	V0590 Hya	10 18 12.7 -22 16 20	RRAB
V1384 Her	16 41 10.7 +08 51 06	SRB	V0591 Hya	10 32 02.8 -14 58 55	SRB
V1385 Her	16 44 11.3 +20 14 37	EA	V0592 Hya	10 48 33.9 -22 44 15	RRC
V1386 Her	16 45 00.7 +28 52 28	EW	V0593 Hya	11 05 21.9 -26 41 04	RRC
V1387 Her	16 47 39.4 +43 04 34	EA	V0594 Hya	11 07 03.9 -32 39 02	RRAB
V1388 Her	16 47 44.3 +40 04 58	EW	V0595 Hya	11 13 50.7 -29 43 40	RRAB
V1389 Her	16 52 49.9 +40 36 03	RRAB	V0596 Hya	11 24 39.1 -29 00 49	RRC
V1390 Her	16 55 48.5 +35 49 43	EA	V0597 Hya	11 57 48.8 -33 35 53	RS
V1391 Her	16 56 00.2 +35 50 41	RRAB	V0598 Hya	11 59 52.4 -28 29 43	RRAB
V1392 Her	16 56 27.3 +14 03 24	EW	V0599 Hya	11 59 59.4 -25 36 14	RRAB
V1393 Her	16 57 44.3 +13 38 18	EW	V0600 Hya	12 25 35.8 -27 05 50	RRC
V1394 Her	16 58 15.1 +14 21 59	EA	V0601 Hya	13 04 42.8 -23 13 37	RRC
V1395 Her	17 03 02.2 +35 51 26	RRAB	V0602 Hya	13 41 00.8 -27 42 33	RRAB
V1396 Her	17 03 56.8 +41 36 42	RRAB	V0603 Hya	13 48 19.2 -29 48 49	RR(B)
V1397 Her	17 07 16.8 +17 25 37	EW	V0604 Hya	13 54 21.2 -24 03 24	RRAB
V1398 Her	17 07 17.7 +13 05 55	SR	V0605 Hya	13 57 02.5 -23 34 49	RRAB
V1399 Her	17 09 13.2 +14 38 10	SRB	V0606 Hya	14 10 25.1 -22 44 48	RRAB
V1400 Her	17 09 57.0 +42 50 17	BY	DN Hyi	01 23 17.2 -79 41 32	BY
V1401 Her	17 12 03.8 +13 00 32	EW	DO Hyi	02 46 06.8 -68 53 26	SRB
V1402 Her	17 15 19.7 +17 58 04	EA	AL LMi	09 23 21.4 +38 38 37	RRC
V1403 Her	17 16 25.0 +14 28 00	EW	AM LMi	09 44 36.3 +41 08 35	RRC
V1404 Her	17 16 29.7 +13 23 15	RS	AN LMi	10 01 13.7 +35 30 14	RRAB
V1405 Her	17 18 43.5 +13 06 19	SR	AO LMi	10 29 25.7 +36 31 45	SRD:
V1406 Her	17 20 50.6 +15 51 16	SR	AP LMi	10 35 36.2 +37 46 38	BY:
V1407 Her	17 21 18.0 +39 22 30	LB	LR Leo	09 27 30.7 +11 07 38	RR(B)
AL Hor	03 34 53.0 -46 40 24	RRAB	LS Leo	09 36 46.4 +12 02 50	EA

Table 1 (continued)

Name	R.A., Decl., 2000.0	Type	Name	R.A., Decl., 2000.0	Type
	h m s o ' "			h m s o ' "	
LT Leo	09 40 42.7 +16 42 18	EA	V0364 Lib	15 09 46.6 -21 47 47	UG:
LU Leo	09 48 37.3 +25 04 29	EW	V0365 Lib	15 14 41.7 -15 59 08	DSCT
LV Leo	09 48 57.3 +17 31 42	RRAB	V0366 Lib	15 18 49.6 -10 00 00	RRC
LW Leo	09 49 32.9 +08 06 29	EA	V0367 Lib	15 19 51.0 -09 50 00	RRC
LX Leo	09 50 27.7 +20 43 05	EW	V0368 Lib	15 37 19.9 -18 00 57	RR(B)
LY Leo	09 55 37.4 +23 13 35	EB	V0401 Lup	14 22 07.3 -54 17 06	RS
LZ Leo	09 57 21.4 +14 12 15	EW	V0402 Lup	14 35 36.6 -53 47 38	RS
MM Leo	10 00 52.2 +24 40 21	BY	V0403 Lup	15 04 28.6 -39 24 26	RS
MN Leo	10 01 34.9 +25 30 00	RRC	V0404 Lup	15 21 03.9 -37 04 41	M
MO Leo	10 08 43.7 +26 03 57	EB	V0405 Lup	15 52 04.5 -37 47 44	RS
MP Leo	10 10 14.8 +16 46 12	EW	V0406 Lup	16 06 49.2 -33 12 35	SRB
MQ Leo	10 10 49.1 +18 56 18	EW	FY Lyn	07 13 05.0 +48 31 51	EW
MR Leo	10 12 00.1 +19 22 00	RRAB	FZ Lyn	07 14 04.8 +44 38 44	EA
MS Leo	10 12 57.3 +10 16 55	EW	GG Lyn	07 14 31.5 +46 20 26	LB
MT Leo	10 22 41.7 +22 53 11	RRAB	GH Lyn	07 14 51.8 +49 56 49	EW
MU Leo	10 24 59.9 +24 30 52	EA	GI Lyn	07 19 23.7 +51 40 42	EW
MV Leo	10 28 00.1 +21 48 14	UGZ+E	GK Lyn	07 21 37.8 +49 32 53	RS
MW Leo	10 50 16.3 +21 53 06	EA	GL Lyn	07 24 12.1 +48 43 01	EW
MX Leo	10 53 14.7 +01 12 01	RRC	GM Lyn	07 25 30.1 +50 56 49	EW
MY Leo	10 54 40.0 +22 41 00	EW	GN Lyn	07 27 24.8 +51 28 34	LB
MZ Leo	10 57 46.6 +09 58 41	EW	GO Lyn	07 30 48.2 +40 40 59	EW
NN Leo	10 58 55.1 +17 22 12	EB	GP Lyn	07 33 08.6 +48 03 54	RRAB
NO Leo	11 00 02.1 +04 42 07	EW	GQ Lyn	07 34 12.8 +48 18 34	EW
NP Leo	11 09 08.3 +00 07 32	EA	GR Lyn	07 35 23.6 +44 58 00	EW
NQ Leo	11 10 10.8 +01 07 33	RRC:	GS Lyn	07 36 47.1 +49 20 44	EW
NR Leo	11 12 33.5 +12 17 35	EB	GT Lyn	07 39 15.4 +44 43 58	EW
NS Leo	11 17 06.0 -00 34 24	RRAB	GU Lyn	07 39 47.1 +42 56 39	EW
NT Leo	11 18 19.3 +16 28 05	EA	GV Lyn	07 41 17.8 +49 28 43	EW
NU Leo	11 19 09.4 +01 57 27	EA	GW Lyn	07 42 08.9 +51 33 18	EA
NV Leo	11 21 05.1 +03 30 56	RR(B)	GX Lyn	07 44 26.1 +41 43 07	EA
NW Leo	11 22 10.3 +25 23 19	EW	GY Lyn	07 45 52.8 +42 03 43	EA
NX Leo	11 22 25.7 +04 28 49	EA	GZ Lyn	07 46 17.9 +44 24 19	RRC
NY Leo	11 24 35.7 +05 59 24	EW	HH Lyn	07 46 58.1 +47 46 19	EA
NZ Leo	11 27 17.2 +10 35 12	EW	HI Lyn	07 47 10.9 +48 53 18	EB
OO Leo	11 27 23.3 +04 42 19	EW	HK Lyn	07 47 25.7 +45 04 35	RRAB
OP Leo	11 28 01.7 +06 01 26	EW	HL Lyn	07 47 50.3 +41 05 22	EW
OQ Leo	11 28 05.7 +06 05 44	EW	HM Lyn	07 48 33.5 +50 50 45	EA
OR Leo	11 30 30.8 -01 01 57	EW	HN Lyn	07 48 47.3 +45 46 44	EW
OS Leo	11 33 37.0 +07 51 29	RS	HO Lyn	07 49 12.0 +41 30 39	EB:
OT Leo	11 37 01.2 -06 00 24	RRC	HP Lyn	07 49 28.6 +49 20 25	EW
OU Leo	11 45 39.9 +14 12 02	EW	HQ Lyn	07 50 11.0 +47 13 55	EW:
OV Leo	11 47 21.0 +15 42 59	EW	HR Lyn	07 51 45.4 +46 02 54	SRD:
OW Leo	11 52 13.6 +18 58 55	EW	HS Lyn	07 53 55.6 +46 20 26	EA
OX Leo	11 56 53.3 +10 31 33	GDOR	HT Lyn	07 54 19.5 +43 02 11	EB
BI Lep	05 24 02.3 -22 47 24	RRAB	HU Lyn	07 55 38.2 +45 58 50	EA
BK Lep	05 31 04.2 -11 02 14	EA	HV Lyn	07 56 42.3 +47 39 18	EA
BL Lep	05 32 58.8 -13 54 00	EW	HW Lyn	07 56 54.9 +47 46 23	EW
BM Lep	05 41 35.6 -13 39 38	EA	HX Lyn	07 57 22.5 +48 07 19	SRD:
BN Lep	05 48 42.5 -16 27 03	RRC	HY Lyn	07 57 49.1 +46 16 23	EB
BO Lep	05 52 51.5 -11 03 11	EA	HZ Lyn	07 58 28.7 +49 04 10	SRD:
BP Lep	05 58 08.8 -11 12 06	EA:/RS	II Lyn	07 58 34.0 +48 59 14	SRD:
BQ Lep	06 04 50.2 -13 14 16	EA	IK Lyn	07 58 44.1 +54 25 14	EW
V0362 Lib	14 43 41.9 -17 55 50	UGSU	IL Lyn	07 58 45.3 +42 11 21	RS
V0363 Lib	15 06 44.5 -08 38 48	RS	IM Lyn	07 58 56.9 +44 52 53	EW

Table 1 (continued)

Name	R.A., Decl., 2000.0	Type	Name	R.A., Decl., 2000.0	Type
	h m s o ' "			h m s o ' "	
IN Lyn	07 59 46.4 +41 04 35	EW	V0975 Mon	06 41 13.0 +09 27 33	EA+IN
IO Lyn	08 01 56.2 +41 01 18	RRAB	V0976 Mon	06 41 20.5 +09 45 36	INB
IP Lyn	08 02 23.5 +51 46 45	EW	V0977 Mon	06 41 23.0 +09 27 27	INB
IQ Lyn	08 02 24.1 +48 09 05	EW	V0978 Mon	06 41 27.1 +09 35 07	INB
IR Lyn	08 02 30.5 +51 54 11	EB	V0979 Mon	06 41 34.6 +07 56 40	CEP(B)
IS Lyn	08 03 27.3 +50 39 49	EA	V0980 Mon	06 47 01.1 -10 05 42	EW
IT Lyn	08 04 52.6 +44 07 24	EW	V0981 Mon	06 48 29.2 -10 14 18	DCEP
IU Lyn	08 06 04.6 +50 20 43	EW	V0982 Mon	06 48 47.1 -02 53 53	EA
IV Lyn	08 06 22.0 +46 17 16	LB	V0983 Mon	06 54 01.7 -07 39 59	SR
IW Lyn	08 07 48.8 +42 03 58	EA	V0984 Mon	06 56 47.9 -11 05 31	EW
IX Lyn	08 08 39.9 +46 43 29	LB	V0960 Mon	06 59 31.6 -04 05 28	FU
IY Lyn	08 11 36.4 +43 38 24	EA	V0985 Mon	07 00 34.0 -02 20 55	CEP(B)
IZ Lyn	08 12 27.7 +42 11 41	EW	V0986 Mon	07 02 47.5 -06 59 02	EB
KK Lyn	08 13 55.1 +43 25 26	EW	V0987 Mon	07 10 28.0 +00 20 26	EW
KL Lyn	08 14 42.9 +51 43 06	EW	V0988 Mon	07 10 29.8 +00 24 06	EW
KM Lyn	08 15 29.1 +51 30 02	BY	V0989 Mon	07 18 28.7 -03 36 39	EW
KN Lyn	08 16 36.4 +47 50 43	EW	V0990 Mon	07 20 07.1 -09 51 19	EA
KO Lyn	08 19 10.5 +35 02 17	EW	V0991 Mon	07 29 04.0 -05 40 31	EA
KP Lyn	08 19 17.6 +41 59 00	DSCT	V0992 Mon	07 37 35.5 -04 21 35	EA
KQ Lyn	08 21 41.7 +46 20 54	SRD:	V0993 Mon	07 47 00.9 -05 20 34	EB
KR Lyn	08 24 33.5 +51 24 41	EW	V0994 Mon	07 53 31.5 -01 33 01	EW
KS Lyn	08 24 45.9 +40 31 32	EW	V0995 Mon	07 56 48.4 -00 39 59	EA
KT Lyn	08 27 41.9 +47 41 29	SR	V0996 Mon	08 03 55.1 -02 46 26	EW
KU Lyn	08 27 51.5 +41 47 19	BY	V0354 Mus	12 21 05.0 -71 16 49	BY
KV Lyn	08 27 55.8 +40 56 28	EW	V0355 Mus	12 24 47.3 -75 03 09	RS
KW Lyn	08 30 47.9 +41 22 23	LB	V0356 Mus	13 17 13.8 -66 05 00	CEP(B)
KX Lyn	08 31 52.2 +38 32 14	RRC	V0491 Nor	15 45 17.9 -53 18 10	RS
KY Lyn	08 32 30.1 +42 14 00	EW	V0492 Nor	15 52 26.7 -55 00 38	EW
KZ Lyn	08 32 49.6 +43 16 02	RRC	V0493 Nor	15 52 38.4 -53 26 15	RS
LL Lyn	08 36 20.9 +46 26 24	SRD:	V0494 Nor	15 54 13.6 -58 55 24	RS
LM Lyn	08 37 53.5 +42 06 56	EW	V0495 Nor	16 02 17.0 -59 44 32	RS
LN Lyn	08 43 28.5 +40 22 48	EB	V0496 Nor	16 06 44.3 -52 02 30	SR:
LO Lyn	08 43 56.7 +43 22 13	RRC	V0497 Nor	16 07 11.8 -51 48 51	M
LP Lyn	08 44 59.8 +44 51 45	BY:	V0498 Nor	16 07 14.7 -60 07 31	SR
LQ Lyn	08 46 10.2 +43 04 31	DSCT	V0499 Nor	16 07 25.8 -53 33 15	M
LR Lyn	08 50 39.5 +43 40 02	RRAB	V0500 Nor	16 08 04.3 -54 32 37	LB
LS Lyn	09 06 00.1 +39 27 58	RRC	V0501 Nor	16 08 42.8 -54 57 23	SR
LT Lyn	09 21 59.4 +35 00 33	EW	V0502 Nor	16 08 47.2 -58 42 26	SR
BE Men	05 53 29.3 -81 56 53	RS	V0503 Nor	16 10 03.2 -50 26 12	RS
BF Men	07 05 09.1 -78 25 18	RS	V0504 Nor	16 10 18.2 -44 44 57	M
V0961 Mon	05 57 08.3 -07 28 15	EA	V0505 Nor	16 10 53.5 -55 42 38	M
V0962 Mon	06 05 27.0 -10 14 33	GDOR	V0506 Nor	16 11 16.5 -54 46 34	M
V0963 Mon	06 09 13.7 -06 43 56	INS	V0507 Nor	16 12 12.5 -54 27 30	EA
V0964 Mon	06 18 31.7 -06 43 30	EB	V0508 Nor	16 12 26.8 -53 49 06	RRAB
V0965 Mon	06 23 26.2 +00 05 46	RRAB	V0509 Nor	16 12 52.4 -54 28 41	EA:/RS
V0966 Mon	06 27 34.8 +09 49 50	CEP(B)	V0510 Nor	16 13 04.1 -53 45 38	SRA
V0967 Mon	06 29 40.4 +07 23 42	EA	V0511 Nor	16 13 12.8 -54 21 43	M
V0968 Mon	06 31 02.1 +03 27 29	RS	V0512 Nor	16 13 22.7 -54 25 05	M
V0969 Mon	06 36 56.3 -05 21 04	BY	V0513 Nor	16 14 14.2 -53 34 47	SR
V0970 Mon	06 39 47.8 -09 44 03	EW	V0514 Nor	16 14 43.0 -53 58 56	EA
V0971 Mon	06 40 22.9 +08 35 52	RS	V0515 Nor	16 14 48.8 -54 02 45	EA
V0972 Mon	06 40 31.2 +09 31 08	INT	V0516 Nor	16 14 56.4 -53 36 27	EA
V0973 Mon	06 41 01.5 +10 14 57	IN	V0517 Nor	16 15 21.3 -53 46 46	M
V0974 Mon	06 41 03.5 +09 31 18	INT	V0518 Nor	16 15 28.8 -54 39 02	LB

Table 1 (continued)

Name	R.A., Decl., 2000.0	Type	Name	R.A., Decl., 2000.0	Type
	h m s o ' "			h m s o ' "	
V0519 Nor	16 15 43.0 -54 11 58	RRAB	V2841 Oph	16 38 41.9 -06 30 19	LB
V0520 Nor	16 15 51.9 -53 59 31	M	V2842 Oph	16 39 56.6 -02 05 40	DSCT
V0521 Nor	16 15 53.6 -54 21 24	M	V2843 Oph	16 42 40.5 -24 24 50	M
V0522 Nor	16 15 59.9 -54 08 33	EA	V2844 Oph	16 42 49.3 +02 56 27	SRA
V0523 Nor	16 16 11.2 -53 38 30	RRAB	V2845 Oph	16 46 18.4 -11 59 21	SR
V0524 Nor	16 16 19.8 -53 59 41	EA	V2846 Oph	16 51 13.1 +10 48 36	EW
V0525 Nor	16 16 21.4 -53 40 47	RRAB	V2847 Oph	16 53 02.1 -01 09 06	DSCT
V0526 Nor	16 16 30.0 -53 55 56	EA	V2848 Oph	16 53 18.6 -16 17 54	UG
V0527 Nor	16 16 35.9 -53 36 38	EA	V2849 Oph	16 54 15.4 +04 21 40	SRA
V0528 Nor	16 16 46.8 -53 41 10	M	V2850 Oph	16 54 55.9 -26 02 43	M
V0529 Nor	16 16 58.9 -53 28 58	EA	V2851 Oph	16 55 32.4 +06 30 56	EW
V0530 Nor	16 17 07.1 -53 32 07	M	V2852 Oph	16 55 38.0 +06 45 15	EB
V0531 Nor	16 17 10.1 -53 29 21	RRAB	V2853 Oph	16 56 39.6 +11 26 33	EW
V0532 Nor	16 17 13.7 -53 38 02	M	V2854 Oph	16 57 09.9 +11 25 36	BY:
V0533 Nor	16 17 22.4 -54 12 39	EA	V2855 Oph	16 57 16.2 +11 47 53	EW
V0534 Nor	16 17 39.3 -53 33 36	M	V2856 Oph	16 57 24.7 +12 00 41	BY:
V0535 Nor	16 18 00.8 -54 03 15	M	V2857 Oph	16 58 09.9 +11 31 53	EW
V0536 Nor	16 18 05.3 -53 50 58	EA	V2858 Oph	16 58 16.8 +11 23 15	BY:
V0537 Nor	16 18 22.9 -57 09 03	SRB	V2859 Oph	16 58 21.1 -24 04 38	SRB
V0538 Nor	16 20 10.4 -54 22 16	SRA:	V2860 Oph	16 58 36.0 +12 03 46	EW
V0539 Nor	16 20 54.2 -53 33 17	DCEP	V2861 Oph	16 58 54.5 +11 46 19	EW
V0540 Nor	16 21 16.0 -53 33 20	EW:	V2862 Oph	16 59 01.7 -15 15 29	XND
V0541 Nor	16 23 00.5 -53 30 12	M	V2863 Oph	17 00 07.1 -18 04 56	RRC
V0542 Nor	16 23 05.7 -51 56 53	RRAB	V2864 Oph	17 00 23.5 +05 01 30	SRB
V0543 Nor	16 23 57.6 -55 54 46	SR	V2865 Oph	17 00 41.2 -24 20 04	M
V0544 Nor	16 24 07.1 -52 31 05	EA	V2866 Oph	17 01 54.5 -00 44 18	SRB
V0545 Nor	16 24 08.3 -52 03 18	EA	V2867 Oph	17 01 57.5 +07 33 32	E/RS
V0546 Nor	16 24 57.2 -51 57 58	EA	V2868 Oph	17 02 05.0 +09 08 39	EB
V0547 Nor	16 25 18.6 -52 05 32	RRAB	V2869 Oph	17 02 26.1 +02 00 19	SRB
V0548 Nor	16 25 28.8 -51 25 18	BY:	V2870 Oph	17 03 11.4 -26 00 42	M
V0549 Nor	16 25 45.6 -52 02 18	EA	V2871 Oph	17 03 39.6 -23 45 22	SR
V0550 Nor	16 26 06.5 -52 05 32	M	V2872 Oph	17 04 09.3 -23 11 14	LB
V0551 Nor	16 26 28.4 -52 09 13	RRAB	V2873 Oph	17 04 25.6 +06 19 32	EW
V0552 Nor	16 30 12.6 -53 28 51	SRA	V2874 Oph	17 04 25.8 -27 02 07	M
V0553 Nor	16 30 57.2 -52 19 41	M	V2875 Oph	17 04 35.6 -19 38 01	SRA
V0554 Nor	16 33 02.5 -54 03 08	M	V2876 Oph	17 05 11.1 -25 24 39	M
FN Oct	05 06 18.5 -86 41 45	RS	V2877 Oph	17 05 18.3 -15 36 41	M
FO Oct	17 19 28.8 -86 38 27	SR	V2878 Oph	17 05 18.5 -23 34 29	SRA
V2825 Oph	16 23 04.7 -01 26 19	LB	V2879 Oph	17 05 27.4 -24 56 59	M
V2826 Oph	16 24 11.9 -22 29 46	SR	V2880 Oph	17 05 29.8 +06 55 01	EW
V2827 Oph	16 26 24.7 -04 49 47	SR	V2881 Oph	17 06 11.2 +01 09 49	EW
V2828 Oph	16 26 58.8 -06 02 31	EW	V2882 Oph	17 06 17.6 -26 32 23	M
V2829 Oph	16 28 00.9 -21 35 22	SRB	V2883 Oph	17 06 43.8 -18 48 42	SR
V2830 Oph	16 28 17.8 -21 46 03	SR	V2884 Oph	17 07 14.9 -26 11 41	M:
V2831 Oph	16 28 39.6 -07 24 22	EW:	V2885 Oph	17 07 35.9 -23 22 40	M
V2832 Oph	16 28 42.3 -07 44 28	RRC	V2886 Oph	17 07 43.8 -18 09 15	SR
V2833 Oph	16 29 34.1 -03 32 01	SRB	V2887 Oph	17 07 54.3 -03 27 04	LB
V2834 Oph	16 29 53.3 -12 01 43	SRB	V2888 Oph	17 08 08.5 -26 22 43	M
V2835 Oph	16 30 14.1 -02 34 01	SRB	V2889 Oph	17 08 46.5 -27 53 14	M
V2836 Oph	16 30 19.5 -02 41 34	SRB	V2890 Oph	17 09 11.1 -02 34 32	SRB
V2837 Oph	16 31 04.4 -24 04 33	INB	V2891 Oph	17 09 19.2 +03 04 18	EW
V2838 Oph	16 31 20.4 -05 16 00	SRB	V2892 Oph	17 09 23.6 -23 03 07	M
V2839 Oph	16 35 08.2 -00 36 34	EB	V2893 Oph	17 10 34.5 -25 32 07	SR
V2840 Oph	16 36 24.4 -06 21 56	LB	V2894 Oph	17 11 02.6 -17 10 27	LB

Table 1 (continued)

Name	R.A., Decl., 2000.0	Type	Name	R.A., Decl., 2000.0	Type
	h m s o ' "			h m s o ' "	
V2895 Oph	17 11 11.7 -25 57 50	SR	V2794 Ori	04 53 58.9 +04 01 13	EW
V2896 Oph	17 11 56.6 -16 30 58	LB	V2795 Ori	04 57 29.5 +00 57 32	EW
V2897 Oph	17 13 01.9 -10 34 42	SR	V2796 Ori	04 58 43.1 +02 35 06	EB
V2898 Oph	17 13 45.2 -18 17 53	SR	V2797 Ori	05 03 01.6 +12 03 34	GDOR
V2899 Oph	17 13 54.0 -03 59 49	SRB	V2798 Ori	05 05 08.1 +06 29 52	RS
V2900 Oph	17 14 09.9 -14 59 59	LB	V2799 Ori	05 06 38.9 -02 16 55	EB
V2901 Oph	17 14 12.2 -17 53 26	LB	V2800 Ori	05 06 40.0 +02 08 25	RS
V2902 Oph	17 14 14.5 -21 26 14	RCB	V2801 Ori	05 07 42.3 +02 57 48	EW
V2903 Oph	17 14 23.0 -04 44 31	SR	V2802 Ori	05 08 51.8 +02 49 16	EW
V2904 Oph	17 15 04.5 -17 04 59	SRB	V2803 Ori	05 09 09.6 +06 33 27	EW
V2905 Oph	17 15 10.2 -15 17 49	M	V2804 Ori	05 11 34.1 -10 34 24	EW
V2906 Oph	17 15 49.9 -17 43 00	SR	V2805 Ori	05 17 12.3 +03 38 35	EA
V2907 Oph	17 17 14.7 -29 15 39	M	V2806 Ori	05 22 47.2 -00 29 14	EA
V2908 Oph	17 17 26.0 -19 04 59	SR	V2807 Ori	05 29 29.5 +03 18 21	BY
V2909 Oph	17 17 32.8 -24 16 41	SR	V2808 Ori	05 30 02.9 -01 30 05	EW
V2910 Oph	17 17 36.8 -25 49 41	M	V2809 Ori	05 30 08.0 +13 24 24	EW
V2911 Oph	17 17 49.5 -17 58 17	SR	V2810 Ori	05 30 20.6 +13 35 42	EW
V2912 Oph	17 17 58.9 -18 06 05	SRB	V2811 Ori	05 33 41.8 +05 04 17	EW
V2913 Oph	17 18 06.5 +09 08 01	SRB	V2812 Ori	05 35 41.1 +11 27 06	EW
V2914 Oph	17 18 30.3 +09 22 44	SRB	V2813 Ori	05 38 45.1 -08 19 59	EW
V2915 Oph	17 19 04.8 -17 28 22	LB	V2814 Ori	05 39 45.6 -00 55 51	RS
V2916 Oph	17 19 27.9 -25 39 36	M:	V2815 Ori	05 43 22.5 +07 01 21	EA
V2917 Oph	17 19 57.7 -17 59 24	SR	V2816 Ori	05 45 17.7 +05 33 19	RS
V2918 Oph	17 20 12.2 -23 05 10	M	V2817 Ori	05 48 22.6 +12 18 26	RS
V2919 Oph	17 20 39.6 -25 50 47	M	V2818 Ori	05 49 59.4 -07 25 54	EW
V2920 Oph	17 20 48.6 +08 45 54	EW	V2819 Ori	05 50 15.2 -03 30 22	EA
V2921 Oph	17 20 55.0 -21 29 20	RV	V2820 Ori	05 50 51.1 +06 25 39	EB
V2922 Oph	17 21 12.9 +04 41 10	LB	V2821 Ori	06 07 42.9 +08 44 38	EB
V2923 Oph	17 21 19.2 +08 37 23	SR	V2822 Ori	06 08 15.6 -01 31 51	EW
V2924 Oph	17 23 34.3 -20 47 55	SR	V2823 Ori	06 09 55.7 +08 09 29	EB
V2925 Oph	17 23 55.4 +09 46 39	RRAB	V2824 Ori	06 11 42.7 -00 46 59	EW
V2926 Oph	17 24 18.9 -16 53 54	M	V2825 Ori	06 14 25.9 -00 31 41	EW
V2927 Oph	17 24 26.4 -17 23 31	M	V2826 Ori	06 15 18.7 +03 47 01	BY
V2928 Oph	17 25 01.2 -17 09 30	M	V2827 Ori	06 18 12.9 +15 26 05	EB
V2929 Oph	17 25 02.6 +10 38 18	SRB	V2828 Ori	06 19 59.9 +19 26 59	NL
V2930 Oph	17 26 34.3 +12 04 31	RRAB	V0621 Peg	00 04 14.6 +31 15 09	EW
V2931 Oph	17 27 31.7 +11 32 14	RRAB	V0622 Peg	00 05 39.5 +22 52 52	EW
V2932 Oph	17 27 34.1 +05 31 10	LB	V0623 Peg	00 06 53.1 +16 46 21	EW
V2933 Oph	17 28 20.1 +03 33 17	EW	V0966 Per	01 36 42.4 +54 15 21	EA
V2934 Oph	17 28 25.3 -21 02 38	M	V0967 Per	01 54 51.3 +54 44 38	EW
V2935 Oph	17 28 25.6 +04 14 34	BY:	V0968 Per	01 55 12.5 +54 42 08	EB
V2936 Oph	17 28 32.8 +03 51 30	BY:	V0969 Per	02 31 37.7 +57 49 11	EW
V2937 Oph	17 28 36.2 +04 14 19	BY:	V0970 Per	02 31 43.9 +56 59 56	EA
V2938 Oph	17 28 39.2 +03 55 19	EW	V0971 Per	02 32 20.6 +58 04 19	EB:
V2939 Oph	17 28 49.3 +08 35 32	CWB	V0972 Per	02 32 26.0 +57 26 42	EW
V2940 Oph	17 28 49.9 +03 52 44	EB	V0973 Per	02 32 45.9 +57 41 47	EW
V2941 Oph	17 28 57.2 +05 19 38	SRB	V0974 Per	02 33 07.1 +57 30 29	EW
V2942 Oph	17 28 59.1 +04 03 34	EW	V0975 Per	02 33 08.2 +57 28 11	EB
V2943 Oph	17 29 11.1 +09 44 52	RRAB	V0976 Per	02 33 29.3 +57 48 32	DSCT
V2944 Oph	17 29 13.4 -18 46 14	NA	V0977 Per	02 33 45.6 +57 19 33	M:
V2945 Oph	17 29 31.2 +04 07 57	EW	V0978 Per	02 34 22.9 +57 25 47	EB
V2946 Oph	17 29 37.7 +03 46 27	EW	V0979 Per	02 34 48.3 +56 59 19	EB
V2947 Oph	17 29 40.1 +04 09 33	EW	V0980 Per	02 34 53.8 +57 56 26	EB
V2948 Oph	17 29 40.6 -19 22 02	SRA	V0981 Per	02 36 28.2 +52 16 31	SR:

Table 1 (continued)

Name	R.A., Decl., 2000.0 h m s o ' "	Type	Name	R.A., Decl., 2000.0 h m s o ' "	Type
V0982 Per	02 38 24.0 +56 31 57	EA	V1036 Per	04 26 03.1 +50 28 33	LB:
V0983 Per	02 42 25.3 +37 09 24	SR	V1037 Per	04 26 39.0 +31 52 28	EW
V0984 Per	02 42 36.5 +49 50 25	LB	V1038 Per	04 26 41.4 +32 15 13	EW
V0985 Per	02 44 30.0 +49 01 25	LB	V1039 Per	04 26 55.7 +32 11 06	EW
V0986 Per	02 44 37.6 +48 03 56	DSCT	V1040 Per	04 27 06.7 +32 15 09	EW
V0987 Per	02 47 14.4 +40 18 04	SR	V1041 Per	04 27 40.4 +47 30 44	LB:
V0988 Per	02 49 18.7 +51 05 11	LB	V1042 Per	04 27 44.5 +32 15 18	EW
V0989 Per	02 50 29.2 +49 22 22	SR:	V1043 Per	04 27 46.3 +31 57 41	E/RS:
V0990 Per	02 52 37.9 +39 20 22	EW	V1044 Per	04 28 03.4 +32 27 47	EW
V0991 Per	02 53 57.7 +46 09 27	RS	V1045 Per	04 28 26.7 +32 28 10	DSCTC
V0992 Per	02 54 40.4 +42 55 40	EA	V1046 Per	04 28 37.1 +31 57 58	UG
V0993 Per	02 56 29.2 +31 52 09	LB	V1047 Per	04 28 39.6 +48 35 55	EA
V0994 Per	02 57 50.1 +49 42 15	EW	V1048 Per	04 28 46.9 +32 00 40	EW
V0995 Per	02 59 17.8 +51 50 25	SR	V1049 Per	04 28 47.3 +32 08 41	EA
V0996 Per	03 00 31.1 +37 59 08	EW	V1050 Per	04 29 15.8 +32 06 33	SR
V0997 Per	03 04 04.2 +44 11 54	EW	V1051 Per	04 31 06.7 +47 02 51	LB
V0998 Per	03 04 04.9 +34 42 57	SR:	V1052 Per	04 32 42.9 +44 37 39	EB
V0999 Per	03 05 24.1 +49 58 33	LB	V1053 Per	04 38 16.5 +46 52 01	LB
V1000 Per	03 07 51.0 +33 07 46	LB	V1054 Per	04 48 02.6 +44 45 53	SR:
V1001 Per	03 14 31.7 +57 00 59	BY	DK Phe	00 04 00.9 -42 43 57	RRAB
V1002 Per	03 15 03.3 +32 30 19	SR:	DL Phe	00 27 42.9 -41 26 16	RS:
V1003 Per	03 15 19.5 +57 04 49	SR:	DM Phe	00 34 06.1 -51 03 01	RS
V1004 Per	03 15 58.2 +57 26 41	DSCT	DN Phe	00 37 05.7 -43 17 43	RRAB
V1005 Per	03 16 18.0 +57 08 59	BY:	DO Phe	00 55 25.3 -49 56 57	RS
V1006 Per	03 16 19.1 +57 03 43	EW	DP Phe	00 57 49.7 -39 35 32	RRC
V1007 Per	03 16 29.3 +57 03 49	EA	DQ Phe	01 01 16.7 -45 56 37	BY
V1008 Per	03 16 30.4 +57 14 02	EW	DR Phe	01 31 40.6 -49 57 19	RRAB
V1009 Per	03 16 49.5 +33 30 15	EW	DS Phe	02 02 36.9 -43 07 56	RRAB
V1010 Per	03 17 52.5 +32 00 12	EW	AV Pic	04 37 00.4 -51 50 27	RS
V1011 Per	03 18 06.6 +32 21 00	EB	AW Pic	05 08 38.7 -56 02 58	RRAB
V1012 Per	03 18 38.5 +57 20 26	EB	AX Pic	05 28 40.1 -53 16 12	RRC
V1013 Per	03 18 50.6 +57 08 22	EW	AY Pic	05 36 00.7 -49 51 53	RS
V1014 Per	03 19 40.5 +40 22 06	SR	AZ Pic	05 53 22.4 -54 17 55	EW
V1015 Per	03 20 43.9 +39 23 48	RS	BB Pic	06 03 24.5 -55 28 21	EA/RS
V1016 Per	03 25 52.9 +43 14 57	E:/RS:	BC Pic	06 13 06.0 -56 20 25	RS
V1017 Per	03 31 41.8 +37 19 53	ACV	IQ Psc	00 15 07.6 -03 20 00	RS
V1018 Per	03 31 48.6 +37 23 37	EA	IR Psc	00 15 55.7 +06 44 45	EW
V1019 Per	03 31 55.8 +37 03 12	EA	IS Psc	00 17 01.6 +16 59 38	EW
V1020 Per	03 41 32.0 +33 07 37	EW	IT Psc	00 20 22.3 +07 34 16	SR
V1021 Per	03 55 32.5 +32 56 53	BY:	IU Psc	00 26 53.9 +17 33 28	LB
V1022 Per	03 55 47.1 +40 41 09	DSCT	IV Psc	00 31 01.7 +19 15 47	EW
V1023 Per	04 01 58.8 +51 23 42	EA	IW Psc	00 40 54.3 +03 36 01	EW
V1024 Per	04 02 39.0 +42 50 44	UG	IX Psc	00 52 56.0 +20 17 30	EW
V1025 Per	04 04 46.3 +51 26 26	EW:	IY Psc	00 54 14.8 +06 41 10	EW
V1026 Per	04 11 04.7 +32 52 12	RRAB	IZ Psc	00 55 14.1 +31 30 22	LB
V1027 Per	04 11 24.0 +49 00 44	EA	KK Psc	00 58 29.8 +13 48 44	EW
V1028 Per	04 15 40.1 +49 19 01	LB	KL Psc	00 58 31.8 +30 21 47	LB
V1029 Per	04 17 28.1 +50 43 05	M	KM Psc	01 01 02.3 +14 46 59	EW
V1030 Per	04 18 18.5 +44 04 05	BY	KN Psc	01 05 44.7 +33 23 28	BY
V1031 Per	04 22 07.0 +50 17 29	LB	KO Psc	01 10 24.1 +27 19 15	DSCT
V1032 Per	04 22 37.6 +51 05 47	SR	KP Psc	01 18 16.7 +30 18 35	BY
V1033 Per	04 24 33.5 +49 29 10	LB	KQ Psc	01 20 33.6 +02 45 47	EA
V1034 Per	04 24 54.5 +49 26 14	SR	KR Psc	01 24 29.0 +30 58 19	LB:
V1035 Per	04 25 46.0 +31 51 39	EW:	KS Psc	01 25 26.9 +02 56 21	RS

Table 1 (continued)

Name	R.A., Decl., 2000.0	Type	Name	R.A., Decl., 2000.0	Type
	h m s o ' "			h m s o ' "	
KT Psc	01 33 36.6 +08 06 32	EW	DG Scl	00 31 00.5 -25 16 52	LB
KU Psc	01 40 35.4 +28 06 50	EB	DH Scl	00 54 41.5 -28 13 55	RRC
V0706 Pup	06 20 43.5 -43 49 45	RS	DI Scl	01 00 12.3 -38 18 38	RS
V0707 Pup	06 46 14.9 -43 19 12	RRC	V1536 Sco	16 06 08.5 -18 51 55	M
V0708 Pup	06 48 47.7 -36 28 53	EW	V1537 Sco	16 06 51.4 -21 51 50	GDOR
V0709 Pup	06 49 30.6 -36 20 44	EW	V1538 Sco	16 08 43.3 -35 02 24	M
V0710 Pup	06 49 52.3 -36 31 41	EW	V1539 Sco	16 09 24.6 -22 57 02	SRB:
V0711 Pup	06 50 01.9 -36 29 22	RRAB	V1540 Sco	16 09 29.2 -15 37 29	EW
V0712 Pup	06 50 44.5 -36 24 58	SXPHE	V1541 Sco	16 09 47.6 -32 58 53	LB
V0713 Pup	06 58 07.2 -38 37 53	M	V1542 Sco	16 10 03.4 -34 14 39	M
V0714 Pup	07 00 00.6 -37 32 31	RRAB	V1543 Sco	16 10 42.5 -36 47 06	LB
V0715 Pup	07 06 53.7 -41 07 34	EA	V1544 Sco	16 11 14.1 -29 21 38	SRB
V0716 Pup	07 15 48.8 -44 05 18	RRC	V1545 Sco	16 11 42.0 -42 00 59	M
V0717 Pup	07 17 49.8 -33 56 40	BY	V1546 Sco	16 11 55.8 -31 05 06	SR
V0718 Pup	07 28 13.9 -12 14 07	EB	V1547 Sco	16 12 01.4 -38 40 28	INT:
V0719 Pup	07 43 42.5 -20 50 20	CEP(B)	V1548 Sco	16 12 24.9 -40 18 42	M
V0720 Pup	07 45 22.3 -24 00 14	EB	V1549 Sco	16 13 01.3 -24 06 55	BY:
V0721 Pup	07 51 27.1 -11 45 28	EA	V1550 Sco	16 13 17.7 -27 59 57	SRB
V0722 Pup	07 51 28.4 -43 28 23	RS	V1551 Sco	16 14 59.7 -16 40 51	RRAB
V0723 Pup	07 51 33.4 -39 51 46	M	V1552 Sco	16 17 15.1 -37 44 24	M
V0724 Pup	07 53 45.1 -36 58 14	DCEP	V1553 Sco	16 20 21.8 -35 41 16	DSCT
V0725 Pup	07 56 36.1 -41 45 26	RS	V1554 Sco	16 20 36.4 -32 24 35	RRAB
V0726 Pup	07 58 57.9 -35 22 17	RS	V1555 Sco	16 20 58.0 -21 31 19	SR
V0727 Pup	07 59 26.5 -11 31 27	EB	V1556 Sco	16 21 28.1 -22 07 17	SRB
V0728 Pup	08 03 18.2 -25 30 06	RRC	V1557 Sco	16 21 42.4 -34 48 37	M
V0729 Pup	08 05 11.0 -34 21 37	DCEP	V1558 Sco	16 22 43.5 -36 23 58	M
V0730 Pup	08 10 24.8 -38 28 25	DCEP	V1559 Sco	16 23 41.3 -31 39 00	M
V0731 Pup	08 10 25.9 -32 31 17	DCEP	V1560 Sco	16 24 18.1 -41 58 09	M
V0732 Pup	08 11 32.1 -28 21 18	RR(B)	V1561 Sco	16 24 18.4 -29 47 42	SRB
V0733 Pup	08 18 07.0 -22 14 08	DSCT	V1562 Sco	16 24 21.7 -32 01 57	M
V0734 Pup	08 18 22.7 -36 40 38	EW	V1563 Sco	16 24 29.1 -37 18 41	M
V0735 Pup	08 22 06.4 -12 02 48	EA	V1564 Sco	16 26 26.4 -34 35 53	M
DU Pyx	08 28 58.5 -36 13 55	DCEP	V1565 Sco	16 26 30.5 -29 07 29	M
DV Pyx	08 29 24.4 -36 37 02	M	V1566 Sco	16 26 39.4 -31 14 37	M
DW Pyx	08 32 19.5 -31 07 04	M	V1567 Sco	16 28 19.9 -30 28 06	SRB
DX Pyx	08 34 26.1 -35 59 07	DCEP	V1568 Sco	16 29 26.4 -30 01 32	SR
DY Pyx	08 34 47.1 -28 35 28	M	V1569 Sco	16 30 54.2 -30 56 25	SR
DZ Pyx	08 47 56.0 -20 25 33	BY	V1570 Sco	16 31 28.8 -32 02 35	M
EE Pyx	08 50 19.5 -28 56 39	RS	V1571 Sco	16 32 05.8 -34 39 21	M
EF Pyx	08 58 16.3 -30 22 02	SR	V1572 Sco	16 33 53.7 -33 56 18	M
EG Pyx	09 21 25.2 -36 28 15	RRAB	V1573 Sco	16 34 17.9 -30 44 52	EW
WZ Ret	03 27 39.7 -58 09 50	RS	V1574 Sco	16 35 27.2 -32 09 36	M
XX Ret	03 31 48.9 -63 31 54	BY	V1575 Sco	16 36 52.4 -34 50 20	M
XY Ret	04 00 37.3 -60 13 59	RS	V1576 Sco	16 36 56.7 -30 56 59	SR
XZ Ret	04 11 55.7 -58 01 47	RS	V1577 Sco	16 37 18.8 -30 18 50	M
YY Ret	04 33 56.5 -61 29 17	RS	V1578 Sco	16 37 33.3 -36 19 27	SR
V5667 Sgr	18 14 25.1 -25 54 35	N	V1579 Sco	16 38 20.0 -30 15 43	SR
V5666 Sgr	18 25 08.8 -22 36 03	NB	V1580 Sco	16 38 26.8 -29 40 11	LB
V5668 Sgr	18 36 56.8 -28 55 40	N	V1581 Sco	16 38 39.2 -30 59 23	M
CY Scl	00 01 57.8 -36 40 43	RRAB	V1582 Sco	16 40 16.4 -26 10 05	M
CZ Scl	00 06 04.0 -29 37 42	EA	V1583 Sco	16 40 34.0 -44 57 56	EB
DD Scl	00 09 44.1 -33 59 21	RRAB	V1584 Sco	16 40 40.2 -34 50 56	M:
DE Scl	00 13 24.4 -28 32 12	RR(B)	V1585 Sco	16 40 53.2 -44 28 23	EA
DF Scl	00 15 41.8 -32 39 55	SR	V1586 Sco	16 40 59.1 -34 21 08	M

Table 1 (continued)

Name	R.A., Decl., 2000.0	Type	Name	R.A., Decl., 2000.0	Type
	h m s o ' "			h m s o ' "	
V1587 Sco	16 41 26.7 -44 23 32	EA	V0573 Ser	15 59 29.8 +02 52 21	EW
V1588 Sco	16 42 54.0 -44 16 15	EB:	V0574 Ser	16 01 28.5 +03 34 26	EW
V1589 Sco	16 43 51.9 -44 28 10	EA	V0575 Ser	16 01 39.9 +03 25 59	RR(B)
V1590 Sco	16 46 26.4 -31 45 42	SR	V0576 Ser	16 04 14.5 +03 04 59	EW
V1591 Sco	16 47 08.4 -31 20 16	SR	V0577 Ser	16 05 09.3 +05 55 23	EW
V1592 Sco	16 48 16.9 -40 37 25	LB	V0578 Ser	16 07 22.0 +10 29 40	EW
V1593 Sco	16 49 00.8 -42 43 42	EA	V0579 Ser	16 11 04.3 +03 28 53	RR(B)
V1594 Sco	16 49 06.3 -33 01 39	SRB	V0580 Ser	16 12 32.5 -00 46 28	SR
V1595 Sco	16 49 44.5 -36 24 22	RS	V0581 Ser	16 12 53.6 -02 20 42	EB:
V1596 Sco	16 49 54.5 -29 34 39	EA	V0582 Ser	16 13 52.4 -00 43 09	EB
V1597 Sco	16 49 56.8 -30 27 00	SRA	V0583 Ser	16 14 34.7 -01 24 30	SRB
V1598 Sco	16 55 42.0 -38 34 39	RRC	V0584 Ser	16 15 06.8 +01 00 23	EW
V1599 Sco	16 58 53.2 -40 28 00	EW	V0585 Ser	16 15 47.6 -02 23 32	LB
V1600 Sco	17 00 42.8 -44 11 58	RRAB	V0586 Ser	16 16 55.4 -00 50 43	SRB
V1601 Sco	17 00 45.9 -44 10 15	EA	V0587 Ser	16 18 40.4 -01 19 14	RRC
V1602 Sco	17 01 06.3 -44 07 44	EA	V0588 Ser	16 19 56.9 -02 18 10	EW
V1603 Sco	17 01 44.6 -42 15 59	EB	V0589 Ser	16 21 58.4 +02 44 27	RRC
V1604 Sco	17 02 06.1 -32 07 04	SRB	V0590 Ser	17 18 50.3 -15 00 41	M
V1605 Sco	17 02 21.3 -33 00 05	M	V0591 Ser	17 19 40.6 -15 11 48	SRB
V1606 Sco	17 02 39.1 -44 18 23	EA	V0592 Ser	17 21 10.2 -13 30 09	M
V1535 Sco	17 03 26.2 -35 04 18	NA:	V0593 Ser	17 21 15.1 -14 38 03	M
V1607 Sco	17 03 28.4 -37 09 48	SRD	V0594 Ser	17 21 22.5 -16 00 16	M
V1608 Sco	17 04 35.4 -44 24 42	RRAB	V0595 Ser	17 21 37.6 -14 03 38	SRA
V1609 Sco	17 04 45.6 -33 12 08	SRA	V0596 Ser	17 24 58.1 -10 29 22	SRB
V1610 Sco	17 04 47.7 -41 42 48	SRB	V0597 Ser	17 29 09.8 -16 00 06	LB
V1611 Sco	17 05 24.5 -38 47 01	EA	V0556 Ser	18 09 03.4 -11 12 34	N
V1612 Sco	17 06 36.9 -39 15 44	EW	BU Sex	10 05 12.1 +05 51 31	EW
V1613 Sco	17 07 11.4 -39 06 46	LB	BV Sex	10 20 40.0 +02 20 40	EW
V1614 Sco	17 09 42.7 -32 48 22	LB	BW Sex	10 21 57.8 -03 43 41	EA
V1615 Sco	17 10 09.6 -43 04 00	SRB	BX Sex	10 22 17.6 -06 37 08	EA
V1616 Sco	17 12 37.5 -39 31 01	RV:	BY Sex	10 30 08.3 +03 36 08	RR(B)
V1617 Sco	17 12 59.3 -38 02 59	SRB	BZ Sex	10 30 19.0 +02 39 30	EW
V1618 Sco	17 14 22.0 -38 08 54	EB	CC Sex	10 32 27.5 -06 47 35	EA
V1534 Sco	17 15 46.9 -31 28 30	ZAND:	CD Sex	10 39 22.7 +01 35 35	EW
V1619 Sco	17 20 35.5 -38 28 17	SRB	CE Sex	10 43 19.0 -02 45 57	EA
V1620 Sco	17 21 09.1 -39 42 10	SRB	CF Sex	10 47 48.7 -03 08 43	RRC
V1621 Sco	17 26 55.9 -31 05 30	LB	CG Sex	10 49 02.6 +01 05 00	RRAB
V1533 Sco	17 33 59.5 -36 06 21	NA	V1375 Tau	03 26 12.2 +09 49 07	EW
V0557 Ser	15 14 35.4 -00 30 00	RRAB	V1376 Tau	03 31 08.4 +07 13 25	BY:
V0558 Ser	15 18 23.6 +00 21 22	RRAB	V1377 Tau	03 39 59.1 +03 14 30	EW
V0559 Ser	15 24 30.2 +20 14 29	RRC	V1378 Tau	03 44 18.7 +14 39 20	EW
V0560 Ser	15 25 47.1 +00 24 10	RRC	V1379 Tau	03 45 34.8 +19 26 18	EW
V0561 Ser	15 26 52.7 -00 53 12	RS	V1380 Tau	03 47 29.9 +23 33 15	UV:
V0562 Ser	15 31 13.0 +17 07 33	EA	V1381 Tau	03 51 39.6 +14 47 48	RS
V0563 Ser	15 34 43.3 -00 29 38	RRAB	V1382 Tau	03 51 57.0 +09 41 29	EW
V0564 Ser	15 35 03.0 +00 14 22	RRC	V1383 Tau	03 52 04.0 +14 17 15	EA:
V0565 Ser	15 35 18.0 +00 14 05	RRAB:	V1384 Tau	03 54 07.3 +07 59 15	DSCT
V0566 Ser	15 39 38.0 +01 11 24	RRAB	V1385 Tau	03 54 25.2 +12 04 08	EW
V0567 Ser	15 41 22.2 -00 23 17	EA	V1386 Tau	03 55 46.3 +07 08 16	EW
V0568 Ser	15 44 49.5 +03 42 54	EW	V1387 Tau	04 00 28.0 +04 21 44	EW
V0569 Ser	15 45 04.3 +17 36 44	RRAB	V1388 Tau	04 04 30.0 +09 35 06	EW
V0570 Ser	15 48 18.6 +08 59 04	EW	V1389 Tau	04 06 59.8 +00 52 44	UGSU
V0571 Ser	15 58 32.5 +18 58 56	EW	V1390 Tau	04 15 53.4 +30 41 27	EW
V0572 Ser	15 59 12.6 +23 45 04	EW	V1391 Tau	04 19 55.8 +01 49 28	EW

Table 1 (continued)

Name	R.A., Decl., 2000.0	Type	Name	R.A., Decl., 2000.0	Type
	h m s o ' "			h m s o ' "	
V1392 Tau	04 26 05.9 +01 26 26	DSCT	V0373 UMa	09 32 40.7 +42 21 08	RRC
V1393 Tau	04 29 04.0 +14 15 46	EW	V0374 UMa	10 22 34.3 +42 37 00	GDOR:
V1394 Tau	04 30 30.5 +19 38 13	EA	V0375 UMa	10 26 37.0 +47 54 27	UGSU
V1395 Tau	04 34 13.8 +28 11 37	EA	V0376 UMa	10 34 18.0 +41 01 04	RS:
V1396 Tau	04 35 24.0 +19 08 20	EW	V0377 UMa	10 50 32.9 +42 08 29	EW
V1397 Tau	04 46 59.9 +22 16 04	EW	V0378 UMa	10 55 20.0 +38 30 39	RRC
V1398 Tau	04 47 04.6 +22 42 00	EA	V0379 UMa	10 57 43.6 +38 46 48	RR(B)
V1399 Tau	04 47 14.7 +22 12 37	EW	V0380 UMa	10 59 57.2 +37 50 20	RR(B)
V1400 Tau	04 47 49.1 +23 13 43	EW	V0381 UMa	11 00 21.5 +36 03 20	RRC
V1401 Tau	04 47 49.8 +23 02 03	BY	V0382 UMa	11 02 31.7 +42 30 40	CEP:
V1402 Tau	04 47 56.3 +23 01 58	EW	V0383 UMa	11 03 08.4 +36 24 02	RRAB
V1403 Tau	04 48 35.8 +22 47 04	EW	V0384 UMa	11 03 08.9 +37 47 49	RRC:
V1404 Tau	04 49 30.6 +22 40 00	EB	V0385 UMa	11 03 30.0 +36 22 47	EW
V1405 Tau	04 49 42.1 +22 50 53	EW	V0386 UMa	11 04 29.2 +38 29 20	EW
V1406 Tau	04 57 44.4 +21 09 52	EB	V0387 UMa	11 05 22.3 +44 27 53	LB:
V1407 Tau	05 20 59.6 +24 46 05	BY	V0388 UMa	11 05 45.9 +36 15 55	EW
V1408 Tau	05 25 05.4 +19 16 39	EW	V0389 UMa	11 10 21.8 +35 46 50	RR(B)
V1409 Tau	05 32 22.3 +25 21 08	EW	V0390 UMa	11 10 26.9 +36 32 44	EA
V1410 Tau	05 41 43.8 +26 06 41	EW	V0391 UMa	11 12 25.6 +39 50 56	RS
V1411 Tau	05 44 32.0 +13 05 36	EW	V0392 UMa	11 12 46.9 +32 46 39	EW
V1412 Tau	05 55 31.8 +28 21 28	EW	V0393 UMa	11 12 59.4 +34 26 08	EW
V1413 Tau	05 56 35.9 +28 20 35	EB	V0394 UMa	11 13 30.0 +35 34 35	RRAB:
V1414 Tau	05 57 46.1 +28 12 45	RRC:	V0395 UMa	11 14 03.8 +31 24 56	EW
V1415 Tau	05 58 54.4 +28 20 26	EA	V0396 UMa	11 20 42.7 +34 47 12	RRC
V1416 Tau	05 59 20.9 +28 23 34	DSCT	V0397 UMa	11 35 25.9 +30 43 18	RRC
V0346 TrA	15 26 49.2 -65 53 36	RS	V0398 UMa	11 48 42.1 +54 43 08	DSCT
V0347 TrA	15 38 30.2 -69 06 25	RRAB	V0399 UMa	11 55 11.3 +46 28 11	DSCTC:
V0348 TrA	15 44 58.7 -62 36 56	DSCT	V0400 UMa	12 53 11.9 +52 58 01	EW
V0349 TrA	15 48 00.5 -68 40 56	M	V0401 UMa	13 00 25.7 +53 03 29	EW
V0350 TrA	15 59 58.0 -64 33 59	RS	V0402 UMa	13 00 51.6 +53 59 56	EW
V0351 TrA	16 09 51.2 -62 12 02	SR	V0403 UMa	13 01 59.4 +54 04 59	EA:
V0352 TrA	16 10 15.0 -66 46 56	M	V0404 UMa	13 08 30.1 +53 17 33	EA
V0353 TrA	16 16 28.4 -60 58 26	SRB	V0405 UMa	13 11 04.7 +54 32 26	RRAB
V0354 TrA	16 16 55.1 -69 56 41	SRA	V0406 UMa	13 11 23.1 +53 17 29	RRAB
V0355 TrA	16 17 32.6 -68 48 30	M	V0407 UMa	13 11 45.2 +52 52 09	RRAB
V0356 TrA	16 20 57.8 -67 11 33	SR	V0408 UMa	13 12 20.8 +53 41 40	RRAB
V0357 TrA	16 25 38.6 -61 48 36	BY	V0409 UMa	13 17 47.4 +53 41 29	RRAB
V0358 TrA	16 32 44.9 -65 34 27	M	V0410 UMa	13 18 51.4 +52 45 42	EW
V0359 TrA	16 36 36.9 -70 09 02	M	V0411 UMa	13 22 53.6 +54 25 47	BY:
V0360 TrA	16 43 36.8 -67 03 34	M	V0412 UMa	13 23 48.7 +54 28 28	L:
V0361 TrA	17 05 42.5 -67 42 41	BY	V0413 UMa	13 26 22.5 +54 32 20	RS
CV Tri	01 42 10.3 +33 17 42	EW	V0414 UMa	13 29 05.2 +52 36 42	EW
CW Tri	01 44 39.4 +33 13 44	SR	V0415 UMa	13 29 14.2 +53 34 47	EA
CX Tri	01 53 47.2 +30 38 44	UG	V0416 UMa	13 30 50.8 +54 07 46	DSCT
CY Tri	02 06 40.2 +33 43 29	EW	V0417 UMa	13 32 24.1 +53 07 56	EA
CZ Tri	02 07 44.2 +30 42 34	EW	V0418 UMa	13 34 14.7 +53 34 13	RRC
DD Tri	02 12 05.5 +30 36 16	BY	V0419 UMa	13 35 32.9 +51 24 36	EW
DE Tri	02 19 53.9 +33 17 01	BY	V0420 UMa	13 35 52.5 +53 31 24	BY
DF Tri	02 33 17.2 +32 04 31	EW	V0421 UMa	13 36 31.0 +53 35 38	EW
EW Tuc	00 28 10.8 -59 19 21	EA	V0422 UMa	13 40 17.2 +51 08 57	EW
V0369 UMa	08 35 50.5 +48 00 52	BY:	V0423 UMa	13 47 09.2 +52 59 21	EW
V0370 UMa	08 40 06.7 +50 18 25	EW	V0424 UMa	13 49 24.9 +53 01 14	EW
V0371 UMa	08 43 37.7 +46 58 24	EW	V0425 UMa	13 53 40.3 +54 16 01	RRAB
V0372 UMa	09 05 08.2 +52 03 51	SR	V0426 UMa	13 56 28.3 +54 29 22	RRAB

Table 1 (continued)

Name	R.A., Decl., 2000.0	Type	Name	R.A., Decl., 2000.0	Type
	h m s o ' "			h m s o ' "	
V0427 UMa	13 56 42.4 +61 30 24	UG	V0611 Vir	11 50 29.4 +05 00 33	EW
V0428 UMa	14 17 06.9 +58 57 33	EA	V0612 Vir	11 51 14.0 +00 45 06	RRAB
V0429 UMa	14 18 55.4 +62 02 58	RRAB	V0613 Vir	11 56 28.6 +01 12 24	RRC
V0430 UMa	14 26 25.7 +57 52 18	ZZ	V0614 Vir	11 56 32.2 +07 17 51	EA
AM UMi	13 10 58.0 +72 53 05	EW	V0615 Vir	12 00 47.9 +00 46 11	RRC
AN UMi	13 16 19.2 +73 28 22	EW	V0616 Vir	12 04 58.5 +06 55 37	EW
AO UMi	13 22 26.6 +70 20 29	RS	V0617 Vir	12 13 29.6 -01 01 52	RRAB
AP UMi	13 42 53.4 +70 01 50	EW	V0618 Vir	12 15 07.8 +00 49 30	RRC
AQ UMi	14 47 44.7 +68 38 37	EW	V0619 Vir	12 18 03.7 +00 14 49	RRAB
AR UMi	15 31 13.7 +70 26 51	EW	V0620 Vir	12 21 48.7 +09 42 03	EW
AS UMi	15 31 47.0 +73 08 11	EA	V0621 Vir	12 22 28.4 -01 02 16	RRAB
AT UMi	15 34 20.5 +72 25 27	EW	V0622 Vir	12 25 01.9 +01 14 08	RRAB
AU UMi	15 38 49.2 +69 00 50	RS	V0623 Vir	12 33 51.3 +01 57 05	EW
AV UMi	15 42 23.9 +72 30 17	SRD	V0624 Vir	12 40 08.6 +12 38 35	EW
AW UMi	15 43 46.3 +70 18 25	RS	V0625 Vir	12 40 46.6 +00 50 06	RRC
AX UMi	15 45 41.0 +80 36 10	EW	V0626 Vir	12 41 09.8 -05 05 01	EA
AY UMi	15 54 59.2 +72 57 36	ELL:	V0627 Vir	12 41 36.6 +01 13 06	RRAB
AZ UMi	16 08 19.4 +70 03 47	RS	V0628 Vir	12 42 18.0 +06 06 53	EW
BB UMi	16 11 41.4 +70 47 26	SR	V0629 Vir	12 43 58.6 +11 07 16	EA
V0519 Vel	08 34 34.0 -41 34 36	CEP(B)	V0630 Vir	12 49 29.0 +03 22 41	RR(B)
V0520 Vel	08 36 11.4 -39 03 42	DCEP:	V0631 Vir	12 57 36.0 +07 49 11	EW
V0521 Vel	08 39 08.6 -37 20 46	SR:	V0632 Vir	12 59 50.8 +01 02 29	EW
V0522 Vel	08 41 22.2 -43 52 56	EW	V0633 Vir	13 02 26.0 +07 18 34	EW
V0523 Vel	08 42 51.5 -49 25 51	EA	V0634 Vir	13 15 37.4 -01 12 30	EA
V0524 Vel	08 58 48.7 -53 03 25	BY	V0635 Vir	13 18 06.6 -00 33 00	RRC
V0525 Vel	08 59 52.4 -41 07 18	RS	V0636 Vir	13 21 30.8 +02 37 37	EA
V0526 Vel	09 03 13.3 -52 02 29	DSCT	V0637 Vir	13 23 12.6 +03 27 54	EW
V0527 Vel	09 04 35.7 -46 33 13	DCEP	V0638 Vir	13 25 47.0 +14 12 03	EA
V0528 Vel	09 04 46.0 -56 25 04	DSCT	V0639 Vir	13 26 19.0 +02 35 22	EW
V0529 Vel	09 08 22.1 -53 30 25	SR:	V0640 Vir	13 26 35.1 +00 20 35	RRAB
V0530 Vel	09 09 32.0 -53 59 16	DCEP	V0641 Vir	13 26 54.0 +07 39 32	EW
V0531 Vel	09 20 25.4 -56 47 45	M	V0642 Vir	13 30 24.9 +13 49 32	EA
V0532 Vel	09 22 49.8 -51 51 39	DCEP	V0643 Vir	13 30 30.3 -15 51 43	EA/RS
V0533 Vel	09 23 39.9 -47 11 14	RS	V0644 Vir	13 31 16.1 +03 34 07	RR(B)
V0534 Vel	09 25 06.2 -43 27 58	RS:	V0645 Vir	13 32 52.9 +00 46 23	RRAB
V0535 Vel	09 26 03.4 -53 03 51	M	V0646 Vir	13 45 13.9 +00 22 40	RRC
V0536 Vel	09 27 57.8 -52 18 58	DCEP	V0647 Vir	13 47 51.8 +07 00 47	EW
V0537 Vel	09 30 05.1 -51 37 25	DCEP	V0648 Vir	13 50 09.1 -00 34 14	RRAB
V0538 Vel	09 43 38.6 -44 37 11	M	V0649 Vir	13 52 31.8 +00 43 51	RRAB
V0539 Vel	09 44 09.4 -56 17 12	EA/NL:	V0650 Vir	13 57 40.2 -12 02 18	RRC
V0540 Vel	09 52 20.0 -54 14 30	DSCT	V0651 Vir	14 00 49.4 -21 40 10	RRAB
V0541 Vel	09 52 21.4 -43 29 40	SRB	V0652 Vir	14 01 39.0 +06 29 17	EW
V0542 Vel	09 56 19.6 -52 56 10	M	V0653 Vir	14 06 06.8 -00 33 57	RRAB
V0543 Vel	10 11 04.1 -51 19 47	BY	V0654 Vir	14 06 43.3 +02 27 15	EW
V0544 Vel	10 18 55.9 -48 25 14	RS	V0655 Vir	14 11 42.1 +00 22 49	RRAB
V0545 Vel	10 35 33.0 -53 52 28	RS	V0656 Vir	14 13 00.8 +06 56 26	EW
V0546 Vel	10 43 17.3 -53 33 17	M	V0657 Vir	14 18 07.4 +00 23 03	RRAB
V0547 Vel	10 44 47.9 -50 53 06	RS	V0658 Vir	14 18 12.2 +01 56 44	EW
V0548 Vel	10 57 19.1 -50 57 52	DSCT	V0659 Vir	14 20 22.4 +03 06 52	RR(B)
V0606 Vir	11 37 55.7 +04 10 19	EB	V0660 Vir	14 22 49.8 +06 41 12	BY
V0607 Vir	11 38 14.2 +01 05 29	RRAB	V0661 Vir	14 23 32.7 +01 59 51	EW
V0608 Vir	11 44 53.7 +00 09 57	EW	V0662 Vir	14 23 56.7 -00 34 28	RRC
V0609 Vir	11 45 42.2 +00 23 15	RRAB	V0663 Vir	14 36 14.8 +01 08 26	RRAB
V0610 Vir	11 47 05.9 +01 14 41	EW	V0664 Vir	14 37 13.4 +00 16 23	RRAB

Table 1 (continued)

Name	R.A., Decl., 2000.0 h m s o ' "	Type	Name	R.A., Decl., 2000.0 h m s o ' "	Type
V0665 Vir	14 41 54.4 -03 24 46	EW	V0669 Vir	15 05 45.4 -00 05 05	RRAB
V0666 Vir	14 46 18.5 +00 13 21	RRAB	V0670 Vir	15 09 16.8 +00 19 47	RRAB
V0667 Vir	14 56 16.1 +04 02 23	EW	AM Vol	07 54 08.7 -65 41 30	RS
V0668 Vir	15 03 37.3 -00 28 13	RRAB	AN Vol	08 27 09.6 -65 04 43	RS

Table 2. Novae and rare-type variables

GCVS	Nova name	GCVS	Nova name
V1830 Aql	Nova Aql 2013	V5666 Sgr	Nova Sgr 2014
V1369 Cen	Nova Cen 2013	V5667 Sgr	Nova Sgr 2015 No. 1
V0962 Cep	Nova Cep 2014	V5668 Sgr	Nova Sgr 2015 No. 2
V2659 Cyg	Nova Cyg 2014	V1533 Sco	Nova Sco 2013
V0339 Del	Nova Del 2013	V1534 Sco	Nova Sco 2014 (type ZAND:)
V0960 Mon	(Type FU)	V1535 Sco	Nova Sco 2015
V2944 Oph	Nova Oph 2015 No. 1	V0556 Ser	Nova Ser 2013

COMMISSIONS 27 AND 42 OF THE IAU
INFORMATION BULLETIN ON VARIABLE STARS

Number 6152

Konkoly Observatory
Budapest
27 October 2015

HU ISSN 0374 – 0676

BAV-RESULTS OF OBSERVATIONS - PHOTOELECTRIC MINIMA OF SELECTED ECLIPSING BINARIES AND MAXIMA OF PULSATING STARS

(BAV MITTEILUNGEN NO. 239)

HÜBSCHER, JOACHIM

Bundesdeutsche Arbeitsgemeinschaft für Veränderliche Sterne e.V. (BAV), Munsterdamm 90, 12169 Berlin, Germany, www.bav-astro.de, publikat@bav-astro.de

In this 81st compilation of BAV results, photoelectric observations obtained mostly in the years 2014 ans 2015 are presented on 512 variable stars giving 838 minima on eclipsing binaries and maxima on pulsating stars. All moments of minima and maxima are heliocentric UTC. The errors are tabulated in column "±". All information about photometers and filters are specified in the columns "Fil" and "Rem". The observations were made at private observatories. The photoelectric measurements and all the light curves with evaluations can be obtained from the office of the BAV for inspection.

Please use the following link for an easy access to all the publications of the BAV including the "Lichtenknecker Database of the BAV": `http://www.bav-astro.de/sfs`.

Table 1: Times of minima of eclipsing binaries

Variable	HJD 24.....	±	Obs	Fil	n	Rem
TW And	56950.3048	0.0060	AG	-I	59	89)
AA And	56928.4110	0.0035	AG	-I	48	89)
	56943.3719	0.0059	AG	-I	39	89)
AP And	56965.2623	0.0029	AG	-I	50	89)
BD And	56924.3528	0.0014	JU	o	70	90)
BX And	56940.4178	0.0117	AG	-I	47	89)
DS And	56934.3374	0.0073	AG	-I	47	89)
GZ And	56924.3860	0.0026	AG	-I	44	89)
	56924.5371	0.0036	AG	-I	44	89)
LM And	56924.4168	0.0082	AG	-I	44	89)
LO And	56916.4148	0.0015	AG	-I	28	89)
	56933.3444	0.0023	AG	-I	47	89)
	56933.5330	0.0014	AG	-I	47	89)
QW And	56917.4619	0.0002	MS FR	o	350	97)
	56983.3729	0.0003	MS FR	o	56	97)
QX And	56934.3783	0.0173	AG	-I	47	89)
	56934.5858	0.0065	AG	-I	47	89)
V355 And	56928.5169	0.0033	AG	-I	51	89)
V363 And	56918.4102	0.0068	AG	-I	42	89)
V372 And	56924.4840	0.0048	AG	-I	44	89)
V376 And	56965.4905	0.0155	AG	-I	60	89)
V392 And	56908.5851	0.0041	AG	-I	45	89)
V404 And	56905.3573	0.0024	AG	-I	40	89)
V425 And	56963.3123	0.0001	MS FR	o	81	97)
V440 And	56986.2883	0.0001	MS FR	o	49	97)
V441 And	56949.3302	0.0001	MS FR	o	64	97)

Table 1: cont.

Variable	HJD 24.....	±	Obs	Fil	n	Rem
V449 And	56932.3542	0.0001	MS FR	o	57	97)
V490 And	56986.2807	0.0007	MS FR	o	45	97)
V525 And	56924.4139	0.0109	AG	-I	44	89)
V527 And	56924.3544	0.0013	AG	-I	50	89)
V530 And	56924.4424	0.0053	AG	-I	44	89)
V543 And	56928.2888	0.0015	AG	-I	51	89)
V547 And	56934.4863	0.0097	AG	-I	47	89)
V566 And	56955.3134	0.0016	AG	-I	29	89)
V571 And	56963.4038	0.0015	AG	-I	40	89)
V575 And	56963.4878	0.0062	AG	-I	39	89)
V613 And	56928.4262	0.0048	AG	-I	49	89)
	56943.4320	0.0034	AG	-I	39	89)
	56960.3118	0.0063	AG	-I	33	89)
V662 And	56933.3781	0.0016	AG	-I	47	89)
V683 And	56908.5605	0.0056	AG	-I	45	89)
V707 And	56928.6215	0.0044	AG	-I	51	89)
	56949.3318	0.0018	AG	-I	37	89)
V712 And	56916.4882	0.0070	AG	-I	28	89)
	56924.3910	0.0042	AG	-I	43	89)
	56924.5716	0.0050	AG	-I	43	89)
	56928.4299	0.0053	AG	-I	51	89)
	56928.6108	0.0053	AG	-I	51	89)
	56940.3586	0.0046	AG	-I	41	89)
	56940.5433	0.0053	AG	-I	41	89)
	56949.3562	0.0045	AG	-I	37	89)
	56949.5417	0.0017	AG	-I	37	89)
CD Aqr	56918.4162	0.0141	AG	-I	29	89)
V417 Aql	56841.4861	0.0012	QU	BVIc	30	91) 2)
	56842.4116	0.0010	QU	BVIc	25	91) 2)
	56854.4462	0.0010	QU	BVIc	17	91) 2)
	56857.4095	0.0006	QU	BIc	46	91) 2)
	56924.4351	0.0007	QU	B	95	91) 2)
	56928.3236	0.0007	QU	B	95	91) 2)
	56929.4349	0.0007	QU	Ic	76	91) 2)
V640 Aql	56814.4677	0.0001	MS FR	o	44	97)
V1817 Aql	56918.4586	0.0040	AG	-I	27	89)
RX Ari	56978.2404	0.0030	AG	-I	42	89)
BN Ari	56978.3105	0.0008	AG	-I	48	89)
	56978.4590	0.0006	AG	-I	48	89)
BO Ari	56978.3850	0.0014	AG	-I	48	89)
	56978.5427	0.0015	AG	-I	46	89)
ZZ Aur	56987.4625	0.0005	MS FR	o	46	97)
	57060.5071	0.0010	AG	-I	35	89)
GX Aur	56918.5337	0.0005	MS FR	o	109	97)
HS Aur	57069.4153	0.0020	AG	-I	24	89)
II Aur	56949.4819	0.0002	MS FR	o	96	97)
IU Aur	57042.2883	0.0004	AG	-I	32	89)
KU Aur	57076.3951	0.0004	JU	o	80	90)
V364 Aur	56929.6264	0.0004	MS FR	o	61	97)
V404 Aur	56691.2689	0.0002	MS FR	o	34	97)
V432 Aur	56628.5648	0.0060	BRW	V	554	91)
V455 Aur	57057.5485	0.0018	AG	-I	48	89)
V459 Aur	57042.3051	0.0012	AG	-I	37	89)
V523 Aur	56984.5877	0.0002	MS FR	o	43	97)
V591 Aur	57060.3663	0.0074	AG	-I	28	89)
V610 Aur	57057.3438	0.0023	AG	-I	44	89)
V620 Aur	57016.4170	0.0003	MS FR	o	49	97)
V641 Aur	57062.3567	0.0009	JU	o	42	90)
FY Boo	56729.4802	0.0001	MS FR	o	53	97)
PY Boo	57066.7037	0.0001	MS FR	o	79	97)
WW Cam	56943.4469	0.0043	AG	-I	48	89)
CV Cam	56978.2631	0.0055	AG	-I	47	89)
DN Cam	56950.3295	0.0054	AG	-I	61	89)
	56950.5803	0.0047	AG	-I	61	89)
NX Cam	56950.3243	0.0096	AG	-I	63	89)
	56950.6136	0.0070	AG	-I	63	89)
OO Cam	56949.2864	0.0029	AG	-I	46	89)
V366 Cam	56950.3560	0.0197	AG	-I	58	89)
V382 Cam	56950.4368	0.0004	AG	-I	57	89)
TX Cnc	57069.3648	0.0011	AG	-I	26	89)
WW Cnc	57035.6867	0.0004	AG	-I	51	89)

Table 1: cont.

Variable	HJD 24.....	±	Obs	Fil	n	Rem
WX Cnc	57057.4336	0.0055	AG	-I	55	89)
IN Cnc	57074.4786	0.0004	AG	-I	57	89)
IO Cnc	57074.4373	0.0016	AG	-I	57	89)
	57074.6089	0.0008	AG	-I	57	89)
IQ Cnc	57074.4363	0.0038	AG	-I	65	89)
LU Cnc	57074.3819	0.0027	AG	-I	66	89)
	57074.5806	0.0017	AG	-I	66	89)
BI CVn	57056.6188	0.0052	AG	-I	73	89)
DR CVn	56728.3209	0.0003	MS FR	o	62	97)
DX CVn	55943.4611	0.0005	MS FR	o	55	94)
	56729.3394	0.0002	MS FR	o	52	97)
GG CVn	57069.4820	0.0002	MS FR	o	75	97)
CM CMa	57000.0486	0.0010	MS FR	V	79	84)
UZ CMi	57074.3264	0.0010	AG	-I	43	89)
XZ CMi	57074.3908	0.0011	AG	-I	45	89)
YY CMi	57074.3107	0.0032	AG	-I	41	89)
AC CMi	57069.3172	0.0025	AG	-I	26	89)
BB CMi	57074.4305	0.0100	AG	-I	45	89)
BF CMi	57074.3312	0.0093	AG	-I	43	89)
BH CMi	57074.4613	0.0075	AG	-I	41	89)
CZ CMi	57061.2977	0.0038	AG	-I	32	89)
DW CMi	56354.4143	0.0003	AG	-I	17	89)
	56713.3313	0.0008	AG	-I	33	89)
	56713.4843	0.0005	AG	-I	33	89)
	56726.4008	0.0013	AG	-I	29	89)
RZ Cas	57061.6567	0.0002	KBL	V	44	95)
TV Cas	56663.4359	0.0030	BRW	V	688	91)
	56924.4508	0.0025	AG	-I	44	89)
TW Cas	56621.5627	0.0060	BRW	V	527	91)
	56924.3763	0.0022	AG	-I	44	89)
	57074.3520	0.0035	JU	o	50	90)
TX Cas	56933.5405	0.0185	AG	-I	51	89)
XX Cas	56924.3675	0.0014	AG	-I	45	89)
ZZ Cas	56905.3482	0.0037	AG	-I	40	89)
	56928.3518	0.0074	AG	-I	51	89)
AE Cas	56949.5505	0.0003	SCI	o	62	90)
BS Cas	56905.3932	0.0013	AG	-I	40	89)
	56905.6131	0.0006	AG	-I	40	89)
DN Cas	56934.3399	0.0055	AG	-I	47	89)
DO Cas	56933.2902	0.0002	AG	-I	50	89)
EG Cas	56950.4442	0.0029	AG	-I	60	89)
EP Cas	56950.4965	0.0013	AG	-I	60	89)
ES Cas	56933.3790	0.0002	MS FR	o	66	97)
EY Cas	56950.2919	0.0015	AG	-I	59	89)
	56950.5339	0.0029	AG	-I	59	89)
GG Cas	56905.3745	0.0095	AG	-I	38	89)
IL Cas	56916.4821	0.0109	AG	-I	25	89)
IQ Cas	56918.3959	0.0002	MS FR	o	293	97)
IR Cas	56918.4784	0.0011	AG	-I	40	89)
KR Cas	56930.4121	0.0129	AG	-I	66	89)
KT Cas	56955.5956	0.0023	AG	-I	61	89)
LR Cas	56908.4047	0.0030	AG	-I	45	89)
MN Cas	56908.5443	0.0013	AG	-I	44	89)
MT Cas	56950.2602	0.0013	AG	-I	59	89)
	56950.4193	0.0015	AG	-I	59	89)
	56950.5733	0.0005	AG	-I	59	89)
OR Cas	56928.4519	0.0028	AG	-I	51	89)
OX Cas	56916.4223	0.0059	AG	-I	28	89)
PV Cas	56908.5063	0.0042	AG	-I	45	89)
QQ Cas	55155.3169	0.0004	RAT RCR	-U-I	165	86)
V345 Cas	56933.5529	0.0003	SCI	o	77	90)
V368 Cas	56978.4254	0.0152	AG	-I	47	89)
V374 Cas	56950.4984	0.0041	AG	-I	59	89)
V375 Cas	56569.3691	0.0060	BRW	V	222	91)
	56907.5165	0.0082	AG	-I	53	89)
V380 Cas	56933.2915	0.0033	AG	-I	52	89)
V381 Cas	56907.5781	0.0047	AG	-I	56	89)
	56970.4343	0.0030	BRW	V	206	91)
V387 Cas	56955.3523	0.0009	AG	-I	27	89)
V389 Cas	56940.5642	0.0059	AG	-I	47	89)
	56965.5118	0.0012	AG	-I	46	89)

Table 1: cont.

Variable	HJD 24.....	±	Obs	Fil	n	Rem
V459 Cas	56934.2993	0.0013	AG	-I	47	89)
	56955.5087	0.0001	AG	-I	53	89)
V520 Cas	56950.3899	0.0026	AG	-I	59	89)
	56950.6348	0.0026	AG	-I	59	89)
V523 Cas	56907.3605	0.0008	AG	-I	56	89)
	56907.4759	0.0008	AG	-I	56	89)
	56907.5923	0.0008	AG	-I	56	89)
V541 Cas	56940.5446	0.0044	AG	-I	44	89)
V544 Cas	56965.5377	0.0110	AG	-I	51	89)
V821 Cas	56908.5163	0.0042	AG	-I	45	89)
V860 Cas	56965.5116	0.0013	AG	-I	43	89)
V959 Cas	56950.2942	0.0032	AG	-I	59	89)
V1001 Cas	56965.5168	0.0051	AG	-I	44	89)
V1007 Cas	56965.5015	0.0012	AG	-I	50	89)
	56965.6686	0.0009	AG	-I	50	89)
V1010 Cas	56949.5416	0.0035	AG	-I	42	89)
V1014 Cas	56955.3364	0.0010	AG	-I	27	89)
V1018 Cas	56955.3637	0.0093	AG	-I	29	89)
V1025 Cas	56950.3517	0.0123	AG	-I	59	89)
V1030 Cas	56965.4688	0.0005	AG	-I	44	89)
	56965.6230	0.0018	AG	-I	44	89)
V1043 Cas	56965.4893	0.0019	AG	-I	43	89)
V1060 Cas	56949.5637	0.0054	AG	-I	42	89)
V1070 Cas	56928.4811	0.0029	AG	-I	51	89)
V1139 Cas	56955.3329	0.0007	AG	-I	30	89)
	56955.4840	0.0044	AG	-I	30	89)
V1175 Cas	56978.5299	0.0041	AG	-I	48	89)
WX Cep	56908.5072	0.0075	AG	-I	45	89)
WY Cep	56928.4401	0.0058	AG	-I	50	89)
	56930.3146	0.0050	AG	-I	66	89)
XX Cep	56907.4267	0.0032	AG	-I	54	89)
XZ Cep	56907.4769	0.0228	AG	-I	56	89)
	56930.4182	0.0239	AG	-I	66	89)
ZZ Cep	56928.4078	0.0022	AG	-I	51	89)
BE Cep	56949.3344	0.0016	AG	-I	44	89)
	56949.5455	0.0012	AG	-I	44	89)
CW Cep	56940.4460	0.0109	AG	-I	40	89)
EE Cep	56893.8764	0.0700	BRW	V	49	91)
EY Cep	56918.3843	0.0051	AG	-I	42	89)
GS Cep	56934.3765	0.0024	AG	-I	40	89)
KP Cep	56934.5889	0.0030	AG	-I	43	89)
NW Cep	56924.4639	0.0129	AG	-I	30	89)
V338 Cep	56907.3638	0.0004	AG	-I	50	89)
	56929.4570	0.0080	AG	-I	31	89)
V383 Cep	56929.3741	0.0130	AG	-I	30	89)
V397 Cep	56916.4322	0.0052	AG	-I	27	89)
	56965.3777	0.0011	AG	-I	53	89)
V833 Cep	56907.4304	0.0044	AG	-I	46	89)
V839 Cep	56928.4934	0.0037	AG	-I	37	89)
V868 Cep	56949.4854	0.0004	AG	-I	46	89)
V919 Cep	56943.3868	0.0074	AG	-I	37	89)
V927 Cep	56908.5210	0.0077	AG	-I	45	89)
V961 Cep	56978.3508	0.0081	AG	-I	43	89)
DG Com	56736.4790	0.0002	MS FR	o	33	97)
LL Com	57066.5373	0.0002	MS FR	o	53	97)
LO Com	56746.4202	0.0001	MS FR	o	46	97)
AV CrB	57069.6208	0.0001	MS FR	o	100	97)
WZ Cyg	56940.4363	0.0010	AG	-I	33	89)
BO Cyg	56932.3533	0.0001	SCI	o	52	90)
DL Cyg	56907.4779	0.0324	AG	-I	50	89)
DO Cyg	56934.5058	0.0035	AG	-I	42	89)
PW Cyg	56924.3893	0.0017	SCI	o	44	90)
	56929.4392	0.0007	SCI	o	43	90)
V366 Cyg	56940.4363	0.0071	AG	-I	27	89)
V370 Cyg	56730.6533	0.0010	MS FR	o	48	97)
	56918.4797	0.0007	AG	-I	61	89)
V388 Cyg	56918.5155	0.0044	AG	-I	35	89)
V401 Cyg	56905.5105	0.0031	AG	-I	32	89)
	56918.3284	0.0014	AG	-I	58	89)
	56929.4007	0.0007	AG	-I	36	89)
	56943.3871	0.0026	AG	-I	40	89)

Table 1: cont.

Variable	HJD 24.....	±	Obs	Fil	n	Rem
V442 Cyg	56918.4750	0.0026	AG	-I	36	89)
V477 Cyg	56929.3982	0.0040	AG	-I	30	89)
V478 Cyg	56910.3804	0.0002	SCI	o	137	90)
	56933.4402	0.0092	AG	-I	32	89)
V512 Cyg	56856.4971	0.0024	SCI	o	106	90)
V541 Cyg	56929.4809	0.0020	AG	-I	27	89)
V642 Cyg	56928.4091	0.0032	AG	-I	40	89)
V680 Cyg	56924.6020	0.0032	AG	-I	30	89)
V753 Cyg	56933.4238	0.0014	AG	-I	52	89)
V850 Cyg	56933.3557	0.0031	AG	-I	52	89)
V859 Cyg	56905.5315	0.0046	AG	-I	35	89)
V865 Cyg	56929.3267	0.0011	AG	-I	37	89)
	56930.4224	0.0007	AG	-I	35	89)
V866 Cyg	56929.4321	0.0117	AG	-I	35	89)
	56930.3228	0.0046	AG	-I	37	89)
V869 Cyg	56937.3139	0.0037	AG	-I	28	89)
V877 Cyg	56905.4827	0.0050	AG	-I	36	89)
	56950.4055	0.0017	FR	-I	66	89)
V884 Cyg	56930.4080	0.0014	AG	-I	38	89)
V885 Cyg	56937.3418	0.0151	AG	-I	29	89)
V909 Cyg	56937.2785	0.0049	AG	-I	29	89)
V912 Cyg	56937.3271	0.0015	AG	-I	34	89)
V931 Cyg	56943.4085	0.0014	AG	-I	40	89)
V934 Cyg	56831.4599	0.0032	SCI	o	61	90)
V941 Cyg	56929.4025	0.0057	AG	-I	38	89)
	56929.4038	0.0062	AG	-I	22	89)
V957 Cyg	56905.4512	0.0054	AG	-I	36	89)
V959 Cyg	56905.3899	0.0026	AG	-I	36	89)
V961 Cyg	56730.6275	0.0002	MS FR	o	48	97)
	56929.3128	0.0010	AG	-I	37	89)
V961 Cyg	56930.3314	0.0018	AG	-I	38	89)
V963 Cyg	56929.4359	0.0013	AG	-I	24	89)
	56929.4372	0.0009	AG	-I	38	89)
V965 Cyg	56905.4265	0.0002	AG	-I	33	89)
	56929.4389	0.0061	AG	-I	38	89)
V974 Cyg	56918.3686	0.0022	AG	-I	60	89)
V1117 Cyg	56905.5545	0.0055	AG	-I	35	89)
V1256 Cyg	56929.2648	0.0002	AG	-I	34	89)
V1401 Cyg	56924.4543	0.0042	AG	-I	30	89)
	56934.5177	0.0056	AG	-I	43	89)
V1411 Cyg	56928.6055	0.0018	AG	-I	40	89)
V1437 Cyg	56950.2854	0.0006	FR	-I	71	89)
	56984.3777	0.0018	FR	-I	33	89)
V1877 Cyg	56937.4254	0.0028	FR	-I	43	89)
V2080 Cyg	56823.5213	0.0008	SCI	o	157	90)
V2278 Cyg	56830.4980	0.0002	SCI	o	89	90)
	56855.4855	0.0002	SCI	o	65	90)
	56871.4085	0.0003	SCI	o	47	90)
	56921.3767	0.0002	SCI	o	36	90)
	56923.3705	0.0006	SCI	o	31	90)
	56931.3068	0.0003	SCI	o	48	90)
	56931.5525	0.0003	SCI	o	48	90)
	56933.3092	0.0021	AG	-I	52	89)
	56933.5323	0.0090	AG	-I	52	89)
	56935.2988	0.0003	SCI	o	32	90)
	56935.5047	0.0005	SCI	o	60	90)
V2280 Cyg	56933.2893	0.0035	AG	-I	52	89)
	56933.4657	0.0013	AG	-I	52	89)
V2282 Cyg	56933.3469	0.0009	AG	-I	52	89)
	56933.5140	0.0019	AG	-I	52	89)
	56934.3549	0.0014	JU	o	82	90)
V2363 Cyg	56933.3360	0.0018	AG	-I	52	89)
	56933.5145	0.0018	AG	-I	52	89)
V2364 Cyg	56933.4565	0.0016	AG	-I	52	89)
V2409 Cyg	56933.3185	0.0013	AG	-I	52	89)
	56933.4999	0.0017	AG	-I	52	89)
V2469 Cyg	56933.4043	0.0011	AG	-I	52	89)
V2509 Cyg	56905.4203	0.0011	AG	-I	34	89)
	56929.4265	0.0010	AG	-I	38	89)
	56930.4186	0.0016	AG	-I	37	89)
V2524 Cyg	56933.4513	0.0004	FR	-I	77	89)

Table 1: cont.

Variable	HJD 24.....	±	Obs	Fil	n	Rem
V2524 Cyg	56935.2564	0.0004	FR	-I	54	89)
V2546 Cyg	56918.3875	0.0054	AG	-I	35	89)
V2551 Cyg	56949.3011	0.0008	AG	-I	24	89)
	56949.4225	0.0022	AG	-I	24	89)
V2552 Cyg	56949.3038	0.0024	AG	-I	23	89)
	56949.4458	0.0006	AG	-I	23	89)
V2562 Cyg	56940.4584	0.0152	AG	-I	29	89)
V2646 Cyg	56924.4646	0.0002	AG	-I	30	89)
	56924.6362	0.0001	AG	-I	30	89)
DM Del	56905.3494	0.0075	AG	-I	39	89)
MR Del	56934.4117	0.0018	AG	-I	27	89)
EX Dra	56897.3473	0.0035	PGL	TG	124	98) 82)
	56927.3692	0.0035	PGL	TG	56	99)
MU Dra	56933.3947	0.0023	AG	-I	52	89)
	56933.5651	0.0028	AG	-I	52	89)
V415 Dra	56933.3084	0.0026	AG	-I	52	89)
	56933.5277	0.0039	AG	-I	52	89)
V422 Dra	56908.3708	0.0056	AG	-I	29	89)
SX Gem	57060.4712	0.0024	AG	-I	35	89)
AF Gem	57057.3074	0.0009	AG	-I	50	89)
AL Gem	57074.5012	0.0036	AG	-I	45	89)
AY Gem	57069.3448	0.0022	AG	-I	26	89)
EL Gem	57028.5425	0.0003	SCI	o	45	90)
EN Gem	57015.5651	0.0006	SCI	o	15	90)
GM Gem	56693.2993	0.0010	MS FR	o	50	97)
HR Gem	56964.6693	0.0022	AG	-I	41	89)
V382 Gem	57057.2825	0.0002	AG	-I	47	89)
V389 Gem	57057.3018	0.0014	AG	-I	55	89)
V396 Gem	57061.3983	0.0054	AG	-I	30	89)
V428 Gem	57057.4119	0.0009	AG	-I	56	89)
IT Her	56908.3343	0.0007	AG	-I	28	89)
	56908.5055	0.0060	AG	-I	28	89)
V643 Her	56908.3801	0.0013	AG	-I	28	89)
V732 Her	56827.4536	0.0002	SCI	o	45	90)
V865 Her	56728.5843	0.0018	MS FR	o	49	97)
V1032 Her	56712.6163	0.0012	MS FR	o	40	97)
V1045 Her	56713.5764	0.0002	MS FR	o	69	97)
V1065 Her	56746.5731	0.0002	MS FR	o	56	97)
RW Lac	56935.3184	0.0003	AG	-I	12	89)
SW Lac	56905.3956	0.0032	AG	-I	41	89)
	56905.5588	0.0017	AG	-I	41	89)
AG Lac	56928.4570	0.0038	AG	-I	40	89)
AI Lac	56949.4183	0.0005	AG	-I	46	89)
AU Lac	56928.4030	0.0014	AG	-I	40	89)
CO Lac	56949.3589	0.0008	JU	o	67	90)
CY Lac	56949.3046	0.0023	AG	-I	46	89)
DG Lac	56916.4991	0.0010	AG	-I	26	89)
EQ Lac	56928.5312	0.0026	AG	-I	40	89)
ES Lac	56916.3590	0.0002	AG	-I	34	89)
	56950.3291	0.0094	AG	-I	41	89)
	56965.4111	0.0040	AG	-I	31	89)
EY Lac	56949.3067	0.0020	AG	-I	46	89)
GX Lac	56924.4269	0.0082	AG	-I	39	89)
IL Lac	56924.4563	0.0036	AG	-I	32	89)
IM Lac	56949.4047	0.0017	AG	-I	46	89)
IU Lac	56934.5795	0.0016	AG	-I	43	89)
IZ Lac	56934.2955	0.0013	AG	-I	42	89)
	56949.4765	0.0043	AG	-I	46	89)
KS Lac	56928.4600	0.0003	AG	-I	39	89)
LY Lac	56928.3593	0.0019	AG	-I	40	89)
NS Lac	56897.4421	0.0003	MS FR	o	43	97)
NW Lac	56924.4873	0.0014	AG	-I	30	89)
PP Lac	56924.4232	0.0004	AG	-I	30	89)
	56924.6238	0.0014	AG	-I	30	89)
	56949.2947	0.0023	AG	-I	46	89)
	56949.4951	0.0017	AG	-I	46	89)
V339 Lac	56928.3855	0.0034	AG	-I	41	89)
V340 Lac	56934.5619	0.0028	AG	-I	43	89)
V344 Lac	56934.4433	0.0022	AG	-I	43	89)
	56934.6401	0.0002	AG	-I	43	89)
	56949.3483	0.0007	AG	-I	46	89)

Table 1: cont.

Variable	HJD 24.....	±	Obs	Fil	n	Rem
V344 Lac	56949.5454	0.0023	AG	-I	46	89)
V441 Lac	56934.2735	0.0009	AG	-I	43	89)
	56934.4287	0.0030	AG	-I	43	89)
	56934.5833	0.0022	AG	-I	43	89)
V474 Lac	56949.4576	0.0022	AG	-I	46	89)
UU Leo	57074.3680	0.0126	AG	-I	66	89)
VZ Leo	57074.5948	0.0049	AG	-I	66	89)
WZ Leo	57074.3255	0.0011	AG	-I	67	89)
GU Leo	57074.4157	0.0007	AG	-I	66	89)
	57074.5931	0.0008	AG	-I	66	89)
RT LMi	56746.3370	0.0001	MS FR	o	43	97)
VW LMi	57056.4780	0.0033	AG	-I	75	89)
	57056.7170	0.0010	AG	-I	75	89)
XX LMi	56745.3687	0.0004	MS FR	o	64	97)
SW Lyn	57057.3567	0.0072	AG	-I	54	89)
	57069.2710	0.0011	AG	-I	25	89)
SX Lyn	57056.5252	0.0150	AG	-I	59	89)
TY Lyn	57069.3504	0.0079	AG	-I	24	89)
UV Lyn	57061.3059	0.0018	AG	-I	34	89)
	57069.3961	0.0015	AG	-I	25	89)
CD Lyn	57061.3016	0.0019	JU	o	47	90)
	57070.4030	0.0060	BRW	V	212	91)
CN Lyn	57056.5812	0.0027	AG	-I	64	89)
	57057.5602	0.0051	AG	-I	52	89)
DZ Lyn	57035.4554	0.0023	AG	-I	49	89)
	57035.6444	0.0012	AG	-I	49	89)
	57057.5695	0.0063	AG	-I	54	89)
FI Lyn	57035.5145	0.0007	AG	-I	47	89)
	57035.7005	0.0003	AG	-I	47	89)
FN Lyn	57042.4241	0.0024	AG	-I	32	89)
AA Lyr	56908.3782	0.0040	AG	-I	30	89)
	56918.4627	0.0001	FR	-I	55	89)
DF Lyr	56908.4547	0.0046	AG	-I	29	89)
DT Lyr	56940.3122	0.0019	AG	-I	47	89)
	56943.4629	0.0012	AG	-I	36	89)
DU Lyr	56908.4601	0.0016	AG	-I	31	89)
ET Lyr	56918.5250	0.0067	AG	-I	59	89)
FL Lyr	56535.4735	0.0018	AG	-I	29	89)
KT Lyr	56770.5409	0.0030	MS FR	o	39	97)
LZ Lyr	56933.3640	0.0018	JU	o	72	90)
NV Lyr	56934.3638	0.0030	FR	-I	45	89)
NY Lyr	56934.2754	0.0003	FR	-I	118	89)
	56934.4976	0.0003	FR	-I	118	89)
OT Lyr	56072.5023	0.0093	AG	-I	24	89)
	56897.5191	0.0230	AG	-I	31	89)
	56964.210	0.005	AG	-I	106	89)
PV Lyr	56937.3492	0.0089	AG	-I	31	89)
	56943.3401	0.0067	AG	-I	40	89)
QU Lyr	56918.3956	0.0053	AG	-I	60	89)
V412 Lyr	56918.4255	0.0007	FR	-I	49	89)
V431 Lyr	56934.2896	0.0005	FR	-I	77	89)
	56934.5126	0.0025	FR	-I	77	89)
V507 Lyr	56736.6200	0.0006	MS FR	o	36	97)
V579 Lyr	56737.5602	0.0002	MS FR	o	65	97)
V580 Lyr	56783.4033	0.0025	MS FR	o	42	97)
VX Mon	56983.5690	0.0001	MS FR	o	51	97)
XZ Mon	57067.3634	0.0001	MS FR	o	56	97)
DQ Mon	57057.0128	0.0060	MS FR	V	37	84)
NS Mon	57061.2903	0.0010	AG	-I	30	89)
V448 Mon	57074.3203	0.0042	AG	-I	37	89)
V452 Mon	57011.5602	0.0016	MS FR	o	40	96)
V634 Mon	56963.6623	0.0007	MS FR	o	69	97)
V906 Mon	57061.3367	0.0050	AG	-I	30	89)
V910 Mon	57074.2678	0.0001	AG	-I	37	89)
V922 Mon	57074.4364	0.0022	AG	-I	44	89)
DX Ori	57015.5865	0.0024	MS FR	o	33	97)
FH Ori	57042.3011	0.0008	AG	-I	24	89)
FT Ori	57069.2731	0.0029	AG	-I	26	89)
V392 Ori	57042.4858	0.0065	AG	-I	34	89)
V2783 Ori	57074.4189	0.0049	AG	-I	37	89)
U Peg	56933.3539	0.0024	AG	-I	51	89)

Table 1: cont.

Variable	HJD 24.....	±	Obs	Fil	n	Rem
U Peg	56933.5422	0.0017	AG	-I	51	89)
UX Peg	56934.3389	0.0054	AG	-I	54	89)
VW Peg	56930.4484	0.0012	AG	-I	67	89)
DF Peg	56891.3667	0.0021	AG	-I	36	89)
DI Peg	56929.3667	0.0023	AG	-I	31	89)
	56930.4362	0.0034	AG	-I	65	89)
DM Peg	56934.3735	0.0121	AG	-I	45	89)
KW Peg	55879.2817	0.0019	BHE	-I	98	85)
V357 Peg	56905.4955	0.0035	AG	-I	40	89)
V404 Peg	56905.3447	0.0003	MS FR	o	28	97)
	56918.3404	0.0059	AG	-I	42	89)
	56918.5486	0.0045	AG	-I	42	89)
	56930.2874	0.0020	AG	-I	67	89)
	56930.4939	0.0013	AG	-I	67	89)
V407 Peg	56930.3776	0.0053	AG	-I	65	89)
RT Per	56943.6120	0.0007	AG	-I	47	89)
RV Per	56978.3598	0.0068	AG	-I	56	89)
AG Per	56934.4986	0.0001	SCI	o	149	90)
	57057.2676	0.0026	AG	-I	38	89)
BP Per	56957.4596	0.0008	SCI	o	110	90)
BR Per	56985.2808	0.0001	MS FR	o	47	97)
DM Per	56950.3106	0.0072	AG	-I	60	89)
HK Per	56984.2846	0.0003	MS FR	o	43	97)
IQ Per	56943.4332	0.0050	AG	-I	48	89)
	56949.4603	0.0081	AG	-I	44	89)
IZ Per	56905.4784	0.0068	AG	-I	40	89)
KL Per	56955.2943	0.0091	AG	-I	30	89)
KN Per	56989.4415	0.0070	BRW	V	202	91)
KR Per	57060.4507	0.0003	AG	-I	30	89)
MS Per	56928.5693	0.0014	MS FR	o	58	97)
V432 Per	56955.4287	0.0021	AG	-I	30	89)
	56965.5848	0.0017	AG	-I	62	89)
	56978.2362	0.0027	AG	-I	42	89)
	56978.4262	0.0025	AG	-I	42	89)
V450 Per	56963.4826	0.0015	AG	-I	40	89)
V505 Per	56934.4935	0.0026	AG	-I	47	89)
V725 Per	56924.5447	0.0084	AG	-I	44	89)
V789 Per	56963.4238	0.0076	AG	-I	41	89)
V871 Per	56940.3398	0.0083	AG	-I	45	89)
V873 Per	56955.3024	0.0015	AG	-I	28	89)
	56955.4502	0.0007	AG	-I	28	89)
	56963.4128	0.0008	AG	-I	37	89)
	56963.5595	0.0015	AG	-I	37	89)
V876 Per	56963.4147	0.0016	AG	-I	38	89)
	56963.5721	0.0004	AG	-I	38	89)
V881 Per	56978.4087	0.0030	AG	-I	45	89)
V887 Per	56965.6234	0.0062	AG	-I	62	89)
V959 Per	56978.4199	0.0017	AG	-I	37	89)
beta Per	57036.305	0.001	VLM	o	140	100)
	57059.243	0.001	VLM	o	250	100) 1)
SU Psc	56943.4667	0.0208	AG	-I	47	89)
DZ Psc	56949.3493	0.0015	AG	-I	45	89)
	56949.5326	0.0022	AG	-I	45	89)
HL Psc	56943.5585	0.0072	AG	-I	48	89)
	56949.4610	0.0084	AG	-I	46	89)
V384 Ser	56924.3124	0.0030	FR	-I	58	89)
V505 Ser	56924.3288	0.0030	FR	-I	46	89)
SV Tau	57061.3747	0.0023	AG	-I	30	89)
AL Tau	56932.5840	0.0002	SCI	o	69	90)
	56964.6263	0.0059	AG	-I	38	89)
AM Tau	57028.4123	0.0002	SCI	o	169	90)
GR Tau	57015.3660	0.0010	QU	V	156	91)
GW Tau	56924.5151	0.0001	SCI	o	143	90)
V781 Tau	56964.5848	0.0004	AG	-I	40	89)
V1260 Tau	56964.6589	0.0037	AG	-I	36	89)
V1374 Tau	56964.6651	0.0008	AG	-I	36	89)
V Tri	56943.5574	0.0052	AG	-I	48	89)
	56949.4112	0.0069	AG	-I	46	89)
X Tri	55856.3930	0.0012	AG	V	57	89)
	56949.3629	0.0018	AG	-I	44	89)
RS Tri	56949.4967	0.0023	AG	-I	46	89)

Table 1: cont.

Variable	HJD 24.....	±	Obs	Fil	n	Rem
RW Tri	55856.2675	0.0010	AG	-I	57	89)
	55856.5009	0.0010	AG	-I	57	89)
WW Tri	56963.5104	0.0017	AG	-I	40	89)
AV Tri	56955.3251	0.0064	AG	-I	29	89)
BC Tri	56949.3299	0.0109	AG	-I	45	89)
CD Tri	56963.4265	0.0020	AG	-I	39	89)
CU Tri	56948.4491	0.0028	MZ	-U-I	120	91)
	57028.3799	0.0030	MZ	-U-I	216	91)
W UMa	57056.4428	0.0014	AG	-I	75	89)
	57056.6092	0.0010	AG	-I	75	89)
VV UMa	57056.6893	0.0021	AG	-I	75	89)
ZZ UMa	57035.6959	0.0004	AG	-I	52	89)
AA UMa	57035.5262	0.0005	AG	-I	50	89)
QT UMa	57035.4491	0.0007	AG	-I	50	89)
	57035.6872	0.0002	AG	-I	50	89)
BP Vul	56929.3385	0.0023	AG	-I	31	89)
BQ Vul	56928.3854	0.0034	FR	-I	46	89)
EV Vul	56926.3425	0.0035	PGL	TG	97	99) 59)
	56926.3425	0.0035	PGL	TB	97	99) 59)
FM Vul	56937.4052	0.0019	AG	-I	33	89)
GI Vul	56905.3675	0.0015	AG	-I	34	89)
1SWASP J225840.47+343746.2	56918.4551	0.0131	AG	-I	42	89)
ASAS J003412+2052.4	56949.3736	0.0036	AG	-I	45	89)
	56949.5434	0.0040	AG	-I	45	89)
ASAS J072000+2543.7	57057.5484	0.0032	AG	-I	49	89)
ASAS J072125+2559.1	57057.4641	0.0031	AG	-I	55	89)
ASAS J194531+2821.4	56795.5271	0.0003	MS FR	o	58	97)
ASAS J210121+0447.9	56540.4244	0.0032	AG	-I	37	89)
CSS J002629.9+421231	56986.2608	0.0010	MS FR	o	67	97)
CSS J002641.1+415921	56986.2365	0.0002	MS FR	o	42	97)
CSS J031004.3+275152	57015.3179	0.0015	FR	-I	72	100)
	57015.4418	0.0011	FR	-I	72	100)
GSC 00163-01415	56990.5927	0.0029	MS FR	o	88	97)
GSC 00189-01660	57074.3955	0.0018	AG	-I	44	89)
GSC 00195-01613	55629.3294	0.0007	RAT RCR	-U-I	105	86)
GSC 00472-02473	56151.5505	0.0035	PGL	V	156	98) 27)
GSC 01337-01137	57069.2874	0.0046	AG	-I	26	89)
GSC 02656-04286	56905.5486	0.0007	AG	-I	34	89)
	56930.3163	0.0060	AG	-I	37	89)
GSC 03151-02485	56534.3789	0.0045	AG	-I	39	89)
GSC 03612-00014	56934.4524	0.0149	AG	-I	43	89)
GSC 03618-00162	56934.4009	0.0057	AG	-I	42	89)
	56934.5227	0.0034	AG	-I	42	89)
	56949.3460	0.0043	AG	-I	46	89)
	56949.4711	0.0047	AG	-I	46	89)
GSC 03618-00448	56934.5106	0.0042	AG	-I	42	89)
	56949.2951	0.0026	AG	-I	46	89)
	56949.5682	0.0046	AG	-I	45	89)
GSC 03619-00047	56924.6373	0.0013	AG	-I	30	89)
GSC 03619-00715	56934.5548	0.0084	AG	-I	41	89)
GSC 03627-00379	56907.5229	0.0240	AG	-I	59	89)
GSC 03688-01184	56955.3240	0.0072	AG	-I	24	89)
GSC 04009-00670	56950.3714	0.0141	AG	-I	59	89)
GSC 04046-00313	55880.5691	0.0002	RAT RCR	-U-I	350	86)
GSC 04049-00327	56949.4671	0.0044	AG	-I	46	89)
GSC 04635-00390	55615.5969	0.0001	RAT RCR	-U-I	270	86)
LINEAR 16156855	56924.3124	0.0013	FR	-I	49	89)
NSV 25911	56928.4766	0.0147	AG	-I	44	89)
NSVS 10363572	57067.5295	0.0003	MS FR	o	87	97)
NSVS 1394144	56916.3733	0.0004	AG	-I	32	89)
NSVS 1750812	56908.4245	0.0020	AG	-I	40	89)
NSVS 1824689	56918.3798	0.0039	AG	-I	42	89)
	56918.5364	0.0022	AG	-I	42	89)
NSVS 1841163	56592.2993	0.0013	AG	-I	57	89)
	56592.5020	0.0003	AG	-I	57	89)
	56644.3812	0.0025	AG	-I	33	89)
	56934.3260	0.0015	AG	-I	47	89)
	56934.5329	0.0028	AG	-I	47	89)
NSVS 188332	56949.3815	0.0201	AG	-I	38	89)
NSVS 1889885	56924.4062	0.0041	AG	-I	44	89)
	56924.5752	0.0143	AG	-I	44	89)

Table 1: cont.

Variable	HJD 24.....	±	Obs	Fil	n	Rem
NSVS 2560518	57035.5761	0.0015	AG	-I	52	89)
NSVS 3769020	56940.5155	0.0111	AG	-I	47	89)
NSVS 3842733	56928.6075	0.0019	AG	-I	51	89)
NSVS 3971593	56940.4695	0.0113	AG	-I	47	89)
NSVS 4116978	56943.3385	0.0036	AG	-I	47	89)
	56943.4963	0.0024	AG	-I	47	89)
	56943.6455	0.0009	AG	-I	47	89)
NSVS 4863977	57035.5289	0.0025	AG	-I	49	89)
NSVS 4873889	57035.5622	0.0016	AG	-I	51	89)
NSVS 503993	56978.3689	0.0043	AG	-I	48	89)
NSVS 5873337	56905.5771	0.0045	AG	-I	38	89)
NSVS 5875899	56905.3875	0.0081	AG	-I	37	89)
NSVS 8500709	56918.3592	0.0057	AG	-I	35	89)
NSVS 8554141	56918.3348	0.0023	AG	-I	35	89)
ROTSE1 J125947.50+365843.6	57056.6666	0.0088	AG	-I	73	89)
STARE aur0 306	57060.3245	0.0022	AG	-I	32	89)
TYC 2964-1200-1	57061.3205	0.0079	AG	-I	32	89)
TYC 3983-1552	55795.4293	0.0240	AG	-I	37	89)
TYC 4047-267-1	56933.4708	0.0024	AG	-I	50	89)
T-Cas0-02013	56928.4425	0.0058	AG	-I	51	89)
UCAC3 213-102451	55643.4776	0.0011	FR	-I	77	89)
	56727.2897	0.0016	FR	-I	71	89)
	56727.4553	0.0009	FR	-I	71	89)
UCAC3 220-058696	55514.6125	0.0005	FR	-I	44	89)
	56712.3628	0.0003	FR	-I	80	89)
	56712.5278	0.0007	FR	-I	80	89)
	56714.3285	0.0010	FR	-I	57	89)
	56714.4930	0.0009	FR	-I	57	89)
U-A2 0900-04405532	56990.6239	0.0012	MS FR	o	68	97)
U-A2 1275-06888047	56984.5967	0.0007	MS FR	o	61	97)
U-B1 1176-0623404	55352.4927	0.0050	SIR	o	147	93)
	55375.4687	0.0050	SIR	o	94	93)
	55380.4860	0.0050	SIR	o	87	93)
	55398.4391	0.0050	SIR	o	95	93)
	55405.4359	0.0050	SIR	o	127	93)
	55451.3834	0.0050	SIR	o	75	93)
U-B1 1177-0635723	55341.5142	0.0030	SIR	o	118	93)
	55352.5033	0.0020	SIR	o	147	93)
	55371.4485	0.0030	SIR	o	170	93)
	55374.4889	0.0030	SIR	o	243	93)
	55385.4809	0.0010	SIR	o	149	93)
U-B1 1177-0635723	55393.4316	0.0020	SIR	o	53	93)
	55408.4023	0.0010	SIR	o	70	93)
	55430.3861	0.0030	SIR	o	77	93)
	55441.3787	0.0010	SIR	o	59	93)
U-B1 1177-0636539	55374.4453	0.0040	SIR	o	242	93)
U-B1 1178-0639212	55374.5103	0.0001	SIR	o	142	93)
	55375.5242	0.0005	SIR	o	76	93)
	55385.4063	0.0006	SIR	o	148	93)
	55393.5183	0.0006	SIR	o	96	93)
	55405.4278	0.0005	SIR	-I	127	93)
	55408.4691	0.0006	SIR	o	105	93)
	55441.4141	0.0005	SIR	o	80	93)
	55443.4418	0.0005	SIR	o	87	93)
U-B1 1400-0455467	56934.4844	0.0191	AG	-I	40	89)

Table 2: Times of maxima of pulsating stars

Variable	HJD 24.....	±	Obs	Ref	Fil	n	Rem
SW And	56268.3783	0.0104	PGL	V	78	101) 6)	
	56929.5549	0.0012	ALH	R	579	92)	
	56933.535	0.001	AG	-I	51	89)	
XX And	56934.4982	0.0024	ALH	o	367	92)	
CC And	56949.3150	0.0014	ALH	V	416	92)	
	56949.4444	0.0018	ALH	V	416	92)	
GP And	56659.2880	0.0010	BRW	V	110	90)	

Table 2: cont.

Variable	HJD 24.....	±	Obs	Ref	Fil	n	Rem
GP And	56957.2506	0.0006	ALH	V	495	92)	
	56957.3287	0.0005	ALH	V	495	92)	
	56957.4072	0.0004	ALH	V	495	92)	
	56957.4863	0.0005	ALH	V	495	92)	
	56957.5649	0.0005	ALH	V	495	92)	
	56958.3616	0.0010	BRW	V	368	91)	
	56958.4411	0.0010	BRW	V	368	91)	
	56958.5189	0.0010	BRW	V	368	91)	
	56958.5976	0.0010	BRW	V	368	91)	
OV And	56886.4071	0.0035	PGL	V	103	99) 23)	
	56917.4664	0.0035	PGL	V	159	99) 21)	
	56948.5249	0.0010	ALH	o	614	92)	
V524 And	56950.3128	0.0010	ALH	o	493	92)	
	56950.4106	0.0015	ALH	o	493	92)	
	56950.5021	0.0011	ALH	o	493	92)	
	56950.5963	0.0012	ALH	o	493	92)	
	56963.4680	0.0010	BRW	V	149	91)	
	56963.5490	0.0030	BRW	V	149	91)	
V544 And	56920.3443	0.0035	PGL	TG	220	99) 63)	
	56920.3443	0.0035	PGL	TR	220	99) 61)	
	56920.3445	0.0035	PGL	TB	220	99) 65)	
	56920.4507	0.0035	PGL	TG	220	99) 62)	
	56920.4509	0.0035	PGL	TR	220	99) 60)	
	56920.4513	0.0035	PGL	TB	220	99) 64)	
	56970.2481	0.0015	ALH	o	280	92)	
	56970.3565	0.0013	ALH	o	280	92)	
RV Ari	56985.3461	0.0006	WLH	-U-I	36	94)	
CR Aur	54405.7108	0.0035	PGL	CV	204	102) 80)	
	54418.6930	0.0035	PGL	CV	59	102) 81)	
	54437.5776	0.0035	PGL	CV	111	102) 77)	
	54447.6193	0.0035	PGL	CV	72	102) 79)	
YZ Boo	56776.4262	0.0035	PGL	TG	87	99) 15)	
	56776.4280	0.0035	PGL	TB	87	99) 15)	
DD Boo	56691.5785	0.0008	MS FR	o	65	97)	
RW Cnc	57074.555	0.001	AG	-I	135	89)	
BI CMi	57074.317	0.001	AG	-I	41	89)	
	57074.442	0.001	AG	-I	41	89)	
V516 Cas	56642.4146	0.0015	MZ	-U-I	191	91)	
	56691.2865	0.0014	MZ	-U-I	99	91)	
	56917.4902	0.0015	MZ	-U-I	112	91)	
	56924.3564	0.0015	MZ	-U-I	87	91)	
V1040 Cas	56897.516	0.002	MS FR	o	57	97)	
	56897.591	0.002	MS FR	o	57	97)	
V1041 Cas	56965.621	0.001	AG	-I	50	89)	
V1057 Cas	56950.519	0.005	AG	-I	59	89)	
V876 Cep	56924.464	0.001	AG	-I	30	89)	
	56924.620	0.001	AG	-I	30	89)	
XX Cyg	56897.5131	0.0104	PGL	V	159	99) 26)	
XZ Cyg	56934.369	0.001	AG	-I	23	89)	
V789 Cyg	56949.3453	0.0003	SCI	o	60	90)	
	56958.3071	0.0002	SCI	o	51	90)	
V791 Cyg	53920.541	0.003	FR	-I	25	87)	
	53992.534	0.003	FR	-I	26	87)	
	54033.391	0.005	FR	-I	93	87) 3)	
	54033.452	0.010	FR	-I	93	87) 4)	
	56984.324	0.004	FR	-I	53	89)	
V1240 Cyg	56816.472	0.002	MS FR	o	63	97)	
V2367 Cyg	56903.4923	0.0010	BRW	V	250	91)	
	56904.3777	0.0020	BRW	V	250	91)	
	56904.5596	0.0020	BRW	V	250	91)	
V2455 Cyg	56867.4869	0.0020	BRW	V	153	91)	
	56867.5832	0.0010	BRW	V	153	91)	
	56914.5926	0.0035	PGL	B	149	99) 7)	
	56914.5930	0.0035	PGL	V	149	99) 7)	
AR Her	56915.4639	0.0035	PGL	V	114	99) 22)	
	56917.3389	0.0035	PGL	B	105	99) 16)	
	56917.3389	0.0035	PGL	R	105	99) 16)	
	56917.3389	0.0035	PGL	V	105	99) 16)	
	56923.4358	0.0035	PGL	V	89	99) 18)	
	56924.3743	0.0035	PGL	V	102	99) 19)	
FY Her	56912.3849	0.0020	MZ	-U-I	115	91)	

Table 2: cont.

Variable	HJD 24.....	±	Obs	Ref	Fil	n	Rem
V392 Her	56918.3390	0.0010	MZ	-U-I	92	91)	
V1139 Her	56858.4985	0.0020	BRW	V	96	91)	
V2109 Her	56820.3839	0.0010	BRW	V	84	91)	
	56820.4173	0.0010	BRW	V	84	91)	
	56820.4350	0.0010	BRW	V	84	91)	
	56824.4371	0.0010	BRW	V	93	91)	
	56838.4404	0.0010	BRW	V	93	91)	
	56838.4918	0.0010	BRW	V	77	91)	
VX Hya	55674.3359	0.0013	FLG	-U-I	58	88)	
GP Leo	57067.570	0.002	MS FR	o	58	97)	
EN Lyn	54075.7054	0.0035	PGE	CV	129	102) 78)	
	54085.6989	0.0035	PGE	CV	55	102) 73)	
	54100.7006	0.0035	PGE	CV	60	102) 76)	
	54120.6991	0.0035	PGE	CV	45	102) 68)	
	54122.5813	0.0035	PGE	CV	56	102) 70)	
	54142.5865	0.0035	PGE	CV	71	102) 67)	
	54147.5923	0.0035	PGE	CV	44	102) 69)	
	54149.4618	0.0035	PGE	CV	70	102) 71)	
	54154.4617	0.0035	PGE	CV	82	102) 72)	
	54169.4644	0.0035	PGE	CV	78	102) 74)	
	54194.4661	0.0035	PGE	CV	64	102) 75)	
WW Lyr	56934.325	0.000	FR	-I	72	89)	
EN Lyr	56940.310	0.001	AG	-I	43	89)	
LX Lyr	56915.3517	0.0010	MZ	-U-I	66	91)	
PU Lyr	56934.407	0.003	FR	-I	68	89)	
V593 Lyr	56890.5044	0.0010	BRW	V	127	91)	
	56890.6077	0.0010	BRW	V	127	91)	
VV Peg	56926.4662	0.0035	PGL	TG	63	99) 28)	
	56926.4667	0.0035	PGL	TB	63	99) 28)	
	56928.4221	0.0016	ALH	o	726	92)	
BH Peg	56897.3665	0.0069	PGL	V	394	83) 25)	
	56903.3541	0.0035	PGL	CV	348	83) 17)	
	56917.4493	0.0035	PGL	V	385	83) 20)	
BP Peg	56917.4229	0.0007	ALH	o	634	92)	
	56917.5308	0.0009	ALH	o	634	92)	
CD Peg	56970.3903	0.0026	MZ	-U-I	53	91) 5)	
DY Peg	56200.3840	0.0035	PGL	V	139	99) 12)	
	56928.4038	0.0056	PGL	TB	133	99) 13)	
	56928.4039	0.0056	PGL	TR	133	99) 13)	
	56928.4043	0.0056	PGL	TG	133	99) 13)	
	56981.3496	0.0035	HPF	V	331	99) 10)	
	56981.4225	0.0035	HPF	V	331	99) 11)	
V536 Peg	56912.5234	0.0010	BRW	V	37	91)	
AR Per	56657.3067	0.0035	PGL	V	60	99) 8)	
	56905.4012	0.0035	PGL	TB	232	99) 9)	
	56905.4012	0.0035	PGL	TG	232	99) 9)	
V371 Per	55849.442	0.007	FR	o	46	100)	
SS Psc	56903.5283	0.0035	PGL	V	116	99) 24)	
	56903.5289	0.0035	PGL	TR	116	99) 24)	
	56903.5414	0.0035	PGL	TB	116	99) 24)	
UU Tri	56706.2859:	0.0022	MZ	-U-I	216	91)	
	57028.4794	0.0024	MZ	-U-I	216	91)	
UX Tri	56886.4710	0.0035	PGL	V	82	99) 66)	
BW Tri	56631.4976	0.0035	MZ	-U-I	46	91)	
	56934.4659	0.0030	MZ	-U-I	129	91)	
	56972.2772	0.0030	MZ	-U-I	120	91)	
BN Vul	56904.4902	0.0069	PGL	TG	443	99) 14)	
	56904.4902	0.0069	PGL	TB	443	99) 14)	
2MASS J19131461+3329277	56934.330	0.002	FR	-I	85	89)	
ASAS J070452+1027.5	56963.3180	0.0002	MS FR	o	170	97)	
GSC 03949-00386	56933.266	0.001	FR	-I	321	89)	
	56933.351	0.001	FR	-I	321	89)	
	56933.460	0.001	FR	-I	321	89)	
	56933.557	0.001	FR	-I	321	89)	
	56933.648 :	0.001	FR	-I	321	89)	
	56935.271	0.002	FR	-I	55	89)	
GSC 04464-00924	56919.3668	0.0020	BRW	V	82	91)	
	56928.3457	0.0010	BRW	V	146	91)	
	56928.4238	0.0010	BRW	V	146	91)	
NSVS 14243430	56879.4154	0.0010	BRW	V	107	91)	
	56879.5041	0.0020	BRW	V	107	91)	

Table 2: cont.

Variable	HJD 24.....	±	Obs	Ref	Fil	n	Rem
TYC 1698-01052-1	56896.4843	0.0035	PGL	V	380	83) 45)	
	56896.5069	0.0035	PGL	V	380	83) 44)	
	56896.5291	0.0035	PGL	V	380	83) 40)	
	56897.3733	0.0035	PGL	V	307	83) 46)	
	56897.3980	0.0035	PGL	V	307	83) 43)	
	56897.4205	0.0035	PGL	V	307	83) 43)	
	56897.4406	0.0035	PGL	V	307	83) 41)	
	56897.4611	0.0035	PGL	V	307	83) 38)	
	56897.4854	0.0035	PGL	V	307	83) 42)	
	56903.3726	0.0035	PGL	o	349	83) 32)	
	56903.3955	0.0035	PGL	o	349	83) 34)	
	56903.4149	0.0035	PGL	o	349	83) 33)	
	56903.4348	0.0035	PGL	o	349	83) 31)	
	56903.4577	0.0035	PGL	o	349	83) 29)	
	56903.4795	0.0035	PGL	o	349	83) 30)	
TYC 1698-01052-1	56904.4118	0.0028	PGL	o	368	83) 36)	
	56904.4310	0.0028	PGL	o	368	83) 41)	
	56904.4550	0.0028	PGL	o	368	83) 37)	
	56904.4800	0.0028	PGL	o	368	83) 39)	
	56904.4989	0.0028	PGL	o	368	83) 35)	
	56905.3668	0.0035	PGL	V	456	83) 52)	
	56905.3668	0.0035	PGL	V	456	83) 52)	
	56905.3893	0.0035	PGL	V	456	83) 52)	
	56905.4105	0.0035	PGL	V	456	83) 50)	
	56905.4337	0.0035	PGL	V	456	83) 47)	
	56905.4557	0.0035	PGL	V	456	83) 46)	
	56905.4771	0.0035	PGL	V	456	83) 48)	
	56905.4985	0.0035	PGL	V	456	83) 49)	
	56905.5226	0.0035	PGL	V	456	83) 53)	
	56917.3179	0.0035	PGL	V	127	83) 51)	
	56917.4010	0.0035	PGL	V	95	83) 49)	
	56917.4652	0.0035	PGL	V	99	83) 52)	
	56920.3150	0.0035	PGL	V	479	83) 57)	
	56920.3955	0.0035	PGL	V	479	83) 53)	
	56920.4186	0.0035	PGL	V	479	83) 54)	
	56920.4412	0.0035	PGL	V	479	83) 55)	
	56920.4627	0.0035	PGL	V	479	83) 56)	
	56920.4875	0.0035	PGL	V	479	83) 58)	
UCAC3 226-130007	56490.478	0.002	FR	-I	119	89)	
	56506.391	0.002	FR	-I	57	89)	

Observers:

AG: Agerer, F., Tiefenbach
ALH: Alich, K., Schaffhausen
BHE: Böhme, D., Nessa
BRW: Braunwarth, H., Hamburg
FLG: Flechsig, G., East Greenbush USA
FR: Frank, P., Velden
HPF: Hopfer, R., Dresden
JU: Jungbluth, H., Karlsruhe
KBL: Kubala, R., Berlin
MS: Moschner, W., Lennestadt
MZ: Maintz, G., Bonn
PGE: Jürss, M., Wittenbeck
PGL: Pagel, L., Klockenhagen
QU: Quester, W., Esslingen
RAT: Rätz, M., Herges-Hallenberg
RCR: Rätz, K., Herges-Hallenberg
SCI: Schmidt, U., Karlsruhe
SIR: Schirmer, J., Harsefeld
VLM: Vollmann, W., Wien AU
WLH: Wollenhaupt, G., Oberwiesenthal

Remarks:

n number of measurements
: uncertain
s secondary minimum
(1) normal minimum
(2) mean error in this case: standard deviation
(3) double maximum: time of the first maximum
(4) double maximum: time of the second maximum
(5) wave in ascent

(6) 9.048 mag
(7) 9.063 mag
(8) 9.805 mag
(9) 9.825 mag
(10) 9.976 mag
(11) 10.024 mag
(12) 10.025 mag
(13) 10.048 mag
(14) 10.218 mag
(15) 10.274 mag
(16) 10.333 mag
(17) 10.379 mag
(18) 10.404 mag
(19) 10.405 mag
(20) 10.458 mag
(21) 10.534 mag
(22) 10.670 mag
(23) 10.726 mag
(24) 10.743 mag
(25) 11.002 mag
(26) 11.022 mag
(27) 11.187 mag
(28) 11.226 mag
(29) 11.269 mag
(30) 11.271 mag
(31) 11.272 mag
(32) 11.276 mag
(33) 11.277 mag
(34) 11.278 mag
(35) 11.281 mag
(36) 11.282 mag
(37) 11.283 mag
(38) 11.285 mag
(39) 11.286 mag
(40) 11.287 mag
(41) 11.289 mag
(42) 11.291 mag
(43) 11.292 mag
(44) 11.295 mag
(45) 11.299 mag
(46) 11.300 mag
(47) 11.302 mag
(48) 11.305 mag
(49) 11.314 mag
(50) 11.315 mag
(51) 11.320 mag
(52) 11.324 mag
(53) 11.328 mag
(54) 11.342 mag
(55) 11.345 mag
(56) 11.349 mag
(57) 11.364 mag
(58) 11.365 mag
(59) 11.667 mag
(60) 12.285 mag
(61) 12.302 mag
(62) 12.413 mag
(63) 12.450 mag
(64) 12.750 mag
(65) 12.784 mag
(66) 12.933 mag
(67) 13.266 mag
(68) 13.267 mag
(69) 13.273 mag
(70) 13.278 mag
(71) 13.289 mag
(72) 13.316 mag
(73) 13.318 mag
(74) 13.323 mag
(75) 13.337 mag
(76) 13.341 mag
(77) 13.358 mag
(78) 13.361 mag
(79) 13.375 mag
(80) 13.631 mag
(81) 13.732 mag
(82) 16.302 mag

Photometers:

(83) CCD camera Artemis 4021
(84) CCD camera FLI Proline 16803
(85) CCD camera Mead DSI Pro 3
(86) CCD camera Moravian G2-1600
(87) CCD camera OES-LcCCD12
(88) CCD camera Sigma 402
(89) CCD camera Sigma 1603
(90) CCD camera ST-7
(91) CCD camera ST-7E
(92) CCD camera ST-8 XMEI
(93) CCD camera ST-8 XME
(94) CCD camera ST-8 XM
(95) CCD camera ST-10 XME
(96) CCD camera STL-11000 M
(97) CCD camera STXL-6303E
(98) CCD camera QHY8
(99) CCD camera QHY8L
(100) camera Canon EOS 450D
(101) camera Canon EOS 1100D
(102) SuperWasp 2048×2048 px

Filters:

o	without filter
V	V-filter
B	B-filter
R	R-filter
Ic	I-filter Cousins
-I	IR cut-off filter
-U	U cut-off filter
CV	CV-filter
TB	TB-filter
TG	TG-filter
TR	TR-filter

References:

BAV Services for Scientists, 2013, `http://www.bav-astro.de/sfs/index.php/`
Lichtenknecker Database of the BAV, `http://www.bav-astro.de/LkDB/index.php/`

ERRATUM FOR IBVS 5959 (BAVM 214)

QQ Cas 54155.3169 RAT RCR has to be deleted

COMMISSIONS 27 AND 42 OF THE IAU
INFORMATION BULLETIN ON VARIABLE STARS

Number 6153

Konkoly Observatory
Budapest
18 November 2015

HU ISSN 0374 – 0676

110 MINIMA TIMINGS OF ECLIPSING BINARIES

PETROPOULOU, M.; GAZEAS, K.; TZOUGANATOS, L.; KARAMPOTSIOU, E.

Department of Astrophysics, Astronomy and Mechanics, National & Kapodistrian University of Athens, Zografos, Athens, Hellas; e-mail: mariapetr90@gmail.com; kgaze@phys.uoa.gr

Observatory and telescope:
T1: 0.4m, f/8 Cassegrain telescope, located at the University of Athens Observatory, at Zografos, Athens, Greece **T2**: 1.2m, f/13 Cassegrain telescope of the National Observatory of Athens, located at the Kryoneri Astronomical Station, at Korinth, Greece.

Detector:	**C1**: ST-10XME CCD camera, KAF-3200ME chip, $16' \times 11'$ and $25' \times 17'$ (using an f/6.3 focal reducer) field of view (FoV) with T1, **C2**: ST-8XMEI CCD camera, KAF-1603ME chip, $15' \times 10'$ FoV with T1, **C3**: ST-8 CCD camera, KAF-1600 chip, $15' \times 10'$ FoV with T1, **C4**: Photometrics CH250 CCD camera, SI502 chip, $2.5' \times 2.5'$ FoV with T2. All CCDs have a Peltier-type cooling system and are equipped with a set of UBVRI filters (Bessell specifications).

Method of data reduction:
Differential photometry

Method of minimum determination:
Kwee & van Woerden (1956)

Table 1: Times of minima of eclipsing binaries

System	HJD	Error	Type	Filters	Remark
HV Aqr	2453575.4741	0.0007	II	BVRI	T1+C3
	2453576.4089	0.0002	I	BVRI	T1+C3
	2453576.5953	0.0005	II	BVRI	T1+C3
	2453577.3462	0.0001	II	BVRI	T1+C3
	2453577.5321	0.0002	I	BVRI	T1+C3
	2453578.4697	0.0001	II	BVRI	T1+C3
	2453579.4047	0.0002	I	BVRI	T1+C3
	2453579.5922	0.0005	II	BVRI	T1+C3

Table 1 – continued from previous page

System	HJD	Error	Type	Filters	Remark
OO Aql	2453984.40663	0.00008	II	B	T1+C3
	2453985.42083	0.00008	II	B	T1+C3
	2454009.23946	0.00012	II	B	T1+C3
	2454034.32515	0.00028	I	B	T1+C3
	2454044.20783	0.00012	II	B	T1+C3
	2454060.17083	0.00021	I	B	T1+C3
	2454061.18491	0.00015	I	B	T1+C3
	2453982.37903	0.00005	II	V	T1+C3
	2453998.34313	0.00005	I	V	T1+C3
	2453999.35674	0.00004	I	V	T1+C3
	2453980.35235	0.00005	II	R	T1+C3
	2453997.32946	0.00004	I	R	T1+C3
	2453986.43442	0.00004	II	I	T1+C3
	2454013.29382	0.00003	II	I	T1+C3
	2454031.28448	0.00005	I	I	T1+C3
	2454064.22605	0.00011	I	I	T1+C3
	2454066.25299	0.00007	I	I	T1+C3
	2454067.26656	0.00011	I	I	T1+C3
V1182 Aql	2453272.3302	0.0002	I	V	T1+C3
FP Boo	2453147.5082	0.0016	II	BVRI	T1+C3
	2453156.4651	0.0016	II	BVRI	T1+C3
	2453439.5467	0.0010	II	VR	T1+C3
	2453446.5938	0.0005	II	VR	T1+C3
	2453447.5537	0.0004	I	VR	T1+C3
	2453448.5118	0.0005	II	VR	T1+C3
	2453506.4744	0.0005	I	BI	T1+C3
	2453507.4367	0.0005	II	BI	T1+C3
SZ Cam	2453298.3965	0.0005	I	R	T1+C3
	2453325.3720	0.0003	I	R	T1+C3
V470 Cam (HS0705+6700)	2452319.26182	0.00004	I	I	T2+C4
	2452319.30950	0.00011	II	I	T2+C4
	2452319.35741	0.00005	I	I	T2+C4
	2452319.40565	0.00011	II	I	T2+C4
	2452320.26681	0.00010	II	I	T2+C4
	2452320.60143	0.00004	I	I	T2+C4
FZ CMa	2453030.3201	0.0003	I	V	T1+C3
	2453037.3233	0.0003	II	R	T1+C3
	2453336.4991	0.0002	II	R	T1+C3
	2453681.4816	0.0002	II	R	T1+C3
AH Cep	2453001.2848	0.0034	I	V	T1+C3
AA Cet	2453687.4389	0.0001	I	R	T1+C3
YY CrB	2452472.2891	0.0002	I	BVRI	T2+C4
	2452473.4190	0.0002	I	BVRI	T2+C4
V700 Cyg	2453234.2964	0.0002	II	BVR	T2+C4
	2453234.4422	0.0003	I	BVR	T2+C4
	2453234.5873	0.0003	II	BVR	T2+C4
	2453238.3654	0.0003	II	BVRI	T1+C3

Table 1 – continued from previous page

System	HJD	Error	Type	Filters	Remark
V700 Cyg	2453238.5112	0.0003	I	BVRI	T1+C3
	2453250.2814	0.0001	II	BVRI	T2+C4
	2453250.4275	0.0002	II	BVRI	T2+C4
	2453250.5721	0.0001	II	BVRI	T2+C4
	2453251.2992	0.0002	II	BVRI	T2+C4
	2453251.4441	0.0001	II	BVRI	T2+C4
	2453251.5885	0.0003	II	VR	T2+C4
V1034 Cyg	2453248.4945	0.0005	II	VRI	T1+C3
	2453279.2643	0.0002	I	VRI	T1+C3
SV Equ	2453178.4311	0.0016	I	BVRI	T1+C3
	2453196.4948	0.0018	II	BVRI	T1+C3
UX Eri	2453686.5115	0.0001	I	R	T1+C3
BG Gem	2456324.9606	0.1276	II	BVRI	T1+C1
	2456371.0612	0.0811	I	BVRI	T1+C1
	2456416.4522	0.1463	II	BVRI	T1+C1
	2456554.7222	0.0372	I	BVRI	T1+C1
	2456600.4005	0.1029	II	BVRI	T1+C1
	2456646.5539	0.0499	I	BVRI	T1+C1
	2456692.0865	0.1191	II	BVRI	T1+C1
	2456737.8613	0.0575	I	BVRI	T1+C1
V345 Gem	2454066.4769	0.0003	II	BVRI	T1+C3
	2454066.6150	0.0003	I	BVRI	T1+C3
	2454067.4391	0.0004	I	BVRI	T1+C3
	2454067.5761	0.0003	II	BVRI	T1+C3
	2454068.5381	0.0002	I	BVRI	T1+C2
	2454068.6748	0.0004	II	V	T1+C2
V918 Her	2456495.3514	0.0003	II	BVRI	T1+C1
	2456497.3558	0.0003	I	BVRI	T1+C1
	2456508.2997	0.0004	I	BVRI	T1+C1
V921 Her	2453256.3965	0.0012	I	VRI	T1+C3
	2453257.2741	0.0008	I	VRI	T1+C3
	2453260.3439	0.0009	II	VRI	T1+C3
	2453264.2957	0.0013	I	VRI	T1+C3
V1003 Her	2456471.5104	0.0006	II	BVRI	T1+C1
	2456488.5271	0.0008	I	BVRI	T1+C1
	2456490.5026	0.0006	I	BVRI	T1+C1
	2456491.4911	0.0006	I	BVRI	T1+C1
	2456492.4759	0.0005	I	BVRI	T1+C1
	2456493.4668	0.0006	I	BVRI	T1+C1
	2456500.3635	0.0010	I	BVRI	T1+C1
	2456501.3530	0.0010	I	BVRI	T1+C1
	2456502.3398	0.0008	I	BVRI	T1+C1
	2456504.3251	0.0013	I	BVRI	T1+C1
ET Leo	2452724.3704	0.0005	II	BVRI	T1+C3
	2452724.5447	0.0015	I	BVRI	T1+C3
XZ Leo	2453034.4919	0.0002	I	BVRI	T1+C3
	2453036.4436	0.0002	I	BVRI	T1+C3

Table 1 – continued from previous page

System	HJD	Error	Type	Filters	Remark
XZ Leo	2453036.6865	0.0006	II	BVRI	T1+C3
	2453051.5635	0.0002	I	BVRI	T1+C3
CW Lyn	2456748.3737	0.0009	II	BVR	T1+C1
	2456768.2720	0.0008	I	BVRI	T1+C1
	2456770.3038	0.0010	II	BVRI	T1+C1
	2456796.3181	0.0006	II	BVRI	T1+C1
DD Mon	2453441.3815	0.0001	I	BVRI	T2+C4
	2453442.2346	0.0003	II	VRI	T2+C4

Explanation of the remarks in the table:

T1, T2, C1, C2, C3 and C4 refer to the instrumentation (telescope and CCD camera) used for each case.

Remarks:

A large number of the above observations were performed utilizing the robotic and remotely controlled telescope at the University of Athens.

Acknowledgements:

Times of minima of contact binaries presented in this work are by-product of the *W UMa Project* (Papers I - VII) (Kreiner et al. 2003; Baran et al. 2004; Zola et al. 2004; Gazeas et al. 2005; Zola et al. 2005; Gazeas et al. 2006; Zola et al. 2010.), which aims in performing accurate photometric and spectroscopic study of eclipsing binaries of W UMa type. In addition, part of this work is a result of the *Contact Binaries Towards Merging (CoBiToM) Project*, initiated and still undergoing at the National and Kapodistrian University of Athens since 2012 (PI: K. Gazeas).

References:

Baran A., Zola S., Rucinski S. M., Kreiner J. M., Siwak M., Drozdz M., 2004, *AcA*, **54**, 195 (Paper II)

Gazeas K., Baran A., Niarchos P., Zola S., Kreiner J.M., et al., 2005, *AcA*, **55**, 123 (Paper IV)

Gazeas K., Niarchos P., Zola S., Kreiner J.M., Rucinski S.M., 2006, *AcA*, **56**, 127 (Paper VI)

Kreiner J. M., Rucinski S. M., Zola S., Niarchos P., Ogloza W., Stachowski G., Baran A., Gazeas K., Drozdz M., Zakrzewski B., Pokrzywka B., Kjurkchieva D., Marchev D., 2003, *A&A*, **412**, 465 (Paper I)

Kwee K., van Woerden H., 1956, *Bulletin of the Astronomical Institutes of the Netherlands*, **12**, 327

Zola S., Rucinski S.M., Baran A., Ogloza W., Pych W., Kreiner J.M., Stachowski G., Gazeas K., Niarchos P., Siwak M., 2004, *AcA*, **54**, 299 (Paper III)

Zola S., Kreiner, J.M., Zakrzewski B., Kjurkchieva D.P., Marchev D.V., Baran A., Rucinski S.M., Ogloza W., Siwak M., Koziel D., Drozdz M., Pokrzywka B., 2005, *AcA*, **55**, 389 (Paper V)

Zola S., Gazeas K., Kreiner J. M., Ogloza W., Siwak M., Koziel-Wierzbowska D., Winiarski M., 2010, *MNRAS*, **408**, 464 (Paper VII)

COMMISSIONS 27 AND 42 OF THE IAU
INFORMATION BULLETIN ON VARIABLE STARS

Number 6154

Konkoly Observatory
Budapest
9 December 2015

HU ISSN 0374 – 0676

OAN-TNT RESULTS OF OBSERVATIONS - PHOTOELECTRIC MINIMA OF SELECTED ECLIPSING BINARIES AND MAXIMA OF PULSATING STARS

PENA, J. H.[1]; RENTERIA, A.[1,2]; VILLARREAL, C.[1,2]; PIÑA, D. S.[2]; SONI, A. A.[2]; TREJO, O.[1]; GUILLEN, J.[2]; VARGAS, K.[2]; GARCIA, C.[2]; MANCERA, P.[3]; PANI, A.[4]; HUEPA, H.[4]; HUEPA, J. L.[4]; STUDENTS FROM THE LATIN AMERICAN SCHOOL OF OBSERVATIONAL ASTRONOMY ESAO-BELA 12, 14 AND 15 AS WELL AS THE STUDENTS FROM THE ADVANCED OBSERVATIONAL COURSES 12, 13, 14 AND 15 AT FACULTAD DE CIENCIAS, UNAM

[1] Instituto de Astronomía, Apartado Postal 70-264, Mexico D. F. 04510, Mexico, jhpena@astro.unam.mx

[2] Facultad de Ciencias, Universidad Nacional Autónoma de México, México D.F., México

[3] Facultad de Ciencias, Universidad Veracruzana, Xalapa, México

[4] Observatorio Astronómico Nacional, Tonantzintla, México

In this first compilation of OAN-TNT results, photoelectric observations of 9 variable stars obtained from 2011 to 2015 are presented giving 50 minima for eclipsing binaries and maxima of pulsating stars. All times of minima and maxima are heliocentric and were determined with a fifth grade polynomial fitting to the light curve. The epoch values and period to determine the $O-C$ were taken from Kholopov et al. (1985) and are given in days. The values in column $O-C$ are determined without incorporation of nonlinear terms. The errors were determined from the RMS of the residuals evaluated for the times of maxima and are about 0.016 day. The accuracy of each point is given by the exposure time and varies between 3 min for the 1 m telescope and 1 min for the smaller telescopes. It may seem contradictory to give a longer integration time to the larger aperture telescope. However, this is done since the mounting of the 10-inch telescope is of an altazimuth type, which does not allow long integration times. For the 1-meter telescope there were around 40,000 counts and for the 10-inch telescope there were 11,000 counts, enough to secure high precision.

The stars' coordinates in Table 1 are epoch 2000 and the V values are given in magnitudes. All information about telescopes, photometers and filters are specified in Tables 2 and 3. In the same Tables the following quantities are listed. Column 1 is the ID, column 2 the time in HJD, N gives the number of data points in each run and Δt is the time span of the run. Observers and reductors are specified in the remarks to the Tables. The observations were made at both the Observatorio Astronomico Nacional at Tonantzintla (TNT) and San Pedro Martir (SPM), both belonging to UNAM. The CCD reduction was done with AstroImageJ (Collins 2012) and the photoelectric observations were reduced using a classical procedure (see Peña et al. 2012 for details). The photoelectric measurements and all the light curves can be requested for inspection.

Table 1: Characteristics of the observed stars

Star	RA (2000)	DEC (2000)	V (mag)	SpType	T_0 (d)	P (d)	Observatory
GP And	00 55 18	+23 09 49.36	10.79	A3	2433861.438	0.0786827	SPM
AD CMi	07 52 47	+01 35 50.50	9.38	F3III	2442429.458	0.12297443	TNT & SPM
AZ CMi	07 44 07	+02 24 19.52	6.47	F0III	2440886.071	0.09526	SPM
KZ Hya	10 50 54	−25 21 14.00	10.06	B9III	2442516.158	0.059510421	TNT
EH Lib	14 58 55	−00 56 53.05	9.38	F0	2433438.608	0.088413245	TNT
SZ Lyn	08 09 35	+44 28 17.61	9.43	F2	2438124.398	0.120534920	TNT & SPM
1 Mon	05 59 01	−09 22 56.01	6.16	F2IV	2441661.167	0.136126	TNT & SPM
AE UMa	09 36 53	+44 04 00.39	11.35	A9	2435604.338	0.086017055	TNT & SPM
W UMa	09 43 45	+55 57 09.00	7.85	F8V	2445765.739	0.33363749	TNT

Table 2: Times of maxima of pulsating stars

ID	HJD−2450000	N	Δt (d)	Telescope	Fil	Detector	$O-C$	Observers/Reductors
GP And	6612.7070	32	0.08	84	V	phot	0.0089	JHP,CVR/JHP
	6614.6748	18	0.09	84	V	phot	0.0097	JHP,CVR/JHP,CVR
AD CMi	6333.8206	202	0.13	m1	G	ST8	0.0127	CVR/CVR
	6346.7301	226	0.12	m1	wo	ST8	0.0099	AOA13/ARL
	6614.9390	20	0.09	84	V	phot	0.0076	JHP,CVR/JHP
	6685.7670	182	0.12	1m	G	8300	0.0063	ESAOBELA14/JHP
	6753.6540	99	0.08	m2		phot	0.0114	AOA14/CGS
AZ CMi	6614.9522	19	0.08	84	V	phot	0.0278	JHP,CVR/JHP,CVR
KZ Hya	7088.7971	155	0.16	m1	V	1001	0.0248	AOA15/KVR
	7088.8565	155	0.16	m1	V	1001	0.0246	AOA15R/KVR
	7089.7493	194	0.12	m1	V	1001	0.0248	AOA15R/DSP
	7112.8385	150	0.13	m1	V	1001	0.0239	DSP/DSP
	7112.7789	150	0.13	m1	V	1001	0.0239	DSP/DSP
	7112.7798			1m	wo	8300	0.0248	OTA,AS/OTA,AS
EH Lib	6354.9736	58	0.10	1m	G	1001	0.0061	CVR,DZR/CVR
	6376.8984	120	0.11	1m	G	1001	0.0045	CVR/CVR
	6753.8916	281	0.15	m1	wo	8300	0.0036	AOA14R/CVR
	7088.8023	114	0.06	c11	wo	8300	0.0049	AOA15R/DSP
	7114.7947	52	0.05	m1	V	1001	0.0038	KVR,JGT/DSP
	7172.7920	55	0.07	84	V	phot	0.0020	JGT,AS/JHP
	7175.7990	32	0.05	84	V	phot	0.0030	AS/JHP
	7177.8310	43	0.09	84	V	phot	0.0015	AS/JHP
SZ Lyn	6333.6440	134	0.21	1m	V	1001	0.0356	AOA13/ARL
	6333.7641						0.0352	AOA13/ARL
	6615.9288	47	0.09	84	V	phot	0.0277	JHP,CVR/JHP
	7044.8220	76	0.12	m2	G	ST8	0.0576	ESAOBELA15/JHP,JGT
	7044.9040	76	0.12	m2	G	ST8	0.0191	ESAOBELA15/JHP,JGT
	7045.7557	313	0.18	m2	G	ST8	0.0270	ESAOBELA15/DSP
	7045.8719			m2	G	ST8	0.0227	ESAOBELA15/DSP
	7049.8522	230	0.12	m2	G	ST8	0.0253	ESAOBELA15/CVR
	7050.8158	222	0.12	m2	G	ST8	0.0247	ESAOBELA15/JGT
1 Mon	6332.7595	158	0.06	1m	V	1001	−0.0678	OTA,AP/ARL
	6610.8688	79	0.12	84	V	phot	−0.0639	JHP,CVR/JHP
AE UMa	5901.9574	58	0.06	84	y	e2v2	0.0029	ARL,JHP/ARL
	5902.0394	58	0.06	84	y	e2v2	−0.0011	ARL,JHP/ARL
	5906.9400	118	0.17	84	V	phot	−0.0035	ARL,JHP/JHP
	5907.0230			84	V	phot	−0.0065	ARL,JHP/JHP
	5950.8077	36	0.20	1m	V	1001	−0.0045	ESAOBELA12/JHP
	5951.7986	37	0.13	1m	V	1001	0.0402	ESAOBELA12/JHP
	5989.8581	13	0.05	1m	V	1001	−0.0058	AOA12/ARL
	5990.7191	44	0.25	1m	V	1001	−0.0050	AOA12/ARL
	5990.8104			1m	V	1001	0.0003	AOA12/ARL
	6361.7207	41	0.19	1m	V	1001	0.0050	AOA13/ARL
	6361.8010	41	0.19	1m	V	1001	−0.0007	AOA13/ARL
	7129.3859	16	0.07	1m	G	8300	−0.0320	AS,OTA/AS

Table 3: Times of minima of eclipsing binaries

ID	HJD−2450000	N	Δt (d)	Telescope	Fil	Detector	$O-C$	Observers/Reductors
W UMa	6680.77	389	0.18	m1	V	1001	0.0805	ESAOBELA14/JHP
	6680.93			m1	V	1001	−0.0931	ESAOBELA14/JHP
	6685.78	180	0.08	m1	V	1001	0.0860	ESAOBELA14/JHP
	7045.77	311	0.70	m1	V	1001	0.0811	ESAOBELA14/JHP
	7050.77	190	0.14	m1	V	1001	0.0765	ESAOBELA15/JHP

Remarks:

1. Telescope	2. Detector	3. Filter
1m - 1m telescope	ST8 - CCD camera ST-8	V - V-filter in UBV system
m1 - 10" Meade telescope	1001 - CCD camera ST-1001	G - Green in RGB set
m2 - 10" Meade telescope	8300 - CCD camera ST-8300	y - y-filter in *uvby* system
c11 - 11" Celestron telescope	phot - *uvby* Photometer	wo - Without filter
84 - 0.84m telescope	e2v2 - CCD camera e2v-4290	

AS: A. A. Soni
OTA: O. Trejo
ARL: A. Renteria
JHP: J. H. Pena
CVR: C. Villarreal
AP: A. Pani
KVR: K. Vargas
DSP: D. S. Piña
JGT: J. Guillen
CGS: C. Garcia

ESAOBELA12: Abril, Valentina; Alberti, Carlos; Aréas, Ligia; Batista, Lester; Buitrago, Juan; García, Ovido; González, Myrian; Ramírez, Ma. Claudia; Recinos, Beatriz; Rodríguez, Anthony; Ruiz, Juan; Soriano, Fatima.

ESAOBELA14: Ordoñez, Norida; Mafla, Katherine; Fajardo, Wilmar; Rojas, Miguel; Cruz, Ignacio; Martínez, Armando; Rojas, Alexander; Rosales, Jennyffer; Garcia, Alan; Fuentes, Walter; Nicolas.

ESAOBELA15: Díaz, Saida; Chaverri, Fabian; Oreamuno, Rafael; Alvarenga, Sandra; Montezuma, Roberto; Delcompare, Paola; Molina, Brian; Gómez, Berenice; Turiján, Benita; Torre, Erika; Alvarado, Jaime.

AOA12: Aguilera, David; Deras, Dan; Espinosa, Marco; Valencia, Karen; Vessi, Pamela; Villarreal, César.

AOA13: A. Soni, Angel; García, Carlos; León, Rubén; Ramírez, Eduardo; Trejo, Oriana.

AOA14: Camargo, José; Flores, Jesús; Galicia, David; García, Carlos; Guillén, Jorge; Muñoz, Andrea; Pérez, Erika; Ramírez, Julio; Segura, Daniel; Serratos, Mario; Yslas, Rodrígo; Zamarrón, Javier.

AOA15: Arellano, Sergio; Díaz López, Julianne; Moreno, Ximena; Ramírez, Juan; Ruíz, Francisco; Téllez, Carlos; Vargas, Karla; Vázquez, Valente.

Acknowledgments: We would like to thank the staff of the observatories for their assistance in securing the observations, A. Díaz, C. Guzmán, F. Ruíz, E. Colorado and F. Angeles for technical support and Daniel Zuñiga who assisted CVR on the night of March, 2013. This work was partially supported by IAU and DGAPA through PE103112 and IN104612. Proofreading was done by J. Miller.

References:

Collins, 2012, Astrophysics Source Code Library, `http://ascl.net/1309.001`
Kholopov et al., 1985, *General Catalog of Variable Stars*, Nauka Publishing House, Moscow
Peña, J. H., Figuera Jaimes, R., Chow, M., Peña Miller R. & Álvarez, M., 2012, *RevMexAA*, **48**, 299

*This version of the paper contains corrections, and differs from the one appeared on-line originally. Date of last modification: Thu May 26 06:48:10 CEST 2016

COMMISSIONS 27 AND 42 OF THE IAU
INFORMATION BULLETIN ON VARIABLE STARS

Number 6155

Konkoly Observatory
Budapest
30 December 2015

HU ISSN 0374 – 0676

THE 81ST NAME-LIST OF VARIABLE STARS. PART II — RA 17^h30^m TO 24^h

KAZAROVETS, E.V.[1]; SAMUS, N.N.[1,2]; DURLEVICH, O.V.[2]; KIREEVA, N.N.[1]; PASTUKHOVA, E.N.[1]

[1] Institute of Astronomy, Russian Academy of Sciences, 48, Pyatnitskaya Str., Moscow 119017, Russia
[helene@inasan.ru, samus@sai.msu.ru, kireeva@sai.msu.ru, pastukhova@sai.msu.ru]

[2] Sternberg Astronomical Institute, M.V. Lomonosov University of Moscow, 13, University Ave., Moscow 119992, Russia
[gcvs@sai.msu.ru]

The first part of the 81st Name-List of Variable Stars (Kazarovets et al. 2015) contained information on 1952 variable stars recently named in the system of designations of the GCVS (General Catalogue of Variable Stars; Samus et al. 2007–2015; `http://www.sai.msu.su/gcvs/gcvs`). Almost all of them are in the right ascension (RA) range between 0^h and 17^h30^m.

The second part of the 81st Name-List of Variable Stars introduces GCVS names for 2091 variable stars, all of them in the RA range between 17^h30^m and 24^h. Among them, there are three Novae quickly named upon requests from the IAU Bureau of Astronomical Telegrams; their names within constellations are not in the order of their RA, but also in the same RA range.

Table 1 of the current Name-List contains the new GCVS name, equatorial coordinates (rounded to an accuracy sufficient for identification), and variability type for each star. The order of stars in Table 1 corresponds to the order of stars in the GCVS, in the alphabetical order of full constellation names. The complete electronic version of the Name-List at `http://www.sai.msu.su/gcvs/gcvs/nl81`, to be presented in the nearest future, will additionally contain variability ranges, light elements, spectral types, identifications with astronomical catalogues, detailed remarks, bibliographic references for the newly named variable stars, accurate coordinates and proper motions (with references to corresponding positional catalogs or sources in the literature). Table 2 presents identification of GCVS names for three Novae with their preliminary designations.

The total number of named variable stars, not counting designated non-existing stars or stars subsequently identified with earlier-named variables, is now 51 853.

This study was supported in part by Russian Foundation for Basic Research and by the Programme "Non-stationary Phenomena of Objects in the Universe" of the Presidium of Russian Academy of Sciences.

References:

Kazarovets, E.V., Samus, N.N., Durlevich, O.V., Kireeva, N.N., Pastukhova, E.N. 2015, *Inform. Bull. Var. Stars*, No. 6151

Samus, N.N., Durlevich, O.V., Goranskij, V.P., Kazarovets, E.V., Kireeva, N.N., Pastukhova, E.N., Zharova, A.V. 2007–2015, *General Catalogue of Variable Stars*, VizieR On-line Data Catalog: B/gcvs

Table 1

Name	R.A., Decl., 2000.0	Type	Name	R.A., Decl., 2000.0	Type
	h m s o ' "			h m s o ' "	
V0763 And	23 00 02.2 +42 35 43	EW	V1837 Aql	19 13 50.7 +02 51 20	CEP(B)
V0764 And	23 00 59.2 +37 47 35	SR	V1838 Aql	19 15 02.1 +07 19 48	UGSU
V0765 And	23 01 16.1 +42 22 22	RRAB	V1839 Aql	19 15 54.0 +09 36 56	LB
V0766 And	23 01 27.6 +42 46 42	EW	V1840 Aql	19 22 07.0 -11 38 33	EW
V0767 And	23 01 48.9 +42 33 27	EW	V1841 Aql	19 27 28.7 +12 32 16	BY
V0768 And	23 03 11.8 +42 39 09	EW:	V1842 Aql	19 27 29.5 +08 54 37	M
V0769 And	23 03 32.0 +42 09 13	RRAB	V1843 Aql	19 37 11.8 +06 28 11	EA
V0770 And	23 07 29.0 +49 02 37	GDOR	V1844 Aql	19 50 25.0 +14 30 50	GDOR
V0771 And	23 09 10.2 +40 44 10	LB	V1845 Aql	19 51 05.9 -03 14 15	RRAB
V0772 And	23 10 53.8 +40 03 24	EW	V1846 Aql	19 51 20.6 +15 14 36	RRC
V0773 And	23 11 21.7 +35 23 52	EW	V1847 Aql	19 53 50.2 -08 47 43	EA
V0774 And	23 17 20.6 +39 21 00	LB	V1848 Aql	19 54 03.2 +10 41 45	RS
V0775 And	23 18 45.9 +38 49 22	EW	V1849 Aql	19 57 53.0 +14 20 18	RS
V0776 And	23 19 36.1 +36 47 01	UGSU	V1850 Aql	19 57 53.4 +04 55 28	RRAB
V0777 And	23 20 11.3 +38 40 20	EA	V1851 Aql	19 57 57.9 +05 28 16	EW
V0778 And	23 21 31.4 +37 49 11	SR	V1852 Aql	19 57 59.1 +14 32 17	EB
V0779 And	23 21 44.1 +39 57 07	EW	V1853 Aql	19 58 04.4 +04 46 53	EW:
V0780 And	23 24 34.2 +36 15 08	LB	V1854 Aql	19 58 04.9 +05 25 51	RRAB
V0781 And	23 35 50.2 +48 43 43	DSCTC	V1855 Aql	19 58 06.1 +04 46 13	EW
V0386 Aps	17 30 15.3 -75 17 49	EW	V1856 Aql	19 58 12.8 +04 56 27	BY:
V0387 Aps	17 30 30.1 -79 08 02	SRB	V1857 Aql	19 58 21.1 +04 43 12	EW
V0388 Aps	17 31 20.0 -71 23 38	SR	V1858 Aql	19 58 26.4 +05 30 42	SR
V0389 Aps	17 35 50.5 -68 21 30	SRA	V1859 Aql	19 58 27.5 +04 46 53	EW
V0390 Aps	17 36 36.0 -71 06 46	E/RS	V1860 Aql	19 58 27.6 +04 54 21	RRAB
V0391 Aps	17 53 36.8 -71 11 12	RRAB	V1861 Aql	19 58 39.5 +05 03 03	EB
V0392 Aps	17 56 20.6 -70 21 44	SRB	V1862 Aql	19 58 42.5 +05 29 12	EW
V0393 Aps	18 00 22.6 -70 26 26	RRC	V1863 Aql	19 58 45.9 +05 26 52	EW
V0394 Aps	18 04 11.2 -71 59 48	CV	V1864 Aql	19 58 52.2 +05 02 54	BY:
V0364 Aqr	20 41 17.7 -04 52 05	EW	V1865 Aql	19 58 59.9 +05 31 37	SR
V0365 Aqr	20 54 09.2 -02 45 34	RS	V1866 Aql	19 59 01.1 +05 11 48	SR:
V0366 Aqr	20 57 38.9 -14 25 44	RPHS	V1867 Aql	19 59 08.2 +04 50 43	EW
V0367 Aqr	21 03 09.2 -01 12 11	RR(B)	V1868 Aql	19 59 10.7 +07 58 38	EA
V0368 Aqr	21 20 46.9 +00 12 37	RR(B)	V1869 Aql	19 59 16.3 +05 29 26	EB
V0369 Aqr	21 26 29.4 -00 20 54	RR(B)	V1870 Aql	19 59 30.9 +05 31 56	LB
V0370 Aqr	21 29 33.6 -00 43 30	RR(B)	V1871 Aql	19 59 47.5 +04 58 48	EW
V0371 Aqr	21 29 52.7 -01 10 19	DSCT	V1872 Aql	19 59 49.6 +04 42 34	BY:
V0372 Aqr	21 41 00.7 +01 09 39	RRC	V1873 Aql	20 00 01.4 +04 56 15	EW
V0373 Aqr	21 56 24.0 +00 56 30	RR(B)	V1874 Aql	20 00 06.2 +04 51 01	EW
V0374 Aqr	22 05 40.0 -08 43 00	EA	V1875 Aql	20 00 07.7 +05 10 50	EW
V0375 Aqr	22 06 54.3 -01 05 15	RR(B)	V1876 Aql	20 00 14.7 +05 17 23	DSCT
V0376 Aqr	22 10 22.0 +02 32 31	EA	V1877 Aql	20 00 20.9 +05 30 11	EW
V0377 Aqr	22 17 52.5 -07 56 24	EA	V1878 Aql	20 00 23.5 +05 05 17	RRC
V0378 Aqr	22 20 29.9 -01 39 58	RS	V1879 Aql	20 00 31.5 +05 00 36	E:/RS
V0379 Aqr	22 22 14.3 +01 01 00	RR(B)	V1880 Aql	20 00 57.8 +05 05 59	EW
V0380 Aqr	22 42 00.1 -00 42 22	RR(B)	V1881 Aql	20 00 58.3 +04 43 37	RRAB
V0381 Aqr	22 55 17.4 -23 17 38	RRC	V1882 Aql	20 00 58.4 +05 18 32	SR
V0382 Aqr	23 12 09.2 -18 55 26	RRC	V1883 Aql	20 01 12.9 +05 19 10	DSCT
V0383 Aqr	23 39 51.3 -16 44 25	RRC	V1884 Aql	20 01 16.7 +05 00 12	EB
V1831 Aql	19 21 50.1 +15 09 25	NA	V1885 Aql	20 01 16.8 +04 41 43	SR:
V1832 Aql	18 44 16.3 -03 48 55	SR	V1886 Aql	20 05 08.4 -02 18 43	EW
V1833 Aql	18 55 42.1 -01 23 06	EA	V1887 Aql	20 05 58.4 -01 59 53	EB
V1834 Aql	19 03 46.0 +16 29 52	SR	V1888 Aql	20 08 39.0 +01 53 44	RRAB
V1835 Aql	19 07 42.4 +00 02 51	RCB	V1889 Aql	20 11 38.9 +16 06 28	DSCTC
V1836 Aql	19 12 13.5 +10 31 29	M	V1890 Aql	20 11 39.6 -02 35 26	BY

Table 1 (continued)

Name	R.A., Decl., 2000.0 h m s o ' "	Type	Name	R.A., Decl., 2000.0 h m s o ' "	Type
V1891 Aql	20 13 17.7 +03 24 02	EB	V1028 Ara	17 56 02.9 -55 40 31	SR
V1892 Aql	20 15 41.7 +04 04 19	SRB	V1029 Ara	17 56 12.1 -48 31 13	RRAB
V1893 Aql	20 17 34.0 +00 31 29	EB	V1030 Ara	17 58 59.0 -46 47 09	M
V1894 Aql	20 23 35.2 -01 45 04	RS	V1031 Ara	17 59 15.1 -52 22 33	RRAB
V1895 Aql	20 29 12.7 +00 30 28	EW	V1032 Ara	17 59 16.1 -56 46 46	SR
V1896 Aql	20 29 34.9 +00 05 26	RRAB	V1033 Ara	17 59 43.0 -55 42 06	SRB
V1897 Aql	20 29 49.4 -00 06 00	EW	V1034 Ara	17 59 56.0 -52 12 08	EA
V1898 Aql	20 30 59.4 +00 22 26	EW	V1035 Ara	18 00 27.4 -54 39 04	EA
V1899 Aql	20 31 10.4 +00 01 40	EW	V1036 Ara	18 00 31.9 -46 59 50	SR
V1900 Aql	20 31 20.9 -00 11 25	RRAB	V1037 Ara	18 01 11.1 -46 35 53	SRB
V1901 Aql	20 31 37.6 -00 05 11	E+AM:	V1038 Ara	18 01 34.4 -50 55 41	SR
V0985 Ara	17 30 03.3 -46 19 18	SR	V1039 Ara	18 02 28.8 -47 55 18	M
V0986 Ara	17 30 14.8 -57 45 51	M	V1040 Ara	18 02 29.0 -52 03 22	EB
V0987 Ara	17 30 15.8 -51 01 20	M	V1041 Ara	18 02 36.8 -48 31 01	M
V0988 Ara	17 31 07.7 -50 16 22	M	V1042 Ara	18 03 00.5 -50 53 18	M
V0989 Ara	17 31 14.0 -57 25 24	SR:	V1043 Ara	18 03 27.5 -47 13 03	M
V0990 Ara	17 31 21.8 -56 50 39	SR	V1044 Ara	18 03 40.8 -51 22 39	SRA
V0991 Ara	17 31 48.1 -51 20 35	M	V1045 Ara	18 03 55.6 -48 44 23	M:
V0992 Ara	17 31 57.4 -53 59 02	M	DN Cap	20 09 06.7 -18 16 05	RVA
V0993 Ara	17 32 29.0 -50 24 37	M	DO Cap	20 21 46.6 -23 41 30	RRC
V0994 Ara	17 32 33.7 -59 52 48	SRB	DP Cap	20 30 37.0 -27 13 50	RRC
V0995 Ara	17 33 24.9 -58 49 59	SRB	DQ Cap	20 30 41.8 -23 57 22	RRAB
V0996 Ara	17 34 01.4 -53 09 37	M	DR Cap	20 31 44.9 -21 58 46	RRC
V0997 Ara	17 35 58.5 -55 27 35	M	DS Cap	20 34 19.5 -25 08 54	RRAB
V0998 Ara	17 36 04.0 -47 10 10	RS	DT Cap	20 36 37.6 -24 05 37	RRAB
V0999 Ara	17 36 13.0 -47 03 12	M	DU Cap	20 39 12.0 -21 24 50	RRAB
V1000 Ara	17 37 04.4 -48 36 43	SR	DV Cap	20 44 39.9 -24 02 43	RRC
V1001 Ara	17 37 49.6 -63 42 01	SRB	DW Cap	20 48 25.1 -20 46 36	RRC
V1002 Ara	17 38 31.8 -56 49 01	SR	DX Cap	21 49 35.2 -23 30 19	RRC
V1003 Ara	17 38 55.1 -56 37 02	SR	V1285 Cas	22 58 16.4 +56 58 33	LB
V1004 Ara	17 39 41.7 -60 20 04	LB	V1286 Cas	23 02 44.3 +57 53 58	EW
V1005 Ara	17 39 55.1 -47 27 40	M	V1287 Cas	23 07 45.7 +54 08 02	EW
V1006 Ara	17 40 20.5 -51 34 08	M	V1288 Cas	23 10 03.2 +58 08 30	EB
V1007 Ara	17 40 21.8 -52 14 42	LB	V1289 Cas	23 12 17.5 +58 58 42	EB
V1008 Ara	17 40 28.4 -51 27 31	LB	V1290 Cas	23 13 17.6 +58 29 30	DSCT
V1009 Ara	17 41 29.7 -51 11 51	M	V1291 Cas	23 28 17.8 +57 28 57	SR
V1010 Ara	17 41 52.6 -47 51 14	M	V1292 Cas	23 29 30.8 +60 31 38	EW
V1011 Ara	17 42 01.7 -46 33 43	RRC	V1293 Cas	23 45 41.8 +66 05 07	EA
V1012 Ara	17 42 38.5 -56 49 40	LB	V1294 Cas	23 47 28.1 +62 26 29	EW
V1013 Ara	17 44 12.0 -47 44 01	M	V1295 Cas	23 52 21.8 +57 27 47	EW
V1014 Ara	17 44 30.7 -48 19 38	M	V0970 Cep	20 15 00.2 +76 54 18	EA
V1015 Ara	17 45 33.8 -50 55 09	M	V0971 Cep	20 32 24.9 +60 28 37	UG
V1016 Ara	17 46 55.8 -50 02 48	SR	V0972 Cep	20 33 08.4 +60 20 06	EW
V1017 Ara	17 47 06.4 -49 24 15	M	V0973 Cep	20 52 31.1 +70 54 40	DSCT
V1018 Ara	17 47 43.8 -51 36 47	SR	V0974 Cep	20 57 30.2 +60 03 09	RS
V1019 Ara	17 48 18.3 -49 56 07	SR	V0975 Cep	21 05 12.3 +69 12 55	UG:
V1020 Ara	17 50 38.7 -47 33 34	M	V0976 Cep	21 39 55.2 +66 04 07	EW
V1021 Ara	17 51 03.2 -52 35 14	M	V0977 Cep	21 40 29.7 +66 26 44	INT:
V1022 Ara	17 51 07.7 -52 53 25	M	V0978 Cep	21 40 30.7 +66 26 03	LB:
V1023 Ara	17 51 52.5 -54 51 53	SR	V0979 Cep	21 40 51.0 +66 03 48	LB
V1024 Ara	17 53 15.9 -51 01 59	SR	V0980 Cep	21 40 57.6 +66 02 26	LB
V1025 Ara	17 53 45.0 -48 52 00	M	V0981 Cep	21 41 23.6 +65 55 38	SRB
V1026 Ara	17 55 16.9 -56 27 04	SRB	V0982 Cep	21 41 33.2 +66 22 20	INT
V1027 Ara	17 55 59.4 -56 42 23	RRC:	V0983 Cep	21 42 12.0 +66 00 25	INT:

Table 1 (continued)

Name	R.A., Decl., 2000.0 h m s o ' "	Type	Name	R.A., Decl., 2000.0 h m s o ' "	Type
V0984 Cep	21 42 21.1 +65 55 41	LB	V2674 Cyg	19 29 31.9 +41 42 10	EA
V0985 Cep	21 42 40.2 +66 13 29	INT:	V2675 Cyg	19 29 34.8 +41 50 54	LB:
V0986 Cep	21 42 42.8 +66 12 28	EB	V2676 Cyg	19 29 38.0 +43 47 51	EW
V0987 Cep	21 42 47.1 +66 04 58	BY:	V2677 Cyg	19 29 39.5 +41 48 38	DSCT
V0988 Cep	21 42 52.6 +66 06 57	INT	V2678 Cyg	19 29 41.3 +42 30 07	EW
V0989 Cep	21 42 53.5 +66 08 05	INT:	V2679 Cyg	19 29 53.6 +43 24 57	EW
V0990 Cep	21 42 59.6 +66 04 34	INT	V2680 Cyg	19 30 27.4 +43 10 32	EB
V0991 Cep	21 43 01.9 +66 06 45	INT:	V2681 Cyg	19 30 52.3 +43 09 56	LB
V0992 Cep	21 43 07.8 +65 57 10	IN:	V2682 Cyg	19 31 07.3 +42 30 24	BY:
V0993 Cep	21 43 11.6 +66 09 11	INT	V2683 Cyg	19 39 02.6 +30 32 08	EB
V0994 Cep	21 43 16.8 +66 05 49	INT:	V2684 Cyg	19 39 55.9 +52 35 10	DSCT
V0995 Cep	21 43 22.9 +66 10 00	IN:	V2685 Cyg	19 41 29.4 +30 51 19	EA
V0996 Cep	21 43 27.0 +66 09 37	IN:	V2686 Cyg	19 50 48.7 +33 12 55	EB
V0997 Cep	21 43 31.8 +66 08 51	INT	V2687 Cyg	19 51 44.8 +37 40 15	EW
V0998 Cep	21 43 36.3 +66 11 33	BY:	V2688 Cyg	19 51 45.1 +37 16 29	EA
V0999 Cep	21 43 37.7 +65 50 49	INT:	V2689 Cyg	19 51 46.5 +37 16 16	EA
V1000 Cep	21 43 52.8 +65 54 28	SRB:	V2690 Cyg	19 51 47.5 +37 16 48	NL
V1001 Cep	21 44 06.3 +66 04 23	INT:	V2691 Cyg	19 51 50.5 +37 19 27	EA
V1002 Cep	21 44 13.2 +65 45 01	EB	V2692 Cyg	19 51 52.9 +37 18 10	EW
V1003 Cep	21 44 28.4 +65 46 37	EW	V2693 Cyg	19 51 54.5 +37 16 26	EW
V1004 Cep	21 44 29.6 +65 48 44	EA	V2694 Cyg	19 54 39.5 +32 56 03	DSCTC
V1005 Cep	21 44 46.5 +66 27 02	SR	V2695 Cyg	19 55 23.8 +37 28 59	DSCT
V1006 Cep	21 44 56.0 +65 45 50	LB	V2696 Cyg	19 55 44.6 +29 31 43	M
V1007 Cep	21 45 15.2 +65 49 24	EW:	V2697 Cyg	19 57 27.5 +43 17 44	EW
V1008 Cep	22 07 56.2 +54 31 06	XP	V2698 Cyg	19 59 06.8 +44 27 40	EA/RS
V1009 Cep	22 08 41.2 +54 33 18	DSCTC	V2699 Cyg	19 59 25.3 +58 33 20	GDOR
V1010 Cep	22 36 15.9 +70 32 04	RS	V2700 Cyg	20 03 18.7 +33 27 00	BCEP
V1011 Cep	22 48 36.3 +58 45 14	EA	V2701 Cyg	20 04 06.2 +41 39 54	EW
V1012 Cep	22 49 55.6 +57 12 10	EA:	V2702 Cyg	20 05 50.6 +30 58 57	DSCT
V1013 Cep	22 50 05.0 +59 00 47	EW	V2703 Cyg	20 08 01.6 +30 52 44	DSCTC
V1014 Cep	22 50 18.6 +56 55 47	SRB:	V2704 Cyg	20 15 16.6 +56 10 06	RS
V1015 Cep	23 05 55.6 +71 44 20	EW	V2705 Cyg	20 32 05.9 +31 17 58	EB
V1016 Cep	23 07 12.9 +71 40 28	DSCTC	V2706 Cyg	20 32 08.8 +31 24 17	DSCT
V1017 Cep	23 56 06.1 +71 00 00	LB	V2707 Cyg	20 32 29.6 +31 21 46	BY:
V1018 Cep	23 57 42.2 +69 01 34	M:	V2708 Cyg	20 32 39.2 +31 11 58	EW
V0754 CrA	18 02 10.6 -38 32 39	LB	V2709 Cyg	20 34 14.5 +50 48 06	NL+ZZ:
V0755 CrA	18 02 44.6 -45 04 30	EW	V2710 Cyg	20 38 06.2 +39 46 00	RS
V0756 CrA	18 25 36.3 -42 13 36	DSCT	V2711 Cyg	20 47 31.6 +30 31 03	M
V0757 CrA	18 52 19.3 -42 43 32	M	V2712 Cyg	20 58 01.5 +35 09 19	DSCTC
V0758 CrA	18 56 54.3 -42 12 27	M	V2713 Cyg	20 59 17.4 +45 06 43	EW
V2660 Cyg	19 19 30.2 +43 47 24	EW	V2714 Cyg	21 00 10.1 +33 59 43	EW
V2661 Cyg	19 20 08.3 +43 51 12	EW	V2715 Cyg	21 00 18.6 +34 21 38	EW
V2662 Cyg	19 27 37.0 +43 51 10	EB	V2716 Cyg	21 00 24.8 +34 09 43	EW
V2663 Cyg	19 28 26.0 +43 32 53	EA	V2717 Cyg	21 00 33.7 +33 30 09	EW
V2664 Cyg	19 28 37.8 +42 17 28	EW	V2718 Cyg	21 00 39.5 +33 33 31	EW
V2665 Cyg	19 28 44.3 +41 48 56	EW	V2719 Cyg	21 00 40.2 +34 01 02	EW
V2666 Cyg	19 28 58.5 +43 23 52	EA	V2720 Cyg	21 00 40.4 +33 56 49	EW
V2667 Cyg	19 29 07.4 +42 37 55	BY:	V2721 Cyg	21 00 41.3 +34 17 40	BY:
V2668 Cyg	19 29 09.5 +41 50 58	EW	V2722 Cyg	21 00 42.0 +33 47 09	EW
V2669 Cyg	19 29 15.9 +43 03 50	EW	V2723 Cyg	21 00 48.9 +33 31 37	EA
V2670 Cyg	19 29 25.0 +41 44 32	EA	V2724 Cyg	21 00 49.9 +34 01 34	EW
V2671 Cyg	19 29 26.6 +42 36 10	LB:	V2725 Cyg	21 00 54.4 +34 11 19	EW
V2672 Cyg	19 29 28.8 +30 26 36	EA	V2726 Cyg	21 00 56.9 +34 11 13	EW
V2673 Cyg	19 29 31.0 +41 54 02	RRC	V2727 Cyg	21 01 00.2 +34 15 58	DCEP:

Table 1 (continued)

Name	R.A., Decl., 2000.0	Type	Name	R.A., Decl., 2000.0	Type
	h m s o ' "			h m s o ' "	
V2728 Cyg	21 01 06.8 +34 23 57	EA:	V2782 Cyg	21 11 47.9 +41 07 47	EA
V2729 Cyg	21 01 12.6 +33 42 03	EB	V2783 Cyg	21 11 55.9 +40 48 12	EW
V2730 Cyg	21 01 19.7 +33 54 12	BY:	V2784 Cyg	21 11 59.0 +41 09 57	EW
V2731 Cyg	21 01 20.0 +33 38 28	EW	V2785 Cyg	21 12 01.9 +40 35 11	EA
V2732 Cyg	21 01 27.9 +33 39 49	EW	V2786 Cyg	21 12 08.4 +40 30 05	RRAB
V2733 Cyg	21 01 28.2 +33 53 54	EA	V2787 Cyg	21 12 11.9 +41 02 42	EB
V2734 Cyg	21 01 33.5 +34 20 34	EA	V2788 Cyg	21 12 18.9 +40 54 15	EW
V2735 Cyg	21 01 36.4 +34 22 33	EA	V2789 Cyg	21 12 21.9 +40 24 33	EW
V2736 Cyg	21 01 41.0 +33 32 24	GDOR	V2790 Cyg	21 12 30.9 +41 14 48	EB
V2737 Cyg	21 01 41.2 +33 49 41	EW	V2791 Cyg	21 12 42.9 +40 56 00	EW
V2738 Cyg	21 01 42.1 +34 11 42	EW	V2792 Cyg	21 12 46.0 +40 54 49	EB
V2739 Cyg	21 01 42.3 +34 12 36	EW	V2793 Cyg	21 12 49.3 +40 31 10	EA
V2740 Cyg	21 01 51.3 +34 00 03	EA	V2794 Cyg	21 12 59.8 +46 59 03	ACV:
V2741 Cyg	21 01 52.9 +34 25 02	EW	V2795 Cyg	21 13 24.8 +40 39 58	EA
V2742 Cyg	21 01 55.0 +45 17 21	SR	V2796 Cyg	21 13 32.6 +40 37 32	EA
V2743 Cyg	21 01 57.2 +34 00 32	EW	V2797 Cyg	21 13 33.7 +40 29 55	EA
V2744 Cyg	21 01 58.7 +34 07 41	EW	V2798 Cyg	21 13 36.5 +41 12 23	EW
V2745 Cyg	21 02 00.0 +34 01 14	EA	V2799 Cyg	21 13 36.7 +47 05 40	DSCTC
V2746 Cyg	21 02 04.2 +34 01 30	EW	V2800 Cyg	21 13 38.4 +47 03 29	EW
V2747 Cyg	21 02 09.5 +34 12 25	EW	V2801 Cyg	21 13 42.5 +40 57 35	EA
V2748 Cyg	21 02 11.6 +34 00 07	EA	V2802 Cyg	21 13 45.5 +41 14 12	EW
V2749 Cyg	21 02 16.3 +34 12 21	RRAB	V2803 Cyg	21 13 49.2 +46 59 42	CWB
V2750 Cyg	21 02 19.9 +33 42 06	EW	V2804 Cyg	21 13 51.4 +47 03 44	ACV:
V2751 Cyg	21 02 20.9 +34 17 00	EW	V2805 Cyg	21 13 56.8 +47 02 34	ACV:
V2752 Cyg	21 02 30.4 +33 46 13	EW	V2806 Cyg	21 13 58.9 +40 33 26	EW
V2753 Cyg	21 02 39.5 +34 19 32	EW	V2807 Cyg	21 14 02.8 +47 00 21	SRB
V2754 Cyg	21 02 45.3 +33 43 09	EW	V2808 Cyg	21 14 05.2 +40 32 44	EB
V2755 Cyg	21 02 57.3 +33 41 59	EW	V2809 Cyg	21 14 07.6 +47 02 26	SRD:
V2756 Cyg	21 03 00.4 +33 51 40	EB	V2810 Cyg	21 14 14.5 +47 01 17	LB
V2757 Cyg	21 03 00.8 +33 55 43	EW	V2811 Cyg	21 14 17.6 +40 53 05	EB
V2758 Cyg	21 03 02.3 +34 10 20	EW	V2812 Cyg	21 14 19.5 +47 02 17	EA
V2759 Cyg	21 03 15.2 +34 16 35	EW	V2813 Cyg	21 14 21.3 +47 05 57	EA
V2760 Cyg	21 03 21.0 +33 43 14	EA	V2814 Cyg	21 14 26.9 +41 07 26	EW
V2761 Cyg	21 03 29.4 +34 14 23	EB	V2815 Cyg	21 14 41.5 +40 26 37	EW
V2762 Cyg	21 03 35.7 +45 45 06	XN	V2816 Cyg	21 14 43.9 +40 28 33	EW
V2763 Cyg	21 03 42.5 +33 53 25	EA	V2817 Cyg	21 14 59.5 +40 44 38	EW
V2764 Cyg	21 03 46.5 +33 59 47	EW	V2818 Cyg	21 15 13.1 +41 03 23	EW
V2765 Cyg	21 03 58.1 +33 47 44	BY:	V2819 Cyg	21 15 15.9 +40 52 40	EW
V2766 Cyg	21 04 03.9 +33 33 07	EW	V2820 Cyg	21 15 21.6 +40 35 54	EW
V2767 Cyg	21 04 22.8 +33 32 21	EA	V2821 Cyg	21 15 22.7 +40 53 11	EA
V2768 Cyg	21 04 29.3 +34 13 44	EW	V2822 Cyg	21 15 28.7 +40 44 30	EW
V2769 Cyg	21 04 59.3 +46 54 10	M	V2823 Cyg	21 15 32.5 +41 01 49	EB
V2770 Cyg	21 06 44.7 +45 51 53	RRC	V2824 Cyg	21 15 36.7 +41 05 15	EW
V2771 Cyg	21 07 09.9 +30 52 35	DSCT	V2825 Cyg	21 15 38.9 +41 15 11	EA
V2772 Cyg	21 09 46.5 +46 43 28	EA	V2826 Cyg	21 15 41.3 +40 29 44	EW
V2773 Cyg	21 10 38.8 +47 12 09	LPB:	V2827 Cyg	21 15 41.6 +40 41 10	EB
V2774 Cyg	21 11 09.2 +40 42 43	EW	V2828 Cyg	21 15 43.5 +40 37 00	EB
V2775 Cyg	21 11 09.6 +41 08 04	EW	V2829 Cyg	21 15 45.3 +41 00 02	EW
V2776 Cyg	21 11 11.9 +40 36 31	EW	V2830 Cyg	21 15 45.5 +40 48 06	EW
V2777 Cyg	21 11 20.0 +41 03 29	EW	V2831 Cyg	21 16 54.2 +41 33 56	SRA:
V2778 Cyg	21 11 24.1 +40 51 11	EW	V2832 Cyg	21 33 20.0 +51 08 19	EW
V2779 Cyg	21 11 33.5 +41 11 18	EW	V2833 Cyg	21 33 21.6 +51 08 57	EW
V2780 Cyg	21 11 40.4 +40 40 37	EW	V2834 Cyg	21 33 42.7 +49 28 15	EW
V2781 Cyg	21 11 46.9 +40 35 15	BY:	V2835 Cyg	21 33 45.1 +49 29 22	DCEP

Table 1 (continued)

Name	R.A., Decl., 2000.0	Type	Name	R.A., Decl., 2000.0	Type
	h m s o ' "			h m s o ' "	
V2836 Cyg	21 33 49.2 +49 29 20	EW	V1409 Her	17 34 27.1 +32 13 31	EB
V2837 Cyg	21 33 49.6 +49 29 35	EW	V1410 Her	17 35 38.6 +32 26 32	DSCT:
V2838 Cyg	21 38 46.4 +48 19 22	DSCT	V1411 Her	17 36 37.4 +17 04 30	SRA
V2839 Cyg	21 47 02.3 +43 19 19	DSCTC	V1412 Her	17 37 23.2 +26 02 51	EB
V2840 Cyg	21 49 13.2 +30 58 06	EW	V1413 Her	17 38 22.6 +26 33 04	EW
V2841 Cyg	21 55 56.5 +50 32 20	EA	V1414 Her	17 38 48.9 +26 34 37	EW
V0340 Del	20 22 51.0 +10 26 29	EW	V1415 Her	17 38 51.3 +25 57 46	EA
V0341 Del	20 23 09.8 +14 06 43	EB	V1416 Her	17 39 00.0 +26 28 29	EW
V0342 Del	20 37 47.6 +16 18 55	EW	V1417 Her	17 39 03.3 +38 41 38	LB
V0343 Del	21 03 23.3 +19 30 56	RS	V1418 Her	17 39 14.1 +26 42 43	EW
V0344 Del	21 08 09.9 +18 33 30	EA	V1419 Her	17 39 14.3 +26 32 02	EW
V0517 Dra	17 30 45.3 +70 31 49	LB	V1420 Her	17 39 52.7 +26 10 20	EW
V0518 Dra	17 33 16.8 +70 42 26	EB	V1421 Her	17 41 41.2 +29 14 13	LB
V0519 Dra	17 34 34.6 +68 29 26	LB	V1422 Her	17 41 43.4 +14 47 05	RRAB
V0520 Dra	17 41 09.4 +66 52 21	EW	V1423 Her	17 41 59.6 +14 26 10	RRAB
V0521 Dra	17 44 10.9 +72 03 03	RS	V1424 Her	17 42 34.8 +33 23 23	EW
V0522 Dra	17 49 04.3 +72 30 10	LB	V1425 Her	17 43 08.9 +21 51 24	RRAB
V0523 Dra	17 50 25.5 +64 19 44	EW	V1426 Her	17 43 14.8 +37 27 15	LB
V0524 Dra	17 52 20.1 +66 14 34	EW	V1427 Her	17 45 18.5 +17 15 32	LB
V0525 Dra	17 54 28.8 +68 49 01	SR	V1428 Her	17 46 25.4 +34 08 45	RRAB
V0526 Dra	18 35 33.9 +60 15 22	LB	V1429 Her	17 47 02.2 +45 39 44	LB
V0527 Dra	18 38 56.2 +60 23 54	EB	V1430 Her	17 47 06.8 +14 44 12	SRA
V0528 Dra	18 39 58.4 +58 55 54	BY	V1431 Her	17 47 54.3 +29 23 42	RRAB
V0529 Dra	18 42 28.1 +48 37 41	UGSU	V1432 Her	17 49 38.7 +30 10 02	RRAB
V0530 Dra	18 48 29.4 +64 23 28	RS	V1433 Her	17 50 04.7 +16 00 01	EW
V0531 Dra	18 54 48.5 +60 35 06	SR:	V1434 Her	17 52 07.0 +37 32 46	EP
V0532 Dra	18 56 02.9 +72 05 39	EW	V1435 Her	17 52 12.0 +37 39 07	EW
V0533 Dra	18 56 07.9 +59 37 45	SR	V1436 Her	17 52 45.1 +35 39 21	SR:
V0534 Dra	19 08 10.5 +49 24 24	EW	V1437 Her	17 53 38.6 +16 40 14	M:
V0535 Dra	19 13 33.3 +70 28 46	LB	V1438 Her	17 54 12.3 +17 28 55	SR
V0536 Dra	19 14 43.5 +60 52 14	UGSU	V1439 Her	17 54 29.5 +14 47 43	LB
V0537 Dra	19 18 32.7 +70 12 35	LB	V1440 Her	17 56 04.0 +46 42 37	DSCTC:
V0538 Dra	19 27 53.7 +77 17 42	EA	V1441 Her	18 02 52.5 +21 31 51	DSCT
V0539 Dra	19 30 00.0 +70 12 37	EW	V1442 Her	18 09 30.3 +32 45 14	RRC
V0540 Dra	19 41 32.6 +71 57 17	EA	V1443 Her	18 13 52.4 +17 14 46	BY
V0541 Dra	19 47 52.6 +72 47 39	EW	V1444 Her	18 16 13.6 +16 24 33	EW
V0542 Dra	19 49 39.9 +70 18 33	EW	V1445 Her	18 16 52.8 +17 57 03	RS
V0543 Dra	19 55 59.7 +69 02 27	LB	V1446 Her	18 18 58.1 +21 05 43	SR
V0544 Dra	20 16 08.5 +70 53 56	BY	V1447 Her	18 27 09.0 +22 49 26	SR
V0545 Dra	20 29 39.4 +73 54 34	RS	V1448 Her	18 35 12.2 +18 40 11	SRB
VY Equ	20 58 49.6 +08 54 05	DSCT	V1449 Her	18 35 56.3 +22 26 40	UG
EQ Gru	21 30 12.1 -44 15 20	RRC	V1450 Her	18 39 00.0 +20 04 02	EW
ER Gru	21 35 31.0 -39 06 31	RRAB	V1451 Her	18 40 07.0 +14 11 45	M
ES Gru	21 38 25.8 -39 44 56	RRC	DI Ind	20 37 49.3 -57 35 32	RRC:
ET Gru	21 46 00.4 -40 15 54	RRAB	DK Ind	20 41 14.5 -50 11 04	M
EU Gru	21 57 36.6 -45 32 37	RRC	DL Ind	21 07 41.0 -58 44 09	RRC
EV Gru	22 10 39.2 -50 49 47	RRC	DM Ind	21 11 35.3 -58 50 15	RRC
EW Gru	22 16 52.4 -51 44 01	RRAB	DN Ind	21 16 20.3 -59 01 57	EW
EX Gru	22 20 40.6 -37 02 16	RRAB	DO Ind	21 19 10.4 -45 22 34	RRC
EY Gru	23 12 14.2 -37 37 20	RRC	DP Ind	21 19 29.0 -52 09 47	SR
EZ Gru	23 19 17.1 -37 40 48	RRC	DQ Ind	21 20 26.4 -58 25 02	EW:
FF Gru	23 19 59.9 -45 00 46	RRAB:	DR Ind	21 20 45.3 -56 49 15	BY:
FG Gru	23 23 42.5 -41 57 24	RRC:	DS Ind	22 04 54.0 -66 34 57	RRAB
V1408 Her	17 31 07.2 +21 23 10	EW	DT Ind	23 21 52.5 -69 42 12	BY

Table 1 (continued)

Name	R.A., Decl., 2000.0	Type	Name	R.A., Decl., 2000.0	Type
	h m s o ' "			h m s o ' "	
V0481 Lac	21 59 17.1 +44 18 58	DSCT	V0535 Lac	22 45 38.1 +51 45 01	BY
V0482 Lac	22 02 10.6 +44 01 23	EW	V0536 Lac	22 45 44.8 +52 18 47	EW
V0483 Lac	22 06 03.0 +46 17 23	EB	V0537 Lac	22 45 48.2 +52 52 38	EW
V0484 Lac	22 11 33.4 +40 41 51	EA	V0538 Lac	22 45 52.6 +50 56 42	DSCTC
V0485 Lac	22 14 17.9 +51 48 06	EW	V0539 Lac	22 46 06.5 +51 54 03	LB:
V0486 Lac	22 14 18.7 +51 42 56	EW:	V0540 Lac	22 46 18.4 +43 52 08	RRC
V0487 Lac	22 15 46.3 +48 39 06	EW	V0541 Lac	22 46 22.5 +52 10 54	LB
V0488 Lac	22 19 19.1 +51 39 35	EW	V0542 Lac	22 46 26.8 +51 08 04	LB
V0489 Lac	22 22 57.1 +51 37 00	EW	V0543 Lac	22 46 32.1 +52 30 20	RRC
V0490 Lac	22 24 31.8 +50 01 41	EB	V0544 Lac	22 46 33.7 +52 11 15	EW
V0491 Lac	22 26 19.2 +52 15 02	DSCT	V0545 Lac	22 46 42.0 +52 22 27	EA
V0492 Lac	22 27 04.3 +44 45 59	EW	V0546 Lac	22 47 01.6 +51 05 19	EA
V0493 Lac	22 28 15.6 +52 24 46	DSCT	V0547 Lac	22 47 21.4 +39 09 22	DSCT
V0494 Lac	22 34 08.7 +44 35 00	LB	V0548 Lac	22 47 27.9 +45 53 30	RRC
V0495 Lac	22 34 16.3 +55 34 24	EA	V0549 Lac	22 47 28.4 +52 39 13	EW
V0496 Lac	22 34 21.5 +55 30 13	EA	V0550 Lac	22 47 53.0 +52 28 50	EW
V0497 Lac	22 34 25.1 +46 35 40	LB	V0551 Lac	22 48 06.0 +52 15 57	EW
V0498 Lac	22 34 29.3 +55 29 03	EW	V0552 Lac	22 48 06.7 +52 09 56	EW
V0499 Lac	22 38 02.5 +36 40 11	SR	V0553 Lac	22 48 07.2 +52 57 47	EW
V0500 Lac	22 38 51.3 +40 03 47	EA	V0554 Lac	22 48 09.5 +52 53 01	LB:
V0501 Lac	22 40 07.7 +39 52 07	LB	V0555 Lac	22 48 11.6 +51 17 13	BY:
V0502 Lac	22 40 56.6 +40 33 53	LB	V0556 Lac	22 48 14.2 +51 44 15	EA
V0503 Lac	22 41 16.6 +44 47 45	EW	V0557 Lac	22 48 15.7 +51 43 33	EA
V0504 Lac	22 41 47.8 +36 24 56	EB	V0558 Lac	22 48 21.0 +52 20 04	LB:
V0505 Lac	22 42 47.7 +45 21 05	EW	V0559 Lac	22 48 25.2 +51 15 11	EW
V0506 Lac	22 42 49.9 +52 27 09	EW	V0560 Lac	22 48 32.5 +50 49 35	EW
V0507 Lac	22 43 00.8 +52 00 17	EW	V0561 Lac	22 48 43.9 +52 48 02	EW
V0508 Lac	22 43 02.8 +52 02 13	LB:	V0562 Lac	22 48 45.2 +51 01 14	EA
V0509 Lac	22 43 03.4 +51 43 19	EW	V0563 Lac	22 48 59.7 +53 07 38	EW
V0510 Lac	22 43 12.7 +52 40 28	EA	V0564 Lac	22 49 02.4 +44 41 00	SRB
V0511 Lac	22 43 18.7 +51 41 21	EW	V0565 Lac	22 49 07.6 +51 59 16	EA
V0512 Lac	22 43 33.3 +52 42 23	EW	V0566 Lac	22 49 11.1 +52 20 35	EW
V0513 Lac	22 43 39.4 +52 10 57	EW	V0567 Lac	22 49 19.8 +51 54 49	LB:
V0514 Lac	22 43 44.0 +51 10 19	EA	V0568 Lac	22 49 21.0 +51 11 09	DSCTC
V0515 Lac	22 44 00.1 +52 44 52	LB	V0569 Lac	22 49 24.4 +52 58 50	EW
V0516 Lac	22 44 03.5 +51 41 57	EW	V0570 Lac	22 49 34.1 +53 04 15	EA
V0517 Lac	22 44 06.1 +52 58 46	EA	V0571 Lac	22 49 37.1 +39 58 12	LB
V0518 Lac	22 44 07.2 +52 47 44	EW	V0572 Lac	22 49 47.5 +53 04 04	EA
V0519 Lac	22 44 19.2 +37 51 51	EW	V0573 Lac	22 49 57.4 +51 25 15	EW
V0520 Lac	22 44 20.1 +52 15 30	EW	V0574 Lac	22 50 05.1 +40 05 44	SR
V0521 Lac	22 44 21.1 +50 59 17	EW	V0575 Lac	22 50 13.7 +52 00 09	EW
V0522 Lac	22 44 25.2 +51 32 04	EA	V0576 Lac	22 50 16.2 +50 53 57	LB:
V0523 Lac	22 44 29.6 +52 05 14	EW	V0577 Lac	22 50 23.0 +51 14 51	SR
V0524 Lac	22 44 37.0 +51 23 27	DSCTC	V0578 Lac	22 50 26.1 +51 50 16	BY
V0525 Lac	22 44 41.4 +49 52 29	EW	V0579 Lac	22 50 26.7 +52 08 17	DSCTC
V0526 Lac	22 44 46.5 +52 49 44	EW	V0580 Lac	22 50 36.8 +52 33 20	EA
V0527 Lac	22 44 47.5 +51 15 17	EW	V0581 Lac	22 50 37.2 +51 51 06	EW
V0528 Lac	22 44 49.6 +51 21 19	EW	V0582 Lac	22 50 45.6 +51 38 42	EW
V0529 Lac	22 45 00.5 +51 42 46	EA	V0583 Lac	22 50 51.5 +52 03 22	EW
V0530 Lac	22 45 13.0 +51 02 27	RRC	V0584 Lac	22 50 55.4 +51 53 31	EW
V0531 Lac	22 45 13.9 +52 50 17	EW	V0585 Lac	22 51 00.3 +51 18 38	EB
V0532 Lac	22 45 27.5 +51 21 11	BY	V0586 Lac	22 51 04.6 +51 20 41	DSCT
V0533 Lac	22 45 28.9 +51 01 43	LB:	V0587 Lac	22 51 10.1 +51 18 56	EA
V0534 Lac	22 45 33.0 +52 40 05	EB	V0588 Lac	22 51 18.0 +51 20 12	EW

Table 1 (continued)

Name	R.A., Decl., 2000.0	Type	Name	R.A., Decl., 2000.0	Type
	h m s o ' "			h m s o ' "	
V0589 Lac	22 51 30.2 +52 55 16	EB	V0643 Lac	22 56 05.4 +53 07 24	EW
V0590 Lac	22 51 32.1 +50 52 17	EA	V0644 Lac	22 56 15.5 +52 03 46	EW
V0591 Lac	22 51 32.5 +52 19 41	EW	V0645 Lac	22 56 28.8 +45 30 44	SR
V0592 Lac	22 51 34.5 +51 01 46	BY	V0646 Lac	22 56 33.8 +52 02 38	EW
V0593 Lac	22 51 36.7 +51 32 45	EA	V0647 Lac	22 56 36.6 +52 33 39	EW:
V0594 Lac	22 51 52.5 +52 38 14	EW	V0648 Lac	22 56 44.4 +53 07 53	BY
V0595 Lac	22 51 54.2 +50 53 37	EA	V0649 Lac	22 56 48.6 +52 10 38	DSCTC
V0596 Lac	22 52 07.1 +51 41 00	EW	V0650 Lac	22 56 52.6 +52 03 33	LB
V0597 Lac	22 52 16.2 +52 07 38	EA	V0651 Lac	22 56 56.6 +51 18 58	EB:
V0598 Lac	22 52 17.6 +51 46 23	BY:	V0652 Lac	22 56 59.7 +51 53 24	EA
V0599 Lac	22 52 21.2 +52 54 28	EW	V0653 Lac	22 57 04.1 +52 09 04	EA
V0600 Lac	22 52 23.0 +52 53 13	EW	V0654 Lac	22 57 08.4 +52 26 32	EB
V0601 Lac	22 52 29.2 +52 44 33	EA	V0655 Lac	22 57 13.5 +52 16 52	EW
V0602 Lac	22 52 30.3 +53 07 33	EA	V0656 Lac	22 57 22.0 +51 36 52	DSCTC:
V0603 Lac	22 52 37.5 +52 43 06	EA	V0657 Lac	22 57 24.6 +51 16 17	EW
V0604 Lac	22 52 42.3 +53 01 33	EW	V0725 Lyr	18 14 26.8 +47 19 10	EW
V0605 Lac	22 52 43.4 +53 04 49	EW:	V0726 Lyr	18 14 48.2 +47 10 03	RRC
V0606 Lac	22 52 47.2 +37 37 35	BY	V0727 Lyr	18 15 24.5 +33 44 53	LB
V0607 Lac	22 52 54.8 +52 35 03	DSCTC	V0728 Lyr	18 16 08.2 +30 10 35	LB
V0608 Lac	22 52 59.3 +53 01 32	RRC:	V0729 Lyr	18 16 29.0 +36 44 56	RRC
V0609 Lac	22 53 01.5 +52 52 41	LB	V0730 Lyr	18 16 46.4 +30 05 08	LB:
V0610 Lac	22 53 30.3 +51 41 12	EB	V0731 Lyr	18 18 43.3 +33 15 58	LB
V0611 Lac	22 53 32.9 +51 52 27	EW	V0732 Lyr	18 21 41.7 +40 04 37	SRB
V0612 Lac	22 53 43.5 +50 59 53	EW	V0733 Lyr	18 23 37.2 +33 32 10	SR
V0613 Lac	22 53 44.3 +51 53 59	EA	V0734 Lyr	18 31 45.0 +40 38 01	LB
V0614 Lac	22 53 44.4 +51 21 14	L	V0735 Lyr	18 32 05.4 +40 29 58	SRB
V0615 Lac	22 53 44.5 +50 56 41	EW	V0736 Lyr	18 34 29.5 +35 04 24	DSCT
V0616 Lac	22 53 47.5 +51 46 24	EW	V0737 Lyr	18 34 57.8 +30 20 22	SR
V0617 Lac	22 53 53.1 +51 35 18	EW	V0738 Lyr	18 35 28.6 +35 53 25	ELL:
V0618 Lac	22 54 09.8 +52 02 11	EW	V0739 Lyr	18 36 33.5 +30 01 01	SR
V0619 Lac	22 54 41.2 +51 47 00	EA	V0740 Lyr	18 36 41.2 +27 55 23	EW
V0620 Lac	22 54 41.8 +51 53 26	LB	V0741 Lyr	18 37 17.7 +29 25 20	LB
V0621 Lac	22 54 43.9 +52 10 55	BY	V0742 Lyr	18 37 51.3 +47 23 23	RCB
V0622 Lac	22 54 50.2 +52 48 11	EW	V0743 Lyr	18 39 39.2 +29 15 49	LB
V0623 Lac	22 54 59.4 +51 40 37	RRC	V0744 Lyr	18 52 31.2 +41 33 11	LB
V0624 Lac	22 55 01.6 +51 23 26	EW	V0745 Lyr	18 54 22.2 +36 51 07	EA
V0625 Lac	22 55 05.4 +52 07 47	EB	V0746 Lyr	19 01 23.1 +39 39 55	BY+UV
V0626 Lac	22 55 08.0 +52 48 16	EW	V0747 Lyr	19 06 34.4 +43 27 35	EB
V0627 Lac	22 55 12.7 +52 11 20	DSCTC	V0748 Lyr	19 10 13.2 +29 12 33	EW
V0628 Lac	22 55 17.5 +52 00 11	RRC	V0749 Lyr	19 11 31.3 +40 46 53	BY:
V0629 Lac	22 55 18.6 +53 03 04	EA	V0750 Lyr	19 11 33.0 +40 24 10	EW
V0630 Lac	22 55 20.8 +51 20 27	EW	V0751 Lyr	19 12 16.4 +40 26 00	RRAB
V0631 Lac	22 55 22.4 +52 40 23	EA	V0752 Lyr	19 12 16.4 +40 30 22	BY:
V0632 Lac	22 55 25.2 +53 06 55	EW	V0753 Lyr	19 12 17.2 +40 47 13	EW
V0633 Lac	22 55 32.5 +52 49 21	EW	V0754 Lyr	19 12 23.3 +40 49 54	EW
V0634 Lac	22 55 38.7 +55 50 44	LB	V0755 Lyr	19 12 32.5 +40 09 58	EA/RS
V0635 Lac	22 55 44.9 +56 28 37	EA:	V0756 Lyr	19 12 42.7 +40 45 49	BY:
V0636 Lac	22 55 47.6 +51 47 51	EB	V0757 Lyr	19 12 47.7 +40 53 35	EA
V0637 Lac	22 55 48.6 +51 15 14	EB	V0758 Lyr	19 12 56.4 +40 36 23	EW
V0638 Lac	22 55 50.9 +50 54 10	LB	V0759 Lyr	19 12 59.2 +40 54 48	EB
V0639 Lac	22 55 51.2 +51 55 15	EA	V0760 Lyr	19 13 14.6 +39 56 08	RS
V0640 Lac	22 55 55.5 +51 01 31	EW	V0761 Lyr	19 13 15.8 +40 08 28	SR:
V0641 Lac	22 55 56.8 +51 46 08	EW	V0762 Lyr	19 13 20.3 +40 45 28	EW
V0642 Lac	22 56 03.5 +52 01 01	BY:	V0763 Lyr	19 13 40.4 +40 49 13	EW

Table 1 (continued)

Name	R.A., Decl., 2000.0	Type	Name	R.A., Decl., 2000.0	Type
	h m s o ' "			h m s o ' "	
V0764 Lyr	19 13 49.3 +40 54 48	EA	V0818 Lyr	19 25 22.0 +43 17 23	EW:
V0765 Lyr	19 13 50.0 +40 55 36	EW	V0819 Lyr	19 25 22.4 +42 19 48	SR:
V0766 Lyr	19 13 55.9 +40 23 51	EW	V0820 Lyr	19 25 27.2 +41 59 51	LB:
V0767 Lyr	19 13 57.7 +40 45 09	EW	V0821 Lyr	19 26 01.1 +43 00 45	EW
V0768 Lyr	19 14 02.2 +40 26 45	EW	V0822 Lyr	19 26 11.5 +43 26 01	BY:
V0769 Lyr	19 14 14.5 +40 08 10	SR:	V0823 Lyr	19 26 22.2 +42 34 10	EW
V0770 Lyr	19 14 27.1 +40 20 01	BY:	V0824 Lyr	19 26 36.0 +42 10 06	LB
V0771 Lyr	19 14 39.6 +40 39 59	EA	V0825 Lyr	19 26 50.7 +42 05 27	LB
V0772 Lyr	19 14 52.8 +41 24 29	BY	V0826 Lyr	19 27 32.2 +42 54 38	EA
V0773 Lyr	19 14 58.5 +40 52 46	EW	DL Mic	20 27 45.7 -28 50 34	RRC
V0774 Lyr	19 15 11.8 +40 49 10	EW	DM Mic	20 37 38.6 -41 51 57	LB
V0775 Lyr	19 15 18.9 +40 45 51	EW	DN Mic	20 45 11.5 -40 49 58	RS
V0776 Lyr	19 15 30.2 +40 23 44	EW	DO Mic	20 45 36.8 -39 49 57	RS
V0777 Lyr	19 15 36.9 +40 46 16	EW	DP Mic	21 12 04.1 -37 00 08	RRAB
V0778 Lyr	19 15 37.3 +40 10 09	EW:	DQ Mic	21 12 19.0 -33 36 21	RS
V0779 Lyr	19 15 38.1 +40 42 32	EB	DR Mic	21 17 30.4 -35 17 58	RRC
V0780 Lyr	19 15 39.9 +40 42 25	EW	DS Mic	21 23 31.4 -30 24 57	RRC
V0781 Lyr	19 15 42.4 +40 49 36	DSCTC	FP Oct	17 55 43.8 -84 08 27	M
V0782 Lyr	19 15 46.0 +40 28 01	EW	FQ Oct	18 35 39.5 -77 22 29	SRB
V0783 Lyr	19 15 50.1 +40 29 55	BY:	FR Oct	19 31 53.0 -78 55 23	M
V0784 Lyr	19 15 57.0 +40 15 08	EW	FS Oct	21 18 47.1 -81 45 18	BY
V0785 Lyr	19 16 11.3 +40 39 10	EB:	FT Oct	21 25 27.5 -81 38 28	BY
V0786 Lyr	19 19 09.1 +42 22 06	LB:	V2949 Oph	17 34 47.7 -24 09 04	N
V0787 Lyr	19 19 11.7 +43 19 18	BY	V2950 Oph	17 30 01.6 +02 25 35	BY:
V0788 Lyr	19 19 21.1 +43 21 55	EB	V2951 Oph	17 30 06.5 +03 38 20	XM
V0789 Lyr	19 19 28.3 +42 05 40	RRC	V2952 Oph	17 30 10.7 +03 36 20	EB
V0790 Lyr	19 19 28.4 +42 37 53	EW	V2953 Oph	17 30 23.5 +04 08 54	EB
V0791 Lyr	19 19 41.7 +43 13 09	EW	V2954 Oph	17 30 24.6 +03 49 51	RRAB
V0792 Lyr	19 19 44.7 +43 09 26	EW	V2955 Oph	17 30 33.8 +03 29 18	EW
V0793 Lyr	19 20 10.4 +43 42 56	RRC	V2956 Oph	17 30 36.9 +09 41 20	RRAB
V0794 Lyr	19 20 17.5 +42 51 41	EA	V2957 Oph	17 31 01.8 +03 35 02	EB
V0795 Lyr	19 20 22.3 +41 49 25	SR:	V2958 Oph	17 31 25.0 +03 22 31	BY:
V0796 Lyr	19 20 25.5 +42 46 26	EW	V2959 Oph	17 31 28.4 +02 18 38	SR
V0797 Lyr	19 20 49.2 +42 25 51	RRC	V2960 Oph	17 31 28.9 +09 26 53	RRC
V0798 Lyr	19 20 52.8 +41 38 26	L:	V2961 Oph	17 31 33.1 +11 17 20	SR
V0799 Lyr	19 20 55.0 +42 36 07	EW	V2962 Oph	17 32 22.9 +09 36 26	RRAB
V0800 Lyr	19 20 58.8 +42 09 19	EW	V2963 Oph	17 32 56.0 -16 21 09	SRB
V0801 Lyr	19 21 09.4 +42 10 55	DSCT	V2964 Oph	17 32 57.3 -17 39 38	SRA
V0802 Lyr	19 21 09.7 +42 58 58	EA	V2965 Oph	17 33 09.0 +03 16 04	EA
V0803 Lyr	19 21 35.4 +42 43 14	EW	V2966 Oph	17 33 49.7 -19 15 32	M
V0804 Lyr	19 21 41.2 +42 04 09	EW:	V2967 Oph	17 34 42.0 +06 29 45	SRB
V0805 Lyr	19 21 49.0 +41 52 34	EW	V2968 Oph	17 34 49.0 -18 39 40	M
V0806 Lyr	19 21 52.9 +41 49 22	EW	V2969 Oph	17 34 50.2 -19 53 48	SRD
V0807 Lyr	19 22 00.7 +41 45 50	EW	V2970 Oph	17 34 57.5 -18 37 31	RRC:
V0808 Lyr	19 22 16.7 +41 57 33	EW	V2971 Oph	17 35 00.6 -18 21 09	EA
V0809 Lyr	19 22 20.1 +42 50 21	EW	V2972 Oph	17 35 03.6 -18 13 20	M
V0810 Lyr	19 22 21.6 +43 29 44	BY:	V2973 Oph	17 35 12.2 +08 57 04	SRB
V0811 Lyr	19 22 30.4 +43 10 29	EA	V2974 Oph	17 35 12.4 -17 46 19	EW
V0812 Lyr	19 22 34.9 +42 47 52	EA	V2975 Oph	17 35 16.9 -17 58 49	RRC
V0813 Lyr	19 23 48.8 +34 50 32	UG:	V2976 Oph	17 35 23.9 -18 08 30	RRAB
V0814 Lyr	19 23 52.9 +43 00 50	EA	V2977 Oph	17 35 24.9 -18 02 24	RRC
V0815 Lyr	19 24 10.5 +42 07 42	BY	V2978 Oph	17 35 34.0 -18 19 53	SR:
V0816 Lyr	19 24 21.8 +42 29 57	EW	V2979 Oph	17 35 39.6 -18 35 36	SR:
V0817 Lyr	19 24 38.6 +43 14 16	DSCT:	V2980 Oph	17 35 41.7 -17 50 15	RRAB

Table 1 (continued)

Name	R.A., Decl., 2000.0	Type	Name	R.A., Decl., 2000.0	Type
	h m s o ' "			h m s o ' "	
V2981 Oph	17 35 44.2 -18 07 14	RRAB	V3035 Oph	17 40 13.6 +04 53 04	RRAB
V2982 Oph	17 35 44.3 +09 07 54	SRB	V3036 Oph	17 40 13.7 +01 32 52	RRC:
V2983 Oph	17 35 45.1 -17 59 29	RRAB	V3037 Oph	17 40 16.1 -29 03 38	XM
V2984 Oph	17 36 01.0 -18 00 35	EB	V3038 Oph	17 40 26.1 +08 32 19	SRB
V2985 Oph	17 36 01.3 -18 32 05	RRAB	V3039 Oph	17 40 27.6 +02 12 35	LB
V2986 Oph	17 36 01.7 -19 09 14	M	V3040 Oph	17 40 29.8 +06 55 42	RRAB
V2987 Oph	17 36 02.9 -18 26 26	RRC	V3041 Oph	17 40 30.2 +01 56 54	SRD:
V2988 Oph	17 36 07.0 -18 37 41	EA	V3042 Oph	17 40 35.5 +06 17 00	RRAB
V2989 Oph	17 36 07.5 -18 08 28	SRA	V3043 Oph	17 40 38.0 +08 52 15	SR
V2990 Oph	17 36 08.2 -18 02 41	SR:	V3044 Oph	17 40 49.0 -18 32 59	M
V2991 Oph	17 36 09.2 -18 16 36	RRAB	V3045 Oph	17 41 01.7 +04 32 18	LB
V2992 Oph	17 36 09.4 +13 03 30	SRB	V3046 Oph	17 41 14.7 -20 16 28	M
V2993 Oph	17 36 14.7 -18 20 16	SR:	V3047 Oph	17 41 18.9 +03 49 26	SR
V2994 Oph	17 36 19.9 -18 37 33	EW	V3048 Oph	17 41 19.1 -18 00 33	M
V2995 Oph	17 36 20.4 -18 06 09	EA	V3049 Oph	17 41 28.3 +08 01 58	SR
V2996 Oph	17 36 24.5 -18 16 35	RRC	V3050 Oph	17 41 29.0 +03 23 44	RRC
V2997 Oph	17 36 32.9 -18 14 51	RRAB	V3051 Oph	17 41 38.0 +03 46 56	EW
V2998 Oph	17 36 34.2 -18 33 06	SR	V3052 Oph	17 41 49.8 +02 50 11	SR:
V2999 Oph	17 36 39.3 -17 50 40	SR:	V3053 Oph	17 41 52.0 +00 14 57	LB
V3000 Oph	17 36 39.5 -18 29 18	EW	V3054 Oph	17 42 14.0 +05 42 45	EB
V3001 Oph	17 36 47.3 -18 14 56	RRC	V3055 Oph	17 42 21.3 +04 18 42	SR
V3002 Oph	17 36 48.3 -18 08 44	RRAB	V3056 Oph	17 42 27.3 +03 38 34	LB
V3003 Oph	17 36 49.3 -17 50 26	RRC	V3057 Oph	17 42 42.6 +03 00 33	LB
V3004 Oph	17 36 49.4 -18 28 09	RRAB	V3058 Oph	17 42 44.9 +04 46 37	EW
V3005 Oph	17 36 59.4 -18 06 27	SRA:	V3059 Oph	17 43 04.1 +02 06 21	SRB
V3006 Oph	17 37 10.5 -18 31 10	RRAB	V3060 Oph	17 43 04.5 +06 54 44	RRAB
V3007 Oph	17 37 10.7 -17 48 08	RRAB	V3061 Oph	17 43 10.2 +03 29 35	SR
V3008 Oph	17 37 13.7 -18 05 59	RRAB	V3062 Oph	17 43 17.5 -18 24 02	M
V3009 Oph	17 37 24.3 +10 34 49	RRAB	V3063 Oph	17 43 48.3 +02 38 24	RRAB
V3010 Oph	17 37 24.8 +03 48 58	SRB	V3064 Oph	17 43 53.0 +06 36 02	EW
V3011 Oph	17 37 31.6 -18 10 08	SR:	V3065 Oph	17 43 54.8 -28 50 10	EW
V3012 Oph	17 37 36.9 -17 46 32	EB	V3066 Oph	17 44 09.2 +05 44 58	SR
V3013 Oph	17 37 39.8 -18 21 16	RRC:	V3067 Oph	17 44 17.9 +10 41 18	SR:
V3014 Oph	17 37 46.2 -17 52 20	RRAB	V3068 Oph	17 44 19.2 +03 25 23	EW:
V3015 Oph	17 37 46.5 +09 59 02	RRC	V3069 Oph	17 44 19.5 +02 24 30	RRC
V3016 Oph	17 38 02.6 -18 17 47	RRAB:	V3070 Oph	17 44 20.7 +00 19 31	RRAB
V3017 Oph	17 38 03.7 -17 50 01	RRAB	V3071 Oph	17 44 22.9 +00 08 23	RRAB
V3018 Oph	17 38 03.9 -18 28 58	RRAB	V3072 Oph	17 44 32.9 +01 34 14	EW
V3019 Oph	17 38 08.5 -17 51 43	RRAB	V3073 Oph	17 44 34.4 -07 51 22	SRB
V3020 Oph	17 38 11.0 -17 08 04	M	V3074 Oph	17 44 39.6 +02 44 18	LB
V3021 Oph	17 38 15.1 -18 01 29	RRAB	V3075 Oph	17 45 00.4 +01 27 41	EB
V3022 Oph	17 38 17.9 -18 32 09	M:	V3076 Oph	17 45 13.7 +05 03 16	LB
V3023 Oph	17 38 18.2 -18 20 01	RRC	V3077 Oph	17 45 18.1 +08 14 21	RRAB
V3024 Oph	17 38 18.7 -18 36 13	RRAB	V3078 Oph	17 45 25.7 +02 16 46	DSCT
V3025 Oph	17 38 22.0 -18 14 53	RRAB	V3079 Oph	17 45 38.1 +01 15 31	RRAB
V3026 Oph	17 38 27.4 -18 23 03	RRAB	V3080 Oph	17 45 40.5 +01 01 59	RRC
V3027 Oph	17 38 28.8 +03 19 37	SRB	V3081 Oph	17 45 49.6 +05 13 50	LB
V3028 Oph	17 38 38.2 -17 46 15	RRAB	V3082 Oph	17 45 57.4 +05 02 46	RRAB
V3029 Oph	17 38 39.8 -18 07 46	RRAB	V3083 Oph	17 46 15.3 +06 14 15	SRB
V3030 Oph	17 39 34.8 +09 49 10	SR	V3084 Oph	17 46 25.4 +03 58 49	RS
V3031 Oph	17 39 53.1 -18 06 34	LB	V3085 Oph	17 46 25.8 +00 15 24	LB
V3032 Oph	17 40 07.8 +04 24 28	LB	V3086 Oph	17 47 19.4 +00 13 54	EW
V3033 Oph	17 40 12.7 +10 12 31	RRAB	V3087 Oph	17 47 23.3 +06 10 27	EW
V3034 Oph	17 40 13.3 +06 02 52	RRAB	V3088 Oph	17 47 42.7 +10 27 10	EW

Table 1 (continued)

Name	R.A., Decl., 2000.0	Type	Name	R.A., Decl., 2000.0	Type
	h m s o ' "			h m s o ' "	
V3089 Oph	17 47 55.1 +08 15 58	EW	V3143 Oph	17 52 28.5 +02 52 47	EA
V3090 Oph	17 47 59.4 +05 46 07	EB	V3144 Oph	17 52 28.7 +07 01 01	EA
V3091 Oph	17 48 06.3 +08 12 54	RRC	V3145 Oph	17 52 31.5 +05 01 18	RRC
V3092 Oph	17 48 09.1 +05 08 33	RRAB	V3146 Oph	17 52 36.7 +00 41 23	EW
V3093 Oph	17 48 09.7 +06 09 10	EW	V3147 Oph	17 52 37.3 +07 20 50	EW
V3094 Oph	17 48 23.1 +06 37 29	SR:	V3148 Oph	17 52 40.6 +08 28 06	EW
V3095 Oph	17 48 29.2 +05 29 17	EA	V3149 Oph	17 52 41.9 +03 04 44	SR
V3096 Oph	17 48 34.3 +06 30 25	EB	V3150 Oph	17 52 44.9 +03 33 40	LB
V3097 Oph	17 48 34.6 +08 09 41	RRC	V3151 Oph	17 52 53.8 +02 15 56	EW
V3098 Oph	17 48 40.0 +08 29 06	RRAB	V3152 Oph	17 52 53.8 +04 24 34	RRC
V3099 Oph	17 48 41.6 -00 24 26	EW	V3153 Oph	17 53 04.0 +06 14 32	SR:
V3100 Oph	17 48 50.1 +05 59 20	LB	V3154 Oph	17 53 04.8 +06 13 46	RRAB
V3101 Oph	17 48 58.3 +02 02 14	EW	V3155 Oph	17 53 07.4 +03 13 39	EB
V3102 Oph	17 49 03.4 +05 06 19	EW	V3156 Oph	17 53 08.5 +04 32 04	RRC
V3103 Oph	17 49 06.6 +01 42 20	LB	V3157 Oph	17 53 22.3 +04 00 01	EW:
V3104 Oph	17 49 11.1 +08 24 26	RRC	V3158 Oph	17 53 32.3 +06 08 35	EW
V3105 Oph	17 49 11.1 +06 03 53	RRAB	V3159 Oph	17 53 43.4 +01 52 36	RRAB
V3106 Oph	17 49 30.2 +04 18 40	LB	V3160 Oph	17 53 44.1 +07 00 53	LB
V3107 Oph	17 49 37.3 +06 51 44	SR:	V3161 Oph	17 53 44.2 +02 37 42	RRC
V3108 Oph	17 49 37.5 +06 55 14	SRB	V3162 Oph	17 53 50.6 +07 13 27	RRC
V3109 Oph	17 49 46.8 +05 30 56	RRAB	V3163 Oph	17 53 50.8 -00 28 46	LB
V3110 Oph	17 49 50.7 -00 11 01	RRC	V3164 Oph	17 53 51.8 +00 28 39	LB
V3111 Oph	17 49 51.7 +07 16 41	EW	V3165 Oph	17 53 52.8 +06 11 26	LB
V3112 Oph	17 49 52.6 +03 30 03	RRC	V3166 Oph	17 53 57.6 +00 58 53	RRAB
V3113 Oph	17 50 00.3 +04 38 18	RRAB	V3167 Oph	17 54 01.9 +01 03 18	EW
V3114 Oph	17 50 02.1 +01 34 35	RRAB	V3168 Oph	17 54 05.1 +00 34 05	LB
V3115 Oph	17 50 10.5 +09 02 35	EW	V3169 Oph	17 54 07.0 +02 04 03	EW:
V3116 Oph	17 50 26.9 +02 19 23	LB	V3170 Oph	17 54 08.4 +00 59 49	EA
V3117 Oph	17 50 43.1 +01 00 26	EW	V3171 Oph	17 54 20.5 +04 52 03	LB
V3118 Oph	17 50 45.5 +01 23 52	RRAB	V3172 Oph	17 54 23.4 +08 13 13	RRAB
V3119 Oph	17 50 46.8 +06 07 58	RRC	V3173 Oph	17 54 23.5 +06 21 45	RRAB
V3120 Oph	17 50 50.8 +07 51 11	SR	V3174 Oph	17 54 24.1 +05 05 45	CWB:
V3121 Oph	17 50 51.5 +02 51 49	EW	V3175 Oph	17 54 24.9 +03 08 53	RRC
V3122 Oph	17 50 53.1 +03 36 12	EB	V3176 Oph	17 54 29.3 +02 03 15	RRC
V3123 Oph	17 50 56.8 +06 21 20	LB	V3177 Oph	17 54 34.5 +04 31 43	RRAB
V3124 Oph	17 50 57.9 -00 16 53	LB	V3178 Oph	17 54 37.7 +07 10 46	DSCT
V3125 Oph	17 50 59.6 +09 44 38	LB	V3179 Oph	17 54 58.6 +02 59 20	LB
V3126 Oph	17 51 16.2 +00 10 28	LB	V3180 Oph	17 55 04.3 +02 25 50	EW
V3127 Oph	17 51 21.0 +02 54 40	RRAB	V3181 Oph	17 55 09.1 +03 16 22	EW:
V3128 Oph	17 51 23.5 +08 25 03	RRAB	V3182 Oph	17 55 10.6 +01 20 48	LB
V3129 Oph	17 51 34.6 +07 40 31	RRC	V3183 Oph	17 55 12.2 +08 30 50	RRC
V3130 Oph	17 51 39.0 +04 32 08	RRC	V3184 Oph	17 55 14.2 +07 55 01	EB
V3131 Oph	17 51 45.0 +03 47 55	LB	V3185 Oph	17 55 22.8 +04 00 23	RRC
V3132 Oph	17 51 45.9 -00 10 59	DSCT	V3186 Oph	17 55 34.5 +07 19 33	EW
V3133 Oph	17 51 48.8 +09 26 34	RRAB	V3187 Oph	17 55 36.0 +09 04 15	RRAB
V3134 Oph	17 51 54.8 +05 26 15	LB	V3188 Oph	17 55 44.1 +05 59 30	RRAB:
V3135 Oph	17 51 57.0 +01 30 51	LB	V3189 Oph	17 55 45.7 +03 39 58	RRAB
V3136 Oph	17 51 59.7 +03 56 23	RRC	V3190 Oph	17 55 50.9 +08 11 10	EW
V3137 Oph	17 52 02.9 +08 49 52	EW	V3191 Oph	17 55 59.6 +04 02 29	SR
V3138 Oph	17 52 05.1 +04 33 22	EA	V3192 Oph	17 56 05.8 +08 11 35	CWA:
V3139 Oph	17 52 11.8 +04 54 39	SR	V3193 Oph	17 56 17.9 +06 22 43	DSCT
V3140 Oph	17 52 18.4 +01 03 07	RRC	V3194 Oph	17 56 19.7 -00 13 56	SRB
V3141 Oph	17 52 24.1 +04 31 58	L	V3195 Oph	17 56 20.9 +03 23 30	SRB
V3142 Oph	17 52 24.7 +09 16 16	RRC	V3196 Oph	17 56 23.5 +05 02 07	EA

Table 1 (continued)

Name	R.A., Decl., 2000.0	Type	Name	R.A., Decl., 2000.0	Type
	h m s o ' "			h m s o ' "	
V3197 Oph	17 56 23.8 -01 17 28	SRB	V3251 Oph	17 59 29.4 +08 45 42	EA
V3198 Oph	17 56 27.8 +02 21 20	LB	V3252 Oph	17 59 33.8 +05 38 58	EW
V3199 Oph	17 56 41.1 +05 53 58	LB	V3253 Oph	17 59 36.9 +01 07 53	SR
V3200 Oph	17 56 49.5 -06 33 50	SR	V3254 Oph	17 59 37.8 +02 19 57	EA
V3201 Oph	17 56 50.8 +01 45 58	EW	V3255 Oph	17 59 39.8 +04 59 52	SR
V3202 Oph	17 56 50.9 +08 08 02	RRC	V3256 Oph	17 59 46.4 +00 03 48	EW
V3203 Oph	17 56 54.1 +02 18 13	EA	V3257 Oph	17 59 47.8 +09 22 42	RRC
V3204 Oph	17 56 54.2 +03 37 53	RRC	V3258 Oph	17 59 48.5 +08 10 48	EW
V3205 Oph	17 56 56.5 +04 19 08	LB	V3259 Oph	18 00 00.7 +07 26 22	LB
V3206 Oph	17 57 00.2 +03 56 42	EW	V3260 Oph	18 00 03.7 +04 41 21	RRAB
V3207 Oph	17 57 01.6 +06 15 25	LB	V3261 Oph	18 00 04.7 +03 17 59	EB
V3208 Oph	17 57 04.2 +01 57 21	SR:	V3262 Oph	18 00 06.6 +02 39 54	RRAB
V3209 Oph	17 57 15.2 +02 19 45	RRAB	V3263 Oph	18 00 07.8 +04 30 27	LB
V3210 Oph	17 57 20.8 +03 36 04	RRAB	V3264 Oph	18 00 07.9 +01 58 19	RRAB
V3211 Oph	17 57 24.0 +02 43 32	SR:	V3265 Oph	18 00 09.9 +01 44 42	SR
V3212 Oph	17 57 26.7 +01 03 17	RRC	V3266 Oph	18 00 12.5 +06 26 26	EW
V3213 Oph	17 57 32.5 +05 19 20	RRC:	V3267 Oph	18 00 23.7 +04 08 24	SRB
V3214 Oph	17 57 40.5 +04 50 51	EB	V3268 Oph	18 00 26.8 +01 23 26	EB
V3215 Oph	17 57 42.3 +04 39 08	EW	V3269 Oph	18 00 32.2 +05 27 11	SRB
V3216 Oph	17 57 42.7 +04 23 59	RRAB	V3270 Oph	18 00 32.7 +06 50 24	LB
V3217 Oph	17 57 43.6 +01 48 12	EB	V3271 Oph	18 00 37.0 +08 55 08	RRAB
V3218 Oph	17 57 44.6 +02 30 44	SRB	V3272 Oph	18 00 37.8 +05 06 01	EA
V3219 Oph	17 57 44.8 +07 32 53	RRC:	V3273 Oph	18 00 51.4 +02 40 56	EB
V3220 Oph	17 57 46.8 +05 55 29	EW	V3274 Oph	18 00 56.9 +09 21 30	LB
V3221 Oph	17 57 58.9 +04 09 48	EB	V3275 Oph	18 00 57.1 +01 39 57	EA
V3222 Oph	17 58 01.3 +05 49 27	EB	V3276 Oph	18 00 59.4 +07 21 22	RRC:
V3223 Oph	17 58 03.9 +03 50 24	EW	V3277 Oph	18 01 00.8 +04 07 52	EW
V3224 Oph	17 58 05.4 +09 02 33	RRAB	V3278 Oph	18 01 05.6 +06 21 14	RRAB
V3225 Oph	17 58 07.9 +00 22 04	LB	V3279 Oph	18 01 06.4 +02 33 48	LB
V3226 Oph	17 58 08.0 +08 22 59	RRAB	V3280 Oph	18 01 10.7 +01 50 53	RRAB:
V3227 Oph	17 58 09.4 +08 05 09	RRAB	V3281 Oph	18 01 32.5 +02 13 50	SR
V3228 Oph	17 58 15.6 +00 50 23	EW	V3282 Oph	18 01 33.2 +02 54 39	EW
V3229 Oph	17 58 20.4 +03 01 58	RRAB	V3283 Oph	18 01 33.4 +03 41 16	LB
V3230 Oph	17 58 21.4 +06 35 09	LB	V3284 Oph	18 01 43.5 +07 23 05	SRB
V3231 Oph	17 58 22.5 +05 53 15	EB	V3285 Oph	18 01 46.6 +08 18 35	EA
V3232 Oph	17 58 22.7 +02 23 25	RRAB:	V3286 Oph	18 01 49.8 +08 27 02	SR
V3233 Oph	17 58 27.7 +03 32 57	RRC	V3287 Oph	18 01 50.7 +03 26 34	LB
V3234 Oph	17 58 28.6 +06 10 01	LB	V3288 Oph	18 01 55.4 +04 22 16	L:
V3235 Oph	17 58 34.0 +02 44 09	EA	V3289 Oph	18 02 01.2 +03 34 57	RRC
V3236 Oph	17 58 34.1 +06 02 57	LB:	V3290 Oph	18 02 03.9 +07 08 07	EW
V3237 Oph	17 58 34.7 +05 01 06	LB	V3291 Oph	18 02 10.7 +00 43 27	EW
V3238 Oph	17 58 40.0 +04 54 17	EB	V3292 Oph	18 02 11.4 +07 26 43	LB
V3239 Oph	17 58 48.5 +07 16 43	EA	V3293 Oph	18 02 12.5 +06 48 14	SRB
V3240 Oph	17 58 50.3 +01 33 36	EB	V3294 Oph	18 02 13.4 +01 32 26	EW
V3241 Oph	17 58 50.5 +01 27 31	RRAB	V3295 Oph	18 02 13.5 +06 53 00	EB
V3242 Oph	17 58 53.9 +02 05 54	EW	V3296 Oph	18 02 14.0 +08 12 18	EW
V3243 Oph	17 58 54.9 +09 27 46	EB	V3297 Oph	18 02 23.1 +08 01 40	RRAB
V3244 Oph	17 58 59.3 +04 20 03	RRC	V3298 Oph	18 02 25.1 +02 06 23	RRAB
V3245 Oph	17 59 11.6 +09 01 53	EA	V3299 Oph	18 02 26.2 +01 54 25	RRAB
V3246 Oph	17 59 12.2 +07 52 05	LB	V3300 Oph	18 02 26.4 +02 47 41	EW
V3247 Oph	17 59 15.9 +05 13 14	RRC	V3301 Oph	18 02 26.9 +03 24 25	RRAB:
V3248 Oph	17 59 19.7 +07 51 05	RRAB	V3302 Oph	18 02 27.3 +01 03 17	SRB
V3249 Oph	17 59 22.5 +05 07 33	EB	V3303 Oph	18 02 29.4 +02 41 24	EB:
V3250 Oph	17 59 29.4 +04 32 33	LB	V3304 Oph	18 02 29.5 +07 12 48	RRAB

Table 1 (continued)

Name	R.A., Decl., 2000.0	Type	Name	R.A., Decl., 2000.0	Type
	h m s o ' "			h m s o ' "	
V3305 Oph	18 02 34.7 +03 23 13	SRB	V3359 Oph	18 05 29.9 +06 07 53	EB
V3306 Oph	18 02 34.9 +00 36 39	SR	V3360 Oph	18 05 33.5 +04 45 55	EB
V3307 Oph	18 02 36.6 +02 00 59	RRAB	V3361 Oph	18 05 35.6 +08 35 00	RRAB
V3308 Oph	18 02 40.4 +01 55 49	EW	V3362 Oph	18 05 36.6 +01 40 10	LB
V3309 Oph	18 02 41.9 +04 33 02	EW	V3363 Oph	18 05 38.0 +02 16 27	DSCT
V3310 Oph	18 02 47.0 +00 00 36	RRC	V3364 Oph	18 05 39.4 +05 10 12	DSCT
V3311 Oph	18 02 50.0 +08 43 58	EW	V3365 Oph	18 05 42.8 +05 20 18	EB
V3312 Oph	18 02 53.2 +04 32 38	EW	V3366 Oph	18 05 46.8 +01 54 11	EW
V3313 Oph	18 02 54.9 +06 34 10	EW	V3367 Oph	18 05 49.5 +07 55 13	SR:
V3314 Oph	18 02 55.8 +05 02 51	EW	V3368 Oph	18 05 52.4 +05 19 30	DSCT
V3315 Oph	18 02 57.1 +06 02 10	EB	V3369 Oph	18 05 54.4 +07 13 48	RRAB
V3316 Oph	18 02 59.8 +07 22 02	LB	V3370 Oph	18 05 54.5 +03 31 56	RRC
V3317 Oph	18 03 06.0 +05 03 01	SRB	V3371 Oph	18 05 56.5 +02 55 28	EW
V3318 Oph	18 03 07.2 +04 20 41	LB	V3372 Oph	18 06 03.4 +02 43 28	SR
V3319 Oph	18 03 10.5 +03 57 15	EW	V3373 Oph	18 06 03.6 +05 03 08	EW
V3320 Oph	18 03 14.6 +03 25 20	EA	V3374 Oph	18 06 05.6 +04 24 37	EW
V3321 Oph	18 03 24.1 +05 16 56	LB	V3375 Oph	18 06 05.8 +05 54 54	RRAB
V3322 Oph	18 03 24.7 +06 40 58	LB	V3376 Oph	18 06 07.6 +02 53 59	LB
V3323 Oph	18 03 35.2 +01 28 45	RRC	V3377 Oph	18 06 07.7 +04 31 44	RRAB
V3324 Oph	18 03 36.3 +02 57 36	EW	V3378 Oph	18 06 12.1 +05 06 38	RRAB:
V3325 Oph	18 03 36.7 +02 18 15	RRC	V3379 Oph	18 06 15.1 +01 49 41	SR
V3326 Oph	18 03 36.7 +05 00 34	BY:	V3380 Oph	18 06 15.3 +07 06 35	RRC
V3327 Oph	18 03 48.1 +01 02 43	LB	V3381 Oph	18 06 18.6 +08 55 21	EB
V3328 Oph	18 03 51.4 +05 48 22	RRAB	V3382 Oph	18 06 30.8 +08 22 06	EB
V3329 Oph	18 03 51.5 +08 05 37	EB	V3383 Oph	18 06 31.8 +03 59 53	SR:
V3330 Oph	18 03 54.7 +07 34 28	SR	V3384 Oph	18 06 32.5 +00 43 56	SRB
V3331 Oph	18 03 58.6 +05 04 18	EW	V3385 Oph	18 06 32.8 +04 29 32	RRAB
V3332 Oph	18 03 59.0 +06 21 30	EW	V3386 Oph	18 06 36.5 +05 00 44	RRAB
V3333 Oph	18 04 04.3 +01 14 26	LB	V3387 Oph	18 06 37.0 +03 38 09	EB
V3334 Oph	18 04 04.7 +03 54 20	LB	V3388 Oph	18 06 37.4 +01 48 57	LB
V3335 Oph	18 04 14.8 +03 38 15	EW	V3389 Oph	18 06 38.4 +08 02 52	EA
V3336 Oph	18 04 16.5 +08 23 39	SRB	V3390 Oph	18 06 39.9 +00 36 47	SRB
V3337 Oph	18 04 20.0 +03 08 58	LB	V3391 Oph	18 06 43.5 +01 36 52	SR:
V3338 Oph	18 04 22.4 +08 12 34	SR	V3392 Oph	18 06 46.4 +08 50 12	SR
V3339 Oph	18 04 25.3 +04 50 51	DSCT	V3393 Oph	18 06 50.4 +02 13 47	SRB
V3340 Oph	18 04 31.1 +03 35 21	EW	V3394 Oph	18 06 51.4 +05 09 30	EW
V3341 Oph	18 04 32.6 +05 13 55	EA	V3395 Oph	18 06 56.2 +06 27 48	RRC
V3342 Oph	18 04 34.0 +04 39 01	EW	V3396 Oph	18 07 05.7 +06 05 15	LB
V3343 Oph	18 04 34.1 +04 43 20	EW	V3397 Oph	18 07 06.4 +02 48 03	RRC
V3344 Oph	18 04 39.6 +07 31 03	RRAB	V3398 Oph	18 07 07.4 +02 10 04	RRC
V3345 Oph	18 04 43.4 +05 53 27	RRAB	V3399 Oph	18 07 12.7 +04 58 10	EW
V3346 Oph	18 04 44.1 +03 20 09	EW	V3400 Oph	18 07 13.6 +04 09 01	RRAB
V3347 Oph	18 04 51.2 +08 03 58	RRC	V3401 Oph	18 07 16.4 +05 16 52	LB
V3348 Oph	18 04 53.5 +05 14 42	RRAB	V3402 Oph	18 07 17.2 +01 23 42	SR:
V3349 Oph	18 04 58.5 +03 46 04	EB	V3403 Oph	18 07 21.5 +05 32 13	SR
V3350 Oph	18 05 00.4 +06 22 51	LB	V3404 Oph	18 07 23.1 +02 32 50	SR:
V3351 Oph	18 05 07.3 +01 17 30	EB	V3405 Oph	18 07 30.1 +03 11 07	RRC
V3352 Oph	18 05 09.3 +03 18 35	RRAB	V3406 Oph	18 07 36.9 +07 26 36	RRC
V3353 Oph	18 05 10.2 +03 01 40	RRC	V3407 Oph	18 07 41.3 +06 45 29	SRB
V3354 Oph	18 05 14.1 +05 02 03	EW	V3408 Oph	18 07 49.7 +05 27 52	EA
V3355 Oph	18 05 24.4 +04 37 01	EW	V3409 Oph	18 07 50.5 +04 36 38	EA
V3356 Oph	18 05 25.9 +01 27 17	EB	V3410 Oph	18 07 50.7 +02 25 20	EW
V3357 Oph	18 05 26.6 +02 13 56	EW	V3411 Oph	18 07 54.6 +02 44 13	LB
V3358 Oph	18 05 27.9 +07 16 51	SRB	V3412 Oph	18 07 55.7 +07 47 12	EA/RS

Table 1 (continued)

Name	R.A., Decl., 2000.0	Type	Name	R.A., Decl., 2000.0	Type
	h m s o ' "			h m s o ' "	
V3413 Oph	18 07 56.0 +04 56 47	EW	V3467 Oph	18 11 05.3 +07 54 03	EW
V3414 Oph	18 07 59.0 +04 45 56	LB	V3468 Oph	18 11 09.7 +03 29 09	RRAB
V3415 Oph	18 08 00.3 +01 17 31	EW:	V3469 Oph	18 11 12.7 +05 26 17	EW
V3416 Oph	18 08 01.1 +01 42 40	RRC:	V3470 Oph	18 11 20.0 +07 16 12	EW:
V3417 Oph	18 08 01.9 +05 23 57	LB	V3471 Oph	18 11 20.6 +02 20 38	EB
V3418 Oph	18 08 03.1 +06 14 14	SRB	V3472 Oph	18 11 22.8 +01 51 10	LB
V3419 Oph	18 08 06.0 +07 40 27	EW	V3473 Oph	18 11 22.9 +03 43 39	RRAB
V3420 Oph	18 08 10.1 +05 40 58	RRC:	V3474 Oph	18 11 25.2 +08 41 15	RRAB
V3421 Oph	18 08 10.3 +04 29 01	RRAB	V3475 Oph	18 11 51.5 +03 50 03	EW
V3422 Oph	18 08 11.2 +03 52 54	RRAB	V3476 Oph	18 12 01.8 +01 45 42	RRC
V3423 Oph	18 08 13.8 +07 41 16	DSCT	V3477 Oph	18 12 07.6 +06 03 44	SRB
V3424 Oph	18 08 14.5 +04 48 00	DSCT:	V3478 Oph	18 12 09.7 +05 18 40	SRB
V3425 Oph	18 08 24.3 +06 28 14	LB	V3479 Oph	18 12 14.4 +09 06 18	SRB
V3426 Oph	18 08 24.3 +05 26 19	LB	V3480 Oph	18 12 21.5 +05 26 56	SRB
V3427 Oph	18 08 30.8 +05 39 12	RRAB	V3481 Oph	18 12 26.4 +02 42 16	EW
V3428 Oph	18 08 32.9 +07 41 49	EW	V3482 Oph	18 12 27.2 +02 46 49	EA
V3429 Oph	18 08 44.6 +05 57 55	SR:	V3483 Oph	18 12 29.3 +05 10 06	LB
V3430 Oph	18 08 54.5 +00 22 37	DSCT:	V3484 Oph	18 12 31.6 +05 21 10	EW
V3431 Oph	18 08 56.0 +05 12 36	SR:	V3485 Oph	18 12 34.1 +03 53 05	LB
V3432 Oph	18 08 56.2 +05 57 10	EW	V3486 Oph	18 12 37.3 +03 49 33	LB
V3433 Oph	18 09 04.4 +07 55 38	RRC:	V3487 Oph	18 12 37.9 +07 18 23	RRAB
V3434 Oph	18 09 04.6 +02 55 12	EA	V3488 Oph	18 12 40.1 +04 45 31	LB
V3435 Oph	18 09 09.1 +05 04 24	EB	V3489 Oph	18 12 40.8 +02 00 07	EW
V3436 Oph	18 09 09.2 +03 47 52	LB	V3490 Oph	18 12 48.1 +03 26 42	LB
V3437 Oph	18 09 09.9 +07 28 10	SRB	V3491 Oph	18 12 50.5 +04 23 38	EB
V3438 Oph	18 09 13.4 +03 24 47	LB	V3492 Oph	18 12 52.2 +02 55 23	RRAB
V3439 Oph	18 09 13.5 +05 50 41	RRC	V3493 Oph	18 12 59.7 +04 20 35	SRB
V3440 Oph	18 09 15.4 +01 51 03	LB	V3494 Oph	18 13 00.2 +06 52 27	EB
V3441 Oph	18 09 18.7 +02 34 54	DSCT	V3495 Oph	18 13 01.9 +03 40 42	LB
V3442 Oph	18 09 23.8 +06 51 48	SRB	V3496 Oph	18 13 06.8 +08 15 49	LB
V3443 Oph	18 09 26.2 +05 35 59	EW	V3497 Oph	18 13 08.6 +05 25 22	SR:
V3444 Oph	18 09 26.7 +03 30 28	LB	V3498 Oph	18 13 13.9 +06 16 55	SRB
V3445 Oph	18 09 27.3 +02 31 40	SRB	V3499 Oph	18 13 16.6 +03 38 17	SR:
V3446 Oph	18 09 27.6 +04 28 51	DSCT	V3500 Oph	18 13 19.2 +01 51 16	EW
V3447 Oph	18 09 42.0 +01 53 15	EW	V3501 Oph	18 13 20.6 +02 03 10	RRAB
V3448 Oph	18 09 46.1 +02 22 34	EW	V3502 Oph	18 13 21.9 +04 20 40	RRAB
V3449 Oph	18 09 48.6 +06 00 38	SRB	V3503 Oph	18 13 27.9 +06 23 12	SR
V3450 Oph	18 09 51.1 +05 03 47	EB	V3504 Oph	18 13 30.9 +03 40 47	EW
V3451 Oph	18 09 53.9 +04 16 08	EA	V3505 Oph	18 13 36.6 +03 28 48	RRAB
V3452 Oph	18 09 59.3 +04 44 29	RRAB	V3506 Oph	18 13 37.3 +06 53 38	SRB
V3453 Oph	18 10 07.8 +07 58 23	SRB	V3507 Oph	18 13 45.0 +06 32 20	RRAB
V3454 Oph	18 10 11.8 +01 23 30	LB	V3508 Oph	18 13 48.9 +03 32 20	LB
V3455 Oph	18 10 13.9 +02 10 07	RRAB	V3509 Oph	18 13 54.9 +04 42 38	EW
V3456 Oph	18 10 16.6 +02 43 51	LB	V3510 Oph	18 13 56.5 +06 22 44	LB
V3457 Oph	18 10 17.4 +08 11 27	EW	V3511 Oph	18 13 58.7 +08 55 44	EB
V3458 Oph	18 10 20.1 +06 02 08	EB	V3512 Oph	18 14 07.6 +09 01 42	SR:
V3459 Oph	18 10 24.6 +05 27 16	EB	V3513 Oph	18 14 12.3 +05 07 31	SRB
V3460 Oph	18 10 29.5 +04 22 49	RRC	V3514 Oph	18 14 22.8 +05 31 31	RRAB
V3461 Oph	18 10 36.7 +02 29 47	LB	V3515 Oph	18 14 22.9 +06 09 56	RRAB
V3462 Oph	18 10 41.0 +00 10 56	LB	V3516 Oph	18 14 24.4 +07 12 52	SRB
V3463 Oph	18 10 46.8 +01 50 53	EW	V3517 Oph	18 14 31.8 +03 32 38	LB
V3464 Oph	18 10 55.7 +06 20 09	EB	V3518 Oph	18 14 53.8 +02 43 10	LB
V3465 Oph	18 10 58.8 +02 03 42	LB	V3519 Oph	18 15 04.2 +07 55 42	RRAB
V3466 Oph	18 10 59.0 +05 07 48	LB	V3520 Oph	18 15 04.3 +03 20 18	EW

Table 1 (continued)

Name	R.A., Decl., 2000.0	Type	Name	R.A., Decl., 2000.0	Type
	h m s o ' "			h m s o ' "	
V3521 Oph	18 15 11.7 +06 47 03	RRAB	V3575 Oph	18 19 34.9 +06 12 10	SR:
V3522 Oph	18 15 13.5 +09 06 08	LB	V3576 Oph	18 19 40.4 +02 56 18	EW
V3523 Oph	18 15 14.5 +07 29 35	SR	V3577 Oph	18 19 47.3 +02 01 03	RRC
V3524 Oph	18 15 21.0 +05 39 10	SR	V3578 Oph	18 19 52.7 +04 16 37	LB
V3525 Oph	18 15 21.2 +02 27 43	SR	V3579 Oph	18 20 00.9 +08 25 10	EW:
V3526 Oph	18 15 21.7 +02 37 50	RRAB	V3580 Oph	18 20 04.1 +04 11 34	EW
V3527 Oph	18 15 26.0 +02 44 39	EW	V3581 Oph	18 20 15.6 +08 03 36	LB
V3528 Oph	18 15 28.2 +06 47 53	EW	V3582 Oph	18 20 19.4 +06 20 06	LB
V3529 Oph	18 15 31.4 +06 19 20	SRB	V3583 Oph	18 20 30.1 +03 48 02	DSCT
V3530 Oph	18 15 31.6 +02 49 17	RRAB	V3584 Oph	18 20 55.1 +04 44 46	EW
V3531 Oph	18 15 38.8 +06 29 59	SRB	V3585 Oph	18 22 03.1 +08 45 51	EB
V3532 Oph	18 15 46.3 +03 01 14	EA	V3586 Oph	18 28 37.3 +03 18 05	RRC
V3533 Oph	18 15 47.0 +05 38 35	RRC	V3587 Oph	18 28 47.5 +03 05 26	EW
V3534 Oph	18 15 47.9 +06 18 41	EB:	V3588 Oph	18 28 54.2 +03 31 05	LB
V3535 Oph	18 15 48.9 +07 08 33	RRAB	V3589 Oph	18 28 55.7 +11 41 47	EW
V3536 Oph	18 15 57.1 +04 07 56	RRC	V3590 Oph	18 29 00.8 +03 12 52	SR:
V3537 Oph	18 15 57.6 +01 20 11	M	V3591 Oph	18 29 01.3 +03 19 59	EA
V3538 Oph	18 16 04.6 +02 37 58	RRC	V3592 Oph	18 29 12.7 +03 13 41	SR:
V3539 Oph	18 16 11.2 +07 21 48	LB	V3593 Oph	18 29 12.7 +03 37 07	SR:
V3540 Oph	18 16 18.4 +06 16 11	SR	V3594 Oph	18 29 13.0 +03 05 02	EW
V3541 Oph	18 16 20.7 +03 15 27	DSCT	V3595 Oph	18 29 16.7 +03 26 56	SR:
V3542 Oph	18 16 23.2 +04 47 26	RRAB	V3596 Oph	18 29 18.1 +03 40 57	LB
V3543 Oph	18 16 27.1 +06 42 56	SR:	V3597 Oph	18 29 30.7 +03 24 30	SR:
V3544 Oph	18 16 28.5 +02 06 02	LB	V3598 Oph	18 29 31.8 +03 28 53	SR:
V3545 Oph	18 16 35.2 +05 34 35	SR	V3599 Oph	18 29 33.7 +03 30 49	SR:
V3546 Oph	18 16 40.1 +06 37 12	SR	V3600 Oph	18 29 37.3 +03 27 52	SR:
V3547 Oph	18 16 45.2 +07 57 50	RRC	V3601 Oph	18 29 40.9 +03 24 35	RRAB
V3548 Oph	18 16 46.2 +08 18 49	LB	V3602 Oph	18 30 06.2 +03 27 22	SR:
V3549 Oph	18 16 50.1 +05 41 14	LB	V3603 Oph	18 30 09.6 +03 25 45	SR:
V3550 Oph	18 16 51.8 +03 17 23	EB	V3604 Oph	18 30 14.0 +03 10 50	SR:
V3551 Oph	18 17 00.7 +04 29 25	LB	V3605 Oph	18 30 16.9 +03 12 11	SR:
V3552 Oph	18 17 03.1 +03 31 15	LB	V3606 Oph	18 30 25.6 +03 40 56	LB
V3553 Oph	18 17 11.4 +06 18 13	RRAB	V3607 Oph	18 30 30.4 +03 31 48	SR:
V3554 Oph	18 17 20.3 +02 04 44	EW	V3608 Oph	18 30 45.1 +03 37 50	SR:
V3555 Oph	18 17 20.6 +06 08 44	EW	V3609 Oph	18 30 46.4 +03 14 57	RRAB
V3556 Oph	18 17 22.4 +05 26 14	LB	V3610 Oph	18 30 47.8 +03 41 01	M
V3557 Oph	18 17 30.5 +08 14 47	EA	V3611 Oph	18 31 05.7 +03 09 43	BY:
V3558 Oph	18 17 32.1 +08 14 16	RRAB	V3612 Oph	18 31 30.5 +03 12 56	SR:
V3559 Oph	18 17 35.2 +08 32 20	EW	V3613 Oph	18 34 43.9 +08 03 39	LB
V3560 Oph	18 17 37.9 +04 58 12	EW	V3614 Oph	18 36 57.5 +09 34 18	EW
V3561 Oph	18 17 52.1 +01 54 48	EB	V3615 Oph	18 37 03.5 +09 42 26	RRAB
V3562 Oph	18 18 00.4 +05 18 06	EA	V3616 Oph	18 37 04.8 +09 14 47	EW
V3563 Oph	18 18 16.3 +02 59 35	LB	V3617 Oph	18 37 05.2 +09 30 38	EW:
V3564 Oph	18 18 31.4 +04 15 22	SRB	V3618 Oph	18 37 13.2 +09 45 13	EW
V3565 Oph	18 18 56.3 +04 40 05	SR	V3619 Oph	18 37 14.7 +10 02 54	EW
V3566 Oph	18 18 57.0 +06 37 53	LB	V3620 Oph	18 37 23.9 +09 16 10	EW
V3567 Oph	18 19 10.5 +03 34 45	CWB	V3621 Oph	18 37 25.0 +09 29 06	EB
V3568 Oph	18 19 17.2 +04 57 27	RRAB	V3622 Oph	18 37 25.4 +09 18 05	EA
V3569 Oph	18 19 18.4 +06 34 41	EW	V3623 Oph	18 37 28.1 +09 44 16	EW
V3570 Oph	18 19 20.3 +04 39 48	EW	V3624 Oph	18 37 37.1 +09 59 21	EW
V3571 Oph	18 19 21.2 +05 17 20	SR:	V3625 Oph	18 37 42.3 +10 00 13	EW
V3572 Oph	18 19 21.4 +06 22 45	EB	V3626 Oph	18 37 44.5 +09 55 59	EB
V3573 Oph	18 19 24.1 +03 03 12	RRC	V3627 Oph	18 37 47.4 +09 34 30	EW:
V3574 Oph	18 19 28.9 +05 37 54	RRAB	V3628 Oph	18 37 52.8 +09 13 07	SR:

Table 1 (continued)

Name	R.A., Decl., 2000.0						Type	Name	R.A., Decl., 2000.0						Type
	h	m	s		o	'	"		h	m	s		o	'	"	
V3629 Oph	18	37	54.3	+09	22	36	SR:	V0443 Pav	18	03	09.8	-58	18	07	RRAB
V3630 Oph	18	38	13.1	+09	49	08	EW	V0444 Pav	18	03	24.6	-57	04	16	RRAB
V3631 Oph	18	38	16.1	+09	31	13	EW	V0445 Pav	18	27	20.4	-62	24	15	BY
V3632 Oph	18	38	20.2	+09	23	52	SXPHE	V0446 Pav	18	28	23.5	-68	11	47	SR
V3633 Oph	18	38	30.7	+09	42	04	EW	V0447 Pav	18	34	26.8	-58	41	29	RRC
V3634 Oph	18	38	39.7	+09	31	56	EB	V0448 Pav	18	51	48.2	-59	53	14	RRAB
V3635 Oph	18	38	45.8	+09	41	54	EW	V0449 Pav	18	57	18.9	-63	21	25	RRAB
V3636 Oph	18	38	54.6	+10	03	37	EW	V0450 Pav	19	35	38.0	-74	09	55	RRC
V3637 Oph	18	38	57.2	+09	13	27	RRAB	V0451 Pav	19	48	53.4	-62	07	53	RS
V3638 Oph	18	38	58.0	+10	02	48	EW	V0452 Pav	20	46	55.6	-66	53	00	RS:
V3639 Oph	18	38	58.7	+09	24	18	RRAB	V0453 Pav	21	27	56.3	-67	02	37	BY:
V3640 Oph	18	39	00.2	+09	57	33	EW	V0624 Peg	21	09	50.5	+13	48	40	UGSU
V3641 Oph	18	39	05.9	+09	34	30	EW	V0625 Peg	21	32	28.1	+24	10	21	EW
V3642 Oph	18	39	13.6	+09	45	08	EB	V0626 Peg	21	38	05.2	+24	02	48	EW
V3643 Oph	18	39	15.6	+09	46	49	EW	V0627 Peg	21	38	06.7	+26	19	57	UGSU
V3644 Oph	18	39	18.4	+09	56	28	EB	V0628 Peg	21	39	14.5	+28	22	41	EA
V3645 Oph	18	39	20.6	+09	44	01	BY:	V0629 Peg	21	41	16.7	+26	58	58	RS
V3646 Oph	18	39	30.9	+10	03	50	EB	V0630 Peg	21	51	27.0	+15	05	38	RRAB
V3647 Oph	18	39	32.4	+09	33	03	RRAB	V0631 Peg	21	59	44.6	+16	57	38	RS
V3648 Oph	18	39	38.1	+10	02	09	SXPHE	V0632 Peg	22	01	44.6	+30	57	08	RRC
V3649 Oph	18	39	40.7	+09	48	18	RRC	V0633 Peg	22	12	48.0	+08	29	58	EW
V3650 Oph	18	39	44.9	+09	54	20	EW	V0634 Peg	22	12	55.2	+12	07	44	EB
V3651 Oph	18	39	45.0	+09	51	24	EW	V0635 Peg	22	15	10.1	+11	11	24	EW
V3652 Oph	18	39	49.2	+10	03	15	EW	V0636 Peg	22	16	50.8	+34	11	07	RS
V3653 Oph	18	39	54.9	+09	13	39	SXPHE	V0637 Peg	22	21	53.4	+28	02	47	EW
V3654 Oph	18	39	56.7	+09	22	14	EW	V0638 Peg	22	23	11.3	+17	45	11	EW
V3655 Oph	18	40	07.9	+09	36	58	EW	V0639 Peg	22	23	11.7	+04	08	51	EW
V3656 Oph	18	40	10.2	+09	59	45	EB	V0640 Peg	22	26	07.9	+06	21	07	EW
V3657 Oph	18	40	15.9	+09	19	47	EW	V0641 Peg	22	28	36.2	+03	05	26	RS
V3658 Oph	18	40	23.2	+10	02	46	DSCT	V0642 Peg	22	29	53.5	+26	14	19	EW
V3659 Oph	18	40	30.8	+09	12	39	EW	V0643 Peg	22	32	35.5	+20	13	48	GDOR
V3660 Oph	18	42	15.6	+08	51	24	EB	V0644 Peg	22	34	34.2	+27	07	45	RS
V0421 Pav	17	42	36.1	-65	54	13	EW	V0645 Peg	22	36	15.5	+06	00	51	EW
V0422 Pav	17	42	40.6	-64	36	51	RRC	V0646 Peg	22	37	08.4	+30	17	23	EW
V0423 Pav	17	43	59.0	-66	10	15	RRAB:	V0647 Peg	22	38	22.3	+32	38	55	RRC
V0424 Pav	17	44	01.3	-66	48	36	M	V0648 Peg	22	40	31.0	+17	43	31	DSCT
V0425 Pav	17	44	54.9	-59	35	27	LB	V0649 Peg	22	42	39.5	+32	09	41	SRD
V0426 Pav	17	45	05.6	-60	30	52	SRB	V0650 Peg	22	43	48.5	+08	09	27	UGSU
V0427 Pav	17	46	08.6	-57	42	05	SR	V0651 Peg	22	44	57.9	+34	16	41	EW
V0428 Pav	17	47	16.9	-57	38	20	M	V0652 Peg	22	46	40.7	+32	46	56	EW
V0429 Pav	17	51	43.8	-57	45	17	RRC	V0653 Peg	22	46	57.7	+34	05	55	EA
V0430 Pav	17	52	31.3	-58	59	26	RRC:	V0654 Peg	22	47	08.0	+34	14	21	EW
V0431 Pav	17	53	03.0	-58	43	50	SRB	V0655 Peg	22	47	17.7	+34	06	37	EW
V0432 Pav	17	55	01.9	-60	05	10	SR	V0656 Peg	22	48	27.6	+34	13	51	EW
V0433 Pav	17	56	34.6	-59	24	27	EW	V0657 Peg	22	48	34.9	+34	15	22	EA
V0434 Pav	17	57	53.9	-57	18	03	EW	V0658 Peg	22	49	47.5	+34	00	56	EB
V0435 Pav	17	58	58.7	-60	08	09	RRAB	V0659 Peg	22	50	10.7	+34	04	56	EW
V0436 Pav	17	59	31.6	-59	03	15	EW	V0660 Peg	22	50	24.0	+14	31	43	RS
V0437 Pav	17	59	51.7	-59	20	00	UG:	V0661 Peg	22	50	28.8	+24	49	31	EB
V0438 Pav	17	59	54.6	-57	26	10	RRAB	V0662 Peg	22	51	48.3	+15	32	04	EW
V0439 Pav	18	00	04.9	-62	22	12	SRB	V0663 Peg	22	52	59.6	+33	54	26	EB
V0440 Pav	18	00	55.8	-63	24	51	RRAB	V0664 Peg	22	53	59.3	+33	33	47	EW
V0441 Pav	18	01	10.2	-58	33	01	RRAB	V0665 Peg	22	56	23.1	+31	42	03	EA
V0442 Pav	18	02	38.6	-66	52	35	SRA	V0666 Peg	22	59	56.2	+14	18	12	EW

Table 1 (continued)

Name	R.A., Decl., 2000.0	Type	Name	R.A., Decl., 2000.0	Type
	h m s o ' "			h m s o ' "	
V0667 Peg	23 03 06.4 +33 51 51	EW	V0402 Sge	19 16 06.3 +19 13 41	SR:
V0668 Peg	23 03 23.9 +31 27 25	SR	V0403 Sge	19 55 19.9 +19 14 07	EW
V0669 Peg	23 06 28.1 +33 40 10	EW	V0404 Sge	19 55 29.4 +21 05 35	EW
V0670 Peg	23 09 11.5 +32 46 20	EA	V0405 Sge	19 55 31.2 +20 31 51	EB
V0671 Peg	23 09 46.4 +22 33 34	BY	V0406 Sge	19 55 33.0 +20 41 43	EW
V0672 Peg	23 09 51.2 +34 59 10	SR	V0407 Sge	19 55 35.9 +20 58 18	DSCT
V0673 Peg	23 10 16.8 +26 43 09	EW	V0408 Sge	19 55 47.8 +21 09 38	EB
V0674 Peg	23 14 54.2 +29 45 51	EW	V0409 Sge	19 55 50.0 +20 30 45	DSCT
V0675 Peg	23 17 00.1 +19 44 56	EW	V5669 Sgr	18 03 32.8 -28 16 05	NA
V0676 Peg	23 18 06.7 +32 12 36	RRAB	V5670 Sgr	17 45 49.1 -28 56 45	EA
V0677 Peg	23 18 16.9 +20 35 36	EA	V5671 Sgr	17 45 54.5 -29 08 13	EB
V0678 Peg	23 19 29.1 +18 01 35	EW	V5672 Sgr	17 46 10.4 -29 03 18	EA
V0679 Peg	23 23 48.3 +26 52 14	EW	V5673 Sgr	17 47 29.8 -28 28 52	EW
V0680 Peg	23 24 29.2 +29 28 39	LB	V5674 Sgr	17 48 08.3 -17 29 21	SR
V0681 Peg	23 27 27.2 +08 55 39	UG	V5675 Sgr	17 50 15.5 -22 23 43	SR
V0682 Peg	23 35 56.6 +08 30 18	EA:	V5676 Sgr	17 50 19.7 -29 30 01	BY
V0683 Peg	23 40 38.8 +09 46 27	EW	V5677 Sgr	17 50 48.6 -28 29 24	EA:
V0684 Peg	23 45 05.3 +12 13 48	EB	V5678 Sgr	17 52 15.1 -22 20 32	XND
V0685 Peg	23 53 19.5 +28 23 50	EW	V5679 Sgr	17 52 55.7 -18 08 36	LB
V0686 Peg	23 57 20.3 +22 51 36	BY	V5680 Sgr	17 54 08.9 -28 20 13	M
DT Phe	23 27 47.0 -46 08 01	RR	V5681 Sgr	17 54 23.1 -29 49 44	RS
DU Phe	23 52 23.9 -42 20 01	RRC	V5682 Sgr	17 54 23.6 -29 49 43	RS
DV Phe	23 58 56.6 -44 40 15	RRC	V5683 Sgr	17 54 28.6 -29 51 05	RS
KV Psc	22 58 09.3 +00 52 17	RRC	V5684 Sgr	17 54 29.5 -29 49 43	BY
KW Psc	22 58 31.8 +05 52 24	EW	V5685 Sgr	17 54 30.2 -29 47 12	RS
KX Psc	23 04 25.9 +06 25 46	UGSU	V5686 Sgr	17 54 49.6 -29 49 34	RS
KY Psc	23 13 32.8 +02 14 05	EA	V5687 Sgr	17 54 51.2 -29 52 51	BY
KZ Psc	23 16 45.0 +06 18 57	RS	V5688 Sgr	17 54 52.3 -29 53 10	EA/RS
LL Psc	23 21 47.1 +00 14 08	RR(B)	V5689 Sgr	17 54 58.5 -29 51 50	RS
AH PsA	21 40 06.9 -26 53 20	RRC	V5690 Sgr	17 55 01.9 -29 49 57	RS
AI PsA	21 53 20.4 -30 39 15	RRAB	V5691 Sgr	17 55 04.9 -29 55 25	BY
AK PsA	21 59 30.9 -36 23 30	RRAB	V5692 Sgr	17 55 08.4 -29 47 36	RS
AL PsA	22 04 42.5 -27 02 34	RRC	V5693 Sgr	17 55 08.7 -29 54 19	RS
AM PsA	22 18 10.3 -31 16 03	SR	V5694 Sgr	17 55 14.7 -29 42 36	BY
AN PsA	22 33 38.7 -33 35 24	RRAB	V5695 Sgr	17 55 53.4 -27 25 58	EA
AO PsA	22 51 31.3 -30 06 13	RRC	V5696 Sgr	17 56 05.7 -27 54 26	EB
AP PsA	22 55 58.8 -27 09 57	RR:	V5697 Sgr	17 56 25.3 -28 01 30	EA
V0385 Sge	19 12 46.7 +19 31 42	SR	V5698 Sgr	17 56 59.1 -17 28 36	M
V0386 Sge	19 12 49.5 +19 20 49	M	V5699 Sgr	17 57 50.9 -29 11 32	EB
V0387 Sge	19 12 52.0 +19 31 12	LB	V5700 Sgr	17 58 30.2 -29 01 59	SRB
V0388 Sge	19 13 08.8 +19 31 58	SR:	V5701 Sgr	18 00 01.3 -28 24 30	M:
V0389 Sge	19 13 17.4 +19 30 38	SR:	V5702 Sgr	18 00 06.6 -16 01 25	M
V0390 Sge	19 13 24.5 +19 25 23	LB	V5703 Sgr	18 00 48.4 -27 36 34	EA/RS
V0391 Sge	19 13 24.9 +19 04 44	SR	V5704 Sgr	18 00 57.2 -33 00 09	EB
V0392 Sge	19 13 42.7 +19 19 11	SR:	V5705 Sgr	18 01 19.0 -36 35 37	SRB
V0393 Sge	19 13 52.6 +19 32 36	SR	V5706 Sgr	18 02 15.8 -31 48 14	M
V0394 Sge	19 14 02.0 +19 02 14	LB	V5707 Sgr	18 02 22.3 -29 58 00	RS
V0395 Sge	19 14 22.2 +19 10 56	SR:	V5708 Sgr	18 02 41.8 -29 55 11	RS
V0396 Sge	19 14 29.3 +19 18 49	SR:	V5709 Sgr	18 02 45.3 -30 01 09	BY
V0397 Sge	19 14 42.2 +19 08 25	LB	V5710 Sgr	18 02 45.4 -29 57 56	RS
V0398 Sge	19 14 42.4 +19 05 08	LB	V5711 Sgr	18 02 46.5 -32 02 40	M
V0399 Sge	19 14 49.8 +19 29 05	SR	V5712 Sgr	18 02 48.5 -29 55 31	BY
V0400 Sge	19 15 13.2 +19 17 57	LB:	V5713 Sgr	18 02 48.6 -29 58 35	RS
V0401 Sge	19 15 31.4 +19 06 32	SR:	V5714 Sgr	18 02 50.9 -32 04 08	M:

Table 1 (continued)

Name	R.A., Decl., 2000.0	Type	Name	R.A., Decl., 2000.0	Type
	h m s o ' "			h m s o ' "	
V5715 Sgr	18 02 51.8 -29 59 59	BY	V5769 Sgr	18 06 08.4 -27 26 39	M
V5716 Sgr	18 02 54.5 -29 51 19	BY	V5770 Sgr	18 06 12.2 -27 42 34	M
V5717 Sgr	18 02 56.0 -29 52 24	RS	V5771 Sgr	18 06 15.5 -28 06 51	M
V5718 Sgr	18 03 00.6 -29 59 47	BY	V5772 Sgr	18 06 19.0 -27 01 00	M
V5719 Sgr	18 03 01.8 -30 07 56	BY	V5773 Sgr	18 06 29.5 -27 47 42	M
V5720 Sgr	18 03 02.4 -27 34 37	M	V5774 Sgr	18 06 31.4 -26 58 58	M
V5721 Sgr	18 03 04.3 -29 54 36	BY	V5775 Sgr	18 06 31.5 -27 16 55	M
V5722 Sgr	18 03 06.0 -27 26 00	M	V5776 Sgr	18 06 47.1 -27 52 43	M
V5723 Sgr	18 03 06.8 -35 57 35	LB	V5777 Sgr	18 06 49.0 -28 15 46	M
V5724 Sgr	18 03 06.9 -27 42 08	M	V5778 Sgr	18 06 51.2 -28 06 51	M
V5725 Sgr	18 03 07.0 -28 05 39	M	V5779 Sgr	18 06 52.1 -29 36 42	RVB
V5726 Sgr	18 03 08.5 -29 48 28	BY	V5780 Sgr	18 06 56.6 -27 58 33	M
V5727 Sgr	18 03 09.4 -29 49 31	RS	V5781 Sgr	18 07 15.0 -27 54 16	M
V5728 Sgr	18 03 11.9 -30 04 59	BY	V5782 Sgr	18 07 19.9 -28 15 01	M
V5729 Sgr	18 03 12.5 -27 35 28	M	V5783 Sgr	18 07 26.2 -28 18 58	M
V5730 Sgr	18 03 12.8 -27 28 07	M	V5784 Sgr	18 07 43.9 -28 13 01	M
V5731 Sgr	18 03 14.2 -29 55 26	RS	V5785 Sgr	18 07 48.2 -28 13 01	M
V5732 Sgr	18 03 15.0 -29 56 25	RS	V5786 Sgr	18 07 50.7 -28 09 16	M
V5733 Sgr	18 03 18.5 -29 57 40	RS	V5787 Sgr	18 07 57.2 -28 16 59	M
V5734 Sgr	18 03 22.8 -27 56 58	M	V5788 Sgr	18 07 57.3 -28 14 48	M
V5735 Sgr	18 03 25.7 -29 55 16	BY	V5789 Sgr	18 08 04.3 -28 10 53	M
V5736 Sgr	18 03 30.9 -29 55 33	BY	V5790 Sgr	18 08 07.0 -28 03 53	M
V5737 Sgr	18 03 36.0 -27 44 04	M	V5791 Sgr	18 08 13.0 -28 02 06	M
V5738 Sgr	18 03 41.7 -22 10 59	DCEP	V5792 Sgr	18 08 32.2 -32 01 53	M
V5739 Sgr	18 03 46.2 -27 43 08	M	V5793 Sgr	18 08 37.7 -28 18 17	M
V5740 Sgr	18 03 52.4 -27 57 23	M	V5794 Sgr	18 08 48.0 -27 22 34	M
V5741 Sgr	18 04 19.2 -27 38 19	RS	V5795 Sgr	18 08 48.2 -27 50 43	M
V5742 Sgr	18 04 19.5 -27 24 47	M	V5796 Sgr	18 08 48.5 -27 49 24	M
V5743 Sgr	18 04 26.5 -27 44 42	RS	V5797 Sgr	18 08 58.0 -27 54 36	M
V5744 Sgr	18 04 30.0 -27 14 18	M	V5798 Sgr	18 09 00.3 -31 13 41	M
V5745 Sgr	18 04 31.7 -27 36 19	BY	V5799 Sgr	18 09 02.5 -27 25 40	M
V5746 Sgr	18 04 35.6 -27 49 26	BY	V5800 Sgr	18 09 14.0 -27 40 22	M
V5747 Sgr	18 04 37.0 -27 42 07	E/RS	V5801 Sgr	18 09 35.7 -27 29 48	M
V5748 Sgr	18 04 43.4 -27 29 36	EA	V5802 Sgr	18 09 41.6 -28 05 03	M
V5749 Sgr	18 04 43.9 -27 28 32	M	V5803 Sgr	18 10 05.6 -27 56 33	M
V5750 Sgr	18 04 47.2 -27 21 46	M	V5804 Sgr	18 10 06.4 -27 46 46	M
V5751 Sgr	18 04 51.7 -27 02 58	M	V5805 Sgr	18 10 10.0 -27 22 55	M
V5752 Sgr	18 04 55.5 -28 38 32	BY	V5806 Sgr	18 10 16.9 -27 30 30	M
V5753 Sgr	18 05 04.7 -28 02 29	M	V5807 Sgr	18 10 46.3 -28 02 29	M
V5754 Sgr	18 05 06.4 -27 32 42	RS	V5808 Sgr	18 10 48.8 -27 56 23	M
V5755 Sgr	18 05 09.6 -27 05 04	M	V5809 Sgr	18 10 51.1 -30 53 20	M
V5756 Sgr	18 05 15.7 -27 16 45	M	V5810 Sgr	18 11 04.1 -27 15 30	M
V5757 Sgr	18 05 20.4 -27 01 40	M	V5811 Sgr	18 11 05.2 -27 30 51	M
V5758 Sgr	18 05 22.6 -27 06 13	M	V5812 Sgr	18 11 49.7 -27 49 02	M
V5759 Sgr	18 05 33.7 -20 20 38	ZAND	V5813 Sgr	18 11 51.1 -27 47 49	M
V5760 Sgr	18 05 40.5 -27 34 28	E+*	V5814 Sgr	18 12 00.0 -27 00 08	M
V5761 Sgr	18 05 47.7 -27 24 13	M	V5815 Sgr	18 12 20.7 -21 06 31	LB
V5762 Sgr	18 05 48.2 -28 36 30	RS	V5816 Sgr	18 12 20.7 -27 43 57	M
V5763 Sgr	18 05 49.6 -28 27 26	EA/RS	V5817 Sgr	18 12 26.2 -27 47 32	M
V5764 Sgr	18 06 02.0 -27 03 17	M	V5818 Sgr	18 12 31.2 -27 11 17	M
V5765 Sgr	18 06 02.7 -27 03 21	M	V5819 Sgr	18 12 48.7 -27 38 54	M
V5766 Sgr	18 06 04.3 -27 39 23	M	V5820 Sgr	18 13 20.8 -27 38 30	M
V5767 Sgr	18 06 04.3 -27 23 45	M	V5821 Sgr	18 13 34.4 -26 24 55	M
V5768 Sgr	18 06 05.4 -26 58 31	M	V5822 Sgr	18 13 47.8 -27 12 22	SRB

Table 1 (continued)

Name	R.A., Decl., 2000.0	Type	Name	R.A., Decl., 2000.0	Type
	h m s o ' "			h m s o ' "	
V5823 Sgr	18 13 51.2 -27 11 26	SR	V1647 Sco	17 56 00.2 -30 42 47	DSCT
V5824 Sgr	18 13 56.5 -27 13 15	M	V1648 Sco	17 56 24.5 -42 22 37	SR
V5825 Sgr	18 15 29.1 -33 06 12	M	V1649 Sco	17 56 54.7 -33 20 42	M
V5826 Sgr	18 19 52.2 -29 16 33	RS	V1650 Sco	17 57 22.3 -44 52 32	M
V5827 Sgr	18 20 01.0 -26 25 59	M	V1651 Sco	17 57 38.6 -42 13 56	M
V5828 Sgr	18 20 19.1 -22 34 58	EB	V1652 Sco	17 57 57.9 -38 54 41	SRB
V5829 Sgr	18 20 21.6 -27 50 26	M	V1653 Sco	17 58 07.2 -33 45 09	M
V5830 Sgr	18 29 22.8 -28 24 02	SRA	V1654 Sco	17 58 18.9 -36 19 17	M
V5831 Sgr	18 32 34.3 -28 33 47	M	DK Scl	23 12 00.4 -28 44 46	RRAB
V5832 Sgr	18 44 14.9 -17 32 34	M	DL Scl	23 14 07.9 -28 32 01	BY:
V5833 Sgr	18 48 07.0 -35 13 42	DSCT	DM Scl	23 46 03.1 -35 35 21	RS
V5834 Sgr	18 59 44.7 -27 19 38	SRD	DN Scl	23 46 48.6 -30 00 30	RRC
V5835 Sgr	19 01 29.9 -35 45 12	RRAB	DO Scl	23 47 35.1 -24 55 08	RRC
V5836 Sgr	19 03 29.1 -33 24 34	RRC	DP Scl	23 57 42.0 -34 01 12	RRAB
V5837 Sgr	19 22 26.3 -22 34 43	DSCT	V0507 Sct	18 29 29.7 -15 03 30	EA
V5838 Sgr	19 27 41.6 -32 32 51	SRA	V0508 Sct	18 29 49.8 -15 02 55	EA
V5839 Sgr	19 28 23.8 -18 52 22	RRC	V0509 Sct	18 30 33.0 -14 30 06	EA
V5840 Sgr	19 28 32.0 -35 07 59	RS	V0510 Sct	18 30 35.0 -14 22 49	EA
V5841 Sgr	19 28 37.7 -33 48 44	SRB	V0511 Sct	18 30 39.7 -15 00 58	EW
V5842 Sgr	19 29 18.4 -19 16 20	M	V0512 Sct	18 30 40.8 -14 28 48	EB
V5843 Sgr	19 29 19.1 -15 11 44	M	V0513 Sct	18 30 40.9 -14 21 36	EB
V5844 Sgr	19 35 03.8 -18 33 57	RS	V0514 Sct	18 30 41.2 -14 00 05	EW
V5845 Sgr	19 52 26.9 -23 17 54	RR(B)	V0515 Sct	18 30 41.4 -15 01 22	EB
V5846 Sgr	19 54 57.7 -23 51 45	EW	V0516 Sct	18 30 41.6 -14 17 12	RRC
V5847 Sgr	20 04 47.8 -37 15 03	RR(B)	V0517 Sct	18 30 42.6 -13 59 41	EB
V5848 Sgr	20 23 01.7 -41 54 49	RRC	V0518 Sct	18 30 44.7 -14 29 17	EW
V5849 Sgr	20 25 01.8 -42 23 48	RRAB	V0519 Sct	18 30 59.7 -15 18 07	EW
V5850 Sgr	18 22 59.3 -19 14 12	N	V0520 Sct	18 31 00.6 -15 04 23	EB
V5851 Sgr	17 43 34.1 -18 07 34	M	V0521 Sct	18 31 04.4 -14 27 12	EA
V1622 Sco	17 32 53.1 -35 54 41	DCEP	V0522 Sct	18 31 04.5 -14 20 47	EA
V1623 Sco	17 36 51.7 -44 20 07	RS	V0523 Sct	18 31 08.7 -14 33 53	EW
V1624 Sco	17 38 26.9 -41 32 51	LB	V0524 Sct	18 31 11.5 -14 27 06	EB
V1625 Sco	17 42 47.5 -43 46 35	SR	V0525 Sct	18 31 11.6 -13 24 01	EB
V1626 Sco	17 43 51.8 -40 45 56	SR	V0526 Sct	18 31 12.1 -13 47 28	EW
V1627 Sco	17 44 58.4 -38 43 50	SR	V0527 Sct	18 31 13.6 -13 23 20	EW
V1628 Sco	17 48 29.9 -42 49 14	M	V0528 Sct	18 31 15.6 -13 13 40	EW
V1629 Sco	17 48 42.9 -38 57 15	SRB	V0529 Sct	18 31 19.1 -13 48 59	EA
V1630 Sco	17 49 08.2 -37 11 14	EW	V0530 Sct	18 31 19.4 -13 12 36	EB
V1631 Sco	17 50 11.3 -32 50 35	M:	V0531 Sct	18 31 22.3 -14 27 44	EW
V1632 Sco	17 50 27.5 -44 25 55	SR	V0532 Sct	18 31 23.6 -13 29 25	EB
V1633 Sco	17 50 45.7 -38 38 01	SRB	V0533 Sct	18 31 27.1 -13 39 45	M
V1634 Sco	17 52 44.6 -39 52 13	SR	V0534 Sct	18 31 29.1 -13 11 15	M
V1635 Sco	17 52 52.7 -38 36 01	M:	V0535 Sct	18 31 29.7 -13 40 50	EW
V1636 Sco	17 53 02.3 -44 57 26	RRAB:	V0536 Sct	18 31 31.1 -14 13 54	EB
V1637 Sco	17 53 03.3 -37 34 05	M:	V0537 Sct	18 31 36.1 -13 50 38	EW
V1638 Sco	17 53 04.7 -42 09 25	M	V0538 Sct	18 31 37.0 -14 25 38	EW
V1639 Sco	17 53 16.0 -32 11 44	M:	V0539 Sct	18 31 37.8 -13 45 03	EB
V1640 Sco	17 53 23.3 -36 06 08	SR	V0540 Sct	18 31 39.2 -13 52 34	EW
V1641 Sco	17 53 36.9 -43 43 58	M	V0541 Sct	18 31 40.6 -13 36 43	EW
V1642 Sco	17 54 10.4 -30 05 35	BY	V0542 Sct	18 31 42.5 -15 01 04	EW
V1643 Sco	17 54 39.4 -43 22 36	EB	V0543 Sct	18 31 47.2 -13 45 39	EW
V1644 Sco	17 54 54.5 -43 01 07	M	V0544 Sct	18 31 47.5 -15 04 01	EA
V1645 Sco	17 55 19.0 -43 11 39	SR	V0545 Sct	18 31 48.7 -13 41 49	EW
V1646 Sco	17 55 51.0 -42 43 58	SR	V0546 Sct	18 31 50.1 -14 59 18	EW

Table 1 (continued)

Name	R.A., Decl., 2000.0						Type	Name	R.A., Decl., 2000.0						Type
	h	m	s	o	’	"			h	m	s	o	’	"	
V0547 Sct	18	31	51.1	-13	19	14	RRAB	V0601 Sct	18	33	26.2	-13	43	17	EW
V0548 Sct	18	31	52.3	-13	39	05	M	V0602 Sct	18	33	27.0	-14	15	23	EW
V0549 Sct	18	31	55.1	-13	19	30	EB	V0603 Sct	18	33	27.9	-13	41	59	EW
V0550 Sct	18	31	55.6	-14	19	19	EW	V0604 Sct	18	33	35.7	-13	50	53	EA
V0551 Sct	18	31	56.5	-14	26	42	EB	V0605 Sct	18	33	41.7	-13	36	02	EW
V0552 Sct	18	31	57.2	-14	21	49	EW	V0606 Sct	18	33	43.0	-13	46	28	EW
V0553 Sct	18	31	57.6	-14	15	30	EB	V0607 Sct	18	33	48.3	-13	53	05	EW
V0554 Sct	18	32	03.7	-15	19	05	EB	V0608 Sct	18	33	59.4	-13	40	49	EW
V0555 Sct	18	32	05.5	-13	47	42	EW	V0609 Sct	18	34	02.4	-13	53	11	EW
V0556 Sct	18	32	05.6	-13	25	39	EA	V0610 Sct	18	36	36.4	-15	06	43	RS
V0557 Sct	18	32	05.6	-15	00	57	EW	V0598 Ser	17	30	47.9	-15	18	02	M
V0558 Sct	18	32	07.3	-13	40	21	EW	V0599 Ser	17	33	36.5	-15	26	31	M:
V0559 Sct	18	32	08.5	-13	29	43	CWB	V0600 Ser	17	35	39.1	-14	42	21	M
V0560 Sct	18	32	08.8	-14	31	58	EA	V0601 Ser	17	35	46.7	-14	40	51	M
V0561 Sct	18	32	10.8	-13	39	53	EW	V0602 Ser	17	36	07.3	-15	09	12	M
V0562 Sct	18	32	12.1	-13	27	31	M	V0603 Ser	17	36	41.3	-15	54	55	M
V0563 Sct	18	32	13.1	-13	53	17	EW	V0604 Ser	17	36	46.5	-15	30	50	M:
V0564 Sct	18	32	15.6	-15	05	56	EB	V0605 Ser	17	38	37.2	-12	47	01	M
V0565 Sct	18	32	16.3	-13	39	03	EB	V0606 Ser	17	40	00.8	-14	54	11	M:
V0566 Sct	18	32	17.1	-14	15	46	EW	V0607 Ser	17	44	43.4	-15	20	14	ELL:
V0567 Sct	18	32	17.7	-13	34	18	EW	V0608 Ser	17	45	09.6	-15	23	30	EW
V0568 Sct	18	32	18.6	-13	11	13	EA	V0609 Ser	17	46	30.4	-14	58	01	M
V0569 Sct	18	32	18.8	-13	25	32	EW	V0610 Ser	17	47	05.2	-13	40	21	M
V0570 Sct	18	32	20.9	-13	50	53	EB	V0611 Ser	17	47	45.2	-13	13	43	EB
V0571 Sct	18	32	23.4	-14	30	30	EB	V0612 Ser	17	52	49.3	-13	52	56	SR
V0572 Sct	18	32	23.4	-13	13	09	M	V0613 Ser	17	57	49.7	-00	17	00	DSCT
V0573 Sct	18	32	23.9	-13	35	16	EB	V0614 Ser	17	58	47.2	-02	05	20	EB
V0574 Sct	18	32	24.3	-13	46	01	EW	V0615 Ser	17	59	59.7	-10	40	23	SR
V0575 Sct	18	32	27.4	-14	17	51	EW	V0616 Ser	18	00	48.7	-00	35	07	SRB
V0576 Sct	18	32	31.9	-13	11	11	EB	V0617 Ser	18	02	13.8	-00	21	45	LB
V0577 Sct	18	32	33.4	-13	26	55	EB	V0618 Ser	18	02	16.7	-00	06	43	SRB
V0578 Sct	18	32	39.3	-13	25	58	EW	V0619 Ser	18	04	39.0	-00	23	37	SR
V0579 Sct	18	32	39.4	-14	28	30	EW	V0620 Ser	18	05	26.1	-00	21	03	SRB
V0580 Sct	18	32	41.8	-13	38	42	EB	V0621 Ser	18	06	04.4	-00	32	05	SR
V0581 Sct	18	32	42.1	-14	33	05	EW	V0622 Ser	18	16	13.3	-00	03	01	EW
V0582 Sct	18	32	44.7	-13	18	41	M	V0623 Ser	18	27	39.6	+01	00	02	EW
V0583 Sct	18	32	48.8	-13	52	32	EW	V0624 Ser	18	28	30.0	+02	51	56	RRAB
V0584 Sct	18	32	49.8	-14	22	21	EW	V0625 Ser	18	28	35.7	+02	59	27	SR:
V0585 Sct	18	32	50.0	-13	14	11	EW	V0626 Ser	18	28	53.8	+02	48	49	SR:
V0586 Sct	18	32	51.3	-14	23	09	EW	V0627 Ser	18	29	08.6	+02	54	16	EA
V0587 Sct	18	32	55.5	-14	13	49	EW	V0628 Ser	18	29	39.9	+02	51	55	SR:
V0588 Sct	18	32	57.6	-14	28	12	EW	V0629 Ser	18	30	26.8	+02	50	17	SR:
V0589 Sct	18	32	59.6	-13	16	22	EW	V0630 Ser	18	31	24.2	+02	52	59	SR:
V0590 Sct	18	33	04.2	-13	16	47	EB	V0631 Ser	18	31	42.9	+02	59	58	SR:
V0591 Sct	18	33	04.6	-13	25	22	EW	V0632 Ser	18	31	49.9	+03	22	46	SR:
V0592 Sct	18	33	05.9	-13	48	55	EA	V0633 Ser	18	31	50.7	+03	32	46	EB
V0593 Sct	18	33	06.8	-13	35	06	EA	V0634 Ser	18	31	54.6	+03	28	50	SR:
V0594 Sct	18	33	07.3	-13	13	40	M	V0635 Ser	18	32	19.0	+02	14	54	RS
V0595 Sct	18	33	08.8	-13	45	41	EB	V0383 Tel	18	11	23.5	-49	46	19	LB
V0596 Sct	18	33	11.9	-13	32	48	EB	V0384 Tel	18	12	15.0	-52	06	55	RRAB
V0597 Sct	18	33	16.6	-13	26	17	EW	V0385 Tel	18	33	15.8	-48	34	38	SRA
V0598 Sct	18	33	21.2	-13	45	47	EW	V0386 Tel	18	47	50.5	-53	34	37	EW
V0599 Sct	18	33	21.5	-14	27	04	EW	V0387 Tel	18	56	48.1	-47	16	29	SRB
V0600 Sct	18	33	25.8	-13	40	47	EW	V0388 Tel	19	22	27.4	-56	22	28	DSCT

Table 1 (continued)

Name	R.A., Decl., 2000.0	Type	Name	R.A., Decl., 2000.0	Type
	h m s o ' "			h m s o ' "	
V0389 Tel	20 04 31.4 -53 52 18	RRC	V0534 Vul	19 54 35.7 +20 44 18	SR:
V0390 Tel	20 22 10.8 -45 18 50	RRC	V0535 Vul	19 54 36.0 +21 09 43	EA
EX Tuc	22 23 11.3 -62 35 52	RS	V0536 Vul	19 54 37.7 +20 23 35	EW
V0517 Vul	19 45 02.2 +24 34 09	BY	V0537 Vul	19 54 42.1 +20 58 03	EW
V0518 Vul	19 52 18.5 +20 53 29	EA	V0538 Vul	19 54 45.5 +21 02 13	SR:
V0519 Vul	19 52 50.6 +20 51 42	DSCT	V0539 Vul	19 54 47.9 +20 56 44	EW
V0520 Vul	19 52 59.0 +20 57 46	EB	V0540 Vul	19 54 49.5 +20 50 41	EW
V0521 Vul	19 53 00.3 +20 59 11	EW	V0541 Vul	19 54 51.2 +20 25 22	EA
V0522 Vul	19 53 04.3 +20 30 36	EW	V0542 Vul	19 55 05.2 +21 17 31	DSCT
V0523 Vul	19 53 11.2 +21 06 22	EW	V0543 Vul	19 55 25.5 +20 31 38	EW
V0524 Vul	19 53 23.2 +21 15 04	RRC	V0544 Vul	19 55 27.3 +20 54 40	EA
V0525 Vul	19 53 26.2 +21 15 33	EW	V0545 Vul	20 32 12.8 +27 42 58	EW
V0526 Vul	19 53 33.0 +20 38 10	EB	V0546 Vul	20 32 28.2 +24 42 59	EB
V0527 Vul	19 53 40.4 +20 38 25	EA	V0547 Vul	20 32 29.1 +27 51 40	EB
V0528 Vul	19 53 57.0 +21 04 27	EW	V0548 Vul	20 32 59.8 +27 47 46	EA/RS:
V0529 Vul	19 53 59.3 +21 07 29	EB	V0549 Vul	20 33 04.1 +27 40 22	EW
V0530 Vul	19 53 59.5 +20 52 52	EA	V0550 Vul	20 40 26.3 +22 05 07	EB
V0531 Vul	19 54 21.6 +29 13 49	SR	V0551 Vul	20 55 05.3 +24 00 51	EW
V0532 Vul	19 54 26.6 +20 34 14	EB	V0552 Vul	21 16 56.6 +21 48 21	EW
V0533 Vul	19 54 35.2 +20 59 22	EW			

Table 2. Novae

GCVS	Nova name
V1831 Aql	Nova Aql 2015
V2949 Oph	Nova Oph 2015 No. 2
V5669 Sgr	Nova Sgr 2015 No. 3
V5850 Sgr	Nova Sgr 2015 No. 4

*This version of the paper contains corrections, and differs from the one appeared on-line originally. Date of last modification: Jan 14 2016

COMMISSIONS 27 AND 42 OF THE IAU
INFORMATION BULLETIN ON VARIABLE STARS

Number 6156

Konkoly Observatory
Budapest
11 January 2016

HU ISSN 0374 – 0676

THE LONG-TERM BINARY SYSTEM VV Cep

POLLMANN, E.[1]; BENNETT, P. D.[2]; HOPKINS, J. L.[3]

[1] International Working Group ASPA, Emil-Nolde-Str. 12, 51375 Leverkusen, Germany, e-mail: ernestospec@hotmail.de

[2] Department of Astronomy & Physics, Saint Mary's University, Halifax, NS B3H 3C3, e-mail: pbennett@ap.smu.ca

[3] 7812 West Clayton Drive, Phoenix, Arizona USA, e-mail: phjeff@hposoft.com

1 Introduction

VV Cep is an eclipsing binary with a period of about 20.4 years that is comprised of an M2Iab primary star and an early B secondary star. A preliminary orbit was announced in 1933 by Harper & Christie (1936), and McLaughlin (1934) described the behaviour of the wide emission lines of Hydrogen and those of ionized CaII, the H & K lines, which were divided by sharp absorption and shifted in velocity, and presented the V/R (violet to red component) ratio for the Hydrogen Balmer lines. In October 1936, McLauglin (1936) announced that the hot star in VV Cep had been eclipsed, establishing the system as an eclipsing binary. Goedicke (1939a,b) carried out the first detailed spectroscopic analysis of this system. Wright (1977) inferred the existence of intermittent mass transfer and an Hα emitting disk. Kawabata et al. (1981) and Moellenhoff & Schaifers (1978, 1981) further described what appeared to be an accretion disk around the B star.

The dimension of the disk around the Be star was determined by Peery (1966) to be less than 1/18 of the diameter of the M supergiant's photosphere, and according to investigations of Hutchings & Wright (1971) it is not spherically symmetrical, but rather is more dense in the direction of the stellar equator, as in the case of a normal Be star. This seems to be quite logical in view of the remarkable stream of gas in this system.

Long-term monitoring of the intensity variations of the V and R emission peaks (the so-called V/R ratio) delivers important information about the peak strength as measure for the mass and/or density of the gas in the disk, expressed as equivalent width (EW) of the emission, and the direction of movement of the corresponding gas region within the disk (Figure 1). The violet and the red (V and R) components into which the emission line of the VV Cep spectrum is split can be linked to the radiation of the gas disk around the Be star. Due to its counterclockwise rotation around the central star, in relation to the line of sight of the observer, it results in a blueshift by moving towards the observer (V component) and a redshift by moving away (R component) from the observer.

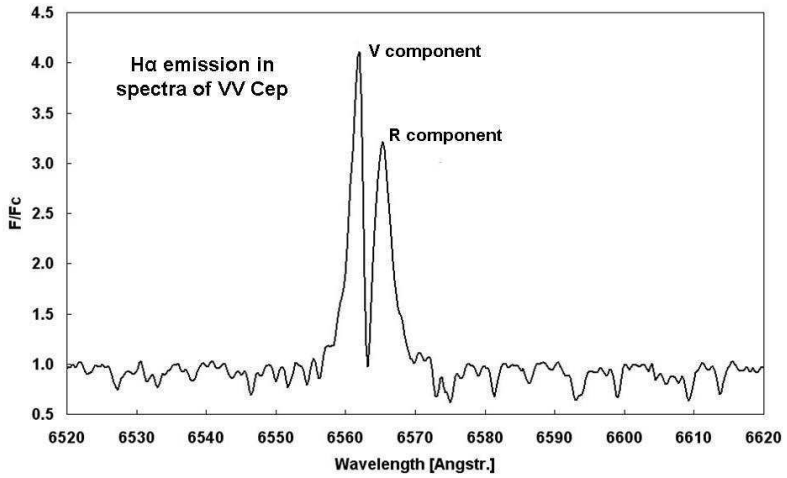

Figure 1. Representative spectrum of VV Cep with its typical Hα emission splitted into two components, the V (blueshifted) and R (redshifted) components.

2 Goals and motivation

According to investigations of Wright (1977), the source of the central absorption in the profile of the Hα emission line is caused by the transferred and absorbed material between observer and shell of the Be star. Because of the mass transfer from the M supergiant towards its Be star companion in the VV Cep system, the presence of the strong Hα emission can be well explained as being created in the outer shell of the companion. The gas stream coming from the M supergiant spiralling around the Be star has to be less dense in the polar regions than around the equator.

Long-term spectroscopic observations clearly outside the eclipses of 1956/57 and 1976–78 have only been published by Wright (1977), Hack et al. (1992) and Moellenhoff & Schaifers (1981). Hα V/R variation from these spectra provide for the first time a rough explanation about a possible quasi-cyclic behavior of the structure of density of the Be star disk, however, even though these data had covered almost the complete orbital phase by measurements, the number of their observations is insufficient for a reliable analysis.

3 Observations

The Hα emission line is the only indication of the presence of the disk. Figure 2 shows monitoring of the Hα equivalent width (EW) since July 1996 until today. The eclipse of the emitting Be star disk by the M supergiant started in March 1997 (JD 2450511) and ended 673 days later. The period from the beginning of the disk coverage (contact 1) up to coverage end (contact 2) lasted 128 days, from first appearance of the disk (contact 3) up to the complete visibility (contact 4) 171 days. The full eclipse period was 373 d. Saito et al. (1980) observed the 1976–78 eclipse with UBV photometry. In that case, totality lasted about 300 days, significantly shorter than the latest eclipse, and the entire event required about 1000 days.

While after the ephemeris of Gaposchkin (1937) ($E_{\rm min}$ = JD 2421070 + 7430 E_0) the mid-point of the eclipse was expected at JD 2450790, the time determined from Figure 2 is JD 2450827, thus with a delay of 37 d. Graczyk et al. (1999) determined the mid-point of the eclipse 1997/99 from UBV photometry at approximately JD 2450855, thus with 65 d delay. Leedjärv et al. (1999) obtained a similar value of 68 d compared with the ephemeris of Gaposchkin (1937) likewise from UBV photometry, as well as optical spectroscopy.

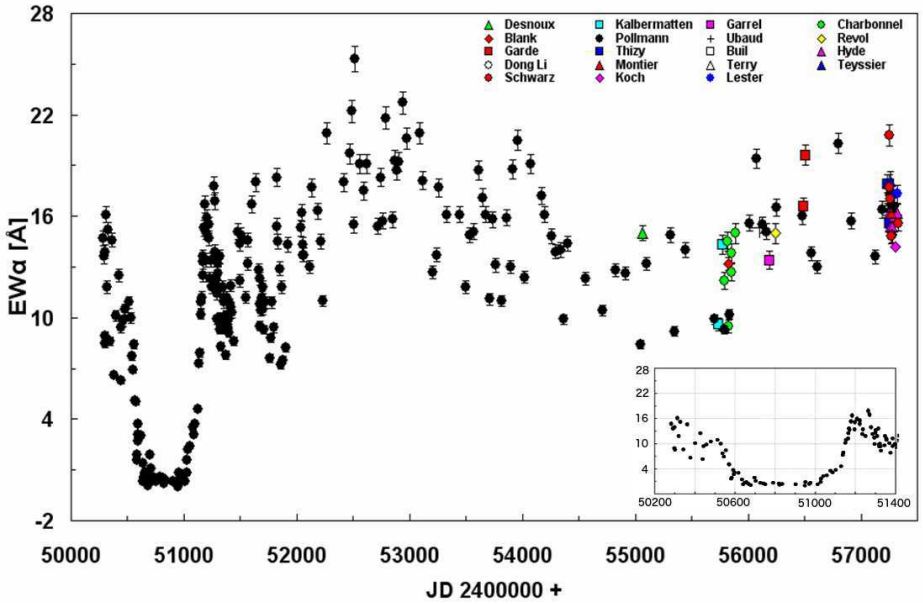

Figure 2. Long-term monitoring of the Hα equivalent width since 1996 until now.

Perhaps the most interesting feature of Figure 2 is the behavior of Hα emission outside of eclipse. Large fluctuations in EW occurred continuously over about 15 years. A possible explanation might be a variable mass accretion from the M supergiant to the accretion disk as described by Wright (1977) and Stencel et al. (1993). However from the findings of this observation material alone, it is not yet possible to judge to what extent these fluctuations are due exclusively to varying contributions by mass transfer between the two components or from the disk itself, or both together.

The amateur community's contribution to the EW and V/R monitoring from July 1996 to November 2015 involved 20 observers of the ARAS group[1]. They used 0.2 m to 0.4 m telescopes with long-slit (in most cases) and échelle spectrographs with spectral resolving power from R = 1000 to R = 22000. Data reduction was performed using MaxIm-DL 3.06 (Diffraction Limited, Sehgal Corp.) for Pollmann's data, while most other amateur data were reduced with software packages developed for amateur spectrographs, such as VSpec3 and IRIS34. Spectral line parameters were measured with the spectral classification software package MK325. No systematic difference in the V/R ratios or the Hα line equivalent widths were found between professional and amateur data.

Measurements of the V/R ratio of Hα by Kawabata et al. (1981) during the 1976–1978 eclipse may indicate that the distribution of matter in the disk is not homogeneous. The stronger violet emission peak may be formed by large density in the left side of the disk

[1] http://www.astrosurf.com/aras

which rotates counterclockwise. Different strengths of the violet and red peaks during the 1997–1999 eclipse can be inferred from the ingress and egress branches of the plot in Figure 2. During ingress, with the disk's left side hidden and its right side in view, on average EW = 11Å. At egress, with the left side emerging from eclipse, EW = 17Å.

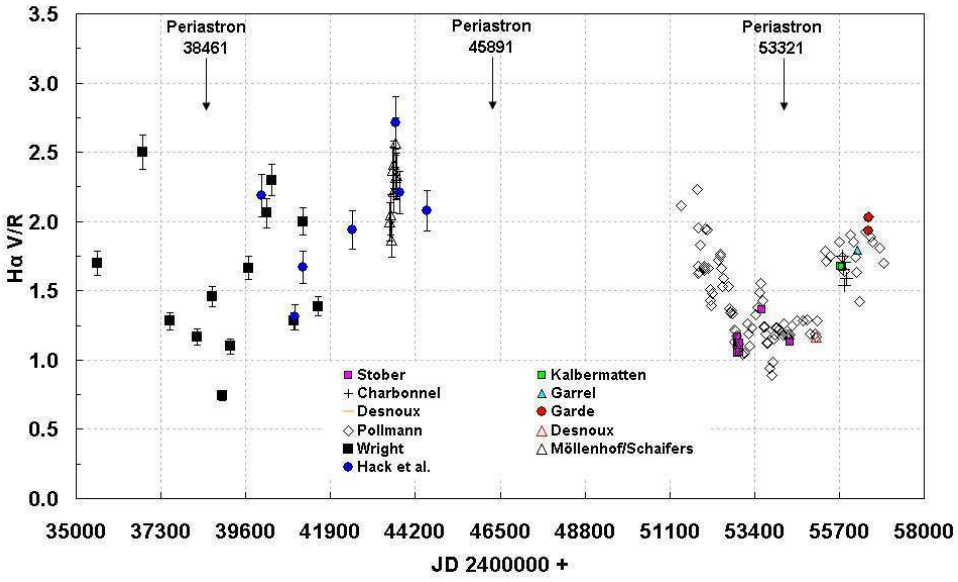

Figure 3. Long-term monitoring of the V/R ratio outside the eclipses of 1956/57 and 1976–78 by Wright (1977), Moellenhoff & Schaifers (1981), Hack et al. (1992) combined with data of the author and the ARAS group since November 2000 (JD 2451413).

4 Results and discussion

The long term monitoring of the variations in intensity of both components (so called V/R relation) results in important information about:

1. emission peak intensity as a measure of the mass or density of the gas in its shell expressed in equivalent width EW of the emission,
2. the direction of motion of the gas shell's region.

A large density of V/R data from the ARAS group has been added since November 2000 (JD 2451413; Figure 3).These additional data points demonstrate how dramatically the V/R relation is changing. The combined data confirm clearly the time evolution of the V/R relation. The V/R variation in Figure 3 asks for a more detailed evaluation about its periodic behavior.

Figure 4 shows a PDM (phase dispersion minimization; Stellingwerf 1978) period analysis of the entire V/R data set in Figure 3, with a dominant period of 3916 d. Figure 5 demonstrates the sine fit of this period to the V/R time behaviour. Figure 5 shows that only the data beginning at JD 2451413 and later are well fit, likely due to the low observation frequency of the time section from JD 2435572 to 2444511 (Wright 1977, Moellenhoff & Schaifers 1981, Hack et al. 1992). In Figure 6, the phase diagram of the 3916 d period

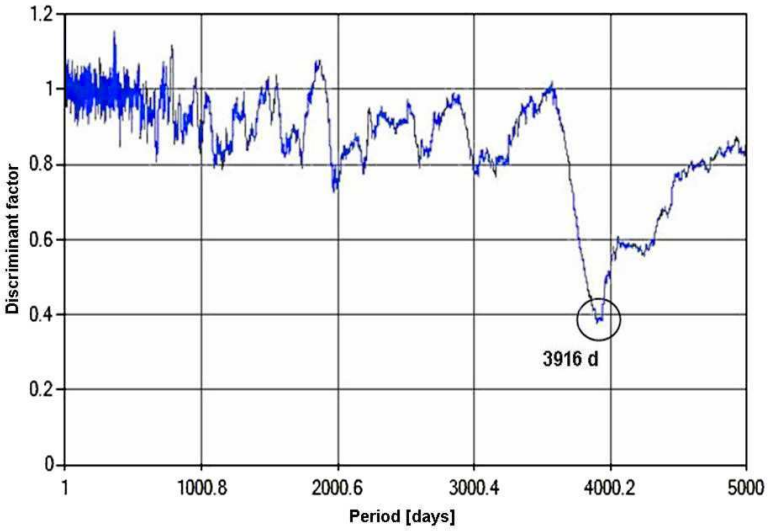

Figure 4. PDM period analysis of all V/R data in Fig. 3

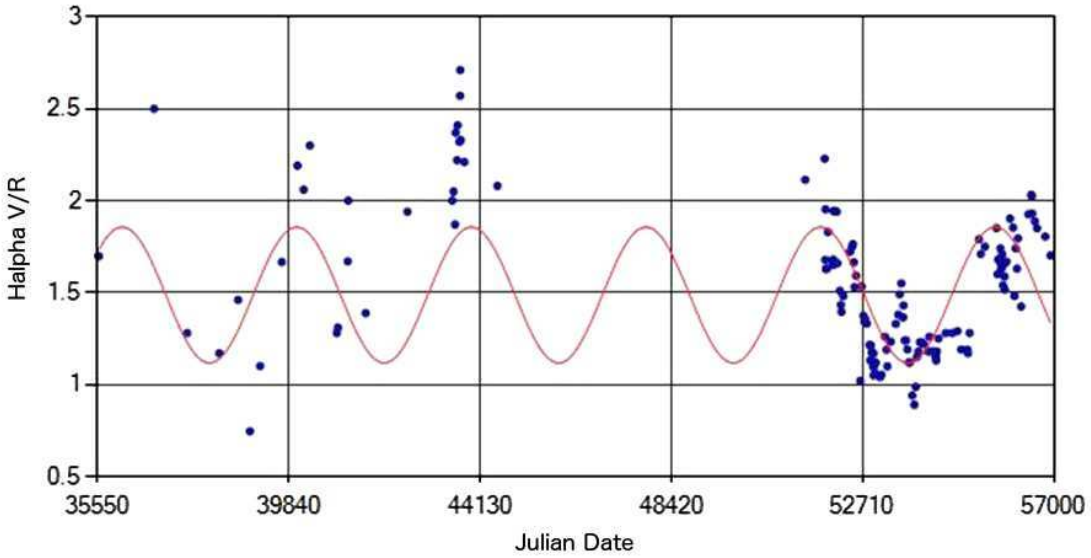

Figure 5. Period-adapted time series of all V/R data in Fig. 3

is shown. It seems to be the half of the orbital period, approximately 7450 d. A possible explanation for that behaviour might be a tidal effect of the M supergiant on the Be star disk during each periastron.

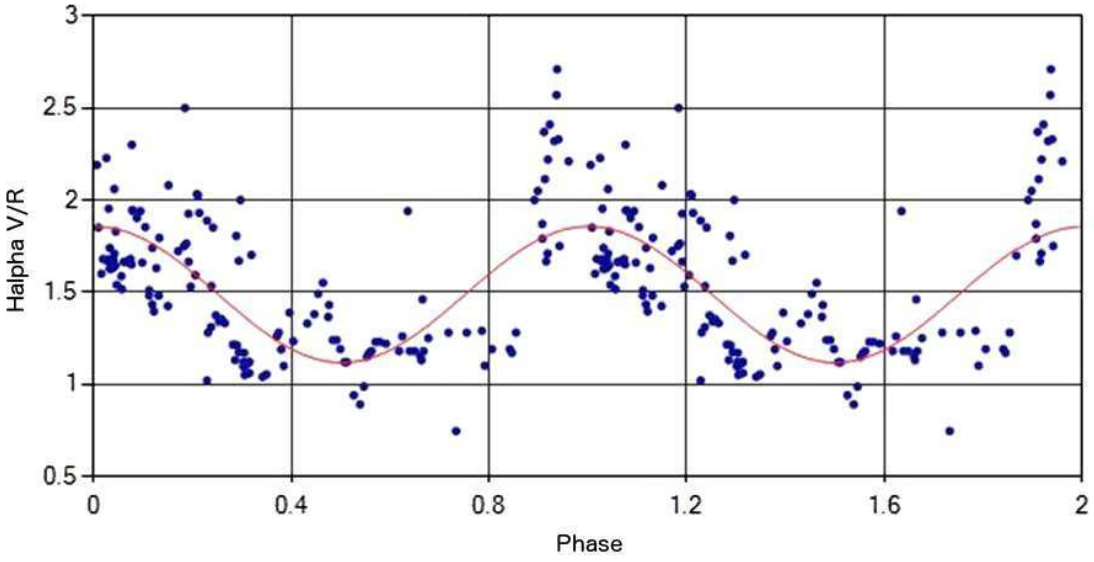

Figure 6. Phase diagram of the PDM period of 3916 days (it seems to be the half of the orbital period).

A further relevant issue is whether there are V/R variations independent of the orbital period. Figure 7 shows the subtraction (residuals) of the 3916 d period from the V/R time series (section JD 2451413 to JD 2456917, the amateur data) and its PDM analysis with the dominant period of 988 d. Figure 8 demonstrates the sine fit of this period to the V/R behaviour of the corresponding time section. Finally, in Figure 9, the corresponding phase diagram of the found 988 d period is shown. This is the first time that amateur observations provide evidence of periodic density variations of a Be star disk in VV Cep. The results of both period analyses are shown in Table 1.

Table 1: Period analysis of VV Cep. Second line is the analysis of the residual after subtracting the orbital period.

V/R Ephemerides	Period [d]	Amplitude	T_0 [d]	RMS [d]
(Half) orbital period	3916 (±44)	0.37 (±0.03)	2435116 (±192)	0.29
Residuals	988 (±15)	0.17 (±0.02)	2451290 (±45)	0.16

The next eclipse in 2017–18 provides excellent opportunities to investigate the binary system VV Cep in very different aspects. This event has triggered a world-wide campaign, resulting in cooperation between both professional astronomy and amateurs, in order to collect photometric and spectroscopic data.

The web page `http://www.ap.smu.ca/~pbennett/vvcep/main.html`, designed by P. Bennett, will give detailed announcements of the different phases of this important eclipsing event.

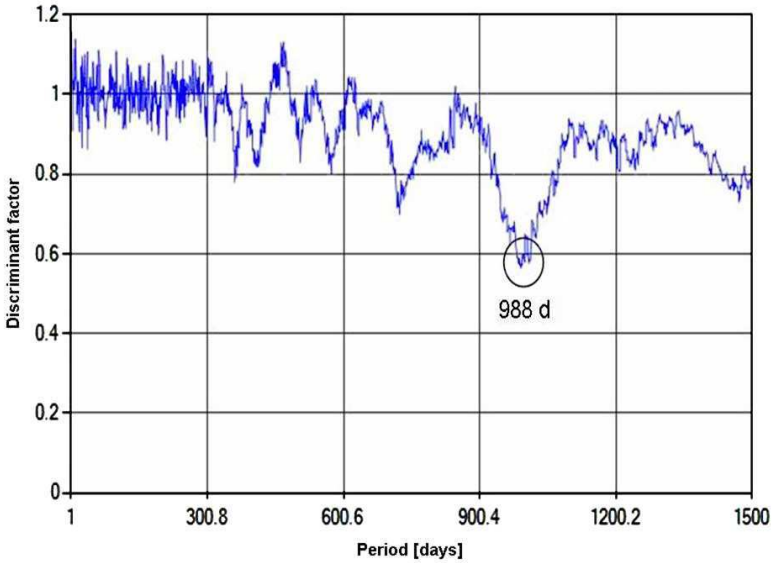

Figure 7. Subtraction (residuals) of the 3916 d period from the V/R time series (section 2451413 to 2456917) and its PDM analysis with the dominant period of 988 days.

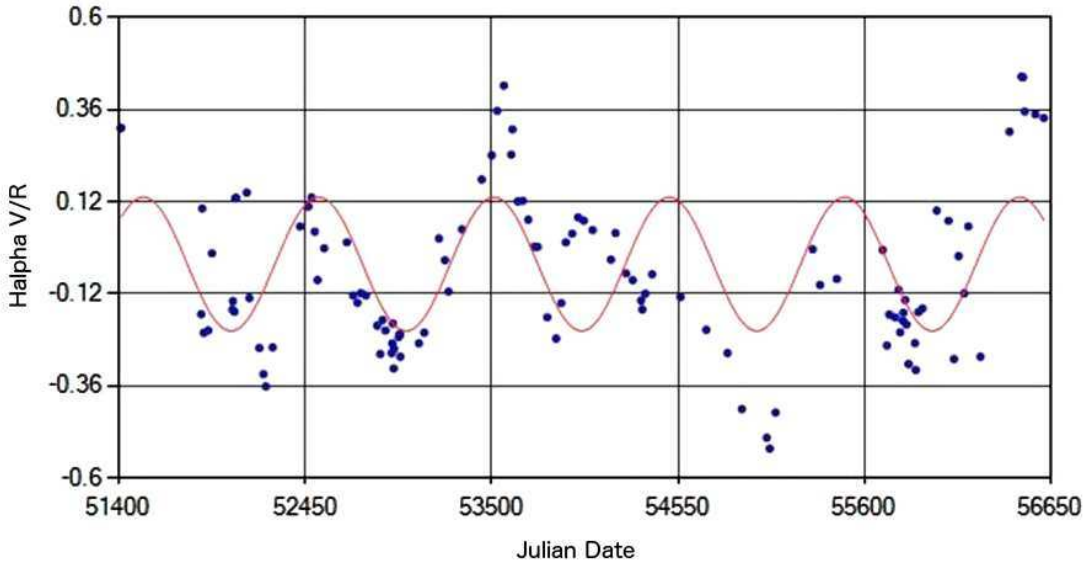

Figure 8. Adjustment of the 988 d period to the corresponding V/R time series.

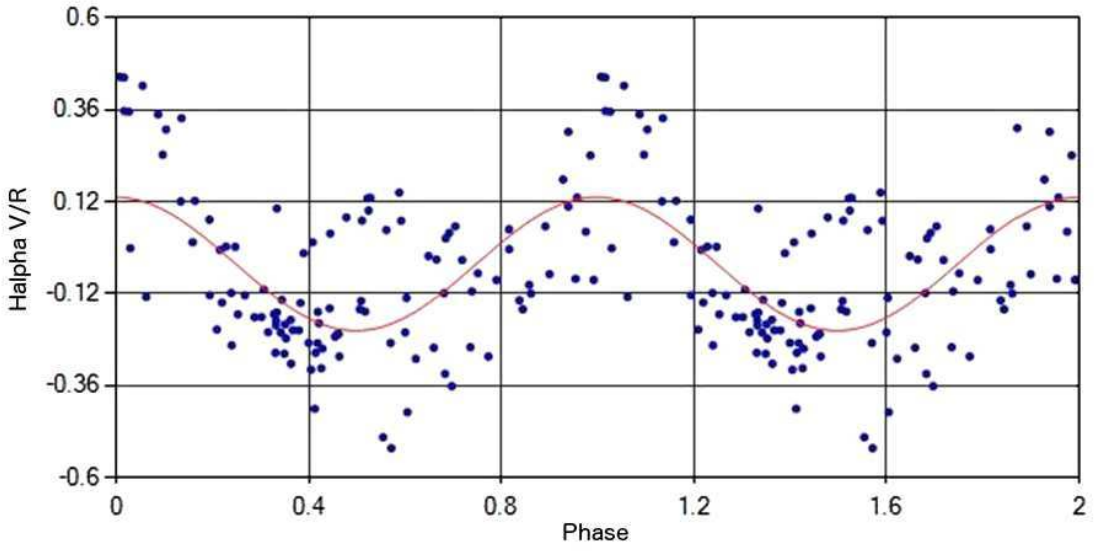

Figure 9. Phase diagram of the found 988 day period.

Acknowledgements: We would like to thank Sara Sawicki for English language improvements.

References:

Gaposchkin, S., 1937, *Harvard Coll. Obs. Circ.*, 421, 1
Goedicke, V. 1939a, *Publ. Obs. Univ. Michigan*, 8. 1
Goedicke, V. 1939b, *Obs.*, **62**, 197
Graczyk D., Mikolajewski, M., Janowski, J.L., 1999, *IBVS*, **4679**
Hack, M., Engin, S., Yilmaz, N., Sedmak, G., Rusconi, L., Boehm, C., 1992, *A&A Suppl. Ser.*, **95**, 589
Harper, W.E. & Christie, W.H., 1936, *P.A.A.S*, **8**, 9
Hutchings, J.B. & Wright, K.O., 1971, *MNRAS*, **155**, 203
Kawabata, S., Saijo, K., Sato, H., Saito, M., 1981, *PASJ*, **33**, 177
Leedjärv, L., Graczyk, D., Mikolajewski, M., Puss, A., 1999, *A&A*, **349**, 511
McLaughlin, D.B. 1934, *ApJ*, **79**, 380
McLaughlin, D.B. 1936, *Harvard Obs. Announcement Card*, 397
Moellenhoff, C., Schaifers, K., 1978, *A&A*, **64**, 253
Moellenhoff, C., Schaifers, K., 1981, *A&A*, **94**, 333
Peery, B.F., Jr., 1966, *ApJ*, **144**, 672
Saito, M., Sato, H., Saijo, K., Hayasaka, T., 1980, *PASJ*, **32**, 163
Stellingwerf, R.F., 1978, *ApJ*, **224**, 953
Stencel, R.E., Potter, D. E., Bauer, W. H., 1993, *PASP*, **105**, 45
Wright, K.O., 1977, *JRASC*, **71**, 152

COMMISSIONS 27 AND 42 OF THE IAU
INFORMATION BULLETIN ON VARIABLE STARS

Number 6157

Konkoly Observatory
Budapest
14 January 2016

HU ISSN 0374 – 0676

BAV-RESULTS OF OBSERVATIONS – PHOTOELECTRIC MINIMA OF SELECTED ECLIPSING BINARIES

(BAV MITTEILUNGEN NO. 241)

HÜBSCHER, JOACHIM

Bundesdeutsche Arbeitsgemeinschaft für Veränderliche Sterne e.V. (BAV), Munsterdamm 90, 12169 Berlin, Germany, www.bav-astro.de, publikat@bav-astro.de

In this 83rd compilation of BAV results, photoelectric observations obtained mostly in the years 2014 ans 2015 are presented on 464 variable stars giving 661 minima of eclipsing binaries. All moments of minima are heliocentric UTC. The errors are tabulated in column "±". All information about photometers and filters are specified in the columns "Fil" and "Rem". The observations were made at private observatories. The photoelectric measurements and all the light curves with evaluations can be obtained from the office of the BAV for inspection.

Please use the following link for an easy access to all the publications of the BAV including the "Lichtenknecker Database of the BAV": `http://www.bav-astro.de/sfs`.

Table 1: Times of minima of eclipsing binaries

Variable	HJD 24.....	±	Obs	Fil	n	Rem
RT And	57199.3952	0.0014	AG	-I	28	11)
TT And	56875.5164:	0.0002	RAT RCR	V	147	9)
AB And	57235.4739	0.0002	AG	-I	21	11)
EP And	56954.5159:	0.0002	RAT RCR	o	102	19)
V613 And	57199.4755	0.0099	AG	-I	27	11)
V683 And	57225.4856	0.0018	AG	-I	33	11)
V346 Aql	57199.4576	0.0018	AG	-I	27	11)
V609 Aql	57210.3839	0.0027	AG	-I	31	11)
V688 Aql	57204.4623	0.0189	AG	-I	31	11)
V1353 Aql	57204.4741	0.0134	AG	-I	31	11)
	57238.4248	0.0030	BRW	V	143	14)
	57255.4042	0.0020	BRW	o	328	4)
V1426 Aql	57213.4961	0.0035	AG	-I	28	11)
V1430 Aql	57219.3755	0.0013	AG	-I	33	11)
	57235.4027	0.0010	BRW	V	113	14)
V1490 Aql	57214.5021	0.0033	AG	-I	30	11)
V1713 Aql	57219.3707	0.0037	AG	-I	33	11)
V1796 Aql	57213.4606	0.0024	AG	-I	28	11)
V1798 Aql	56831.5140	0.0008	RAT RCR	V	111	9)
V1808 Aql	57210.4528	0.0026	AG	-I	30	11)
V1817 Aql	56489.3815	0.0010	AG	-I	25	11)
V1828 Aql	56156.4185	0.0001	RAT RCR	Rc	68	9)
	56158.4053	0.0001	RAT RCR	Rc	65	9)
	56159.3438	0.0004	RAT RCR	Rc	99	9)
	56159.3986	0.0001	RAT RCR	Rc	99	9)
SX Aur	57091.3757	0.0027	AG	-I	25	11)
AH Aur	57089.3666	0.0014	JU	o	46	13)

Table 1: cont.

Variable	HJD 24.....	±	Obs	Fil	n	Rem
HL Aur	57080.3597	0.0015	AG	-I	34	11)
IM Aur	57091.3681	0.0126	AG	-I	23	11)
IY Aur	57101.3876	0.0130	AG	-I	19	11)
KO Aur	57080.2537	0.0014	AG	-I	58	11)
KU Aur	56729.3445	0.0001	RAT RCR	V	88	9)
SS Boo	57106.5296	0.0193	AG	-I	35	11)
UW Boo	57100.6189	0.0020	AG	-I	43	11)
VW Boo	57154.4514	0.0027	AG	-I	33	11)
AC Boo	57094.4834	0.0001	SCI	o	77	13)
	57094.6595	0.0001	SCI	o	79	13)
	57123.3778	0.0004	KBL	o	63	20)
	57154.3991	0.0001	SCI	o	118	13)
	57154.5764	0.0001	SCI	o	142	13)
BG Boo	56794.4743	0.0040	MZ	-I	100	14)
CK Boo	57154.4411	0.0034	AG	-I	27	11)
CV Boo	57153.5197	0.0013	AG	-I	32	11)
DU Boo	57100.5466	0.0066	AG	-I	44	11)
EF Boo	57150.5063	0.0019	AG	-I	32	11)
	57151.3475	0.0011	AG	-I	30	11)
	57153.4495	0.0022	AG	-I	32	11)
EL Boo	57154.4535	0.0052	AG	-I	32	11)
FP Boo	57097.4591	0.0031	AG	-I	41	11)
GK Boo	57106.3962	0.0011	AG	-I	37	11)
	57106.6339	0.0011	AG	-I	37	11)
GT Boo	57106.5123	0.0082	AG	-I	35	11)
	57130.4088	0.0004	MS FR	o	34	17)
GV Boo	57119.4489	0.0005	MS FR	o	79	17)
HH Boo	57100.4486	0.0037	AG	-I	43	11)
	57100.6044	0.0009	AG	-I	43	11)
IO Boo	56767.4440	0.0010	RAT RCR	V	85	9)
LM Boo	57134.4358	0.0002	MS FR	o	102	17)
MN Boo	57150.4088	0.0073	AG	-I	33	11)
	57153.5070	0.0023	AG	-I	32	11)
MV Boo	57106.4512	0.0092	AG	-I	37	11)
NX Boo	57066.8874	0.0009	MS FR	V	23	7)
	57121.3842	0.0003	MS FR	o	62	17)
PT Boo	57097.5519	0.0072	AG	-I	41	11)
	57100.4525	0.0032	AG	-I	38	11)
PU Boo	57097.5704	0.0058	AG	-I	39	11)
	57100.4627	0.0115	AG	-I	38	11)
PY Boo	57123.4254	0.0001	MS FR	o	105	17)
PZ Boo	57100.4767	0.0015	AG	-I	38	11)
QQ Boo	57097.3737	0.0025	AG	-I	43	11)
	57097.5146	0.0008	AG	-I	43	11)
	57100.4154	0.0007	AG	-I	38	11)
	57100.5551	0.0007	AG	-I	38	11)
QT Boo	57100.3887	0.0022	AG	-I	38	11)
	57100.5357	0.0042	AG	-I	38	11)
QW Boo	57097.5074	0.0007	AG	-I	39	11)
	57100.4545	0.0502	AG	-I	38	11)
	57100.5601	0.0011	AG	-I	38	11)
QX Boo	57097.4918	0.0008	AG	-I	37	11)
QY Boo	57097.4593	0.0040	AG	-I	30	11)
	57100.5345	0.0043	AG	-I	38	11)
V339 Boo	57097.5477	0.0022	AG	-I	39	11)
	57100.4634	0.0164	AG	-I	38	11)
	57100.6280	0.0021	AG	-I	38	11)
SV Cam	57080.4040	0.0008	AG	-I	55	11)
AL Cam	57091.3401	0.0089	AG	-I	50	11)
AW Cam	57080.2994	0.0010	AG	-I	37	11)
AZ Cam	57090.4130	0.0069	AG	-I	46	11)
FN Cam	57091.5770	0.0068	AG	-I	50	11)
NR Cam	57091.2973	0.0016	AG	-I	59	11)
	57091.4242	0.0017	AG	-I	59	11)
	57091.5539	0.0042	AG	-I	59	11)
	57091.6789	0.0005	AG	-I	59	11)
NU Cam	57090.4514	0.0033	AG	-I	42	11)
V455 Cam	57080.3605	0.0015	AG	-I	37	11)
V474 Cam	57100.3213	0.0007	AG	-I	30	11)
	57100.4832	0.0010	AG	-I	30	11)
V503 Cam	56744.5876	0.0002	RAT RCR	V	258	9)

Table 1: cont.

Variable	HJD 24.....	±	Obs	Fil	n	Rem
V514 Cam	57091.4485	0.0028	AG	-I	50	11)
	57091.6305	0.0031	AG	-I	50	11)
TX Cnc	57091.3846	0.0001	SCI	o	169	13)
	57091.5748	0.0001	SCI	o	83	13)
WW Cnc	56726.5642	0.0001	RAT RCR	V	160	9)
WY Cnc	57080.5528	0.0012	AG	-I	40	11)
XZ Cnc	57097.3588	0.0039	AG	-I	31	11)
AC Cnc	57093.3523	0.0006	SCI	o	112	13)
	57093.4989	0.0006	SCI	o	46	13)
ES Cnc	57089.4723	0.0010	MS FR	o	60	8)
	57094.3326	0.0003	SCI	o	46	13)
FF Cnc	57101.3821	0.0001	FR	-I	66	11)
HS Cnc	57089.5172	0.0017	MS FR	o	60	8)
IM Cnc	57089.4472	0.0007	MS FR	o	62	8)
KY Cnc	57090.4407	0.0076	AG	-I	40	11)
RS CVn	57089.4340	0.0035	FR	-I	54	11)
	57101.4264	0.0065	AG	-I	55	11)
BO CVn	57100.3255	0.0008	AG	-I	45	11)
	57100.5843	0.0009	AG	-I	45	11)
DF CVn	57097.3441	0.0027	AG	-I	37	11)
	57097.5076	0.0019	AG	-I	37	11)
	57100.4500	0.0021	AG	-I	45	11)
	57100.6104	0.0012	AG	-I	45	11)
DM CVn	57125.4302	0.0003	MS FR	o	61	17)
GG CVn	57066.9750	0.0010	MS FR	V	21	7)
	57122.3578	0.0005	MS FR	o	45	17)
CR CMa	57062.6965	0.0015	MS FR	V	19	7)
	57112.9430	0.0002	MS FR	V	27	6)
	57117.9359	0.0001	MS FR	V	58	6)
EE CMa	57096.9120	0.0005	MS FR	V	69	6) 2)
	57104.9496	0.0015	MS FR	V	83	6)
AK CMi	57097.4264	0.0008	AG	-I	23	11)
BB CMi	57101.3894	0.0010	QU	V	97	14) 1)
AE Cas	57260.4082	0.0008	JU	o	65	13)
AX Cas	57082.3695	0.0017	JU	o	60	13)
IR Cas	57206.4098	0.0021	AG	-I	34	11)
	57207.4340	0.0057	AG	-I	26	11)
V381 Cas	57238.4050	0.0022	JU	o	65	13)
V1107 Cas	57082.3090	0.0007	JU	o	60	13)
SU Cep	57179.5277	0.0013	AG	-I	25	11)
WY Cep	57151.3973	0.0016	AG	-I	22	11)
XX Cep	57219.4778	0.0199	AG	-I	33	11)
XY Cep	57250.4949	0.0040	BRW	V	79	14)
AH Cep	57206.5138	0.0073	AG	-I	34	11)
NN Cep	57219.5030	0.0075	AG	-I	33	11)
	57220.5324	0.0057	AG	-I	31	11)
V397 Cep	57158.498	0.016	AG	-I	39	11)
	57206.5051	0.0104	AG	-I	34	11)
	57207.4529	0.0100	AG	-I	29	11)
V749 Cep	57179.4336	0.0094	AG	-I	25	11)
V833 Cep	57199.4490	0.0024	AG	-I	29	11)
V885 Cep	56917.4967	0.0010	RAT RCR	V	101	9)
V887 Cep	56862.5068	0.0003	RAT RCR	V	132	9)
V888 Cep	56917.4627	0.0005	RAT RCR	V	230	9)
V895 Cep	57206.4745	0.0199	AG	-I	34	11)
V919 Cep	57205.4645	0.0096	AG	-I	27	11)
RW Com	57100.4088	0.0037	AG	-I	43	11)
	57100.5252	0.0018	AG	-I	43	11)
	57100.6445	0.0009	AG	-I	43	11)
RZ Com	57100.3347	0.0041	AG	-I	39	11)
	57100.5025	0.0010	AG	-I	39	11)
LO Com	57100.5046	0.0027	AG	-I	43	11)
	57100.6435	0.0023	AG	-I	43	11)
LP Com	57100.3837	0.0040	AG	-I	42	11)
	57100.5442	0.0059	AG	-I	42	11)
LQ Com	57100.4660	0.0010	AG	-I	42	11)
	57100.6413	0.0018	AG	-I	42	11)
MR Com	56712.4387	0.0002	MS FR	o	55	17)
RW CrB	57154.4596	0.0018	AG	-I	32	11)
BR CrB	57106.4604	0.0066	AG	-I	36	11)
WZ Cyg	57179.4825	0.0017	AG	-I	25	11)

Table 1: cont.

Variable	HJD 24.....	±	Obs	Fil	n	Rem
ZZ Cyg	57178.4754	0.0013	AG	-I	30	11)
BO Cyg	56924.4483	0.0003	RAT RCR	V	195	9)
BR Cyg	57158.4492	0.0047	AG	-I	40	11)
CG Cyg	57179.5066	0.0010	AG	-I	23	11)
DK Cyg	57205.5122	0.0030	AG	-I	27	11)
GO Cyg	57178.4835	0.0084	AG	-I	31	11)
KR Cyg	57198.4295	0.0006	AG	-I	28	11)
	57214.4880	0.0002	FR	-I	47	11)
	57219.5606	0.0006	FR	-I	123	11)
	57225.4742	0.0002	FR	-I	61	11)
MR Cyg	57214.4752	0.0070	AG	-I	30	11)
V345 Cyg	56933.4042	0.0002	RAT RCR	o	168	19)
V366 Cyg	56918.5106	0.0002	RAT RCR	V	223	9)
V382 Cyg	57178.4438	0.0059	AG	-I	32	11)
V388 Cyg	57199.4157	0.0028	AG	-I	29	11)
	57208.4398	0.0091	AG	-I	33	11)
	57220.4624	0.0002	SCI	o	124	13)
V401 Cyg	57176.4723	0.0011	AG	-I	28	11)
V442 Cyg	57178.5450	0.0007	AG	-I	30	11)
V456 Cyg	57204.5084	0.0020	AG	-I	31	11)
V463 Cyg	57210.4530	0.0190	AG	-I	31	11)
V466 Cyg	57198.5283	0.0011	AG	-I	28	11)
V469 Cyg	57248.5980	0.0003	FR	-I	154	11)
V477 Cyg	57220.4226	0.0053	AG	-I	31	11)
V488 Cyg	57198.3941	0.0021	AG	-I	27	11)
	57219.4146	0.0006	FR	-I	78	11)
V490 Cyg	57198.4753	0.0010	AG	-I	24	11)
	57214.4369	0.0002	FR	-I	32	11)
V541 Cyg	57198.5271	0.0026	AG	-I	28	11)
V548 Cyg	57210.4901	0.0035	AG	-I	31	11)
	57210.4909	0.0030	BRW	V	120	14)
	57210.4919	0.0060	BRW	B	115	14)
V664 Cyg	56924.4731	0.0002	RAT RCR	V	168	9)
V687 Cyg	57198.5020	0.0017	AG	-I	28	11)
V700 Cyg	57204.4356	0.0009	AG	-I	31	11)
V725 Cyg	57219.4580	0.0029	FR	-I	40	11)
V728 Cyg	57204.4234	0.0028	AG	-I	31	11)
V745 Cyg	57257.5331	0.0001	FR	-I	70	11)
	57264.3819	0.0002	FR	-I	72	11)
V788 Cyg	57243.3857	0.0010	BRW	V	142	14)
V796 Cyg	57205.4882	0.0044	AG	-I	27	11)
	57219.4992	0.0046	AG	-I	33	11)
	57225.4240	0.0032	AG	-I	33	11)
V836 Cyg	57198.4282	0.0020	AG	-I	28	11)
V859 Cyg	57176.4784	0.0020	AG	-I	26	11)
V865 Cyg	54212.5833	0.0001	MS FR	o	78	15)
V873 Cyg	57242.5676	0.0007	FR	-I	79	11)
V885 Cyg	57214.4345	0.0092	AG	-I	30	11)
V891 Cyg	57176.5087	0.0023	AG	-I	30	11)
V1018 Cyg	56841.4975	0.0003	RAT RCR	V	119	9)
V1034 Cyg	57207.5212	0.0103	AG	-I	27	11)
V1061 Cyg	57225.4797	0.0021	AG	-I	31	11)
V1073 Cyg	57214.3977	0.0064	AG	-I	30	11)
V1437 Cyg	57242.5473	0.0005	FR	-I	78	11)
V1823 Cyg	57248.5088	0.0002	FR	-I	62	11)
V2021 Cyg	57208.4727	0.0028	AG	-I	34	11)
V2083 Cyg	57205.5106	0.0059	AG	-I	27	11)
V2181 Cyg	56933.3333	0.0005	RAT RCR	o	158	19)
	57219.5010	0.0002	FR	-I	58	11)
	57225.5228	0.0011	FR	-I	80	11)
V2197 Cyg	57208.4558	0.0019	AG	-I	32	11)
V2247 Cyg	57207.4775	0.0014	AG	-I	23	11)
V2278 Cyg	57215.4204	0.0003	SCI	o	30	13)
V2282 Cyg	57225.4509	0.0013	JU	o	60	13)
V2364 Cyg	57161.4249	0.0050	AG	-I	21	11)
V2477 Cyg	57176.4197	0.0006	AG	-I	30	11)
V2486 Cyg	57204.4805	0.0100	AG	-I	30	11)
V2490 Cyg	56505.4441	0.0002	RAT RCR	V	143	9)
V2517 Cyg	57206.4715	0.0054	AG	-I	34	11)
V2520 Cyg	57178.4022	0.0018	AG	-I	32	11)
V2529 Cyg	57213.4837	0.0078	AG	-I	30	11)

Table 1: cont.

Variable	HJD 24.....	±	Obs	Fil	n	Rem
V2545 Cyg	56954.3930	0.0004	RAT RCR	o	125	19)
V2549 Cyg	57178.4459	0.0010	AG	-I	28	11)
V2551 Cyg	56891.5075	0.0002	RAT RCR	V	187	9)
	56891.6288	0.0009	RAT RCR	V	187	9)
	56897.4442	0.0003	RAT RCR	V	180	9)
	56897.5655	0.0002	RAT RCR	V	180	9)
	57176.4747	0.0016	AG	-I	31	11)
V2552 Cyg	57176.4315	0.0010	AG	-I	26	11)
V2562 Cyg	57198.4988	0.0097	AG	-I	27	11)
V2619 Cyg	57198.4640	0.0202	AG	-I	28	11)
V2643 Cyg	56853.5138	0.0004	RAT RCR	V	127	9)
	57214.5269	0.0057	AG	-I	30	11)
DM Del	57225.4752	0.0033	AG	-I	33	11)
KO Del	57207.5214	0.0015	AG	-I	24	11)
MR Del	55174.3110	0.0002	RAT RCR	V	87	9)
	56175.3554	0.0001	RAT RCR	V	102	9)
	57214.5586	0.0005	AG	-I	29	11)
OZ Del	57205.4618	0.0156	AG	-I	27	11)
PY Del	57225.3871	0.0060	AG	-I	33	11)
Z Dra	57090.3899	0.0022	AG	-I	45	11)
TZ Dra	56937.3168	0.0002	RAT RCR	o	126	19)
	57214.4475	0.0013	JU	o	65	13)
XY Dra	57137.3797	0.0007	SCI	o	34	13)
AX Dra	57097.3656	0.0037	AG	-I	44	11)
BH Dra	57204.5198	0.0002	SCI	o	100	13)
EF Dra	56725.5941	0.0003	RAT RCR	V	173	9)
FX Dra	57106.4550	0.0086	AG	-I	37	11)
HP Dra	57132.5141	0.0001	SCI	o	150	13)
	57213.4146	0.0038	AG	-I	31	11)
V341 Dra	57100.3831	0.0033	AG	-I	45	11)
V347 Dra	56723.5609	0.0002	RAT RCR	V	200	9)
V357 Dra	57097.4395	0.0018	AG	-I	35	11)
V388 Dra	56727.5021	0.0003	RAT RCR	V	251	9)
V391 Dra	57161.4280	0.0004	AG	-I	25	11)
V400 Dra	56742.4868	0.0003	RAT RCR	V	194	9)
V422 Dra	57179.4652	0.0082	AG	-I	25	11)
	57199.4444	0.0176	AG	-I	29	11)
V423 Dra	57210.4969	0.0053	AG	-I	31	11)
WW Gem	57074.3946	0.0003	WTR	o	142	12)
YY Gem	56334.5087	0.0001	RAT RCR	V	200	9)
	56725.3640	0.0001	RAT RCR	V	102	9)
	56731.4705	0.0001	RAT RCR	V	212	9)
AL Gem	57070.2835	0.0010	DIE	o	28	3)
FQ Gem	57061.0682	0.0008	MS FR	V	27	6)
GW Gem	57080.3185	0.0040	AG	-I	43	11)
GX Gem	57091.4323	0.0065	AG	-I	32	11)
V410 Gem	57101.3517	0.0029	AG	-I	26	11)
RX Her	57178.4576	0.0037	AG	-I	32	11)
TT Her	57153.4547	0.0105	AG	-I	32	11)
TX Her	57161.4227	0.0008	AG	-I	25	11)
UX Her	57198.4866	0.0175	AG	-I	28	11)
	57205.4530	0.0008	JU	o	57	13)
AK Her	57158.5166	0.0041	AG	-I	41	11)
BO Her	57198.4138	0.0069	AG	-I	28	11)
CC Her	57179.4677	0.0304	AG	-I	25	11)
DH Her	57176.4277	0.0050	AG	-I	26	11)
DP Her	57123.5865	0.0002	MS FR	o	52	17)
FN Her	57178.5314	0.0017	AG	-I	30	11)
IM Her	54207.3699:	0.0200	MS FR	o	82	15)
LT Her	57179.4535	0.0014	AG	-I	25	11)
PW Her	57154.3650	0.0025	AG	-I	42	11)
V342 Her	57203.4916	0.0192	AG	-I	34	11)
V359 Her	57122.6317	0.0002	SCI	o	118	13)
V450 Her	57154.4493	0.0028	AG	-I	33	11)
	57206.4938	0.0002	SCI	o	151	13)
V687 Her	57134.5075	0.0002	MS FR	o	63	17)
	57135.4714	0.0002	SCI	o	33	13)
	57170.5107	0.0003	MS FR	V	34	16)
	57199.4480	0.0001	SCI	o	40	13)
V732 Her	57133.5262	0.0004	SCI	o	50	13)
	57158.5368	0.0001	SCI	o	46	13)

Table 1: cont.

Variable	HJD 24.....	±	Obs	Fil	n	Rem
V733 Her	57121.5735	0.0001	MS FR	o	67	17)
V829 Her	56764.5417	0.0001	RAT RCR	V	154	9)
V842 Her	57106.4474	0.0023	AG	-I	37	11)
V861 Her	57128.3754	0.0004	MS FR	o	49	17)
V899 Her	57125.4787	0.0002	SCI	o	140	13)
V1003 Her	57225.405	0.005	AG	-I	33	11)
V1021 Her	57100.4239	0.0046	AG	-I	38	11)
V1023 Her	57100.4319	0.0029	AG	-I	38	11)
	57100.5892	0.0019	AG	-I	38	11)
V1039 Her	57135.4872	0.0002	MS FR	o	62	17)
V1045 Her	57127.4132	0.0002	MS FR	o	65	17)
V1047 Her	57210.4382	0.0014	JU	o	66	13)
V1049 Her	57114.6349	0.0016	MS FR	V	16	16)
	57176.4545	0.0026	AG	-I	27	11)
V1053 Her	57131.3901	0.0001	MS FR	o	75	17)
	57136.5701	0.0007	MS FR	V	15	16)
	57158.4428	0.0001	MS FR	o	86	17)
V1055 Her	57178.4604	0.0014	JU	o	74	13)
V1057 Her	57143.8279	0.0005	MS FR	V	31	6)
V1071 Her	57136.3993	0.0002	MS FR	o	52	17)
V1073 Her	57158.4949	0.0018	AG	-I	41	11)
V1095 Her	57133.4363	0.0001	MS FR	o	46	17)
	57136.5504	0.0018	MS FR	V	18	16)
	57143.8202	0.0003	MS FR	V	31	6)
V1096 Her	57133.3970	0.0004	MS FR	o	77	17)
	57136.5356	0.0019	MS FR	V	18	16)
	57143.7767	0.0007	MS FR	V	30	6)
V1097 Her	57158.4023	0.0032	AG	-I	41	11)
V1102 Her	57114.6101	0.0018	MS FR	V	16	16)
V1119 Her	57178.5077	0.0102	AG	-I	32	11)
V1140 Her	57097.4084	0.0063	AG	-I	40	11)
	57097.5855	0.0016	AG	-I	40	11)
V1148 Her	57100.3955	0.0011	AG	-I	38	11)
	57100.5368	0.0006	AG	-I	38	11)
V1167 Her	57158.4365	0.0055	AG	-I	41	11)
V1179 Her	57178.4275	0.0020	AG	-I	30	11)
V1185 Her	57106.4459	0.0035	AG	-I	37	11)
	57106.6245	0.0021	AG	-I	37	11)
V1298 Her	57179.4683	0.0021	AG	-I	25	11)
V1321 Her	57150.4096	0.0042	AG	-I	31	11)
	57153.4954	0.0034	AG	-I	32	11)
V1355 Her	56802.5021	0.0002	RAT RCR	V	112	9)
AV Hya	57090.3630	0.0003	AG	-I	36	11)
	57091.3911	0.0021	AG	V	49	11)
DF Hya	57101.3305	0.0015	AG	-I	45	11)
	57101.4932	0.0006	AG	-I	45	11)
EU Hya	57090.4541	0.0027	AG	-I	25	11)
FG Hya	57097.3480	0.0021	AG	-I	29	11)
V409 Hya	57101.3089	0.0131	AG	-I	34	11)
V519 Hya	57101.4593	0.0015	AG	-I	34	11)
RW Lac	57220.5454	0.0026	AG	-I	31	11)
SW Lac	57205.4341	0.0007	AG	-I	26	11)
	57214.4155	0.0008	AG	-I	29	11)
UW Lac	57248.5309	0.0050	BRW	V	293	14)
VX Lac	57214.4459	0.0014	AG	-I	29	11)
VY Lac	57205.5129	0.0064	AG	-I	27	11)
AW Lac	57206.5160	0.0046	AG	-I	34	11)
CO Lac	57225.4141	0.0047	AG	-I	32	11)
CS Lac	57219.5146	0.0105	AG	-I	33	11)
DG Lac	57225.4135	0.0059	AG	-I	32	11)
ES Lac	57213.4390	0.0176	AG	-I	30	11)
V364 Lac	57214.4923	0.0072	AG	-I	29	11)
	57225.4482	0.0045	AG	-I	32	11)
Y Leo	57097.4782	0.0011	AG	-I	36	11)
RT Leo	57091.4765	0.0149	AG	-I	45	11)
UV Leo	57090.5035	0.0010	AG	-I	45	11)
UZ Leo	57090.3818	0.0057	AG	-I	45	11)
	57094.4009	0.0010	QU	V	150	14) 1)
WY Leo	57091.4675	0.0219	AG	-I	44	11)
	57101.4434	0.0001	SCI	o	37	13)
	57106.4296	0.0012	FR	-I	64	11)

Table 1: cont.

Variable	HJD 24.....	±	Obs	Fil	n	Rem
XY Leo	57080.4143	0.0015	AG	-I	50	11)
	57080.5552	0.0019	AG	-I	50	11)
XZ Leo	57080.5284	0.0011	AG	-I	48	11)
AL Leo	57080.4189	0.0010	AG	-I	55	11)
AM Leo	57100.4242	0.0006	AG	-I	43	11)
	57100.6059	0.0014	AG	-I	43	11)
AP Leo	57102.4393	0.0010	QU	V	120	14)
ET Leo	57132.4159	0.0023	JU	o	56	13)
XY LMi	57097.4966	0.0026	AG	-I	41	11)
AG LMi	57080.4915	0.0011	AG	-I	54	11)
FU Lib	57114.6075	0.0020	MS FR	V	14	16)
RY Lyn	56726.4368	0.0001	RAT RCR	V	71	9)
	57135.4120	0.0006	JU	o	68	13)
RZ Lyn	55988.3392	0.0017	SCI	o	76	13)
SW Lyn	57067.3373	0.0010	DIE	o	26	3)
	57090.5248	0.0027	AG	-I	34	11)
UU Lyn	57093.3862	0.0013	JU	o	67	13)
	57101.5835	0.0071	AG	-I	60	11)
	57134.3783	0.0017	JU	o	80	13)
DE Lyn	57136.4045	0.0014	JU	o	64	13)
DY Lyn	57090.4888	0.0035	AG	-I	34	11)
EL Lyn	57101.4090	0.0011	AG	-I	55	11)
FG Lyn	57101.4459	0.0185	AG	-I	31	11)
FN Lyn	56706.5316	0.0015	RAT RCR	V	205	9)
FO Lyn	57101.4487	0.0045	AG	-I	58	11)
FP Lyn	57101.4357	0.0041	AG	-I	59	11)
	57101.6149	0.0020	AG	-I	59	11)
FU Lyn	57101.4804	0.0021	AG	-I	60	11)
TT Lyr	57199.5345	0.0029	AG	-I	29	11)
UZ Lyr	57214.3972	0.0027	AG	-I	30	11)
AA Lyr	57258.3390	0.0030	BRW	V	97	4)
DT Lyr	57158.5615	0.0001	MS FR	o	57	17)
FL Lyr	57158.4242	0.0037	AG	-I	41	11)
HT Lyr	56797.4769	0.0035	MS FR	o	113	17)
	57122.4521	0.0003	MS FR	o	84	17)
	57144.8643	0.0003	MS FR	V	38	6)
MZ Lyr	57144.8596	0.0006	MS FR	V	38	16)
NY Lyr	57131.5341	0.0001	MS FR	o	70	17)
V563 Lyr	57170.5186	0.0029	MS FR	V	25	16)
	57179.4655	0.0064	AG	-I	25	11)
V574 Lyr	57256.4285	0.0007	JU	o	64	13)
V576 Lyr	57126.6071	0.0004	MS FR	V	25	16)
V579 Lyr	57133.4920	0.0001	MS FR	o	43	17)
	57204.4217	0.0011	JU	o	52	13)
V592 Lyr	57143.5612	0.0005	MS FR	V	33	16)
V656 Lyr	57143.5110	0.0007	MS FR	V	33	16)
VX Mon	57065.0519	0.0012	MS FR	V	38	6)
XZ Mon	57069.9899	0.0035	MS FR	V	32	6)
AN Mon	57073.3615	0.0003	WTR	o	116	12)
CF Mon	57065.0035	0.0001	MS FR	V	42	6)
MX Mon	57094.3494	0.0008	MZ	-I	63	14)
V448 Mon	57070.4028	0.0010	QU	V	85	14) 1)
	57093.3346	0.0020	QU	V	155	14) 1)
V453 Mon	57061.6683	0.0048	MS FR	V	24	6)
	57062.6921	0.0017	MS FR	V	18	6)
V494 Mon	57061.0447	0.0003	MS FR	V	38	6)
V498 Mon	57101.3213	0.0043	AG	-I	20	11)
V514 Mon	57064.1096	0.0010	MS FR	V	35	6)
V868 Mon	57101.3762	0.0007	AG	-I	23	11)
V906 Mon	57018.3740	0.0006	RAT RCR	V	91	9)
V456 Oph	57198.5113	0.0014	AG	-I	28	11)
V501 Oph	57213.5024	0.0013	AG	-I	29	11)
V508 Oph	57176.4462	0.0009	AG	-I	31	11)
V839 Oph	56781.5159	0.0001	RAT RCR	V	150	9)
	57205.4519	0.0021	AG	-I	27	11)
V2563 Oph	57220.4779	0.0023	AG	-I	31	11)
V2612 Oph	57207.3981	0.0008	AG	-I	29	11)
V2713 Oph	57178.4182	0.0018	AG	-I	32	11)
V1363 Ori	56985.3815	0.0015	RAT RCR	V	65	9)
VW Peg	57225.4559	0.0114	AG	-I	33	11)
BK Peg	57217.5066	0.0069	PGL	o	299	10)

Table 1: cont.

Variable	HJD 24.....	±	Obs	Fil	n	Rem
GP Peg	57235.4809	0.0011	AG	-I	19	11)
V365 Peg	57220.4572	0.0097	AG	-I	31	11)
V404 Peg	57225.3901	0.0040	AG	-I	33	11)
V478 Peg	57235.4127	0.0027	AG	-I	19	11)
V489 Peg	56858.4984	0.0008	RAT RCR	V	126	9)
V596 Peg	56877.4727	0.0002	RAT RCR	V	153	9)
RY Per	57263.5548	0.0100	BRW	V	152	4)
NZ Per	56935.5168	0.0004	RAT RCR	o	170	19)
b Per	57034.50	0.000	VLM	o	18	18)
RV Psc	57000.4379	0.0002	RAT RCR	V	45	9)
DV Psc	56221.3789	0.0001	RAT RCR	V	216	9)
V Sge	57219.4382	0.0033	AG	-I	31	11)
	57220.4758	0.0073	AG	-I	31	11)
SY Sge	57206.4953	0.0031	AG	-I	33	11)
CU Sge	57203.4780	0.0056	AG	-I	33	11)
GN Sge	57207.4962	0.0159	AG	-I	28	11)
V380 Sge	57210.4129	0.0100	AG	-I	31	11)
V382 Sge	57210.5140	0.0040	AG	-I	31	11)
AO Ser	57153.4472	0.0141	AG	-I	32	11)
AQ Ser	57176.4503	0.0023	AG	-I	31	11)
LX Ser	57132.3919	0.0003	NIC	V	52	5)
	57135.4023	0.0002	NIC	o	60	5)
V384 Ser	57122.3618	0.0003	FR	-I	89	11)
	57122.4959	0.0002	FR	-I	89	11)
	57133.5137	0.0001	FR	-I	83	11)
	57134.4542	0.0002	FR	-I	78	11)
	57134.5884	0.0001	FR	-I	78	11)
	57153.3994	0.0003	FR	-I	81	11)
	57153.5338	0.0004	FR	-I	81	11)
	57158.3709	0.0034	AG	-I	41	11)
	57158.5038	0.0036	AG	-I	40	11)
	57238.4509	0.0002	FR	-I	45	11)
	57241.4065	0.0002	FR	-I	37	11)
V505 Ser	57122.4934	0.0005	FR	-I	87	11)
	57133.3928	0.0007	FR	-I	62	11)
	57134.3831	0.0010	FR	-I	66	11)
	57153.4725	0.0023	FR	-I	46	11)
	57158.4245	0.0118	AG	-I	41	11)
	57238.4204	0.0006	FR	-I	53	11)
	57241.3921	0.0005	FR	-I	44	11)
Y Sex	57091.4879	0.0018	AG	V	49	11)
VY Sex	56727.3692	0.0003	RAT RCR	V	78	9)
WX Sex	57091.3290	0.0006	AG	-I	49	11)
	57091.5498	0.0048	AG	-I	49	11)
WY Sex	56712.4098	0.0002	RAT RCR	V	79	9)
EQ Tau	56963.4344	0.0005	RAT RCR	o	114	19)
GR Tau	57036.2088	0.0008	DIE	o	18	3)
V1128 Tau	56986.3574	0.0002	RAT RCR	V	92	9)
VW Tri	56987.5276	0.0005	RAT RCR	V	162	9)
BX Tri	56942.3823	0.0004	RAT RCR	-U-I	158	9)
RW UMa	57101.3978	0.0006	AG	-I	119	11)
TY UMa	57094.3920	0.0011	JU	o	73	13)
UY UMa	57120.4107	0.0013	JU	o	75	13)
	57176.4390	0.0017	JU	o	60	13)
AF UMa	57080.5151	0.0009	AG	-I	51	11)
AW UMa	57090.4059	0.0062	AG	-I	45	11)
BS UMa	56397.3861	0.0001	RAT RCR	R	115	9)
	56746.5445	0.0001	RAT RCR	o	154	9)
ES UMa	57080.4987	0.0012	AG	-I	51	11)
GT UMa	57080.6298	0.0033	AG	-I	47	11)
OT UMa	56729.5088	0.0003	RAT RCR	V	233	9)
QT UMa	56728.5957	0.0001	RAT RCR	V	228	9)
	57090.3807	0.0007	AG	-I	39	11)
V342 UMa	57091.4856	0.0019	JU	o	80	13)
V354 UMa	57097.4494	0.0049	AG	-I	35	11)
	57100.3855	0.0026	AG	-I	43	11)
	57100.5326	0.0031	AG	-I	43	11)
RU UMi	57091.3558	0.0070	AG	-I	50	11)
	57091.6179	0.0016	AG	-I	50	11)
RZ UMi	57161.4048	0.0021	AG	-I	22	11)
VW UMi	56713.5686	0.0003	RAT RCR	V	244	9)

Table 1: cont.

Variable	HJD 24.....	±	Obs	Fil	n	Rem
VY UMi	56712.5388	0.0001	RAT RCR	V	222	9)
	56712.7014	0.0001	RAT RCR	V	222	9)
	56772.4138	0.0001	RAT RCR	V	222	9)
	56772.5763	0.0001	RAT RCR	V	222	9)
ZZ UMi	56730.4542	0.0002	RAT RCR	V	225	9)
CG Vir	57178.4570	0.0007	QU	V	110	14) 1)
V355 Vir	57100.4958	0.0008	FR	-I	81	11)
Z Vul	57220.4518	0.0006	AG	-I	31	11)
RR Vul	57258.4541	0.0030	BRW	V	111	4)
RS Vul	57220.4949	0.0075	AG	-I	31	11)
AT Vul	57208.3911	0.0083	AG	-I	34	11)
AW Vul	57214.4724	0.0011	AG	-I	30	11)
BE Vul	56842.5075	0.0001	RAT RCR	V	132	9)
	57199.4823	0.0016	AG	-I	29	11)
BP Vul	57219.3820	0.0013	AG	-I	32	11)
	57220.3905	0.0018	AG	-I	31	11)
BS Vul	57199.4236	0.0070	AG	-I	28	11)
BU Vul	57213.4781	0.0017	AG	-I	31	11)
CD Vul	57199.4501	0.0020	AG	-I	28	11)
DR Vul	57210.4846	0.0039	AG	-I	31	11)
	57219.4881	0.0035	AG	-I	33	11)
	57220.4800	0.0043	AG	-I	30	11)
EV Vul	57208.5329	0.0023	AG	-I	34	11)
	57225.4824	0.0112	AG	-I	33	11)
	57225.4853	0.0010	BRW	V	367	14)
	57256.5312	0.0040	BRW	o	235	4)
	57256.5312	0.0040	BRW	o	235	4)
FR Vul	57206.4287	0.0072	AG	-I	34	11)
GP Vul	57204.4298	0.0029	AG	-I	31	11)
V491 Vul	57225.4937	0.0062	AG	-I	33	11)
V495 Vul	57210.4492	0.0030	AG	-I	31	11)
V502 Vul	56483.4173	0.0004	RAT RCR	V	139	9)
ASAS J072018-1942.8	57096.9077	0.0015	MS FR	V	71	6)
ASAS J115328+0551.6	57080.3891	0.0008	FR	-I	40	11)
	57100.4647	0.0009	FR	-I	67	11)
ASAS J165940+1510.0	57135.4875	0.0005	MS FR	o	41	17)
ASAS J214320+2215.2	57220.4955	0.0123	AG	-I	31	11)
ASAS J220226+4831.3	56534.4416	0.0023	AG	-I	40	11)
	56534.5811	0.0017	AG	-I	40	11)
	56539.3926	0.0018	AG	-I	44	11)
	56539.5244	0.0036	AG	-I	44	11)
	56568.3996	0.0117	AG	-I	38	11)
	56568.5378	0.0070	AG	-I	38	11)
	57214.3840	0.0047	AG	-I	30	11)
	57214.5160	0.0015	AG	-I	30	11)
CSS J005610.9+411701	56949.2606	0.0002	MS FR	o	48	17)
	56949.4011	0.0012	MS FR	o	48	17)
CSS J083156.6+174315	57101.4551	0.0015	FR	-I	57	11)
CSS J181349.1+384235	57122.5204	0.0007	MS FR	o	52	17)
CSS J181430.8+380754	57122.5405	0.0007	MS FR	o	50	17)
CSS J184544.8+401721	57170.5622	0.0008	MS FR	V	33	16)
FASTT 1007	57220.5294	0.0016	AG	-I	31	11)
GSC 00238-00793	57091.4448	0.0044	AG	-I	48	11)
GSC 00279-00822	57080.3600	0.0004	FR	-I	40	11)
	57100.3653	0.0004	FR	-I	101	11)
	57100.5533	0.0006	FR	-I	101	11)
GSC 00811-01992	57066.4053	0.0005	MS FR	o	104	17)
GSC 01383-01601	57101.4074	0.0003	FR	-I	104	11)
	57101.5400	0.0002	FR	-I	104	11)
GSC 01403-01508	57105.4443	0.0003	SCI	o	97	13)
	57106.4524	0.0004	SCI	o	81	13)
GSC 01934-00130	57080.5227	0.0024	AG	-I	36	11)
GSC 02671-02330	57198.4039	0.0013	AG	-I	27	11)
GSC 02695-03163	56937.4601	0.0030	FR	-I	116	11)
GSC 02888-00780	57013.4684	0.0004	MS FR	o	73	17)
	57032.3831	0.0005	MS FR	V	42	16)
GSC 03335-00288	56928.3902	0.0005	MS FR	o	60	17)
GSC 03433-00277	54206.3539	0.0024	JU	o	100	13)
	56397.4848	0.0023	JU	o	84	13)
GSC 03453-00892	57097.4796	0.0044	AG	-I	43	11)
GSC 03483-01820	57100.4687	0.0067	AG	-I	38	11)

Table 1: cont.

Variable	HJD 24.....	±	Obs	Fil	n	Rem
GSC 03547-02849	56933.5527	0.0118	AG	-I	47	11)
GSC 03948-02316	56933.2883	0.0008	FR	-I	97	11)
	56933.5168	0.0006	FR	-I	97	11)
GSC 03949-00631	56933.3806	0.0010	FR	-I	77	11)
GSC 03949-01667	56933.3034	0.0005	FR	-I	101	11)
	56933.4689	0.0008	FR	-I	101	11)
	56935.2948	0.0011	FR	-I	22	11)
GSC 03950-00707	56891.4612	0.0006	RAT RCR	V	186	9)
GSC 04254-01666	55446.6314	0.0008	RAT RCR	-I	299	9)
Linear 16562635	57170.5211	0.0009	MS FR	V	32	16)
Linear 8489525	57089.3827	0.0021	FR	-I	38	11)
NSVS 10105062	57097.2971	0.0005	FR	-I	47	11)
	57101.3628	0.0007	FR	-I	72	11)
	57101.4837	0.0004	FR	-I	72	11)
NSVS 1108888	56742.4225	0.0005	RAT RCR	V	195	9)
	56771.5726	0.0005	RAT RCR	V	154	9)
NSVS 2837573	56495.4391	0.0001	RAT RCR	V	175	9)
	56496.4851	0.0001	RAT RCR	V	179	9)
NSVS 3067305	57210.5579	0.0014	AG	-I	30	11)
NSVS 3068865	57210.4206	0.0025	AG	-I	30	11)
NSVS 4873889	57090.4617	0.0101	AG	-I	39	11)
NSVS 5777463	57213.4371	0.0060	AG	-I	30	11)
NSVS 6066802	57208.4310	0.0013	AG	-I	33	11)
NSVS 6707166	56932.4719	0.0007	MS FR	o	52	17)
	56985.2597	0.0007	MS FR	o	40	17)
NSVS 755884	56744.4900	0.0005	RAT RCR	V	230	9)
	56744.6435	0.0005	RAT RCR	V	230	9)
NSVS 777749	56737.5226	0.0006	RAT RCR	V	228	9)
NSVS 8353928	57220.4282	0.0144	AG	-I	31	11)
NSVS 8713121	57205.4022	0.0022	AG	-I	27	11)
	57214.4444	0.0040	AG	-I	30	11)
SAVS 224247+452103	57205.5158	0.0043	AG	-I	27	11)
TYC 0945-0345	57179.5197	0.0061	AG	-I	25	11)
TYC 1077-1127	57199.5379	0.0017	AG	-I	27	11)
TYC 2038-0800	57158.4829	0.0045	AG	-I	38	11)
TYC 2679-0233	56568.3928	0.0047	AG	-I	32	11)
	57207.5032	0.0076	AG	-I	29	11)
TYC 2917-0440	56654.3821	0.0058	AG	-I	52	11)
TYC 3269-0662	56940.4665	0.0251	AG	-I	47	11)
TYC 3414-0117	57101.4489	0.0105	AG	-I	31	11)
TYC 3454-1194	57097.3578	0.0032	AG	-I	43	11)
	57097.5070	0.0024	AG	-I	43	11)
	57101.3264	0.0020	AG	-I	83	11)
	57101.4697	0.0028	AG	-I	83	11)
	57101.6203	0.0084	AG	-I	83	11)
TYC 3929-1500	57179.4968	0.0030	AG	-I	25	11)
	57199.3876	0.0006	AG	-I	29	11)
TYC 4537-0765	57080.4709	0.0008	AG	-I	55	11)
T-And0-16341	56917.3690	0.0002	MS FR	o	243	17)
UCAC3 213-102451	57106.4484	0.0005	FR	-I	62	11)
UCAC3 231-242192	55830.4900	0.0013	FR	-I	80	11)
	56521.5835	0.0010	FR	-I	69	11)
UCAC3 231-243155	56928.3261	0.0005	FR	-I	36	11)
UCAC3 232-231268	54648.4686	0.0013	FR	-I	43	11)
	55791.5441	0.0019	FR	-I	33	11)
	56928.2617	0.0012	FR	-I	127	11)
UCAC3 298-137891	56933.4170	0.0020	FR	-I	104	11)
	56933.5881	0.0013	FR	-I	104	11)
VSX J200942.2+345102	57248.3584	0.0010	FR	-I	151	11)
	57248.5342	0.0004	FR	-I	151	11)
VSX J201223.3+344140	55482.3893	0.0006	FR	-I	111	11)
	55836.4467	0.0004	FR	-I	89	11)
	55874.3144	0.0008	FR	-I	142	11)
	57248.4973	0.0003	FR	-I	103	11)
VSX J220917.2+543726	57206.4093	0.0064	AG	-I	34	11)

Observers:

AG:	Agerer, F., Tiefenbach
BRW:	Braunwarth, H., Hamburg
DIE:	Dietrich, M., Radebeul
FR:	Frank, P., Velden
JU:	Jungbluth, H., Karlsruhe
KBL:	Kubala, R., Berlin
MS:	Moschner, W., Lennestadt
MZ:	Maintz, G., Bonn
NIC:	Nickel, O., Mainz
PGL:	Pagel, L., Klockenhagen
QU:	Quester, W., Esslingen
RAT:	Rätz, M., Herges-Hallenberg
RCR:	Rätz, K., Herges-Hallenberg
SCI:	Schmidt, U., Karlsruhe
VLM:	Vollmann, W., Wien AU
WTR:	Walter, F., München

Remarks:

n	number of measurements
:	uncertain
s	secondary minimum
(1)	normal minimum
(2)	mean error in this case: standard deviation

Photometers:

(3)	CCC camera ATIK 314 L+
(4)	CCC camera ATIK 383 L
(5)	CCC camera ATIK 460 exm
(6)	CCD camera FLI Proline 16803
(7)	CCD camera FLI PL6303E
(8)	CCD camera KAF-6303E
(9)	CCD camera Moravian G2-1600
(10)	CCD camera QHY8L
(11)	CCD camera Sigma 1603
(12)	CCD camera ST-6
(13)	CCD camera ST-7
(14)	CCD camera ST-7 E
(15)	CCD camera ST-9 XE
(16)	CCD camera STL-11000 M
(17)	CCD camera STXL-6303E
(18)	camera Canon EOS 450D
(19)	camera Canon EOS 600D
(20)	camera Canon EOS 1100D

Filters:

o	without filter
V	V-filter
B	B-filter
R	R-filter
Rc	R-filter Cousins
-I	IR cut-off filter
-U	U cut-off filter

References:

BAV Services for Scientists, 2013, `http://www.bav-astro.de/sfs/index.php/`
Lichtenknecker Database of the BAV, `http://www.bav-astro.de/LkDB/index.php/`

ERRATUM FOR IBVS 6152 (BAVM 239)

V2109 Her six maxima, the star name is wrong, correctly: V1209 Her

COMMISSIONS 27 AND 42 OF THE IAU
INFORMATION BULLETIN ON VARIABLE STARS

Number 6158

Konkoly Observatory
Budapest
22 January 2016

HU ISSN 0374 – 0676

106 MINIMA TIMINGS OF ECLIPSING BINARIES

KARAMPOTSIOU, E.; GAZEAS, K.; PETROPOULOU, M.; TZOUGANATOS, L.

Department of Astrophysics, Astronomy and Mechanics, National & Kapodistrian University of Athens, Zografos, Athens, Hellas; e-mail: sevi.kar@gmail.com; kgaze@phys.uoa.gr

Observatory and telescope:
T1: 0.4m, f/8 Cassegrain telescope, located at the University of Athens Observatory, at Zografos, Athens, Greece **T2**: 1.2m, f/13 Cassegrain telescope of the National Observatory of Athens, located at the Kryoneri Astronomical Station, at Korinth, Greece.

Detector:	**C1**: ST-10XME CCD camera, KAF-3200ME chip, $16' \times 11'$ and $25' \times 17'$ (using an f/6.3 focal reducer) field of view (FoV) with T1, **C2**: ST-8XMEI CCD camera, KAF-1603ME chip, $15' \times 10'$ FoV with T1, **C3**: ST-8 CCD camera, KAF-1600 chip, $15' \times 10'$ FoV with T1, **C4**: Photometrics CH250 CCD camera, SI502 chip, $2.5' \times 2.5'$ FoV with T2. All CCDs have a Peltier-type cooling system and are equipped with a set of UBVRI filters (Bessell specifications).

Method of data reduction:
Differential photometry

Method of minimum determination:
Kwee & van Woerden (1956).

Times of minima:

Star name	Time of min. HJD 2400000+	Error	Type	Filter	Rem.
HS Aqr	56527.4507	0.0006	I	BVRI	T1+C1
	56528.5181	0.0007	II	BVRI	T1+C1
	56533.4893	0.0006	II	BVRI	T1+C1
	56535.2661	0.0006	I	BVRI	T1+C1
	56537.3963	0.0003	I	BVRI	T1+C1
	56538.4605	0.0005	II	BVRI	T1+C1
	56541.3082	0.0007	II	BVRI	T1+C1
	56542.3688	0.0003	I	BVRI	T1+C1
	56543.4338	0.0005	II	BVRI	T1+C1

Times of minima:					
Star name	Time of min. HJD 2400000+	Error	Type	Filter	Rem.
HV Aqr	52534.2955	0.0006	I	BVRI	T1+C3
	52534.4824	0.0004	II	BVRI	T1+C3
	52535.4188	0.0003	I	BVRI	T1+C3
	52537.2909	0.0004	I	BVRI	T1+C3
V417 Aql	52469.37720	0.0005	I	BVRI	T2+C4
	52469.56290	0.0001	II	BVRI	T2+C4
	52470.48820	0.0005	I	BVRI	T2+C4
AH Aur	52978.4309	0.0011	I	VRI	T1+C3
	52992.5153	0.0002	II	VRI	T1+C3
	53113.3245	0.0011	I	VRI	T1+C3
VZ CVn	56437.4781	0.0002	I	BVRI	T1+C1
	56440.4260	0.0003	II	BVRI	T1+C1
	56443.3762	0.0003	I	BVRI	T1+C1
	56453.4858	0.0004	I	BVRI	T1+C1
	56459.3827	0.0001	I	BVRI	T1+C1
V387 Cyg	53138.4923	0.0001	I	BVRI	T1+C3
	53186.5372	0.0001	I	BVRI	T1+C3
	53187.4939	0.0003	II	BVRI	T1+C3
V401 Cyg	53532.3419	0.0003	I	BI	T2+C4
	53533.5079	0.0003	I	BVRI	T2+C4
	53534.3829	0.0001	II	BVRI	T2+C4
EF Dra	56564.2482	0.0006	I	BVRI	T1+C1
	56565.3049	0.0003	II	BVRI	T1+C1
	56567.4235	0.0006	II	BVRI	T1+C1
	56572.3018	0.0003	I	BVRI	T1+C1
	56576.3312	0.0003	II	BVRI	T1+C1
	56577.3884	0.0006	I	BVRI	T1+C1
WX Eri	56235.4376	0.0005	II	BVRI	T1+C1
	56242.4342	0.0001	I	BVRI	T1+C1
GSC 00104-00634	56680.4139	0.0007	I	BVRI	T1+C1
V1038 Her	53488.3777	0.0002	II	V	T1+C3
	53488.5131	0.0001	I	V	T1+C3
	53508.3588	0.0002	I	RI	T1+C3
	53508.4913	0.0002	II	RI	T1+C3
NSV 13431	52538.4061	0.0016	II	BVRI	T1+C3
	52539.2880	0.0014	II	BVRI	T1+C3
	53178.4357	0.0020	I	BVRI	T1+C3
	53196.4951	0.0013	II	BVRI	T1+C3
V839 Oph	53153.4211	0.0002	II	BVRI	T1+C3
	53154.4434	0.0001	I	BVRI	T1+C3
	53162.4190	0.0001	II	BVRI	T1+C3
	53166.5094	0.0002	II	BVRI	T1+C3
	53168.5544	0.0002	II	BVRI	T1+C3
	53193.5036	0.0001	II	BVRI	T1+C3
	53194.3217	0.0002	II	BVRI	T1+C3
V839 Oph	53194.5259	0.0002	I	BVRI	T1+C3
	53195.3435	0.0002	I	BVRI	T1+C3
	53195.5488	0.0003	II	BVRI	T1+C3

Times of minima:					
Star name	Time of min. HJD 2400000+	Error	Type	Filter	Rem.
V2357 Oph	53440.5196	0.0005	I	BVRI	T2+C4
	53441.5597	0.0006	II	BVRI	T2+C4
	53442.5965	0.0007	I	BVRI	T2+C4
ET Ori	56266.4598	0.0006	I	BVRI	T1+C1
	56305.4476	0.0005	II	BVRI	T1+C1
	56356.3224	0.0002	I	BVRI	T1+C1
	56357.2731	0.0002	I	BVRI	T1+C1
V1363 Ori	52705.2324	0.0005	I	BVRI	T1+C3
	52695.2984	0.0008	I	BVRI	T1+C3
	53433.2473	0.0010	II	BVRI	T1+C3
	53436.2638	0.0012	II	BVRI	T1+C3
	53447.2824	0.0007	I	BVRI	T1+C3
V351 Peg	53583.5548	0.0003	II	BVRI	T1+C3
	53584.4452	0.0003	I	BVRI	T1+C3
	53586.5209	0.0003	II	BVRI	T1+C3
	53590.3783	0.0004	I	BVRI	T1+C3
	53591.5649	0.0003	I	BVRI	T1+C3
IQ Per	53679.47568	0.00005	I	R	T1+C3
	53685.5207	0.0001	II	R	T1+C3
TY Pup	56714.3402	0.0003	I	BVRI	T1+C1
	56730.3147	0.0005	II	R	T1+C1
	56737.2797	0.0003	I	BVRI	T1+C1
CC Ser	52753.5651	0.0003	I	VRI	T1+C3
	52760.5331	0.0004	II	VRI	T1+C3
GW Tau	51946.2544	0.0002	I	VRI	T1+C3
USNO A2.0 1275-10788218	57155.5391	0.0022	I	VR	T1+C1
	57156.4173	0.0014	I	R	T1+C1
	57156.5635	0.0008	II	R	T1+C1
	57157.4500	0.0023	II	R	T1+C1
USNO A2.0 1275-10794124	57155.5058	0.0011	I	VR	T1+C1
	57156.5043	0.0010	II	VR	T1+C1
	57157.4992	0.0018	I	VR	T1+C1
USNO A2.0 1275-10811543	57155.4843	0.0011	I	VR	T1+C1
	57156.4800	0.0010	II	VR	T1+C1
	57157.4708	0.0011	I	VR	T1+C1
	57158.4621	0.0015	II	VR	T1+C1
	57159.4607	0.0015	I	VR	T1+C1
USNO A2.0 1275-10813091	57155.4190	0.0009	I	VR	T1+C1
	57155.5562	0.0014	II	VR	T1+C1
	57156.3996	0.0011	II	VR	T1+C1
	57156.5447	0.0009	I	VR	T1+C1
	57157.5260	0.0009	II	V	T1+C1
	57157.3925	0.0014	I	VR	T1+C1
	57158.5124	0.0011	I	VR	T1+C1
	57159.4876	0.0007	II	R	T1+C1
USNO A2.0 1275-10815489	57155.5562	0.0014	I	R	T1+C1
	57157.4441	0.0018	I	V	T1+C1

Times of minima:					
Star name	Time of min. HJD 2400000+	Error	Type	Filter	Rem.
2MASS J06260661+2755581	52978.5564	0.0011	I	VRI	T1+C3
	54203.3416	0.0002	I	R	T1+C2

Explanation of the remarks in the table:

T1, T2, C1, C2, C3 and C4 refer to the instrumentation (telescope and CCD camera) used for each case.

Remarks:

The systems GSC 00104-00634, USNO-A2.0 1275-10788218, USNO-A2.0 1275-10794124, USNO-A2.0 1275-10811543, USNO-A2.0 1275-10813091, USNO-A2.0 1275-10815489 are recently discovered eclipsing binaries, announced by Gazeas & Karampotsiou (2015) and Karampotsiou & Gazeas (2015). A large number of the above observations were performed utilizing the robotic and remotely controlled telescope at the University of Athens.

Acknowledgements:

Times of minima of contact binaries presented in this work are by-product of the *W UMa Project* (Papers I - VII) (Kreiner et al. 2003; Baran et al. 2004; Zola et al. 2004; Gazeas et al. 2005; Zola et al. 2005; Gazeas et al. 2006; Zola et al. 2010.), which aims at performing accurate photometric and spectroscopic study of eclipsing binaries of W UMa type. In addition, part of this work is a result of the *Contact Binaries Towards Merging (CoBiToM) Project*, initiated in 2012 and still undergoing at the National and Kapodistrian University of Athens since (PI: K. Gazeas).

References:

Baran A., Zola S., Rucinski S. M., Kreiner J. M., Siwak M., Drozdz M., 2004, *AcA*, **54**, 195 (Paper II)

Gazeas K., Baran A., Niarchos P., Zola S., Kreiner J.M., et al., 2005, *AcA*, **55**, 123 (Paper IV)

Gazeas K., Niarchos, P., Zola S., Kreiner J.M., Rucinski S.M., 2006, *AcA*, **56**, 127 (Paper VI)

Gazeas K., Karampotsiou E., 2015, *IBVS*, **6200**, Report No. 6

Karampotsiou E., Gazeas K., 2015, *IBVS*, **6200**, Report No. 7

Kreiner J. M., Rucinski S. M., Zola S., Niarchos P., Ogloza W., Stachowski G., Baran A., Gazeas K., Drozdz M., Zakrzewski B., Pokrzywka B., Kjurkchieva D., Marchev D., 2003, *A&A*, **412**, 465 (Paper I)

Kwee K., van Woerden H., 1956, *Bulletin of the Astronomical Institutes of the Netherlands*, **12**, 327

Zola S., Rucinski S.M., Baran A., Ogloza W., Pych W., Kreiner J.M., Stachowski G., Gazeas K., Niarchos P., Siwak M., 2004, *AcA*, **54**, 299 (Paper III)

Zola S., Kreiner, J.M., Zakrzewski B., Kjurkchieva D.P., Marchev D.V., Baran A., Rucinski S.M., Ogloza W., Siwak M., Koziel D., Drozdz M., Pokrzywka B., 2005, *AcA*, **55**, 389 (Paper V)

Zola S., Gazeas K., Kreiner J. M., Ogloza W., Siwak M., Koziel-Wierzbowska D., Winiarski M., 2010, *MNRAS*, **408**, 464 (Paper VII)

COMMISSIONS 27 AND 42 OF THE IAU
INFORMATION BULLETIN ON VARIABLE STARS

Number 6159

Konkoly Observatory
Budapest
22 January 2016

HU ISSN 0374 – 0676

VARIABLES IN THE GLOBULAR CLUSTER M12 (NGC 6218)

KINMAN, T. D.

Kitt Peak National Observatory, NOAO,[1] P.O.Box 26732, Tucson, Arizona 85726, USA,
email: kinman@noao.edu

Messier 12 (NGC 6218) is a moderately low metallicity ([Fe/H] = −1.33) globular cluster which belongs to the inner Galactic halo. Only a few variables were known in it until a recent survey by Kaluzny et al. (2015) (hereafter KAL) found 36 variables in its field. All but two of these are new and twenty are shown by their proper motions to be members of the cluster. This paper reviews the known cluster variable candidates in M12 and also five more variable sources in the cluster field that are taken from the GUVV2 catalog of *GALEX* far-ultraviolet variables (Wheatley et. al., 2008).

Two of the variables in M12 have been known for some time: one is a W Vir star with a 15-day period (Clement et al. 1988) and the other is a W Ursa Majoris star with a period of 0.2431 days (von Braun et al., 2002). Besides these, Malakhova et al. (1997) suggested that two RR Lyrae candidates are also cluster members and identified them on their finding chart as V2, (V = 14.85, $B-V$ = 0.57) and V3, (V = 15.11, $B-V$ = 0.58). Their suggestion that these stars are variables was based solely on their place in their color-magnitude diagram; they gave no photometric evidence. In the proper motion study of M12 by Zloczewski et al. (2012) (hereafter ZLO), V2 has coordinates RA = 251.°76088 Dec = −1.°90454 and is a non-member. V3 consists of two member stars (separation 1.1 arcsec) with coordinates 251.°80799,−01.°914043 (V = 15.78, $B-V$ = 0.98) and 251.809007, −01.914341 (V = 15.59, $B-V$ = 0.20); they have a combined magnitude and color of V = 14.97 and $B-V$ = 0.47. Neither object is included in KAL's list of 36 variables in the M12 field and so there is no evidence that they are variables. KAL do, however. include the EW variables found by von Braun et al. (2002) but none of the X-ray sources in the M12 field given by Lu et al. (2009) or the single *GALEX* source in M12 given by Schiavon et al. (2012).

The Second *GALEX* Ultraviolet Variability Catalog (GUVV-2) of Wheatley et al. (2008) has 5 sources (Nos. 333 to 337 inclusive) in a 1.2 degree diameter field centered on M12. These variables all lie within 5 arcmin of the cluster center given by Goldsbury et al., (2010). They occupy an area that is only 2% of the observed GUVV-2 field of M12; this makes it very likely that they are all cluster members.

Table 1 gives the data for these 5 GUVV-2 sources. The nearest ZLO stars to these sources are given in the footnotes to this table in which the distances (in arcsec) between these *GALEX* sources and ZLO stars are given in parentheses. It is surprising that if

[1]The National Optical Astronomy Observatories are operated by the Association of Universities for Research in Astronomy, Inc., under cooperative agreement with the National Science Foundation

we identify these ZLO stars with the *GALEX* variables, none of them correspond to the variables listed by KAL. Also in this case, they would have $(NUV - V)_0$ and $(B - V)_0$ colors that would not be those expected for globular cluster stars except that No 333 might possibly be a blue straggler. The lack of identifications of any of the *GALEX* variables with the stars in ZLO and KAL suggests that neither of these compilations are complete.

For example, J164714.5-020046 and J164719.0-015229 are two candidate variables that are 3.86 and 4.59 arcmin respectively from the cluster center. The first of these is 1.2 arcsec from a cluster member in ZLO with $V = 16.06$ and $(B - V) = 0.09$; it seems very likely that it is a cluster variable although it is not given by KAL. The second candidate is within 0.7 arcsec of a 17th magnitude star with a proper motion of 7 mas y^{-1} listed by Fedorov et al. (2011) but not by ZLO or KAL; its proper motion shows that it is not a cluster member. The ephemerides and light curves of these two variables were derived from data given in the CSS Survey (Drake et al. 2009).

The ephemerides of the two variables are:

Min = HJD 2453632.2877 ; $P = 4.951404$ days for J164714.5-020046, and

Min = HJD 2454004.9723 ; $P = 0.277440$ days for J164719.0-015229.

The light-curves of these two variables are given in Fig. 1.

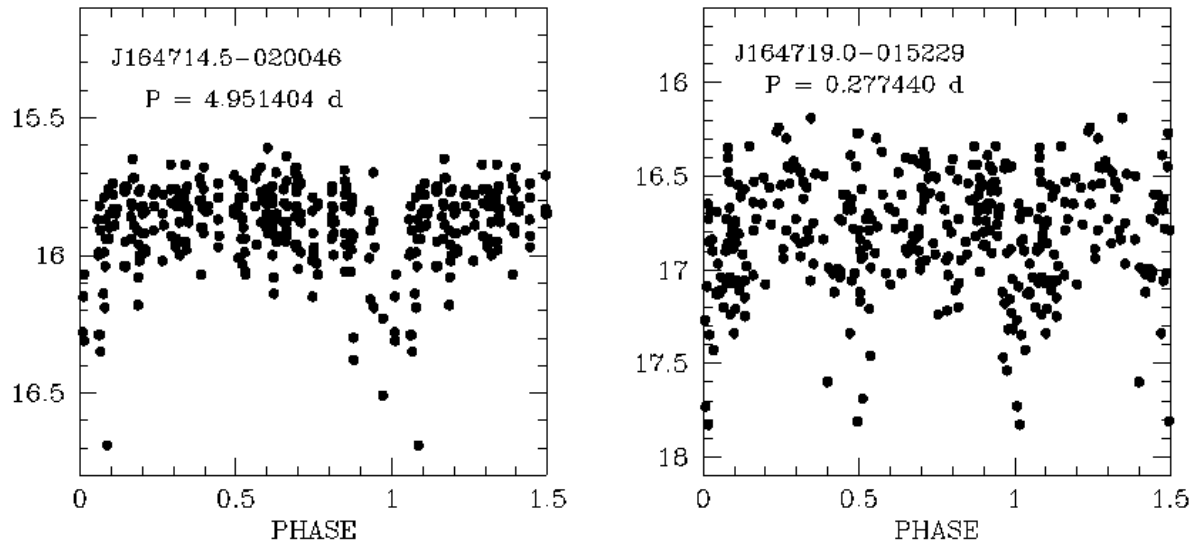

Figure 1. Light curves for variables J164714.5-020046 and J164719.0-015229.

Table 1. Data for GUVV-2 variables in M12 field.

No.	Identification	R.A. (J2000)	Dec.	NUV (mag.)	Ampl. (mag.)	$(NUV - V)_0$ (mag.)	R^a (arcmin)
333[b]	J164714.3-020035.7	251.80958	−2.00992	19.77	1.09	+1.54	3.16
334[c]	J164718.2-015603.4	251.82583	−1.93428	17.31	1.16	−1.30	1.13
335[d]	J164718.8-015221.4	251.82833	−1.87261	19.38	1.03	−1.09	4.70
336[e]	J164725.0-015505.9	251.85417	−1.91831	19.02	0.88	−1.20	3.26
337[f]	J164727.8-020040.7	251.86583	−2.01131	18.37	2.11	−0.56	5.08

[a] Radial distance in arcmin from cluster center.
[b] 251.81002, −2.00930 (2.65), $V = 18.22$, $B - V = 0.65$ (member);
[c] 251.82527, −1.93485 (2.89), $V = 19.13$, $B - V = 0.81$ (member);
[d] 251.82827, −1.87651 (14.04), $V = 20.40$, $B - V = 0.92$ (member);
[e] 251.85442, −1.91819 (1.03), $V = 20.00$, $B - V = 0.89$ (member);
[f] 251.86600, −2.01089 (1.90), $V = 19.94$, $B - V = 0.80$ (member).

Acknowledgements: The CSS survey is funded by NASA under Grant No. NNG05GF22G issued through the Science Mission Directorate Near-Earth Objects Observations Program, The CRTS survey is supported by the NSF under grants AST-0909182 and AST-1313422.

References:

Clement, C., Sawyer-Hogg, H., Yee, A., 1988, *AJ*, **96**, 1642
Drake, A. J., et. al, 2009, *ApJ*, **696**, 870
Fedorov, P., Akhmetov, V., Bobylev, V., 2011, *MNRAS*, **416**, 403
Goldsbury, R., Richer, H., Anderson, J., Dotter, A. et al., 2010, *AJ*, **140**, 1830
Kaluzny, J., Thompson, I., Narloch, W., Pych, W., Rozyczka, M., 2015, *AcA*, **65**, 267
Lu, T.-N., Kong, A., Bassa, C., Verbunt, F., Lewin, W., Anderson, S., Pooley, D., 2009, *ApJ*, **705**, 175
Malakhova, Yu., Gerashchenko, A., Kadla, Z., 1997, *IBVS*, 4434
Schiavon, R., Dalessandro, E., Sohn, S., Rood, R. et al., 2012, *AJ*, **143**, 121
von Braun, K., Mateo, M., Chiboucas, K., Athey, A., Hurley-Keller, D., 2002, *AJ*, **124**, 2067
Wheatley, J., Welsh, B., Browne, S., 2008, *AJ*, **136**, 259
Zloczewski, K., Kaluzny, J., Rozycka, M., Krzeminski, W., Mazur, B., 2012, *AcA*, **62**, 357

*This version of the paper contains corrections, and differs from the one appeared on-line originally. Date of last modification: Feb 27 2016

COMMISSIONS 27 AND 42 OF THE IAU
INFORMATION BULLETIN ON VARIABLE STARS

Number 6160

Konkoly Observatory
Budapest
11 February 2016

HU ISSN 0374 – 0676

TWO NEW BLAZHKO STARS: XZ UMi AND VX Scl

SKARKA, M.[1,2]; DOLINSKÝ, J.[3]; JURYŠEK, J.[2,4,5]; HOŇKOVÁ[2], K.; MAŠEK, M.[2,4]; LIŠKA, J.[2,3]; ZEJDA, M.[2,3]

[1] Konkoly Observatory, Research Centre for Astronomy and Earth Sciences, Hungarian Academy of Sciences, H-1121 Budapest, Konkoly Thege Miklós út 15-17, Hungary, e-mail: marek.skarka@csfk.mta.hu

[2] Variable Star and Exoplanet Section of the Czech Astronomical Society, Valašské Meziříčí, Vsetínská 78, Valašské Meziříčí, 757 01, Czech Republic

[3] Department of Theoretical Physics and Astrophysics, Masaryk University, Kotlářská 2, 611 37 Brno, Czech Republic

[4] Institute of Physics, Czech Academy of Sciences, Na Slovance 1999/2, 182 21 Praha, Czech Republic

[5] Astronomical Institute, Faculty of Mathematics and Physics, Charles University in Prague, V Holešovičkách 2, Praha 8, 180 00 Praha, Czech Republic

1 Introduction

Amplitude and phase modulation of the light curves of pulsating stars is quite common. In RR Lyrae stars pulsating in the fundamental mode almost every other star is considered to show some kind of modulation (Jurcsik et al. 2009; Benkő et al. 2010). The nature of this phenomenon, called the Blazhko effect (Blažko 1907), and its observed characteristics are still poorly understood (see e.g. Kovács 2009, 2015, and Szabó 2014). Also the reasons why some of the stars are modulated, and some not, are not clear (e.g. Skarka 2014b).

We give a brief note about a discovery of modulation in two RRab stars XZ UMi and VX Scl. The targets were observed as a part of the Czech RR Lyrae Observational Project (Skarka et al. 2013; Skarka et al. 2015). In both stars we observed scattering around maximum light which is typical of Blazhko stars. Because our data were insufficient for reliable confirmation of the Blazhko effect and determination of the modulation period, publicly available data from sky surveys archives were utilized.

2 XZ UMi

Variability of XZ UMi was firstly noted by Wils et al. (2006) in NSVS data (Wozniak et al. 2004, 148 data points, time span of one year). We observed this star in seven nights from December 2014 to April 2015 at Masaryk University Observatory (MUO), Brno, Czech Republic, with a 24inch Newtonian telescope equipped with MII G2-4000 camera. We obtained about 450 data points in Johnson-Cousins BVR_cI_c filters. For the sake of clarity we give only data for B-filter, because the modulation is most apparent in this filter. Identification of comparison stars can be found in Table 1 and in the left panel of Fig. 1.

Table 1: Cross-identification of XZ UMi and comparison stars. Coordinates and magnitudes come from the UCAC4 (APASS photometry) catalogue (Zacharias et al. 2013).

ID UCAC4	RA(2000)	DEC(2000)	V [mag]	$B-V$ [mag]
XZ UMi				
824-016693	14 39 51.623	+74 45 02.08	11.884	0.732
comp star				
824-016709	14 41 10.264	+74 36 29.03	11.772	0.895
check star				
824-016696	14 40 18.613	+74 40 37.14	12.032	1.055

From the top panel of Fig. 2 it is apparent that XZ UMi is a Blazhko star with very distinct amplitude modulation. From our measurements we estimate the pulsation period as 0.58521(2) d (we used Period04 software, Lenz & Breger 2005). This value is slightly different from the NSVS-based pulsation period (0.58506(2) d). Although both values are determined on the basis of not optimal data samples, the difference of $1.5{\cdot}10^{-4}$ d could indicate period change.

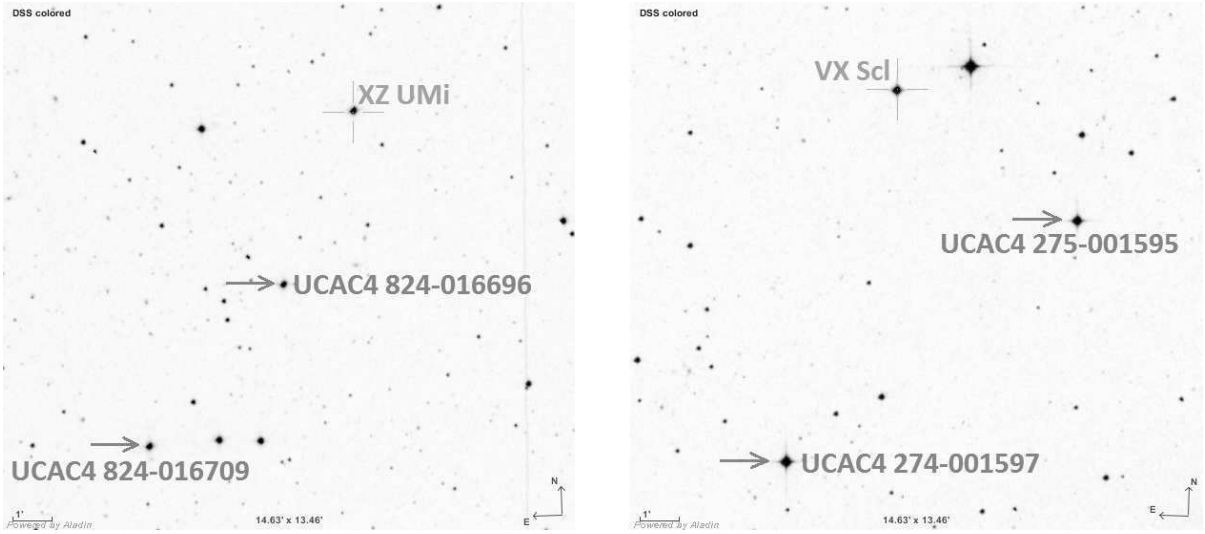

Figure 1. Identification of stars used as comparison and check stars.

Our data are insufficient for the determination of modulation period, but in the NSVS survey data a side peak just next to the basic pulsation frequency was identified after removing the only two detectable pulsation components (Fig. 3, top panel). The separation between the basic pulsation peak (in this figure highlighted by the dashed line) and the side peak is 0.0243(1) c/d. Blazhko period is then 41.1(2) d. The detected frequencies in NSVS data set are in Table 2.

3 VX Scl

This star was suspected of modulation by Skarka (2014a). We observed it in 9 nights (2014 - 2015) using FRAM (F(/Ph)otometric Robotic Atmospheric Monitor, Ebr et al.

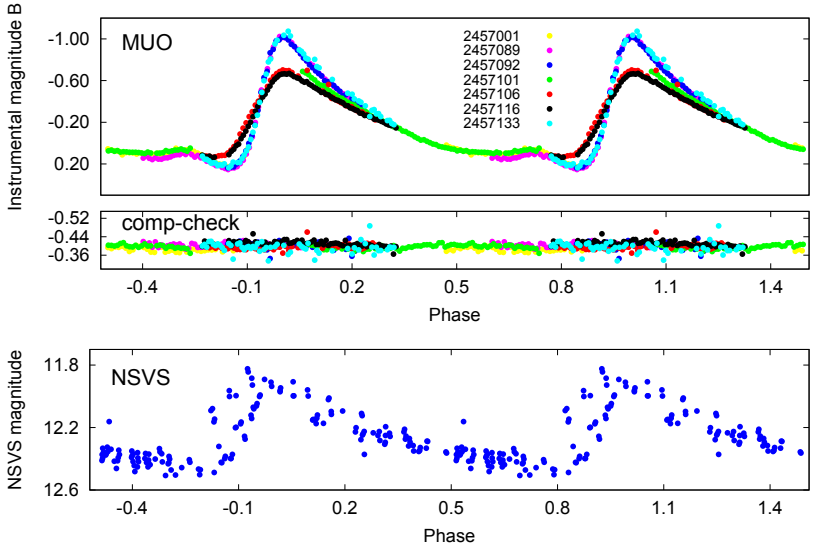

Figure 2. XZ UMi data phased with period of 0.58521(2) d and zero epoch 2457092.4632(9).

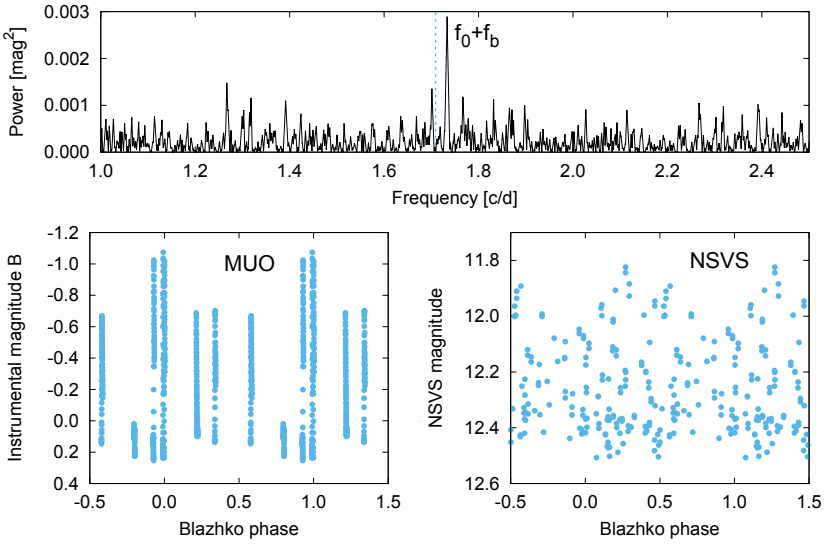

Figure 3. The top panel shows NSVS frequency spectra of XZ UMi after extraction of detectable pulsation components (f_0 and $2f_0$), while the bottom panels show the data phased with the Blazhko period. The location of the basic pulsation frequency f_0 is marked by the dashed line in the top panel.

Table 2: Frequencies detected in the NSVS data of XZ UMi.

ID	f [c/d]	A [mag]	ϕ [rad]
f_0	1.70915(5)	0.196(7)	2.06(5)
$f_0 + f_b$	1.7334(2)	0.062(7)	0.36(11)
$2f_0$	3.4185(1)	0.086(7)	4.92(2)

Table 3: VX Scl and comparison stars.

ID UCAC4	RA(2000)	DEC(2000)	V [mag]	$B-V$ [mag]
VX Scl				
275-001600	01 35 23.658	−35 07 42.57	11.928	0.311
comp star				
275-001595	01 35 01.127	−35 11 01.03	11.587	0.470
check star				
274-001597	01 35 37.542	−35 17 10.53	11.021	0.565

2014) - a 300/3000 mm Schmidt-Cassegrain telescope placed near Malargüe at the Pierre Auger Observatory, Argentina. This telescope is equipped with MII G2-1600 camera with *BVRI* filters. We obtained more than 300 data points in each of the filters, but we show only data in *V*-filter because in this filter we got the largest number of measurements around maxima.

The scatter around maximum light suggests modulation (Fig. 4). However, our data were insufficient to certainly decide about the Blazhko effect and for determination of the modulation period. Fortunately, VX Scl was observed by the SuperWASP survey in 2006 and 2007 (Pollacco et al. 2006).

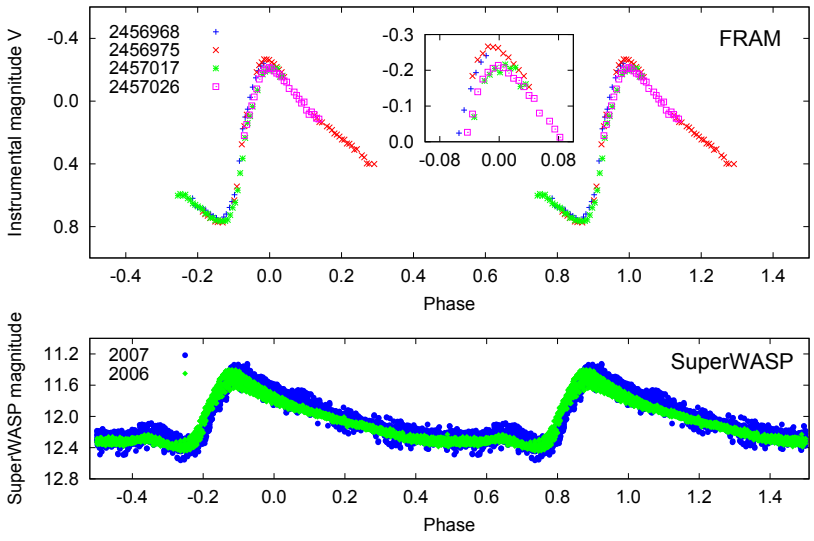

Figure 4. VX Scl data phased with the basic pulsation period of $1/f_0 = 0.637061(1)$ d and zero epoch 2456975.6521(5). Only data from four nights are shown in the top panel for better clarity.

Skarka (2014a) did not analyse SuperWASP data because they did not fulfil high demands for his analysis. We removed all data points with the uncertainty higher than 0.02 mag. Only data from camera 221 were used for frequency analysis (7712 points, time span of two years). After removing detectable pulsation components ($kf_0 = k \cdot 1.569708(2)$ c/d, where $k = \langle 1, 7 \rangle$) side peaks near f_0, $2f_0$[1] were revealed (see the top panel of Fig. 5 where the frequency spectrum around f_0 is shown). The spacing is 0.01486(4) c/d which is equivalent to modulation period of 67.3(2) d. SuperWASP data phased with the modulation period are shown in the bottom panel of Fig. 5. The modulation envelope

[1]When analysing seasons separately, in the first part of the data also $3f_0 + f_b$ was detected.

created from maximum magnitudes with amplitude of about 0.15 mag is well apparent.

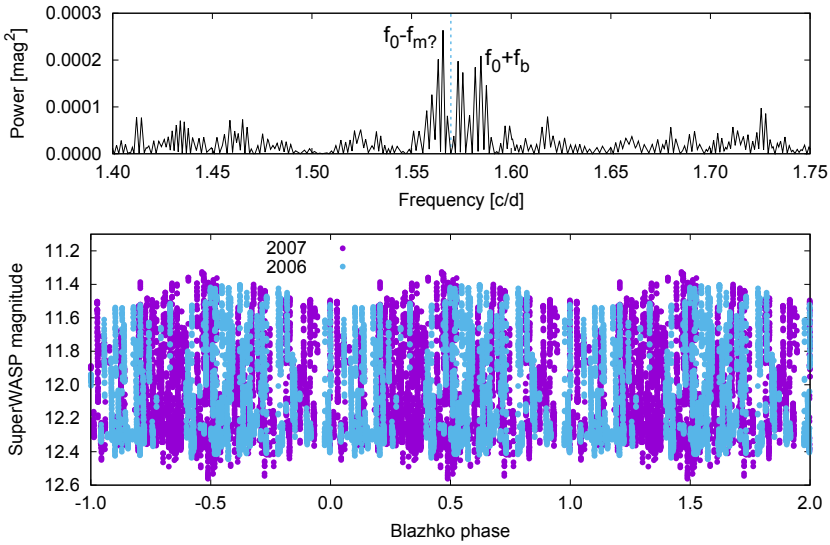

Figure 5. Frequency spectrum of VX Scl based on SuperWASP data after subtraction of seven detectable main pulsation components with position of f_0 highlighted by the dashed line (top panel). The bottom panel shows SuperWASP data phased with the modulation period of 67.3 d.

The full light-curve solution for SuperWASP data is given in Table 4. Beside these peaks, additional peaks appeared near 0.001, 4, 5, and 7 c/d when both seasons were analysed together. The peaks were not detected in the first part of the data. Therefore we suspect them from the artificial nature arising from the shifts between seasons and nights in the second part of the data (see the bottom part of Fig. 4 from where it is apparent that the data from season 2007 have significantly larger scatter than from the season 2006).

The basic pulsation period of VX Scl is probably slowly changing which could be deduced from the bottom panel of Fig. 4 where data from both seasons are shifted in phase. In addition, bunch of peaks close to f_0 supports this hypothesis. Alternatively, we cannot exclude that VX Scl could be multi-modulated Blazhko star – the closest nearly-equidistant peaks to f_0 indicate the modulation period of about 274 d[2] (peak marked as $f_0 - f_{m?}$ in Table 4). However, for more reliable analysis larger data sets would be needed, because the separation of the peaks from f_0 is only twice the Rayleigh criterion.

4 Conclusions

Presented analysis showed that RRab stars XZ UMi and VX Scl are modulated with periods of 41.1 d and 67.3 d, respectively. The attention to these targets was brought on the basis of our original measurements. The results for both stars should be considered as preliminary estimates because both targets probably show more complex behaviour. From our figures it is apparent that the pulsation period of both stars could be variable. In VX Scl we have a suspicion of either double modulation with additional Blazhko component with a period of about 274 d, or of secular period change apparent in SuperWASP data. In both targets better data sets are needed for more reliable analysis.

[2]No corresponding peaks were detectable near kf_0.

Table 4: Frequencies identified in the SuperWASP data of VX Scl.

ID	f [c/d]	A [mag]	ϕ [rad]
f_0	1.569708(2)	0.3148(11)	4.758(1)
$f_0 - f_{\rm m?}$	1.56606(3)	0.0246(10)	2.55(1)
$f_0 + f_{\rm b}$	1.58457(4)	0.0161(9)	1.56(2)
$2f_0$	3.139315(5)	0.1381(8)	6.001(1)
$2f_0 + f_{\rm b}$	3.15401(7)	0.0093(8)	1.17(2)
$3f_0$	4.709001(5)	0.1074(8)	2.412(1)
$4f_0$	6.278645(8)	0.0742(8)	3.462(2)
$5f_0$	7.84835(1)	0.0489(8)	0.674(2)
$6f_0$	9.41799(3)	0.0239(8)	1.182(7)
$7f_0$	10.98767(6)	0.0113(8)	5.57(1)

Acknowledgement: MS acknowledges the support of the postdoctoral fellowship programme of the Hungarian Academy of Sciences at the Konkoly Observatory as a host institution. This research made use of the International Variable Star Index (VSX) database, operated at AAVSO, Cambridge, Massachusetts, USA. Support of MUNI/A/1110/2014 and LH14300 is acknowledged (JL, MZ). The operation of the robotic telescope FRAM has been supported by the grants of the Ministry of Education of the Czech Republic (MSMT-CR LG13007 and LG15014) and by the grant No. 14-17501S of the Czech Science Foundation. This paper makes use of data from the DR1 of the WASP data as provided by the WASP consortium, and the computing and storage facilities at the CERIT Scientific Cloud, reg. no. CZ.1.05/3.2.00/08.0144 which is operated by Masaryk University, Czech Republic.

References:

Benkő, J. M., Kolenberg, K., Szabó, R., et al. 2010, *MNRAS*, **409**, 1585
Blažko S. 1907, *AN*, **175**, 325
Ebr, J., Janeček, P., Prouza, M., et al. 2014, *RMxAC*, **45**, 114
Jurcsik, J., Sódor, Á., Szeidl, B., et al. 2009, *MNRAS*, **400**, 1006
Kovács, G. 2009, *AIP Conf. Ser.*, **1170**, 261
Kovács, G. 2015, *arXiv:1512.05722*
Lenz, P., & Breger, M. 2005, *Communications in Asteroseismology*, **146**, 53
Pojmanski, G. 2002, *AcA*, **52**, 397
Pollacco, D. L., Skillen, I., Collier Cameron, A., et al. 2006, *PASP*, **118**, 1407
Skarka, M., Honkova, K., & Jurysek, J. 2013, *IBVS*, **6051**, 1
Skarka, M. 2014a, *A&A*, **562**, A90
Skarka, M. 2014b, *MNRAS*, **445**, 1584
Skarka, M., Liska, J., Dreveny, R., & Auer, R. F. 2015, *Open European Journal on Variable Stars*, **169**, 36
Szabó, R. 2014, *IAU Symposium*, **301**, 241
Wils, P., Lloyd, C., & Bernhard, K. 2006, *MNRAS*, **368**, 1757
Woźniak, P. R., Vestrand, W. T., Akerlof, C. W., et al. 2004, *AJ*, **127**, 2436
Zacharias, N., Finch, C. T., Girard, T. M., et al. 2013, *AJ*, **145**, 44

COMMISSIONS 27 AND 42 OF THE IAU
INFORMATION BULLETIN ON VARIABLE STARS

Number 6161

Konkoly Observatory
Budapest
8 March 2016

HU ISSN 0374 – 0676

Announcement

CONSTRAINING SOLAR/STELLAR ACTIVITY AND MAGNETICALLY-DRIVEN VARIABILITY

FABBIAN, DAMIAN[1]; SIMONIELLO, ROSARIA[2]

[1] Max-Planck-Institut für Sonnensytemforschung (MPS), 37077 Göttingen, Germany

[2] Geneva Observatory, University of Geneva, Maillettes 51, 1290, Sauverny, Switzerland

A splinter session *Constraining Solar/Stellar Activity and Magnetically-Driven Variability* will be held at the Cool Stars 19 meeting in Uppsala, Sweden, on June 7th and on June 9th, 2016.

Co-chairs: Damian Fabbian & Rosaria Simoniello, SOC members: R. Collet; S. Criscuoli; H. Korhonen; N. Krivova; K. Oláh; A. Shapiro; A. Vidotto; N. Vitas

SCIENTIFIC MOTIVATION

The richness of solar observations, for which continuous monitoring is now available at extremely high spatial resolution and throughout the electromagnetic spectrum (e.g., HINODE, SDO), is complemented by a wealth of new spectro-polarimetric observations and information at increasing spatial and temporal resolution in the new era of statistical studies based on unprecedentedly huge samples of stars observed from space-borne observatories like *Kepler* and *CoRoT*. Together with the results of advanced theoretical and computational tools and the availability of massively-parallel supercomputers, these new data are rapidly changing our view of stellar magnetic activity and variability throughout stellar evolution.

Solar-like stars are known to show chromospheric activity similar to that on the Sun, e.g. in the Ca II H and K emission indicators. Magnetic activity shows erratic, multi- or single-periodic behaviour, interrupted by long quiescent periods (grand minima). What is the origin of this broad range of variability in stellar activity and how does it relate to solar variability and activity? In solar-like stars, the cyclic activity is ascribed to a dynamo mechanism maintained through differential rotation at the tachocline. However, the tachocline moves towards increasing depths with later spectral types, disappearing around spectral-type M4. Thus, a direct comparison between the stellar activity in solar-type with lower-mass stars is essential for the understanding of the effect of stellar mass on the resulting magnetic activity through a dynamo mechanism.

This Splinter is aimed at offering a synthetic view of the recent progresses in the domain of variability of stellar magnetism from different perspectives. We invite astrophysicists to present their latest results on this topic, in particular in relation to the solar-stellar

connection and the intimate interplay between magnetic activity and variability of our Sun and cool stars.

Key questions/scientific motivation:

- How does the Sun's variability and activity compare to that of other solar-like stars?
- What do we know about magnetically-driven variability and activity in FGK-type stars of different evolutionary stages?

In particular, the different sessions will focus on:

1. Solar/stellar variability: observational properties and theory
2. Stellar magnetic fields and their impact on the surrounding environment
3. Rotation/activity relation from stellar survey and theory
4. Constraining solar/stellar dynamo theory

We kindly invite solar and stellar astrophysicists to present their latest results on this topic, in particular in relation to the solar-stellar connection and on the peculiarities and common features between magnetic activity and variability of our Sun and cool stars.

Please consider attending and contributing and save the dates to your diary.

Abstract submission deadline: Friday, April 29th, 2016

For contributed talks, you can already send your abstract through the splinter webpage: http://www.mso.anu.edu.au/∼remo/cs19/splinters/stellar-var/

For posters, please note that abstracts should be submitted during the compulsory registration to the plenary session via the CS19 website at http://www.coolstars19.com/

Further announcements about this splinter session will follow soon including confirmed invited speakers and other relevant instructions.

http://www.mso.anu.edu.au/∼remo/cs19/splinters/stellar-var/

COMMISSIONS 27 AND 42 OF THE IAU
INFORMATION BULLETIN ON VARIABLE STARS

Number 6162

Konkoly Observatory
Budapest
8 March 2016

HU ISSN 0374 – 0676

PHOTOMETRIC EVOLUTION OF THE 2016 OUTBURST OF RECURRENT NOVA LMC 1968: THE FIRST THREE WEEKS

MUNARI, U.[1]; WALTER, F. M.[2]; HAMBSCH, F.-J.[3]; FRIGO, A.[3]

[1] INAF Osservatorio Astronomico di Padova, Sede di Asiago, I-36032 Asiago (VI), Italy

[2] Dept. of Physics and Astronomy, Stony Brook University, Stony Brook, NY 11794-3800, USA

[3] ANS Collaboration, c/o Astronomical Observatory, 36012 Asiago (VI), Italy

When Nova LMC 1968 (= LMCN 1968-12a = Nova Men 1968; Sievers 1970) erupted again in 1990 (as Nova LMC 1990 N.2 = LMCN 1990-02a = LMC V1341; Liller 1990), it became the first recurrent nova known in LMC (Shore et al. 1991). Further outbursts of Nova LMC 1968 were observed in 2002 (by the ASAS-3 survey, Pojmanski 2002), and in 2010 (by the OGLE survey, Mroz et al. 2014). A fifth eruption, detected in OGLE real-time data, has just been announced by Mroz and Udalski (2016). In this paper we present and discuss our extensive B,V,$R_{\rm C}$,$I_{\rm C}$ photometry of the first three weeks of 2016 event, while further observations are in progress.

We have obtained optical photometry of the nova with the (a) SMARTS 1.3-m telescope + ANDICAM from CTIO (Chile), which data are reduced against nightly observations of all-sky standard stars (Walter et al. 2012), and with (b) a 0.4-m robotic telescope operated by ANS Collaboration in Atacama (Chile), which data are reduced against a local photometric sequence extracted from the all-sky APASS survey (Henden et al. 2012, Munari et al. 2014). Two faint field stars are located within ∼2 arcsec of the nova, a fact not appreciated in previous outbursts whose published photometry refers to the combined (non-deconvolved) light of the nova and of these two nearby field stars. The combined magnitude of the two field stars is B=18.79, V=18.26, $R_{\rm C}$=17.86, and $I_{\rm C}$=17.49. In Figure 1 we present our non-deconvolved B,V,$R_{\rm C}$,$I_{\rm C}$ photometry of the 2016 outburst (measured through a 11-arcsec aperture on both telescopes), while deconvolved SMARTS photometry (PSF-fitting) is plotted in Figure 2, and both sets of data are listed in Table 1 (available electronically only). No deconvolution is possible for SMARTS JD=2457414.65 observation because of the ∼3 arcsec seeing affecting it. ANS photometry is not deconvolved because of the focal length too short for a meaningful PSF-fitting. In both figures, the continuous line is the deconvolved OGLE $I_{\rm C}$-band photometry for the 2010 outburst, plotted for reference. A similar comparison with other outbursts and/or other wavelengths is not possible because the published photometry is very scanty, with only a few points being – at best – available per outburst.

The decline rates for the first week of the 2016 outburst are 0.57 mag day^{-1} in $R_{\rm C}$, 0.53 in $I_{\rm C}$, 0.50 in B, and 0.45 in V. The corresponding classical t_2 and t_3 decline times are 3.5 and 5.2 days in $R_{\rm C}$, 3.8 and 5.7 in $I_{\rm C}$, 4.0 and 5.9 in B, and 4.5 and 6.7 in V. The

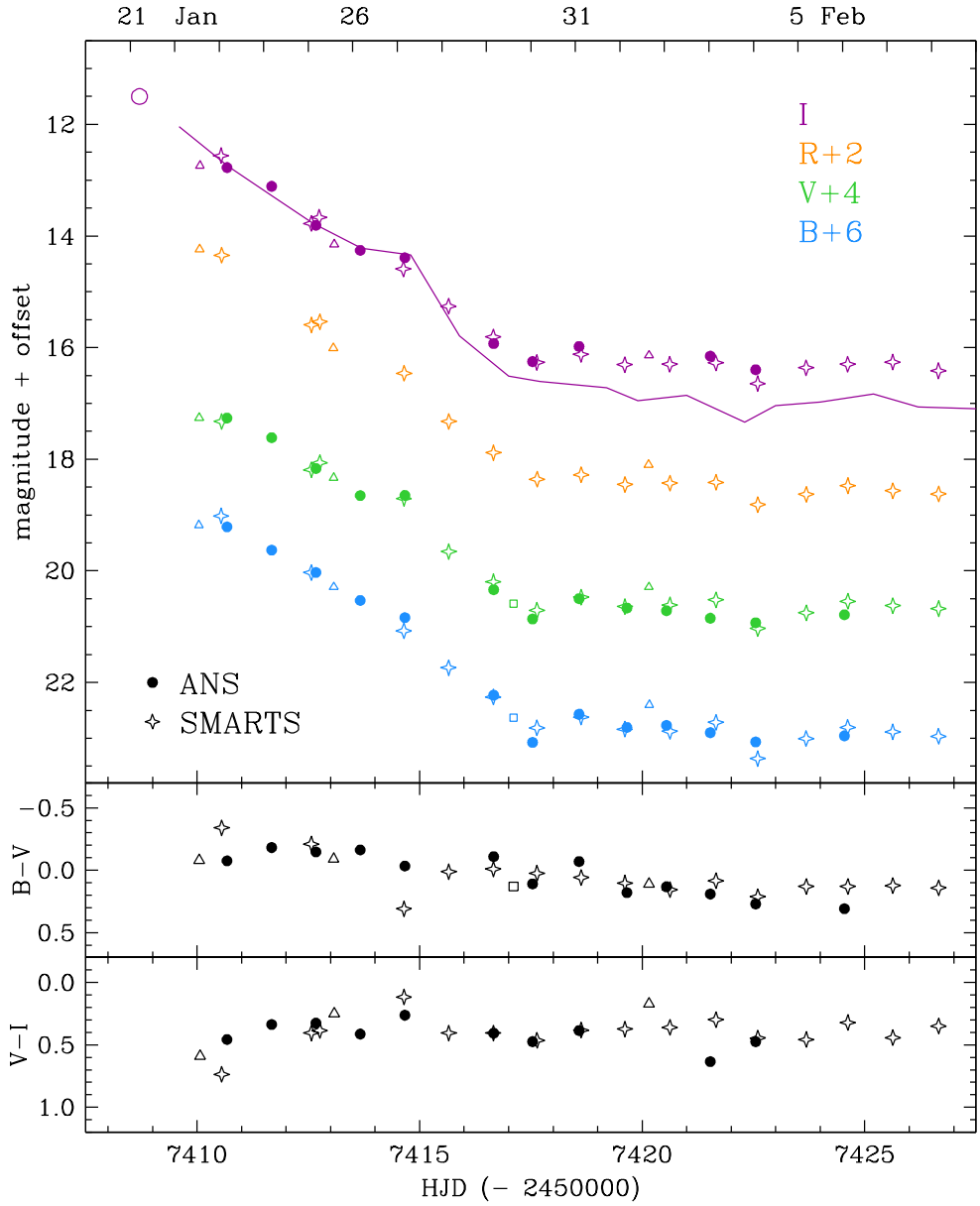

Figure 1. Non-deconvolved BVR_CI_C photometry of the 2016 outburst of Nova LMC 1968. The open circle is the I_C-band discovery observation by Mroz and Udalski (2016), and the line is the I_C-band light curve of the 2010 outburst (from Mroz et al. 2014). Triangles and squares are observations by Kaur et al. (2016) and Darnley and Williams (2016), respectively.

2016 outburst is characterized by a striking similarity to that of 2010, at least for the I_C light curve, as illustrated in Figures 1 and 2. In addition to the identical decline rates, the ∼1 day *plateau* the nova went through between 26 and 27 Jan 2016, is similarly present in the 2010 light curve, and coincides with the first appearance of super-soft X-ray emission in 2016 Swift observations of the nova (Page et al. 2016). The detection of emerging super-soft emission indicates the ejecta were turning optically thin and therefore exposed to the hard radiation field of the central white dwarf. The consequent input of ionizing photons spreading through the ejecta, counter-balanced for a short time the recombination and delayed by ∼1 day the resumption of the fast decline, which is driven by the dilution

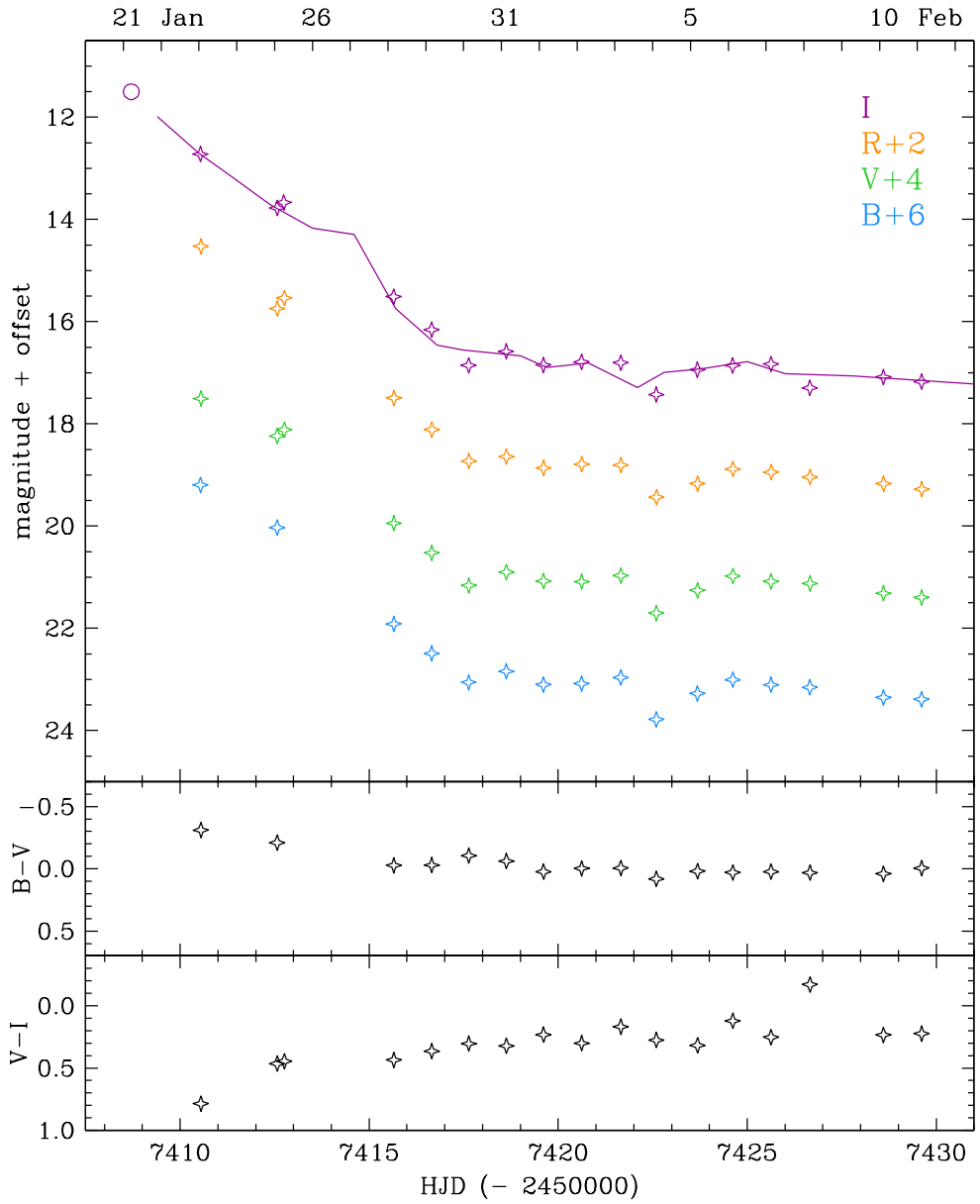

Figure 2. Deconvolved SMARTS BVR_CI_C photometry of the 2016 outburst of Nova LMC 1968. The open circle and the line have the same meaning as in Figure 1.

of the rapidly expanding ejecta. The fast decline lasted for only a few more days, until the system brightness became sustained primarily by the direct emission from the central white dwarf. This phase corresponds to the marked flattening of the light curve after January 30. As illustrated in Figure 2, the brightness of the nova during this phase is identical in the 2016 and 2010 events, signifying identical conditions for the white dwarf and the ongoing nuclear burning at its surface. Intriguing is the dent visible in all bands between February 3 and 4, similarly present in the 2010 light curve.

For the 2010 eruption, Mroz et al. (2014) report the nova being at normal $I_C \sim 19$ mag quiescent brightness on 19.2 November and at $I_C \sim 12$ mag (possibly saturated) on the next observation two days later, on 21.2 November, and estimate in $I_C \sim 11.5$ the peak magnitude supposedly reached around 20.2 November. Mroz and Udalski (2016)

quote their $I_{\rm C} = 11.5$ mag discovery observation on 21.2 January 2016 as saturated. Its position on the light curve of Figure 1 suggests however that the saturation is probaby only marginal. It is also at the same level of the peak brightness estimated by Mroz et al. (2014) for the 2010 event. Considering the identical 2010 and 2016 light curves, it seems reasonable to assume that the nova reached its maximum $I_{\rm C} \sim 11.5$ brightness on 21.2 January 2016. Adopting for LMC a 18.5 mag distance modulus and a $E_{B-V} = 0.08$ mag reddening, the corresponding absolute magnitude is $M_I = -7.15$ mag. By low order extrapolation to 21.2 January of the color evolutions depicted in Figures 1 and 2, the peak brightness attained by the nova in the other bands can be estimated as $R_{\rm C} \sim 11.3$, $B \sim 12.0$ and $V \sim 12.2$. As already noted by Sekiguchi et al. (1990) for the 1990 outburst, these magnitudes are much fainter than expected – for LMC distance and reddening – on the basis of magnitude-at-maximum/rate-of-decline (MMRD) relations, like the most recent one by Downes and Duerbeck (2000) that predicts an observed $V_{\rm peak} \sim 9$ mag.

Only small portions of the light curve were mapped during previous outbursts. Given the identical $I_{\rm C}$ light curve for 2010 and 2016 eruptions, we may assume that the light curves in other bands are similar from outburst to outburst, in particular their decline rates. The time intervals elapsed between the 2016, 2010, 2002, 1990, and 1968 events are then 1888.4, 2961.2, 4621.7, and 7728.3 days, respectively (uncertainties ± 0.6 days). Considering that (*i*) the 2010 outburst was missed altogether by the community, and it was recovered only by inspecting years later the archived OGLE data (Mroz et al. 2014), (*ii*) OGLE-IV is in operation only by a few years, and (*iii*) inter-season gaps in the OGLE monitoring of LMC last for ~ 100 days, we may conclude that several more outbursts of Nova LMC 1968 have probably gone missed. A recurrence period of ~ 955 days would decently fit both the OGLE inter-season gaps and the observed intervals between previous outbursts. If correct, this would place Nova LMC 1968 among those with the shortest known recurrence period, between M31N 2008-12a (∼1 year) and M31N 1963-09c (∼5 years; Shafter et al. 2015).

References:

Darnley, M. J., Williams, S. C. 2016, *ATel*, **8616**
Downes, R. A., Duerbeck, H. W. 2000, *AJ*, **120**, 2007
Henden, A. et al. 2012, *JAVSO*, **40**, 430
Kaur, A., et al. 2016, *ATel*, **8626**
Liller, W. 1990, *IAUC*, **4964**
Mroz, P., et al. 2014, *MNRAS*, **443**, 784
Mroz, P., Udalski, A. 2016, *ATel*, **8578**
Munari, U. et al. 2014, *AJ*, **148**, 81
Page, K. L. et al. 2016, *ATel*, **8615**
Pojmanski, G. 2002, *AcA*, **52**, 397
Sekiguchi, K., et al. 1990, *MNRAS*, **245**, 28P
Shafter, A. W. et al. 2015, *ApJS*, **216**, 34
Shore, S. N. et al. 1991, *ApJ*, **370**, 193
Sievers, J. 1970, *IBVS*, **448**
Walter, F. M., et al. 2012, *PASP*, **124**, 1057

COMMISSIONS 27 AND 42 OF THE IAU
INFORMATION BULLETIN ON VARIABLE STARS

Number 6163

Konkoly Observatory
Budapest
9 March 2016

HU ISSN 0374 – 0676

MULTIPERIODIC VARIABILITY OF THE PULSATING STAR GSC 0476-1362

GAZEAS, K.[1]; ILIOPOULOS, I.[2]

[1] Department of Astrophysics, Astronomy and Mechanics, University of Athens, GR-157 84, Zografos, Athens, Greece

[2] AKTIS Astronomical Observatory, Oreokastro GR 57013, Thessaloniki, Greece

The variability of GSC 0476-1362 was discovered by one of the authors (I. I.) on September 29, 2007, while studying a series of unfiltered 5-min exposures of the nearby 12-mag planetary nebula NGC 6781 (Gazeas & Iliopoulos 2014).

GSC 0476-1362 (TYC 476-1362-1) is located in the constellation of Aquila, and its equatorial coordinates are: RA = $19^{\rm h}17^{\rm m}27\overset{\rm s}{.}2$ and Dec = $+06°29'49.9''$ (J2000). It is listed in the GSC and TYC2 catalogue as a non-variable star with VTmag=11.48 and color index $(B-V)_{\rm Tycho}$=0.63, based on TYC2 magnitudes (Tycho photometry, not corrected for interstellar reddening). This color index corresponds to the rough value of $B-V=0.57$ in Johnson's photometric system, i.e. to a spectral type of F9, however with quite large uncertainty. 2MASS color index gives a value of $J-H=0.22$ (Cutri et al. 2003), which corresponds to a spectral type of F3-F5. The photometric light curves show a multi-periodic pulsating variable, possibly of δ *Sct* type. Being unable to find any previously recorded variability for this star, we decided to undertake photometric observations in the optical R-band between 2007 and 2009.

Photometric observations were obtained from AKTIS Astronomical Observatory (private), located in Thessaloniki, Greece. The site of the observatory is typically suburban with mediocre seeing and transparency. The first observations in 2007 were obtained with a 102 mm f/9 apochromatic refractor, while for the observations in 2008 and 2009 a 127 mm f/7.5 apochromatic refractor was used. In all cases the detector was a SBIG-ST8XME CCD camera. The 2007 configuration resulted in a 34×51 arcmin non-vignetted field of view. A 20×25 arcmin sample of the entire FOV is presented in Fig. 1, where the variable (GSC 0476-1362, $V=11.48$ mag) and main comparison (GSC 0476-1816, $V=12.39$ mag) stars are shown. In order to compensate for the small diameter of the telescope, the R filter was used in all observations, taking advantage of the higher sensitivity of the CCD camera in this spectral region. The star GSC 0476-1816 served as the comparison star (C), while several other stars in the field were used in order to check and confirm its brightness stability.

In total 369 exposures were obtained in 11 nights, during the period of October-November 2007. The early photometric analysis of the data showed quite a confusing situation of pulsating frequencies, due to ±1 c/d alias and the small number of data.

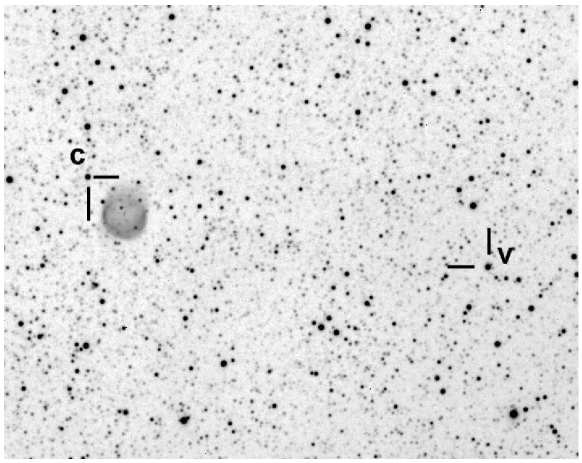

Figure 1. A cropped 20×25 arcmin sample of the original images, where variable (V) and comparison (C) stars are shown, together with the planetary nebula NGC 6781. North is up and East to the left.

Archival data from ASAS automated sky survey (Pojmański 2002) were added in our analysis without any significant improvement, since they were taken sporadically. The archival data set consists of a sum of 237 observations, which are randomly scattered along 8 years between 1998-2006, lacking any continuous time-series acquisition.

Follow up observations obtained in 2008, concluding with 530 exposures in 17 nights. This data set resulted in a stronger signal of the pulsation frequencies on the Fourier analysis and established a better determination of the pulsating behavior of GSC 0476-1362. However, signal-to-noise on the frequency spectrum was still low in the data and the multi-periodicity on top of the ±1 c/d alias was rendering the discrimination of the pulsation frequencies a complicated task. It was clear that longer duration observations were necessary in order to determine the exact pulsation frequencies of this star.

Longer time-series observations were obtained in 2009. In total, 401 exposures were obtained during 6 nights in 2009. This time the Fourier analysis gave a clear picture of the existing pulsation frequencies, as the data were better in quality and longer in duration with no interruptions. In our study, the effort to add all data together (1537 data points) and perform a combined analysis resulted in more accurate values. The complete log for all observations between 1998 and 2009 is given in Table 1.

All images were processed and analyzed with the MIRA AP package (Mirametrics, Inc. 1990-2005). The overall range of light variation is about 0.2 mag, while the amplitude of pulsation during the observing runs was of the order of 0.08 mag. The error in magnitude estimation is typically of the order of 0.02 mag in each individual night. Our observations were not transformed to a standard photometric system.

We performed the standard Fourier analysis with Period04 software package (Lenz & Breger 2005), applying a multi-frequency sine-wave fitting. The frequency search was performed on the original data, in the interval from 0 to 50 c/d, with a frequency step smaller than 10^{-3} c/d. After each successful detection, the most dominant frequency was prewhitened from the original data. The results of the frequency analysis are presented in Table 2. In this table we give the identification number of each frequency with their values, as well as the amplitude, phase shift and signal-to-noise ratio (S/N) of each one of them. Errors on these values were calculated following Breger et al. (1999) and Montgomery & O'Donoghue (1999). The errors in the table are expressed in units of

Table 1: Observational log.

Date	HJD 2450000+	Number of data points	Filter	Obs.
1998 - 2006	1286-3896	237	V	ASAS
2007-10-03	4377	29	R	AKTIS
2007-10-14	4388	26	R	AKTIS
2007-10-15	4389	29	R	AKTIS
2007-10-16	4390	52	R	AKTIS
2007-10-17	4391	49	R	AKTIS
2007-10-25	4399	18	R	AKTIS
2007-10-29	4403	43	R	AKTIS
2007-11-06	4411	26	R	AKTIS
2007-11-11	4416	40	R	AKTIS
2007-11-13	4418	28	R	AKTIS
2007-11-21	4426	29	R	AKTIS
Total in 2007	4377-4426	369	R	AKTIS
2008-10-01	4741	24	R	AKTIS
2008-10-06	4746	11	R	AKTIS
2008-10-07	4747	23	R	AKTIS
2008-10-13	4753	50	R	AKTIS
2008-10-16	4756	40	R	AKTIS
2008-10-20	4760	41	R	AKTIS
2008-10-22	4762	5	R	AKTIS
2008-10-23	4763	53	R	AKTIS
2008-10-28	4768	20	R	AKTIS
2008-11-02	4773	48	R	AKTIS
2008-11-03	4774	32	R	AKTIS
2008-11-04	4775	43	R	AKTIS
2008-11-11	4782	20	R	AKTIS
2008-11-12	4783	45	R	AKTIS
2008-11-13	4784	12	R	AKTIS
2008-11-20	4791	35	R	AKTIS
2008-11-27	4798	28	R	AKTIS
Total in 2008	4741-4798	530	R	AKTIS
2009-06-16	4999	42	R	AKTIS
2009-07-01	5014	23	R	AKTIS
2009-07-13	5026	84	R	AKTIS
2009-07-14	5027	96	R	AKTIS
2009-07-20	5033	90	R	AKTIS
2009-08-18	5062	66	R	AKTIS
Total in 2009	4999-5062	401	R	AKTIS

last decimal places quoted, given in parentheses after each value. In our analysis we adopt a significance criterion of amplitude S/N of 4.0, following Breger et al. (1993). We calculated amplitudes and phases up to a certain order, since the amplitudes of the higher order frequencies went below the significance level. We repeated the same procedure using the data sets obtained in 2007, 2008 and 2009 individually, as well as using ASAS data alone.

The significance (S/N) of the first four detected frequencies seem to remain at the same level in the data sets obtained in 2007 and 2008.

As expected, the better quality data were obtained with the larger telescope in 2008 and 2009 and therefore we trust more the results obtained from the combined analysis. Especially the long-duration time series obtained in 2009 reduced significantly the ± 1 c/d alias from the early data, resulting in accurate and definite determination of the three main pulsation frequencies with high S/N values. Searching for frequencies using all data together results in low S/N values, as the ASAS data add noise to the overall data set. Therefore, the solution from the combined data set are not presented, since they add no

Table 2: Results derived from the Fourier analysis of all the observed data.

Dataset	Frequency	f [c/d]	A [mag]	ϕ [deg]	S/N
ASAS	f_1	7.28146 (2)	0.0451 (48)	29 (6)	7.4
	f_2	7.43831 (3)	0.0312 (48)	30 (8)	5.1
	f_3	8.08597 (3)	0.0324 (48)	168 (8)	5.4
	$2f_1$	14.56291 (3)	0.0271 (48)	154 (9)	4.3
2007	f_1	7.28010 (42)	0.0330 (12)	224 (2)	16.5
	f_2	7.43723 (46)	0.0299 (12)	181 (2)	15.1
	f_3	8.08675 (42)	0.0331 (12)	79 (2)	16.2
	$2f_1$	14.56020 (52)	0.0268 (12)	195 (2)	9.7
2008	f_1	7.28058 (23)	0.0412 (9)	45 (1)	15.8
	f_2	7.43776 (34)	0.0281 (9)	243 (2)	10.8
	f_3	8.08669 (30)	0.0324 (9)	204 (1)	12.9
	$2f_1$	14.56115 (37)	0.0258 (9)	188 (2)	11.1
	$3f_1$	21.84173 (96)	0.0065 (9)	1 (8)	3.4
2009	f_1	7.28104 (15)	0.0462 (7)	354 (1)	32.0
	f_2	7.43879 (18)	0.0375 (7)	221 (1)	25.4
	f_3	8.08514 (31)	0.0220 (7)	2 (2)	13.1
	$2f_1$	14.56208 (28)	0.0242 (7)	111 (1)	9.5
	$3f_1$	21.84399 (11)	0.0056 (7)	79 (7)	4.7

The errors in all values are expressed in units of last decimal places quoted, given in parentheses after each value.

useful information.

In Figures 2-5 we present samples of the time-series of the original data, over-plotted with the predicted light curve, as calculated with the recovered frequencies, listed in Table 2.

Figure 6 presents the Fourier (amplitude) spectra of all available data, showing the dominant frequency and its harmonics (f_1, $2f_1$ and $3f_1$). Two more detected frequencies are shown in the same plots (f_2 and f_3), and the effect of a possible alias on f_3.

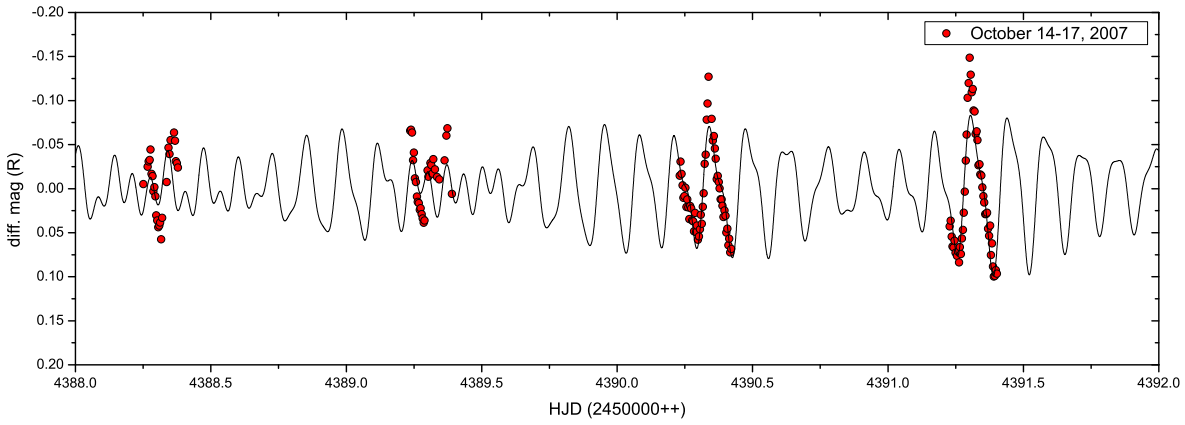

Figure 2. Observed and predicted light curve, according to the data taken on October 14-17, 2007.

The light curves of the pulsating star GSC 0476-1362 displays multi-periodic behaviour, which cannot be described by a single frequency. At least three frequencies (f_1, f_2 and f_3) seem to be real, as they are prominent with high S/N ratio, according to the results given in Table 2. The main frequency f_1 is so strong that the first and second harmonics

($2f_1$ and $3f_1$) were apparent in the Fourier spectrum. Higher order frequencies have low S/N ratio and they are subject to be either unrealistic or aliases of the main frequencies.

Following the detection criteria as established by Loumos & Deeming (1978), we find that the difference between all detected frequencies is larger than the value of $1.5/T$ (where T corresponds to the time interval in each data set). This is an extra proof or at least strong evidence that all detected frequencies are real.

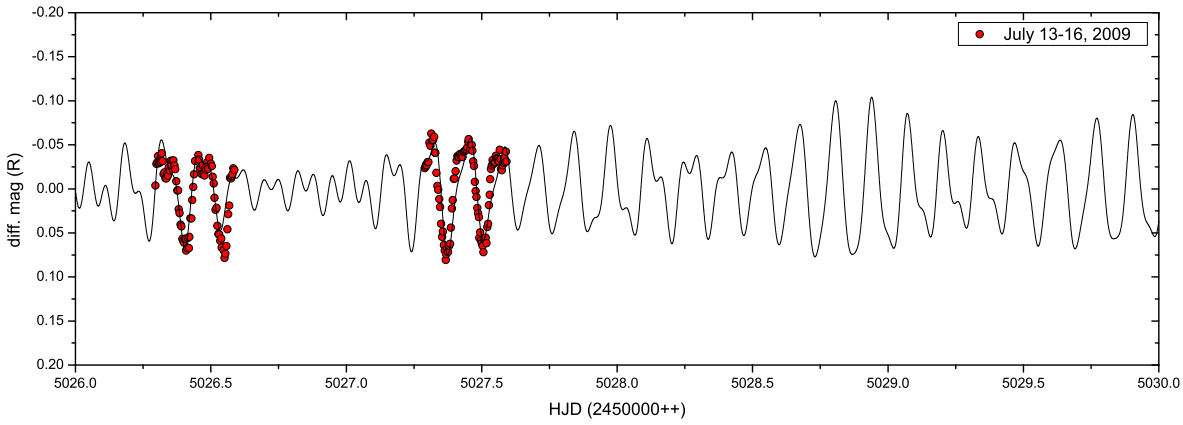

Figure 3. Observed and predicted light curve, according to the data taken on July 13-16, 2009.

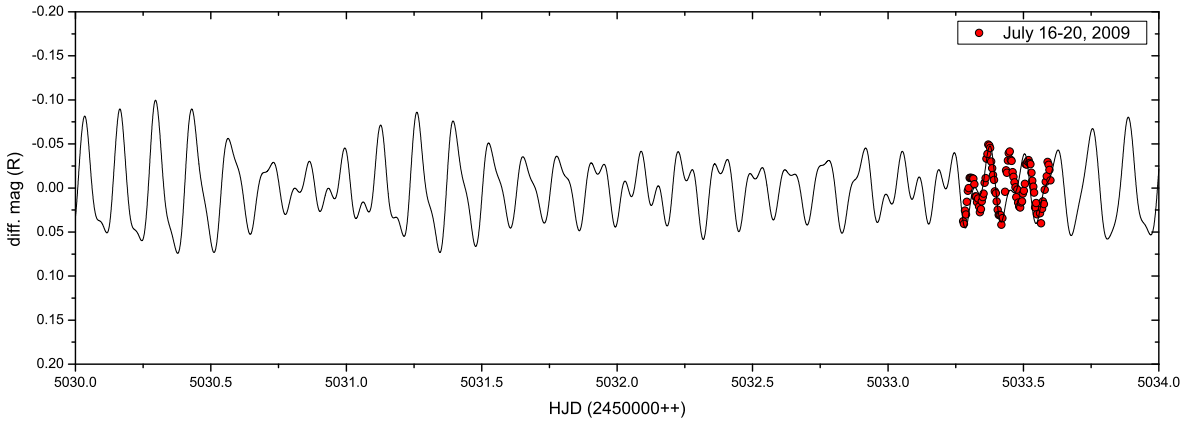

Figure 4. Observed and predicted light curve, according to the data taken on July 13-16, 2009.

Since our data sets consist of single-band photometry, we cannot conclude about the nature of the frequencies (radial or non-radial), as this information requires multi-band photometry. However, we notice that the frequency ratios which are found in this study do not follow the same pattern as the typical radial pulsators. The detected frequencies

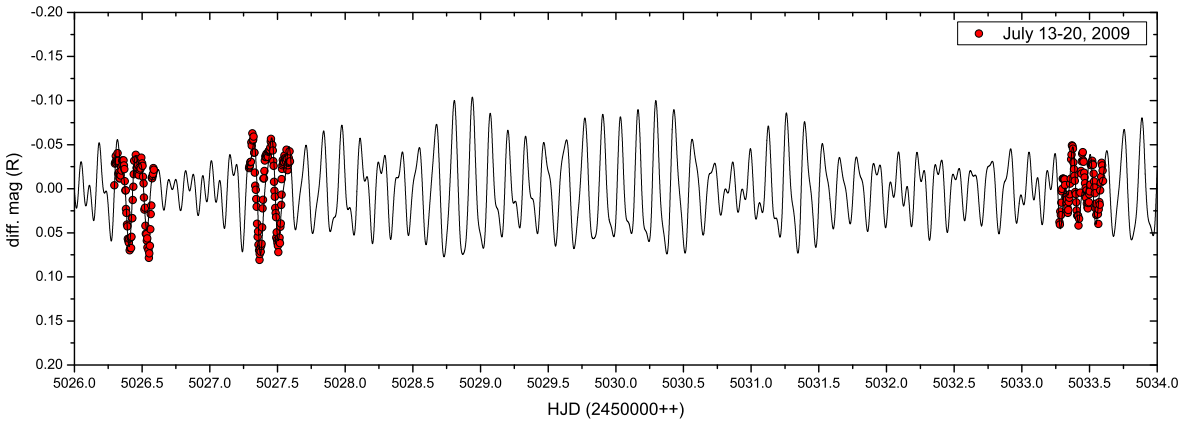

Figure 5. Observed and predicted light curve, according to the data taken on July 13-20, 2009.

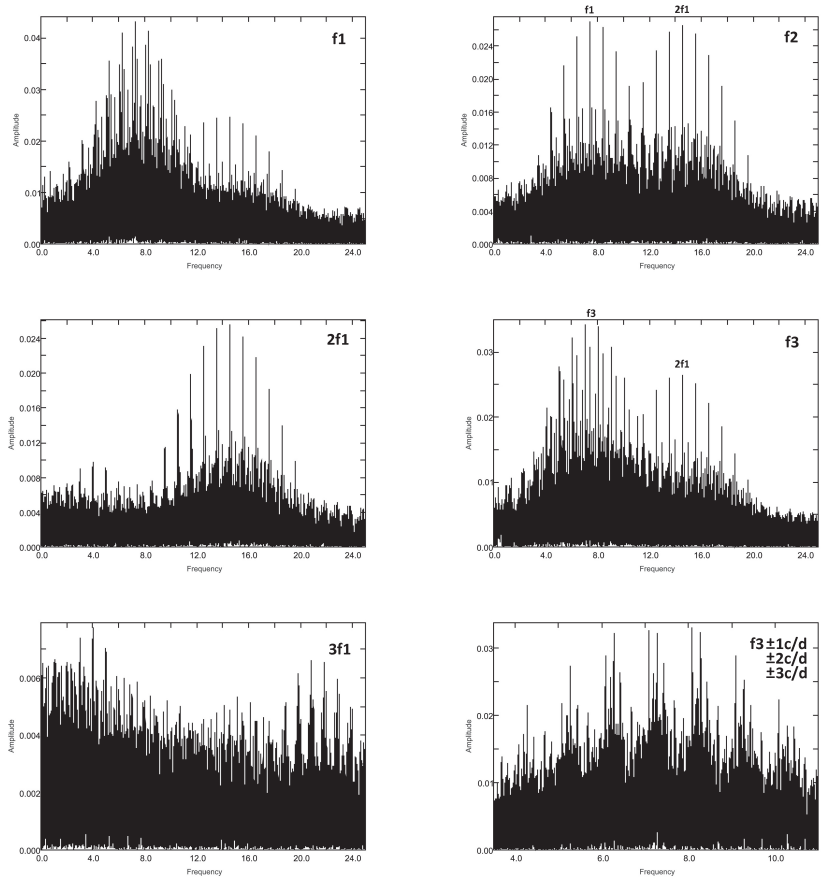

Figure 6. Fourier (amplitude) spectra of all available data, showing the dominant frequency and its harmonics, as well as two more detected frequencies and the effect of a possible alias. Units in x-axis are in cycles/day (c/d) while in y-axis are in magnitudes (mag).

give the ratios: $f_1/f_2 = 0.98$, $f_1/f_3 = 0.90$ and $f_2/f_3 = 0.92$, which are significantly higher than the value of 0.76-0.78, which is typical of radial pulsation modes (Jurcsik et al. 2006, Pigulski et al. 2006 and Poretti et al. 2005). This suggests that at least two of the detected frequencies are not radial pulsation modes. Although it is expected that high-order radial modes in multi-periodic pulsators can produce similar ratios (Breger 2000), they are usually not strong enough to be detected, as they are strongly damped in these stars.

Acknowledgements: We wish to thank Dr. K. Kolenberg and Dr. A. Liakos for the fruitful discussion during the data analysis and the layout preparation. We are also grateful to the anonymous referee for the useful comments, which helped towards the improvement of this manuscript.

References:

Breger, M., Stich, J., Garrido, R., et al. 1993, *A&A*, **271**, 482
Breger, M., Handler, G., Garrido, R., et al. 1999, *A&A*, **349**, 225
Breger, M. 2000, *ASPC*, **210**, 3
Cutri, R.M. et al. 2003, *yCat*, **2246**, 0 VizieR On-line Data Catalog: II/311
Gazeas K., Iliopoulos I., 2014, *IBVS*, **6200**, 5
Jurcsik J., Szeidl B., Váradi M., et al. 2006, *A&A*, **445**, 617
Lenz, P., Breger, M. 2005, *CoAst*, **146**, 53
Loumos, G.L. & Deeming, T.J. 1978, *ApSS*, **56**, 285
MIRA AP, *Advanced Image Processing Software for Astronomy*, Mirametrics, Inc. 1990-2005
Montgomery, M.H., O'Donoghue, D. 1999, *Delta Scuti Star Newsletter*, **13**, 28
Pigulski A., Kolaczkowski Z., Ramza T., and Narwid A., 2006, Mem. S.A.It. **77**, 223
Pojmański, G. 2002, *Acta Astr.*, **52**, 397
Poretti E., Suárez J.C., Niarchos P.G., Gazeas K., et al. 2005, *A&A*, **440**, 1097

COMMISSIONS 27 AND 42 OF THE IAU
INFORMATION BULLETIN ON VARIABLE STARS

Number 6164

Konkoly Observatory
Budapest
9 March 2016

HU ISSN 0374 – 0676

CCD MINIMA FOR SELECTED ECLIPSING BINARIES IN 2015

NELSON, ROBERT H.

1393 Garvin Street, Prince George, BC, Canada, V2M 3Z1 email: bob.nelson@shaw.ca

Observatory and telescope:
Sylvester Robotic Observatory (SyRO): 33 cm f/4.5 Newtonian on a Paramount ME

Detector:	SyRO: SBIG ST-10XME, 6.8′ pixels, 34.4″× 23.2″ FOV, $-10^\circ < T < -30^\circ$C

Method of data reduction:
Bias and dark subtraction, flat-fielding using light-box flats; aperture photometry– all using MIRA, by Mirametrics. Check stars were used throughout.

Method of minimum determination:
Digital tracing paper method, bisection of chords, curve fitting, and (occasionally) Kwee and van Woerden (1956)

Times of minima:						
Star name	Time of min. HJD 2400000+	Error	Type	Filter	$O-C$ [day]	Rem.
V0566 And	57352.6129	0.0003	EW	c	−0.0348	
G2822-1558 And	57353.6523	0.0002	EA	c	−0.0001	
RX Ari	57308.7469	0.0004	EA/DM	R	−0.0109	
AH Aur	57372.73435	0.0005	EW/DW	R	−0.0121	
V0599 Aur	57373.59485	0.0005	EW	c	−0.0170	
TY Boo	57099.7924	0.0002	EW/KW	c	−0.0037	
TZ Boo	57081.9603	0.0002	EW/KW	R	0.0020	
FI Boo	57130.7838	0.0003	EW	R	−0.0070	
KP Boo	57053.9405	0.0004	EB	R	0.0108	
QT Boo	57124.7948	0.0005	EW	c	0.0000	
AO Cam	57308.9177	0.0003	EW/KW	V	0.0019	
FN Cam	57352.9537	0.0001	EW	V	0.0012	
V0335 Cam	57315.77	0.01	EA	c	−0.0003	
V0403 Cam	57352.7429	0.0003	EW	c	0.0252	
CW Cas	57351.6131	0.0002	EW/KW	R	−0.0008	
V0608 Cas	57254.9347	0.0001	E	c	−0.0011	
V1063 Cas	57355.682	0.003	EW	c	0.0799	
V1160 Cas	57256.8831	0.0002	EA	c	−0.0008	
V0737 Cep	57182.8999	0.0001	EW	c	−0.0017	
V0814 Cep	57144.8828	0.001	na	c	−0.0307	
V0849 Cep	57334.6034	0.0002	EA	c	0.0018	
V0959 Cep	57310.6359	0.0006	EW/DW	c	−0.0255	
TX Cnc	57350.9761	0.0001	EW/KW	R	−0.0018	
EH Cnc	57353.846	0.002	EW	c	−0.0010	
IT Cnc	57071.7262	0.0003	EW	c	−0.0030	
G1936-0040 Cnc	57372.87253	0.0005	ESD-EC	c	0.0026	
RW Com	57096.8470	0.0003	EW/KW	R	0.0003	
CC Com	57071.8296	0.0001	EW/KW	c	−0.0013	
LR Com	57084.8813	0.0003	EA	c	0.0054	
YY CrB	57074.9458	0.0001	EW	V	0.0056	
AS CrB	57097.8485	0.0003	EW	c	0.0090	
BO CVn	57105.7589	0.0002	EW	R	−0.0013	
DL CVn	57121.7205	0.0002	EB	c	0.0005	
DX CVn	57053.8386	0.0004	EW?	R	−0.0123	
FQ CVn	57372.97511	0.0007	EW?	c	−0.0147	
FV CVn	57119.8307	0.0002	EW?	c	−0.0014	
GM CVn	57352.0223	0.0004	EW	c	0.0008	
G2530-1069 CVn	57346.9728	0.0003	EW	c	0.0003	
G2530-1069 CVn	57119.7279	0.0002	EW	c	0.0018	
V0628 Cyg	57164.886	0.002	EW	c	0.0015	
V1034 Cyg	57213.8702	0.0005	EB/SD:	I	−0.0021	
V1191 Cyg	57170.8519	0.0005	EW/KW	c	−0.0001	
V2477 Cyg	57153.8529	0.0002	EW	VRI	0.0003	
V2477 Cyg	57152.9192	0.0001	EW	VRI	0.0003	
V2477 Cyg	57150.8966	0.0003	EW	VRI	0.0012	
V2477 Cyg	57145.9165	0.0001	EW	R	0.0021	
V2517 Cyg	57118.9692	0.0002	EA	R	0.0048	

Times of minima:						
Star name	Time of min. HJD 2400000+	Error	Type	Filter	$O-C$ [day]	Rem.
Z Dra	57068.6705	0.0002	EA/SD	VRI	0.0018	
BL Dra	57179.8114	0.0004	EW	c	0.0000	
BW Dra	57120.7280	0.002	EW/KW	V	−0.0375	
EF Dra	57159.8118	0.0003	EW	R	0.0116	
V0341 Dra	57121.8405	0.0002	EA	R	−0.0007	
V0402 Dra	57141.949	0.002	EW	R	0.0000	
G3897-1017 Dra	57151.7917	0.0003	EW	c	0.0036	
G3913-0160 Dra	57135.9436	0.0002	E	c	0.0000	
G3929-1500 Dra	57158.7691	0.0003	EW	c	−0.0404	
G4421-0400 Dra	57150.7630	0.0002	EW	c	−0.0081	
G4448-1301 Dra	57154.8071	0.0002	EW	c	−0.0004	
V0402 Gem	57365.7279	0.0004	EW	c	0.0073	
G1886-1869 Gem	57344.8993	0.0002	EC	c	0.0059	
IT Her	57154.9044	0.0003	E	c	−0.0032	
V0728 Her	57130.9124	0.0003	EW/KW	c	−0.0012	
V0829 Her	57131.8304	0.0003	EW/KW	c	0.0019	
V0857 Her	57075.9632	0.0005	EW	c	0.0000	
V0921 Her	57119.9522	0.0002	EB	R	0.0139	
V1023 Her	57122.822	0.002	EW	c	−0.0023	
V1047 Her	57118.8694	0.0002	EW	c	0.0008	
V1067 Her	57122.9473	0.0003	EW	c	0.0114	
V1101 Her	57183.8328	0.0001	EW	c	0.0003	
V1103 Her	57097.9779	0.0003	EW	c	0.0112	
V1104 Her	57157.7794	0.0002	EW	c	−0.0038	
V1175 Her	57120.8844	0.0004	EW	c	0.0204	
V1197 Her	57156.7867	0.0002	EW	c	0.0005	
V1261 Her	57147.8060	0.0003	EW?	c	−0.0091	
G2093-1834 Her	57169.7898	0.0003	EB	c	0.0000	
UV Leo	57078.8006	0.0001	EA/DW	V	−0.0002	
CE Leo	57101.7420	0.0002	EW/KW	c	0.0118	
G1965-0735 Leo	57084.6568	0.0002	EB	R	−0.0057	
XX LMi	57081.6606	0.0003	EW	c	−0.0066	
V0653 Lyr	57144.806	0.0003	EW	c	0.0026	
V2790 Ori	57346.8874	0.0002	EW/KW	c	0.0073	
BN Peg	57224.7770	0.0005	EA	VRI	−0.0032	
BN Peg	57254.7348	0.0003	EA	VRI	−0.0039	
KR Per	57354.789	0.002	EB/KE	c	−0.0053	
KW Per	57286.7954	0.0003	EB/SD	c	−0.0007	
V0432 Per	57310.754	0.001	EW/DW	VRI	0.0011	
CP Psc	57354.615	0.001	EB:	R	0.0036	
GW Psc	57332.7228	0.0002	EW	c	0.0115	
HL Psc	57365.5982	0.0002	EB/RS	c	0.0017	
HN Psc	57258.8694	0.0007	EW	c	−0.0422	
HO Psc	57320.7440	0.0002	EW	c	−0.0005	
AU Ser	57084.9700	0.0001	EW/KW	c	0.0026	
AU Ser	57135.7953	0.0003	EW/KW:	c	0.0031	
EQ Tau	57326.800	0.001	EW/DW	c	0.0013	

Times of minima:

Star name	Time of min. HJD 2400000+	Error	Type	Filter	$O-C$ [day]	Rem.
V1241 Tau	57351.7894	0.0002	EA/SD	VRI	−0.0054	
G1804-0539 Tau	57346.7745	0.0002	E	c	−0.0037	
UX UMa	57081.8536	0.0002	EA/WD	c	0.0011	
ES UMa	57097.6854	0.0001	EW	R	0.0004	
HH UMa	57344.996	0.002	EW?	c	0.0028	
NU UMa	57079.794	0.003	EA	V	−0.0024	
OQ UMa	57078.8912	0.0002	EW	c	−0.0054	
G3807-0759 UMa	57089.7522	0.0002	EW+EA	R	0.0133	
WW UMi	57080.8015	0.0004	EB	c	0.0164	
G0289-0144 Vir	57131.7373	0.0005	EW	c	0.0000	

Remarks:

To save space, GSC star names have been shortened to a leading "G" only; times of minimum are heliocentric Julian dates with the leading 24 removed.
$O-C$ values were computed using elements computed from the $O-C$ database listed in the references (Nelson, 2015).

Acknowledgements:

Thanks are due to Environment Canada for the website satellite views (see reference below) that were essential in predicting clear times for observing runs in this cloudy locale. Thanks are also due to Attilla Danko for his Clear Sky Charts, (see below). This research has made use of the SIMBAD database, operated at CDS, Strasbourg, France

References:

Danko, A., Clear Sky Charts, `http://cleardarksky.com/`
Kwee, K.K., van Woerden, H., 1956, B.A.N. 12, (464), 327
Nelson, R.H., 2015, O-C Files, `http://www.aavso.org/bob-nelsons-o-c-files`
Satellite Images for North America, `http://weather.gc.ca/`

COMMISSIONS 27 AND 42 OF THE IAU
INFORMATION BULLETIN ON VARIABLE STARS

Number 6165

Konkoly Observatory
Budapest
10 April 2016

HU ISSN 0374 – 0676

107 MINIMA TIMINGS OF ECLIPSING BINARIES

TZOUGANATOS, L.; GAZEAS, K.; KARAMPOTSIOU, E.; PETROPOULOU, M.

Department of Astrophysics, Astronomy and Mechanics, National & Kapodistrian University of Athens, Zografos, Athens, Hellas; e-mail: tzouganatosle@gmail.com; kgaze@phys.uoa.gr

Observatory and telescope:
T1: 0.4m, f/8 Cassegrain telescope, located at the University of Athens Observatory, at Zografos, Athens, Greece **T2**: 1.2m, f/13 Cassegrain telescope of the National Observatory of Athens, located at the Kryoneri Astronomical Station, at Korinth, Greece.

Detector:	**C1**: ST-10XME CCD camera, KAF-3200ME chip, $16' \times 11'$ and $25' \times 17'$ (using an f/6.3 focal reducer) field of view (FoV) with T1, **C2**: ST-8XMEI CCD camera, KAF-1603ME chip, $15' \times 10'$ FoV with T1, **C3**: ST-8 CCD camera, KAF-1600 chip, $15' \times 10'$ FoV with T1, **C4**: Photometrics CH250 CCD camera, SI502 chip, $2.5' \times 2.5'$ FoV with T2. All CCDs have a Peltier-type cooling system and are equipped with a set of UBVRI filters (Bessell specifications).

Method of data reduction:
Differential photometry

Method of minimum determination:
Kwee & van Woerden (1956).

Times of minima:

Star name	Time of min. HJD 2400000+	Error	Type	Filter	Rem.
V395 And	56437.4754	0.0002	I	$BVRI$	T1+C1
	56440.4240	0.0003	II	$BVRI$	T1+C1
	56443.3740	0.0003	I	$BVRI$	T1+C1
	56453.4839	0.0004	I	$BVRI$	T1+C1
	56459.3817	0.0001	I	$BVRI$	T1+C1
XZ Aql	56486.4291	0.0001	I	$BVRI$	T1+C1
	56487.4987	0.0010	II	$BVRI$	T1+C1

Times of minima:					
Star name	Time of min. HJD 2400000+	Error	Type	Filter	Rem.
XZ Aql	2456516.3781	0.0001	I	$BVRI$	T1+C1
	2456517.4474	0.0010	II	$BVRI$	T1+C1
	2456531.3526	0.0002	I	$BVRI$	T1+C1
	2456532.4234	0.0010	II	$BVRI$	T1+C1
AR Aur	2452993.4143	0.0003	I	VRI	T1+C3
	2453301.4461	0.0004	II	R	T1+C3
V402 Aur	2452654.4595	0.0016	I	$BVRI$	T1+C3
	2452655.3588	0.0016	II	$BVRI$	T1+C3
	2452668.3348	0.0008	I	$BVRI$	T1+C3
V410 Aur	2452992.3830	0.0003	I	VRI	T1+C3
	2453331.2675	0.0004	I	VRI	T1+C3
	2453331.4466	0.0006	II	VRI	T1+C3
	2453331.6339	0.0003	I	VRI	T1+C3
	2453332.3659	0.0001	I	RI	T1+C3
	2453332.5468	0.0001	II	RI	T1+C3
	2453336.3962	0.0001	I	V	T1+C3
	2453351.2296	0.0003	II	V	T1+C3
	2453351.4160	0.0001	I	V	T1+C3
	2453351.5962	0.0002	II	V	T1+C3
	2453352.3293	0.0007	II	B	T1+C3
	2453352.5148	0.0004	I	B	T1+C3
	2453353.2480	0.0008	I	B	T1+C3
	2453353.4301	0.0006	II	B	T1+C3
	2453353.6148	0.0004	I	B	T1+C3
	2453375.2274	0.0007	I	V	T1+C3
CK Boo	2453218.3282	0.0006	II	VRI	T1+C3
	2453221.3431	0.0012	I	VRI	T1+C3
	2453231.2888	0.0005	I	$BVRI$	T1+C3
	2453421.6473	0.0003	I	$BVRI$	T1+C3
	2453422.5394	0.0006	II	$BVRI$	T1+C3
	2453423.6042	0.0004	II	$BVRI$	T1+C3
	2453425.5546	0.0003	I	$BVRI$	T1+C3
XY Boo	2456666.6369	0.0002	II	$BVRI$	T1+C1
	2456679.6067	0.0002	II	$BVRI$	T1+C1
	2456680.5324	0.0003	I	$BVRI$	T1+C1
	2456687.5726	0.0003	I	$BVRI$	T1+C1
	2456699.6181	0.0002	II	$BVRI$	T1+C1
	2456701.6554	0.0004	I	$BVRI$	T1+C1
	2456707.5837	0.0004	I	$BVRI$	T1+C1
V445 Cep	2456578.4395	0.0003	II	$BVRI$	T1+C1
	2456579.3631	0.0002	II	$BVRI$	T1+C1
	2456580.2681	0.0002	II	$BVRI$	T1+C1
	2456580.4463	0.0002	I	$BVRI$	T1+C1
	2456581.3574	0.0002	I	$BVRI$	T1+C1
	2456584.3062	0.0002	II	$BVRI$	T1+C2
TZ Dra	2452424.4357	0.0002	I	I	T1+C3
	2452446.5163	0.0009	II	I	T1+C3

Times of minima:					
Star name	Time of min. HJD 2400000+	Error	Type	Filter	Rem.
GSC 4778-0001	2451880.4857	0.0003	II	V	T1+C3
	2451896.4618	0.0007	II	V	T1+C3
	2452639.4307	0.0003	II	V	T1+C3
	2452671.3862	0.0004	II	V	T1+C3
	2452697.3500	0.0004	I	V	T1+C3
	2453342.4534	0.0013	II	V	T1+C3
	2453376.4057	0.0003	I	V	T1+C3
	2453382.3983	0.0004	II	V	T1+C3
TX Her	2453858.51923	0.00004	I	VI	T1+C3
	2453859.54918	0.00006	II	VI	T1+C3
V899 Her	2456733.5874	0.0003	I	$BVRI$	T1+C1
	2456734.6402	0.0003	II	$BVRI$	T1+C1
	2456735.4849	0.0004	II	VRI	T1+C1
	2456736.5362	0.0002	I	$BVRI$	T1+C1
	2456737.5899	0.0003	II	$BVRI$	T1+C1
	2456738.6364	0.0003	I	$BVRI$	T1+C1
	2456756.5390	0.0003	II	$BVRI$	T1+C1
	2456758.4336	0.0003	I	$BVRI$	T1+C1
	2456766.4414	0.0003	I	$BVRI$	T1+C1
AQ Psc	2452968.3678	0.0003	I	$BVRI$	T2+C4
DZ Psc	2452170.3860	0.0002	II	R	T1+C3
	2452177.3437	0.0002	II	R	T1+C3
	2452177.5259	0.0002	I	R	T1+C3
	2452178.4413	0.0003	II	V	T1+C3
	2452186.3132	0.0002	I	B	T1+C3
	2452186.4972	0.0005	II	B	T1+C3
	2452187.4107	0.0003	I	I	T1+C3
	2452188.3258	0.0004	II	V	T1+C3
	2452192.3538	0.0004	II	V	T1+C3
	2452192.5358	0.0003	I	V	T1+C3
	2452193.4528	0.0003	II	I	T1+C3
	2452206.2672	0.0002	II	R	T1+C3
	2452206.4486	0.0003	I	R	T1+C3
VY Sex	2453499.3807	0.0006	II	$BVRI$	T1+C3
	2453500.2668	0.0005	II	$BVRI$	T1+C3
YY Sgr	2452839.3849	0.0002	I	V	T1+C3
V505 Sgr	2452837.6016	0.0029	I	$BVRI$	T1+C3
	2452843.3891	0.0029	I	VRI	T1+C3
	2453263.3029	0.0001	I	R	T1+C3
HH UMa	2456674.5499	0.0003	I	$BVRI$	T1+C1
	2456668.5399	0.0006	I	$BVRI$	T1+C1
	2456657.4628	0.0006	II	$BVRI$	T1+C1
	2456657.6496	0.0005	I	$BVRI$	T1+C1
	2456678.4854	0.0007	II	$BVRI$	T1+C1
	2456665.5334	0.0006	I	$BVRI$	T1+C1
	2456667.6007	0.0014	II	VRI	T1+C1
	2456403.4410	0.0014	I	$BVRI$	T1+C1

Times of minima:					
Star name	Time of min. HJD 2400000+	Error	Type	Filter	Rem.
HH UMa	2456655.5860	0.0017	II	$BVRI$	T1+C1
	2456667.4126	0.0005	I	VRI	T1+C1
	2456678.6809	0.0007	I	$BVRI$	T1+C1
MS Vir	2452723.5689	0.0005	II	$BVRI$	T1+C3
	2452726.5359	0.0004	I	$BVRI$	T1+C3
	2452765.4372	0.0014	II	$BVRI$	T1+C3

Explanation of the remarks in the table:

T1, T2, C1, C2, C3 and C4 refer to the instrumentation (telescope and CCD camera) used for each case.

Remarks:

A large number of the above observations were performed utilizing the robotic and remotely controlled telescope at the University of Athens.

Acknowledgements:

Times of minima of contact binaries presented in this work are by-product of the *W UMa Project* (Papers I - VII) (Kreiner et al. 2003; Baran et al. 2004; Zola et al. 2004; Gazeas et al. 2005; Zola et al. 2005; Gazeas et al. 2006; Zola et al. 2010.), which aims at performing accurate photometric and spectroscopic study of eclipsing binaries of W UMa type. In addition, part of this work is a result of the *Contact Binaries Towards Merging (CoBiToM) Project*, initiated in 2012 and still undergoing at the National and Kapodistrian University of Athens (PI: K.Gazeas).

References:

Baran A., Zola S., Rucinski S. M., Kreiner J. M., Siwak M., Drozdz M., 2004, *AcA*, **54**, 195 (Paper II)

Gazeas K., Baran A., Niarchos P., Zola S., Kreiner J.M., et al., 2005, *AcA*, **55**, 123 (Paper IV)

Gazeas K., Niarchos P., Zola S., Kreiner J.M., Rucinski S.M., 2006, *AcA*, **56**, 127 (Paper VI)

Kreiner J. M., Rucinski S. M., Zola S., Niarchos P., Ogloza W., Stachowski G., Baran A., Gazeas K., Drozdz M., Zakrzewski B., Pokrzywka B., Kjurkchieva D., Marchev D., 2003, *A&A*, **412**, 465 (Paper I)

Kwee K., van Woerden H., 1956, *Bulletin of the Astronomical Institutes of the Netherlands*, **12**, 327

Zola S., Rucinski S.M., Baran A., Ogloza W., Pych W., Kreiner J.M., Stachowski G., Gazeas K., Niarchos P., Siwak M., 2004, *AcA*, **54**, 299 (Paper III)

Zola S., Kreiner J.M., Zakrzewski B., Kjurkchieva D.P., Marchev D.V., Baran A., Rucinski S.M., Ogloza W., Siwak M., Koziel D., Drozdz M., Pokrzywka B., 2005, *AcA*, **55**, 389 (Paper V)

Zola S., Gazeas K., Kreiner J. M., Ogloza W., Siwak M., Koziel-Wierzbowska D., Winiarski M., 2010, *MNRAS*, **408**, 464 (Paper VII)

COMMISSIONS 27 AND 42 OF THE IAU
INFORMATION BULLETIN ON VARIABLE STARS

Number 6166

Konkoly Observatory
Budapest
24 April 2016

HU ISSN 0374 – 0676

USING APASS STANDARDS TO TRANSFORM CCD OBSERVATIONS: APPLICATION TO NEW AND OLD OBSERVATIONS OF MT Cam

TERRELL, DIRK[1,2]; GROSS, JOHN[2]; COONEY, WALTER R., JR.[3]

[1] Department of Space Studies, Southwest Research Institute, 1050 Walnut St., Suite 300, Boulder, CO, USA, 80302

[2] Sonoita Research Observatory, 705 W. Millbrook Lane, Tucson, AZ USA, 85704

[3] Sonoita Research Observatory, 19523 Salado Creek Ct., Cypress, TX USA, 77433

e-mail: terrell@boulder.swri.edu; johngross3@msn.com; waltc111@att.net

The variability of MT Camelopardalis was reported by Nakajima et al. (2004), and identified as a W UMa binary with a period of 0.3662 days. The light curve appeared to have complete eclipses and was placed in the observing queue at Sonoita Research Observatory (SRO) in late 2004. A reasonably complete light curve was observed in the Johnson V passband. In early 2016, MT Cam was again observed at SRO, this time in the Johnson B and V passbands, and the Cousins I passband. Complete light curves in all passbands were obtained.

While it has been customary to make observations of eclipsing binary stars as differential magnitudes of the target star against a comparison star, the observations reported herein have been transformed to the standard (Vega) system using on-chip standards from data release 9 of the AAVSO Photometric All-Sky Survey (hereafter, APASS; Henden et al., 2012). The CCD images were first reduced in the usual manner by subtracting bias and dark frames and flatfielding in IRAF. Point-spread function (PSF) photometry on the reduced images was then performed with the SExtractor and PSFEx software (Bertin & Arnouts, 1996) to get instrumental magnitudes for all detected stars in each frame.

Transformation of the instrumental magnitudes to the standard system for the 2016 observations was straightforward. Normally one will observe a target field and several standard star fields (Landolt, 1992; 2009) during the night to get a set of transformation coefficients for the night. With the availability of the APASS catalog, there is a high probability that several standards in the 10^{th} to 16^{th} magnitude range will be in the target field itself, making it unnecessary to move the telescope away from the target field. Not only does this allow for more observations of the target star, it also allows for more observations of standard stars. It also allows the transformation coefficients to be determined for each frame. Observations in at least two passbands enable a least squares fit between the standard magnitudes of suitable APASS stars in each frame and their instrumental magnitudes and colors of the form:

$$M = \mu \times m + \epsilon \times c + \xi$$

where M is the standard magnitude, m is the instrumental magnitude, c is the instrumental color, and μ,ϵ,ξ are the transformation coefficients. Figure 1 shows the instrumental versus APASS magnitudes and the residuals from the fit for a typical frame. Once the transformation coefficients have been determined, instrumental photometry of objects in the frame can be transformed onto the standard system. Because the MT Cam field is reasonably crowded, many APASS stars are available for use. We used APASS stars with photometric errors of 0.05 mag or less, and usually had 20 or more standards on each frame for each fit. To avoid potential problems with long-period variable stars, we rejected stars that showed large residuals (greater than 0.05 mag) in the fit. Comparison of the transformed magnitudes and colors for those APASS stars not used in the fit with their APASS catalog values, as well as Tycho photometry for the brighter stars, showed good agreement.

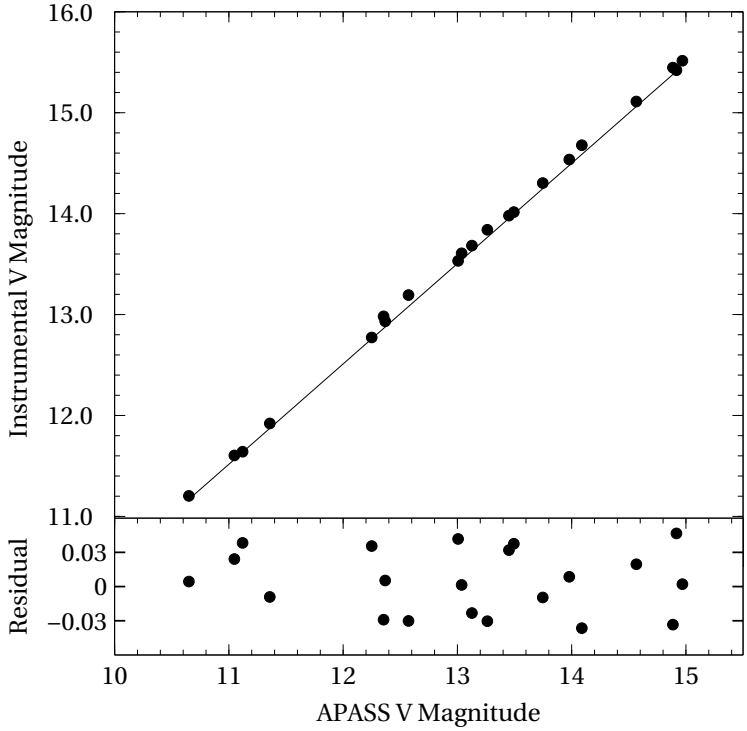

Figure 1. Instrumental V versus APASS V magnitudes and the residuals from the fit to data for a typical frame. The solid line represents only the linear portion of the fit. The residuals are for the full fit, including the color term, and clearly show that the color term is important.

Unfortunately, the 2004 observations were made only in the V passband, since at the time we were not concerned with their transformation onto the standard system. With no instrumental colors available, we substituted the catalog colors of the stars for the instrumental colors in order to be able to make the transformation onto the standard system. Of course, this approach means that for stars without APASS colors the transformation cannot be made, but all of the stars of interest to the current study have APASS colors, so we can get the transformed V magnitudes. While somewhat unorthodox, this approach seemed to work well when we checked the resulting V magnitudes for APASS stars not used in the fit against their APASS values. In order to reduce the noise in the 2004 observations, we measured the V magnitude of a comparison star, GSC 3736-00851,

Table 1. Parameters for MT Cam.

Parameter	Value
T_1 (K)	5368 (assumed)
T_2 (K)	5222± 5
i (°)	82.3±0.3
Ω_1	6.41±0.02
q	2.88±0.02
HJD_0	2453291.1269±0.0002
P (days)	0.366136±0.000002
dP/dt	$1.6 \times 10^{-9} \pm 1.1 \times 10^{-9}$
$L_1/(L_1+L_2)_B$	0.316±0.002
$L_1/(L_1+L_2)_V$	0.307±0.002
$L_1/(L_1+L_2)_{I_C}$	0.297±0.002

on all frames and formed the mean of those measurements to get V=11.35 ± 0.01. (The APASS catalog gives V=11.36 ± 0.04.) We then formed differential magnitudes between MT Cam and GSC 3736-00851 on each frame, and then added the mean V magnitude for GSC 3736-00851 to get the final V magnitudes for MT Cam.

The photometry was then analyzed with the 2013 version of the Wilson-Devinney program (hereafter, WD; Wilson & Devinney, 1971; Wilson, 1979). The light curves show an overcontact morphology, and therefore we used WD in mode 3 (Leung & Wilson, 1977). The 2013 version of WD can compute several quantities automatically, such as curve-dependent weights and local limb darkening coefficients, and we employed these features. The mean effective temperature of the primary was set to 5368 K based on the APASS $B-V$ value of 0.79±0.03. The adjusted parameters were orbital inclination (i), mean effective temperature of the secondary (T_2), surface potential of the primary (Ω_1), mass ratio (q), reference epoch (HJD_0), orbital period (P), first time derivative of the orbital period (dP/dt), and the bandpass luminosities of the primary (L_{1B}, L_{1V}, L_{1I_C}). Table 1 shows the final parameters from the solution. Figure 2 shows the fit to the 2004 observations and Figure 3 shows the fits to the 2016 observations. Figure 4 shows the system at secondary eclipse. The observations are available from the IBVS web site as file 6166-t2.txt.

The analysis shows that indeed the eclipses are complete, with the slightly deeper eclipse (0.02 mag in B) showing totality, so we find the cooler star to be the more massive one. The light curves do show variability between the 2004 and the 2016 observations, presumably due to spots on one or both stars, so the relative depths of the eclipses may change over time, even changing which eclipse is deeper. So, while our solution technically makes this a W-type system, light curve changes could easily make the system look like an A-type system (which is what the Nakajima et al. (2004) observations appear to show). We did not attempt to perform any solutions with spots on the stars. Our purpose in publishing these observations and a preliminary analysis now is to show that with complete eclipses, this is a system that is a very rewarding target for radial velocity observations.

Our solution does show a marginal detection of a period change, $dP/dt = 1.6 \times 10^{-9} \pm 1.1 \times 10^{-9}$. Although it is not surprising to find W UMa systems with period variability (Nelson et al., 2014), future observations will be needed to confirm and characterize the nature of MT Cam's period variability.

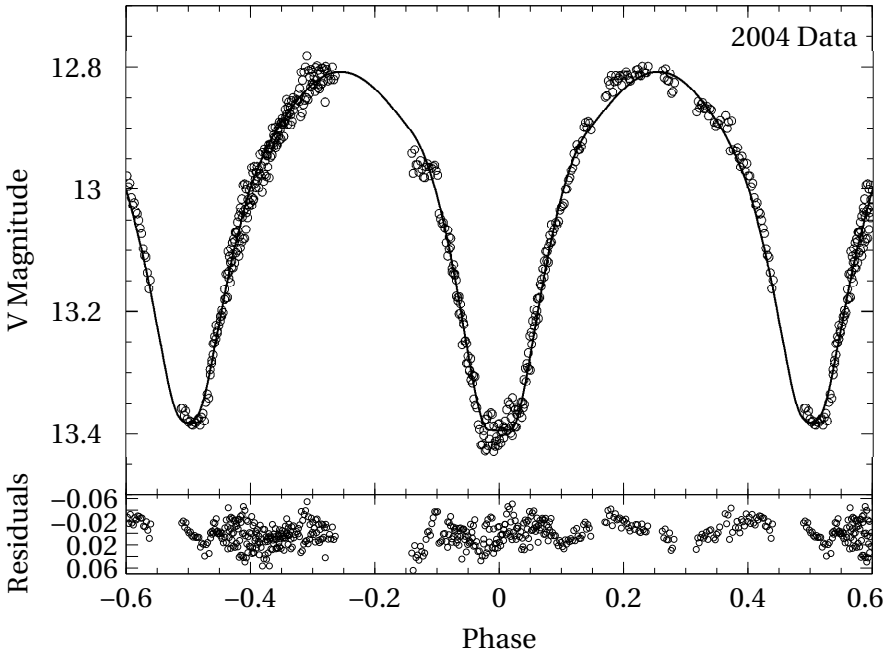

Figure 2. The 2004 V light curve of MT Cam and the fit from the WD solution (solid line). The residuals of the fit are shown at the bottom.

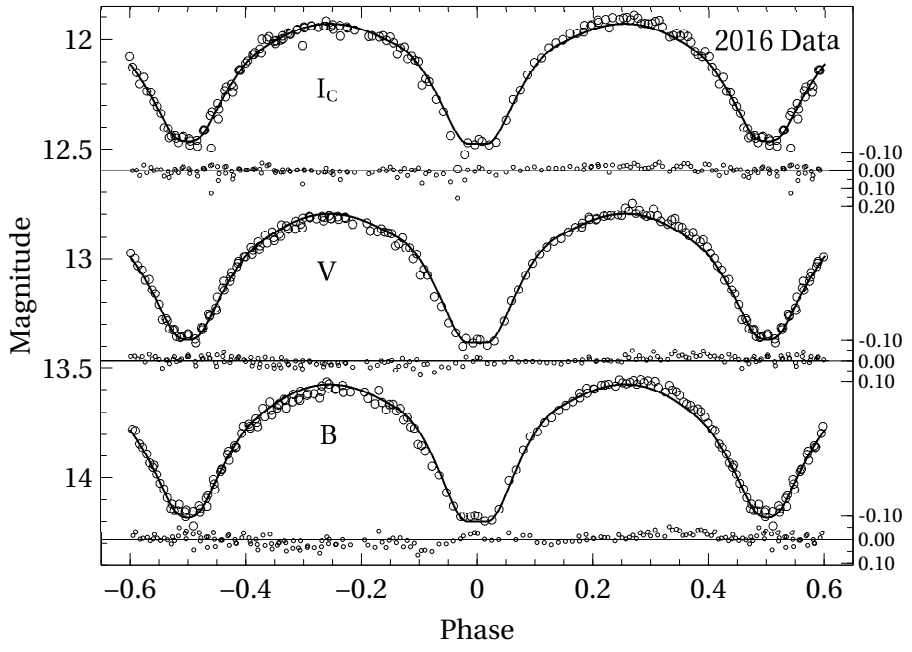

Figure 3. The 2016 B, V and I_C light curves of MT Cam and the fits from the WD solution (solid lines). The residuals from the fits are shown below each light curve.

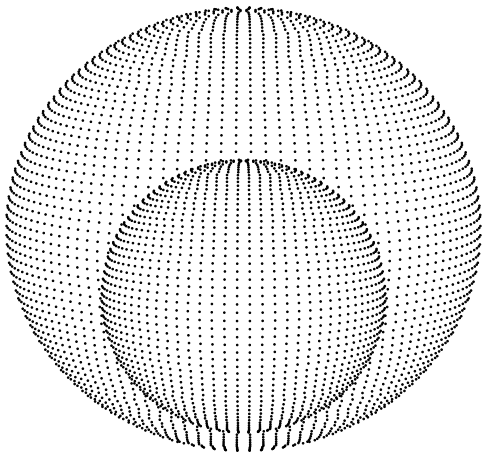

Figure 4. The appearance of MT Cam at the time of secondary eclipse.

Because the eclipses are complete, the mass ratio should be relatively well-determined (Terrell & Wilson, 2005), and if spectroscopic observations could only reveal one component's spectral lines, a full solution for the system's absolute parameters could still be achieved. Note also that since our observations are on the standard system, such a solution could also include a direct estimate of the distance to the system (Wilson, 2008) as part of the analysis. Versions of WD since 2013 can include the distance to the system as a model parameter, thus eliminating the need to make any simplifying assumptions (such as spherical stars), dependence on stellar evolution models (e.g., Klagyivik & Csizmadia, 2004), or statistically derived period-color-luminosity relations (Rucinski, 1996). Given the lack of radial velocities for the system, we can only characterize our solution as preliminary, but the complete eclipses and standardized photometry make future radial velocity observations even more valuable.

In conclusion, we have shown how the availability of APASS standards not only makes new observations easier to transform onto the standard system, they also enable the reanalysis of existing observations to transform them as well, even in the case where the existing observations were made in only one filter. Just as all-sky astrometric catalogs have made it possible to easily perform plate solutions for CCD observations, APASS now makes it easy to place photometric observations onto the standard system.

Acknowledgement: This research was made possible through the use of the AAVSO Photometric All-Sky Survey (APASS), funded by the Robert Martin Ayers Sciences Fund and U.S. National Science Foundation grant 1412587.

References:

Bertin, E. & Arnouts, S., 1996, *A&AS*, **117**, 393
Henden, A. A., Levine, S. E., Terrell, D., Smith, T. C. & Welch, D., 2012, *JAAVSO*, **40**, 430
Klagyivik, P. & Csizmadia, S., 2004, *ASP Conf. Ser.*, **318**, 195
Landolt, A., 1992, *AJ*, **104**, 340
Landolt, A., 2009, *AJ*, **137**, 4186
Leung, K.-C., & Wilson, R.E., 1977, *ApJ*, **211**, 853
Nakajima, K., Yoshida, S., Ohkura, N., & Kadota, K., 2004, *IBVS*, **5600**
Nelson, R. H., Terrell, D. & Milone, E. F., 2014, *New Astr. Rev.*, **59**, 1
Rucinski, S., 1996, *ASP Conf. Ser.*, **90**, 270
Terrell, D. & Wilson, R. E., 2005, *ApSpSc*, **296**, 221
Wilson, R. E., 1979, *ApJ*, **234**, 1054
Wilson, R. E., 2008, *ApJ*, **672**, 575
Wilson, R. E. & Devinney, E. J., 1971, *ApJ*, **166**, 605

COMMISSIONS 27 AND 42 OF THE IAU
INFORMATION BULLETIN ON VARIABLE STARS

Number 6167

Konkoly Observatory
Budapest
20 May 2016

HU ISSN 0374 – 0676

MINIMA TIMES OF SELECTED ECLIPSING BINARIES

PARIMUCHA, Š.[1]; DUBOVSKÝ, P.[2]; KUDAK, V.[1]; PERIG, V.[3]

[1] Institute of Physics, Faculty of Science, P.J. Šafárik University in Košice, The Slovak Republic; e-mail: stefan.parimucha@upjs.sk

[2] Vihorlat Observatory in Humenné, The Slovak Republic; e-mail: var@kozmos.sk

[3] Laboratory of Space Research, Uzhhorod National University, Ukraine

Observatory and telescope:
Kolonica Observatory: ZIGA - 508/3454 Planewave CDK20, C11 - 280/2800 Celestron, C14 - 356/3910 Celestron EdgeHD, VNT 1000/9000 Cassegrain Uzhhorod Observatory: T400 - 400/1500 Newton, BRC-250/1268 Takahashi refractor

Detector:	G4 - Moravian Instruments G4-16000, G2 - Moravian Instruments G2-1600, FLI - FLI PL1001E, U9 - Apogee Alta U9

Method of data reduction:
All observations were reduced and photometry was performed using C-Munipack package (http://c-munipack.sourceforge.net/)

Method of minimum determination:
The minima times were computed by the method proposed in Mikulášek et al. (2006)

Times of minima:					
Star name	Time of min. HJD 2400000+	Error	Type	Filter	Rem.
UU And	57259.5005	0.0005	I	V	ZIGA-G4
	57262.4723	0.0001	I	V	ZIGA-G4
	57326.3846	0.0002	I	V	ZIGA-G4
	57332.3301	0.0002	I	VI	ZIGA-G4
	57410.3555	0.0009	II	R	T400+FLI
AB And	57326.2448	0.0001	II	V	ZIGA-G4
AD And	57220.4121	0.0001	II	V	ZIGA-G4
	57326.4291	0.0002	I	V	ZIGA-G4
BD And	57223.3892	0.0003	I	V	ZIGA-G4
	57253.4779	0.0004	II	V	ZIGA-G4
	57265.5134	0.0001	II	V	ZIGA-G4
	57267.3649	0.0001	II	V	ZIGA-G4
EP And	56940.3681	0.0001	I	VR	C11+G2
	56959.5630	0.0002	II	VR	C11+G2
	57067.2588	0.0001	I	V	ZIGA-G4
GZ And	56510.4804	0.0002	I	V	C11+G2
	56905.4767	0.0002	I	VI	C11+G2
LO And	56917.5562	0.0001	I	V	C14+G2
	57215.4412	0.0001	I	V	ZIGA-G4
	57264.4465	0.0001	II	V	C11+G2
SS Ari	56942.5297	0.0006	I	VI	C11+G2
CL Aur	57326.4883	0.0002	II	V	ZIGA-G4
TY Boo	56432.3592	0.0007	II	VR	C11+G2
	57185.4219	0.0001	I	VI	ZIGA-G4
TZ Boo	57480.4528	0.0004	I	VR	ZIGA-G4
XY Boo	56401.4951	0.0007	I	VI	C11+G2
	57029.6075	0.0001	I	VI	C11+G2
AC Boo	57088.4916	0.0001	I	VI	C11+G2
	57135.5445	0.0001	I	VI	C11+G2
	57176.4290	0.0002	I	VI	ZIGA-G4
	57484.4752	0.0001	I	VI	C11+G2
GK Boo	57452.5398	0.0009	I		BRC+U9
SV Cam	56966.5348	0.0002	I	VI	C11+G2
AO Cam	56967.4707	0.0001	II	VI	C11+G2
	57098.2769	0.0001	I	V	C11+G2
	57327.5574	0.0001	I	VI	C11+G2
CD Cam	56746.3933	0.0003	I		C11+G2
	57102.4945	0.0003	I	V	C11+G2
	57122.3628	0.0004	I	VI	C11+G2
DN Cam	57102.3169	0.0008	I	BV	C11+G2
NR Cam	56958.4917	0.0002	I	VI	C11+G2
	56958.6175	0.0003	II	VI	C11+G2
	57029.4992	0.0001	II	R	C11+G2
	57065.4533	0.0002	II	V	ZIGA-G4
	57065.5806	0.0001	I	V	ZIGA-G4

Times of minima:					
Star name	Time of min. HJD 2400000+	Error	Type	Filter	Rem.
NR Cam	57102.3000	0.0001	I	V	ZIGA-G4
	57065.4274	0.0001	II	V	ZIGA-G4
	57065.5560	0.0001	I	V	ZIGA-G4
TX Cnc	56709.4565	0.0002	I	VR	C11+G2
	57071.2804	0.0002	I	V	ZIGA-G4
EH Cnc	56629.6066	0.0003	I	VI	C11+G2
	57071.2579	0.0002	II	VI	C11+G2
BI CVn	56423.4374	0.0007	II	V	C11+G2
	57036.6389	0.0002	II	VI	C11+G2
	57070.4505	0.0001	II	VI	C11+G2
TW Cas	57251.4656	0.0001	I	V	ZIGA-G4
	57251.4656	0.0001	I	V	ZIGA-G4
	57266.4629	0.0003	I	VR	ZIGA-G4
BS Cas	56929.3988	0.0002	II	VI	C11+G2
	56959.5694	0.0005	I	VR	ZIGA-G4
	56967.2780	0.0002	II	VR	ZIGA-G4
	57245.4309	0.0001	I	VI	C11+G2
	57279.3462	0.0001	I	VI	C11+G2
CW Cas	56929.2859	0.0001	I	VI	C14+G2
	57214.5052	0.0001	II	VR	ZIGA-G4
	57246.5494	0.0001	I	VI	C14+G2
DO Cas	57326.2926	0.0001	I	V	ZIGA-G4
	57327.3201	0.0006	II	RI	ZIGA-G4
	57328.3470	0.0001	I	VR	ZIGA-G4
	57330.4008	0.0001	I	VR	ZIGA-G4
	57331.4296	0.0001	II	VR	ZIGA-G4
V523 Cas	56942.2958	0.0001	I	VI	C11+G2
	57328.2410	0.0001	I	VI	C11+G2
	57328.3588	0.0001	II	VI	C11+G2
VW Cep	57464.5077	0.0002	I		BRC+U9
	57472.5801	0.0004	I	B	T400+FLI
WZ Cep	57069.2614	0.0002	II	V	ZIGA-G4
	57069.4703	0.0002	I	V	ZIGA-G4
	57244.3759	0.0002	I	VI	C11+G2
GW Cep	56709.3311	0.0001	II	VR	C11+G2
	57068.3367	0.0002	II	V	ZIGA-G4
	57068.4954	0.0002	I	V	ZIGA-G4
	57105.3216	0.0001	II	V	ZIGA-G4
	57105.4809	0.0001	I	V	ZIGA-G4
	57244.4911	0.0001	I	VI	C11+G2
	57248.4769	0.0002	II	VR	ZIGA-G4
	57249.4333	0.0002	II	VR	ZIGA-G4
	57250.3900	0.0002	II	VR	ZIGA-G4
	57250.5490	0.0001	I	VR	ZIGA-G4

Times of minima:					
Star name	Time of min. HJD 2400000+	Error	Type	Filter	Rem.
RW Com	56421.4720	0.0006	II	V	C11+G2
	57067.6530	0.0002	I	VR	C11+G2
	57071.4510	0.0002	II	V	ZIGA-G4
	57071.5685	0.0002	I	V	ZIGA-G4
RZ Com	57099.3183	0.0003	I	V	C11+G2
SS Com	56424.4098	0.0010	I	VI	C11+G2
CC Com	56423.3464	0.0002	I	V	C11+G2
	57067.5263	0.0002	I	V	ZIGA-G4
	57067.6362	0.0002	II	V	ZIGA-G4
	57098.4223	0.0002	I	V	ZIGA-G4
	57098.5320	0.0002	II	V	ZIGA-G4
	57477.4483	0.0001	II	VR	ZIGA-G4
V401 Cyg	57181.4211	0.0001	I	VI	ZIGA-G4
V1191 Cyg	56424.5123	0.0009	I	R	C11+G2
	56432.5028	0.0008	II	R	C11+G2
	56461.4929	0.0011	I	R	C11+G2
	56942.3915	0.0002	II	VI	C11+G2
	57180.4120	0.0003	I	VI	ZIGA-G4
V1918 Cyg	56420.4878	0.0007	I	VR	C11+G2
	56433.5004	0.0009	II	VR	C11+G2
	57154.4972	0.0002	II	VI	C11+G2
	57183.4197	0.0001	II	VI	ZIGA-G4
	57214.4073	0.0002	II	VI	C11+G2
	57241.4711	0.0001	I	VR	ZIGA-G4
	57242.5042	0.0001	II	VR	ZIGA-G4
BE Dra	57135.4101	0.0004	II	VI	C11+G2
	57188.4382	0.0002	I	VI	ZIGA-G4
CM Dra	56079.4780	0.0001	II		C14+G2
	56199.3429	0.0001	I		VNT+FLI
	56351.5499	0.0001	I		C14+G2
	56356.6234	0.0001	I		C14+G2
	56476.4852	0.0001	II		C14+G2
	56478.3884	0.0001	I		C14+G2
	56823.3899	0.0001	I		C14+G2
	57065.6537	0.0001	I		C14+G2
	57206.4448	0.0001	I		C14+G2
	57258.4488	0.0001	I		C14+G2
EF Dra	56787.5016	0.0004	II	VI	C11+G2
	57136.4913	0.0004	II	VI	C11+G2
	57188.4350	0.0003	I	VI	C11+G2
FU Dra	56541.3208	0.0001	II	V	C11+G2
	57085.4362	0.0003	II	V	C11+G2
	57099.3899	0.0002	I	V	ZIGA-G4
	57099.5444	0.0001	II	V	ZIGA-G4
	57214.4095	0.0001	I	VI	ZIGA-G4

Times of minima:					
Star name	Time of min. HJD 2400000+	Error	Type	Filter	Rem.
AK Her	57461.5928	0.0002	I	R	T400+FLI
V728 Her	56421.3762	0.0018	I	VI	C11+G2
	57151.4160	0.0007	I	VI	C11+G2
	57221.4028	0.0002	II	VR	ZIGA-G4
	57184.4051	0.0002	I	VI	ZIGA-G4
	57240.4899	0.0001	I	VR	ZIGA-G4
	57255.3349	0.0003	II	V	ZIGA-G4
V829 Her	56433.4239	0.0006	I	V	C11+G2
	57154.3966	0.0002	I	VI	C11+G2
V857 Her	56429.4211	0.0022	II	VR	C11+G2
	57207.4502	0.0002	I	VI	C11+G2
V1024 Her	57452.5663	0.0006	I		BRC+U9
PP Lac	56540.3095	0.0002	I	V	C11+G2
	56943.4774	0.0002	I	VI	C11+G2
	57206.4406	0.0001	II	VI	ZIGA-G4
	57224.4922	0.0001	II	VR	ZIGA-G4
	57226.4981	0.0001	II	VR	ZIGA-G4
	57228.5037	0.0001	II	VR	ZIGA-G4
	57235.5236	0.0001	I	VR	ZIGA-G4
V344 Lac	56614.3740	0.0002	II		C14+G2
CE Leo	56993.4812	0.0004	II	VR	C11+G2
	57071.3991	0.0004	I	VI	C11+G2
RT LMi	56709.5948	0.0002	I	VR	C11+G2
	56744.4673	0.0002	I	V	C11+G2
	57068.3912	0.0002	I	VR	C11+G2
	57070.2649	0.0002	I	V	ZIGA-G4
	57070.4532	0.0002	II	V	ZIGA-G4
	57070.6398	0.0002	I	V	ZIGA-G4
	57091.2607	0.0002	I	V	ZIGA-G4
	57091.4488	0.0002	II	V	ZIGA-G4
UV Lyn	57482.3110	0.0001	II	B	T400+FLI
V714 Mon	56624.5981	0.0001	I	V	C11+G2
	57069.3544	0.0002	I	VI	C11+G2
V508 Oph	56463.4192	0.0004	I	R	C11+G2
	57105.5927	0.0001	II	V	C11+G2
	57185.4113	0.0001	I	VI	C11+G2
BB Peg	57243.4654	0.0002	II	VR	ZIGA-G4
	57246.3572	0.0002	II	VR	ZIGA-G4
	57243.5364	0.0002	I	VR	ZIGA-G4
BX Peg	56943.3347	0.0002	I	VI	C11+G2
	57214.4983	0.0001	I	VI	C11+G2
DI Peg	57327.2750	0.0002	I	VI	C11+G2
V432 Per	56957.5359	0.0002	I	VR	C11+G2
	56990.3088	0.0002	II	VR	ZIGA-G4
	56990.4995	0.0002	I	VR	ZIGA-G4

Times of minima:					
Star name	Time of min. HJD 2400000+	Error	Type	Filter	Rem.
V432 Per	56991.2662	0.0002	II	VR	ZIGA-G4
	56991.4589	0.0001	I	VR	ZIGA-G4
	57264.5491	0.0001	I	VI	C11+G2
V449 Per	57424.2593	0.0007	II	R	T400+FLI
DV Psc	56573.4163	0.0001	I	VR	C14+G2
	56956.3076	0.0001	I	VR	VNT+FLI
	56956.4638	0.0002	II	VR	VNT+FLI
	57279.3459	0.0002	I	VR	ZIGA-G4
	57283.3572	0.0002	I	VR	ZIGA-G4
	57287.3673	0.0002	II	VR	ZIGA-G4
	57287.5216	0.0002	I	VR	ZIGA-G4
EX Psc	56573.3387	0.0002	II	VR	C14+G2
	56573.4787	0.0004	I	VR	C14+G2
	56927.3706	0.0012	II	VR	VNT+FLI
	56927.5164	0.0012	I	VR	VNT+FLI
	56928.5294	0.0006	II	VR	VNT+FLI
	56956.3190	0.0003	II	VR	VNT+FLI
	56956.4633	0.0002	I	VR	VNT+FLI
	57279.3791	0.0009	II	VR	ZIGA-G4
	57283.4338	0.0007	II	VR	ZIGA-G4
	57287.3413	0.0013	II	VR	ZIGA-G4
	57287.4878	0.0008	I	VR	ZIGA-G4
AU Ser	56787.3675	0.0001	I	VR	C11+G2
	57246.3338	0.0001	II	VR	C11+G2
	57480.5515	0.0007	II	V	ZIGA-G4
AH Tau	57327.4187	0.0001	I	VI	C11+G2
CT Tau	57036.4846	0.0002	I	VI	C11+G2
EQ Tau	56905.5767	0.0002	I	VI	C11+G2
	57070.2768	0.0002	II	VI	C11+G2
XY UMa	57482.3782	0.0007	II	B	T400+FLI
AA UMa	57069.4640	0.0002	I	VI	C11+G2
	57332.5537	0.0002	I	VI	ZIGA-G4
	57479.5459	0.0002	I	VI	ZIGA-G4
HH UMa	56614.6573	0.0008	II	I	C11+G2
	57123.4527	0.0002	II	I	C11+G2
	57326.5954	0.0001	II	V	ZIGA-G4
	57480.3614	0.0001	I	V	ZIGA-G4
	57484.4910	0.0002	I	VR	ZIGA-G4
TV UMi	57258.4037	0.0007	I	VR	ZIGA-G4
	57263.3889	0.0008	I	VR	ZIGA-G4
	57264.4280	0.0005	II	VR	ZIGA-G4
AZ Vir	57136.3367	0.0002	II	VI	C11+G2

Explanation of the remarks in the table:
Remarks give information on the observatory and used instrument. If two filters are given, we publish weighted average times of minima from the given filters.

Remarks:
Minima types are calculated according to elements given in Up-to-date Linear Elements of Eclipsing Binaries database (Kreiner, 2004).

Acknowledgements:
This paper was supported by the APVV-15-0458 grant and the VVGS-2016 -72608 internal grant of the Faculty of Science, P.J. Šafárik University in Košice.

References:

Kreiner, J.M., 2004, *Acta Astronomica*, 54, 207

Mikulášek, Z., Wolf, M., Zejda, M., Pecharová, P., 2006, *Astrophysics and Space Science*, 304, 363

COMMISSIONS 27 AND 42 OF THE IAU
INFORMATION BULLETIN ON VARIABLE STARS
Number 6168

Konkoly Observatory
Budapest
25 May 2016
HU ISSN 0374 – 0676

BG CMi TIME KEEPING

BONNARDEAU, MICHEL

MBCAA Observatory, Le Pavillon, 38930 Lalley, France, email: arzelier1@free.fr

BG Canis Minoris (RA=$07^{\rm h}31^{\rm m}29\overset{\rm s}{.}00$, DEC=$+09°56'23\overset{''}{.}1$, J2000) is an intermediate polar (a cataclysmic system in which the white dwarf is magnetized enough to moderate the accretion). Its magnitude is around 14.5. The orbital motion has a period of $P_{\rm orb}$ = 3.235 hr, and gives a modulation visible by photometry.

There is also a modulation of the light curves with a period $P_{\rm spin}$ = 913 s. This modulation is usually interpreted as being due to the spin of the white dwarf. However this is not firmly established: the spin period may be twice $P_{\rm spin}$, with both poles visible (Patterson & Thomas, 1993), or the observed modulation may be synodic, with the spin period being actually shorter (Norton et al., 1992).

According to Pych et al. (1996) and references therein, the period $P_{\rm spin}$ is decreasing, so there is a spin-up of the white dwarf. However, according to Kim et al. (2005, hereafter K05), the rate of this spin-up is decreasing.

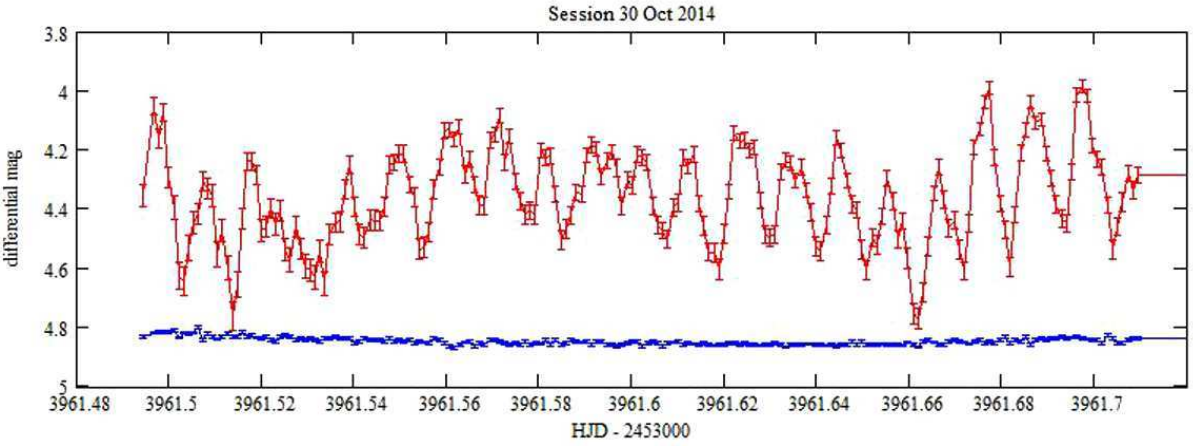

Figure 1. Upper light curve: BG CMi, lower one: the check star shifted by +4.2 mag. The error bars are the quadratic sum of the 1σ statistical uncertainties on the variable/check star and on the comparison star.

Observations

Photometric observations of BG CMi were carried out over twelve seasons, from 2005 to 2016, with a 203 mm f/6.3 Schmidt-Cassegrain telescope, a clear filter and an SBIG ST7E camera (KAF401E CCD). The exposures were 60 s long. For the aperture differential photometry, the comparison star is GSC 768-01373. Over 49 nights 5161 useful images were obtained. A check star, GSC 768-01665, is used to compare the standard deviations to the statistical uncertainties so as to make sure that the systematic errors are low. An example of the light curve is given in Fig. 1.

O-C analysis of the P_{spin} modulation

The light curves are searched for pulses due to the P_{spin} modulation. $N = 254$ well defined pulses are found. These pulses are then fitted with the

$$t(E) = T + PE + BE^2 \tag{1}$$

quadratic ephemeris, where E is the cycle number, minimizing S:

$$S = \sqrt{\frac{\sum_{i=0}^{N-1} (t_i - T - PE_i - BE_i^2)^2/\delta t_i}{\sum_{i=0}^{N-1} 1/\delta t_i}} \tag{2}$$

where the t_i are the HJD of the pulses and the δt_i their uncertainties.

Solution(s) are searched for using a Monte Carlo algorithm. This has the advantage over the least squares method of readily revealing cycle counting ambiguities. It works the following way:

make 10 runs (or more) of the following:

- make 1 millions trials (or more) of the following:
  - select randomly a set of T, P, B;
  - compute the cycle number E_i of each pulse;
  - compute S;
- retain the set of T, P, B that gives the smallest S.

The sets of T, P, B are randomly selected in the following ranges:

- $T = [\text{the first pulse} - P_{\mathrm{spin}}/2 : \text{the first pulse} + P_{\mathrm{spin}}/2]$
- $P = [P_{\mathrm{spin}} - P_{\mathrm{spin}}/1000 : P_{\mathrm{spin}} + P_{\mathrm{spin}}/1000]$
- $B = [-40 \times 10^{-13} : 0]$

For each run, the same number of cycles is always obtained, 375,969, between the first and the last pulses. So there is no cycle ambiguity. The adopted values for T, P, B are the average values of the runs, and the adopted values for the uncertainties are the standard deviations:

$$T = 2453449.38837(48)\,\mathrm{HJD} = 2453449.389105\,\mathrm{HJD_{TDB}} \tag{3}$$

$$P = 0.0105726046(47)\,\mathrm{d} \tag{4}$$

$$B = -1.41(11) \times 10^{-13}\,\mathrm{d}. \tag{5}$$

The white dwarf is then spinning up with $\dot{P} = 2B/P = -2.67 \times 10^{-11}$ in a time scale $P/2|\dot{P}| = 543$ kyr.

The ephemeris (1) is precise enough to be applied with no cycle ambiguity to the 2002-2005 data of K05. The cycle numbers run from −76,998 to −4,194.

The spin-up rate in the ephemeris (1) is quite smaller than the one obtained from 1982-1996 observations (Pych et al., 1996),

$$t(e) = T_{\rm P96} + P_{\rm P96}e + B_{\rm P96}e^2, \tag{6}$$

with

$$T_{\rm P96} = 2445020.2800(2)\,{\rm HJD} = 2445020.2806\,{\rm HJD_{TDB}} \tag{7}$$

$$P_{\rm P96} = 0.010572992(2)\,{\rm d} \tag{8}$$

$$B_{\rm P96} = -3.83(4) \times 10^{-13}\,{\rm d}. \tag{9}$$

When the ephemeris (6) is applied to the 2002-2005 data of K05, the first pulse is at the epoch number $-720,254$, with an ambiguity of ± 1 or more cycles.

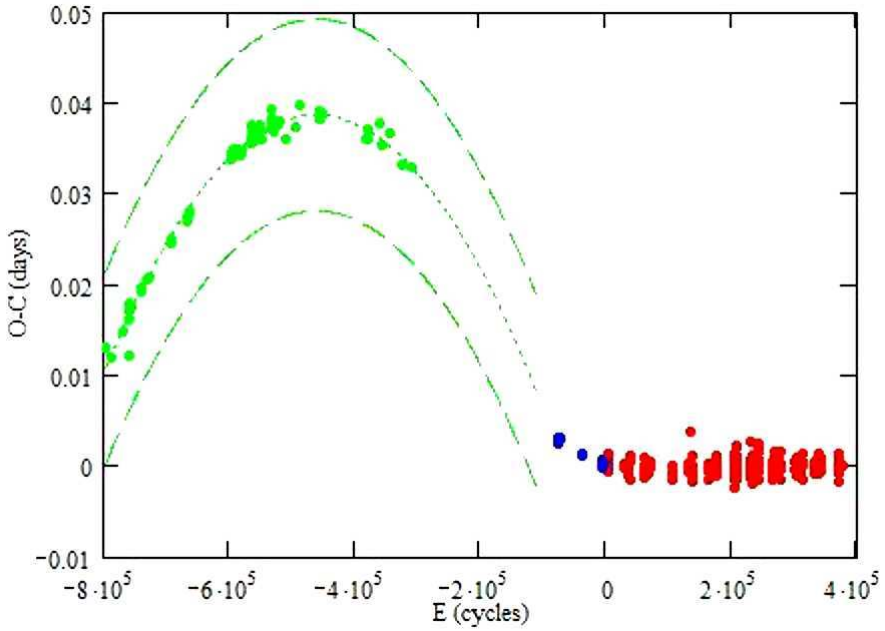

Figure 2. Red dots: present data, Blue: K05, Green: Pych et al (1996) with the first pulse between the epochs $-720,254$ and $-76,998$. Green dotted line: ephemeris (2) with $E = e + E_0$, upper dashed line: with $E = e + E_0 + 1$, lower dashed line: with $E = e + E_0 - 1$.

Besides the heliocentric correction, there are smaller corrections to be taken into account (Eastman et al., 2010), in particular the leap seconds due to the Earth rotation slowing down. The leap second correction at the time of the ephemeris (1), in 2005, is 32 s, and 36 s in 2016. And at the time of ephemeris (2), in 1982, it is 20 s, and 30 s in 1996. The barycentric effect of Jupiter and Saturn is neglected as it is only ±4 s and

cyclic (unlike the leap seconds that keep accumulating), and the other general relativistic corrections are much smaller. (And there is also 32.184 s to be added to obtain $\mathrm{BJD_{TDB}}$.)

This gives the O−C diagram in Fig. 2, computed from the ephemeris (1).

Between 1996 and 2005 there was a change of regime, from the ephemeris (6) to the ephemeris (1). Unfortunately, this was not observed, except by K05 who captured the end of this episode.

Fourier analysis of the orbital modulation

The light curves are inspected to look for the orbital dips, and they are found in phase with the orbital ephemeris of K05.

The light curves are analysed with the Period04 software program (Lenz & Breger, 2005), which provides simultaneously sine-wave fitting and least-squares fitting algorithms, around the frequency $1/P_{\mathrm{orb}}$. Besides $1/P_{\mathrm{orb}}$, up to 6 harmonics are used to fit the orbital modulation. This yields the orbital period:

$$P_{\mathrm{orb}} = 0.134748376(74)\,\mathrm{d} \tag{10}$$

which is in agreement with the period of K05 (the uncertainty is given by the Period04 Monte Carlo simulation).

Fourier analysis of the residuals

As the P_{spin} period is varying, the data are analysed season by season (so the variation is not too important): for each season an average P_{spin} period is computed from the ephemeris (1) and the Period04 program is used to derived the amplitude and phase. The same is done for 2 harmonics (actually, the amplitudes of these 2 harmonics are very small: the modulation is quasi-sinusoidal).

The data are then prewhitened with this fit for the P_{spin} modulation and with the fit for the orbital modulation, yielding a Fourier spectrum of the residuals for the season.

These Fourier spectra show many variations from one season to the other. But it is not clear which have physical causes. Actually, such features were already observed (Patterson & Thomas, 1993, Garlick et al., 1994, de Martino et al., 1995). All these spectra for each season are summed, resulting in a spectrum for the whole set of observations, prewhitened with the P_{spin} and the orbital modulations. Most of the variations cancel out, and a fairly strong peak shows up with two fainter ones, as shown in Figure 3.

The peak (1) corresponds to a period of 1083 s. It was already observed by Patterson & Thomas (1993) who interpreted it as the sideband $1/P_{\mathrm{spin}} - 2/P_{\mathrm{orb}}$.

The peak (2) corresponds to a period of 1309 s. It has not been reported by other observers. It could be the sideband $1/P_{\mathrm{spin}} - 4/P_{\mathrm{orb}}$.

The peak (3) corresponds to a period of 835 s. This is close to the signal at 847 s reported by Norton et al. (1992) and Choi et al. (2007) in X-ray, but unseen in optical band except by Garlick et al. (1994), and which was interpreted as the sideband $1/P_{\mathrm{spin}} + 1/P_{\mathrm{orb}}$.

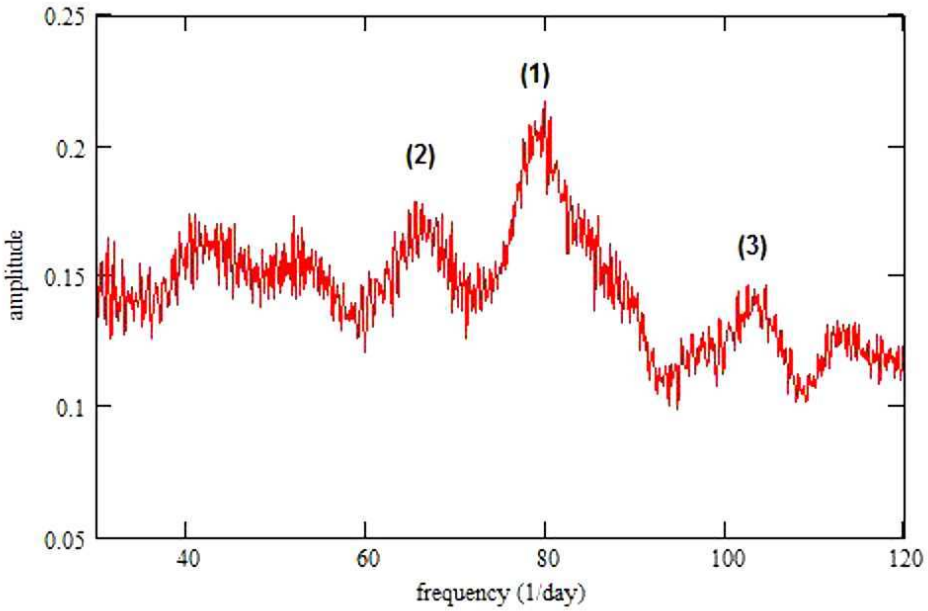

Figure 3. Sum of the spectra of the residuals for the twelve seasons.

References:

Choi C.-S., Dotani T., Kim Y., Ryu D., 2007, *New Astronomy*, **12**, 622
de Martino D. et al., 1995, *A&A*, **298**, 849
Eastman J., Siverd R., Gaudi B.S., 2010, *PASP*, **122**, 935
Garlick M.A. et al., 1994, *MNRAS*, **267**, 1095
Kim Y.G., Andronov I.L., Park S.S., Jeon Y.B., 2005, *A&A*, **441**, 663
Lenz P., Breger M., 2005, *Comm. Asteroseismology*, **146**, 53
Norton A.J., McHardy I.M., Lehto H.J., Watson M.G., 1992, *MNRAS*, **258**, 697
Patterson J., Thomas G., 1993, *PASP*, **105**, 59
Pych W., Semeniuk I., Olech A., Ruszkowski M., 1996, *Acta Astronomica*, **46**, 279

COMMISSIONS 27 AND 42 OF THE IAU
INFORMATION BULLETIN ON VARIABLE STARS

Number 6169

Konkoly Observatory
Budapest
26 May 2016

HU ISSN 0374 – 0676

MONITORING THE RADIAL VELOCITY OF HeI 6678 OF γ Cas

POLLMANN, ERNST

International Working Group ASPA, Emil-Nolde-Str. 12, 51375 Leverkusen, Germany

Introduction

The Be star γ Cas (27 Cas, HD 5394, HR 264) is a primary component of a spectroscopic binary and is the very first Be star known, discovered by Secchi (1887). Spectroscopically γ Cas has been investigated mostly in the Balmer lines, mainly in Hα. Recent studies considered He and Fe II lines as well as the kinematics of the circumstellar shell (Hanuschik, 1994, Smith, 1995). The HeI 6678 line has an important diagnostic value of activity close to the star's surface. Investigations of Smith (1995), Harmanec et al. (2000), Harmanec (2002), Pollmann & Stober (2007) and Pollmann (2009) give detailed information about the long-term behaviour of the equivalent widths of the HeI 6678 emission line.

In the context of the investigations concerning the periodic behaviour of the ratio V/R of the relative intensities of the violet component I_v to the red component I_r of the HeI 6678 emission line in γ Cas (Fig. 1), as it was described by Pollmann & Guarro (2015), a clearly detectable and clear variation of its radial velocity with a spectral resolving power of 10000 to 20000 were noticed. The HeI 6678 emission is formed close to stars photosphere and, therefore, it should be possible to measure RV without restructuring or turbulence effects, as in the outer region of the disk at Hα. Harmanec et al. (2000) (H2000 hereafter) argued that there are at different times "migrating sub-features" moving across the Hα line profile which affect the blue and red wings.

Against this background, the RV monitoring of the HeI 6678 absorption core of γ Cas will offer an opportunity to observe an "undisturbed" process. The BeSS data base[1] provides the use of corresponding γ Cas HeI 6678 spectra of observers of the ARAS group[2] from the years 2000 to 2016. Altogether 112 spectra of that time period were usedfor the investigation presented here, 52 BeSS spectra (observers are mentioned the caption to Fig. 2) from Sept. 2000 (JD 2451810) to Feb. 2016 (JD 2457442), 15 spectra of the Pollmann & Guarro (2015) paper, and 45 further spectra of the author (not all in BeSS). All RV data used in the analysis present here are available at: `http://astrospectroscopy.de/media/files/RV_data_gamcas.txtt`.

[1] `http://basebe.obspm.fr/basebe/`
[2] `http://www.astrosurf.com/aras`

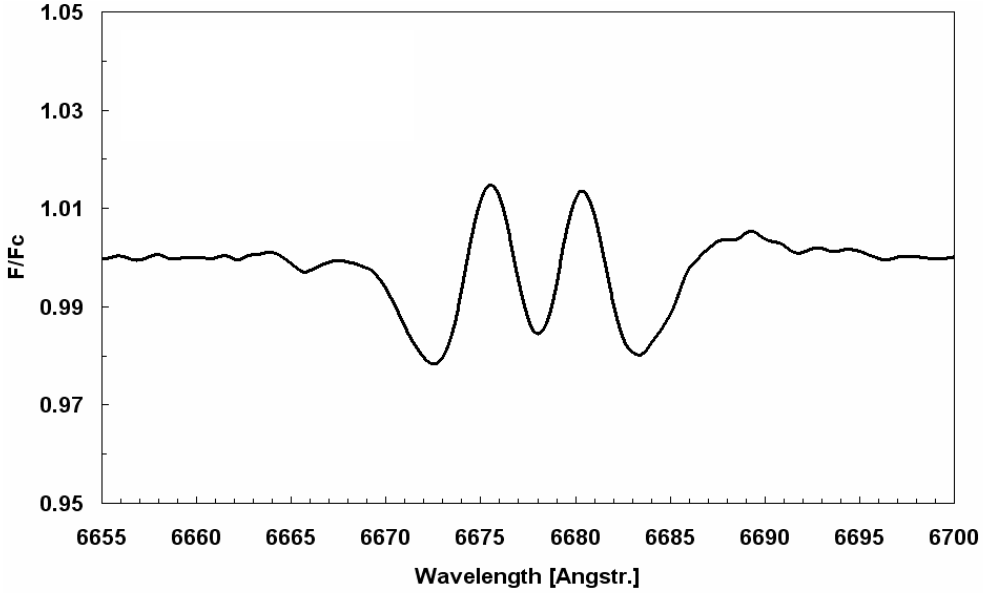

Figure 1. Example spectrum of the HeI 6678 emission of γ Cas, taken by the author November 01, 2015 with a LHIRES III spectrograph (R ca. 17000)

Observations

The spectra for the RV measurements of the HeI 6678 line presented here, were taken at different locations with 20 cm Newtonian and 40 cm Schmidt-Cassegrain telescopes. Spectrographs with spectral resolving powers of 10000 to 20000 were used. The signal to noise ratio of these spectra were of the order of magnitude S/N ca. 200-300. The spectra have been reduced with standard procedures (instr. response, normalisation, wavelength calibration) using the program VSPEC[3].

The evaluation of the heliocentric RV was performed by the profile mirror method. This method measures the Doppler shift of spectra by correlation of the spectral lines with their mirroring around the laboratory wavelength, and is particularly suitable for the evaluation of asymmetrical lines within exactly specified profile ranges.

Results

With the HeI 6678 RV of these spectra, along with Fig. 2 of the H2000 paper, it was possible to design a total overview of the RV time behaviour since 1993 (Fig. 2). The time base of 22 years in that long-term overview with the BeSS data starting from September 2000 demonstrates the continuation of the RV process from where the H2000 measurements ended.

[3]http://www.astrosurf.com/vdesnoux

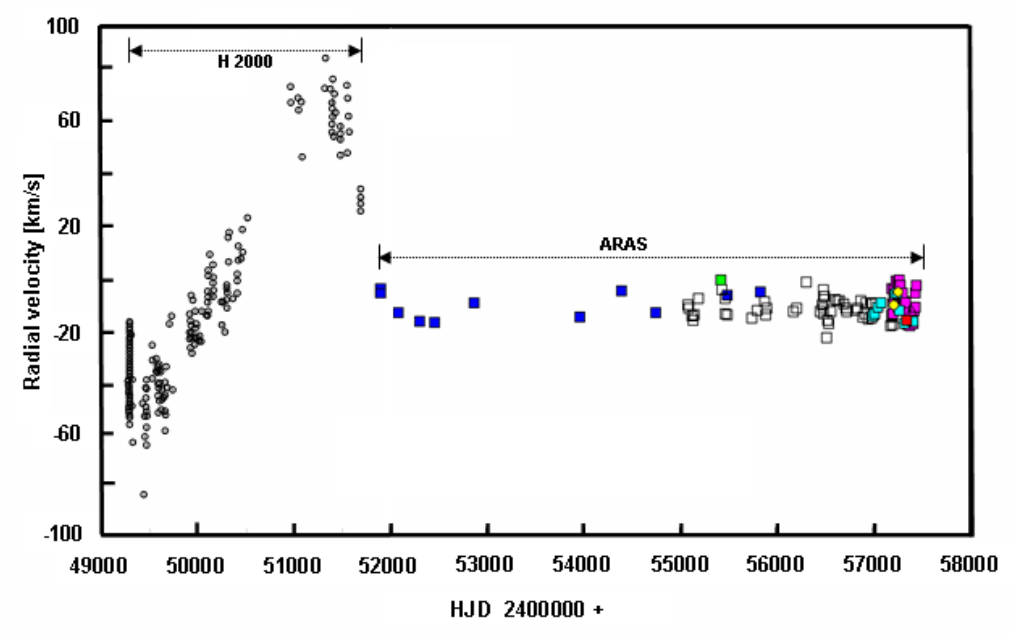

Figure 2. The compound long-term monitoring of RV measurements of H2000 (open circles), and the monitoring of observers of the ARAS group: Pollmann (open squares), Guarro (magenta squares), Lester (turquoise squares), Montier (yellow squares), Houpert (red squares), Buil (blue squares), Thizy (green squares), Berardi (open triangle)

	Period	Semi-amplitude	Epoch T_0 (JD)	RMS
H2000	203.59±? d	7.0 ± 1.5 km/s	2450578.7±?	8.95 km/s
ARAS	202.2 ± 0.6 d	4.44 ± 0.51 km/s	2451740.89 ± 14.3	3.6 km/s

Table 1: Result comparison of the analysis of H2000 and ARAS.

The first surprise is that after the RV (H2000) maximum with +90 km/s (approx. JD 2451300, May 1999), our campaign clearly shows the RV at a more or less constant level between 0.5 and −20 km/s. This overall RV behaviour leads to the question of the physical causes within this ring-like Helium zone, the answers to which cannot be given here. But at least it was interesting to see, whether the periodic behaviour of the HeI 6678 RV between Sept. 1993 and Sept. 2000, found by H2000, has changed. In order to find this out, a PDM (Phase Dispersion Minimization) analysis (Stellingwerf, 1978) of our data from Sept. 2000 to Dec. 2015 has been performed. The result with a clearly detectable period of 202 d is shown in Fig. 3. The corresponding phase diagram is shown in Fig. 4.

Table 1 shows the comparison of the period, semi-amplitude, epoch T_0 and RMS, measured as result of the ARAS analysis and the results of H2000.

Discussion

With our instruments nowadays we were able to achieve primarily a much better signal to noise ratio (S/N) than H2000. In addition the application of the spline filtering inter-

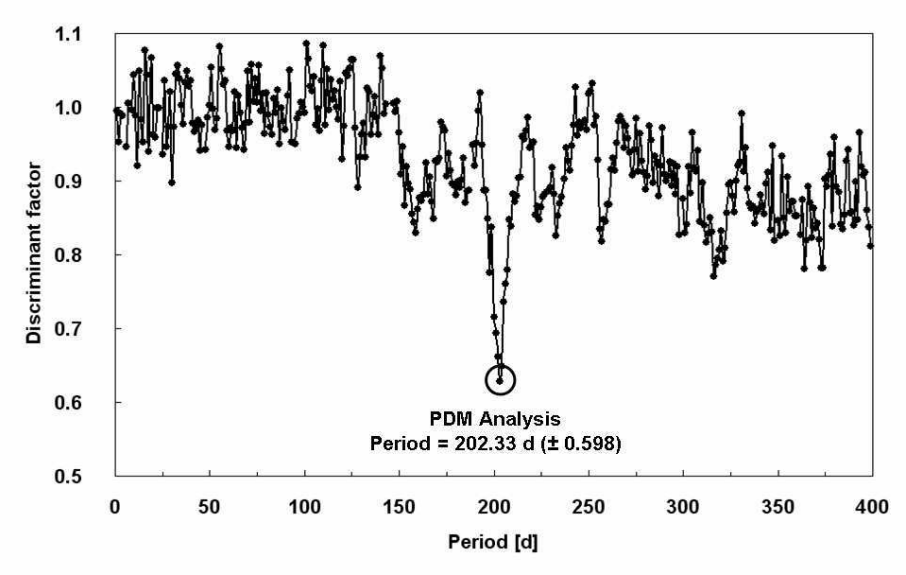

Figure 3. The PDM analysis of the ARAS RV data from Sept. 2000 to Dec. 2015 with a clearly detectable period of 202.33 days.

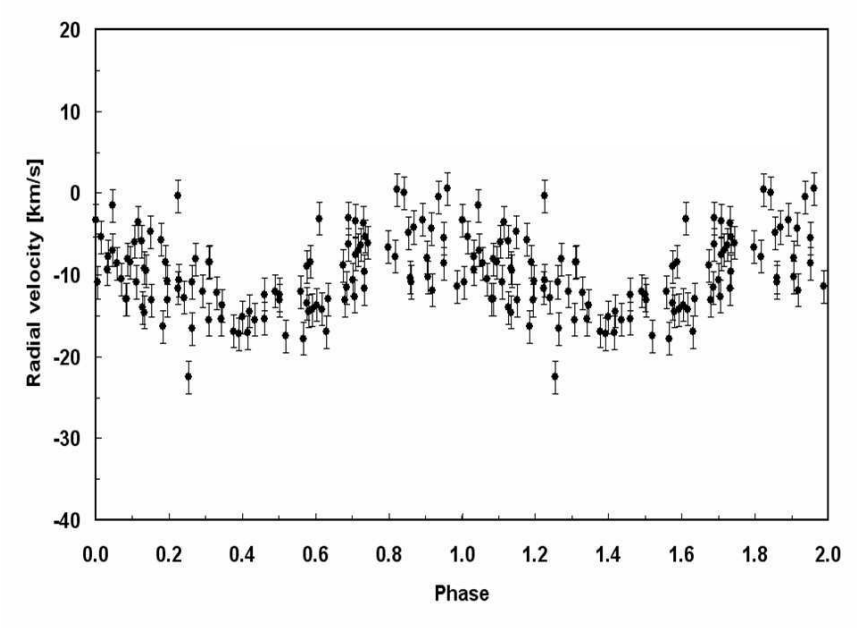

Figure 4. Phase diagram of the found period of the PDM analysis in Fig. 3

polation of the program VSPEC enables in small limits by adjustment of very carefully adapted spline coefficients, to smooth the line profile (ca. factor 1.1 to 1.2 of the normalized continuum), without any modification of the spectral information itself. The use of that tool leads to an improvement of the accuracy of the RV determination. With the results in Figs. 3 & 4, this campaign confirms a clearly detectable phase behaviour with a period very close to the period of H2000, in spite of very different RV time behaviour, shown in Fig. 2. It is difficult to judge, whether the small difference of 1.39 km/s established by H2000 and the period found in this analysis, is really significant. Maybe the small difference between the period is caused by the very strong change of the RV amplitude (Fig. 2) during the observation period of H2000. I want to emphasize that with our spectra we achieved a much better RMS (3.6 km/s) than H2000 (8.95 km/s).

Acknowledgements

I am grateful to Sara and Carl Sawicki (Alpine, Texas, USA) for their helpful improvements and suggestions in language.

References:

Hanuschik, R. W., 1994, *IAUS*, **162**, 265
Harmanec, P., Habuda, P., Stefl, S., Hadrava, P., Korcakova, D., Koubsky, P., Krticka, J., Kubat, J., Skoda, P., Slechta, M., Wolf, M., 2000, *A&A*, **364**, L85
Harmanec, P., 2002, *ASP Conference Series*, **279**, 221
Pollmann, E., 2009, *Be Star Newsletter*, **39**, 32
Pollmann, E., Guarro Flo, J., 2015, *IBVS*, **6103**
Pollmann, E., Stober, B., 2007, *Be Star Newsletter*, **38**, 8
Secchi, A. 1867, *Astron. Nachrichten*, **68**, 63
Smith, M. A., 1995, *ApJ*, **442**, 812
Stellingwerf, R. F., 1978, *ApJ*, **224**, 953

COMMISSIONS 27 AND 42 OF THE IAU
INFORMATION BULLETIN ON VARIABLE STARS

Number 6170

Konkoly Observatory
Budapest
31 May 2016

HU ISSN 0374 – 0676

HISTORIC LIGHT CURVE OF V890 Cas

NESCI, R.

INAF/IAPS, via Fosso del Cavaliere 100, 00133 Roma, Italy, e-mail: roberto.nesci@iaps.inaf.it

Introduction

The star V890 Cas (01:07:44.6 +59:03:02, J2000) was discovered to be variable by the Japanese amateur astronomer Akira Takao (Kita-kyushu, Japan) in the year 2001 with an average (unfiltered) ∼13 mag (Kazarovets et al. 2003). It is a strong infrared source, detected by IRAS, 2MASS, MSX, WISE, AKARI. Wright et al. (2009) report this star as Hα emitter, listed in the IPHAS survey as ERSO 27, with a spectral type SX/6e: no special remarks were reported by the authors on this star, though they were aware of its variability. This star is flagged as a Mira-type variable in the General Catalog of Variable Stars (Samus et al. 2013) but without a quoted period.

In the Asiago plate archive I found 87 plates of the Schmidt telescope (65/92/215) taken with I-N emulsion and RG5 filter, reproducing the Cousins I_C band. These plates, centred on γ Cas, were taken between 1967 and 1984, in the framework of a large project of search for late-type variables on the Galactic equator (Maffei 1975, 1977; Gasperoni et al. 1991). Most plates of γ Cas ranged from 1967 to 1975 with a typical limiting magnitude of I ∼15 in the USNO-B1 scale. Blue plates were also secured on the same night in most cases for comparison. The results of the red variables search for the γ Cas field have never been published, at variance with the other fields (M16/M17, γ Cyg, IC 1805).

Comparison sequence

To determine the light curve of V890 Cas I used the digitized version of the plates, made with an EPSON 1680 Pro of the University of Perugia at 1600 dpi in transparency mode (Nesci et al. 2014). Sixteen nearby stars were selected from the USNO-B1 catalog, ranging from I=11 to I=15, to provide a photometric sequence covering the full variability range, and aperture photometry was made with IRAF/apphot. The stars brighter than I ∼11 are overexposed, with a "decrease" of intensity in the very central pixels, as if they were somehow solarized. V890 Cas at maximum is brighter than this limit, showing a dip in the centre. Stars are generally not well detected below I ∼15, so fainter values are very uncertain and must be better considered as upper limits. A finding chart is shown in Fig. 1.

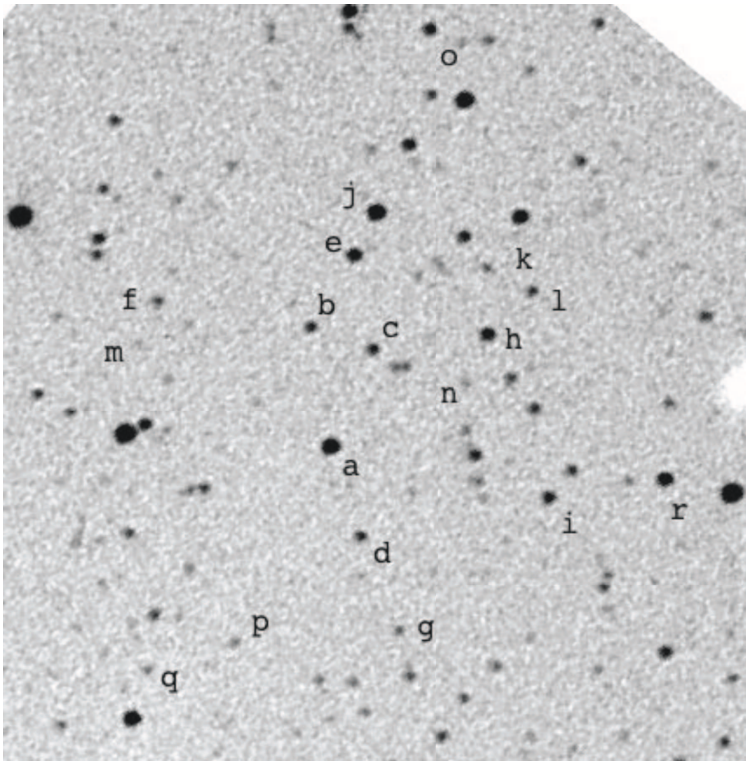

Figure 1. Finding chart of the comparison stars around V890 Cas. The variable is labelled a and is at maximum (I=11.29).

A parabolic fit to the instrumental *vs* catalog magnitudes in the useful range provided a good calibration curve, with typical rms deviations of 0.14 magnitudes. To increase the photometric accuracy, I intercalibrated the reference stars from the whole set of plates and computed again the calibration curve for each plate, finding a substantial decrease of the rms deviation (0.09) of the parabolic fit to the instrumental magnitudes. Then I compared the magnitudes so derived (Asiago magnitudes) with the original (USNO-B1) ones: the differences were always small (rms 0.065 mag) save for two stars (i and l), with differences >0.2 mag. The internal spread of the measured magnitudes of these stars in the dataset is not larger than the other ones, so there is no reason to suppose that they are variable: I assume therefore a mistake in the USNO-B1, which is anyway within the quoted catalog accuracy (0.4 mag). As a check, I made a comparison of the Asiago magnitudes with those in the UCAC4 catalog: 15 of the reference stars are present in this catalog, but only 10 have an *i'*-band magnitude. A scatter plot of the Asiago magnitudes with the UCAC4 *i'* ones gives a linear fit with slope 1, with a zero point offset of 0.75 mag, UCAC4 magnitudes being fainter: an offset is expected because the *i'* zero point is on the Sloan magnitude scale, not on the Cousins (Vega) one. The two discrepant stars (i and l) have UCAC4 magnitudes in agreement with the Asiago ones, taking the offset into account, confirming the self-consistency of our comparison sequence.

A further check was attempted with the GSC2.3.2 catalog: unfortunately only 6 stars of the sequence have an N magnitude in this catalog. On average, Asiago magnitudes are 0.3 mag brighter than the GSC2 values and a linear correlation has a slope of 1.09, again supporting the goodness of the intercalibration. V890 Cas is present in both USNO-B1 and GSC2.3.2 with magnitude 13.63 and 13.99 respectively, consistently with the offset

found for the comparison stars. Table 1 reports the J2000 coordinates (in degrees), the star labels, the original USNO-B1 I magnitudes, the intercalibrated (Asiago) I magnitudes, the UCAC4 i' magnitudes and the GSC2.3.2 N magnitudes.

The intercalibration process was also used to estimate the photometric error to be assigned to the variable at different magnitude levels. The rms deviations of each star with respect to its average value is reported in Fig. 2: as expected, it increases for fainter stars, ranging from 0.1 at I=11 to 0.2 at I=15. For I <11 the error may be larger due to saturation problems.

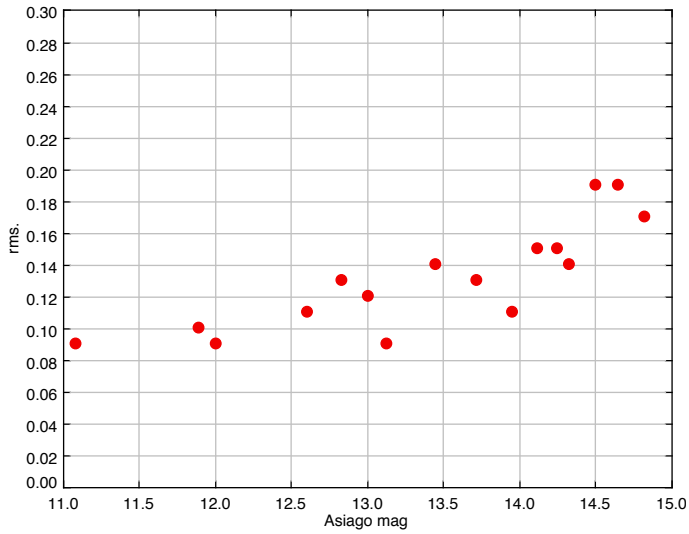

Figure 2. The trend of the rms deviation of the comparison stars as a function of the star magnitude.

Light curve

The light curve of V890 Cas between 1967 and 1975, when the coverage was well sampled (81 points), is reported in Fig. 3. The whole data set is listed in the electronic table. I have checked the quality of the plates where the star is faintest finding them of good quality.

The shape of the light curve is typical of Mira variables; both maxima and minima do not reach strictly the same magnitude in each cycle. These features are present in several other Miras (e.g. Templeton et al. 2005; Kiss & Szatmáry 2002).

To derive the best period I adopted the DFT technique (Deeming 1975): both the original Deeming's FORTRAN code and the Period04 code (Lenz and Breger 2005) were used for the analysis. The power density spectrum is reported in Fig. 4 and shows a strong main peak at 0.002028 d^{-1} (493 d), with a full width at half maximum of about 40 days. The spectrum also shows a few minor peaks: this is not unexpected because it is well known that Mira variables are not strictly periodic nor with constant overall variability amplitude: in a Fourier transform this is numerically indicated with the presence of further lower amplitude frequencies. The sampling (window) function shows basically a peak around the yearly frequency, as expected, and its alias at double frequency. A clear monthly frequency is also present, due to the fact that the Schmidt telescope was

not used around the full Moon. These frequencies do not interfere significantly with the stellar light curve frequencies.

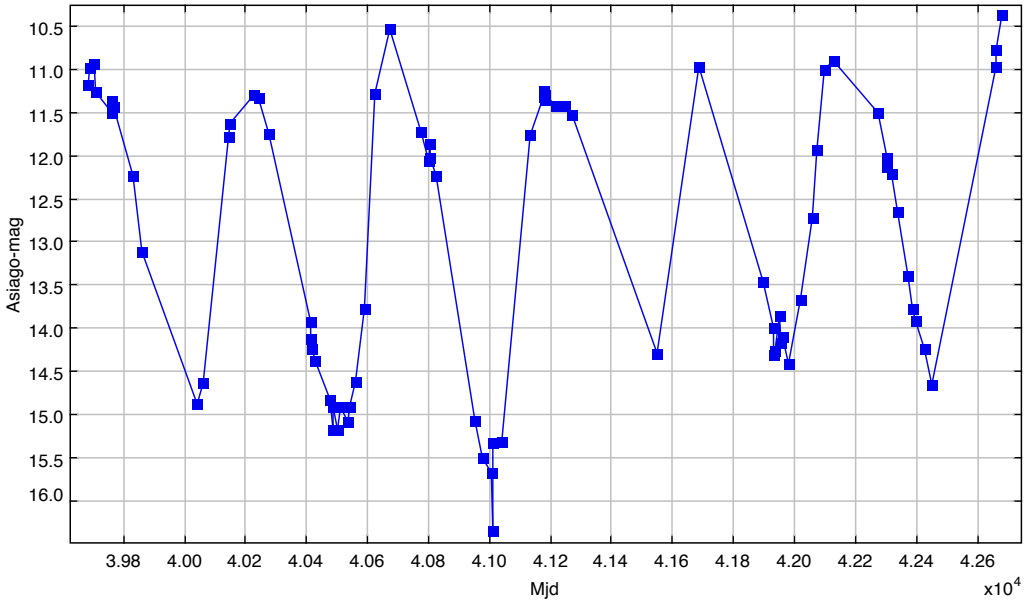

Figure 3. The light curve of V890 Cas in the years 1967-75. The observations cover 7 maxima and 2998 days.

The phased light curve based on the main frequency is reported in the lower panel of Fig. 5 and shows a dispersion larger than the expected photometric errors. Doubling the adopted period gives the phased light curve shown in the upper panel of the same figure. From the comparison of the two curves it is not evident that doubling the period produces a significant improvement.

For a deeper analysis, I subtracted the best fitting sinusoidal light curve of 493 d from the observed data and performed a new DFT analysis of the residuals: the power spectrum is shown in Fig. 6.

The strongest peak has a period of about 3700 days, longer than the available baseline and therefore of limited physical meaning: noticeably, several other low frequencies of comparable intensity are present, up to a frequency double than the basic 0.002028 d^{-1} of the original light curve. A fit of the residuals with the 3700 days period shows an rms deviation of 0.4 mag (see Fig. 7).

It seems therefore unlikely that this star undergoes amplitude variations, like e.g. R Cyg (Kiss & Szatmáry 2002).

Period check and color index

Adopting a period of 493 d, the resulting ephemeris for the maxima is MJD= $n \times 493 +$ 40228. A first check of the ephemeris was made using 6 Asiago data in the years 1981-84, which were not used in determining the period. The data of 1981 were quite fainter than the expected values, while the maximum of 1984 (n=5) was well predicted.

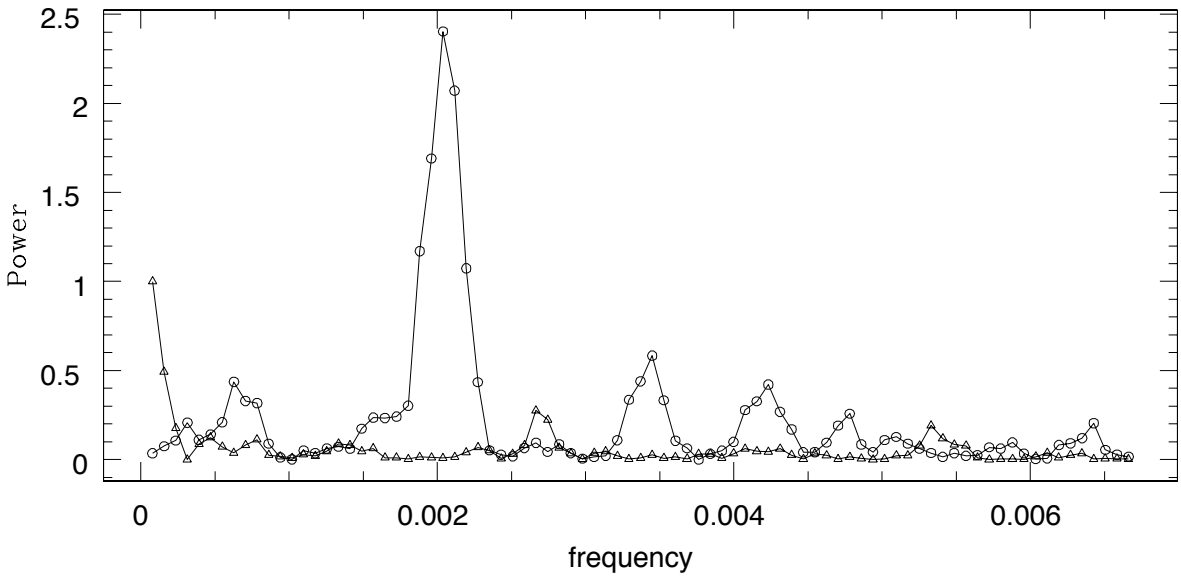

Figure 4. The power spectrum of the light curve of V890 Cas: circles refer to the star while open triangles are the window function.

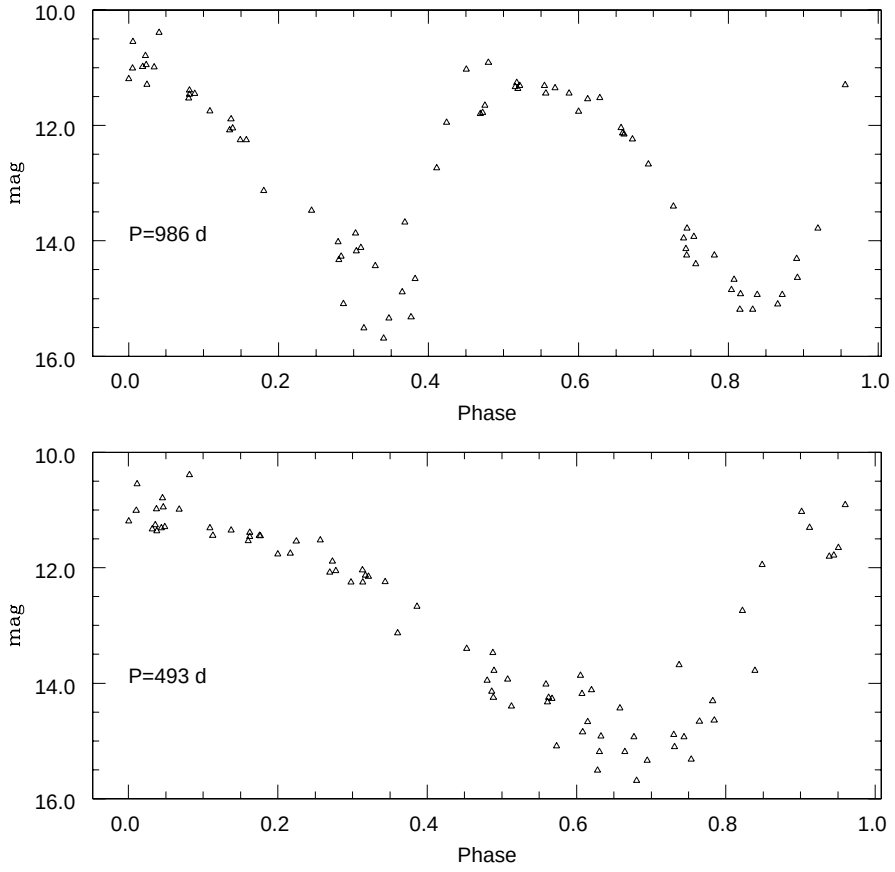

Figure 5. Lower panel: the phased light curve of V890 Cas in the years 1967-1975 adopting the period of 493 days. Upper panel: the phased light curve adopting a doubled period of 986 d.

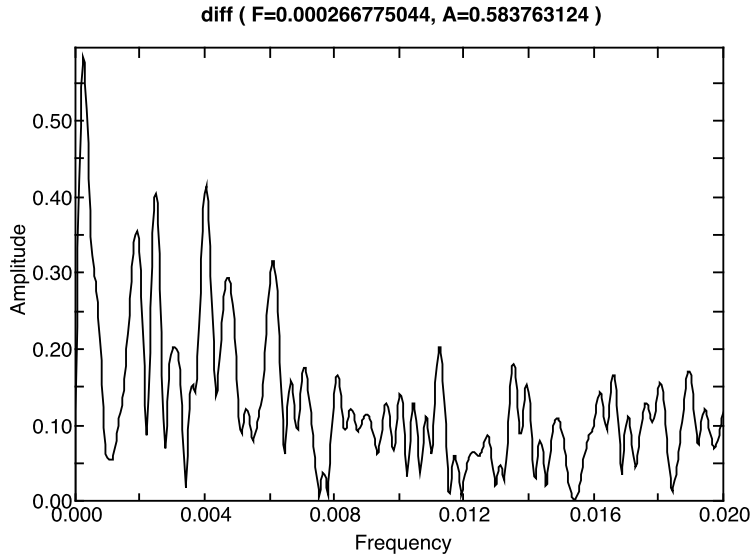

Figure 6. The power density spectrum of the light curve after subtraction of the best-fit sinusoidal curve of 493 d period.

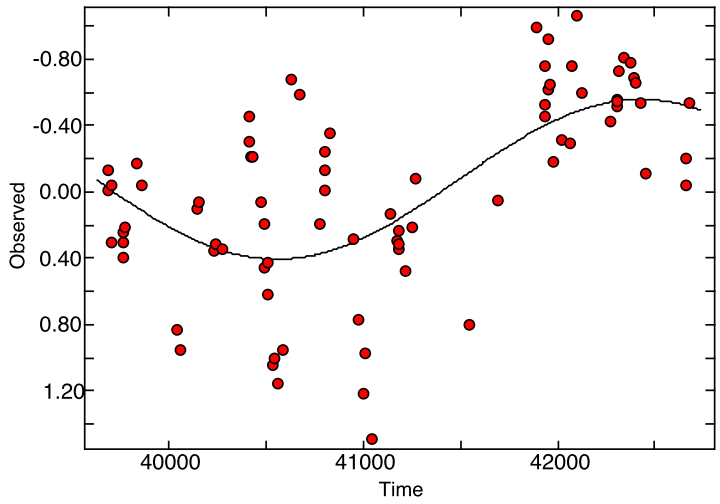

Figure 7. The light curve of V890 Cas after subtraction of the main sinusoidal component of 493 d period. Strong residuals with respect to a 3700 d long term component are evident, suggesting its limited relevance.

A second check can be done using the POSS N plate, taken on 1993-09-07 (MJD ∼49237) used for the USNO-B1 catalog: at that epoch the star was at phase 0.38 and its magnitude fits nicely in the falling branch of the phased light curve (Fig. 5). This test is however ambiguous because a good fit would also be found if the phase were around 0.7.

A better check can be done using the photometric data form VSNET archive (T. Kato, VSNET) which cover about one year and record densely a maximum around MJD 52169. This is about 24 cycles after the adopted epoch MJD 40228. These VSNET magnitudes are quoted as CCD-unfiltered, without indication of the comparison stars adopted, so it is not possible to include them in the Asiago dataset and perform an all-inclusive DFT analysis, due to the certain presence of a systematic offset in the magnitudes. Taking the above quoted ephemeris, the nearest maximum around MJD 52169 would be either at 52060 (cycle 24) or 52553 (cycle 25): agreement with the first date would require an average period of 497 d (0.00201 d^{-1}), well within the resolution of the main Asiago peak.

A DFT analysis of the VSNET data alone gives a best period of 445 d (frequency 0.002245), suggesting that small period changes at 10% level happen in this star. It is not unusual for long period variables not to be strictly periodic: as discussed above, also in the Asiago dataset there are indications in this sense.

I looked for the star in the Asiago blue plates around the maxima but it was always below the detection threshold (B∼18).

A measure of the color index of V890 Cas around maximum can be made using a plate taken on 1984-12-25 in the R band (103aE+RG1): in the same night, plates were taken also in the other bands (U, B, V) but the star was not visible. Using the USNO-B1 $R1$ magnitudes for comparison the result is R=16.21, giving $R - I$=4.99 (±0.3), a result fully consistent with the very late spectral type of the star. This is also in broad agreement with the result reported by Wright et al. (2009) $r' - i'$=5.46, which correspond to $R_C - I_C$=5.67 (Jester et al. 2005), measured when the star was in a fainter (i'=14.7) and probably cooler state.

Overall, the ∼17 years time span of the Asiago archive plates fully support the Mira-type variability of V890 Cas indicated by the VSNET data.

Table 1. Comparison stars for V890 Cas

RA2000 degrees	DEC2000 degrees	ident	USNO I mag	Asiago I mag	UCAC4 i' mag	GSC2.3.2 N mag
16.9424	+59.0800	b	13.00	12.97	13.769	
16.9136	+59.0724	c	12.71	12.80	13.593	
16.9239	+59.0281	d	13.16	13.10		
16.9198	+59.0966	e	11.81	11.88	12.507	
17.0143	+59.0882	f	13.74	13.70	14.349	
16.9088	+59.0052	g	13.99	14.12	14.889	14.28
16.8588	+59.0755	h	11.97	11.98	12.645	
16.8338	+59.0353	i	12.23	12.58	13.320	
16.9092	+59.1068	j	11.21	11.09	11.248	
16.8576	+59.0917	k	13.94	13.94		14.22
16.8365	+59.0854	l	13.65	13.43	14.148	
17.0249	+59.0777	m	14.98	14.90		15.37
16.8704	+59.0640	n	14.58	14.53		14.87
16.8639	+59.1466	o	14.76	14.70		
16.9862	+59.0045	p	14.32	14.35	15.010	14.63
17.0277	+58.9988	q	14.28	14.26		14.55

References:

Deeming, T. J., 1975, *Ap&SS*, **36**, 137
Gasperoni, V., Maffei, P., Tosti, G., 1991, *IBVS*, **3573**
Jester, S., Schneider, D. P., Richards, G. T., et al., 2005, *AJ*, **130**, 873
Kato, T., `http://www.kusastro.kyoto-u.ac.jp/vsnet//Mail/vsnet-newvar/msg01062.html`
Kazarovets, E. V., et al., 2003, *IBVS*, **5422**
Kiss, L. L., & Szatmáry, K., 2002, *A&A*, **390**, 585
Lenz, P. & Breger M., 2005, *CoAst*, **146**, 53
Maffei, P., 1975, *IBVS*, **985**
Maffei, P., 1977, *IBVS*, **1302**
Nesci, R., Bagaglia M., Nucciarelli G., 2014, Astroplate 2014, Edited by Linda Mišková and Stanislav Vítek. Published by the Institute of Chemical Technology, Prague, 2014, p.75
Samus, N. N. et al., 2013, VizieR On-line Data Catalog B/gcvs
Templeton, M. R., Mattei, J. A., Willson, L. A., 2005, *AJ*, **130**, 776
Wright, N. J., Barlow, M. J., Greimel, R., et al., 2009, *MNRAS*, **400**, 1413

COMMISSIONS 27 AND 42 OF THE IAU
INFORMATION BULLETIN ON VARIABLE STARS

Number 6171

Konkoly Observatory
Budapest
1 June 2016

HU ISSN 0374 – 0676

THE AD BINARY IN THE MULTIPLE SYSTEM η Mus

BLACKFORD, M.G.[1]; BUTLAND, R.J.[1,2]; BUDDING, E.[1,2,3,4]

[1] Variable Stars South (VSS); Royal Astronomical Society of New Zealand, Private Bag, Wellington

[2] Department of Physics and Astronomy, University of Canterbury, NZ

[3] School of Chemical and Physical Sciences, Victoria University of Wellington, Private Bag, Wellington

[4] Carter Observatory, 40 Salamanca Rd., Kelburn, Wellington, NZ

Introduction

An account of the multiple star η Mus (HD 114911, HIP 64661, HR 4993) was given by Budding et al. (2013). The light is dominated by the young close binary ($V \sim 4.8$-4.9, $B-V \approx -0.08$, $U-B \approx -0.34$), which is a B8V type partially eclipsing system composed of two stars of measurably the same mass though with apparently somewhat different rotation speeds (see also Bakış et al. 2007). The 7.3 magnitude visual companion η Mus B (CD −67 1384B) appears about 58″ NW of the close binary, while a 10th mag (J) closer companion (η Mus C = DUN 131C) is found ∼3″ SE of the main pair. Butland & Budding (2011) announced the likely presence of another, optically unresolved, star in the system, sufficiently close to the central binary to disturb its γ-velocity on a ∼2000 d period. The sky location, HIPPARCOS distance of 124 ± 9 pc, and proper motions ($\mu_\alpha \cos\delta = -36.92$; $\mu_\delta = -10.63$ mas y^{-1}), make the system a likely member of the Lower Centaurus Crux (LCC) concentration (Blaauw 1964; de Zeeuw et al. 1999) of the Sco-Cen OB2 Association, within the Gould's Belt giant star formation region (Nitschelm 2004), and so of interest in the context of stellar formation and dynamical interaction theory.

After considering HIPPARCOS data, other sources and background literature, Budding et al. (2013) gave an updated ephemeris for the eclipsing system as

$$\text{Min I} = 2453874.2708 + 2.396318E. \quad (1)$$

A brief discussion of the (∼12 km s^{-1}) difference in radial velocity between the A and B components found by Bakış et al. (2007) was given by Butland & Budding (2011), who argued that this difference would probably disappear when averaged over the orbital period of the new star ('η Mus D'). Butland & Budding, however, appealed for further observations to clarify details of the poorly known properties of this inner system.

New data and analysis

The VSS group, affiliated to the RASNZ, responded with timings of the eclipse minima, summarized in Table 1. These findings are plotted in Fig. 1, together with a theoretical curve showing calculated times of minima for corresponding phases of the deduced orbit of the close binary η Mus A about the centre of gravity of the AD putative binary. Further details on these timings are available from the VSS via M.G.B.

Table 1: Adopted times of minimum with estimated errors

Date	Type	HJD (obs.)	Error
110610	Sec	2455723.0212	0.0024
110803	Pri	2455776.9387	0.0027
120402	Sec	2456020.1765	0.0020
120508	Sec	2456056.1213	0.0021
120607	Pri	2456086.0760	0.0020
130312	Pri	2456364.0529	0.0021
140515	Pri	2456792.9890	0.0016
150706	Pri	2457209.9407	0.0016
160228	Pri	2457447.1754	0.0014
160305	Sec	2457453.1664	0.0015

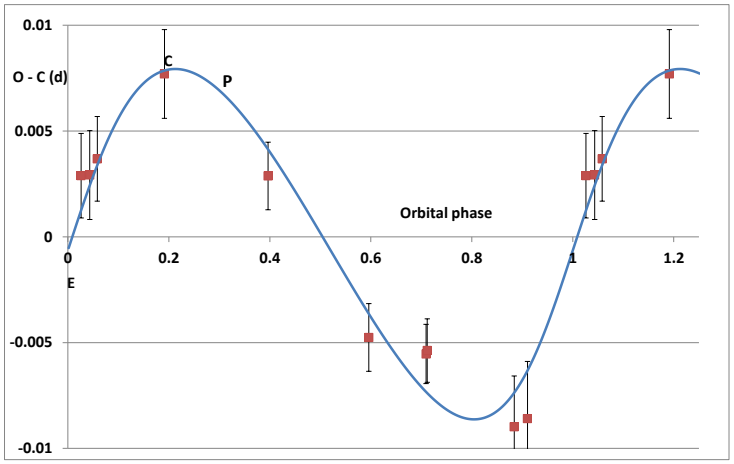

Figure 1. Optimal curve fitting applied to the O–C data for η Mus, as collected by M.G.B. The model orbit is phased from the reference epoch E. Its shape depends on the eccentricity parameters (e, M_0), which locate the periastron at P. Model phases are related to the observed times of minima, using the epoch and period given in Table 1, through the displacement $\Delta\phi_0$ from the conjunction at C.

In the meantime, further observations of the system were made using the HERCULES spectrograph and 1m McLellan Telescope of the Mt John University Observatory. These

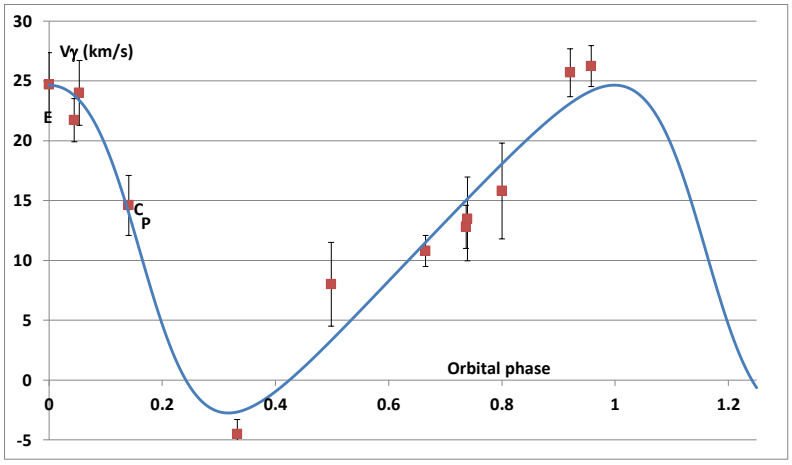

Figure 2. Optimal curve fitting applied to measured γ-velocities for η Mus over the last 10 years. Observational phases are reckoned from the epoch E, here at the origin, but displaced from the conjunction C by about the same shift $\Delta\phi_0$ as for the O–Cs. The periastron position P, dependent on the fitted eccentricity parameters, appears closer to the conjunction C than in the O–C fitting.

are shown in Fig. 2, together with a model similarly derived from optimal curve-fitting procedures. The corresponding data are listed in Table 2. The masses of the components of η Mus being measurably the same, the system velocity can be easily determined by taking the average of line pairs towards elongation. Typically 4 HeI lines were used for this purpose, together with H_β; lines which are conveniently located in the échelle field (see Budding et al. 2013, for further details).

The two programs FITRV and FITOMC optimize separate sets of fitting parameters, but of course these should be related as they refer to the same orbit. Results are thus collected together in Table 3. The epoch of equation (1) was adopted as a reference point for both analyses, as was a period of 2090 d for the orbit of η Mus AD, derived from averages of preliminary fittings of both data-sets. Even so, small differences arise from the separate fittings: for example, the (projected) distance travelled in the period $P_{\rm AD}$ with the spectroscopic velocity amplitude $K_{\rm A}$ is greater than goes with the photometric light travel amplitude $A \sin i$. Parameter errors on the order of 10% may accommodate such differences, though the scale of errors estimated from the fitting programs (Table 1) are somewhat lower than that. Note that the inclination i is not derivable from O–C or radial velocity data. The value in Table 1 comes from photometric analysis of η Mus A given by Budding et al. (2013), and adopted for the η Mus AD orbit.

The fittings agree on a moderate eccentricity to the orbit, and the value $e = 0.29$, retained from Butland & Budding (2011), is supported by the present data-sets. The shapes of the curves are dependent on the orientation parameter (cf. Irwin 1952a,b), usually associated with the longitude of periastron ω, but the related mean anomaly at the conjunction phase (M_0: inferior conjunction of the less massive η Mus D) is more convenient in the computation. There is some difference in the preferred orientation of the ellipse between the two analyses, the v_γ periastron seemingly occurring $\sim$0.1 in phase before that of the O–Cs (Figs. 1 & 2). The values of M_0 and its corresponding ω given in Table 1 are then adopted means. The shift of the apsidal line with respect to the line

Table 2: Adopted system (γ) radial velocities with estimated errors at the listed (mean) heliocentric Julian dates. Also shown is the number (No.) of separate spectrograms used for each mean date of observation.

Mean HJD 2450000+	No.	γ vel.	Error
3874.27	16	24.7	2.7
3967.31	1	21.7	1.8
3985.88	1	24.1	2.7
5413.59	2	12.8	1.8
5418.79	3	13.5	3.5
5546.09	2	15.8	4.0
5797.82	3	25.7	2.0
5875.99	6	26.1	1.7
6258.11	2	14.6	2.5
6669.74	3	-4.5	1.2
7005.64	3	8.0	3.5
7354.35	3	10.8	1.3

of sight being set, the angle $\Delta\phi_0$ relates this latter reference direction to the epoch from which observational phases are initially reckoned. Both data-sets point to $\Delta\phi_0 \approx 300$ deg from the conjunction. The positive shift in the average line of sight position of the AD system to the focus of η Mus A's ellipse Δz_0 is about 0.001 light days greater than would correspond with Irwin's (1952a) formula ($Ae \sin\omega \sin i$). This is less than the O–C mean timing error ($\delta\tau$), but it may indicate a small error in the adopted period of η Mus A.

Although the separate data-sets and analyses produce comparable results, the scatter of the observed points in average-parameter curves is larger than expected and we cannot rule out some additional variation beyond a two-body model in the AD system. This point, and the minor inconsistencies in the present relatively small radial velocity and O–C data-sets, should be checked on the basis of more observations, and this interesting multiple star is worthy of continued review.

Acknowledgement: The authors would like to thank the Director and Staff of the Mt John University Observatory for supporting the petrographical observations reported in this paper, as well as the Director of VSS for similar photometric support to our Southern Binaries Programme, of which these studies of η Mus are a part.

Table 3: Orbital parameter set for η Mus A's projected orbit about the centre of gravity of the AD system from the combined O–C and γ-velocity data. The feasible datum error estimates δv_γ in velocity and $\delta\tau$ in time give rise to acceptable χ^2/ν values for the fittings shown in Figs. 1 & 2, but these would deteriorate to $\chi^2/\nu \sim 2$ or greater, with the average M_0 and $\Delta\phi_0$ values of the table, suggesting higher datum errors than assigned.

Parameter	Value	Error
Epoch E (HJD)	2453874.2708	
$P_{\rm AD}$ (d)	2090	50
$K_{\rm A}$ (km/s)	13.7	1.2
$v_{\gamma{\rm AD}}$	11.3	0.8
A sin i (AU)	1.50	0.13
i (deg)	77.9	
e	0.29	0.1
ω (deg)	40	20
M_0 (deg)	30	20
$\Delta\phi_0$(deg) (O–C)	300	10
Δz_0 (l.d.)	0.0028	0.0003
δv_γ (km/s)	2.5	
$\delta\tau$ (d)	0.002	
χ^2/ν (v_γ)	1.08	
χ^2/ν (O–C)	1.17	

References:

Bakış, V., Bakış, H., Eker, Z., Demircan, O., 2007, *MNRAS*, **382**, 609
Blaauw, A., 1964, *IAUS*, **20**, 50
Budding, E., Butland, R.J., Blackford, M., 2013, *PASA*, **30**, 37
Butland, R., Budding, E., 2011, *IBVS*, **6004**
de Zeeuw, P.T., Hoogerwerf, R., de Bruijne, J.H.J., et al., 1999, *AJ*, **117**, 354
Irwin, J.B., 1952a, *ApJ*, **116**, 211
Irwin, J.B., 1952b, *ApJ*, **116**, 218
Nitschelm, C., 2004, *ASPC*, **318**, 291

COMMISSIONS 27 AND 42 OF THE IAU
INFORMATION BULLETIN ON VARIABLE STARS
Number 6172

Konkoly Observatory
Budapest
20 June 2016
HU ISSN 0374 – 0676

LONG-TERM RADIAL VELOCITY MONITORING OF THE HeI 6678 LINE OF ζ TAURI

POLLMANN, ERNST

International Working Group ASPA, Emil-Nolde-Str. 12, 51375 Leverkusen, Germany

Introduction

The binary star ζ Tau, one of the brightest Be stars in the northern sky, shows cyclic behaviour in the radial velocity (RV) variations on several distinct time scales. It is also a spectroscopic binary with a 133 d orbital period established by Harmanec (1984). Its orbital RV variations are superimposed on the cyclic long-term and short-term ones. ζ Tau also shows cyclic behaviour in the radial velocity of the HeI 6678 Å absorption line. As far as we know the first long-term investigation (time period 1993–2005) of the RV of the HeI 6678 absorption line has been performed by Stefl et al. (2007). That monitoring until about 2007 led to the estimation of a long-term period of 1503 d.

Observations

The spectra for the RV measurements of the HeI 6678 line presented here were taken with 20 cm Newtonian- and 40 cm Schmidt-Cassegrain telescopes. Spectrographs with spectral resolving power of 10000 to 20000 were used. The signal to noise ratio of these spectra was of the order of magnitude $S/N = 200-300$. The spectra have been reduced with standard procedures (instrument response, normalisation, wavelength calibration) by use of the program VSPEC[1]. The evaluation of the heliocentric RV was performed by the profile mirror method. This method measures the Doppler shift of spectra by correlation of the spectral line with their mirroring around the laboratory wavelength, and is particularly suitable for the evaluation of asymmetrical lines within exactly specified profile ranges.

Long-term changes

We will compare the 1503 d period of Stefl et al. (2007) with our results covering approximately 15 years (December 2000 to February 2016). Such a long investigation interval was possible because we combine radial velocity data from Ruzdjak et al. (2009) with our data of the ARAS group[2]. This long-term monitoring is shown in Fig. 1. In order to

[1] http://www.astrosurf.com/vdesnoux
[2] http://www.astrosurf.com/aras/

recognize the separate cyclic behaviour of the Ruzdjak et al. (2009) data and the ARAS data, the corresponding separate phase plots are shown in Figs. 2 and 3. The overlay of both periods is shown in Fig. 4. For this analysis the program AVE[3] was used.

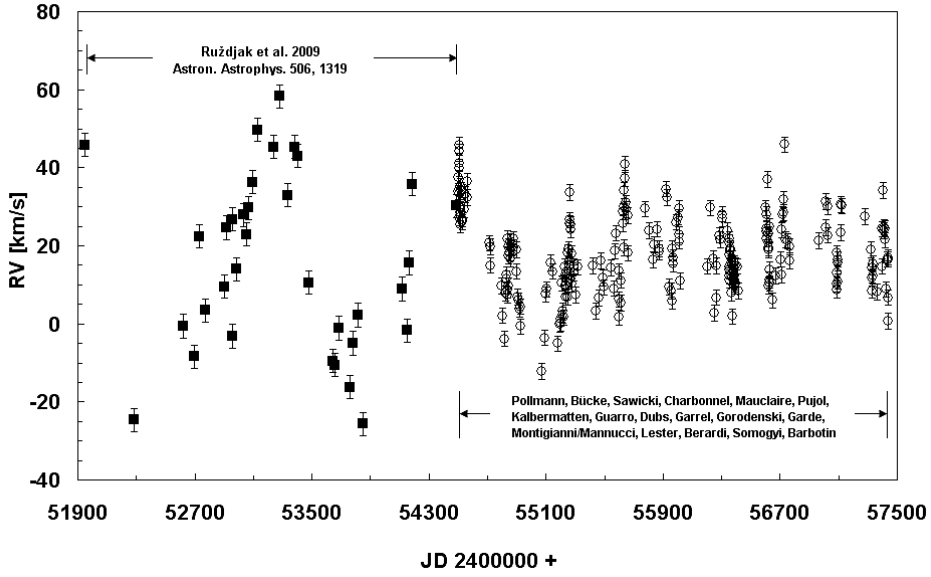

Figure 1. RV Long-term monitoring of the HeI 6678 line from December 2000 to February 2016.

The RV comparison of these three time intervals, P = 1503 d for 1993–2005 (Stefl et al. 2007), P = 1325 d for 2001–2008 (Ruzdjak et al. 2009), and P = 1190 d for 2008–2016 (this paper), points out that the long-term RV period has constantly decreased at least since 1993 .

Orbital variations

One of the most interesting studies of the RV variations in the spectrum of ζ Tau is the paper by Ruzdjak et al. (2009). We were fortunate to start a long-term observing campaign of the HeI 6678 line at the time when the investigations of the researchers of the mentioned paper ended, approximately at JD 2454500. Our findings on the HeI 6678 RV orbital variability of 132.2 d ($\pm$ 0.8) and 131.3 d ($\pm$ 0.9) received with different analysis programs (Pollmann et al. 2012) are very close to those of Ruzdjak et al. (2009) for the most important parameters.

Short-term variations

The HeI 6678 absorption line of ζ Tau consists of a strong central shell absorption, which is overlaid by a rotation-broadened photospheric component with a projected rotation velocity $v \sin i$ = 320 km/s. The profile of this absorption line shows weak but sharp features which cross periodically through the entire line profile. These features are observed as small absorption "bumps", generally moving through the line profile from blue to red.

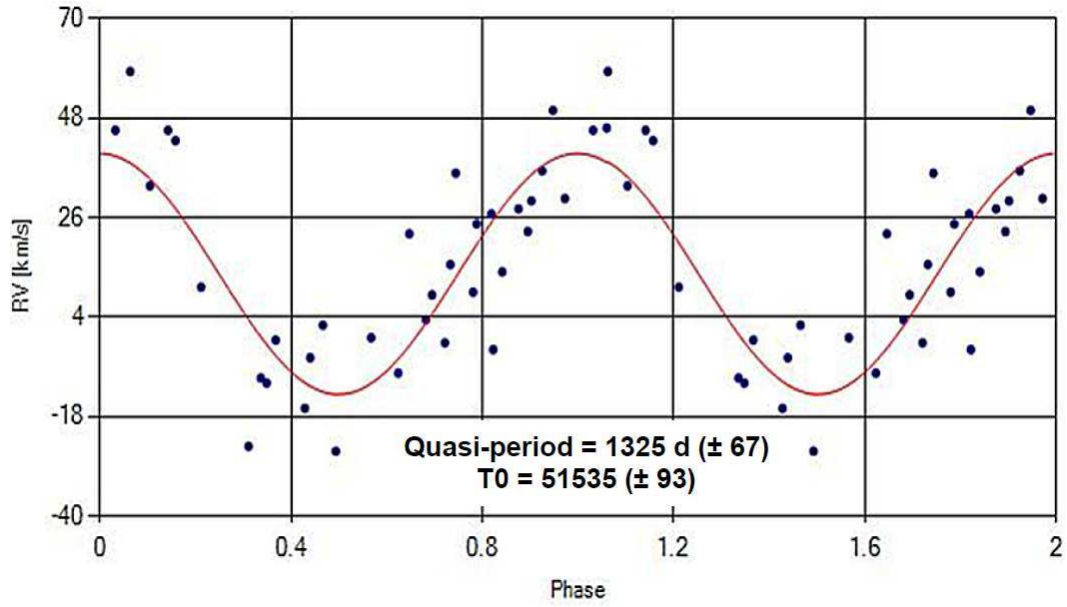

Figure 2. RV variation (period = 1325 d (± 67), starting from T_0 = JD 2451535) of Ruzdjak et al. (2009) data in Fig. 1.

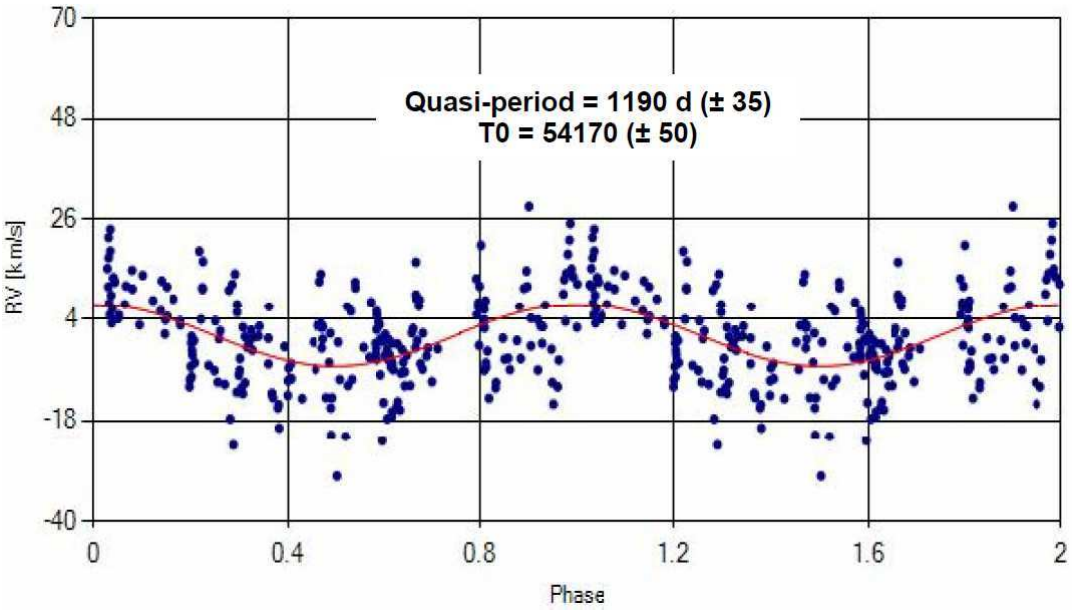

Figure 3. RV variation (period = 1190 d (± 35), starting from T_0 = JD 2454170) of ARAS data in Fig. 1.

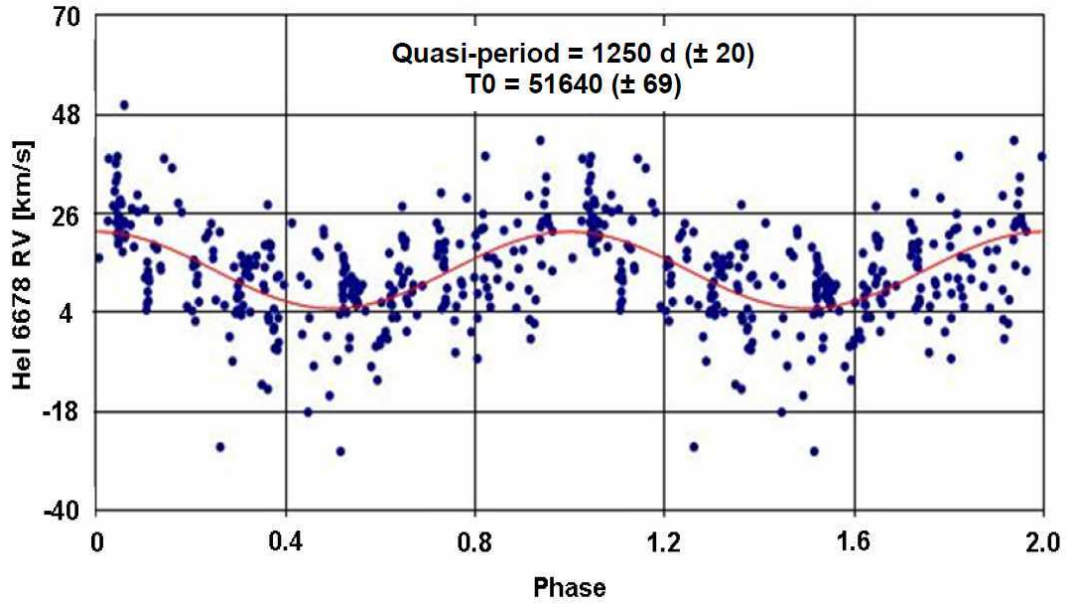

Figure 4. RV variation (period = 1250 d (± 20), starting from T_0 = JD 2451640) of the ARAS & Ruzdjak et al. (2009) data in Fig. 1.

Such a profile could be the result of stellar rotation and dark or bright regions (star spots) on the surface of the star (Yang et al. 1990; Balona 1991, 1995), or by circumstellar material orbiting the primary component (Vogt & Penrod 1983; Harmanec 1989). Local density enhancement in certain regions between the circumstellar gas disk and the star could be another possible cause of this phenomenon.

Short-term RV measurements of the HeI 6678 line have been performed by the author with a LHIRES III spectrograph (R=17000) at the C14 telescope of the Vereinigung Sternfreunde Köln (Germany) on three nights: 2012/11/16, 2013/01/11 and 2013/01/12. We took ten individual spectra with exposure times between 300–350 s. The signal to noise ratio of the sum spectrum was in general > 1000.

The results of these RV measurements are shown in Figs. 5a-b and 6a-b. Figure 5a (top) shows the RV short-term behaviour of the HeI 6678 line during the nights 2012/11/16, 2013/01/11 and 2013/01/12. Figure 5b (middle) shows the result of a period analysis of the RVs, i.e. 0.499 days. Figure 6a (top) shows the RV short-term behaviour of the HeI 6678 line on two nights: 2013/12/02 and 2013/12/03. Figure 6b (middle) shows the result of a period analysis of the RVs, i.e. 0.469 days period, and Fig. 6c (bottom) shows the corresponding phase plot.

The spectrograph used for these measurements was firmly mounted on the telescope and moved with it. In order to take into account possible effects of flexture, the author measured the RV of the Hα line in the spectrum of Aldebaran (α Tau, dec = +16°) on a similar hour angle. The results are shown in Fig. 7.

The spectra were likewise evaluated with the mirror method. As can be seen, there is a small RV trend with increasing hour angle, in the order of 1km/s, a magnitude (smaller than the RV variation) which is negligibly small compared with the RV variability in ζ Tau. The error bar indicates the reproducibility accuracy of repeated evaluations (3 times).

[3] `http://astrogea.org/soft/ave/aveint.htm`

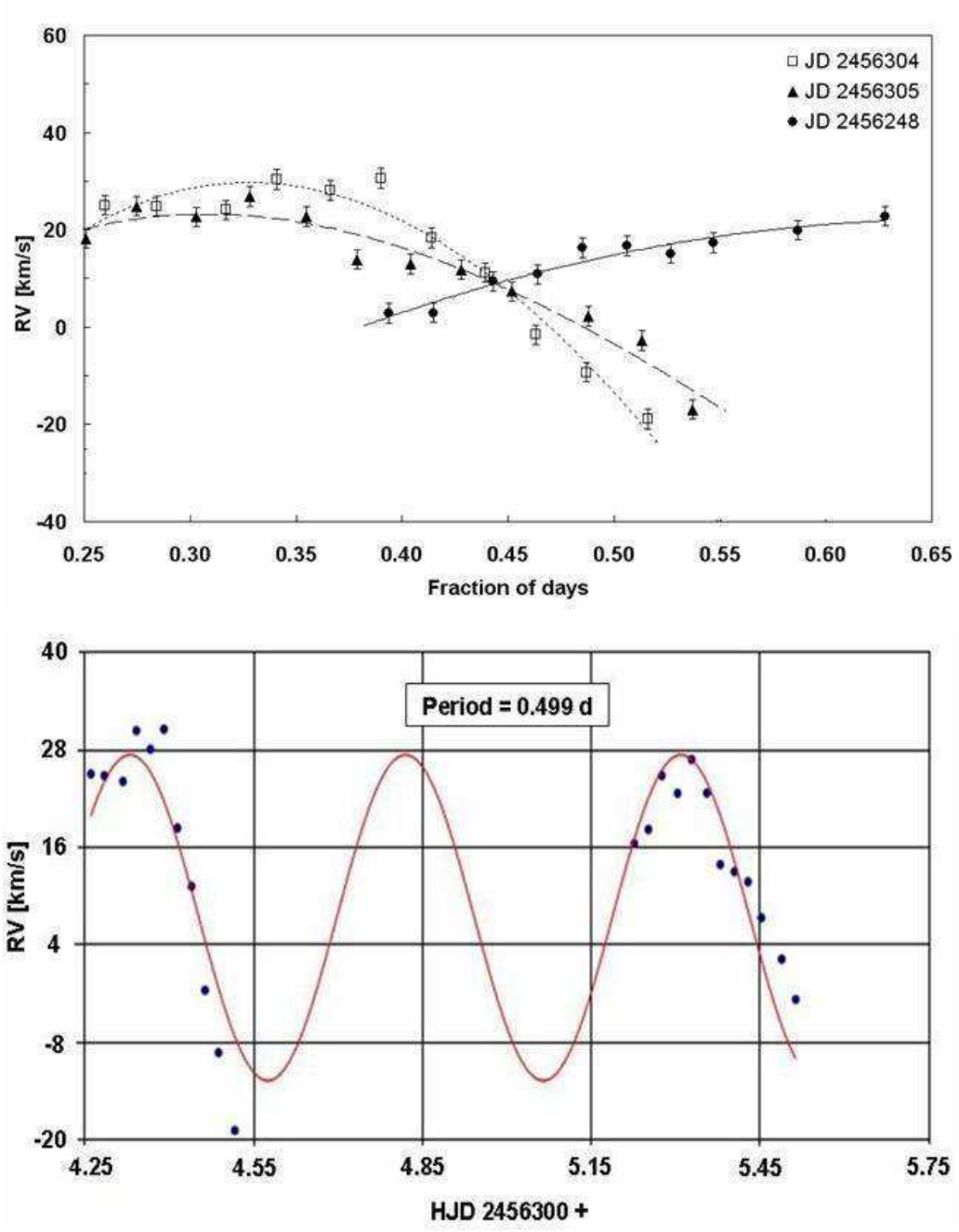

Figure 5. Short-term RV observations of the HeI 6678 line on three nights: 2012/11/16, 2013/01/11 and 2013/01/12.

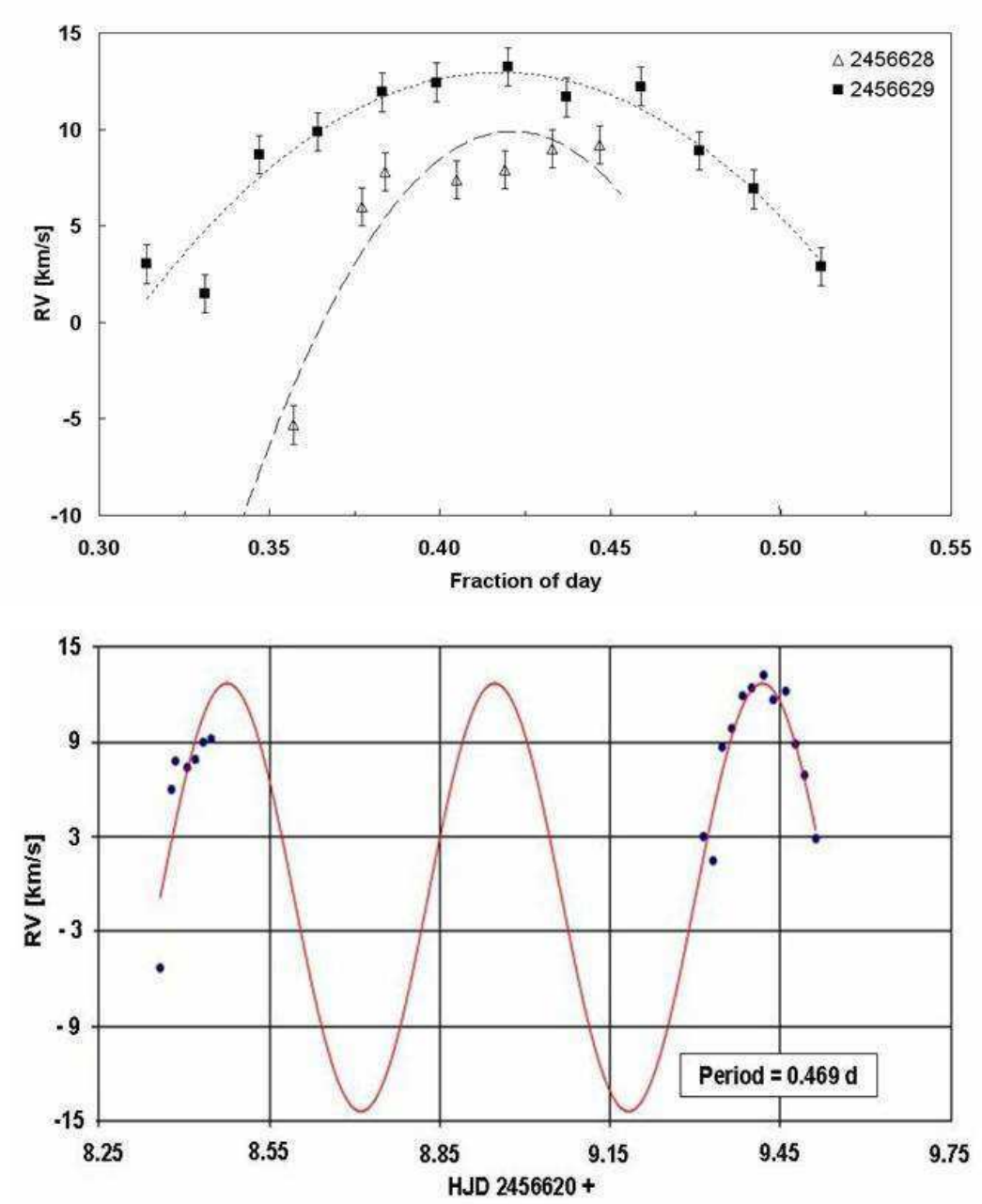

Figure 6. Short-term RV observations of the HeI 6678 line on two nights: 2013/12/02 and 2013/12/03.

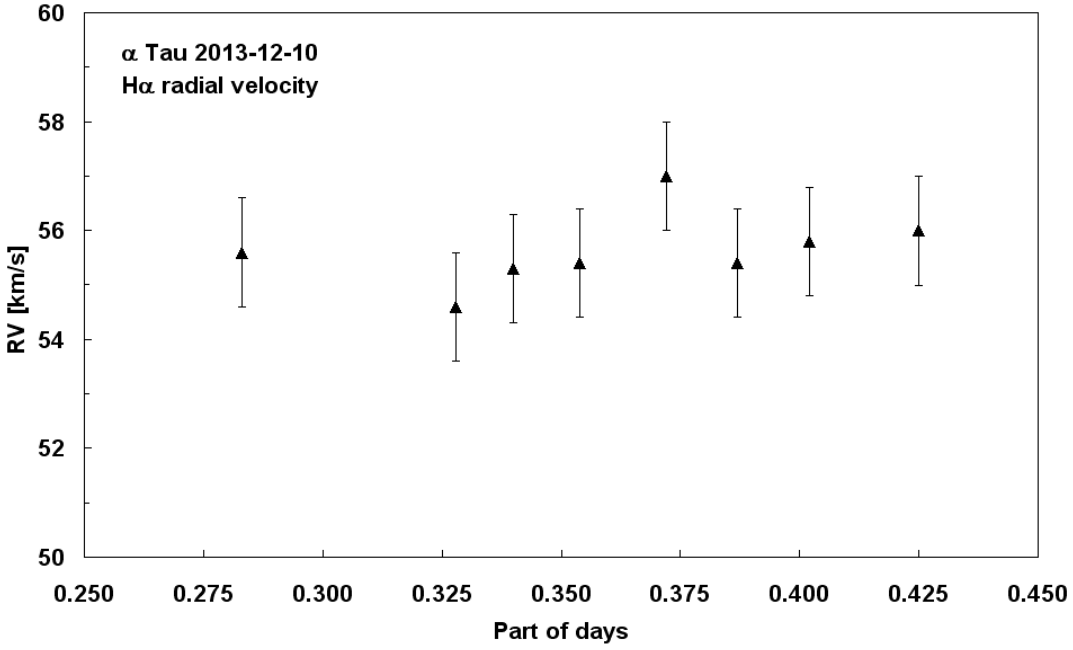

Figure 7. Check measurements of the RV stability at α Tau for comparable hour angles of ζ Tau.

Discussion

Attempts to detect long-term cyclic RV variations of the HeI 6678 absorption line in the spectrum of ζ Tau (Stefl et al. (2007) found quasi-period = 1503 d; Ruzdjak et al. (2009) found quasi-period = 1325 d ($\pm$ 67); we found quasi-period = 1190 d ($\pm$ 35)) points out that the long-term RV period at least since 1993 has constantly decreased. We also confirmed the overlaid medium-term RV period of 133 d corresponding to the orbital period of the binary already established in the past by Harmanec (1984), Ruzdjak et al. (2009), Pollmann, Mauclaire & Bücke (2012). Finally, we also distinguished short-term RV variations. All, long-, medium- and short-term variations have to be taken into account for a complete study of the variability of ζ Tau.

Whether the short-term cyclic variations we found are connected with the assumed combination of stellar rotation and dark or bright ranges (spots) on the surface, or with orbital circumstellar material around the primary star (as mentioned above) remains unclear. We cannot conclude on the nature of these variations from a study of just one line, therefore we intend to extend this study in the future.

Acknowledgements: I am grateful to Sara and Carl Sawicki (Alpine, Texas, USA) for their helpful improvements and suggestions in language. I am grateful too to Prof. Dr. Anatoly Miroshnichenko (University of North Carolina at Greensboro) for his comprehensive support improving this work in several aspects.

References:

Balona, L. A. 1991, Proc. ESO Conf. and Workshop 36, Rapid Variability of OB Stars: Nature and Diagnostic Value, ed. D. Baade (Garching: ESO), 249
Balona, L. A. 1995, *MNRAS*, **277**, 1547
Harmanec, P. 1984, *Bull. Astron. Inst. Czechoslovakia*, **35**, 164
Harmanec, P. 1989, *Bull. Astron. Inst. Czechoslovakia*, **40**, 201
Pollmann, E., Mauclaire, B., Bücke, R., 2012, *IBVS*, **6099**
Ruzdjak, D. et al. 2009, *A&A*, **506**, 1319
Stefl, S. et al. 2007, *ASP Conf. Ser.*, **361**, 274
Vogt, S. S., Penrod, G. D. 1983, *ApJ*, **275**, 661
Yang, S., Walker, G. A. H., Hill, G. M., Harmanec, P. 1990, *ApJS*, **74**, 595

COMMISSIONS 27 AND 42 OF THE IAU
INFORMATION BULLETIN ON VARIABLE STARS

Number 6173

Konkoly Observatory
Budapest
21 June 2016

HU ISSN 0374 – 0676

SPOTTED STARS AS CEPHEID IMPOSTORS OBSERVED WITH K2

VIDA, K.[1]; PLACHY, E.[1]; MOLNÁR, L.[1]; KRISKOVICS, L.[1]; KLAGYIVIK, P.[1]; HAJDU, T.[2]; KOVÁCS, O. E.[1,2]; SZABÓ, R.[1]

[1] Konkoly Observatory, Research Centre for Astronomy and Earth Sciences, Konkoly Thege Miklós út 15-17, H-1121 Budapest, Hungary

[2] Department of Astronomy, Eötvös University, Pázmány Péter sétány 1/A, H-1117 Budapest, Hungary

E-mail: vidakris@konkoly.hu, plachy@konkoly.hu

1 Introduction

Distinguishing Cepheids from rotational variables or eclipsing binary stars in ground-based photometric measurements is often a difficult task. Recent space missions revealed that a high percentage of stars labeled as Cepheid candidates based on sparse photometric survey data are misclassified (Szabó et al. 2011, Poretti et al. 2015). In this paper we present the analysis of three stars that were previously identified, erroneously, as potential Cepheid variables. The stars were observed by the *Kepler* space telescope in Campaigns 0 and 2 of the K2 mission (Howell et al. 2014).

The targets were selected based on existing classifications in ground-based surveys (Molnár et al. 2014, Plachy et al. 2016). All of three stars were observed by the All Sky Automated Survey[1] (ASAS; Pojmanski 1997). ASAS 064003+2825.6 was classified as a possible classical Cepheid, ASAS J162402-2910.8 as a Type II Cepheid, while ASAS J162308-2301.0 as either a Type II Cepheid or an eclipsing binary (Pojmanski 2002). However, the latter two stars were also identified as optical counterparts of the X-ray sources 1RXS J162402.5-291042 and 1RXS J162308.8-230046, respectively, by Berdnikov & Pastukhova (2008), and a new identification as RS CVn-type variables was suggested.

2 Data reduction

We applied the Extended Aperture Photometry (Klagyivik et al. 2016) on target pixel files provided by NASA Kepler Guest Observer Office to minimize the effects of spacecraft movements and collect all the available flux using the PyKE software (Still & Barclay 2012). We did not apply self-flat-fielding (SFF) correction to the data. The SFF algorithm in PyKE uses smoothing to separate the (slower) stellar variation from the instrumental variations, but we could not satisfactorily smooth out the flares and fit the periodic variations simultaneously. Light curves with EPIC (Ecliptic Plane Input Catalog) numbers and folded light curves are displayed in Fig. 1.

[1] http://www.astrouw.edu.pl/asas/

ASAS J064003+2825.6 (EPIC 202064452) was observed during Campaign 0 that was a full-length engineering test run for the K2 mission. During the first 16 days the telescope did not achieve fine pointing that led to gaps in the data and somewhat lower photometric accuracy. *Kepler* eventually went into safe mode that lasted for 24 days. After the observations restarted, data were collected for an additional 35 days, this time in fine pointing mode. As the star fell on one of the outer modules, its position varied in excess of 2 pixels due to the attitude changes of *Kepler*, causing small jumps and outlier points in the light curves coincident with the attitude control maneuvers. These jumps are also present in the detrended light curve produced by Armstrong et al. (2015).

ASAS J162402-2910.8 (EPIC 202571062) and ASAS J162308-2301.0 (EPIC 204264833) were observed during Campaign 2. *Kepler* collected data for 78 days, almost continuously. The first star was close to the edge of the field-of-view, therefore suffers from jumps and outliers, whereas the second was near to the center and is mostly unaffected by instrumental errors.

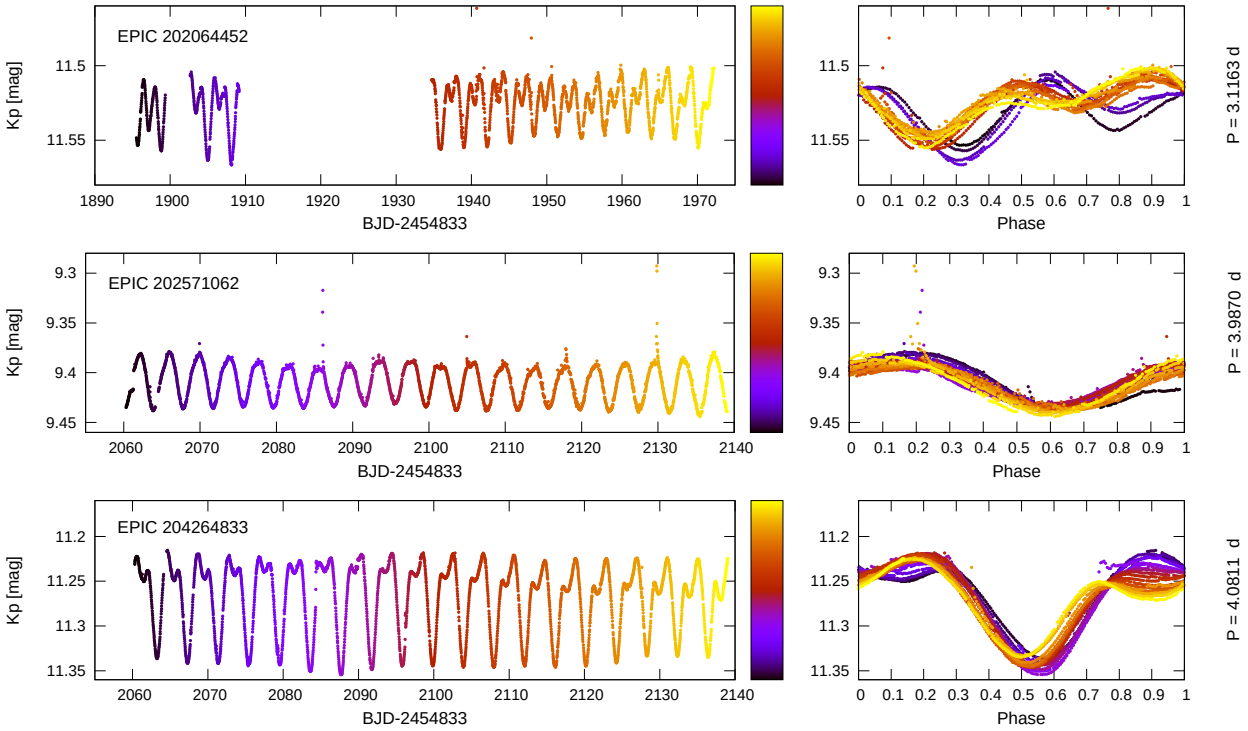

Figure 1. Light curves and folded light curves. Colors indicate the time evolution of the light curves. Periods were calculated with the Period04 software (Lenz & Breger 2005).

3 Analysis

The visual inspection of *Kepler* light curves suggests that these stars are not Cepheids: the cycle-to-cycle changes in the light curve shapes is typical of spotted stars (Kővári & Oláh 2014). In order to support the classification of the target stars we calculated the O–C values based on the times of minima in the light curves, that are presented in Fig. 2.

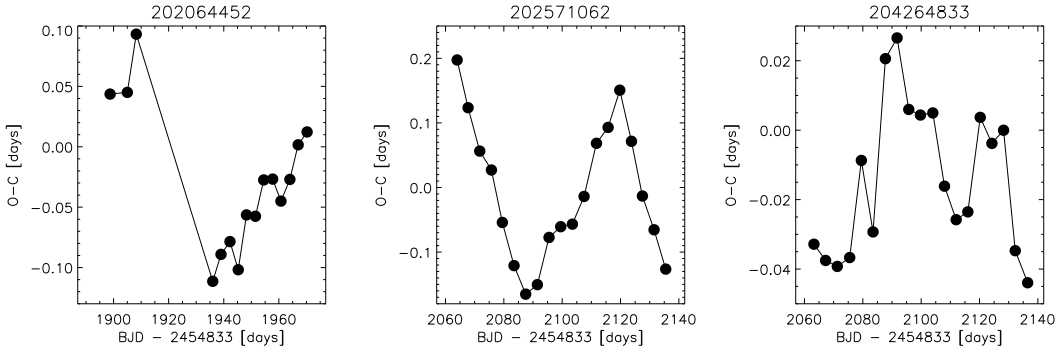

Figure 2. O–C diagrams of the three target stars.

EPIC 202064452 (ASAS J064003+2825.6, TYC 1892-1190-1) has a later-type nearby star according to SDSS images with a separation of 8.3″, but as this object is fainter by ≈ 6 magnitudes, it does not have much contribution to the observed light curve changes. In the catalogue of Schmidt et al. (2011) it was identified as a classical Cepheid with $P = 3.09580$ d, $T_{\rm eff} = 5050$ K, and $\log g = 4.41$. Our period analysis found an average period of $P_{\rm K2} = 3.1163$ d, but as a result of light curve evolution and the 25.6 day-long gap in the observation, the period of Schmidt et al. (2011), based on several years, describes our dataset better.

The light curve shows several flares, in total 5, during the $\approx$1146 hours of observation.

The observations also suggest two synchronously shifting active longitudes roughly on opposite hemispheres. At the beginning of the observations, the two nests were found around 0.2 and 0.7 phases, while around the end of the run, they shifted to 0.3 and 0.8. Also, the second active region became more prominent at the end of the observing run.

The O–C diagram (left panel of Fig. 2) shows a jump near the middle of the observations, which is in agreement with two active longitudes.

EPIC 202571062 (ASAS J162402-2910.8, HD 147611) is probably a wide binary (or multiple) system according to the 2MASS observations (Skrutskie et al. 2006). Torres et al. (2006) identified the object with spectral type of K7Ve and with $v \sin i = 9.7$ km s^{-1}.

This star also exhibits several (at least six) flaring events during the 78 days of observations, the major ones of which seem to concentrate around the same phase (≈ 0.2), which is a fairly common phenomenon on flaring cool dwarfs (cf. e.g., Vida et al. 2016). Note however, that due to the low number of detected flares, this cannot be stated quantitatively. The second major event could also be a sympathetic flare (i.e., a flare resulting from a transient phenomenon occurring elsewhere on the stellar surface, see Fig. 3).

Here, the longitudes of the active regions seem to be more stable, however, the O–C diagram of the times of minima (middle panel of Fig. 2) suggests large-amplitude, periodic variations.

EPIC 204264833 (ASAS J162308-2301.0) is a K5V type star in the solar neighbourhood (Riaz et al. 2006). Our period analysis yielded $P_{\rm rot} = 4.0811$ d. The light curve is

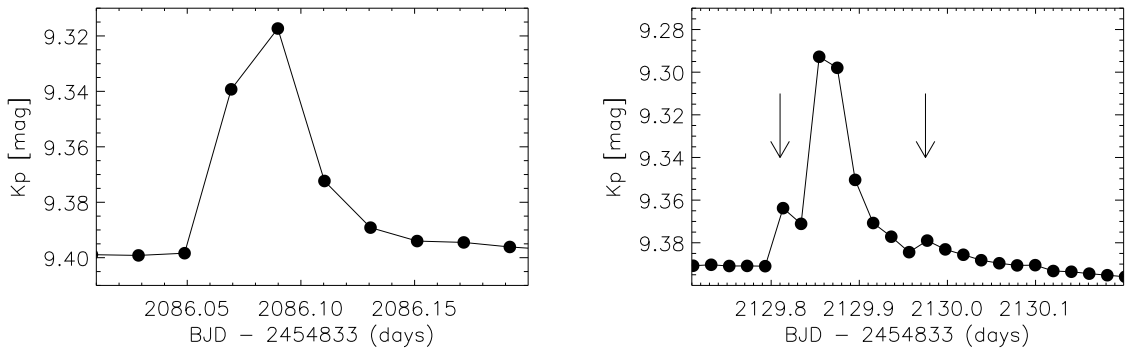

Figure 3. The two major flare events of EPIC 202571062. On the second panel, the arrows indicate possible sympathetic flares.

W-shaped, the changes are probably caused by two spotted regions (of which the more prominent being more stable in time), that is supported by the O–C diagram (right panel of Fig. 2), which shows relatively large variations in short timescale. Only weak flaring activity can be seen in the data.

4 Conclusions

According to K2 light curves, none of the analysed stars are Cepheid variables. The light curve shapes and the O–C diagrams suggest that their light variations are caused by stellar activity (i.e., spots on the surface) and probably not by stellar eclipses or ellipsoidal light variations in binary systems.

Acknowledgements:

This work has used K2 targets selected and proposed by the RR Lyrae and Cepheid Working Group of the *Kepler* Asteroseismic Science Consortium (proposal numbers GO0051 and GO2041). Funding for the *Kepler* and K2 missions is provided by the NASA Science Mission directorate. This project has been supported by the Lendület-2009, the Lendület-2012 (LP2012-31) and the LP2014-17 Programs of the Hungarian Academy of Sciences, and by the NKFIH K-115709 and PD-116175 grants of the Hungarian National Research, Development and Innovation Office. L.M. was supported by the János Bolyai Research Scholarship of the Hungarian Academy of Sciences.The authors acknowledge support from the Hungarian Research Grants OTKA K-109276, OTKA K-113117 and the ESA PECS Contract No. 4000110889/14/NL/NDe.

This research leading to these results has received funding from the European Community's Seventh Framework Programme (FP7/2007-2013) under grant agreements no. 312844 (SPACEINN) and no. 269194 (IRSES/ASK).

This work made use of PyKE (Still & Barclay 2012), a software package for the reduction and analysis of *Kepler* data. This open source software project is developed and distributed by the NASA Kepler Guest Observer Office. This research has made use of the SIMBAD database, operated at CDS, Strasbourg (France).

References:

Armstrong, D. J., et al., 2015, *A&A*, **579**, A19
Berdnikov, L. N., Pastukhova, E. N., 2008, *PZ*, **28**, 9
Howell, S. B., et al. 2014, *PASP*, **126**, 398
Klagyivik, P., et al. 2016, in prep.
Kővári, Zs., Oláh, K., 2014, *Space Sci. Rev*, **186**, 457
Lenz, P., Breger, M., 2005, *CoAst.*, **146**, 53
Molnár, L., Plachy, E., Szabó, R., 2014, *IBVS*, **6108**, 1
Plachy, E., et al., 2016, *CoKon*, **105**, 19
Pojmanski, G., 1997, *AcA*, **47**, 467
Pojmanski, G., 2002, *AcA*, **52**, 397
Poretti, E., et al., 2015, *MNRAS*, **454**, 849
Riaz, B., et al., 2006, *AJ*, **132**, 866
Schmidt, E. G., et al., 2011, *AJ*, **141**, 53
Skrutskie, M. F., et al., 2006, *AJ*, **131**, 1163
Still, M., Barclay, T., 2012, Astrophysics Source Code Library, ascl:1208.004
Szabó, R., et al., 2011, *MNRAS*, **413**, 2709
Torres, C. A. O., et al., 2006, *A&A*, **460**, 695
Vida, K., et al., 2016, *A&A*, **590**, A11

COMMISSIONS 27 AND 42 OF THE IAU
INFORMATION BULLETIN ON VARIABLE STARS

Number 6174

Konkoly Observatory
Budapest
23 June 2016

HU ISSN 0374 – 0676

CONFIRMATION OF THE MAGNETIC NATURE OF THE δ SCUTI STAR HD 21190

HUBRIG, S.[1]; SCHÖLLER, M.[2]

[1] Leibniz-Institut für Astrophysik, An der Sternwarte 16, 14482 Potsdam, Germany, e-mail: shubrig@aip.de

[2] European Southern Observatory, Karl-Schwarzschild-Str. 2, 85748 Garching, Germany

Using time-series photometry of the δ Scuti star HD 21190 obtained by the *Hipparcos* mission, Koen et al. (2001) discovered a variability period of 3.6 h. According to these authors, the spectral classification of this star is F2 III SrEuSi: based on the strength of Sr II, Eu II, and Si II lines, making it the most evolved Ap star known. González et al. (2008) presented a search for pulsational line profile variations in high time-resolution UVES spectra of HD 21190 and could show that this star presents the best known example of a δ Scuti star with moving bumps in its line profiles characteristic of higher-order overtone pulsation. Indications that a few Ap stars can show a hybrid δ Sct – γ Dor variability were reported by Balona et al. (2011) who used *Kepler* observations of stars in the δ Scuti instability strip.

On the other hand, pulsations of δ Scuti type among Ap stars are not expected from a theoretical point of view. The models by Saio (2005) led to a clear prediction that lower radial overtone pulsation modes typical of δ Scuti stars are suppressed by the magnetic field in Ap stars. Obviously, magnetic field measurements in this type of pulsating stars with Ap characteristics are of utmost importance to understand the interplay between the magnetism and the physical processes taking place inside the stars.

The first measurement of a longitudinal magnetic field in HD 21190 was presented by Kurtz et al. (2008) who used the multi-mode instrument FORS 1 mounted at the 8-m Kueyen telescope of the VLT with the GRISM 600B. This multi-mode instrument is equipped with polarization analyzing optics, comprising super-achromatic half-wave and quarter-wave phase retarder plates, and a Wollaston prism with a beam divergence of 22″ in standard resolution mode. A detailed description of the assessment of the longitudinal magnetic field measurements using this instrument is given by Hubrig et al. (2016). The measurements revealed the rather weak longitudinal magnetic field $\langle B_z \rangle = 47 \pm 13$ G.

Since the longitudinal field strength depends on the viewing aspect and typically is variable with rotation in Ap stars, further observations were needed to confirm the detection. We succeeded to reobserve HD 21190 with FORS 2 at the VLT on 2016 March 15 using the same instrumental setup as in 2008. A magnetic field detection at a significance level of more than 4σ ($\langle B_{\rm z} \rangle_{\rm all} = -254 \pm 59$ G) was achieved for HD 21190 using for the measurements the entire spectrum, and at a significance level of more than 3σ ($\langle B_{\rm z} \rangle_{\rm hyd} = -237 \pm 75$ G) using the hydrogen lines. To obtain an independent error estimate, we applied Monte Carlo bootstrapping tests, where we generated 250 000 statistical

variations of the original dataset by the bootstrapping technique, and analyzed the resulting distribution $P(\langle B_z \rangle)$ of the regression results. Mean and standard deviation of this distribution are identified with the most likely mean longitudinal magnetic field and its 1σ error, respectively. The measurement uncertainties obtained before and after the Monte Carlo bootstrapping tests were found to be in close agreement. In Fig. 1 we present the distributions from our Monte Carlo bootstrapping tests for our data set.

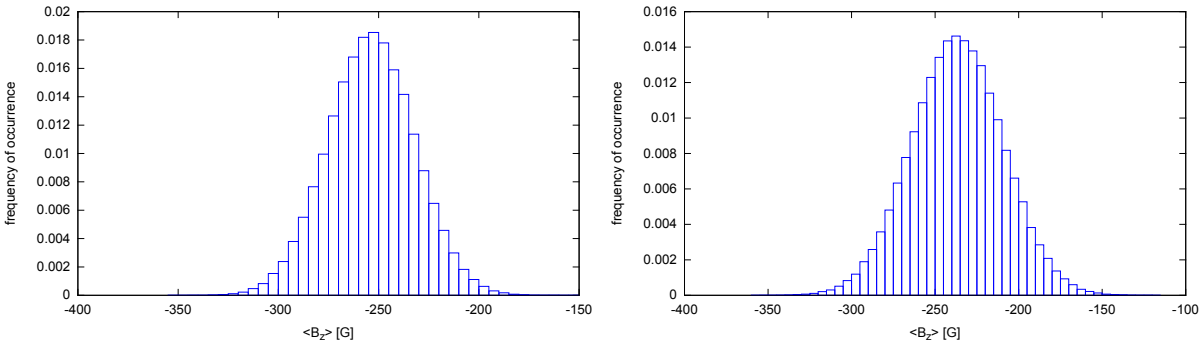

Figure 1. Distributions from our Monte Carlo bootstrapping tests for the data set of HD 21190 from 2016 March using the entire spectrum (left panel) and only the hydrogen lines (right panel).

We note that there is no known case of an Ap star with a significant magnetic field that shows δ Scuti pulsations. Neiner & Lampens (2015) recently obtained two spectropolarimetric observations of the *Kepler* δ Sct – γ Dor hybrid candidate HD 188774. Only one observation showed a weak signal of about 76 G. Furthermore, the target did not show any Ap characteristics as the abundance analysis did not reveal any chemical peculiarity and no chemical spots were identified.

The confirmation of the presence of a magnetic field in HD 21190 shows that δ Scuti pulsations can indeed exist in stars with a magnetic field. Further observations are needed to determine the magnetic field geometry and the polar field strength of this currently unique star.

References:

Balona, L. A., Cunha, M. S., Kurtz, D. W., *et al.*, 2011, *MNRAS*, **410**, 517
González, J. F., Hubrig, S., Kurtz, D. W., *et al.*, 2008, *MNRAS*, **384**, 1140
Hubrig, S., Scholz, K., Hamann, W.-R., *et al.*, 2016, *MNRAS*, **458**, 3381
Koen, C., Kurtz, D. W., Gray, R. O,. *et al.*, 2001, *MNRAS*, **326**, 387
Kurtz, D. W., Hubrig, S., González, J. F., *et al.*, 2008, *MNRAS*, **386**, 1750
Neiner, C., Lampens, P., 2015, *MNRAS*, **454**, L86
Saio, H., 2005, *MNRAS*, **360**, 1022

COMMISSIONS 27 AND 42 OF THE IAU
INFORMATION BULLETIN ON VARIABLE STARS

Number 6175

Konkoly Observatory
Budapest
27 June 2016

HU ISSN 0374 – 0676

METAL-RICH OR MISCLASSIFIED? THE CASE OF FOUR RR LYRAE STARS

MOLNÁR, L.[1]; JUHÁSZ[1,2], Á. L.; PLACHY, E.[1]; SZABÓ, R.[1]

[1] Konkoly Observatory, Research Centre for Astronomy and Earth Sciences, Konkoly Thege Miklós út 15-17, H-1121 Budapest, Hungary

[2] Department of Astronomy, Eötvös Loránd University, Pázmány Péter sétány 1/a, H-1117 Budapest, Hungary

e-mail: molnar.laszlo@csfk.mta.hu

1 Introduction

RR Lyrae stars are old, usually metal-poor, population II stars, currently evolving on the horizontal branch, and crossing the classical instability strip. Most of them, the RRab stars, pulsate in the fundamental mode and have well recognisable light curves, with a very short and steep ascending branch and a long descending branch that often, but not always, exhibits a strong bump feature before reaching minimum light. First-overtone pulsators, members the RRc subclass, display a comparatively more sinusoidal light curve that is usually less asymmetric, and often features a notable depression, or hump, before maximum light. (Quasi-continuous observations of space photometric missions provided numerous textbook examples of RR Lyrae light curves: we refer the reader to the works by Benkő et al. 2010, 2014, Moskalik et al. 2015, Nemec et al. 2011, Szabó et al. 2014, and references therein.)

The light curve shape of RR Lyrae stars strongly depends on the physical parameters of the star, therefore photometric data can be exploited to derive those properties. Jurcsik & Kovacs (1996, JK96 hereafter) derived a formula to calculate the [Fe/H] indices of RRab stars from the pulsation period and the ϕ_{31} Fourier coefficients, defined as the $\phi_{31} = \phi_3 - 3\,\phi_1$ relative phase difference by Simon & Lee (1981). A similar relation was determined for RRc stars by Morgan et al. (2007), and later modified by Nemec et al. (2013), who also provided an updated formula for RRab stars observed in the passband of the *Kepler* space telescope. We note that the accuracy of the JK96 formula is limited for very low- and high-metallicity stars (see, e.g., Nemec et al. 2013).

While most RR Lyrae stars are metal-poor, with negative [Fe/H] indices (see, e.g. Feast et al. 2008), some may reach metallicities close to solar, such as AV Peg (–0.08), RW TrA (–0.13) from the HIPPARCOS sample (Feast et al. 2008) or V839 Cyg (-0.05 ± 0.14) and V784 Cyg (-0.05 ± 0.10) in the original *Kepler* sample (Nemec et al. 2013). Another interesting example is the short-period, high-metallicity star TV Lib (with ($P = 0.26962$ d, and [Fe/H] = –0.17) that nevertheless displays very characteristic RRab light variations (Clube et al. 1969, Kovács 2005).

During the target search for the K2 mission of the *Kepler* space telescope (Howell et al. 2014; Plachy et al. 2016) we encountered one star, V397 Gem, whose photometric metallicity appeared to be extremely high, [Fe/H] = 0.42, based on the NSVS light curve (Northern Sky Variability Survey, Hoffmann et al. 2009) and the original formula of JK96. V397 Gem also displayed a very short pulsation period of $P = 0.294$ d, considering that it was classified as an RRab star by Wils et al. (2006). After a literature search, we found three more examples in the measurements of the All-Sky Automated Sky Survey (ASAS), based on the work of Szczygieł et al. (2009). All three stars were classified as RRab ones, have short periods (between 0.3–0.35 d) and [Fe/H] indices consistently above +0.5, based on methods of both JK96 and Sandage (2004). The folded light curves of the four stars are displayed in Fig. 1.

The apparently extremely high metallicity suggests that these stars cannot be RRab stars, and the calculated values are simply erroneous. Alternate possibilities include high-amplitude δ Scuti stars; their rare, high-mass variants, the AC And-type pulsators; and RRc stars with unusually asymmetric, sawtooth-like light curves that mislead the (semi-)automated classification schemes of the surveys. In this paper we examine whether these objects could be misclassified RRc stars.

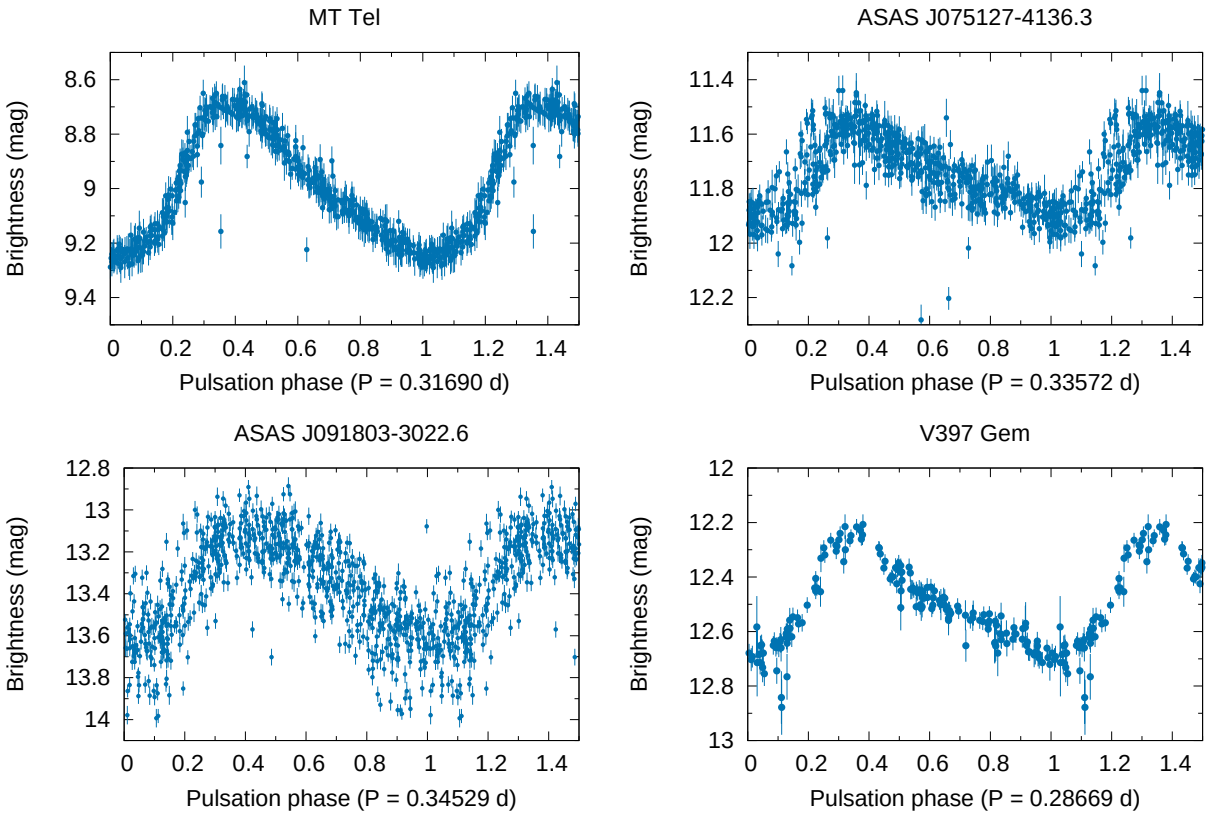

Figure 1. Folded light curves of the four RR Lyrae stars. Data were obtained by the NSVS survey for V397 Gem, and by the ASAS survey for the other three stars.

2 Photometric metallicities

As a first step, we recalculated the photometric [Fe/H] incides of the stars, using equation (4) of Nemec et al. (2013) which is an adjusted version of the Morgan et al. (2007) relation, with the addition of four RRc stars observed by *Kepler* during the original mission. In all four cases we derived indices typical of RR Lyrae stars, between –1.70 and –2.14. One of the four stars, MT Tel was actually known to be a first-overtone star, but even Przybylski (1967) mentioned in the discovery paper that the star displayed an unusually asymmetric light curve for an RRc star. Our value, [Fe/H] = –1.97, agrees relatively well with the one derived by Feast et al. (2008) who calculated it to be –1.85. These findings suggest (although do not prove) that the stars are potentially misclassified in the works of Wils et al. (2006) and Szczygieł et al. (2009), rather than being extremely metal-rich ones.

Table 1: Properties of the four RR Lyrae stars. $[Fe/H]_{RRab}$ and $[Fe/H]_{RRc}$ columns are the photometric metallicity values obtained from the equations for fundamental-mode and first-overtone stars, respectively.

Name	RA_{2000} h:m:s	Dec_{2000} d:m:s	V mag	Period d	$[Fe/H]_{RRab}$	$[Fe/H]_{RRc}$
V397 Gem	06:22:44.3	+18:31:53.4	12.1	0.28669	0.42	−1.70
MT Tel	19:02:12.0	-46:39:11.9	8.94	0.31690	0.66/1.04	−1.97
J075127–4136.3	07:51:27.4	–41:36:17.9	11.86	0.33572	0.95/1.13	−2.11
J091803–3022.6	09:17:59.6	–30:23:34.0	12.06	0.34529	1.51/0.85	−2.14

3 Fourier coefficients

We calculated the various Fourier coefficients of the four stars and plotted them against the OGLE-IV bulge sample and a collection of RRab stars observed by the ASAS and SuperWASP surveys in Fig. 2 (Skarka 2014). The OGLE data, published by Soszyński et al. (2014), were collected in the I band, and we converted their coefficients to V with the conversion formulae of Morgan et al. (1998). We note that the c indices indicate that here the ϕ_{21} and ϕ_{31} phase differences were converted to cosine-based Fourier parameters: $\phi^c_{21} = \phi^s_{21} + \pi/2$ and $\phi^c_{31} = \phi^s_{31} - \pi$.

We also highlighted three known high-metallicity stars in the plot with black circles for comparison with the stars we found. The two longer-period ones, RW TrA and AV Peg, fall into the RRab loci in all four plots. The third one, TV Lib, has already been known as a very peculiar star, especially because of its very short period, and it is an outlier in three out of four panels here too.

Based on the positions of the four stars, we can summarise tour findings as follows:

- V397 Gem, the star with the shortest period out of the four, falls into the region that is populated, sparsely, by both classes. Based on the Fourier coefficients alone, the classification of this star is still uncertain. Together with the photometric metallicity values, the RRc classification is more plausible, but not definitive.
- MT Tel is also close to the overlapping region in three out of four panels, but the low ϕ^c_{31} confirms that it is an RRc star, albeit an unusual one, as it has been already established in previous works.

- ASAS J075127–4136.3 is another star that falls into the overlapping either-or region in the first three panels. The photometric metallicity and the ϕ_{31}^{c} value together suggest that the star is likely a first overtone pulsator rather than a fundamental-mode one, but our classification is uncertain.
- ASAS J091803–3022.6, the star with the longest period and lowest R_{21} ratio, falls squarely into the RRc loci, confirming that it is indeed a first-overtone star.

We note that the classification of the OGLE-IV observations was based on fitting light curve templates typical of the RRab and RRc classes to the data. Hence it is entirely possible that some stars with highly asymmetric, sawtooth-like, short-period variations, similar to the ones shown in Fig. 1, were identified as RRab stars in that sample too.

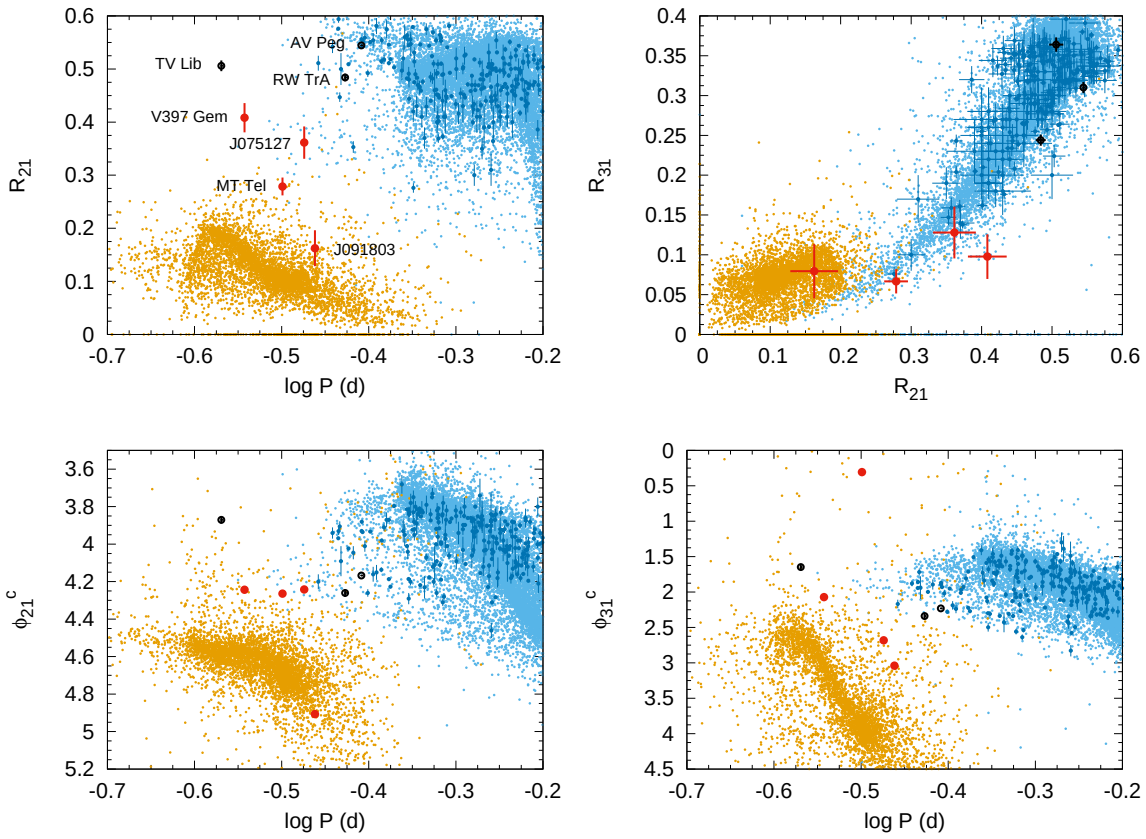

Figure 2. Fourier coefficients of bulge RRab (light blue) and RRc (orange) stars from OGLE-IV, field RRab stars (dark blue), and the four stars from this paper (red). Known high-metallicity RRab stars are marked with black circles. Uncertainties for the OGLE-IV data were not provided.

4 Conclusions

The analysis of these four stars highlights the limits of the photometric methods in variable star classification. Out of the four stars we examined, MT Tel was already known to be an RRc star, yet the classification scheme of ASAS labeled it as a fundamental-mode star. We showed that another star, ASAS J091803-3022.6 was also misclassified and is in fact an RRc star, but in this case the error be plausibly attributed to the low photometric

quality of the ASAS data. In both cases the reclassification also provided us with [Fe/H] indices that are common for RR Lyrae stars, instead of the apparently extremely high (and therefore likely erroneous) values calculated by Szczygieł et al. (2009).

The case of the other two stars, V397 Gem and ASAS J075127-4136.3, is less simple. The period–Fourier-coefficient parameter space contains multiple outlier points, from both subclasses: V397 Gem and ASAS J075127-4136.3 are prime examples of these stars (as is TV Lib). While we prefer the RRc classification for both stars, spectroscopic observations will be needed to decide between the two, very different [Fe/H] indices we obtained from photometry. We also note that in the case of V397 Gem, high-precision photometry from the *Kepler* space telescope might be able to help, as the low-amplitude additional mode content of RRc and RRab stars are different (see, e.g., Benkő et al. 2014, Moskalik et al. 2015, Molnár 2016) but the investigation of the K2 data will be part of a separate study.

Acknowledgements: L. M. was supported by the János Bolyai Research Scholarship and the INKP 2015/1 travel grant of the Hungarian Academy of Sciences. This work has been supported by the NKFIH K-115709 and PD-116175 grants of the Hungarian National Research, Development and Innovation Office, and by the Lendület Programme of the Hungarian Academy of Sciences under grant number LP2014-17. The research leading to these results has received funding from the ESA PECS Contract No. 4000110889/14/NL/NDe and the European Community's Seventh Framework Programme (FP7/2007-2013) under grant agreements no. 269194 (IRSES/ASK) and no. 312844 (SPACEINN). This research has made use of the SIMBAD database, operated at CDS, Strasbourg (France), and NASA's Astrophysics Data System Bibliographic Services.

References:

Benkő, J. M., et al., 2010, *MNRAS*, **409**, 1585
Benkő, J. M., Plachy, E., Szabó, R., Molnár, L., Kolláth, Z., 2014, *ApJS*, **213**, 31
Clube, S. V. M., Evans, D. S., Jones, D. H. P., 1969, *Mem. RAS*, **72**, 101
Feast, M. W., Laney, C. D., Kinman, T. D., van Leeuwen, F., Whitelock, P. A., 2008, *MNRAS*, **386**, 2115
Hoffman, D. I., Harrison, T. E., McNamara, B. J., 2009, *AJ*, **138**, 466
Howell, S. B., et al., 2014, *PASP*, **126**, 398
Jurcsik, J., Kovacs, G., 1996, *A&A*, **312**, 111
Kovács, G., 2005, *A&A*, **438**, 227
Molnár, L., 2016, *CoKon*, **105**, 11
Morgan, S. M., Simet, M., Bargenquast, S., 1998, *AcA*, **48**, 341
Morgan, S. M., Wahl, J. N., Wieckhorst, R. M., 2007, *MNRAS*, **374**, 1421
Moskalik, P. A., 2015, *MNRAS*, **447**, 2348
Nemec, J. M., et al., 2011, *MNRAS*, **417**, 1022
Nemec, J. M., et al., 2013, *ApJ*, **773**, 181
Plachy, E., Molnár, L., Szabó, R., Kolenberg, K., Bányai, E., 2016, *CoKon*, **105**, 19
Przybylski, A., 1967, *MNRAS*, **136**, 185
Sandage, A., 2004, *AJ*, **128**, 858
Simon, N. R., Lee, A. S., 1981, *ApJ*, **248**, 291
Skarka, M., 2014, *MNRAS*, **445**, 1584
Soszyński, I., et al., 2014, *AcA*, **64**, 177
Szabó, R., et al., 2014, *A&A*, **570**, A100
Szczygieł, D. M., Pojmański, G., Pilecki, B., 2009, *AcA*, **59**, 137
Wils, P., Lloyd, C., Bernhard, K., 2006, *MNRAS*, **368**, 1757

COMMISSIONS 27 AND 42 OF THE IAU
INFORMATION BULLETIN ON VARIABLE STARS

Number 6176

Konkoly Observatory
Budapest
6 July 2016

HU ISSN 0374 – 0676

HISTORICAL LIGHT CURVE AND THE 2016 OUTBURST OF THE SYMBIOTIC STAR StHα 169

MUNARI, ULISSE[1]; GRAZIANI, MAURO[2]; JURDANA-ŠEPIĆ, RAJKA[3]

[1] INAF Osservatorio Astronomico di Padova, Sede di Asiago, I-36032 Asiago (VI), Italy

[2] ANS Collaboration, c/o Astronomical Observatory, 36012 Asiago (VI), Italy

[3] Physics Department, University of Rijeka, Radmile Matejčić, 51000, Rijeka, Croatia

StHα 169 (J2000 α=19$^{\rm h}$49$^{\rm m}$57$^{\rm s}$.59, δ=+46°15′20″.6) was discovered by Stephenson (1986) during an objective prism search for emission line objects away from the Galactic plane. No information was logged on the type of spectrum or intensity of Hα emission, only its magnitude was recorded as $m_V > 13.5$. The symbiotic nature of StHα 169 was recognized by Downes & Keyes (1988) in the course of a spectroscopic survey of Stephenson (1986) objects. Their spectrum shows Balmer, HeI and HeII 4686 emission lines superimposed on the absorption spectrum of an M2 giant, similarly to what recently reported by Li et al. (2015) from a LAMOST survey spectrum. The classification by Downes & Keyes (1988) prompted the inclusion of the star in the catalog of symbiotic stars compiled by Belczyński et al. (2000). Henden & Munari (2008) reported $UBVRI$ photometry at three epochs in 2001, their mean values being V=13.68, $U-B$=+0.952, $B-V$=+1.64, $V-R_{\rm C}$=+1.04, and $V-I_{\rm C}$=+2.14. Pigulski et al. (2009) obtained V,$I_{\rm C}$ photometry of StHα 169 from June 2006 to Jan 2008, with mean values V=13.44 and $V-I_{\rm C}$=+2.03. Their short focal length did not resolve StHα 169 from a nearby field star, 10 arcsec to the East, for which Henden & Munari (2006) give V=16.606, $U-B$=+0.946, $B-V$=+1.208, $V-R_{\rm C}$=+0.745, and $V-I_{\rm C}$=+1.519. Correcting the Pigulski et al. (2009) photometry of StHα 169 for the contribution of this nearby field star provides V=13.50 and $V-I_{\rm C}$=+2.05, close to the 2001 values measured by Henden & Munari (2008). The star is situated within the field of view of the planet-hunter *Kepler* space mission. According to Ramsay et al. (2014) the *Kepler* unfiltered, white-light 2009-2013 data shows a quasi-periodic behaviour with a mean period of 34 days and an amplitude of a few per cent superimposed on a stable mean brightness, consistent with a low amplitude variability intrinsic to the cool giant. To a good approximation, this is all what is known about StHα 169, which can thus be appropriately labelled as one of the poorest studied symbiotic stars. We have been continuously monitoring StHα 169 since 2005, both photometrically and spectroscopically, and have recently reported on it entering an outburst state during 2016 (Munari & Graziani 2016).

$BVR_{\rm C}I_{\rm C}$ optical photometry of StHα 169 is regularly obtained with ANS Collaboration telescope N. 73, a 0.30-m f/10 Meade LX200 telescope located in Alfonsine (Ravenna, Italy). It is equipped with $UBVR_{\rm C}I_{\rm C}$ Astrodon filters. The CCD is a Finger Lake Instruments MAXCAM CM9-1E 512×512 array, 20 μm pixels ≡ 1.37″/pix, with a field of

view of $11' \times 11'$. Image quality and plate scale allow full separation of the variable from the nearby field star above described, to the point that no difference is found between the results obtained with aperture photometry or PSF-fitting. The local photometric sequence, calibrated by Henden & Munari (2006) against Landolt equatorial standards, was used throughout the whole observing campaign, ensuing a high consistency of the data. Our BVR_CI_C photometry of StHα 169 is given in Table 1 (available electronic only), where the quoted uncertainties are the total error budget, which quadratically combines the measurement error on the variable with the error associated to the transformation from the local to the standard photometric system (as defined by the photometric comparison sequence). A detailed description of ANS Collaboration telescopes operation and data reduction is provided by Munari et al. (2012) and Munari & Moretti (2012).

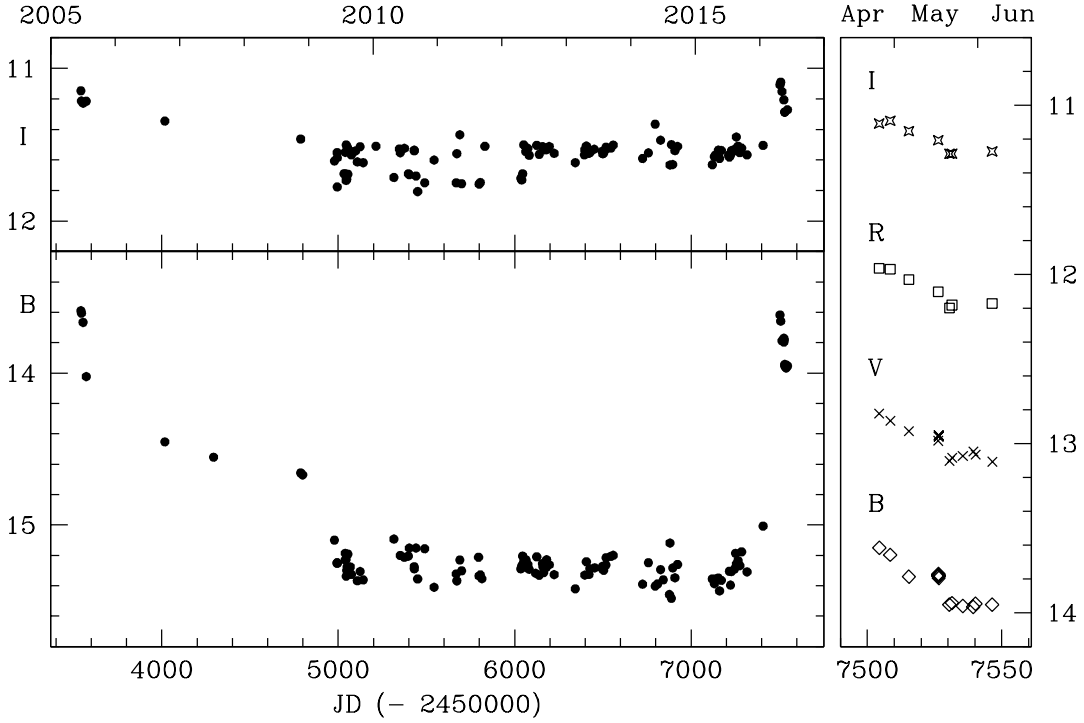

Figure 1. *Left:* overall 2005-2016 light curves in the B and I_C bands of StHα 169. *Right:* a zoom in all four BVR_CI_C bands on the 2016 outburst.

The 2005-2016 light curve of StHα 169 based on the data in Table 1 is presented in Figure 1. During 2005-2009 the variable appears declining from a large amplitude outburst ($\Delta B \sim$2 mag), which maximum could have occurred at an earlier date but later than mid-2001 when the photometric observations by Henden & Munari (2008) found it in quiescence. The amplitude of the outburst decreases with increasing wavelength (down to $\Delta I_C \sim$0.45 mag), as typical in symbiotic stars where the cool giant is usually a passive bystander of the eruption. From mid-2009 to Jan 2016, StHα 169 has remained at flat quiescence, and when the observations resumed in April 2016 we found the object declining from maximum during a new outburst. The start of the current outburst could be marked by the last observation of the previous observing season, on 2016 Jan 21, when StHα 169 appears already brighter than any other previous B-band quiescence observations (cf Figure 1). The recorded peak brightness for both the 2005 and 2016 outbursts is the same (B=13.6), as it is the same the initial fast decline. Only continued monitoring will

reveal if the current outburst will replicate the behaviour of the previous eruption that was characterized by a much slower rate during the last magnitude of decline.

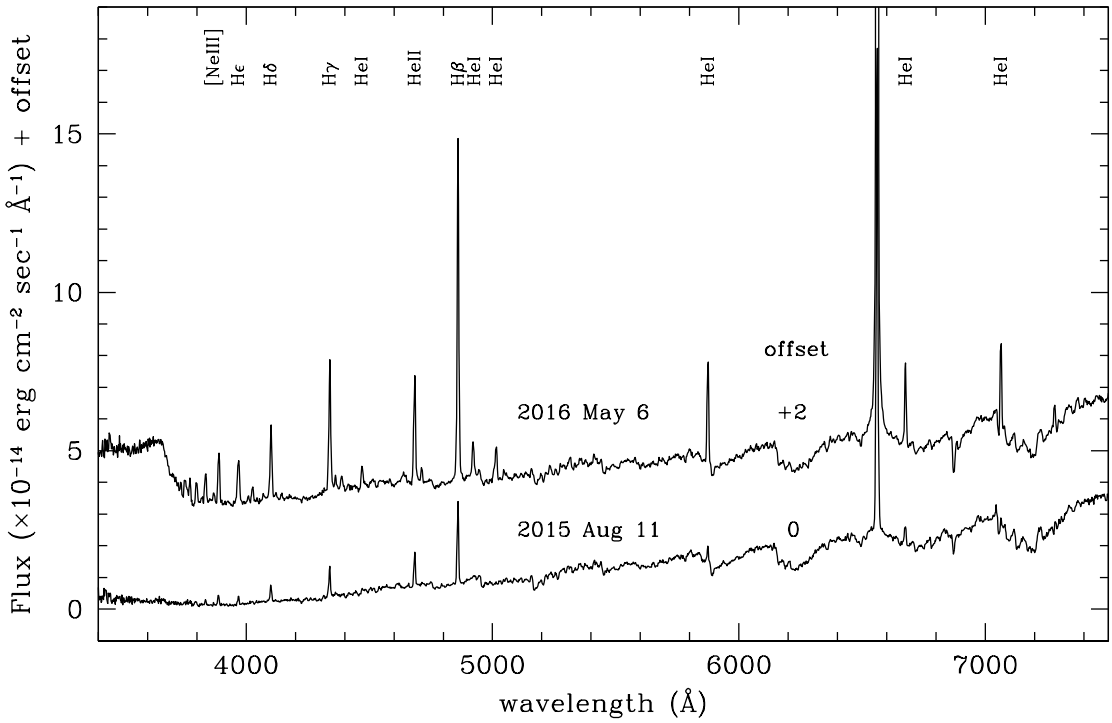

Figure 2. Fluxed low resolution spectra of StHα 169. The one for 2015 Aug 11 is typical of quiescence conditions, that for 2016 May 6 shows the appearance during the current outburst.

Low resolution spectra of StHα 169 are regularly obtained with the 1.22m telescope + B&C spectrograph operated in Asiago by the Department of Physics and Astronomy of the University of Padova. Figure 2 compares our last spectrum of StHα 169 during the preceding quiescence with one obtained during the current outburst. In outburst, a strong blue continuum overwhelms the M giant absorption spectrum short of 5800 Å, and the Balmer continuum turns into strong emission. The [NeV] 3426 and the OVI Raman scattering at 6825 Å, that are weakly present in quiescence, are gone. During outburst, the emission lines have largely increased their integrated flux, Balmer lines by 7×, HeII 4686 by 4.5× and HeI by 9×. The width of the emission lines remains sharp and the same as in quiescence, and no P-Cyg profile is visible.

To put our 2005-2016 CCD observations in a broader context, we have searched via the DASCH database the Harvard plate archive for historical data on StHα 169. We found the star to have been positively recorded on 94 blue sensitive Harvard plates. The corresponding light curve is plotted in Figure 3, where the original DASCH data have been shifted by +0.14 mag to match the modern B-band CCD scale. This shift has been derived by comparing the DASCH B-band magnitudes for the photometric comparison sequence around StHα 169 with the values published by Henden and Munari (2006). The shifted DASCH magnitudes are listed in Table 2 (available electronic only). The 1897-1951 light curve in Figure 3 is characterized by a series of brightenings superimposed on a general decline in brightness that affected StHα 169 until 1916, when the star settled on a quiescence characterized by the same mean B=15.29 value that we measured for

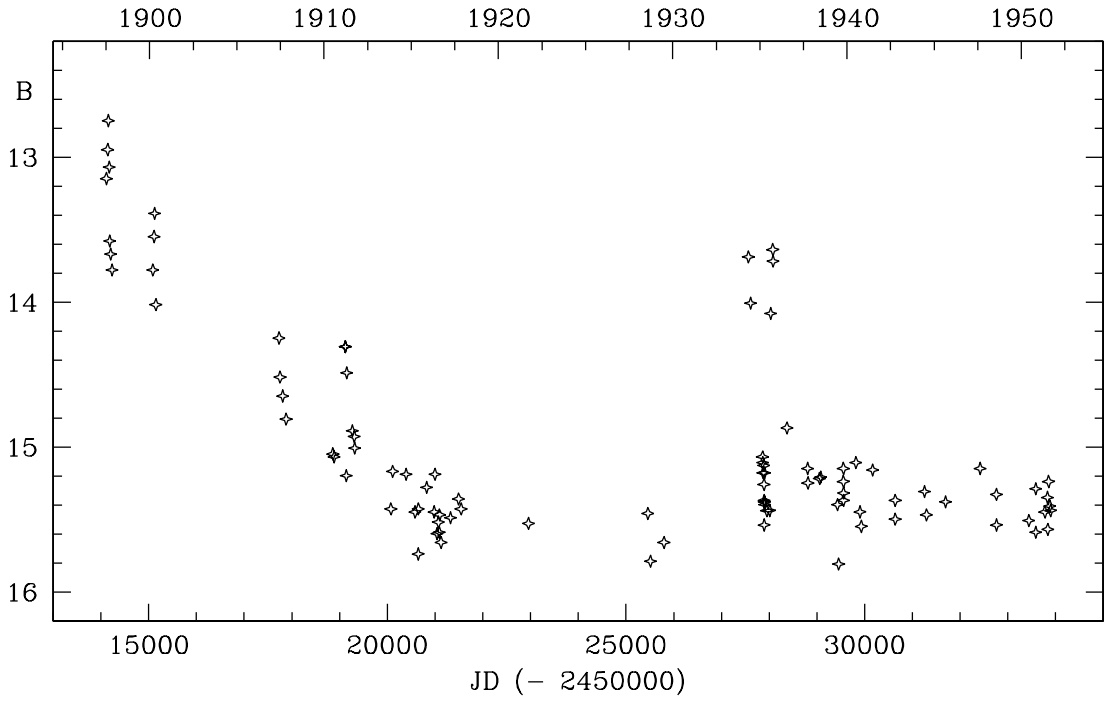

Figure 3. *B*-band historical light curve of StHα 169 from Harvard plates.

quiescence during 2009-2015. Two rapidly evolving outbursts were recorded in 1934 and 1935, both peaking at B ∼13.7 about 510 days apart. Such peak brightness is remarkably similar to the B=13.6 value characterizing both the 2005 and the 2016 events we have observed (cf Figure 1).

Acknowledgements: We thank Alison Doane, Curator of Astronomical Photographs at the Harvard College Observatory, for granting us access to DASCH database (partially supported from NSF grants AST-0407380, AST-0909073, and AST-1313370). We also acknowledge the assistance by S. Dallaporta, L. Baldinelli and A. Maitan (ANS Collaboration) with some of the photometric measurements reported in this paper.

References:

Belczyński K., et al., 2000, *A&AS*, **146**, 407
Downes R. A., Keyes C. D., 1988, *AJ*, **96**, 777
Henden A., Munari U., 2006, *A&A*, **458**, 339
Henden A., Munari U., 2008, *BaltA*, **17**, 293
Li J., et al., 2015, *RAA*, **15**, 1332
Munari U., Moretti S., 2012, *BaltA*, **21**, 22
Munari U., et al., 2012, *BaltA*, **21**, 13
Munari U., Graziani M., 2016, *ATel*, **9036**
Pigulski A., Pojmański G., Pilecki B., Szczygieł D. M., 2009, *AcA*, **59**, 33
Ramsay G., Hakala P., Howell S. B., 2014, *MNRAS*, **442**, 489
Stephenson C. B., 1986, *ApJ*, **300**, 779

COMMISSIONS 27 AND 42 OF THE IAU
INFORMATION BULLETIN ON VARIABLE STARS

Number 6177

Konkoly Observatory
Budapest
7 July 2016

HU ISSN 0374 – 0676

ON THE ORBITAL PERIOD OF THE EXOPLANET WASP-39 b†

MACIEJEWSKI, G.[1]; GINSKI, CH.[2,3]; GILBERT, H.[2]; MUGRAUER, M.[2]; NEUHAEUSER, R.[2]

[1] Centre for Astronomy, Faculty of Physics, Astronomy and Informatics, Nicolaus Copernicus University, Grudziadzka 5, 87-100 Toruń, Poland, e-mail: gmac@umk.pl

[2] Astrophysikalisches Institut und Universitäts-Sternwarte, Schillergässchen 2–3, D–07745 Jena, Germany

[3] Sterrewacht Leiden, PO Box 9513, Niels Bohr weg 2, NL–2300RA Leiden, the Netherlands

The WASP-39 system is composed of a G8 main-sequence star and a bloated Saturn-mass planet on a 4.06 d circular orbit (Faedi et al. 2011). Ricci et al. (2015) acquired three new light curves with 0.8-2.2 m telescopes and refined system parameters. In Maciejewski et al. (2016), we have revisited the system parameters by modelling two new high-precision light curves obtained with 2 m telescopes. We have found that the orbital period of WASP-39 b is shorter by 3 seconds compared to the value determined by Ricci et al. (2015). In this research note, we present a new transit light curve acquired in 2016, i.e. about 200 epochs after observations of Ricci et al. (2015) and about 380 epochs after observations of Maciejewski et al. (2016). In addition, we also present an unpublished transit light curve acquired in 2011. We used those data together with the literature ones to verify the orbital period of WASP-39 b and refine its transit ephemeris.

The new transit light curve was acquired on 2016 April 29 with the 0.6 m Cassegrain telescope located at the Centre for Astronomy of the Nicolaus Copernicus University in Piwnice, near Toruń (Poland). An SBIG STL-1001 CCD camera with 1024×1024 24-μm size pixels was used as detector. The instrumental setup offers the field of view of $11\farcm8 \times 11\farcm8$. To achieve a higher precision for transit timing, the observations were carried out without any filter (in so called white light). The maximum of a spectral response was found to fall between V and R bands. The sky conditions were photometric. The archival light curve was obtained on 2011 April 19 with the 0.9/0.6 m Schmidt Teleskop Kamera (Mugrauer & Berthold 2010) at the University Observatory Jena (Germany). The sky was clear, and observations were done through a Bessel R filter. The detailed log of observations is given in Table 1.

We used the AstroImageJ package (AIJ, Collins et al. 2016) to process the data. The scientific exposures were corrected with dark current and flat field calibration frames. Timestamps were converted to barycentric Julian dates in barycentric dynamical time ($\mathrm{BJD_{TDB}}$). Differential aperture photometry was applied to produce the light curves. The aperture radius and a set of comparison stars were optimized to achieve the smallest photometric scatter for the target star. The light curves were simultaneously detrended against the airmass, position on the matrix, time, and seeing. The light curve of 2016

†Partly based on observations obtained with telescopes of the University Observatory Jena, which is operated by the Astrophysical Institute of the Friedrich-Schiller-University.

Table 1: Details on individual observing runs.

Date	UT start - end	Airmass	$t_{\rm exp}$ [s]	$N_{\rm exp}$	Γ	pnr	$T_{\rm mid}$ (BJD$_{\rm TDB}$)
2011 Apr 19	20:56 - 01:03	2.45 → 1.71 → 1.80	60	196	0.82	4.10	$2455671.4470^{+0.0010}_{-0.0011}$
2016 Apr 29	20:58 - 01:40	2.04 → 1.81 → 2.62	15	789	3.02	3.33	$2457508.48959^{+0.00063}_{-0.00063}$

Date is given for the beginning of a run. Airmass shows changes of the airmass during a run. $t_{\rm exp}$ is the exposure time used. $N_{\rm exp}$ is the number of exposures. Γ is the median number of exposures per minute. pnr is the photometric scatter in parts per thousand of the normalized flux per minute of observation, based on a definition given in Fulton et al. (2011). $T_{\rm mid}$ is the mid-transit time.

April 29 was also detrended against a meridian flip close to the middle of the transit. The fluxes in both time series were normalized to unity for out-of-transit brightness. The mid-transit times were determined with the Transit Analysis Package (TAP, Gazak et al. 2012). In the fitting procedure, we used the system parameters (the orbital inclination, scaled semi-major axis, and planet-to-star radii ratio) from Maciejewski et al. (2016) as Gaussian priors with their uncertainties as 1-σ penalties. The limb darkening coefficients of the quadratic law were interpolated from tables of Claret & Bloemen (2011) and allowed to vary under Gaussian penalty of $\sigma = 0.1$. To account for possible trends in a total error budget, the intercept and slope of the out-of-transit brightness were free parameters. The best-fitting values and their 1-σ uncertainties were calculated as median and the 15.9 and 85.1 percentile values of marginalized posteriori probability distributions of ten Markov chain Monte Carlo walks with 10^6 steps each. New light curves[1] with the best-fitting models are plotted in Fig. 1.

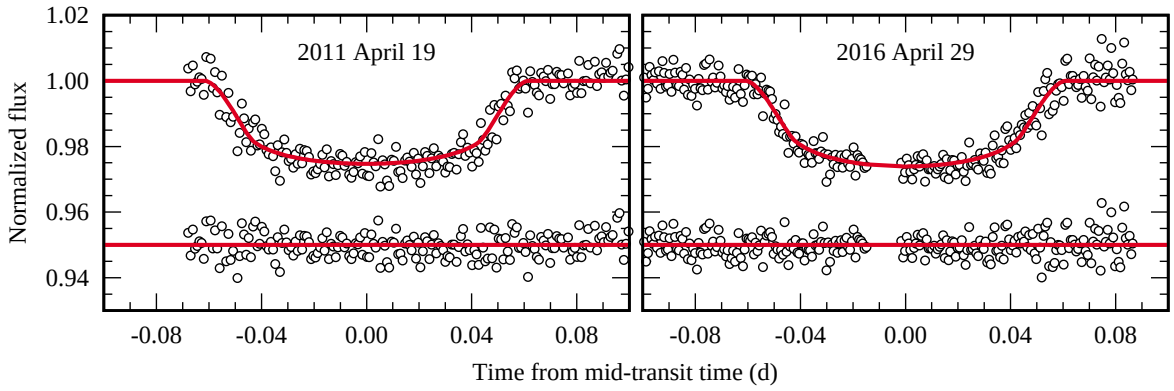

Figure 1. New transit light curves for WASP-39 b. The original light curve acquired on 2016 April 29 was binned into 1 minute intervals.

New mid-transit times, given in Table 1, were combined with the literature determinations from Faedi et al. (2011) and Maciejewski et al. (2016) in order to refine the transit ephemeris. Using the least-squares method, we derived

$$\mathrm{T_{mid}(BJD_{TDB})} = (2455342.96933 \pm 0.00033) + (4\overset{\mathrm{d}}{.}0552807 \pm 0\overset{\mathrm{d}}{.}0000015) \times E, \qquad (1)$$

where E is a transit number starting from the initial epoch given by Faedi et al. (2011). The goodness of the fit $\chi^2_{\rm red}$ was found to be equal to 1.11. The mid-transit time for epoch 0 is 1.5 times more precise than that one reported in Maciejewski et al. (2016).

[1]The photometric time series are available online at `http://www.home.umk.pl/~gmac/TTV`

The orbital period was found to be longer by 0.35 s and 2.3 times more precise than the value given in Maciejewski et al. (2016). A plot of residuals for transit timing is shown in Fig. 2. The mid-transit times of Ricci et al. (2015) are 11-14 σ outliers, and were skipped in calculations.

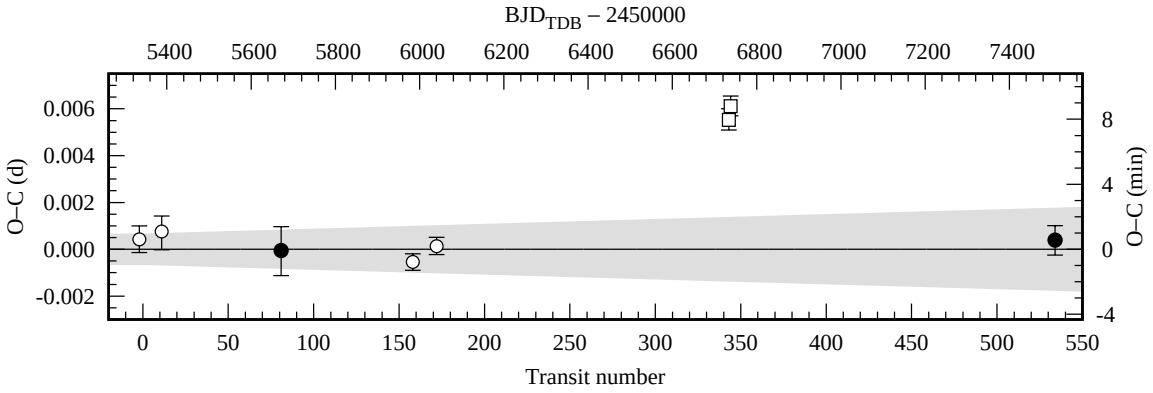

Figure 2. Transit timing residuals from a linear ephemeris. Filled dots are two new determinations reported in this note. Open circles mark the literature points from Faedi et al. (2011) and Maciejewski et al. (2016). Open squares show outlying mid-transit times of Ricci et al. (2015). The gray area shows propagation of the ephemeris uncertainties at a 95.5% confidence level.

Our new observations refined the transit ephemeris for WASP-39 b and confirm that the orbital period is shorter than that one reported in Ricci et al. (2015). The mid-transit times of Ricci et al. (2015) are shifted by some systematic effect, the source of which could be an incorrect time survey during observing runs or errors in the conversion of timestamps. We found that the linear ephemeris reproduces observed mid-transit times satisfactorily, giving no hint of any variations in transit timing.

Acknowledgements: CG and MM want to thank the German Science Foundation (DFG) for support in grant MU2695/13-1. We would like to acknowledge financial support from the Thuringian government (B 515-07010) for the STK CCD camera used in this project.

References:

Claret, A., & Bloemen, S., 2011, *A&A*, **529**, A75
Collins, K.A., Kielkopf, J.F., Stassun, K.G., 2016, *arXiv:1601.02622*
Faedi, F., Barros, S.C.C., Anderson., D.R., et al., 2011, *A&A*, **531**, A40
Fulton, B. J., Shporer, A., Winn, J. N., et al., 2011, *AJ*, **142**, 84
Gazak, J. Z., Johnson, J. A., Tonry, J., et al., 2012, *Advances in Astronomy*, ID 697967
Maciejewski, G., Dimitrov, D., Mancini., L., et al., 2016, *AcA*, **66**, 55
Mugrauer, M., Berthold, T, 2010, *Astron. Nachr.*, **331**, 449
Ricci, D., Ramón-Fox, F.G., Ayala-Loera, C., et al., 2015, *PASP*, **127**, 143

COMMISSIONS 27 AND 42 OF THE IAU
INFORMATION BULLETIN ON VARIABLE STARS

Number 6178

Konkoly Observatory
Budapest
25 July 2016

HU ISSN 0374 – 0676

DISCOVERY OF A NEW PULSATING MASS-ACCRETING COMPONENT IN THE ALGOL-TYPE SYSTEM VY Hya

GUNSRIWIWAT, K.[1]; MKRTICHIAN, D.E.[2]

[1] Department of Physics and Materials Science, Faculty of Science, Chiang Mai University, Muang, 50200 Chiang Mai, Thailand

[2] National Astronomical Research Institute of Thailand, 191 Siriphanich Bldg., Huay Kaew Rd., Suthep, Muang, 50200 Chiang Mai, Thailand

So called oEA stars (**o**scillating **E**clipsing **A**lgol stars), according to classification (Mkrtichian et al. 2002, 2004), consist of A-F spectral type oscillating mass-accreting components of the semi-detached Algol type eclipsing binary systems. These stars are former low-mass secondaries of evolved close binary systems which passed through the first mass-transfer exchange and finally settled on the main sequence. These mass-accreting components lie inside the classical instability strip of δ Scuti and related stars. Since 2002, when the oEA group was classified, dozens of oEA stars have been discovered.

VY Hya is a semi-detached (Algol-type) close binary system with an A3 V primary component and 2.0011799-day orbital period (Brancewicz & Dworak, 1980). The spectral class of the primary and the semi-detached configuration of binary system pin up it into the instability strip of δ Scuti-type and related stars. We include it to the target list of the "Thai Sky Survey for oEA Stars" (THASSOS) in order to search for pulsations.

The photometric observations of VY Hya were obtained during 4 nights (15-18 March 2014) with an Apogee Alta F42 CCD camera attached to the 0.6-meter Thai Southern Hemisphere Telescope (TST) PROMPT8 at Cerro Tololo Inter-American Observatory (CTIO). 20 second exposures through B filter were used.

All stars in the field of view were reduced by Maxim DL5 program using aperture photometry. Comparison and check stars for VY Hya are listed in Table 1. Phased differential light curve folded with the period of 2.0011799 days is plotted in Figure 1. As seen, all observations were obtained during out-of-eclipse orbital phases optimal for searching for pulsations. To extract pulsational variations, slow orbital light variations for every night were removed using low-order polynomial fits and residuals were merged.

Table 1: Data on VY Hya, comparison and check stars.

Star	RA (J2000)	DEC (J2000)	B
VY Hya	$0^{\rm h}20^{\rm m}16\overset{\rm s}{.}0$	$-23°09'05\overset{''}{.}2$	10.61
HD89638 (Comparison Star)	$10^{\rm h}20^{\rm m}13\overset{\rm s}{.}2$	$-23°06'09\overset{''}{.}3$	8.43
HD89581 (Check Star)	$10^{\rm h}19^{\rm m}48\overset{\rm s}{.}8$	$-22°58'16\overset{''}{.}6$	8.96

The residuals from the orbital light curve of VY Hya shown in Figure 2 exhibits strong amplitude modulation indicating multiperiodicity of pulsations.

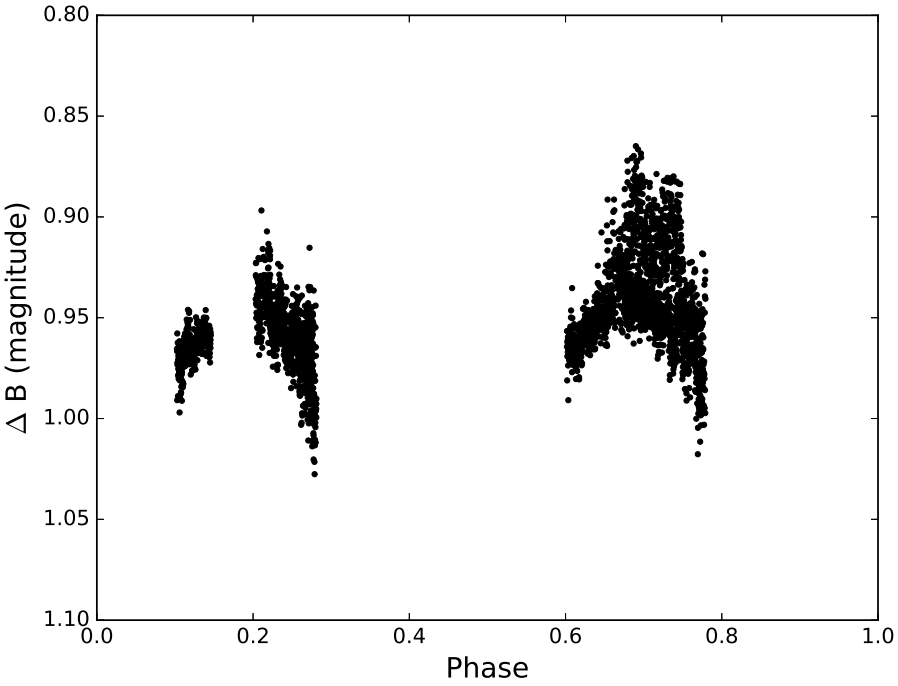

Figure 1. The phased B-filter light curve of VY Hya folded on the period of 2.0011799 days.

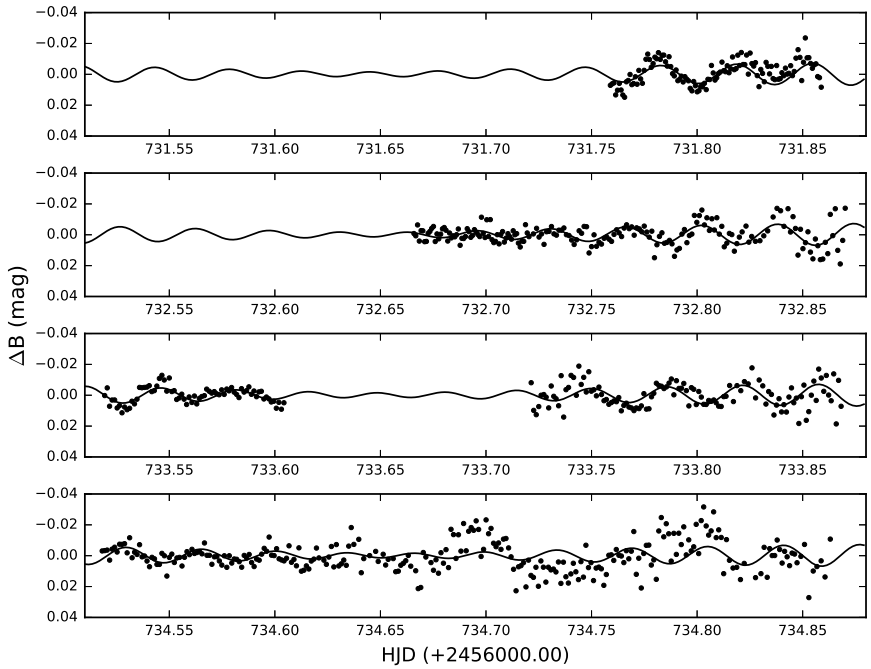

Figure 2. The nightly residual light variations (time zero point is HJD 2456000+).

Discrete Fourier Transform (DFT) analysis was applied to the all residual data to find the pulsation frequencies of the primary component. The signal pre-whitening technique was used for consecutive detection of signals in the data. The steps of DFT analyses and consecutive prewhitening of VY Hya are shown in Figure 3 from top to bottom. Two oscillation frequencies, listed in Table 2, were detected.

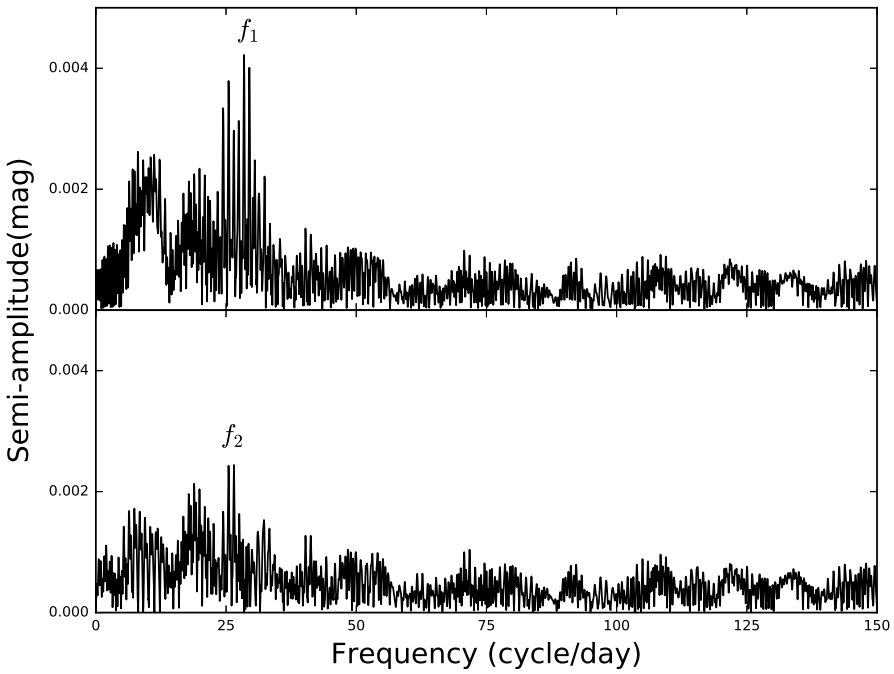

Figure 3. The DFT amplitude spectrum of the residual light curve of the primary component (top) and after the pre-whitening procedure (bottom).

Table 2: Pulsation frequencies and amplitudes.

Frequency (c/d)	Amplitude (mag)
F_1=28.44±0.01	0.0043±0.0004
F_2=26.50±0.02	0.0024±0.0004

We conclude that the primary component of VY Hya is a new member of the oEA group of pulsating mass-accreting components of Algols.

Acknowledgements: Department of Physics and Materials Science Chiang Mai University thanked for support. This work is a part of research activity of the National Astronomical Research Institute of Thailand (NARIT).

References:

Brancewicz, H. K., Dworak, T. Z., 1980, *AcA*, **30**, 501
Mkrtichian D. et al., 2002, *ASP Conf. Ser.*, **259**, 96
Mkrtichian, D.E., Kusakin, A.V., Rodriguez, E., et al., 2004, *A&A*, **419**, 1015

COMMISSIONS 27 AND 42 OF THE IAU
INFORMATION BULLETIN ON VARIABLE STARS

Number 6179

Konkoly Observatory
Budapest
5 August 2016

HU ISSN 0374 – 0676

VARIABILITY OF THE He I 6678 EMISSION IN δ Sco

POLLMANN, ERNST

International Working Group ASPA, Emil-Nolde-Str. 12, 51375 Leverkusen, Germany

Introduction

δ Scorpii (HD143275, HR5953) is a 2.3 magnitude Be binary star whose binarity was discovered interferometrically by McAlister (1978). But its binary nature was first reported by Innes (1901). The star was first classified as a Be star when it showed an emission profile on the wings of an absorption core of a spectrum taken in 1990 by Coté & van Kerkwijk (1993) and is now considered to be a typical B0.3 IV star.

This binary system with its large eccentric orbit ($e > 0.9$) (Tango et al. 2009) exhibits a strong mass loss that has resulted in a circumstellar gaseous disk formation. He I lines are good tracers of matter very close to the star, where temperature and density are the highest and ionisation is the strongest. The He I 6678 line profile of δ Sco suggests that one sees some optically-thick outflow and a lot of matter in the line of sight. The outflow should add more mass to the disk and as a result, the disk will gradually grow outwards. This is very interesting since the inclination angle of the circumstellar disk is about 45°[36°, Miroshnichenko et al. (2013); 38°± 5°Miroshnichenko et al. (2001); 48.5°± 6.6°Hartkopf et al. (1996); 70°, Bedding (1993)].

During each periastron (period = 10.8 years) some ring material may flow from the primary's Roche lobe into the secondary's Roche lobe. During that process the disk becomes denser and single-, double- or triple peak profiles may be observable. Outside of each periastron the He 6678 line is emitted in an extended rotating elliptical disk or ring around the central star, where the ring is not centered on the central star.

The situation might be more complex since the companion is triggering the disk/ring formation or destruction through tidal effect on the circumstellar disk/ring. There seems to be two physical effects going on in δ Sco: one is the ejection of material from the photosphere, the other is the formation of "blobs" of gas in the disk or ring(s) probably from viscosity effects. The blobs rotate in a more or less Keplerian mode, eventually to fall back closer to the star (Miroshnichenko, personal communication 07/2004).

As to further studies of the physical properties of δ Sco's disk, I refer to the following important publications: Properties of the δ Sco circumstellar disk from continuum modelling, Carciofi et al. (2006); Disk geometry and kinematics before the 2011 periastron, Maillard et al. (2011); Imaging disk distortion of Be binary system δ Scorpii near periastron, Che et al. (2012); The circumstellar disk evolution after the periastron, Meilland et al. (2013).

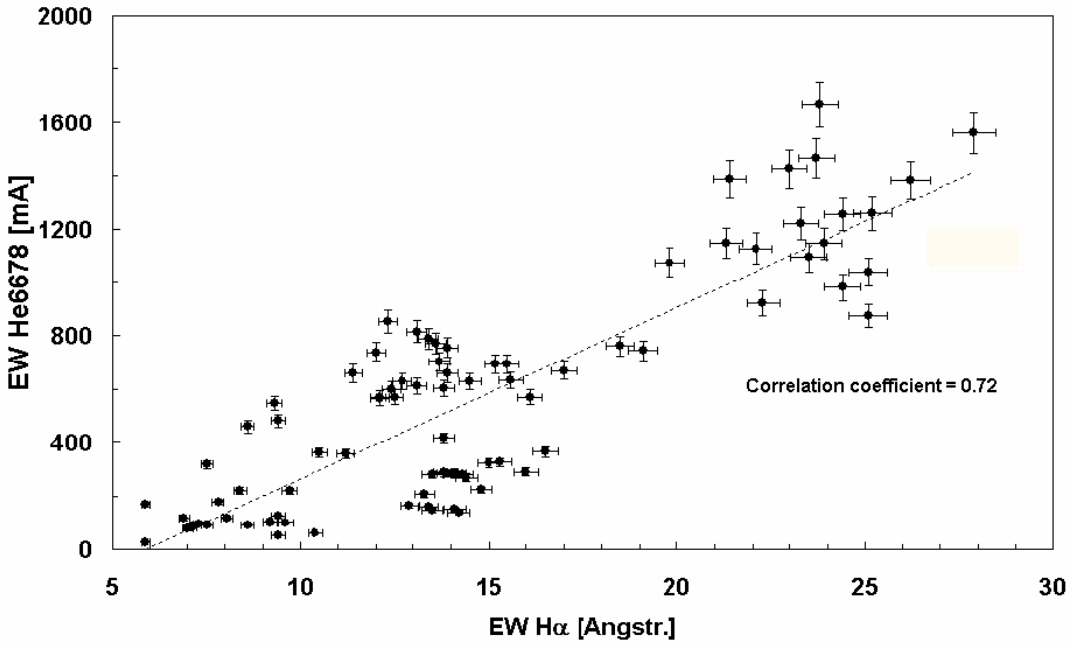

Figure 1. Correlation between the equivalent width of He I 6678 and Hα from April 2005 to April 2016.

Observation and results

Following the generally accepted assumption that the disk of this binary system is being fed due to outbursts of matter ejected from the stellar surface (Miroshnichenko et al., 2003), and since the He I 6678 line forms near the photosphere of the primary component one can expect a correlation between the equivalent width (EW) of the Hα and and He I 6678 lines (Fig. 1). Such a correlation might be interpreted as a result of a disk feeding process. However we cannot exclude that this reflects only contemporaneous density variations within the line formation zones.

This study of a correlation between Hα and He I 6678 EWs (Fig. 1) and of the behaviour of the He I 6678 line profiles have been performed by the author at the observatory of the Vereinigung der Sternfreunde Köln (Germany) with a C14 40 cm Schmidt-Cassegrain-telescope, the slit-grating-spectrograph LHIRES III with a spectral resolving power $R \sim$ 17000 and a CCD-camera (768×512 pixel, pixel size 9 μm, this instrumental configuration provides spectra within the range from 6500 to 6700 Å), in collaboration with observers of the ARAS group[1] at different locations, different telescopes (apertures between 20 and 40 cm) and different spectrographs with spectral resolving powers of 10000 to 20000 (signal-to-noise ratios, S/N of these spectra are ca. 200–300).

With exposure times of 300 to 350 sec for an individual spectrum, the S/N in a sum spectrum of 10 individual spectra reached values mostly more than 1000. The spectra have been reduced manually with standard procedures (instr. response, normalisation,

[1] http://www.astrosurf.com/aras

wavelength calibration) by using the programs Maxim-DL[2], VSpec[3] and MK32[4].

Since April 2005, during every observing season, the observed correlation impressively supports the existence of this disk-feeding process, in which the slope of the linear fit shown in Fig. 1 reflects the quantitative correlation.

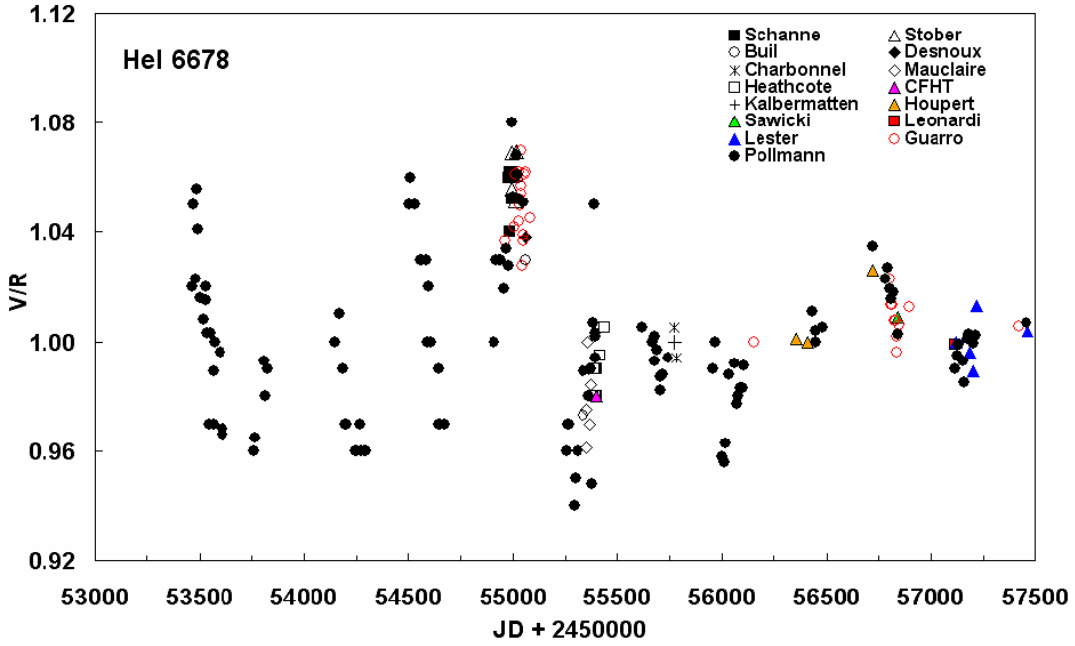

Figure 2. Long-term monitoring of the V/R ratio from April 2005 to March 2016.

In addition to the variability of the EWs (measured and analysed in the same spectra) the He I 6678 line double-peaked profile exhibits a variable V/R ratio that is the relative intensity of the violet component I_V to the red component I_R. For the first time it was possible to analyse eleven complete cycles of the V/R variations from April 2005 to March 2016 (Fig. 2). In the earlier seasons, merely the descent could be measured. On this occasion I emphasize that, among others, members of the ARAS group, made a significant contribution to the frequent observations.

The V/R measurements of these eleven cycles presented here permitted an analysis of possible periodicities. For the analysis of the period (Fig. 3) and the phase diagram (Fig. 4) the method of the PDM [phase dispersion minimization of Stellingwerf (1978)] within the program package AVE[5] was used.

As very clear result the period of 553 d (± 2.3) with the output epoch T_0 = JD 2453794 (± 7.8) could be found. The V/R ratio has been measured of course only in the spectra for which the double peak profiles are apparent. In the light of that result it is interesting to have a look on the cyclic behaviour of the Hα EW within our long-term monitoring of that star from July 2000 to May 2015 (see Fig. 5). After subtracting the long-term wave of approx. 9 years in the upper left panel of Fig. 5, I could derive a period of 509 days (lower left, upper and lower right panels of Fig. 5), which is very close to the period of

[2]http://www.cyanogen.com
[3]http://www.astrosurf.com/vdesnoux
[4]http://www.appstate.edu/ grayro/spectrum/spectrum276/
[5]http://astrogea.org/soft/ave/aveint.htm

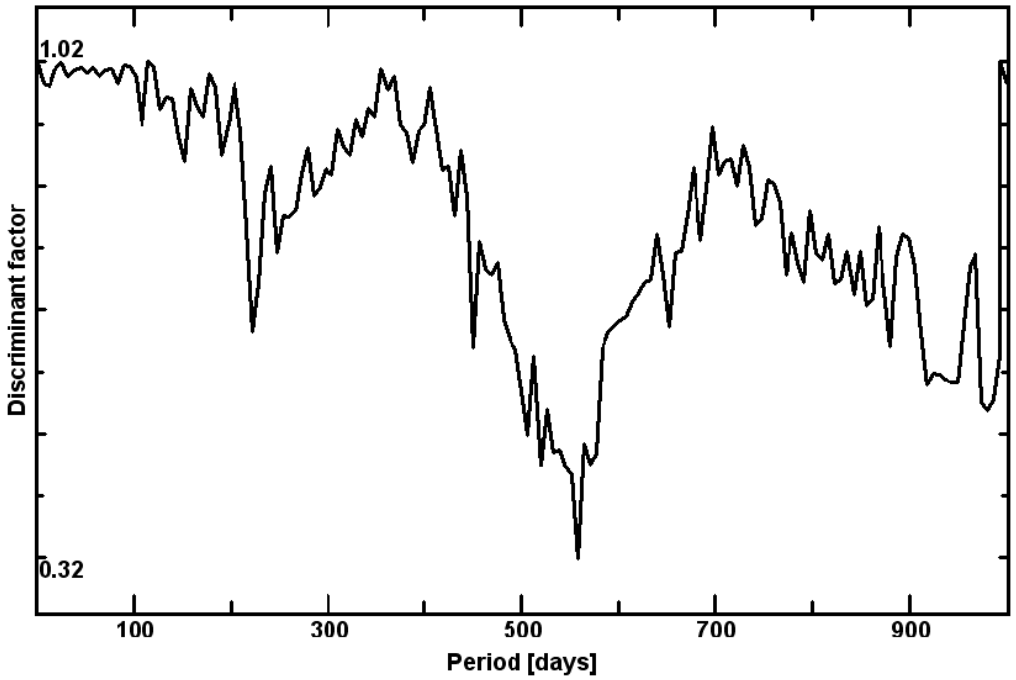

Figure 3. The method of the PDM analysis revealed a period of 553 d in the V/R data in Fig. 2.

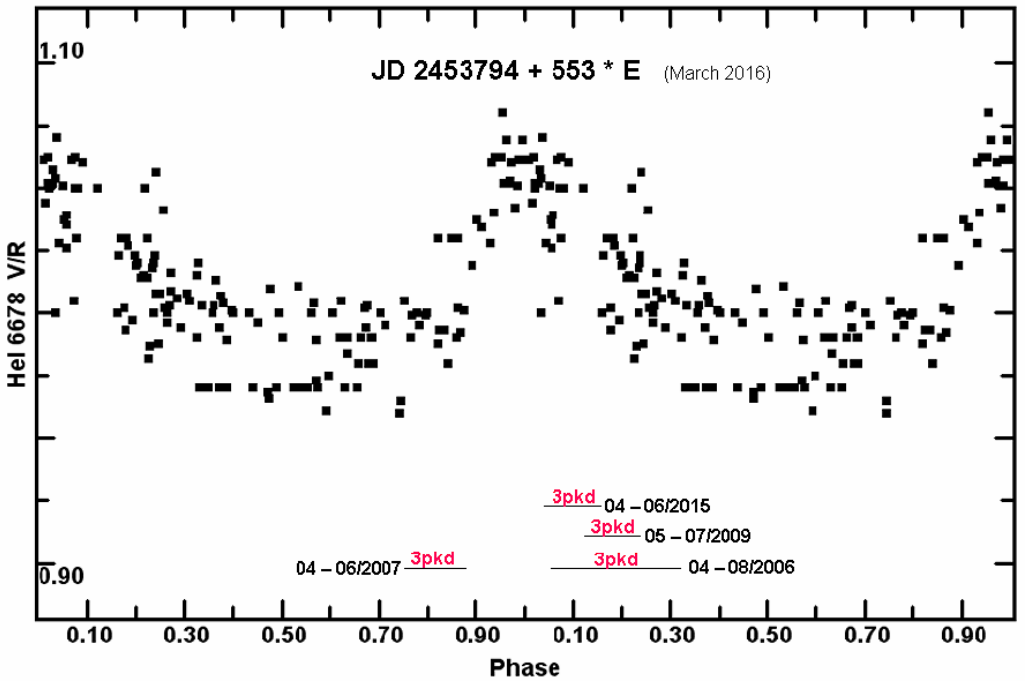

Figure 4. Phase diagram of the V/R data folded on the period of 553 d with $T_0 = 2453794$ and the marked phase sections of the triple-peak appearance (3pkd).

He I 6678 derived in this paper. These close coincidences of the periodic behaviour led to the suspicion of identical physical causes. The long-term behaviour of the Hα emission of δ Sco might be studied in a further paper.

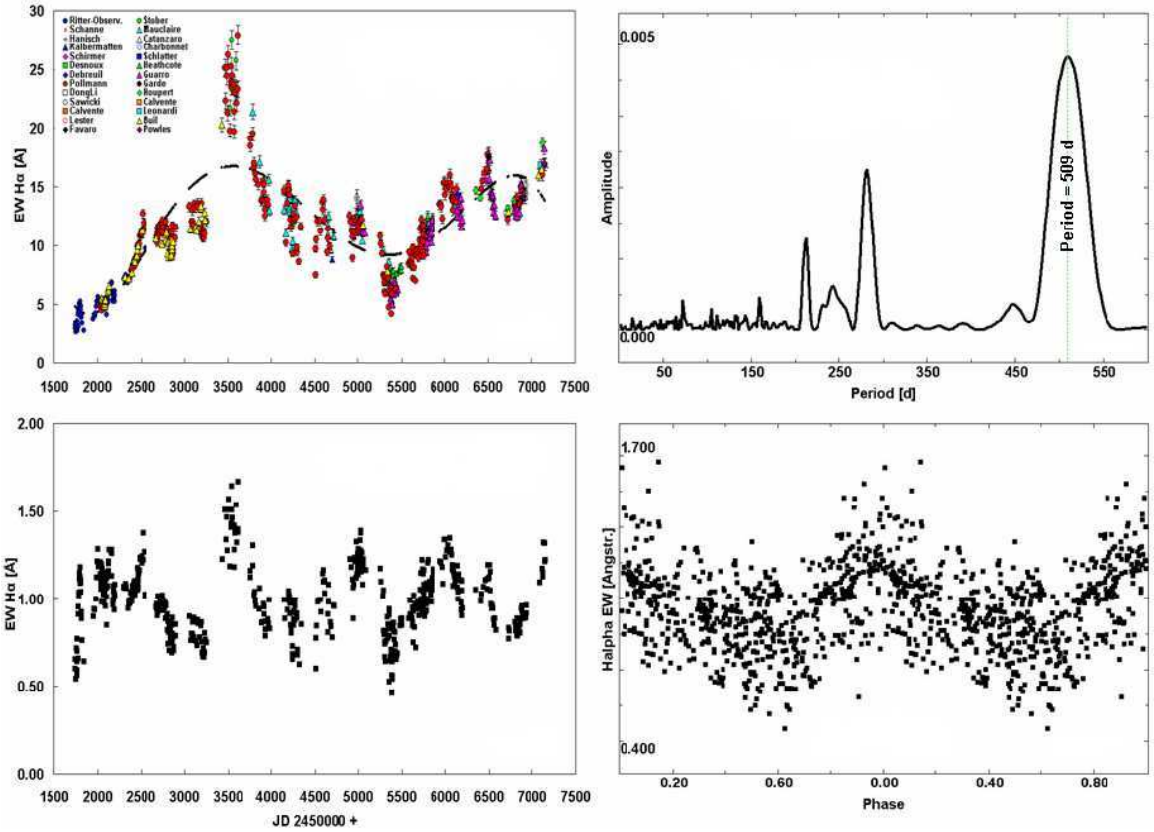

Figure 5. (Upper left) δ Sco Hα monitoring and long-term variations (period approx. 9 years). (Lower left) Long-term variation removed EW of Fig. 1 divided through the long-term variation. (Upper right) Period analysis of the long-term removed data in the lower left panel. (Lower right) Phase diagram of the 509 d period.

An inspection of the spectra shown in Fig. 6 shows that the third emission component (the triple-peak profile) was observed within the phase intervals $\sim$ 0.06 to $\sim$ 0.3 (04-08/2006), $\sim$ 0.75 (04/2007), $\sim$ 0.1 to $\sim$ 0.24 (05-07/2009) and $\sim$ 0.03 to $\sim$ 0.13 (04-06/2015). marked (in red, as 3pkd) in Fig. 4. The last triple peak phase from April to June 2016 (approx. JD 2457114 to 2457175) was observed very weakly as a consequence of the very low emission intensity.

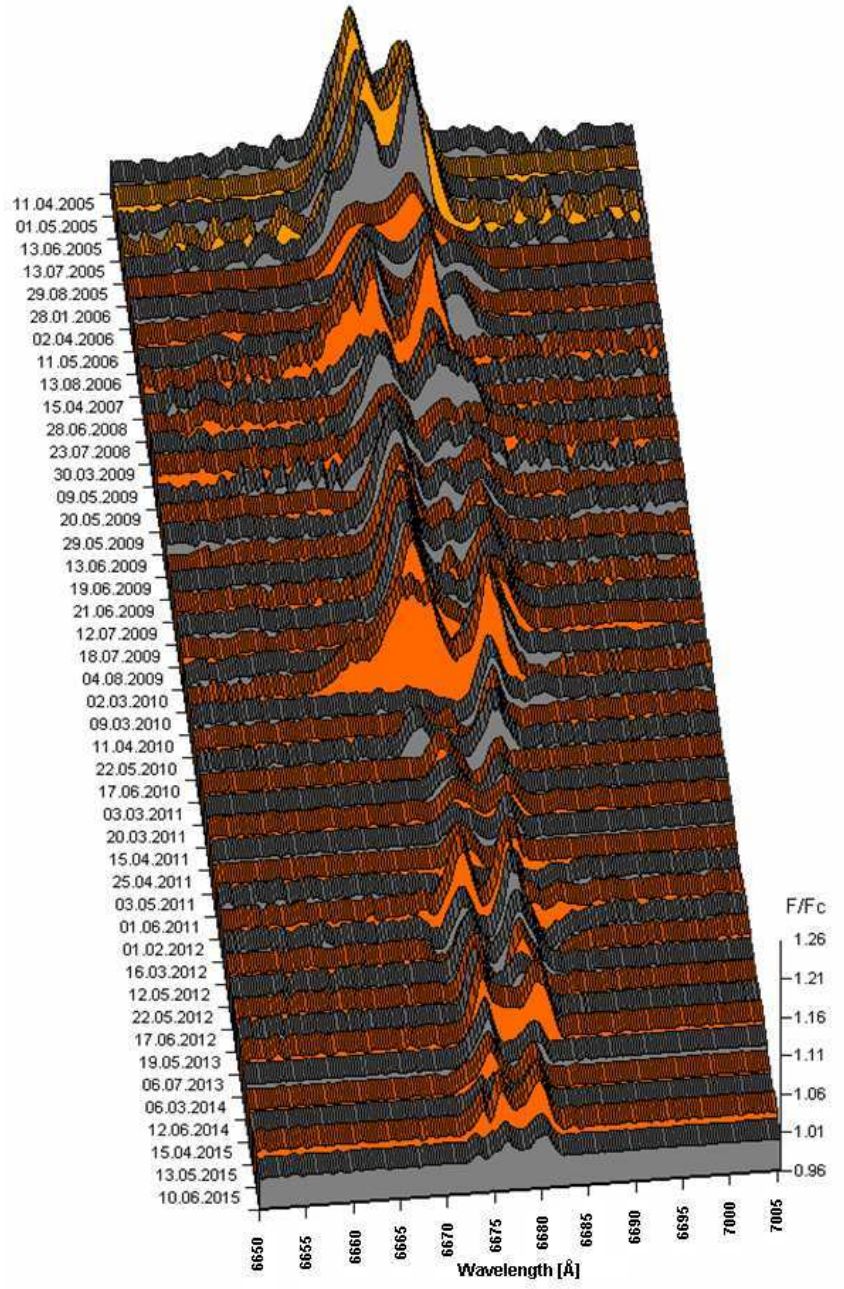

Figure 6. Three-dimensional plot to show the appearance of the third emission component (the triple-peak profile), observed within the phase interval ~ 0.06 to ~ 0.3 (04-08/2006), ~ 0.75 (04/2007), ~ 0.1 to ~ 0.24 (05-07/2009) and ~ 0.03 to ~ 0.13 (04-06/2015).

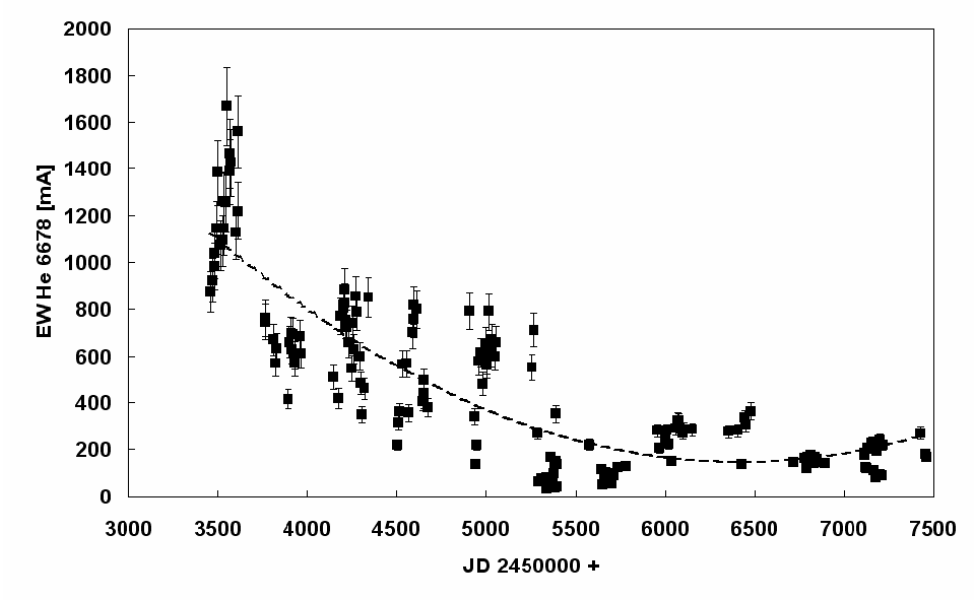

Figure 7. Long-term monitoring of the He I 6678 emission line EW from April 2005 to March 2016.

The plot of the emission intensity long-term monitoring as EW of He I 6678 versus time in Fig. 7 confirms this fact with the EW being at minimum at that time. One can state that there is no certain phase preference for the appearance of this bizarre and mystery line profile characteristics, in the He I 6678 emission of the spectra of δ Sco. This might be due to the presence of a density enhancement sometimes in front of the star and sometimes hidden behind it at other phases.

References:

Bedding, T., R., 1993, *AJ*, **106**, 768
Carciofi, A. C. et al., 2006, *ApJ*, **652**, 1617
Che, X. et al., 2012, *ApJ*, **757**, 29
Coté, J., van Kerkwijk, M. H., 1993, *A&A*, **274**, 870
Hartkopf, W. L., Mason, B., D., McAlister, H., A., 1996, *AJ*, **111**, 370
Innes, R. T. A., 1901, *MNRAS*, **61**, 414
McAlister, H. A., 1978, *ApJ*, **225**, 932
Meilland, A. et al., 2011, *A&A*, **532**, A80
Miroshnichenko, A. S., Fabregat, J., Bjorkman, K. S. Knauth, D. C., Morrison, N. D., Tarasov, A., E., Reig, P., Negueruela, I., Blay, P., 2001, *A&A*, **377**, 485
Miroshnichenko, A. S. et al., 2003, *A&A*, **408**, 305
Miroshnichenko, A. S. et al., 2013, *ApJ*, **766**, 119
Stellingwerf, R. F., 1978, *ApJ*, **224**, 953
Tango, W. J. Davis, J., Jacob, A. P., Mendez, A., North, J. R., O'Byrne, J. W., Seneta, E. B., Tuthill, P., G, 2009, *MNRAS*, **396**, 842

*This version of the paper contains corrections, and differs from the one appeared on-line originally. Date of last modification: Aug 24 08:41:17 CEST 2016

COMMISSIONS 27 AND 42 OF THE IAU
INFORMATION BULLETIN ON VARIABLE STARS

Number 6180

Konkoly Observatory
Budapest
18 August 2016

HU ISSN 0374 – 0676

RW ARIETIS, AN ECLIPSING RR LYRAE STAR?

ODELL, ANDREW P.[1]; SREEDHAR, Y. HARSHA[2]

[1] Dept of Physics and Astronomy, Northern Arizona University, Flagstaff, AZ 86011, USA, e-mail: Andy.Odell@nau.edu

[2] Indian Institute of Astrophysics, Koramangala, Bangalore 560034, India, e-mail: yuvrajharsha@gmail.com

1 Introduction

RW Arietis is a typical RRc star, thus a core-helium burning, post-RGB star pulsating in the radial first overtone (period ≈ 0.3543 days, amplitude in $V \approx 0.540$ mag); normally these stars have a stable period and light curve behavior. Variability of the star was discovered by Detre (1937), who found an alias (0.26141 days) of the true period, which was corrected by Notni (1962) to 0.3543184 days.

Wiśniewski (1971) brought attention to RW Ari when he announced what appeared to be eclipses on three of his 19 nights of photoelectric observations in 1966-7[1]. He suggested an orbital period of 3.1754 days, with the companion star being perhaps a blue giant or young B-type star, based on eclipse depth and color change. He acknowledged that this is difficult to understand, since the RR Lyr component would have gone through the red giant phase, and presumably destroyed a close companion. However, Wiśnewski should have noticed that on another night when a primary eclipse was expected, it was not seen, and a bright blue companion would have diluted the pulsation amplitude, also not seen.

Abt & Wiśniewski (1972) searched for evidence of orbital motion by obtaining spectra of RW Ari at presumably the same pulsation phase, but separated by half the purported orbital period, and found a radial velocity difference of 35 $\mathrm{km\,s^{-1}}$. Unbeknown to these authors, the pulsation period had changed and their phasing was not correct (see sections 3 and 5). Also in response to Wiśnewski's claim, Edwards (1978) and Goranskij & Shugarov (1979) (GS79 in tables) separately undertook photometric observations to confirm or deny the 3.17 days period, both ruling out that possibility.

If confirmed, RW Ari would be the first true RR Lyr star in an eclipsing binary. Others have been suggested, including TU UMa, VX Her, RZ Cet, and OGLE-BLG-02792; the first has a possible period of 23 years, the second and third have not been confirmed, and the final one has a mass much too small to be a classical RR Lyr star (see Liska 2016). The observation of a mass and radius could resolve the discrepancy between RR Lyr masses derived from stellar evolutionary and pulsation models.

[1] Wiśniewski's data is available from Bookmyer et al. (1977), two nights of which, taken in April 1969, cannot be RW Ari, as it was behind the sun at that time

We realized that a wealth of photometric measurements exists in surveys (such as Super-WASP), and that if eclipses occur with any short period, evidence should be easy to obtain from them. In addition, Lowell Observatory agreed to use its robotic NASAcam to visit the star once per hour to also attempt to discover eclipses. No further eclipses were seen in any of the data sets (see section 2). This allows us to put a lower limit on the orbital period of at least 25 days, and almost certainly eliminate one longer than this, as well.

Since we have many new timings of maximum and minimum light, as well as excellent light and radial velocity curves, we decided to collect all this information and make it available to the community, which is the purpose of this paper (see sections 3, 4, and 5).

2 Attempt to Find Eclipses

Wiśniewski (1971) claimed that RW Ari exhibited an eclipse ingress on April 16, 1966 (JD 2439384) that lasted for two hours. He advocated an orbital period of 3.1754 days based on two additional nights that might have shown a primary and a secondary eclipse, but this was ruled out by two subsequent studies: Edwards (1978) and GS79. However, these studies left open the the possibility that some other period might be appropriate, but with no idea when to observe again. We realized that several all-sky survey archives could be searched for evidence of eclipses, and with very little effort. Table 1 lists all the sources of photometric data we could find.

Table 1. Photometric Datasets

Source	Years	Number of points	Sigma (mag)
Detre	1936-1937	294	0.16
Wiśniewski	1966-1967	107	0.04
Penston	1970	29	0.04
GS79	1976-1978	256	0.10
Edwards	1976-1978	657	0.03
NSVS	1999-2000	220	0.10
ASAS	2002-2010	211	0.10
CSS	2004-2011	252	0.08
Pi Of The Sky	2006-2009	1272	0.15
Super-WASP	2006-2009	5249	0.03
Lowell NASAcam	2011-2016	1194	0.004

NSVS = Northern Sky Variability Survey (Wozniak et al. 2004)
ASAS = All Sky Automated Survey (Pojmanski 2002)
CSS = Catalina Sky Survey (Drake et al. 2014)
Pi Of The Sky (Mankiewicz et al., 2014)

The survey with the highest quality and quantity of photometry is the Super-WASP (Wide Angle Search for Planets; see Pollacco et al. 2006). Richard West (personal comm.) graciously and quickly supplied over 3000 useful measures from the 2006-7 season, and another 2200 from 2008-9. Unfortunately, after eliminating the measures with greater than 5% error, no obvious deviations from the RR Lyr light curve emerged.

We also undertook observations with the Lowell Observatory 0.8-m telescope with NASAcam in robotic mode (Buie 2010) using the B filter, obtaining one image each available hour, during 2011-12 season, which amounts to an additional 1100 measures. With an eclipse lasting at least three hours, and probably four, this would catch either a primary or secondary eclipse if it happened. Again unfortunately, no eclipses were seen.

Our entire set of photometric observations are given in Table 8, as HJD and magnitude: (for filters B, V, R, and I). (The table is available through the IBVS website as `6180-t8.txt`.) Since the Super-WASP data has not been released for stars within 20° of the equator, we also make available that photometry in Table 9, as HJD and unfiltered magnitude. (This table is also available through the IBVS website as `6180-t9.txt`.)

This lack of eclipses meant we could not find an orbital period or predict another eclipse. So we decided to see what periods we could eliminate with this data set, by writing a FORTRAN program which would consider periods starting at Wiśniewski's 3.17 days, and work upward, folding the SuperWASP and NASAcam times of no eclipse, and looking for the largest gap in time. The trial period was incremented by 0.14 minute up to 5.17 days, and then 1.4 minutes up to 25 days.

The lower panel of Fig. 1 shows the largest gap (in hours) in a possible light curve as a function of period. If the gap is less than three hours, then that assumed period can be ruled out. With longer gaps, the probability of an eclipse being able to hide in them can be estimated as the length of the gap, minus three hours, divided by the period, which is displayed in Fig. 1 top panel. Large gaps appear at exact integer numbers of days, as the eclipse could take place always during daylight hours. So, for example, if the period were exactly 5.0 days, the largest gap would be about 10 hours, during daylight, and the eclipse missed. If the period were just 1.5 minutes longer or shorter than 5.0 days, the eclipse would migrate into the night, and have been observed sometime during our coverage. However, the probability the orbital period would be that close to 5.0 days is at the 0.02% level.

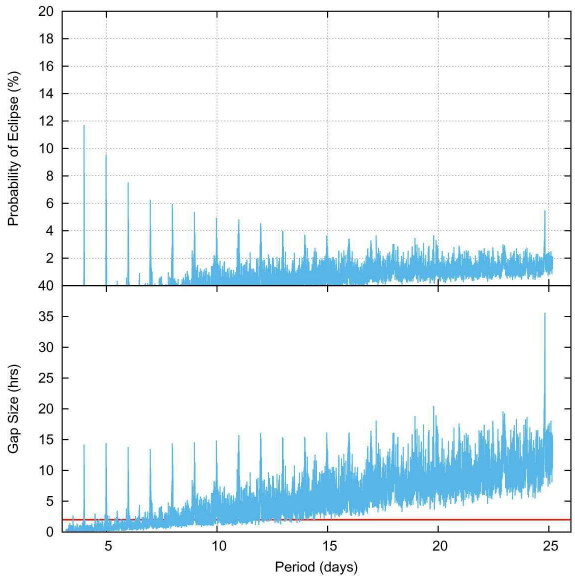

Figure 1. Bottom panel - the size of the largest gap in hours, as a function of assumed (folding) period in days. Top panel - the probability of missing an eclipse (percentage which the largest gap (minus 3 hours) is, of the assumed period).

We find that no period of less than eight days could harbor an eclipse at all, and up to 25 days, the gap was so small there was only a 2% chance we would have missed one. For longer periods yet, eclipses are very unlikely, and most likely ruled out with the many other photometric studies and surveys which also exhibit no eclipses.

A much longer orbital period cannot be ruled out; indeed it becomes more likely, due to larger uncovered gaps. However, it also becomes much less likely that the orbit would be oriented edge-on to the level necessary. Discouraged by this eventuality, we decided to study the RR Lyr pulsations instead, to which the rest of this paper is devoted.

3 Pulsation Period Changes and Ephemeris

3.1 Ephemeris for the timings from Lowell Observatory

In anticipation of finding eclipses for RW Ari which would affect the RR Lyr light curve, we decided to obtain a full, high quality light curve in BVRI on 21 October, 2011 with Lowell Observatory's NASAcam (see section 3). We continued to record full light curves on additional nights, to monitor any period or light curve changes. While many light curves have been made over the years, there has been a problem fitting all of them with one period (see Todoran 1988). Ultimately we derived timings of maximum and/or minimum light on 13 additional nights between 2011 and 2016, as well as a few timings from the B filter alone (details given in section 3).

The light curve of RW Ari seems to remain quite constant over the years, but it has a very broad maximum (see section 3). Thus we determined that minimum light occurs at phase 0.55, and used timings of that as well, adjusting the cycle count by that fraction. The method of finding the time of maximum or minimum is a method developed for eclipsing binary stars by Kwee & van Woerden (1956). Essentially the light curve is folded about a time, so the rising branch falls over the descending branch, and the folding time adjusted to obtain the best correlation (here done by eye). In a few instances, maximum or minimum was not well covered, and the timing was determined by overlaying the phased light curve with the night of 26 September, 2013 as a template, and adjusting the assumed phase zero time until the two curves coincided optimally.

Our results are shown in Table 2, where the estimated cycle number E, HJD, and $(O-C)$ residual in minutes are given. Col. 4 indicates the standard deviation of the times derived from the 4-filter light curves, typically under 5 minutes, and col. 5 gives the UT date. A minimum timing is indicated by a cycle number with the fraction 0.55 added. We quickly saw that the data from the 2011-12 season is incompatible with the later timings; a period change must have occurred after the 2011-12 observing season. We fit the timings after this (and without the two timings in February 2015; see below) with a linear ephemeris, which is

$$\mathrm{HJD}_{\mathrm{max}} = 2455854.753(2) + 0.3543113(7)\mathrm{E} \qquad (1)$$

(uncertainty in the last digit is given in parentheses). The RMS of the $(O-C)$s for the fit data is 5.1 minutes, consistent with our estimated uncertainty of the timings.

The $(O-C)$ residuals from eq. 1 are plotted in Fig. 2a (lower left panel). It can be seen that two epochs do not fit the trend within the expected errors, and these were not used to derive eq. 1. The first is around HJD 2455900, which we take to be due to a period change, and the second is two measures at HJD 2457100. These latter timings show a residual of about 20 minutes, whereas the uncertainty in the average of four filters is about four minutes. We have no explanation for this (but see section 5); when measurements were again possible, the phase and period were back to what they were before the anomaly. We checked the data from those nights and could find no problems; indeed the timings for other stars from those nights were within a minute of the predicted ones.

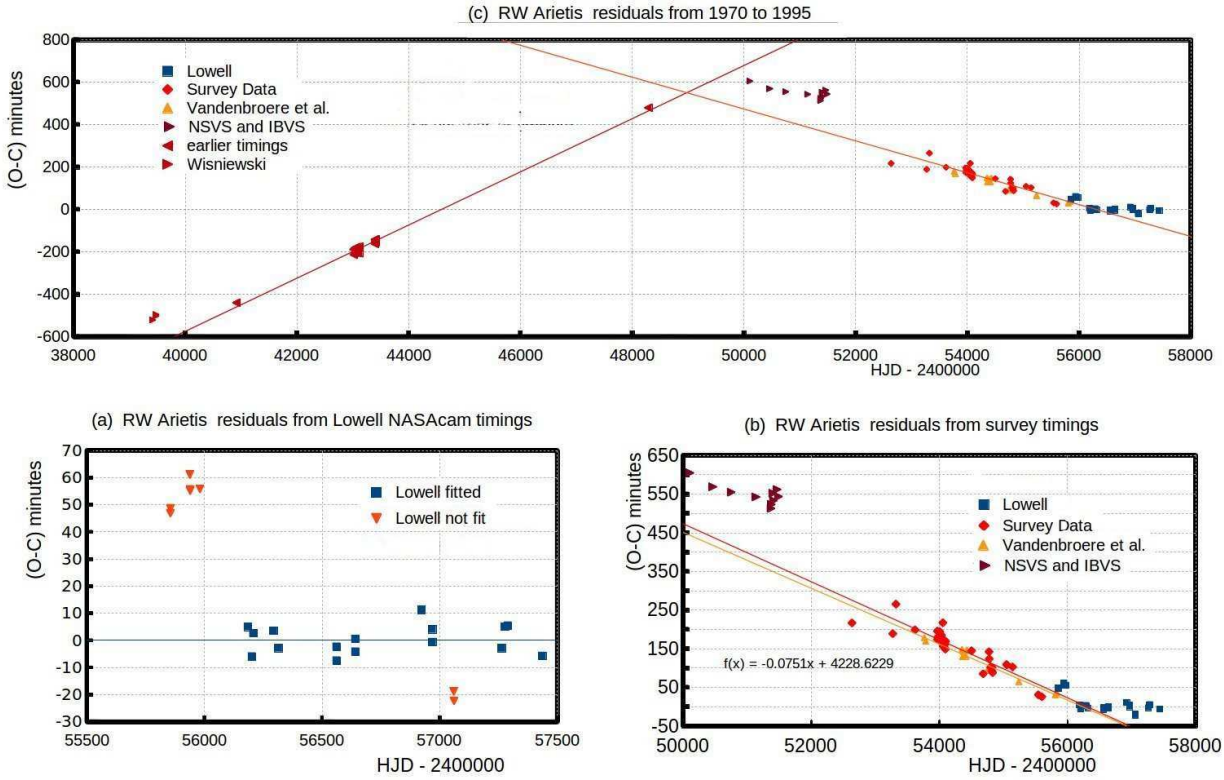

Figure 2. Top panel: The $(O-C)$ diagram including timings from 1966 to 2016; $(O-C)$ is the residual between the observed times of extrema and those computed from eq. 1; Lower left panel: The $(O-C)$ diagram for the 2012-16 NASAcam timings, still based on eq 1; Lower right panel: The $(O-C)$ diagram including the timings from survey data, still based on eq. 1.

Table 2 Ephemeris timings from NASAcam light curves.

Cycle	HJD −2400000	$(O-C)$ min	Quality min	UT date
4464.55	57436.5893	−5.3	3.6	02/18/16†
4462.00	57435.6860	−5.1	2.9	02/17/16†
4050.00	57289.7173	5.8	6.9	09/25/15†
4016.55	57277.8653	5.0	5.9	09/12/15
3977.00	57263.8468	−2.5	2.3	08/29/15
3403.55	57060.6535	−22.0	4.2	02/07/15*
3401.00	57059.7524	−18.6	4.4	02/06/15*,†
3144.55	56968.9019	−0.4	3.3	11/06/14
3144.00	56968.7103	4.3	5.7	11/06/14
3015.00	56923.0091	11.4	1.8	09/23/14†
2221.55	56641.8701	−4.1	5.2	12/15/13
2221.00	56641.6785	0.6	5.0	12/15/13
1996.00	56561.9529	−7.4	7.2	09/26/13
1995.55	56561.7970	−2.3	3.9	09/26/13
1298.00	56314.6468	−2.9	1.8	01/22/13
1238.55	56293.5867	3.5	2.2	01/01/13
997.00	56208.0029	2.6	**	10/08/12
979.55	56201.8135	−6.0	**	10/01/12
931.00	56184.6200	4.9	**	09/14/12
355.00	55980.5720	55.7	**	02/23/12*
237.00	55938.7628	55.0	2.1	01/11/12*
236.55	55938.6030	55.5	3.6	01/10/12*
234.00	55937.7040	61.0	6.9	01/10/12*
0.55	55854.9807	48.5	4.7	10/20/11*
0.00	55854.7853	46.8	4.0	10/20/11*
−164.00	55796.6780	46.4	**	08/23/11*
−212.00	55779.6710	46.3	**	08/06/11*

†timing derived by fitting template from 9/26/2013 (see text).
*not used in fit for eq. 1, which was used to compute $(O-C)$.
**used only B measures: 10/08/12 and 10/01/12 used one night each; 9/14/12 combined 2 nights; 2/23/12 combined 8 nights; 8/23/11 and 8/06/11 combined 3 nights each.

3.2 Ephemeris for the timings from survey data

To investigate the period change and extend the ephemeris back in time, we extracted timings from the archival survey datasets shown in Table 1, extending back to 2004, and they confirm that the period indeed had been different before 2011. After doing this we discovered timings made by Vandenbroere & Salmon (2009), which exhibit the same period as our survey results, thus verifying the period change. The ephemeris for the years 2004-2011 which we derive from those timings is

$$\mathrm{HJD}_{\mathrm{max}} = 2455854.763(6) + 0.3542890(1)\mathrm{E}, \tag{2}$$

and the RMS residual from that fit is then 15.8 minutes. This is compatible with an estimate of the precision of the survey timings, and is consistent with Vandenbroere & Salmon (2009), the RMS of which is 14.4 minutes. Fig. 2b (lower right panel) shows the $(O-C)$ residuals (still based on eq. 1) extended back to 1996.

There is another problem, however, in that the Lowell timing residuals from 2011-12 season are above the line fit to the survey data by about 25 to 50 minutes, and this discrepancy appears to have been increasing with time. When one recalls that the expected precision of these measures is about five minutes, this is highly significant, and again, we have no explanation for it (but see section 5).

Table 3 Ephemeris timings from survey light curves.

Cycle	HJD −2400000	$(O-C)$ min	Source
−723.00	55598.6035	−11.9	CSS 2010-11
−875.00	55544.7516	−11.8	CSS 2010-11
−2012.55	55141.7556	24.6	CSS 2009-10
−2264.00	55052.6671	22.2	Super-WASP
−2278.00	55047.7072	22.4	Super-WASP
−2894.00	54829.4370	−17.8	Super-WASP
−2914.00	54822.3600	−5.1	Super-WASP
−2925.00	54818.4560	−14.9	Super-WASP
−2976.00	54800.3930	−6.6	Super-WASP
−3040.55	54777.5380	13.1	Super-WASP
−3048.55	54774.7164	31.4	CSS 2008-09
−3816.55	54502.6071	9.8	CSS 2007-08
−4966.00	54095.3600	−2.2	Super-WASP
−4994.00	54085.4340	−10.7	Super-WASP
−4997.00	54084.3780	−0.8	Super-WASP
−5000.00	54083.3100	−8.2	Super-WASP
−5022.00	54075.5200	−1.9	Super-WASP
−5025.00	54074.4450	−19.4	Super-WASP
−5039.00	54069.4930	−7.8	Super-WASP
−5042.00	54068.4270	−12.3	Super-WASP
−5045.00	54067.3710	−2.4	Super-WASP
−5073.00	54057.4400	−18.1	Super-WASP
−5083.55	54053.7449	42.3	CSS 2006-7
−5146.00	54031.5950	8.0	Super-WASP
−5174.00	54021.6690	−0.5	Super-WASP
−5177.00	54020.6075	1.5	Super-WASP
−5211.00	54008.5600	−0.9	Super-WASP
−5219.00	54005.7270	1.0	Super-WASP
−5222.00	54004.6730	13.7	Super-WASP
−5225.00	54003.6110	15.0	Super-WASP
−5239.00	53998.6420	2.1	Super-WASP
−5242.00	53997.5750	−3.8	Super-WASP
−5253.00	53993.6815	1.5	Super-WASP
−5270.00	53987.6520	−8.0	Super-WASP
−5304.00	53975.6100	−2.5	Super-WASP
−5318.00	53970.6460	−8.2	Super-WASP
−5321.00	53969.5980	13.2	Super-WASP
−6308.00	53619.8950	−14.5	CSS 2005-6
−7149.55	53321.7712	25.5	CSS 2004-5
−12321.00	51489.6606	141.3	NSVS*
−12384.00	51467.3517	157.6	IBVS 5017*
−12546.00	51409.9334	123.9	NSVS*
−12580.00	51397.8999	141.7	NSVS*
−12642.00	51375.9126	110.9	NSVS*

*not used in fit for eq. 2, which was used to compute $(O-C)$.

3.3 Ephemeris for timings between 1996 and 2001

There is a gap in the available timings of about three years before 2004 but the NSVS allows some estimates between 1996 and 2001, as well as five timings taken from IBVS between 1996 and 1999. As shown at the end of Table 3, these timings are inconsistent with the ephemeris given in eq. 2, the residuals being over two hours. Therefore there must have been another period change within that gap.

An ephemeris can be derived from these timings, which differs from those before and

after, and is represented by

$$\mathrm{HJD}_{\max} = 2455855.00(4) + 0.354301(3)\mathrm{E}. \quad (3)$$

Table 4 shows the timings and the residuals, which have an RMS of 16.1 min. The next earlier timing, given in the last line of that table, has a residual of over three hours, showing that another period change must have occurred.

Table 4 Ephemeris timings between 1996 and 2000.

Cycle	HJD −2400000	$(O-C)$ min	Source
−12321.00	51489.6606	10.0	NSVS
−12384.00	51467.3517	27.4	IBVS 5017
−12546.00	51409.9334	−3.6	NSVS
−12580.00	51397.8999	14.8	NSVS
−12642.00	51375.9126	−14.9	NSVS
−12656.00	51370.9450	−25.6	A.Paschke, ROTSE
−13310.00	51139.2460	−5.5	IBVS 4712
−14410.00	50749.5120	−9.5	IBVS 4606
−15215.00	50464.3012	−7.2	IBVS 4562
−16228.00	50105.4089	14.0	IBVS 4382
−21359.00	48287.3500	−187.4	Hübscher et al. (1992)*

*not used in fit for eq. 3, which was used to compute $(O-C)$.

3.4 Ephemeris for timings between 1972 and 1996

Before 1996, timings are sparse back to the discovery paper, but we managed to find an ephemeris which fit well the ones between 1970 and 1991, which is

$$\mathrm{HJD}_{\max} = 2455855.73(2) + 0.3543421(5)\mathrm{E}. \quad (4)$$

The RMS residual of those timings from this ephemeris is 12.7 minutes, lower than we have any right to expect. Thus, contrary to several published suggestions, the period seems to have been constant for over 20 years. Fig. 2c (upper panel) shows the $(O-C)$ residuals (still based on eq. 1) extended back to 1966. Table 5 contains the timings and residuals from this even earlier epoch.

3.5 Ephemeris for timings before 1972

When Detre (1937) discovered RW Ari to be variable, he derived an alias (0.2614151 days) to the true period. Though his dataset is not very good by today's standards, being photographic magnitudes, it is useful in determining the ephemeris at that early epoch. Notni (1962) observed the star photoelectrically in 1959, and published a new ephemeris with the approximately correct period of 0.3543184 days. He promised to publish his actual data, but that evidently was never done. Todoran (1988) found a period compatible with the data of Detre, Wiśniewsi, and Penston of 0.3543145 days, but this is incompatible with Notni's period.

We find that Todoran probably made a cycle count error by adding one cycle to the gap between Detre and Wiśniewski's data. We have derived a new ephemeris for those years:

$$\mathrm{HJD}_{\max} = 2455854.99(2) + 0.3543241(3)\mathrm{E}. \quad (5)$$

While this and Todoran's ephemeris (with different cycle count) fit the early photometry equally well, ours fits Detre's considerably better, and so we adopt it here.

Table 5 Ephemeris timings between 1970 and 1991.

Cycle	HJD −2400000	$(O-C)$ min	Source
−21359.00	48287.3500	15.2	Hübscher et al. (1992)
−35128.00	43408.4040	2.1	GCVS
−35139.00	43404.5004	−6.3	GS79
−35142.00	43403.4460	6.1	GS79
−35156.00	43398.4814	0.7	GS79
−35166.00	43394.9280	−13.7	Edwards
−35177.55	43390.8500	7.4	Edwards
−35948.55	43117.6530	8.5	Edwards
−35962.55	43112.6900	5.3	Edwards
−35971.00	43109.6770	−21.7	Edwards
−36086.55	43068.7620	−5.2	Edwards
−36098.00	43064.6800	−15.3	Edwards
−36100.55	43063.7960	12.9	Edwards
−36166.00	43040.5900	−7.7	GS79
−36175.00	43037.4150	12.5	GS79
−36185.00	43033.8550	−11.3	Edwards
−36230.00	43017.9050	−18.0	Edwards
−36233.00	43016.8430	−16.5	Edwards
−36251.00	43010.4820	8.2	GS79
−42163.00	40915.6190	19.4	Penston
−42165.00	40914.9090	17.5	Penston
−46224.00	39476.7173	137.1	Wiśniewski*
−46227.00	39475.6592	144.1	Wiśniewski*
−46401.00	39413.9913	126.3	Wiśniewski*

*not used in fit for eq. 4, which was used to compute $(O-C)$.

We can use Notni's ephemeris to estimate a timing for his epoch:

$$\mathrm{HJD}_{\max} = 2428183.324 + 0.3543184 \times 24501 = 2436864.4791 \tag{6}$$

which corresponds to UT 23 Oct, 1959 23:30. Note this is NOT an actual timing from Notni, but a time which fits his ephemeris, and is therefore possible. The phase of this time, based on Todoran's ephemeris, is 0.325, which is incompatible. The phase derived from eq. 5 is also incompatible, being 0.561. Without finding Notni's actual data, we cannot decide whether this indicates another period change, or some problem with that data.

Lastly, we note the excellent fit of Penston's data to eq. 5, but the large residuals of about 18 minutes based on eq. 4 suggest that the period change in 1972 took place somewhat after Penston recorded her data. It is possible that the Harvard Plate Collection[2] could shed light on the behavior of the star in these gaps, but plates from that part of the sky have not yet been scanned.

It is clear that the star has changed its period at least three and possibly four or five times since its discovery, and it is clear that anomalous (but not seemingly periodic) excursions in timings occur, which means the star should be monitored in the future, to extend and verify these behaviors.

[2] `http://dasch.rc.fas.harvard.edu/project.php`

4 The Light Curve

On UT 20 Oct, 2011 we used NASAcam at Lowell Observatory to obtain light curves of RW Ari in B, V, R, and I filters. The images were processed using IRAF[3] for overscan, zero, and flat field corrections. Magnitudes were extracted with IRAF task QPHOT, and corrected approximately to standard values by using the average of the comparison stars listed in Table 6. The magnitudes of the comparison stars were measured by observing Landolt field 92 on UT 26 Sept, 2013, to produce a final light curve, shown in Fig. 3 for the V filter.

Table 6 Stars used from NASACam images.

Object	Purpose	B magnitude	V magnitude	Comments
RW Ari	Target	12.40-12.96	12.06-12.48	RA $2^h16^m03\overset{s}{.}7$ dec $+17°31'04''$
BD +16 262	Comp 1	11.72	11.01	22^s W and $22''$ S
BD +15 264	Comp 2	11.63	10.96	13^s E and $3'$ N
Un-named	Check	12.65	12.03	$1\overset{s}{.}8$ E and $6''$ S

The light curve shows a broad maximum, a slow decline in brightness, a rather narrower minimum at phase 0.55, and a more rapid rise to maximum. On the rising branch the star remains constant for about 25 minutes (phase 0.815 to 0.865), thus it exhibits a stillstand. The check star used was the companion star about 1.8^s to the east, which is a mid-F star of similar color to RW Ari, and its magnitude is shown also in Fig. 3.

The lower panel shows the $(B-V)$ color, which is bluest at phase 0.00 when the star is brightest, and reddest at phase 0.55 when the star is faintest. Light curves at additional 13 epochs over the next five years show no differences from the one presented in Fig. 3, after being corrected to consistent phase; no measures in B filter or in Super-WASP data show any deviation. The light curve appears to be quite repeatable over at least 10 years.

5 Radial Velocities

Spectra were taken with the Boller and Chivens spectrograph on the Bok 2.3-m telescope at Steward Observatory on Kitt Peak AZ during 2012-2014. We used this instrument configured with the 832 lines/mm grating in second order, which yields a dispersion of 0.72 Å/pix (50 $\mathrm{km\,s^{-1}}$), and a 1.5 arcsec entrance slit, which gives a resolution of 0.88Å. The camera was the Loral thinned, back-illuminated 1200×800 chip binned 1×2, so the effective 2-pixel resolution was undersampled at 1.44Å, or 100 $\mathrm{km\,s^{-1}}$ over the region 3850-4700Å. The exposure time of 10 minutes yielded a S/N of about 100. Six HeAr comparison spectra were taken before and after each pair of target spectra, and averaged, for wavelength calibration.

The spectra were reduced with IRAF, and task FXCOR was used to derive radial velocities by cross-correlating with the template spectrum (Image 0067 from 4 Nov 2014), which was of HD222368 (an F7V star with heliocentric radial velocity +5.95 $\mathrm{km\,s^{-1}}$). Table 7 gives the image number, HJD (minus 2400000), phase based on the listed ephemeris, the radial velocity, and the formal error from FXCOR. Fig. 4 shows the resulting radial velocity curve; spectra from UT 11 Jan, 2012 were included to help fill the gap near phase

[3]The Image Reduction and Analysis Facility, a general purpose software package for astronomical data, written and supported by the IRAF programming group of the National Optical Astronomy Observatories (NOAO) in Tucson, AZ.

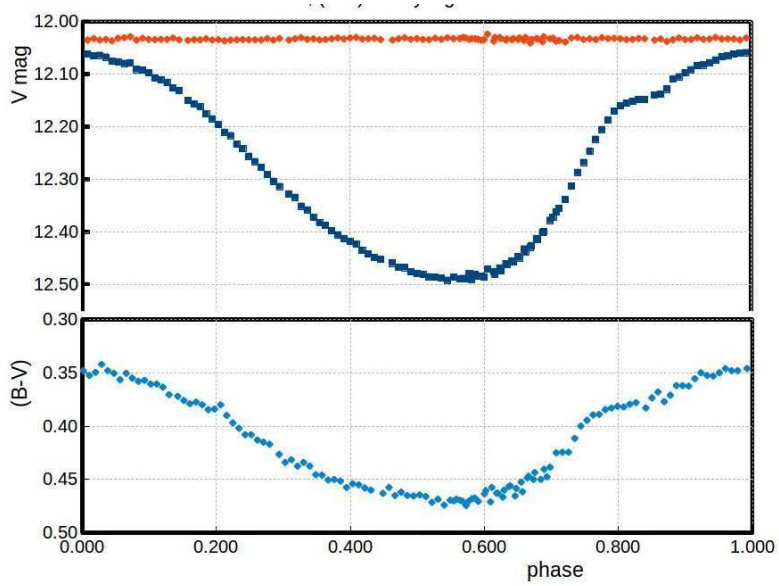

Figure 3. The V and $(B-V)$ light curves derived from images obtained on October 20, 2011 with NASAcam.

0.80 when the velocity was rapidly decreasing. The radial velocities from Jeffery et al. (2007) are also plotted, but with their phase updated. The individual spectra are available in a web database through the IBVS website as a gzipped tar archive `6180.tar.gz`.) When used only with hydrogen lines (Hγ, Hδ, Hϵ and Hζ), the velocities were consistently 7 $\mathrm{km\,s^{-1}}$ redward, and when used only with lines other than hydrogen, were 3 $\mathrm{km\,s^{-1}}$ blueward of the tabulated values.

The median heliocentric velocity is -47.5 $\mathrm{km\,s^{-1}}$, which would induce a period change of +4.8 seconds due to Doppler shift, as suggested by Davies et al. (2014).

Along with the spectra used for Table 7, we obtained radial velocities on two additional nights in 2012 and two in December 2013, but these velocities appeared to be anomalous, in that there were jumps in the velocity curve which would not make sense for a single star. It is remotely possible that this is evidence of a light travel time effect in a binary system, but the orbit would need to be highly elliptical and oriented in a special way to our line of sight.

The final problem with radial velocities of this star is the measurements of Abt & Wiśniewski (1972), who found a discrepancy of 35 $\mathrm{km\,s^{-1}}$ on two nights chosen to have the same pulsation phase, but different orbital phases. However, there was a period change in the pulsation before the spectra were obtained, and in fact, the conditions on phase were not met (see section 3). Even so, the second measure is given by them as -11 $\mathrm{km\,s^{-1}}$, which is much bluer than any we obtained. One possibility was that the companion star was inadvertently measured, which has roughly this velocity.

With thoughts of some problem with the velocity measurements, we obtained the original photographic spectra from Kitt Peak, and digitally scanned them, so they could be treated with IRAF. This was an interesting exercise, because many weak lines popped out in the scanned spectra that were lost when looking at the plates. The first thing we noticed was that six spectra were obtained in 1972, one of which was underexposed, one was of the companion star (which is obviously a mid-F type), and four were of RW Ari.

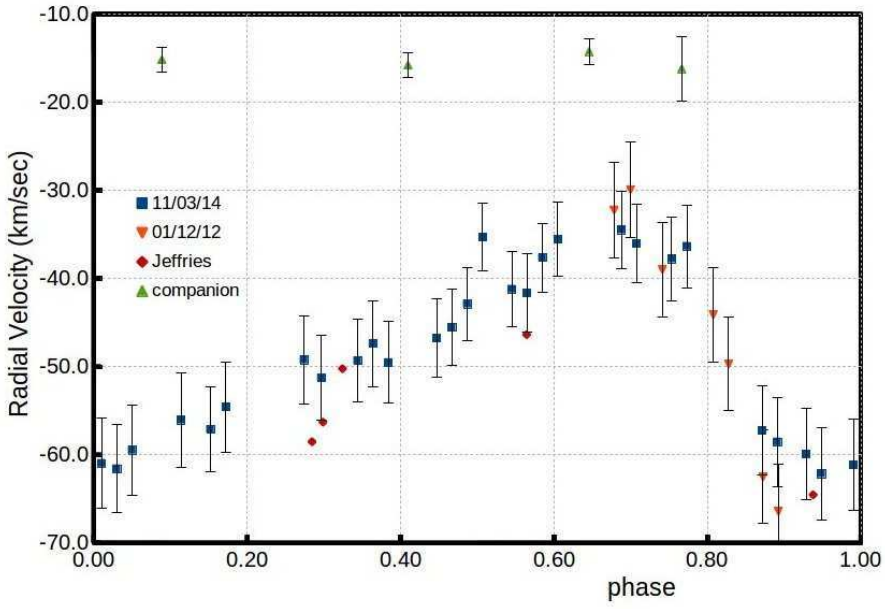

Figure 4. The radial velocity curve derived from spectra from UT 3 Nov, 2014 and UT 12 Jan, 2012. The four radial velocities above -20 km s^{-1} are for the companion star, which while not an RV standard, appears to have constant velocity.

We reduced the spectra twice, once using Abt's eight comparison lines and five stellar lines (Hγ, Hδ, Ca II K, Hζ, and Hϵ), and once using all the lines in both the comparison and stellar spectra (over 50 of each). We used IRAF task RVID to derive velocities, and both methods agree well with the photographic measurements. Even the companion's velocity agrees with the ones we measured here. Thus we are unable to find any explanation for the anomaly in the spectra themselves.

6 Conclusions

Although RW Ari has long been suspected of being in an eclipsing binary system, we find that this is almost certainly not the case. Except under extremely unusual circumstances, an eclipse would have been seen by now, with the plethora of photometric measurements that have been made of the star.

The star remains an interesting object in itself. It has changed its period abruptly several times since being discovered, at least around 1968, 1994, 2002, and 2011. It also exhibits anomalous behavior on a short timescale, where for a few nights to a few months, the light curve appears shifted in phase from the normal ephemeris before and after. One possible explanation for this phenomenon was suggested by Learned et al. (2008), ie that an advanced civilization could modulate pulsating star phase as a means of communication. If this is the explanation for RW Ari, we have no clue what message we are being sent.

Odell (2012) has shown that BW Vul, the largest amplitude β Cephei star, shows similar discreet changes in period. Sweigart and Renzini (1979) demonstrated that mixing events in the semiconvective zone or in convective overshoot in horizontal branch models

Table 7 Measured radial velocities for RW Ari.

Image	HJD (mid) −2400000	phase*	RV helio km s^{-1}	uncertainty km s^{-1}	Comments
	3 Nov 2014				
21	56965.6185	0.274	−49.2	4.9	
22	56965.6265	0.297	−51.3	4.8	
35	56965.6432	0.344	−49.3	4.7	
36	56965.6503	0.364	−47.4	4.8	
37	56965.6575	0.384	−49.5	4.6	
38	56965.6665	0.410	−15.8	1.4	companion
51	56965.6798	0.447	−46.7	4.5	
52	56965.6868	0.467	−45.5	4.3	
53	56965.6939	0.487	−42.9	4.2	
54	56965.7010	0.507	−35.3	3.8	
67	56965.7145	0.545	−41.2	4.3	
68	56965.7215	0.565	−41.6	4.4	
69	56965.7286	0.585	−37.6	3.9	
70	56965.7357	0.605	−35.5	4.2	
83	56965.7501	0.646	−14.2	1.5	companion
96	56965.7650	0.688	−34.5	4.4	
97	56965.7721	0.708	−36.1	4.4	
110	56965.7883	0.753	−37.8	4.7	
111	56965.7954	0.773	−36.3	4.7	
143	56965.8301	0.871	−57.2	5.1	
144	56965.8372	0.891	−58.5	5.1	
157	56965.8505	0.929	−59.9	5.1	
158	56965.8575	0.949	−62.2	5.3	
171	56965.8722	0.990	−61.1	5.2	
172	56965.8793	0.010	−61.0	5.1	
173	56965.8863	0.030	−61.6	5.0	
174	56965.8934	0.050	−59.5	5.1	
187	56965.9071	0.089	−15.2	1.4	companion
188	56965.9160	0.114	−56.1	5.4	
201	56965.9296	0.152	−57.1	4.9	
202	56965.9367	0.172	−54.6	5.1	
	11 Jan 2012				
7	55937.5900	0.678	−32.2	5.4	
8	55937.5976	0.700	−29.9	5.4	
21	55937.6122	0.741	−39.0	5.4	
22	55937.6212	0.766	−16.2	3.7	companion
35	55937.6358	0.807	−44.1	5.4	
36	55937.6429	0.828	−49.7	5.3	
49	55937.6587	0.872	−62.5	5.3	
50	55937.6658	0.892	−66.4	5.3	

*The phases for 3 November, 2014 were calculated from the light curve from three nights later, ie phase 0 = HJD 56968.7103. The phases for 11 January, 2012 were calculated from the light curve from the same night, ie phase 0 = HJD 55937.7040. 'companion' indicates a spectrum of the photometric check star.

could produce period changes in RR Lyr stars such as we observe for RW Ari.

The light curve of RW Ari is rather typical of an RRc star, roughly sinusoidal, but with a steeper rise in brightness than fall. It shows a stillstand of about a half hour during the rise time. Even though the period changes in strange ways, the light curve repeats itself quite well.

The radial velocity of the star shows a typical RR Lyr behavior, but there are nights

when the velocity appears quite different than expected. While this could be a problem with the observations (A-type stars are notably difficult to measure velocities for), it could also indicate a long-period binary orbit, but that would require a very specific orientation of the orbit.

As in most similar studies, more work needs to be done on the star, in particular, continued monitoring for period changes and erratic behavior of the pulsation cycle. Future sky surveys could prove extremely valuable in this endeavor.

Acknowledgements: We would like to thank Lowell Observatory for making time available on their 0.8-m telescope, and Steward Observatory for time allocated on the Bok 2.2-m telescope. We especially appreciate Robert West's effort to supply us with SuperWASP photometry, which was essential for the work done here. We thank Helmut Abt for loaning his spectra from Kitt Peak. We benefited from discussions with Eckhart Spalding, Horace Smith, and Sebastian Otero, as well as Jacqueline Vandenbroere and Chris Sterken. This research has made use of the SIMBAD database, operated at CDS, Strasbourg, France.

References:

Abt, H. A., Wiśniewski, W. Z., 1972, *IBVS*, **697**
Agerer, F., Dahm, M., Hübscher, J., 1999, *IBVS*, **4712**
Agerer, F., Dahm, M., Hübscher, J., 2001, *IBVS*, **5017**
Agerer, F., Hübscher, J., 1996, *IBVS*, **4382**
Agerer, F., Hübscher, J., 1998, *IBVS*, **4562**
Agerer, F., Hübscher, J., 1998, *IBVS*, **4606**
Bookmyer, B. B. et al., 1977, *RMxAA*, **2**, 235
Buie, M. W., 2010, *Adv. in Astron.*, AID:130172
Davies, G. R. et al., 2014, *MNRAS*, **445**, L94
Detre, L., 1937, *AN*, **262**, 81
Drake, A. J., et al., 2014, *ApJS*, **213**, 9
Edwards, D. A., 1978, *A photometric investigation of the variable RW Arietis*, master thesis, University of Texas, Austin, USA
Goranskij, V. P., Shugarov, S. Y., 1979, *Peremennye Zvezdy*, **21**, 211 (GS79)
Hübscher, J., Agerer, F., Mundry, E., 1992, *BAV Mitt.*, **60**, 1
Jeffery, E. J. et al., 2007, *ApJS*, **171**, 512
Kwee, K. K., van Woerden H. 1956, *BAN*, **12**, 327
Learned, J. G., Kudritzki, R-P., Pakvasa1, S., Zee A. 2008, arXiv:0809.0339
Liska, J., Skarka, M., Hajkova, P., & Auer, R. F. 2016, arXiv:1601.03082
Mankiewicz, L., et al., 2014, *RMxAC*, **45**, 7
Notni, P., 1962, *Mitteilungen über Veränderliche Sterne*, **1**, 667
Odell, A. P., 2012, *A&A*, **544**, A28
Pojmanski, G., 2002, *AcA*, **52**, 397
Pollacco, D. L. et al., 2006, *PASP*, **118**, 1407
Sweigart, A. V. & Renzini, A., 1979, *A&A*, **71**, 66
Todoran, I., 1988, *IBVS*, **3149**
Vandenbroere, J. & Salmon, G., 2009, *GEOS Circular RR*, **38**
Wiśniewski, W. Z., 1971, *AcA*, **21**, 307
Wozniak, P. R., et al., 2004, *AJ*, **127**, 2436

COMMISSIONS 27 AND 42 OF THE IAU
INFORMATION BULLETIN ON VARIABLE STARS

Number 6181

Konkoly Observatory
Budapest
8 September 2016

HU ISSN 0374 – 0676

FO Aqr TIME KEEPING

BONNARDEAU, MICHEL

MBCAA Observatory, Le Pavillon, 38930 Lalley, France, email: arzelier1@free.fr

FO Aquarii (RA=$22^{\rm h}17^{\rm m}55\overset{\rm s}{.}39$ DEC=$-08°21'03\overset{''}{.}8$, J2000) is an intermediate polar, that is a subclass of cataclysmic systems in which the white dwarf is magnetized enough to modulate the accretion. Furthermore, the period of rotation (or spin) of the white dwarf is shorter than the orbital period. FO Aqr is one of the brightest of its kind.

The orbital period of FO Aqr is $P_{\rm orb} = 4.85$ hr, the rotation period of the white dwarf is $P_{\rm rot} = 1254$ s (Patterson et al., 1998, hereafter P98). They are visible as modulations in optical photometry, the rotation modulation being fairly strong with an amplitude of 0.2 mag. Some faint and random sideband modulations may show up; however, following e.g. P98 and Williams (2003 hereafter W03), they will be neglected in the analysis that will follow.

Twelve seasons of photometric monitoring, from 2004 to 2015, are to be presented and compared with previous observations. The analysis is similar to the one in Bonnardeau (2015) for AO Psc.

Observations

The observations were carried out with a 203 mm f/6.3 Schmidt-Cassegrain telescope, without filter and an SBIG ST7E camera (KAF401E CCD, which is mostly red sensitive). The exposures were 60 s long. For the differential photometry, the comparison star is UCAC4 409-138153 (or GSC 5803-398) with $r' = 10.596 \pm 0.02$. A total of 5328 useful images were obtained over 49 nights. Figure 1 shows an example of a light curve.

Analysis of the modulations

The magnitudes as a function of time t are fitted by the following $H(t)$ function:

$$H(t) = A_0 + H_{\rm rot}(t) + H_{\rm orb}(t)$$

where A_0 is a constant, $H_{\rm rot}(t)$ is the rotation modulation:

$$H_{\rm rot}(t) = A_{rot}[\cos(\pi(t - t_{\rm rot})/P_{\rm rot}]^2$$

and $H_{\rm orb}(t)$ is the orbital modulation:

$$H_{\rm orb}(t) = A_{\rm orb}[1 + \cos(2\pi(t - t_{\rm orb})/P_{\rm orb})]$$

The $H(t)$ function is fitted to the observations using a Monte Carlo method to test the parameters relative to the timing, and, for each trial, the amplitudes are determined by a least-squares method. The fits are weighted with the uncertainties on the observations. This is done season by season and the results are listed in Table 1.

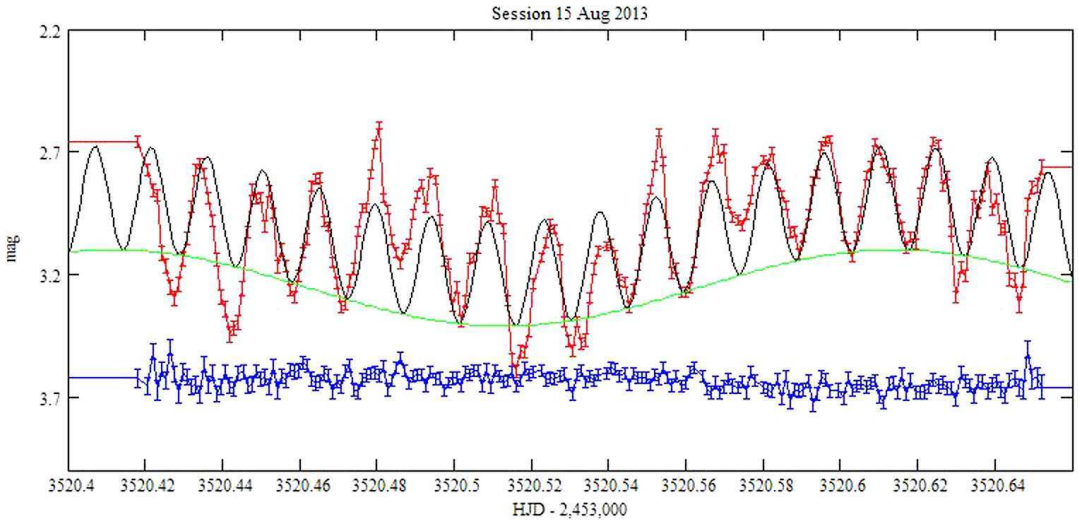

Figure 1. Upper light curve: FO Aqr, lower one: the check star UCAC4 409-138161. The error bars are the quadratic sum of the 1-sigma statistical uncertainties on the comparison star and, respectively, on the variable star or the check star. Dark line: $H(t)$ function, green line: $H_{\rm orb}(t) + A_0$ function.

Table 1: Results of the fits and cycle counts

Season	$t_{\rm orb}$	$\Delta N_{\rm orb}$	$t_{\rm rot}$	$\Delta N_{\rm rot}$	A_0	$A_{\rm orb}$	$A_{\rm rot}$
2004	249.55091	(a)	245.48796	(b)	2.828	0.103	−0.194
	±0.00069		±0.00007		±0.029	±0.001	±0.004
2005	695.29533	2206	695.37821	30988	2.864	0.126	−0.213
	±0.00042		±0.00008		±0.039	±0.008	±0.008
2006	916.5548	1095	999.44714	20944	2.932	0.058	−0.237
	±0.0012		±0.00006		±0.044	±0.001	±0.009
2007	1294.6062	1871	1350.43570	24176	2.887	0.059	−0.242
	±0.0013		±0.00009		±0.032	±0.004	±0.006
2008	1682.56750	1920	1682.55057	22876	2.763	0.137	−0.234
	±0.00061		±0.00005		±0.016	±0.001	±0.002
2009	2058.60433	1861	2058.59430	25902	2.864	0.148	−0.194
	±0.00056		±0.00010		±0.022	±0.003	±0.003
2010	2478.49376	2078	2416.51837	24654	2.749	0.147	−0.220
	±0.00030		±0.00010		±0.013	±0.006	±0.003
2011	2745.5946	1322	2794.59157	26042	2.835	0.083	−0.209
	±0.0035		±0.00015		±0.020	±0.001	±0.003
2012	3125.4822	1880	3167.42265	25681	2.887	0.102	−0.261
	±0.0014		±0.00005		±0.019	±0.001	±0.003
2013	3520.5132	1955	3520.43653	24316	2.900	0.121	−0.331
	±0.0014		±0.00010		±0.023	±0.002	±0.005
2014	3830.4561	1534	3887.58892	25290	2.957	0.021	−0.288
	±0.0069		±0.00005		±0.020	±0.001	±0.004
2015	4214.5996	1901	4327.40413	30295	2.903	0.100	−0.359
	±0.0015		±0.00005		±0.020	±0.001	±0.004

$t_{\rm xxx}$ in BJD − 2,453,000
$\Delta N_{\rm xxx}$ number of cycles from the previous season
(a) 12,478 cycles from the last observation of P98, 41,902 cycles from the origin of P98.
(b) 582,866 cycles from the origin of W03, see text.

Analysis of the orbital minima

The orbital modulation gives orbital minima $t_{\rm orb}$ (Figure 1 shows one of them). There are 70 orbital minima available: 54 from P98, 3 from Kruszewski & Semeniuk (1998), 1 from Kennedy et al (2016), and 12 from this work. They span 34 yr and 61,525 orbits.

These minima are converted in BJD using the on-line tool of the University of Ohio. They are fitted with the linear ephemeris $t_{\rm orb}(e) = T_{\rm orb} + P_{\rm orb} \cdot e$ using a Monte Carlo method. The results are:

$$T_{\rm orb} = 2444782.870469 \pm 0.000056 \text{ BJD}$$

$$P_{\rm orb} = 0.2020594932 \pm 0.0000000025 \text{ day}$$

This is compatible with the ephemeris of P98, with an improved precision. The resulting $O - C$ diagram shows only noise.

Analysis of the rotation maxima

The rotation modulation gives rotation maxima $t_{\rm rot}$ (Figure 1 shows a number of them). The last observations of rotation maxima before my measurements are the ones from W03 in 1992, 1997, 1998, 2001 and 2002. The cycle count for these measurements can be computed from the ephemeris of W03: 281,276 for 1992, 405,380 for 1997, 433,342 for 1998. For 2001 the cycle count is ambiguous, it is either 510,202 or 510,203. The number of cycles between 2001 and 2002 is 21,089.

The number of cycles between the 2002 observation of W03 and my first measurement, in 2004, is also ambiguous: it is either 51,574 or 51,573.

I fit together the W03 observations and mine with a quadratic ephemeris $t_{\rm rot}(e) = T_{\rm rot} + P_{\rm rot} \cdot e + b_{\rm rot} \cdot e^2$. Because of the ambiguities in the cycle counting, there are 4 different ways to do the fit. The residuals of the 4 fits are shown in the $O - C$ diagram of Figure 2.

The fit that gives the least residuals and the smoothest ones is for the 2001 measurement of W03 at cycle number 510,203 and for 51,574 cycles between the 2002 measurement and my 2004 measurement.

Actually, W03 considered 3 different values for the cycle count for the 2001 measurement (and not 2). So I also considered the 2001 measurement with the cycle count numbers 510,201 and 510,204. The 4 extra fits give residuals that are larger than the ones shown in Figure 2.

So, by interpolation, the ambiguities of the cycle count are lifted.

There are 140 rotation maxima available:

- 114 from P98 and 7 from Kruszewski & Semeniuk (1998) whose cycle numbers can be calculated from the ephemeris of W03;
- 1 from Andronov et al. (2005) (there are a V measurement and a R measurement and a combination of both; I used this last one), at -1259 cycles from my 2004 observation and 581,607 cycles from the origin of W03;
- 1 from Kennedy et al. (2016) at 8,601 cycles from my 2014 observations and 842,336 cycles from the origin of W03;

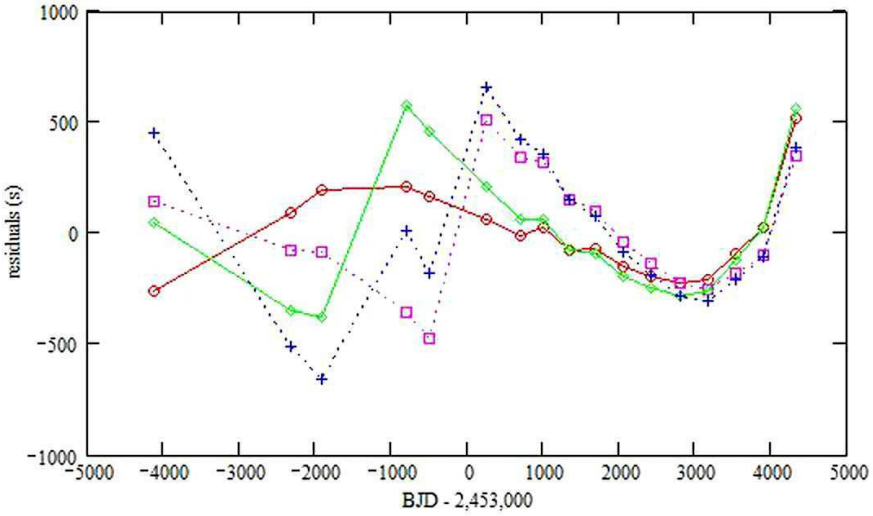

Figure 2. Red circles: the residuals for 2001 at cycle number 510,203 and 2004 at 51,574 cycles from 2002, magenta squares with dotted line: same for 2001 and 2004 at 51,573 cycles from 2002, green diamonds: 2001 at cycle number 510,202 and 2004 at 51,574 cycles from 2002, blue crosses with dotted line: same for 2001 and 2004 at 51,573 cycles from 2002.

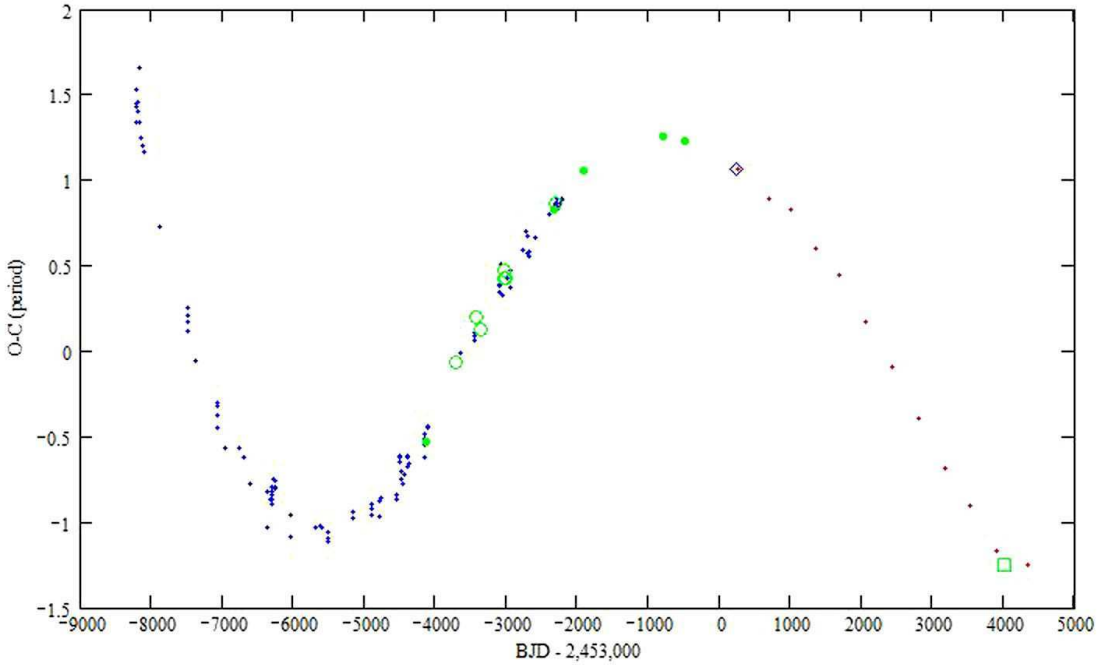

Figure 3. Blue dots: the data from P98, green dots: the W03 observations, green circles: Kruszewski & Semeniuk (1998), blue diamond: Andronov et al. (2005), green square: Kennedy et al. (2016), red dots: this work.

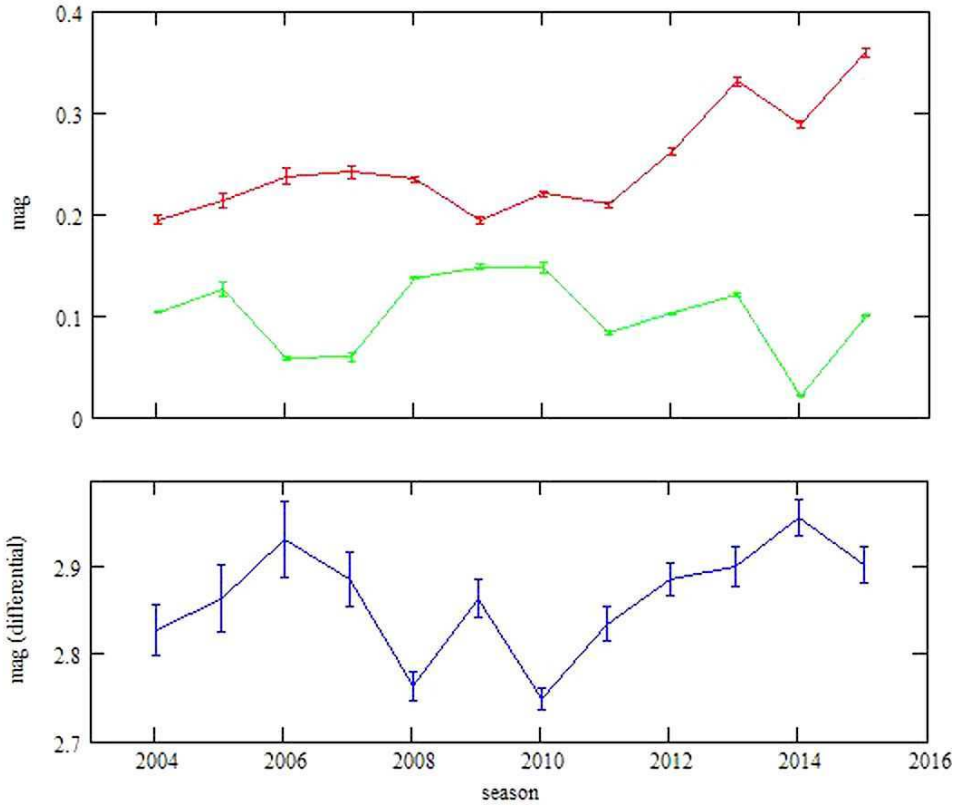

Figure 4. Red: $-A_{\rm rot}$, green: $A_{\rm orb}$, blue: A_0 (may be approximatively transformed into r' non-differential mag by adding the r' mag of the comparison star).

- 5 from W03 and 12 from this work, whose cycle numbers have been determined above. These data span 34 years and 864,030 rotations.

The 140 times of maxima are converted in BJD and are fitted with the same quadratic ephemeris as above. The results of the Monte Carlo are:

$$T_{\rm rot} = 2444782.8967 \pm 0.0016 \text{ BJD}$$

$$P_{\rm rot} = 1254.48379 \pm 0.00092 \text{ s}$$

$$b_{\rm rot} = -1.002 \cdot 10^{-12} \pm 0.021 \cdot 10^{-12} \text{ day}$$

The resulting $O-C$ diagram is shown in Figure 3.

The period of rotation of the white dwarf is decreasing at a rate $P'_{\rm rot} = 2b_{\rm rot}/P_{\rm rot} = -1.380 \cdot 10^{-10} \pm 0.029 \cdot 10^{-10}$, over a time scale $P_{\rm rot}/2P'_{\rm rot} = -144$ kyr (about the same as for AO Psc, see Bonnardeau, 2015). The $O-C$ diagram may suggest an oscillation with a time scale of about 25 yr; this is not due to a third body as the residuals for the orbital ephemeris show no modulation.

Amplitude variations

The variations of the amplitudes do not show any obvious trend or correlation, except for $A_{\rm rot}$ which stayed nearly constant at -0.2 mag from 2004 to 2011, then reached -0.35 mag in 2015, as shown in Figure 4.

However, a preliminary result for the season 2016 is that FO Aqr has fainted by about 1.5 mag; see also Littlefield et al. (2016a,b,c).

Acknowledgment: The use of the on-line tool of the University of Ohio to convert HJD to BJD, at `http://astroutils.astronomy.ohio-state.edu/time/hjd2bjd.html`, is acknowledged.

References:

Andronov, I.L., Ostrova, N.I. and Burwitz, V., 2005, *ASP Conf. Ser.*, **335**, 229
Bonnardeau, M., 2015, *IBVS*, 6146
Kennedy M.R. et al., 2016, *MNRAS*, **459**, 3622
Kruszewski A. and Semeniuk, I., 1998, *AcA*, **48**, 757
Littlefield, C. et al., 2016a, *ATEL* 9216
Littlefield, C. et al., 2016b, *ATEL* 9225
Littlefield, C. et al., 2016c, `http://arxiv.org/abs/1609.01026`
Patterson, J. et al., 1998, *PASP*, **110**, 415
Williams, G., 2003, *PASP*, **115**, 618

COMMISSIONS 27 AND 42 OF THE IAU
INFORMATION BULLETIN ON VARIABLE STARS

Number 6182

Konkoly Observatory
Budapest
8 September 2016

HU ISSN 0374 – 0676

DETECTION OF MULTIPERIODIC OSCILLATIONS IN THE MASS-ACCRETING COMPONENT OF GQ TrA

MKRTICHIAN, D.E.[1]; GUNSRIWIWAT, K.[2]; KOMONJINDA, S.[2]

[1] National Astronomical Research Institute of Thailand, 191 Siriphanich Bldg., Huay Kaew Rd., Suthep, Muang, 50200 Chiang Mai, Thailand.

[2] Department of Physics and Materials Science, Faculty of Science, Chiang Mai University, Muang, 50200 Chiang Mai, Thailand

The "**Tha**i **S**ky **S**urvey for **o**EA **S**tars" (THASSOS) project is focused on searching for and studies of new mass-accreting pulsating components of a semi-detached Algol-type systems, the class called oEA stars (Mkrtichian et al., 2002, 2004). From the point of view of stellar evolution, this class of pulsating stars is different from pulsating δ Scuti type stars in the detached eclipsing binary systems, showing similar pulsational characteristics.

GQ TrA is a southern semi-detached Algol type eclipsing binary system with A3V primary component and 2.339450-day orbital period. It was discovered and classified as an Algol type star by Hoffmeister (1949).

The new CCD photometric observations for GQ TrA were obtained during 7 nights from 16 to 22 April 2014 using the Thai Southern Hemisphere Telescope (TST, PROMPT-8) at Cerro Tololo Inter-American Observatory (CTIO) in Chile. Ten second exposures through B-filter were used. All stars in the field of view were reduced by MaxIm DL 5 software using aperture photometry, TYC 9049-1892-1 star (RA = $16^{\rm h}22^{\rm m}07\overset{\rm s}{.}19$ DEC= $-65°46'34\overset{''}{.}7$) was used as a comparison star. Phased differential light curve folded according to HJD = 2452501.01 + 2.339450 × E is shown in Figure 1. Times of GQ TrA light minima were measured using quadratic polynomial fitting method. The Heliocentric Julian Day (HJD) of a primary minimum measured on 18 April 2014 is 2456765.7942.

The pulsations variations were searched for in the out-of-eclipse parts of light curves after removal of slow orbital variations using the low order polynomial fits. Residual light curves are shown in Figure 2. The periodic variations in the residual data were analysed using the Period04 software (Lenz & Breger, 2005). We use a Discrete Fourier Transform (DFT) and pre-whitening technique for consecutive detection of signals in the data. The steps of DFT analyses and consecutive pre-whitenings of found frequencies are shown in Figure 3 from top to bottom. We detected eight oscillation frequencies in the interval of 39.0 - 47.9 c/d (30-36.9 min). Frequencies are listed in Table 1.

Conclusion: We found a new time of primary minima. We conclude that GQ TrA is a new member of oEA group of pulsators, showing a rich spectrum of relatively high amplitude, low-degree oscillations. It is a promising target for further photometric and especially spectroscopic line profile detection of the full (low- and high-degree) spectrum of non-radial oscillations.

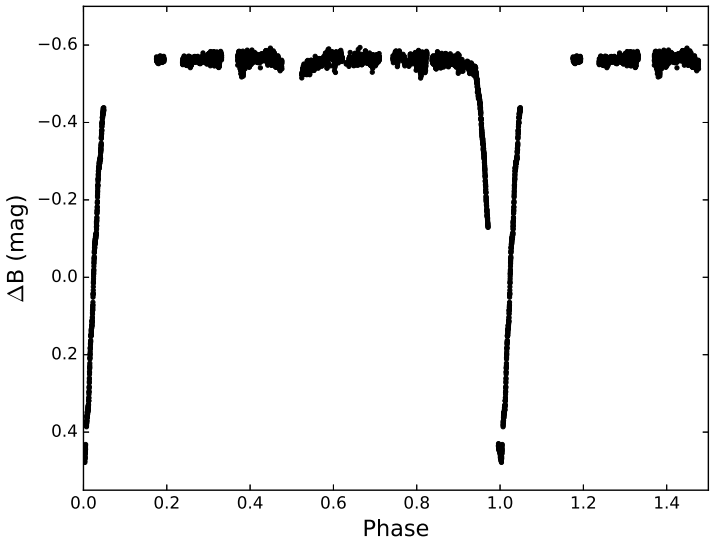

Figure 1. The phased B-filter light curve of GQ TrA folded with the period of 2.339450 days.

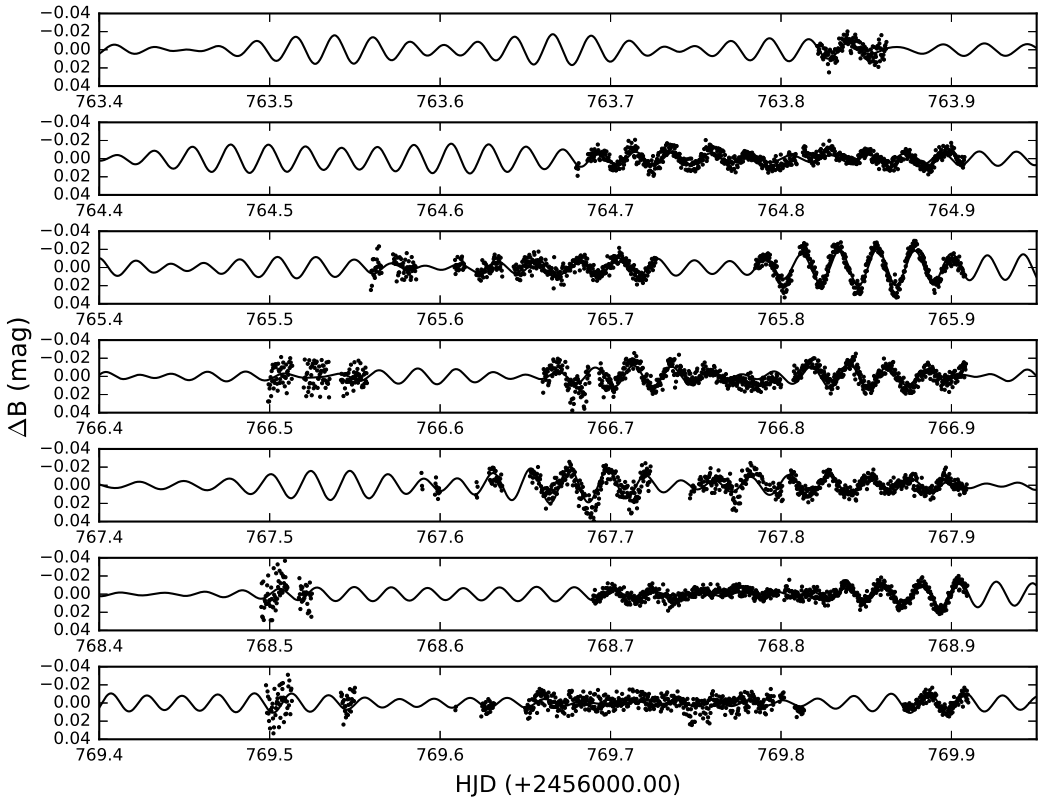

Figure 2. The nightly residual light variations (HJD time zero point is 2456000+).

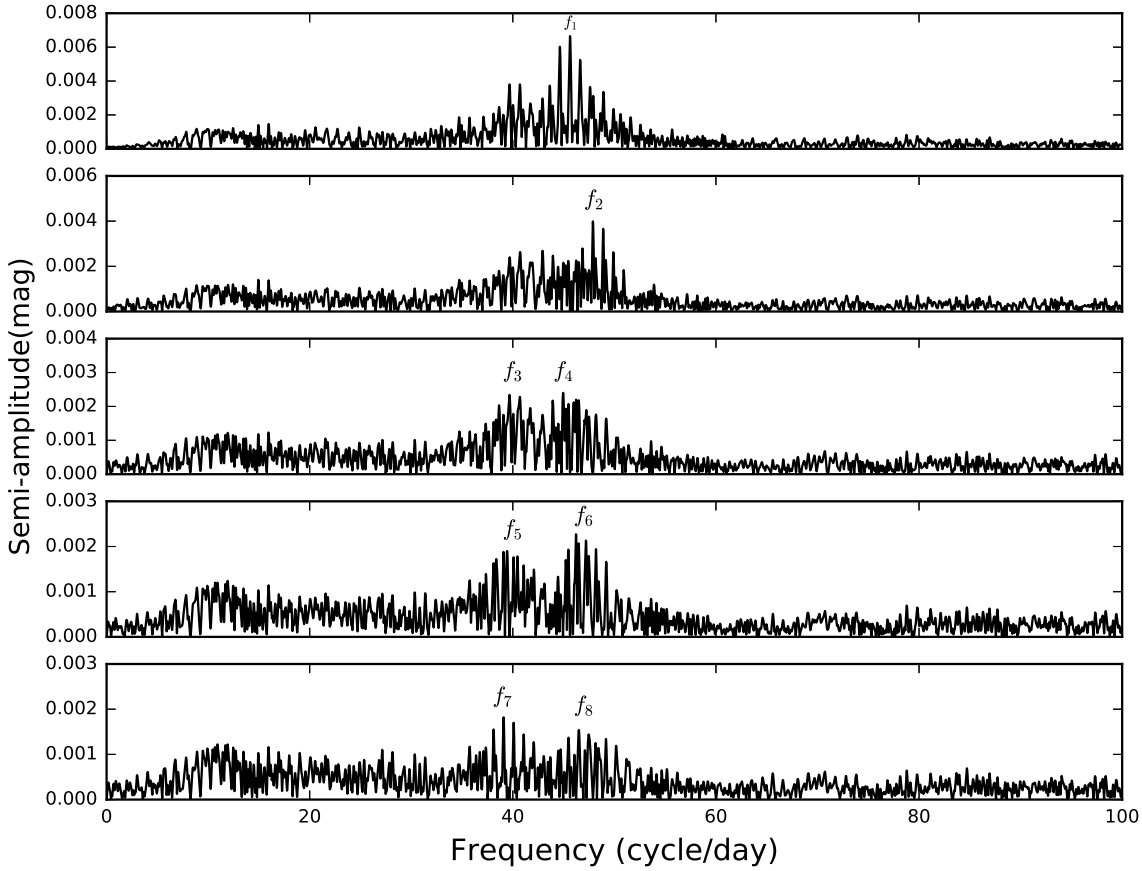

Figure 3. The DFT amplitude spectra of the primary component after consecutive (from top to bottom) pre-whitening procedures.

Table 1: Pulsation frequencies and amplitudes.

Frequency (c/d)/(σ)	Amplitude (mag)/(σ)
f_1=45.644(2)	0.0060(1)
f_2=47.900(3)	0.0044(1)
f_3=44.954(4)	0.0028(1)
f_4=39.669(4)	0.0033(1)
f_5=46.201(6)	0.0020(1)
f_6=39.409(5)	0.0023(1)
f_7=39.094(6)	0.0020(1)
f_8=46.542(5)	0.0024(1)

Acknowledgements: This work was a part of the research activity supported by the National Astronomical Research Institute of Thailand (NARIT), Ministry of Science and Technology of Thailand.

References:

Hoffmeister C., 1949, *Erg. AN*, **12**, No. 1
Lenz P., Breger M., 2005, *Communications in Asteroseismology*, **146**, 53
Mkrtichian D. et al., 2002, *ASP Conf. Ser.*, **259**, 96
Mkrtichian, D.E., Kusakin, A.V., Rodriguez, E., et al., 2004, *A&A*, **419**, 1015

COMMISSIONS G1 AND G4 OF THE IAU
INFORMATION BULLETIN ON VARIABLE STARS
Volume 62 Number 6183 DOI: 10.22444/IBVS.6183

Konkoly Observatory
Budapest
13 September 2016

HU ISSN 0374 – 0676

GH Lib: A MULTI-PERIODIC MIRA, NOT AN ECLIPSING BINARY

SIVIERO, ALESSANDRO[1]; MUNARI, ULISSE[2]; RIGHETTI, GIAN LUIGI[3]; GRAZIANI, MAURO[3]

[1] Dipartimento di Fisica ed Astronomia, Universitá di Padova, 36012 Asiago (VI), Italy

[2] INAF Osservatorio Astronomico di Padova, Sede di Asiago, I-36032 Asiago (VI), Italy

[3] ANS Collaboration, c/o Astronomical Observatory, 36012 Asiago (VI), Italy

GH Lib (≡BV 1623, $\alpha = 14^{\rm h}36^{\rm m}07\overset{\rm s}{.}82$, $\delta = -24°21'50\overset{''}{.}9$ J2000) was discovered on sky patrol plates as a variable star and classified as an eclipsing binary of the Algol type by Carter (1975), who remarked that too few minima were observed to derive an orbital period. Based on Carter's report, Kukarkin et al. (1977) included GH Lib in the General Catalog of Variable stars and Malkov et al. (2006) in their compilation of eclipsing binaries, where no information appear in addition to what already given in the discovery paper.

Intrigued by the lack of suitable follow-up observations, we have obtained photometric and spectroscopic observations of GH Lib from 2012 to 2016. They show GH Lib to be an oxygen-rich Mira variable, of the multi-period type, and not an eclipsing variable. In spite the conclusion by Kharchenko (1985) that nearly all Miras with a peak magnitude brighter than 14 have already been discovered, here we have a brand new Mira variable peaking at V=11 mag.

V and $R_{\rm C}$ optical photometry of GH Lib has been obtained with two ANS Collaboration 0.30-m f/10 Meade LX200 telescopes located in Granarolo (Bologna, Italy) and Alfonsine (Ravenna, Italy). Aperture photometry was carried out at both telescopes against the same local photometric sequence extracted from the APASS survey (Henden et al. 2012). The photometry we collected on GH Lib during 50 independent nights, is given in Table 1 (provided as online data to the paper). Our V-band data are plotted in Figure 1 together with archive V-band data extracted from the ASAS database (Pojmanski 1997).

The light curve of GH Lib in Figure 1 is that of a Mira pulsating with more than one periodicity. A Fourier analysis using the code by Deeming (1975), shows the main period to be 157 days, with the following ephemeris providing times of maxima in the V band:

$$\mathrm{JD}^{V}_{\rm max,primary} = 2454299 + 157 \times E \qquad (1)$$

where E is the progressive cycle number. The corresponding phased light curve is given in Figure 2. The several branches which are clearly visible in Figure 2, the ∼1 mag spread similarly present at all phases, and the apparently regular up-and-downs in the peak brightness along the 157 day cycles in Figure 1, all points to the presence of a second periodicity. We have searched the *residuals* from the mean light curve in Figure 2 (the red continuous curve) and again performed a Fourier analysis that returned 1180 days as

– by large margin – the strongest peak. The following ephemeris provides the maxima for this secondary periodicity:

$$\mathrm{JD}^{V}_{\mathrm{max,secondary}} = 2454225 + 1180 \times E \quad (2)$$

The sinusoidal combination of these two pulsation periods is over-plotted to the data as the continuous line in Figure 1, with an amplitude of 3.5 mag for the 157 day and 1.0 mag for the 1180 day cycle. The total amplitude of variation of GH Lib is 4.5 mag in V. Secondary periods have been observed in several pulsating M giants, either of the Mira (Percy and Bagby 1999) or semi-regular types (Kiss et al. 1999). In the majority of cases, however, the cycle-to-cycle differences seems due to low-frequency stochastic variability (Eddington and Plakidis 1929, Percy and Colivas 1999, Templeton and Karovska 2009) and not to secondary periods.

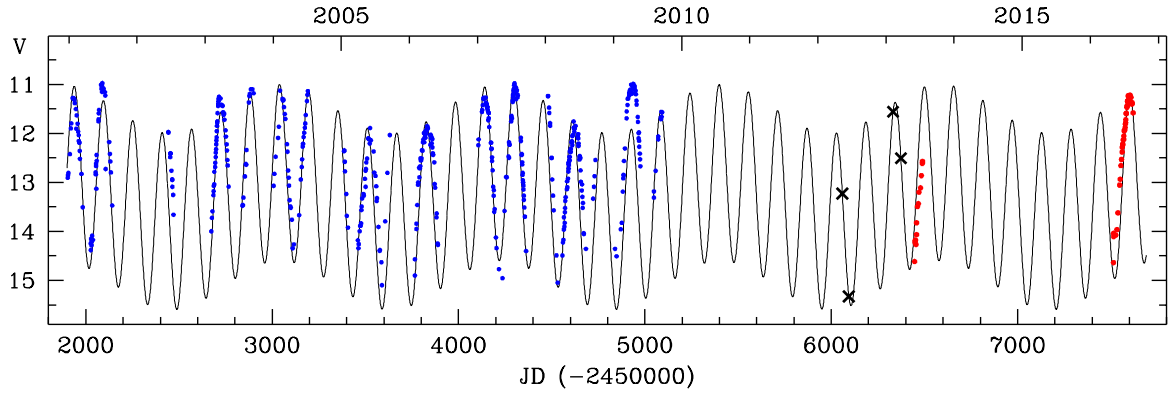

Figure 1. Long-term V-band light curve of GH Lib obtained by combining our observations (JD>2456400, in red) with ASAS archive data (JD<2455200, in blue). The bi-periodic curve is the sinusoid combination of ephemerides 1 and 2. The four crosses mark the time of the spectra in Figure 3.

Four low resolution spectra of GH Lib have been obtained at different epochs with the 1.22m telescope + B&C spectrograph operated in Asiago by the Department of Physics and Astronomy of the University of Padova. The spectra cover the 3400-8000 Å range at a dispersion of 2.3 Å/pix, and have been treated in a standard fashion in IRAF, including correction for bias, dark and flat fields, subtraction of sky background, and wavelength calibration. Flux calibration has been achieved via spectrophotometric standard stars observed during the same nights as GH Lib itself. The spectra are shown in Figure 3, and their corresponding position in the pulsation light curve of GH Lib is marked with crosses in Figure 1. By lucky coincidence, two of the four spectra were obtained very close to the maximum and minimum along the 157-day cycle, and the remaining two at the same 0.20 phase. The continuum of the spectra at maximum and minimum are perfectly fitted by those of M2III and M7III spectral type standards, respectively, and by an M5III at 0.20 phase.

The primary period of 157 days places GH Lib close to the short term border in the period distribution for Miras. Among the 5202 Miras with a pulsation period listed in the General Catalog of Variable Stars (GCVS) at the time of writing, only 4% of the oxygen-rich type (M spectral type) have a period shorter than GH Lib. An amplitude of 4.5 magnitudes and a M2III-M7III spectral range are similar – according to the GCVS compilation – to those exhibited by other Miras of equivalent pulsation periods.

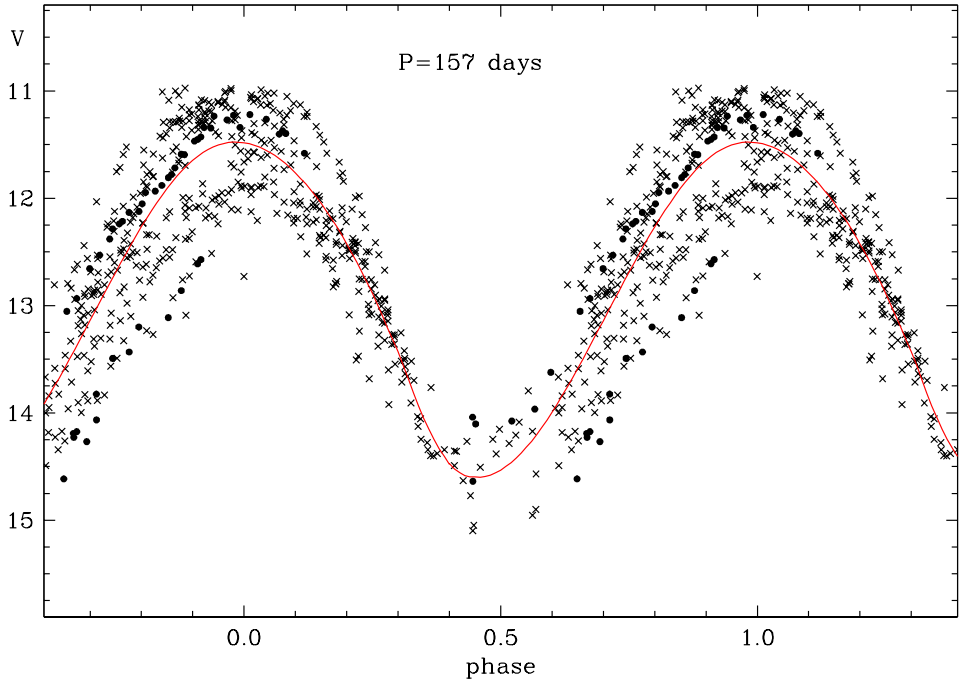

Figure 2. ASAS data (crosses) and our V-band observations (dots) of GH Lib folded with the main pulsation period of 157 days, following ephemeris 1. The continuous curve is a spline fit to the data.

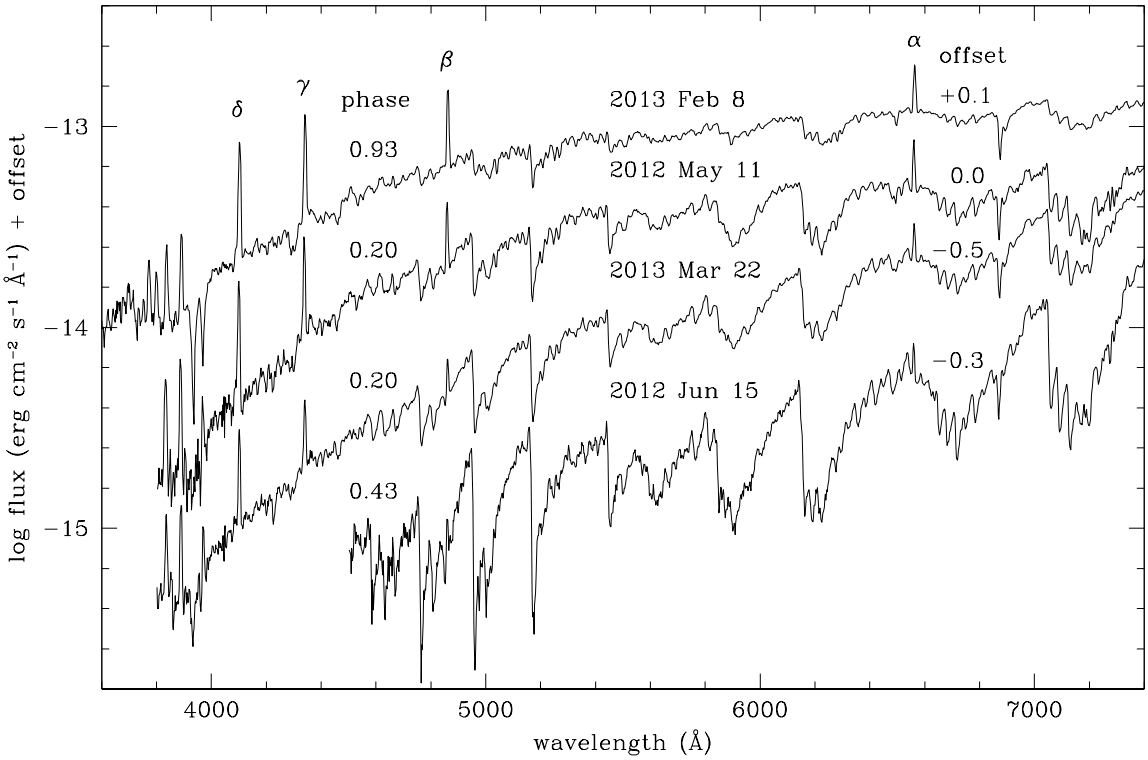

Figure 3. Spectra of GH Lib at four distinct epochs. To enhance visibility, an offset in ordinates is applied as indicated. The phase is relative to the main pulsation period of 157 days, following ephemeris 1.

What is not typical is the large intensity of the Hα and Hβ emission lines visible in the spectra of GH Lib in Figure 3. Lower Balmer lines do not generally stand in prominent emission in low resolution spectra of Mira variables, the strongest observed emission being that of Hδ (Joy 1926). The reason for such an anomalous ratio in the intensity of Balmer emission lines is due to the overlapping absorption by TiO bands (Scott 1945). Shortwards of 4300 Å there is essentially no absorption band from TiO, and therefore Hδ (4100 Å), H8 (3889 Å) and H9 (3835 Å) can emerge unabsorbed through the stellar atmosphere (Merrill et al. 1962). On the contrary, at the redder wavelengths of Hα and Hβ the absorption from many strong and overlapping TiO bands effectively blocks the emergence of radiation from internal atmospheric layers.

In Miras, the ionization of hydrogen responsible for the observed emission lines occurs in a shock region in the atmosphere (Joy 1947, Merrill 1955), where infalling material from the previous pulsation cycle collides with that moving outward from the following cycle (Fox et al. 1984, Gillet et al. 1985). This shock region is usually located deep in the atmosphere, well below the region from where TiO absorption originates (de Laverny and Magnan 1995). In GH Lib, the Hδ/Hγ/Hβ/Hα intensity ratio is 1.00/1.34/1.44/1.48, 1.00/1.51/1.88/4.84, and 1.00/1.17/1.51/3.25 for the 2013 Feb 8, 2012 May 11, and 2013 Mar 22 spectra in Figure 3, respectively. For comparison, this same ratio measured on some spectra of *o* Cet (obtained with the same instrumentation as for GH Lib) is 1.00/0.40/0.05/0.62 (similar numbers are tabulated by Crowe and Garrison (1988) for a large sample of southern Miras). We conclude that the region of Balmer line formation in GH Lib seems located at a larger radius (more external atmospheric layers) than in typical Miras, as if mixed with and not deeply below the region where absorption by TiO molecules occurs, which poses the interesting question of how TiO can survive in the same place where hydrogen is collisionally ionized (comparing the 6.8 eV ionization potential for TiO with that of hydrogen, 13.6 eV). The relative location within the atmosphere of GH Lib of the regions where Balmer emission lines and TiO absorption bands form should be investigated via radial velocities from high-resolution spectra.

References:

Carter, B. S., 1975, *IBVS*, **994**
Crowe, R. A., Garrison, R. F., 1988, *ApJS*, **66**, 69 DOI
Deeming, T. J., 1975, *Ap&SS*, **36**, 137 DOI
de Laverny, P., Magnan, C., 1995, *ASPC*, **83**, 419
Eddington, A. S., Plakidis, L. 1929, *MNRAS*, **90**, 65 DOI
Fox, M. W., et al., 1984, *ApJ*, **286**, 337 DOI
Gillet, D., et al. 1985, *A&A*, **150**, 89
Henden, A., et al., 2012, *JAAVSO*, **40**, 430
Joy, A. H. 1926, *ApJ*, **63**, 281 DOI
Joy, A. H. 1947, *ApJ*, **106**, 288 DOI
Kharchenko, N. V., 1985, *Sov. Astr. Lett.*, **11**, 25
Kiss, L. L., et al., 1999, *A&A*, **346**, 542
Kukarkin, B. V., Kholopov, P. N., Kireeva, N. N., 1977, *ASSL*, **64**, 131 DOI
Malkov, O. Yu., Oblak, E., Snegireva, E. A., Torra, J., 2006, *A&A*, **446**, 785 DOI
Merrill, P. W., 1955, *PASP*, **67**, 199 DOI
Merrill, P. W., et al., 1962, *ApJ*, **136**, 21 DOI
Percy, J. H., Bagby, D. H., 1999, *PASP*, **111**, 203 DOI
Percy, J. H., Colivas, T., 1999, *PASP*, **111**, 94 DOI

Pojmanski, G., 1997, *AcA*, **47**, 467
Scott, R. M., 1945, *ApJ*, **101**, 71 DOI
Templeton, M. R., Karovska, M. 2009, *ApJ*, **691**, 1470 DOI

COMMISSIONS G1 AND G4 OF THE IAU
INFORMATION BULLETIN ON VARIABLE STARS
Volume 62 Number 6184 DOI: 10.22444/IBVS.6184

Konkoly Observatory
Budapest
23 September 2016

HU ISSN 0374 – 0676

WHITE DWARF PERIOD TABLES I. PULSATORS WITH HYDROGEN-DOMINATED ATMOSPHERES

BOGNÁR, ZS.; SÓDOR, Á.

Konkoly Observatory, MTA Research Centre for Astronomy and Earth Sciences, Konkoly Thege Miklós út 15-17, H–1121 Budapest

e-mail: bognar.zsofia@csfk.mta.hu

1 Introduction

The tradition of collecting and publishing the main photometric and physical parameters of pulsating white dwarf (WD) stars, together with their observed pulsation periods, amplitudes and their references, goes back to 1995. Bradley (1995) collected this information on the ZZ Ceti (or DAV), V777 Her (or DBV), interacting binary white dwarf (IBWD) stars, and also on the pulsating PG 1159-type (or DOV) and planetary nebula nucleus variable (PNNV) stars known at that time. Two updates followed this paper published in 1998 and 2000, respectively (Bradley 1998, 2000). After that time, online-only updates were presented for the white dwarf community in 2001[1], in 2005[2] and in 2010[3]. The last source lists the ZZ Ceti stars only (155 items).

In the meantime, dividing the hot (pre-)white dwarf pulsators into DOV and PNNV classes have become obsolete, and now the denomination GW Vir stars is used instead for all the post-AGB stars showing nonradial g-mode pulsations (Quirion et al. 2007). Nevertheless, new groups of pulsating white dwarfs have been discovered, like the extremely low-mass DA pulsators (ELM-DAVs), the hot DAV stars, the DQV stars and the pulsating, mixed-atmosphere, extremely low-mass white dwarf precursors (pre-ELM WD variables). ZZ Ceti variables in detached white dwarf plus main-sequence (MS) binaries have also become known. Considering the new groups, the newly discovered members of the 'classical' ZZ Ceti, V777 Her and GW Vir groups, and also the new observational results on the formerly known pulsators, the update of the white dwarf data tables is now appropriate.

In this paper, taking the relatively large number of white dwarf variables and the considerable observational information on them into account, we focus on their most populated subgroup, that is, on the variables with hydrogen-dominated atmospheres only. Thus, we collected the main stellar parameters and pulsational properties with references of the 'classical' ZZ Ceti stars, the ZZ Ceti variables in detached WD plus MS binaries, the ELM-DAV and hot DAV stars.

[1] http://astro.if.ufrgs.br/wdtab.htm; by Kepler de Souza Oliveira Filho
[2] http://whitedwarf.org/tables/; webpage of the White Dwarf Research Corporation
[3] http://astro.if.ufrgs.br/zzceti.htm; by Kepler de Souza Oliveira Filho

2 Data collection and structure of the data tables

Table 1 lists the ZZ Ceti variables in detached white dwarf plus main-sequence binaries. This list of seven variables is based on the paper of Pyrzas et al. (2015).

Table 2 summarizes the observational results on the seven extremely low-mass DA pulsators presented in the papers of Hermes et al. (2012, 2013b,d); Bell et al. (2015b) and Kilic et al. (2015).

The hot DAV stars are listed in Table 3, a new group consisting of three members discovered by the work of Kurtz et al. (2008, 2013).

Finally, we list the members of the most populated subgroup of white dwarf pulsators with hydrogen atmospheres, the 'classical' ZZ Ceti stars, in Table 4. These objects can be treated as products of single-star evolution, in contrast to the ELM-DAV or ZZ Ceti stars in WD+MS binaries. We started the data collection with the 136 DAVs listed and refereed in the review paper of Fontaine & Brassard (2008). We then complemented this list with the ZZ Ceti stars reported by Stobie et al. (1997); Castanheira et al. (2010); Hermes et al. (2011); Sayres et al. (2012); Kepler et al. (2012); Castanheira et al. (2013); Hermes et al. (2013a); Greiss et al. (2014); Green et al. (2015); Gentile Fusillo et al. (2016); Greiss et al. (2016) and Bell et al. (2016). We closed the data collection with this last paper published on arxiv.org on 7th July, 2016. Altogether, 180 ZZ Ceti stars are listed in Table 4.

All tables follow the same structure specified below.

- Identifiers: the first column shows the star's identifier in WD (J)HHMM±DDM(M) format, while the second column shows another identifier used in the literature or can be used to identify the object in the SIMBAD database (Wenger et al. 2000). The identifiers in parentheses are not recognized by SIMBAD, but used in the literature.
- Third and fourth columns: right ascension (RA) and declination (DEC) in the equatorial coordinate system (epoch J2000.0) from the SIMBAD database. The objects are arranged according to increasing right ascensions.
- Fifth and sixth columns: effective temperature ($T_{\rm eff}$) and surface gravity ($\log g$) values. In the case of ZZ Ceti stars in Table 4, most of the objects can be found either in the database of Gianninas et al. (2011) or Tremblay et al. (2011) with their spectroscopic atmospheric parameters determined by one-dimensional model atmospheres and by the use of the ML2/α=0.8 version of the mixing-length theory. We corrected these $T_{\rm eff}$ and $\log g$ values according to the findings of Tremblay et al. (2013) based on radiation-hydrodynamics three-dimensional simulations of convective DA stellar atmospheres. We denoted the resulting values with G or T in superscript at the corresponding effective temperatures referring to the source of the original atmospheric parameters. In all the other cases, the source of the $T_{\rm eff}$ and $\log g$ values is the paper referred to in the last column, which is practically the paper reporting the discovery of the given pulsator.
- Seventh column: the V magnitude of the star in the SIMBAD database. If there is no such data in SIMBAD, we list its g magnitude, or, in absence of both V and g magnitudes, its brightness in B band.
- Eight and ninth (last) columns: pulsation period (in second) with Fourier amplitude (in milli-modulation amplitude, mma) values arranged according to increasing periods, and the corresponding references. We applied the

$$1\,\mathrm{mma} = 1/1.086\,\mathrm{mmag} = 0.1\% = 1\,\mathrm{ppt}$$

conversion to convert the amplitudes published if necessary.

Our data collection strategy was to use the NASA's Astrophysics Data System (ADS) to search for publications referring to a given object and looked for papers publishing pulsation periods and their Fourier amplitudes. In some instances, only period values were presented. In such cases, we abstained from making estimates on the amplitudes by the Fourier spectra presented (if any), thus we listed the periods only.

We aimed at collecting linearly independent pulsation frequencies alone, thus, if a frequency was denoted as a combination term in the literature, we did not add it to the period list. Such cases are indicated in parentheses by the following remarks after the periods and amplitudes: '+C' – there are additional linear combinations (including harmonics) reported; '+SH' – additional subharmonics ($\sim n/2f_i$) present in the data. '+R' denotes that frequency components, which may be results of rotational splitting are also detected. In addition, the 'iR' remark means that the period list contains rotationally split frequencies, while 'iC?' denotes that our list may contains combination terms.

3 What is new?

One of the most conspicuous improvements we made comparing to the previous versions of white dwarf data tables is the completion of the object list with newly discovered pulsators both in the formerly known group of classical ZZ Ceti stars and in the newly established groups of hydrogen-atmosphere white dwarf pulsators.

Another relevant improvement concerns the periods listed. The authors restricted to the presentation of one set of periods, or just a representative period range, per object in the previously published white dwarf data tables. In contrast, we attempted to collect all different period lists existing in the literature for an object, that is, observational results from different epochs. We also emphasize this choice with the title selection of our catalogue 'White Dwarf Period Tables' instead of the 'White Dwarf Data Tables' used previously. This also implies that we present the almost complete bibliography of the observations of hydrogen-atmosphere pulsating white dwarf stars starting from 1968.

The different periods observed at different epochs can be the result e.g. of the different lengths and qualities of the data sets analysed, however, especially in the case of the ZZ Ceti stars being close to the red edge of the instability domain, short time-scale variations in the amplitudes of the excited modes are common. That is, pulsation modes never seen before can be excited to an observable level, while others can vanish from one observational run to another. Eventually, comparing the different sets of periods from different runs, it can result in a more complete set of pulsation periods, which is essential for detailed asteroseismic investigations.

Smaller, but also significant improvements that we checked and corrected the star identifiers if it was necessary, in order to publish at least one identifier per star which can be found in the SIMBAD database. In essence, this affected the Sloan Digital Sky Survey (SDSS) identifiers, where the use of the correct format, including all the necessary decimals is crucial. We also note that in many cases the WD (J)HHMM±DDM(M) identifiers used in the literature are not found in SIMBAD, thus, especially in the publication of a new discovery, we recommend the indication of another identifier existing in the database (if any), or at least the equatorial coordinates of the object to make the identification of the new pulsator clear and easy. At last, as we mentioned in Sect. 2, we revised and updated the effective temperature and surface gravity values of the classical ZZ Ceti stars.

Table 1: ZZ Ceti stars in detached white dwarf plus main-sequence binaries.

Identifiers		RA	DEC	$T_{\rm eff}$	$\log g$	V	Period/Amplitude	References
WD (SDSS)	Other	(h m s)	(° ′ ″)	(K)	(dex)	(mag)	(s/mma)	
0049-011	SDSS J005208.42-005134.7	00 52 08	−00 51 35	12 300	8.46	18.3 (g)	1077.2/4.0; 1093.8/4.0	Pyrzas et al. (2015)
(J0111+000)	SDSS J011123.90+000935.2	01 11 24	+00 09 35	12 320	7.50	18.4 (g)	366.5/9.1; 510.2/18.9; 583.2/16.3; 631.6/28.0; 883.6/15.9	Pyrzas et al. (2015)
0201+004	SDSS J020351.29+004025.0	02 03 51	+00 40 25	10 790	8.17	19.4 (g)	398.8/11.9; 683.9/15.2; 957.0/38.5	Pyrzas et al. (2015)
(J0824+1723)	SDSS J082429.01+172345.4	08 24 29	+17 23 45	11 430	8.21	18.3 (g)	513.9/9.2; 623.7/20.4; 807.2/13.9; 987.9/12.0	Pyrzas et al. (2015)
(1043+0603)	SDSS J104358.59+060320.9	10 43 59	+06 03 21	11 170	8.19	18.7 (g)	164.9/6.6; 292.5/5.3; 324.7/28.8; 634.4/8.5	Pyrzas et al. (2015)
(J1117-1255)	SDSS J111710.53-125540.9	11 17 11	−12 55 41	11 300	8.29	19.7 (g)	835.8/21.9	Pyrzas et al. (2015)
(J1136+0409)	SDSS J113655.18+040952.6	11 36 55	+04 09 53	11 700	7.99	17.1	182.2/4.4; 276.5/8.3	Pyrzas et al. (2015)
							160.8/0.4; 162.2/1.2; 163.7/0.4; 181.3/1.8; 201.8/0.5; 274.9/3.5; 279.4/2.3; 284.2/0.2; 337.7/0.8; 351.1/0.7; 395.9/0.4; 474.5/0.4 (iR)	Hermes et al. (2015)

Table 2: Extremely low-mass DA pulsators.

WD (SDSS)	Identifiers Other	RA (h m s)	DEC (° ′ ″)	$T_{\rm eff}$ (K)	$\log g$ (dex)	V (mag)	Period/Amplitude (s/mma)	References
(J1112+1117)	SDSS J111215.82+111745.0	11 12 16	+11 17 45	9 590	6.36	16.3	107.6/0.4; 134.3/0.4; 1792.9/3.3; 1884.6/4.7; 2258.5/7.5; 2539.7/6.8; 2855.7/3.6	Hermes et al. (2013d)
(J1518+0658)	SDSS J151826.68+065813.2	15 18 27	+06 58 13	9 900	6.80	17.6 (g)	1335.3/13.6; 1956.4/18.1; 2134.0/14.2; 2268.2/21.6; 2714.3/21.6; 2799.1/35.4; 3848.2/15.7	Hermes et al. (2013d)
							1318.8/12.9; 1956.3/18.1; 2210.0/19.9; 2413.1/15.6; 2796.0/41.1; 2802.8/26.4; 3683.7/17.7	Hermes et al. (2013d)
(J1614+1912)	SDSS J161431.28+191219.4	16 14 31	+19 12 19	8 880	6.66	16.4 (g)	1184.1/3.2; 1262.7/5.9	Hermes et al. (2013b)
(J1618+3854)	SDSS J161831.69+385415.1	16 18 32	+38 54 15	9 140	6.83	19.7 (g)	2543.0/16.0; 4935.2/56.3; 6125.9/25.5	Bell et al. (2015b)
–	PSR J1738+0333	17 38 54	+03 33 11	9 130	6.55	21.3	1788.0/12.7; 2656.0/11.5; 3057.0/12.2	Kilic et al. (2015)
(J1840+6423)	SDSS J184037.78+642312.3	18 40 38	+64 23 12	9 100	6.22	18.9 (g)	1578.6/29.5; 2376.0/48.8; 4445.9/65.9	Hermes et al. (2012)
(J2228+3623)	SDSS J222859.93+362359.6	22 28 60	+36 24 00	7 870	6.03	16.9 (g)	3254.5/2.3; 4178.3/6.3; 6234.9/1.9	Hermes et al. (2013b)

Table 3: Hot DAV stars.

Identifiers		RA	DEC	$T_{\rm eff}$	$\log g$	V	Period/Amplitude	References
WD	Other	(h m s)	(° ′ ″)	(K)	(dex)	(mag)	(s/mma)	
0101+145	SDSS J010415.99+144857.4	01 04 16	+14 48 57	29 980	7.38	18.8 (g)	159.0/4.0	Kurtz et al. (2008)
0232-097A	SDSS J023520.02-093456.3	02 35 20	−09 34 56	30 110	7.30	17.8 (g)	705.0/15.6	Kurtz et al. (2008)
1017-138	–	10 19 52	−14 07 34	32 600	7.80	14.6	624.0/1.0	Kurtz et al. (2013)

Table 4: List of ZZ Ceti stars.

WD	Identifiers Other	RA (h m s)	DEC (° ′ ″)	$T_{\rm eff}$ (K)	$\log g$ (dex)	V (mag)	Period/Amplitude (s/mma)	References
(J0000-0046)	SDSS J000006.75-004654.0	00 00 07	−00 46 54	$10\,620^{T}$	8.18	18.8 (g)	584.8/15.9; 601.4/9.0; 611.4/23.0	Castanheira et al. (2007)
(J0018+0031)	SDSS J001836.11+003151.1	00 18 36	00 31 53	$11\,530^{T}$	8.04	17.4 (g)	257.9/5.8	Mullally et al. (2005)
							149.9/3.7; 257.3/6.0	Castanheira & Kepler (2009)
0016-258	MCT 0016-2553	00 18 45	−25 36 42	$11\,060^{G}$	8.06	16.1	1152.4/8.1	Gianninas et al. (2006)
–	HE 0031-5525	00 33 36	−55 08 39	11 480	7.65	15.7 (g)	274.9/1.5; 276.9/4.8; 329.5/2.5	Castanheira et al. (2006)
0036+312	G 132-12	00 39 04	31 31 37	$12\,480^{G}$	8.00	16.2	212.7/4.3	Gianninas et al. (2006)
0041+006	SDSS J004345.78+005549.9	00 43 46	00 55 50	$12\,130^{T}$	8.14	18.7 (g)	258.2/6.7	Castanheira et al. (2010)
(J0048+1521) 0046+150	SDSS J004855.17+152148.7	00 48 55	15 21 49	$11\,280^{T}$	8.17	18.7 (g)	615.3/24.8	Mullally et al. (2005)
							323.1/14.8; 333.2/8.6; 609.8/22.1; 636.4/8.7; 672.3/8.5; 698.4/18.3	Romero et al. (2013)
0049-473	EC 00497-4723	00 52 01	−47 07 09	–	–	16.5	500.0/7.0; 722.0/23.0; 867.0/17.0; 1083.0/12.0; 1182.0/9.0	Stobie et al. (1997) (periods and amplitudes: Castanheira & Kepler 2009)
(J0102-0032) 0059-008	SDSS J010207.17-003259.4 LP 586-51	01 02 07	−00 33 00	$10\,850^{T}$	8.18	18.2	830.3/29.2; 926.1/37.2	Mukadam et al. (2004)
							752.2/19.4; 830.3/35.1; 926.3/34.7; 1043.4/15.3	Mukadam et al. (2006)
							796.1/75.1	Gentile Fusillo et al. (2016)
0104-464	BPM 30551	01 06 54	−46 08 54	$11\,240^{G}$	8.16	15.4	606.8; 682.7; 744.7; 840.2; ∼11mma	Hesser et al. (1976)
(J0111+0018)	SDSS J011100.63+001807.2	01 11 01	00 18 07	$11\,490^{T}$	8.08	18.8 (g)	255.3/15.6; 292.3/21.9	Mukadam et al. (2004)
							255.5/13.0; 293.0/22.1 (+C)	Castanheira & Kepler (2009)
							255.7/14.3; 292.9/25.7 (+C)	Hermes et al. (2013c)
0120+002	SDSS J012234.68+003025.8	01 22 35	00 30 26	$11\,650^{T}$	7.94	16.8 (g)	121.1/1.5; 200.8/1.3; 358.6/1.2	Castanheira et al. (2010)
–	SDSS J012950.44-101842.0	01 29 50	−10 18 42	11 910	8.00	18.4 (g)	147.4/2.3; 193.8/2.9	Castanheira et al. (2010)
0132-014	SDSS J013440.94-010902.3	01 34 41	−01 09 02	$10\,260^{T}$	7.82	18.1 (g)	1212.0/45.4	Gentile Fusillo et al. (2016)

Table 4: continued.

WD	Identifiers Other	RA (h m s)	DEC (° ′ ″)	$T_{\rm eff}$ (K)	$\log g$ (dex)	V (mag)	Period/Amplitude (s/mma)	References
0133-116	Ross 548	01 36 14	−11 20 33	12 300^{G}	8.03	14.2	212.9; 273.0; ∼2–11mma	Lasker & Hesser (1971)
							212.8/5.1; 213.1/8.6; 274.3/5.8; 274.8/3.7 (iR)	Stover et al. (1977)
							212.8/4.8; 213.1/8.4; 274.3/5.3; 274.8/3.7	Stover et al. (1980)
							187.0/∼1; 212.8/2.1; 213.1/3.3; 274.3/2.2; 274.8/1.3; 320.0/∼1; 333.0/∼1	Kepler et al. (1995a)
							187.3/0.9; 212.8/4.1; 213.1/6.2; 274.3; 274.8; 318.1/0.9; 333.6/0.6	Mukadam et al. (2003)
							187.3/0.9; 213.0/5.4; 274.5/3.5; 318.1/1.1; 333.6/1.3	Castanheira & Kepler (2009)
							186.5/0.3; 186.7/0.4; 186.9/0.5; 212.8/4.4; 213.0/1.0; 213.1/6.6; 274.3/4.2; 274.5/0.7; 274.8/3.2; 317.0/0.4; 318.1/0.4; 319.2/0.4; 333.6/0.6; 334.5/0.3; 335.3/0.3; 336.2/0.3	Mukadam et al. (2013)
							186.9/0.9; 212.8/4.1; 212.9/1.4; 213.1/6.6; 217.8/0.3; 274.3/4.3; 274.5/1.2; 274.8/3.1; 318.1/0.7; 318.8/0.3; 333.6/0.6	Giammichele et al. (2015)
0145-221	MCT 0145-2211	01 47 22	−21 56 51	11 850^{G}	8.15	14.9	462.2/25.0; 727.9/19.0; 823.2/17.0	Fontaine et al. (2003) (amplitudes: Mukadam et al. 2006)
–	(HS 0210+3302)	02 13 06	33 16 10	11 920	7.39	15.8 (B)	189.4/4.7; 207.5/3.7	Voss et al. (2007)
(J0214-0823) 0211-086	SDSS J021406.78-082318.4	02 14 07	−08 23 18	11 580^{T}	7.86	17.9 (g)	263.5/7.1; 297.5/16.0; 347.1/8.3; 348.1/8.5	Mukadam et al. (2004)
							263.2/7.0; 297.1/15.7; 347.3/6.6 (+C)	Castanheira & Kepler (2009)
0235+069	HS 0235+0655	02 38 33	07 08 10	10 950	7.75	16.6 (B)	1283.7/4.2	Voss et al. (2007)

Table 4: continued.

WD	Identifiers Other	RA (h m s)	DEC (° ′ ″)	$T_{\rm eff}$ (K)	$\log g$ (dex)	V (mag)	Period/Amplitude (s/mma)	References
–	SDSS J024922.35-010006.7	02 49 22	−01 00 07	11 030^{T}	8.19	18.9	1005.6/5.6; 1045.2/10.9	Castanheira et al. (2006)
0246+326	KUV 02464+3239	02 49 28	32 51 13	11 620^{G}	8.13	15.8	831.6	Fontaine et al. (2001)
							619.3/4.3; 777.6/6.0; 828.7/12.6; 866.2/10.3; 993.2/14.3; 1250.3/4.8	Bognár et al. (2009)
–	SDSS J030153.81+054020.0	03 01 54	05 40 20	11 470	8.09	18.1 (g)	300.8/24.9	Castanheira et al. (2010)
(J0303-0808) 0300-086A	SDSS J030325.22-080834.9	03 03 25	−08 08 35	11 260^{T}	8.40	18.8 (g)	707.0/4.1; 1128.0/3.5	Castanheira et al. (2007)
(J0318+0030) 0316+003	SDSS J031847.09+003029.9	03 18 47	00 30 30	11 150^{T}	8.18	17.8 (g)	536.1/10.6; 587.1/10.1; 826.4/21.1	Mukadam et al. (2004)
							536.1/11.1; 587.1/10.6; 695.0/8.9; 826.4/27.3; 844.9/15.3	Mukadam et al. (2006)
							969.0/21.8; 746.4/21.1	Gentile Fusillo et al. (2016)
(0332-0049) 0330-010	SDSS J033236.61-004918.3	03 32 37	−00 49 18	10 940^{T}	8.05	18.2 (g)	767.5/15.1	Mukadam et al. (2004)
							402.0/4.1; 765.0/15.2; 938.4/6.7; 1143.7/7.4	Mukadam et al. (2006)
0341-459	BPM 31594	03 43 29	−45 49 04	11 500^{G}	8.05	15.0	314.0(?); 617.0	McGraw (1976)
							617.3 (+C,SH)	O'Donoghue (1986)
							416.1(?)/5.0; 617.9/9–65 (+C,SH)	O'Donoghue et al. (1992)
0344+073	KUV 03442+0719	03 46 51	07 28 03	10 870^{G}	7.78	16.2 (B)	1384.9/7.6	Gianninas et al. (2006)
							428.7/5.0; 431.8/3.9; 908.6/4.5; 972.9/2.2; 976.0/5.1; 976.6/1.8; 1023.9/1.8; 1031.2/2.6; 1097.5/2.2; 1136.5/5.2; 1139.6/4.3; 1167.1/2.8; 1185.6/2.8; 1192.6/2.0; 1237.4/2.7; 1238.0/2.6; 1250.4/5.4; 1287.0/6.0; 1289.6/1.5; 1323.3/10.6; 1326.8/2.6; 1349.2/9.6; 1396.1/1.8; 1403.7/3.7; 1423.7/2.7; 1508.8/5.9; 1686.5/2.3; 1806.8/1.8; 2425.7/1.7; 2439.0/4.0; 2494.8/4.7 (+R,C)	Su et al. (2014a)

Table 4: continued.

WD	Identifiers Other	RA (h m s)	DEC (° ′ ″)	$T_{\rm eff}$ (K)	$\log g$ (dex)	V (mag)	Period/Amplitude (s/mma)	References
–	HE 0344-1207	03 47 07	−11 58 09	11 470	8.28	17.0 (B)	392.9/21.1; 461.0/11.4; 762.2/18.9	Voss et al. (2007)
(J0349+1036)	SDSS J034939.35+103649.9	03 49 39	10 36 50	11 720	8.40	16.6 (g)	184.5/3.8	Castanheira et al. (2013)
0416+272	HL Tau 76	04 18 57	27 17 48	11 470^{G}	7.92	14.1	747.4	Landolt (1968)
							626.0; 663.0; 746.0 (+C,SH)	Page (1972)
							494.2; 746.2 (+C)	Fitch (1973)
							359.0/8.1; 383.0/21.8; 450.0/7.3; 494.0/30.2; 541.0/40.5; 597.0/15.6; 657.0/11.2; 781.0/9.9; 796.0/9.7; 933.0/25.2; 1065.0/19.9 (iC?)	Dolez (1998)
							382.5/16.5; 493.2/7.1; 494.2/4.4; 541.0/28.5; 541.8/8.1; 542.5/7.0; 596.8/14.6; 597.1/4.5; 598.6/3.6; 659.5/10.7; 660.1/7.4; 661.4/9.3; 661.9/7.6; 662.3/10.8; 662.8/3.5; 663.6/11.9; 664.2/15.0; 792.7/4.1; 794.1/5.1; 795.7/3.6; 796.4/3.7; 798.3/4.0; 799.1/5.2; 930.6/3.6; 933.2/3.2; 971.6/3.9; 974.4/5.0; 976.4/6.5; 979.2/4.3; 1060.2/7.7; 1061.8/11.4; 1062.6/3.2; 1067.5/9.7; 1070.8/9.6; 1390.8/3.6 (+C,R)	Dolez et al. (2006)
0417+361	G 38-29	04 20 17	36 16 27	11 160^{G}	7.89	15.6	923.9; 1021.9 (+C)	McGraw & Robinson (1975)
							413.3/3.1; 432.4/3.6; 544.9/6.1; 547.0/7.0; 548.9/4.8; 706.0/18.4; 709.2/6.0; 840.4/5.2; 900.0/10.6; 922.7/5.9; 945.4/12.3; 962.1/8.1; 963.6/4.6; 980.1/11.4; 989.7/10.0; 1002.2/7.1; 1016.2/5.8; 1081.8/5.0; 1086.8/3.9; 1089.4/5.2 (+C)	Thompson et al. (2009)
0455+553	G 191-16	04 59 27	55 25 21	11 440^{G}	8.04	16.0	588.2; 666.7; 882.6 (+C)	McGraw et al. (1981)
							892.9 (+C,SH)	Vauclair et al. (1989)
(0502+540)	LP 119-10	05 02 34	54 01 09	11 400	8.24	15.2	873.6/12.7	Green et al. (2015)

Table 4: continued.

WD	Identifiers Other	RA (h m s)	DEC (° ′ ″)	$T_{\rm eff}$ (K)	$\log g$ (dex)	V (mag)	Period/Amplitude (s/mma)	References
0507+045	(HS 0507+0435) HS 0507+0434B	05 10 14	04 38 55	12 010^G	8.19	15.3	278.4/12.8; 355.1/22.0; 445.2/7.3; 558.7/19.0 (+C)	Jordan et al. (1998)
							354.9/10.9; 355.4/4.7; 355.8/25.7; 444.6/12.6; 445.3/3.0; 446.1/14.7; 555.3/18.6; 556.6/6.3; 557.6/17.1; 743.4/8.4 (+C,iR)	Handler & Romero-Colmenero (2001) (also in Handler et al. 2002)
							286.1/3.6; 354.9/6.8; 355.8/22.7; 444.8/13.6; 446.2/11.0; 557.7/18.7; 743.0/13.9 (+C,iR)	Kotak et al. (2002)
							355.8/24.0; 446.2/13.9; 555.3/16.6; 743.4/7.6	Castanheira & Kepler (2009)
							354.9/15.8; 355.3/2.5; 355.8/12.6; 444.7/5.3; 445.3/2.8; 446.1/13.8; 555.3/14.3; 556.5/6.7; 557.8/15.0; 654.8/11.0; 655.9/5.8; 657.1/10.6; 695.6/17.4; 699.6/15.2; 746.1/13.0; 748.6/10.5; 750.3/10.9; 999.7/3.0 (+C,iR)	Fu et al. (2013)
0517+307	GD 66	05 20 38	30 48 24	12 210^G	8.10	15.6	197.0/6.0; 256.0/5.0; 273.0/20.0; 304.0/10.0	Dolez et al. (1983)
							196.7; 271.4; 301.4; 810.4 (+C)	Fontaine et al. (1985)
							197.2/1.8; 197.6/4.2; 198.1/2.7; 255.9/3.4; 256.2/2.5; 271.2/2.9; 271.7/16.7; 272.2/2.5; 302.8/11.3; 518.6/1.8; 523.3/2.3 (+C,iR)	Yeates et al. (2005)
							197.4/5.4; 256.0/3.8; 271.7/17.0; 302.8/11.4 (+C)	Castanheira & Kepler (2009)
0532-560	HE 0532-5605	05 33 07	−56 03 53	11 510^G	8.42	16.0	586.4; 688.8	Fontaine et al. (2003)
							522.4/2.1; 563.7/2.5; 599.7/2.5; 686.1/5.5; 723.7/7.8; 753.8/4.8; 822.3/3.4; 881.7/2.9	Castanheira & Kepler (2009)
(0702+440)	PM J07029+4406	07 02 59	44 06 54	11 000	8.29	15.1	1366.4/1.0	Green et al. (2015)

Table 4: continued.

WD	Identifiers Other	RA (h m s)	DEC (° ′ ″)	$T_{\rm eff}$ (K)	$\log g$ (dex)	V (mag)	Period/Amplitude (s/mma)	References
–	(HS 0733+4119) SDSS J073707.99+411227.6	07 37 08	41 12 28	11 160	7.72	15.8 (g)	468.8/19.4; 656.2/38.7; 747.4/20.3	Voss et al. (2007)
(J0756+2020)	SDSS J075617.54+202010.2	07 56 18	20 20 10	11 830^T	8.13	18.3 (g)	199.5/6.8	Mullally et al. (2005)
(J0815+4437)	SDSS J081531.75+443710.3	08 15 32	44 37 10	11 840^T	8.21	19.3 (g)	258.3/6.2; 311.3/9.3; 311.7/22.0; 511.5/7.3; 787.5/6.6	Mukadam et al. (2004)
							258.3/6.8; 309.0/10.2; 311.7/18.9; 787.5/7.2	Mukadam et al. (2006)
(J0818+3131)	SDSS J081828.98+313153.0	08 18 29	31 31 53	11 820^T	8.13	17.4 (g)	202.3/3.3; 253.3/2.9	Mullally et al. (2005)
(0825+0329)	SDSS J082518.86+032927.8	08 25 19	03 29 28	12 120^T	8.15	17.5 (g)	303.0/3.8; 334.0/6.9; 481.0/4.5; 664.0/11–12; 704.0/6.0; 826.0/5.3	Kepler et al. (2005)
(J0825+4119)	SDSS J082547.00+411900.0	08 25 47	41 19 00	11 510^T	8.37	18.5 (g)	611.0/11.2; 653.4/17.1	Mukadam et al. (2004)
–	SDSS J083203.98+142942.3 (EPIC 211596649)	08 32 04	14 29 42	11 230	7.94	18.9 (g)	not published yet	Bell et al.(2016)
0836+404	KUV 08368+4026	08 40 08	40 15 04	12 010^G	8.13	15.6 (g)	494.5/6.0; 618.0/17.4	Vauclair et al. (1997)
							257.3/9.0; 362.5/2.0; 307.9/10.0; 400.1/5.0; 519.9/4.0; 778.8/5.0 (+C)	Dolez et al. (1999)
							257.2/11.5; 257.3/11.6; 257.3/10.4; 307.9/7.2; 308.0/14.1; 308.1/4.5; 362.3/3.7; 362.5/3.3; 399.9/8.0; 400.2/10.7; 463.1/2.4; 505.7/4.0; 506.0/8.2; 506.2/2.9; 779.0/5.2; 780.9/4.2; 782.0/2.4 (+C,iR)	Li et al. (2015)
–	SDSS J084054.14+145709.0 (EPIC 211629697)	08 40 54	14 57 09	10 570	7.92	18.3 (g)	487.0/1.6; 1095–1309 s	Bell et al.(2016)
(J0842+3707)	SDSS J084220.73+370701.7	08 42 21	37 07 02	11 620^T	7.88	18.8 (g)	309.3/17.9	Mukadam et al. (2004)
							212.3/5.2; 309.3/18.0; 321.1/4.4	Mukadam et al. (2006)
(0843+0431)	SDSS J084314.05+043131.6	08 43 14	04 31 32	11 220^T	8.09	17.8 (g)	373.0/10.4; 1049.0/11.4; 1085.0/7.4	Kepler et al. (2005)
(J0847+4510)	SDSS J084746.82+451006.3	08 47 47	45 10 06	11 690^T	8.12	18.3 (g)	201.0/7.3	Mukadam et al. (2004)

Table 4: continued.

WD	Identifiers Other	RA (h m s)	DEC (° ′ ″)	$T_{\rm eff}$ (K)	$\log g$ (dex)	V (mag)	Period/Amplitude (s/mma)	References
							123.4/3.0; 200.5/7.0	Mukadam et al. (2006)
(0851+0605)	SDSS J085128.17+060551.1	08 51 28	06 05 51	11 300^T	8.05	16.8 (g)	326/22.4	Kepler et al. (2005)
(J0853+0005) 0850+002	SDSS J085325.55+000514.2	08 53 26	00 05 14	11 950^T	8.15	18.2 (g)	264.4/4.0	Castanheira et al. (2007)
(J0855+0635)	SDSS J085507.29+063540.9	08 55 07	06 35 41	10 970^T	8.22	17.2 (g)	433.0/15.0; 850.0/44.0	Castanheira et al. (2007)
–	SDSS J085648.33+185804.9 (EPIC 211916160)	08 56 48	18 58 05	11 900	8.23	18.9 (g)	not published yet	Bell et al.(2016)
–	SDSS J090041.08+190714.3 (EPIC 211926430)	09 00 41	19 07 14	11 690	8.09	17.6 (g)	not published yet	Bell et al.(2016)
0858+363	GD 99	09 01 49	36 07 08	12 110^G	8.20	14.6	–	McGraw & Robinson (1976)
							105.2/2.0; 223.6/2.9; 228.9/4.5; 633.1/2.0; 853.2/2.4; 924.7/1.7; 976.0/2.1; 1007.0/6.5; 1058.0/8.3; 1088.0/4.3; 1151.0/1.9	Mukadam et al. (2006)
							223.9/2.6; 228.7/6.3; 1026.1/4.3; 1058.1/7.6	Bognár et al. (2007)
–	SDSS J090231.76+183554.9 (EPIC 211891315)	09 02 32	18 35 55	11 310	8.03	19.4 (g)	486.0/11.9; 562.1/19.9; 756.4/22.2; 978.8/11.2	Bell et al.(2016)
(J0906-0024)	SDSS J090624.26-002428.2	09 06 24	−00 24 28	11 260^T	8.07	17.7 (g)	266.6/7.6; 457.9/9.5; 574.5/23.7; 618.8/9.1; 769.4/26.1	Mukadam et al. (2004)
(0911+0310)	SDSS J091118.42+031045.1	09 11 18	03 10 45	11 630^T	8.14	18.4 (g)	176.0/11.1; 347.0/17.4; 352.0–353.0/27.7–26.9; 388.0/12.3; 420.0/12.6; 757.0/16.4	Kepler et al. (2005)
(J0913+4036)	SDSS J091312.74+403628.7	09 13 13	40 36 29	11 850^T	8.09	17.6 (g)	203.9/3.8; 260.3/16.5; 288.7/12.4; 320.5/14.7	Mullally et al. (2005)
(J0916+3855)	SDSS J091635.07+385546.2	09 16 35	38 55 46	11 320^T	8.04	16.6 (g)	238.1/10.8; 447.7/14.4; 485.1/32.9; 747.2/9.1	Castanheira et al. (2007)
(0917+0926)	SDSS J091731.00+092638.1 EQ J0917+0926	09 17 31	09 26 38	11 340^T	8.09	18.1 (g)	212.0/8.0; 259.0/10.2; 289.0/16.1	Kepler et al. (2005)

Table 4: continued.

WD	Identifiers Other	RA (h m s)	DEC (° ′ ″)	$T_{\rm eff}$ (K)	$\log g$ (dex)	V (mag)	Period/Amplitude (s/mma)	References
(J0923+0120) 0920+015	SDSS J092329.81+012020.0	09 23 30	01 20 20	11 190^{T}	8.38	18.3 (g)	595.2/7.4	Mukadam et al. (2004)
							655.7/4.4; 668.9/3.5	Mukadam et al. (2006)
							595.1/2.7; 1436.4/1.4; 2032.3;	Romero et al. (2013)
0921+354	G 117-B15A	09 24 15	35 16 51	12 420^{G}	8.12	15.5	1311.0	Richer & Ulrych (1974)
							216.0; 271.7; 307.7	McGraw & Robinson (1976)
							215.2/23.9; 271.0/7.3; 304.4/8.1 (+C)	Kepler et al. (1982)
							215.2/20.2; 270.5/5.6; 304.1/6.3 (+C)	Kepler et al. (1995c)
							215.2/17.4; 270.5/6.1; 304.1/7.5 (+C)	Castanheira & Kepler (2008)
(J0925+0509)	SDSS J092511.60+050932.4	09 25 12	05 09 33	10 830^{T}	8.21	15.2 (g)	1127.1/3.2; 1264.3/3.1	Castanheira et al. (2010)
							1159.0/2.7; 1341.0/4.0	Romero et al. (2013)
(J0939+5609) 0936+563	SDSS J093944.89+560940.2	09 39 45	56 09 40	11 690^{T}	8.29	18.7 (g)	249.9/7.2	Mukadam et al. (2004)
							48.5/5.9(?); 249.9/7.2	Mukadam et al. (2006)
(J0940+0052)	SDSS J094000.27+005207.1	09 40 00	00 52 07	10 590^{T}	8.34	18.1 (g)	255.0/17.1; 255.8/8.0	Castanheira et al. (2013)
(J0942+5733) 0938+577	SDSS J094213.13+573342.5	09 42 13	57 33 43	11 360^{T}	8.12	17.4 (g)	451.0/18.4; 550.5/12.2; 694.7/37.7	Mukadam et al. (2004)
							273.0/9.0; 550.5/12.3; 694.7/37.7; 909.4/7.7	Mukadam et al. (2006)
(0949-0000) 0946+002	SDSS J094917.04-000023.6	09 49 17	−00 00 24	11 130^{T}	8.21	18.8 (g)	213.3/6.0; 363.2/12.5; 364.0/7.3; 365.2/17.7; 516.6/16.2; 634.2/5.1; 711.6/6.0	Mukadam et al. (2004)
0951+132	HS 0951+1312	09 53 45	12 58 30	12 010^{G}	8.05	16.5 (g)	208.0/9.3; 258.6/3.6; 281.6/8.8	Mukadam et al. (2004)
							208.0/9.4; 258.0/3.6; 282.2/9.0; 311.7/2.7	Mukadam et al. (2006)
0952+182	HS 0952+1816	09 55 11	18 02 15	11 390^{G}	8.11	16.3 (g)	853.8/3.9; 1159.7/4.8; 1466.0/4.5	Mukadam et al. (2004)
							674.7/3.0; 790.0/2.9; 883.0/3.6;	Mukadam et al. (2006)

Table 4: continued.

WD	Identifiers Other	RA (h m s)	DEC (° ′ ″)	$T_{\rm eff}$ (K)	$\log g$ (dex)	V (mag)	Period/Amplitude (s/mma)	References
							945.9/10.4; 1150.0/4.8; 1160.9/7.9	
(J0958+0130) 0955+017	SDSS J095833.13+013049.3	09 58 33	01 30 49	11 730^{T}	8.08	16.7 (g)	203.7/2.5; 264.4/4.7	Mukadam et al. (2004)
							121.2/1.6; 203.7/2.5; 264.4/4.7	Mukadam et al. (2006)
(J0959+0238)	SDSS J095936.96+023828.4	09 59 37	02 38 29	11 830^{T}	8.06	18.5	194.7/7.2; 283.4/13.0	Castanheira et al. (2010)
(J1002+5818)	SDSS J100238.58+581835.9	10 02 39	58 18 36	11 440^{T}	8.11	18.3 (g)	268.2/6.8; 304.6/5.3	Mullally et al. (2005)
(J1007+5245) 1004+529	SDSS J100718.26+524519.8	10 07 18	52 45 20	11 390^{T}	8.12	18.9 (g)	152.8/5.8; 258.8/11.0; 290.1/7.7; 323.1/10.4 (iC?)	Mullally et al. (2005)
(J1015+5954)	SDSS J101519.65+595430.5	10 15 20	59 54 31	11 440^{T}	8.06	18.0 (g)	213.0/9.8; 292.4/8.5; 401.7/20.8; 453.7/15.8; 1116.5/12.6	Mukadam et al. (2004)
							139.2/4.6; 145.5/3.1; 292.4–294.0/8.6–9.1; 399.7–401.7/19.2–21.4; 453.8–456.1/15.5–19.6; 769.9–768.4/5.7–7.5	Mukadam et al. (2006)
(J1015+0306) 1013+033	SDSS J101548.01+030648.4	10 15 48	03 06 48	11 630^{T}	8.12	15.7 (g)	194.7/5.8; 255.7/7.3; 270.0/8.4	Mukadam et al. (2004)
1039+412	HS 1039+4112 PB 520	10 42 34	40 57 15	11 730^{G}	8.12	16.1 (g)	837.3/26.0; 855.5/55.2 (+C)	Silvotti et al. (2005)
1047+335	–	10 50 46	33 15 48	11 310^{G}	8.09	16.5 (g)	767.5/27.7	Green et al. (2015)
(J1054+5307) 1051+533B	SDSS J105449.87+530759.1	10 54 50	53 07 59	10 960^{T}	7.96	17.9 (g)	444.6/16.0; 869.1/37.4	Mullally et al. (2005)
(J1056-0006)	SDSS J105612.32-000621.7	10 56 12	−00 06 22	11 130^{T}	7.91	17.5 (g)	314.2/11.0; 474.4/22.9; 942.2/62.3	Mukadam et al. (2004)
							603.0/11.5; 670.6/12.0; 925.4/60.3; 1024.9/31.6	Mukadam et al. (2006)
(J1105-1613)	SDSS J110525.70-161328.3	11 05 26	−16 13 29	11 670	8.23	17.5 (g)	192.7/12.1; 298.3/7.1	Castanheira et al. (2010)
(1106+0115) 1103+015	SDSS J110623.40+011520.8	11 06 23	01 15 21	10 920^{T}	7.90	18.4 (g)	842.0/9.4; 973.0/10.8	Kepler et al. (2005)
1116+026	GD 133	11 19 12	02 20 33	12 430^{G}	8.10	14.6	115.9/1.5; 120.4/4.6; 146.9/1.1	Silvotti et al. (2006)

Table 4: continued.

WD	Identifiers Other	RA (h m s)	DEC (° ′ ″)	$T_{\rm eff}$ (K)	$\log g$ (dex)	V (mag)	Period/Amplitude (s/mma)	References
(J1122+0358)	SDSS J112221.10+035822.4	11 22 21	03 58 22	11 030^{T}	7.91	18.2 (g)	859.0/34.3; 996.1/17.9	Mukadam et al. (2004)
							740.1/10.0; 859.1/34.6; 996.1/17.3	Mukadam et al. (2006)
(J1125+0345)	SDSS J112542.84+034506.3	11 25 43	03 45 06	11 600^{T}	7.95	18.1 (g)	208.6/2.8; 265.5/7.2; 265.8/3.3	Mukadam et al. (2004)
							208.6/2.8; 265.5/7.1; 265.8/3.3; 335.1/2.8	Mukadam et al. (2006)
1126-222	EC 11266-2217	11 29 12	−22 33 44	12 010^{G}	8.08	16.2	215.7–218.3/3.7–8.1; 234.1/4.49; 275.7–277.6/7.7–7.0; 386.4/4.0; 402.7/3.0	Voss et al. (2006)
(J1136-0136)	SDSS J113604.01-013658.1	11 36 04	−01 36 58	11 780^{T}	8.05	17.8 (g)	260.8/2.5	Castanheira et al. (2010)
1137+423	KUV 11370+4222	11 39 41	42 05 19	11 940^{G}	8.17	16.5 (g)	257.2/5.8; 292.2/2.7; 462.9/3.5	Vauclair et al. (1997)
							139.0/2.6; 257.9/18.3; 280.8/2.7; 293.8/3.0; 394.1/4.5; 398.1/2.5; 402.1/2.4; 462.8/8.4; 762.4/2.8; 811.8/2.5 (+C,iR)	Su et al. (2014b)
1149+057	PG 1149+057	11 51 54	05 28 40	11 060^{G}	8.06	15.4	1023.5/10.5	Voss et al. (2006)
1150-153	EC 11507-1519	11 53 15	−15 36 36	12 440^{G}	8.20	16.0	249.6/7.7	Gianninas et al. (2006)
							191.7/3.6; 249.4/4.7	Voss et al. (2007)
(J1157+0553)	SDSS J115707.43+055303.6	11 57 07	05 53 04	11 040^{T}	8.04	17.6 (g)	436.1/3.9; 458.7/4.2; 748.5/5.6; 826.2/8.1; 918.9/15.9; 1056.2/5.8	Mukadam et al. (2004)
(J1200-0251)	SDSS J120054.55-025107.0	12 00 55	−02 51 07	11 970^{T}	8.24	18.2 (g)	257.1/6.7; 271.3/13.1; 294.1/6.7; 304.8/23.7	Castanheira et al. (2013)
1159+803	G 255-2	12 01 45	80 04 59	11 440^{G}	8.14	16.0	384.6; 476.2; 689.7/36.0; 840.3/36.0	Vauclair et al. (1981)
							399; 461; 573; 608; 660; 681; 764; 810; 855; 906 (+R)	Fu et al. (2002)
							568.5/6.6; 607.9/13.1; 681.2/24.9; 775.2/15.2; 819.7/11.3; 855.4/11.2; 898.5/9.4	Mukadam et al. (2006)

Table 4: continued.

WD	Identifiers Other	RA (h m s)	DEC (° ′ ″)	$T_{\rm eff}$ (K)	$\log g$ (dex)	V (mag)	Period/Amplitude (s/mma)	References
							568.5/16.5; 681.2/27.7; 773.4/12.7; 985.2/4.8	Mukadam et al. (2006)
(1216+0922)	SDSS J121628.55+092246.4	12 16 29	09 22 46	$11\,240^{T}$	8.25	18.6 (g)	409.0/30.1; 570.0/24.6; 626.0/21.6; 823.0/45.2; 840.0/42.0; 967.0/20.5	Kepler et al. (2005)
(J1218+0042) 1215+009	–	12 18 31	00 42 16	$11\,170^{T}$	8.06	18.5 (g)	100.0/11.0; 152.0/5.1; 175.0/10.0; 258.0–259.0/8.2–16.0	Kepler et al. (2005)
(1222-0243)	SDSS J122229.57-024332.5	12 22 30	−02 43 33	$11\,380^{T}$	8.19	16.7 (g)	198.0/7.3; 396.0/22.0	Kepler et al. (2005)
1236-495	BPM 37093	12 38 50	−49 48 00	$11\,620^{G}$	8.69	14.0	600.0/4.0	Kanaan et al. (1992)
							560.0; 583.0; 614.0	Kanaan et al. (1998)
							512.0; 532.0; 548.0; 565.0; 582.0; 608.0; 615.0; 635.0; 649.0	Kanaan et al. (2000)
							511.7; 531.1; 548.4; 564.1; 582.0; 600.7; 613.5; 635.1	Metcalfe et al. (2004)
							511.7/0.7; 531.1/1.2; 548.4–549.2/0.8–1.1; 562.6/0.9; 565.5–565.9/0.5–1.2; 582.0/1.0; 600.7/0.9; 613.5/1.1; 633.2–633.5/1.1–1.3; 636.7–637.2/0.7–1.7; 660.8/0.5 (iR?)	Kanaan et al. (2005)
(1247+310)	–	∼ 12 47	∼ 31 00	12 110	8.43	17.2	364.6/2.0	Green et al. (2015)
1250+041	HS 1249+0426	12 52 15	04 10 43	$12\,160^{G}$	8.21	16.0 (g)	288.9/7.6	Voss et al. (2006)
(1255+0211) 1253+024	SDSS J125535.41+021116.0	12 55 35	02 11 16	$11\,580^{T}$	8.15	19.1 (g)	812.0/16.4; 897.0/31.7; 1002.0/21.7	Kepler et al. (2005)
(J1257+0124) 1254+016	SDSS J125710.50+012422.9	12 57 11	01 24 23	$11\,490^{T}$	8.30	18.7	905.8/46.7	Castanheira et al. (2006)
							377.8/6.6; 398.1/6.7; 466.3/8.9; 507.1/8.4; 644.5/21.9; 786.9/8.9; 946.3/10.5; 1070.5/7.9	Romero et al. (2013)
1258+013 (1301+0107)	HE 1258+0123	13 01 11	01 07 40	$11\,420^{G}$	8.02	16.3	439.2; 528.5; 744.6; 1092.1	Bergeron et al. (2004)
							628.0/15.2; 882.0/17.6	Kepler et al. (2005)

Table 4: continued.

WD	Identifiers Other	RA (h m s)	DEC (° ′ ″)	$T_{\rm eff}$ (K)	$\log g$ (dex)	V (mag)	Period/Amplitude (s/mma)	References
							439.2/9.8; 528.5/9.3; 628.0/15.2; 744.6/22.9; 881.5/17.6; 1092.1/14.1	Castanheira & Kepler (2009)
1307+354	GD 154	13 09 58	35 09 47	11 120^G	8.07	15.3	1186.1 (+C,SH)	Robinson et al. (1978)
							402.6/2.7; 1084.0/5.6; 1088.6/5.0; 1183.5/4.6; 1186.5/16.7; 1190.5/6.3; 1092.1/3.0 (+C,iR)	Pfeiffer et al. (1995) (also in Pfeiffer et al. 1996)
							402.5; 596.1; 597.2; 1125.1; 1129.5; 1133.4; 1271.4 (+C,iR)	Hürkal et al. (2005)
							402.6/3.8; 1085.1/4.2; 1088.5/4.8; 1131.8/4.5; 1156.7/5.3; 1160.7/6.3; 1186.0/7.5; 1191.7/9.1; 1238.2/5.0; 1244.2/4.8 (+C,iR)	Paparó et al. (2013)
(1310-0159) 1307-017	–	13 10 08	−01 59 56	10 940^T	7.76	17.7 (g)	280.0/6.6–9.2; 310.0/6.4; 349.6/17.6	Kepler et al. (2005)
1321+013	SDSS J132350.28+010304.2	13 23 50	01 03 04	11 380^T	8.45	18.5 (g)	495.4/4.1; 549.8/6.7; 590.1/7.1; 612.2/11.9; 636.4/4.8; 671.1/4.4; 698.6/4.3; 831.1/4.6; 884.2/4.1	Kepler et al. (2012)
							432.5/5.1; 497.4/6.4; 525.0/3.6; 550.5/8.6; 564.6/18.3; 590.1/7.1; 603.6/8.3; 612.2/11.9; 636.4/4.8; 656.0/15.3; 675.4/6.4; 698.6/4.3; 731.6/5.2; 831.1/4.6; 884.2/4.1	Romero et al. (2013)
(J1337+0104) 1334+013	–	13 37 14	01 04 44	11 460^T	8.64	18.6 (g)	715.0/10.0	Kepler et al. (2005)
(J1338-0023) 1335-001	SDSS J133831.74-002328.0	13 38 32	−00 23 28	11 900^T	8.07	17.1 (g)	119.7/1.8; 196.9/4.0	Castanheira et al. (2010)
–	(EPIC 229227292)	13 42 12	−07 35 40	11 190	8.02	16.7 (Kp)	289.3; 370.7; 514.1; 800–1250 s	Bell et al.(2016)
1342-237	EC 13429-2342	13 45 46	−23 57 10	11 000^G	8.02	16.0	982.0/5.2; 1177.0/6.2	Voss et al. (2006)
(J1345-0055) 1343-006	SDSS J134550.93-005536.5	13 45 51	−00 55 36	11 760^T	8.10	16.7 (g)	195.2/5.5; 195.5/3.9; 254.4/2.4 (iR?)	Mukadam et al. (2004)

Table 4: continued.

WD	Identifiers Other	RA (h m s)	DEC (° ′ ″)	$T_{\rm eff}$ (K)	$\log g$ (dex)	V (mag)	Period/Amplitude (s/mma)	References
1349+552	LP 133-144	13 51 20	54 57 43	$12\,150^{G}$	7.97	15.7 (g)	209.2; 304.5; 306.9; 327.3	Bergeron et al. (2004)
							140.5/0.7; 179.4/0.7; 179.5/0.4; 179.7/0.5; 209.0/1.2; 209.2/11.8; 209.4/1.1; 270.4/2.2; 270.6/3.8; 270.9/3.7; 305.6/3.3; 305.9/4.2; 306.2/1.3; 327.3/3.0 (+C,iR)	Bognár et al. (2016)
1350+656	G 238-53	13 52 11	65 24 57	$12\,130^{G}$	7.97	15.5	206.0	Fontaine & Wesemael (1984)
							122.2/2.0	Mullally et al. (2008)
(J1354+0108) 1352+013	SDSS J135459.89+010819.3	13 55 00	01 08 19	$11\,650^{T}$	8.03	16.4 (g)	127.8/1.5; 173.3/1.1; 198.3/6.0; 291.6/2.2; 322.9/1.9	Mukadam et al. (2004)
(J1355+5454)	SDSS J135531.03+545404.5	13 55 31	54 54 05	$11\,480^{T}$	7.93	18.6 (g)	324.0/21.8	Mullally et al. (2005)
1401-147	EC 14012-1446	14 03 57	−15 01 11	$12\,020^{G}$	8.18	15.7	399.0/13.0; 530.0/15.0; 610.0/57.0; 724.0/21.0; 937.0/11.0 (+C)	Stobie et al. (1995) (amplitudes: Mukadam et al. 2006)
							399.2/7.4; 529.8/13.4; 608.6/7.6; 612.1/36.4; 615.8/11.4; 673.8/2.8; 678.9/6.1; 683.0/3.5; 715.2/11.8; 716.9/7.9; 722.1/44.1; 723.6/10.4; 727.0/5.1; 728.9/9.9; 769.8/43.2; 771.8/9.4; 775.6/5.8; 882.7/3.1; 1217.6/7.7 (+C,iR)	Handler et al. (2008)
							398.9/12.1; 530.1/16.7; 610.4/54.3; 678.6/7.6; 722.9/22.9; 769.1/51.7; 882.7/2.9; 937.2/11.0; 1217.4/7.5	Castanheira & Kepler (2009)
							350.1/2.0; 398.7/2.1; 399.2/12.7; 433.9/4.7; 528.8/3.8; 529.8/20.7; 530.9/1.5; 537.6/6.4; 563.4/7.2; 612.0/25.7; 615.8/3.1; 645.9/7.9; 657.2/2.2; 705.0/1.2; 805.5/1.2; 865.1/1.9; 905.6/2.2; 979.3/1.7; 1069.1/2.7 (+C,iR)	Provencal et al. (2012)
							821.3; 935.4; 964.7; 1035.4; 1104.2; 1136.5; 1163.2; 1219.8; 1298.9; 1332.9; 1384.9; 1418.4;	Provencal et al. (2012) (average periods 2004–2008)

Table 4: continued.

WD	Identifiers Other	RA (h m s)	DEC (° ′ ″)	$T_{\rm eff}$ (K)	$\log g$ (dex)	V (mag)	Period/Amplitude (s/mma)	References
							1463.7; 1548.2; 1633.6; 1775.0; 1860.4; 1887.5; 2304.9; 2505.4; 2738.1; 2856.2	
							350.1; 398.7; 399.2; 433.9; 528.8; 529.8; 530.9; 537.6; 563.4; 608.5; 612.1; 615.9; 645.9; 657.2; 673.8; 678.5; 683.0; 705.0; 714.8; 716.9; 721.9; 723.6; 727.1; 729.2; 769.3; 771.8; 775.6; 805.5; 865.1; 882.7; 905.6; 979.3; 1069.1; 1217.4 (iR)	Chen & Li (2014)
(1408+0445) 1406+050	SDSS J140859.46+044554.7	14 08 59	04 45 55	$10\,920^{T}$	7.99	17.9 (g)	764.0/11.1; 849.0/24.3; 1038.0/12.0	Kepler et al. (2005)
(J1417+0058) 1414+012	SDSS J141708.81+005827.2	14 17 09	00 58 27	$11\,000^{T}$	8.01	18.0 (g)	812.5/31.5; 894.5/44.0	Mukadam et al. (2004)
							522.0/14.9; 749.4/17.9; 812.5/32.1; 894.6/42.8; 980.0/11.3	Mukadam et al. (2006)
1422+095	GD 165	14 24 39	09 17 14	$12\,220^{G}$	8.11	14.3	120.0; 193.0; 240.0; 649.0; 775.0; 870.0; 1316.0; 1820.0 (iC?)	Bergeron & McGraw (1990)
							107.7/0.4; 114.3/0.6; 120.4/6.1; 146.4/0.5; 166.2/0.4; 192.7/4.8; 249.7/0.7; 321.2/0.5 (+R)	Bergeron et al. (1993)
							114.2/0.4; 114.4/0.2; 120.3/1.1; 120.4/5.1; 120.4/1.6; 146.3/0.4; 146.4/0.2; 168.2/0.3; 192.6/2.3; 192.7/2.3; 192.8/0.6; 250.2/0.6; 250.3/0.2 (iR)	Giammichele et al. (2015)
1429-037	HE 1429-0343	14 32 03	−03 56 38	$11\,290^{G}$	8.00	15.8	450.1/10.2; 829.3/18.3; 969.0/12.7; 1084.9/16.3	Silvotti et al. (2005)
1425-811	L 19-2	14 33 08	−81 20 15	$12\,070^{G}$	8.13	13.0	113.6; 192.4	McGraw (1977)
							113.3/0.6; 113.8/2.4; 114.2(?)/0.3; 118.5/2.0; 118.7/1.2; 118.9(?)/0.3; 143.0(?)/0.3; 143.4/0.6; 192.1/0.8; 192.6/6.5; 193.1/0.9; 348.7/0.5;	O'Donoghue & Warner (1982)

Table 4: continued.

WD	Identifiers Other	RA (h m s)	DEC (° ′ ″)	$T_{\rm eff}$ (K)	$\log g$ (dex)	V (mag)	Period/Amplitude (s/mma)	References
							350.1/1.1 (iR)	
							113.3/0.3; 113.8/1.8; 118.4/0.3; 118.5/1.6; 118.7/1.2; 143.0/0.3; 143.4/0.4; 143.8/0.2; 192.2/1.2; 192.6/5.5; 193.1/1.0; 348.7/0.3; 350.2/0.9 (iR)	Yeates et al. (2005)
(J1443+0134) 1440+017	SDSS J144330.93+013405.8	14 43 31	01 34 06	$10\,450^{T}$	7.85	18.7 (g)	968.9/7.5; 1085.0/5.2	Mukadam et al. (2004)
(J1502-0001) 1459+001	SDSS J150207.02-000147.1	15 02 07	−00 01 47	$11\,090^{T}$	7.75	18.7 (g)	313.6/13.1; 418.2/14.9; 581.9/11.1; 629.5/32.6; 687.5/12.0	Mukadam et al. (2004)
							141.0/14.9; 415.0/16.7; 603.0/28.1; 658.0/27.0	Kepler et al. (2005)
(J1524-0030)	SDSS J152403.25-003022.9	15 24 03	−00 30 23	–	–	15.8 (g)	434.0/47.8; 873.2/111.5	Mukadam et al. (2004)
							255.2/17.9; 498.6/21.6; 717.5/28.3; 873.3/110.8	Mukadam et al. (2006)
							340.1/3.5; 400.9/5.4; 427.3/4.4; 503.2/8.4; 505.1/5.2; 505.5/10.1; 507.4/10.9; 578.6/5.9; 582.0/5.1; 620.8/5.8; 665.5/4.2; 780.3/9.4; 833.1/25.7; 840.5/9.4; 877.7/6.8 (+C,iR)	Handler et al. (2008a)
1526+558	–	15 28 09	55 39 15	$10\,860^{G}$	7.73	17.1 (B)	648.9/36.8	Green et al. (2015)
–	HS 1531+7436	15 30 35	74 26 04	$13\,270^{G}$	8.49	16.4	112.5/4.2	Voss et al. (2006)
(J1533-0206)	SDSS J153332.96-020655.7	15 33 33	−02 06 56	$11\,390^{T}$	8.04	16.4 (g)	257.8/4.3; 260.6/5.3	Castanheira et al. (2006)
1541+650	PG 1541+650	15 41 45	64 53 53	$11\,560^{G}$	8.12	15.6 (g)	467.0/3.0; 564.0/15.0; 689.0/45.0; 757.0/14.0 (+C)	Vauclair et al. (2000)
1559+369	Ross 808	16 01 23	36 48 35	$11\,120^{G}$	7.98	14.4	833.0	McGraw & Robinson (1976)
							404.5/2.1; 511.3/4.6; 745.1/4.2; 796.3/3.8; 877.9/4.3; 907.6/5.9; 956.5/3.5; 1079.1/2.6	Castanheira & Kepler (2009)

Table 4: continued.

WD	Identifiers Other	RA (h m s)	DEC (° ′ ″)	$T_{\rm eff}$ (K)	$\log g$ (dex)	V (mag)	Period/Amplitude (s/mma)	References
							404.5/2.0; 511.3/4.5; 629.2/1.9; 632.2/3.4; 745.1/4.0; 796.3/4.0; 842.7/2.8; 860.2/3.5; 875.1/3.7; 878.5/3.6; 898.7/3.6; 908.4/7.6; 911.5/3.2; 914.7/3.9; 915.8/5.5; 922.5/3.4; 952.4/3.4; 960.5/3.7; 1011.4/2.5; 1040.1/3.3; 1042.1/2.9; 1066.7/2.2; 1091.1/2.4; 1144.0/2.5; 2459.1/2.2 (+C,iR)	Thompson et al. (2009)
1607+205	–	16 09 44	20 23 11	11 140^{G}	7.81	17.4	1928.5/1.8	Green et al. (2015)
(J1612+0830)	SDSS J161218.08+083028.1	16 12 18	08 30 28	12 030	8.46	17.8 (g)	115.2/5.1; 117.2/4.1	Castanheira et al. (2013)
(J1617+4324)	SDSS J161737.63+432443.8	16 17 38	43 24 44	11 070^{T}	8.07	18.4 (g)	626.3/24.1; 889.6/36.6	Mukadam et al. (2004)
							626.3/15.4; 661.7/21.2; 889.7/36.6	Mukadam et al. (2006)
(J1618-0023) 1616-002	SDSS J161837.25-002302.7	16 18 37	−00 23 03	10 860	8.16	19.3 (g)	644.0/5.4	Castanheira et al. (2006)
–	HS 1625+1231	16 28 13	12 24 53	11 690^{G}	8.06	16.1 (g)	385.2/17.0; 533.6/23.6; 862.9/48.9	Voss et al. (2006)
(J1641+3521)	SDSS J164115.61+352140.6	16 41 16	35 21 41	11 230	8.43	19.1	809.3/27.3	Castanheira et al. (2006)
1647+591	G 226-29	16 48 26	59 03 23	12 510^{G}	8.35	12.2	109.1/3.0; 109.3/1.0; 109.5/3.0 (iR)	Kepler et al. (1983)
							109.1/2.5; 109.3/1.1; 109.5/2.8 (iR)	Kepler et al. (1995b)
(J1650+3010)	SDSS J165020.53+301021.2	16 50 21	30 10 21	10 830^{T}	8.43	18.1 (g)	339.1/14.7	Castanheira et al. (2007)
1659+662	GD 518	16 59 15	66 10 33	11 760^{G}	8.97	16.5 (B)	440.2; 513.2; 583.7; 0.8–4.1mma	Hermes et al. (2013a)
(J1700+3549)	SDSS J170055.38+354951.1	17 00 55	35 49 51	11 230^{T}	7.94	17.3 (g)	450.5/19.3; 893.4/54.7; 955.3/20.4	Mukadam et al. (2004)
							552.6/9.3; 893.4/54.3; 955.3/20.3; 1164.4/11.4	Mukadam et al. (2006)
(J1711+6541) 1711+657	SDSS J171113.01+654158.3	17 11 13	65 41 58	11 130^{T}	8.47	16.9 (g)	606.3/5.2; 690.2/3.3; 1248.2/3.2	Mukadam et al. (2004)
							234.0/1.2; 606.3/5.2; 690.2/3.3; 1248.2/3.2	Mukadam et al. (2006)
							214.3/1.7; 561.5/3.0; 612.6/5.7;	Mukadam et al. (2006)

Table 4: continued.

WD	Identifiers Other	RA (h m s)	DEC (° ′ ″)	$T_{\rm eff}$ (K)	$\log g$ (dex)	V (mag)	Period/Amplitude (s/mma)	References
							934.8/2.9; 1186.6/3.3	
1714-547	BPM 24754	17 19 02	−54 45 54	10 840^{G}	7.93	15.6	978.0–1176.0/22.6–6.1	Giovannini et al. (1998)
							643.7; 1045.1; 1234.1; 1356.6	Romero et al. (2012)
(J1724+5835) 1723+586	SDSS J172428.42+583539.0	17 24 28	58 35 39	11 640^{T}	7.88	17.6 (g)	189.2/3.2; 279.5/8.3; 337.9/5.9	Mukadam et al. (2004)
(J1732+5905) 1731+591	SDSS J173235.19+590533.4	17 32 35	59 05 33	10 770^{T}	7.97	18.7 (g)	1122.4/10.2; 1248.4/22.5	Mukadam et al. (2004)
							1090.0/8.0; 1336.0/7.8	Mukadam et al. (2006)
–	HS 1824+6000	18 24 44	60 02 00	11 520^{G}	7.73	15.7 (B)	294.3/8.8; 384.4/3.3; 304.4/7.7; 329.6/13.6	Voss et al. (2006)
							173.7; 224.7; 225.1; 286.1; 320.9; 363.5	Steinfadt et al. (2008)
1855+338	G 207-9	18 57 30	33 57 25	12 080^{G}	8.37	14.6	259.1; 292.0; 318.0; 557.4; 738.6 (iC?)	Robinson & McGraw (1976)
							129.4/1.1; 196.1/1.3; 290.9/1.1; 291.9/11.0; 292.9/1.7; 305.2/0.4; 317.8/0.5; 595.7/2.2; 599.8/1.2; 623.8/1.2; 626.8/0.9 (+C,iR)	Bognár et al. (2016)
–	(KIC 7594781)	19 08 36	43 16 42	11 730	8.11	18.6 (g)	283.8/17.8	Greiss et al. (2016)
–	(KIC 10132702)	19 13 41	47 09 31	11 940	8.12	18.8 (g)	853.5/28.1	Greiss et al. (2016)
(J1916+3938)	KIC 4552982	19 16 44	39 38 50	11 130	8.34	17.7	823.9/3.8; 834.1/3.2; 934.5/3.6; 968.9/4.4; 1089.0/2.5; 1169.9/2.3; 1436.7/2.4	Hermes et al. (2011)
							360.5/0.16; 361.6/0.16; 362.6/0.94; 788.2/0.05; 828.3/0.14; 866.1/0.16; 907.6/0.14; 950.5/0.16; 982.2/0.09; 1014.2/0.08; 1053.7/0.06; 1100.9/0.05; 1158.2/0.07; 1200.2/0.04; 1244.7/0.05; 1289.2/0.11; 1301.7/0.08; 1333.2/0.07; 1363.0/0.07; 1498.3/0.08 (iR)	Bell et al. (2015a)
–	(KIC 4357037) SDSS J191719.16+392718.8	19 17 19	39 27 19	10 950	8.11	18.2 (g)	323.4/13.0	Greiss et al. (2016)

Table 4: continued.

WD	Identifiers Other	RA (h m s)	DEC (° ′ ″)	$T_{\rm eff}$ (K)	$\log g$ (dex)	V (mag)	Period/Amplitude (s/mma)	References
–	KIC 8293193	19 17 55	44 13 26	12 650	8.01	18.4 (g)	310.9/27.9	Greiss et al. (2016)
–	KIC 11911480	19 20 25	50 17 22	12 160	7.94	18.1 (g)	172.9; 173.0; 202.5; 202.6; 259.1; 259.3; 259.4; 290.6; 290.8; 291.0; 324.1; 324.3; 324.5; 0.9–21.8mma (+C,iR)	Greiss et al. (2014)
–	(KIC 4362927)	19 23 49	39 29 33	11 140	7.84	19.4 (g)	723.6/25.3	Greiss et al. (2016)
1935+276	G 185-32	19 37 14	27 43 19	12 470^{G}	8.10	13.0	70.8; 141.4; 215.1 (iC,SH?)	McGraw et al. (1981)
							70.9/1.8; 72.5/1.2; 141.8/1.6; 215.7/2.7; 300.0/1.9; 301.3/1.9; 370.1/2.2; 560.0/1.7	Kepler et al. (2000)
							72.5/0.9; 72.9/0.4; 141.2/0.4; 141.9/1.4; 181.9/0.03; 212.8/0.5; 215.7/1.9; 264.2/0.5; 266.2/0.4; 299.8/1.0; 301.4/1.1; 370.2/1.6; 454.6/0.4; 537.6/0.6; 651.7/0.7 (+C,iR?)	Castanheira et al. (2004)
							72.6/0.7; 141.9/1.5; 215.7/1.9; 301.6/1.5; 370.2/1.3 (+C)	Thompson et al. (2004)
–	(KIC 9162396)	19 39 07	45 33 34	11 070	8.06	18.5 (g)	766.0/14.1	Greiss et al. (2016)
–	(KIC 7766212)	19 44 06	43 27 22	11 890	8.01	16.8 (g)	322.0/6.7	Greiss et al. (2016)
–	(KISJ1945+4455)	19 45 42	44 55 11	11 590	8.04	17.2 (g)	255.9/19.0	Greiss et al. (2016)
1950+250	GD 385	19 52 28	25 09 29	11 820^{G}	8.07	15.1	178.9; 228.8; 254.3; 273.0; 386.4; 535.6; 648.9 (+C)	Fontaine et al. (1980)
							126.0/3.3; 172.0/4.3; 192.0/6.5; 252.0/17.4; 546.0/11.9; 691.5/17.4 (iC?)	Vauclair & Bonazzola (1981)
							128.1/3.7; 256.1/11.4; 256.3/10.9 (iR?)	Kepler (1984)
1959+059	GD 226	20 02 13	06 07 38	10 730^{G}	8.06	16.4	1350.4/5.7	Voss et al. (2007)

Table 4: continued.

WD	Identifiers Other	RA (h m s)	DEC (° ′ ″)	$T_{\rm eff}$ (K)	$\log g$ (dex)	V (mag)	Period/Amplitude (s/mma)	References
2102+233	–	21 04 53	23 33 22	12 040	8.36	15.9 (g)	∼800.0/26.0	Sayres et al. (2012)
(J2128-0007)	SDSS J212808.49-000750.8	21 28 08	−00 07 51	11 420^{T}	8.24	18.0	274.9/11.0; 289.0/9.7; 302.2/17.1	Castanheira et al. (2006)
(J2135-0743) 2132-079	SDSS J213530.32-074330.7	21 35 30	−07 43 31	10 900^{T}	7.96	18.7	281.8/13.3; 299.9/22.9; 323.2/13.0; 510.6/16.8; 565.4/49.8	Castanheira et al. (2006)
–	SDSS J214723.73-001358.4	21 47 24	−00 13 58	11 990	7.92	19.1	199.8/3.9	Castanheira et al. (2010)
2148+539	G 232-38	21 49 59	54 08 39	11 590^{G}	8.02	16.4	741.6; 984.0; 1147.4	Gianninas et al. (2005)
2148-291	–	21 51 40	−28 56 53	11 490^{G}	8.06	15.9	260.8/12.6	Gianninas et al. (2006)
2151-077	SDSS J215354.11-073121.9	21 53 54	−07 31 22	11 910^{T}	8.27	18.7	210.2/5.6	Castanheira et al. (2006)
–	SDSS J215628.26-004617.2	21 56 28	−00 46 17	10 680^{T}	8.01	18.3 (g)	1234.0/31.4; 1478.0/27.0	Gentile Fusillo et al. (2016)
(J2159+1322)	SDSS J215905.52+132255.7	21 59 06	13 22 56	11 370^{T}	8.69	18.9 (g)	683.7/11.7; 801.0/15.1	Mullally et al. (2005)
(J2208+0654)	SDSS J220830.02+065448.7	22 08 30	06 54 49	11 100	8.49	17.9 (g)	668.1/4.1; 757.2/4.4	Castanheira et al. (2013)
(J2209-0919)	SDSS J220915.84-091942.5	22 09 16	−09 19 43	11 630^{T}	8.30	18.4 (g)	447.9/10.8; 789.3/10.4; 894.7/43.9	Castanheira et al. (2010)
(J2214-0025)	SDSS J221458.37-002511.7	22 14 58	−00 25 12	11 650^{T}	8.30	17.9 (g)	195.2/6.1; 255.2/13.1	Mullally et al. (2005)
(J2231+1346)	SDSS J223135.71+134652.8	22 31 36	13 46 53	11 060^{T}	7.89	18.7	382.4/14.6; 548.7/13.7; 619.7/18.9; 627.0/26.3; 707.5/17.1	Castanheira et al. (2006)
–	SDSS J223726.86-010110.9	22 37 27	−01 01 11	11 380^{T}	7.97	18.9 (g)	392.3/44.7; 774.4/80.1	Gentile Fusillo et al. (2016)
2254+126	GD 244	22 56 46	12 52 50	11 760^{G}	8.09	15.6	307.0; 294.6; 256.3; 203.3 (+C)	Fontaine et al. (2001)
							203.0/4.0; 256.2/6.7; 256.6/12.3; 306.6/5.0; 307.1/20.2; 906.1/1.7 (+C,iR)	Yeates et al. (2005)
2303+242	PG 2303+242	23 06 18	24 32 08	11 500^{G}	8.07	15.5	570.7/8.0; 623.4/15.0; 675.4/8.0; 794.5/56.0; 900.5/16.0 (+C,iR)	Vauclair et al. (1987)
							210.9/1.4; 227.5/1.4; 234.5/1.3; 254.2/1.2; 279.1/1.4; 299.5/1.4; 380.1/1.2; 394.3/8.4; 434.0/1.6; 453.2/2.5; 462.8/1.6; 482.6/5.8; 539.8/4.7; 577.9/11.9; 611.3/5.8;	Vauclair et al. (1992)

Table 4: continued.

WD	Identifiers Other	RA (h m s)	DEC (° ′ ″)	$T_{\rm eff}$ (K)	$\log g$ (dex)	V (mag)	Period/Amplitude (s/mma)	References
							682.6/1.2; 707.7/1.2; 758.5/1.6; 835.9/2.9; 955.3/3.5; 1043.5/2.1; 1241.2/3.1 (+C)	
							206.1/2.3; 211.3/2.1; 234.1/3.2; 261.8/2.3; 322.5/3.1; 390.7/2.8; 394.4/7.3; 452.2/2.2; 578.1/2.8; 616.4/31.3; 654.6/2.5; 656.0/2.7; 671.6/2.2; 711.5/2.0; 776.6/2.5; 852.3/6.1; 857.8/4.9; 863.8/7.4; 873.2/3.9; 965.3/19.7; 1066.1/2.2; 1705.0/1.6; 2046.7/3.1; 2234.6/3.3 (+C,iR)	Pakštienė et al. (2011)
–	SDSS J230726.66-084700.3	23 07 27	−08 47 00	10 970^T	8.21	18.9	617.0/12.5; 1212.2/25.6	Castanheira et al. (2006)
2326+049	G 29-38	23 28 48	05 14 54	11 910^G	8.17	13.0	612.9; 677.0; 824.7; 930.9; 1015.5 (+C)	McGraw & Robinson (1975)
							283.8; 615.2	Winget et al. (1990)
							186.1/25.0; 242.9/31.5; 267.9/32.6; 614.9/119.5	Patterson et al. (1991)
							284.0; 400.4; 500.0; 615.0 (+C,R)	Kleinman (1995)
							110.0; 177.0; 237.0; 284.0; 355.0; 400.0; 500.0; 552.0; 610.0; 649.0; 678.0; 730.0; 771.0; 809.0; 860.0; 894.0; 915.0; 1147.0; 1240.0 (+C,R)	Kleinman et al. (1998)
							218.7/1.5; 283.9/4.8; 363.5/4.7; 400.5/9.1; 496.2/7.9; 614.4/32.8; 655.1/6.1; 770.8/5.1; 809.4/30.1; 859.6/24.6; 894.0/14.0; 1150.5/3.6; 1185.6/3.4; 1239.9/1.9 (+C,R)	Castanheira & Kepler (2009) (mean values from different observing campaigns)
(J2334+0103)	SDSS J233458.71+010303.1	23 34 59	01 03 03	11 400	7.99	19.2 (g)	923.2/40.4	Castanheira et al. (2007)
2336-079	GD 1212	23 38 51	−07 41 20	10 970^G	8.03	13.3	1160.7/5.4	Gianninas et al. (2006)
							369.8/0.2; 371.1/0.1; 828.2/0.5; 843.0/0.5; 849.1/0.2; 857.5/0.5; 871.1/0.2; 956.9/0.2; 987.0/1.0;	Hermes et al. (2014)

Table 4: continued.

WD	Identifiers Other	RA (h m s)	DEC (° ′ ″)	$T_{\rm eff}$ (K)	$\log g$ (dex)	V (mag)	Period/Amplitude (s/mma)	References
							1008.1/0.3; 1025.3/0.5; 1048.2/0.1; 1063.1/0.6; 1086.1/0.2; 1098.4/1.0; 1125.4/0.2; 1147.1/0.5; 1166.7/0.2; 1180.4/0.9; 1190.5/2.1; 1220.8/0.2 (+C)	
2347+128	G 30-20	23 49 53	13 06 13	11 150^{G}	8.01	16.1	1068.0/13.8	Mukadam et al. (2002)
(J2350-0054)	SDSS J235040.72-005430.9	23 50 41	−00 54 31	10 290^{T}	8.14	18.1 (g)	273.3/6.2; 304.3/17.0; 391.1/7.5	Mukadam et al. (2004)
							206.7/3.2; 273.3/6.3; 304.3/17.0; 391.1/7.5	Mukadam et al. (2006)
2348-244	EC 23487-2424	23 51 22	−24 08 17	11 560^{G}	8.09	15.5 (B)	804.5/19.3; 868.2/12.8; 989.3/11.0; 993.0/37.7 (+C)	Stobie et al. (1993)
							508.1/15.0; 878.8/34.0	Thompson et al. (2005)

Notes. $^{(G)}$ The effective temperature ($T_{\rm eff}$) and surface gravity ($\log g$) values are provided by Gianninas et al. (2011), and then corrected according to the results of Tremblay et al. (2013). $^{(T)}$ The effective temperature ($T_{\rm eff}$) and surface gravity ($\log g$) values are provided by Tremblay et al. (2011), and then corrected according to the results of Tremblay et al. (2013).

Acknowledgements: The financial support of the Hungarian National Research, Development and Innovation Office (NKFIH) grant K-115709 is acknowledged. Á.S. was supported by the János Bolyai Research Scholarship of the Hungarian Academy of Sciences. This research has made use of the SIMBAD database, operated at CDS, Strasbourg, France, and NASA's Astrophysics Data System Bibliographic Services.

References:

Bell, K. J., Hermes, J. J., Bischoff-Kim, A., et al., 2015a, *ApJ*, **809**, 14 DOI
Bell, K. J., Hermes, J. J., Montgomery, M. H., et al., 2016, arXiv:1607.01392 DOI
Bell, K. J., Kepler, S. O., Montgomery, M. H., et al., 2015b, *ASP Conf. Ser.*, **493**, 217
Bergeron, P., Fontaine, G., Billères, M., Boudreault, S., & Green, E. M., 2004, *ApJ*, **600**, 404 DOI
Bergeron, P., Fontaine, G., Brassard, P., et al., 1993, *AJ*, **106**, 1987 DOI
Bergeron, P. & McGraw, J. T., 1990, *ApJ*, **352**, L45 DOI
Bognár, Zs., Paparó, M., Bradley, P. A., & Bischoff-Kim, A., 2009, *MNRAS*, **399**, 1954 DOI
Bognár, Zs., Paparó, M., Molnár, L., et al., 2016, *MNRAS*, **461**, 4059 DOI
Bognár, Zs., Paparó, M., Steininger, B., & Virághalmy, G., 2007, *Communications in Asteroseismology*, **150**, 251 DOI
Bradley, P. A., 1995, *Baltic Astronomy*, **4**, 536
Bradley, P. A., 1998, *Baltic Astronomy*, **7**, 355
Bradley, P. A., 2000, *Baltic Astronomy*, **9**, 485
Castanheira, B. G. & Kepler, S. O., 2008, *MNRAS*, **385**, 430 DOI
Castanheira, B. G. & Kepler, S. O., 2009, *MNRAS*, **396**, 1709 DOI
Castanheira, B. G., Kepler, S. O., Costa, A. F. M., et al., 2007, *A&A*, **462**, 989 DOI
Castanheira, B. G., Kepler, S. O., Kleinman, S. J., Nitta, A., & Fraga, L., 2010, *MNRAS*, **405**, 2561 DOI
Castanheira, B. G., Kepler, S. O., Kleinman, S. J., Nitta, A., & Fraga, L., 2013, *MNRAS*, **430**, 50 DOI
Castanheira, B. G., Kepler, S. O., Moskalik, P., et al., 2004, *A&A*, **413**, 623 DOI
Castanheira, B. G., Kepler, S. O., Mullally, F., et al., 2006, *A&A*, **450**, 227 DOI
Chen, Y. H. & Li, Y., 2014, *MNRAS*, **443**, 3477 DOI
Dolez, N., 1998, *Baltic Astronomy*, **7**, 153
Dolez, N., Vauclair, G., & Chevreton, M., 1983, *A&A*, **121**, L23
Dolez, N., Vauclair, G., Kleinman, S. J., et al., 2006, *A&A*, **446**, 237 DOI
Dolez, N., Vauclair, G., Xiao-Bin, Z., Chevreton, M., & Handler, G., 1999, *ASP Conf. Ser.*, **169**, 129
Fitch, W. S., 1973, *ApJ*, **181**, L95 DOI
Fontaine, G., Bergeron, P., Billères, M., & Charpinet, S., 2003, *ApJ*, **591**, 1184 DOI
Fontaine, G., Bergeron, P., Brassard, P., Billères, M., & Charpinet, S., 2001, *ApJ*, **557**, 792 DOI
Fontaine, G. & Brassard, P., 2008, *PASP*, **120**, 1043 DOI
Fontaine, G., Lacombe, P., McGraw, J. T., et al., 1980, *ApJ*, **239**, 898 DOI
Fontaine, G. & Wesemael, F., 1984, *AJ*, **89**, 1728 DOI
Fontaine, G., Wesemael, F., Bergeron, P., et al., 1985, *ApJ*, **294**, 339 DOI
Fu, J.-N., Dolez, N., Vauclair, G., et al., 2013, *MNRAS*, **429**, 1585 DOI
Fu, J.-N., Vauclair, G., Dolez, N., Jiang, S.-Y., & Chevreton, M., 2002, *ASP Conf. Ser.*, **259**, 378

Gentile Fusillo, N. P., Hermes, J. J., & Gänsicke, B. T., 2016, *MNRAS*, **455**, 2295 DOI
Giammichele, N., Fontaine, G., Bergeron, P., et al., 2015, *ApJ*, **815**, 56 DOI
Gianninas, A., Bergeron, P., & Fontaine, G., 2005, *ApJ*, **631**, 1100 DOI
Gianninas, A., Bergeron, P., & Fontaine, G., 2006, *AJ*, **132**, 831 DOI
Gianninas, A., Bergeron, P., & Ruiz, M. T., 2011, *ApJ*, **743**, 138 DOI
Giovannini, O., Kepler, S. O., Kanaan, A., Costa, A. F. M., & Koester, D., 1998, *A&A*, **329**, L13
Green, E. M., Limoges, M.-M., Gianninas, A., et al., 2015, *ASP Conf. Ser.*, **493**, 237
Greiss, S., Gänsicke, B. T., Hermes, J. J., et al., 2014, *MNRAS*, **438**, 3086 DOI
Greiss, S., Hermes, J. J., Gänsicke, B. T., et al., 2016, *MNRAS*, **457**, 2855 DOI
Handler, G., Provencal, J. L., Lendl, M., Montgomery, M. H., & Beck, P. G., 2008a, *Communications in Asteroseismology*, **156**, 18
Handler, G. & Romero-Colmenero, E., 2001, *ASP Conf. Ser.*, **226**, 313
Handler, G., Romero-Colmenero, E., & Montgomery, M. H., 2002, *MNRAS*, **335**, 399 DOI
Handler, G., Romero-Colmenero, E., Provencal, J. L., et al., 2008, *MNRAS*, **388**, 1444 DOI
Hermes, J. J., Charpinet, S., Barclay, T., et al., 2014, *ApJ*, **789**, 85 DOI
Hermes, J. J., Gänsicke, B. T., Bischoff-Kim, A., et al., 2015, *MNRAS*, **451**, 1701 DOI
Hermes, J. J., Kepler, S. O., Castanheira, B. G., et al., 2013a, *ApJ*, **771**, L2 DOI
Hermes, J. J., Montgomery, M. H., Gianninas, A., et al., 2013b, *MNRAS*, **436**, 3573 DOI
Hermes, J. J., Montgomery, M. H., Mullally, F., Winget, D. E., & Bischoff-Kim, A., 2013c, *ApJ*, **766**, 42 DOI
Hermes, J. J., Montgomery, M. H., Winget, D. E., et al., 2013d, *ApJ*, **765**, 102 DOI
Hermes, J. J., Montgomery, M. H., Winget, D. E., et al., 2012, *ApJ*, **750**, L28 DOI
Hermes, J. J., Mullally, F., Ostensen, R. H., et al., 2011, *ApJ*, **741**, L16 DOI
Hesser, J. E., Lasker, B. M., & Neupert, H. E., 1976, *ApJ*, **209**, 853 DOI
Hürkal, D. Ö., Handler, G., Steininger, B. A., & Reed, M. D., 2005, *ASP Conf. Ser.*, **334**, 577
Jordan, S., Koester, D., Vauclair, G., et al., 1998, *A&A*, **330**, 277
Kanaan, A., Kepler, S. O., Giovannini, O., & Diaz, M., 1992, *ApJ*, **390**, L89 DOI
Kanaan, A., Kepler, S. O., Giovannini, O., et al., 1998, *Baltic Astronomy*, **7**, 183
Kanaan, A., Nitta, A., Winget, D. E., et al., 2005, *A&A*, **432**, 219 DOI
Kanaan, A., Nitta-Kleinman, A., Winget, D. E., et al., 2000, *Baltic Astronomy*, **9**, 87
Kepler, S. O., 1984, *ApJ*, **278**, 754 DOI
Kepler, S. O., Castanheira, B. G., Saraiva, M. F. O., et al., 2005, *A&A*, **442**, 629 DOI
Kepler, S. O., Giovannini, O., Costa, A. F. M., et al., 1995a, *Baltic Astronomy*, **4**, 238
Kepler, S. O., Giovannini, O., Wood, M. A., et al., 1995b, *ApJ*, **447**, 874 DOI
Kepler, S. O., Nather, R. E., McGraw, J. T., & Robinson, E. L., 1982, *ApJ*, **254**, 676 DOI
Kepler, S. O., Pelisoli, I., Peçanha, V., et al., 2012, *ApJ*, **757**, 177 DOI
Kepler, S. O., Robinson, E. L., Koester, D., et al., 2000, *Baltic Astronomy*, **9**, 59
Kepler, S. O., Robinson, E. L., & Nather, R. E., 1983, *ApJ*, **271**, 744 DOI
Kepler, S. O., Winget, D. E., Nather, R. E., et al., 1995c, *Baltic Astronomy*, **4**, 221
Kilic, M., Hermes, J. J., Gianninas, A., & Brown, W. R., 2015, *MNRAS*, **446**, L26 DOI
Kleinman, S. J., 1995, *Baltic Astronomy*, **4**, 270
Kleinman, S. J., Nather, R. E., Winget, D. E., et al., 1998, *ApJ*, **495**, 424 DOI
Kotak, R., van Kerkwijk, M. H., & Clemens, J. C., 2002, *A&A*, **388**, 219 DOI

Kurtz, D. W., Shibahashi, H., Dhillon, V. S., Marsh, T. R., & Littlefair, S. P., 2008, *MNRAS*, **389**, 1771 DOI
Kurtz, D. W., Shibahashi, H., Dhillon, V. S., et al., 2013, *MNRAS*, **432**, 1632 DOI
Landolt, A. U., 1968, *ApJ*, **153**, 151 DOI
Lasker, B. M. & Hesser, J. E., 1971, *ApJ*, **163**, L89 DOI
Li, C., Fu, J.-N., Vauclair, G., et al., 2015, *MNRAS*, **449**, 3360 DOI
McGraw, J. T., 1976, *ApJ*, **210**, L35 DOI
McGraw, J. T., 1977, *ApJ*, **214**, L123 DOI
McGraw, J. T., Fontaine, G., Lacombe, P., et al., 1981, *ApJ*, **250**, 349 DOI
McGraw, J. T. & Robinson, E. L., 1975, *ApJ*, **200**, L89 DOI
McGraw, J. T. & Robinson, E. L., 1976, *ApJ*, **205**, L155 DOI
Metcalfe, T. S., Montgomery, M. H., & Kanaan, A., 2004, *ApJ*, **605**, L133 DOI
Mukadam, A. S., Bischoff-Kim, A., Fraser, O., et al., 2013, *ApJ*, **771**, 17 DOI
Mukadam, A. S., Kepler, S. O., Winget, D. E., & Bergeron, P., 2002, *ApJ*, **580**, 429 DOI
Mukadam, A. S., Kepler, S. O., Winget, D. E., et al., 2003, *Baltic Astronomy*, **12**, 71
Mukadam, A. S., Montgomery, M. H., Winget, D. E., Kepler, S. O., & Clemens, J. C., 2006, *ApJ*, **640**, 956 DOI
Mukadam, A. S., Mullally, F., Nather, R. E., et al., 2004, *ApJ*, **607**, 982 DOI
Mullally, F., Thompson, S. E., Castanheira, B. G., et al., 2005, *ApJ*, **625**, 966 DOI
Mullally, F., Winget, D. E., Degennaro, S., et al., 2008, *ApJ*, **676**, 573 DOI
O'Donoghue, D., 1986, *NATO Advanced Science Institutes (ASI) Series C*, **169**, ed. D. O. Gough, p. 467
O'Donoghue, D., Warner, B., & Cropper, M., 1992, *MNRAS*, **258**, 415 DOI
O'Donoghue, D. E. & Warner, B., 1982, *MNRAS*, **200**, 563 DOI
Page, C. G., 1972, *MNRAS*, **159**, P25 DOI
Pakštienė, E., Solheim, J.-E., Handler, G., et al., 2011, *MNRAS*, **415**, 1322 DOI
Paparó, M., Bognár, Zs., Plachy, E., Molnár, L., & Bradley, P. A., 2013, *MNRAS*, **432**, 598 DOI
Patterson, J., Zuckerman, B., Becklin, E. E., Tholen, D. J., & Hawarden, T., 1991, *ApJ*, **374**, 330 DOI
Pfeiffer, B., Vauclair, G., Dolez, N., et al., 1996, *A&A*, **314**, 182
Pfeiffer, B., Vauclair, G., Dolez, N., et al., 1995, *Baltic Astronomy*, **4**, 245
Provencal, J. L., Montgomery, M. H., Kanaan, A., et al., 2012, *ApJ*, **751**, 91 DOI
Pyrzas, S., Gänsicke, B. T., Hermes, J. J., et al., 2015, *MNRAS*, **447**, 691 DOI
Quirion, P.-O., Fontaine, G., & Brassard, P., 2007, *ApJS*, **171**, 219 DOI
Richer, H. B. & Ulrych, T. J., 1974, *ApJ*, **192**, 719 DOI
Robinson, E. L. & McGraw, J. T., 1976, *ApJ*, **207**, L37 DOI
Robinson, E. L., Stover, R. J., Nather, R. E., & McGraw, J. T., 1978, *ApJ*, **220**, 614 DOI
Romero, A. D., Córsico, A. H., Althaus, L. G., et al., 2012, *MNRAS*, **420**, 1462 DOI
Romero, A. D., Kepler, S. O., Córsico, A. H., Althaus, L. G., & Fraga, L., 2013, *ApJ*, **779**, 58 DOI
Sayres, C., Subasavage, J. P., Bergeron, P., et al., 2012, *AJ*, **143**, 103 DOI
Silvotti, R., Pavlov, M., Fontaine, G., Marsh, T., & Dhillon, V., 2006, *Mem. Soc. Astron. Italiana*, **77**, 486
Silvotti, R., Voss, B., Bruni, I., et al., 2005, *A&A*, **443**, 195 DOI
Steinfadt, J. D. R., Bildsten, L., Ofek, E. O., & Kulkarni, S. R., 2008, *PASP*, **120**, 1103 DOI
Stobie, R. S., Chen, A., O'Donoghue, D., & Kilkenny, D., 1993, *MNRAS*, **263**, L13 DOI

Stobie, R. S., Kilkenny, D., Koen, C., & O'Donoghue, D., 1997, *The Third Conference on Faint Blue Stars*, ed. A. G. D. Philip, J. Liebert, R. Saffer, & D. S. Hayes, p. 497
Stobie, R. S., O'Donoghue, D., Ashley, R., et al., 1995, *MNRAS*, **272**, L21 DOI
Stover, R. J., Nather, R. E., Robinson, E. L., Hesser, J. E., & Lasker, B. M., 1980, *ApJ*, **240**, 865 DOI
Stover, R. J., Robinson, E. L., & Nather, R. E., 1977, *PASP*, **89**, 912 DOI
Su, J., Li, Y., & Fu, J.-N., 2014a, *New A*, **33**, 52 DOI
Su, J., Li, Y., Fu, J.-N., & Li, C., 2014b, *MNRAS*, **437**, 2566 DOI
Thompson, S. E., Clemens, J. C., & Koester, D., 2005, *ASP Conf. Ser.*, **334**, 471
Thompson, S. E., Clemens, J. C., van Kerkwijk, M. H., O'Brien, M. S., & Koester, D., 2004, *ApJ*, **610**, 1001 DOI
Thompson, S. E., Provençal, J. L., Kanaan, A., et al., 2009, *Journal of Physics Conference Series*, **172**, 012067 DOI
Tremblay, P.-E., Bergeron, P., & Gianninas, A., 2011, *ApJ*, **730**, 128 DOI
Tremblay, P.-E., Ludwig, H.-G., Steffen, M., & Freytag, B., 2013, *A&A*, **559**, A104 DOI
Vauclair, G., Belmonte, J. A., Pfeiffer, B., et al., 1992, *A&A*, **264**, 547
Vauclair, G. & Bonazzola, S., 1981, *ApJ*, **246**, 947 DOI
Vauclair, G., Dolez, N., & Chevreton, M., 1981, *A&A*, **103**, L17
Vauclair, G., Dolez, N., & Chevreton, M., 1987, *A&A*, **175**, L13
Vauclair, G., Dolez, N., Fu, J. N., & Chevreton, M., 1997, *A&A*, **322**, 155
Vauclair, G., Dolez, N., Fu, J.-N., et al., 2000, *Baltic Astronomy*, **9**, 133
Vauclair, G., Goupil, M. J., Baglin, A., Auvergne, M., & Chevreton, M., 1989, *A&A*, **215**, L17
Voss, B., Koester, D., Ostensen, R., et al., 2006, *A&A*, **450**, 1061 DOI
Voss, B., Koester, D., Ostensen, R., et al., 2007, *ASP Conf. Ser.*, **372**, 583
Wenger, M., Ochsenbein, F., Egret, D., et al., 2000, *A&AS*, **143**, 9 DOI
Winget, D. E., Nather, R. E., Clemens, J. C., et al., 1990, *ApJ*, **357**, 630 DOI
Yeates, C. M., Clemens, J. C., Thompson, S. E., & Mullally, F., 2005, *ApJ*, **635**, 1239 DOI

COMMISSIONS G1 AND G4 OF THE IAU
INFORMATION BULLETIN ON VARIABLE STARS
Volume 62 Number 6185 DOI: 10.22444/IBVS.6185

Konkoly Observatory
Budapest
18 October 2016

HU ISSN 0374 – 0676

DETECTION OF NEW PULSATIONS IN THE roAp STAR HD 177765

HOLDSWORTH, DANIEL L.

Jeremiah Horrocks Institute, University of Central Lancashire, Preston PR1 2HE, UK
e-mail: dlholdsworth@uclan.ac.uk

Introduction

The rapidly oscillating Ap (roAp) stars were first identified by Kurtz (1982). They show high-overtone ($n > 15$) low-degree ($\ell \leq 2$) non-radial modes, with periods between about 5-23 min. In most cases, pulsations are thought to be driven by the κ-mechanism acting in the H I ionisation zone, with evidence that turbulent pressure may be the driving mechanism in a subset of the stars (Cunha et al. 2013). Due to the intrinsic nature of the roAp stars, they are an ideal class of pulsator to study the interaction between pulsations, rotation, chemical stratification and strong global magnetic fields. To date, there are 61 known roAp stars (see Smalley et al. 2016).

HD 177765 (J2000 α=19$^{\rm h}$07$^{\rm m}$09$^{\rm s}$.78, δ=−26°19′54″.5; V = 9.15; $T_{\rm eff}$ = 8000 K, $\log g$ = 3.8, Alentiev et al. 2012) was shown to be a roAp star by Alentiev et al. (2012) through the analysis of high-resolution spectra obtained with VLT/UVES over a period of 66 min. Previous attempts to identify pulsations in photometric data have failed (e.g. Martinez & Kurtz 1994; Holdsworth 2015) due to the inherent low-amplitude of the variability ($7 - 150\,{\rm m\,s^{-1}}$; Alentiev et al. 2012). However, with the precision afforded by the *Kepler* space telescope, we are able to confirm the spectroscopic observations, and identify two further pulsation frequencies in this star.

Observations and Data Reduction

HD 177765 was observed during Campaign 7 of the K2 mission in long cadence (LC) mode (through proposals GO7030 & GO7061). Observations cover a period of 81.32 d (2015 October - 2015 December) and consist of 3720 data points. Due to the systematics in the raw K2 data, data processed by the pipeline of Vanderburg & Johnson (2014) was used for the analysis. The top panel of Figure 1 shows the pipeline processed light curve. As can be seen, there are some instrumental artefacts remaining in the light curve at the start of the observations; these data points were disregarded from the analysis. We also removed data points which were obvious outliers from the mean light curve. The resultant light curve consists of 3614 data points.

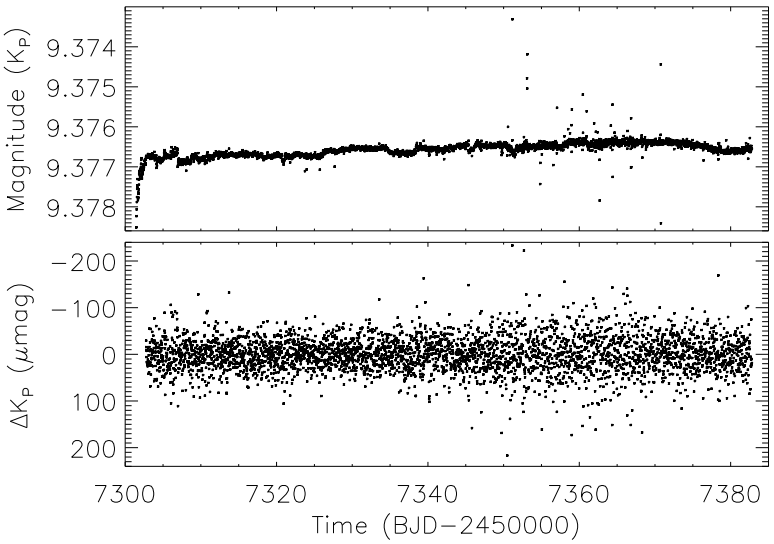

Figure 1. Top panel: K2 light curve reduced with the Vanderburg & Johnson (2014) pipeline. Bottom panel: the prewhitened light curve which was used for the pulsation analysis.

To be able to attain the best signal-to-noise ratio for the pulsation frequencies, we prewhitened the final light curve to remove all low-frequency signals, to a maximum of $10\,\mathrm{d}^{-1}$, which have an amplitude of $2.5\,\mu$mag or greater (the approximate noise level surrounding the pulsations). There is a significant frequency gap between the prewhitened region and the pulsations such that this process does not affect the astrophysical signal. The result of this process is shown in the bottom panel of Figure 1.

Analysis

Although HD 177765 was observed in LC mode, there is no ambiguity in differentiating between an alias peak and a true peak as the principal pulsation frequency is known from spectroscopic observations. We therefore assume that the two newly identified peaks are in the same frequency range, as is seen in other multifrequency roAp stars. Further to this, the peaks are well defined; alias peaks show a 'ragged' structure as a result of Nyquist-frequency crossings, thus implying ν_2 and ν_3 are the true pulsation frequencies as this is not the case. Figure 2 shows the periodogram of the light curve where the true pulsations are found. Note that the amplitudes presented are suppressed due to undersampling of the pulsations, which are above the LC Nyquist frequency.

Analysis of the pulsations was conducted following the methodology of Kurtz (1985), with the results of a non-linear least-squares fit to the three frequencies shown in Table 1. There are no rotationally split sidelobes associated with any of the identified peaks, which are expected with the oblique pulsator model (Kurtz 1982; Bigot & Kurtz 2011). However, this is not surprising for HD 177765 due to the expected long rotation period of the star. Mathys et al. (1997) measured a constant mean magnetic field modulus for the star over two years of observations, suggesting the rotation period of the star is much longer than their time base.

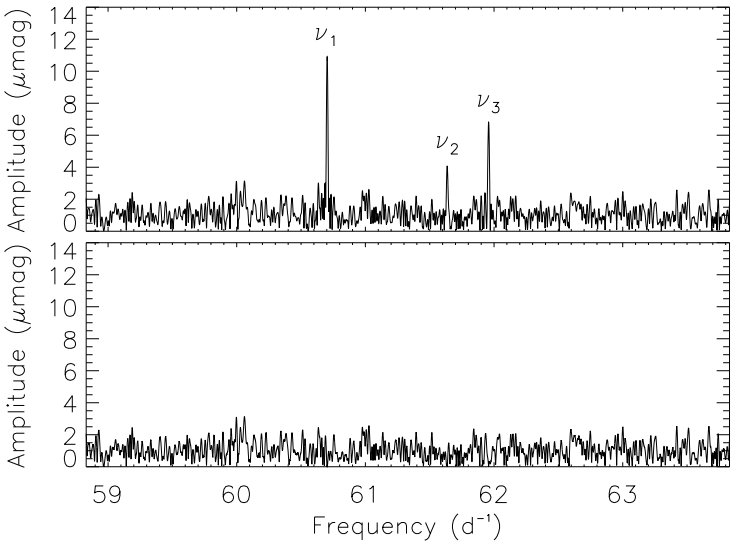

Figure 2. Top panel: periodogram of the K2 data showing the three identified frequencies, as listed in Table 1. Bottom panel: periodogram of the same data after the three identified peaks are removed showing no further significant peaks, and confirming the peaks to be the correct frequencies.

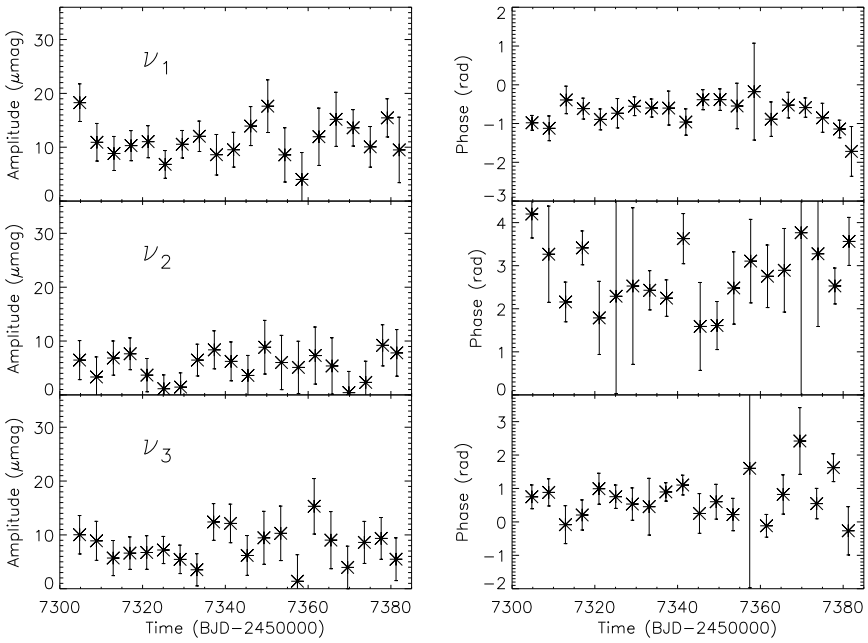

Figure 3. Left column: pulsation amplitude as a function of time for each identified mode. Right column: pulsation phase as a function of time for each identified mode. There is no trend in either parameter, indicating a long rotation period and stable pulsations.

Table 1. The results of a non-linear least-squares fit to the K2 light curve. The zero-point for the phases is BJD−245 7342.7892.

ID	Frequency (d^{-1})	Amplitude (μmag)	Phase (rad)
ν_1	60.7029 ± 0.0005	11.0 ± 0.8	-2.69 ± 0.08
ν_2	61.6362 ± 0.0013	4.2 ± 0.8	1.35 ± 0.20
ν_3	61.9580 ± 0.0009	6.8 ± 0.8	2.36 ± 0.12

To test the stability of the pulsation modes, we divided the data into sections of 250 pulsation cycles (for each mode separately) and computed the amplitude and phase of the pulsation. This number of pulsation cycles allowed us to well resolve ν_2 and ν_3. None of the pulsation modes show a variation in amplitude or phase, as shown in Figure 3. This is consistent with the long rotation period as the amplitude is not modulated with rotation, nor does the phase change at quadrature (cf. figure 15 of Holdsworth et al. (2016) for examples of amplitude and phase modulations). Finally, there is no long-term drift in the phase that would indicate frequency variability, as phase and frequency are coupled.

To perform an asteroseismic analysis on HD 177765 requires knowledge of the large frequency separation, $\Delta\nu$, which varies between $\sim 6.9\,d^{-1}$ for main-sequence A stars (for modes of (n, ℓ) and $(n+1, \ell)$), and $\sim 3.5\,d^{-1}$ for slightly evolved stars (Heller & Kawaler 1988; Shibahashi & Saio 1985). Through the analysis of their spectra, Alentiev et al. (2012) derive a luminosity of $\log L/L_\odot = 1.15$, and thus expect a large separation of $\Delta\nu \sim 4.3\,d^{-1}$ for HD 177765. However, the separations of the pulsations presented here are: $\nu_2 - \nu_1 = 0.933 \pm 0.002\,d^{-1}$, $\nu_3 - \nu_1 = 1.255 \pm 0.001\,d^{-1}$, and $\nu_3 - \nu_2 = 0.321 \pm 0.002\,d^{-1}$. The frequency difference between these values and those expected are too large for any of the frequency separations to be considered to be $\Delta\nu$.

The newly identified peaks are not indicative of rotation as the peaks are not equally split and do not agree with the results of Mathys et al. (1997) mentioned above.

There is the possibility, however, that these newly detected pulsations are of different ℓ values. Kurtz, Elkin & Mathys (2006) argued for a new type of variability in the upper atmospheres of the roAp stars. Through VLT/UVES observations, they found eight out of nine of their target stars showed radial velocity variations at frequencies not seen in photometric data. One of their hypotheses was higher ℓ pulsations high in the atmosphere which are averaged out in photometric observations of the continuum. It is plausible that *Kepler* observations have the precision to detect these higher degree modes. Further high-resolution, time-resoled spectra, over a significant time-base, are required for HD 177765 to resolve the peaks and confirm this theory.

Conclusions

For the first time, we have shown HD 177765 to be a multiperiodic roAp star. Analysis of the K2 photometric light curve has allowed us to identify the principal frequency to a much higher precision than was obtained previously. Two further pulsation frequencies have been identified above the noise in the periodogram, the first detection of these frequencies. The lack of rotational sidelobes to the pulsations, as expected by the oblique pulsator model, shows this star has a rotation period longer than 81 d, a result consistent with the literature. The frequency difference between the modes is not expected to be the large frequency separation required for an asteroseismic analysis of HD 177765.

References:

Alentiev D., et al., 2012, *MNRAS*, **421**, L82 DOI
Bigot L., Kurtz D. W., 2011, *A&A*, **536**, A73 DOI
Cunha M. S., et al., 2013, *MNRAS*, **436**, 1639 DOI
Heller C. H., Kawaler S. D., 1988, *ApJ*, **329**, L43 DOI
Holdsworth D. L., 2015, PhD thesis, Keele University
Holdsworth D. L., et al., 2016, *MNRAS*, **462**, 876 DOI
Kurtz D. W., 1982, *MNRAS*, **200**, 807 DOI
Kurtz D. W., 1985, *MNRAS*, **213**, 773 DOI
Kurtz D. W., Elkin V. G., Mathys G., 2006, *MNRAS*, **370**, 1274 DOI
Martinez P., Kurtz D. W., 1994, *MNRAS*, **271**, 129 DOI
Mathys G., et al., 1997, *A&AS*, **123**, 353 DOI
Shibahashi H., Saio H., 1985, *PASJ*, **37**, 245
Smalley B., et al., 2015, *MNRAS*, **452**, 3334 DOI
Vanderburg A., Johnson J. A., 2014, *PASP*, **126**, 948 DOI

COMMISSIONS G1 AND G4 OF THE IAU
INFORMATION BULLETIN ON VARIABLE STARS
Volume 62 Number 6186 DOI: 10.22444/IBVS.6186

Konkoly Observatory
Budapest
2 November 2016

HU ISSN 0374 – 0676

PULSATIONAL STABILITY OF THE SX Phe STAR AE UMa

PEÑA, J.H.[1,2,3]; RENTERÍA, A.[1,3]; VILLARREAL, C.[1,3]; PIÑA, D.S.[1,3]; SONI, A.A.[3]; GUILLEN, J.[3]; VARGAS, K.[3]; TREJO, O.[1]

[1] Instituto de Astronomía, Universidad Nacional Autónoma de México, México D.F.
e-mail: jhpena@astro.unam.mx

[2] Observatorio Astronómico Nacional, Tonantzintla

[3] Facultad de Ciencias, Universidad Nacional Autónoma de México

1 Motivation

Soon after we started this research program into high amplitude Delta Scuti stars (HADS) in 2011, we presented our ideas at the Obergurgl Conference held in Austria the following year. There we stated that our motivation was to find out how far we could go with the observation of faint stellar objects utilizing the Astronomical Observatory of Tonantzintla, Mexico, since the site no longer has optimum conditions for astronomical observations. This observatory has a 1–m diameter telescope and several smaller 10-inch telescopes all provided with CCD cameras. All are used mostly for the training of students and we are currently seeking scientific observational programs to increase their educational experience. This was the motivation for the present study. The star AE UMa was chosen because of the following characteristics: short period of variation (0.086 d), high-amplitude variation (0.44 mag) and relative brightness (11.35 mag). These make it an ideal test object for both the telescopes and the instrumentation.

AE Ursae Majoris was first reported to be a variable star by Geyer et al. (1955). Tsesevich and Filatov reported some results in 1956 and 1960, but the type of variability could not be determined from their visual observations. In 1973 Tsesevich determined that this star was a dwarf cepheid. Other studies were later carried out by several authors (Szeidl 1974, Broglia & Conconi 1975, Rodríguez et al. 1992, Hintz et al. 1997).

AE UMa is listed as an SX Phoenicis star (Garcia et al. 1995 and the GCVS). Hence it is considered to be a metal-poor, Population II star (unlike the most common dwarf cepheids which are Population I). Before this classification AE UMa was considered to be a double-mode dwarf Cepheid or a high-amplitude δ Scuti star (HADS), which are not Population II type stars. Rodríguez et al. (1992), using a δm_1 metal calibration for metal abundance, reported [M/H]= -0.3, and Hintz et al. (1997) give values of [M/H] between -0.1 and -0.4. He also mentions that "no kinematic information is available for AE UMa; however, its galactic coordinates, might lead one to conclude that it is possible a halo object and should therefore be grouped with the SX Phe stars".

Table 1: Log of observing seasons of AE UMa.

Date(yr/mo/day)	Telescope	Observers
11/12/0506	0.84 m	arl, jhp
11/12/1011	0.84 m	arl, jhp
12/01/2324	1.0 m	ESAOBELA12
12/01/2425	1.0 m	ESAOBELA12
12/03/0203	1.0 m	AoA12
12/03/0304	1.0 m	AoA12
13/03/0910	1.0 m	aas, err
13/04/1617	1.0 m	aas, ota
16/04/0102	1.0 m	jg

Notes: arl, A. Rentería; jhp, J. H. Peña; aas, A. A. Soni; ota, O. Trejo; err, E. Ramírez; jg, J. Guillen; ESAOBELA12: V. Abril, C. Alberti, L. Aréas, L. Batista, J. Buitrago, O. García, M, González, C. Ramírez, B. Recinos, A. Rodríguez, J. Ruiz, F. Soriano; AoA12: D. Aguilera, D. Deras, M. Espinosa, K. Valencia, P. Vessi, C. Villarreal

The most relevant studies of AE UMa are those of Szeidl (2001), Pocs & Szeidl (2001) and Zhou (2001) who found that the fundamental period of AE UMa had been essentially constant for 60 years in accordance with the theoretical expectation. They stated that the constancy of the fundamental period suggested that the star was in the post-main sequence evolutionary state. They also found that the first overtone period was decreasing at a rate of $(1/P_1)(dP_1/dt) = -7.3 \times 10^{-8}\mathrm{y}^{-1}$.

Szeidl (2001) found that small long-term variations in the amplitudes had been present for the previous 25 years. After these two studies the only significant analysis was done by Coates & Landes (2008) who, utilizing the same data set as Pocs & Szeidl (2001) and using the beat-curve approach, deduced detailed and quite precise information about the fundamental and first overtone periods of AE UMa and confirmed the values found by Pocs & Szeidl (2001) for the rates of change (assumed constant) of the periods, which are similar in magnitude to those of other Pop. I radially pulsating δ Scuti stars (Breger & Pamyatnykh 1998). In addition, because they had access to times of maxima for the star post-1998, they were able to extend the work of Pocs & Szeidl (2001) and deduce that there were possible sudden jumps in both the periods in approximately 1996, thus adding AE UMa to VZ Cnc (Arellano Ferro et al. 1994) as a radially pulsating δ Scuti star which has possible sudden jumps in period.

In addition, without any analysis, AE UMa has been extensively observed in monitoring campaigns to acquire new times of maximum light of pulsating stars. These times of maximum light of AE UMa have been compiled for behavior monitoring.

2 Observations

Although the new times of maximum light of this star have been reported elsewhere (Peña et al., 2015) here we present the detailed procedure for acquiring the data. These were all taken at both sites of the Observatorio Astronómico Nacional, at Tonantzintla (TNT) and San Pedro Mártir, México (SPM). At TNT the 1 m telescope was utilized provided with a CCD SBIG STL-1001E camera. At SPM two detectors were employed, a CCD camera and a spectrophotometer in the $uvby - \beta$ system was attached to the 0.84 m telescope. The log of observation is presented in Table 1.

Table 2: New times of maxima of AE UMa.

Time of Maximum (HJD)	Telescope	Filter	Observatory
2455901.9574	0.84 m	y	SPM
2455902.0394	0.84 m	y	SPM
2455906.9400	0.84 m	V	SPM
2455907.0230	0.84 m	V	SPM
2455950.8077	1.0 m	V	TNT
2455951.7985	1.0 m	V	TNT
2455989.8581	1.0 m	V	TNT
2455990.7191	1.0 m	V	TNT
2455990.8104	1.0 m	V	TNT
2456361.7207	1.0 m	V	TNT
2456361.8010	1.0 m	V	TNT
2457129.3859	1.0 m	G	TNT
2457480.7170	1.0 m	G	TNT
2457480.7995	1.0 m	G	TNT

Table 3: Transformation coefficients obtained for the observed season.

season	B	D	F	J	H	I	L
Dec 2011	0.054	0.967	1.058	0.041	1.030	0.161	−0.888

2.1 Data acquisition and reduction at TNT

During all the observational nights the following procedure was utilized. Sequence strings in the V filter were obtained. The integration time for the 1 m telescope was 3 min; there were around 40,000 counts for the 1 m telescope, enough to secure high precision. The reduction work was done with AstroImageJ (Collins 2012). This software is easy to use. It is free and works well on the most common computing platforms. With the CCD photometry two reference stars were utilized whenever possible in a differential photometry mode. The results were obtained from the difference $V_{\rm variable} - V_{\rm reference}$ and the scatter calculated from the difference $V_{\rm reference1} - V_{\rm reference2}$. Light curves were also obtained. The newly obtained times of maximum light are presented in Table 2.

2.2 Data acquisition and reduction at SPM

During the night of the observations at SPM the following procedure was utilized: each measurement consisted of at least five ten-second integrations of each star and one ten-second integration of the sky for the *uvby* filters and the narrow and wide filters that define Hβ. Individual uncertainties were determined by calculating the standard deviations of the fluxes in each filter for each star. The percentual error in each measurement is, of course, a function of both the spectral type and the brightness of each star, but they were observed long enough to secure sufficient photons to get a S/N ratio of accuracy of $N/\sqrt{N}$ of 0.01 mag in all cases. A series of standard stars was also observed on this night to transform the data into the standard system. The reduction procedure was done with the numerical packages NABAPHOT (Arellano-Ferro & Parrao 1988). The chosen standard system was that defined by the standard values of Olsen (1983) although for

the standard bright stars some were also taken from the Astronomical Almanac (2006). The transformation equations are those defined by Crawford & Barnes (1970) and by Crawford & Mander (1966).

The coefficients defined by the following equations and that adjusted the data to the standard system are:

$$\begin{aligned} V_{\rm std} &= A + B(b-y)_{\rm inst} + y_{\rm inst} \\ (b-y)_{\rm std} &= C + D(b-y)_{\rm inst} \\ m_{1_{\rm std}} &= E + F(m_1)_{\rm inst} + J(b-y)_{\rm inst} \\ c_{1_{\rm std}} &= G + H(c_1)_{\rm inst} + I(b-y)_{\rm inst} \\ H\beta_{\rm std} &= K + L(H\beta)_{\rm inst} \end{aligned}$$

In these equations the coefficients D, F, H and L are the slope coefficients for $(b-y)$, m_1, c_1 and β, respectively. The coefficients B, J and I are the color terms of V, m_1, and c_1. The averaged transformation coefficients of each night are listed in Table 3. Errors were evaluated using of the twenty-three standard stars observed. These uncertainties were calculated through the differences in magnitude and colors, for (V, $b-y$, m_1, c_1 and β) as (0.052, 0.0075, 0.0094, 0.025, 0.032), respectively which provide a numerical evaluation of our uncertainties. Emphasis is made on the large range of the standard stars in the magnitude and color values: V (5.45, 8.40); $(b-y)$ (-0.19, 0.63); m_1 (0.10, 0.66); c_1 (0.19, 0.91) and β (2.609, 2.828).

Table 4 lists the photometric values of the observed star. In this table, column 1 reports the time of the observation in HJD, columns 2 to 5 the Strömgren values V, $(b-y)$, m_1 and c_1, respectively; column 6, Hβ.

3 Frequency Content

The frequency content of the pulsation of AE UMa was determined utilizing two different data sets: i) the light curves of Rodríguez et al. (1992) and those presented in the current paper and ii) the compiled list of times of maximum light, including the newly acquired ones.

3.1 Time Series Analysis

We were lucky that this star was observed in the $uvby-\beta$ photometric system in 1986 and 1987 by Rodríguez et al. (1992) at the Sierra Nevada Observatory, Spain, with a twin spectrophotometer like the one we used in 2011 at SPM Observatory, México, some twenty-five years later. Rodríguez et al. (1992) published their observations in magnitude differences AE UMa $-$ BD $+ 44^\circ$ 1898 so, transformation into the standard system was immediate. Furthermore, observations were reported in V and B filters by Broglia & Conconi (1975). In section 2.2 we described in detail the transformation followed to obtain the reported observations of the present study. The whole V sample is constituted of 1299 data points in the V filter in four seasons covering a time span of 38 years.

Utilizing the period proposed by Pocs & Szeidl (2001) we calculated the phase for each $uvby-\beta$ data point and plotted magnitude V and color indexes in a diagram, Figure 1. We should here mention the impressive result of how well all the magnitude and color

Table 4: $uvby-\beta$ photoelectric photometry of AE UMa.

HJD	V	$(b-y)$	m_1	c_1	β
-2455900					
6.8611	11.035	0.130	0.148		2.708
6.8636	11.048	0.155	0.137	0.888	2.778
6.8684	11.100	0.143	0.132	0.846	2.770
6.8709	11.122	0.159	0.113		2.793
6.8728	11.110	0.185	0.130	0.923	
6.8738	11.142	0.174	0.153	0.870	
6.8753	11.192	0.149	0.166	0.941	
6.8764	11.222	0.161	0.142	0.906	
6.8776	11.182	0.202	0.095	0.981	
6.8784	11.235	0.162	0.130		
6.8794	11.203	0.226	0.071	0.972	
6.8804	11.233	0.201	0.113	0.929	
6.8847	11.271	0.195	0.153	0.834	
6.8857	11.297	0.199	0.118	0.795	
6.8871	11.297	0.216	0.142	0.767	
6.8878	11.303	0.212	0.104	0.897	
6.8889	11.330		0.198	0.681	
6.8902	11.339		0.209	0.847	
6.8913	11.351	0.162	0.221	0.764	
6.8920	11.323	0.200	0.145	0.811	
6.8930	11.388	0.218	0.697		
6.8940	11.383		0.196	0.718	
6.8969	11.354	0.233	0.073		
6.8977	11.387	0.197	0.183	0.804	
6.8991	11.365	0.212	0.125	0.831	
6.9003	11.390	0.188	0.203	0.732	
6.9015	11.391	0.194	0.197	0.715	
6.9022	11.382	0.225	0.077	0.857	
6.9033	11.415	0.197	0.193	0.704	
6.9047		0.211	0.156	0.740	
6.9057	11.400	0.229	0.152	0.731	
6.9063	11.417	0.209	0.185		
6.9076	11.433	0.209	0.131	0.841	
6.9087	11.406		0.062	0.815	
6.9109	11.430	0.221	0.120	0.859	
6.9115	11.435	0.191	0.191	0.847	
6.9125	11.413	0.224	0.125		
6.9134	11.418	0.233	0.108	0.796	
6.9155	11.440	0.230	0.080	0.825	
6.9170	11.436	0.210	0.117	0.767	
6.9178	11.415	0.242	0.099	0.751	
6.9191	11.446	0.218	0.091	0.768	
6.9206	11.414	0.254	0.045	0.832	
6.9246	11.369	0.219	0.148	0.700	
6.9254	11.361	0.201	0.189	0.795	

Table 4: Continued.

HJD	V	$(b-y)$	m_1	c_1	β
-2455900					
6.9271	11.339	0.210	0.089	0.848	
6.9283	11.277	0.247	0.065	0.869	
6.9294	11.270	0.221	0.090	0.864	
6.9301	11.222	0.203	0.131	0.777	
6.9320	11.167	0.163	0.133	0.822	
6.9332	11.164	0.102	0.221	0.735	
6.9344	11.065	0.115	0.194	0.824	
6.9350	10.989	0.151	0.115	0.914	
6.9364	10.909	0.127	0.140	1.054	
6.9378	10.845	0.138	0.105	1.114	
6.9402	10.849	0.093	0.130	1.058	
6.9409	10.830	0.084	0.192	0.911	
6.9420	10.852	0.070	0.209	1.015	
6.9427	10.847	0.086	0.177	1.086	
6.9438	10.881	0.076	0.179	0.979	
6.9454	10.899	0.092	0.167	1.042	
6.9465	10.919	0.092	0.173	0.995	
6.9472	10.912	0.125	0.141	1.005	
6.9484	10.952	0.100	0.177	1.049	
6.9498	10.987	0.091	0.196	1.037	
6.9523	11.038	0.138	0.153	0.969	
6.9531	11.061	0.111	0.168	0.953	
6.9544	11.057	0.160	0.116	0.943	
6.9555	11.083	0.146	0.153	0.997	
6.9568	11.109	0.146	0.160	1.049	
6.9575	11.112	0.161	0.126	1.014	
6.9587	11.122	0.185	0.110	0.967	
6.9603	11.172	0.183	0.064	1.100	
6.9620	11.165	0.215	0.048	1.043	
6.9627	11.165	0.183	0.150	0.975	
6.9643	11.227	0.173	0.143	0.863	
6.9656	11.212	0.204	0.121	0.806	
6.9681	11.263	0.198	0.150	0.767	
6.9688	11.284	0.182	0.179	0.736	
6.9699	11.325		0.258	0.742	
6.9706	11.279	0.205	0.108	0.842	
6.9719	11.295	0.213	0.120	0.814	
6.9732	11.322	0.206	0.156	0.656	
6.9744	11.307	0.220	0.132	0.711	
6.9751	11.314	0.222	0.142	0.754	
6.9763	11.393		0.227	0.776	
6.9775	11.399		0.200	0.736	
6.9800	11.415		0.214	0.650	
6.9808	11.380	0.219	0.117		
6.9836	11.377	0.218	0.126	0.787	

Table 4: Continued.

HJD	V	$(b-y)$	m_1	c_1	β
-2455900					
6.9849	11.396	0.216	0.141	0.714	
6.9858	11.402	0.212	0.165	0.670	
6.9870	11.426	0.213	0.180	0.608	
6.9883	11.397		0.119	0.767	
6.9895	11.380		0.077	0.748	
6.9905	11.452	0.205	0.116		
6.9919	11.478	0.197	0.130	0.606	
6.9931	11.488	0.174	0.194	0.640	
6.9963	11.414		0.080	0.726	
6.9970	11.479	0.194	0.165	0.763	
6.9984	11.457	0.199	0.193	0.682	
6.9991	11.428		0.058	0.725	
7.0002	11.430		0.096	0.812	
7.0012	11.432		0.067	0.739	
7.0121	11.294	0.142	0.185	0.818	
7.0198	10.980	0.082	0.162	0.940	
7.0214	10.944	0.065	0.211	0.946	
7.0232	10.925	0.075	0.178	1.018	
7.0256	10.939	0.082	0.181	0.992	
7.0270	10.953	0.093	0.172	1.038	

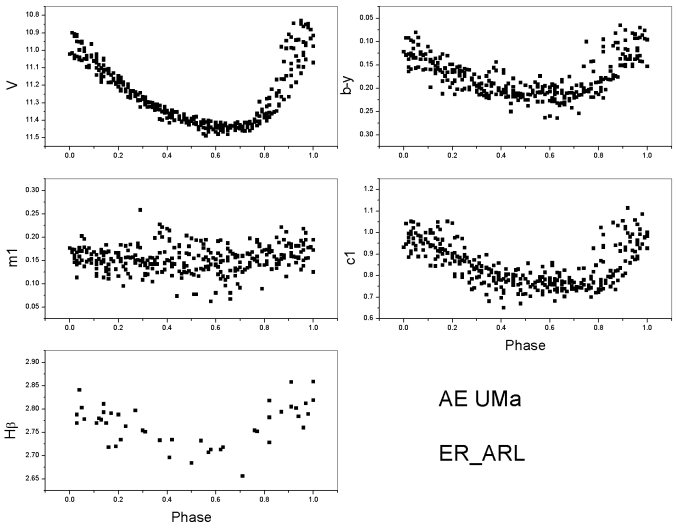

Figure 1. Phase plot of the $uvby-\beta$ photometry of Rodríguez et al. (1992) and that of the present paper. The time span between both sets is 25 years. The period considered is 0.086017053 d.

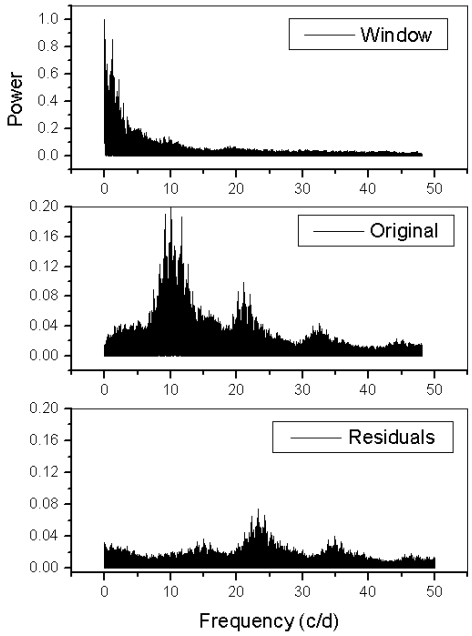

Figure 2. Periodogram of V magnitude of $uvby-\beta$ photometry of Rodríguez et al. (1992) and data from the present paper in Period04. Top, Window function; middle, original data; bottom, residuals.

indexes conform the phase with the period used here. A few points were completely out of the general pattern; we discarded them and were left with a sample of 356 $uvby-\beta$ data points.

The first method utilized to determine the frequency content of AE UMa was Period04 (Lenz & Breger 2005), a well-known method widely utilized by the δ Scuti star community. For the 1299 V points of the sample we selected a frequency range between 0 and 50 c/d. We ran the method twice and obtained the results listed in Table 5 and represented graphically in Figure 2, with these other characteristics: Zero point: 11.2871229; Residuals: 0.0584757486. The comparison of the observations with the predictions were astonishing given the long time basis of 38 years.

The same data set was tested in Period04 with the period proposed by Pocs & Szeidl (2001). The obtained results are frequency 11.6253822 c/d; amplitude, 0.22205636 mag; phase, 0.819373 mag with a zero point 11.287086 and a residual of 0.079247, which demonstrate the goodness of the Period04 proposed period.

An absolute verification of the constancy of the period for at least the last 25 years was done through the $uvby-\beta$ photometry carried out by Rodríguez et al. (1992, starting in 1986 and continuing in 1987 over twenty nights) and that observed by us in 2011, 25 years later. A phase was calculated for both seasons with a total of 356 points; the resulting diagram is shown in Figure 1. As can be seen this discards the supposition of a double mode variable although there is some evidence of a variable amplitude. This also rules out a secular variation of the period.

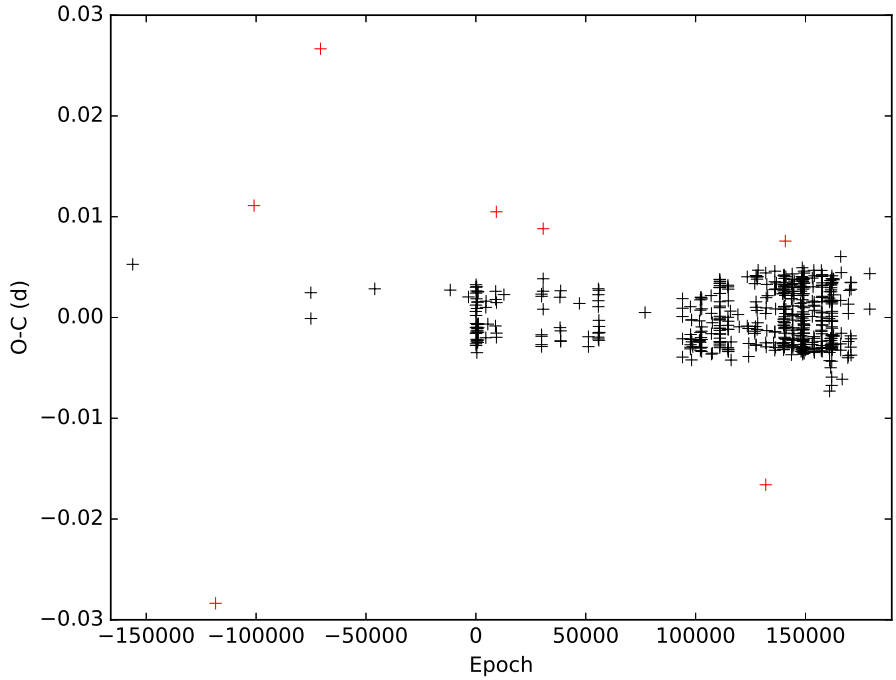

Figure 3. O–C distributions vs time. A large scatter is caused by reduction or observation procedure and not inherent to behaviour of the star.

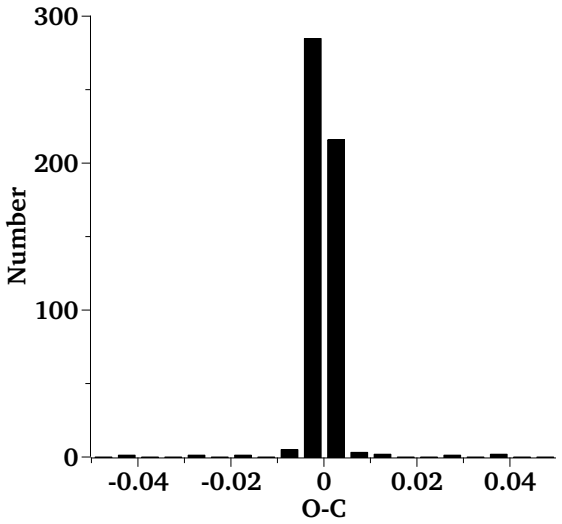

Figure 4. O–C distributions in an histogram. The values at the wings were discarded.

Table 5: Output of the PERIOD04 package with time series of the V data of AE UMa

Nr	Frequency (c/d)	Amplitude (mag)	Phase
F1	$11.6253822 \pm 5.9 \times 10^{-7}$	0.214 ± 0.004	0.775 ± 0.003
F2	$23.2514162 \pm 2.0 \times 10^{-7}$	0.077 ± 0.004	0.275 ± 0.009

Table 6: AE UMa ephemeris equations.

Author	T_0	P	β
Pocs and Szeidl (2001)	2442062.5824	0.086017076	
Zhou (2001)	2442062.5827	0.08601585	5.71034×10^{-12}
PERIOD04		0.086018677	
MSDR	2442062.5824	0.086017072	
PDDM	2456746.6464	0.086017069	

3.2 O–C Methods

Before calculating the coefficients of the ephemeris equation, we studied the existing literature related to AE UMa. Several authors have conducted studies of the O–C behaviour of this particular object and, in this preliminary stage, we took the existing equation and reproduced the diagrams with our updated list of times of maxima taken from the literature plus the data that we acquired.

The principal works on AE UMa are those of Pocs & Szeidl (2001) and Zhou (2001). They are presented in Table 6. In the first one the authors find this star varying with a constant period for more than half a century. On the other hand, Zhou (2001) finds a varying period (his equation 14).

Pocs & Szeidl (2001) took all the O–C values, into account with the exception of Filatov's data (124 maxima, time interval of 61 years) and they arrived at the following quadratic polynomial fit

$$\begin{aligned} O-C &= (2.2 \pm 2.6) \times 10^{-4} - (1.71 \pm 0.53) \times 10^{-8} E \\ &+ (0.053 \pm 0.053) \times 10^{-12} E^2 \end{aligned}$$

Since then, the only studies of the analysis of the pulsation of AE UMa were done by Coates & Landes (2008), and Niu et al. (2013) which merely confirmed the constancy of the period of pulsation of AE UMa. There have been numerous reports on the times of maxima of this star. Those previously observed by us (Peña et al., 2015) are presented in Table 2 along with the newly observed maxima.

With an increased time basis (more than 28114 days (77 years) or 326845 cycles and 512 times of maxima compiled) we tested the reported calculations. What was immediately obvious was the exceedingly large spread in the O–C values (Figure 3). Those in the earlier stages had already been discarded by Pocs & Szeidl (2001) and Zhou (2001). However, a large scatter in the $O-C$ values was found with more recent data which did not exist on the earlier studies. To diminish the scatter the following was done: a histogram of the O–C values was calculated and the standard deviation was evaluated (Figure 4). From the graphical representation of the O–C differences vs. time those values with large spread from the mean became conspicuous. These were discarded. Some, the old ones, were those that the previous authors had also eliminated. If they are not considered, this eliminates the large spread and makes it possible to determine a more logical behaviour of the star.

3.3 Minimization of the standard deviation of the O–C residuals (MSDR)

The second method for period determination utilizes as criteria of goodness, the minimization of the standard deviation of the $O - C$ residuals (see Peña et al. 2016 for a detailed description).

This method is based on O–C standard deviation minimization. We considered a set 508 data points of $T_{\max}$. These are presented in Figure 5. This data set covers a time span of 77 years.

A mean period was determined in the differences of two or three times of maxima that were observed on the same night with an associated standard deviation. We swept the period between this limits. The output was a straight line with some values of the deviation of the O–C residuals clearly diminishing. We swept again for a closer period range around this feature calculating 5000 steps which gives the sufficient accuracy provided by the time span of the observations. The obtained precision of one millionth provides the new period and the limits for the iteration. In each iteration, the O–C standard deviation was calculated. We chose to be the best period that which showed the minimum standard deviation (Figure 5). The resulting equation is:

$$T_{max} = (2442062.5824 \pm 3 \times 10^{-3}) + (0.086017072 \pm 2 \times 10^{-9}) \times E$$

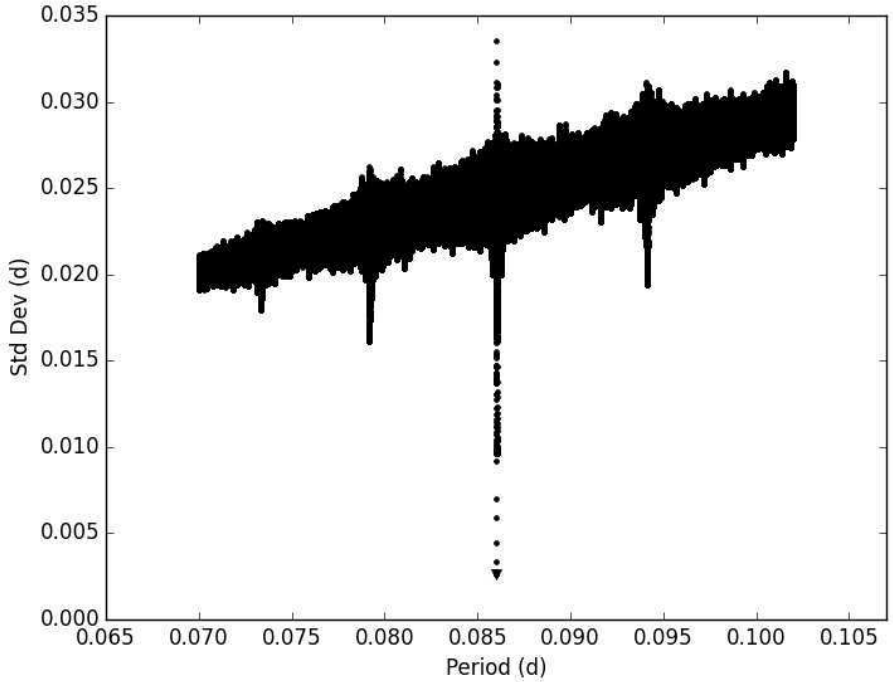

Figure 5. Standard deviation vs. Period. The minimum, clearly discerned, served to determine the best period.

3.4 Period determination through an O–C differences minimization (PDDM)

As in the case of BO Lyn (Peña et al. 2016), we employed a method based on the idea of searching the minimization of the chord length which links all the points in the O–C diagram for different values of changing periods, looking for the best period which corresponds to the minimum chord length.

A set of 508 times of maxima was considered to perform this analysis. These times are those remaining after the analysis of the histogram in Section 3.2. Two hundred and sixty-six consecutive pairs of times of maxima were used to calculate the average period and the standard deviation, being the resulting period and deviation 0.0857 d and 0.0039 d, respectively. Taking this into consideration, we can fix an interval span in which the period is located in 0.0856 ± 0.0039 days. Maintaining a period precision of a billionth and taking the interval span period into consideration, 7.9×10^6 periods were used to perform this method. The T_0 used to calculate the O–C diagrams is 2456746.6464, the final of Hübscher & Lehmann (2015). Then the best period is the one with the smallest chord length and it is shown in Figure 6. The resulting linear ephemerides equation is

$$T_{\max} = 2456746.6464 + 0.086017069 \times E$$

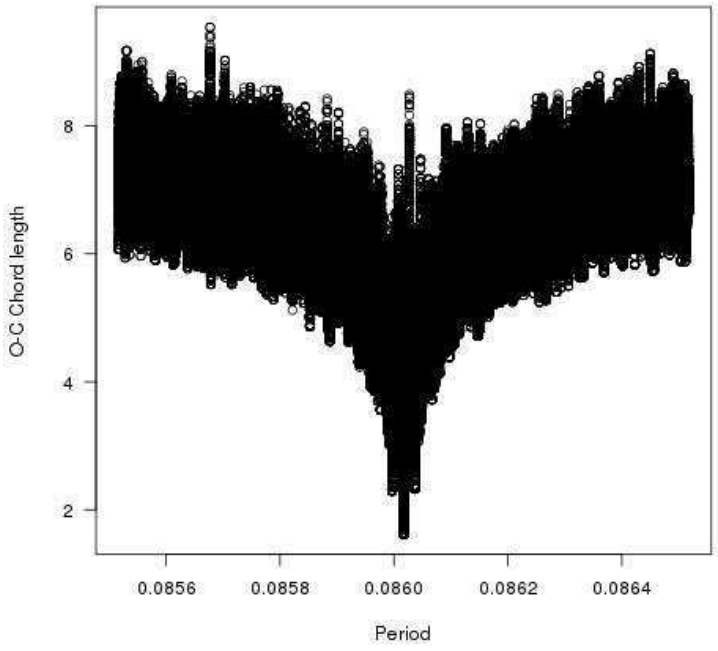

Figure 6. Period determination through an O–C differences minimization, PDDM.

4 Physical Parameters

Determining physical parameters for the stars is not a simple task. The advantage of intermediate band photometry is that, if it is well calibrated and used together with the

Table 7: Reddening and unreddened parameters of AE UMa

Phase	$E(b-y)$	$(b-y)_0$	m_0	c_0	Hβ	V_0	M_V	DM	Dist	[Fe/H]
0.05	0.000	0.131	0.160	0.966	2.796	11.00	1.03	9.98	989	
0.15	0.000	0.158	0.144	0.941	2.765	11.12	0.79	10.33	1165	
0.25	0.015	0.161	0.161	0.864	2.771	11.16	1.54	9.62	838	
0.35	0.009	0.187	0.153	0.805	2.746	11.28	1.72	9.56	815	
0.45	0.000	0.211	0.151	0.768	2.715	11.38	1.38	10.00	1001	−0.246
0.55	0.000	0.216	0.146	0.768	2.709	11.43	1.20	10.22	1108	−0.287
0.65	0.007	0.209	0.139	0.764	2.716	11.41	1.44	9.97	988	−0.430
0.75	0.000	0.207	0.154	0.769	2.721	11.41	1.53	9.88	946	
0.85	0.017	0.140	0.168	0.833	2.801	11.18	2.27	8.91	606	
0.95	0.000	0.132	0.168	0.949	2.797	11.00	1.19	9.81	915	

theoretical models, it can be utilized to infer the physical conditions of the stars.

The whole $uvby-\beta$ sample consisted of some 360 data points. In both data sets the weak point was the subset of Hβ photometry. Rodríguez et al. (1992) observed only 58 data points and in 2011 our Hβ sample consisted of only four data points.

With the advantages of the empirical calibrations of Balona and Shobbrook (1984) and Nissen (1988), based on the earlier papers of Crawford for stars of different spectral type stars for $uvby-\beta$ photometry, we determined reddening and unreddened indexes. These, combined with theoretical models such as those of Lester, Gray & Kurucz (1986, hereinafter LGK86), determined physical parameters such as surface gravity and effective temperature. These calibrations have already been described and used in previous analyses (Peña & Peniche 1994; Peña & Sareyan 2006).

As was described at the end of section O–C Analysis, a remarkable phasing was accomplished with the two $uvby-\beta$ photometric seasons observed twenty-five years apart. In order to calculate the reddening and unreddened colors and in view of the poorness of the Hβ data of both seasons, we calculated mean averages in phase bins of steps of 0.1. To follow the behavior of Hβ we overlapped the V curve and discarded seven points which were out of the general trend of the variation.

The application of Nissen's prescription gave, for the values averaged in phase bins, the corresponding unreddened values that were presented in Table 7. This Table lists, in the first column, the phase. Subsequent columns present the reddening, the unreddened indexes, the unreddened magnitude, the absolute magnitude, the distance modulus, and distance and, in the last column, the metallicity [Fe/H] for the stages when the star was of spectral type F.

Mean values were calculated for $E(b-y)$, Distance Modulus and distance for two cases: i) the whole data sample and ii) in phase limits between 0.3 and 0.8, which is customary for pulsating stars to avoid the maximum. It gave, for the whole cycle, values of 0.005 ± 0.007; 9.83 ± 0.40 and 937 ± 158 for $E(b-y)$, DM and distance (in pc), respectively, whereas for the mentioned phase limits we obtained, 0.03 ± 0.04; 9.92 ± 0.24 and 972 ± 106 respectively. The uncertainty is merely the standard deviation. In the case of the reddening, most of the values in the spectral type in the F stage of AE UMa produced negative $E(b-y)$ values which is unphysical. In those cases we forced the reddening to be zero in which case the $(b-y)$ index is the same.

Once the unreddened colors are known, it is possible to determine some physical pa-

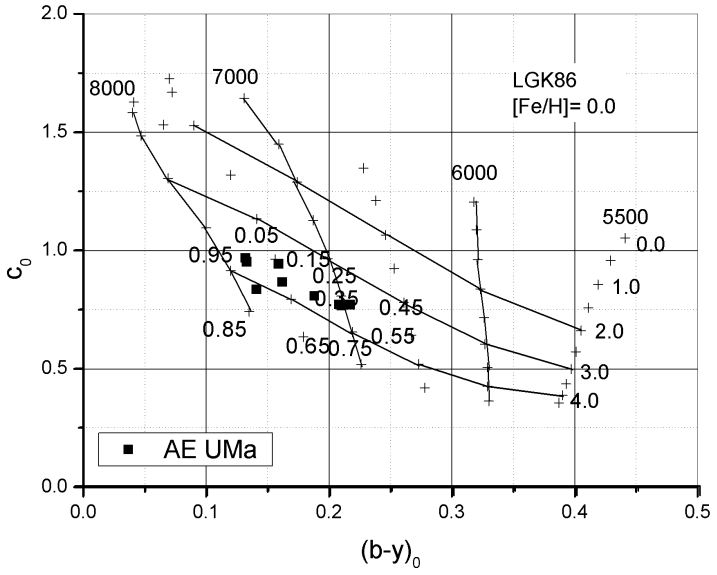

Figure 7. Cycle variation of AE UMa in the theoretical grids of LGK86.

rameters (log T_e and log g) from a direct comparison with the models developed. A metallicity has to be assumed. We mentioned in the Introduction that with respect to the metallic content, Rodríguez et al. (1992), using a δm_1 metal calibration for metal abundance, reported [M/H] $= -0.3$, and Hintz et al. (1997) give values of [M/H] between -0.1 and -0.4. McNamara (1997) reports [M/H] $= -0.5$ for AE UMa. We, utilizing the same data as Rodríguez et al. (1992) and with the same technique, obviously arrived at the same results. In the phase bins the star shows the F nature in three different phases, 0.45, 0.55 and 0.65 and a mean value [Fe/H] of -0.321 is obtained. All of these determined values fit the [Fe/H] vs. $\log P$ relationship of McNamara (1997) (his Figure 1) adequately, corroborating the assumed metallicity of AE UMa.

LGK86 calculated their model outputs for several metallicities. Particularly in the case of AE UMa, for which we determined mean metallicity of [Fe/H] $= -0.32 \pm 0.10$, there are two models which were applicable, either [Fe/H] 0.0 or -0.5. We tested both since our determined mean metallicity of [Fe/H] -0.32 ± 0.10 lies in between.

The temperature of the star was determined from its positions in the LGK86 grids (Figure 8) and is listed in Table 8 for both metallicities. The reddening $E(B-V)$ was calculated utilizing the well-known relation $E(b-y) = 0.7 \times E(B-V)$. Table 9 presents a summary of the compiled characteristics.

5 Conclusions

New times of maximum light have been gathered for the HADS AE UMa, from CCD photometry at the Tonantzintla and $uvby-\beta$ photometry at the San Pedro Mártir Observatories, Mexico. With the inclusion of these maxima and those gathered from

Table 8: Effective temperature of AE UMa.

phase		T_e	T_e		OP&J	$\log g$
	[Fe/H]	0.0	−0.5	mean		−0.5
0.05		7800	7100	7450	7822	3.4
0.15		7500	7200	7350	7553	3.5
0.25		7500	7200	7350	7605	3.8
0.35		7200	7000	7100	7388	3.8
0.45		6800	7500	7150	7119	3.5
0.55		6800	7500	7150	7067	3.5
0.65		7100	7700	7600	7128	3.8
0.75		7000	7500	7250	7171	3.5
0.85		7700	7400	7550	7866	4.1
0.95		7700	7400	7550	7831	3.8

Table 9: Compiled characteristics for AE UMa.

Spectral Type	A9
Galactic longitude	176.1978
Galactic latitude	+47.7071
Distance [pc]	972
Reddening [mag] $E(b-y)$	0.005 ± 0.007
Reddening [mag] $E(B-V)$	0.034
Parallaxes [mas]	5.74
Distance modulus [mag]	7.92
Log T_e	3.85
Log g	3.8

the literature, the ephemerides proposed by Pocs & Szeidl (2001) was slightly modified because a larger time span was available. This result is confirmed from the time series $uvby-\beta$ data separated 25 years apart. Two other methods were employed to determine the frequency content of the star. A sinusoidal behaviour of the residuals can be discerned. Thus, the binary nature of AE UMa, indicated by other authors has been tightened up with the new times of maxima determined. Hence, the solution for AE UMa is valid since it is supported by a longer time string. The residuals indicate that this star might have the same sinusoidal behavior as AN Lyn (Peña et al. (2015) or BO Lyn (Peña et al. 2016) which would indicate a binary nature. Some physical parameters were determined for AE UMa from $uvby-\beta$ photometry from the literature (Rodríguez et al. 1992) and that presented in this study. The obvious recommendation is to gather more observations that, in the long run could prove or discard this binary assumption.

Acknowledgements:

We thank the staff of the OAN at TNT and SPM for their assistance in securing the observations. This work was partially supported by PAPIIT IN106615 and PAPIME PE113016. AR thanks the IA for allowing the telescope time at SPM. Typing and proofreading were done by J. Orta, and J. Miller, respectively. C. Guzmán, F. Ruíz and A. Díaz assisted us in the computing. This research has made use of the Simbad databases operated at CDS, Strasbourg, France and NASA ADS Astronomy Query Form.

References:

Arellano Ferro, A. Nuñez, N. S., Avila, J. J., Trejoluna, J. J., 1994, *RMxAA*, **29**, 218
Arellano Ferro, A., Parrao, L., 1988, IA-UNAM Reporte Técnico, 57
Nautical Almanac Office, 2006, *Astronomical Almanac*
Balona, L. A., Shobbrook, R. R., 1984, *MNRAS*, **211**, 375 DOI
Breger, M., Pamyatnykh A.A., 1998, *A&A*, **332**, 958
Broglia, P., Conconi, P. 1975, *A&AS*, **22**, 243
Coates, D.W., Landes, H., 2008, *Comm. in Asteroseismology*, **153**, 8 DOI
Collins, K., 2012, *Astrophysics Source Code Library*, ascl:1309.001
Crawford, D. L., Barnes, J. V., 1970, *AJ*, **75**, 978 DOI
Crawford, D. L., Mander, J., 1966, *AJ*, **71**, 114 DOI
Filatov, G. S., 1960, *Astron. Tsirk.*, **215**, 20
Garcia, J. R., Cebral, J. R., Scoccimarro, E. R., et al. 1995, *A&AS*, **109**, 201
Geyer, E., Kippenhahn, R., Strohmeier, W., 1955, *Kleine Veröff. Bamberg*, **11**
Hintz, E. G., Hintz, M. L., Jones, M. D., 1997, *PASP*, **109**, 1073 DOI
Hübscher, J., Lehmann, P., 2015, *IBVS*, **6149**
Lenz, P., Breger, M., 2005, *Comm. in Asteroseismology*, **146**, 53 DOI
Lester, J. B., Gray, R. O., & Kurucz, R. L., 1986, *ApJS*, **61**, 509 DOI
Nissen, P., 1988, *A&A*, **199**, 146
Niu, J. S., Fu, J. N., Yang, X. H., & Zong, W. K., 2013, arXiv:1304.3772v2
Olsen, E. H., 1983, *A&AS*, **54**, 55
Peña, J. H., Peniche, R., 1994, *RMxAA*, **28**, 139
Peña, J. H., Sareyan, J. P., 2006, *RMxAA*, **42**, 179
Peña, J. H., Rentería, A. Villarreal, C. et al., 2015, *IBVS*, **6154**
Peña, J. H., et al., 2016, *RMxAA*, **52**, 385
Pocs, M. D., Szeidl, B., 2001, *A&A*, **368**, 880 DOI
Rodriguez, E., Rolland, A., Lopez de Coca, P., Garcia-Lobo, E., Sedano, J. L., 1992, *A&AS*, **93**, 189
Szeidl, B., 1974, *IBVS*, **903**
Szeidl, B., 2001, *Comm. in Asteroseismology*, **140**, 56
Tsesevich, V. P., 1956, *Astron. Tsirk.*, **170**
Tsesevich, V. P., 1973, *Astron. Tsirk.*, **775**, 2
Zhou, A.-Y., 2001, *A&A*, **374**, 235 DOI

COMMISSIONS G1 AND G4 OF THE IAU
INFORMATION BULLETIN ON VARIABLE STARS
Volume 62 Number 6187 DOI: 10.22444/IBVS.6187

Konkoly Observatory
Budapest
8 November 2016

HU ISSN 0374 – 0676

NEW FLARE STARS AND FLARES OF THE KNOWN ONES IN ORION

NATSVLISHVILI, REZO[1]; KOCHIASHVILI, IA[1,2]; KOCHIASHVILI, NINO[1]

[1] Eugene Kharadze Abastumani Astrophysical Observatory, Ilia State University, Kakutsa Cholokashvili Ave 3/5, Tbilisi 0162, Georgia

[2] Dark Cosmology Centre, Niels Bohr Institute, University of Copenhagen, Juliane Maries Vej 30, DK-2100 Copenhagen Ø, Denmark

Observations of red dwarf flare stars were initiated in the Abastumani Astrophysical Observatory in 1969 (Kiladze, 1972). Regions rich in red dwarf stars were selected: the area around Orion Trapezium, and the stellar cluster of Pleiades have been chosen to ensure efficiency of observations. The objective of the investigation was to establish the character of time distribution of flares and to study the flare mechanism in red dwarf stars.

Observations were obtained with photographic method using photo-plates of Kodak and ORWO, on the wide-field (circular field with diameter of $4°50'$) Maksutov system 70/100/210 cm Meniscus-type telescope of the Abastumani observatory by means of multiple exposure method.

Observational data containing information about flare stars and their flares obtained after processing photographic observations in 1969-1986 around Orion Trapezium has been published in the cumulative catalogue of flare stars in the Orion region (Natsvlishvili, 1991), where complete information about known (for that period) 490 flare stars and their 654 flares included. Out of these, 125 new flare stars and 182 flares of known flare stars were fixed in the Abastumani Astrophysical Observatory. Star AB461=TZ Ori turned out to be a short-period Cepheid (Natsvlishvili, 1994). After the publication of this catalogue new photographic material was obtained using the same methodology. On the basis of the new observations, data about newly revealed flare stars and the flares from known flare stars are presented in this article. This material, that was obtained in quite separate time interval, could be used for investigation of possible cyclic nature of the flare activity of red dwarf stars.

Estimations of photometric parameters of flare stars in normal conditions and the ones of flares were made using the sequence of the photometric standard stars (Andrews, 1970) existing in the Orion Trapezium area.

As a result of reexamining the 1989-1998 astrophotographic plates for the Orion Nebula Region, 12 new flare stars and 7 flares for known flare stars around Orion Trapezium have been revealed. For the new flare stars, the Abastumani numbering (AB) has been extended (Natsvlishvili, 1984). Flare parameters for the new flare stars are given in Table 1. In Table 2 parameters of the repeated flares are presented; numbering for these objects in the table are given according to "A Catalog of Flare Stars in Orion Nebula

Region" (Natsvlishvili, 1991). The identification charts of the newly detected flare stars are presented in Figure 1. The flare stars numbered AB146, AB148, AB149 and AB152 in Table 1 are known Orion variables: V1426 Ori, V1485 Ori, NW Ori and OU Ori, respectively. Flare star AB151 represents the microwave radio source JCMTSEJ053540.0-060838 (Di Francesco et al., 2008).

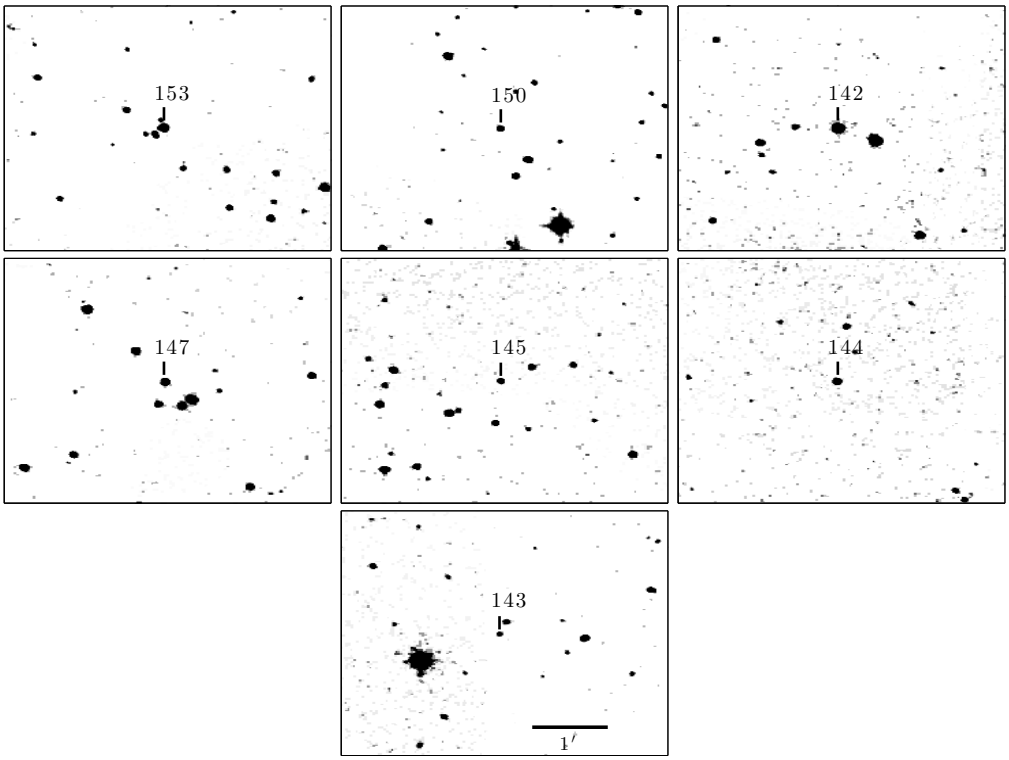

Figure 1. Identification charts for new the flare stars.

Table 1: New flare stars in Orion

#	RA(2000)	DEC(2000)	m_{pg}	Δm_{pg}	Date
AB142	$05^h29^m25^s.19$	$-04°30'44''.9$	$14^m.8$	$2^m.2$	16.11.1996
AB143	05 32 03.04	−06 42 01.5	20.5	4.6	28.02.1998
AB144	05 32 48.40	−04 41 42.1	17.4	1.7	17.11.1996
AB145	05 33 57.88	−04 35 42.7	20.4	3.5	20.11.1996
AB146	05 34 17.56	−06 03 38.2	16.9	2.0	28.02.1998
AB147	05 34 49.30	−05 04 36.6	17.8	2.3	18.11.1996
AB148	05 35 08.02	−05 36 46.4	18.3	1.6	17.11.1996
AB149	05 35 30.16	−06 03 02.6	16.7	1.4	21.02.1993
AB150	05 35 36.64	−03 13 00.3	20.0	4.2	22.02.1993
AB151	05 35 40.00	−06 08 38.0	20.8	4.0	31.10.1995
AB152	05 35 50.47	−05 51 42.2	15.6	1.5	02.12.1997
AB153	05 36 26.06	−03 13 54.0	16.0	2.7	15.11.1996

Table 2: Repeated flares in Orion

#	RA(2000)	DEC(2000)	$m_{\rm pg}$	$\Delta m_{\rm pg}$	Date
AB188	$05^{\rm h}34^{\rm m}29\overset{\rm s}{.}07$	$-06°38'51\overset{''}{.}8$	$16\overset{\rm m}{.}2$	$1\overset{\rm m}{.}3$	16.11.1996
AB209	05 34 41.46	−05 47 56.1	16.1	1.1	02.03.1989
AB222	05 34 47.52	−05 46 30.2	16.5	1.2	31.10.1995
AB273	05 35 25.11	−06 47 56.6	14.7	0.8	26.03.1992
AB363	05 36 20.56	−07 05 31.8	16.8	3.1	15.11.1996
AB386	05 36 40.69	−06 52 04.5	17.3	1.7	18.12.1989
AB401	05 36 59.80	−05 23 40.9	16.0	2.2	27.03.1989

References:

Andrews, A.D., 1970, *Bol. Obs. Tonantzintla y Tacubaya*, **5**, 195
Di Francesco, J., et. al., 2008, *ApJS*, **175**, 277 DOI
Kiladze, R.I., 1972, *IBVS*, **670**, 1
Natsvlishvili, R. Sh., 1984, *IBVS*, **2565**, 1
Natsvlishvili, R. Sh., 1991, *Afz*, **34**, 107
Natsvlishvili, R. Sh., 1994, *Afz*, **37**, 367

COMMISSIONS G1 AND G4 OF THE IAU
INFORMATION BULLETIN ON VARIABLE STARS
Volume 62 Number 6188 DOI: 10.22444/IBVS.6188

Konkoly Observatory
Budapest
10 November 2016

HU ISSN 0374 – 0676

AN INVESTIGATION OF THE RCB STAR CANDIDATE GDS J0702414-023501

HÜMMERICH, S.[1,2]; BERNHARD, K.[1,2]

[1] Bundesdeutsche Arbeitsgemeinschaft für Veränderliche Sterne e.V. (BAV), Berlin, Germany; e-mail: ernham@rz-online.de

[2] American Association of Variable Star Observers (AAVSO), Cambridge, USA

R Coronae Borealis (hereafter RCB) stars are hydrogen-deficient, carbon-rich supergiant stars. Their photometric variability is characterised by unpredictable fading events (up to ∼8 magnitudes (V)), which are thought to be caused by the formation of carbon dust (e.g. Clayton 2012). RCB stars have been shown to possess warm and bright circumstellar shells, which are readily detected at mid-infrared wavelengths. Therefore, near- and mid-infrared colour-colour diagrams and cuts can be employed as a viable and efficient method of identifying new RCB candidates (cf. e.g. Feast (1997); Alcock et al. (2001); and Tisserand (2012)).

Using the above mentioned colour selection criteria, the star 2MASS J07024146-0235017 was included into the 'Catalogue enriched with R CrB stars' by Tisserand (2012). No time series photometry had been available for this object until the advent of the Bochum Galactic Disk Survey (GDS hereafter), which has been monitoring stars in a 6°wide strip along the Galactic plane and comprises photometry for stars in the magnitude range $8 < r' < 18$ mag and $7 < i' < 17$ mag. For more information on the GDS, the reader is referred to Haas et al. (2012) and Hackstein et al. (2015).

Hackstein et al. (2015) present a sample of 64 151 variable sources identified in the GDS. Among them is 2MASS J07024146-0235017, which is listed under the designation GDS J0702414-023501 with a mean magnitude of 14.15 mag (i') and an amplitude of 4.96 mag (i'). No variability type was proposed by the aforementioned authors. Basic data and archival photometry of GDS J0702414-023501 are presented in Table 1; positional information was derived from the 2MASS catalogue (Skrutskie et al. 2006).

We have investigated the object because of its inclusion in the Tisserand (2012) catalogue and the observed, large-amplitude variability in GDS data. The light curve based on the current data release (Hackstein et al. 2015) is shown in Figure 1; only i' data are available for this object. Although there are only 71 data points scattered over a time span of ∼1600 days, it becomes obvious that the star's range of variability is large (approximate range of $12.5\,\mathrm{mag} < i' < 17\,\mathrm{mag}$). Furthermore, the light curve is reminiscent of an RCB variable and seems to provide evidence against a Mira or RV Tauri classification – two types of variables that, according to our experience, contaminate the RCB-enriched catalogue of Tisserand (2012). In particular, the light curve indicates that the star's brightness has been more or less constant for about 160 days around HJD 2456300, hovering around a mean magnitude of ∼16.5 mag (i'). Because of the available data, GDS J0702414-023501

Table 1: Table 1. Basic data and archival photometry of GDS J0702414-023501.

ID	GDS J0702414-023501, 2MASS J07024146-0235017, IRAS 07001-0230, CGCS 6197
pos (RA, Dec; J2000)	$07^{\rm h}02^{\rm m}41\overset{\rm s}{.}461$, $-02°35'01\overset{''}{.}76$
J, H, K_s (2MASS)	11.957 mag, 9.417 mag, 7.402 mag
$W1$, $W2$, $W3$, $W4$ (WISE)	5.075 mag, 3.124 mag, 2.193 mag, 1.563 mag
[9μm], [18μm] (AKARI)	8.509 Jy, 3.101 Jy
[12μm], [25μm], [60μm] (IRAS)	5.045 Jy, 2.387 Jy, 0.548 Jy

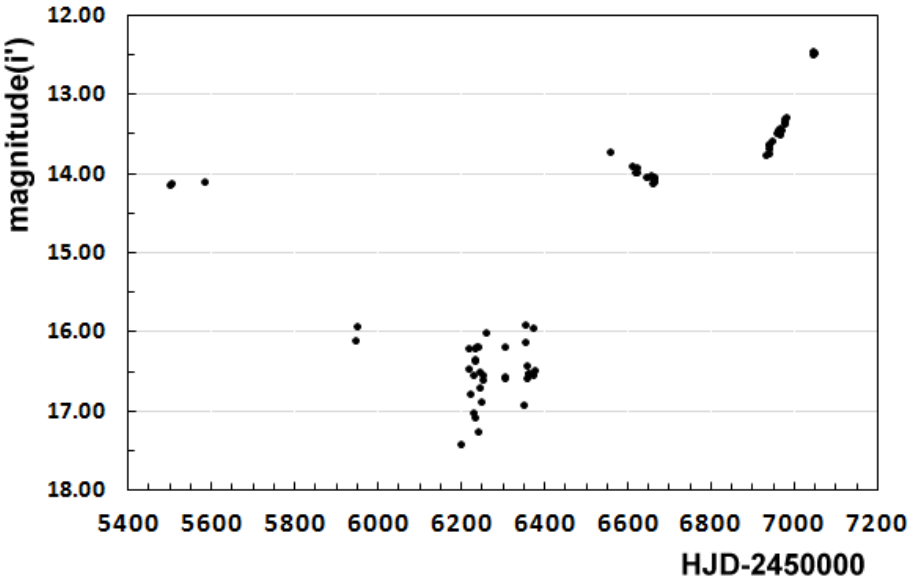

Figure 1. The GDS i' light curve of GDS J0702414-023501, based on the current data release (Hackstein et al. 2015).

has been listed as an RCB candidate (variability type RCB:) in the AAVSO International Variable Star Index (VSX; Watson 2006).

We have searched sky survey plate archives for the existence of exposures of the sky region of our interest (Figure 2). Unfortunately, no images are available that show the star in a very bright state, as recorded by the GDS. Nevertheless, the star is considerably brighter on I-band sky survey plates from 1997 than it was in 1985 (two rightmost panels in Figure 2).

Based on the calculations of Schlafly and Finkbeiner (2011), we estimate an interstellar extinction of $A_V \approx 2.2$ mag and $E_{B-V} \approx 0.7$ mag for the sky area of our interest. Dereddened magnitudes in the 2MASS J, H, Ks and WISE $W1$ and $W2$ bands (Cutri et al. 2012) were derived from the aforementioned source, which were used in the construction of the following colour-colour plots.

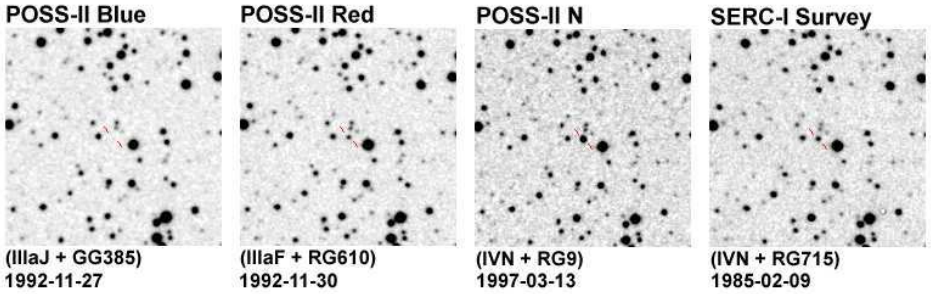

Figure 2. GDS J0702414-023501 on archival sky survey plates (position of the star is indicated). The captions provide information on emulsions and filters used, as well as the epoch the plate was taken.

A $(J-H)$ vs. $(H-K_{\rm s})$ diagram is shown in Figure 3. The RCB candidate GDS J0702414-023501 is indicated by the red and green dots which denote the loci of the star based on, respectively, reddened and unreddened magnitudes. Also shown are several confirmed RCB variables (open symbols), Mira variables (filled symbols) and the RV Tauri star UY Ara (cross). Classifications were taken from the GCVS (Samus et al. 2007-2016) and VSX online databases; data were drawn from the 2MASS catalogue.

The Mira variables approximately follow the positions of SMC carbon stars (solid line), as computed by Westerlund et al. (1991) and employed in this particular context by Tisserand et al. (2004). The very red, carbon-rich Mira V831 Mon is roughly situated on an extension of this line. The RCB stars, however, follow the dashed line, which illustrates the loci of a combination of two blackbodies representing the photosphere of the star (∼5500 K) and the dust shell (∼900 K), as employed by Feast (1997). The represented flux ranges from 'all star' (lower, left end) to 'all shell' (upper, right end).

The position of GDS J0702414-023501 is reminiscent of the positions of RCB variables during deep obscuration minima (cf. e.g. the position of UW Cen during deep minima, indicated by the small crosses in Fig. 1 of Feast (1997)).

Figure 4 shows the $(W2-W3)$ vs. $(W3-W4)$ diagram and has been based on WISE data. Stars and symbols are the same as in Figure 3. Selection cut (1) of Tisserand (2012), which effectively identifies objects with a shell signal, is indicated by the dashed lines. Only the confirmed RCB variables and GDS J0702414-023501 are well inside the indicated area.

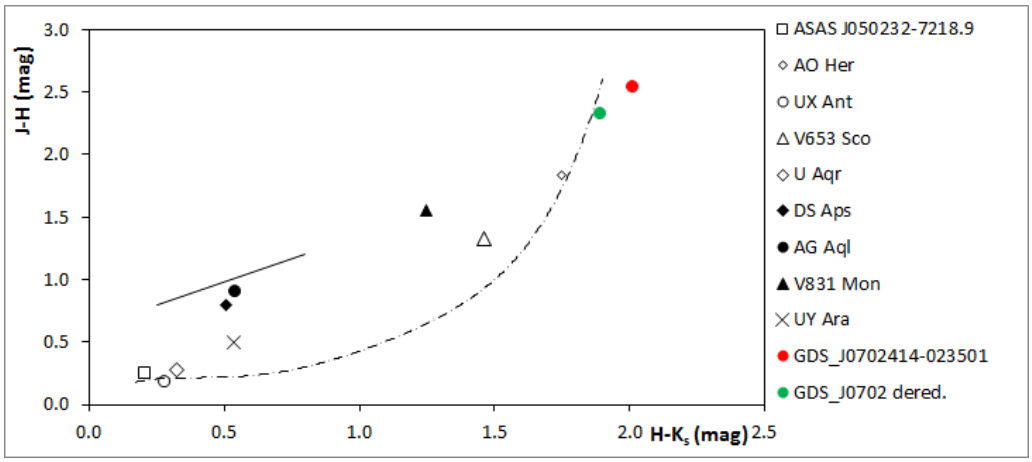

Figure 3. $(J-H)$ vs. $(H-K_s)$ diagram, indicating the positions of GDS J0702414-023501 (red and green dots) and several confirmed RCB variables (open symbols), Mira variables (filled symbols) and the RV Tauri star UY Ara (cross). See text for details.

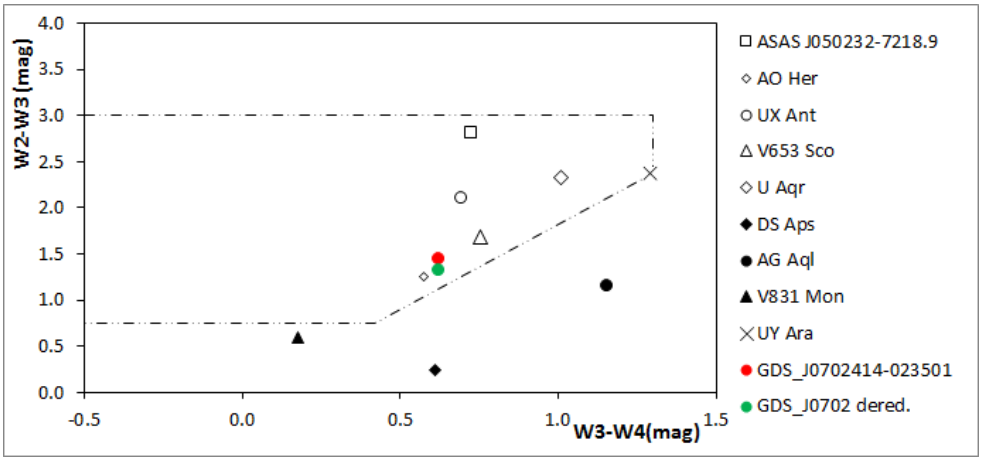

Figure 4. $(W2-W3)$ vs. $(W3-W4)$ diagram, indicating the positions of GDS J0702414-023501 (red and green dots) and several confirmed RCB variables (open symbols), Mira variables (filled symbols) and the RV Tauri star UY Ara (cross). See text for details.

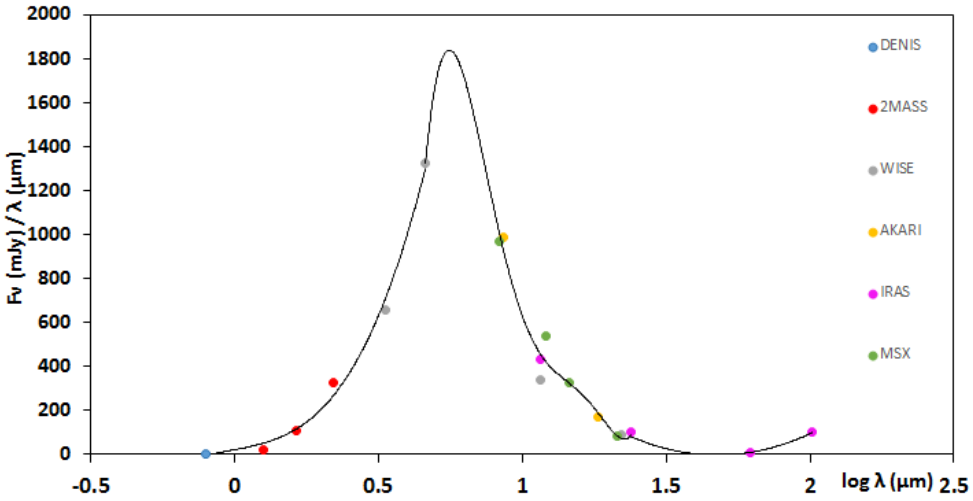

Figure 5. Spectral energy distribution of GDS J0702414-023501, based on data from various catalogues, as indicated in the inset legend. The solid line indicates a polynomial fit of 6th order.

The spectral energy distribution (SED) is shown in Figure 5, which has been based on data obtained with the VizieR Photometry viewer[1]. The data have not been corrected for line-of-sight extinction. Note that the IRAS value at 100 μm denotes an upper limit. An IR excess due to the presence of warm dust is clearly visible. However, the SED differs from that of typical RCB stars in that there is no indication of cold dust (cf. e.g. Fig. 6 of Tisserand et al. 2009). This does not necessarily exclude an RCB classification, as the amount and temperature of dust around the star is related to the frequency and duration of obscuration events. However, it casts doubt on the proposed variability type.

The IRAS source 07001-0230 lies 15.″1 distant from the 2MASS position of GDS J0702414-023501. Interestingly, IRAS 07001-0230 was identified as a carbon star on ground of its infrared colours by Guglielmo et al. (1993) and later entered the General Catalogue of Carbon Stars as CGCS 6197 (Alksnis et al. 2001). The identification of IRAS 07001-0230 with 2MASS J07024146-0235017 = GDS J0702414-023501 seems secure (MacConnell 1993; Chen et al. 2012). In MacConnell (1993), a V magnitude of 20.0 mag is indicated for IRAS 07001-0230, which elicits the following remark from B. Skiff: "CGCS 6197, too faint (mi=16.7)". This may be taken as a hint at the large amplitude of variability observed in GDS J0702414-023501, which has been found as bright a 12.5 mag (i').

In order to shed more light on the nature of our object of interest, new and hitherto unpublished GDS data were procured (M. Hackstein, private communication), which have been based on an improved reduction procedure and extend the time baseline by ∼600 days (Figure 6). Furthermore, the new data also boast measurements in r', thereby allowing an investigation of the colour index evolution (Figure 6, bottom panel).

The new data indicate that about 300 days after the rise to $i' \sim 12.5$ mag (at which point the hitherto available dataset terminates), a rather sharp drop in brightness takes place. Another ∼300 days later, several datapoints suggest a further drop or rise in brightness. Moreover, the new and improved data reduction procedure significantly reduced the number of faint datapoints around HJD 2456300; what formerly looked like a phase of

[1]http://vizier.u-strasbg.fr/vizier/sed/

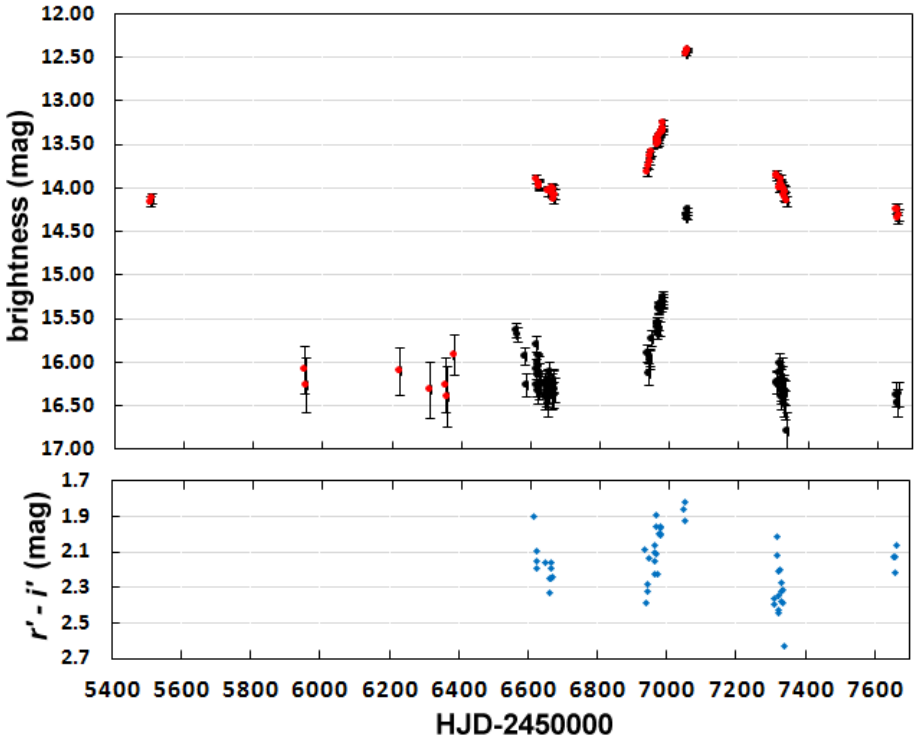

Figure 6. The GDS light and colour curves of GDS J0702414-023501, based on recent, newly reduced and as yet unpublished GDS data (M. Hackstein, private communication). Red and black dots indicate, respectively, GDS i' and r' data.

approximately constant brightness (cf. Figure 1) is now down to some scattered data points and the light curve shape during this part is open to conjecture.

Generally, RCB stars show very diverse and sometimes peculiar light curves. However, the new GDS light and colour curves are strongly reminiscent of a Mira-type variable. Although the star has passed the selection criteria of Tisserand (2012) and is a confirmed carbon star, an RCB classification seems therefore unlikely; as has been pointed out above, Mira variables are known to contaminate the candidate list of Tisserand (2012).

Taking into account all available data, we propose GDS J0702414-023501 as a long-period variable of the Mira type. However, further photometric and spectroscopic studies are needed to reach a final conclusion.

Acknowledgements: We thank Moritz Hackstein (Ruhr-Universität Bochum, Germany) for providing us with the most recent and newly reduced GDS observations, and the referee for helpful suggestions and valuable advice. This research has made use of the VizieR database, operated at CDS, Strasbourg, France.

References:

Alcock, C., et al., 2001, *ApJ*, **554**, 298 DOI
Alksnis, A., et al., 2001, *BaltA*, **10**, 1
Chen, P.S., et al., 2012, *AJ*, **143**, 36 DOI
Clayton, G.C., 2012, *JAVSO*, **40**, 539
Cutri, R.M., et al., 2012, *WISE All-Sky Data Release*, VizieR Online Data Catalogue (`http://cdsarc.u-strasbg.fr/viz-bin/Cat?II/311`)
Feast, M.W., 1997, *MNRAS*, **285**, 339 DOI
Guglielmo, F., 1993, *A&AS*, **99**, 31
Haas, M., et al., 2012, *AN*, **333**, 706 DOI
Hackstein, M., et al., 2015, *AN*, **336**, 590 DOI
MacConnell, D.J., 1993, VizieR Online Data Catalogue (`http://cdsarc.u-strasbg.fr/viz-bin/VizieR?-source=III/170B`)
Samus, N.N., et al., 2007-2016, *General Catalogue of Variable Stars*, VizieR Online Data Catalogue (`http://cdsarc.u-strasbg.fr/viz-bin/Cat?B/gcvs`)
Schlafly, E.F., & Finkbeiner, D.P., 2011, *ApJ*, **737**, 103 DOI
Skrutskie, M.F., et al., 2006, *AJ*, **131**, 1163 DOI
Tisserand, P., et al., 2004, *A&A*, **424**, 245 DOI
Tisserand, P., et al., 2009, *A&A*, **501**, 985 DOI
Tisserand, P., 2012, *A&A*, **539**, A51 DOI
Watson, C.L., 2006, *SASS*, **25**, 47
Westerlund, B.E., et al., 1991, *A&AS*, **91**, 425

COMMISSIONS G1 AND G4 OF THE IAU
INFORMATION BULLETIN ON VARIABLE STARS
Volume 62 Number 6189 DOI: 10.22444/IBVS.6189

Konkoly Observatory
Budapest
25 November 2016

HU ISSN 0374 – 0676

V620 Oph = CoRoT 104190253 – A MISCLASSIFIED RR LYRAE STAR

BENKŐ, J. M.

Konkoly Observatory, MTA CSFK, 1121 Budapest, Konkoly Thege u. 15-17. Hungary
e-mail: benko@konkoly.hu

While I was reading the recently appeared CoRoT Legacy Book (CoRoT Team, 2016) I noticed the figures A.1 and A.2 in the paper of Ollivier et al. (2016). The authors call the attention to a rare but possible failure of the jump detection algorithm of the CoRoT data pipeline. If a large amplitude variable star has similar period than the CoRoT satellite South Atlantic Anomaly passing through rate (0.499 d), this could lead to a false jump detection and the algorithm heavily distorts the light curve. The effect is illustrated with the case of the RR Lyrae star CoRoT 104190253. Since the CoRoT Variable star Classifier (CVC, Debosscher et al. 2009) uses the processed light curves, this star was not classified as an RR Lyrae star. So it has not been reported by any of the specific CoRoT RR Lyrae studies nor by the two review papers (Szabó et al. 2014, Benkő et al. 2016).

1 History and classification

The SIMBAD database contains a Mira variable star V620 Oph at the position of CoRoT 104190253 (α_{2000}=18$^{\rm h}$33$^{\rm m}$47$^{\rm s}$.35, δ_{2000}=+9°06′58″.608). The literature of V620 Oph is rather poor. Its variable nature was discovered by Hoffmeister (1936) who later gave the finding chart as well (Hoffmeister, 1957). The only additional paper which mentioned the star is the work of Kinnunen & Skiff (2000), which provides proper positions for many variable stars. No specific study of V620 Oph has been found.

The star was observed by the CoRoT satellite (Baglin 2006, 2016) in its fourth long run towards the Galactic centre direction (LRc04) between 07 July and 29 September 2009 (84 days). After the first two days the observation was taken in oversampled mode which means 32 sec sampling rate. This resulted in more than 19 000 individual data points[1]. Considering the data it is immediately visible that the Mira classification is wrong. The period, the amplitude, and the light curve shape are all typical of a fundamentally pulsating RR Lyrae (RRab) star (Fig. 1).

[1]The CoRoT N2 reduced data used this work can be downloaded from the IAS CoRoT Public Archive site at http://idoc-corot.ias.u-psud.fr/sitools/client-user/COROT_N2_PUBLIC_DATA/project-index.html

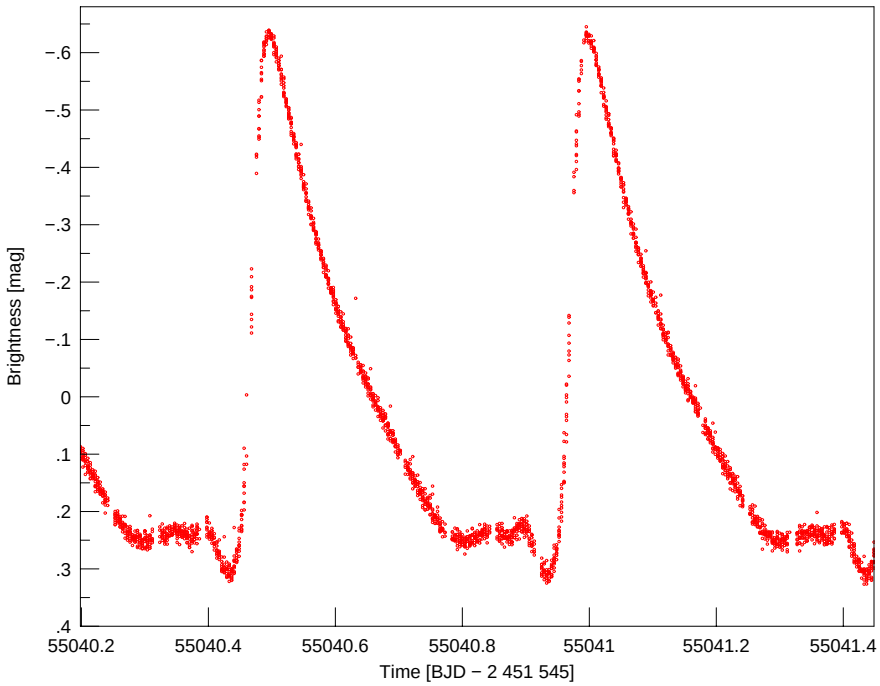

Figure 1. A light curve part of the CoRoT observation of V620 Oph.

2 Data analysis and results

The data was selected, processed, and analyzed in the same way as it was described in Benkő et al. (2016). The main pulsation period P_0 is 0.501743±0.000003 d and the Fourier amplitude of the main frequency in CoRoT instrumental magnitude scale is $A(f_0) = 0.3284 \pm 0.0005$ mag. All the errors given in this paper are estimated with the Monte Carlo Simulation tool of Period04 program package (Lenz & Breger 2005).

The light curve does not show any serious modulation effects but the Fourier analysis shows some. If I pre-whiten the data with the main pulsation frequency and its harmonics the residual spectrum is dominated by side peaks around the harmonics and a highly significant (S/N=12.2) peak in the low frequency regime at $f' = 0.016 \pm 0.013$ d^{-1}. The side peak distances from the harmonics and f' frequency itself determine a possible ∼60 d-long modulation.

The reality of such a long period modulation needs a careful check which can distinguish it from the possible similar time-scale instrumental trends. For this purpose I chose the Period04 amplitude/phase variation calculation tool which is sensitive for finding small amplitude or phase modulations (Nemec et al. 2011, 2013). To test the method dependence on the bin size I run the program twice using either 3 days-long or 5 days-long bin sizes. The results concerning the amplitude and phase of the main pulsation frequency are shown in Fig. 2.

The variation is clearly seen in both panels of the figure. The different symbols (which denote the two bin sizes) show the same curve shape demonstrating that the variation is independent of the used bin sizes. The amplitude and phase variation curves are highly (anti)correlated which strengthen the reality of the effect. Fourier spectra of these curves

yield a period of $P = 41.2 \pm 11$ d which is in agreement with the result of the above light curve Fourier analysis. The huge period error of both methods is on the one hand due to the small number of covered cycles (~ 2), on the other hand because of the irregularity of the cycles. The observed two Blazhko cycles have different amplitude and phase variation curves suggesting multiperiodic and/or irregular nature of the effect. It is not a surprise because it was recently demonstrated that the multiperiodic Blazhko effects are very common (Benkő et al. 2014).

The amplitude of this amplitude variation is $\Delta A_1 = 0.042 \pm 0.001$ mag while the amplitude of the phase variation is $\Delta\phi_1 = 0.0018 \pm 0.0008$. Here I used the definition of Nemec et al. (2013) for ΔA_1 and $\Delta\phi_1$, the phases defined as in Lenz & Breger (2005) that is they should be multiplied by 2π for obtaining the phases in radian. The amplitude of the detected variations is low but not extremely: V620 Oph values are between the parameters of the two *Kepler* Blazhko stars KIC 11125706 and V838 Cyg (Nemec et al. 2013). (Here I assumed that the CoRoT white light amplitudes are similar to those that the *Kepler* unfiltered ones.) Otherwise, this star shows the smallest amplitude Blazhko effect among the non-blended CoRoT RRab stars.

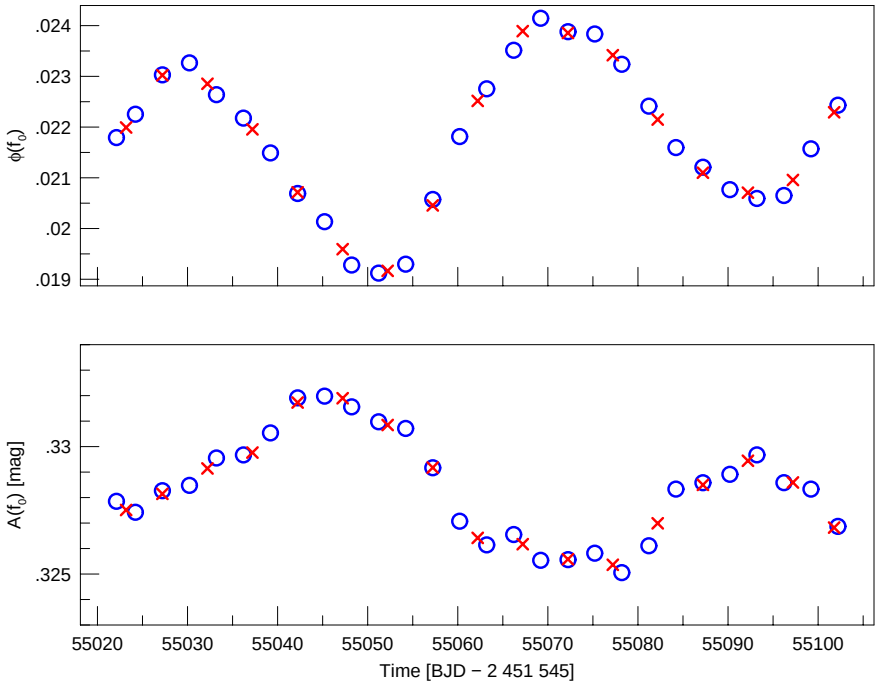

Figure 2. The amplitude (bottom) and phase variation (top) of the main pulsation frequency f_0. Phase units are rad/2π. The open circles denote the result obtained using 3 days-long bin size while x symbols show the 5 days-long bin size result. The error of the individual data points is smaller than the symbol sizes.

3 Conclusion

In this short paper I demonstrated that the formerly misclassified V620 Oph is a fundamental-mode pulsating RR Lyrae star showing a small amplitude but real Blazhko effect. The effect has possible multiperiodic or irregular character.

The lesson from the accidental finding of the star is that some RR Lyrae stars with similar period might be hidden in the CoRoT archive. This is the first and the only identified RR Lyrae star within the period range of 0.4853-0.5385 d. In turn the maximum of the period distribution function of Galactic RR Lyrae stars (0.556 d, see e.g. Soszyński et al. 2011) is near of this interval.

Acknowledgements: The author thanks K. Nagy for polishing the English style of the paper. This research has been supported partially by the NKFIH Grant K-115709.

References:

Baglin, A., Fridlund, M., 2006, in The CoRoT Mission Pre-Launch Status – Stellar Seismology and Planet Finding, ESA SP-1306, p. 11

Baglin, A., Lam-Trong, T., Vandermarcq, O., Donny, C., & Burgaud, S., 2016, in The CoRoT Legacy Book, (EDP Sciences), p. 11 DOI

Benkő, J. M., Plachy, E., Szabó, R. et al., 2014, *ApJS*, **213**, 31 DOI

Benkő, J. M., Szabó, R., Derekas, A., & Sódor, Á., 2016, *MNRAS*, in press, arXiv:1608.06418 DOI

Debosscher, J., Sarro, L. M., López, M. et al., 2009, *A&A*, **506**, 519 DOI

CoRoT Team, 2016, The CoRoT Legacy Book, EDP Sciences DOI

Hoffmeister, C., 1936, *AN*, **259**, 37 DOI

Hoffmeister, C., 1957, *Mitteil. Veränd. Sterne*, No. 245

Kinnunen, T. & Skiff, B. A., 2000, *IBVS*, No. 4864

Lenz, P. & Breger, M., 2005, CoAst, 146, 53 DOI

Nemec, J. M., Smolec, R., Benkő, J. M. et al., 2011, *MNRAS*, **417**, 1022 DOI

Nemec, J. M., Cohen, J. G., Ripepi, V. et al., 2013, *ApJ*, **773**, 181 DOI

Ollivier, M., Deru, A., Chaintreuil, S. et al., 2016, in The CoRoT Legacy Book, EDP Sciences, p. 41 DOI

Soszyński, I., Dziembowski, W. A., Udalski, A. et al., 2011, *Acta Astron.*, **61**, 1

Szabó, R., Benkő, J. M., Paparó, M. et al., 2014, *A&A*, **570**, A100 DOI

COMMISSIONS G1 AND G4 OF THE IAU
INFORMATION BULLETIN ON VARIABLE STARS
Volume 62 Number 6190 DOI: 10.22444/IBVS.6190

Konkoly Observatory
Budapest
15 December 2016

HU ISSN 0374 – 0676

NEW R CORONAE BOREALIS AND DY PERSEI CANDIDATES IN THE SMC

NIKZAT, F.[1,2]; CATELAN, M.[1,2]

[1] Instituto de Astrofísica, Facultad de Física, Pontificia Universidad Católica de Chile, Av. Vicuña Mackenna 4860, 782-0436 Macul, Santiago, Chile; e-mail: fnikzat@astro.puc.cl, mcatelan@astro.puc.cl

[2] Millennium Institute of Astrophysics, Santiago, Chile

R Coronae Borealis (RCB) stars are C-rich, H-deficient red supergiants that undergo dramatic dimming episodes at irregular intervals. The dimming episodes are caused by self-obscuration by dust, occurring as a consequence of mass loss events (e.g., Lambert & Rao 1994; Clayton 1996, 2012; Catelan & Smith 2015, and references therein). The purpose of this contribution is to report on a new search for RCB stars in the Small Magellanic Cloud (SMC), carried out using VI light curves from the OGLE project (Soszyński et al. 2011). To detect candidates, the VI light curves of all SMC red variable stars were visually inspected, and compared against templates from the literature. New RCB candidates were detected in the process, which had previously been classified as semi-regular or Mira variables. Additionally, DY Persei candidates were also identified. Compared to their RCB counterparts, the DY Per stars tend to be cooler, have slower decline rates, and more symmetrical declines (e.g., Začs et al. 2007; Catelan & Smith 2015, and references therein). If confirmed, these detections would lead to a significant increase in the number of known RCB + DY Per stars in the SMC.

The RCB stars have traditionally been classified as eruptive variables, due to their massive ejection episodes. However, they may also be classified as *self-eclipsing variable stars*, because of the self-obscuration due to formation of carbon dust around the star during mass loss events. Consequently, the RCB stars show a deep drop in their light curves which is a distinguishing characteristic of this class of variables. Since the dust forms in discrete clouds, the declines only occur when dust condenses along our line of sight.

The evolutionary origin of the RCB stars is not understood yet. Two scenarios have been proposed for their formation (Iben et al. 1996; Saio & Jeffery 2002): a merger of two white dwarfs or a final He-shell flash of the central object of a planetary nebula-hosting post-asymptotic giant branch (AGB) star. In the latter case, they would represent so-called "born-again stars," to the extent that they would constitute (pre-) white dwarf stars that have been brought back to giant dimensions (Renzini 1990); in the former, they would be low-mass analogs of the same process that is believed to result in type Ia supernovae.

RCB stars are rare, with only about a hundred currently known (Tisserand et al. 2016), of which roughly one quarter are found in the Magellanic Clouds (Tisserand et al. 2013). To properly understand their evolutionary origin, more RCB stars in different

environments with different metallicities are required. Furthermore, AGB stars are known as one of the main producers of dust to the interstellar medium (ISM), and likewise RCB stars may also significantly contribute to the dust enrichment of the ISM. As dust has different behavior in different environments, building significant samples of low-metallicity RCB stars can provide useful constraints on the role such stars may have played in the course of cosmic history.

In this note, we present new RCB candidates found in the relatively low-metallicity environment of the SMC, based on an analysis of the morphology of the light curves of red variables published by the OGLE team. Their names and coordinates are provided in Table 1. To date, only three RCB and three DY Per stars have been confirmed in the SMC (Tisserand et al. 2009), with an additional two RCB plus three DY Per candidates also having been reported in the literature (Kraemer et al. 2005; Tisserand et al. 2009). Most recently, a new RCB candidate, Gaia16aau, was discovered using Gaia data (Tisserand et al. 2016).

The catalog data for red variable stars in the SMC are available online from the OGLE project.[1] The data were taken with the 1.3-meter Warsaw telescope at Las Campanas Observatory, northern Chile, in the course of the OGLE-III campaigns (Soszyński et al. 2011). All VI light curves were visually inspected, in a search for dramatic, non-periodic drops in brightness that might be indicative of RCB-like behavior. Our results are summarized in Table 1 and Figures 1 through 14. In total, we present two new RCB (Fig. 1) and 63 new DY Per (Figs. 2-14) candidates. A third RCB candidate was also identified, and will be discussed later in this note.

For completeness, previously confirmed and candidate RCB and DY Per stars in the SMC are also listed in Table 2. Among these, three confirmed DY Per stars (OGLE-SMC-LPV-03068, OGLE-SMC-LPV-04633, OGLE-SMC-LPV-11903) and three DY Per candidates (OGLE-SMC-LPV-05023, OGLE-SMC-LPV-06616, OGLE-SMC-LPV-12291) from the EROS2 project (Tisserand et al. 2009) were detected in the OGLE data. Their corresponding light curves are shown in Figures 15 and 16 for the confirmed and candidate DY Per stars, respectively. Note that we include OGLE-SMC-LPV-05007 among the DY Per candidates in this paper, even though it was rejected by Tisserand et al. (2009) due to the presence of strong TiO bands. However, the light curve morphology bears some resemblance to those of other C-rich stars, and indeed the star has been classified as a C-star in the OGLE-III catalog. This star may thus be an interesting example of what might perhaps be called a "borderline" DY Per-like star, not clearly conforming to the canonical DY Per classification scheme. Its coordinates are given in the bottom row of Table 2.

We emphasize, in this context, that OGLE-SMC-LPV-11903[2] (EROS2-SMC-DYPer-3), which has previously been classified as a DY Per star based on spectroscopic data, presents a light curve morphology that is strongly reminiscent of an RCB star (Fig. 15). This may also hint at the possibility of a "transitional" DY Per/RCB status. The latter might be consistent with the presence of an evolutionary sequence among hydrogen-deficient carbon stars, as suggested by Saio & Jeffery (2002) and supported by De Marco et al. (2002) and Schaefer (2016).

We also note that, while OGLE-SMC-LPV-03068 (EROS2-SMC-DYPer-2) is classified as an O-type LPV in the OGLE-III catalog, it has already been spectroscopically confirmed to be a DY Per C-star (see Tisserand et al. 2004, 2009). The star's light curve, as shown in Figure 15, is indeed consistent with that expected for a C-star.

[1] ftp://ftp.astrouw.edu.pl/ogle/ogle3/OIII-CVS/smc/lpv/

[2] Note that the OGLE-2 ID for this star is missing in the OGLE-III catalog.

We were able to match the spectroscopic RCB candidate MSX-SMC-014 (Kraemer et al. 2005; Tisserand et al. 2009) to OGLE-SMC-LPV-05719; the light curve is shown in Figure 17. We point out that this light curve bears some resemblance to that of OGLE-SMC-LPV-17611; in both cases, we see several photometric declines during the OGLE-III monitoring, and the time interval between adjacent minima/maxima is roughly similar (Fig. 17). We accordingly propose OGLE-SMC-LPV-17611 as an additional candidate RCB star in the SMC.

To close, we note that, in our work, we have only used light curve morphology as indicative of potential RCB/DY Per status. Follow-up observations, both photometric and spectroscopic, are required in order to conclusively establish the nature of our candidates.

Acknowledgments: We warmly thank the referee, E. J. Montiel, for his thoughtful report. Support for this project is provided by the Ministry for the Economy, Development, and Tourism's Millennium Science Initiative through grant IC 120009, awarded to the Millennium Institute of Astrophysics (MAS); by Proyecto Basal PFB-06/2007; by CONICYT's PCI program through grant DPI20140066; and by FONDECYT grants #1141141. FN is grateful for financial support by Proyecto Gemini CONICYT grants #32130013 and #32140036.

References:

Catelan, M., Smith, H. A., 2015, *Pulsating Stars* (Wiley-VCH)
Clayton, G. C., 1996, *PASP*, **108**, 225 DOI
Clayton, G. C., 2012, *JAAVSO*, **40**, 539
De Marco, O., Clayton, G. C., Herwig, F., et al., 2002, *AJ*, **123**, 3387 DOI
Iben, I., Tutukov, A. V., Yungelson, L. R., 1996, *ApJ*, **456**, 750 DOI
Kraemer, K. E., Sloan, G. C., Wood, P. R., et al., 2005, *ApJ*, **631**, L147 DOI
Lambert, D. L., & Rao, N. K., 1994, *JApA*, **15**, 47 DOI
Renzini, A., 1990, *ASPC*, **11**, 549
Saio, H., & Jeffery, C. S., 2002, *MNRAS*, **333**, 121 DOI
Schaefer, B. E., 2016, *MNRAS*, **460**, 1233 DOI
Soszyński, I., Udalski, A., Szymański, M. K., et al., 2011, *AcA*, **61**, 217
Tisserand, P., Clayton, G. C., Welch, D. L., et al., 2013, *A&A*, **551**, A77 DOI
Tisserand, P., Marquette, J. B., Beaulieu, J. P., et al., 2004, *A&A*, **424**, 245 DOI
Tisserand, P., Wood, P. R., Marquette, J. B., et al., 2009, *A&A*, **501**, 985 DOI
Tisserand, P., Wyrzykowski, L., Clayton, G., et al., 2016, *ATel*, **8681**, 1
Začs, L., Mondal, S., Chen, W. P., et al., 2007, *A&A*, **472**, 247 DOI

Table 1: New RCB and DY Per candidates in the SMC

New RCB candidates (*this note*)				
OGLE-SMC-LPV-01019	00:31:16.77	−73:56:48.6		SRV
OGLE-SMC-LPV-06216	00:47:05.33	−72:34:30.5	MACHO-208.15801.1	SRV
OGLE-SMC-LPV-17611	01:09:21.69	−71:24:35.1		Mira
New DY Per candidates (*this note*)				
OGLE-SMC-LPV-00190	00:23:58.50	−73:37:54.9		Mira
OGLE-SMC-LPV-00486	00:27:10.92	−73:24:30.3		Mira
OGLE-SMC-LPV-00492	00:27:14.50	−73:36:42.4		Mira
OGLE-SMC-LPV-00666	00:28:34.78	−74:05:41.9		SRV
OGLE-SMC-LPV-00799	00:29:42.22	−73:19:11.1		SRV
OGLE-SMC-LPV-02715	00:39:13.28	−73:57:05.9		SRV
OGLE-SMC-LPV-03078	00:40:16.26	−73:01:15.5		Mira
OGLE-SMC-LPV-03315	00:40:55.61	−72:47:49.4		Mira
OGLE-SMC-LPV-03429	00:41:16.95	−72:52:16.8	MACHO-213.15398.77	Mira
OGLE-SMC-LPV-03593	00:41:42.45	−72:58:53.7	MACHO-213.15453.892	Mira
OGLE-SMC-LPV-03810	00:42:16.10	−72:57:32.6		SRV
OGLE-SMC-LPV-04208	00:43:09.58	−73:09:20.1		Mira
OGLE-SMC-LPV-04575	00:43:56.94	−73:56:08.0		Mira
OGLE-SMC-LPV-05322	00:45:33.00	−73:05:12.1	MACHO-212.15679.930	Mira
OGLE-SMC-LPV-05801	00:46:23.52	−72:37:39.8		Mira
OGLE-SMC-LPV-06089	00:46:50.78	−71:47:39.4		SRV
OGLE-SMC-LPV-06156	00:46:59.11	−73:25:18.8	MACHO-212.15788.31	SRV
OGLE-SMC-LPV-06572	00:47:37.82	−73:00:13.3	MACHO-212.15795.25	SRV
OGLE-SMC-LPV-06962	00:48:12.30	−72:41:18.6		SRV
OGLE-SMC-LPV-07113	00:48:27.01	−72:45:55.5	MACHO-208.15855.5029	Mira
OGLE-SMC-LPV-07354	00:48:50.92	−73:14:02.3		SRV
OGLE-SMC-LPV-07375	00:48:52.49	−73:08:56.8	MACHO-212.15907.28	Mira
OGLE-SMC-LPV-07665	00:49:20.53	−72:34:11.8	MACHO-208.15915.2828	Mira
OGLE-SMC-LPV-07829	00:49:34.97	−73:18:18.5	MACHO-212.15904.2217	SRV
OGLE-SMC-LPV-08192	00:50:12.59	−72:33:42.3	MACHO-208.15972.2547	SRV
OGLE-SMC-LPV-08390	00:50:31.29	−72:29:13.1	MACHO-208.15973.50	Mira
OGLE-SMC-LPV-08445	00:50:37.00	−73:08:53.7		SRV
OGLE-SMC-LPV-08741	00:51:04.65	−72:01:37.6		SRV
OGLE-SMC-LPV-08803	00:51:10.37	−72:27:42.8		Mira
OGLE-SMC-LPV-08931	00:51:23.06	−72:36:16.4		SRV
OGLE-SMC-LPV-09350	00:51:58.14	−73:43:35.3		SRV
OGLE-SMC-LPV-09801	00:52:40.18	−72:47:27.7	MACHO-207.16140.490	Mira
OGLE-SMC-LPV-10280	00:53:23.12	−72:04:22.4		SRV
OGLE-SMC-LPV-10436	00:53:37.31	−72:34:35.2	MACHO-207.16200.324	Mira
OGLE-SMC-LPV-10465	00:53:40.01	−72:52:18.7		SRV
OGLE-SMC-LPV-10816	00:54:10.75	−73:03:03.1	MACHO-211.16250.24	SRV
OGLE-SMC-LPV-11279	00:54:54.11	−73:03:18.2	MACHO-211.16250.4090	Mira
OGLE-SMC-LPV-11698	00:55:34.14	−72:40:29.4	MACHO-207.16313.24	SRV
OGLE-SMC-LPV-11806	00:55:44.47	−72:54:40.8		Mira
OGLE-SMC-LPV-12043	00:56:10.05	−72:28:41.9		Mira
OGLE-SMC-LPV-12119	00:56:16.38	−72:16:41.4	MACHO-207.16376.687	Mira
OGLE-SMC-LPV-12304	00:56:36.77	−73:32:55.5		SRV
OGLE-SMC-LPV-12427	00:56:50.29	−72:25:08.7	MACHO-207.16373.675	Mira
OGLE-SMC-LPV-13205	00:58:20.78	−72:55:02.1	MACHO-211.16480.1110	SRV
OGLE-SMC-LPV-13251	00:58:26.59	−73:40:35.0		SRV
OGLE-SMC-LPV-13320	00:58:34.86	−73:32:10.9		SRV
OGLE-SMC-LPV-13323	00:58:35.18	−72:59:35.6	MACHO-211.16479.2	SRV
OGLE-SMC-LPV-13676	00:59:15.78	−72:27:54.6	MACHO-207.16544.36	Mira
OGLE-SMC-LPV-13739	00:59:21.90	−72:11:13.4		SRV
OGLE-SMC-LPV-13749	00:59:23.36	−73:56:01.0		SRV
OGLE-SMC-LPV-14197	01:00:15.67	−72:22:26.2	MACHO-207.16602.106	SRV
OGLE-SMC-LPV-14205	01:00:16.84	−72:55:18.1		Mira
OGLE-SMC-LPV-14322	01:00:31.66	−72:14:49.1	MACHO-207.16604.926	Mira
OGLE-SMC-LPV-14778	01:01:26.59	−72:47:41.2		Mira
OGLE-SMC-LPV-14991	01:01:54.59	−72:58:22.4	MACHO-211.16707.28	Mira
OGLE-SMC-LPV-16113	01:04:39.84	−72:49:48.2		Mira

Table 1: cont.

Star name	Ra (J2000)	DEC (J2000)	Other ID	Subtype
OGLE-SMC-LPV-16844	01:06:53.07	−73:46:00.2		Mira
OGLE-SMC-LPV-16850	01:06:54.81	−72:24:41.2		Mira
OGLE-SMC-LPV-17194	01:08:01.14	−72:53:17.4		SRV
OGLE-SMC-LPV-17267	01:08:12.97	−72:52:44.0		Mira
OGLE-SMC-LPV-17976	01:10:53.22	−72:14:46.0		SRV
OGLE-SMC-LPV-18657	01:15:09.88	−72:05:51.3		Mira
OGLE-SMC-LPV-19032	01:18:48.06	−72:27:43.7		Mira

Table 2: Known RCB and DY Per stars in the SMC

Star name	RA (J2000)	DEC (J2000)	Other ID
RCB and DY Per confirmed			
EROS2-SMC-RCB-1	00:37:47.11	−73:39:02.3	RAW-21
EROS2-SMC-RCB-2	00:48:22.96	−73:41:04.7	RAW-476
EROS2-SMC-RCB-3	00:57:18.15	−72:42:35.2	MACHO-207.16426.1662
EROS2-SMC-DYPer-1	00:44:07.50	−72:44:16.4	RAW-233
			MACHO-208.15571.60
			OGLE-SMC-LPV-04633
EROS2-SMC-DYPer-2	00:40:14.72	−74:11:21.6	[MH95]-431
			OGLE-SMC-LPV-03068
EROS2-SMC-DYPer-3	00:55:54.97	−72:35:12.27	RAW-961
			OGLE2-SMC-SC7-368043
			OGLE-SMC-LPV-11903
RCB and DY Per candidates			
EROS2-SMC-RCB-4	01:04:52.89	−72:04:02.64	OGLE2-SMC-SC10-107856
MSX-SMC-014	00:46:16.33	−74:11:13.6	OGLE-SMC-LPV-05719
Gaia16aau	00:50:10.67	−69:43:57.9	[MH95]-580
			OGLE-SMC710.08.1
EROS2-SMC-DYPer-4	00:56:35.47	−71:32:32.66	[MH95]-672
			OGLE-SMC-LPV-12291
EROS2-SMC-DYPer-5	00:47:41.71	−73:06:16.38	RAW-421
			MACHO-212.15793.25
			OGLE-SMC-LPV-06616
EROS2-SMC-DYPer-6	00:44:56.40	−73:12:25.02	MACHO-212.15621.153
			OGLE-SMC-LPV-05023
"Borderline" DY Per-like candidate (*see text*)			
sm0101n-16084	00:44:54.02	−73:15:30.02	MACHO-212.15620.713
			OGLE-SMC-LPV-05007

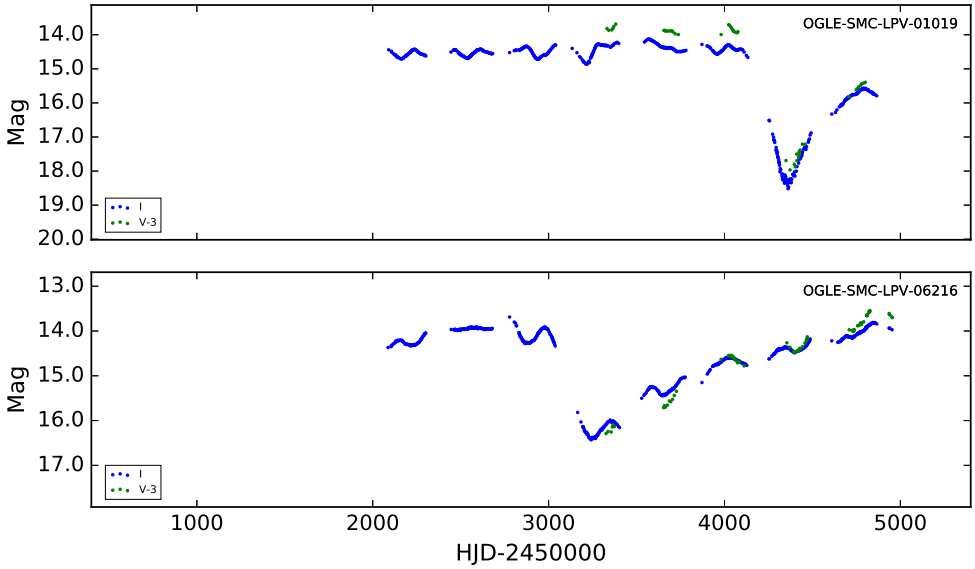

Figure 1. Light curves in I (*blue*) and V (*green*) of two new RCB candidates in the SMC.

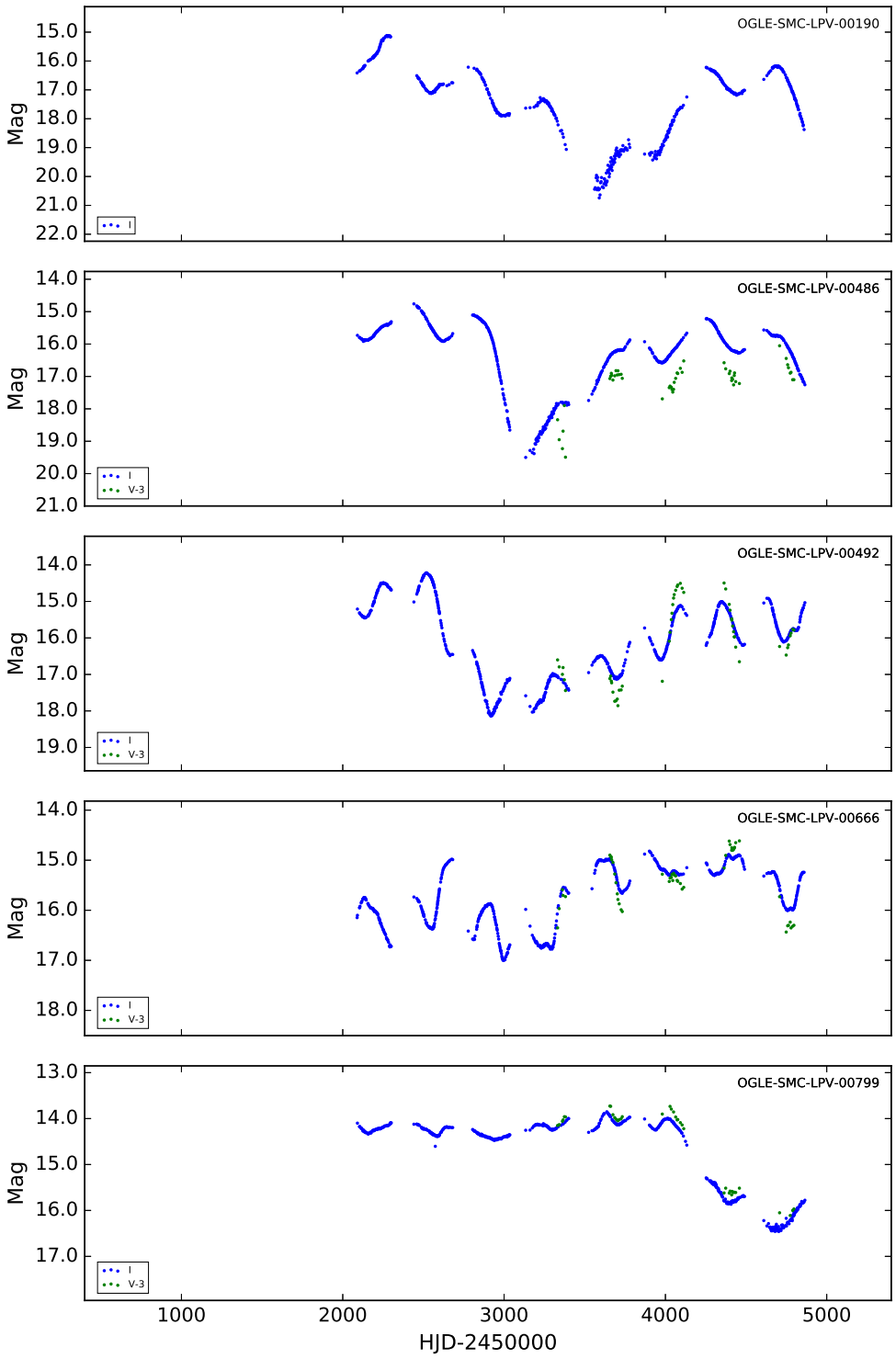

Figure 2. Light curves in I (*blue*) and V (*green*) of new DY Per candidates in the SMC.

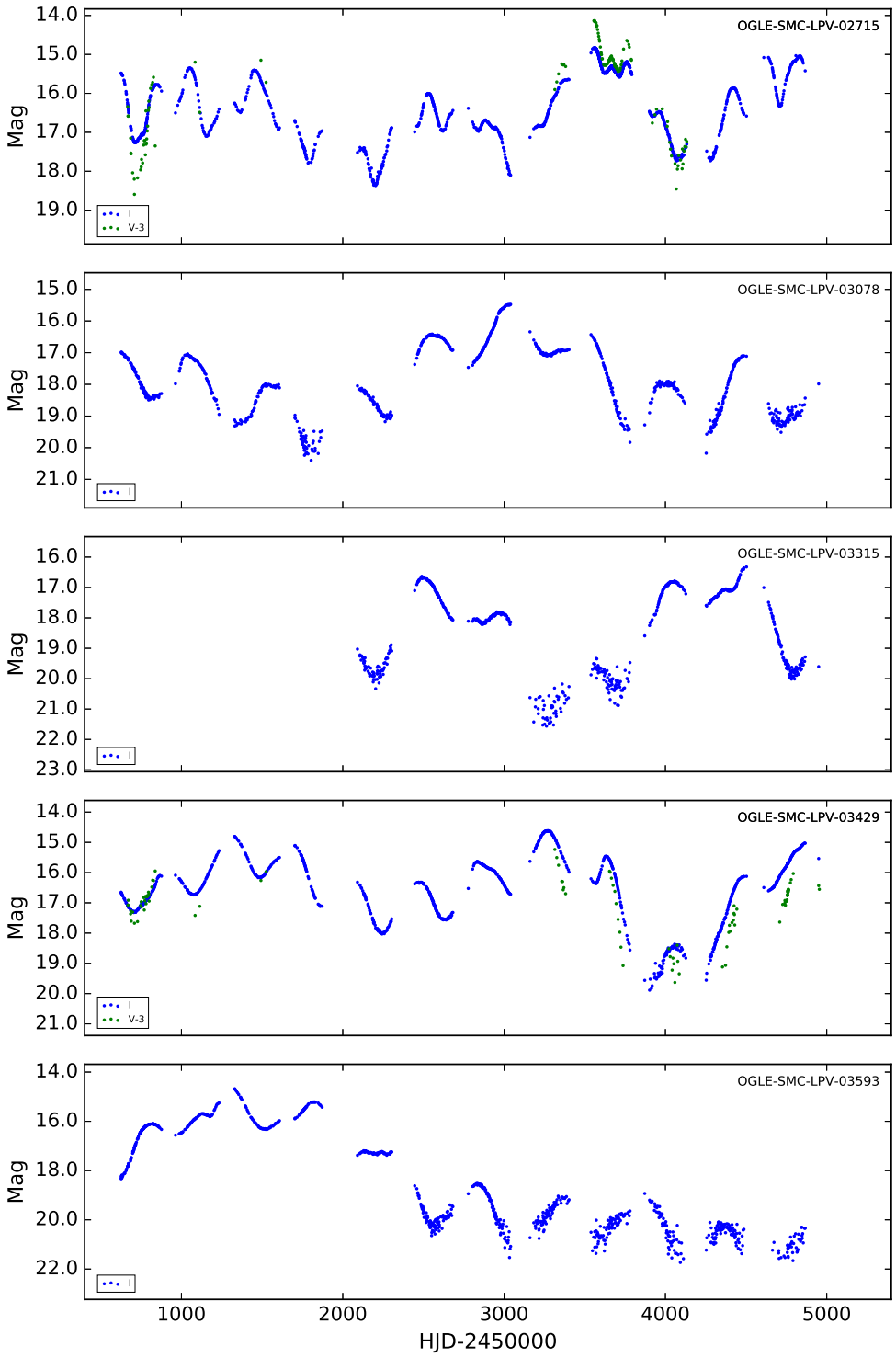

Figure 3. Light curves in I (*blue*) and V (*green*) of new DY Per candidates in the SMC.

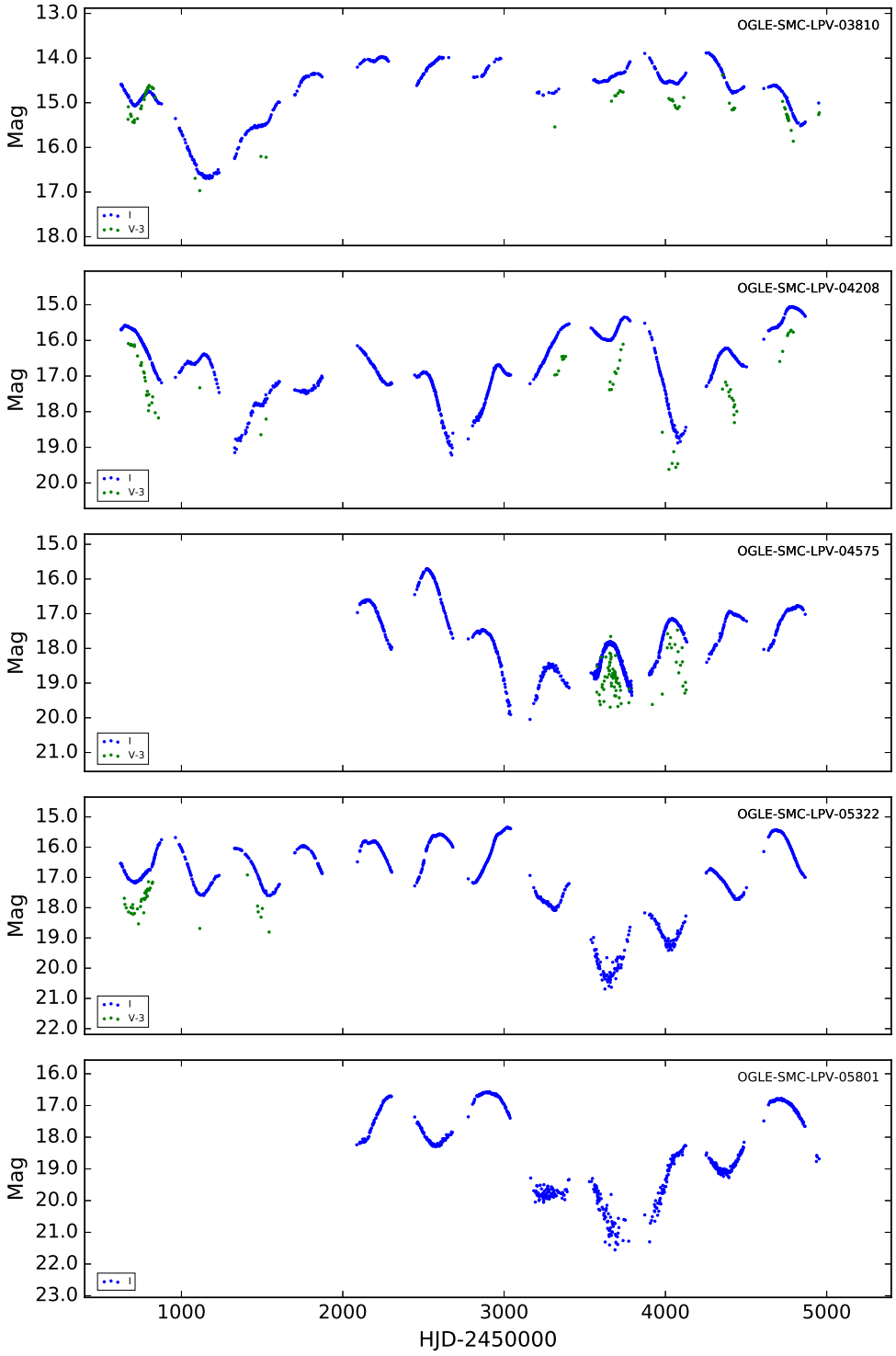

Figure 4. Light curves in I (*blue*) and V (*green*) of new DY Per candidates in the SMC.

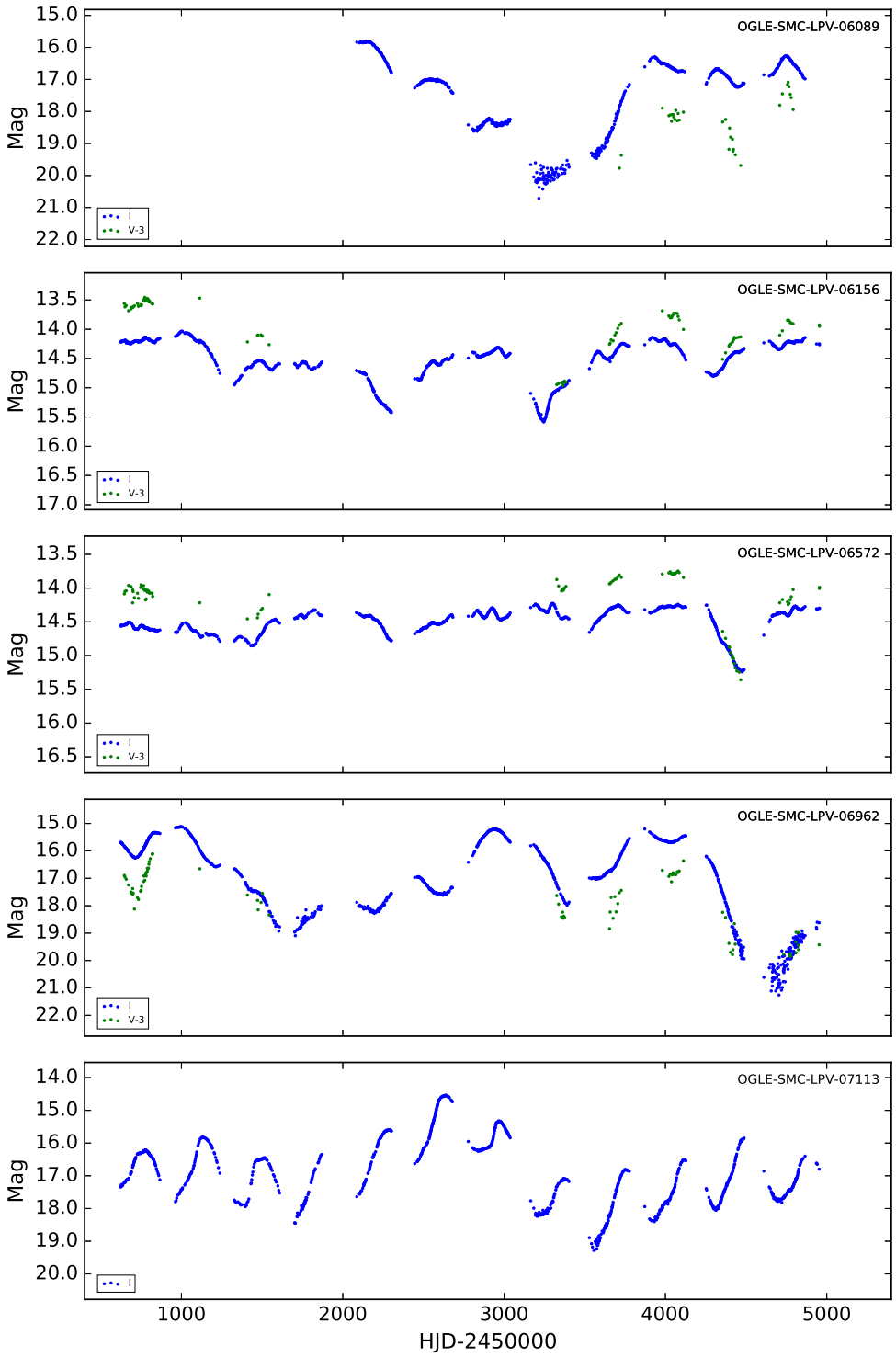

Figure 5. Light curves in I (*blue*) and V (*green*) of new DY Per candidates in the SMC.

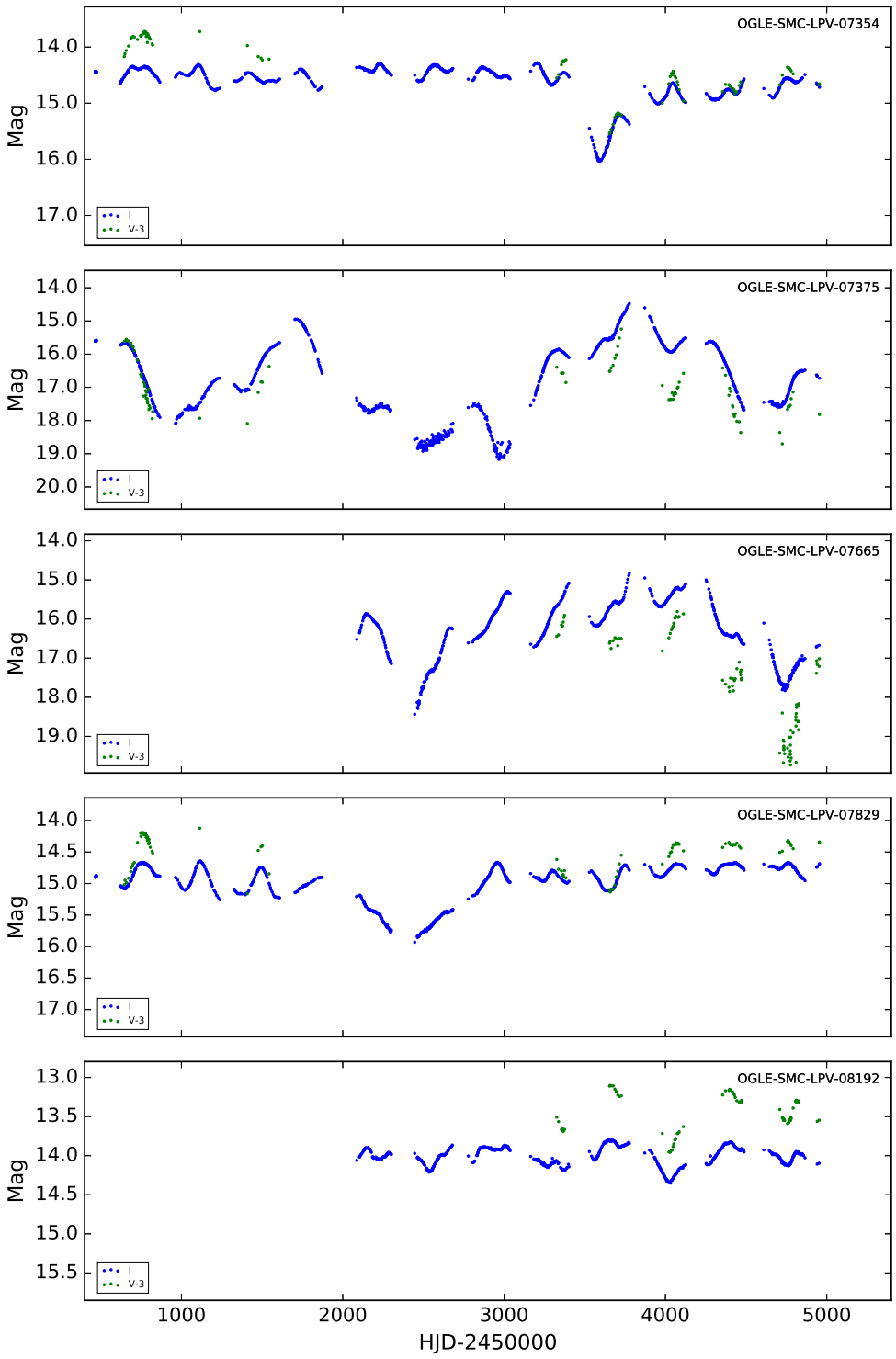

Figure 6. Light curves in I (*blue*) and V (*green*) of new DY Per candidates in the SMC.

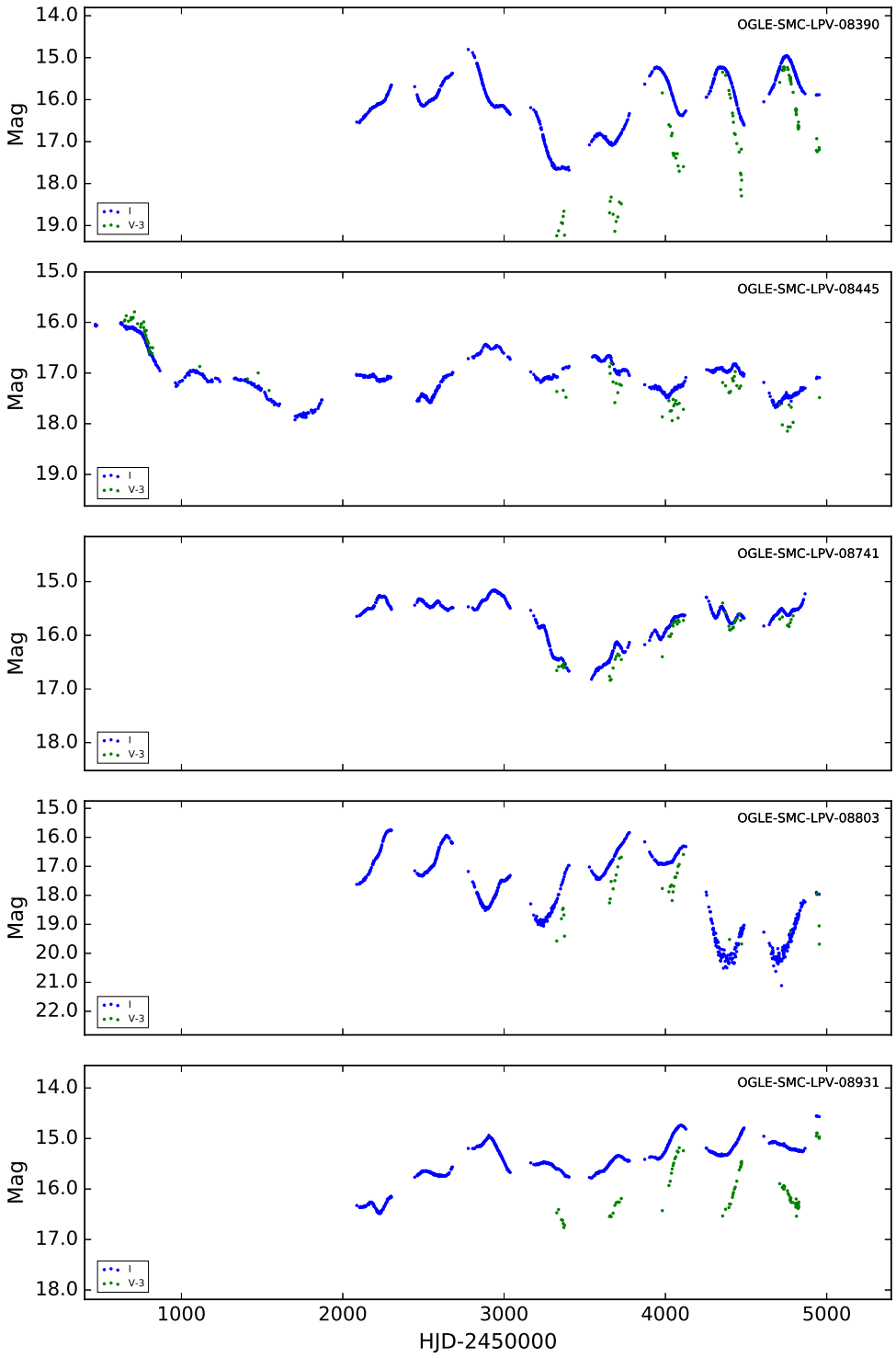

Figure 7. Light curves in I (*blue*) and V (*green*) of new DY Per candidates in the SMC.

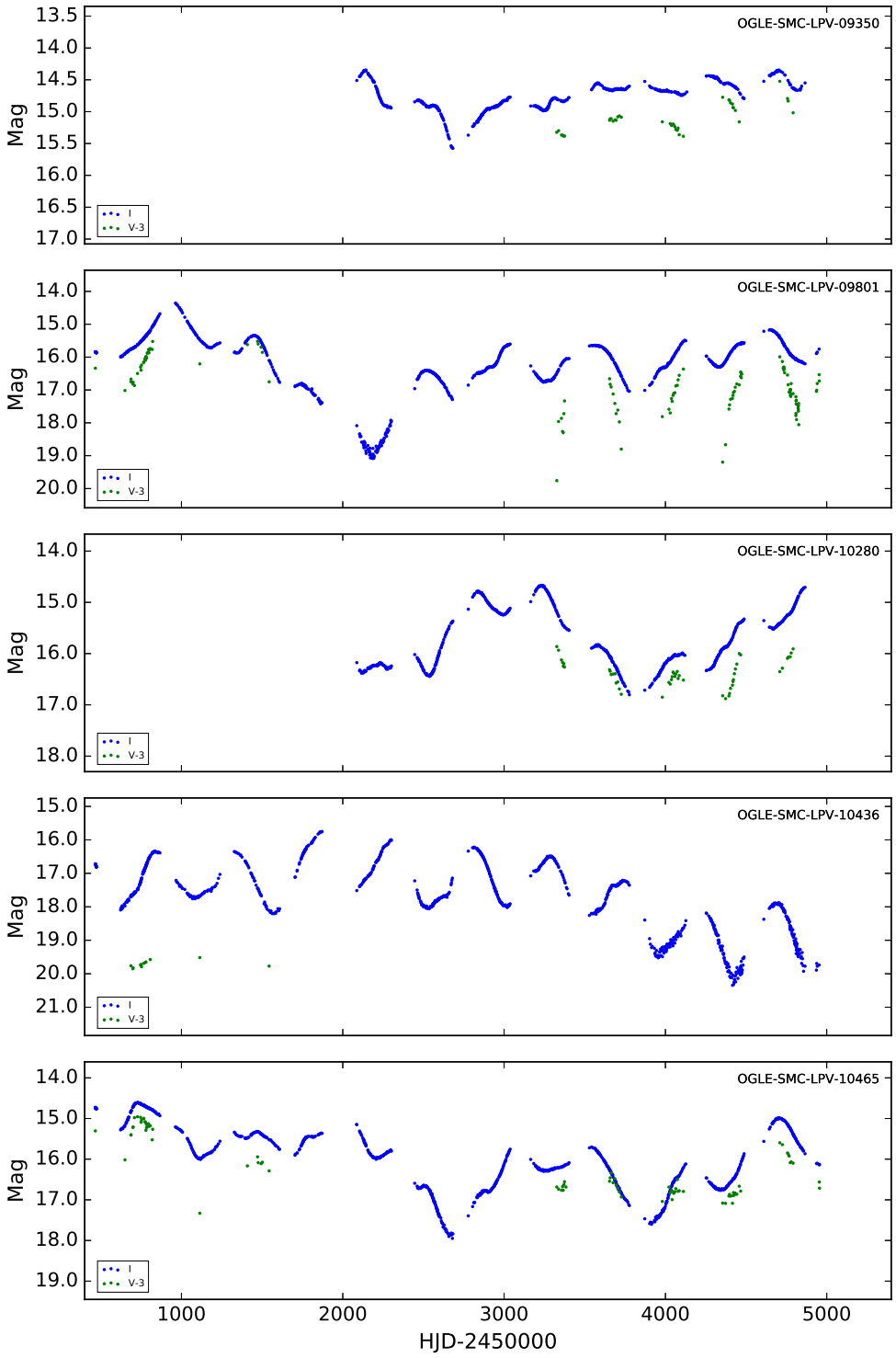

Figure 8. Light curves in I (*blue*) and V (*green*) of new DY Per candidates in the SMC.

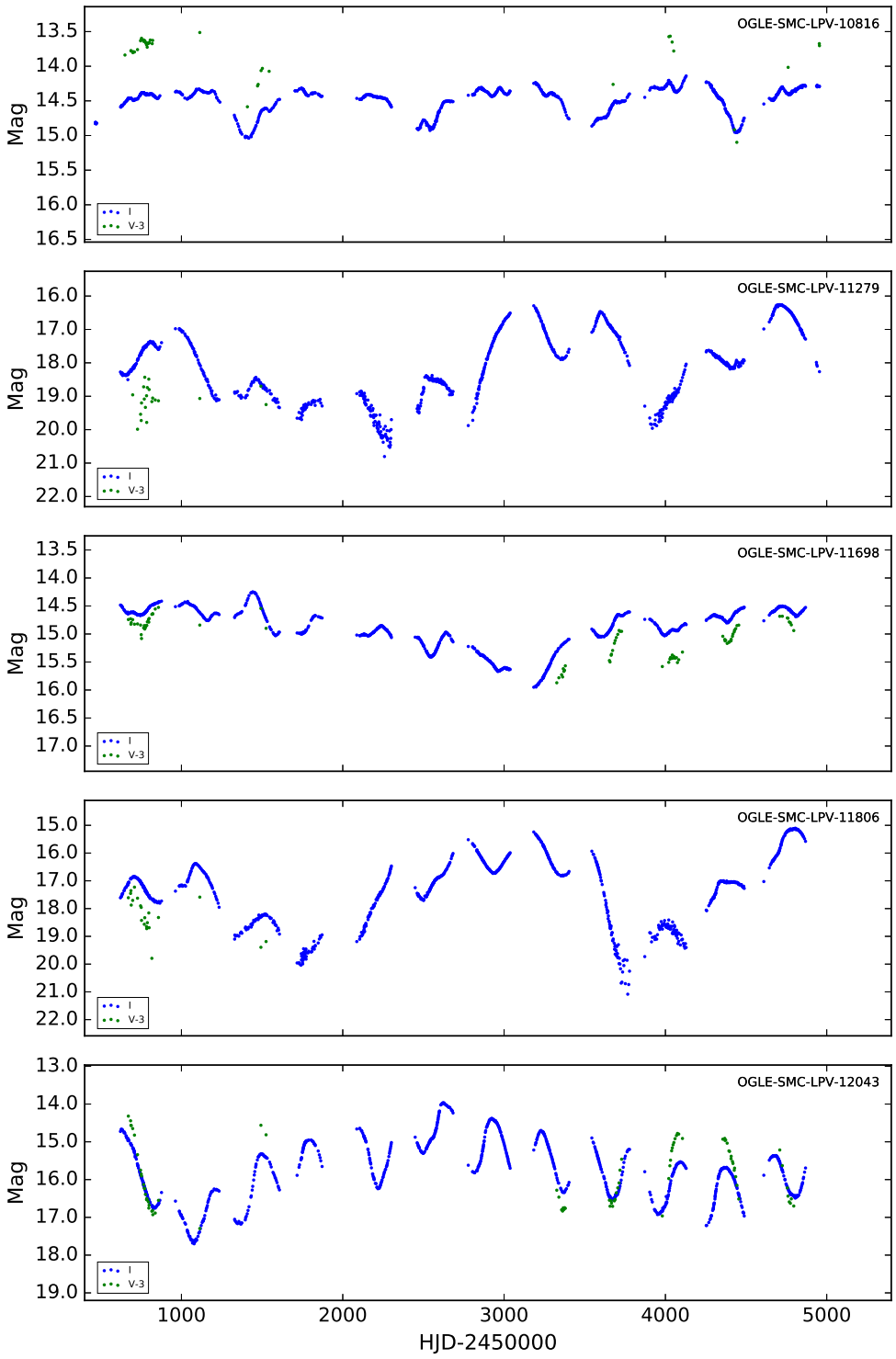

Figure 9. Light curves in I (*blue*) and V (*green*) of new DY Per candidates in the SMC.

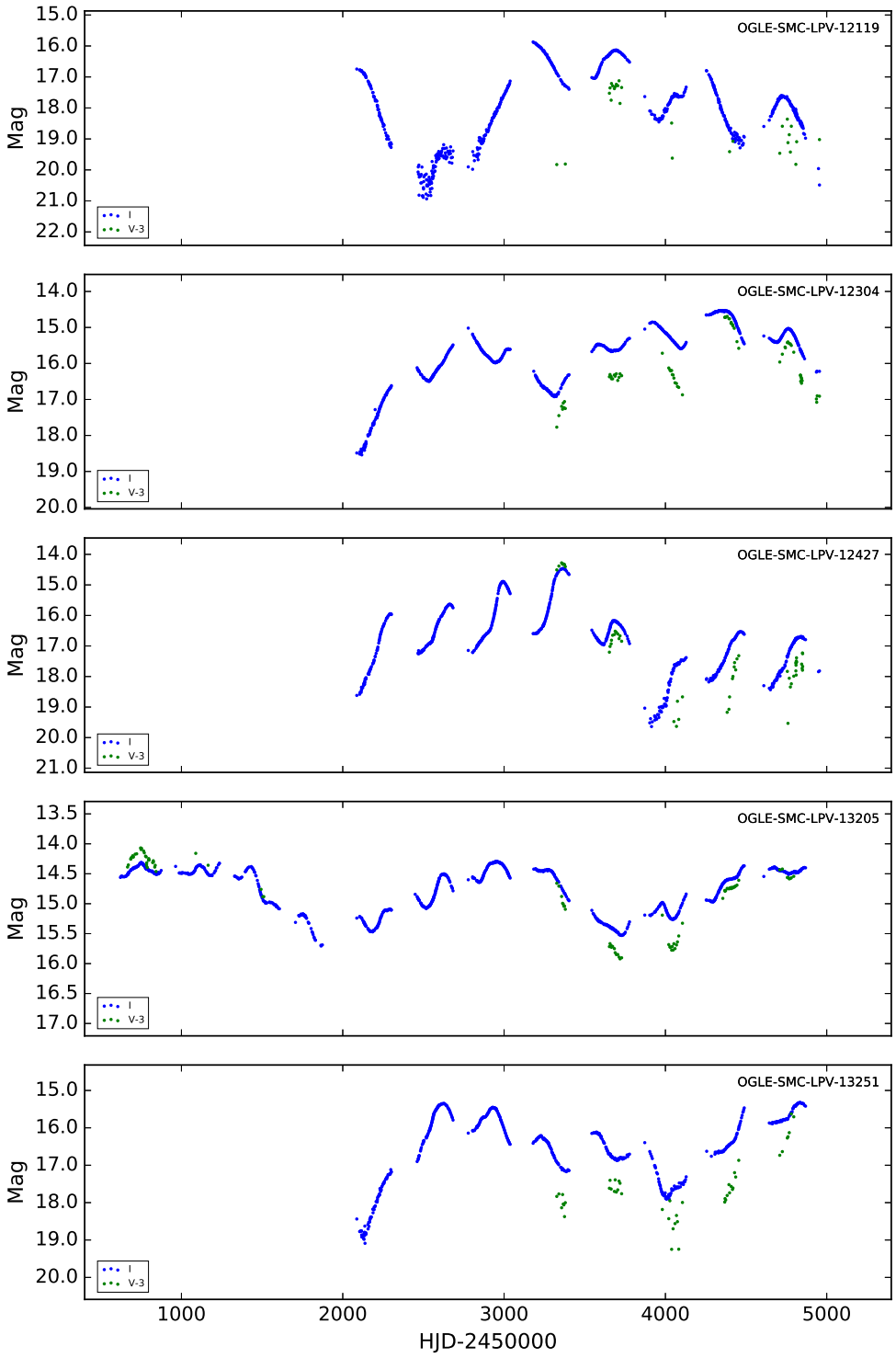

Figure 10. Light curves in I (*blue*) and V (*green*) of new DY Per candidates in the SMC.

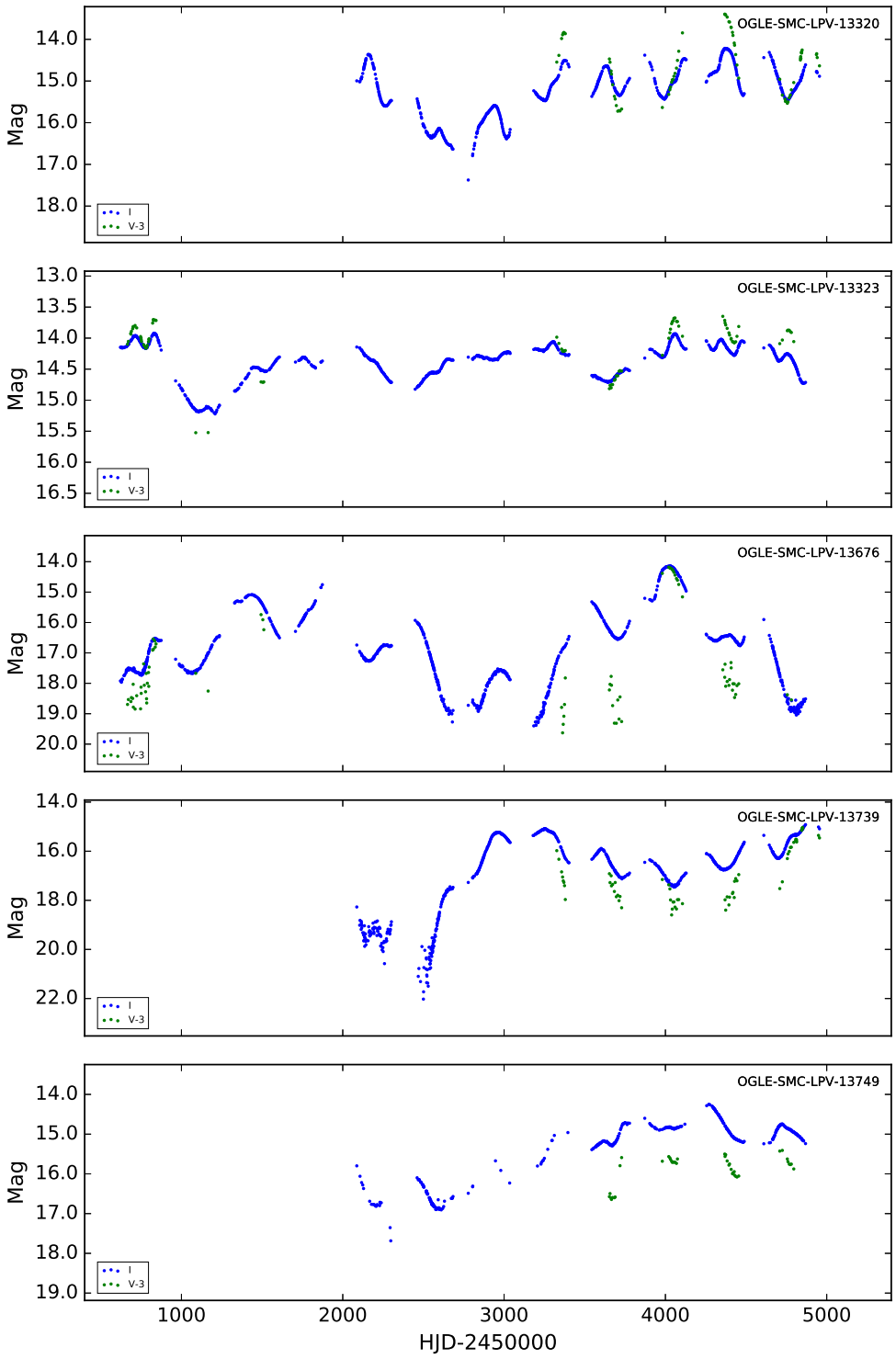

Figure 11. Light curves in I (*blue*) and V (*green*) of new DY Per candidates in the SMC.

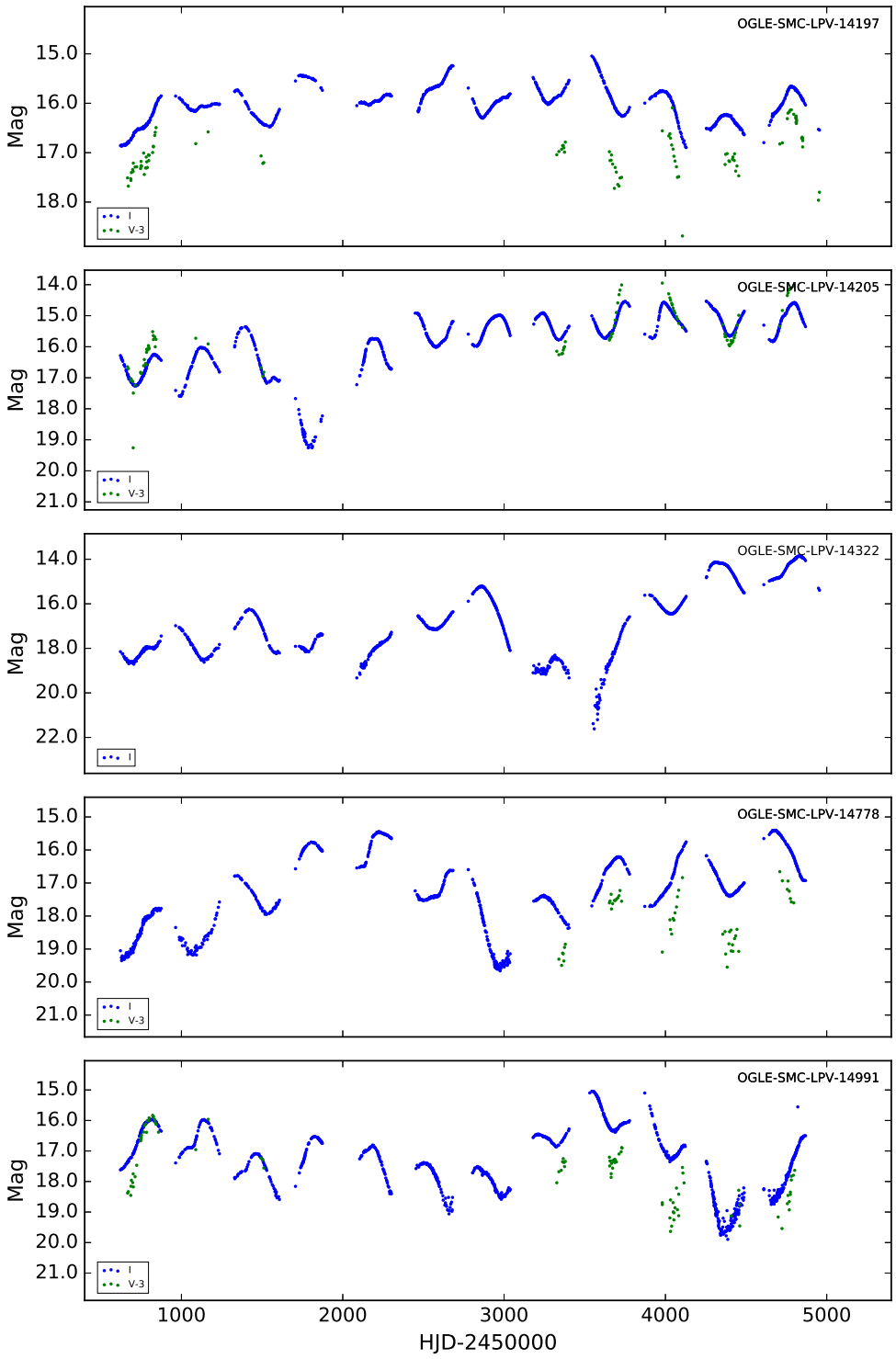

Figure 12. Light curves in I (*blue*) and V (*green*) of new DY Per candidates in the SMC.

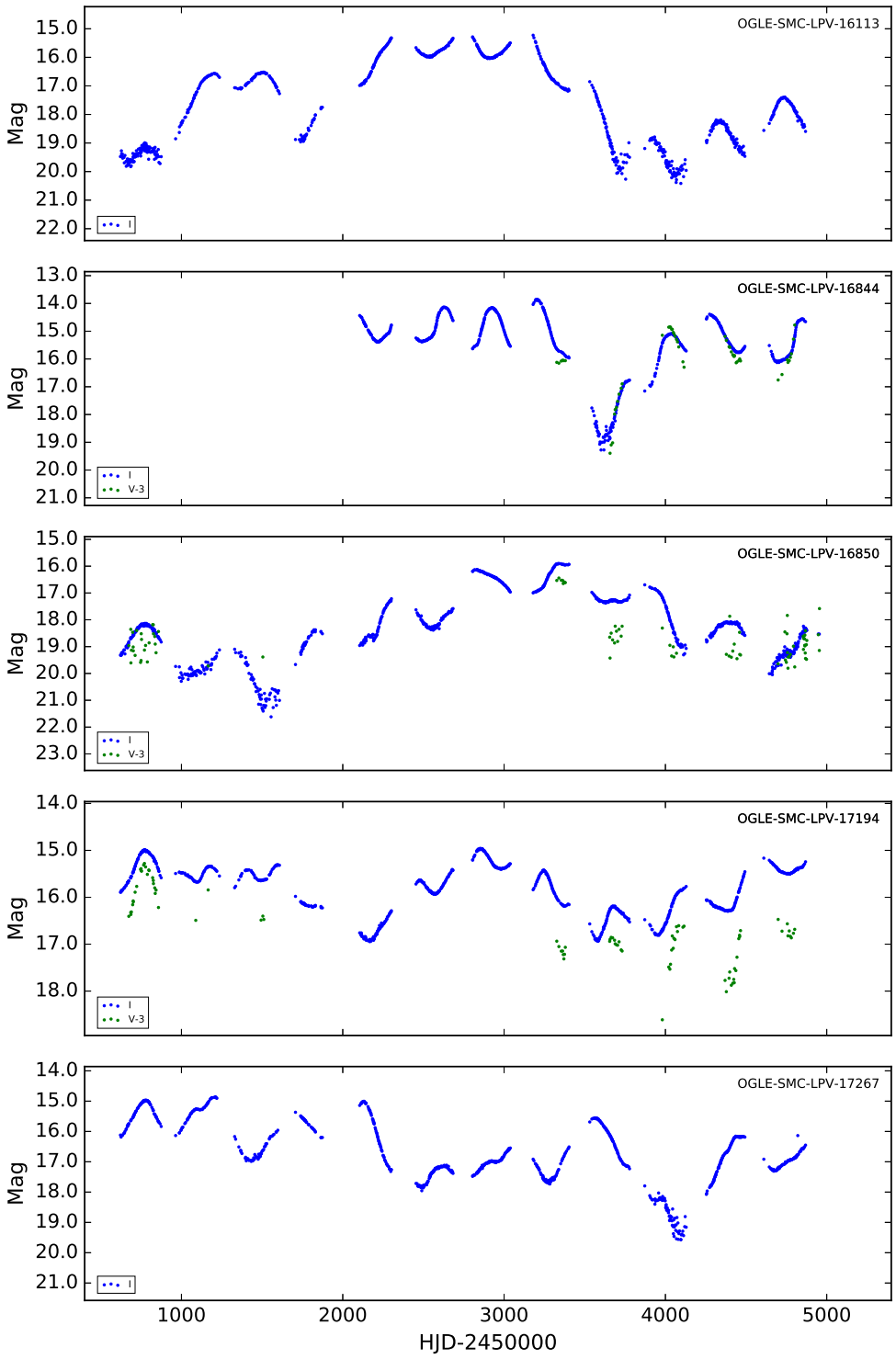

Figure 13. Light curves in I (*blue*) and V (*green*) of new DY Per candidates in the SMC.

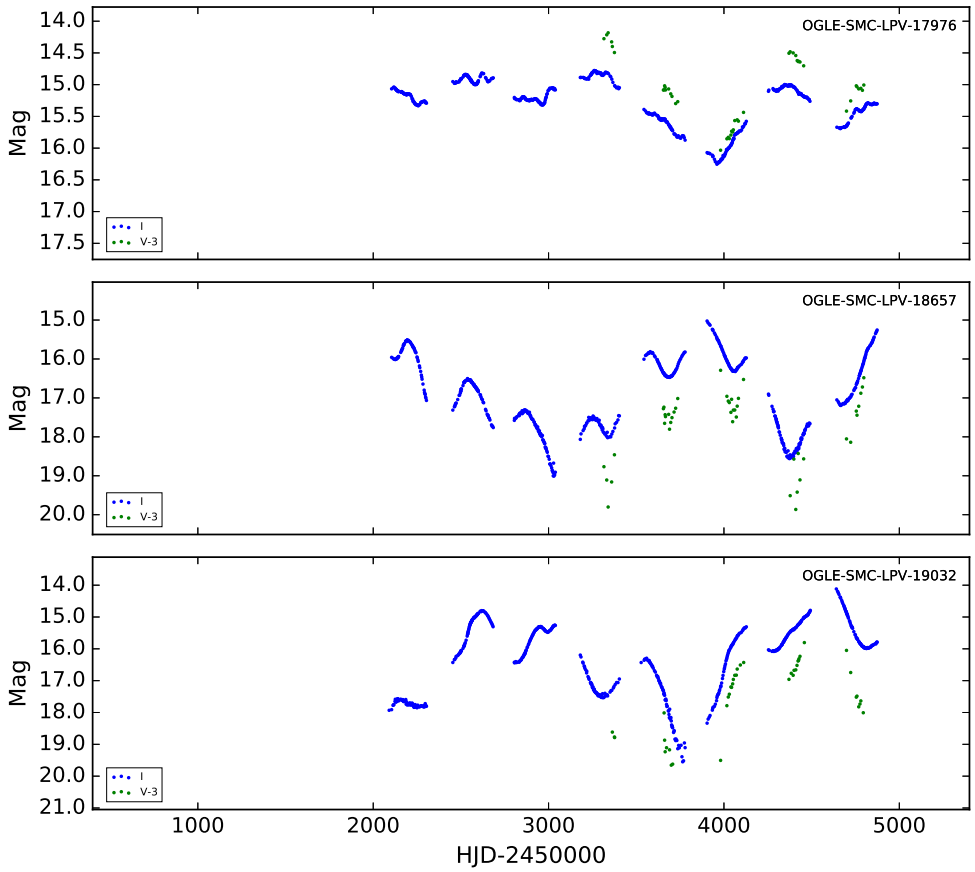

Figure 14. Light curves in I (*blue*) and V (*green*) of new DY Per candidates in the SMC.

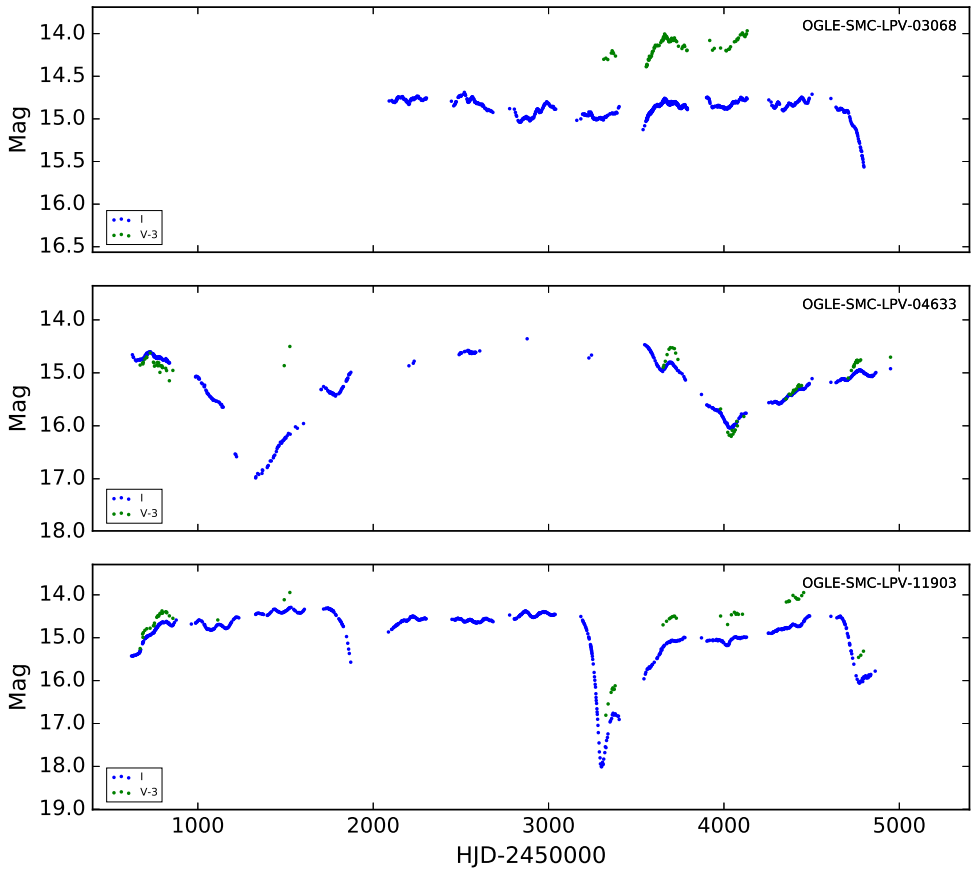

Figure 15. Light curves in I (*blue*) and V (*green*) of previously confirmed DY Per stars in the SMC (Tisserand et al. 2009), identified in this paper using OGLE data. Note the RCB-like light curve shape of OGLE-SMC-LPV-11903.

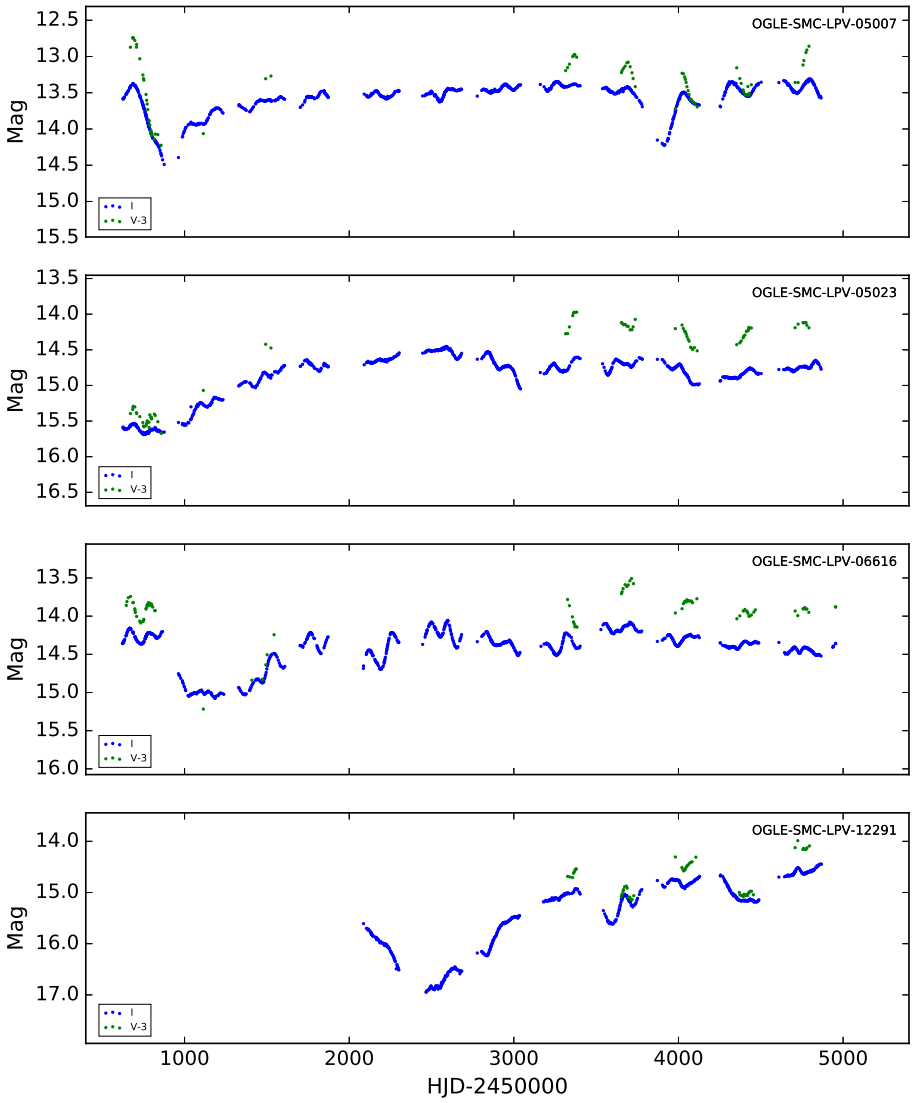

Figure 16. Light curves in I (*blue*) and V (*green*) of candidate DY Per stars in the SMC (Tisserand et al. 2009), identified in this paper using OGLE data. Note that we include in this plot the "borderline" DY Per-like star OGLE-SMC-LPV-05007 (see text for details).

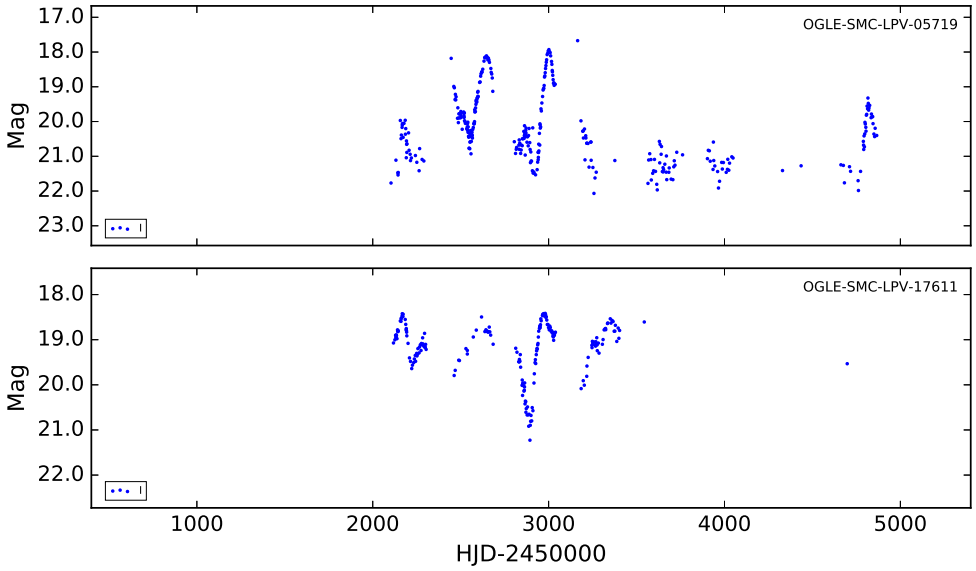

Figure 17. (*Upper panel*): light curve in I (*blue*) of a known RCB candidate in the SMC (MSX-SMC-014; Kraemer et al. 2005), identified in this paper as OGLE-SMC-LPV-05719. (*Bottom panel*): our new RCB candidate OGLE-SMC-LPV-17611.

COMMISSIONS G1 AND G4 OF THE IAU
INFORMATION BULLETIN ON VARIABLE STARS
Volume 62 Number 6191 DOI: 10.22444/IBVS.6191

Konkoly Observatory
Budapest
2 January 2017
HU ISSN 0374 – 0676

NEW TIMES OF MINIMA OF SOME ECLIPSING BINARY STARS

BULUT, İ.[1,3]; KABAŞ, A.[2,3]; NEHİR, Ç.[2,3]; ALLAK, S.[1,3]; NESLİHAN, K.[2,3]; YILAN, E.[1,3]; DOĞAN, M.[1,3]; GÜNEŞ, M.[2,3]; BULUT, A.[2,3]; DEMİRCAN, O.[1,3]

[1] Department of Space Sciences and Technologies, Faculty of Arts and Sciences, Çanakkale Onsekiz Mart University, Terzioğlu Kampüsü, TR-17020, Çanakkale, Turkey; e-mail: ibulut@comu.edu.tr

[2] Department of Physics, Faculty of Arts and Sciences, Çanakkale Onsekiz Mart University, Terzioğlu Kampüsü, TR-17020, Çanakkale, Turkey

[3] Astrophysics Research Centre and Observatory, Çanakkale Onsekiz Mart University, Terzioğlu Kampüsü, TR-17020, Çanakkale, Turkey

Observatory and telescope:
30-cm Schmidt-Cassegrain (T30), 40-cm Cassegrain-Schmidt (T40), 0.6-m Ritchey-Chrétien (T60) and 122-cm Cassegrain-Nasmyth (T122) telescopes of Çanakkale Onsekiz Mart University Observatory, Çanakkale.

Detector:	Apogee ALTA U47 CCD camera, Peltier cooling, E2V CCD47-10 chip, $15' \times 15'$ FOV, 1024×1024 pixels. Apogee ALTA U42 CCD camera, Peltier cooling, E2V CCD47-10 chip, $15' \times 15'$ FOV, 2048×2048 pixels. ST237 camera, Peltier cooling, TC237 chip, $11' \times 8'$ FOV, 640×480 pixels. STL1001E camera, Peltier cooling, KAF-1001E chip, $28' \times 28'$ FOV, 1024×1024 pixels.

Method of data reduction:
Reduction of the CCD frames was made with C-MUNIPACK software (`http://c-munipack.sourceforge.net/`).

Method of minimum determination:
The minima times were computed with the Kwee – van Woerden method (Kwee & van Woerden, 1956).

Times of minima:

Star name	Time of min. HJD 2400000+	Error	Type	Filter	Rem.
CN And	57244.4176	0.0003	II	*BVR*	T60
	57251.3595	0.0003	II	*BVR*	T60
	57254.3652	0.0002	I	*BVR*	T60
V376 And	57362.4344	0.0001	II	*VR*	T40
	57364.4204	0.0002	I	*BVR*	T40
OO Aql	57240.5483	0.0001	II	*BVR*	T60
	57247.3888	0.0001	I	*BVR*	T60
	57260.3130	0.0002	II	*BVR*	T60
SS Ari	57385.2454	0.0011	I	*BVR*	T30
	57385.3541	0.0021	II	*BVR*	T30
	57634.5158	0.0002	II	*VR*	T40
	57637.5596	0.0002	I	*VR*	T40
	57655.4241	0.0014	I	*VR*	T40
XY Boo	56384.4471	0.0002	I	*BVR*	T122
	56387.4123	0.0002	I	*BVR*	T122
	56387.5998	0.0001	II	*BV*	T122
	56448.3711	0.0002	II	*BV*	T122
	57126.4146	0.0003	I	*BVR*	T30
	57162.3595	0.0001	I	*BR*	T30
	57188.4856	0.0003	II	*B*	T30
BI CVn	57125.3925	0.0002	II	*BVR*	T30
	57125.5822	0.0001	I	*BVR*	T30
	57141.3373	0.0003	I	*BVR*	T30
	57141.5297	0.0003	II	*BVR*	T30
	57151.3264	0.0002	I	*BVR*	T30
	57151.5190	0.0002	II	*BVR*	T30
	57152.4788	0.0002	I	*BVR*	T30
VW Cep	57331.3372	0.0002	II	*BVR*	T30
	57343.3032	0.0001	II	*BVR*	T30
	57343.4462	0.0003	I	*BVR*	T30
	57593.4838	0.0033	II	*BVR*	T40
	57600.4120	0.0012	I	*BVR*	T40
RW Com	57099.4578	0.0002	I	*BVR*	T30
	57129.3634	0.0002	I	*BVR*	T30
	57129.4818	0.0001	II	*BVR*	T30
	57134.3478	0.0002	I	*BVR*	T30
V401 Cyg	57230.3695	0.0002	I	*BVR*	T30
	57231.5354	0.0003	I	*BVR*	T30
	57256.3101	0.0006	II	*BVR*	T30
	57258.3377	0.0003	I	*BVR*	T30

Times of minima:

Star name	Time of min. HJD 2400000+	Error	Type	Filter	Rem.
V2150 Cyg	56945.3872	0.0004	I	*BVR*	T30
	56950.3830	0.0005	II	*BVR*	T30
	57255.3538	0.0004	I	*BVR*	T30
	57620.4085	0.0004	II	*BVR*	T40
	57624.3005	0.0007	II	*BVR*	T40
	57632.2891	0.0006	I	*BVR*	T40
CM Dra	57168.3932	0.0002	I	*BVR*	T30
EZ Hya	57231.5354	0.0004	II	*BVR*	T40
	57476.2982	0.0003	I	*BVR*	T40
	57478.3242	0.0003	II	*BVR*	T40
V502 Oph	57123.3120	0.0002	I	*BVR*	T30
	57124.3758	0.0002	II	*BVR*	T30
	57130.3193	0.0007	I	*BVR*	T30
	57131.4254	0.0002	II	*BVR*	T30
	57495.5418	0.0003	II	*BVR*	T30
	57498.5442	0.0003	I	*BVR*	T30
	57505.5824	0.0004	II	*BVR*	T40
	57509.3875	0.0002	I	*BVR*	T40
	57542.4681	0.0005	I	*BVR*	T40
	57543.3749	0.0002	I	*BVR*	T40
	57544.5107	0.0008	II	*BVR*	T40
	57582.3674	0.0002	I	*BVR*	T40
U Peg	57362.2868	0.0001	II	*BVR*	T30
	57384.2106	0.0001		*BVR*	T30
BX Peg	57252.4269	0.0001	I	*BVR*	T30
	57495.5418	0.0003	I	*BVR*	T40
	57498.5442	0.0003	I	*BVR*	T40
	57509.3875	0.0003	I	*BVR*	T40
OU Ser	57173.4168	0.0006	II	*BVR*	T30
	57174.4622	0.0003	I	*BVR*	T30
W UMa	57476.3183	0.0003	I	*BVR*	T30
	57476.4853	0.0001	II	*BVR*	T30
	57496.3362	0.0001	I	*BVR*	T30
	57496.5031	0.0001	II	*BVR*	T30
	57523.3605	0.0001	I	*BVR*	T30

Times of minima:					
Star name	Time of min. HJD 2400000+	Error	Type	Filter	Rem.
AW UMa	57123.3120	0.0002	I	*BVR*	T30
	57124.3758	0.0023	II	*BVR*	T30
	57130.3193	0.0007	I	*BVR*	T30
	57131.4254	0.0002	II	*BVR*	T30
HN UMa	57385.5690	0.0005	I	*BVR*	T60

Explanation of the remarks in the table:

In the Remarks column of Times of Minima table, telescopes used in the observations are given.

Remarks:

We present 80 minima times of 19 eclipsing binaries.

Acknowledgements:

This study has been supported by the Turkish TÜBİTAK under the Grant No. 114F166.

Reference:

Kwee, K. K., van Woerden, H., 1956, *Bull. Astron. Inst. Netherlands*, **12**, 327

COMMISSIONS G1 AND G4 OF THE IAU
INFORMATION BULLETIN ON VARIABLE STARS
Volume 62 Number 6192 DOI: 10.22444/IBVS.6192

Konkoly Observatory
Budapest
2 January 2017

HU ISSN 0374 – 0676

V2477 Cyg — A W–TYPE CONTACT ECLIPSING BINARY

NELSON, ROBERT H.[1,2]

[1] 393 Garvin Street, Prince George, BC, Canada, V2M 3Z1
email: bob.nelson@shaw.ca

[2] Guest investigator, Dominion Astrophysical Observatory, Herzberg Institute of Astrophysics, National Research Council of Canada

The variability of V2477 Cyg (NSV 13016 = NSVS 3227395 = HD 239379 = TYC 3945–1423–1), amongst many others, was discovered photographically by Hoffmeister (1963) as part of the Sonneberg Survey (Gessner 1966). The former gave coordinates and a finder chart, described the system as a short period variable, and designated it as S 7891. Skiff (1999) identified many Sonneberg variables, amongst them S 7891, giving accurate coordinates and associating them with existing names. The first accessible elements (epoch, period) were published by Otero & Wils (2005), who also classified the system as EW, and listed the magnitude range and spectral type. Since then, there have been a number of eclipse timings, but no light curve analysis.

In order to rectify this lack, the author first secured, in April of 2015 and again in September of 2016, a total of 6 medium resolution (R∼10000 on average) spectra of V2477 Cyg at the Dominion Astrophysical Observatory (DAO) in Victoria, British Columbia, Canada using the Cassegrain spectrograph attached to the 1.85 m Plaskett Telescope. He used the 21181 grating with 1800 lines/mm, blazed at 5000 Å giving a reciprocal linear dispersion of 10 Å/mm in the first order. The wavelength ranged from 5000 to 5260 Å, approximately. A log of observations is given in Table 1. The following elements were used for both radial velocity (RV) and photometric phasing:

$$JD(\mathrm{Hel})_{\mathrm{MinI}} = 2457176.2636 + 0.3112515\,\mathrm{E} \qquad (1)$$

Frame reduction was performed by software 'RaVeRe' (Nelson 2009). See Nelson et al. (2014) for further details. The normalized spectra are reproduced in Fig. 1, sorted by phase. Note towards the right the strong neutral iron lines (at 5167.487 and 5171.595 Å) and the strong neutral magnesium triplet (at 5167.33, 5172.68, and 5183.61 Å).

Radial velocities were determined using the Rucinski broadening functions (Rucinski 2004, Nelson 2010b, Nelson et al. 2014). An Excel worksheet with built-in macros (written by him) was used to do the necessary RV conversions to geocentric and back to heliocentric values (Nelson 2010a). The resulting RV determinations are also presented in Table 1. These results were corrected 5.2% up for the 2015 data, but only 1% for the 2016 data (owing to the shorter exposure times) to allow for the small phase smearing. Correction was achieved by dividing the RVs by the factor $f = (\sin X)/X$; where $X = 2\pi t/P$, where t denotes exposure time and P denotes the orbital period. For spherical stars, this

Table 1: Log of DAO observations.

DAO Image No.	Mid Time (HJD–2400000, d)	Exposure (sec)	Phase at mid-exp	RV_1 (km/s)	RV_2 (km/s)
13277	57299.7801	2400	0.839	+189.4(6.2)	−123.5(7.9)
13286	57299.8831	2400	0.169	−269.2(5.6)	+72.6(7.9)
13321	57300.6639	2400	0.678	+207.5(7.9)	−150.8(7.8)
13335	57300.8815	2400	0.377	−193.9(3.7)	+56.4(4.5)
9359	57646.7883	1200	0.719	+219.5(8.6)	−141.3(7.0)
9489	57652.8783	900	0.285	−267.4(6.5)	+76.9(9.7)

correction is exact; in other cases, it can be shown to be close enough for any deviation to fall below observational errors. The mean rms errors for RV_1 and RV_2 are 6.4 and 7.5 km/s, respectively, and the overall rms deviation from the (sinusoidal) curves of best fit is 9.7 km/s. The best fit yielded the values $K_1 = 256.6(1.1)$ km/s, $K_2 = 118.1(1.1)$ km/s and $V_\gamma = -30.5(0.6)$ km/s, and thus a mass ratio $q_{\rm sp} = K_1/K_2 = M_2/M_1 = 2.17(2)$.

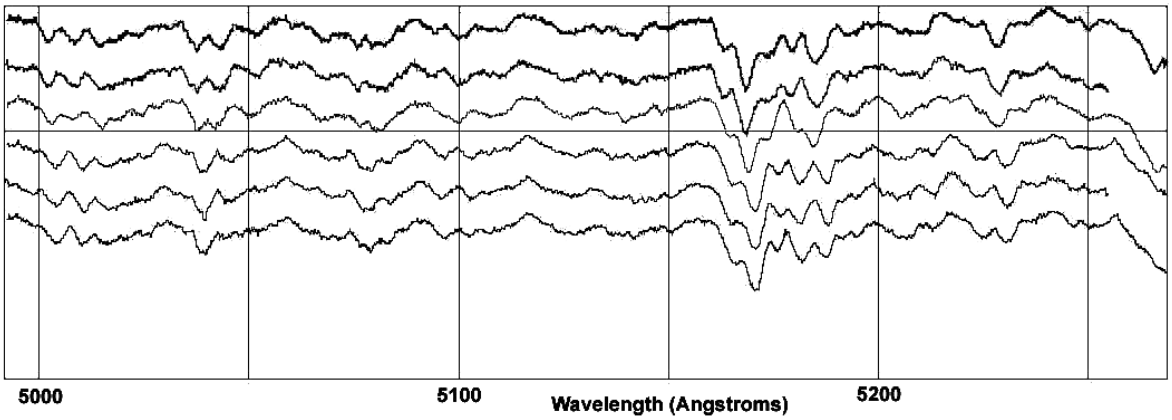

Figure 1. V2477 Cyg spectra at phases 0.169, 0.285, 0.377, 0.678, 0.719, 0.839 (from top to bottom).

Representative broadening functions, at phases 0.285 and 0.719 are depicted in Figs. 2 and 3, respectively. Smoothing by a Gaussian filter is routinely done in order to centroid the peak values for determining the RVs.

In May 8-11 of 2015, the author took a total of 201 frames in V, 204 in R_C and 199 in the I_C band at his private observatory in Prince George, BC, Canada. The telescope was a 33 cm f/4.5 Newtonian on a Paramount ME mount; the camera was a SBIG ST-10XME. Standard reductions were then applied. The variable, comparison and check stars are listed in Table 2. The coordinates and magnitudes for V2477 Cyg are from the Tycho Catalogue (Hog et al. 2000), those for the other two stars are from the GSC catalogue.

The author used the 2003 version of the Wilson-Devinney (WD) light curve and RV analysis program with Kurucz atmospheres (Wilson & Devinney 1971, Wilson 1990, Kallrath et al. 1998) as implemented in the Windows front-end software `WDwint` (Nelson 2009) to analyze the data. To get started, the spectral type F8 (taken from SIMBAD, no reference given; main sequence assumed) was adopted. Interpolated tables from Cox (2000) gave a temperature $T_1 = 6250 \pm 216$ K and $\log g = 4.367 \pm 0.006$. (The quoted er-

Table 2: Details of the variable, comparison and check stars.

Object	GSC	RA (J2000)	Dec (J2000)	V (mag)	$B-V$ (mag)
Variable	3945-1423	$20^{\rm h}18^{\rm m}58\overset{\rm s}{.}9357$	$56°36'19\overset{''}{.}272$	10.00(3)	+0.67(5)
Comparison	3495-1732	$20^{\rm h}19^{\rm m}33\overset{\rm s}{.}13$	$56°34'16\overset{''}{.}33$	10.44(5)	+1.063
Check	3945-1197	$20^{\rm h}18^{\rm m}52\overset{\rm s}{.}0$	$56°31'32\overset{''}{.}0$	10.7	N/A

rors refer to one and one half spectral sub-classes.) An interpolation program by Terrell (1994, available from Nelson 2009) gave the Van Hamme (1993) limb darkening values; and finally, a logarithmic (LD = 2) law for the limb darkening coefficients was selected, appropriate for temperatures < 8500 K (ibid.). The limb darkening coefficients are listed in Table 3. (The values for the second star are based on the later-determined temperature of 5880 K and assumed spectral type of G1.) Convective envelopes for both stars were used, appropriate for cooler stars (hence values gravity exponent $g = 0.32$ and albedo $A = 0.500$ were used for each).

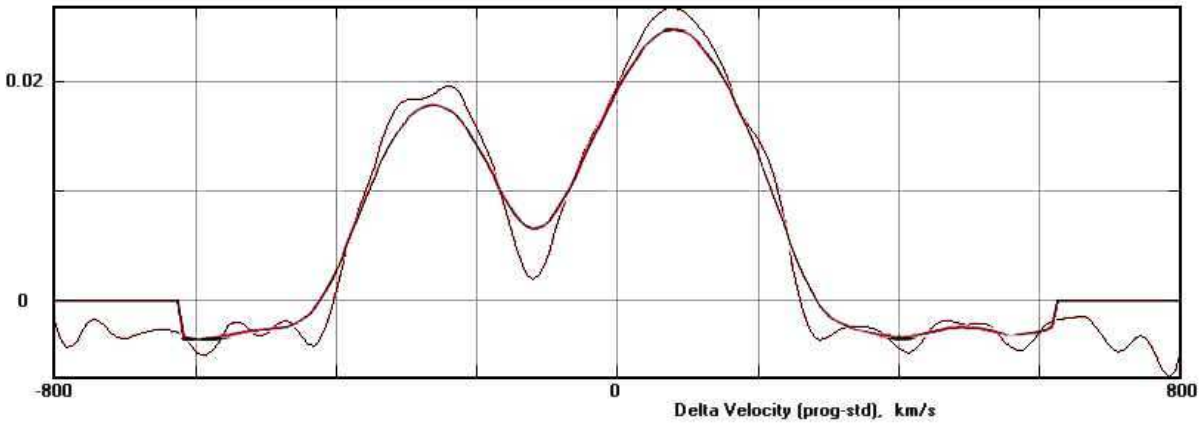

Figure 2. Broadening function at phase 0.285–smoothed and unsmoothed.

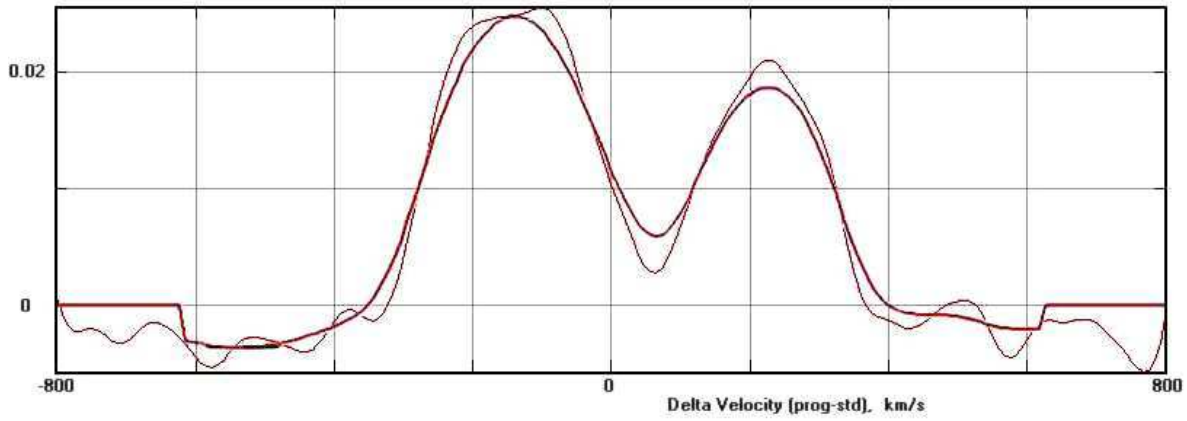

Figure 3. Broadening function at phase 0.719–smoothed and unsmoothed.

Table 3: Limb darkening values from Van Hamme (1993).

Band	x_1	x_2	y_1	y_2
Bol	0.647	0.647	0.179	0.214
V	0.790	0.755	0.164	0.242
R_C	0.723	0.684	0.203	0.260
I_C	0.637	0.600	0.212	0.254

From the GCVS 4 designation (EW) and from the shape of the light curve, mode 3 (contact binary) mode was used. Early on, it was noted that the maxima between eclipses were slightly unequal. This is the O'Connell effect (Davidge & Milone 1984, and references therein) and is usually explained by the presence of one or more star spots. Because of the only slight difference between Max I (phase 0.25) and Max II (phase 0.75), a solution was first sought with no spots; later on, one was added first to star 2, and then to star 1. The latter gave better results and was adopted. In any case, the spotted solution gave only a marginal improvement in the fit. However, both unspotted and spotted solutions are presented in Table 4, even though the values are identical in most cases.

Convergence by the method of multiple subsets was reached in a small number of iterations. (The subsets were: (a, i, Ω_1, L_1), (i, T_2, q), and (V_γ, i, Ω_1). Almost immediately, it was realized that a solution was impossible without third light (el_3). Therefore third light was added to the preliminary fitting, and that parameter was added to the third subset. Also, only values of the inclination near 90° were possible, with 90° always giving the best fit. In view of the fact that differential corrections always suggested non-physical corrections, the inclination was not varied thereafter.

Detailed reflections were tried, with $n_{\rm ref}$ = 1-3, but there was little—if any—difference in the fit from the simple treatment. There are certain uncertainties in the process (see Csizmadia et al. 2013, Kurucz 2000). On the other hand, the solution is very weakly dependent on the exact values used.

In the first set of iterations (i.e., with no spot), when a fit was near, the sigmas for each dataset were adjusted, based on the output of WD (viz. computed from the sum of residuals for each dataset plus number of points).

The model is presented in Table 4. For the most part, the error estimates are those provided by the WD routines and are known to be low; however, it is a common practice to quote these values and we do so now. Also, estimating the uncertainties in temperatures T_1 and T_2 is somewhat problematic. A common practice is to quote the temperature difference over—say—one and one half spectral sub-classes (assuming that the classification is good to one or two spectral sub-classes, the precision being unknown). In addition, various different calibrations have been made (Cox 2000, page 388–390 and references therein, and Flower 1996), and the variations between the various calibrations can be significant. If the classification is ± one sub-class, an uncertainty of ± 200 K to the absolute temperatures of each, would be reasonable. (The modelling error in temperature T_2, *relative to* T_1, is indicated by the WD output to be much smaller, around 5 K.)

The light curve data and the fitted curves are depicted in Figures 4-6. The residuals (in the sense observed-calculated) are also plotted, shifted upwards by 0.45 units.

The radial velocities are shown in Fig. 7. A three-dimensional representation from Binary Maker 3 (Bradstreet 1993) is shown in Fig. 8.

Table 4: Wilson-Devinney parameters.

WD	No spot	Spot		
Quantity	Value	Value	error	Unit
Temperature T_1	6250	6250	[fixed]	K
Temperature T_2	5879	5880	5	K
$q = m_2/m_1$	1.919	1.919	0.002	—
Potential $\Omega_1 = \Omega_2$	5.026	5.026	0.003	—
Inclination, i	90	90	[fixed]	deg
Semi-maj. axis, a	2.39	2.39	0.03	$R_\odot$
V_γ	−28.9	−30.1	2.7	km/s
Fill-out, f	0.1204	0.1204	—	—
Spot co-latitude	—	75	10	deg
Spot longitude	—	147	2	deg
Spot radius	—	18	2	deg
Spot temp. factor	—	0.976	0.002	—
el (V)	0.085	0.085	0.002	—
el (R_C)	0.084	0.084	0.002	—
el (I_C)	0.083	0.083	0.002	—
$L_1/(L_1 + L_2)$ (V)	0.4198	0.4196	0.0007	—
$L_1/(L_1 + L_2)$ (R_C)	0.4094	0.4093	0.0006	—
$L_1/(L_1 + L_2)$ (I_C)	0.4013	0.4012	0.0007	—
r_1 (pole)	0.3130	0.3130	0.0004	orb. rad.
r_1 (side)	0.3283	0.3283	0.0005	orb. rad.
r_1 (back)	0.3675	0.3675	0.0008	orb. rad.
r_2 (pole)	0.4204	0.4204	0.0003	orb. rad.
r_2 (side)	0.4483	0.4483	0.0004	orb. rad.
r_2 (back)	0.4805	0.4805	0.0006	orb. rad.
Phase shift	−0.0007	−0.0007	0.0001	—
$\Sigma\omega^2_{\rm res}$	0.06952	0.06335	—	—

The WD output fundamental parameters and errors are listed in Table 5. Corresponding values from the spotted and unspotted solutions agreed within the displayed digits in all cases, so therefore only one set of values is given. Most of the errors are output or derived estimates from the WD routines. From Kallrath & Milone (1998), the fill-out factor is $f = (\Omega_{\rm I} - \Omega)/(\Omega_{\rm I} - \Omega_{\rm O})$, where Ω is the modified Kopal potential of the system, $\Omega_{\rm I}$ is that of the inner Lagrangian surface, and $\Omega_{\rm O}$, that of the outer Lagrangian surface, was also calculated.

To determine the distance r, the analysis proceeded as follows: first the WD routine gave the absolute bolometric magnitudes of each component; these were then converted to the absolute visual (V) magnitudes of both, $M_{V,1}$ and $M_{V,2}$, using the bolometric corrections BC = –0.160 and –0.190 for stars 1 and 2 respectively. The latter were taken from interpolated tables constructed from Cox (2000). The absolute V magnitude was then computed in the usual way, getting $M_V = 4.14 \pm 0.03$ magnitudes. The apparent magnitude in the V passband was $V = 10.00 \pm 0.03$, taken from the Tycho values (Hog, et al., 2000) and converted to a Johnson magnitude using relations due to Henden (2001). The colour excess (in $B - V$) was obtained in the usual way, by subtracting the tabular value of $B - V$ (for that spectral class) from the observed (converted Tycho) value. This

gave E$[B-V] = 0.18$ magnitudes. However, reference to the dust tables of Schlegel et al. (1998) revealed a value of E$[B-V] = 0.2823$ for those galactic coordinates. Since the E$[B-V]$ values have been derived from full-sky far-infrared measurements, they therefore apply to objects outside of the Galaxy; this value of E$[B-V]$ so derived then represents an upper limit for closer objects within the Galaxy. Hence the lower value of 0.18 is reasonable, and was adopted. (An uncertainty of—say—half this amount was used in the error calculation for distance.)

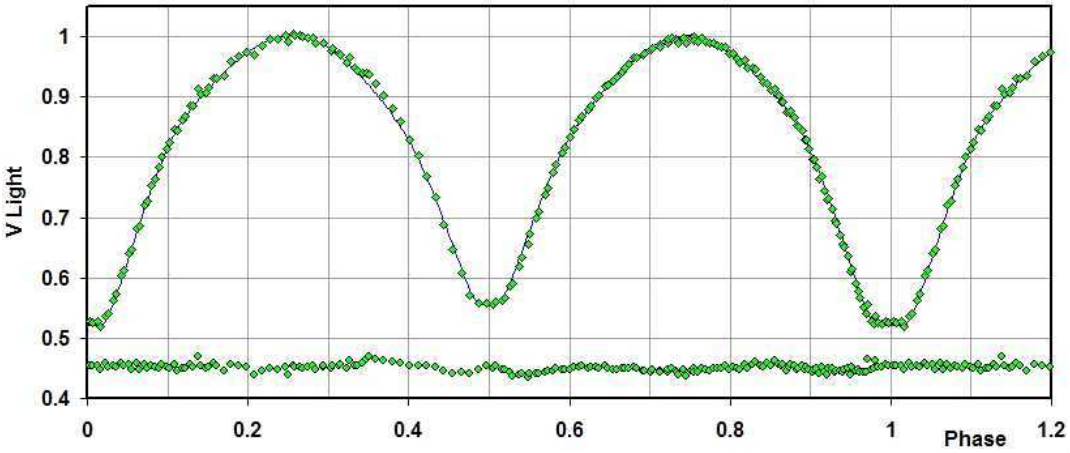

Figure 4. V light curves for V2477 Cyg – data, WD fit, and residuals.

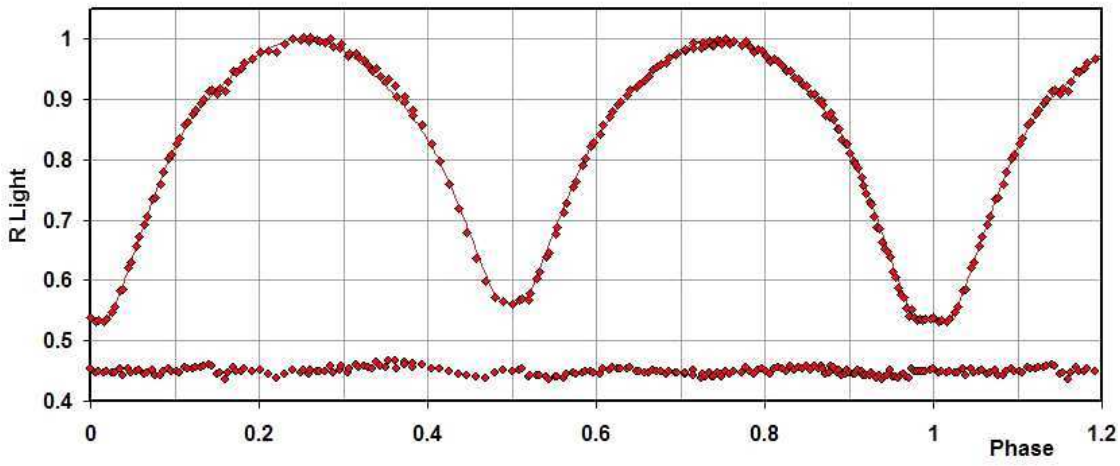

Figure 5. R_C light curves for V2477 Cyg – data, WD fit, and residuals.

Galactic extinction was obtained from the usual relation $A_V = R\mathrm{E}[B-V]$, using $R = 3.1$ for the reddening coefficient. Hence, distance $r = 112$ pc was calculated from the standard relation:

$$r = 10^{0.2(V-M_V-A_V+5)} \text{ pc} \qquad (2)$$

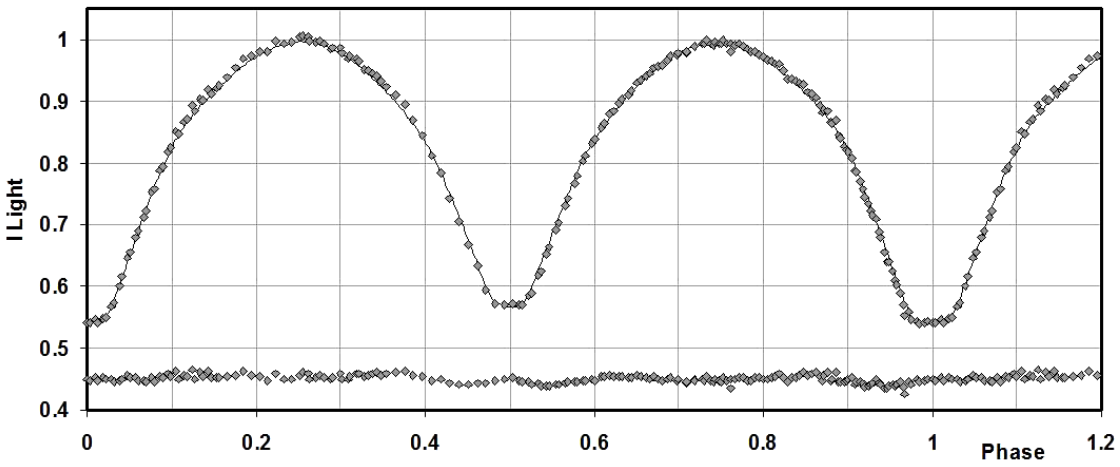

Figure 6. I_C light curves for V2477 Cyg – data, WD fit, and residuals.

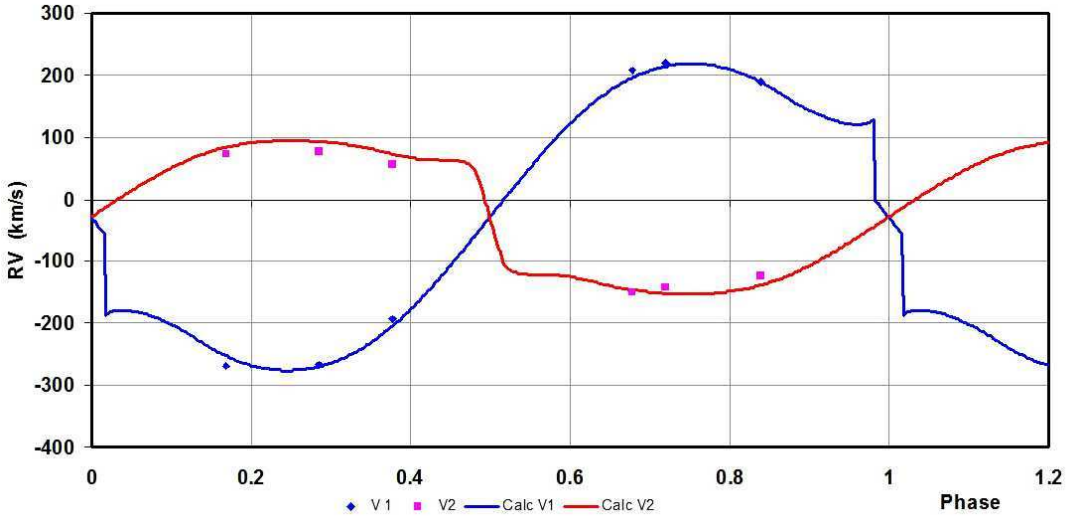

Figure 7. Radial velocity curves for V2477 Cyg – data and WD fit.

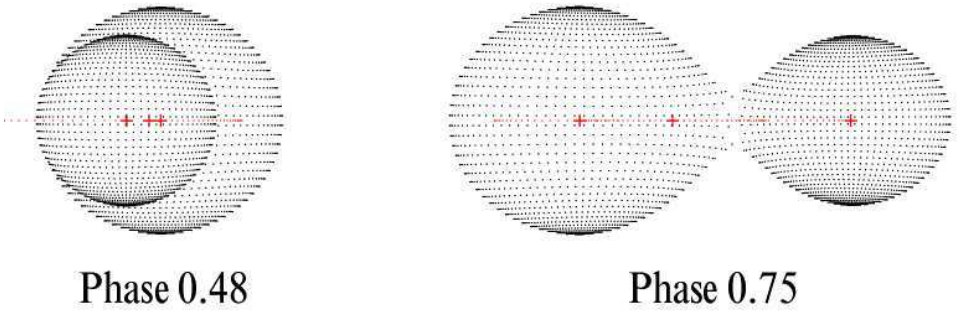

Figure 8. Binary Maker 3 representation of the system – at phases 0.48 and 0.75.

Table 5: Fundamental parameters.

Quantity	Value	Error	unit
Temperature, T_1	6250	200	K
Temperature, T_2	5880	200	K
Mass, m_1	0.65	0.02	$M_\odot$
Mass, m_2	1.24	0.02	$M_\odot$
Radius, R_1	0.81	0.01	$R_\odot$
Radius, R_2	1.08	0.01	$R_\odot$
$M_{\rm bol,1}$	4.91	0.02	mag
$M_{\rm bol,2}$	4.55	0.02	mag
log g_1	4.43	0.01	cgs
log g_2	4.47	0.01	cgs
Luminosity, L_1	0.895	0.02	$L_\odot$
Luminosity, L_2	1.25	0.02	$L_\odot$
Fill-out factor	0.12	0.005	—
Distance, r	112	15	pc

The errors were assigned as follows: $\delta M_{\rm bol,1} = \delta M_{\rm bol,2} = 0.014$, $\delta BC_1 = \delta BC_2 = 0.015$ (the variation of 1.5 spectral sub-classes), $\delta V = 0.03$, $\delta E(B–V) = 0.07$, all in magnitudes, and $\delta R = 0.1$. Combining the errors rigorously (i.e., by adding the variances) yielded an estimated error in r of 15 pc.

Some comments regarding the period variation are in order. An eclipse timing difference ($O - C$) plot is depicted in Fig. 9. It will be seen that even though the existing points, almost all derived using CCD detectors, display considerable scatter, it is still possible to fit a quadratic relation. (Notes: for determining the elements of equation 1, a tangent line was used, and the open square represents a rejected datum.) But what should one do with the original point from 1999 (at cycle 0)?

Rucinski et al. (2007 and references therein) showed that, for close binaries, a third component is very common. So therefore the light time effect (LiTE) (whereby the orbiting pair makes an orbit about the common centre of mass, and the light information may be advanced or retarded due to varying distance to the observer), may play a role in the period variation. Irwin (1952, 1959) provided the equations for computing the theoretical period variation, based on the period of the third star, P_3 and other orbital parameters.

Using these equations, it is possible to fit not one but many (at least seven) different LiTE relations to all the points using periods P3 ranging from 14 to 35 years. It is obvious that no definitive solution for the orbital parameters of the putative third star orbit will be possible without many new points spanning perhaps a decade or more. However the point is that it is at least plausible that the light time effect exists and that the point at 0,0 is not aberrant. The $O - C$ file may be found online at Nelson (2016).

In conclusion, the fundamental parameters of this system have been determined. It has been shown to have a low degree of contact, expressed by the fill-out parameter $f = 0.120$. This is typical for a W-type contact binary (Rucinski 1974). Also, the existence a significant third light is consistent with the high proportion of contact binaries having a third component (Rucinski 2007, and references therein).

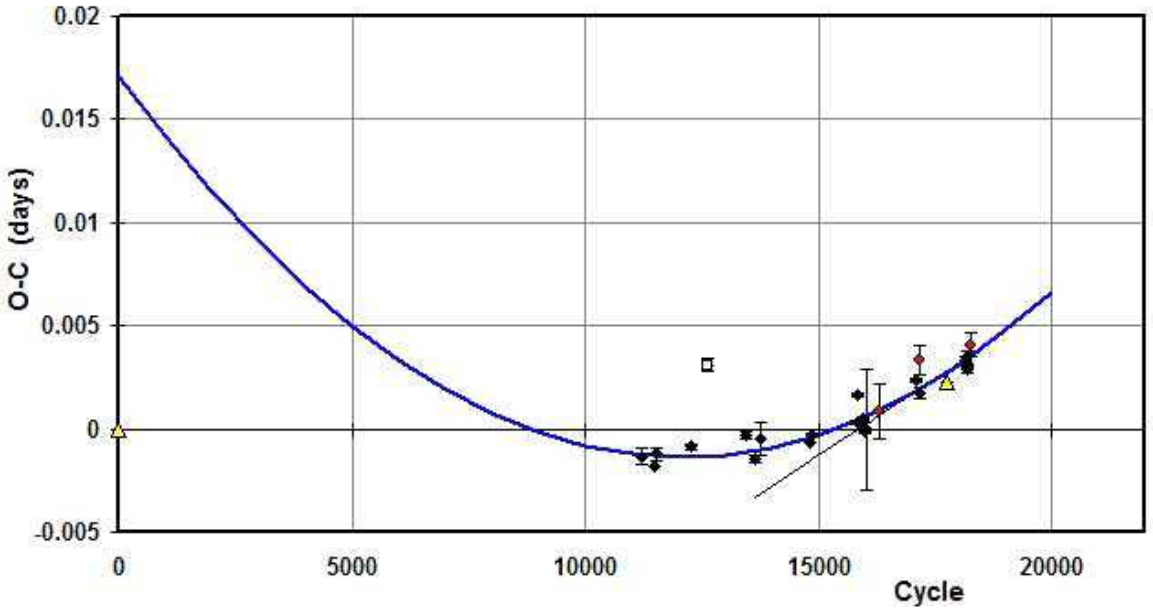

Figure 9. V2477 Cyg – eclipse timing $(O-C)$ diagram with a quadratic fit for points after cycle 10000.

No evidence of the third star was seen in the spectra. This is hardly surprising because of the relatively weak contribution from the third light. Because the relative flux at phases 0.25 and 0.75 has been normalized to close to unity, quantity l_3 represents the fractional contribution to the flux there (Wilson 1998, page 5). Assuming isotropic radiation from the third star, then its luminosity may be estimated by $\mathrm{el}_3 \times$(total luminosity of system) $= 0.04 \times 2.1 = 0.08$. If the companion is a main sequence star, this would make it a red dwarf of spectral type M1–M2—far too faint to register in the spectra above the noise.

It is somewhat troubling that the spectroscopic mass ratio $q_{\mathrm{sp}} = 2.17(2)$ differs significantly from that derived by the light curve modelling, $q_{\mathrm{ptm}} = 1.919(2)$. In view of the fact that the eclipses are total, we may trust the photometric value (Terrell & Wilson 2005). Moreover, the excellent fit of theoretical to observed light curves (Figs. 4-6) gives one confidence in the photometric value. But why is the spectroscopic value deviant?

It is tempting to believe that more spectra would clarify the situation, but there is much to be said for these spectra: they have a high signal-to-noise ratio, with continuum levels ranging from 20,000 to over 50,000; unlike some cases, the spectra reproduced in Fig. 1 display highly significant shifts over phase; the broadening functions, as reproduced in Figs. 2 and 3, are robust, with low noise and little to compromise the RV extraction; and finally, all estimates for the RV errors lie somewhat less than 10 km/s, typical in this work.

Although it has been argued that the contribution from the third star is low, it seems possible that its light has contaminated the spectra, distorting the RV determination.

Whatever the cause of the disparity, it seems safe to assume that the photometric mass ratio is more reliable and that the derived fundamental parameters are reliable.

Acknowledgements: It is a pleasure to thank the staff members at the DAO (especially Dmitry Monin and David Bohlender) for their usual splendid help and assistance.

References:

Bradstreet, D.H., 1993, "Binary Maker 2.0 - An Interactive Graphical Tool for Preliminary Light Curve Analysis", in Milone, E.F. (ed.) Light Curve Modelling of Eclipsing Binary Stars, pp 151-166 (Springer, New York, N.Y.)

Cox, A.N., ed, 2000, Allen's Astrophysical Quantities, 4th ed., (Springer, New York, NY)

Csizmadia, S., Pasternacki, T., Dreyer, C., Cabrera, A., Erikson, A., Rauer, H., 2013, *A&A*, **549**, A9 DOI

Davidge, T.J., Milone, E.F., 1984, *ApJS*, **55**, 571 DOI

Flower, P.J., 1996, *ApJ*, **469**, 355 DOI

Gessner, H., 1966, *Veröff. Sternwarte Sonneberg*, **7**, 61

Henden, A., 2001, `http://www.tass-survey.org/tass/catalogs/tycho.old.html`

Hoffmeister, C. von, 1963, *AN*, **287**, 169 DOI

Hog, E., et al., 2000, *A&A*, **355**, L27

Irwin, J.B., 1952, *ApJ*, **116**, 211 DOI

Irwin, J.B., 1959, *AJ*, **64**, 149 DOI

Kallrath, J., Milone, E.F., 1998, Eclipsing Binary Stars–Modeling and Analysis (Springer-Verlag) DOI

Kallrath, J., Milone, E.F., Terrell, D., Young, A.T., 1998, *ApJ*, **508**, 308 DOI

Kurucz, R.L., 2000, *Baltic Astron.*, **11**, 101

Nelson, R.H., 2009, software by Bob Nelson, `http://members.shaw.ca/bob.nelson/software1.htm`

Nelson, R.H., 2010a, spreadsheets by Bob Nelson, `http://members.shaw.ca/bob.nelson/spreadsheets1.htm`

Nelson, R.H., 2010b, "Spectroscopy for Eclipsing Binary Analysis" in The Alt-Az Initiative, Telescope Mirror & Instrument Developments (Collins Foundation Press, Santa Margarita, CA), R.M. Genet, J.M. Johnson and V. Wallen (eds)

Nelson, R.H., 2016, Bob Nelson's $O-C$ Files, `http://www.aavso.org/bob-nelsons-o-c-files`

Nelson, R. H., Şenavcı, H.V. Baştürk, Ö., Bahar, E., 2014, *New Astron.*, **29**, 57 DOI

Otero, S.A., Wils, P., 2005, *IBVS*, **5630**

Rucinski, S. M., 1974, *AcA*, **24**, 119

Rucinski, S. M., 2004, *IAUS*, **215**, 17

Rucinski, S. M., Pribulla, T., and van Kerkwijk, M.H., 2007, *AJ*, **134**, 2353 DOI

Schlegel, D.J., Finkbeiner, D.P., Davis, M., 1998, *ApJ*, **500**, 525 DOI

Skiff, B.A., 1999, *IBVS*, **4720**

Terrell, D., 1994, Van Hamme Limb Darkening Tables, vers. 1.1.

Terrell, D. Wilson, R.E., 2005, *ApSS*, **296**, 221 DOI

Van Hamme, W., 1993, *AJ*, **106**, 2096 DOI

Wilson, R.E., Devinney, E.J., 1971, *ApJ*, **166**, 605 DOI

Wilson, R.E., 1990, *ApJ*, **356**, 613 DOI

Wilson, R.E., 1998, Documentation of Eclipsing Binary Computer Model (available from the author)

COMMISSIONS G1 AND G4 OF THE IAU
INFORMATION BULLETIN ON VARIABLE STARS
Volume 62 Number 6193 DOI: 10.22444/IBVS.6193

Konkoly Observatory
Budapest
5 January 2017
HU ISSN 0374 – 0676

MINIMA OF ECCENTRIC ECLIPSING SYSTEMS OBSERVED FROM MT. SUHORA

OGŁOZA, W.; DRÓŻDŻ, M.; KREINER, J.M.; STACHOWSKI, G.; †WINIARSKI, M.; ZAKRZEWSKI, B.

Mt. Suhora Observatory, Pedagogical University of Cracow, Poland; e-mail: ogloza@up.krakow.pl

Observatory and telescope:

Three different instruments from Mt. Suhora Observatory (`www.as.up.krakow.pl`) were used. Tel-1: 60 cm Zeiss telescope (detector at primary focus), Tel-2: 20 cm Ritchey-Chrétien, and the portable Tel-3: 3 cm wide-field objective.

Detector:	Tel-1: Apogee Aspen C47, Tel-2: SBIG-ST10XME, Tel-3: Atik 314L

Method of data reduction:

Reduction of the CCD frames was made in the usual way using CMUNIPACK[1] package.

Method of minimum determination:

The minima times were computed with Kwee & van Woerden (1956) method and a digital implementation of the tracing paper method (Szafraniec, 1948).

Times of minima:

Star name	Time of min. HJD 2400000+	Error	Type	Filter	Rem.
AG Ari	57267.5364	.0006	II	R	
BW Boo	57373.6051	.0003	I	V	
EQ Boo	56742.523 :		I	V	TP
EQ Boo	57128.4153	.0005	I	V	
WW Cam	57389.2219	.0001	I	V	
WW Cam	57390.3412	.0002	II	V	
AS Cam	57134.4299	.0004	II	V	
AS Cam	57345.6019	.0002	I	V	
OO Cam	56210.46 :		II	V	TP
OO Cam	56742.3389	.0023	I	V	
OO Cam	57091.4563	.0009	I	V	

[1]Webpage: (`c-munipack.sourceforge.net`)

Times of minima:					
Star name	Time of min. HJD 2400000+	Error	Type	Filter	Rem.
V361 Cam	56496.5450		I	R	TP
V361 Cam	56522.504		I	R	TP
V361 Cam	56643.536		I	R	TP
V361 Cam	56980.253 :		I	R	TP
V469 Cam	56369.5266	.0010	II	V	TP
V469 Cam	56666.3427	.0002	II	V	
V469 Cam	56696.4014 :		I	V	TP
AR CMa	57391.4453	.0006	II	V	
DR CMi	56739.349 :		I	V	TP
OX Cas	56097.4406	.0001	II	V	
OX Cas	57368.2814		I	V	
PV Cas	56481.3943	.0001	II	V	
PV Cas	56571.5077	.0001	I	V	
PV Cas	57161.4176	.0003	I	V	
PV Cas	57266.4436	.0004	I	V	
PV Cas	57532.5135	.0003	I	V	
PV Cas	57658.5486	.0001	I	V	
V381 Cas	57354.5380	.0004	I	V	
V381 Cas	57388.5507	.0004	II	V	
V744 Cas	56482.4226	.0001	I	V	
V775 Cas	57185.4691	.0050	I	V	
V785 Cas	57331.5490	.0002	I	V	
V785 Cas	57335.4840	.0005	II	V	
V799 Cas	56997.5077	.0002	I	V	
V821 Cas	56985.3438	.0005	II	V	
V821 Cas	57176.4811	.0006	II	V	
V821 Cas	57376.4595	.0002	II	V	
V1018 Cas	55927.5371	.0001	I	V	
V1018 Cas	56581.4052	.0041	II	V	TP
V1018 Cas	56930.602 :		I	V	TP
V1066 Cas	56581.5534	.0036	II	V	TP
V1066 Cas	56585.3143	.0030	I	V	
V1103 Cas	57388.2775	.0004	I	V	
V1137 Cas	56441.4969	.0020	II	V	
V1137 Cas	56645.2754	.0089	II	V	
V1137 Cas	56938.4949	.0006	I	V	
V1141 Cas	56586.460		I	V	
CO Cep	56498.4453	.0012	II	R	TP
CO Cep	56587.1898	.0010	I	R	TP
CW Cep	56996.4418	.0002	I	V	
CW Cep	57299.3821	.0006	I	V	
EK Cep	57134.5466	.0002	I	V	
EK Cep	57267.381	.005	I	V	
EY Cep	56671.2250		II	V	
V397 Cep	57135.5546	.0050	II	V	
V397 Cep	57136.5084	.0008	I	V	
V397 Cep	57352.5742	.0003	II	V	
V731 Cep	56320.3967	.0001	II	V	DKW
V731 Cep	57376.2982	.0002	II	V	

Times of minima:					
Star name	Time of min. HJD 2400000+	Error	Type	Filter	Rem.
V743 Cep	56177.560	.012	I	V	
V743 Cep	56219.595	.005	I	V	
V743 Cep	56892.4423	.0050	I	V	
V881 Cep	56967.3013	.0007	I	V	
V881 Cep	57373.3699	.0004	I	V	
V881 Cep	57387.3735	.0006	I	V	
V897 Cep	57099.307 :		II	V	TP
V898 Cep	56766.391		II	V	
V898 Cep	56858.373 :		II	V	TP
V898 Cep	57389.2621	.0003	I	V	
V919 Cep	56966.5539	.0007	I	V	
V919 Cep	57254.5283	.0002	II	V	
V919 Cep	57255.4670	.0002	I	V	
V922 Cep	56867.4754 :		II	V	TP
V922 Cep	56965.4884	.0002	I	V	
V922 Cep	57396.5752	.0003	II	V	
Y Cyg	56542.4057	.0001	II	R	
Y Cyg	56569.3803	.0001	II	R	
MY Cyg	57646.4763		II	V	
V477 Cyg	57267.3605	.0003	II	V	
V478 Cyg	57123.5766		II	V	
V490 Cyg	56246.3910	.0001	I	V	DKW
V490 Cyg	56889.4749	.0001	I	V	
V490 Cyg	57125.5026	.0005	I	V	
V796 Cyg	57122.5626	.0003	I	V	
V796 Cyg	57254.3589	.0003	I	V	
V2544 Cyg	57256.3846	.0002	II	V	
V2647 Cyg	57096.6573 :		I	V	TP
V2647 Cyg	57098.5856 :		II	V	TP
BY Del	56615.3340	.0060	I	V	
BF Dra	57097.236 :		I	V	TP
CM Dra	57391.6303	.0001	I	V	
NS Dra	56649.32	.61	I	V	
V410 Gem	57387.6370	.0009	II	V	
V410 Gem	57389.3844	.0002	I	V	
V994A Her	56188.3700	.0010	I	V	BD
KW Hya	56267.6201	.0001	I	V	DKW
OZ Hya	57388.6050	.0010	I	V	
CO Lac	56888.4539	.0003	I	V	
MZ Lac	56964.5589	.0001	I	R	
V340 Lac	56615.5438 :		I	V	TP
V398 Lac	56502.3980	.0034	I	V	TP
V398 Lac	56580.3261	.0056	II	V	TP
RU Mon	55142.9028	.0007	I	V	IU
AO Mon	57364.5876	.0007	I	V	
AO Mon	57365.5506	.0003	II	V	
V521 Mon	57388.5675	.0003	I	V	

Times of minima:					
Star name	Time of min. HJD 2400000+	Error	Type	Filter	Rem.
V451 Oph	57137.4936	.0007	I	V	
BK Peg	57648.4353 :	.0001	II	V	
AG Per	57639.5209	.0005	I	R	
AG Per	57641.5486	.0001	I	V	
AG Per	57642.5134	.0001	II	V	
IM Per	57332.4937	.0006	I	V	
IM Per	57643.5776	.0002	I	V	
IQ Per	51912.3225	.0001	II	V	DKW
IQ Per	51932.4087	.0004	I	V	
IQ Per	57297.3766	.0004	I	V	
IQ Per	57332.2478	.0003	I	V	
NO Per	57390.5915	.0007	I	V	
V751 Per	57386.5054	.0003	I	V	
V370 Sge	56826.367 :		II	V	TP
V370 Sge	57139.573 :		I	V	TP
V413 Ser	56160.4185		II	V	
V1260 Tau	57388.2578	.0004	I	V	
V1260 Tau	57391.2628	.0006	II	V	
PS UMa	56431.516 :		I	V	SZ
BP Vul	56175.4753	.0001	II	V	DKW
BP Vul	57246.5443	.0001	II	V	
DR Vul	56483.4675	.0001	II	V	
DR Vul	57220.4809	.0005	I	V	
DR Vul	57352.2874	.0005	II	V	
FQ Vul	56499.5237	.0020	II	V	TP
FW Vul	57221.4807	.0003	II	V	
V491 Vul	56857.3449 :		I	V	TP
V495 Vul	57246.4241	.0002	I	V	
V495 Vul	57391.1996	.0001	II	V	

Explanation of the remarks in the table:

Times of minima determined by the digital tracing paper method are marked by 'TP'. ':' marks uncertain. 'DKW', 'BD', 'IU' and 'SZ' mark observations made by D. Koziel-Wierzbowska, B. Dyduch, I. Ulman and S. Zola respectively.

Acknowledgements:

Observations at Mt. Suhora were partially supported by Polish NCN grant no. 2011/03/D/ST9/01808.

References:

Kreiner, J.M., 2004, *Acta Astron.*, **54**, 207
Kwee, K. K. & van Woerden, H., 1956, *BAN*, **12**, 327
Szafraniec, R., 1948, *Acta Astron. ser. C*, **4**, 81

COMMISSIONS G1 AND G4 OF THE IAU
INFORMATION BULLETIN ON VARIABLE STARS
Volume 62 Number 6194 DOI: 10.22444/IBVS.6194

Konkoly Observatory
Budapest
10 January 2017

HU ISSN 0374 – 0676

SEARCH FOR VARIABILITY OF FIVE CENTRAL STARS OF PLANETARY NEBULAE

PAUNZEN, E.[1]; NETOPIL, M.[1]; RODE-PAUNZEN, M.[2]

[1] Department of Theoretical Physics and Astrophysics, Masaryk University, Kotlářská 2, 611 37 Brno, Czech Republic

[2] Institut für Astrophysik der Universität Wien, Türkenschanzstr. 17, A-1180 Wien, Austria

Introduction

Planetary nebulae (PN) are the next-to-last stages of evolution of stars with main sequence masses between 0.8 and 8 $M_{\odot}$. As the core slowly collapses, the outer layers are ejected forming the typical nebula-like structures. Nowadays it is beyond doubt that there is a connection between binary central stars and PN shaping (Hillwig et al. 2016). However, due to projection effects, even a spherical symmetric shape does not imply an apparent single star nature. It is therefore important to search for signs of binarity using photometric time series. One would either expect classical eclipses or reflection effects due to the orbital motion of the components.

Another type of variability is attributed to variations in the stellar wind, but also pulsation of some objects has been suggested as a possible explanation (Handler et al. 1997). These variations have been found in all type of PN central stars. For example, HD 35914, the variable central star of the PN IC 418 shows two distinct kinds of variability: irregular light modulation with a time scale of days (amplitude of about 0.3 mag), as well as cyclic variations with a time scale of hours (0.02 mag).

De Marco et al. (2008) summarized the back then known variability properties of PNe (Figure 4 therein) including all above described mechanisms. The observed periods range up to three days with amplitudes up to two magnitudes.

Here, we present photometric observations of five central stars of PNe, Kronberger PN J1944.9+2245, NGC 6853, NGC 7008, NGC 7076, and NGC 7354 in order to search for variability on time scale from hours to days. We were not able to detect any signs of variability with upper limits between 0.01 and 0.12 mag, respectively.

Observations and data reduction

The observations were performed in August and September 2010 at the Hvar Observatory, University of Zagreb (Croatia), using the 1 m Austrian-Croatian Telescope (ACT). The

Table 1: Observation log and results. Kronberger PN J1944.9+2245 was also investigated for variations in four nights on the time scale of hours (second line).

PN	V [mag]	HJD(start) 2455792+	HJD(end) 2455792+	N	Upper Limit [mag]
J1944.9+2245	15.8	0.44241	10.37849	42	0.12
J1944.9+2245		44.25059	49.27524	131	0.10
NGC 6853	14.1	0.45868	45.31385	52	0.08
NGC 7008	12.8	0.47488	49.40449	64	0.01
NGC 7076	13.4	0.48364	44.41168	38	0.06
NGC 7354	16.1	0.49543	49.42055	44	0.07

telescope was equipped with an Apogee Alta U47 CCD camera of 1024×1024 pixels, resulting in a field-of-view of about $3'$ square. The integration times for the observations in the Bessell I filter system were set between 45 and 120 s, depending on the weather conditions and the brightness of the target. After the basic CCD reductions (bias-subtraction and flat fielding), we applied aperture photometry within IRAF because all targets are in non-crowded fields. The sizes of the applied apertures were inspected manually for all observations to minimize the effects of the surrounding nebula. The further reduction steps were performed using the standard technique for time series CCD observations.

In each field, there were at least seven comparison stars of similar brightness as the target. The differential light curves derived from at least five comparison stars within the field were used for the time-series analysis. This should guarantee eliminating possible unknown instrumental effects. All differential light curves were examined in more detail using the Phase-Dispersion-Minimization method (PDM) within the software Peranso (Paunzen & Vanmunster 2016). An analysis with a discrete Fourier algorithm gave the same noise level over the searched frequency range as PDM.

Analysis and conclusions

For all five targets, we searched for long-term variations on the time scales of days. For this, three to five consecutive observations in one night were secured. The time-series analysis was performed using all individual measurements, but also for the mean of all individual nights. In Table 1, the results are summarized. We were not able to detect any statistically significant ($4\,\sigma$ above the noise level) signal in the light curves. The upper limits range from 0.01 to 0.12 mag. Hillwig et al. (2015) presented variability caused by binarity for the central star of Abell 65. The amplitude in the I filter for this object is about one magnitude with a period very close to one day. In addition, the characteristics for other known binaries among PN central stars are very similar (De Marco et al. 2008). Therefore we conclude that none of the investigated objects shows eclipses and irradiation effects on the investigated time scale of up to 50 days.

The object Kronberger PN J1944.9+2245 was also investigated during four nights searching for variation on a time scale up to a few hours. The noise level is rather high (0.1 mag) compared to the cyclic variations (0.02 mag) found by Handler et al. (1997) for the central star of IC 418. We can therefore not exclude such variations for this object.

We encourage further photometric observations of PN central stars to detect to-date unknown binary systems which is a perfect suited project for smaller telescopes. The

expected variations can reach even up to a few magnitudes which is observable in non-perfect conditions and sites. With the prospects of precise parallaxes and thus distances from the Gaia, such observations will significantly contribute to our knowledge of PNe.

Acknowledgements: The work was supported by the Czech Grant Agency under the project 14-26115P.

References:

De Marco, O., Hillwig, T. C., Smith, A. J., 2008, *AJ*, **136**, 323 DOI
Handler, G., et al., 1997, *A&A*, **320**, 125
Hillwig, T. C., et al., 2015, *AJ*, **150**, 30 DOI
Hillwig, T. C., et al., 2016, *ApJ*, **832**, 125 DOI
Paunzen, E., Vanmunster, T., 2016, *AN*, **337**, 239 DOI

COMMISSIONS G1 AND G4 OF THE IAU
INFORMATION BULLETIN ON VARIABLE STARS
Volume 62 Number 6195 DOI: 10.22444/IBVS.6195

Konkoly Observatory
Budapest
20 January 2017
HU ISSN 0374 – 0676

CCD MINIMA FOR SELECTED ECLIPSING BINARIES IN 2016

NELSON, R. H.

1393 Garvin Street, Prince George, BC, Canada, V2M 3Z1 e-mail: bob.nelson@shaw.ca

Observatory and telescope:
Sylvester Robotic Observatory (SyRO): 33 cm f/4.5 Newtonian on a Paramount ME

Detector:	SyRO: SBIG ST-10XME, 6.8″ pixels, 34.4′×23.2′ FOV, $-10 < T < -30^{\circ}$ C

Method of data reduction:
Bias and dark subtraction, flat-fielding using light-box flats; aperture photometry– all using MIRA, by Mirametrics. Check stars were used throughout.

Method of minimum determination:
Digital tracing paper method, bisection of chords, curve fitting, and (occasionally) Kwee and van Woerden (1956)

Times of minima:						
Star name	Time of min. HJD 2400000+	Error	Type	Filter	$O-C$ [day]	Rem.
QX And	57734.6099	0.0002	I	c	0.0016	
V0527 And	57654.7928	0.0003	I	c	0.0020	
V1747 Aql	57521.9096	0.0003	I	c	0.0023	
SS Ari	57699.6733	0.0003	I	R	−0.0061	
BN Ari	57702.6294	0.0003	I	VRI	−0.0003	
BN Ari	57707.5698	0.0007	II	VRI	0.0006	
BN Ari	57707.7187	0.0002	I	VRI	−0.0002	
BN Ari	57728.6745	0.0005	I	VRI	−0.0001	
BN Ari	57729.5727	0.0003	I	VRI	−0.0000	
BN Ari	57730.621	0.0002	II	VRI	0.0005	
V0410 Aur	57738.5905	0.0002	I	R	0.0000	
V0644 Aur	57734.74	0.0002	I	c	−0.0001	
TY Boo	57477.829	0.0002	I	c	−0.0006	
TZ Boo	57439.8916	0.0002	I	R	0.0007	
TZ Boo	57753.1011	0.0003	II	R	0.0020	
CK Boo	57498.7485	0.0008	I	c	−0.0047	
GI Boo	57514.7897	0.0002	I	c	0.0033	
GN Boo	57476.8355	0.0001	I	c	−0.0059	
GQ Boo	57439.988	0.0004	II	c	−0.0019	
GQ Boo	57498.8367	0.0002	II	c	−0.0030	
GR Boo	57465.8222	0.0003	II	c	−0.0005	
GR Boo	57492.7537	0.0003	I	c	−0.0008	
GS Boo	57463.8021	0.0003	II	c	0.0009	
HH Boo	57487.7804	0.0002	I	c	−0.0024	
HH Boo	57499.7308	0.0002	II	c	−0.0019	
IK Boo	57497.7395	0.0002	I	c	−0.0079	
QT Boo	57493.788	0.002	I	c	−0.0035	
AO Cam	57672.798	0.0002	II	c	−0.0008	
CV Cam	57747.622	0.0002	II	R	0.0003	
LR Cam	57671.9582	0.0001	I	R	0.0048	
NR Cam	57707.8518	0.0003	II	c	−0.0006	
NX Cam	57739.6351	0.0006	II	c	0.0004	
V0337 Cam	57736.5865	0.0003	I	R	−0.0005	
V0383 Cam	57625.9666	0.0003	II	c	−0.0002	
V0403 Cam	57737.7574	0.0003	II	c	0.0014	
V0474 Cam	57729.8173	0.0003	II	c	−0.0008	
G3715-0043 Cam	57739.6261	0.0006	0	c	0.0000	
TW Cas	57619.9773	0.0002	I	VRI	0.0020	
ZZ Cas	57617.8966	0.0001	I	c	0.0025	
BS Cas	57615.8603	0.0001	I	c	0.0001	
EY Cas	57637.8343	0.0002	I	c	−0.0028	
IR Cas	57672.6806	0.0002	I	VRI	−0.0002	
IR Cas	57673.7035	0.0002	II	VRI	0.0017	
V0375 Cas	57625.8179	0.0001	I	R	−0.0034	
V1063 Cas	57645.8468	0.0002	II	c	0.0004	
V1139 Cas	57483.7239	0.0002	II	c	0.0005	
V0736 Cep	57619.7376	0.0006	I	VRI	−0.0004	
G4500-0730 Cep	57661.635	0.0002	II	c	0.0001	

Times of minima:						
Star name	Time of min. HJD 2400000+	Error	Type	Filter	$O-C$ [day]	Rem.
BX CMi	57425.6877	0.0002	I	R	0.0005	
DS CMi	57441.6687	0.0005	I	c	0.0003	
EH Cnc	57730.9149	0.0001	II	c	0.0018	
IU Cnc	57463.6988	0.0002	I	c	0.0051	
G1936-0040 Cnc	57738.8988	0.0002	II	c	0.0002	
UX CVn	57454.7799	0.0003	I	c	−0.0012	
DH CVn	57723.9964	0.0006	II	c	−0.0001	
DR CVn	57480.7116	0.0005	II	VRI	−0.0074	
DX CVn	57443.9182	0.0002	II	c	0.0008	
EL CVn	57476.713	0.002	I	R	−0.0006	
FV CVn	57433.9306	0.0003	II	c	−0.0002	
G2530-1069 CVn	57747.0468	0.0002	I	c	0.0007	
RW Com	57425.8104	0.0004	I	c	−0.0008	
RZ Com	57478.7858	0.0001	I	R	0.0046	
SS Com	57479.7958	0.0003	II	c	0.0002	
CM Com	57477.722	0.0003	I	c	−0.0018	
AS CrB	57441.9686	0.0002	II	c	0.0044	
AV CrB	57478.8942	0.0001	I	c	−0.0020	
V0401 Cyg	57487.9323	0.0002	I	c	−0.0070	
V0687 Cyg	57510.9305	0.0001	I	c	−0.0030	
V0859 Cyg	57530.8584	0.0002	II	c	0.0009	
V2197 Cyg	57514.918	0.0001	I	c	−0.0008	
V2282 Cyg	57510.839	0.0002	II	c	−0.0000	
V2364 Cyg	57498.9433	0.0006	I	c	−0.0016	
V2477 Cyg	57499.9633	0.0001	I	R	−0.0001	
BV Dra	57463.9201	0.0003	I	V	−0.0005	
BW Dra	57463.8751	0.0005	II	V	0.0019	
EF Dra	57515.7979	0.0005	I	c	0.0025	
GQ Dra	57483.8383	0.0002	I	V	0.0006	
IV Dra	57492.8669	0.0004	II	c	0.0056	
V0415 Dra	57492.9764	0.0004	I	c	−0.0030	
G3870-1172 Dra	57448.8752	0.0002	II	c	0.0009	
G3870-1172 Dra	57497.8737	0.0001	II	R	0.0015	
G3881-0579 Dra	57465.9382	0.0001	II	c	0.0007	
G3929-1500 Dra	57522.817	0.0002	II	c	−0.0013	
G4215-1480 Dra	57480.8837	0.0002	I	c	0.0000	
G4439-1124 Dra	57499.8687	0.0004	I	c	0.0055	
G4439-1124 Dra	57516.7866	0.0008	II	c	0.0011	
V0415 Gem	57734.8607	0.0004	II	c	−0.0004	
G1886-1869 Gem	57738.765	0.0005	I	c	−0.0007	
V1036 Her	57521.8043	0.0002	II	c	0.0018	
V1067 Her	57479.9096	0.0002	II	c	−0.0001	
V1103 Her	57475.863	0.0003	I	c	−0.0006	
V1167 Her	57475.9724	0.0004	I	R	0.0027	
V1198 Her	57524.8347	0.0003	I	c	0.0026	
V1284 Her	57513.8723	0.0001	I	c	0.0001	
V1286 Her	57493.8911	0.0002	I	c	−0.0050	
V1289 Her	57511.9014	0.0001	I	c	−0.0005	

Times of minima:						
Star name	Time of min. HJD 2400000+	Error	Type	Filter	$O-C$ [day]	Rem.
V1302 Her	57522.912	0.0003	I	c	0.0010	
V1333 Her	57481.9646	0.0001	II	c	0.0001	
SW Lac	57674.6566	0.0002	I	R	0.0022	
UZ Leo	57731.003	0.0001	II	V	0.0032	
ET Leo	57738.9741	0.0003	II	R	0.0005	
XX LMi	57454.6765	0.0003	I	c	−0.0019	
AG LMi	57442.6695	0.0002	I	c	0.0001	
SW Lyn	57735.8821	0.0002	I	c	0.0031	
CL Lyn	57735.7652	0.0003	I	c	−0.0007	
DE Lyn	57728.7772	0.0003	II	c	−0.0019	
FO Lyn	57728.9316	0.0002	II	c	0.0001	
PY Lyr	57508.964	0.002	I	c	0.0000	
V0563 Lyr	57481.8633	0.0002	I	c	−0.0004	
V0579 Lyr	57477.927	0.001	I	c	−0.0016	
V0653 Lyr	57476.9573	0.0001	I	c	0.0003	
V0927 Mon	57737.8363	0.0003	II	c	0.0000	
V0508 Oph	57497.965	0.0002	II	R	0.0030	
V2713 Oph	57480.9854	0.0003	I	c	0.0005	
V0517 Ori	57747.778	0.002	I	c	0.0004	
V1833 Ori	57746.7359	0.0005	I	c	−0.0004	
V1848 Ori	57389.684	0.0002	I	c	0.0012	
V2762 Ori	57730.794	0.0002	I	I	−0.0003	
DK Peg	57646.8229	0.0003	I	c	0.0022	
V0523 Peg	57637.7164	0.0002	II	c	0.0002	
V0535 Peg	57624.7678	0.0003	I	c	0.0047	
V0576 Peg	57615.7732	0.0002	I	c	−0.0012	
V0619 Peg	57624.8949	0.0002	I	R	0.0005	
RT Per	57618.8972	0.0001	I	c	0.0014	
RT Per	57646.928	0.0001	I	c	0.0016	
V0881 Per	57626.8723	0.0002	II	c	−0.0013	
DZ Psc	57653.8041	0.0003	I	c	0.0052	
HL Psc	57731.5992	0.0005	II	c	−0.0065	
HO Psc	57742.5931	0.0004	II	c	0.0009	
V0384 Ser	57513.7615	0.0001	I	c	−0.0025	
AH Tau	57635.9722	0.0008	II	c	−0.0019	
EQ Tau	57737.6095	0.0002	II	c	−0.0005	
V0781 Tau	57751.6673	0.0002	I	R	−0.0016	
V1241 Tau	57672.867	0.002	II	VRI	−0.0056	
V1332 Tau	57742.7253	0.0005	II	c	−0.0013	
XY UMa	57427.7634	0.0003	II	R	−0.0005	
AA UMa	57707.9965	0.0001	I	c	0.0042	
HH UMa	57437.744	0.0002	II	R	0.0014	
LP UMa	57453.716	0.0004	I	c	−0.0045	
MQ UMa	57746.8928	0.0002	I	c	0.0088	
MT UMa	57735.9896	0.0005	I	c	−0.0005	
NU UMa	57448.8067	0.0003	I	V	0.0009	
G4386-0604 UMa	57747.9238	0.0002	I	R	−0.0041	
KN Vul	57516.9138	0.0003	I	c	0.0004	

Remarks:

To save space, GSC star names have been shortened to a leading "G" only; times of minimum are heliocentric Julian dates with the leading 24 removed.
$O-C$ values were computed using elements computed from the $O-C$ database listed in the references (Nelson, 2016).

Acknowledgements:

Thanks are due to Environment Canada for the website satellite views (see reference below) that were essential in predicting clear times for observing runs in this cloudy locale. Thanks are also due to Attilla Danko for his 'Clear Sky Charts', (see below). This research has made use of the SIMBAD database, operated at CDS, Strasbourg, France.

References:

Danko, A., Clear Sky Charts, `http://cleardarksky.com/`
Kwee, K.K., & van Woerden, H., 1956, B.A.N. 12, 327
Nelson, R.H. 2016, Bob Nelson's O-C Files, `http://www.aavso.org/bob-nelsons-o-c-files`
Satellite Images for North America, `http://weather.gc.ca/`

COMMISSIONS G1 AND G4 OF THE IAU
INFORMATION BULLETIN ON VARIABLE STARS
Volume 62 Number 6196 DOI: 10.22444/IBVS.6196

Konkoly Observatory
Budapest
20 January 2017
HU ISSN 0374 – 0676

BAV-RESULTS OF OBSERVATIONS - PHOTOELECTRIC MINIMA OF SELECTED ECLIPSING BINARIES AND MAXIMA OF PULSATING STARS

(BAV MITTEILUNGEN NO. 244)

HÜBSCHER, JOACHIM

Bundesdeutsche Arbeitsgemeinschaft für Veränderliche Sterne e.V. (BAV), Munsterdamm 90, 12169 Berlin, Germany, www.bav-astro.de, publikat@bav-astro.de

In this 86th compilation of BAV results, photoelectric observations obtained mostly in the years 2015 and 2016 are presented on 1,063 variable stars giving 1,850 minima of eclipsing binaries. All moments of minima are heliocentric UTC. The errors are tabulated in column "±". All information about photometers and filters are specified in the columns "Fil" and "Rem". The observations were made at private observatories. The photoelectric measurements and all the light curves with evaluations can be obtained from the office of the BAV for inspection.

Please use the following link for an easy access to all the publications of the BAV including the "Lichtenknecker Database of the BAV": `http://www.bav-astro.de/sfs`.

Table 1: Times of minima of eclipsing binaries

Variable	HJD 24.....	±	Obs	sec	Fil	n	Rem
RT And	57327.3783	0.0005	AG		-I	57	10)
RT And	57588.3844	0.0014	AG		-I	37	10)
UU And	57305.5745	0.0019	AG		-I	42	10)
WZ And	57328.4914	0.0047	AG		-I	62	10)
XZ And	57290.4019	0.0007	AG		-I	35	10)
XZ And	57305.3316	0.0019	AG		-I	46	10)
AA And	57257.5634	0.0038	AG		-I	38	10)
AA And	57590.4593	0.0015	AG		-I	35	10)
AB And	57590.4285	0.0008	AG		-I	35	10)
AD And	57293.3906	0.0013	JU		o	75	12)
AD And	57577.4151	0.0005	AG		-I	31	10)
AP And	57295.4185	0.0001	SCI		o	33	12)
AP And	57299.3865	0.0001	SCI	s	o	71	12)
BD And	57590.4718	0.0035	AG		-I	26	10)
BX And	57299.4630	0.0059	AG		-I	52	10)
BX And	57328.4439	0.0049	AG		-I	69	10)
CN And	57244.4158	0.0134	AG		-I	35	10)
CN And	57264.5456	0.0053	AG		-I	57	10)
CU And	57261.4342	0.0009	AG		-I	37	10)
CZ And	57261.4424	0.0227	AG		-I	37	10)
DS And	57276.4007	0.0076	AG		-I	46	10)
EX And	57590.3958	0.0001	AG		-I	26	10)
GZ And	57290.4067	0.0002	AG		-I	38	10)
GZ And	57290.5579	0.0012	AG		-I	38	10)
GZ And	57296.3541	0.0076	AG		-I	74	10)
GZ And	57296.5060	0.0036	AG		-I	74	10)

GZ And	57296.6593	0.0001	AG		-I	74	10)
GZ And	57299.4046	0.0027	AG		-I	50	10)
GZ And	57299.5564	0.0052	AG		-I	50	10)
LM And	57290.5482	0.0011	AG		-I	41	10)
LO And	57242.4515	0.0038	AG		-I	39	10)
LO And	57577.4303	0.0004	AG		-I	31	10)
LO And	57590.5542	0.0073	AG		-I	26	10)
QX And	56590.4187	0.0004	MS FR		o	30	9)
QX And	57276.4794	0.0094	AG		-I	46	10)
QX And	57342.4270	0.0002	SCI		o	57	12)
QX And	57342.6326	0.0004	SCI	s	o	66	12)
V355 And	57256.4488	0.0064	AG		-I	42	10)
V363 And	57297.3275	0.0017	AG		-I	56	10)
V372 And	57296.5233	0.0128	AG		-I	74	10)
V372 And	57299.4685	0.0160	AG		-I	50	10)
V376 And	57305.3251	0.0003	AG		-I	44	10)
V392 And	57242.3974	0.0145	AG		-I	39	10)
V392 And	57246.4484	0.0079	AG		-I	36	10)
V392 And	57248.4744	0.0148	AG		-I	45	10)
V404 And	57245.3974	0.0041	AG		-I	35	10)
V412 And	57577.5050	0.0005	AG		-I	31	10)
V449 And	57276.6235	0.0001	MS FR		V	64	3)
V452 And	57355.4342	0.0001	MS		L	86	8)
V477 And	57305.3690	0.0027	AG		-I	39	10)
V477 And	57305.5509	0.0042	AG		-I	39	10)
V480 And	57305.4228	0.0039	AG		-I	40	10)
V483 And	57244.3828	0.0033	AG		-I	35	10)
V483 And	57244.5399	0.0097	AG		-I	35	10)
V484 And	57305.3125	0.0017	AG		-I	41	10)
V506 And	57305.3214	0.0024	AG		-I	38	10)
V506 And	57305.4934	0.0010	AG		-I	38	10)
V506 And	57328.3320	0.0009	AG		-I	60	10)
V506 And	57328.5049	0.0024	AG		-I	60	10)
V508 And	57305.4169	0.0170	AG		-I	38	10)
V508 And	57328.2899	0.0010	AG		-I	62	10)
V509 And	57305.3664	0.0076	AG		-I	39	10)
V509 And	57305.5201	0.0101	AG		-I	39	10)
V512 And	57305.2797		AG		-I	36	10)
V512 And	57328.3850	0.0005	AG		-I	65	10)
V523 And	57328.6357	0.0034	AG		-I	62	10)
V527 And	57305.5077	0.0036	AG		-I	49	10)
V543 And	57278.4539	0.0009	AG		-I	52	10)
V546 And	57385.4285	0.0002	RAT RCR		V	13	6)
V547 And	57276.4304	0.0128	AG		-I	46	10)
V565 And	57290.4559	0.0013	AG		-I	39	10)
V566 And	57294.3505	0.0018	AG		-I	32	10)
V575 And	57294.3372	0.0047	AG		-I	34	10)
V597 And	57261.4678	0.0017	AG		-I	37	10)
V600 And	57261.4061	0.0020	AG		-I	37	10)
V613 And	57338.2873	0.0057	AG		-I	43	10)
V613 And	57577.4497	0.0015	AG		-I	28	10)
V638 And	57590.5017	0.0008	AG		-I	26	10)
V649 And	57590.5338	0.0017	AG		-I	26	10)
V651 And	57261.5332	0.0014	AG		-I	37	10)
V651 And	57590.4784	0.0003	AG		-I	26	10)
V662 And	57242.5334	0.0018	AG		-I	39	10)
V662 And	57577.4473	0.0021	AG		-I	31	10)
V667 And	57577.5485	0.0036	AG		-I	31	10)
V678 And	57577.4864	0.0007	AG		-I	31	10)
V680 And	57577.5123	0.0007	AG		-I	31	10)
V680 And	57590.4191	0.0013	AG		-I	26	10)
V683 And	57577.4557	0.0017	AG		-I	30	10)
V692 And	57590.3888	0.0004	AG		-I	26	10)
V692 And	57590.5582	0.0049	AG		-I	26	10)
V707 And	57244.4295	0.0049	AG		-I	32	10)
V707 And	57257.3720	0.0028	AG		-I	38	10)
V707 And	57266.4350	0.0126	AG		-I	48	10)
V707 And	57297.4952	0.0095	AG		-I	58	10)
V707 And	57345.3816	0.0008	AG		-I	40	10)
V712 And	57242.3663	0.0065	AG		-I	41	10)
V712 And	57242.5479	0.0051	AG		-I	41	10)
V712 And	57244.3912	0.0032	AG		-I	32	10)
V712 And	57244.5702	0.0043	AG		-I	32	10)

V712 And	57257.4243	0.0038	AG	-I	38	10)
V712 And	57257.6052	0.0004	AG	-I	38	10)
V712 And	57266.4224	0.0073	AG	-I	47	10)
V712 And	57266.6027	0.0021	AG	-I	47	10)
V712 And	57297.4449	0.0061	AG	-I	58	10)
V712 And	57297.6337	0.0046	AG	-I	58	10)
V756 And	57276.5818	0.0002	MS FR	V	50	3)
CX Aqr	57298.3261	0.0028	AG	-I	27	10)
CX Aqr	57330.2957	0.0002	DIE	o	30	20)
DD Aqr	57287.5018	0.0035	AG	-I	34	10)
GS Aqr	57353.3013	0.0012	MS	V	27	8)
HS Aqr	57241.5452	0.0075	AG	-I	34	10)
HS Aqr	57588.4721	0.0008	AG	-I	35	10)
MO Aqr	57257.5442	0.0051	AG	-I	35	10)
FK Aql	57577.4780	0.0008	AG	-I	29	10)
KO Aql	57247.4975	0.0013	AG	-I	26	10)
KP Aql	57257.4430	0.0025	AG	-I	43	10)
OO Aql	57240.5479	0.0025	AG	-I	37	10)
OO Aql	57256.5114	0.0029	AG	-I	32	10)
OP Aql	57580.5508	0.0001	AG	-I	26	10)
V346 Aql	57563.4526	0.0022	AG	-I	23	10)
V415 Aql	57265.4647	0.0080	AG	-I	36	10)
V415 Aql	57563.4685	0.0022	AG	-I	28	10)
V417 Aql	57580.4445	0.0006	AG	-I	32	10)
V609 Aql	57241.4494	0.0052	AG	-I	35	10)
V609 Aql	57257.3821	0.0011	AG	-I	33	10)
V609 Aql	57562.4643	0.0015	AG	-I	26	10)
V616 Aql	57210.4343	0.0002	MS	o	23	9)
V640 Aql	57256.4279	0.0046	AG	-I	31	10)
V640 Aql	57580.5295	0.0009	AG	-I	26	10)
V694 Aql	57256.4836	0.0017	AG	-I	30	10)
V699 Aql	57256.4454	0.0021	AG	-I	30	10)
V699 Aql	57580.4543	0.0005	AG	-I	26	10)
V714 Aql	57580.5059	0.0007	AG	-I	26	10)
V719 Aql	57256.3759	0.0018	AG	-I	31	10)
V719 Aql	57580.4228	0.0020	AG	-I	25	10)
V760 Aql	57580.4606	0.0003	AG	-I	26	10)
V784 Aql	57257.3401	0.0005	AG	-I	53	10)
V784 Aql	57563.5267	0.0007	AG	-I	23	10)
V864 Aql	57257.4247	0.0044	AG	-I	33	10)
V889 Aql	57240.5348	0.0059	AG	-I	37	10)
V889 Aql	57592.4553	0.0040	BRW	V	14	2)
V1045 Aql	57256.5254	0.0016	AG	-I	32	10)
V1096 Aql	57256.4719	0.0089	AG	-I	32	10)
V1096 Aql	57257.5847	0.0027	AG	-I	33	10)
V1168 Aql	57563.4743	0.0007	AG	-I	23	10)
V1299 Aql	57563.4687	0.0022	AG	-I	23	10)
V1331 Aql	57257.4079	0.0103	AG	-I	24	10)
V1353 Aql	57306.3346	0.0030	BRW	V	23	2)
V1353 Aql	57562.4171	0.0024	AG	-I	25	10)
V1430 Aql	57564.4908	0.0023	AG	-I	28	10)
V1461 Aql	57266.3774	0.0041	AG	-I	29	10)
V1542 Aql	57563.5148	0.0004	AG	-I	23	10)
V1695 Aql	57257.4198	0.0040	AG	-I	29	10)
V1700 Aql	57256.4390	0.0119	AG	-I	39	10)
V1713 Aql	57580.4152	0.0036	AG	-I	31	10)
V1714 Aql	57256.4113	0.0011	AG	-I	30	10)
V1714 Aql	57580.4572	0.0004	AG	-I	26	10)
V1747 Aql	57580.5267	0.0009	AG	-I	32	10)
V1796 Aql	57579.4179	0.0006	AG	-I	28	10)
V1799 Aql	57266.4766	0.0014	AG	-I	34	10)
V1808 Aql	57580.4317	0.0016	AG	-I	32	10)
V1814 Aql	57237.5129	0.0046	AG	-I	35	10)
V1817 Aql	57240.4632	0.0057	AG	-I	37	10)
V1817 Aql	57580.4432	0.0009	AG	-I	31	10)
V1825 Aql	57247.4717	0.0060	AG	-I	38	10)
V1825 Aql	57577.4869	0.0007	AG	-I	29	10)
V1826 Aql	57241.4907	0.0128	AG	-I	35	10)
V1826 Aql	57579.4620	0.0019	AG	-I	29	10)
RS Ari	53229.2893	0.0440	PGL		13	21) SWASP
RS Ari	54056.7978	0.0264	PGL		32	21) SWASP
RX Ari	57329.3394	0.0053	AG	-I	62	10)
SS Ari	57345.4640	0.0012	AG	-I	44	10)

TX Ari	57287.3954	0.0025	AG		-I	42	10)
XZ Ari	57287.4304	0.0041	AG		-I	45	10)
XZ Ari	57287.5602	0.0010	AG		-I	45	10)
AG Ari	57329.4558	0.0078	AG		-I	57	10)
AL Ari	57397.2919	0.0040	BRW		V	14	2)
BM Ari	57329.3473	0.0017	AG		-I	58	10)
BM Ari	57329.5875	0.0049	AG		-I	58	10)
BN Ari	57329.3179	0.0007	AG		-I	58	10)
BN Ari	57329.4677	0.0014	AG		-I	58	10)
BN Ari	57329.6165	0.0011	AG		-I	58	10)
BO Ari	57329.3517	0.0019	AG		-I	58	10)
BO Ari	57329.5101	0.0014	AG		-I	58	10)
BO Ari	57329.6691	0.0032	AG		-I	58	10)
BQ Ari	57385.3403	0.0017	AG		-I	48	10)
BQ Ari	57385.4823	0.0024	AG		-I	48	10)
CL Ari	57364.2766	0.0185	AG		-I	82	10)
ZZ Aur	57343.3813	0.0047	AG		-I	35	10)
ZZ Aur	57364.4238	0.0079	AG		-I	91	10)
ZZ Aur	57379.4515	0.0014	MS		V	80	3)
AH Aur	57383.3611	0.0035	AG		-I	66	10)
AH Aur	57383.6055	0.0022	AG		-I	66	10)
BF Aur	57345.6199	0.0013	AG		-I	58	10)
CQ Aur	54213.8015	0.1275	PGL			22	21) SWASP
EP Aur	57383.4135	0.0003	AG		-I	66	10)
HL Aur	57098.4126	0.0001	RAT RCR		V	91	6)
HL Aur	57385.3858	0.0006	AG		-I	65	10)
HR Aur	57384.4101	0.0029	AG		-I	61	10)
HS Aur	57383.5103	0.0051	AG		-I	71	10)
IU Aur	57385.5674	0.0078	AG		-I	82	10)
IY Aur	53253.5011	0.0364	PGL			30	21) SWASP
V404 Aur	57364.4997	0.0059	AG		-I	90	10)
V410 Aur	57384.3263	0.0065	AG		-I	53	10)
V410 Aur	57384.5094	0.0033	AG		-I	53	10)
V425 Aur	57384.5122	0.0158	AG		-I	55	10)
V432 Aur	57306.5275	0.0100	BRW		U	10	2)
V432 Aur	57306.5476	0.0080	BRW		B	12	2)
V432 Aur	57306.5483	0.0100	BRW		V	12	2)
V432 Aur	57383.5907	0.0094	AG		-I	65	10)
V455 Aur	57414.5757	0.0022	AG		-I	43	10)
V459 Aur	57384.4752	0.0039	AG		-I	62	10)
V591 Aur	57343.3292		AG		-I	36	10)
V591 Aur	57345.5491	0.0016	AG		-I	59	10)
V594 Aur	57345.3733	0.0005	AG		-I	54	10)
V609 Aur	57364.4190	0.0054	AG		-I	90	10)
V609 Aur	57364.6557	0.0009	AG		-I	90	10)
V610 Aur	57383.5971	0.0255	AG		-I	67	10)
V620 Aur	57343.3757	0.0012	AG		-I	37	10)
V620 Aur	57364.4236	0.0032	AG		-I	91	10)
V620 Aur	57379.4551:	0.0003	MS		V	80	3)
V623 Aur	57364.4035	0.0026	AG		-I	90	10)
V627 Aur	57364.3311	0.0031	AG		-I	90	10)
V627 Aur	57364.5258	0.0077	AG		-I	90	10)
V641 Aur	57364.2762	0.0011	AG		-I	88	10)
V641 Aur	57364.5294	0.0018	AG		-I	88	10)
V644 Aur	57383.5376	0.0012	AG		-I	66	10)
V648 Aur	57101.4035	0.0007	RAT RCR	s	V	12	6)
SU Boo	57128.4521	0.0016	AG		-I	45	10)
TU Boo	57466.4003	0.0006	AG		-I	45	10)
TU Boo	57466.5636	0.0010	AG		-I	45	10)
TX Boo	57128.5144	0.0091	AG		-I	44	10)
TX Boo	57500.5266	0.0119	AG		-I	42	10)
TY Boo	57128.4950	0.0014	AG		-I	45	10)
TY Boo	57464.5087	0.0007	AG		-I	37	10)
TZ Boo	57121.4834	0.0059	AG		-I	29	10)
TZ Boo	57489.3689	0.0024	AG		-I	46	10)
TZ Boo	57489.5190	0.0025	AG		-I	46	10)
UW Boo	57517.5723	0.0015	AG		-I	32	10)
VW Boo	57125.3602	0.0007	AG		-I	41	10)
VW Boo	57125.5305	0.0009	AG		-I	41	10)
VW Boo	57516.4552	0.0012	AG		-I	35	10)
XY Boo	57119.4699	0.0030	AG		-I	30	10)
XY Boo	57128.3624	0.0046	AG		-I	46	10)
XY Boo	57128.5489	0.0048	AG		-I	46	10)

XY Boo	57489.4823	0.0057	AG		-I	43	10)
XY Boo	57516.5324	0.0023	AG		-I	36	10)
AC Boo	53141.5856	0.0044	PGL			53	21) SWASP
AC Boo	53142.4662	0.0037	PGL				21) SWASP
AC Boo	53143.5193	0.0027	PGL			74	21) SWASP
AC Boo	53144.5841	0.0058	PGL			47	21) SWASP
AC Boo	53146.5173	0.0058	PGL			67	21) SWASP
AC Boo	53150.4194	0.0033	PGL			54	21) SWASP
AC Boo	57119.5079	0.0016	AG		-I	30	10)
AC Boo	57464.3846	0.0011	AG		-I	47	10)
AC Boo	57464.5605	0.0005	AG		-I	47	10)
AC Boo	57474.4295	0.0001	SCI		o	12	12)
AC Boo	57474.6061	0.0001	SCI	s	o	73	12)
AC Boo	57499.4528	0.0001	SCI		o	14	12)
AC Boo	57499.6338	0.0001	SCI	s	o	48	12)
AC Boo	57512.4027	0.0020	BRW		V	60	2)
AD Boo	57128.4198	0.0027	AG		-I	46	10)
CK Boo	57133.4870	0.0032	AG		-I	44	10)
CK Boo	57516.5065	0.0028	AG		-I	36	10)
EF Boo	57464.4197	0.0019	AG		-I	47	10)
EF Boo	57464.6306	0.0016	AG		-I	47	10)
EL Boo	57132.5384	0.0089	AG		-I	40	10)
EM Boo	57131.4273	0.0110	AG		-I	36	10)
ET Boo	57119.4683	0.0024	AG		-I	30	10)
ET Boo	57464.5642	0.0019	AG		-I	47	10)
ET Boo	57475.5298	0.0030	BRW		V	50	2)
EW Boo	57119.4461	0.0052	AG		-I	30	10)
EW Boo	57500.5669	0.0048	AG		-I	44	10)
FP Boo	56719.6017	0.0002	MS		o	16	9)
FP Boo	56730.4837	0.0002	MS FR		o	39	9)
FP Boo	57489.4192	0.0138	AG		-I	46	10)
GG Boo	57132.3977	0.0059	AG		-I	40	10)
GH Boo	57466.5104	0.0022	AG		-I	47	10)
GK Boo	57128.3718	0.0018	AG		-I	45	10)
GK Boo	57128.6108	0.0001	AG		-I	45	10)
GK Boo	57134.3455	0.0026	AG		-I	36	10)
GK Boo	57134.5826	0.0005	AG		-I	36	10)
GK Boo	57137.4502	0.0010	AG		-I	37	10)
GK Boo	57464.4861	0.0013	AG		-I	47	10)
GL Boo	57128.4615	0.0283	AG		-I	46	10)
GL Boo	57136.426	0.011	AG		-I	56	10)
GL Boo	57518.5310	0.0015	AG		-I	66	10)
GN Boo	57123.3566	0.0008	AG		-I	39	10)
GN Boo	57123.5093	0.0027	AG		-I	39	10)
GN Boo	57128.4822	0.0017	AG		-I	45	10)
GN Boo	57137.3819	0.0021	AG		-I	37	10)
GN Boo	57137.5307	0.0009	AG		-I	37	10)
GN Boo	57464.4703	0.0010	AG		-I	37	10)
GN Boo	57464.6193	0.0017	AG		-I	37	10)
GN Boo	57500.3607	0.0026	AG		-I	44	10)
GN Boo	57500.5120	0.0010	AG		-I	44	10)
GP Boo	57131.4808	0.0086	AG		-I	36	10)
GP Boo	57133.5326	0.0062	AG		-I	48	10)
GP Boo	57499.5205	0.0080	AG		-I	50	10)
GP Boo	57517.5333	0.0071	AG		-I	27	10)
GQ Boo	57500.3764	0.0014	AG		-I	44	10)
GQ Boo	57500.5688	0.0019	AG		-I	44	10)
GQ Boo	57517.4922	0.0019	AG		-I	27	10)
GR Boo	57500.4763	0.0007	AG		-I	44	10)
GR Boo	57517.4265	0.0011	AG		-I	27	10)
GS Boo	57464.4296	0.0016	AG		-I	37	10)
GU Boo	57464.4126	0.0010	AG		-I	36	10)
GU Boo	57464.6559	0.0003	AG		-I	36	10)
GV Boo	57446.4702	0.0003	MS		o	14	9)
GW Boo	57119.4516	0.0034	AG		-I	30	10)
GW Boo	57128.4893	0.0031	AG		-I	46	10)
GW Boo	57489.4087	0.0031	AG		-I	43	10)
GW Boo	57516.5166	0.0028	AG		-I	36	10)
GX Boo	57466.5359	0.0077	AG		-I	44	10)
HH Boo	57121.4784	0.0020	AG		-I	29	10)
HH Boo	57464.3602	0.0031	AG		-I	47	10)
HH Boo	57464.5179	0.0014	AG		-I	47	10)
HH Boo	57517.4179	0.0023	AG		-I	32	10)

HH Boo	57517.5730	0.0017	AG		-I	32	10)
IK Boo	57466.3677	0.0039	AG		-I	45	10)
IK Boo	57466.5176	0.0009	AG		-I	45	10)
IN Boo	57466.3837	0.0005	AG		-I	45	10)
IN Boo	57466.5274	0.0008	AG		-I	45	10)
IN Boo	57466.6693	0.0002	AG		-I	45	10)
IO Boo	57102.4467	0.0002	RAT RCR		V	56	6)
IO Boo	57466.3264	0.0029	AG		-I	47	10)
IO Boo	57466.4618	0.0010	AG		-I	47	10)
IO Boo	57466.5990	0.0013	AG		-I	47	10)
IX Boo	57466.4471	0.0020	AG		-I	43	10)
IX Boo	57466.6252	0.0014	AG		-I	43	10)
KO Boo	57466.4910	0.0045	AG		-I	39	10)
KW Boo	57128.5219	0.0040	AG		-I	45	10)
LM Boo	57500.3993	0.0024	AG		-I	43	10)
LM Boo	57500.5640	0.0014	AG		-I	43	10)
LM Boo	57517.4510	0.0008	AG		-I	27	10)
MN Boo	57464.4435	0.0036	AG		-I	47	10)
MN Boo	57464.6393	0.0011	AG		-I	47	10)
NX Boo	57128.4153	0.0012	AG		-I	42	10)
NX Boo	57128.5399	0.0045	AG		-I	42	10)
NX Boo	57464.4353	0.0019	AG		-I	36	10)
NX Boo	57464.5581	0.0016	AG		-I	36	10)
OQ Boo	57500.4752	0.0097	AG		-I	43	10)
OQ Boo	57517.3862	0.0003	AG		-I	26	10)
PU Boo	57489.3887	0.0026	AG		-I	46	10)
V376 Boo	57464.5345	0.0026	AG		-I	36	10)
Y Cam	57328.6246	0.0002	RAT RCR		V	26	6)
Y Cam	57414.5752	0.0054	AG		-I	53	10)
SS Cam	57338.7940	0.0200	AG		-I	12	10)
SV Cam	57296.2808	0.0013	AG		-I	74	10)
SV Cam	57296.5795	0.0042	AG		-I	74	10)
SV Cam	57466.4935	0.0016	AG		-I	56	10)
UU Cam	57474.3973	0.0043	AG		-I	54	10)
WW Cam	57275.5033	0.0001	RAT RCR		V	20	6)
XZ Cam	57284.4964	0.0015	RAT RCR		V	13	6)
AL Cam	57474.5687	0.0017	AG		-I	45	10)
AS Cam	57278.5274	0.0066	AG		-I	55	10)
AS Cam	57297.5742	0.0051	AG		-I	58	10)
AT Cam	57328.3035	0.0064	AG		-I	68	10)
AT Cam	57385.5343	0.0002	RAT RCR		V	26	6)
AW Cam	57364.5431	0.0085	AG		-I	82	10)
AY Cam	57299.5448	0.0089	AG		-I	56	10)
AY Cam	57466.3809	0.0042	AG		-I	56	10)
CP Cam	57296.5121	0.0010	AG		-I	71	10)
DI Cam	57474.4526	0.0274	AG		V	54	10)
DN Cam	57297.4025	0.0024	AG		-I	58	10)
DN Cam	57297.6532	0.0006	AG		-I	58	10)
FN Cam	57409.4939	0.0033	AG		-I	37	10)
LR Cam	57278.4122	0.0038	AG		-I	53	10)
LR Cam	57278.6241	0.0015	AG		-I	53	10)
LR Cam	57297.2935	0.0020	AG		-I	58	10)
LR Cam	57297.5132	0.0043	AG		-I	58	10)
NO Cam	57474.4439	0.0010	AG		-I	54	10)
NR Cam	57299.3330	0.0012	AG		-I	34	10)
NR Cam	57299.4584	0.0012	AG		-I	34	10)
NR Cam	57299.5889	0.0021	AG		-I	34	10)
NR Cam	57466.2959	0.0018	AG		-I	56	10)
NR Cam	57466.4252	0.0021	AG		-I	56	10)
NR Cam	57466.5542	0.0027	AG		-I	56	10)
NS Cam	57299.3761	0.0029	AG		-I	36	10)
NU Cam	57466.5415	0.0104	AG		-I	56	10)
NX Cam	57338.2982	0.0066	AG		-I	68	10)
NX Cam	57338.6109	0.0058	AG		-I	68	10)
OO Cam	57298.4066	0.0058	AG		-I	28	10)
OQ Cam	57270.4614	0.0001	RAT RCR	s	V	13	6)
OQ Cam	57296.2957	0.0010	AG		-I	71	10)
OQ Cam	57296.5118	0.0006	AG		-I	71	10)
OQ Cam	57298.4832	0.0041	AG		-I	46	10)
OQ Cam	57327.3804	0.0003	RAT RCR	s	V	99	6)
QU Cam	57281.4601	0.0010	RAT RCR		V	96	6)
V337 Cam	57295.3893	0.0014	AG		-I	64	10)
V362 Cam	57294.4201	0.0005	RAT RCR		V	25	6)

V366 Cam	57297.6009	0.0098	AG		-I	58	10)
V366 Cam	57305.3369	0.0118	AG		-I	44	10)
V369 Cam	57307.5767	0.0002	RAT RCR		V	15	6)
V382 Cam	57329.3322	0.0014	AG		-I	59	10)
V389 Cam	57278.3119	0.0033	AG		-I	53	10)
V389 Cam	57278.5324	0.0030	AG		-I	53	10)
V389 Cam	57297.4462	0.0002	RAT RCR		V	21	6)
V403 Cam	57328.3988	0.0108	AG		-I	68	10)
V403 Cam	57328.6059	0.0070	AG		-I	68	10)
V428 Cam	57299.3228	0.0026	AG		-I	32	10)
V428 Cam	57299.4678	0.0018	AG		-I	32	10)
V444 Cam	57299.4259	0.0022	AG		-I	34	10)
V444 Cam	57299.6075	0.0023	AG		-I	34	10)
V452 Cam	57099.5207	0.0005	RAT RCR		V	22	6)
V452 Cam	57364.4167	0.0014	AG		-I	81	10)
V452 Cam	57364.6102	0.0014	AG		-I	81	10)
V455 Cam	57100.3924	0.0002	RAT RCR		V	10	6)
V473 Cam	57091.4158	0.0001	RAT RCR	s	V	27	6)
V473 Cam	57091.5638	0.0001	RAT RCR		V	27	6)
V474 Cam	57409.4933	0.0017	AG		-I	39	10)
V475 Cam	57299.4628	0.0175	AG		-I	33	10)
V478 Cam	57299.4181	0.0037	AG		-I	68	10)
V479 Cam	57299.2748	0.0006	AG		-I	35	10)
V479 Cam	57299.4370	0.0010	AG		-I	35	10)
V479 Cam	57299.5987	0.0001	AG		-I	35	10)
V488 Cam	57299.3727	0.0020	AG		-I	36	10)
V488 Cam	57299.5014	0.0008	AG		-I	35	10)
V489 Cam	57276.5124	0.0017	AG		-I	45	10)
V489 Cam	57414.4082	0.0008	AG		-I	54	10)
V499 Cam	57345.4292	0.0014	AG		-I	58	10)
V508 Cam	57100.4729	0.0015	RAT RCR	s	V	19	6)
V508 Cam	57100.6166	0.0010	RAT RCR		V	19	6)
V514 Cam	57474.4993	0.0010	AG		-I	44	10)
V517 Cam	57131.3984	0.0098	AG		-I	36	10)
V530 Cam	57474.5754	0.0090	AG		-I	54	10)
TY Cnc	57131.3826	0.0011	AG		-I	19	10)
WW Cnc	57457.5213	0.0013	AG		-I	40	10)
WX Cnc	57409.4923	0.0025	AG		-I	38	10)
WY Cnc	57465.3797	0.0015	AG		-I	42	10)
AD Cnc	57131.4027	0.0020	AG		-I	19	10)
AH Cnc	56693.4478	0.0002	MS FR		o	45	9)
AO Cnc	57131.4268	0.0014	AG		-I	19	10)
EH Cnc	57364.5075	0.0003	RAT RCR		V	17	6)
GQ Cnc	57414.3070	0.0012	AG		-I	58	10)
GQ Cnc	57414.5183	0.0011	AG		-I	58	10)
IL Cnc	57414.3818	0.0005	AG		-I	31	10)
IL Cnc	57414.5167	0.0007	AG		-I	31	10)
IM Cnc	57414.3515	0.0017	AG		-I	49	10)
IT Cnc	57414.2969	0.0016	AG		-I	42	10)
IT Cnc	57414.4756	0.0029	AG		-I	42	10)
KY Cnc	57465.4033	0.0049	AG		-I	35	10)
VZ CVn	57133.3512	0.0017	AG		-I	46	10)
VZ CVn	57141.3559	0.0027	AG		-I	14	10)
VZ CVn	57464.4405	0.0010	AG		-I	47	10)
YZ CVn	57466.5289	0.0055	AG		-I	47	10)
BI CVn	57465.4213	0.0056	AG		-I	49	10)
BI CVn	57465.6096	0.0021	AG		-I	49	10)
BI CVn	57489.4319	0.0015	AG		-I	41	10)
BI CVn	57489.6259	0.0004	AG		-I	41	10)
BO CVn	57464.3632	0.0003	AG		-I	47	10)
BO CVn	57464.6202	0.0017	AG		-I	47	10)
CI CVn	57517.5615	0.0008	AG		-I	32	10)
DF CVn	57132.4859	0.0016	AG		-I	37	10)
DF CVn	57465.4285	0.0034	AG		-I	49	10)
DF CVn	57465.5913	0.0010	AG		-I	49	10)
DF CVn	57489.4541	0.0009	AG		-I	41	10)
DF CVn	57489.6174	0.0001	AG		-I	41	10)
DF CVn	57514.4618	0.0014	AG		-I	36	10)
DH CVn	57132.4952	0.0012	AG		-I	37	10)
DH CVn	57489.5208	0.0009	AG		-I	41	10)
DH CVn	57499.3982	0.0017	AG		-I	50	10)
DH CVn	57499.5806	0.0009	AG		-I	50	10)
DH CVn	57514.3952	0.0009	AG		-I	36	10)

DH CVn	57514.5771	0.0027	AG	-I	36	10)
DI CVn	57132.3671	0.0009	AG	-I	37	10)
DI CVn	57132.5199	0.0001	AG	-I	37	10)
DI CVn	57514.3654	0.0013	AG	-I	36	10)
DI CVn	57514.5188	0.0010	AG	-I	36	10)
DK CVn	57514.3562	0.0004	AG	-I	36	10)
DL CVn	57489.5221	0.0038	AG	-I	41	10)
DL CVn	57499.4799	0.0027	AG	-I	50	10)
DQ CVn	57132.3900	0.0021	AG	-I	37	10)
DQ CVn	57489.4003	0.0041	AG	-I	41	10)
DQ CVn	57499.4824	0.0032	AG	-I	50	10)
DQ CVn	57514.4660	0.0014	AG	-I	36	10)
DR CVn	57132.4062	0.0018	AG	-I	37	10)
DR CVn	57132.5632	0.0035	AG	-I	37	10)
DR CVn	57489.4413	0.0050	AG	-I	41	10)
DR CVn	57489.5953	0.0021	AG	-I	41	10)
DR CVn	57499.4651	0.0072	AG	-I	50	10)
DR CVn	57514.4480	0.0019	AG	-I	36	10)
DU CVn	57514.4873	0.0011	AG	-I	36	10)
DX CVn	57132.4632	0.0025	AG	-I	37	10)
DX CVn	57489.4839	0.0019	AG	-I	41	10)
DX CVn	57499.4896	0.0003	AG	-I	50	10)
EN CVn	57128.5684	0.0032	AG	-I	46	10)
EO CVn	57489.3842	0.0012	AG	-I	41	10)
EO CVn	57489.5655	0.0014	AG	-I	41	10)
EO CVn	57499.4349	0.0012	AG	-I	50	10)
EX CVn	57132.3651	0.0022	AG	-I	37	10)
EX CVn	57132.5018	0.0013	AG	-I	37	10)
EX CVn	57465.5090	0.0026	AG	-I	48	10)
EX CVn	57465.6391	0.0026	AG	-I	48	10)
EX CVn	57489.4806	0.0015	AG	-I	41	10)
EX CVn	57489.6217	0.0002	AG	-I	41	10)
EX CVn	57514.4252	0.0008	AG	-I	36	10)
EX CVn	57514.5646	0.0011	AG	-I	36	10)
EY CVn	57132.3808	0.0018	AG	-I	37	10)
EY CVn	57132.5521	0.0011	AG	-I	37	10)
EY CVn	57489.4616	0.0027	AG	-I	41	10)
EY CVn	57499.3988	0.0020	AG	-I	50	10)
EY CVn	57499.5732	0.0041	AG	-I	50	10)
FN CVn	57128.3776	0.0063	AG	-I	46	10)
GG CVn	57448.4843	0.0002	MS	o	90	9)
GG CVn	57466.4311	0.0021	AG	-I	45	10)
GG CVn	57466.6241	0.0008	AG	-I	45	10)
GM CVn	57119.5361	0.0036	AG	-I	30	10)
GM CVn	57464.5003	0.0023	AG	-I	47	10)
CM CMa	57051.0174	0.0010	MS FR	V	65	3)
CM CMa	57061.0428	0.0010	MS FR	V	41	3)
EE CMa	57087.9808	0.0020	MS FR	V	93	3)
AM CMi	57459.3055	0.0040	BRW	V	13	2)
AM CMi	57464.390	0.003	BRW	V	15	2)
BB CMi	56730.3349	0.0003	MS FR	o	44	9)
SX Cas	54367.4120	0.2559	PGL		96	21) SWASP
TW Cas	57261.4643	0.0034	AG	-I	49	10)
TX Cas	57296.4637	0.0414	AG	-I	74	10)
XX Cas	57266.3831	0.0195	AG	-I	47	10)
ZZ Cas	57245.4588	0.0070	AG	-I	36	10)
ZZ Cas	57590.5413	0.0026	AG	-I	35	10)
AB Cas	57266.3297	0.0011	AG	-I	48	10)
AL Cas	56590.3105	0.0001	MS FR	o	46	9)
AX Cas	57265.4799	0.0015	AG	-I	29	10)
AX Cas	57366.3433	0.0007	JU	o	78	12)
BH Cas	57266.5381	0.0023	AG	-I	35	10)
BS Cas	57265.4715	0.0008	AG	-I	29	10)
BS Cas	57364.3572	0.0012	JU	o	10	12)
BS Cas	57457.2936	0.0003	SCI	o	44	12)
BZ Cas	57264.5818	0.0001	RAT RCR	V	16	6)
CC Cas	57364.31	0.040	AG	-I	60	10)
CW Cas	57330.4082	0.0010	AG	-I	28	10)
DN Cas	57298.3240	0.0139	AG	-I	45	10)
DN Cas	57299.4670	0.0062	AG	-I	52	10)
DO Cas	57295.4824	0.0006	AG	-I	63	10)
DZ Cas	57329.3579	0.0028	AG	-I	44	10)
EG Cas	57266.5600	0.0013	AG	-I	35	10)

EG Cas	57294.3658	0.0048	AG	-I	51	10)
EG Cas	57307.5272	0.0002	SCI	o	58	12)
EI Cas	57322.3858	0.0014	AG	-I	25	10)
EP Cas	57266.5177	0.0027	AG	-I	35	10)
EP Cas	57294.5802	0.0008	AG	-I	52	10)
EP Cas	57297.4297	0.0026	AG	-I	30	10)
EP Cas	57329.5592	0.0019	AG	-I	44	10)
EY Cas	57322.3790	0.0014	AG	-I	24	10)
EY Cas	57329.3681	0.0023	AG	-I	45	10)
EY Cas	57329.6087	0.0017	AG	-I	45	10)
GG Cas	57307.5196	0.0100	BRW	U	78	2)
GG Cas	57307.5231	0.0100	BRW	V	16	2)
GG Cas	57307.5293	0.0100	BRW	B	12	2)
GG Cas	57322.5559	0.0090	BRW	V	10	2)
GG Cas	57322.5784	0.0090	BRW	B	10	2)
GG Cas	57322.5784	0.0090	BRW	U	10	2)
GG Cas	57405.2454	0.0040	BRW	V	15	2)
GH Cas	57260.4949	0.0019	AG	-I	30	10)
GK Cas	57260.4517	0.0033	AG	-I	30	10)
GT Cas	57329.3619	0.0030	AG	-I	45	10)
GU Cas	57291.4440	0.0040	BRW	V	15	2)
GU Cas	57322.3777	0.0023	AG	-I	25	10)
GU Cas	57322.4725	0.0030	BRW	V	18	2)
IL Cas	57275.4769	0.0060	BRW	V	36	2)
IQ Cas	57265.4965	0.0064	AG	-I	30	10)
IR Cas	57261.5483	0.0050	AG	-I	37	10)
IS Cas	57266.3699	0.0027	AG	-I	35	10)
LR Cas	57260.4087	0.0196	AG	-I	39	10)
MN Cas	57278.5173	0.0121	AG	-I	56	10)
MS Cas	57322.3690	0.0008	AG	-I	25	10)
MS Cas	57329.4039	0.0022	AG	-I	44	10)
MT Cas	57297.4095		AG	-I	29	10)
MT Cas	57322.3625	0.0006	AG	-I	28	10)
MT Cas	57364.2629	0.0004	AG	-I	42	10)
MT Cas	57364.4204	0.0018	AG	-I	42	10)
MW Cas	57364.2448	0.0141	AG	-I	43	10)
NU Cas	57329.4092	0.0040	AG	-I	43	10)
NZ Cas	57330.4381	0.0028	AG	-I	27	10)
OR Cas	57329.5707	0.0020	AG	-I	43	10)
OR Cas	57356.3551	0.0002	MS	-U-I	45	8)
OX Cas	57242.5248	0.0131	AG	-I	41	10)
OX Cas	57247.5032	0.0130	AG	-I	39	10)
OX Cas	57257.4647	0.0110	AG	-I	38	10)
OX Cas	57298.5699	0.0021	AG	-I	45	10)
OX Cas	57328.4435	0.0050	AG	-I	57	10)
OX Cas	57409.3087	0.0022	JU	o	10	12)
PV Cas	57265.6028	0.0017	AG	-I	46	10)
PV Cas	57294.4503	0.0010	BRW	V	38	2)
PV Cas	57294.4510	0.0022	AG	-I	53	10)
PV Cas	57574.5255	0.0006	AG	-I	27	10)
PV Cas	57588.5303	0.0008	AG	-I	36	10)
QQ Cas	57327.3696	0.0037	AG	-I	63	10)
QQ Cas	57329.5155	0.0083	AG	-I	44	10)
V345 Cas	57261.4044	0.0035	AG	-I	37	10)
V355 Cas	57297.4713	0.0007	AG	-I	32	10)
V360 Cas	57297.5155	0.0012	AG	-I	32	10)
V361 Cas	57322.3843	0.0029	AG	-I	26	10)
V361 Cas	57354.3392	0.0018	MS	V	90	8)
V374 Cas	57266.5506	0.0009	AG	-I	35	10)
V375 Cas	57265.5606	0.0068	AG	-I	46	10)
V375 Cas	57590.4531	0.0009	AG	-I	35	10)
V380 Cas	57245.4657	0.0084	AG	-I	36	10)
V381 Cas	57244.5437	0.0064	AG	-I	36	10)
V381 Cas	57245.3861	0.0035	AG	-I	36	10)
V381 Cas	57265.4950	0.0074	AG	-I	46	10)
V381 Cas	57266.3377	0.0020	AG	-I	47	10)
V381 Cas	57307.3972	0.0014	JU	o	82	12)
V389 Cas	57257.4074	0.0062	AG	-I	38	10)
V396 Cas	57328.3233	0.0055	AG	-I	47	10)
V445 Cas	57264.5708	0.0087	AG	-I	56	10)
V448 Cas	57356.3797	0.0003	MS	V	46	8)
V471 Cas	57260.3384	0.0001	AG	-I	30	10)
V471 Cas	57260.5399	0.0020	AG	-I	30	10)

V471 Cas	57265.3507	0.0015	AG		-I	29	10)
V471 Cas	57265.5501	0.0005	AG		-I	29	10)
V471 Cas	57384.4277	0.0004	SCI		o	49	12)
V473 Cas	57265.3323	0.0003	AG		-I	29	10)
V473 Cas	57265.5403	0.0001	AG		-I	29	10)
V520 Cas	57266.5755	0.0012	AG		-I	35	10)
V520 Cas	57376.2967	0.0014	JU	s	o	11	12)
V523 Cas	57244.5788	0.0007	AG		-I	36	10)
V523 Cas	57245.3970	0.0007	AG		-I	36	10)
V523 Cas	57245.5133	0.0020	AG		-I	36	10)
V523 Cas	57266.4287	0.0014	AG		-I	47	10)
V523 Cas	57266.5463	0.0021	AG		-I	47	10)
V541 Cas	57294.4737	0.0021	AG		-I	54	10)
V608 Cas	57383.5114	0.0001	SCI		o	83	12)
V646 Cas	57305.4187	0.0010	AG		-I	38	10)
V651 Cas	57294.5434	0.0020	AG		-I	54	10)
V651 Cas	57297.5348	0.0003	AG		-I	32	10)
V765 Cas	57260.5055	0.0029	AG		-I	30	10)
V766 Cas	57265.5269	0.0081	AG		-I	46	10)
V766 Cas	57287.5376	0.0045	AG		-I	40	10)
V821 Cas	57246.5359	0.0052	AG		-I	37	10)
V959 Cas	57297.5348	0.0006	AG		-I	29	10)
V961 Cas	57329.4085	0.0102	AG		-I	43	10)
V1010 Cas	57244.4662	0.0117	AG		-I	33	10)
V1011 Cas	57330.3269	0.0065	AG		-I	28	10)
V1031 Cas	57343.4488	0.0006	AG		-I	30	10)
V1044 Cas	57245.4055	0.0005	AG		-I	36	10)
V1049 Cas	57246.5339	0.0134	AG		-I	36	10)
V1053 Cas	57356.4128	0.0024	MS		-U-I	45	8)
V1060 Cas	57246.4866	0.0093	AG		-I	37	10)
V1061 Cas	57264.4569	0.0347	AG		-I	57	10)
V1062 Cas	57278.5590	0.0160	AG		-I	57	10)
V1070 Cas	57295.3928	0.0012	AG		-I	59	10)
V1094 Cas	57265.4196	0.0017	AG		-I	29	10)
V1107 Cas	55473.2788	0.0004	MS FR		o	76	17)
V1107 Cas	55473.4162	0.0003	MS FR		o	76	17)
V1107 Cas	55820.3757	0.0004	MS FR		o	93	17)
V1107 Cas	57265.3601	0.0034	AG		-I	29	10)
V1107 Cas	57265.4940	0.0006	AG		-I	29	10)
V1107 Cas	57366.3821	0.0008	JU		o	78	12)
V1115 Cas	57260.4753	0.0022	AG		-I	30	10)
V1115 Cas	57265.4874	0.0026	AG		-I	29	10)
V1138 Cas	53251.3769	0.0005	MS FR		o	67	15)
V1138 Cas	57265.4649	0.0034	AG		-I	29	10)
V1139 Cas	57265.3576	0.0015	AG		-I	29	10)
V1139 Cas	57265.5068	0.0015	AG		-I	29	10)
V1166 Cas	57298.5153	0.0026	AG		-I	42	10)
V1175 Cas	57329.4337	0.0057	AG		-I	59	10)
V1186 Cas	57261.5607	0.0022	AG		-I	37	10)
V1248 Cas	57266.5010	0.0033	AG		-I	35	10)
V1248 Cas	57322.4442	0.0038	AG		-I	25	10)
V1254 Cas	57266.4906	0.0040	AG		-I	35	10)
V1261 Cas	57329.4357	0.0022	AG		-I	43	10)
V1261 Cas	57329.5924	0.0013	AG		-I	43	10)
V1287 Cas	57261.4746	0.0027	AG		-I	37	10)
V1292 Cas	57266.4850	0.0007	AG		-I	35	10)
V1295 Cas	57266.4506	0.0091	AG		-I	35	10)
V1295 Cas	57329.4481	0.0097	AG		-I	44	10)
SU Cep	57305.2736	0.0008	AG		-I	41	10)
SU Cep	57564.4282	0.0006	AG		-I	29	10)
VW Cep	57123.4424	0.0045	AG		-I	37	10)
VW Cep	57123.5819	0.0018	AG		-I	37	10)
VW Cep	57516.4154	0.0037	AG		-I	36	10)
VW Cep	57516.5521	0.0023	AG		-I	36	10)
VZ Cep	57131.4828	0.0024	AG		-I	36	10)
VZ Cep	57295.3796	0.0001	AG		-I	51	10)
VZ Cep	57518.4428	0.0013	AG		-I	35	10)
WW Cep	57327.4568	0.0022	AG		-I	49	10)
WX Cep	57256.4926	0.0082	AG		-I	42	10)
WY Cep	57297.5368	0.0034	AG		-I	50	10)
WZ Cep	57264.4118	0.0003	RAT RCR		V	43	6)
XX Cep	57295.4289	0.0030	BRW		V	50	2)
XY Cep	57264.3667	0.0043	AG		-I	57	10)

XZ Cep	57246.4586	0.0302	AG		-I	37	10)
XZ Cep	57297.4217	0.0199	AG		-I	50	10)
ZZ Cep	57260.3871	0.0023	AG		-I	43	10)
AI Cep	57287.3860	0.0169	AG		-I	38	10)
BE Cep	57265.5048	0.0015	AG		-I	46	10)
BE Cep	57294.3619	0.0019	AG		-I	48	10)
BE Cep	57294.5790	0.0032	AG		-I	48	10)
BE Cep	57298.6085	0.0006	AG		-I	18	10)
CQ Cep	57261.5754	0.0070	AG		-I	49	10)
CW Cep	57247.5267	0.0060	AG		-I	37	10)
CX Cep	57338.4150	0.0362	AG		-I	66	10)
EF Cep	57474.4380	0.0020	AG		-I	54	10)
EG Cep	57123.5428	0.0028	AG		-I	38	10)
EG Cep	57516.4884	0.0018	AG		-I	36	10)
EG Cep	57518.3961	0.0017	AG		-I	34	10)
EI Cep	57125.5398	0.0138	AG		-I	43	10)
EI Cep	57256.3562	0.0012	AG		-I	64	10)
EK Cep	57256.4980	0.0117	AG		-I	42	10)
EK Cep	57568.4697	0.0015	AG		V	17	10)
EY Cep	57385.5566	0.0016	AG		-I	67	10)
GK Cep	57131.5122	0.0067	AG		-I	36	10)
GS Cep	57246.3643	0.0008	AG		-I	37	10)
GT Cep	57260.3970	0.0037	AG		-I	43	10)
IP Cep	57327.6010	0.0032	AG		-I	47	10)
KP Cep	57296.4548	0.0017	AG		-I	31	10)
NW Cep	57242.4299	0.0142	AG		-I	41	10)
V338 Cep	57330.3482	0.0032	AG		-I	30	10)
V383 Cep	57240.4992	0.0081	AG		-I	37	10)
V397 Cep	57517.4351	0.0024	AG		-I	31	10)
V397 Cep	57518.3954	0.0024	AG		-I	35	10)
V397 Cep	57590.4730	0.0016	AG		-I	35	10)
V736 Cep	57244.4324	0.0050	AG		-I	31	10)
V736 Cep	57564.4106	0.0030	AG		-I	29	10)
V737 Cep	57568.4563	0.0029	AG		-I	16	10)
V744 Cep	57327.4213	0.0008	AG		-I	48	10)
V746 Cep	57298.5350	0.0002	RAT	RCR	V	20	6)
V746 Cep	57327.5162	0.0051	AG		-I	47	10)
V806 Cep	57474.5295	0.0042	AG		-I	54	10)
V808 Cep	57080.3878	0.0003	RAT	RCR	V	11	6)
V813 Cep	57588.4574	0.0009	AG		-I	21	10)
V835 Cep	57588.5038	0.0013	AG		-I	21	10)
V836 Cep	57588.4609	0.0009	AG		-I	21	10)
V837 Cep	57588.4963	0.0015	AG		-I	21	10)
V849 Cep	57327.5000	0.0016	AG		-I	48	10)
V863 Cep	57327.5458	0.0154	AG		-I	48	10)
V868 Cep	57131.5700	0.0015	AG		-I	19	10)
V868 Cep	57338.3089	0.0008	AG		-I	66	10)
V875 Cep	57210.5315	0.0003	RAT	RCR	V	14	6)
V890 Cep	57264.5722	0.0032	AG		-I	54	10)
V890 Cep	57265.5437	0.0187	AG		-I	46	10)
V890 Cep	57266.5191	0.0096	AG		-I	48	10)
V898 Cep	57246.4698	0.0269	AG		-I	37	10)
V900 Cep	57294.5875	0.0009	AG		-I	76	10)
V909 Cep	57274.4196	0.0004	RAT	RCR s	V	14	6)
V917 Cep	57327.4380	0.0024	AG		-I	47	10)
V917 Cep	57343.4980	0.0019	AG		-I	31	10)
V923 Cep	57307.3026	0.0003	RAT	RCR	V	13	6)
V927 Cep	57296.4929	0.0084	AG		-I	69	10)
V930 Cep	57327.3463	0.0037	AG		-I	47	10)
V930 Cep	57327.5407	0.0060	AG		-I	46	10)
V930 Cep	57343.4910	0.0024	AG		V	29	10)
V944 Cep	57238.3224	0.0033	AG		-I	62	10)
V944 Cep	57297.3502	0.0188	AG		-I	54	10)
V944 Cep	57579.4547	0.0024	AG		-I	29	10)
V959 Cep	57343.3908	0.0018	AG		V	29	10)
V961 Cep	57256.5008	0.0086	AG		-I	42	10)
V972 Cep	57588.4775	0.0010	AG		-I	21	10)
RW Com	57121.4118	0.0008	AG		-I	32	10)
RW Com	57121.5315	0.0032	AG		-I	32	10)
RW Com	57465.3269	0.0018	AG		-I	49	10)
RW Com	57465.4470	0.0008	AG		-I	49	10)
RW Com	57465.5661	0.0015	AG		-I	49	10)
RZ Com	57125.3834	0.0010	AG		-I	34	10)

RZ Com	57125.5517	0.0006	AG		-I	34	10)
RZ Com	57464.3990	0.0017	AG		-I	47	10)
RZ Com	57464.5685	0.0009	AG		-I	47	10)
SS Com	57475.4611	0.0001	SCI		o	10	12)
UX Com	57119.4391	0.0061	AG		-I	30	10)
UX Com	57465.4837	0.0215	AG		-I	47	10)
CN Com	57133.4736	0.0032	AG		-I	48	10)
EK Com	57465.4279	0.0024	AG		-I	47	10)
EK Com	57465.5615	0.0023	AG		-I	47	10)
LL Com	56719.4362	0.0001	MS		o	22	9)
LL Com	57465.5221	0.0013	AG		-I	47	10)
LO Com	57465.6153	0.0007	AG		-I	49	10)
LO Com	57489.3802	0.0005	JU	s	o	56	12)
LQ Com	57465.5017	0.0049	AG		-I	49	10)
LR Com	57464.4657	0.0022	AG		-I	47	10)
MM Com	57465.4661	0.0020	AG		-I	47	10)
MM Com	57465.6174	0.0012	AG		-I	47	10)
MR Com	57465.4856	0.0012	AG		-I	47	10)
MW Com	57123.5349	0.0067	AG		-I	37	10)
NV Com	57123.4062	0.0003	RAT RCR		V	88	6)
NV Com	57465.3682	0.0024	AG		-I	46	10)
NV Com	57465.5478	0.0029	AG		-I	46	10)
U CrB	57128.4970	0.0116	AG		-I	45	10)
RT CrB	57131.4371	0.0106	AG		-I	36	10)
RW CrB	57125.4002	0.0095	AG		-I	42	10)
RW CrB	57131.5812	0.0019	AG		-I	36	10)
RW CrB	57137.3925	0.0011	AG		-I	37	10)
RW CrB	57500.6007	0.0010	AG		-I	44	10)
TU CrB	57125.4582	0.0007	AG		-I	34	10)
TU CrB	57133.5263	0.0013	AG		-I	37	10)
TW CrB	57131.6102	0.0006	AG		-I	33	10)
TW CrB	57132.4935	0.0023	AG		-I	36	10)
TW CrB	57514.3799	0.0011	AG		-I	35	10)
TW CrB	57515.5569	0.0016	AG		-I	35	10)
YY CrB	57123.5230	0.0028	AG		-I	38	10)
YY CrB	57489.5371	0.0018	AG		-I	46	10)
AM CrB	57125.3568	0.0006	AG		-I	33	10)
AM CrB	57133.4472	0.0075	AG		-I	38	10)
AR CrB	57131.5397	0.0018	AG		-I	33	10)
AR CrB	57514.3878	0.0025	AG		-I	35	10)
AR CrB	57514.5832	0.0020	AG		-I	35	10)
AR CrB	57515.3776	0.0035	AG		-I	35	10)
AR CrB	57515.5771	0.0004	AG		-I	35	10)
AR CrB	57517.3690	0.0015	AG		-I	33	10)
AR CrB	57517.5654	0.0006	AG		-I	33	10)
AS CrB	57125.4466	0.0016	AG		-I	34	10)
AS CrB	57133.4409	0.0022	AG		-I	38	10)
AY CrB	57464.4939	0.0015	AG		-I	37	10)
BR CrB	57489.5421	0.0127	AG		-I	46	10)
BX CrB	57133.4880	0.0025	AG		-I	38	10)
CL CrB	57125.4020	0.0007	AG		-I	33	10)
CL CrB	57125.5601	0.0023	AG		-I	33	10)
CL CrB	57133.3717	0.0021	AG		-I	38	10)
CL CrB	57133.5300	0.0008	AG		-I	38	10)
Y Cyg	57240.5650	0.0057	AG		-I	37	10)
UW Cyg	57189.5199	0.0003	RAT RCR		V	10	6)
UW Cyg	57265.4386	0.0038	AG		-I	39	10)
WW Cyg	57245.5519	0.0017	AG		-I	36	10)
WZ Cyg	57563.4790	0.0004	AG		-I	28	10)
ZZ Cyg	57294.4611	0.0081	AG		-I	36	10)
ZZ Cyg	57564.4435	0.0008	AG		-I	29	10)
BR Cyg	57298.3698	0.0029	AG		-I	27	10)
CG Cyg	57240.4118	0.0012	AG		-I	37	10)
CG Cyg	57305.4209	0.0010	AG		-I	36	10)
CG Cyg	57577.4430	0.0012	AG		-I	29	10)
CV Cyg	57256.4264	0.0072	AG		-I	38	10)
CV Cyg	57579.4744	0.0003	AG		V	35	10)
CV Cyg	57579.4756	0.0001	SCI	s	o	93	12)
DK Cyg	57607.4909	0.0001	SCI	s	o	13	12)
DL Cyg	57588.5653	0.0080	AG		-I	51	10)
DO Cyg	57241.4711	0.0002	SCI	s	o	12	12)
DP Cyg	57338.4725	0.0055	AG		-I	66	10)
EN Cyg	57562.4452	0.0003	AG		-I	41	10)

KR Cyg	57574.5243	0.0003	AG		-I	28	10)
KV Cyg	57574.4870	0.0005	AG		-I	27	10)
MR Cyg	57562.4597	0.0008	AG		-I	26	10)
V366 Cyg	57237.4528	0.0042	AG		-I	35	10)
V366 Cyg	57260.4662	0.0072	AG		-I	40	10)
V366 Cyg	57580.5067	0.0016	AG		-I	31	10)
V382 Cyg	57574.3965	0.0031	AG		-I	28	10)
V388 Cyg	57564.4983	0.0021	AG		-I	24	10)
V393 Cyg	57260.4868	0.0068	AG		-I	37	10)
V398 Cyg	57307.5616	0.0030	FR	s	-I	15	10)
V401 Cyg	57295.3440	0.0001	RAT RCR	s	V	10	6)
V401 Cyg	57562.5213	0.0011	AG		-I	26	10)
V442 Cyg	57332.4373	0.0077	AG		R	35	10)
V442 Cyg	57332.4383	0.0032	AG		V	31	10)
V447 Cyg	57574.4506	0.0017	AG		-I	27	10)
V456 Cyg	57266.4456	0.0024	AG		-I	47	10)
V463 Cyg	57589.5045	0.0001	SCI		o	18	12)
V466 Cyg	57546.4189	0.0011	AG		-I	24	10)
V466 Cyg	57587.4720	0.0001	SCI	s	o	12	12)
V477 Cyg	57238.4980	0.0010	AG		-I	39	10)
V477 Cyg	57241.5456	0.0038	AG		-I	35	10)
V477 Cyg	57292.4784	0.0030	BRW		V	95	2)
V477 Cyg	57292.4800	0.0050	BRW		U	90	2)
V477 Cyg	57292.5009	0.0020	BRW		B	99	2)
V477 Cyg	57579.5108	0.0013	AG		-I	29	10)
V478 Cyg	57247.4477	0.0099	AG		-I	37	10)
V478 Cyg	57574.4555	0.0021	AG		-I	27	10)
V484 Cyg	57256.4377	0.0004	SCI		o	44	12)
V498 Cyg	57266.4339	0.0176	AG		-I	47	10)
V499 Cyg	57332.3835	0.0009	AG		-I	39	10)
V505 Cyg	57574.4654	0.0017	AG		-I	27	10)
V526 Cyg	57577.4823	0.0002	SCI	s	o	63	12)
V536 Cyg	57296.3241	0.0033	AG		-I	32	10)
V628 Cyg	57296.3420	0.0015	AG		-I	32	10)
V675 Cyg	57131.5413	0.0009	AG		-I	18	10)
V680 Cyg	57261.5572	0.0072	AG		-I	49	10)
V680 Cyg	57287.3390	0.0084	AG		-I	37	10)
V687 Cyg	57577.5104	0.0007	AG		-I	29	10)
V703 Cyg	57296.4310	0.0018	AG		-I	32	10)
V728 Cyg	57206.4825	0.0002	RAT RCR		V	13	6)
V787 Cyg	57247.3810	0.0015	AG		-I	40	10)
V787 Cyg	57574.4836	0.0004	AG		-I	28	10)
V788 Cyg	57339.4	0.1	VLM		V		19)
V796 Cyg	57516.4748	0.0036	AG		-I	32	10)
V796 Cyg	57590.5190	0.0014	AG		-I	35	10)
V822 Cyg	57574.4318	0.0004	AG		-I	27	10)
V822 Cyg	57579.5027	0.0001	AG		-I	35	10)
V824 Cyg	57574.4465	0.0011	AG		-I	27	10)
V828 Cyg	57260.3650	0.0065	AG		-I	40	10)
V836 Cyg	57574.4643	0.0026	AG		-I	27	10)
V841 Cyg	57562.4570	0.0004	AG		V	42	10)
V874 Cyg	57562.4598	0.0002	AG		-I	42	10)
V885 Cyg	57580.5033	0.0017	AG		-I	31	10)
V889 Cyg	57244.4173	0.0149	AG		-I	43	10)
V889 Cyg	57563.4212	0.0004	AG		-I	28	10)
V891 Cyg	57300.3817	0.0040	BRW		U	47	2)
V891 Cyg	57300.3829	0.0030	BRW		B	59	2)
V891 Cyg	57300.3848	0.0040	BRW		V	58	2)
V891 Cyg	57580.5314	0.0011	AG		-I	31	10)
V891 Cyg	57582.4398	0.0020	BRW		V	25	2)
V909 Cyg	57244.4669	0.0051	AG		-I	43	10)
V909 Cyg	57568.4884	0.0008	AG		-I	20	10)
V909 Cyg	57582.5146	0.0010	BRW		V	78	2)
V912 Cyg	57579.4850	0.0005	AG		-I	35	10)
V974 Cyg	57562.4529	0.0004	AG		-I	42	10)
V1011 Cyg	57579.5029	0.0008	AG		-I	34	10)
V1018 Cyg	57579.4520	0.0006	AG		V	35	10)
V1034 Cyg	57298.3757	0.0002	RAT RCR		V	10	6)
V1061 Cyg	57366.2818	0.0050	BRW		V	19	2)
V1083 Cyg	57261.5098	0.0096	AG		-I	49	10)
V1083 Cyg	57287.5158	0.0065	AG		-I	36	10)
V1143 Cyg	57278.3199	0.0019	AG		-I	57	10)
V1171 Cyg	57247.5475	0.0056	AG		-I	36	10)

V1171 Cyg	57579.4486	0.0005	AG		V	35	10)
V1193 Cyg	57588.4970	0.0005	AG		-I	21	10)
V1345 Cyg	57293.4612	0.0020	MZ		-I	16	13)
V1345 Cyg	57306.3194	0.0020	MZ		-I	17	13)
V1356 Cyg	57278.4798	0.0094	AG		-I	44	10)
V1401 Cyg	57564.4748	0.0014	AG		-I	21	10)
V1411 Cyg	57277.3643	0.0002	RAT RCR		V	10	6)
V1414 Cyg	57564.4245	0.0011	AG		-I	21	10)
V1417 Cyg	57564.4702	0.0013	AG		-I	21	10)
V1815 Cyg	57298.3243	0.0050	WTR	s	o	90	11)
V1815 Cyg	57564.5118	0.0016	AG		-I	22	10)
V1823 Cyg	57265.4339	0.0002	FR	s	-I	74	10)
V1877 Cyg	57287.4719	0.0007	FR	s	-I	63	10)
V1877 Cyg	57297.5317	0.0008	FR		-I	72	10)
V1877 Cyg	57298.3933	0.0004	FR		-I	51	10)
V1877 Cyg	57307.3021	0.0006	FR	s	-I	84	10)
V2021 Cyg	57307.3828	0.0007	FR		-I	64	10)
V2021 Cyg	57577.4824	0.0008	AG		-I	29	10)
V2247 Cyg	57298.4598	0.0013	FR	s	-I	87	10)
V2263 Cyg	57296.3719	0.0031	AG		-I	31	10)
V2477 Cyg	57563.4584	0.0006	AG		-I	28	10)
V2517 Cyg	57181.4694	0.0002	RAT RCR		V	14	6)
V2517 Cyg	57563.4199	0.0018	AG		-I	28	10)
V2520 Cyg	57238.4130	0.0040	AG		-I	39	10)
V2520 Cyg	57588.4448	0.0015	AG		-I	37	10)
V2524 Cyg	57588.4989	0.0008	AG		-I	21	10)
V2545 Cyg	57332.4558	0.0044	AG		-I	33	10)
V2552 Cyg	57563.4225	0.0013	AG		-I	28	10)
V2554 Cyg	57563.5009	0.0016	AG		-I	28	10)
V2558 Cyg	57287.3216	0.0003	FR		-I	82	10)
V2558 Cyg	57297.6119	0.0007	FR		-I	13	10)
V2558 Cyg	57307.4327	0.0004	FR		-I	66	10)
V2646 Cyg	57131.5916	0.0024	AG		-I	19	10)
V2657 Cyg	57131.5941	0.0009	AG		-I	19	10)
V2657 Cyg	57564.4982	0.0019	AG		-I	21	10)
W Del	57237.4328	0.0076	AG		-I	36	10)
TY Del	57237.5481	0.0021	AG		-I	36	10)
AL Del	57231.5087	0.0006	MS		-U-I	39	8)
AV Del	57257.4764	0.0125	AG		-I	37	10)
BY Del	57257.5183	0.0140	AG		-I	33	10)
CR Del	57204.5134	0.0007	MS		o	20	9)
DK Del	57257.4250	0.0034	AG		-I	33	10)
EX Del	57257.5142	0.0010	AG		-I	33	10)
FZ Del	57238.4576	0.0013	AG		-I	39	10)
FZ Del	57241.5909	0.0003	AG		-I	35	10)
FZ Del	57588.5557	0.0010	AG		-I	36	10)
LY Del	57264.5161	0.0031	AG		-I	41	10)
MR Del	56174.3110	0.0002	RAT RCR		V	87	6)
MR Del	57240.3821	0.0016	AG		-I	37	10)
MR Del	57574.5237	0.0017	AG		-I	26	10)
OX Del	57264.4053	0.0187	AG		-I	57	10)
OZ Del	57204.5412	0.0005	RAT RCR		V	13	6)
PP Del	57260.4946	0.0113	AG		-I	43	10)
Z Dra	57409.3904	0.0025	AG		-I	38	10)
RR Dra	57238.5025	0.0001	RAT RCR		V	17	6)
RX Dra	57136.4939	0.0078	AG		-I	31	10)
RX Dra	57562.4643	0.0008	AG		-I	26	10)
RZ Dra	57128.3891	0.0105	AG		-I	46	10)
RZ Dra	57261.4227	0.0021	AG		-I	32	10)
RZ Dra	57515.3789	0.0012	AG		-I	35	10)
TW Dra	57474.4108	0.0022	AG		-I	45	10)
TZ Dra	57136.5032	0.0021	AG		-I	31	10)
TZ Dra	57515.3959	0.0036	AG		-I	34	10)
UZ Dra	57123.4373	0.0030	AG		-I	38	10)
UZ Dra	57516.4247	0.0011	AG		-I	36	10)
AI Dra	57123.5849	0.0017	AG		-I	34	10)
AI Dra	57134.3720	0.0028	AG		-I	36	10)
AI Dra	57499.4145	0.0124	AG		-I	50	10)
AX Dra	57474.3382	0.0031	AG		-I	45	10)
AX Dra	57474.6259	0.0001	AG		-I	45	10)
BF Dra	57248.3955	0.0118	AG		-I	45	10)
BF Dra	57265.4023	0.0038	AG		-I	35	10)
BF Dra	57517.4582	0.0230	AG		-I	32	10)

BH Dra	57134.5466	0.0013	AG		-I	30	10)
BH Dra	57293.5425	0.0002	SCI	s	o	10	12)
BH Dra	57563.4150	0.0011	AG		-I	28	10)
BS Dra	57134.3592	0.0013	AG		-I	36	10)
BU Dra	57295.5153	0.0002	SCI		o	74	12)
BU Dra	57474.5327	0.0023	AG		-I	44	10)
BU Dra	57543.4479	0.0030	BRW		V	26	2)
CV Dra	57134.5318	0.0022	AG		-I	36	10)
CV Dra	57500.4594	0.0056	AG		-I	42	10)
EF Dra	57102.5663	0.0002	RAT RCR	s	V	16	6)
FU Dra	57121.4737	0.0012	AG		-I	31	10)
FU Dra	57474.3529	0.0004	AG		-I	44	10)
FU Dra	57474.5031	0.0017	AG		-I	44	10)
FX Dra	57137.4872	0.0103	AG		-I	37	10)
FX Dra	57500.4624	0.0058	AG		-I	45	10)
GM Dra	57132.5148	0.0033	AG		-I	40	10)
GM Dra	57514.4431	0.0047	AG		-I	35	10)
GQ Dra	57128.4581	0.0065	AG		-I	42	10)
GQ Dra	57489.6000	0.0002	SCI	s	o	11	12)
GQ Dra	57499.5401	0.0150	AG		-I	48	10)
KZ Dra	57246.4941	0.0002	RAT RCR		V	15	6)
LN Dra	57516.4281	0.0016	AG		-I	36	10)
NN Dra	57070.5879	0.0002	RAT RCR		V	15	6)
NU Dra	57128.4822	0.0002	RAT RCR		V	19	6)
V341 Dra	57515.4684	0.0084	AG		-I	35	10)
V372 Dra	57125.4317	0.0016	AG		-I	43	10)
V372 Dra	57137.4400	0.0024	AG		-I	37	10)
V372 Dra	57499.4363	0.0021	AG		-I	50	10)
V374 Dra	57134.4987	0.0057	AG		-I	36	10)
V374 Dra	57136.5175	0.0067	AG		-I	31	10)
V374 Dra	57500.4395	0.0137	AG		-I	42	10)
V421 Dra	57297.4603	0.0207	AG		-I	58	10)
V423 Dra	57568.4394	0.0043	AG		-I	16	10)
V425 Dra	57297.6472	0.0021	AG		-I	58	10)
V437 Dra	57588.5328	0.0020	AG		-I	21	10)
V438 Dra	57153.5783	0.0009	RAT RCR		V	19	6)
V444 Dra	57568.4430	0.0030	AG		-I	19	10)
V471 Dra	57474.3937	0.0039	AG		-I	44	10)
V471 Dra	57474.5535	0.0028	AG		-I	44	10)
V509 Dra	57132.3973	0.0086	AG		-I	40	10)
V1738 Dra	57500.5382	0.0298	AG		-I	42	10)
S Equ	57241.4558	0.0015	AG		-I	35	10)
S Equ	57588.5054	0.0005	AG		-I	36	10)
SX Gem	57414.4917	0.0013	AG		-I	40	10)
AI Gem	57384.6361	0.0031	AG		-I	54	10)
AY Gem	57414.4079	0.0005	AG		-I	41	10)
AZ Gem	57384.5092	0.0009	AG		-I	51	10)
BD Gem	57385.3790	0.0005	AG		-I	33	10)
DP Gem	57383.3679	0.0042	AG		-I	65	10)
DP Gem	57383.6480	0.0038	AG		-I	65	10)
FG Gem	57384.3500	0.0042	AG		-I	50	10)
KQ Gem	57385.3451	0.0009	AG		-I	34	10)
KV Gem	57384.4938	0.0014	AG		-I	49	10)
V402 Gem	57385.2915	0.0017	AG		-I	38	10)
V402 Gem	57385.4916	0.0018	AG		-I	38	10)
V404 Gem	57384.4511	0.0011	AG		-I	49	10)
V404 Gem	57384.6234	0.0013	AG		-I	49	10)
V405 Gem	57384.4816	0.0038	AG		-I	49	10)
V414 Gem	57384.4990	0.0060	AG		V	53	10)
V415 Gem	57384.4296	0.0012	AG		-I	50	10)
V415 Gem	57384.6068	0.0035	AG		-I	50	10)
V428 Gem	57414.4604	0.0045	AG		-I	47	10)
RX Her	57579.5249	0.0013	AG		-I	28	10)
SZ Her	57136.5365	0.0019	AG		-I	31	10)
SZ Her	57514.4978	0.0010	AG		-I	35	10)
BO Her	57574.4252	0.0031	AG		-I	28	10)
CC Her	57518.4856	0.0007	AG		-I	33	10)
DD Her	57516.3826	0.0069	AG		-I	32	10)
ES Her	57516.3977	0.0027	AG		-I	32	10)
FW Her	57517.5335	0.0004	SCI	s	o	23	12)
GU Her	57500.5607	0.0100	BRW		V	21	2)
HS Her	57245.5232	0.0056	AG		-I	36	10)
MM Her	57579.4564	0.0008	AG		-I	29	10)

MT Her	57546.4552	0.0043	AG		-I	24	10)
MX Her	57518.5018	0.0008	AG		-I	34	10)
V338 Her	57132.5288	0.0013	AG		-I	36	10)
V338 Her	57516.4247	0.0034	AG		-I	36	10)
V342 Her	57516.4949	0.0028	AG		-I	32	10)
V359 Her	57131.3933	0.0031	AG		-I	36	10)
V359 Her	57137.5449	0.0100	AG		-I	36	10)
V450 Her	57132.5476	0.0093	AG		-I	39	10)
V450 Her	57499.4533	0.0123	AG		-I	47	10)
V501 Her	57518.4235	0.0022	AG		-I	35	10)
V502 Her	57515.3768	0.0006	AG		-I	31	10)
V502 Her	57515.5613	0.0020	AG		-I	31	10)
V728 Her	57134.4484	0.0046	AG		-I	35	10)
V728 Her	57137.5127	0.0067	AG		-I	37	10)
V728 Her	57517.3791	0.0011	AG		-I	33	10)
V731 Her	57462.4675	0.0003	MS		o	16	9)
V732 Her	57513.4360	0.0003	SCI		o	64	12)
V732 Her	57515.5916	0.0005	SCI		o	59	12)
V732 Her	57528.4481	0.0005	SCI		o	53	12)
V842 Her	57500.3444	0.0027	AG		-I	44	10)
V842 Her	57500.5493	0.0008	AG		-I	44	10)
V861 Her	57514.3628	0.0002	SCI		o	34	12)
V861 Her	57514.5381	0.0004	SCI	s	o	53	12)
V878 Her	57131.5003	0.0019	AG		-I	36	10)
V878 Her	57137.5883	0.0029	AG		-I	37	10)
V878 Her	57499.4844	0.0019	AG		-I	48	10)
V883 Her	57516.4319	0.0060	AG		-I	32	10)
V994 Her	57590.4201	0.0016	AG		-I	35	10)
V1055 Her	57134.4573	0.0028	AG		-I	35	10)
V1055 Her	57134.6141	0.0006	AG		-I	35	10)
V1055 Her	57137.4621	0.0032	AG		-I	37	10)
V1055 Her	57517.5224	0.0022	AG		-I	33	10)
V1063 Her	57518.4628	0.0059	AG		-I	35	10)
V1066 Her	57518.3732	0.0005	AG		-I	34	10)
V1068 Her	57518.4795	0.0016	AG		-I	34	10)
V1069 Her	57518.4115	0.0019	AG		-I	34	10)
V1071 Her	57518.4845	0.0020	AG		-I	34	10)
V1073 Her	57516.4894	0.0011	AG		-I	34	10)
V1095 Her	57446.6312	0.0002	MS		o	16	9)
V1096 Her	57446.6327	0.0003	MS		o	16	9)
V1097 Her	57546.4975	0.0014	AG		-I	24	10)
V1098 Her	57518.5082	0.0011	AG		-I	34	10)
V1100 Her	57515.5188	0.0023	AG		-I	31	10)
V1101 Her	57514.4548	0.0042	AG		-I	35	10)
V1101 Her	57515.4136	0.0031	AG		-I	35	10)
V1101 Her	57518.4740	0.0015	AG		-I	34	10)
V1103 Her	57515.4874	0.0019	AG		-I	31	10)
V1104 Her	57518.3932	0.0020	AG		-I	34	10)
V1104 Her	57518.5075	0.0003	AG		-I	34	10)
V1106 Her	57516.4158	0.0008	AG		-I	32	10)
V1106 Her	57516.5463	0.0017	AG		-I	32	10)
V1147 Her	57125.3426	0.0006	AG		-I	35	10)
V1147 Her	57125.4723	0.0010	AG		-I	35	10)
V1147 Her	57125.5982	0.0016	AG		-I	35	10)
V1147 Her	57133.3621	0.0016	AG		-I	38	10)
V1147 Her	57133.4866	0.0004	AG		-I	38	10)
V1160 Her	57125.5118	0.0008	AG		-I	35	10)
V1160 Her	57133.4085	0.0018	AG		-I	38	10)
V1160 Her	57133.5971	0.0006	AG		-I	38	10)
V1167 Her	57518.5047	0.0012	AG		-I	32	10)
V1170 Her	57125.4906	0.0015	AG		-I	34	10)
V1170 Her	57133.3592	0.0040	AG		-I	37	10)
V1170 Her	57133.5630	0.0019	AG		-I	37	10)
V1181 Her	57133.5032	0.0024	AG		-I	38	10)
V1181 Her	57149.5119	0.0002	RAT	RCR	V	15	6)
V1185 Her	57134.5118	0.0021	AG		-I	36	10)
V1185 Her	57500.4239	0.0035	AG		-I	44	10)
V1185 Her	57500.6044	0.0005	AG		-I	44	10)
V1198 Her	57125.3850	0.0050	AG		-I	41	10)
V1198 Her	57125.5676	0.0032	AG		-I	41	10)
V1198 Her	57133.3819	0.0041	AG		-I	38	10)
V1198 Her	57133.5682	0.0026	AG		-I	38	10)
V1198 Her	57134.4744	0.0038	AG		-I	36	10)

V1198 Her	57489.3790	0.0064	AG		-I	46	10)
V1198 Her	57489.5616	0.0030	AG		-I	46	10)
V1238 Her	57128.4143	0.0027	AG		-I	44	10)
V1238 Her	57128.5993	0.0014	AG		-I	44	10)
V1238 Her	57500.4181	0.0018	AG		-I	41	10)
V1238 Her	57500.6020	0.0002	AG		-I	41	10)
V1284 Her	57515.3909	0.0031	AG		-I	31	10)
V1284 Her	57515.5581	0.0005	AG		-I	31	10)
V1286 Her	57515.4820	0.0017	AG		-I	31	10)
V1289 Her	57136.4419	0.0016	AG		-I	31	10)
V1289 Her	57515.4710	0.0011	AG		-I	31	10)
V1298 Her	57564.4370	0.0014	AG		-I	25	10)
V1300 Her	57515.4463	0.0016	AG		-I	31	10)
V1302 Her	57132.4458	0.0029	AG		-I	36	10)
V1302 Her	57516.4307	0.0120	AG		-I	36	10)
V1309 Her	57132.5591	0.0028	AG		-I	36	10)
V1309 Her	57516.5008	0.0060	AG		-I	36	10)
V1310 Her	57515.3878	0.0015	AG		-I	31	10)
V1315 Her	57515.5340	0.0007	AG		-I	31	10)
V1321 Her	57514.4005	0.0023	AG		-I	35	10)
V1321 Her	57514.5445	0.0017	AG		-I	35	10)
V1321 Her	57515.4298	0.0027	AG		-I	35	10)
V1321 Her	57515.5726	0.0033	AG		-I	35	10)
V1321 Her	57518.3710	0.0028	AG		-I	34	10)
V1321 Her	57518.5189	0.0021	AG		-I	34	10)
V1327 Her	57516.5599	0.0014	AG		-I	32	10)
V1331 Her	57515.5345	0.0042	AG		-I	31	10)
V1333 Her	57518.4875	0.0016	AG		-I	34	10)
V1435 Her	57515.4221	0.0014	AG		-I	31	10)
u Her	57136.4584	0.0087	AG		-I	31	10)
u Her	57253.3610		VLM		V		18)
u Her	57254.376		VLM		V		18)
TY Hya	57457.4514	0.0098	AG		-I	39	10)
AV Hya	57457.3529	0.0029	AG		-I	39	10)
CU Hya	57131.3585	0.0013	AG		-I	19	10)
DF Hya	57131.4152	0.0017	AG		-I	19	10)
V409 Hya	57074.3891	0.0002	RAT RCR		V	12	6)
V409 Hya	57457.4072	0.0043	AG		-I	35	10)
SW Lac	57328.2733	0.0003	DIE		o	29	20)
TW Lac	57131.5038	0.0014	AG		-I	19	10)
TW Lac	57286.4180	0.0001	MS		-U-I	46	8)
UW Lac	57264.4034	0.0050	BRW		V	16	2)
VV Lac	57345.5258	0.0014	AG		-I	38	10)
VX Lac	57574.4030	0.0004	AG		-I	27	10)
VY Lac	57330.3803	0.0015	AG		-I	31	10)
VY Lac	57590.4781	0.0005	AG		-I	35	10)
AG Lac	57345.5335	0.0005	AG		-I	50	10)
AG Lac	57564.4153	0.0001	AG		-I	20	10)
AI Lac	57564.4175	0.0004	AG		-I	20	10)
AR Lac	57327.3146	0.0093	AG		-I	51	10)
AW Lac	57562.5191	0.0018	AG		-I	26	10)
CM Lac	57247.4693	0.0021	AG		-I	40	10)
CO Lac	57296.3535	0.0011	JU	s	o	79	12)
EK Lac	57201.4700	0.0002	MS		o	20	9)
EM Lac	57298.5930	0.0016	AG		-I	19	10)
EP Lac	57283.5274	0.0004	MS		-U-I	48	8)
ER Lac	57357.3465	0.0004	MS		-U-I	57	8)
ES Lac	57237.4478	0.0115	AG		-I	36	10)
EU Lac	57131.5736	0.0020	AG		-I	19	10)
EY Lac	57286.4412	0.0003	MS		-U-I	44	8)
HR Lac	57214.4888	0.0003	MS		o	23	9)
HR Lac	57283.5711	0.0005	MS		-U-I	44	8)
IL Lac	57131.5290	0.0105	AG		-I	19	10)
IP Lac	57564.5457	0.0004	AG		-I	20	10)
IU Lac	57345.4591	0.0012	AG		-I	49	10)
KU Lac	57345.3214	0.0013	AG		-I	48	10)
LU Lac	57258.4318	0.0002	MS		-U-I	49	8)
LZ Lac	57338.4117	0.0046	AG		-I	65	10)
LZ Lac	57345.2932	0.0031	AG		-I	47	10)
NR Lac	57258.4449	0.0004	MS		-U-I	50	8)
PP Lac	57298.5055	0.0029	AG		-I	18	10)
PP Lac	57338.4222	0.0011	AG		-I	66	10)
PP Lac	57338.6222	0.0007	AG		-I	66	10)

PP Lac	57345.4422	0.0004	AG		-I	50	10)
V339 Lac	57296.4955	0.0025	AG		-I	31	10)
V344 Lac	57131.5455	0.0021	AG		-I	19	10)
V344 Lac	57357.2812	0.0013	MS		-U-I	60	8)
V402 Lac	57237.5428	0.0063	AG		-I	36	10)
V441 Lac	57345.4458	0.0017	AG		-I	47	10)
V459 Lac	57261.4281	0.0003	AG		-I	37	10)
V474 Lac	57338.2445	0.0038	AG		-I	65	10)
V474 Lac	57338.6180	0.0048	AG		-I	65	10)
V485 Lac	55051.4151	0.0024	FR		-I	63	10)
V488 Lac	57357.4090	0.0007	MS		-U-I	60	3)
V489 Lac	57258.4546	0.0011	MS	s	-U-I	49	8)
V489 Lac	57345.4047	0.0025	AG		-I	48	10)
V505 Lac	57590.3826	0.0009	AG		-I	35	10)
V505 Lac	57590.5467	0.0015	AG		-I	35	10)
V525 Lac	57261.3692	0.0016	AG		-I	37	10)
V525 Lac	57261.5357	0.0047	AG		-I	37	10)
UV Leo	57457.4550	0.0011	AG		-I	45	10)
UZ Leo	57457.5112	0.0035	AG		-I	45	10)
WY Leo	57465.3853	0.0001	SCI		o	88	12)
XY Leo	57457.4284	0.0023	AG		-I	60	10)
XY Leo	57457.5700	0.0038	AG		-I	60	10)
XZ Leo	57457.5499	0.0029	AG		-I	60	10)
AG Leo	57496.3931	0.0050	BRW		V	41	2)
AM Leo	57466.4033	0.0025	AG		-I	50	10)
AM Leo	57466.5864	0.0017	AG		-I	50	10)
AM Leo	57475.3652	0.0020	BRW		V	33	2)
AM Leo	57476.4634	0.0010	BRW		V	48	2)
AP Leo	57466.3129	0.0024	AG		-I	47	10)
AP Leo	57466.5257	0.0034	AG		-I	47	10)
FM Leo	54911.3841:	0.0006	MS FR		o	12	17)
HI Leo	57079.4064	0.0002	RAT RCR	s	V	68	6)
RT LMi	57128.3778	0.0001	RAT RCR	s	V	58	6)
VW LMi	57457.3854	0.0048	AG		-I	46	10)
VW LMi	57457.6264	0.0025	AG		-I	46	10)
XY LMi	57457.4897	0.0048	AG		-I	47	10)
AG LMi	57101.5574	0.0001	RAT RCR		V	17	6)
AG LMi	57457.6199	0.0034	AG		-I	45	10)
RZ Lyn	57121.4756	0.0055	AG		-I	22	10)
RZ Lyn	57414.4971	0.0032	AG		-I	42	10)
RZ Lyn	57457.5263	0.0038	AG		-I	39	10)
RZ Lyn	57464.4073	0.0016	JU		o	79	12)
SW Lyn	57414.4929	0.0016	AG		-I	53	10)
SW Lyn	57474.3928	0.0007	DIE		o	25	1)
UV Lyn	57414.4586	0.0016	AG		-I	52	10)
BG Lyn	57384.3906	0.0030	AG		-I	64	10)
CN Lyn	57409.5525	0.0033	AG		-I	39	10)
DE Lyn	57466.3246	0.0002	SCI	s	o	10	12)
DY Lyn	57409.5861	0.0005	AG		-I	38	10)
DZ Lyn	57409.5045	0.0066	AG		-I	38	10)
DZ Lyn	57414.4185	0.0036	AG		-I	53	10)
FI Lyn	57409.5232	0.0026	AG		-I	38	10)
TZ Lyr	56507.4501	0.0009	FR		V	67	18)
TZ Lyr	57136.4871	0.0065	AG		-I	31	10)
TZ Lyr	57515.3900	0.0017	AG		-I	34	10)
UZ Lyr	57577.5166	0.0009	AG		-I	29	10)
DU Lyr	57283.4369	0.0003	MS		-U-I	29	8)
FL Lyr	57562.4747	0.0013	AG		-I	26	10)
HY Lyr	57516.3920	0.0010	AG		-I	32	10)
HY Lyr	57516.5767	0.0005	AG		-I	32	10)
V406 Lyr	57585.4328	0.0020	BRW		V	13	2)
V563 Lyr	57518.5453	0.0016	AG		-I	32	10)
V569 Lyr	57297.3191	0.0002	RAT RCR		V	13	6)
V582 Lyr	57261.3703	0.0001	MS FR		-U-I	77	3)
V596 Lyr	57343.3063	0.0003	MS		V	38	3)
V639 Lyr	57516.5000	0.0035	AG		-I	32	10)
beta Lyr	57227.146		VLM	s	V	70	18)
beta Lyr	57246.557		VLM		V	70	18)
DQ Mon	54842.4614	0.0003	MS FR		o	64	17)
V634 Mon	53069.4301	0.0007	MS FR		o	12	16)
U Oph	57251.429		VLM		V		18)
U Oph	57252.266		VLM	s	V		18)
RV Oph	57546.4976	0.0011	AG		-I	24	10)

V456 Oph	57546.4848	0.0007	AG		-I	24	10)
V501 Oph	57546.4783	0.0016	AG		-I	24	10)
V566 Oph	57248.3887	0.0023	AG		-I	34	10)
V566 Oph	57546.4139	0.0031	AG		-I	24	10)
V2610 Oph	57248.3890	0.0103	AG		-I	28	10)
V2612 Oph	57546.4910	0.0011	AG		-I	24	10)
V2713 Oph	57546.4539	0.0027	AG		-I	24	10)
BM Ori	57360.489		VLM		V	20	18)
V392 Ori	57414.3071	0.0092	AG		-I	40	10)
V641 Ori	56596.4890	0.0006	MS FR	s	o	50	9)
V1633 Ori	57373.8259	0.0001	MS		V	14	4)
V1633 Ori	57378.4231	0.0003	MS		L	14	8)
V2793 Ori	57373.7947	0.0003	MS		V	14	4)
V2793 Ori	57434.7223	0.0001	MS		V	14	4)
U Peg	57294.4506	0.0014	AG		-I	56	10)
U Peg	57294.6364	0.0016	AG		-I	56	10)
UX Peg	57246.3535	0.0001	AG		-I	37	10)
BB Peg	57329.3235	0.0011	DIE		o	36	20)
BG Peg	57338.3856	0.0050	AG		-I	45	10)
BK Peg	57217.5066	0.0069	PGL		V	29	7)
BK Peg	57261.4224	0.0063	AG		-I	48	10)
BN Peg	57241.5462	0.0099	AG		-I	35	10)
BX Peg	57260.4856	0.0002	SCI	s	o	57	12)
BX Peg	57260.6244	0.0001	SCI		o	44	12)
BX Peg	57299.3233	0.0010	WTR		o	77	11)
BY Peg	57297.5307	0.0007	MS FR		-U-I	10	3)
CC Peg	57297.4441	0.0003	MS FR		-U-I	18	3)
CU Peg	57355.3488	0.0002	MS		-U-I	39	8)
DI Peg	57278.5163	0.0058	AG		-I	56	10)
GP Peg	57238.4099	0.0029	AG		-I	38	10)
GP Peg	57364.2631	0.0019	AG		-I	40	10)
GP Peg	57577.4348	0.0013	AG		-I	27	10)
IP Peg	57261.4431	0.0004	SCI		o	35	12)
IP Peg	57261.5238	0.0003	SCI	s	o	86	12)
IP Peg	57265.3969	0.0008	SCI		o	68	12)
IP Peg	57265.4687	0.0003	SCI	s	o	71	12)
IP Peg	57265.5532	0.0007	SCI		o	68	12)
IP Peg	57265.6286	0.0003	SCI	s	o	24	12)
IP Peg	57269.3536	0.0008	SCI		o	27	12)
IP Peg	57269.4315	0.0003	SCI	s	o	66	12)
IP Peg	57269.5086	0.0003	SCI		o	63	12)
IP Peg	57269.5927	0.0009	SCI	s	o	71	12)
IP Peg	57293.3986	0.0002	SCI		o	13	12)
IP Peg	57300.3604	0.0003	SCI		o	34	12)
IP Peg	57307.3218	0.0003	SCI		o	23	12)
IP Peg	57322.3517	0.0006	SCI		o	14	12)
IP Peg	57342.2825	0.0003	SCI		o	61	12)
IP Peg	57383.2583	0.0003	SCI		o	58	12)
V357 Peg	57261.5324	0.0019	AG		-I	48	10)
V357 Peg	57276.5718	0.0029	AG		-I	45	10)
V357 Peg	57278.3076	0.0003	AG		-I	57	10)
V357 Peg	57278.5972	0.0016	AG		-I	57	10)
V404 Peg	57241.5239	0.0068	AG		-I	35	10)
V404 Peg	57242.3637	0.0020	AG		-I	41	10)
V404 Peg	57242.5686	0.0059	AG		-I	40	10)
V404 Peg	57354.2746	0.0018	MS		V	38	8)
V404 Peg	57590.4791	0.0025	AG		-I	35	10)
V407 Peg	57276.5272	0.0066	AG		-I	45	10)
V407 Peg	57278.4378	0.0046	AG		-I	56	10)
V421 Peg	57294.4972	0.0044	AG		-I	55	10)
V421 Peg	57305.3026	0.0038	AG		-I	43	10)
V481 Peg	57246.4762	0.0027	AG		-I	37	10)
V481 Peg	57248.3761	0.0037	AG		-I	45	10)
V481 Peg	57248.5858	0.0062	AG		-I	45	10)
V481 Peg	57260.4022	0.0054	AG		-I	43	10)
V481 Peg	57299.4417	0.0056	AG		-I	38	10)
V535 Peg	57241.5198	0.0013	AG		-I	35	10)
V535 Peg	57242.4884	0.0025	AG		-I	41	10)
V535 Peg	57577.4479	0.0005	AG		-I	29	10)
V560 Peg	57238.5794	0.0003	AG		-I	38	10)
V560 Peg	57364.2693	0.0083	AG		-I	40	10)
V560 Peg	57577.4553	0.0028	AG		-I	27	10)
V560 Peg	57590.4233	0.0017	AG		-I	34	10)

V619 Peg	57298.3710	0.0039	AG		-I	27	10)
RT Per	57276.5827	0.0007	AG		-I	45	10)
RT Per	57345.3868	0.0007	JU		o	59	12)
RV Per	57343.4569	0.0029	AG		-I	35	10)
AG Per	57364.5787	0.0116	AG		-I	75	10)
AG Per	57414.3277	0.0079	AG		-I	37	10)
AY Per	57406.3318	0.0070	BRW		V	21	2)
BO Per	56596.3790	0.0002	MS FR		o	64	9)
DK Per	57260.4647	0.0056	AG		-I	30	10)
DK Per	57265.4081	0.0002	AG		-I	29	10)
DM Per	57295.3757	0.0047	AG		-I	59	10)
IQ Per	57338.2754	0.0145	AG		-I	68	10)
IQ Per	57343.5052	0.0081	AG		-I	33	10)
IQ Per	57384.5562	0.0020	AG		-I	43	10)
IT Per	57327.3925	0.0120	AG		-I	82	10)
IT Per	57413.2812	0.0015	JU		o	75	12)
IU Per	57276.4119	0.0023	AG		-I	44	10)
IZ Per	57294.5310	0.0177	AG		-I	57	10)
KQ Per	55135.3167:	0.0200	MS FR		o	45	17)
KQ Per	57329.3939	0.0005	FR		-I	69	10)
KQ Per	57466.4822	0.0020	FR	s	-I	46	10)
KR Per	57329.3943	0.0029	AG		-I	59	10)
KW Per	57276.5518	0.0014	AG		-I	45	10)
LX Per	57385.3411	0.0079	AG		-I	47	10)
V432 Per	57276.4469	0.0015	AG		-I	44	10)
V432 Per	57299.4449	0.0018	AG		-I	54	10)
V432 Per	57328.3846	0.0026	AG		-I	67	10)
V432 Per	57328.5751	0.0024	AG		-I	67	10)
V505 Per	57295.4760	0.0041	AG		-I	63	10)
V570 Per	57338.5811	0.0034	AG		-I	68	10)
V723 Per	57260.5757	0.0041	AG		-I	29	10)
V736 Per	57327.4020	0.0082	AG		-I	80	10)
V740 Per	57343.3563	0.0014	AG		-I	34	10)
V740 Per	57343.5436	0.0005	AG		-I	34	10)
V740 Per	57364.2491	0.0046	AG		-I	75	10)
V740 Per	57364.4311	0.0039	AG		-I	75	10)
V740 Per	57364.6180	0.0049	AG		-I	75	10)
V871 Per	57327.3853	0.0044	AG		-I	82	10)
V873 Per	57327.3226	0.0027	AG		-I	84	10)
V873 Per	57327.4703	0.0013	AG		-I	84	10)
V873 Per	57327.6172	0.0014	AG		-I	84	10)
V881 Per	57328.3960	0.0017	AG		-I	70	10)
V881 Per	57328.6026	0.0020	AG		-I	70	10)
V881 Per	57383.4043	0.0005	RAT RCR		V	68	6)
V887 Per	57299.3625	0.0049	AG		-I	54	10)
V930 Per	57330.5664	0.0013	FR		-I	71	10)
V951 Per	57343.4112	0.0020	AG		-I	30	10)
V959 Per	57345.4784	0.0009	AG		-I	60	10)
V967 Per	57260.4091	0.0024	AG		-I	30	10)
V967 Per	57260.5836	0.0021	AG		-I	30	10)
V968 Per	57260.3383	0.0020	AG		-I	30	10)
beta Per	57360.302		VLM		V	60	18)
beta Per	57383.240		VLM		V	52	18)
RV Psc	57364.4099	0.0005	RAT RCR		V	62	6)
SU Psc	57364.4383	0.0136	AG		-I	57	10)
UV Psc	57343.4300	0.0011	AG		-I	31	10)
VZ Psc	57298.3958	0.0028	AG		-I	27	10)
AQ Psc	57343.4585	0.0027	AG		-I	31	10)
DS Psc	57328.3284	0.0003	RAT RCR		V	11	6)
DZ Psc	57338.3744	0.0042	AG		-I	56	10)
DZ Psc	57338.5562	0.0037	AG		-I	56	10)
ET Psc	57343.4682	0.0012	AG		-I	32	10)
EW Psc	57284.3864	0.0004	RAT RCR		V	70	6)
FY Psc	57305.4157	0.0005	AG		-I	40	10)
FY Psc	57328.3918	0.0006	AG		-I	63	10)
FY Psc	57328.5696	0.0023	AG		-I	63	10)
GO Psc	57328.3562	0.0055	AG		-I	62	10)
GO Psc	57328.5693	0.0052	AG		-I	62	10)
GT Psc	57328.3531	0.0142	AG		-I	62	10)
HL Psc	57297.5208	0.0093	AG		-I	56	10)
HL Psc	57329.4679	0.0027	AG		-I	54	10)
HO Psc	57329.3497	0.0012	AG		-I	51	10)
HO Psc	57329.5128	0.0021	AG		-I	51	10)

U Sge	57241.4635	0.0030	AG		-I	34	10)
V Sge	57580.4042	0.0034	AG		-I	32	10)
CU Sge	57568.4396	0.0005	AG		-I	17	10)
CW Sge	57299.4329	0.0067	AG		-I	34	10)
V375 Sge	57246.3847	0.0047	AG		-I	37	10)
V375 Sge	57247.4352	0.0085	AG		-I	38	10)
V375 Sge	57579.3859	0.0009	AG		-I	29	10)
V382 Sge	57579.5006	0.0018	AG		-I	29	10)
AO Ser	57514.4213	0.0022	AG		-I	35	10)
AU Ser	57136.5691	0.0020	AG		-I	31	10)
AU Ser	57514.3682	0.0016	AG		-I	35	10)
AU Ser	57514.5613	0.0008	AG		-I	35	10)
AU Ser	57515.5275	0.0008	AG		-I	35	10)
BI Ser	57514.4046	0.0052	AG		-I	32	10)
EG Ser	57244.4684	0.0048	AG		-I	24	10)
V384 Ser	57132.4396	0.0022	AG		-I	37	10)
V384 Ser	57132.5732	0.0026	AG		-I	37	10)
V384 Ser	57266.3980	0.0004	FR	s	-I	78	10)
V384 Ser	57499.3842	0.0002	FR	s	-I	11	10)
V384 Ser	57499.5191	0.0002	FR		-I	11	10)
V384 Ser	57508.3868	0.0001	FR		-I	15	10)
V384 Ser	57508.5205	0.0001	FR	s	-I	15	10)
V384 Ser	57514.4331	0.0001	FR	s	-I	14	10)
V384 Ser	57514.4351	0.0038	AG		-I	35	10)
V384 Ser	57514.5660	0.0018	AG		-I	35	10)
V384 Ser	57514.5677	0.0001	FR		-I	14	10)
V384 Ser	57515.3725	0.0010	AG		-I	35	10)
V384 Ser	57515.3740	0.0001	FR		-I	63	10)
V384 Ser	57515.5092	0.0017	AG		-I	35	10)
V384 Ser	57516.4489	0.0001	FR		-I	13	10)
V384 Ser	57516.5825	0.0005	FR	s	-I	13	10)
V384 Ser	57517.3889	0.0002	FR	s	-I	12	10)
V384 Ser	57517.5243	0.0003	FR		-I	12	10)
V505 Ser	57132.4016	0.0012	AG		-I	37	10)
V505 Ser	57187.3919	0.0015	MS FR		I	20	3)
V505 Ser	57187.3924	0.0006	MS FR		B	17	3)
V505 Ser	57187.3939	0.0008	MS FR		V	18	3)
V505 Ser	57266.3966	0.0018	FR	s	-I	41	10)
V505 Ser	57499.5030	0.0003	FR		-I	15	10)
V505 Ser	57508.4205	0.0003	FR		-I	91	10)
V505 Ser	57510.6259	0.0005	MS FR	s	V	13	3)
V505 Ser	57510.6301	0.0012	MS FR	s	R	13	3)
V505 Ser	57510.6349	0.0012	MS FR	s	I	12	3)
V505 Ser	57514.3658	0.0004	FR		-I	92	10)
V505 Ser	57514.3675	0.0010	AG		-I	35	10)
V505 Ser	57515.3563	0.0004	FR		-I	44	10)
V505 Ser	57515.3564		AG		-I	35	10)
V505 Ser	57516.3480	0.0005	FR		-I	13	10)
V505 Ser	57517.3370	0.0007	FR		-I	13	10)
V505 Ser	57547.5581	0.0005	MS FR		R	15	3)
V505 Ser	57547.5583	0.0007	MS FR		V	14	3)
V505 Ser	57579.4669	0.0007	MS FR	s	V	10	3)
V505 Ser	57579.4683	0.0011	MS FR	s	B	12	3)
V505 Ser	57579.4692	0.0015	MS FR	s	R	10	3)
V505 Ser	57579.4787	0.0014	MS FR	s	I	10	3)
Y Sex	57474.3653	0.0016	AG		-I	33	10)
WW Sex	57474.3533	0.0024	AG		-I	31	10)
WY Sex	57119.4767	0.0015	AG		-I	21	10)
RZ Tau	57383.3697	0.0025	AG		-I	60	10)
RZ Tau	57383.5768	0.0019	AG		-I	60	10)
WY Tau	57383.5508	0.0015	AG		-I	66	10)
AM Tau	57446.4105	0.0002	SCI		o	73	12)
AN Tau	57364.5960	0.0044	AG		-I	70	10)
CT Tau	57383.5691	0.0022	AG		-I	64	10)
CT Tau	57384.5671	0.0058	AG		-I	61	10)
EQ Tau	57383.2923	0.0021	AG		-I	54	10)
EQ Tau	57383.4629	0.0019	AG		-I	54	10)
GR Tau	57383.3137	0.0075	AG		-I	55	10)
GR Tau	57383.5221	0.0030	AG		-I	55	10)
V781 Tau	57383.3043	0.0015	AG		-I	71	10)
V781 Tau	57383.4783	0.0019	AG		-I	71	10)
V781 Tau	57383.6463	0.0034	AG		-I	71	10)
V781 Tau	57384.3374	0.0030	AG		-I	61	10)

V781 Tau	57384.5138	0.0021	AG		-I	61	10)
V781 Tau	57384.6834	0.0032	AG		-I	61	10)
V1112 Tau	57361.1820	0.0032	MS		o	33	3)
V1123 Tau	57343.4381	0.0013	AG		-I	32	10)
V1123 Tau	57385.2345	0.0003	AG		-I	59	10)
V1123 Tau	57385.4313	0.0036	AG		-I	59	10)
V1128 Tau	57385.3272	0.0009	AG		-I	51	10)
V1128 Tau	57385.4781	0.0012	AG		-I	51	10)
V1370 Tau	57383.3732	0.0010	AG		-I	66	10)
V1370 Tau	57383.5240	0.0013	AG		-I	66	10)
V Tri	55889.3137	0.0011	BHE		-I	19	5)
V Tri	57297.3158	0.0018	AG		-I	58	10)
V Tri	57297.6059	0.0087	AG		-I	58	10)
V Tri	57329.5020	0.0025	AG		-I	55	10)
X Tri	57338.4626	0.0040	AG		-I	66	10)
RS Tri	57329.3697	0.0027	AG		-I	55	10)
RW Tri	57287.4518	0.0002	AG		-I	46	10)
BC Tri	57329.4119	0.0227	AG		-I	55	10)
BC Tri	57329.4270	0.0010	RAT RCR		V	33	6)
BQ Tri	57294.3386	0.0028	AG		-I	34	10)
BU Tri	57294.4029	0.0012	AG		-I	31	10)
BV Tri	57294.4030	0.0037	AG		-I	31	10)
BX Tri	57294.3870	0.0025	AG		-I	30	10)
BX Tri	57294.4872	0.0025	AG		-I	30	10)
CD Tri	57287.4401	0.0039	AG		-I	43	10)
CD Tri	57294.4503	0.0027	AG		-I	27	10)
CL Tri	57287.3576	0.0014	AG		-I	47	10)
CM Tri	57294.5272	0.0003	AG		-I	31	10)
CN Tri	57287.5125	0.0024	AG		-I	43	10)
CS Tri	57287.5782	0.0040	AG		-I	45	10)
CU Tri	53271.694	0.003	MZ			72	21) SWASP
CU Tri	54068.4036	0.0030	MZ	s		54	21) SWASP
W UMa	57465.4755	0.0004	AG		-I	38	10)
RW UMa	57134.3795	0.0039	AG		-I	59	10)
TY UMa	57487.4163	0.0012	JU		o	53	12)
UY UMa	57465.4137	0.0021	JU	s	o	80	12)
VV UMa	57125.4262	0.0001	RAT RCR		V	18	6)
XZ UMa	57121.5064	0.0027	AG		-I	20	10)
XZ UMa	57465.5907	0.0016	AG		-I	51	10)
AA UMa	57414.4745	0.0035	AG		-I	58	10)
AW UMa	57121.5557	0.0013	AG		-I	28	10)
AW UMa	57474.5082	0.0080	AG		-I	52	10)
BS UMa	57134.5053	0.0001	RAT RCR		o	16	6)
ES UMa	57409.4461	0.0015	AG		-I	39	10)
KM UMa	56731.3227	0.0003	MS FR		o	22	9)
KM UMa	56744.3415	0.0005	MS FR		o	20	9)
NU UMa	57465.3272	0.0007	AG		-I	46	10)
PW UMa	57098.6724	0.0006	RAT RCR		V	18	6)
QT UMa	57121.3985	0.0010	AG		-I	23	10)
QT UMa	57132.5256	0.0001	RAT RCR		V	18	6)
QT UMa	57465.4249	0.0025	AG		-I	39	10)
V354 UMa	57499.4000	0.0067	AG		-I	50	10)
V354 UMa	57499.5503	0.0042	AG		-I	50	10)
RT UMi	57121.5110	0.0038	AG		-I	31	10)
RT UMi	57517.5430	0.0054	AG		-I	33	10)
RU UMi	57465.3641	0.0006	AG		-I	49	10)
RU UMi	57465.6233	0.0080	AG		-I	49	10)
VY UMi	57079.5934	0.0002	RAT RCR	s	V	23	6)
VY UMi	57120.4319	0.0005	RAT RCR		V	14	6)
AL UMi	57164.5789	0.0030	RAT RCR	s	V	17	6)
AG Vir	57489.4991	0.0040	BRW		V	51	2)
AG Vir	57499.4540	0.0020	BRW		V	53	2)
AH Vir	57515.4082	0.0020	BRW		V	26	2)
AH Vir	57516.4290	0.0020	BRW		V	41	2)
AW Vir	57123.5282	0.0022	AG		-I	28	10)
AW Vir	57125.4737	0.0016	AG		-I	42	10)
AW Vir	57514.5181	0.0016	AG		-I	35	10)
AW Vir	57518.4123	0.0012	AG		-I	35	10)
AX Vir	57125.3925	0.0107	AG		-I	42	10)
AX Vir	57518.4571	0.0009	AG		-I	35	10)
AZ Vir	57125.4976	0.0013	AG		-I	40	10)
BF Vir	57132.4858	0.0184	AG		-I	39	10)
BF Vir	57516.5082	0.0022	AG		-I	35	10)

BH Vir	57132.5288	0.0024	AG		-I	40	10)
BH Vir	57514.4155	0.0022	AG		-I	35	10)
HT Vir	57125.5007	0.0030	AG		-I	40	10)
HT Vir	57514.4217	0.0028	AG		-I	35	10)
HW Vir	57515.3762	0.0060	WTR		o	10	11)
HW Vir	57516.3683	0.0010	WTR	s	o	10	11)
HY Vir	57133.3874	0.0152	AG		-I	47	10)
NN Vir	57133.4113	0.0063	AG		-I	44	10)
NN Vir	57518.4435	0.0011	AG		-I	35	10)
PY Vir	57125.5041	0.0007	AG		-I	37	10)
PY Vir	57517.3599	0.0020	WTR	s	o	99	11)
V415 Vir	57123.5056	0.0071	AG		-I	35	10)
V415 Vir	57489.3689	0.0050	AG		-I	44	10)
V415 Vir	57489.5481	0.0029	AG		-I	44	10)
V467 Vir	57133.5017	0.0082	AG		-I	43	10)
V637 Vir	57514.3918	0.0045	AG		-I	35	10)
V639 Vir	57514.3586	0.0009	AG		-I	35	10)
V639 Vir	57514.5397	0.0035	AG		-I	35	10)
Z Vul	57247.4561	0.0022	AG		-I	39	10)
Z Vul	57274.4626	0.0040	BRW		V	84	2)
Z Vul	57274.4634	0.0020	BRW		U	91	2)
Z Vul	57274.4665	0.0030	BRW		B	93	2)
RR Vul	57248.3581	0.0014	AG		-I	46	10)
AT Vul	57588.5270	0.0028	AG		-I	37	10)
AW Vul	57256.4069	0.0012	AG		-I	42	10)
AW Vul	57568.5025	0.0004	AG		-I	20	10)
AX Vul	57256.5054	0.0030	AG		-I	42	10)
AX Vul	57579.4653	0.0008	AG		-I	29	10)
AY Vul	57285.3765	0.0001	MS		-U-I	46	8)
BE Vul	57563.4396	0.0040	AG		-I	27	10)
BO Vul	57588.5579	0.0035	AG		-I	37	10)
BP Vul	57574.4630	0.0009	AG		-I	28	10)
BP Vul	57577.4134	0.0008	AG		-I	29	10)
BU Vul	57237.3766	0.0005	AG		-I	36	10)
BU Vul	57563.4088	0.0010	AG		-I	28	10)
DR Vul	57237.4958	0.0042	AG		-I	36	10)
DR Vul	57238.4883	0.0034	AG		-I	38	10)
EO Vul	57231.4517	0.0006	MS		-U-I	41	8)
EO Vul	57285.3606	0.0007	MS		-U-I	47	8)
FR Vul	57546.4395	0.0029	AG		-I	24	10)
FR Vul	57562.4511	0.0002	AG		V	42	10)
V473 Vul	57178.5068	0.0002	RAT RCR		V	14	6)
V495 Vul	57237.4985	0.0039	AG		-I	36	10)
V495 Vul	57564.5131	0.0026	AG		-I	27	10)
V502 Vul	57265.5623	0.0127	AG		-I	46	10)
V552 Vul	55071.3534	0.0042	AG		-I	53	10)
V552 Vul	55071.5608	0.0045	AG		-I	53	10)
V552 Vul	55791.5567	0.0013	AG		-I	31	10)
V552 Vul	55806.5301	0.0013	AG		-I	29	10)
V552 Vul	55807.5804	0.0026	AG		-I	31	10)
1SWASP J212624.19+325248.7	57238.4844	0.0137	AG		-I	39	10)
1SWASP J225840.47+343746.2	57590.5011	0.0030	AG		-I	34	10)
2MASS J22194689+5142524	55141.4582	0.0025	FR		-I	95	10)
2MASS J23391561+5615109	57354.3977	0.0013	MS		V	39	8)
ASAS J003412+2052.4	57338.3192	0.0065	AG		-I	56	10)
ASAS J003412+2052.4	57338.4809	0.0046	AG		-I	56	10)
ASAS J033627+1726.9	57343.3463	0.0051	AG		-I	29	10)
ASAS J034521+1635.0	57383.4280	0.0030	AG		-I	51	10)
ASAS J061335+4914.1	57385.3552	0.0109	AG		-I	65	10)
ASAS J061335+4914.1	57385.5428	0.0022	AG		-I	65	10)
ASAS J072000+2543.7	57414.3551	0.0007	AG		-I	49	10)
ASAS J072125+2559.1	57414.3903	0.0021	AG		-I	50	10)
ASAS J072333-1554.2	57117.9532	0.0003	MS FR		V	56	3)
ASAS J072740+2623.1	57414.4148	0.0031	AG		-I	43	10)
ASAS J085128+2527.9	57414.5955	0.0025	AG		-I	57	10)
ASAS J161240+0827.0	57518.4130	0.0022	AG		-I	33	10)
ASAS J175529+2131.4	57579.4863	0.0034	AG		-I	29	10)
ASAS J184327+0841.5	57546.4620	0.0021	AG		-I	24	10)
ASAS J190505+0537.2	57579.4308	0.0013	AG		-I	28	10)
ASAS J191314+2028.9	57579.4767	0.0022	AG		-I	29	10)
ASAS J191745+0846.9	57579.4074	0.0016	AG		-I	28	10)
ASAS J193711+1148.2	57256.5529	0.0071	AG		-I	38	10)
ASAS J194531+2821.4	55372.4346	0.0004	MS FR		o	41	17)

ASAS J201225+0959.4	57577.5104	0.0024	AG		-I	29	10)
ASAS J205122+2724.8	57237.5158	0.0109	AG		-I	36	10)
ASAS J205847+2731.9	57248.3496	0.0008	AG		-I	46	10)
ASAS J205847+2731.9	57248.4846	0.0010	AG		-I	46	10)
ASAS J220226+4831.3	57562.5081	0.0007	AG		-I	26	10)
CI NGC7789XZD3	56933.2875	0.0003	MS FR	s	o	35	9)
CI NGC7789XZD3	56933.4574	0.0004	MS FR		o	36	9)
CSS J025828.6+370907	57328.4391	0.0008	AG		-I	68	10)
CSS J025828.6+370907	57328.6472	0.0011	AG		-I	68	10)
CSS J083927.1+233535	57448.3022	0.0002	MS		o	27	9)
CSS J083954.1+232016	57414.3940	0.0032	AG		-I	48	10)
CSS J083954.1+232016	57448.3150	0.0004	MS		o	27	9)
CSS J083954.1+232016	57462.3719	0.0003	MS		o	16	9)
CSS J160111.8+251634	57122.5002	0.0013	FR		-I	10	10)
CSS J160111.8+251634	57133.4268	0.0019	FR		-I	12	10)
CSS J160111.8+251634	57133.5914	0.0004	FR	s	-I	12	10)
CSS J160111.8+251634	57134.4201	0.0009	FR		-I	15	10)
CSS J160111.8+251634	57134.5824	0.0006	FR	s	-I	15	10)
CSS J160111.8+251634	57153.4500	0.0005	FR	s	-I	13	10)
CSS J160111.8+251634	57241.4957	0.0015	FR	s	-I	94	10)
CSS J160111.8+251634	57266.3196	0.0011	FR	s	-I	75	10)
CSS J160111.8+251634	57499.5077	0.0008	FR		-I	12	10)
CSS J160111.8+251634	57508.4449	0.0006	FR		-I	13	10)
CSS J160111.8+251634	57514.4036	0.0008	FR		-I	14	10)
CSS J160111.8+251634	57514.5711	0.0008	FR	s	-I	14	10)
CSS J160111.8+251634	57515.3971	0.0008	FR		-I	60	10)
CSS J160111.8+251634	57516.3919	0.0010	FR		-I	13	10)
CSS J160111.8+251634	57516.5560	0.0007	FR	s	-I	30	10)
CSS J160111.8+251634	57517.3841	0.0012	FR		-I	11	10)
CSS J160111.8+251634	57517.5503	0.0005	FR	s	-I	11	10)
CSS J174400.0+342105	57515.4569	0.0040	AG		-I	31	10)
CSS J175458.2+372902	57515.4447	0.0034	AG		-I	31	10)
CSS J180001.1+401611	57515.4343	0.0020	AG		-I	31	10)
CSS J180001.1+401611	57515.5581	0.0020	AG		-I	31	10)
CSS J181106.8+490858	57518.4921	0.0044	AG		-I	34	10)
GSC 00158-01247	54842.4567	0.0009	MS FR		o	63	17)
GSC 01337-01137	57414.2785	0.0030	AG		-I	41	10)
GSC 01403-01508	57106.4524	0.0004	SCI		o	81	12)
GSC 02313-01533	57294.4047	0.0030	AG		-I	34	10)
GSC 02423-00517	57384.4767	0.0059	AG		-I	60	10)
GSC 02423-00517	57384.6616	0.0043	AG		-I	60	10)
GSC 03453-00892	57134.4507	0.0067	AG		-I	34	10)
GSC 03619-03058	55141.5133	0.0005	FR	s	-I	77	10)
GSC 03627-00379	57338.4266	0.0088	AG		-I	43	10)
GSC 03715-00043	56167.5397	0.0029	AG		-I	29	10)
GSC 03715-00043	56950.3337	0.0200	AG		-I	57	10)
GSC 03715-00043	56950.5705	0.0083	AG		-I	57	10)
GSC 03715-00043	57338.3591	0.0062	AG		-I	68	10)
GSC 03715-00043	57338.5877	0.0057	AG		-I	68	10)
GSC 03899-00384	57132.3973	0.0086	AG		-I	40	10)
GSC 04049-00327	57298.3893	0.0144	AG		-I	28	10)
GSC 04190-01948	57296.3400	0.0001	SCI	s	o	66	12)
GSC 04372-00831	55887.5847	0.0036	AG		-I	74	10)
LINEAR 7532224	55309.3842	0.0039	AG		-I	59	10)
LINEAR 7532224	55309.5127	0.0040	AG		-I	59	10)
LINEAR 7532224	56012.4541	0.0014	AG		-I	49	10)
LINEAR 7532224	56012.5766	0.0022	AG		-I	49	10)
LINEAR 7532224	57489.3872	0.0019	AG		-I	41	10)
LINEAR 7532224	57489.5121	0.0024	AG		-I	41	10)
LINEAR 7532224	57499.3728	0.0051	AG		-I	50	10)
LINEAR 7532224	57499.4970	0.0032	AG		-I	50	10)
LINEAR 7532224	57514.4134	0.0010	AG		-I	36	10)
LINEAR 7532224	57514.5404	0.0005	AG		-I	36	10)
LINEAR 20961058	57518.4874	0.0016	AG		-I	34	10)
NSV 12079	57562.4431	0.0011	AG		-I	42	10)
NSV 13339	57264.3680	0.0092	AG		-I	57	10)
NSV 13339	57264.5434	0.0080	AG		-I	57	10)
NSV 15495	55858.2686	0.0004	MS FR		o	37	14)
NSVS 109935	57296.4371	0.0007	AG		-I	74	10)
NSVS 503993	57329.4032	0.0056	AG		-I	59	10)
NSVS 503993	57329.5824	0.0089	AG		-I	59	10)
NSVS 710419	57414.2857	0.0010	AG		-I	48	10)
NSVS 710419	57414.4654	0.0029	AG		-I	48	10)

NSVS 296349	57245.5386	0.0027	AG		-I	36	10)
NSVS 889633	57466.3990	0.0079	AG		-I	56	10)
NSVS 889633	57466.5739	0.0058	AG		-I	56	10)
NSVS 1203826	57248.3433	0.0007	AG		-I	43	10)
NSVS 1203826	57248.5612	0.0063	AG		-I	43	10)
NSVS 1203826	57265.4900	0.0101	AG		-I	35	10)
NSVS 1206916	57248.4454	0.0156	AG		-I	45	10)
NSVS 1206916	57265.4049	0.0071	AG		-I	35	10)
NSVS 1206916	57517.4397	0.0072	AG		-I	32	10)
NSVS 1296445	57518.3758	0.0032	AG		-I	34	10)
NSVS 1304738	57297.5664	0.0058	AG		-I	58	10)
NSVS 1305379	57518.4520	0.0013	AG		-I	34	10)
NSVS 1541003	57294.5995	0.0023	AG		-I	52	10)
NSVS 1541648	57294.4839	0.0030	AG		-I	50	10)
NSVS 1557555	57364.2251	0.0015	AG		-I	43	10)
NSVS 1557555	57364.3620	0.0008	AG		-I	43	10)
NSVS 1622436	57260.3560	0.0027	AG		-I	40	10)
NSVS 1691305	57265.5764	0.0038	AG		-I	46	10)
NSVS 1748410	57294.3916	0.0015	AG		-I	56	10)
NSVS 1750812	57294.3871	0.0016	AG		-I	49	10)
NSVS 1750812	57294.5725	0.0014	AG		-I	49	10)
NSVS 1776195	57276.4319	0.0138	AG		-I	45	10)
NSVS 1776195	57276.6072	0.0054	AG		-I	45	10)
NSVS 1824689	57364.2353	0.0036	AG		-I	53	10)
NSVS 1824689	57364.3862	0.0024	AG		-I	53	10)
NSVS 1824689	57364.5467	0.0010	AG		-I	53	10)
NSVS 1828214	57364.4021	0.0038	AG		-I	50	10)
NSVS 1841163	57298.2993	0.0025	AG		-I	43	10)
NSVS 1841163	57298.5000	0.0031	AG		-I	43	10)
NSVS 1841163	57299.3235	0.0036	AG		-I	52	10)
NSVS 1841163	57299.5283	0.0025	AG		-I	52	10)
NSVS 1851662	57296.3065	0.0022	AG		-I	73	10)
NSVS 1851662	57296.4779	0.0011	AG		-I	73	10)
NSVS 1851662	57296.6527	0.0040	AG		-I	73	10)
NSVS 1913053	57295.4905	0.0007	AG		-I	57	10)
NSVS 1916718	57295.4514	0.0009	AG		-I	57	10)
NSVS 1916718	57295.6363	0.0020	AG		-I	57	10)
NSVS 1925038	57295.5021	0.0007	AG		-I	62	10)
NSVS 1958258	57338.3045	0.0099	AG		-I	68	10)
NSVS 2200550	57328.4852	0.0082	AG		-I	68	10)
NSVS 2256852	57385.3482	0.0039	AG		-I	51	10)
NSVS 2256852	57385.5310	0.0101	AG		-I	51	10)
NSVS 2432620	57409.4657	0.0172	AG		-I	38	10)
NSVS 2745595	57474.3808	0.0025	AG		-I	44	10)
NSVS 2745595	57474.5168	0.0028	AG		-I	44	10)
NSVS 2871290	57546.3956	0.0001	SCI	s	o	13	12)
NSVS 2908283	57514.4967	0.0050	AG		-I	35	10)
NSVS 2918200	57500.5981	0.0011	AG		-I	42	10)
NSVS 3115945	57516.4605	0.0100	AG		-I	36	10)
NSVS 3769020	57257.5362	0.0140	AG		-I	38	10)
NSVS 3842733	57278.4821	0.0205	AG		-I	52	10)
NSVS 3960184	57305.4926	0.0094	AG		-I	46	10)
NSVS 3971593	57299.4679	0.0050	AG		-I	52	10)
NSVS 3971593	57328.3198	0.0043	AG		-I	69	10)
NSVS 4116978	57276.4790	0.0046	AG		-I	45	10)
NSVS 4116978	57276.6326	0.0005	AG		-I	45	10)
NSVS 4147261	57328.4160	0.0014	AG		-I	69	10)
NSVS 4147261	57328.6209	0.0016	AG		-I	69	10)
NSVS 4179530	57338.5625	0.0314	AG		-I	65	10)
NSVS 4179530	57385.5310	0.0244	AG		-I	51	10)
NSVS 4280338	57345.3269	0.0009	AG		-I	57	10)
NSVS 4502253	57385.3586	0.0037	AG		-I	65	10)
NSVS 4524426	57343.5504	0.0052	AG		-I	37	10)
NSVS 4524601	57343.4529	0.0021	AG		-I	35	10)
NSVS 4524601	57379.5372	0.0003	MS		V	80	3)
NSVS 4776916	57409.5464	0.0122	AG		-I	38	10)
NSVS 4873889	57465.4865	0.0091	AG		-I	39	10)
NSVS 4989337	57515.4920	0.0034	AG		-I	27	10)
NSVS 4992380	57515.5084	0.0017	AG		-I	27	10)
NSVS 5811775	57238.5066	0.0089	AG		-I	39	10)
NSVS 6109324	57574.4736	0.0021	AG		-I	27	10)
NSVS 6156390	57295.4644	0.0035	AG		-I	48	10)
NSVS 7169040	57384.4318	0.0034	AG		-I	60	10)

NSVS 7328383	57457.4098	0.0004	FR		V	12	10)
NSVS 7328383	57457.5452	0.0004	FR	s	-I	12	10)
NSVS 7442379	57457.4121	0.0044	AG		-I	40	10)
NSVS 7442379	57457.5791	0.0032	AG		-I	40	10)
NSVS 9000641	57354.3847	0.0009	MS		V	38	8)
NSVS 9064677	57298.3913	0.0041	AG		-I	27	10)
NSVS 10123419	57414.4168	0.0033	AG		-I	42	10)
NSVS 13120542	57466.4370	0.0087	AG		-I	46	10)
ROTSE1 J125947.50+365843.6	57465.5887	0.0190	AG		-I	49	10)
ROTSE1 J130705.50+365757.1	57465.4938	0.0185	AG		-I	49	10)
ROTSE1 J143602.90+370529.4	57464.4508	0.0124	AG		-I	47	10)
ROTSE1 J143602.90+370529.4	57464.5963	0.0088	AG		-I	47	10)
ROTSE1 J144443.28+255752.4	57518.4752	0.0067	AG		-I	35	10)
ROTSE1 J175527.44+440654.3	57516.4212	0.0120	AG		-I	36	10)
ROTSE1 J175632.30+324803.2	55648.6053	0.0009	MS FR		o	12	17)
ROTSE1 J175632.30+324803.2	55670.4977	0.0030	AG		-I	35	10)
ROTSE1 J175632.30+324803.2	55673.4880	0.0028	AG		-I	35	10)
ROTSE1 J175632.30+324803.2	57516.4114	0.0022	AG		-I	32	10)
ROTSE1 J175632.30+324803.2	57516.5692	0.0014	AG		-I	32	10)
ROTSE1 J175725.72+461548.1	57514.4384	0.0059	AG		-I	35	10)
ROTSE1 J181032.62+403847.4	57136.4856	0.0035	AG		-I	31	10)
ROTSE1 J185226.53+445527.8	57343.2735	0.0016	MS		V	36	3)
SAVS 224247+452103	57330.4264	0.0012	AG		-I	31	10)
SAVS 224833+584522	57240.5394	0.0063	AG		-I	37	10)
STARE aur0 1096	57384.5797	0.0131	AG		-I	55	10)
TSVSC1 TN-N311213120-111-6	57329.5139	0.0063	AG		-I	44	10)
TYC 2019-1037	57136.4502	0.0074	AG		-I	31	10)
TYC 2679-0233	54706.5213	0.0008	FR		-I	61	10)
TYC 2679-0233	54718.4720	0.0010	FR		-I	59	10)
TYC 2679-0233	55805.5546	0.0008	FR	s	-I	12	10)
TYC 2917-0440	57384.6117	0.0110	AG		-I	55	10)
TYC 2964-1200-1	57384.3992	0.0025	AG		-I	64	10)
TYC 2964-1200-1	57384.6100	0.0019	AG		-I	64	10)
TYC 3101-1180	57132.3892	0.0032	AG		-I	36	10)
TYC 3101-1180	57132.5591	0.0032	AG		-I	36	10)
TYC 3454-1194	57134.3817	0.0016	AG		-I	34	10)
TYC 3454-1194	57134.5288	0.0024	AG		-I	34	10)
TYC 3481-1550	57464.6209	0.0058	AG		-I	47	10)
TYC 3897-0897	57134.4706	0.0027	AG		-I	36	10)
TYC 3897-0897	57134.4706	0.0027	AG		-I	36	10)
TYC 3897-0897	57136.5276	0.0086	AG		-I	31	10)
TYC 3897-0897	57136.5276	0.0086	AG		-I	31	10)
TYC 3897-1017	57134.4243	0.0043	AG		-I	36	10)
TYC 3897-1017	57134.4243	0.0043	AG		-I	36	10)
TYC 3897-1017	57136.5667	0.0059	AG		-I	31	10)
TYC 3897-1017	57136.5667	0.0059	AG		-I	31	10)
TYC 3900-0116	57125.5557	0.0061	AG		-I	43	10)
TYC 3900-0116	57132.5052	0.0081	AG		-I	40	10)
TYC 4034-1405	57296.3590	0.0015	AG		-I	74	10)
T-Per1-01259	57327.3170	0.0084	AG		-I	80	10)
T-Per1-01259	57327.4854	0.0060	AG		-I	80	10)
T-Per1-01259	57327.6575	0.0064	AG		-I	80	10)
UCAC3 248-155839	55857.3689	0.0011	FR		-I	55	10)
UCAC3 248-155839	56934.3126	0.0006	FR	s	-I	55	10)
UCAC3 248-155839	56934.4650	0.0009	FR		-I	55	10)
UCAC3 248-156543	55857.3649	0.0014	FR	s	-I	53	10)
UCAC3 248-156543	56934.4032	0.0005	FR		-I	10	10)
UCAC3 274-028753	57276.7037:	0.0030	MS FR		V	51	3)
UCAC3 274-028768	57276.7028:	0.0030	MS FR		V	78	3)
VSX J030845.1+423719	57276.4394	0.0151	AG		-I	44	10)
VSX J030845.1+423719	57328.2767	0.0027	AG		-I	71	10)
VSX J030845.1+423719	57328.4639	0.0031	AG		-I	71	10)
VSX J030845.1+423719	57328.6514	0.0020	AG		-I	71	10)
VSX J200942.2+345102	57265.3161	0.0009	FR		-I	12	10)
VSX J200942.2+345102	57265.4969	0.0007	FR	s	-I	12	10)
VSX J201223.3+344140	57265.348	0.001	FR	s	-I	12	10)
VSX J201223.3+344140	57265.5382	0.0005	FR		-I	12	10)
VSX J202530.6+372547	57574.4851	0.0017	AG		-I	27	10)
VSX J212615.0+455338	57261.4088	0.0063	AG		-I	49	10)
VSX J212615.0+455338	57287.4071	0.0078	AG		-I	36	10)
VSX J214004.5+273835	57297.4207	0.0001	MS FR		-U-I	17	3)
VSX J220917.2+543726	57562.4693	0.0027	AG		-I	26	10)

Observers:

AG:	Agerer, F., Tiefenbach
ALH:	Alich, C., Schaffhausen (CH)
BHE:	Böhme, D., Nessa
BRW:	Braunwarth, H., Hamburg
DIE:	Dietrich, M., Radebeul
FR:	Frank, P., Velden
JU:	Jungbluth, H., Karlsruhe
MS:	Moschner, W., Lennestadt
MZ:	Maintz, G., Bonn
PGL:	Pagel, L., Klockenhagen
RAT:	Rätz, M., Herges-Hallenberg
RCR:	Rätz, K., Herges-Hallenberg
SCI:	Schmidt, U., Karlsruhe
VLM:	Vollmann, W., Wien AU
WTR:	Walter, F., München

Remarks:

n	number of measurements
:	uncertain
s	secondary minimum

Photometers:

(1)	CCC camera ATIK 314 L+
(2)	CCC camera ATIK 383 L
(3)	CCD camera FLI Proline 16803
(4)	CCD camera FLI PL6303E
(5)	CCD camera Meade DSI Pro 2
(6)	CCD camera Moravian G2-1600
(7)	CCD camera QHY8L
(8)	CCD camera STL-11000 M
(9)	CCD camera STXL-6303E
(10)	CCD camera Sigma 1603
(11)	CCD camera ST-6
(12)	CCD camera ST-7
(13)	CCD camera ST-7 E
(14)	CCD camera ST-8 XMEI
(15)	CCD camera ST-9
(16)	CCD camera ST-9 E
(17)	CCD camera ST-9 XE
(18)	camera Canon EOS 450D
(19)	camera Canon EOS 600D
(20)	camera Canon EOS 70D
(21)	SuperWASP

Filters:

o	without filter
V	V-filter
B	B-filter
R	R-filter
U	U-filter
I	I-filter
L	-U-I cut-off filter
Rc	R-filter Cousins
-I	IR cut-off filter
-U	U cut-off filter
L	-U-I cut-off filter

References:

BAV Services for Scientists, 2013, `http://www.bav-astro.de/sfs/index.php/`
Lichtenknecker Database of the BAV, `http://www.bav-astro.de/LkDB/index.php/`

ERRATUM FOR IBVS 6026 (BAVM 225)

V Tri 55889.2774 BHE has to be deleted

ERRATUM FOR IBVS 6157 (BAVM 241)

MR Del 55174.3110 RAT RCR has to be deleted

COMMISSIONS G1 AND G4 OF THE IAU
INFORMATION BULLETIN ON VARIABLE STARS
Volume 62 Number 6197 DOI: 10.22444/IBVS.6197

Konkoly Observatory
Budapest
6 February 2017

HU ISSN 0374 – 0676

ADDITIONAL OBSERVATIONS OF THE 1943 ECLIPSE OF TYC 2505-672-1

OSBORN, W.; MILLS, O.F.

Yerkes Observatory, 373 W. Geneva St., Williams Bay WI 53191, U.S.A., e-mail: Wayne.Osborn@cmich.edu

Rodriguez et al. (2016) and Lipunov et al. (2016) recently reported independent discovery of an unusual eclipsing binary, TYC 2505-672-1. The star shows deep eclipses that last about 3.5 years and occur every 69 years, making it the eclipsing binary with the longest period known. The period was determined from observations of an eclipse in 2012 – 2014 and a second eclipse about 1943 seen on archival photographic plates at Harvard. and released as part of the DASCH project (Los et al. 2011). Those plates, however, only partially sampled the 1943 eclipse and such data as its eclipse depth, duration and mid-eclipse epoch were just approximate.

We have searched the Yerkes Observatory plate archive for additional observations of TYC 2505-672-1, particularly in the years around the 1943 eclipse. We located 27 plates showing the field and reaching sufficiently deep to be useful. The epochs range from 1915 to 1956. Included are two red plates taken in 1943; all other plates were unfiltered photographic (blue) ones with most being pairs taken on the same night.

A comparison sequence of surrounding stars was established using magnitudes from the Tycho, Nomad and ASCC catalogs. The adopted B, V and R magnitudes, some of which have uncertainties of up to 0.3 mag., are given in Table 1.

Eye estimates of the magnitude of TYC 2505-672-1 were made for each of the plates. The star was not visible on the two 1943 red plates and we determined the faintest magnitudes seen. The results are given in Table 2, listing the two red plates last. To aid comparison with the light curves published by Rodriguez et al. (2016) and Lipunov et al. (2016), the approximate colors of TYC 2505-672-1 of $B - V = 1.7$ and $V - R = 0.9$ have been used to estimate the equivalent V magnitudes from the corresponding blue and red measures. These are listed in the final column of Table 2.

Table 1: Comparison star sequence.

Star	GSC1 No.	B	V	R
A	2504-00723	9.4	8.4	7.8
B	2505-00438	11.5	10.8	10.4
X	2505-00435	12.1	11.6	11.3
C	2505-00703	13.3	12.3	11.7
D	2505-00347	13.8	13.1	13.0
E	2505-00630	15.0	14.0	14.1
F	2505-00332	15.3	14.1	13.8

Table 2: Yerkes archival photographic observations of TYC 2505-672-1.

Plate	Date	Type	Mag.	V
10B-961	1915-05-05	Blue	12.6	10.9
6B-961	1915-05-05	Blue	12.5	10.8
P-T231	1918-04-01	Blue	12.3	10.6
P-A239	1918-04-09	Blue	12.6	10.9
P-T239	1918-04-09	Blue	12.6	10.9
P-50A	1932-02-05	Blue	12.7	11.0
P-114A	1932-02-28	Blue	12.5	10.8
P-115B	1932-02-28	Blue	12.5	10.8
P-128A	1932-03-05	Blue	12.6	10.9
P-129B	1932-03-05	Blue	12.6	10.9
P-216A	1932-03-11	Blue	12.5	10.8
P-217B	1932-03-11	Blue	12.4	10.7
P-394A	1932-05-01	Blue	12.6	10.9
P-395B	1932-05-01	Blue	12.6	10.9
P-430A	1932-05-23	Blue	12.6	10.9
P-431B	1932-05-23	Blue	12.3	10.6
10R-1367	1937-08-10	Blue	12.7	11.0
CA-640	1951-02-10	Blue	12.5	10.8
CA-644	1951-02-10	Blue	12.5	10.8
Co-C026	1951-05-08	Blue	12.5	10.8
Co-C028	1951-05-08	Blue	12.5	10.8
CA-1988	1952-01-31	Blue	12.4	10.7
CA-2011	1952-02-18	Blue	12.4	10.7
Co 10-75	1956-03-11	Blue	12.4	10.7
Co 10-76	1956-03-11	Blue	12.6	10.9
D-1669	1943-02-08	Red	>12.0	>12.9
D-1690	1943-03-08	Red	>13.8	>14.7

All of the blue plates were outside of eclipse, and their derived magnitudes scatter about 12.5 with a standard deviation of 0.10 mag. The two red plates taken during eclipse have limiting R magnitudes of about 12.0 and 13.8, equivalent to approximately 12.9 and 14.7 respectively in V and 14.6 and 16.4 in B. These results confirm both the deep nature of the 1943 eclipse and that mid-eclipse was near the epoch found by Rodriguez et al. (2016). This is illustrated in the light curve from 1910 to 1970, shown in Figure 1. Plotted are our derived B magnitudes (large circles), our approximate limiting B values (lines) and the blue magnitudes from Harvard plates from the DASCH project (Grindlay et al. 2009, Los et al. 2011) database (dots).

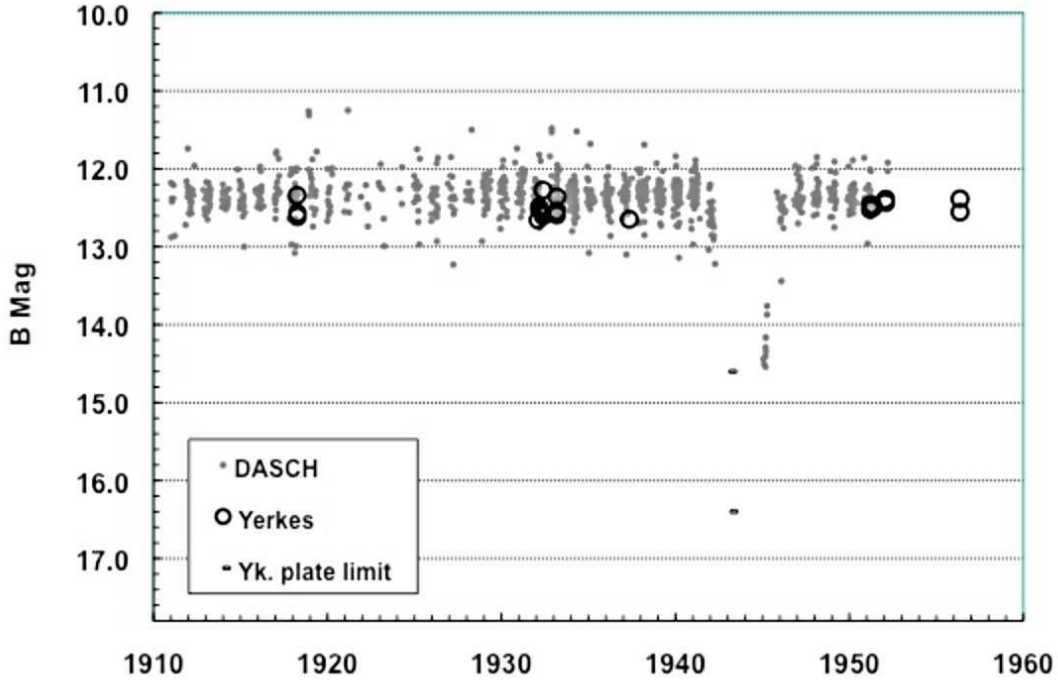

Figure 1. The light curve of TYC 2505-672-1 from 1910 to 1960.

References:

Grindlay, J. et al. 2009, *ASPC*, **410**, 101
Lipunov, V. E. et al. 2016, *A&A*, 588, A90 DOI
Los, E. et al. 2011, *ASPC*, **442**, 269
Rodriguez, J. E. et al. 2016, *AJ*, **151**, 123 DOI

COMMISSIONS G1 AND G4 OF THE IAU
INFORMATION BULLETIN ON VARIABLE STARS
Volume 62 Number 6198 DOI: 10.22444/IBVS.6198

Konkoly Observatory
Budapest
24 February 2017

HU ISSN 0374 – 0676

A TIME SERIES OF BV PHOTOMETRY AND Hα EMISSION FLUXES OF THE ECLIPSING BINARY VV Cep

POLLMANN, E.[1]; VOLLMANN, W.[2]; BENNETT, P.D.[3]

[1] Emil-Nolde Straße 12, 51375 Leverkusen, Germany

[2] Dammäckergasse 28/D1/20, A-1210 Wien, Austria

[3] Department of Physics & Atmospheric Science, Dalhousie University, Halifax, Nova Scotia, Canada

Introduction

The VV Cep binary is a red supergiant of mass 15–20 $M_{\odot}$, with a hot, presumably main-sequence, early B-type companion of comparable mass. The two stars are sufficiently well separated that Roche lobe mass transfer does not occur at present, and given the high orbital eccentricity ($e = 0.346$, Wright 1977), probably has not occurred over the evolutionary history of the system. (The orbits of binaries undergoing Roche lobe mass transfer rapidly circularize). In the ultraviolet (UV), the hot companion appears embedded in a region of circumstellar gas, as inferred from the veiled appearance of the UV spectrum (the spectrum of the naked B-star is never seen). The gas around the companion is probably a result of wind accretion from the massive wind of the M supergiant. In VV Cep, Hα emission is especially prominent, with peak fluxes of ∼10—30 times that of the (M star) continuum. This Hα emission exhibits radial velocity behaviour opposite to that of the M supergiant, implying a source near the hot companion (Wright 1977). Even though this emission declines sharply for higher Balmer lines, at times Balmer emission remains visible from levels up to $n \sim 16$. Balmer continuum emission is often observed at wavelengths shortward of 3700 Å, and at times, is strong enough to dominate this part of the UV spectrum (Bennett & Bauer 2015). In the UV, lines of Fe II also appear strongly in emission, and are probably pumped by Lyman-α and Lyman-β emission (Bennett & Bauer 2015). The great width of these Fe II emission lines (with wings out to ∼300 km s^{-1}) suggests the line-forming region is in Keplerian rotation around the B star companion, as these velocities are far larger than any other observed in the circumstellar environment of VV Cep. Although the source of the companion's emission spectrum is usually attributed to "accretion" of circumstellar gas from the M star onto the hot star, it is likely that the emission luminosity comes not from the release of gravitational energy, but from recombination of circumstellar hydrogen photoionized by the B star's Lyman continuum.

The Hα emission is variable on both short timescales and longer timescales of several years. The slow variability in Hα flux appears to correlate with the orbital separation of the two stars, with larger emission flux seen when the companion is near periastron (Bennett, private communication).

Observations

VV Cep is a 5th magnitude system of variable visual brightness, with V magnitudes ranging from 4.9–5.4. Due to its high declination (+64°), VV Cep is circumpolar and well-suited for year-round observations at northern mid-latitude sites. In preparation for the VV Cep international campaign, contemporaneous observations of B and V band DSLR photometry and Hα emission equivalent width (EW) have been obtained over the past eight years.

The V band photometry was obtained by W. Vollmann (DSLR, AAVSO+BAV), B. Hassforther (DSLR, BAV-Germany) and G. Samolyk (CCD, AAVSO data base). W. Vollmann and G. Samolyk also obtained B photometry, concurrent with the DSLR V observations. However because of the lower DSLR pixel sensitivity in Vollmann's B photometry, these data are inevitably not as precise, nor as accurate, as the V photometry. Vollmann used the Johnson B brightness of the reference stars, but did not transform to the Johnson B system, and that process resulted in an offset in the derived B magnitudes compared to Samolyk's more accurate Johnson B magnitudes. Data reduction was performed using MaxIm-DL 3.06 (Diffraction Limited, Sehgal Corporation) for Pollmann's data, while data from other amateur observers were reduced with software packages developed for amateur spectrographs, such as SpcAudace3, Audela4, VSpec5, and IRIS36.

The Hα EW study used 86 spectra, obtained by members of the ARAS spectroscopy group between July 2004 and October 2016, at times with simultaneous V band photometry. These Hα spectra were obtained with 0.2m to 0.4m telescopes with a long-slit (in most cases) and echelle spectrographs with resolutions of R = 1000–22000. All spectra included the 6400–6700 Å region, with a S/N of ∼100 for the continuum near 6600 Å. Spectral line parameters were measured with the spectral classification software package MK32. The EWs reported here included the entire Hα emission profile (including both red and blue components) from 6550–6571 Å. Since the Hα emission originates from a different source (the B-type companion) than the optical continuum of the M supergiant, the EWs calculated relative to the M stars (variable) continuum were corrected for this variability in order to provide a reliable estimate of total Hα emission flux. This correction was done by scaling the previously calculated Hα EWs by a factor of $10^{-0.4\Delta V}$, where $\Delta V = V - \overline{V}$ and $\overline{V}$ is the mean magnitude of the out-of-eclipse V time series.

Results

Here we present the data and analyses.

Figures 1, 2, and 3 show the time series of the V and B data, and the Hα emission fluxes (Hα emission EWs, corrected for continuum variability). These observations are from July 2004 to October 2016 (JD 2455500 to 2458000), or from orbital phases of 0.625–0.961, measured from mid-eclipse.

Figure 4 compares VV Cep Hα emission fluxes to simultaneous V band photometry from July 2004 to October 2016 (JD 2455500–2458000).

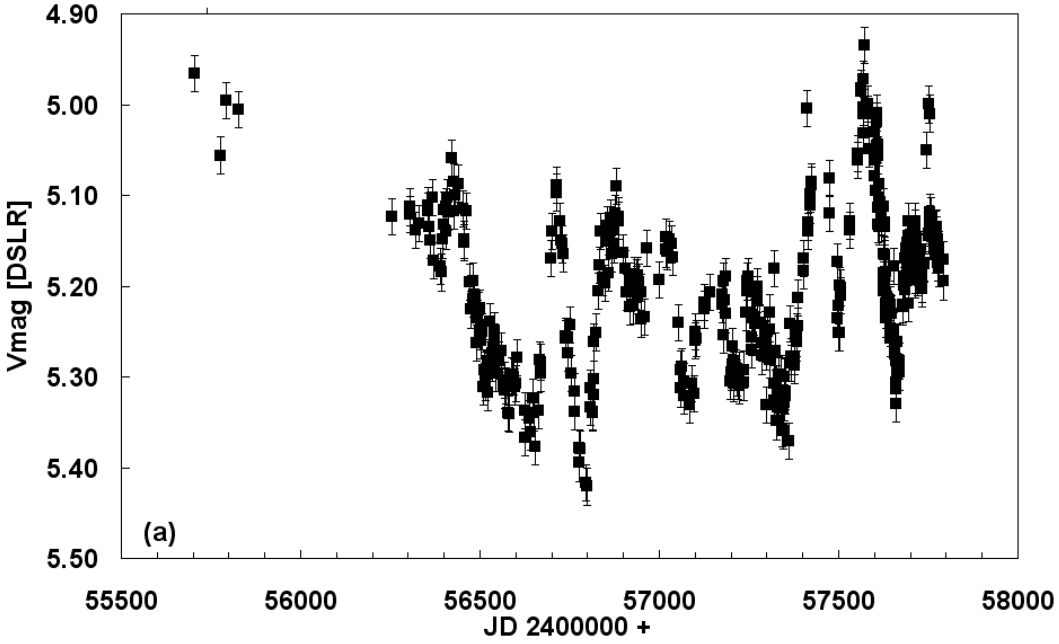

Figure 1. VV Cep DSLR V magnitudes: July 2004 to October 2016.

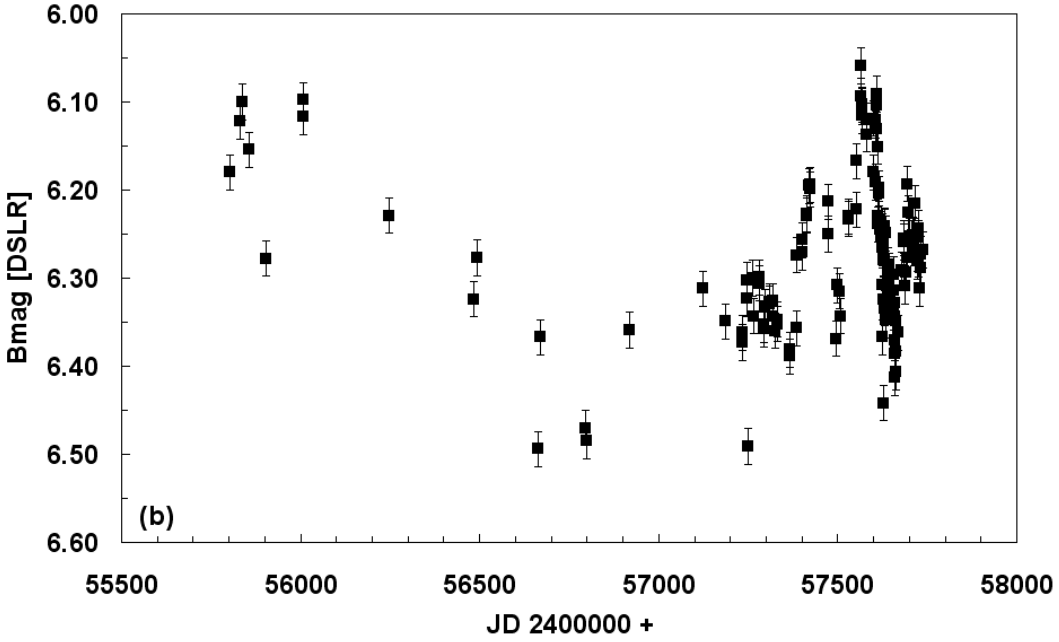

Figure 2. VV Cep B magnitudes: July 2004 to October 2016.

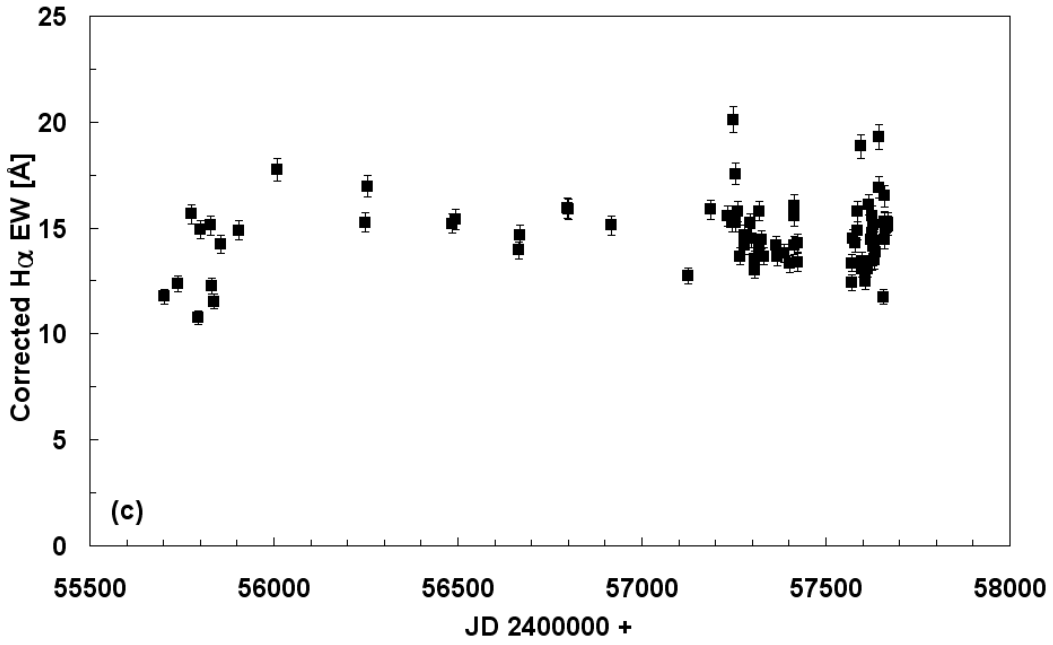

Figure 3. VV Cep Hα emission fluxes: July 2004 to October 2016.

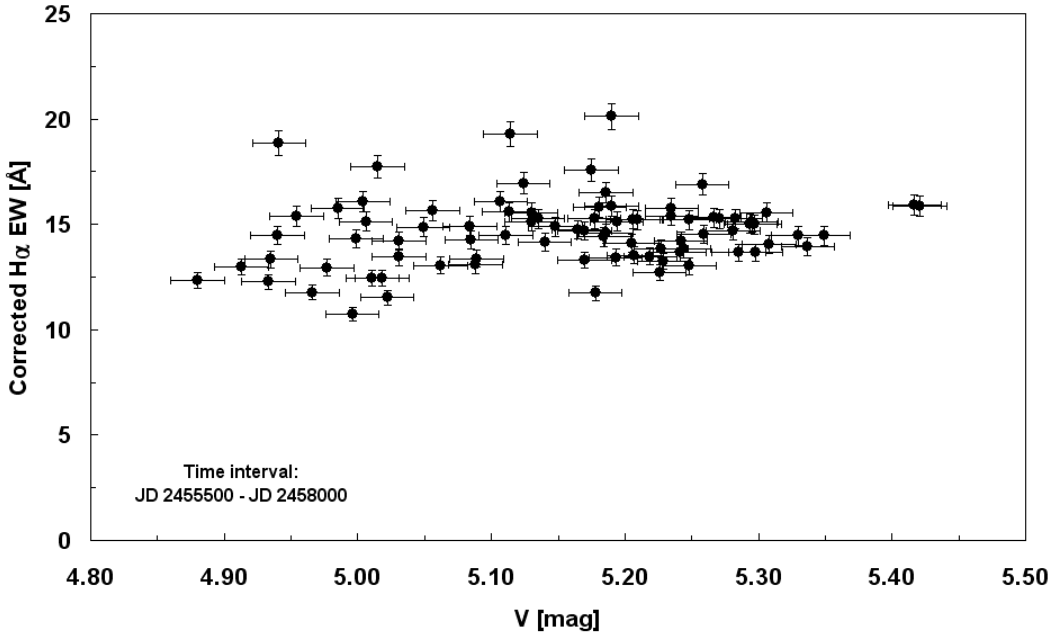

Figure 4. VV Cep Hα emission fluxes versus DSLR V magnitude.

Figure 5 shows the power spectrum of the V photometry of VV Cep obtained using the Period04 code (Lenz & Breger 2005). The strongest peaks in the power spectrum of the V photometry are near 145 and 656 days. The first period lies close to the 150 day period first proposed by Hayasaka et al. (1971) and is almost certainly real. The second period is about one-half of the time spanned by the vast majority (406 out of 412 points) of the photometry, and may be an artifact resulting from long-term variations over this period.

Figure 6 shows the corresponding phase diagram of the V photometry produced by program AVE (Barberá 1998), of Figure 1, phased with a 145.5 day period. Many other periods have been reported in the literature over the years: e.g., periods of 60, 110, 114, 116, and 280 days (Graczyk et al. 1999; Saito et al. 1980; McCook et al. 1978; Baldinelli et al. 1979; Pfeiffer et al. 1989), and it apparent from Figure 5 that there is significant power at other frequencies with periods longer than about 30 days, and especially longer than 100 days. This behaviour suggests the short-term variability is somewhat irregular in nature, and probably has a substantial stochastic component. Indeed, the plot of the V variability, phased to a period of 145.5 days (Figure 6), shows a substantial fraction of this variability remains unexplained by this regular short-period oscillation.

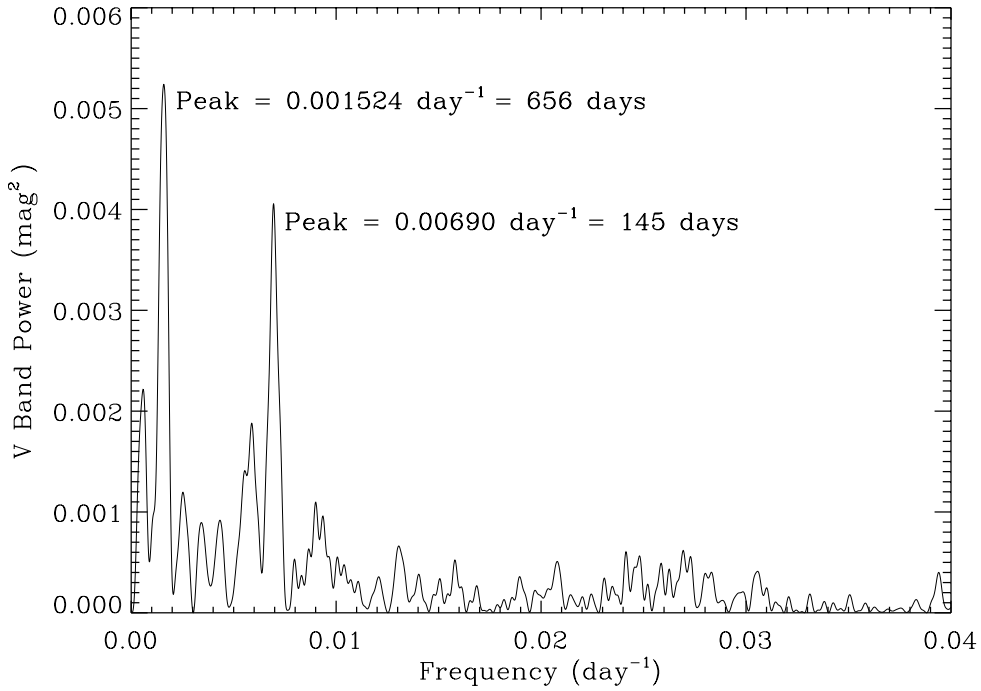

Figure 5. Power spectrum of V band photometry of VV Cep. The peak of 656 days may be an artifact due to the finite length of the time series; the second prominent peak at 145 days is probably real and due to intrinsic pulsation of the M supergiant.

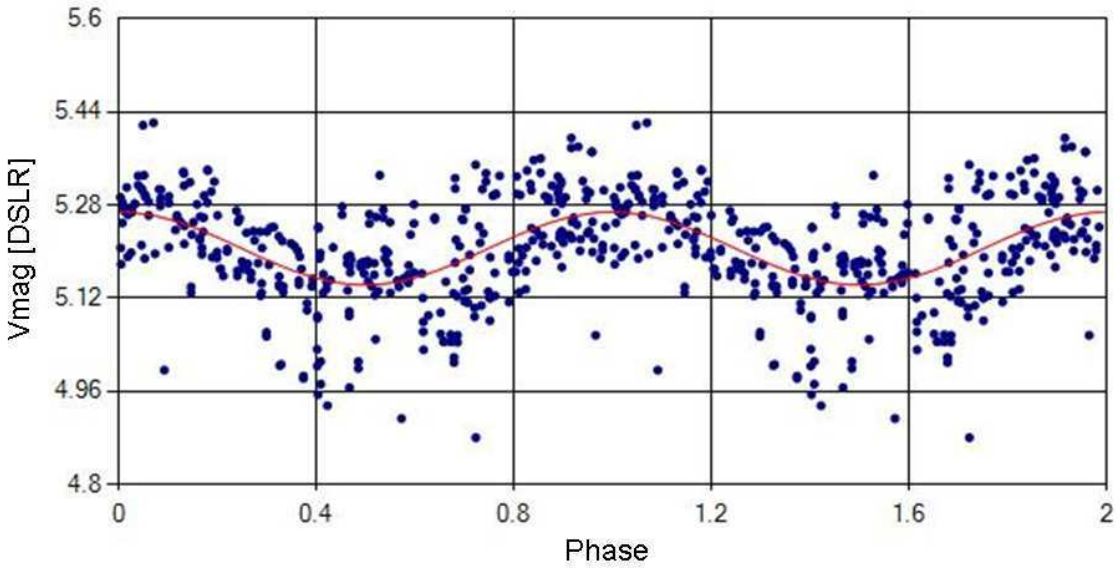

Figure 6. AVE phase diagram of the V photometry of Figure 1, with a fitted period of 145.5 ± 1.2 days, and epoch JD 2456750.

Conclusions

The observations presented here span the period from JD 2455500 to 2458000, corresponding to orbital phases 0.625–0.961. The amplitude of the photometric variability is $\Delta V \approx 0.4$–0.5 mag, whereas the amplitude of the total eclipse of the B star is only is $\Delta V \approx 0.15$ mag. The period and photometric amplitude of the variability is quite similar to that resulting from irregular pulsation in other, single late-type supergiants. We confirm the peak power of this pulsation lies near a period of 145 days. A second, longer period of 656 days may be an artifact arising from the finite length of the time series. All of this strongly suggests that the photometric variability observed for VV Cep is intrinsic, and due to irregular pulsation of the M star. The source of the variability of Hα, originating from an accretion region around the hot companion, remains unclear and the time sampling of these Hα observations are too sparse to permit a meaningful period analysis.

Acknowledgements

We are grateful to Sara and Carl Sawicki (Alpine, Texas, USA) for their helpful improvements and suggestions in language. We are grateful to the observers of the ARAS spectroscopy group for contributing Hα spectra of VV Cep. We wish to thank Bela Hassforther (Deutsche Arbeitsgemeinschaft Veränderliche Sterne, BAV) for supplying additional V photometry. Finally, we acknowledge, with thanks, the use of variable star observations contributed to the AAVSO International Database by Gerard Samolyk.

Observers of the ARAS Spectroscopy Group

J. N. Terry, B. Koch, O. Thizy, E. Betrand, O. Garde, F. Teyssier, T. Lester, J. Foster, Ch. Buil, M. Schwarz, J. Guarro, D. Hyde, E. Pollmann.
ARAS website — `http://www.astrosurf.com/aras/`

References:

Baldinelli, L., Ghedini, S., Marmi, S. 1979, *IBVS*, **1675**
Barberá, R. 1999, `AVE` code, version 2.51, `http://astrogea.org/soft/ave/aveint.htm`
Bennett, P.D., Bauer, W.H. 2015, *ASSL*, **408**, 85 DOI
Graczyk, D., Mikolajewski, M., Janowski, J. L. 1999, *IBVS*, **4679**
Harmanec, P., 1983, *Hvar Obs. Bull.*, **7**, 55
Hayasaka, T., Saijo, K. , Sato, H., Saito, M., Kitamura, M. 1977, *Tokyo Astr. Bull. Second Series*, **247**, 2865
Hutchings, J. B., Wright, K. O. 1971, *MNRAS*, **155**, 203 DOI
Lenz, P., Breger, M. 2005, *Comm. in Asteroseismology*, **146**, 53 DOI
McCook, G., P., Guinan, E., F. 1978, *IBVS*, **1385**
Pfeiffer, R. J., Maffei, J. C. 1989, *BAAS*, **21**, 792
Saito, M., Sato, H., Saijo, K., Hayasaka, T. 1980, *PASJ*, **32**, 163-177
Wright, K.O. 1977, *JRASC*, **71**, 152

COMMISSIONS G1 AND G4 OF THE IAU
INFORMATION BULLETIN ON VARIABLE STARS
Volume 62 Number 6199 DOI: 10.22444/IBVS.6199

Konkoly Observatory
Budapest
24 February 2017
HU ISSN 0374 – 0676

OBSERVATIONS OF VARIABLES

Date: 19 August 2014

Reported by:
Hojjatpanah, S. - Department of Physics, Biruni Observatory, Shiraz University, P.O. Box 71454, Shiraz, Iran,
Mousavi, N. - Department of Physics, Biruni Observatory, Shiraz University, P.O. Box 71454, Shiraz, Iran
Kazemi, S. - Department of Physics, Biruni Observatory, Shiraz University, P.O. Box 71454, Shiraz, Iran

Name of the object:

AE UMa

Remarks:

The data were reduced by using dark, bias, flat-field frames and differential photometry method was used in order to data reduction. The times of maxima listed in IBVS 6199-t2.txt were calculated by fitting a parabolic curve to the data around the maxima.

Date: 27 April 2015

Reported by:
Pollmann, E. - International Working Group "Active Spectroscopy in Astronomy", 51375 Leverkusen, Germany, ernestospec@hotmail.de
Leonardi, M. - Observatory "Cotoletta", Gorgonzola (Milano), Italy, mleonardi10@gmail.com

Name of the object:

28 Tau

Remarks:

Within the time span January 2012 to February 2015 a group of 24 observers of the ARAS community (`http://www.astrosurf.com/aras/`) was successful in documenting four periastron passages of the Be binary 28 Tau. The main purpose of the campaign was to observe the change in radial velocity (RV, `6199-f2.jpg` – the figures are available in the online version) along with the V/R ratio of the Hα double peak profile (`6199-f3.jpg`). For this campaign Littrow spectrographs of the type LHIRES III with different spectral resolving power R from 8000 to 17000 resp. were used. The reproducibility of our Hα RV measurements of one spectrum during one night can be indicated by application of the line profile mirror method with ± 2 km/s.

Our observation results represent only the Be-shell time period JD 2459942 to 2457083. With our campaign we were particularly interested in seeing what happens with changes of the V/R ratio around the minimum radial velocity epoch near the periastron as a consequence of the attractive force of the secondary in the 218-d-binary. Our detailed Hα RV representation in `6199-f4.jpg` shows a clear jump in the positive (red shift) direction around JD 2457060, which is similar to that found in the RV data (JD 2452860 to 2454186) of Nemravova et al. (2010).

Because of this unusual jump in our observations, we checked this RV behaviour with the line FeII 6516 Å, which is formed closer to the central star, and to compare it to the RV at the outer (Hα) radius of the disk. In `6199-f5.jpg` we see an impressive indication that in fact the FeII 6516 RV is decreasing more or less evenly and undisturbed to the periastron at approx. JD 2457076.4. According to the recently determined orbital elements (e.g.: $e = 0.596$; $\omega = 148°$; $T_{\rm periastron} = 2440040\overset{\rm d}{.}4$) by Nemravova et al. (2010) at the Hα absorption core, we had to expect this periastron at JD 2457077.0 .

The unusual V/R variation as an appearance of two separate minimum components (at JD 2457060 & 2457076) near the periastron in `6199-f6.jpg` seems to indicate a distortion and deformation process of the two disks (Hirata 2007 & Tanaka et al. 2007).

In spite of this blur in the periastron time definition, we tried to calculate a period analysis both of RV and V/R. First, `6199-f7.jpg` shows the PDM (phase dispersed minimization) RV period calculation of all observed periastron in this paper, which led to a period of 227.4 days. `6199-f8.jpg` shows the corresponding phase diagram. Our larger period results from the fact that we were able to observe in detail RV as well as V/R within certain periastron campaigns, which led to a larger dispersion of the exact periastron time itself. The more or less sharp V/R definition in our observations (except for the last monitored periastron), reflects [with the PDM period analysis (`6199-f9.jpg`) and its phase diagram (`6199-f10.jpg`)] fairly exactly the 217.9 day orbital period of Katahira et al. (1996) and Nemravova et al. (2010).

The following ARAS observer contributed with their spectra: Th. Garrel, C. Sawicki, J. Montier, J. S. Devaux, M. Pujol, M. Leonardi, V. Desnaux, P. Berardi, Ch. Buil, K. Graham, B. Mauclaire, F. Houpert, E. Pollmann, N. Montigiani, M. Mannucci, J. N. Therry, J. Guarro, Th. Lemoult, O. Garde, St. Charbonnel, T. Lester, A. Favaro, Dong Li, P. Fosanelli.

Date: 18 November 2015

Reported by:

Gazeas, K. - Department of Astrophysics, Astronomy and Mechanics, National and Kapodistrian University of Athens, GR 15784, Zografos, Athens, Greece, kgaze@phys.uoa.gr

Name of the object:

GSC 03122-02426

Remarks:

Detected on 28 September 2012 in the FoV of V563 Lyr.

RA(J2000)	Dec(J2000)	type
18 45 44.86	+40 17 20.2	EW

Magnitude	Period	Epoch
14.9(Rmag -USNO A2.0)	0.30050(9)	2456200.2458(7)

Cross-identification(s):

GSC 03122:02426 = TYC 3122-2426-1 = 2MASS J18454487+4017197 = USNO-A2.0 1275-10327334 = GSC2.2 N030012326476 = CSS J184544.8+401722

Name of the object:

GSC 05581-00047

Remarks:

Detected on 24 May 2015 in the FoV of the blazar PKS 1510-089

RA(J2000)	Dec(J2000)	type
15 13 16.41	-09 08 41.4	RRLyr

Magnitude	Period	Epoch
14.1(Rmag -USNO A2.0)	0.36869(5)	2457163.4136(5)

Cross-identification(s):

GSC 05581:00047 = USNO-A2.0 0750-08849885 = GSC2.2 S2310211460 = 2MASS J15131640-0908413 = HE 1510-0857 = CSS J151316.4-090841

Date: 8 June 2016

Reported by:

Rocchi, G. - Porziano Astronomical Observatory, piazza S. Chiara 2, 06081 Assisi, Perugia, Italy
Spogli, C. - Porziano Astronomical Observatory, piazza S. Chiara 2, 06081 Assisi, Perugia, Italy
Fagotti, P. - Porziano Astronomical Observatory, piazza S. Chiara 2, 06081 Assisi, Perugia, Italy
Ciprini, S. - Agenzia Spaziale Italiana (ASI) Science Data Center, via del Politecnico snc, 00133 Rome, Italy & INFN Perugia Section, via Pascoli, 06123 Perugia, Italy, stefano.ciprini.asdc@gmail.com
Vergari, D. - Porziano Astronomical Observatory, piazza S. Chiara 2, 06081 Assisi, Perugia, Italy
Brunozzi, P. - Porziano Astronomical Observatory, piazza S. Chiara 2, 06081 Assisi, Perugia, Italy

Name of the object:

V720 Cas

Remarks:

A total of 40 observations from 2013 January 3 to December 23, and 37 observations from 2014 January 01 to October 9 of the semiregular pulsating carbon star V720 Cas have been obtained in the V (Johnson) photometric band. Our observations are obtained in the context of a long-term variability study of a sample of dwarf novae and long-period variable stars at the Porziano Astronomical Observatory, Mount Subasio, Assisi, Italy. Our data confirms the period of 455 days.

V720 Cas (also known as IRAS 00422+5310, TAV 0042+53, CGCS 105, GSC 3655.01254, 2MASS J00450706+5326473, WISE J004507.06+532647.7) was initially classified as a carbon star from low resolution IRAS spectra (Olnon et al. 1986) in the 8-22μm mid-infrared band by Little-Marenin et al. (1987). A carbon star is a late-type bright and red AGB giant star whose atmosphere contains more carbon than oxygen, those combining in the upper layers of the star forming CO and consuming all the oxygen in the atmosphere. Free carbon atoms form other carbon compounds, giving the star a pitchy atmosphere and a strikingly ruby red appearance. They are particularly bright at IR and millimetre bands. Beyond IRAS, V720 Cas was, in fact, observed also by the WISE and AKARI infrared space satellites. The IRAS low-resolution mid-IR spectrum class is 4.5, the flux density $F_{12\mu\mathrm{m}} = 16.3\,\mathrm{Jy}$, the mid-IR color indices are $[25-12] = -0.751$ mag and $[60-25] = -0.991$ mag while was not possible to detect OH maser lines (Sivagnanam et al. 1990). Noguchi et al. (1991) presented first $JHKL$ bands and 3.1μm (SiC) photometry. Rudolf (1993) analysed about 300 Sonneberg observatory plates to reveal semiregular variation in the light curve with cycle lengths of 420 days (for the interval 1971-1986) and 456 days (from 1988). Later Kazarovets and Samus (1997) describes variations for V720 Cas spanning from $P = 9.6$ mag to $P = 12.5$ mag ($P = 374$nm filter). The observation of hydrogen cyanide (HCN) in the millimetre spectrum of V720 Cas with the IRAM 30m millimeter telescope, has confirmed the carbon-rich character (Groenewegen et al. 2002a). The star has $m_{(bol)} = 8.08$, $M_{(bol)} = -5.00$ and distance from earth of 4.11 kpc, while the gas mass loss rate, derived from the CO spectral line, is $dM/dt^{(gas)} = 3.61 \times 10^{-6}$ $M_\odot$ yr^{-1}, and the dust mass loss, derived from the IRAS 60μm flux density, is $dM/dt^{(dust)} = 9.80 \times 10^{-9}$ $M_\odot$ yr^{-1} (Groenevegen et al. 2002b). The star was more recently observed also in near-IR bands: $J = 7.28 \pm 0.02$, $H = 5.62 \pm 0.02$, $K = 4.41 \pm 0.02$ (Chen et al. 2012).

Our observations have been collected with the 110 mm refractor ED telescope of the Porziano Observatory equipped with a SBIG CCD Camera (Kodak KAF 402 ME 762×512 pixel) and standard V Johnson broad band filter (Bessell 1979). The exposure time was 240s or 300s. The CCD frames were first corrected for debiasing and flat-fielding, then processed for aperture photometry. To calibrate the V magnitudes we used stars in the Tycho-2 catalogue (Høg et al. 2000). In the year 2013 the star varied in luminosity from 14.14 ± 0.05 to 12.81 ± 0.04 with an amplitude of 1.33 mag. In 2014 the variation was of 2 magnitudes from 13.72 ± 0.01 to $11.72 + 0.02$.

The period analysis of our 2013-2014 total light curve is performed using the Lomb-Scargle periodogram (LSP) technique (Lomb 1976, Scargle 1982). Our analysis results in dominating periodic signal peak (Fig. 3) corresponding to a period of 455 days, in agreement with the findings of Rudolf (1993). Figure 1 shows the finding chart with the comparison stars used for the photometry. Table 1 reports the V photometric Tycho-2 values and standard deviations for the selected comparison stars. Table 2 gives the V magnitudes of V720 Cas, and the Figure 2 presents the V light curve of V720 Cas during the 2013-2014 interval. Finally Figure 3 includes a plot of the LSP of our light curve.

Date: 5 August 2016

Reported by:
Garcia, Jose Garcia - Tamarindo, 5, 41089 Dos Hermanas, Sevilla, Spain, garciados@infonegocio.com
Parsamian, Elma S. - V. Ambartsumian Byurakan Astrophysical Observatory, Armenia, elma@sci.am, eparsam@bao.sci.am

Name of the object:
V1118 Ori

Remarks:
Variability of V1118 Ori was discovered in 1983 (Hurst, Chanal, 1984), and the star was soon recognized as an EXor or Subfuor (Parsamian & Gasparian, 1987, Herbig, 1990). After reaching maximum brightness, EXors usually keep their brightness constant with some fluctuations for several months and then fade to minimum. During the outburst the stellar spectra have strong emissions which become less intensive in quiet state. The evidence, that V1118 Ori was not included in the catalog of Hα emission stars in the region of the Orion Nebula (Parsamian, Chavira, 1982) speaks in favour of that V1118 Ori was not a strong Hα variable before the first outburst. Till to now only two stars – V1118 Ori and V1143 Ori – have been known as EXors in the Orion association region. It seems that the activity of such kind is very short in the life of T Tau stars, although the duration of each outburst is about 1.5-2.0 years. We have information on outbursts for the years 1983-1984 (Kosai, 1983, Hurst et al. 1984, Parsamian & Gasparian, 1987), 1988-1990 (Parsamian et al., 1993, 1996), 1992-1994 (Garcia Garcia, Mampaso & Parsamian, 1995, Parsamian et al., 2002), 1996-1998 (Hayakawa et al., 1998, Garcia Garcia & Parsamian, 2000), 2004-2006 (Waagen et al., 2005, Williams et al. 2005, Garcia Garcia et al., 2006), 2007-2008 (Garcia Garcia & Parsamian, 2008). A new outburst took place in September 2015 (Giannini et al., 2016). Our observations cover the period 2014-2016 (Fig. 1). During this period the brightness of the star changed from $V = 17.1$ and reached a maximum of $V = 13.8$ in 13.11.2015. It seems that the outburst frequency become lower during last years. Further observations would show behaviour of star during this outburst. Our observations are going to be continued.

Date: 14 September 2016

Reported by:
Essam, Ahmed - Astronomy Department, National Research Institute of Astronomy and Geophysics (NRIAG) 11421 Helwan, Egypt, essam60@yahoo.com
Elsadek, Mohamed - Astronomy Department, NRIAG, 11421 Helwan, Egypt
Shokry, Ahmed - Astronomy Department, NRIAG, 11421 Helwan, Egypt
Darwish, Mohamed - Astronomy Department, NRIAG, 11421 Helwan, Egypt

Name of the object:
GSC2.3 N1Y0039176

Remarks:

RA(J2000)	Dec(J2000)	Type	Vmag.	Period	Epoch
20 00 46.395	+05 47 47.97	EW	17.18-17.85	0.276853 d	2457602.5001 ±0.0

Variation of the star was first reported at the AAVSO Variable Star Index (VSX): `https://www.aavso.org/vsx/index.php?view=detail.top&oid=473895`.
All the observations have been carried out by using the EEV CCD 42-40 camera with a format of 2048×2048 pixels, cooled by liquid nitrogen attached on the Newtonian focus of the 1.88-m Kottamia reflector telescope in Egypt.
the location of Kottamia Astronomical Observatory (KAO) as follows:
Latitude: 29°56′02.″43 N
Longitude: 31°49′40.″10 E
Height: 467 m
International code = 088

Cross-identification(s):
GSC2.3 N1Y0039176 = 2MASS J20004638+0547475 = USNO-B1.0 0957-0507660

Date: 21 September 2016

Reported by:
Essam, Ahmed - Astronomy Department, National Research Institute of Astronomy and Geophysics (NRIAG) 11421 Helwan, Egypt, essam60@yahoo.com
Elsadek, Mohamed - Astronomy Department, NRIAG, 11421 Helwan, Egypt

Name of the object:
1SWASP J200059.78+054408.9

Remarks:

RA(J2000)	Dec(J2000)	Type	Vmag.	Period	Epoch
20 00 59.78	+05 44 08.9	EW	15.014-15.737	0.205691 d	2457604.37104 ±0.0010

Variation of the star was discovered by Lohr et al. (2013).
All the observations have been carried out by using the EEV CCD 42-40 camera with a format of 2048×2048 pixels, cooled by liquid nitrogen attached on the Newtonian focus of the 1.88-m Kottamia reflector telescope in Egypt.
the location of Kottamia Astronomical Observatory (KAO) as follows:
Latitude: 29°56′02.″43 N
Longitude: 31°49′40.″10 E
Height: 467 m
International code = 088

Cross-identification(s):
1SWASP J200059.78+054408.9 = UCAC4 479-113657 = 2MASS J20005975+0544073

Date: 23 January 2017

Reported by:
Ziaali, E. - Research Institute for Astronomy and Astrophysics of Maragha (RIAAM), Maragha, East Azerbaijan, Iran, P.O. Box: 55177-36698, ziaali29me@gmail.com
Kermani, M.H. - Research Institute for Applied Physics and Astronomy, University of Tabriz, 29 Bahman Blvd, Tabriz, Iran, P.O. Box: 5166616471, kermani@tabrizu.ac.ir
Ebadi, H. - Department of Theoretical Physics and Astrophysics, University of Tabriz, Tabriz, Iran, P.O. Box: 51666-16471, hosseinebadi@tabrizu.ac.ir

Name of the object:

V0367 Cam

Remarks:

RA(J2000)	Dec(J2000)	Type
$04^{\rm h}40^{\rm m}55\overset{\rm s}{.}1822$	$+53°38'06\overset{''}{.}524$	DSCT

Observatory and Telescope:
Observatory of Research Institute for Astronomy and Astrophysics of Maragha (RIAAM), Iran (Longitude: 46.238°E, Latitude: 37.3835°N, Elevation: 1472.29 meters) a 12-inch Cassegrain Mead telescope

Detector:
SBIG STX–16803 CCD camera, 16 million pixels (4096×4096 pix) with a pixel length of 9 μm and field of view of 42 arcmin^2.

Filter(s):
Johnson V and R filters

Date(s) of observation(s):
The V band observations of V0367 Cam were carried out on 22 and 23 October and 4 November 2016 and the R band observations of V0367 Cam were carried out on 23 October and 4 November 2016.

Comparison star(s):
TYC 3733-390-1 (2MASS J04413568+5335117)

Check star(s):
ChK1: GSC 03733-00063
ChK2: GSC 03733-00152
ChK3: GSC 03733-00327

Transformed to a standard system (Johnson $UBVRI$).
Standard stars (field) used: BD+53 796C

V0367 Cam (also known as GSC 03733-01115, 2MASS J04405518+5338066, TYC 3733- 1115-1) was discovered in 2006 by Otero (2007) as a DSCT star with a period of 0.121596 d. Again it was confirmed as a DSCT star by Kazarovets et al. (2011) in The 80th Name-list of Variable Stars. V0367 Cam was observed in 2013 and the epochs were reported by Wils et al. (2014) The light curves of GSC 03733-01115 were extracted using MaxIm Dl version 5.03 software independently for each filter.

We searched for the main pulsation frequencies and their harmonics. The period analysis was performed using Period04 software (Lenz & Breger 2005) for obtaining exact results. The analysis of the original dataset confirmed the large contribution of the average value of f_1 term, i.e., 8.2144 d^{-1} on two filters and the period of 0.121737 d was obtained. Considering of the residuals reveals the first harmonic of f_1, averaged on V and R filters as $2f_1 = 16.3889$ d^{-1}.

Acknowledgements:
This work has been supported financially by Research Institute for Astronomy and Astrophysics of Maragha (RIAAM) and also we thank Rahim Heidarnia from RIAAM for his kind assistance in doing observations. We further acknowledge Research Institute for Applied Physics and Astronomy (RIAPA) of University of Tabriz.

References:

Bessell, F.M., 1979, *PASP*, **91**, 589 DOI
Chen, P.S., Yang X. H., 2012, *AJ*, **143**, 36 DOI
Garcia Garcia, J., Mampaso, A., Parsamian E., 1995, *IBVS*, **4268**
Garcia Garcia, J., Parsamian, E. S., 2000, *IBVS*, **4925**
Garcia Garcia, J., Parsamian, E. S., 2008, *IBVS*, **5829**
Garcia Garcia, J., Parsamian, E. S., Velazquez J.C. et al., 2006, *IBVS*, **5691**
Giannini, T., Lorenzetti, D., Antoniucci, S. et al., 2016, *ApJL*, **819**, L5 DOI
Groenewegen, M.A.T., Sevenster, M., Spoon H.W.W., & Pérez, I., 2002a, *A&A*, **390**, 501 DOI
Groenewegen, M.A.T., Sevenster, M., Spoon H.W.W., & Pérez, I., 2002b, *A&A*, **390**, 511 DOI
Hayakawa T., Ueda T., Uemura M., et al., 1998, *IBVS*, **4615**
Herbig, G.H., 1990, Low Mass Star Formation and Pre-Main Sequence Objects, ed. Bo Reipurth, Munchen, 223
Hirata, R., 2007, *ASP Conf. Ser.*, **361**, 267
Høg, E., Fabricius, C., Makarov, V.V., et al., 2000, *A&A*, **355**, L27
Hurst, G.M., Chanal, D., et al., 1984, *IAU Circ.*, **3924**
Katahira, J.-I., Hirata, R., Ito, M., Katoh, M., Ballereau, D., Chauville, J., 1996, *PASJ*, **48**, 317 DOI
Kazarovets, E. V. et al, 2011, *IBVS*, **5969**
Kazarovets, E.V., Samus, N.N., 1997, *IBVS*, **4471**
Kosai, H., 1983, *IAU Circ.*, **3763**
Lenz, P., Breger, M., 2005, *CoAst*, **146**, 53 DOI
Little-Marenin, I.R., Ramsay, M.E, Stephenson, C.B, Little, S.J, Price, S. D., 1987, *AJ*, **93**, 663 DOI
Lohr, M. E., Norton, A. J., Kolb, U. C., Maxted, P. F. L., Todd, I., West, R. G., 2013, *A&A*, **549**, A86 DOI
Lomb, N.R., 1976, *Ap&SS*, **39**, 447 DOI
Nemravova, J., Harmanec, P., Kubat, J., Koubsky, P., Iliev, L., Yang, S., Ribeiro, J., Slechta, M., Kotkova, L., Wolf, M., Skoda, P., 2010, *A&A*, **516**, A80 DOI
Noguchi, K., Sun, J., & Wang, G., 1991, *PASJ*, **43**, 275
Olnon, F.M., Raimond, E., Neugebauer, G., et al., 1986, *A&AS*, **65**, 607
Otero, S. A., 2007, *Open European Journal on Variable Stars*, **56**, 1
Parsamian, E.S., Chavira, E., 1982, *Bol. Inst. Tonantzintla*, **3**, 69
Parsamian, E.S., Gasparian, K.G., 1987, *Astrophysics*, **27**, 598 DOI
Parsamian, E.S., Gasparian, K.G., Oganian G.B. et al., 1996, *Astrophysics*, **39**, 201 DOI
Parsamian, E.S., Ibragimov, M.A., Oganian G.B. et al., 1993, *Astrophysics*, **36**, 12 DOI
Parsamian, E. S., Mujica, R., Corral L., et al., 2002, *Astrophysics*, **45**, 393 DOI
Rudolf, E., 1993, *Mitt. Veränderliche Sterne*, **12**, 165
Scargle, J.D., 1982, *ApJ*, **263**, 835 DOI
Sivagnanam, P., Le Squeren, A.M., Minh, F.T., & Braz M.A., 1990, *A&A*, **233**, 112
Tanaka, K., Sadakane, K., Narusava, S.-Y., et al., 2007, *PASJ*, **59**, L35 DOI
Waagen, E. O., Williams, P., de Scala, G. et al., 2005, *IAU Circ.*, **8626**
Wils, P. et al., 2014, *IBVS*, **6122**
Williams, P., Bembrick, C., Lee, S., 2005, *IAU Circ.*, **8460**

COMMISSIONS G1 AND G4 OF THE IAU
INFORMATION BULLETIN ON VARIABLE STARS
Volume 62 Number 6200 DOI: 10.22444/IBVS.6200

Konkoly Observatory
Budapest
24 February 2017

HU ISSN 0374 – 0676

REPORTS ON NEW DISCOVERIES

Date: 04 July 2014
Observer(s) and affiliation(s): Martignoni, Massimiliano - Stazione Astronomica Betelgeuse, Magnago, Milano, Italy, massimiliano.martignoni@alice.it

RA(J2000)	**Dec(J2000)**	**type**	**Mag.**
17 17 45.37	11 09 32.5	DSCT	13.15 - 13.35 (V)
Period		**Epoch**	
0.217045 d		2456745.613	
Cross-identification(s): UCAC4 506-065333 = CSS J171745.4+110932			

Remark: UCAC4 506-065333 is a DSCT type pulsating variable star in the field of view of V452 Oph. It was observed with a 0.25 m Schmidt-Cassegrain telescope (f/10) of the Stazione Astronomica Betelgeuse in Magnago, Italy equipped with a 512×512 pixels Kodak KAF261E CCD cooled to (typ.) −20°C; 1.6 arcsec per pixel (1×1 binning); 14′×14′ field of view, with V and R_C photometric filters. As comparison and check stars were used UCAC4 506-065387 and UCAC4 506-065389. A total of 119 measurements in V band and 94 in R_C band were collected; reduction to the standard photometric system was not performed.

Date: 15 August 2014
Observer(s) and affiliation(s): Essam, Ahmed - Astronomy Department, National Research Institute of Astronomy and Geophysics (NRIAG), 11421 Helwan, Egypt, address:essam60@yahoo.com

RA(J2000)	**Dec(J2000)**	**type**	**Mag.**
15 58 28.08	–02 57 53.6	EW	15.03 - 15.74 (V)
Period		**Epoch**	
0.361456 d		2456827.46801 ± 0.000334	
Cross-identification(s): UCAC4 436-062932 = 2MASS J15582807-0257536 = CSS J155828.1-025753 = USNO-B1.0 0870-0361232			

Remark: All the observations have been carried out by using the EEV CCD 42-40 camera with a format of 2048×2048 pixels, cooled by liquid nitrogen attached on the Newtonian focus of the 1.88 m Kottamia reflector telescope in Egypt. Comparison star: UCAC4 436-062934. Check star: GSC 0502300278.

Date: 15 December 2014

Observer(s) and affiliation(s):
Liakos, A. - National Observatory of Athens, Institute for Astronomy, Astrophysics, Space Applications, and Remote Sensing, Palaia Penteli, Athens, Hellas (Greece), alliakos@noa.gr
Dakanalis, I. - National and Kapodistrian University of Athens, Department of Astrophysics, Astronomy and Mechanics, Zografos, Athens, Hellas (Greece); National Observatory of Athens, Institute for Astronomy, Astrophysics, Space Applications, and Remote Sensing
Niarchos, P. - National and Kapodistrian University of Athens, Department of Astrophysics, Astronomy and Mechanics, pniarcho@phys.uoa.gr

RA(J2000)	**Dec(J2000)**	**type**	**Mag.**
20 27 52.536	+24 41 30.96	EW?	14.9 (R)

Period	**Epoch**
0.35806(7) d	2455391.447(1)

Cross-identification(s):
USNO-A2.0 1125-16060074 = 2MASS 20275251+2441305

RA(J2000)	**Dec(J2000)**	**type**	**Mag.**
20 28 36.715	+24 56 04.70	RR	13.1 (R)

Period	**Epoch**
0.3468(2) d	2455392.337(3)

Cross-identification(s):
USNO-A2.0 1125-16097188 = NOMAD1 1149-0516720

Remark: Both stars detected in the FoV of AW Vul and the newly discovered variable (marked as NV1 in the finding chart) 2MASS J20275736+2453029 (Liakos & Niarchos 2010).

Date: 15 December 2014

Observer(s) and affiliation(s):
Liakos, A. - National Observatory of Athens, Institute for Astronomy, Astrophysics, Space Applications, and Remote Sensing, Palaia Penteli, Athens, Hellas (Greece), alliakos@noa.gr
Nanouris, N. - National Observatory of Athens, Institute for Astronomy, Astrophysics, Space Applications, and Remote Sensing, Palaia Penteli, Athens, Hellas (Greece), nanouris@noa.gr

RA(J2000)	**Dec(J2000)**	**type**	**Mag.**
22 19 10.737	+70 55 55.94	S	19.7 (R)

Period	**Epoch**
Multiperiodic	–

Cross-identification(s):
NOMAD1 1609-0153378 = USNO B1.0 1609-0151173

RA(J2000)	**Dec(J2000)**	**type**	**Mag.**
22 19 47.743	+70 57 55.88	EA	17.6 (R)

Period	**Epoch**
–	–

Cross-identification(s):
NOMAD1 1609-0153459 = USNO B1.0 1609-0151253

Remark: Both stars detected in the FoV of the planetary nebula PNG 111.0+11.6. The C-K light curve is given for comparison. NOMAD1 1609-0153378 shows variations on ~ 2 d and $\sim 2-3$ h timescales, therefore it has been classified as "S – Unstudied variable star with rapid light changes".
NOMAD1 1609-0153459: a single primary and a potential secondary eclipse has been observed, ~ 2.1 days apart.

Date: 19 December 2014
Observer(s) and affiliation(s): Gazeas, K. - Department of Astrophysics, Astronomy and Mechanics, National and Kapodistrian University of Athens, GR 15784, Zografos, Athens, Greece, kgaze@phys.uoa.gr Iliopoulos, I., AKTIS Astronomical Observatory, Oreokastro GR 57013, Thessaloniki, Greece

RA(J2000)	**Dec(J2000)**	**type**	**Mag.**
19 17 27.07	+06 29 51.7	DSCT	10.4 (R)

Period	**Epoch**
0.13727(1) d	2455062.4224(5)

Cross-identification(s):
GSC 0476-1362 = TYC 0476-1362-1

Remark: Detected on 29 September 2007 in the FoV of NGC 6781. Epoch refers to maximum light.

Date: 7 February 2015
Observer(s) and affiliation(s): Gazeas, K. - Department of Astrophysics, Astronomy and Mechanics, National and Kapodistrian University of Athens, GR 15784, Zografos, Athens, Greece, kgaze@phys.uoa.gr Karampotsiou, E. - Department of Astrophysics, Astronomy and Mechanics, National and Kapodistrian University of Athens, GR 15784, Zografos, Athens, Greece, sevi.kar@gmail.com

RA(J2000)	**Dec(J2000)**	**type**	**Mag.**
05 21 08.24	+03 02 51.9	EA	11.33 ($V_{\rm T}$ - TYC2)

Period	**Epoch**
–	2456680.4139(7)

Cross-identification(s):
GSC 0104-0634 = TYC 0104-0634-1

Remark: Detected on 22 January 2014 in the FoV of 1SWASP J052036.84+030402.1.

RA(J2000)	**Dec(J2000)**	**type**	**Mag.**
07 33 35.77	−20 44 37.2	EA	12.19 ($V_{\rm T}$ -TYC2)

Period	**Epoch**
–	2456730.22(5)

Cross-identification(s):
GSC 5991-1106 = TYC 5991-1106-1

Remark: Detected on 13 March 2014 in the FoV of TY Pup.

RA(J2000)	**Dec(J2000)**	**type**	**Mag.**
07 32 38.99	−20 46 52.1	DSCT	11.14 ($V_{\rm T}$ - TYC2)

Period	**Epoch**
0.18236(2)	2456714.2422(5)

Cross-identification(s):
GSC 5991-1727 = TYC 5991-1727-1

Remark: Detected on 19 February 2014 in the FoV of TY Pup. Epoch refers to maximum light.

RA(J2000)	**Dec(J2000)**	**type**	**Mag.**
07 32 44.65	−20 43 11.6	DSCT	11.48 ($V_{\rm T}$ -TYC2)

Period	**Epoch**
0.04954(5)	2456719.3069(2)

Cross-identification(s):
GSC 5991-1865 = TYC 5991-1865-1

Remark: Detected on 2 March 2014 in the FoV of TY Pup. Epoch refers to maximum light.

Date: 10 June 2015

Observer(s) and affiliation(s):
Karampotsiou, E. - Department of Astrophysics, Astronomy and Mechanics, National and Kapodistrian University of Athens, GR 15784, Zografos, Athens, Greece, sevi.kar@gmail.com
Gazeas, K. - Department of Astrophysics, Astronomy and Mechanics, National and Kapodistrian University of Athens, GR 15784, Zografos, Athens, Greece, kgaze@phys.uoa.gr

RA(J2000)	**Dec(J2000)**	**type**	**Mag.**
19 08 03.875	+37 53 59315	EW	15.0 (Rmag - USNO-A2.0)

Period	**Epoch**
0.2812(3)	2457155.419(1)

Cross-identification(s):
USNO-
A2.0 1275-10813091 = GSC2.2 N030320212363 = 2MASS 19080387+3753591 = SDSS J190803.87+375359.1 = KIC 2557987

Remark: Detected on 12th May 2015 in the FoV of KIC 2835289. Differential magnitudes are given with respect to a sum of several comparison stars in the field.

RA(J2000)	**Dec(J2000)**	**type**	**Mag.**
19 08 00.309	+38 01 57.20	EW	15.4 (Rmag - USNO-A2.0)

Period	**Epoch**
0.3974(3)	2457155.484(1)

Cross-identification(s):
USNO-
A2.0 1275-10811543 = GSC2.2 N030320219127 = 2MASS 19080032+3801570 = SDSS J190800.33+380157.1 = KIC 2835711

Remark: Detected on 12th May 2015 in the FoV of KIC 2835289. Differential magnitudes are given with respect to a sum of several comparison stars in the field.

RA(J2000)	**Dec(J2000)**	**type**	**Mag.**
19 07 19.580	+37 55 15.74	EW	16.0 (Rmag - USNO-A2.0)

Period	**Epoch**
0.2850(3)	2457155.506(1)

Cross-identification(s):
USNO-
A2.0 1275-10794124 = GSC2.2 N030320213311 = 2MASS 19071959+3755155 = SDSS J190719.58+375515.6 = KIC 2696006

Remark: Detected on 12th May 2015 in the FoV of KIC 2835289. Differential magnitudes are given with respect to a sum of several comparison stars in the field.

RA(J2000)	**Dec(J2000)**	**type**	**Mag.**
19 07 05.799	+37 54 34.77	EW	16.4 (Rmag - USNO-A2.0)

Period	**Epoch**
0.2921(6)	2457155.539(2)

Cross-identification(s):
USNO-
A2.0 1275-10788218 = GSC2.2 N030320212746 = 2MASS 19070579+3754343 = SDSS J190705.80+375434.3 = KIC 2695854

Remark: Detected on 12th May 2015 in the FoV of KIC 2835289. Differential magnitudes are given with respect to a sum of several comparison stars in the field.

RA(J2000)	**Dec(J2000)**	**type**	**Mag.**
19 08 09.638	+37 56 16.85	EW	16.1 (Rmag - USNO-A2.0)

Period	**Epoch**
0.2691(8)	2457155.556(1)

Cross-identification(s):
USNO-
A2.0 1275-10815489 = GSC2.2 N030320214179 = 2MASS 19080965+3756163 = SDSS J190809.64+375616.3 = KIC 2696645

Remark: Detected on 12th May 2015 in the FoV of KIC 2835289. Differential magnitudes are given with respect to a sum of several comparison stars in the field.

Date: 10 November 2015

Observer(s) and affiliation(s):
Gazeas, K. - Department of Astrophysics, Astronomy and Mechanics, National and Kapodistrian University of Athens, GR 15784, Zografos, Athens, Greece, kgaze phys.uoa.gr

RA(J2000)	**Dec(J2000)**	**type**	**Mag.**
20 32 24.06	+05 16 28.1	EW	7.9(Vmag-USNO-A2.0)

Period	**Epoch**
0.3682(1)	2456495.6525(9)

Cross-identification(s):
HD 195634 = GSC 0518-1033 = SAO 125914 = 2MASS J20322406+0516281 = USNO-A2.0 0900-18660708

Remark: Detected 21 July 2013 in the FoV of MR Del.

RA(J2000)	**Dec(J2000)**	**type**	**Mag.**
06 03 37.68	+27 35 11.4	EW	12.9(Rmag - USNO A2.0)

Period	**Epoch**
0.50316(2)	2456401.2640(9)

Cross-identification(s):
2MASS J06033762+2735111 = USNO-A2.0 1125-03275240 = GSC N22213109574 = USNO-B1.0 1175-0139046

Remark: Detected 12 November 2012 in the FoV of BG Gem.

Date: 9 May 2016

Observer(s) and affiliation(s):
Liska, J. - Department of Theoretical Physics and Astrophysics, Masaryk University, Kotlarska 2, 611 37 Brno, Czech Republic, jiriliska@post.cz
Janik, J. - Department of Theoretical Physics and Astrophysics, Masaryk University, Kotlarska 2, 611 37 Brno, Czech Republic, honza@physics.muni.cz
Zejda, M. - Department of Theoretical Physics and Astrophysics, Masaryk University, Kotlarska 2, 611 37 Brno, Czech Republic, zejda@physics.muni.cz

RA(J2000)	**Dec(J2000)**	**type**	**Mag.**
14 09 07.15	-45 18 18.0	probably RR Lyrae star of RRab type	17.35(2) mag (R) = mean V-C value + USNO R magnitude of Comparison star

Period	**Epoch**
-	2457478.771(2) HJD (maximum)
Cross-identification(s):	
CzeV843 Cen	

Remark: Variability detected 31 March 2016 in the FOV of V834 Cen. The CzeV843 Cen is in the vicinity (about 3.5 arcsec) of a star USNO-A2 0375-20155518 with similar brightness (CzeV843 Cen is about 0.3 mag fainter in R-band). Therefore, it is a blend for many of sky surveys. Observations were performed with the Danish 1.54-m telescope at La Silla, Chile in two nights. Another information is present in the CzeV catalogue http://var2.astro.cz/czev.php. Possible pulsation period can be 0.43 or 0.64 d.

Date: 12 September 2016

Observer(s) and affiliation(s):
Essam, A. - Astronomy Department, National Research Institute of Astronomy and Geophysics (NRIAG), 11421 Helwan, Egypt, essam60@yahoo.com
El-Sadek, M. A. - Astronomy Department, NRIAG, 11421 Helwan, Egypt
Shokry, A. - Astronomy Department, NRIAG, 11421 Helwan, Egypt
Darwish, M. S. - Astronomy Department, NRIAG, 11421 Helwan, Egypt

RA(J2000)	**Dec(J2000)**	**type**	**Mag.**
20 00 59.917	+05 44 11.93	EW	14.807-15.348
Period		**Epoch**	
0.20569 d		2457602.5177±0.0010	
Cross-identification(s):			
UCAC4 479-113658 = 2MASS J20005992+0544120 = GSC2.3 N1Y0035356			

Remark: All the observations have been carried out by using the EEV CCD 42-40 camera with a format of 2048×2048 pixels, cooled by liquid nitrogen attached on the Newtonian focus of the 1.88-m Kottamia reflector telescope in Egypt.
the location of Kottamia Astronomical Observatory (KAO) as follows:
Latitude: 29°56′02.″43 N
Longitude: 31°49′40.″10 E
Height: 467 m
International code = 088

Date: 12 September 2016

Observer(s) and affiliation(s):
El-Sadek, M. A. - Astronomy Department, National Research Institute of Astronomy and Geophysics (NRIAG), 11421 Helwan, Egypt,
Essam, A. - Astronomy Department, NRIAG, 11421 Helwan, Egypt, essam60@yahoo.com
Shokry, A. - Astronomy Department, NRIAG, 11421 Helwan, Egypt
Saad, S. - Astronomy Department, NRIAG, 11421 Helwan, Egypt
Darwish, M. S. - Astronomy Department, NRIAG, 11421 Helwan, Egypt

RA(J2000)	**Dec(J2000)**	**type**	**Mag.**
20 01 07.694	+05 42 21.68	EW	16.07-16.52
Period		**Epoch**	
0.35292 d		2457604.4082±0.0006	
Cross-identification(s):			
UCAC4 479-113711 = 2MASS J20010770+0542216 = USNO-B1.0 0957-0508120			

Remark: All the observations have been carried out by using the EEV CCD 42-40 camera with a format of 2048×2048 pixels, cooled by liquid nitrogen attached on the Newtonian focus of the 1.88-m Kottamia reflector telescope in Egypt.

the location of Kottamia Astronomical Observatory (KAO) as follows:
Latitude: 29°56′02.″43 N
Longitude: 31°49′40.″10 E
Height: 467 m
International code = 088

Date: 6 October 2016
Observer(s) and affiliation(s): Csizmadia, Sz. - Deutsches Zentrum für Luft- und Raumfahrt, Institut für Planetenforschung, D-12489 Berlin, Rutherfordstrasse 2., Germany, szilard.csizmadia@dlr.de Sedaghati, E. - Deutsches Zentrum für Luft- und Raumfahrt, Institut für Planetenforschung, D-12489 Berlin, Rutherfordstrasse 2., Germany; European Southern Observatory, Karl-Schwarzschild-Strasse 2, D-85748 Garching bei München, Germany; Zentrum für Astronomie und Astrophysik, TU Berlin, Hardenbergstr. 36, 10623 Berlin, Germany, esedagha@eso.org Boffin, H. M. J. - European Southern Observatory, Karl-Schwarzschild-Strasse 2, D-85748 Garching bei München, Germany, hboffin@eso.org

RA(J2000)	**Dec(J2000)**	**type**	**Mag.**
09 53 42.692	-45 43 15.95	δ Scuti	V = 13.67 mag

Period	**Epoch**
∼0.1 d	2457418.705

Cross-identification(s):
2MASS 09534278-4543166

Remark: The target was a comparison-star candidate for the spectrophotometric observations of two transits of WASP-19b. Although the differential light curve of the comparison – check star shows some airmass-effect, the variability of 2MASS 09534278-4543166 is clearly visible on both nights when we observed it. The peak-to-peak amplitude is 0.04 magnitude and a main period of ∼0.1 days can be suspected. The $J - K$ colour index is 0.217 (based on the 2MASS Point Source Catalogue). Neglecting interstellar reddening, this corresponds approximately ∼F3 spectral type. The period, the colour index and overall light curve shape suggest a δ Scuti type variable. The object is not listed as a known variable star in GCVS, Catalina Survey or VSX as of the submission date of this note. Figure 1 shows the observed light curve. Notice that the star has a close companion (Fig. 44) and because we did spectroscopic observations with FORS2 (and then we obtained spectrophotometric light curves convolving the spectra with different filter functions) and since the the companion was in the same aperture as the target star, we cannot decide whether the brighter or the fainter star is the variable, but we suspect that brighter one produces the observed light-variation.

Fig. 45. - The light curve of the variable star with solid line on the nights 30 January 2016 (JD 2 457 418) and 29 February 2016 (JD 2 457 448). The dashed curves show the differential light curves of the comparison and the check star. The plotted differential magnitude-curves were shifted by some constant values for sake of clarity.

Acknowledgements: Sz. Cs. acknowledges the Hungarian OTKA Grant K113117.

Reference:

Liakos, A., Niarchos, P., 2010, IBVS, 5998, 3